



UiT The Arctic University of Norway

Faculty of Science and Technology

Department of Chemistry

Marine natural product inspired synthesis towards new antimicrobial and antifouling agents

Synthesis and biological evaluation of novel synthetic mimics of marine eusynstyelamides and studies towards the synthesis of the marine natural product aspergilone A.

Manuel Karl Langer

A dissertation for the degree of Philosophiae Doctor

June 2022

It's still magic even if you know how it's done.

Acknowledgements

It is 2:30 am, and the sun's starting to seep inside our living room/improvised office. Seems like a good time to hail a bunch of people, who travelled alongside me on this winding and bumpy road called a Ph.D. It has sometimes been a hell of a ride.

Firstly, my gratitude goes to Annette, who was still willing to hire me after I decided against her open position in the first place. It was a great pleasure to work under your guidance! I appreciate the freedom and responsibilities you gave me and encouraging me to sometimes aim for more than the bare minimum. I am also grateful for you giving me the opportunity to stay a little longer in Tromsø

Thanks go to my Co-supervisors: Klara, Morten and Marianne for the valuable scientific discussion. Further mention goes to the AntifoMar project, for providing the funding for my research. As a special part of the project, I want to thank Aatur and Hymonti for running all those biological assays and never complaining when I asked for another one. I also want to thank Trude for running all the RBC assays for me. I'd also like to thank the CHOCO group for letting me draw upon their resources and some memorable retreats, even though I've been working on a totally different project.

Special thanks go to Prof. Thomas Wirth for inviting me to Cardiff and giving me the chance to learn about flow chemistry. A big thanks goes to the whole research group for welcoming me so warmheartedly. Jakob, thank you for showing me around in the lab and more importantly the Valleys and the Brecon Beacons. I am indebted to Bethan Winterson for sharing her knowledge about flow chemistry and letting me to see a great mind at work.

A big thanks goes to all my proof-readers Sasha, Phil, Hanna, and Marc. Sasha, thank you so much for working your way through the first draft and many barely improved ones afterwards. I know it was a stony way and a despairing one at times - but Dobby is free now! Thank you, Phil, for your valuable comments and corrections.

To my colleagues in general for a good work environment, laughter, trash-talk and helping in various kinds of troubleshooting. I want to thank the engineers, Jostein Johansen, Truls Ingebrigtsen, Frederic Alan Leeson and Arnfinn Kvarsnes, for keeping this place up and running.

To all those friends made along the way. To Sasha, thanks for being so tidy in the lab. I'm looking forward to tricking you into yet another adventure. To Harald for patiently listening to my, at first, gibberish Norwegian, to Yngve for some well planned and terribly executed trips, to Karen and Jenny for many climbing sessions, and to so many more not listed here. To the Red Cross, which provided yet another, totally different opportunity to develop myself.

I am extending my gratitude to all my old friends left behind in Germany. The same for my parents, who always supported me in whatever I was doing and had my back, regardless of where I chose to settle down.

And finally, to the most important person in the story, my partner Hanna Bähr who has shared only God knows (literally) how many years of her life with me. Thank you for practically forcing me to this beautiful place by following your own dreams and the snow. There are so many things I wouldn't have gotten in touch with, if it hadn't been for you. I am looking forward to many new adventures, wherever life may take us.

Manuel Langer
June 2022, Tromsø, Norway

Abstract

Natural products (NPs) have been a major source for the development of new small molecule drugs in modern medicine. While today's clinical agents almost exclusively originate from NPs from terrestrial sources, marine natural products (MNPs) have started to become of bigger interest over the last five decades, due to greater accessibility of the latter. Technological advances have allowed for extended marine bioprospecting and together with new organisms, a wealth of new bioactive MNPs have been discovered. Despite that, only four MNPs or derivatives thereof are currently in clinical use, leaving a rich pool of bioactives largely untapped.

The focus of the presented thesis is on two MNPs, the eusynstyelamides and aspergilone A, showing antimicrobial and anticancer/antifouling activity, respectively. Thus, these MNPs target pressing health and economical challenges – antimicrobial resistance and marine fouling.

The eusynstyelamides share the pharmacophore of cationic antimicrobial peptides (AMPs), which makes them potential candidates for the development of new antimicrobials. Our aim was to investigate if small-molecule amphipathic eusynstyelamide derivatives can mimic the antimicrobial activity of AMPs.

Almost 100 mimics of the eusynstyelamides were synthesized and tested for their antimicrobial potency and haemolytic activity. Tetrasubstituted, amphipathic barbiturates and hydantoins were the two main structural classes. Barbiturates were found to deliver the most active structures, whereas hydantoins had a better activity-toxicity balance. *N*-propyl hydrocarbon linkers were the most versatile and *n*-butyl linkers were the most active when combined with guanidyl cationic groups. The most active derivatives exhibited MIC values of 2-8 µg/mL against multi-resistant clinical isolates. In the future, the pharmacokinetic properties of the most promising mimics should be analyzed, to elucidate which refinements need to be made and additional core structures could be evaluated to potentially improve the potency even further.

Aspergilone A exhibits antifouling activity and shows additional selective *in vitro* cytotoxicity. This dual activity and aspergilone A's structural resemblance to other NPs sparked our interest.

The synthesis of aspergilone A has not been described, therefore we aimed to develop an enantioselective synthetic route towards aspergilone A, with *ent*-phenol A as a key intermediate, initiating a program to develop antifouling agents. Phenol A, the enantiomer of *ent*-phenol A, is a structural motif found in a number of other NPs and is thus of additional interest for the potential synthesis of the latter.

The synthetic efforts led to a stereocontrolled and adaptable synthesis of *ent*-phenol A, which allows for the construction of all four stereoisomers of the latter without any changes to the protocol. *ent*-phenol A was obtained enantiopure in >99% ee and 5% yield over 7 steps. The new approach towards *ent*-

phenol A can be a first step towards a future total synthesis of aspergilone A, and related NPs, and subsequent structure-activity relationship (SAR) studies.

Summary of papers and author contributions

Paper I

Amphipathic Barbiturates as Mimics of Antimicrobial Peptides and the Marine Natural Products Eusynstyelamides with Activity against Multi-resistant Clinical Isolates.

Marianne H. Paulsen, Magnus Engqvist, Dominik Ausbacher, Trude Anderssen, **Manuel K. Langer**, Tor Haug, Glenn R. Morello, Laura E. Liikanen, Hans-Matti Blencke, Johan Isaksson, Eric Juskewitz, Annette Bayer, and Morten B. Strøm, *J. Med. Chem.* **2021**, 64, 11395–11417.

Paper Summary:

In paper I we introduced amphipathic tetrasubstituted barbituric acid derivatives as mimics for the marine antimicrobials eusynstyelamides. The compounds were designed to fulfil the pharmacophore model derived from antimicrobial peptides, with the compounds having a net charge of +2 and two lipophilic groups. A new synthetic route was developed consisting of 6-8 steps, delivering a total of 16 compounds. We obtained highly active compounds against Gram-positive and Gram-negative strains, including a panel of 30 antibiotic resistant clinical isolates. The mode of action was studied *in vitro* and *in silico* with MD simulations. The *in vivo* activity in a mouse model was demonstrated for one derivative.

My contribution:

I proposed the convergent synthetic route, carried out all associated experiments and wrote the respective paragraph in the Supporting Information. I contributed to the synthesis of PI-2d, PI-3d, PI-6f, PI-7f, and purity determination of several final guanidyl derivatives.

Paper II

A concise SAR-analysis of antimicrobial cationic amphipathic barbiturates for an improved activity-toxicity profile – submitted to *Eur. J. Med. Chem.*

Manuel K. Langer,[#] Aatur Rahman,[#] Hymonti Dey, Trude Anderssen, Francesco Zilioli, Tor Haug, Hans-Matti Blencke, Klara Stensvåg, Morten B. Strøm, Annette Bayer

Paper Summary

In paper II we studied the structure-activity relationship of the amphipathic barbiturates from paper I in detail, by successively varying the cationic groups, hydrocarbon linkers and lipophilic side chains. We devised a shorter and more versatile synthetic strategy to allow for the efficient synthesis of a diverse library. A total of 59 compounds were obtained, all of which were evaluated for their antimicrobial

potency and haemolytic activity. We found guanidines and amines delivering highest broad-spectrum activity and the lipophilic side chains being the main contributor to antimicrobial potency. *n*-Propyl hydrocarbon linkers delivered the best balance between potency and toxicity. The guanidine derivative **3bG** demonstrated a strong membranolytic effect on the outer and inner membrane.

My contribution:

I have designed the 5 series of compounds and decided on the composition of each series. I developed and optimized all synthetic protocols. I synthesized all compounds and collected the analytical data except for PII-2eA, PII-2eG, PII-3eA, PII-3eG, PII-4bG, PII-4(e-h)A, PII-4(e-g)G, PII-5(b-d)A, PII-5fA, PII-5fG. For the aforementioned compounds, I have supervised the synthesis and data collection. I have analyzed and interpreted all analytical data. I contributed to the analysis and contextualization of MIC and RBC values and initiated the studies on the counterion effect. I wrote the first draft of the manuscript, except for the paragraph on mode of action studies and was responsible for editing the later versions. I did not carry out the biological experiments.

Paper III

Hydantoins as a Promising Platform for the Development of Tetrasubstituted, Amphipathic Antimicrobials with Membranolytic Properties – Manuscript

Manuel K. Langer, Ataur Rahman, Hymonti Dey, Trude Anderssen, Hans-Matti Blencke, Tor Haug, Klara Stensvåg, Morten B. Strøm, Annette Bayer

Paper Summary

In paper III we transferred our most promising combination of lipophilic group, hydrocarbon linkers and cationic groups to five new core structures. We identified hydantoin as a new, promising platform for the construction of tetrasubstituted, amphipathic antimicrobials. A total of 20 hydantoin derivatives were synthesized and evaluated for their antimicrobial potency and haemolytic activity. We found that hydantoins generally showed low haemolytic toxicity, also for derivatives with broad-spectrum activity. Initial mode of actions studies suggested guanidine **2bG** to have a strong membranolytic effect.

My contribution:

I have designed all final derivatives, proposed and developed the synthetic strategies and carried out all the chemical synthesis and analyzed and interpreted all analytical data. I contributed to the analysis and contextualization of MIC and RBC values. I wrote the first draft of the manuscript, except for the paragraph on the mode of action studies and was responsible for editing the later versions. I did not carry out the biological experiments.

Paper IV

Stereocontrolled and Adaptable Synthesis of *ent*-Phenol A – one Protocol for the Formal Synthesis of All Four Stereoisomers – Manuscript

Manuel K. Langer, Annette Bayer

Paper Summary

Paper IV describes the stereoselective synthesis of *ent*-phenol A, a key intermediate in the synthesis of the marine antifouling and anticancer compound aspergilone A. The approach allows for the total control of both stereocenters and thereby the facile access to all four stereoisomers. Phenol A, the enantiomer of *ent*-phenol A, is found in most members of the citrinin-type azaphilone family, a structurally related class of polyketides, thus opening for the access to a range of other natural products and analogues thereof.

My contribution

I chose the target structure and developed the synthetic strategy. I carried out all the experimental work and data analysis. I have written the first draft of the manuscript and was responsible for editing the later versions.

Table of Contents

Acknowledgements	II
Abstract	IV
Summary of papers and author contributions	VI
Abbreviations	XI
1 Introduction	1
1.1 Aim of the thesis.....	3
1.2 Outline.....	4
2 Background relevant for this thesis	5
2.1 Natural products: the template for drugs.....	5
2.2 Sources of NPs.....	6
2.2.1 Terrestrial: Fungi and Plants.....	6
2.2.2 Marine sources.....	7
2.2.3 Challenges in NP guided drug discovery	9
2.3 Part A: Eusynstyelamides and their potential as antimicrobial agents	11
2.3.1 The need for new antimicrobials.....	11
2.3.2 The eusynstyelamides: promising marine antimicrobials.....	11
2.3.3 Antimicrobial peptides	12
2.3.4 Mechanism of Action of AMPs.....	13
2.3.5 AMPs in clinical use.....	15
2.3.6 Towards the development of SMAMPs	16
2.3.7 Resistance to AMPs and SMAMPs	19
2.4 Part B: Aspergilone A, an interesting azaphilone	23
2.4.1 The importance of marine biofouling.....	23
2.4.2 General characteristics of azaphilones	23
2.4.3 Citrinin-type azaphilones	24
2.4.4 Synthesis of the azaphilone core and citrinin-type derivatives.....	25
3 General discussion of results from the thesis	29
3.1 1 st Generation of <i>N,N'</i> -dialkylated-5,5-disubstituted barbiturates (paper I).....	29
3.1.1 Introduction	29
3.1.2 Summary of the synthetic work.....	31
3.1.3 Summary of the biological studies.....	33
3.2 2 nd Generation of <i>N,N'</i> -dialkylated-5,5-disubstituted barbiturates (paper II)	36
3.2.1 Introduction	36
3.2.2 Design of the compounds and the synthetic strategy	36

3.2.3	Synthesis.....	37
3.2.4	Summary of biological results	40
3.2.5	Additional results not included in paper II	42
3.3	3 rd Generation: Varying core structures with focus on hydantoins (paper III)	44
3.3.1	Introduction and scaffold design.....	44
3.3.2	Summary of the synthetic work.....	44
3.3.3	Summary of the biological studies.....	50
3.3.4	Additional biological results not included in paper III.....	51
3.4	Comparison of the antibacterial compounds investigated.....	53
3.4.1	Scaffold contribution	53
3.4.2	Contribution of the lipophilic side chains.....	54
3.4.3	Combinations of linkers and cationic groups.....	55
3.4.4	Summary of Part A.....	58
3.5	Towards the total synthesis of Aspergilone A (paper IV).....	59
3.5.1	Introduction	59
3.5.2	Retrosynthetic analysis	59
3.5.3	Synthesis.....	60
3.5.4	Additional results not included in paper IV.....	62
3.5.5	Summary of Part B.....	67
4	Conclusion and Outlook.....	68
5	Experimental Details.....	69
5.1	General methods.....	69
5.1.1	PII: Attempted amidine synthesis	70
5.1.2	Additional compounds connected to paper III	71
5.1.3	Synthesis of aspergilone A under continuous flow.....	78
6	References.....	81
7	Appendix.....	95
7.1	NMR spectra.....	95
7.2	SFC traces.....	108
7.3	IR spectra	109

Abbreviations

AF	Antifouling
AMP(s)	Antimicrobial peptide(s)
AMR	Antimicrobial resistance
APD	Antimicrobial Peptide Database
aq	aqueous
B ₂ pin ₂	bis(pinacolato)diborane
Boc	<i>tert</i> -butyl carbonate
BPR	Back pressure regulator
CC ₅₀	Cytotoxic concentration to reduce cell viability by 50%
CDI	1,1'-Carbonyldiimidazole
COSY	Homonuclear correlated spectroscopy
DCC	<i>N,N'</i> -cyclohexylcarbodiimide
DCM	Dichloromethane
DDD	Drug discovery and development
DDQ	2,3-dichloro-5,6-dicyanoquinone
DIAD	Diisopropyl azodicarboxylate
DIBAL-H	Diisobutylaluminium hydride
DIC	<i>N,N'</i> -diisopropylcarbodiimide
DIPEA	<i>N,N</i> -diisopropylethylamine
DFT	Density functional theory
DMI	1,3-Dimethyl-2-imidazolidinone
DMF	<i>N,N</i> -dimethylformamide
DMSO	Dimethyl sulfoxide
DNA	Desoxyribonucleic acid
DNP	The Dictionary of Natural Products
EC ₅₀	Effective concentration to produce 50% of the maximum response
EG	Ethylene glycol
EtOAc	Ethyl acetate
FDA	Food and Drug administration
GM	Geometric mean
HMBC	Heteronuclear single quantum coherence
HRMS	High resolution mass spectrometry
HTS	High throughput screening

IC ₅₀	Inhibitory concentration required for 50% inhibition in vitro
ID	Inner diameter
IM	Inner membrane
<i>i</i> PrOBpin	2-isopropylboronic acid, pinacol ester
LA	Lewis Acid
LD ₅₀	Lethal dosage required to kill 50% of the organism of interest
LPS	Lipopolysaccharide
LTA	Lipoteichoic acid
MIC	Minimum inhibitory concentration
MNP(s)	Marine natural product(s)
MoA	Mode of action
MS	Mass spectrometry
MS/MS	Tandem mass spectrometry
MTBE	Methyl <i>tert</i> -butyl ether
MTD	Maximal tolerated dose
NaHMDS	Sodium bis(trimethylsilyl)amide
NCE	New chemical entity
NMR	Nuclear magnetic resonance
NP(s)	Natural Product(s)
NPD	Natural product discovery
NPN	1- <i>N</i> -phenylnaphthylamine
o ₂ s	Over to steps
OM	Outer membrane
dppf	1,1'-Bis(diphenylphosphino)ferrocene
PE	Petrol ether
PEEK	Polyether ether ketone
PEG-400	Polyethylene glycol 400
PL(s)	Phospholipid(s)
PTC	Phase-transfer catalysis/catalyst
PTFE	Polytetrafluoroethylene
RBC	Red blood cell
ROESY	Rotating frame Overhauser Enhancement Spectroscopy
RP-HPLC	Reversed phase high performance liquid chromatography
r.t.	room temperature

SAR	Structure-activity relationship
SFC	Supercritical flow chromatography
SI	Selectivity index given by (EC ₅₀ /MIC)
SMAMP	Synthetic mimic of antimicrobial peptides
T	Temperature
TA	Teichoic acid
TBAB	Tetra- <i>n</i> -butylammonium bromide
TBAI	Tetra- <i>n</i> -butylammonium iodide
TEG	Triethylene glycol
TFA	2,2,2-Trifluoro acetic acid
THF	Tetrahydrofurane
TMSCl/I	Trimethylsilyl chloride/iodide
TosMIC	<i>p</i> -Toluenesulfonylmethyl isocyanate
t _r	Residence time
UV	Ultraviolet
μ-wave	Microwave

1 Introduction

Natural products (NPs), in particular secondary metabolites, have been used for medical purposes over several millennia and laid the foundation of modern drug discovery and development (DDD). According to Newman et al. out of the 1394 small molecule drugs, approved between the beginning of 1981 and the end of 2019, 699 were either (modified) NPs or based on the pharmacophore of a NP, amounting to a total of 50% of all approvals.¹ In terms of clinical indications, 65% of all antibacterial and 73% of all anticancer compounds were derived from natural sources.^{2, 3}

NPs have additional pharmaceutical applications outside of DDD. While not always occupying a leading role, NPs serve as a source for new pesticides,⁴ are used as food additives in the form of spices and antioxidants to ensure freshness and longevity,⁵ as well as being widely used in cosmetics in the form of essential oils.⁶

A potential rich source for NPs is marine based organisms. However, despite the majority of earth's surface being covered by water, only in the last four decades this untapped source has gained increasing attention with less than 1% of all marketed drugs being of marine origin.⁷ Despite the wealth of compounds found, many are not investigated beyond the elucidation of their structure and the establishment of their bioactivity. This opens up opportunities to find a natural "blueprint" as a starting point in the development of new synthetic drugs for today's pressing clinical indications.

To investigate and improve the bioactivity of NPs it is often advantageous to either synthesize the natural product itself or to make synthetic analogues. Analogues often have less complex structures or have defined variations, to only study certain structural features at a time. Derivatives of NPs can either be used to elucidate the pharmacophore needed for biological activity, or, if the mode of action (MoA) is already known, to reduce the NP to its most elemental features.

The present thesis focuses on synthetic efforts towards compound libraries derived from two marine natural products (MNPs), one with antimicrobial and one with anticancer/antifouling (AF) activity, which address pressing health and economical questions in modern society. 1.27 million deaths were linked directly to infections caused by antimicrobial resistant (AMR) bacteria in 2019,⁸ with a projected death toll of 10 million by year 2050.⁹ Cancer claims almost 10 million deaths per year and is the first or second leading cause of death before age 70 in 60% of all countries.¹⁰ Marine biofouling describes the attachment of micro- and macroorganisms to submerged man-made structures.¹¹ Fouling has a major impact on the fuel consumption of marine vessels,¹² and thereby a huge financial impact on the shipping industry.

Members of the eusynstyelamide family (Figure 1, left) were isolated from marine based organisms at the Australian shore and in the Barrents sea and displayed mediocre antimicrobial activity with a minimum inhibitory concentration (MIC) of 6.25-25 $\mu\text{g/mL}$ against *Staphylococcus aureus*, *Escherichia coli* and *Pseudomonas aeruginosa*.^{13, 14}

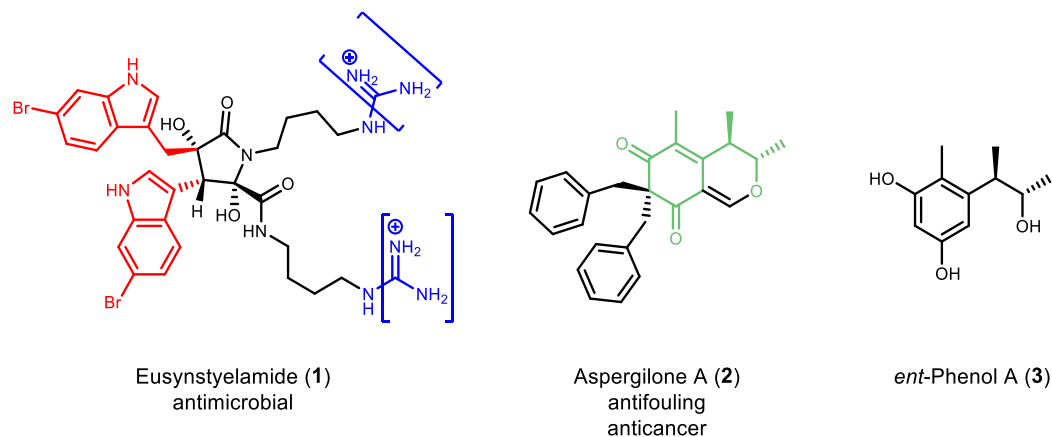


Figure 1. Left: General structure of the eusynstyelamides *ent*-B, D, E and F is shown. The lipophilic part is shown in red and the hydrophilic part in blue. Brackets indicate the possible combinations of an amino and guanidino group found in the different family members.¹⁴ Middle: The structure of aspergilone A is shown, with the *ent*-phenol A partial structure shown in green. Right: The structure of *ent*-phenol A.

They feature two lipophilic 6-bromoindol moieties (red) and two cationic groups either being primary amines, guanidines or a mixture of the two (blue), bound to a central heterocycle. Their amphipathic nature is closely related to that of synthetic mimics of antimicrobial peptides (SMAMPs),¹⁵ which are highly promising candidates as broad-spectrum antibiotics,¹⁵ and fulfills the pharmacophore model of small cationic peptides (AMPs).¹⁶ With AMR being on the rise¹⁷ the demand for new antimicrobial agents is higher than ever. The eusynstyelamides can serve as a valuable structural starting point for the development of new SMAMPs with broad-spectrum antimicrobial activity.

Aspergilone A (2) (Figure 1, middle) is a member of the azaphilone family and was isolated from a marine-derived fungus which was associated with a gorgonian in the South China Sea.¹⁸ It exhibited in vitro cytotoxicity against three tumor cell lines with IC_{50} values of 3.2-37 $\mu\text{g/mL}$.¹⁸ Additional potential AF activity with a EC_{50} value of 7.68 $\mu\text{g/mL}$ was reported. Synthetic access to aspergilone A would give the possibility to study its structure-activity relationships (SAR) and potentially identify new lead compounds. Aspergilone A contains an *ent*-phenol A (3) partial structure (Figure 1, right) and the enantiomer (phenol A) is found in a range of azaphilones, which is the parental class of NPs. If *ent*-phenol A can be incorporated as a synthetic intermediate, it might facilitate the easier access to further azaphilones.

1.1 Aim of the thesis

The aim of the work was two parted: A) The development of new synthetic mimics of the marine antimicrobials **1** preserving the amphipathic nature of the natural product exhibited by two lipophilic and two cationic groups. B) The development of a synthetic strategy towards the MNP **2** with **3** as a key intermediate, enabling an easy-to-build compound library for future SAR studies.

For part A, the marine antimicrobials **1** served as structural starting point. To study mimics of the NP we divided this part into three sub-projects (Figure 2), each focusing on one generation of mimics and the following questions in order:

- (1) Can the butyrolactam core of the eusynstyelamides be simplified by replacement with a barbituric acid and will that, when correctly decorated with cationic and lipophilic groups, provide an amphipathic structure with antimicrobial activity?
- (2) Which combination of structural components (linker, lipophilic side chain, cationic group) delivers the best balance between antimicrobial potency and haemolytic activity?
- (3) Can the barbituric acid core structure be substituted by other heterocycles, and how will this affect the bioactivity?

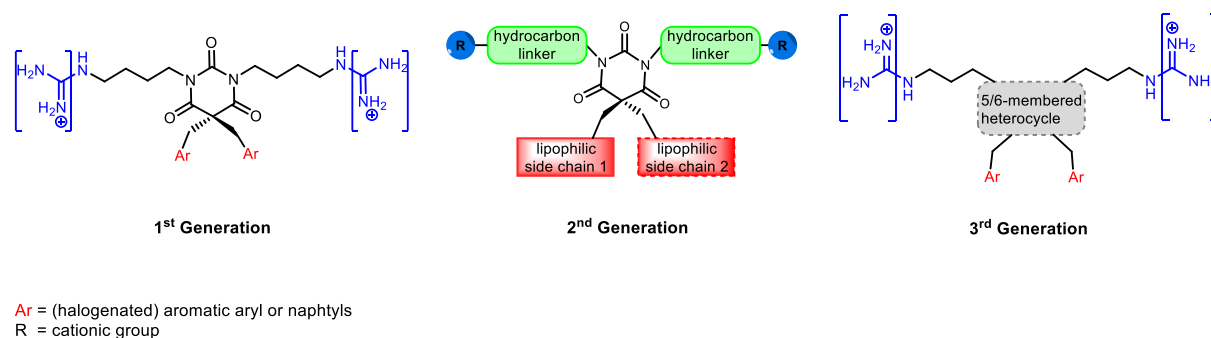


Figure 2. General structures of the eusynstyelamide mimics investigated in this study. For all structures two identical cationic groups were used. Brackets indicate that either two amino or two guanidino groups were used. Left: General structure of the 1st generation of mimics. Ar = (pseudo)halogenated phenyl or naphthyl groups. Middle: General structure of the 2nd generation of mimics. R = cationic head group consisting of 1° - 4° amines, guanidyl and pyridinyl. Hydrocarbon linkers consisted of linear chains containing 2-6 carbons or cyclobutyl and cyclohexyl groups. As lipophilic side chains two identical or a mixture of two different substituted aryls, heteroaryls and linear hydrocarbons were used. Right: General structure of the 3rd generation of mimics. Ar = (pseudo)halogenated phenyl or naphthyl moieties.

For part B, we aimed for a concise and robust synthetic strategy towards **2** via *ent*-phenol A (**3**) as a key intermediate, allowing for multiple points of derivatization for a future compound library (Figure 3). Of particular interest was the facile access and control of the stereocenters (orange oval). Introduction of substituted aryl groups (olive box) should happen as late as possible to facilitate the synthesis of a larger compound library. Further points of interest were the removal of the methyl group (blue oval) and the introduction of a substituent at C-8 (red oval).¹⁹

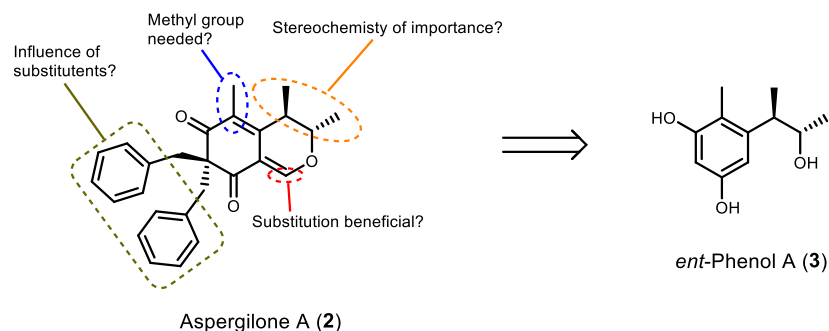


Figure 3. Structure of aspergilone A (2) with possible points for derivatization and the key intermediate *ent*-phenol A (3).

1.2 Outline

The thesis is divided into several sections. Chapter 1 states the motivation and aim of this investigation. Chapter 2 summarizes the relevant background for the thesis. In subchapter 2.1, a brief summary of the impact of NPs on the development of modern medicine is given, followed by describing general sources of natural bioactives and closing with a comment on the obstacles posed by NPs in drug discovery. Subchapter 2.2 describes the main sources of NPs. The two NPs relevant to this work are presented in subchapter 2.3 and 2.4, including structural peculiarities, biological activity, and their MoA, if known. Chapter 3 summarizes the findings, which are further elaborated in paper I-IV. The three subchapters (3.1-3.4) are dedicated to the investigation of the mimics of the eusynstyelamides. Subchapter 3.5 contains the studies on aspergilone A, including additional information not reported in paper IV. Chapter 4 gives a short conclusion and an outlook. Experimental procedures, references and the appendix, including additional data, can be found in chapters 5, 6 and 7, respectively. All structures, which can be found in the papers I-IV are denoted with the same code as in the corresponding paper and carry the prefix **PI**, **PII**, **PIII** or **PIV**, indicating in which paper they can be found. All other molecules are numbered consecutively in order of their appearance in the thesis.

2 Background relevant for this thesis

2.1 Natural products: the template for drugs

The term NP is commonly used for small molecules from natural sources. A number of NPs are secondary metabolites, indicating that the respective compounds originate from non-vital metabolic pathways in the organism of interest.^{7,20} Many NPs have elaborate chemical structures and often exhibit multiple, nevertheless specific biological activities. The biological activity of NPs has been utilized for thousands of years in traditional, often plant based, medicine, long before any of the bioactive compounds had been isolated and studied as single molecules.^{7,21}

Penicillin, being isolated from *Penicillium notatum* in 1929 by Fleming²² and commercialized in the 1940s,^{23,24} can be considered the starting point of natural product based DDD.⁷ In the years, which were to come, most of the major pharmaceutical industries at the time initiated natural product discovery (NPD) programs, focusing on antibacterial and antifungal compounds, as well as anti-infectious agents.⁷ During the course of those programs, additional lead compounds for various clinical indications were identified, including cancer, hypercholesteremia and tissue rejection.^{25,26}

Many of the industrial NPD departments had been reduced or shut down in the early 1990s, which is often correlated to the emergence of combinatorial chemistry and automated high throughput screening (HTS).²⁷ Despite the initial enthusiasm it was quickly realized that combinatorial libraries were intrinsically limited in chemical space and could not deliver as many new chemical entities (NCEs) as anticipated, due to the libraries lacking the structural complexity found in nature.^{7,28} This is well exemplified by the kinase inhibitor sorfendib. It is the only NCE being obtained from combinatorial chemistry and being approved by the U.S Food and Drug Administration (FDA) as of 2010.²⁸ Meanwhile, the total number of approved small-molecule NCEs has been reduced from the 1980s (more than 60/year) to an average of 23 NCEs/year in the period between 2001-2010.^{1,21} This reduction in clinically approved NCEs coincides with the scaling down of industrial NPD programs.

The realization that combinatorial chemistry on its own would not generate enough novel synthetic drugs has led to a renewed focus on NPs.²⁹ Using the structural richness of NPs as basis together with modern combinatorial methods, led to the so called diversity-oriented synthesis.²¹ In this now common approach, privileged structures or structural subunits found in a wide range of diverse bioactive NPs, are identified and used as starting points for building combinatorial libraries.^{21,28} The value NPs still hold is further exemplified by two NP derivatives having been number one and four of the best selling drugs in the US between 1992 and 2017, namely the hypocholesterolemic drug atorvastatin (tradename: Lipitor) and the beta-2-adrenergic agent advair.¹

2.2 Sources of NPs

The Dictionary of Natural Products (DNP) lists over 300,000 NPs from all possible sources,² among the listed are ~55,000 (~18%) from marine sources according to The Dictionary of Marine Natural Products (MDNP), a subset of the DNP database.³⁰ The difference seems quite surprising, given the fact that around 70% of the earth's surface is covered by water. Even though pharmaceutical companies and research institutions had been aware of the great biodiversity found in the oceans, sampling of marine sources is accompanied by the requirement of special equipment, and therefore much higher costs.²¹ However, technological advances during the last decades have allowed for the exploration of so far unreachable territories and increased the cost-efficiency.²¹ In the ten years from 1977 to 1987 around 2500 marine natural products (MNPs) had been reported,²¹ whereas 1407 new compounds had been listed in 2020 alone,³¹ the numbers steadily increasing over the years.³² The late onset of exploration of marine sources is also reflected by the fact that less than five MNPs (including derivatives thereof) were approved for clinical use, as of 2016.³³ In the following some important examples of NPs from terrestrial and marine sources are given.

2.2.1 Terrestrial: Fungi and Plants

Fungi and plants have been used by mankind for several millennia as food, in preparation of alcoholic beverages (yeasts) and as medication in traditional medicine.⁷ Later, they were also recognized as a rich source for the isolation of bioactive NPs, of which four are presented here (Figure 4). Isolated from a

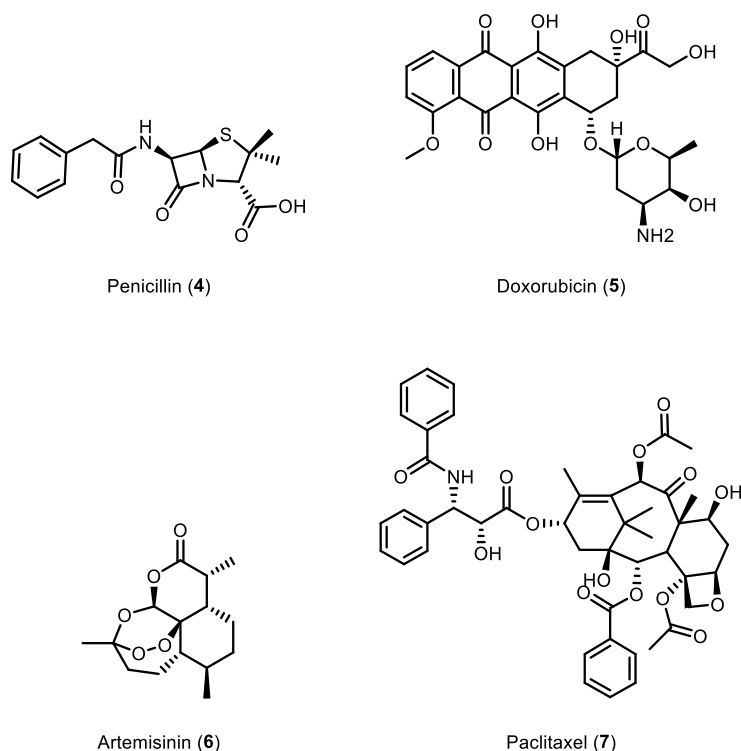


Figure 4. Structures of penicillin (4), doxorubicin (5), artemisinin (6) and paclitaxel (7).

fungus, as noted before, the undoubtedly most famous natural product is the β -lactam containing penicillin (4) (Figure 4). Its isolation paved the way for the “golden age” of the antibiotics, leading to the discovery of other antibiotics of fungal origin, including the structural classes of norcaridins, carbapenems and monobactams.⁷

Doxorubicin (5), an anthracycline, is used to treat acute leukemia, lung cancer, thyroid cancer, soft tissue and bone sarcomas, and both Hodgkins and non-Hodgkins

lymphomas.^{27, 34} It was first isolated in 1969 from *Streptomyces peucetius* var. *caesius*³⁵ and belongs to the daunomycin family.

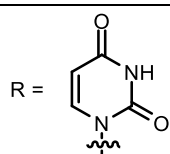
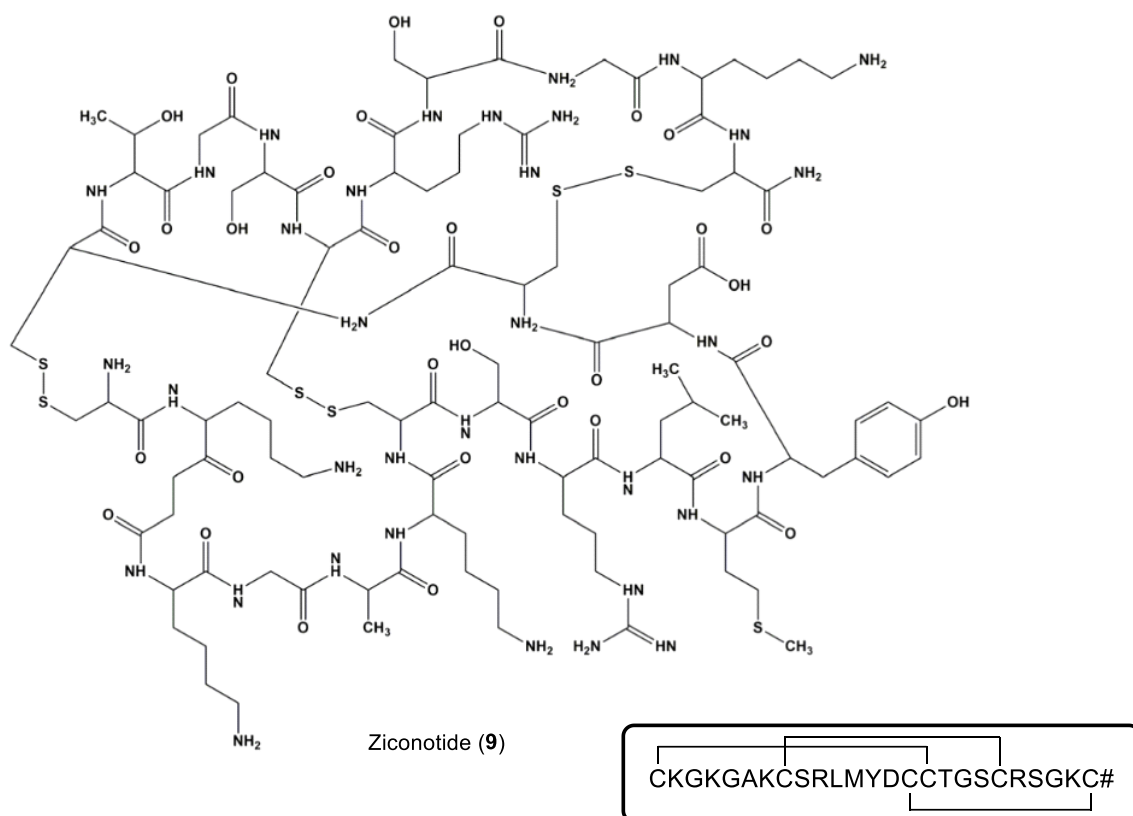
One very important plant-based NP is artemisinin (**6**). The NP had been used unknowingly, when employing its producer plant, *Artemisia annua*, for fever treatment in traditional Chinese medicine. In 1967, during a search for new antimalarial drugs among traditional remedies in China, the plant had been rediscovered and artemisinin (**6**) was eventually isolated from *A. annua* in 1972.³⁶ As of today, **6** is an approved antimalarial drug, together with some of its synthetic derivatives.³⁷ The discovery of **6** had been a breakthrough, due to the emerging resistance in many tropical regions against the antimalarials chloroquine and mefloquine, both being derivatives of the NP quinine.²¹

Paclitaxel (**7**) (tradenname: Taxol) is a member of the taxane family and was originally isolated in 1971 from the bark of the Pacific yew *Taxus brevifolia* Nutt.^{38, 39} It took another 20 years for it to be approved for clinical use against ovarian cancer in 1992 and breast cancer in 1994.^{1, 21} Its importance is reflected by annual sales of over \$1 billion and has inspired the development of many analogues, broadening its use in cancer therapy.^{21, 38}

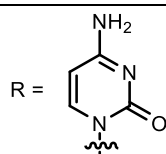
2.2.2 Marine sources

A report from 2012 stated that a total of four MNPs or derivatives thereof (**9**, **12-14**, Figure 5) had been approved for clinical use and another 13 had been in clinical trials.⁷ Of the four being marketed, three compounds were FDA approved and one was registered in the EU. As of writing, the picture has not changed much in terms of approvals, but increasingly more MNPs are in pre-clinical investigations.³³ The majority of the candidates being approved or in clinical trials are (potential) anticancer drugs. This clinical indication being so prevalent, can often be traced back to the funding bodies' interest in the development of new chemotherapeutics.^{40, 41}

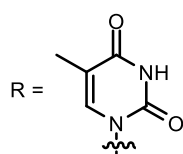
Despite the focus on new anti-cancer drugs, the analgesic ziconotide (**9**) (Prialt®) (Figure 5), approved in 2004, became the first MNP in clinical use without any modifications.³³ It is a 25-mer cyclic peptide and was first isolated from cone snails (*Conus magus*) in 1985, alongside other peptides.⁴² Ziconotide's neurotoxic activity is based on reversibly blocking N-type calcium channels located at the dorsal horn of the spinal cord,^{43, 44} by binding to the presynaptic channels and reducing the release of neurotransmitter. Importantly, it does not produce tolerance upon reoccurring application in contrast to opiates, which lead to desensitization of the patient over time, presenting a major drawback.⁴⁵ Around 200 analogues had been synthesized and evaluated for their pharmaceutical potential, but eventually the parent compound was chosen for commercialisation.³³



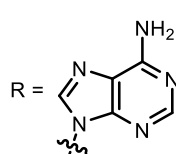
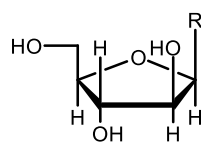
Spongouridine (10)



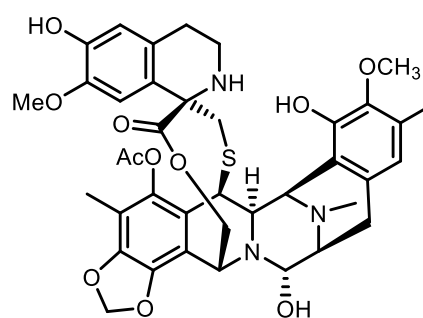
Cytarabine (Ara-C) (12)



Spongothymidine (11)



Vidarabine (Ara-A) (13)



Trabectedin (14)

Figure 5. Structures of ziconotide (9), spongouridine (10), spongothymidine (11), cytarabine (12), vidarabine (13) and trabectedin (14). The sequential one letter code of peptide (9) is given in the black box. Structure (9) was reproduced with permission from Lee et al., *Mar. Drugs* 2015, 13(8), 4967-4984.⁴⁶

One of the first notable discoveries of bioactive compounds from marine sources can be traced back to *C*-nucleosides spongouridine (10) and spongothymidine (11) (Figure 5), obtained from a Caribbean sponge (*Tethya crypta*) in the early 1950s.⁴⁷⁻⁴⁹ While the NPs were not introduced into clinical use, a synthetic derivative, cytarabine (12, Ara-C), was FDA approved in 1969 as a chemotherapeutic agent. 12 is converted intracellularly into cytosine arabinoside triphosphate that competes with the endogenous substrate deoxycytidine triphosphate, resulting in inhibition of the DNA polymerase and DNA synthesis.⁵⁰ Chemically substituting the cytosine with an adenine delivered vidarabine (13, Ara-A), which was commercialized as an antiviral compound. When first introduced to the market, 13 was

manufactured synthetically, but in later years it was also found in the Mediterranean sea (*Eunicella cavolini*),⁵¹ thus being a true MNP in clinical use.³³

The fourth MNP currently in clinical use is trabectedin (**14**) (tradename: Yondelis®, ET-743), found in a tunicate (*Ecteinascidia turbinata*) in the Caribbean and Mediterranean sea.^{52, 53} It was first approved in the European Union for treatment of soft tissue sarcoma⁵⁴ and relapsed platinum-sensitive ovarian cancer.⁵⁵ The structural basis is formed by three fused tetrahydroisoquinoline units through a 10-member lactone bridge and **14** can now be obtained by semisynthesis from safracin B cyano.^{50, 56} The MoA was not fully elucidated, but **14** is hypothesized to bind to the DNA minor groove by a covalent reversible bond and to interact with different binding proteins of the Nucleotide Excision Repair machinery.⁵⁰

These examples demonstrate that MNPs are indeed a valuable source of novel drug candidates and are worth investing more resources into their exploration.

2.2.3 Challenges in NP guided drug discovery

As successful as NPs have been in drug discovery, they face certain challenges in their development phase. Historically, when a microorganism was not cultivatable (less than 1% of all microorganisms observed spectroscopically²¹), it was practically impossible to study that organism and any secondary metabolites it might produce. This challenge has been alleviated somewhat by improved culturing procedures, allowing for the parallel growth of slow- and fast-growing organisms.²¹ If organisms are still not culturable, modern genomics can be used for identification of the organism and with increasing knowledge of gene clusters coding for certain groups of NPs (e.g. polyketide synthase for polyketides), the relevant genes can be identified and expressed by modern cloning techniques.²¹

A previous difficulty was the compatibility of NP crude extracts with HTS. Given the complexity of the extracts, one or many compounds may be present, interfering with the readout by, for instance, autofluorescence or UV absorption. Some NPs can also directly interfere with the assay by means of nonspecific interactions, thus masking the compounds of interest. For example, plant tannins can interfere with enzyme-based assays by complexation of the enzymes⁵⁷ and fatty acids in high concentrations are nonspecific binders due to their detergent-like properties.⁵⁸ Prefractionation techniques and novel, orthogonal screening setups can help to mitigate this problem and largely eliminate false-positive results.²⁷

Even if none of the compounds in a mixture are likely to interfere with the assay, the problem of isolation of inactive and previously reported NPs arises, complicating the isolation of novel NPs. A known method to overcome this obstacle is a process called dereplication.⁵⁹ Before commencing with bioassay-guided isolation, crude extracts are often analyzed by reversed-phase high performance liquid chromatography (RP-HPLC) coupled to a mass spectrometer, usually producing MS/MS fragment ions, and a fraction collector. All UV and MS data of active fractions from a primary screen, can be analyzed against databases of known compounds and the fractions containing known compounds can be excluded

from following isolation procedures.²⁷ Despite these new methods being available, it was estimated that it takes \$US 50,000 and three months of work to identify a new bioactive NP from any source (some being more challenging than others).⁶⁰

A last obstacle to mention is the intrinsic property of NPs, which make them interesting in the first place: their often novel and complex skeletons. While NPs frequently offer highly distinct bioactivity, due to their unique structures, total synthesis is often not trivial. Curiously enough, this sometimes daunting task has led to many organic chemists taking on the challenge and synthesizing intricate structures, thereby greatly advancing not only drug development, but also organic chemistry itself.⁶¹ Linking total synthesis with combinatorial methods and improved fermentation processes has advanced natural product guided DDD and is likely to continue doing so.

2.3 Part A: Eusynstyelamides and their potential as antimicrobial agents

2.3.1 The need for new antimicrobials

Since the commercial introduction of penicillin, resistant bacteria have started to develop resistance more rapidly. The “golden age” of the antibiotics has passed over 50 years ago and the development of new antimicrobials has been reduced dramatically. AMR has become a major global issue, inflicting numerous deaths and leading to high communal costs for health care systems. Many factors are driving the development of AMR, but the most common ones being listed are related to antibiotics: their overprescription in clinical practice, the uncontrolled use of them in many parts of the world and massive amounts of antibiotics used in animal husbandry and for agricultural applications.⁶² Large quantities of sub-lethal amounts of antibiotics in the soil and water, create thereby an ideal environment for bacteria to develop resistance.⁶³

To tackle the rising AMR, the World Health Organization has enacted a global action plan, which defines major steps to be taken in the future.⁶⁴ At the core of the action plan are stricter regulations for the controlled use of antibiotics and the development of new antimicrobial agents, preferentially with broad-spectrum activity.

In the following chapters an interesting antimicrobial MNP is discussed and linked to AMPs, a promising class of new antimicrobials.

2.3.2 The eusynstyelamides: promising marine antimicrobials

The eusynstyelamide family consists of seven members (A-F) (Figure 6) that were found in the Australian ascidian *Eusynstyela latericius*¹³ (**1a-1c**) and the arctic bryozoan *Tegella cf. spitzbergensis*¹⁴ (**1d-1g**) in the Barents sea. The authors were only able to elucidate the relative stereochemistry of **1a-1c** and *ent*-eusynstyelamide B **1d** was found to be the enantiomer of **1b**. All compounds displayed mild antimicrobial activity against *S. aureus* (MIC: 4.4-12.5 µg/mL) except for **1c**. Eusynstyelamides **1d-1g** demonstrated additional low activity against *E. coli* and *P. aeruginosa* (MIC: 12.5-25.0 µg/mL). All members of the family feature two lipophilic 6-bromoindol moieties (red) and two cationic groups (blue), which are either guanidines (**1a-1d**), amines (**1e**) or a combination of the two (**1f, 1g**). The central scaffold is a 4-hydroxybutyrolactam ring, having a total of three stereogenic centers. The eusynstyelamides have their biogenetic origin from arginine and tryptophan and are structurally similar to other marine natural products such as anchinopeptolide (4-hydroxybutyrolactam core and arginine derived),⁶⁵ baretin (derived from arginine and tryptophan),⁶⁶ and the leptoclinidamines (6-bromoindole and arginine containing).⁶⁷ A biosynthetic route towards the eusynstyelamides involving the dimerization of two modified dipeptides has been suggested.¹³ The dipeptides are likely to have originate from an α -keto acid, which is derived from tryptophan and agmatine. Racemic **1a** had been synthesized from 6-bromoindole, methyl glycidate and Boc-protected agmatine in a total yield of 13% over 6 steps.⁶⁸

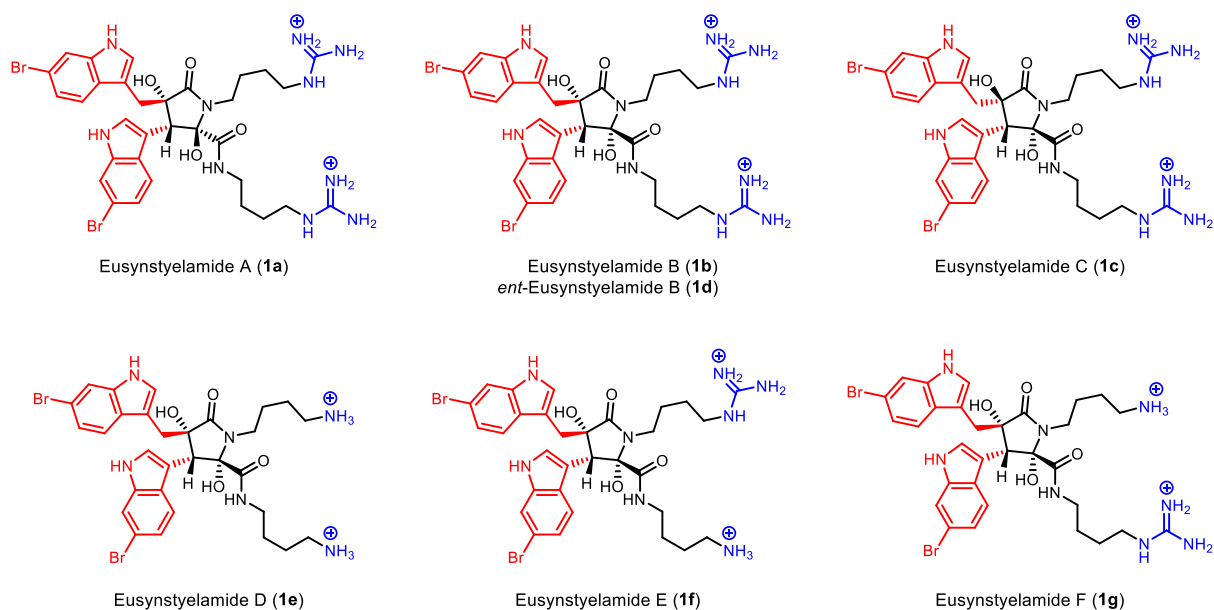


Figure 6. Structures of eusynstyelamides A-F (**1a-1g**). The relative stereochemistry is shown. *Ent*-eusynstyelamide B (**1d**) is the enantiomer of eusynstyelamide B (**1b**). The cationic part is shown in blue and the lipophilic part in red.

The amphipathic nature of the eusynstyelamides satisfies the pharmacophore model of small cationic antimicrobial peptides (AMPs). The model suggests that AMPs need at least two lipophilic and two cationic groups to exert antimicrobial activity.¹⁶ AMPs are a very promising class of potential antibiotics and more details of AMPs and the pharmacophore model are given in the next chapter.

2.3.3 Antimicrobial peptides

Since their first isolation in 1970,⁶⁹ cationic antimicrobial peptides have been found throughout all animal kingdoms and practically in all tissues investigated.⁷⁰⁻⁷² Today, over 3300 AMPs can be found in the Antimicrobial Peptide Database (APD), displaying a wide range of activities besides being antimicrobial.⁷³ AMPs have a range of proposed benefits when considered as antimicrobial agents, including slow resistance development, unique targets and the ability to modulate the immune response.^{72, 74, 75} The very diverse group of AMPs is hard to classify, but the following four major ways are frequently used in literature: source, activity, structural characteristics and amino acid-rich species.⁷⁶ Most commonly, the classification by structure is used, which encompasses β -sheets, α -helices, loops and extended helices.⁷⁷

AMPs are usually defined as peptides consisting of 10-50 amino acids, displaying at physiological pH an overall net positive charge (+2 to +9), which originates from multiple arginine and lysine residues, and having at least 30% hydrophobic residues.^{71, 78} The lipophilic residues originate mainly from the aromatic amino acids tryptophane and phenylalanine, but aliphatic amino acid residues such as valine and isoleucine are found as well.^{75, 79} By folding into one of the aforementioned structures, AMPs achieve a segregation of the lipophilic and the cationic parts, giving rise to highly amphipathic structures.⁸⁰ Folding can occur in free media or upon contact with the negatively charged membranes of

microbes. Some of the most thoroughly investigated AMPs are lactoferricin B, maganin-2, β -defensins, nisin A and polymyxin E.⁷⁵

2.3.4 Mechanism of Action of AMPs

Many AMPs are active against a broad range of bacteria due to their rather unspecific MoA. Most known antimicrobial compound classes target specific enzymes or cellular processes, such as DNA-topoisomerase complexes in DNA replication (fluoroquinolones), transpeptidases in cell wall synthesis (β -lactams) or inhibition of the 50S and 30S subunit of the ribosome in protein synthesis (macrolides and tetracyclines).⁸¹ In contrast, AMPs interfere with the bacterial membrane resulting in damage, thinning or disruption.⁷⁵

The attraction of AMPs towards bacterial membranes arises from the fundamental differences between bacterial and mammalian membranes. Mammalian cells are mostly constituted of phospholipids (PLs) of zwitter- and anionic character.^{82, 83} Due to the anionic PLs being confined to the inner leaflet of the membrane,⁸⁴ eucaryotic cells display a neutral net surface charge. Bacterial membranes typically have an overall negative charge due to incorporation of lipoteichoic- and teichoic acids (LTA and TA) (Gram-positive bacteria) and lipopolysaccharides (LPS), enriched with lipids carrying anionic head groups (Gram-negative bacteria). The differences in membrane structure of Gram-positive and Gram-negative bacteria are illustrated in Figure 7.⁸⁵

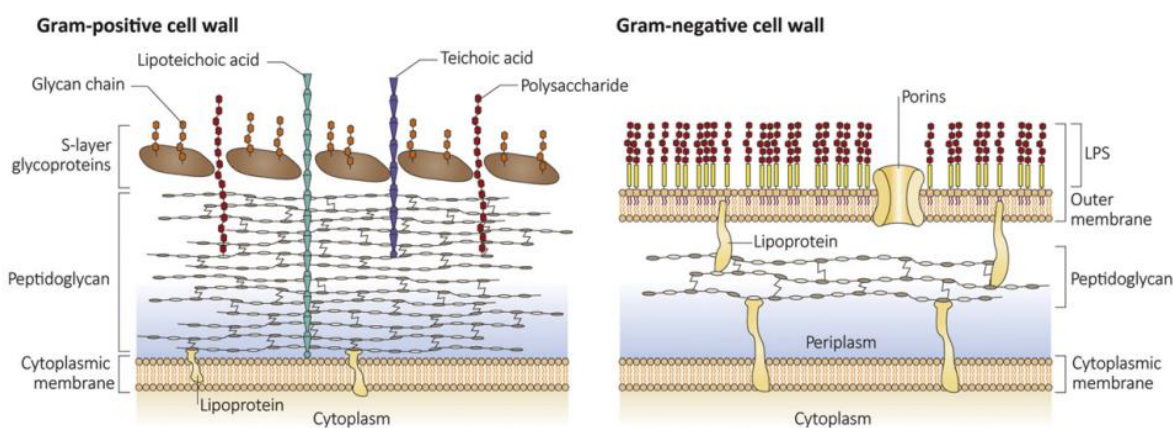


Figure 7. The figure shows a schematic view of cell envelopes of exemplarily Gram-positive and Gram-negative bacterial cells. Reprinted from Depelteau et al., *Encyclopedia of Microbiology (Fourth Edition)*, 2019, 348-360, with permission from Elsevier.⁸⁵

The cationic part of AMPs can interact electrostatically with the negatively charged membranes. Despite the favorable interactions, AMPs still have to cross the outer membrane (OM) of Gram-negative bacteria to reach the cytoplasmic membrane, their primary target. This explains the observation that Gram-negative bacteria are usually more difficult to target using membrane active agents.⁸⁶

Multiple models of the membrane disruption process have been proposed, but the complete mechanisms are yet to be elucidated and are likely to vary for different peptides.⁷² Nevertheless, two main events are

suggested to take place. First, the AMPs attach to and accumulate on the cytoplasmic membrane – a process that often leads to a change in the secondary structure – until the AMP concentration reaches a certain threshold and then the AMPs start to enter or traverse the membrane.⁸⁷ The eventual membrane disruption proceeds *via* a range of different mechanism, which predominantly are described by the carpet model (Figure 8, A), the barrel stave model (Figure 8, B) or the toroidal pore model (Figure 8, C).⁷⁶

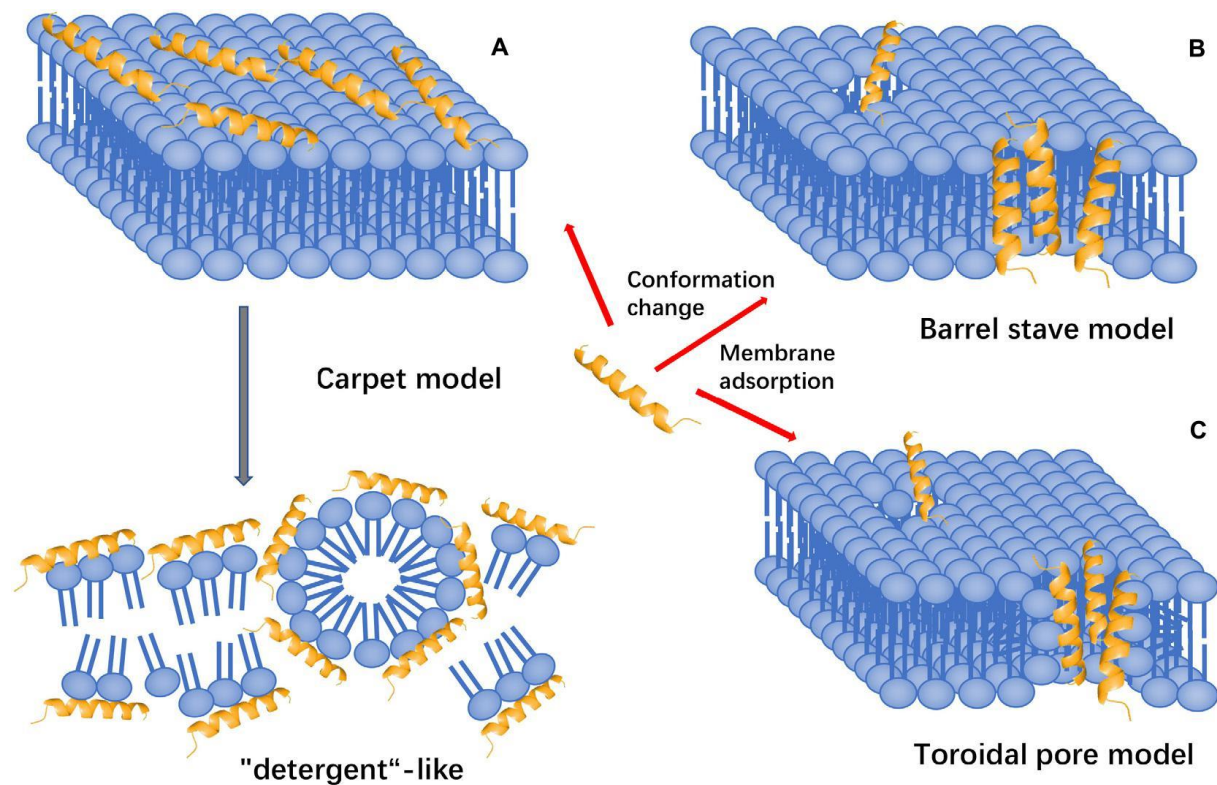


Figure 8. Proposed mechanisms of action of AMPs. A: carpet model, B: barrel stave model, C: toroidal pore model. Reproduced with permission from Huan *et al. Frontiers in Microbiology* 2020, 11.⁷⁶

In the carpet model (A) the AMPs align parallel to the cell membrane, their hydrophilic side facing the aqueous environment and the lipophilic side embedded into the membrane. As given by the name, the AMPs form a carpet on the cell membrane and destroy the latter eventually in a dispersion-like manner.^{72, 76, 88} A point worth mentioning here is that the peptides do not form any quaternary structures as opposed to the other two models (see below).

In the barrel stave model (B), a number of AMPs form a “barrel-like” ring around an aqueous pore. The “stave” term describes singular transmembrane spokes within the barrel⁷² and the peptides are thereby aligned parallel to the phospholipids. The orientation of the phospholipids remains undisturbed. The hydrophobic sites of the AMPs are directed towards the membrane and the hydrophilic sites face into the aqueous pore, creating the pore lining. This arrangement leads to a minimal exposure of the peptide hydrophilic residues to the hydrophobic membrane interior.⁷² Formation of the channels can result in cytoplasmic outflow⁷⁶ or, upon relaxation of the pore, transportation of peptides to the inner membrane leaflet.⁷²

The primary difference between the toroidal pore model (C), also known as the wormhole model, and the barrel stave model (B) is that in the former AMPs are intercalated with lipids in the transmembrane channel. It has been regarded as a supramolecular complex and represents a membrane spanning pore, lined with polar peptide surfaces as well as phospholipid head groups.⁷² Association of α -helical AMPs to the outside of the membranes induces a positive curvature strain, leading to the phospholipids bending inwards, forming the toroidal pore complex.⁷² The pores tend to have short lifetimes and upon disintegration some of the peptides are released into the interior of the cell. It has been suggested as one of the mechanisms operating when AMPs cross the membrane and reach intracellular targets.^{72, 89}

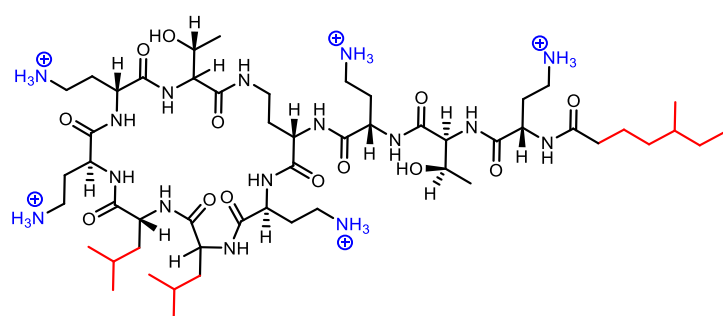
While not as prominent, two additional models are worth mentioning. The electroporation model suggests that cationic AMPs are effectively “pulled” into the cell, based on the negative transmembrane electrochemical potential.⁹⁰ Lastly, the sinking raft model, in which peptides being bound to the outer surface of the membrane cause a mass imbalance, resulting in distress and bending of the membrane. This process creates transient pores, through which the AMPs can translocate over the membrane into the cytoplasm.⁹⁰

It should be mentioned that AMPs can also have intracellular targets. Without going into detail, the four most common targets are listed as follows⁷⁶: (1) Inhibition of protein synthesis by interfering with key enzymes in either the protein transcription, translation or assembly step (Peptide PR-3⁹¹); (2) Inhibition of nucleic acid biosynthesis by affecting key enzymes (indolicidin⁹²); (3) Inhibition of proteases expressed by bacteria (histatin 5⁷⁶); (4) Inhibition of cell division by inhibiting DNA replication and DNA damage response (butorin 2^{93, 94})

2.3.5 AMPs in clinical use

AMPs have some major drawbacks when used as drugs, including often high toxicity, low bioavailability, proteolytic stability and they often fail to demonstrate superiority in clinical studies.⁷⁵ Nevertheless, some AMPs have been approved for clinical use, mostly for topical treatments, of which two are briefly discussed here.

Colistin (**15**) (polymyxin E) (Figure 9) is a member of the polymyxins, a class of non-ribosomal, cyclic



Colistin / Polymyxin E (15)

Figure 9. Structure of colistin (**15**). Cationic residues are marked in blue and lipophilic residues in red.

oligopeptide antimicrobials. The class consists of five members (polymyxins A-E), of which only the aforementioned and polymyxin B are currently in clinical use.⁹⁵ Isolated in 1947 in Japan (*Paenibacillus polymyxa* subsp. *Colistinus*),⁹⁶ colistin was approved for treatment of infectious diarrhea and urinary

tract infections by the FDA in 1959. As a consequence of increase in reports of nephro- and neurotoxicity, prescription levels dropped significantly.⁹⁷ Due to developing multidrug resistance of *P. aeruginosa*, *Acinetobacter baumannii*, and *Klebsiella pneumoniae*, **15** has re-emerged as a last-line treatment, but resistance against colistin is known as well. Colistin usually exhibits MIC values of 0.25-1.0 µg/mL against *E. coli* (ATCC 25922) and 0.5-2 µg/mL against *P. aeruginosa* (ATCC 27853).⁹⁸ **15** acts primarily on the bacterial membrane with a similar MoA as AMPs (*vide supra*). Additional reported MoAs of colistin are the so-called vesicle-vesicle contact, leading to osmotic imbalance and cell death, and the generation of reactive oxygen species.⁹⁵ The cyclic nature of colistin and the incorporation of the unnatural amino acid ornithine into the primary sequence increase its *in vivo* stability.

The second compound worth mentioning is the cyclic antimicrobial lipopeptide daptomycin (**16**) (Figure 10). **16** was first discovered in the 1980s, but was not developed further due to adverse effects on skeletal muscle.⁷⁵ The FDA finally approved daptomycin in 2003 for the treatment of infections caused by Gram-positive bacteria, as it also proved to be effective against methicillin-resistant *S. aureus* (MIC⁹⁹: 1 µg/mL). Structurally, **16** is derived from depsipeptide and consists of 13 amino acid residues, many of them being non-proteinogenic and D-amino acids. Daptomycin is notably different from the AMPs discussed before, having a net charge of -3. The overall negative charge influences the MoA, which was suggested

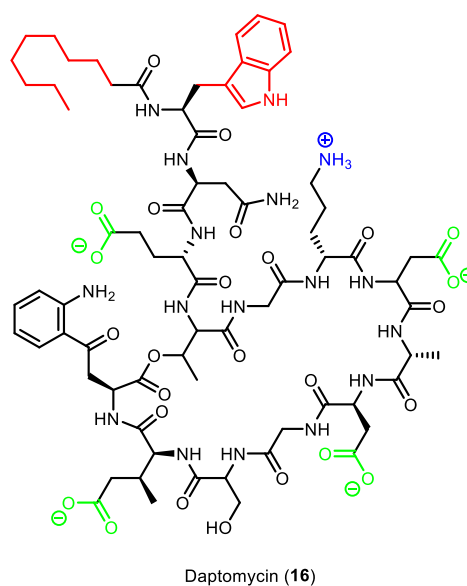


Figure 10. Structure of daptomycin (**16**). Anionic residues are shown in green, cationic residues are shown in blue and lipophilic residues are shown in red.

to involve formation of micelles in the presence of Ca²⁺ ions, masking its negative charge. The micelles subsequently dissociate in proximity to the membrane, into which **16** then can insert. The formation of micelles represents an effective way of bypassing the negatively charged layer of LPS.¹⁰⁰

Both examples demonstrate that it is often not the antimicrobial activity of AMPs and related natural derivatives, but rather their toxicity halting their application and restricting them to topical treatment.⁷⁵

2.3.6 Towards the development of SMAMPs

To overcome the shortcomings of AMPs in clinical use, a number of research groups have channeled their efforts during the last two decades into mitigating the former ones by developing synthetic mimics of AMPs (SMAMPs). The main contributors to the activity and toxicity of SMAMPs are their overall charge and hydrophobicity, as well as the segregation of the charged and hydrophobic sites.^{87, 101} This

led to researchers trying to replicate the function of AMPs, rather than their primary structure when constructing SMAMPs. It has been realized that it is often a thin line between activity and toxicity and increased antimicrobial activity frequently coincides with high toxicity. An interesting finding was made by Strøm et al. in 2003, when they determined the minimum motif for AMPs to exert antimicrobial activity.¹⁶ In their study, a minimum of two cationic and two lipophilic groups was necessary to achieve activity against Gram-positive bacteria, whereas for Gram-negative strains either two bulky lipophilic groups or a third smaller one was needed.

Over the years, a wide variety of AMP mimics have been reported, including peptidomimetics (α -peptides, β 3-peptides, peptoids, β -peptoids, α/β -peptides, peptide/peptoid hybrids, α -AA peptides, γ -AA peptides, α -oligoacyllysines, and β -oligoacyllysines)¹⁰² and small molecule peptidomimetics.¹⁰³ A comprehensive review of the latter was given by Kumar and co-workers¹⁰⁴ and Ghosh et al.¹⁰³ In the following, a selection of small molecule mimics, having molecular weights of <1000 Da, is presented.

Tew and deGrado had been very prolific in the field, developing several interesting structures (Figure 11).¹⁰⁵⁻¹¹⁶ One of their major developments were amide linked aryls **17**, shown in Figure 11 (left).¹⁰⁹ They achieved topical amphiphilicity by an extensive intramolecular network of hydrogen bonds, rigidifying the structure. In earlier studies, they had used urea linkages¹⁰⁷ and a central pyrimidine instead of the dimethoxyphenyl group.¹⁰⁸ All derivatives displayed high antimicrobial activity (MIC: <1 μ M) against *S. aureus* and *E. coli*, but varied in toxicity. Only when the central structure could not contribute to the H-bonding network, the antimicrobial activity was clearly diminished.

Another set of compounds was based on phenyleneethylene, connecting two benzene rings to a central benzene ring by acetylene, being the first SMAMP with a full carbon backbone (Figure 11, middle). The outer benzene rings could carry additional substituents and the most active structure **18** had the cationic amines tethered to the outer phenyl rings by ethyl linkers (Figure 11, middle). It was found that shorter linkers impaired the selectivity of the compounds for bacterial cells and oligomeric derivatives did not exhibit any antimicrobial activity.¹¹³ Another development of the all-carbon backbone mimics is shown in Figure 11 (right).¹¹⁴ The central aromatic moiety was varied between benzene, naphthalene and phenyl benzene, eventually delivering the most active derivative **19**, for which a naphthyl core and a total net charge of +6 was utilized. In a follow up study, they could show that the incorporation of an amide linkage in the hydrophobic region of similar derivatives disrupted the facial amphiphilicity and led to the loss of broad-spectrum activity.¹¹⁵

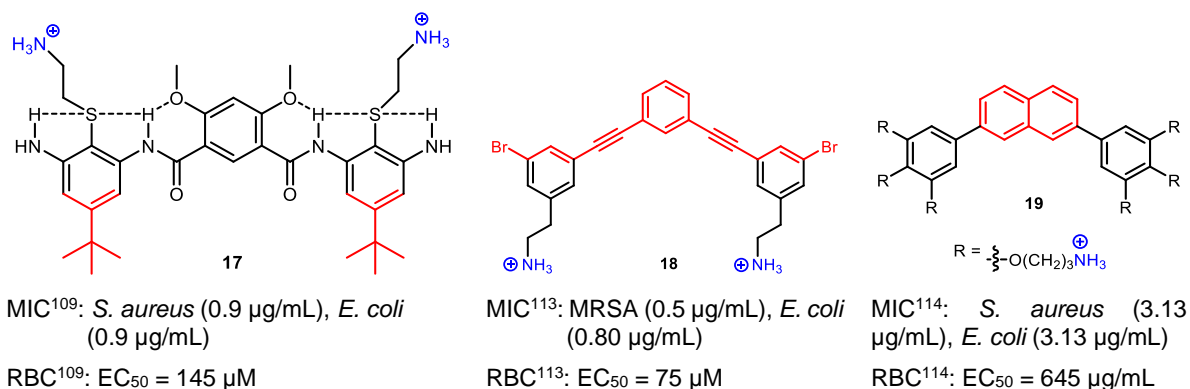


Figure 11. Structures of AMP mimics developed by Tew and deGrado. The cationic part is shown in blue and the lipophilic part in red. RBC = Red blood cells. EC₅₀: The concentration required to cause 50% lysis of a suspension of red blood cells.

Two interesting series of compounds were developed by Pfeffer and coworkers^{117, 121-123} and Savage and coworkers.^{124, 125} Rigidity was achieved by using a norbornane (Figure 12, left) and fused tetracyclic cholic acid (Figure 12, right, cholic acid is shown in green), respectively. Norbornane derivative **20** had been found to be the most active of a series of derivatives with no observed toxicity to mammalian cells. They found that imidazolium and pyridinium cationic groups delivered compounds with low activity, as did compounds with only one cationic guanidine group. Replacement of the cyclic 1,3-dioxolane with substituted benzyl ethers delivered potent structures, but with high toxicity against human embryonic kidney cells (HEK293). One point to make is that the NBD fluorophore (Figure 12, left, red part) in derivative **20** impeded the activity only to a minor extent, although impaired activity of the bioactive often is a concern when working with fluorophores. Savage and coworkers based their mimics on cholic acid (Figure 12, right; cholic acid is shown in green), an inherently amphipathic compound, to mimic polymyxin B.¹⁰³ Polymyxin B binds to lipid A, acting as a sensitizer for the membrane. Savage and coworkers hypothesized that their derivatives would be able to do the same, which they were able to

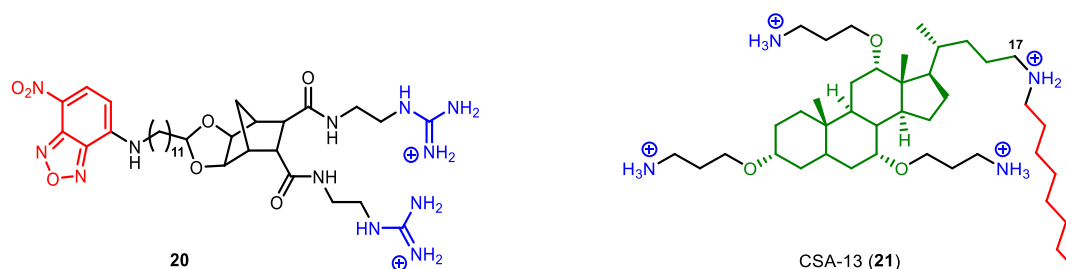
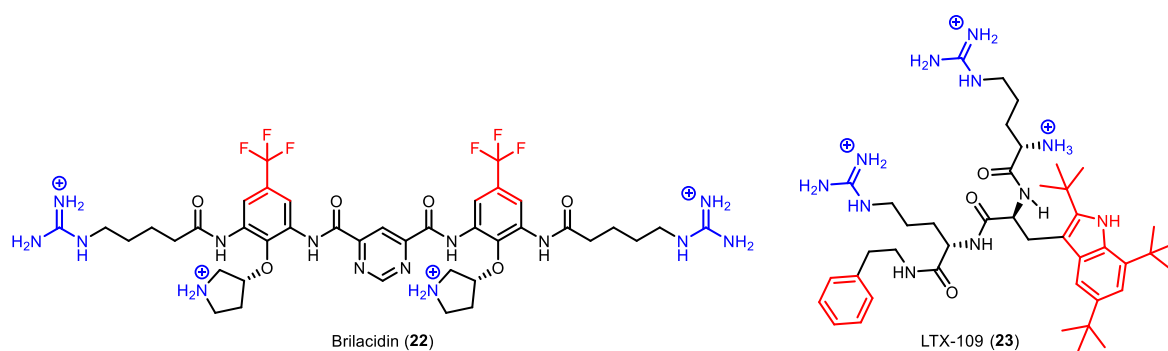


Figure 12. Molecular designs of **20** by Pfeffer and coworkers¹¹⁷ and **21** by Savage and coworkers.¹¹⁸ The cationic part is shown in blue and the lipophilic part in red. Cholic acid is shown in green. HEK = human embryonic kidney cells. RBC = Red blood cells. CC₅₀: Concentration at which 50% of all cells lost viability. EC₅₀: The concentration required to cause 50% lysis of a suspension of red blood cells. LD₅₀: The concentration required to cause 50% death of the organism studied.

proof eventually.¹⁰³

Later, they could refine their mimics by introducing a lipid tail to C-17, resulting in the highly bactericidal compound CSA-13 (**21**), alongside many other derivatives, which were less active.¹²⁶

Lastly, two more peptide-like structures are worth mentioning. The arylamide foldamer brilacidin (**22**) (Figure 13, left) was developed by deGrado and co-workers using coarse grained simulations.¹²⁷ Brilacidin's MoA was found to be similar to daptomycin and LL-37 and **22** surpassed the latter ones in terms of activity.¹⁰³ Evaluated for its anti-infective properties, **22** has recently completed clinical Phase-II studies for acute bacterial skin and skin structure infections, as well as for the prevention of oral mucositis in cancer patients.¹²⁸ LTX-109 (**23**) was inspired by the AMP lactoferricin and was developed by Lytix Biopharma in 2008.¹²⁹ It consists of three amino acids and is believed to have improved proteolytic stability due to its synthetic modifications and small size. **23** has recently completed clinical Phase-II studies for topical treatment of impetigo, nasal decolonization and mild diabetic foot



MIC¹³¹: MRSA (0.5-1.0 µg/mL), *E. coli* (1-2 µg/mL)

RBC¹³¹: EC₅₀ = >500 µg/mL

MIC¹³²: *S. aureus* (2 µg/mL), *E. coli* (3 µg/mL), *P. aeruginosa* (8 µg/mL)

RBC¹³²: EC₅₀ = 175 µg/mL

Figure 13. Structures of Brilacidin (**22**) and LTX-109 (**23**). Both have successfully completed Phase-II clinical trials. The cationic part is shown in blue and the lipophilic part in red. RBC = Red blood cells. EC₅₀: The concentration required to cause 50% lysis of a suspension of red blood cells.

ulcers.^{103, 104} Currently, **23** is developed further under the name of AMC-109.¹³⁰

These examples demonstrate the efforts put into the development of new SMAMPs, but despite many promising mimics being reported and some of them being in clinical trials, there is still a big need for further developments.

2.3.7 Resistance to AMPs and SMAMPs

AMPs have been believed to have a low potential to induce resistance due to the lack of specific enzymatic target. Additionally, AMPs have a sharp onset of activity and high maximum killing effect, resulting in a very narrow mutation selection window and therefore resistance to AMPs is less likely to evolve.⁷⁴ Nevertheless, bacteria have found a number of mechanisms to reduce their susceptibility to AMP type agents and emerging resistance against colistin has been reported.⁹⁷

Two main mechanisms of resistance can be distinguished: constitutive and inducible resistance.⁷² Constitutive (passive) mechanisms consist of electrostatic shielding, changes in membrane potential during growth and biofilm formation. Inducible mechanisms include substitution, modification and acylation of membrane molecules, expression of proteolytic enzymes and efflux pumps.⁸⁷

Many of the inducible mechanisms are directed towards the reduction of the overall negative surface charge to inhibit binding of AMPs, usually by the covalent attachment of a cationic molecule to parts of the membrane.^{133, 134} While modification of the membrane is common for Gram-positive and Gram-negative bacteria, the compounds incorporated into the membrane differ for both types of microbes, due to the differences in their membrane structure. Some possible modifications of the OM in Gram-negative bacteria are shown in Figure 14. Gram-negative bacteria can attach cationic 4-aminoarabinose (L-Ara4N) to lipid A, which is the innermost part of the LPS layer, by means of a phosphodiester bond to the anomeric carbon of L-Ara4N.

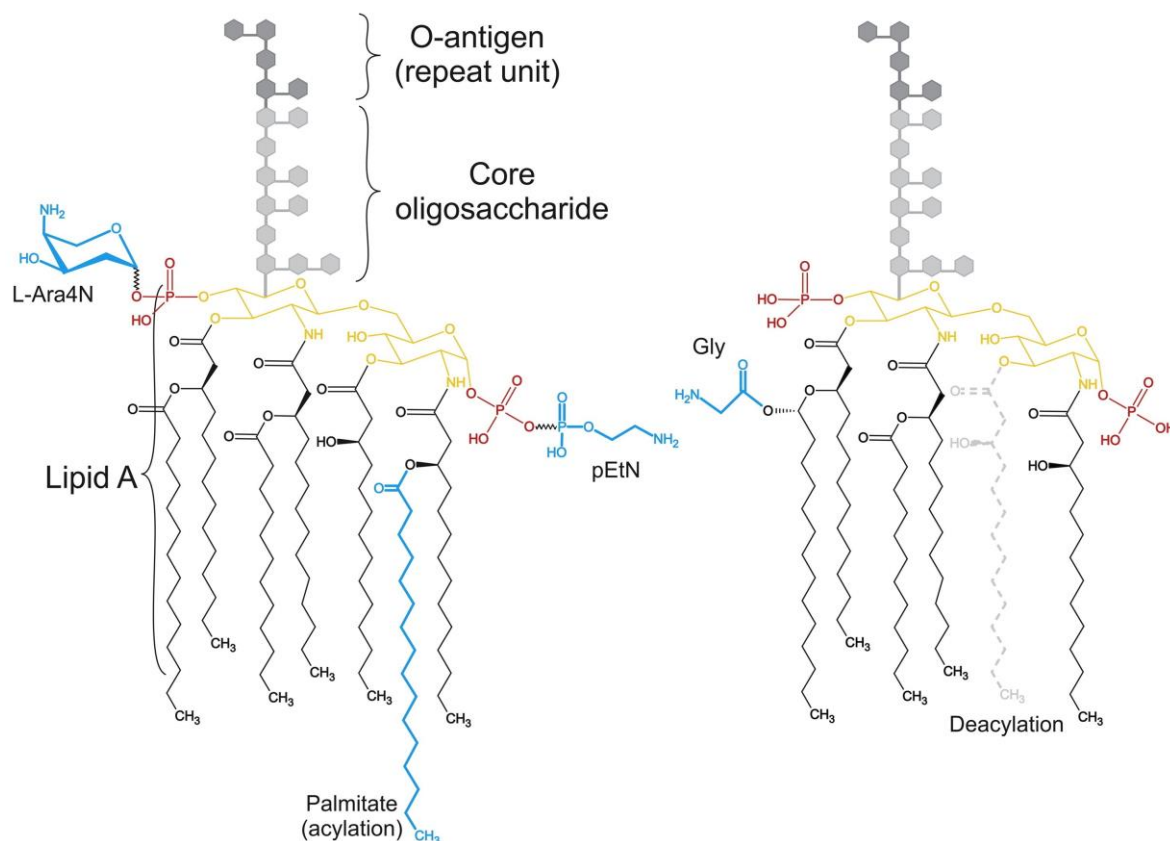


Figure 14. Major lipid A modifications in Gram-negative bacteria and substituents: L-Ara4N (4-aminoarabinose), pEtN (phosphoethanolamine), glycylation (incorporation of glycine), acylation (incorporation of palmitate), deacylation (removal of long-chain fatty-acid). Reprinted from Maria-Neto, S., et al., "Understanding bacterial resistance to antimicrobial peptides: From the surface to deep inside." *Biochim. Biophys. Acta* **2015**, 1848 (11, Part B), 3078-3088, with permission from Elsevier.¹³⁴

The overall negative surface charge gets thereby reduced and the charge attraction of AMPs to the membrane diminished.¹³³ Other modifications of lipid A include: acylation (incorporation of palmitate), phosphoethanolamine bound to phosphate groups and glycylation (incorporation of glycine).¹³⁴ Another type of modification is the removal of long-chain fatty-acids (deacylation) from the lipid A layer.

Gram-positive bacteria, lacking an OM, have a thick layer of peptidoglycan with LTAs as the outermost layer. The most frequent modification is esterification of LTA with D-alanine, effectively reducing the surface charge (Figure 15).¹³⁵ The D-alanylation may also alter the LTA conformation, increasing the cell wall density and flexibility, and acting as a physical barrier to linear AMPs.¹³⁴ On that note, general thickening of the cell wall has also been observed as a resistance mechanism against AMPs.¹³⁶ While all these modifications can occur, the changes in membrane composition are usually associated with fitness costs,^{137, 138} and may be difficult to maintain for the bacteria over an extended period of time.

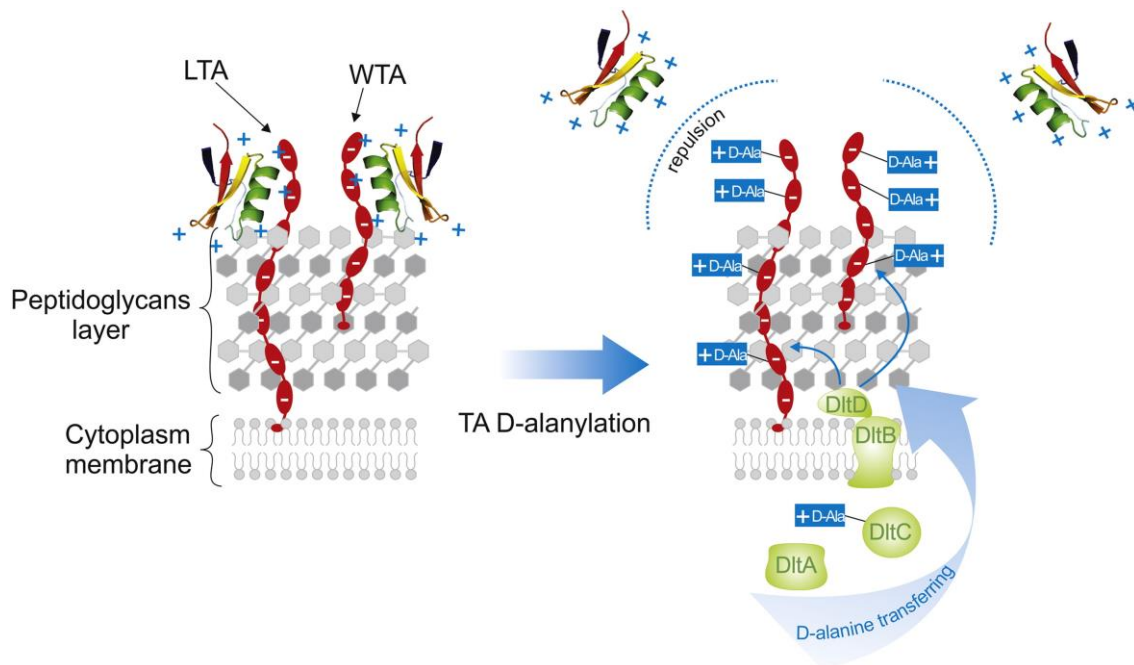


Figure 15. Illustration of the D-alanylation of teichoic acids in Gram-positive bacteria. Left: Interaction between the unmodified TAs and cationic AMPs. Right: Repulsion of the modified TAs and cationic AMPs. Reprinted from Maria-Neto, S., et al., "Understanding bacterial resistance to antimicrobial peptides: From the surface to deep inside." *Biochim. Biophys. Acta* **2015**, 1848 (11, Part B), 3078-3088, with permission from Elsevier.¹³⁴

The discussion of AMR in the context of AMPs and SMAMPs is partially ethical in nature as well. Some voices have been raised, questioning, if resistance induced by SMAMPs could affect our immune system, due to the similar MoA of AMPs belonging to the immune system and AMP-based drug candidates. A scenario with increased resistance against the innate immune system would, if it were to happen, undoubtedly be critical and the current estimations of future deaths caused by AMR would multiply. However, one could argue that bacteria did not become resistant against the immune system of higher forms of life over the course of millions of years. This might partially be due to the immune systems in vertebrates evolving, but they certainly do so at a much slower rate than bacteria express new

resistances. One possible explanation of the slow buildup of resistance could be that the AMPs act in a multitude of ways besides membranolytic, but there are still many factors not being understood.

There are indications that resistance to AMPs can be induced, as demonstrated by nisin, a 34-mer AMP, which has been used as a food biopreservative over decades. A few examples of emerging resistance to nisin have been reported, however, only under laboratory conditions.¹³⁹

Based on the knowledge we have today, it is not possible to predict if widespread resistance against AMPs and their mimics will develop and how this resistance would affect the efficiency of our immune system. The development of new SMAMPs possibly raises the stakes and researchers in the field need to consider their ethical responsibilities.

2.4 Part B: Aspergilone A, an interesting azaphilone

2.4.1 The importance of marine biofouling

Marine biofouling describes the undesired accumulation of living organisms, including microorganisms, animals and plants, on submerged man-made surfaces.^{11, 140} Fouling on ship hulls increases the roughness of the hull's surface and thereby the frictional resistance, resulting in markedly higher fuel consumption.¹⁴¹ As maritime transportation drives 80-90% of the global trade, the shipping industry suffers huge economic losses per year, due to fouling on ship hulls.^{142, 143} The most successful way of preventing fouling is the use of tributyltin-based coatings. However, the general toxicity of tin organyls towards non-target species has led to their ban in 2008.¹⁴⁰ Similar substances are often strictly regulated as well, due to their environmental risks.¹⁴⁰ Consequently, there is an urgent demand for finding alternative AF agents.

One promising source are, yet again, NPs, produced by marine organisms to prevent fouling on their outside. The marine polyketide aspergilone A (**2**) had been shown to exhibit cytotoxic and AF activity. This dual activity and especially the latter has sparked our interest in **2** and the citrinin-type azaphilones in general. In the following chapters, the parental class, that is the polyketides azaphilones, are briefly introduced and some examples from the citrinin-type subclass are given. The chapter closes with a short discussion on the efforts undertaken towards the synthesis of the azaphilone core and citrinin-type azaphilones.

2.4.2 General characteristics of azaphilones

Polyketides are one of the structurally most diverse classes of NPs, spanning from simple aromatics to highly complex structures, while fungi have been regarded as a major source of bioactive polyketides.¹⁴⁴ Azaphilones are polyketides isolated from fungi with a wide range of biological activities including antimicrobial, anti-oxidative, anti-inflammatory, cytotoxic, AF, anticancer and enzyme inhibition.^{18, 144, 146, 147} Many of these activities were related to the general ability of azaphilones to react with amine groups, which are ubiquitously found in amino acids, proteins and nucleic acids in the human body, to form vinylogous γ -pyridones.¹⁴⁷ These adducts can easily be detected, due to the color changing to red, when the pyrane oxygen is replaced with a nitrogen.¹⁴⁸ Structurally, the azaphilones feature an isochroman scaffold, a bicyclic pyrone-quinone core and at least one quaternary carbon (Figure 16, green dot).¹⁴⁶ Currently, over 600 naturally occurring azaphilones have been isolated and grouped into up to 18 categories, based on their structure.^{144, 146} A comprehensive illustration of the structural

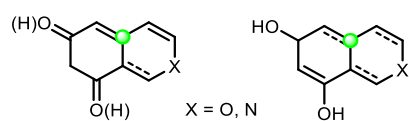


Figure 16. Azaphilone scaffold.

characteristics of all subclasses was given very recently by Chen et al.,¹⁴⁴ restricting the subdivision to 13 classes. Some groups have focused on the efficient construction of the azaphilone core structure,¹⁴⁹⁻¹⁵³ but there are still many structures not having been investigated synthetically.

2.4.3 Citrinin-type azaphilones

One important azaphilone subclass are the citrinin-type azaphilones (Figure 17). The common core, which is shared by all members, is a bicyclic bisphenol-pyrane structure without any mandatory substituents (Figure 17, red box).¹⁴⁴ The classes eponym, (–)-citrinin (**24a**), is possibly the most extensively investigated azaphilone and is produced by several fungal species of genera *Penicillium*, *Monascus*, and *Aspergillus*.^{18, 154-159} **24a** was first isolated in 1931,¹⁶⁰ and it was not before 1963 that the absolute configuration^{161, 162} and the tautomeric configuration¹⁶³ were proposed. The absolute configuration was confirmed in 1971 by X-ray diffraction studies.^{146, 164} Albeit its antimicrobial activity being acknowledged,¹⁵⁹ it is more commonly considered a hazardous contaminant of foods and feeds, just like other mycotoxins.^{159, 165-167}

Most members of the citrinin subclass can be classified based on their degree of polymerization of the citrinin core (Figure 17, red box). Four main categories have been suggested¹⁴⁶: (1) monomeric congeners (Figure 17, blue oval), including (–)-citrinin (**24a**) (2) citrinin dimers containing three to five rings (Figure 17, orange oval), such as penidicitrinin B (**27**)¹⁶⁸ (3) 7,7'-carbon-bridged citrinin dimers (Figure 17, yellow oval), for example dicitrinone A-C (**29a-c**),¹⁶⁹ (4) citrinin trimers containing six or more rings (Figure 17, green oval), such as tricitrinol B (**30**).¹⁷⁰

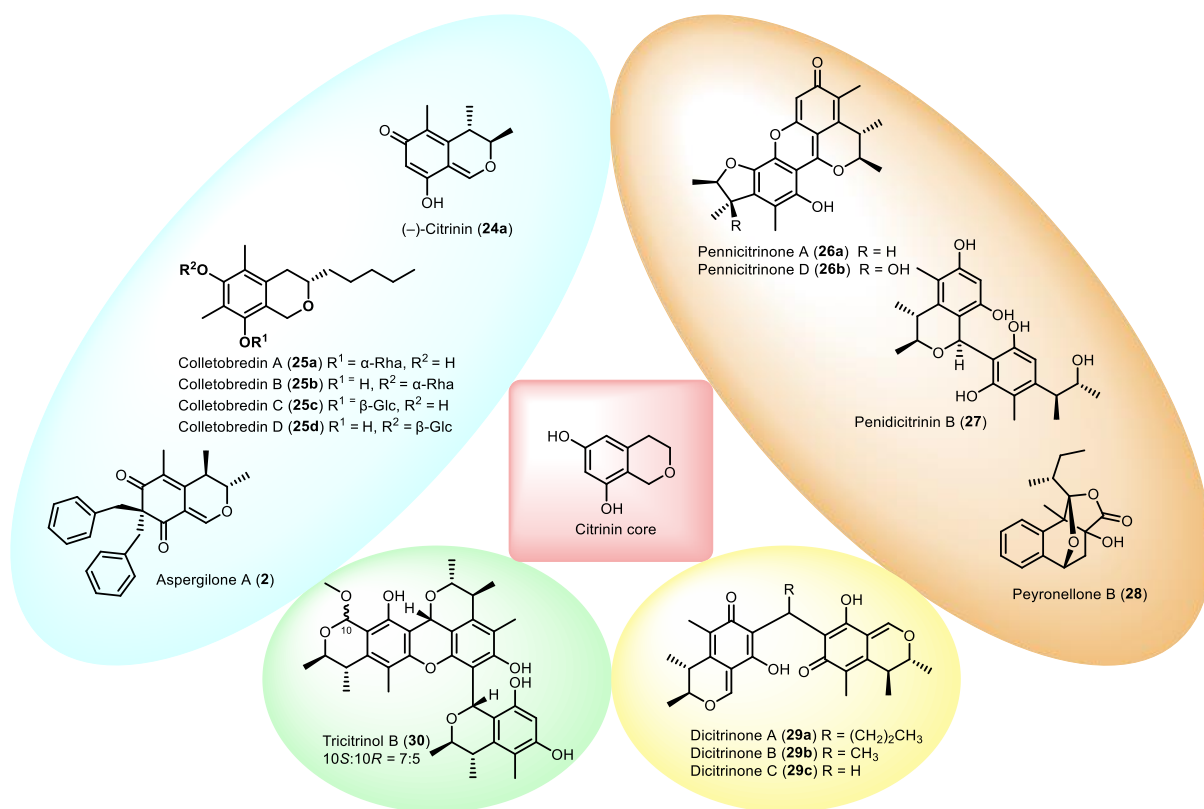


Figure 17. The citrinin core structure and several examples from the citrinin subclass of azaphilones.

As briefly touched upon before, **2** was isolated in 2011 from the marine derived fungus *Aspergillus* sp., which was associated with a gorgonian *Dichotella gemmacea* in the South China Sea.¹⁸ **2** exhibited *in vitro* cytotoxicity against HL-60 human promyelocytic leukemia (IC₅₀ = 3.2 μg/mL), MCF-7 human breast adenocarcinoma (IC₅₀ = 25.0 μg/mL) and A-549 human lung carcinoma (IC₅₀ = 37 μg/mL).¹⁸ Additional potential AF activity with an EC₅₀ value of 7.68 μg/mL was reported.¹⁸ Its dimer, aspergilone B, features a rarely found methylene bridge and had been inactive in the biological assays stated above.¹⁸ Monomeric colletobredins A-D (**25a-d**) were extracted from the cultural broth of *Colletotrichum aotearoa* BCRC 09F0161, which is a fungal endophyte residing in the leaves of an endemic Formosan plant *Bredia oldhamii* Hook. f. (Melastomataceae).¹⁷¹ **25a-d** were the first isochroman glycosides being reported and showed weak inhibition of NO production in activated macrophages.¹⁷¹

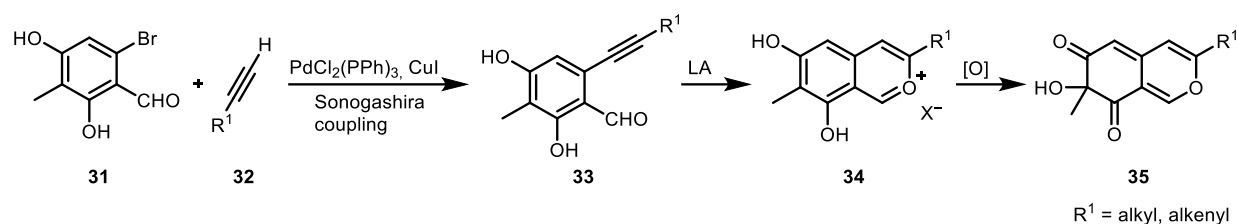
Pennicitrinones A (**26a**) and D (**26b**), isolated from *Penicillium citrinum* in 2006 and *P. notatum* B-52 in 2009, were the first examples of coupling products of **24a** and 2,3,4-trimethyl-5,7-dihydroxy-2,3-dihydrobenzofuran.^{172, 173} Penidicitrinin B (**27**), found in the volcan ash-derived fungus *P. citrinum* HGY1-5, exhibited an interesting linkage between a decarboxydihydrocitrinin and phenol A.¹⁶⁸ Isolated from *Peyronellaea glomerata* in 2018, peyronellone B (**28**) featured a rare tetracyclic caged structure, supposedly derived from a Diels-Alder cycloaddition between the azaphilone and pyruvic acid.¹⁷⁴ A significant hypoxia-protective effect of the same magnitude as verapamil was reported.¹⁷⁴

The unique carbon-bridged dicitrinones A and B (**29a** and **29b**) were isolated as a mixture of two atropisomers from *P. citrinum* IIGY1-5.¹⁶⁹ The *n*-propyl (**29a**) and methyl (**29b**) substituents on the bridging carbon restricted the free rotation, an effect that was not observed for methylene bridged **29c**. Derivative **29b** demonstrated the strongest cytotoxic effects against two leukemia cell lines.

Tricitrinol B (**30**) is the first known citrinin trimer and was isolated in 2011 from *P. citrinum*.¹⁷⁰ The pentacyclic partial structure was hypothesized to have formed from two citrinin monomers *via* a heterocyclic Diels-Alder reaction, followed by the coupling to a third citrinin unit. **30** was found to be a 7:5 mixture of the 10*S* and 10*R* diastereomers and showed comparatively good activity against 17 tumor cells with low IC₅₀ values in the range of 1-10 μM.¹⁷⁰

2.4.4 Synthesis of the azaphilone core and citrinin-type derivatives

Approximately 25 total syntheses of members of the azaphilone family have been reported, including racemic and enantioselective approaches.^{144, 146, 175} While azaphilones have diverse structures, pyronoquinones and pyrylium salts are highly relevant intermediates or precursors for the synthesis of the former.^{150-152, 176} A general synthesis towards the azaphilone core is outlined in Scheme 1.



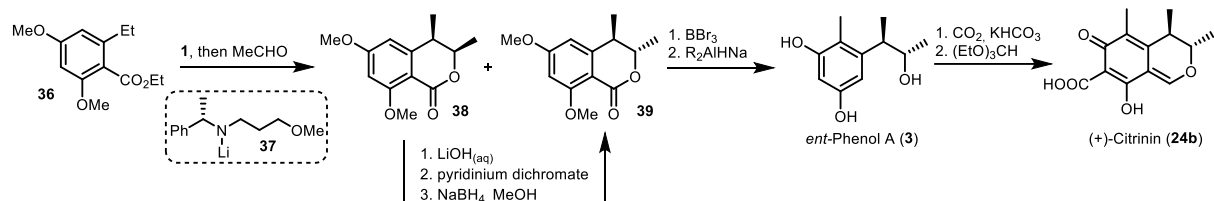
Scheme 1. General synthetic strategy towards the azaphilone core. LA = Lewis Acid. Reprinted with permission from *Chem. Rev.* 2013, 113, 4755–4811.¹⁴⁶

Readily available alkynes **32** were coupled under Sonogashira conditions with the substituted 2-bromobenzaldehyde **31** to yield *o*-alkynylbenzaldehyde **33**.¹⁵² Under Lewis Acid (LA) catalysis (Au(III) or Cu(II)) the 2-benzopyrylium salts **34** were formed, and the latter ones were subsequently oxidized by 2-iodoxybenzoic acid (IBX)^{150, 151} or lead tetraacetate (Pb(OAc)₄)^{177, 178} to the desired isochromene **35**.¹⁷⁹ An alternative approach towards chloroazaphilone reported by Wei et al., utilized a one-pot HClO₄/HOAc mediated condensation of an aromatic aldehyde with an aliphatic ketone to the pyrylium salt and subsequent Pb(OAc)₄ mediated oxidation delivered chloroazaphilone.¹⁴⁹ Starting from a similar intermediate, but using a chemoenzymatic strategy, Pyser et al. could access both stereoisomers of the azaphilone core **35** in a high yields and enantiomeric excess.¹⁸⁰

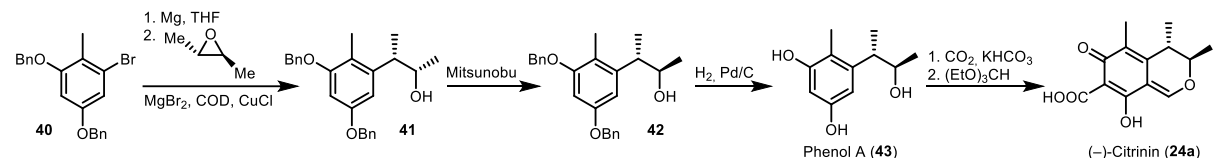
Only a handful of total syntheses of the citrinin-type analogues have been reported until now, differing from the approach shown in Scheme 1. Some partial syntheses of (–)-citrinin **24a** starting from phenol A, a degradation product of the former,^{181–183} and various synthetic analogues were reported.^{19, 181, 183, 184} Only one year after the first report of a diastereoselective total synthesis of citrinin in 1986,¹⁸⁵ the same researchers developed an enantioselective modification towards the unnatural analogue (+)-citrinin (**24b**) (Scheme 2, top).¹⁸⁶ Starting from *o*-ethylbenzoic acid ethyl ester **36**, they could generate an enantioenriched *o*-toluate carbanion, which, upon reaction with acetaldehyde, delivered an unfavorable 3:1 mixture of *erythro*-**38** and *threo*-lactones **39**. *Erythro*-lactone **38** could be converted into the desired *threo*-lactone **39** by a three-step sequence including hydrolysis, oxidation of the secondary alcohol to the ketone and subsequent stereoselective reduction with sodium borohydride. During the process they did not observe any noteworthy racemization. Cleavage of the phenolic methyl ethers with boron tribromide (BBr₃) and ensuing reduction with bis(2-methoxyethoxy)aluminium hydride delivered **3**. As previously reported,^{181, 183} carboxylation of **3** with carbon dioxide and followed by treatment with triethyl orthoformate furnished enantiopure **24b**. Despite having made the unnatural enantiomer of citrinin, their strategy would allow for the synthesis of **24a** as well, using the enantiomer of the chiral base **37**.

Rödel et al.¹⁸⁷ started from bromobenzene **40** to prepare the corresponding aryl Grignard reagent (Scheme 2, middle). Treatment of the aryl Grignard with (2*S*)-*trans*-(–)-2,3-dimethyloxirane,^{188, 189} and 1,5-dicyclooctadienecopper(I) and magnesium bromide as catalysts, delivered *erythro*-alcohol **41**. Needing the *threo*-configuration, they utilized a Mitsunobu reaction to invert the configuration at C-2 to produce diastereomer **42**. Removal of the benzyl protecting groups by palladium mediated hydrogenation delivered phenol A (**43**).

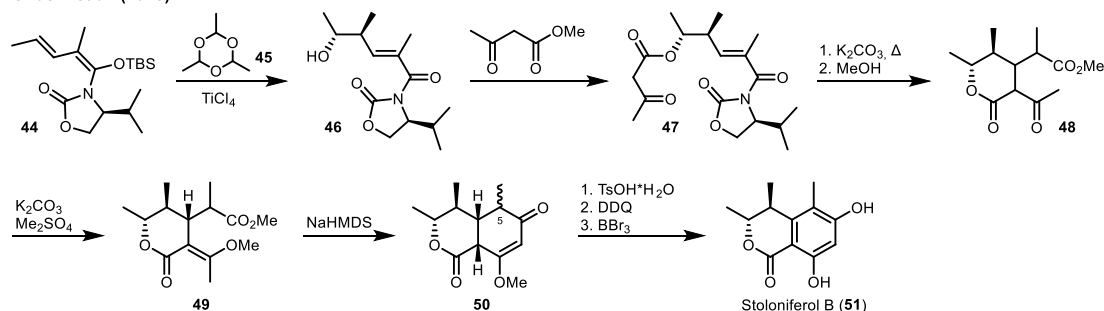
Regan et al. (1987)



Rödel et al. (1995)



Ohashi et al. (2018)



Scheme 2. Synthetic routes towards the unnatural (+)-citrinin (**24b**), natural (–)-citrinin (**24a**) and stoloniferol B (**51**). R = 2-methoxyethoxy.

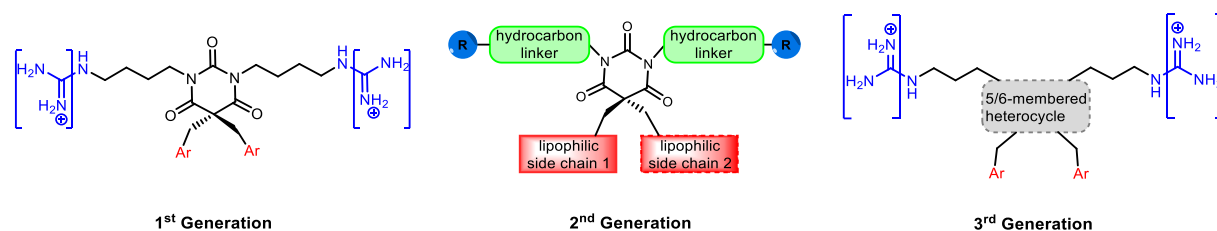
The same sequence, as used by Regan et al., furnished **24a** in 99% ee. While delivering the enantiopure natural product, the need for adjusting one of the stereocenters after its introduction added additional synthetic steps.

Only recently three more members of the citrinin-type azaphilones were prepared by Ohashi et al.¹⁹⁰ They first have synthesized stoloniferol B (**51**), which then was used as the starting point for the synthesis of penicitol A and fusaraisochromanone, culminating in the structural revision of the latter. Not starting from a benzene derivative, they utilized a vinylogous Mukaiyama aldol reaction between **44** and paraldehyde **45** (Scheme 2, bottom), achieving excellent stereoselectivity for the *threo*-adduct **46**. The conversion of alcohol **46** to acetoacetate **47**, utilizing methyl acetoacetate, proceeded smoothly via a ketene intermediate. Upon removal of the chiral auxiliary under basic conditions, they obtained a bislactone which was converted into methyl ester **48** by methanolysis. Enol ether **49** was formed from β-ketolactone **48** by treatment with K₂CO₃ and dimethyl sulfate. For the formation of cyclohexenone **50**, the γ-position of the β-methoxy-α,β-unsaturated carbonyl of **49** was deprotonated with sodium hexamethyldisilazide (NaHMDS) to trigger a vinylogous Dieckmann cyclization. The authors obtained a mixture of C-5 epimers **50** and found that the (*R*)-epimer delivered considerably higher yields in the subsequent oxidation with 2,3-dichloro-5,6-dicyanoquinone (DDQ) to the corresponding phenol. The unfavorable C-5 (*S*)-epimer could be epimerized under acidic conditions with *p*-toluene sulfonic acid (*p*-TsOH), prior to the oxidation. Lastly, de-*O*-methylation with BBr₃ completed the first total synthesis of **51**.

These examples illustrate the efforts put forward to access citrinin-type azaphilones. Enantioselective syntheses of **24a** and **24b** have been achieved, but in both cases the absolute configuration of one stereocenter needed to be adjusted after its introduction. The enantioselective Mukaiyama aldol reaction is an elegant way to introduce the stereocenters, but since it is substrate controlled, it calls for the construction of different starting materials if other diastereomers were to be synthesized.

3 General discussion of results from the thesis

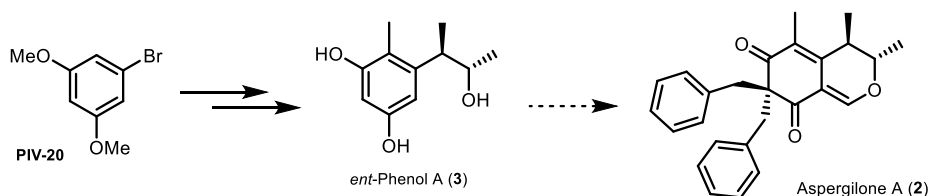
In the following chapters 3.1-3.4, the synthesis and evaluation of eusynstyelamide mimics is discussed (part A in chapter 1.1 Aim of the thesis). Three generations of compounds were developed (Figure 18) to address the research questions formulated in the aim: (1) Can the butyrolactam core be replaced without the compound losing its antimicrobial activity (1st generation); (2) What structural combinations are the most favorable (2nd generation) and (3) Will the findings transfer to other core structures (3rd generation). The insights gained from each generation of compounds are compiled in papers I – III.



Ar = (halogenated) aromatic aryl or naphthyls
R = cationic group

Figure 18. Generations of the compounds developed and studied in this thesis.

In chapter 3.5 the retrosynthetic analysis of aspergilone A (**2**) and the forward synthesis towards the intermediate *ent*-phenol A (**3**) are discussed (part B in chapter 1.1 Aim of the thesis) (Scheme 3). The current progress of our efforts is presented and the challenges ahead are pointed out. The synthetic achievements are summarized in paper IV.



Scheme 3. General approach towards aspergilone A (**2**) via *ent*-phenol A (**3**).

3.1 1st Generation of *N,N'*-dialkylated-5,5-disubstituted barbiturates (paper I)

3.1.1 Introduction

To study mimics of the eusynstyelamides, a decision needed to be made on which structural features were to be investigated. As stated before, the eusynstyelamides fulfill the pharmacophore model of AMPs¹⁶ and we therefore hypothesized that their amphipathic nature was of greater importance than their butyrolactam core (Figure 19, left). Although a racemic synthesis of eusynstyelamide A was published in 2010,⁶⁸ the dihydroxybutyrolactam ring seemed too complex to allow for the efficient construction of a compound library.

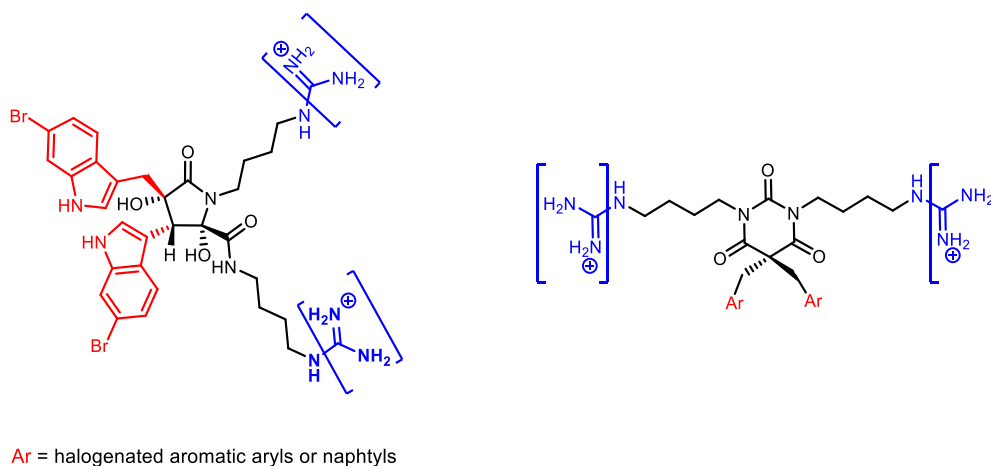


Figure 19. Left: General structure of the eusynstyelamides. Right: General structure of the barbituric acid mimics. Brackets indicate the presence of either the amido or guanidino group.

We reasoned further that if the core of the eusynstyelamides is not part of the pharmacophore according to the model,¹⁶ it should be interchangeable. We, therefore, decided to replace the dihydroxybutyrolactam ring with a much simpler barbituric acid core (Figure 19, right).

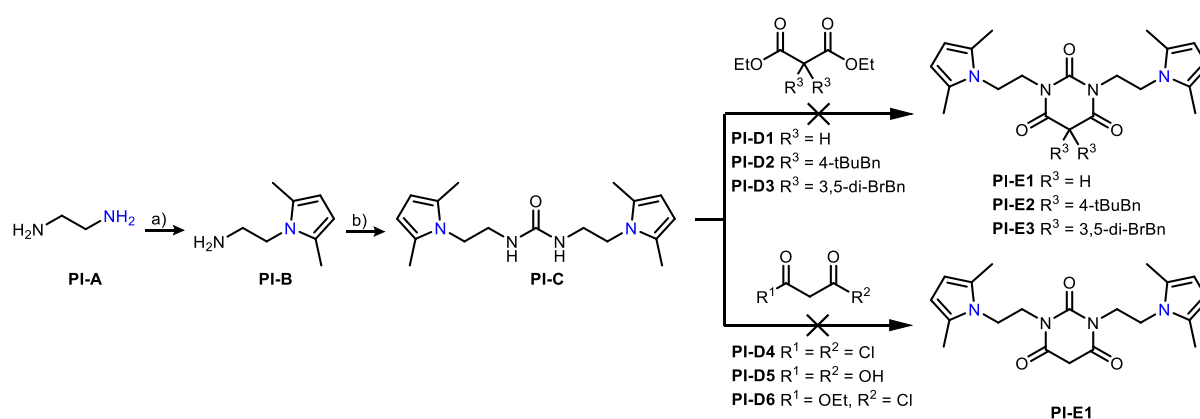
Barbituric acid, commonly known as barbiturate, offered several advantages: (1) Barbituric acid is an achiral, well-known building block in drug design¹⁹¹ and is found in drugs, which are used for a wide range of clinical indications.¹⁹²⁻²⁰⁰ (2) Many synthetic methods for the *de novo* synthesis²⁰¹⁻²⁰⁵ and modification^{202, 205-207} of barbituric acids are reported. (3) The substitution pattern allows for segregation of the cationic and lipophilic sides. (4) The *trans*-relationship of the lipophilic side chains in eusynstyelamides¹⁴ could be retained by the gem-dibenylation of the tetrahedral carbon of the barbituric acid.

Using the 5,5-disubstituted barbituric acid as a premise for further planning, the *n*-butyl hydrocarbon linkers required to be attached to the imide nitrogens. We decided to incorporate either two amine or two guanidino groups, but no combination of the two. Coinciding with the naturally occurring 6-bromoindole in eusynstyelamides, several groups have reported the successful introduction of (pseudo)halo aryls in SMAMPs, albeit the use of aromatic heterocycles is rare.²⁰⁸⁻²¹¹ In medicinal chemistry, halogens and especially fluorine are often introduced into aromatic systems to retard or even prevent metabolic degradation by oxidation, hydroxylation or epoxidation of the aromatic ring.^{212, 213} We therefore decided to focus on promising halogenated side chains, which were evaluated in previous studies of our co-workers.²¹⁴⁻²¹⁶ Those included 3,5-bis(trifluoromethyl)benzyl, 3,5-dibromobenzyl, 4-bromo-3-chlorobenzyl, 4-fluoro-1-naphthyl, 2-naphthyl, 4-(*tert*-butyl)benzyl, 4-(trifluoromethyl)benzyl and 3,5-bis(*tert*-butyl)benzyl.

3.1.2 Summary of the synthetic work

We attempted to develop a convergent synthesis to quickly access the tetrasubstituted barbiturates by coupling *N,N'*-dialkylated ureas with dialkylated diethyl malonates (Scheme 4 and **PI**, *Supporting Information*). The idea was to have various derivatives of both building blocks to be able to synthesize the target barbiturates in two steps on demand. We chose an *n*-ethyl linker over the intended *n*-butyl linker because longer chains may hamper the cyclisation under basic conditions. 2,5-dimethylpyrrole was chosen as the protecting group to reduce the number of potential reactive centers and due to its stability under a wide range of conditions.

Starting from ethylenediamine, hexane-2,5-dione and catalytic amounts of chloramine-T, we could access the mono 2,5-dimethylpyrrole protected diamine **PI-B** in 93% yield. Two equivalents of the primary amine readily reacted with 1,1'-carbonyldiimidazole (CDI) to deliver *N,N'*-disubstituted urea **PI-C** in 78% yield. CDI served here as a safer alternative to phosgene. We then tried to cyclize **PI-C** with substituted and unsubstituted diethyl malonate derivatives **PI-D1** to **PI-D3** (Scheme 4, upper pathway).

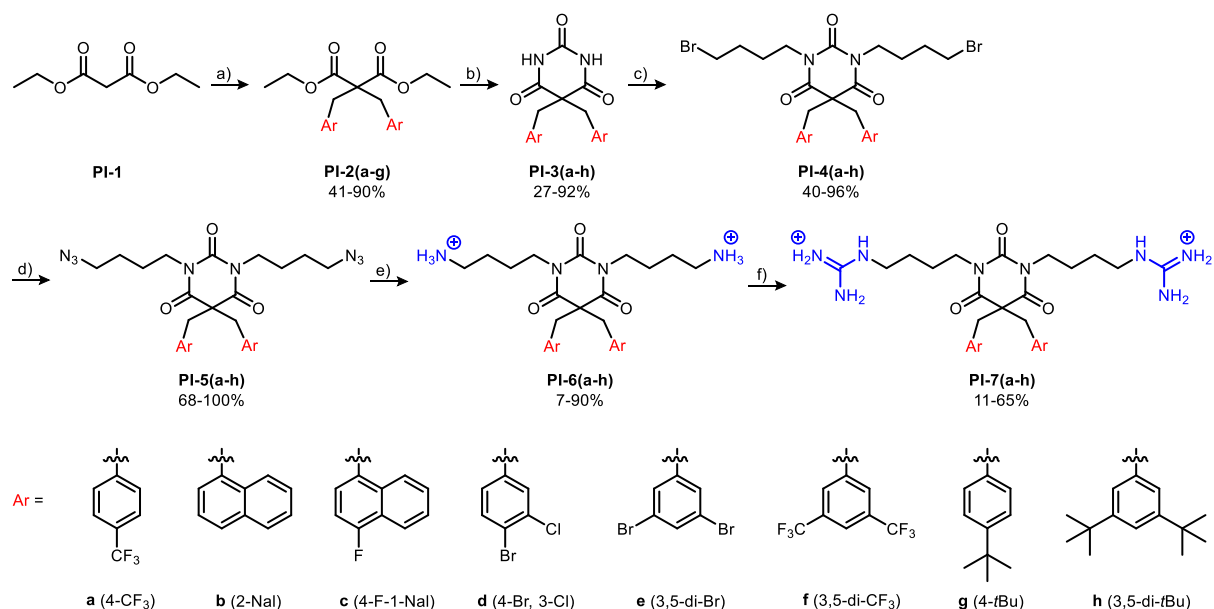


Scheme 4. Unsuccessful strategy towards di- and tetra-substituted barbituric acid derivatives. Reaction conditions: a) hexane-2,5-dione, chloramine-T, MeCN, r.t., 1 h, 93%; b) CDI, DIPEA, DCM, r.t., 18 h, 78%. Adapted with permission from *Paulsen et al., J. Med. Chem. 2021, 64, 15, 11395–11417*.²¹⁷

Neither strongly basic conditions (KO^tBu, Na, NaH) to activate the urea, nor strongly Lewis acidic conditions (Al(Me)₃, TiCl₄, Ti(OⁱPr)₄, BF₃·OEt₂) to activate the malonate led to any conversion to **PI-E**. Employing NaH under μ -wave irradiation led mostly to decomposition of the starting material and delivered fragments of the product. We changed the strategy to the use of more reactive carboxylic acid derivatives (Scheme 4, lower pathway). Unsubstituted malonic acid was treated with *N,N'*-diisopropylcarbodiimide (DIC) or *N,N'*-dicyclohexylcarbodiimide (DCC), followed by the *N,N'*-dialkylated urea **PI-C** but no reaction took place. Reasoning that the *O*-acylisourea intermediate was not electrophilic enough, we decided to employ highly electrophilic acid chlorides. Treating **PI-C** with malonyl chloride led to an insoluble solid, most likely being a polymer. As the di-acid chloride was too electrophilic, we speculated that ethyl malonyl chloride would form one amide bond with the urea at

low temperature and then cyclize to form the barbiturate upon warming. Unfortunately, slow addition of ethyl malonyl chloride to a solution of **PI-C** at $-78\text{ }^{\circ}\text{C}$ yielded only some of the mono addition product and mostly the di substituted urea. The lack of either reactivity or control of the reaction pathway led to abandonment of this approach.

We were able to synthesize the target structures according to a sequence developed by co-workers (Scheme 5). Diethyl malonate **PI-1** was dialkylated with the respective aryl or naphthyl bromides in moderate to excellent yields. Ensuing NaH mediated cyclisation with urea in dimethylformamide (DMF) delivered the 5,5-disubstituted barbiturates **PI-3(a-h)** in 27-92% yields. *N,N'*-dialkylation was carried out with an excess of 1,4-dibromobutane in the presence of K_2CO_3 in DMF to deliver the tetrasubstituted barbiturates **PI-4(a-h)**. $\text{S}_{\text{N}}2$ substitution of the bromides to the corresponding azides **PI-5(a-h)** proceeded in moderate to quantitative yields (68-100%). Reduction of the azides with NaBH_4 and a catalytic amount of propane-1,3-dithiol, followed by addition of Boc_2O delivered the *N*-Boc protected amines. Boc protection was crucial to obtain the compounds in high purity and meaningful yields. TFA mediated Boc removal gave the primary amine barbiturates **PI-6(a-h)**. The yields ranged from 7-90% for the three-step process starting from azides **PI-5(a-h)**. The amines could be converted into the respective Boc-protected guanidine barbiturates **PI-7(a-h)** by employing *N*-Boc-1*H*-pyrazole-1-carboxamide in THF. The Boc-protected intermediates were purified before treatment with TFA in DCM to yield the desired barbiturates **PI-7(a-h)** in 11-65% yields over two steps (o2s).



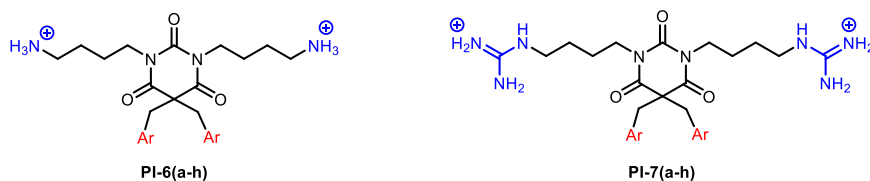
Scheme 5. Successful synthetic strategy towards the 1st generation mimics. Experimental conditions: (a) ArCH_2Br , base, DMF; (b) urea (dry), NaH, DMF (dry); (c) 1,4-dibromobutane, K_2CO_3 , DMF; (d) NaN_3 , DMF; (e) (i) NaBH_4 , 1,3-propanedithiol, THF:isopropanol 1:1 then (ii) Boc_2O ; (iii) $\text{CH}_2\text{Cl}_2/\text{TFA}$; (f) (i) *N*-Boc-1*H*-pyrazole-1-carboxamide, THF; (ii) $\text{CH}_2\text{Cl}_2/\text{TFA}$. Purified using C-18 flash chromatography. Adapted with permission from J. Med. Chem. 2021, 64, 15, 11395–11417.

3.1.3 Summary of the biological studies

MIC evaluation

All compounds were screened against antibiotic susceptible laboratory strains (Table 1) and 30 multi-resistant clinical isolates. Both screenings delivered the same trends, of which some are highlighted in the following summary. As a measure of systemic toxicity, the EC₅₀ values of the haemolysis of human red blood cells (RBC) were used.

Table 1. Antimicrobial activity (MIC in µg/mL) against bacterial reference strains and haemolytic activity against human RBC (EC₅₀ in µg/mL) for all compounds in paper I.



Entry	Comp. ID	Ar	ClogP	Antimicrobial activity				EC ₅₀
				S. a	C. g	E. c	P. a	
1	PI-6a	(4-CF ₃)	3.52	64	4	128	64	>398
2	PI-6b	(2-Nal)	3.82	8	1	16	16	250
3	PI-6c	(4-F-1-Nal)	3.96	4	1	16	8	160
4	PI-6d	(4-Br, 3-Cl)	4.08	4	1	4	8	172
5	PI-6e	(3,5-di-Br)	4.37	4	1	16	16	79
6	PI-6f	(3,5-di-CF ₃)	4.41	16	4	4	8	177
7	PI-6g	(4- <i>t</i> Bu)	4.47	4	1	2	4	145
8	PI-6h	(3,5-di- <i>t</i> Bu)	6.29	1	0.25	8	64	<5
9	PI-7a	(4-CF ₃)	3.52	2	0.25	8	64	>449
10	PI-7b	(2-Nal)	3.82	1	0.25	1	8	133
11	PI-7c	(4-F-1-Nal)	3.96	1	0.25	1	4	90
12	PI-7d	(4-Br, 3-Cl)	4.08	0.5	0.25	2	8	77
13	PI-7e	(3,5-di-Br)	4.37	1	0.25	2	4	62
14	PI-7f	(3,5-di-CF ₃)	4.41	2	2	2	8	98
15	PI-7g	(4- <i>t</i> Bu)	4.47	1	<0.13	2	4	77
16	PI-7h	(3,5-di- <i>t</i> Bu)	6.29	1	0.25	4	4	<6
17	Oxytetracycline			0.65	0.65	2.5	20	

Bacterial reference strains: S. a – *Staphylococcus aureus* ATCC 9144, C. g – *Corynebacterium glutamicum* ATCC 13032, E. c – *Escherichia coli* ATCC 25922, and P. a – *Pseudomonas aeruginosa* PA01, DSM 19880 (ATCC 15692). ^aSide chain Clog P was calculated for a substituted toluene, 1-methyl-Nal, or 2-methyl-Nal (ChemBioDraw Ultra v19.0.0.1.28). ^b Values given as *greater than* correspond to the highest concentration (500 µM) tested in the RBC assay.

The amine guanidines **PI-6** (entries 1-8) were generally less potent and less haemolytic than their guanidyl counterparts **PI-7** (entries 9-16). Most of the derivatives showed a higher potency against Gram-positive strains compared to Gram-negative strains. The potency for all strains, regardless of the cationic head group, increased with higher CLogP values of the lipophilic side chains and the haemolytic activity followed the same trend. Only amine **PI-6f** (3,5-di-CF₃, entry 6) and guanidine **PI-7f** (3,5-di-CF₃, entry 14) were notably less active than the lipophilicity of the side chains would suggest. Of note, barbiturates **PI-6e** and **PI-7e** (3,5-di-Br, entries 5 and 13), having the same substitution pattern as

PI-6f/7f (3,5-di-CF₃, entries 6/14), were 2-4-fold more potent than the latter ones. The electron withdrawing CF₃ groups may lead to an unfavorable polarization of the aromatic ring and thereby impair its ability to interact with the lipid membrane. Derivatives carrying 3,5-bis-(*tert*-butyl) groups, **PI-6h** (entry 8) and **PI-7h** (entry 16), were highly active but too haemolytic for systemic application.

The most promising mimics were the amine barbiturate **PI-6e** (3,5-di-Br, entry 5) and the guanidine derivatives **PI-7c** (4-F-1-Nal, entry 11), **PI-7e** (3,5-di-Br, entry 13) and **PI-7g** (4-*t*Bu, entry 15), due to their good broad-spectrum activity and limited haemolytic activity.

In vivo studies

Having established the general activity of our compounds against antibiotic susceptible strains and multidrug resistant clinical isolates, we tested the *in vivo* efficiency of guanidyl derivative **PI-7e** (3,5-di-Br). Using an established murine peritonitis model, we could show that **PI-7e** (3,5-di-Br) led to a 1.7-log (98%) decrease in bacterial load of *E. coli* for a single treatment of 1.4 mg/kg. The same treatment led to a 1.0-log (90%) reduction in bacterial load of *K. pneumoniae* compared to a vehicle negative control. Despite those promising results the maximal tolerated dose (MTD) of 7 mg/kg poses some limitation. Further pharmacokinetic and administrative studies may help to mitigate that limitation.

MoA studies

Compounds **PI-6e** (3,5-di-Br) and **PI-7e** (3,5-di-Br) were used to study the bacterial viability and membrane integrity utilizing two luciferase-based biosensor assays in *Bacillus subtilis* 168 and *E. coli* HB101.^{218,219} Both compounds exhibited an immediate and strong membranolytic effect for both strains in a concentration-dependent manner. The Gram-positive *B. subtilis* seemed to be affected faster than Gram-negative *E. coli*.

For *B. subtilis* a membranolytic effect was observed as soon as the viability of bacterial cells was reduced. For *E. coli* the correspondence was not as linear. For both compounds the bacterial viability decreased in a concentration-dependent manner. The membranolytic effect, however, was much slower leading to a suggested total metabolic shutdown according to viability assay, while a substantial part of the bacterial population had an intact membrane. This finding was most pronounced for guanidyl derivative **PI-7e** (3,5-di-Br) and may indicate an additional target along with the cytoplasmic membrane.

Conformational analysis and membrane interaction simulations

To further investigate the interaction of our amphipathic barbiturates with the bacterial membrane surface, we determined the most stable conformers in aqueous solution by density functional theory (DFT) geometry optimization and nuclear magnetic resonance (NMR) spectroscopy and carried out a membrane interaction simulation.

We found three minimum energy conformations for guanidine **PI-7e** (3,5-di-Br) mainly differing in the orientation of the lipophilic side chains. Conformation **PI-7e_{up}**, in which the side chains and the barbituric acid were forming a W-shape, had the lowest energy followed by **PI-7e_{up-down}**, where one side

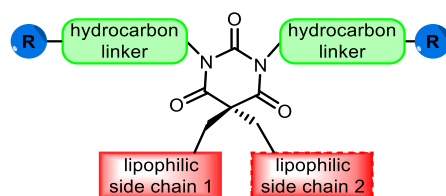
chain was pointing up and one down, and **PI-7e_{down}**, in which both side chains were pointing down, respectively. Analysis of the rotating frame Overhauser enhancement spectroscopy (ROESY) interactions in NMR confirmed a geometrical arrangement similar to **PI-7e_{up}**. The presence of a micelle forming agent (sodium dodecyl sulfate, SDS) led only to minor changes in the spatial arrangement, namely the *n*-butyl linkers being closer to the lipophilic side chains.

To further investigate the membrane interactions we used molecular dynamics simulations with an *E. coli* inner membrane (IM) model²²⁰ for selected compounds. In a simpler model, the membrane can be envisioned as a phospholipid bilayer with a pad of water above and underneath. At the start of the simulation, the compounds were placed above the lipid bilayer in the water pad, having the **up** conformation. The system was then allowed to evolve for a total of 260 ns. Most of the barbiturates inserted rapidly (between 7-35 ns) into the membrane and resided there for the rest of the simulation. For several compounds, a single change from the **up** to the **up-down** conformation was observed during the simulation. Only **PI-6a** (4-CF₃) exhibited more conformational flexibility, shifting multiple times between the **up** and the **up-down** orientation. Additionally, **PI-6a** (4-CF₃) did not remain in the bilayer after the first insertion but left the membrane and re-inserted several times. This fluctuating behavior may account for the low activity (MIC: 128 μg/mL) of **PI-6a** (4-CF₃) against *E. coli*.

3.2 2nd Generation of *N,N'*-dialkylated-5,5-disubstituted barbiturates (paper II)

3.2.1 Introduction

Having established the *in vitro* and *in vivo* efficiency of the new tetrasubstituted barbiturates, we wanted to improve the therapeutic index (balance between antimicrobial potency and haemolytic activity), in search of further lead structures with potential broad-spectrum application. We planned a 2nd generation of derivatives having the general structure shown in Figure 20. We wanted to keep the barbituric acid core unaltered, while systematically investigating the contribution of the cationic groups, linkers and lipophilic side chains towards the compounds' antimicrobial potency and haemolytic activity. The compounds of the 1st generation had shown similar trends of potency against antibiotic susceptible and resistant strains. We therefore decide to only screen against susceptible strains, which reduced the workload substantially.



2nd Generation

Figure 20. General structure of the 2nd generation mimics of the eusynstyelamides.

3.2.2 Design of the compounds and the synthetic strategy

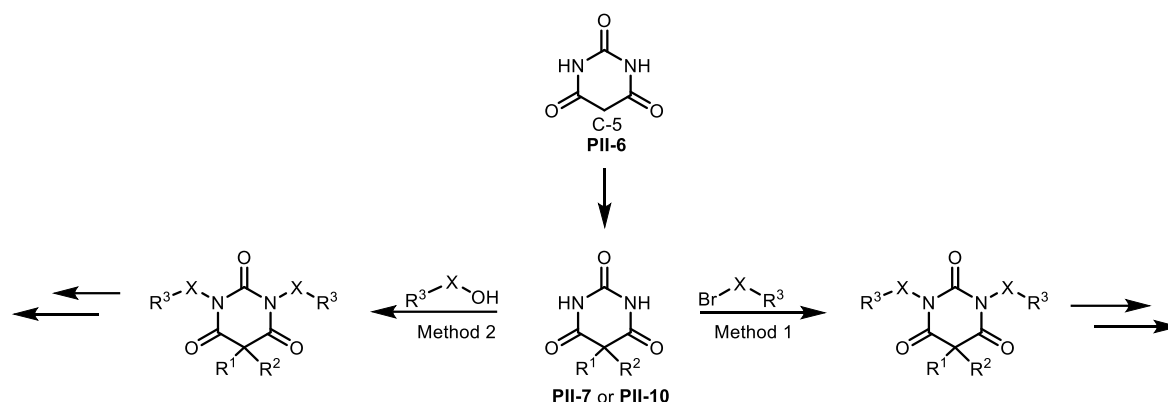
The compounds were grouped into 5 series varying one moiety at a time, while keeping the rest of the molecule unaltered. The focus of each series was as follows: (1) cationic groups, (2) new lipophilic side chains, (3) a combination of two different lipophilic side chains (the side chains were selected based on the screening results from paper I and paper II, *series 2*), (4) different hydrocarbon linkers and (5) combinations of the most promising structural elements from *series 1-4*.

In the following discussion a capital A denotes R³ = amine and a capital G denotes R³ = guanidine in the compound codes. If the descriptor is omitted, both the amine and the guanidine derivatives are being referred to.

3.2.3 Synthesis

3.2.3.1 General synthetic strategy

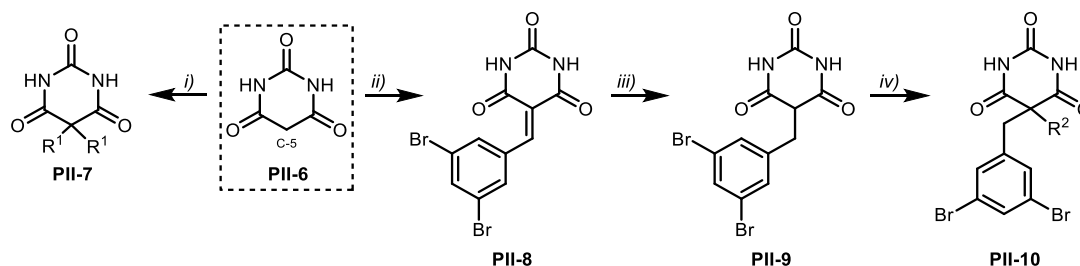
To account for the greater number of derivatives needed, we envisioned a shorter synthetic approach (Scheme 6), consisting of three main steps: (1) C-5 dialkylation of barbituric acid **PII-6** to obtain 5,5-disubstituted derivatives **PII-7** ($R^1 = R^2$) and **PII-10** ($R^1 \neq R^2$); (2) *N,N'*-dialkylation of **PII-7** and **PII-10** and (3) further transformations. For each step we used different methods, depending on the target structures and the availability of starting materials. In the following chapters the synthesis of all target structures is presented in more detail.



Scheme 6. New synthetic strategy towards tetrasubstituted barbiturates. Method 1: S_N2 alkylation with alkyl bromides. Method 2: Mitsunobu reaction.

3.2.3.2 C-5 dialkylation of barbituric acid

Commercially available barbituric acid **PII-6** could be 5,5-dialkylated with either benzyl or alkyl halides in the presence of sodium bicarbonate in PEG-400 at elevated temperatures to deliver compounds **PII-7** in 5-92% yield (Scheme 7). The synthesis of mono-5-substituted barbituric acids is only possible by utilizing indirect methods, as the alkylated barbiturate **PII-9** is more nucleophilic than the unsubstituted barbituric acid **PII-6**.²²¹ Therefore, a Knoevenagel condensation between 3,5-dibromobenzaldehyde and barbituric acid **PII-6** was utilized to deliver **PII-8** and the latter one could be reduced with NaBH_4 in ethanol to 5-mono-alkylated barbiturate **PII-9**.



Scheme 7. Synthesis of core structures **PII-7** and **PII-10**. Reaction conditions: *i*) Alkylating agent, NaHCO_3 , PEG-400, 45-100 °C, 5-92%; *ii*) 3,5-dibromobenzaldehyde, $\text{H}_2\text{O}/\text{EtOH}$ (3:1), 105 °C, 58%; *iii*) NaBH_4 , EtOH, 70 °C, 80%; *iv*) Alkylating agent, NaHCO_3 , PEG-400, 50-100 °C, 5-61%.

Next, using the aforementioned alkylation conditions, differently 5,5-disubstituted barbiturates **PII-10** could be obtained. The yields ranged from 2-28% for the three-step process.

3.2.3.3 *N,N'*-dialkylation and further transformations

To introduce the alkyl linkers, we wanted to use either alkyl halides (Scheme 6, method 1) or aliphatic alcohols (method 2) in a Mitsunobu reaction. As many aliphatic amino alcohols are commercially available, this approach presents a straightforward way to quickly introduce different types of linkers. An additional advantage of the second method is the possibility to use secondary and tertiary alcohols, whereas the corresponding alkyl halides are challenging substrates.

Having the desired intermediates **PII-7** and **PII-10** in hand, we could use one of two methods to introduce alkyl linkers as shown in Figure 21. For *series 1*, 3,5-dibromobenzyl containing barbiturate was treated with 1-bromo-4-chlorobutane under basic conditions to introduce the linker bearing a halogen leaving group (method 1). The terminal chlorine could be substituted with a suitable amine (R³) to yield compounds **PII-1(a-d)**.

For *series 2* and *3*, either *N*-Boc-4-amino-1-butanol or *N,N'*-di-Boc-4-guanidino-1-butanol was used as the alkylation reagent to yield the final amine and guanidine groups, respectively (Scheme 6, method 2). The alcohols could be coupled with 5,5-disubstituted barbiturates **PII-7** and **PII-10** under Mitsunobu conditions with PPh₃ and diisopropyl azodicarboxylate (DIAD) in DCM. The resulting products were treated with TFA in DCM to remove the Boc protecting groups and deliver the final compounds **PII-2(a-f)** and **PII-3(a-g)**.

The same synthetic protocol (method 2) was used for *series 4*, only utilizing commercially available *N*-Boc protected amino alcohols as coupling partners. After removal of the Boc group, the primary amines **PII-4(a-g)A** could be guanylated by use of commercially available *N,N'*-di-Boc-1*H*-pyrazole-1-carboxamide. Ensuing TFA mediated Boc removal delivered the final guanidyl barbiturates **PII-4(a-g)G**.

For *series 5*, we reverted to method 1, employing *N*-Boc-3-bromopropylamine under basic conditions for the *N,N'*-dialkylation. The previously attempted Mitsunobu protocol did deliver the desired products, but in some cases purification posed a major issue. After acidic removal of the Boc groups the obtained amine barbiturates **PII-5(a-g)A** could be converted to their guanidyl counterparts **PII-5(a-g)G** as described for the compounds in *series 4*.

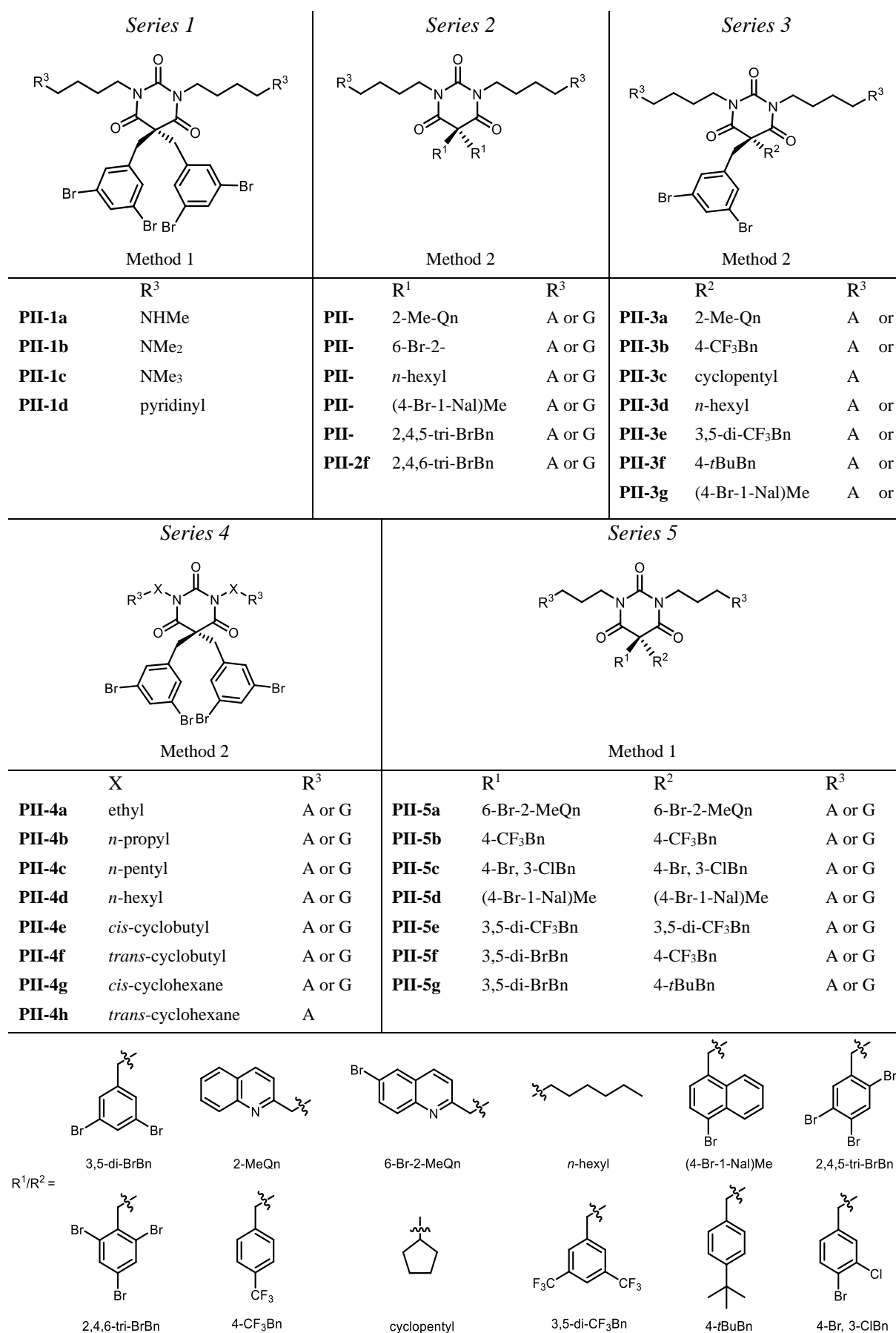


Figure 21. Overview of all synthesized derivatives. For R³ a capital A denotes amine groups and a capital G denotes guanidine groups.

On a short note, the Mitsunobu reaction (method 2) usually delivered higher and more reproducible yields than when using alkyl halides (method 1). Only derivatives with extensively brominated side chains suffered from low solubility and therefore reduced yields. For some derivatives, removal of the reduced DIAD, which is formed during the course of the Mitsunobu reaction, by column chromatography proved to be challenging. The problem could be mitigated by trituration of the final products with Et₂O.

In summary, our newly devised synthetic strategy could deliver both amine and guanidyl barbiturates in as little as 3 steps in the case of identical lipophilic side chains.

3.2.4 Summary of biological results

MIC studies

59 compounds were evaluated for their antimicrobial potency expressed by their MIC values and their systemic toxicity expressed by the EC₅₀ values for haemolysis in the RBC assay. A selection of compounds is given in Table 2 and in the following, some of the major trends are pointed out. A full overview of all MIC values is shown in Tables 1-5 in paper II.

Series 1

(Poly)-methylation of the primary amines led to the loss of activity against *P. aeruginosa*, supposedly due to the lower effective charge of the cationic groups (Table 2, entries 1 and 3). Previously employed amine and guanidine head groups delivered the highest broad-spectrum activity.

Series 2 and 3:

As found before, the antimicrobial potency and haemolytic activity were mainly influenced by the lipophilicity of the side chains. The higher the lipophilicity, the more potent and the more haemolytic the compounds were. CLogP values of the side chains exceeding 4.50, led to high haemolytic activity and an unfavorable solubility profile. The combination of two different lipophilic side chains proved to be an effective way to “fine-tune” the overall lipophilicity.

Series 4:

N-pentyl, *n*-hexyl, cyclobutyl and cyclohexyl linkers exhibited similarly high antimicrobial potency, but demonstrated comparatively high haemolytic activity. The least haemolytic combination was an *n*-propyl linker and a guanidine head group, followed by an ethyl linker and a guanidine head group. Interestingly, the guanidyl derivatives with ethyl and *n*-propyl linkers demonstrated a decrease in haemolytic activity compared to their amine counterparts. This trend opposed our previous findings in paper I, where guanidyl derivatives bearing *n*-butyl linkers were more haemolytic than their amine analogues.

Series 5:

The most promising combination for broad-spectrum activity was an *n*-propyl linker and guanidyl cationic group. Using this combination, either, barbiturates carrying two identical or two different lipophilic groups, could be converted to promising candidates with low haemolytic toxicity (Table 2, entries 4-6).

Several promising compounds could be identified (Table 2), of which some were mainly active and selective towards the Gram-positive strains (entries 1-2), others being active against Gram-positive strains and *E. coli* (entries 3-4) or all tested strains (entries 5-6). Selectivity was evaluated by means of the selectivity index (SI = EC₅₀/MIC), which is a measurement of the preference of a given compound towards bacterial cells. The higher the SI value is, the better is the selectivity towards bacterial cells.

Table 2. Antimicrobial activity (MIC in µg/mL) against bacterial reference strains, haemolytic activity against human RBC (EC₅₀ in µg/mL) and selectivity index (SI = EC₅₀/MIC) for selected compounds from paper II.

Entry	Comp. ID	Antimicrobial activity				EC ₅₀ ^a	SI (EC ₅₀ /MIC) ^b			
		S. a	B. s	E. c	P. a		S. a	B. s	E. c	P. a
1	PII-1c	4	8	128	256	>539	>135	>67	–	–
2	PII-3aG	2	4	32	32	450	225	113	–	–
3	PII-1d	2	4	8	128	>559	>280	>140	>70	–
4	PII-5gG	1	1	2	16	169	>169	>169	85	11
5	PII-4bG	2	2	4	8	187	93	93	47	23
6	PII-5eG	4	2	8	16	445	111	222	56	28
7	Ciprofloxacin	0.06	0.03	0.03	0.25					

Bacterial reference strains: S. a – *Staphylococcus aureus* ATCC 9144, B.s – *Bacillus subtilis* 168, E. c – *Escherichia coli* ATCC 25922, and P. a – *Pseudomonas aeruginosa* ATCC 27853. ^a Values given as *greater than* correspond to the highest concentration (500 µM) tested in the RBC assay. ^b No SI was calculated if the MIC was >16 µg/mL. –: not determined. SI values >20 are considered good.

Counterion effect

When the CLogP value of the lipophilic side chains rose above 4, the water solubility of the respective derivatives dropped below 1 mg/mL. For basic active pharmaceutical ingredients hydrochloride salts are the most used²²² and known to improve water solubility.²²³ We chose five amine and six guanidine barbiturates in the form of their di-TFA salts, of which three amines and four guanidines were not water

soluble. After conversion into their di-HCl salts, all amine and two additional guanidyl derivatives became water soluble. The MIC and RBC values were evaluated again, revealing only slight changes in their haemolytic toxicity for most of the derivatives. The changes could mostly be attributed to the lower molecular weight of the di-HCl salts compared to the di-TFA salts. Interestingly, most of the derivatives demonstrated slightly better antimicrobial potency against the Gram-positive strains by 1-2 titer steps. One possible explanation could be a change in the dissociation rate of the anionic counterions, leaving the cationic head groups more exposed and thereby enhancing their ability to interact with the negatively charged bacterial membrane.

Mode of Action

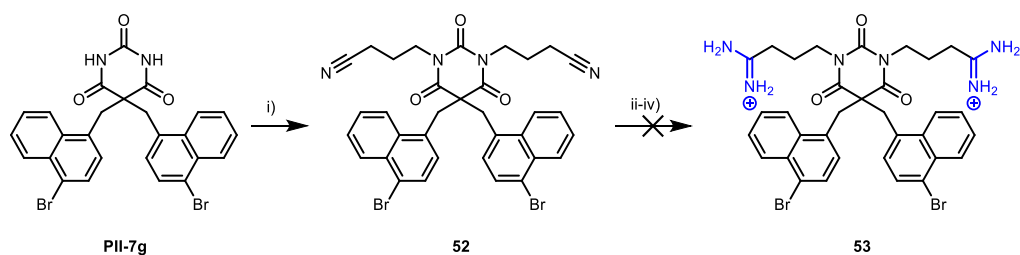
In paper I we had already demonstrated the membranolytic effects of *N,N'*-dialkylated-5,5-disubstituted barbiturates. We now investigated additional 17 narrow-spectrum barbiturates against Gram-positive strains and 14 broad-spectrum derivatives, spanning the chemical space employed in this study. Using again our luciferase-based biosensor assays, we could confirm the concentration-dependent membrane disruption of practically all compounds tested for the cytoplasmic membrane in *B. subtilis* and *E. coli*. Additionally, broad-spectrum barbiturate **PII-3bG** (3,5-di-BrBn; 4-CF₃Bn) was evaluated for its effect on the OM of *E. coli*, by using the hydrophobic 1-*N*-phenylnaphthylamine (NPN) fluorescent probe. For low concentrations (0.8x MIC) the permeability of the OM increased, but the bacterial cells were still viable. At higher compound concentrations (6.4-12.8x MIC) the OM was disrupted at a similar rate as the IM. The additional results in this paper suggest a concentration-dependent disruption of the OM and IM as the primary mode of action.

3.2.5 Additional results not included in paper II

When first investigating the behavior of different cationic groups, amidines were considered as a very interesting link between the primary amines and guanidines. From the methods available, the Pinner reaction is one of the oldest.²²⁴⁻²²⁶ It proceeds through the formation of an imino ether hydrochloride (known as Pinner salts) from a nitrile precursor, by treatment with gaseous HCl in an alcoholic solvent. Pinner salts can react with a range of nucleophiles, including ammonia to produce primary amidines.²²⁴

The 5,5-dibenzylated barbituric acids **PII-7** were *N,N*-dialkylated with 4-bromobutanenitrile in 7-85% yields under the conditions used in method 1 (*vide supra*) (Scheme 8, exemplified with **PII-7g**). Interestingly, the yields were usually lower compared to the alkylations using *N*-Boc-3-bromopropylamine.

Having the nitrile containing barbituric acid derivative **52** in hand, we employed slightly modified Pinner reaction conditions to convert the nitriles into amidines. We decided to use HCl dissolved in anhydrous MeOH instead of gaseous HCl, followed by ammonia in methanol. Unfortunately, we could identify neither the imino ether nor the final amidine. Using a similar pathway, we employed NaOMe in MeOH, followed by the addition of NH₄Cl, which yielded only traces of the desired amidine.



Scheme 8. Attempted synthesis of amidine **53**. Reaction conditions: i) 4-bromobutanenitrile, K_2CO_3 , TBAI, acetone, $50\text{ }^\circ\text{C}$, 72 h, 49%; ii) HCl (1.25 M in MeOH), 1,4-dioxane (dry), MeOH (dry), $0\text{-}25\text{ }^\circ\text{C}$, 2 d then NH_3 (7 N in MeOH), $25\text{ }^\circ\text{C}$, 24 h; 0% iii) NaOMe, NH_4Cl , MeOH (dry), $0\text{-}25\text{ }^\circ\text{C}$, 4 d, 0%; iv) $AlMe_3$, NH_4Cl , $0\text{-}105\text{ }^\circ\text{C}$, 48 h, 0%.

Next, we tried chloro(methyl)aluminum amide, freshly prepared from $Al(Me)_3$ (trimethylaluminum) and NH_4Cl ,^{227, 228} but found only unidentified products, potentially formed by decomposition. As none of the procedures discussed above could deliver the desired amidines, we decided to exclude amidines from our study.

3.3 3rd Generation: Varying core structures with focus on hydantoins (paper III)

3.3.1 Introduction and scaffold design

After the thorough investigation of the structural components of the amphipathic barbiturates, we were interested in how the central scaffold influences the compounds' biological behavior. To that end, we decided to transfer our previously employed substitution pattern to five heterocycles (**PIII-(2-5)** and **PIII-15**), which were structurally related to barbituric acid **PII-4bA** (Figure 22).

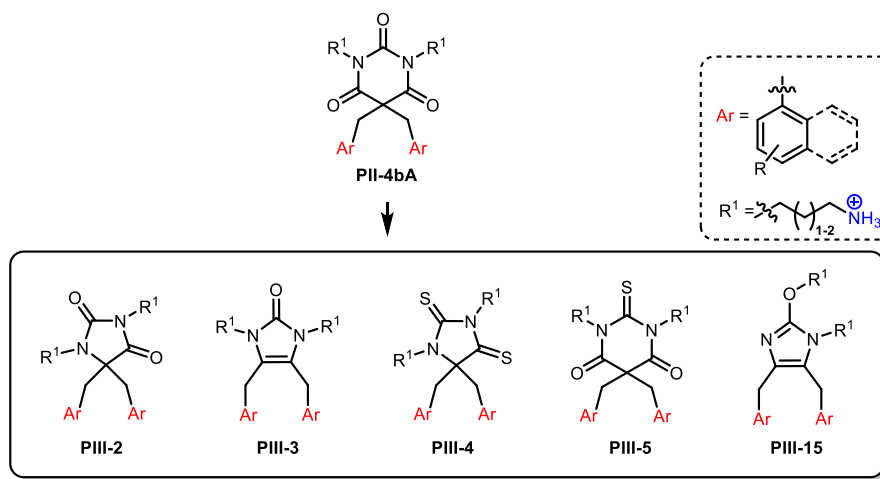
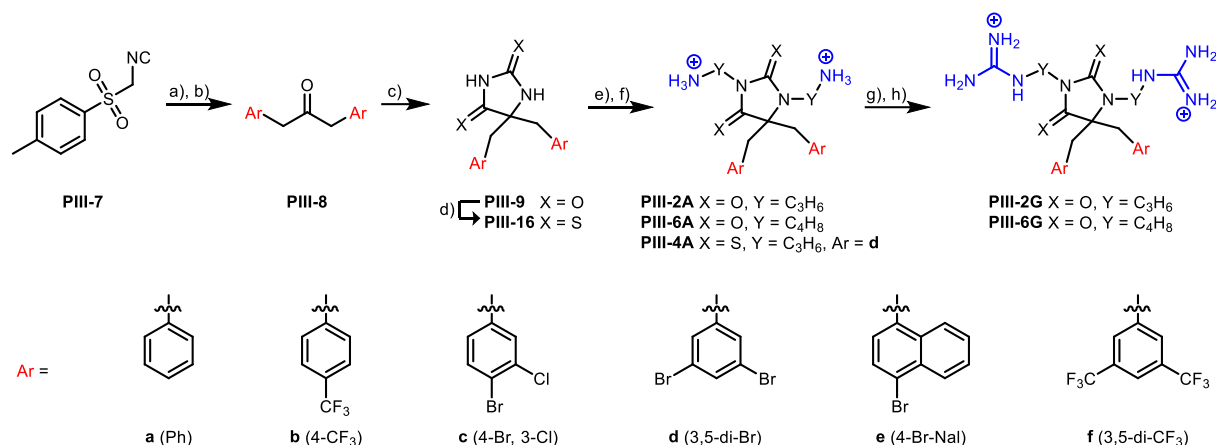


Figure 22. Core structures **PIII-(2-5)** and **PIII-15** used in this study. *Ar* = lipophilic side chain, *R*¹ = *n*-alkyl linker with a cationic head group.

Imidazolidine-2,4-dione **PIII-2**, commonly known as hydantoin, was chosen, as it is a well-known scaffold in medicinal chemistry,²²⁹⁻²³⁴ but is rarely used in antimicrobial agents.^{208, 235-237} 4-imidazolidin-2-one **PIII-3** was chosen, since it was likely to adopt a different geometry in solution and is more lipophilic by one order of magnitude. Sulfur is found in a variety of different drugs,²³⁸⁻²⁴² including prominent antimicrobials such as penicillins and cephalosporines.²⁴³ While the sulfur atom often is part of a heterocyclic structure, we wanted to probe its influence when incorporated in an amide (**PIII-4**) or urea type bond (**PIII-5**). We did not account for 2-(hydroxy)-1*H*-imidazol **PIII-15** in our original library design, but **PIII-15** was obtained as a side product during synthesis. After having evaluated all the core structures, we wanted to build a small library with the most promising core-structure: the hydantoin, then being the basis for the 3rd generation of derivatives.

3.3.2 Summary of the synthetic work

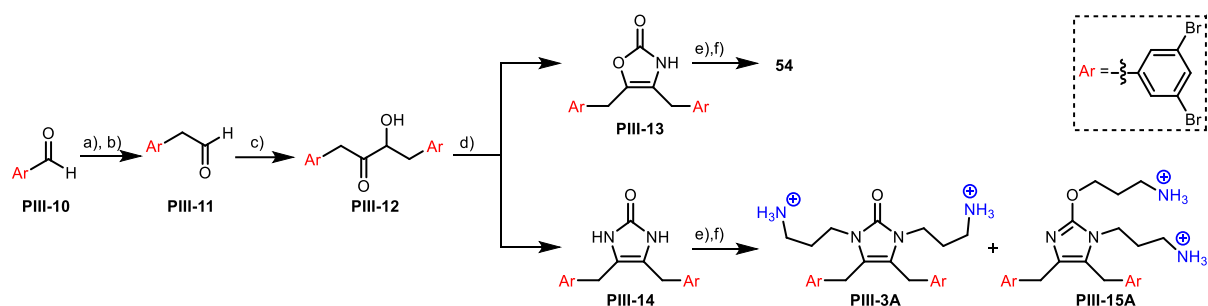
The synthetic strategies towards the tetrasubstituted hydantoins **PIII-2** and 4-imidazolidin-2-one **PIII-3** are shown in Scheme 9 and Scheme 10, respectively. Direct substitution of the commercially available hydantoin is feasible, but regioselectivity is likely to pose a problem, due to the relatively high p*K*_a values of the imidic *N*-3 proton and the C-5 protons. Therefore, we decided on the *de novo* synthesis of the hydantoins (Scheme 9).



Scheme 9. Synthetic strategy towards the target hydantoin **PIII-2**, **PIII-6** and **PIII-4A**. The following compounds were obtained: **PIII-2** Ar = **a-f**; **PIII-6** Ar = **b, c, d, f**; **PIII-4A** Ar = **d**. Reaction conditions: a) ArCH₂Br, TBAB or TBAI, DCM, NaOH(aq) (20-35 wt%), r.t.; b) HCl(conc), DCM/THF, r.t., 53-69% o2s; c) KCN, NH₄CO₃, KOAc, DMSO or KCN, NH₄CO₃, EtOH/H₂O, 60-75 °C, 45-85%; d) Lawesson's reagent, 1,4-Dioxane, 115 °C, 82%; e) *N*-Boc-3-bromopropylamine or *N*-Boc-4-bromobutylamine, Cs₂CO₃, TBAI, acetone, 65 °C then f) TFA, DCM, r.t., 45-85% o2s; g) *N,N'*-di-Boc-1*H*-pyrazole-1-carboxamide, DIPEA, THF, 45 °C then h) TFA, DCM, r.t., 33-91% o2s.

In short, *p*-toluenesulfonylmethyl isocyanate (TosMIC) was α,α -dibenzylated and ensuing acidic hydrolysis delivered ketones **PIII-8**. Employment of modified Bucherer-Bergs conditions delivered the respective hydantoin **PIII-9**. Treatment of the hydantoin of choice with the Lawesson's reagent delivered 2,4-dithiohydantoin **PIII-16**. Using a slightly altered version of the alkylation protocol reported in paper II, utilizing primary alkyl bromides, we obtained the *N,N'*-dialkylated derivatives. Treatment of the latter ones with TFA in DCM delivered the primary amines **PIII-2A**, **PIII-6A** and **PIII-4A**. Conversion of the amines into the respective guanidines **PIII-2G** and **PIII-6G** proceeded as described before.

Tetrasubstituted 4-imidazolidin-2-one **PIII-3A** can be obtained from the respective substituted hydantoin by means of a cationic 1,2-benzyl shift (for details see paper III, Supporting Information). We could demonstrate the general applicability of this method, but the purity of the final products was unsatisfactory. Therefore, we developed the synthetic route shown in Scheme 10.

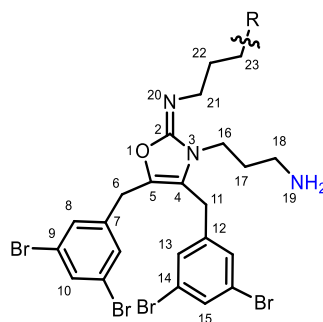


Scheme 10. Synthetic strategy towards tetrasubstituted 4-imidazolidin-2-one **PIII-3A**, its constitutional isomer **PIII-15A** and unresolved structure **54**. Ar = 3,5-dibromophenyl. a) Ph₃P(Cl)CH₂OCH₃, NaHMDS, THF (dry), -78 °C to r.t., 91%; *E/Z* = 1.5/1.0; b) TMSCl, NaI, MeCN (dry), r.t., 60%; c) 3-benzyl-5-(2-hydroxyethyl)-4-methylthiazolium chloride, Et₃N, PEG-400 (dry), 80 °C, 39%; d) urea, AcOH, PEG-400 (dry), 130 °C, 18% for **PIII-13** and 39% for **PIII-14**; e) *N*-Boc-3-bromopropylamine, K₂CO₃, (*n*-hexadecyl)tri-*n*-butylphosphonium bromide, toluene:water 1:1, μ -wave, 130-150 °C then f) TFA, DCM, r.t., 6-19% o2s.

Briefly, commercially available 3,5-dibromobenzaldehyde **PIII-10** could be homologated to **PIII-11** by a sequence of a Wittig reaction, followed by acidic enol-ether cleavage. Aldehyde **PIII-11** was transformed to the α -hydroxy ketone **PIII-12** by a thiazolium salt catalyzed benzoin-type condensation. In the following condensation reaction with urea the desired 4-imidazolidin-2-one **PIII-14** was obtained. Unexpectedly, 4-oxazolin-2-one **PIII-13** was formed as a side product. Utilizing phase-transfer catalysis (PTC), **PIII-13** and **PIII-15** were alkylated under μ -wave irradiation, and subsequent TFA mediated Boc removal delivered derivatives **PIII-3A**, **PIII-15A** and **54**.

Starting from diethyl 2,2-bis(3,5-dibromobenzyl)malonate **PI-2e** and thiourea, we could obtain 5,5-dibenzylated 2-thiobarbituric acid **PIII-18**, utilizing the conditions described in **PI** for the synthesis of the barbiturate core (compounds **PI-3**). *N,N'*-dialkylation with *N*-Boc-3-bromopropylamine proceeded as described before, as did Boc removal with TFA in DCM to deliver 2-thiobarbituric acid **PIII-5A** (Figure 22, Ar = 3,5-dibromobenzyl, R¹ = *n*-propylamine). It should be noted that desulfurization had occurred during the final two steps of the synthesis, yielding a mixture of 2-thiobarbituric acid **PIII-5A** and barbituric acid **PII-4bA** in a ratio of 2.4:1.0. The mixture was inseparable and was tested as such.

Table 3. NMR data¹ of compound **54** and a possible structure. R = unknown, but likely to contain a nitrogen bound to the C-23. *m/z* corresponds to the mass of the fragment including C-23.



54

m/z = 673.8647

Pos.	δ_C mult.	δ_H (<i>J</i> in Hz)	HMBC	Pos.	δ_C mult.	δ_H (<i>J</i> in Hz)	HMBC
1	–	–		13	131.4, CH	7.25, d (1.7)	C-11, C-13, C-14, C-15
2	141.6, -C	–		14	124.1, -C	–	
3	–	–		15	133.3, CH	7.52, t (1.7)	C-13, C-14
4	129.8, -C	–		16	43.4, CH ₂	4.13-4.06, m	C-2, C-4, C-17, C-18
5	137.6, -C	–		17	29.5, CH ₂	1.97-1.85, m	C-16, C-18
6	29.1, CH ₂	4.14, s	C-4, C-5, C-7, C-8, C-9	18	37.9, CH ₂	3.00-2.90, m	C-16, C-17
7	143.1, -C	–		19	–	–	
8	131.1, CH	7.08, d (1.7)	C-6, C-8' C-9, C-10	20	–	–	
9	124.4, -C	–		21	32.6, CH ₂	3.21, t (7.0)	C-2, C-20, C-21
10	133.8, CH	7.57, t (1.7)	C-8, C-9	22	28.5, CH ₂	2.06, p (7.1)	C-19, C-21
11	32.4, CH ₂	3.93, s	C-4, C-5, C-12, C-13	23	39.0, CH ₂	3.13, t (7.0)	C-19, C-20
12	144.5, -C	–		24	–	–	

¹Measured at 400 MHz (¹H) and 101 MHz (¹³C).

Unfortunately, the structure of **54** could not be determined unambiguously. ^1H - and ^{13}C -NMR suggested a structure as shown in Table 3.

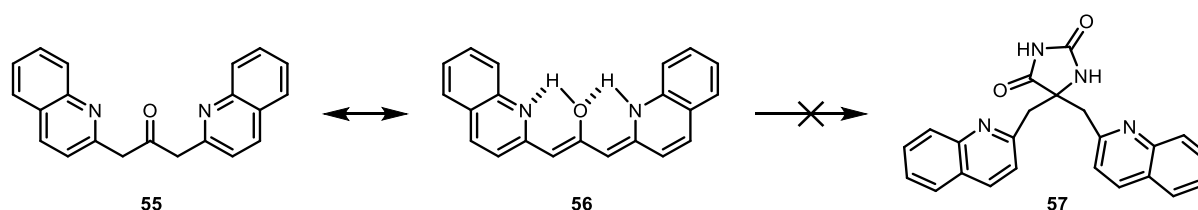
A total of 11 carbons between 124-145 ppm and 8 aliphatic carbons was obtained. The splitting of the aromatic protons in ^1H -NMR clearly showed that two 3,5-dibromobenzyl rings were present. HMBC correlation suggested that they were attached to two different carbon centers at 137.6 ppm (C-5) and 129.8 ppm (C-4), respectively. Based on HMBC correlations of the methylene protons H-6 and H-11, those two carbons had to be attached to heteroatoms. ^1H and COSY data clearly showed the presence of two *n*-propyl groups and the splitting pattern of H-16 and H-21 indicated that C-16 and C-21 were bound to a flat, rigid scaffold. Thus C-2 (141.6 ppm) needed to be sp^2 hybridized and was likely to be double bound to nitrogen N-20.

A possible mechanism for the formation of **54** would be that the Boc group of *N*-Boc-3-bromopropylamine was cleaved under μ -wave irradiation²⁴⁴⁻²⁴⁶ and the primary amine underwent a condensation reaction with the carbonyl of 4-oxazolin-2-one **PIII-3A**. The fate of the terminal bromine remained however unknown. The isotope pattern in HRMS clearly showed the presence of only four bromine atoms. No sensible molecular formula could be delineated from the observed mass ($m/z = 706.8684$), even when MS/MS fragments had been taken into account. Chemical shifts of the hydrogens H-23 indicated a heteroatom bound to carbon C-23. IR data showed the absence of hydroxyl groups, limiting somewhat the identity of the substituent R. A crystal structure could settle that issue but could not be obtained due to time constraints.

Further synthetic curiosities

Stability of 1,3-bis(quinoline-2-yl)acetone **55**

We tried to synthesize hydantoin derivatives with previously utilized quinoline and 6-bromoquinoline as side chains (Scheme 11).



Scheme 11. Most stable isomer of the ketone **55**.

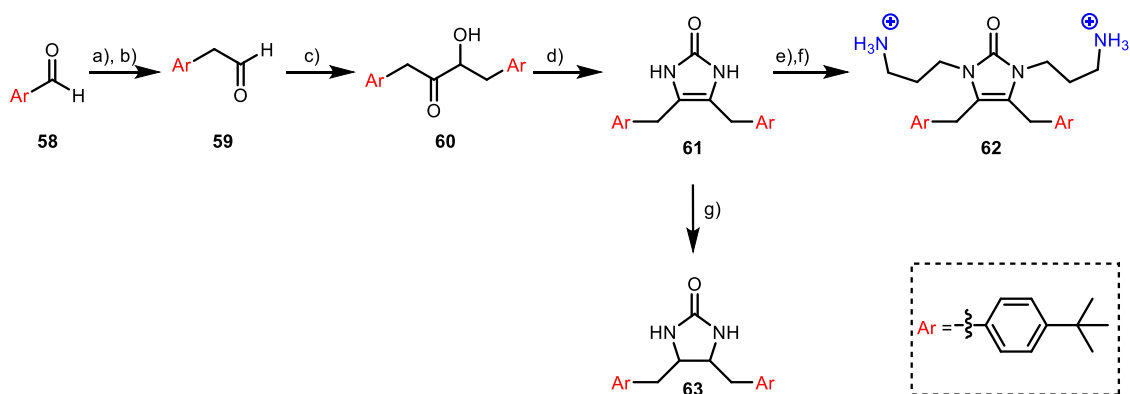
After treatment of the diarylated TosMIC derivative with HCl we obtained the target mass of 1,3-bis(quinolin-2-yl)acetone **55** in HRMS, but the NMR was difficult to interpret and the compound lacked the characteristic carbonyl signal in ^{13}C -NMR. Gawinecki et. al have reported tautomer **56** as being the most stable in solution.²⁴⁷ We believe to have obtained the same tautomer, as we did not observe a carbonyl band in IR. Interestingly, neither a strong OH stretching vibration was found, but the intensity might have been reduced by the intramolecular H-bonds. We subjected (the presumed) compound **56** to

our developed Bucherer-Bergs conditions but did not detect any formation of hydantoin **57**. It remains unknown if the tautomer is too stable and would not revert to the ketone, thus not acting as an electrophile or if we plainly had another structure to begin with.

Synthesis of aldehyde **PIII-11**

Our first approach towards the homologated aldehyde **PIII-11** was *via* nitrile formation from 3,5-dibromobenzyl bromide reacting with sodium cyanide and subsequent reduction to the aldehyde. We screened a range of conditions and reducing agents including diisobutylaluminium hydride (DIBAL-H), Raney Nickel and Ni-Al alloy. Only DIBAL-H yielded some product, but the yields did not exceed 20%. This is a very good example that demonstrates that well-known textbook transformations do not always work, even when utilizing seemingly simple substrates.

Another point to mention is that we had faced some difficulties in the homologation of aldehyde **PIII-10** to **PIII-11** in the synthesis of **PIII-3A**. These complications led to the consideration of using a more facile substrate to develop the synthetic route. We, therefore, used 4-(*tert*-butyl)benzaldehyde **58** to develop the conditions for each synthetic step (Scheme 12), which then needed to be transferred to aldehyde **PIII-10**. The yields for each step, excluding the Wittig reaction, were considerably higher and the homologated aldehyde **59** could be readily purified on silica gel. Additionally, neither 4-oxazolin-2-one formation in the urea condensation step to 4-imidazolidin-2-on **61**, nor *O*-alkylation in the penultimate step were observed. This demonstrates the generality of the synthetic approach and that 3,5-dibromobenzaldehyde had been a challenging substrate.



Scheme 12. Synthetic strategy towards tetrasubstituted 4-imidazolidin-2-one **62**. Ar = 4-(*tert*-butyl)phenyl. a) $\text{Ph}_3\text{P}(\text{Cl})\text{CH}_2\text{OCH}_3$, NaHMDS, THF (dry), -78°C to r.t., 97%; $E/Z = 1.9/1.0$; b) $(\text{COCl})_2$, EtOH, H_2O , CHCl_3 , 0°C to r.t., 73%; c) 3-benzyl-5-(2-hydroxyethyl)-4-methylthiazolium chloride, Et_3N , PEG-400 (dry), 80°C , 77%; d) urea, AcOH, PEG-400 (dry), 130°C , 61%; e) *N*-Boc-3-bromopropylamine, K_2CO_3 , (*n*-hexadecyl)tri-*n*-butylphosphonium bromide, toluene:water 1:1, μ -wave, 130 - 150°C then f) TFA, DCM, r.t., 26% o2s; g) Et_3SiH , TFA, 0 to 50°C , 33%.

We also managed to hydrogenate **61** with a mixture of TFA and Et_3SiH ²⁴⁸ to obtain the saturated, cyclic urea **63**, but low yields and difficult purification led us abolishing this approach. Using Pd/C and Pt/C for hydrogenation, no reaction was observed and only employing PtO_2 resulted in 20% conversion of the double bond to the alkane.

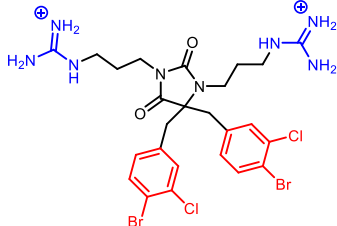
3.3.3 Summary of the biological studies

MIC studies

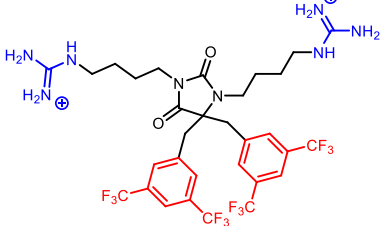
A total of 26 compounds were evaluated for their antimicrobial potency and haemolytic activity, utilizing the same assays as in section 3.2.4. Some selected compounds are shown in Table 4 and the major findings are discussed below. A full overview of MIC data can be found in paper III, Table 1 and Table 2.

When thioamides or thioureas were incorporated, the compounds became less haemolytic and less active against Gram-negative *P. aeruginosa* or unstable as in the case of **PIII-5A**. The hydantoin series proved to be in general less haemolytic than 4-imidazolidin-2-ones **PIII-3A** or 2-(hydroxy)-1*H*-imidazol **PIII-15A**. The potencies within the hydantoin series followed the trends as discussed in paper II, namely guanidine derivatives being more potent and haemolytic than amine derivatives for an *n*-butyl linker and less potent against Gram-negative *P. aeruginosa* and less haemolytic for *n*-propyl linkers. Interestingly, all compounds had EC₅₀ values >200 µg/mL, except for **PIII-2eA** (EC₅₀: 69 µg/mL). Three promising candidates are compiled in Table 4 showing, again, compounds being selective against two (entry 1), three (entry 2) or all four strains (entry 4) of our test panel, as determined by the SI.

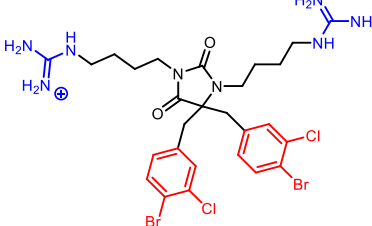
Table 4. Antimicrobial activity (MIC in µg/mL) against bacterial reference strains, haemolytic activity against human red blood cells (EC₅₀ in µg/mL) and selectivity index (SI = EC₅₀/MIC) for selected compounds from paper III.



PIII-2cG



PIII-6fG



PIII-6cG

Entry	Comp. ID	Antimicrobial activity				EC ₅₀	SI (EC ₅₀ /MIC) ^a			
		S. a	B. s	E. c	P. a		S. a	B. s	E. c	P. a
1	PIII-2cG	2	2	32	64	>467	>234	>234	–	–
2	PIII-6fG	2	2	8	32	384	192	192	48	–
3	PIII-6cG	4	2	16	8	347	87	172	22	44
4	Ciprofloxacin	0.06	0.03	0.03	0.25					

Bacterial reference strains: S. a – *Staphylococcus aureus* ATCC 9144, B.s – *Bacillus subtilis* 168, E. c – *Escherichia coli* ATCC 25922, and P. a – *Pseudomonas aeruginosa* ATCC 27853. ^aNo SI was calculated if the MIC was >16 µg/mL. –: not determined. SI values >20 are considered good.

Mode of Action

Having established the antimicrobial activity of tetrasubstituted, amphipathic hydantoin, we wanted to confirm the suspected membranolytic properties of the compounds by using the same biosensor assay as in paper II. We investigated 13 hydantoin in *B. subtilis* and six hydantoin with broad-spectrum activity in *E. coli*. In general, the compounds affected the viability and membrane integrity of both strains in a concentration-dependent manner. The derivatives usually acted faster in the case of Gram-

positive *B. subtilis*. OM permeability in *E. coli* was investigated using the NPN fluorescent probe. Broad-spectrum hydantoin **PIII-2dA** (3,5-di-Br) increased OM permeability at low concentrations (0.4x MIC), but the viability of *E. coli* was not affected. At higher concentrations (1.6-3.2x MIC) low fluorescence levels were detected, suggesting either rapid disruption of the OM before the measurement had started or an intact OM. At the same time, the viability of the bacteria was clearly compromised. It seems most likely that the OM is disrupted equally fast as the IM, however further studies need to be conducted to exclude the possibility of the hydantoins simply translocating over the OM at higher concentrations.

3.3.4 Additional biological results not included in paper III

During the development of the synthetic route towards the target structures and buildup of the library for paper III, we obtained some side products which were also amphipathic. They were not included in paper III for the lack of comparability with the compounds being discussed there. Nevertheless, these compounds were tested against our panel of antibiotic susceptible strains (Table 5).

4-imidazolidin-2-one **62** was active against all strains (MIC: 2-4 $\mu\text{g/mL}$), but rather haemolytic. Guanylated derivative **63** and mono *N*-alkylated derivative **64** had virtually the same antimicrobial potency and haemolytic activity as their di-amine analogue **PIII-3A**. It seemed that for the 4-imidazolidin-2-one core a single positive charge is enough to provide good antimicrobial activity. If the same core was *O*-alkylated, 2-hydroxyimidazole derivative **65**, the activity against *P. aeruginosa* was reduced 4-fold (MIC: 32 $\mu\text{g/mL}$) and the haemolytic activity was almost doubled (EC_{50} : 30 $\mu\text{g/mL}$). Most surprisingly, the simple change from a nitrogen (**64**) to an oxygen (**66**) reduced the overall potency and haemolytic activity drastically. It might be that the N-H proton in compounds **64** and **65** form hydrogen bonds to the TA in the membrane of Gram-positive strains, thus compensating for the lack of a second cationic head group. In the absence of the H-bond donor group in derivative **66** the interaction between TA and the compound is reduced and therefore also the potency. Additionally, a single positive charge in **66** might not be enough to effectively interact with the OM in Gram-negative bacteria, resulting in the compound not being able to cross the OM and thus being virtually inactive. Compound **54** was very active against all strains, including *P. aeruginosa* (MIC: 2 $\mu\text{g/mL}$), but was just as haemolytic as the 4-imidazolidin-2-one **PIII-3A** and 2-hydroxyimidazol **PIII-15A** derivatives. However, it is unknown if the compound carries two positive charges or only one, due to the lack of structural information. The mono-cationic hydantoin **67** was expectedly less potent than the di-cationic analogue **PIII-9cA**, but almost three times as haemolytic for unknown reasons. Further studies need to be conducted to fully unravel the mechanisms at play.

Table 5. Antimicrobial activity (MIC in $\mu\text{g/mL}$) against bacterial reference strains, haemolytic activity against human RBC (EC_{50} in $\mu\text{g/mL}$) and selectivity index ($\text{SI} = \text{EC}_{50}/\text{MIC}$) for compounds not included in paper III.

Code	Core	R^1	ClogP^a	Antimicrobial activity				EC_{50}	$\text{SI} (\text{EC}_{50}/\text{MIC})^b$			
				S. a	B. s	E. c	P. a		S. a	B. s	E. c	P. a
62		(4- <i>t</i> BuBn)	-0.47	4	2	16	8	40	10	20	3	5
63		3,5-di-BrBn	-0.47	2	1	4	8	48	24	48	12	6
64		3,5-di-BrBn	-0.47	4	2	4	8	51	13	26	13	6
65		3,5-di-BrBn	0.26	4	4	4	32	30	8	8	8	-
66		3,5-di-BrBn	-0.23	16	8	64	>64	351	22	44	-	-
54		3,5-di-BrBn	-0.30	2	2	4	2	47	24	24	12	24
67		4-Br, 3-ClBn	-1.69	16	8	16	64	132	8	17	8	-

Bacterial reference strains: S. a – *Staphylococcus aureus* ATCC 9144, B. s – *Bacillus subtilis* 168, E. c – *Escherichia coli* ATCC 25922, and P. a – *Pseudomonas aeruginosa* ATCC 27853. ^a ClogP values were calculated for the unsubstituted central heterocycle (calculated with ChemBioDraw Ultra v19.0.0.1.28). ^bNo SI was calculated if the MIC was $>16 \mu\text{g/mL}$. –: not determined. SI values >20 are considered good.

3.4 Comparison of the antibacterial compounds investigated

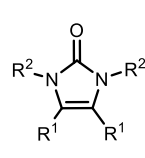
In our previous analysis (*vide supra*), we have mainly discussed activity trends of a series of compounds for a given bacterial strain and used the same approach when comparing selectivity index (SI)_{geo} values. This is a useful approach, if only one strain at a time is considered, but does not fully reflect the antimicrobial potential of an agent against multiple strains. In the following chapter we wanted to compare the compounds reported in papers I-III according to their potential broad-spectrum activity. Some care must be taken in the comparison, as MIC data from paper I was obtained from a different lab than MIC data in papers II and III. During re-testing of selected compounds from paper I, we observed slightly higher MIC values than before, but never more than one titer step as such, this should not influence the general trends highlighted in the following discussion.

For the purpose of comparing potential broad-spectrum activity the geometric mean (GM) of individual MIC values is a valuable tool for representing the average activity of a compound against different strains.²⁴⁹ Since we were interested in broad-spectrum activity when we calculated the GM, MIC data of the Gram-positive strains *C. difficile* and *B. subtilis* was excluded, as they are considered clinically not as important. (Note: for Table 6, MIC data for *B. subtilis* is included in the GM). We chose this selection to make sure that a low GM could only be achieved if a compound is active against Gram-negative strains, which was one of our main interests, due to wide-spread resistance in Gram-negative bacteria. For inactive compounds, a cut-off at MIC: 128 µg/mL was set. Furthermore, when using the GM, the haemolytic toxicity cannot be disregarded. Only compounds with the combination of a low GM and high EC₅₀ values (at least >100 µg/mL) are of general interest, as they have a good enough selectivity towards bacterial cells. The data is summarized in Table 6 and Figure 23 to Figure 26 and areas of interest are color coded to aid the readers understanding (green: good, yellow: medium, red: bad, white: not potent). We tried to find the best compounds from individual series and finally indicate the most promising mimics developed in this work.

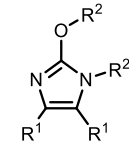
3.4.1 Scaffold contribution

Table 6 focuses on the contribution of the core structure. We chose 3,5-dibromobenzyl as the lipophilic side chain and *n*-propyl linkers carrying amine cationic groups. Compounds in entries 1-2 had the best broad-spectrum activity with GM values of 2.8 µg/mL but were also the most haemolytic. One reason could be the lipophilic side chains being attached to two vicinal sp² hybridized carbons, providing more spatial separation and altered dihedral angle between the side chains. The planar geometry of the sp² centers locks the benzyl groups to the bottom side of the ring, preventing the adoption of a W-shape as observed for the barbiturates (see **PI**: Conformational Analysis and Membrane Interaction Simulations). By confining the hydrophobic bulk to one side of the ring, the structures may interact more efficiently with the hydrophobic membranes.

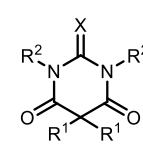
Table 6. The table shows the MIC, GM and EC₅₀ values in µg/mL for six different core structures having the same linkers, lipophilic side chains and cationic groups. The selectivity index SI is given by (EC₅₀/GM).



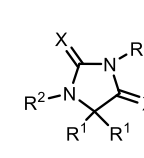
PIII-3A



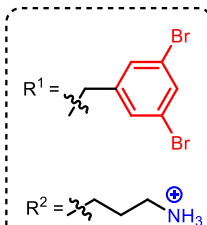
PIII-15A



PII-4bA X = O
PIII-5A X = S



PIII-2dA X = O
PIII-4A X = S



Entry	Compound	ClogP ^a	Antimicrobial activity				EC ₅₀	GM	SI
			S. a	B. s	E. c	P. a			
1	PIII-3A	-0.47	2	1	4	8	52	2.83	18.4
2	PIII-15A	0.26	2	2	4	4	44	2.83	15.5
3	PII-4bA	-1.44	4	4	8	8	99	5.66	17.5
4 ^b	PIII-5A	n.d.	8	4	4	16	305	6.73	45.3
5	PIII-2dA	-1.69	8	4	16	8	344	8.00	43
6	PIII-4A	-1.22	8	8	16	32	385	13.45	28.6

Bacterial reference strains: S. a – *Staphylococcus aureus* ATCC 9144, B.s – *Bacillus subtilis* 168, E. c – *Escherichia coli* ATCC 25922, and P. a – *Pseudomonas aeruginosa* ATCC 27853. GM = Geometric Mean. SI = Selectivity Index. ^a CLogP was calculated for the respective tetrasubstituted core structure (calculated with ChemBioDraw Ultra v19.0.0.1.28). ^bMixture of 2.4:1.0 (**PIII-5A**:**PII-4bG**). n.d. = not determined.

(Thio-)barbiturate derivatives (entries 3-4) were less active by a factor of two. Interestingly, incorporation of one sulfur rendered **PIII-5A** only slightly less active than **PII-4bA**, but the selectivity index was almost three times better and the overall haemolytic activity was very low (EC₅₀: 305 µg/mL). One has to keep in mind that entry 5 describes a 2:1 mixture of **PIII-5A** and **PIII-4bA**, so a pure sample of 2-thio-barbituric acid might show an even stronger effect. The chemical instability of **PIII-5A** is, however, a major drawback for therapeutical applications. The least active and haemolytic scaffolds were the hydantoin and 2,4-dithiohydantoin (entries 5-6). Di-thiolation (entry 6) led to a 4-fold drop in potency against *P. aeruginosa* (entry 5) and had only a minor effect on the haemolytic activity.

In summary, the hydantoin appeared to be the superior scaffold. While not exerting as good antimicrobial potency as the barbiturates or 4-imidazolidin-2-ones, its selectivity for bacterial membranes was markedly higher than any of the other two scaffolds. The second-best choice among the scaffolds was barbituric acid, followed by 4-imidazolidin-2-one. All other scaffolds were not of interest, due to too low potency, too high haemolytic activity or chemical instability. Of note, the barbiturate derivatives were most facile to access synthetically.

3.4.2 Contribution of the lipophilic side chains

Next, we evaluated the performance of the 4-(trifluoromethyl)benzyl (4-CF₃), 4-bromo-3-chlorobenzyl (4-Br, 3-Cl), 3,5-dibromobenzyl (3,5-di-Br) and 3,5-bis(trifluoromethyl)benzyl (3,5-di-CF₃) side chains, when combined with various scaffold structures and linkers, by plotting the GM of the MIC values for each analogue against its EC₅₀ values (Figure 23). Derivatives having a GM <16 µg/mL and EC₅₀ >100 µg/mL were of general interest (Figure 23, green area). From Figure 23 we can conclude that the most potent and most haemolytic side chain was 3,5-dibromobenzyl (black triangles).

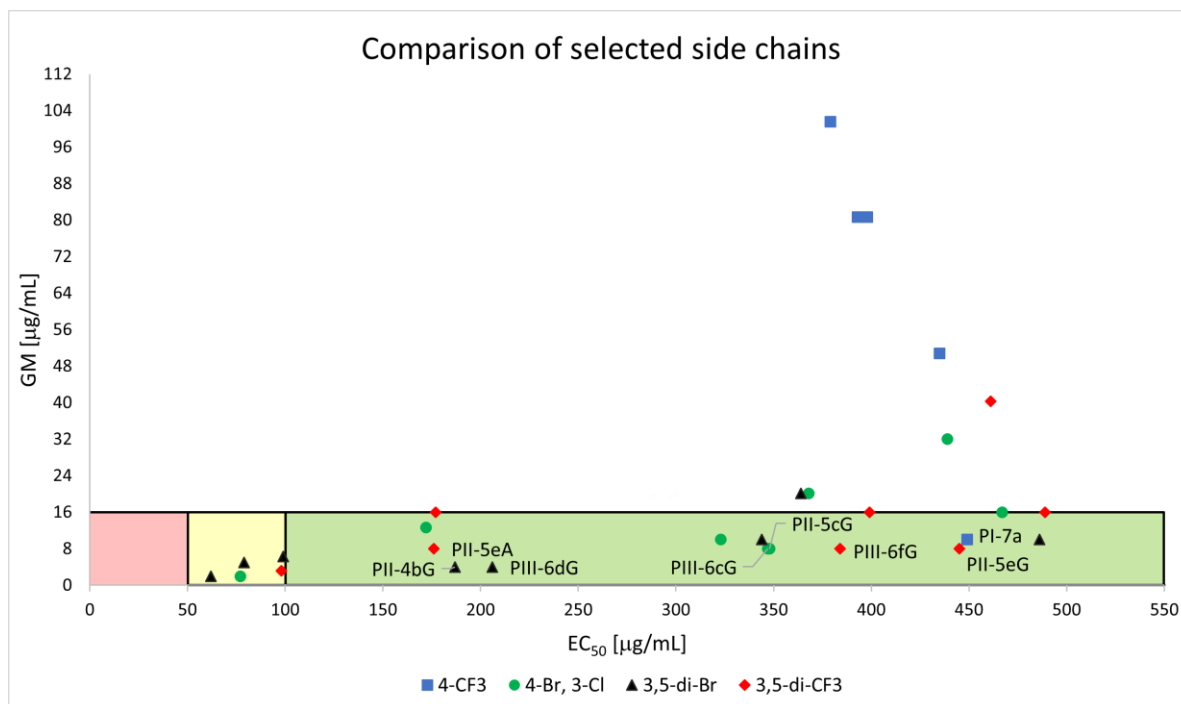


Figure 23. Distribution of all compounds featuring (4-CF₃), (4-Br, 3-Cl), (3,5-di-Br) or (3,5-di-CF₃) side chains based on their EC₅₀ (in µg/mL) values and the GM (in µg/mL) of the MIC values against *S. aureus*, *E. coli* and *P. aeruginosa*. Red: high haemolytic activity (EC₅₀: <50 µg/mL), Yellow: medium haemolytic activity (EC₅₀: 50-100 µg/mL), Green: low haemolytic activity (EC₅₀: >100 µg/mL), White: low antimicrobial potency (GM: >16 µg/mL).

3,5-di-Br was closely followed by 3,5-bis(trifluoromethyl)benzyl (red diamonds) and 4-bromo-3-chlorobenzyl (green dots), which performed quite similarly on average. The by far least potent and least haemolytic side chain was the 4-(trifluoromethyl)benzyl (blue squares), with derivative **PI-7a** (barbiturate, *n*-butyl, guanidyl) being the only one having a GM of <16 µg/mL. As mentioned earlier, this was well in accordance with the CLogP values of those side chains, with 3,5-bis(trifluoromethyl)benzyl being the only exception.

The most promising lipophilic side chain was 3,5-di-Br, as demonstrated by derivatives **PII-4bG** and **PIII-6dG** (black triangles). 4-Br, 3-Cl and 3,5-di-CF₃ performed similarly, which is exemplified by mimics **PII-5cG** and **PIII-6cG** (green dots) and **PII-5eA**, **PIII-6fG** and **PII-5eG** (red diamonds), respectively. The 4-CF₃ exhibited generally too low antimicrobial potency to be of general broad-spectrum interest. Of the aforementioned derivatives, **PIII-6fG** and **PII-5eG** exhibited the highest selectivity towards bacterial cells.

3.4.3 Combinations of linkers and cationic groups

We wanted to compare all compounds having *n*-butyl linkers and amine cationic groups (Figure 24), *n*-butyl linkers and guanidine cationic groups (Figure 25) and *n*-propyl linkers and either amine or guanidine cationic groups (Figure 26). Focusing first on mimics with *n*-butyl linkers and amine head groups, it became clear from Figure 24 that approximately half of all the compounds had GM values <16 µg/mL and only 50% out of those had EC₅₀ >100 µg/mL values in addition.

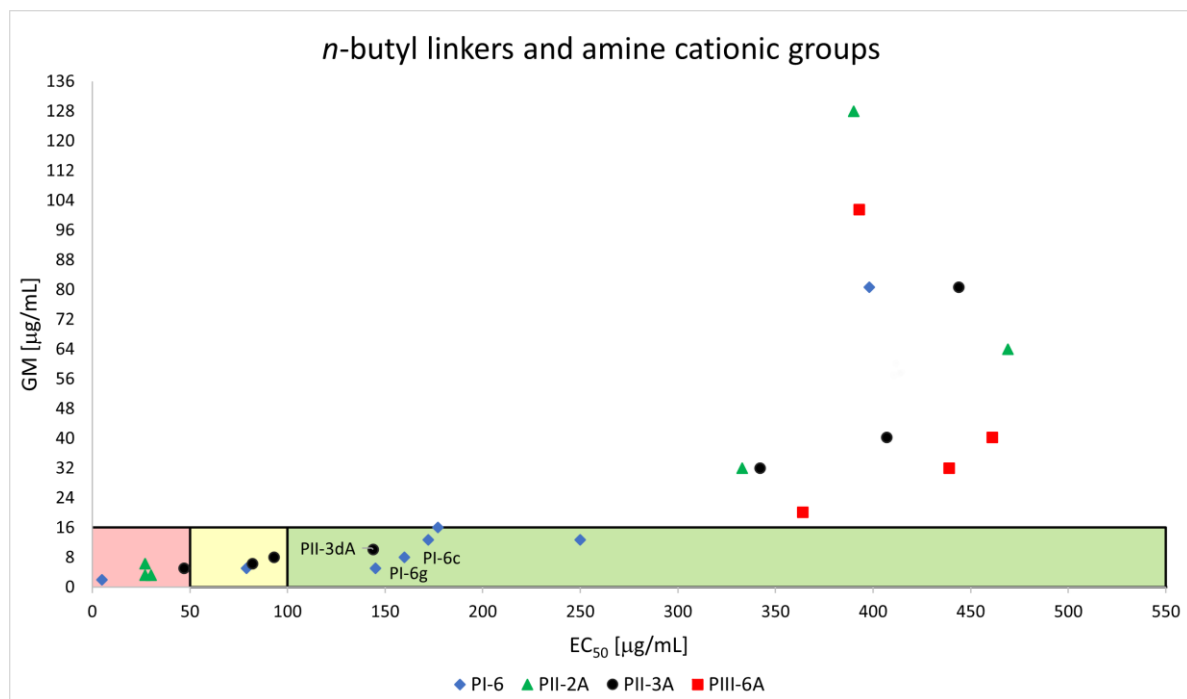


Figure 24. Distribution of all compounds investigated in this thesis having an *n*-butyl linker and amine head groups based on their EC₅₀ (in µg/mL) values and the GM (in µg/mL) of the MIC values against *S. aureus*, *E. coli* and *P. aeruginosa*. Red: high haemolytic activity (EC₅₀: <50 µg/mL), Yellow: medium haemolytic activity (EC₅₀: 50-100 µg/mL), Green: low haemolytic activity (EC₅₀: >100 µg/mL), White: low antimicrobial potency (GM: >16 µg/mL).

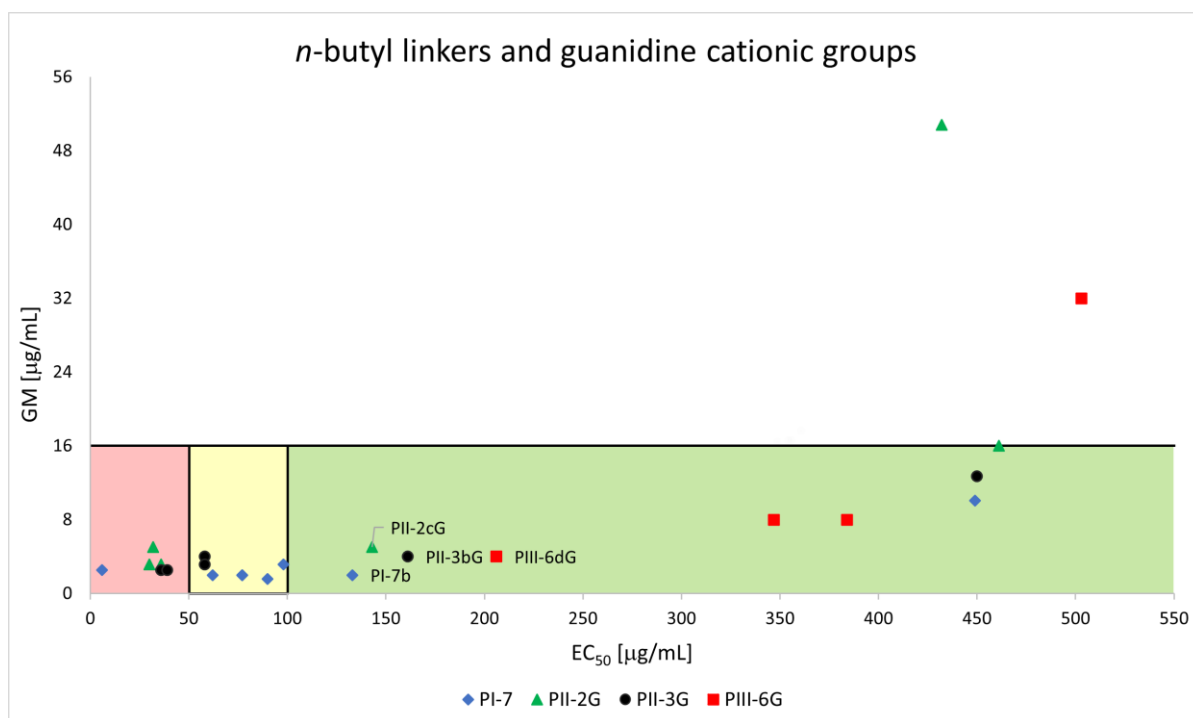


Figure 25. Distribution of all compounds investigated in this thesis having an *n*-butyl linker and guanidyl head groups based on their EC₅₀ (in µg/mL) values and the GM (in µg/mL) of the MIC values against *S. aureus*, *E. coli* and *P. aeruginosa*. Red: high haemolytic activity (EC₅₀: <50 µg/mL), Yellow: medium haemolytic activity (EC₅₀: 50-100 µg/mL), Green: low haemolytic activity (EC₅₀: >100 µg/mL), White: low antimicrobial potency (GM: >16 µg/mL).

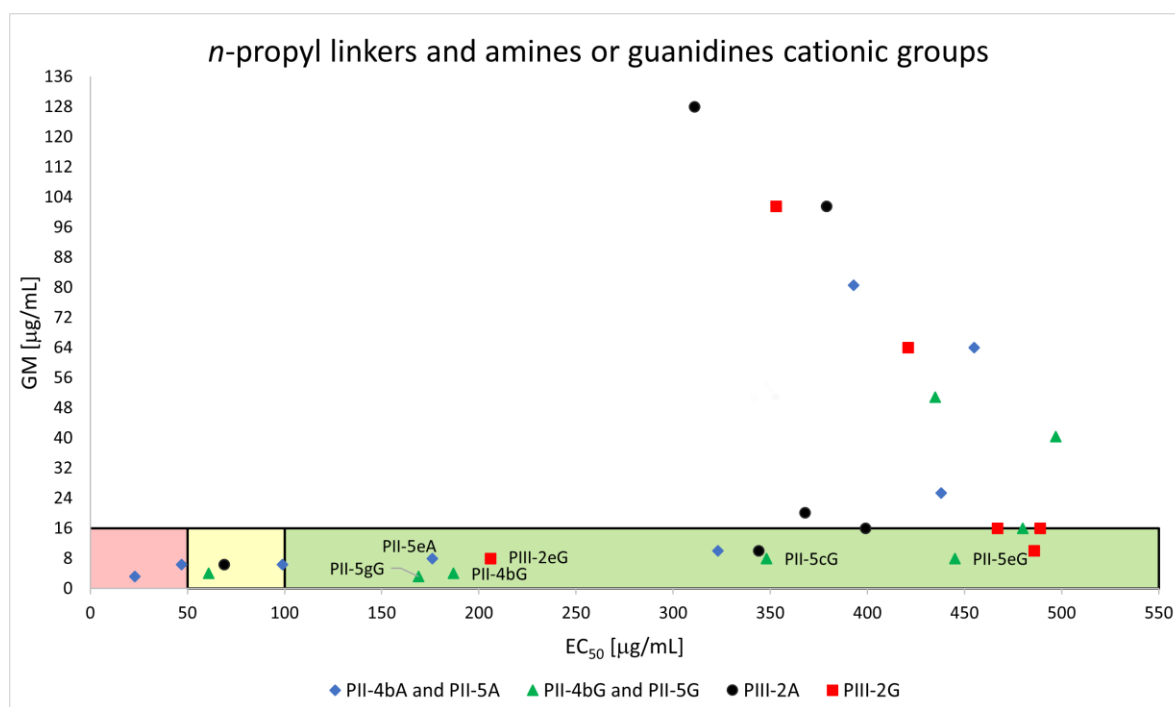


Figure 26. Distribution of all compounds investigated in this thesis having an *n*-propyl linker and amine or guanidyl head groups based on their EC_{50} (in $\mu\text{g/mL}$) values and the GM (in $\mu\text{g/mL}$) of the MIC values against *S. aureus*, *E. coli* and *P. aeruginosa*. Red: high haemolytic activity (EC_{50} : $<50 \mu\text{g/mL}$), Yellow: medium haemolytic activity (EC_{50} : $50\text{--}100 \mu\text{g/mL}$), Green: low haemolytic activity (EC_{50} : $>100 \mu\text{g/mL}$), White: low antimicrobial potency (GM: $>16 \mu\text{g/mL}$).

None of the hydantoin (red squares) could be considered potent in this evaluation, whereas almost all barbiturates from paper I (blue diamonds) were deemed potent. Many of the barbiturates evaluated in paper II (black dots and green triangles) were also considered potent, but the majority of those were too haemolytic. The best derivatives were barbiturates **PI-6g** (4-*t*Bu), **PI-6c** (4-F-Nal) and **PII-3dA** (3,5-di-Br and *n*-hexyl).

Moving on to structures with *n*-butyl linkers and guanidine cationic groups (Figure 25), we found only two derivatives without antimicrobial potency. This illustrates very well, as already discussed in each paper individually, that the guanidyl derivatives were more potent than their amine counterparts for *n*-butyl linkers, regardless of the central scaffold. While many mimics were potent, just a few had low haemolytic activity in addition. The hydantoin derivatives (red squares) were again the least haemolytic on average. The most promising compounds were barbiturates **PI-7b** (2-Nal), **PII-3bG** (3,5-di-Br; 4-CF₃) and **PII-2cG** (*n*-hexyl) and hydantoin **PIII-6dG** (3,5-di-Br).

Lastly, we compared all compounds having *n*-propyl linkers and either an amine or a guanidine cationic group (Figure 26). Most of the barbiturates (blue diamonds and green triangles) were below our threshold for antimicrobial activity. For the hydantoin (black dots and red squares) approximately half of the compounds could be considered antimicrobial. Of the potent derivatives, barbiturates **PII-5gG** (3,5-di-Br and 4-*t*Bu), **PII-4bG** (3,5-di-Br), **PII-5cG** (4-Br, 3-Cl), **PII-5eA** (3,5-di-CF₃) and **PII-5eG** (3,5-di-CF₃) and hydantoin **PIII-2eG** (4-Br-1-Nal) were the most relevant mimics.

3.4.4 Summary of Part A

We have developed 99 mimics of the eusynstyelamide family, of which most were potent against the Gram-positive strains *S. aureus* and *B. subtilis*. Selectivity against the Gram-negative strains *E. coli* and *P. aeruginosa* was dependent on the combination of the core structure, the hydrophobic volume and the nature of the cationic groups.

We found that all structural parts (the core, the linkers, the lipophilic side chains, the cationic groups) contributed to the overall antimicrobial potency and haemolytic activity of the compounds. In very general terms, the haemolytic activity would rise with increasing potency in a given series of compounds. The core seemed to set a certain “baseline” for the potency, which then could be modified mainly by the choice of the lipophilic side chain. The most versatile linkers were *n*-propyl and *n*-butyl hydrocarbons. Longer aliphatic chains and cyclic hydrocarbons led to high haemolytic activity. We found that amine and guanidine groups delivered the most potent broad-spectrum mimics. Methylated amines and guanidines, in contrast, lacked potency against Gram-negative *P. aeruginosa*. The guanidine group seemed to be the most promising, but its potency was dependent on the choice of the *n*-alkyl linker. This emphasizes the fact that the biological performance of each structural part is contextual and therefore, it was difficult to point out the best of each in an absolute sense. While it was challenging to identify a single best analogue, the barbiturate derivatives **PI-7b**, **PII-4bG** and **PII-5gG** and the hydantoin derivative **PIII-6dG** were among the most promising derivatives (Figure 27).

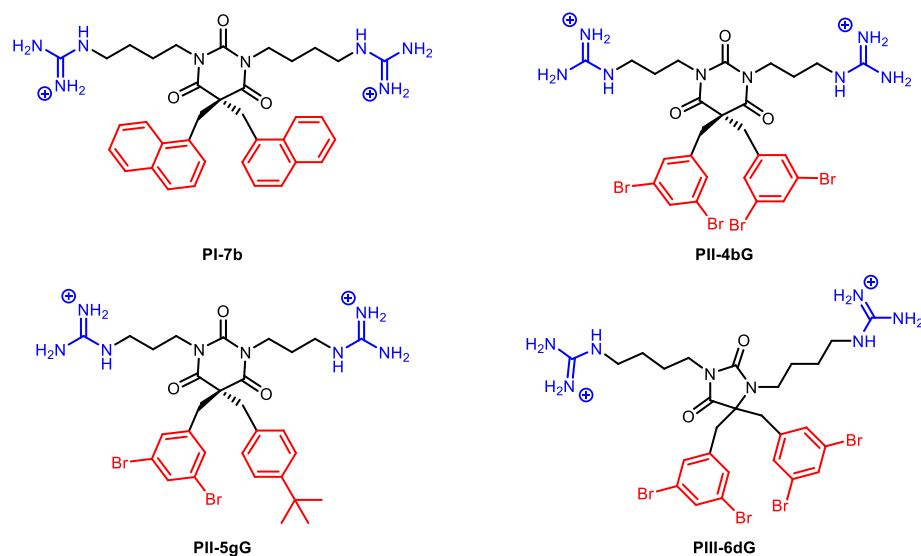


Figure 27. A selection of the most promising mimics developed in this thesis.

3.5 Towards the total synthesis of Aspergilone A (paper IV)

3.5.1 Introduction

As stated in the introduction, aspergilone A (**2**) exhibits AF and anticancer activity.¹⁸ We found this dual activity intriguing and set out to study the SAR of **2** qualitatively. To that end, we decided to develop a synthetic route towards **2**, which would allow for the synthesis of many derivatives, without major adjustments to the protocol.

Our first aim was to devise a concise and stereoselective synthetic route towards the intermediate *ent*-phenol A (**3**). **3** was chosen as an intermediate, based on the published syntheses of structurally related citrinin (**24a** and **24b**) (Scheme 2 in Section 2.4.4). Having gained access to **3**, we would then opt for the synthesis of aspergilone A (**2**), followed by the synthesis of analogues to establish early SARs. Many derivatives are conceivable and some possible analogues **68-71** are shown in Figure 28. We deemed the replacement of the benzyl groups in compound **69** and investigation of all stereoisomers of derivative **71** as particularly interesting.

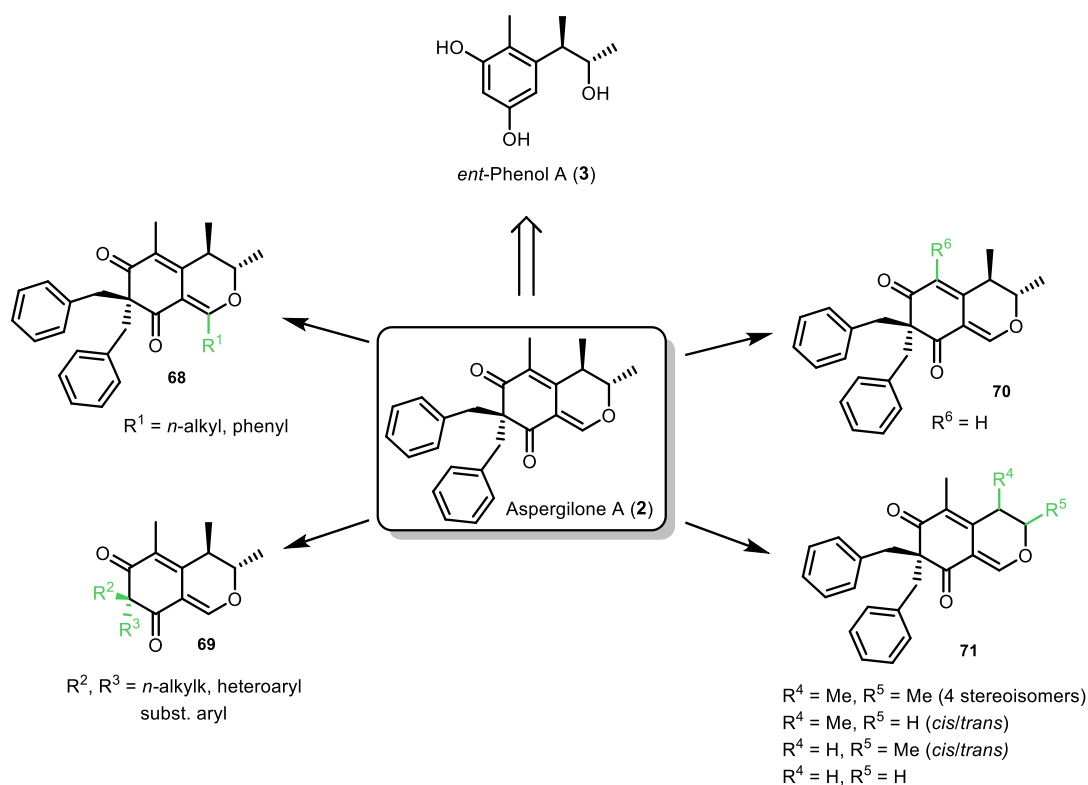
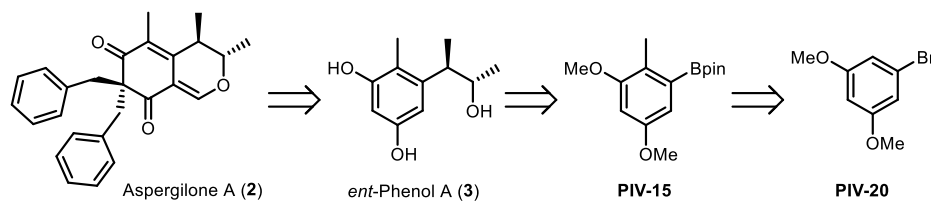


Figure 28. Structure of aspergilone A (**2**), *ent*-phenol A (**3**) and some possible derivatives **68-71**.

3.5.2 Retrosynthetic analysis

Our retrosynthetic analysis of **2** is presented in Scheme 13. We assumed that **2** would be accessible from intermediate *ent*-phenol A (**3**) by a three-step sequence of para-formylation, ring closure¹⁸¹⁻¹⁸³ and α,α -dibenylation of the resulting 1,3-diketone. **3** would be obtainable from the aryl boronic acid pinacol ester **PIV-15**. The disconnection corresponds to the key transformation of our strategy – two sequential

substrate-controlled, stereoselective homologations of the boronic acid pinacol ester **PIV-15**, followed by oxidation to the secondary alcohol. **PIV-15** would be disconnected to the corresponding 1-bromo-3,5-dimethoxybenzene **PIV-20**, corresponding to three sequential transformations encompassing formylation, deoxygenation and borylation with a boronic acid pinacol ester.



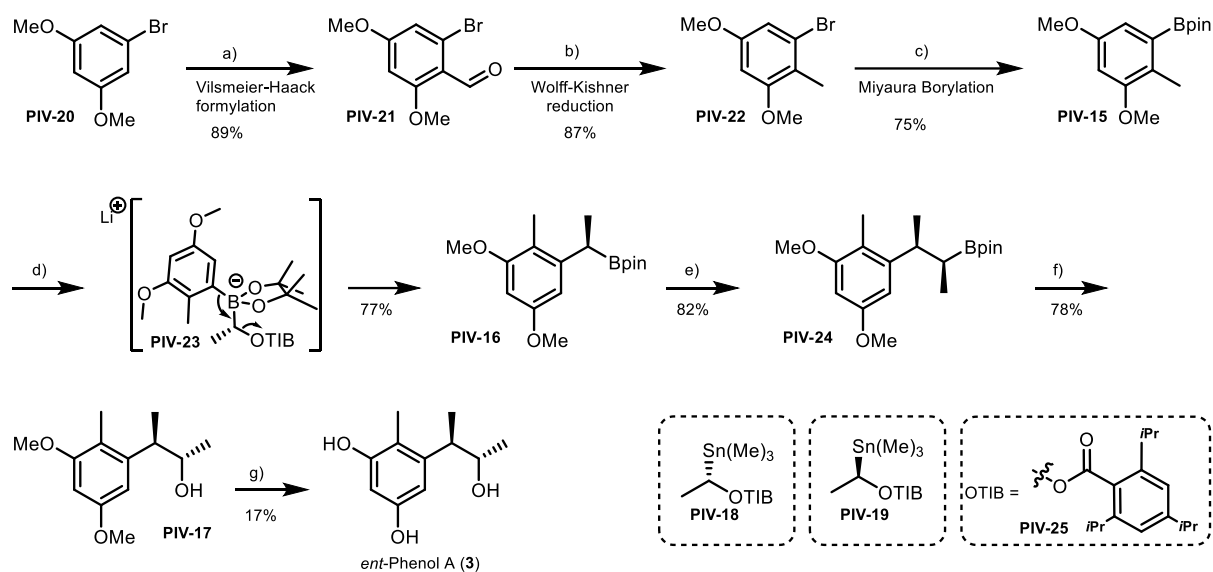
Scheme 13. Retrosynthetic analysis of aspergilone A (**2**).

3.5.3 Synthesis

We started from commercially available 1-bromo-3,5-dimethoxybenzene **PIV-20**, utilizing a modified literature protocol for the Vilsmeier-Haack formylation (Scheme 14).²⁵⁰ Aldehyde **PIV-21** was obtained in 89% yield. The following Wolff-Kishner reduction of aldehyde **PIV-21** was carried out under μ -wave irradiation, to reduce the amount of hydrazine needed.²⁵¹ Glycols had previously been used as solvents in this reduction,²⁵² but due to low solubility of aldehyde **PIV-21** in pure PEG-400, we introduced toluene as a co-solvent. Formation of the hydrazone prior to the addition of KOH proved to be beneficial and we were able to obtain deoxygenated **PIV-22** in 87% yield.

Aryl bromide **PIV-22** could be converted in a good yield (75%) into the respective aryl boronic acid pinacol ester (Ar-Bpin) **PIV-15** using Pd(dppf)Cl₂, bis(pinacolato)diboron (B₂pin₂) and potassium acetate under standard Miyaura borylation conditions. Ar-Bpin **PIV-15** was used as the starting material for the key transformation – a stereospecific 1,2-boronate rearrangement.

We treated (*S*)-tin benzoate **PIV-18** with *n*-BuLi at -78 °C to deliver the chiral secondary alkyl lithium.^{253, 254} Upon addition of Ar-Bpin **PIV-15** to the alkyl lithium, boronate complex **PIV-23** was formed. On warming, the aryl moiety can undergo a 1,2-migration, while the benzoate **25** acts as a leaving group. The stereochemical outcome is defined by the elimination step that requires an antiperiplanar arrangement of the aryl group and the benzoate leaving group **PIV-25** in boronate complex **PIV-23**. Higher temperatures and Lewis acids are known to enhance the rate of the rearrangement.²⁵⁵ Heating to 60 °C and the addition of 1.5 eq MgBr₂ in methanol were imperative to obtain benzyl boronic acid ester **PIV-16** in yields of up to 77%. Using (*R*)-tin benzoate **PIV-19** for the next homologation, we obtained alkylboronic acid pinacol ester **PIV-24** in up to 82% yield, without the need for a Lewis acid or additional heating. Intriguingly, we occasionally obtained the oxidation product of **PIV-16** (the alcohol) from both homologation steps as a side product.



Scheme 14. Synthetic strategy for the synthesis of *ent*-Phenol A (**3**). Reaction conditions: a) POCl₃, DMF (dry), 75 °C, 18 h, 89%; b) N₂H₄ (80% in water), toluene, μ -wave, 90 °C, 15 min, *then* KOH, PEG-400, μ -wave, 110 °C, 25 min, 87%; c) B₂pin₂, KOAc, PdCl₂dppf (3 mol%), 1,4-dioxane (dry), 90 °C, 40 h, 75%; d) i) **PIV-18**, *n*-BuLi, MTBE (dry), -78 °C, 75 min, ii) **PIV-15**, -78 °C, 4 h, iii) MgBr₂ (1.0 M in dry MeOH), -78 °C to 60 °C, 24 h, 77%; e) i) **PIV-19**, *n*-BuLi, MTBE (dry), -78 °C, 60 min, ii) **PIV-16**, -78 °C, 60 min, *then* -41 °C, 60 min, *then* r.t., 3.0 h, 82%; f) 2 N NaOH_(aq), H₂O₂ (30% in water), 0 °C to r.t., 2 h, 78%; g) NaH, DMI, r.t., 30 min, *then* (TMS)₂S, μ -wave, 220 °C, 22min, 17%.

The mechanisms leading to the formation of the alcohol could not be elucidated in due time, but we found out that partial racemization had taken place, reducing the ee values to 4-39%.

Oxidation of the boronic acid pinacol ester **PIV-24** to the alcohol **PIV-17** was achieved in good yields (78%) under standard conditions with 30% H₂O_{2(aq)} and a 2 M NaOH_(aq) solution. Analysis of **PIV-17** with chiral supercritical fluid chromatography (SFC) validated the presence of a single stereoisomer. We could show that a small sample of **PIV-17** slowly racemized when treated with sulfuric acid, similar to phenol A.¹⁶⁰ Racemization is believed to occur *via* a phenonium ion, which is formed through the elimination of water.

Typical methods for the cleavage of aryl methyl ethers use a range of Lewis acidic reagents. To prevent the acid-catalyzed racemization of alcohol **PIV-17** during cleavage of the aryl methyl ethers, we envisioned to use boronic acid pinacol ester **PIV-24** as starting material. We were reasoning that without the hydroxyl group, no water elimination would be possible and racemization would not take place.¹⁸⁵ Before employing **PIV-24**, we used intermediate **PIV-15**, which was more readily available, as the model compound to test typical procedures for the cleavage of aryl methyl ethers,^{256, 257} including BBr₃, AlCl₃ with NaI or TMSI. Most of the test reactions led to either selective removal of the pinacol ester or decomposition of the starting material. Only AlCl₃ and *N,N*-dimethylaniline in toluene under microwave irradiation delivered the desired product in 35% NMR yield at most.²⁵⁸ Discouraged by the low yields on our model compound, we decided to start from alcohol **PIV-17** and use basic conditions to avoid racemization. The counterattack reagent hexamethyldisilathian ((Me₃Si)₂S) seemed to be a good choice²⁵⁹ and we achieved up to 60% NMR yield, when using 3,5-dimethoxybenzyl alcohol as a

model system. Employing our optimized conditions on alcohol **PIV-17** delivered *ent*-phenol A (**3**) as a single stereoisomer, albeit in very low yields (17%). The optical rotation of **3** was $[\alpha] = +34.5^\circ$, supporting the fact that we had prepared the enantiomer of phenol A ($[\alpha] = -36.4^\circ$).²⁶⁰ Due to time constraints, the remaining synthetic steps towards aspergilone A (**2**), that is a three-step sequence of formylation, ring closure to the isochroman scaffold and α,α -dibenylation, could not be attempted.

3.5.4 Additional results not included in paper IV

In parallel to the development of the synthetic route above, we tried to transfer the synthesis from batch to continuous flow. These results are not included in paper IV and are discussed in this chapter.

Flow chemistry is not a new concept, but it has been receiving considerably more attention from the research community in recent years. Flow chemistry has some distinct advantages including faster reaction times, controlled use of highly reactive intermediates, less side product formation and many others.²⁶¹ Multistep processes are more easily controlled²⁶² and continuous flow gives rise to chemical transformations that are not feasible in batch.²⁶³ Despite those advantages, natural product synthesis is still dominated by “classical” chemistry and only a few syntheses are found, where flow chemistry constitutes the primary technique.²⁶⁴ We wanted to tackle this shortcoming and envisioned a transfer of our synthetic strategy to continuous flow. First, we focused on studying each step individually, before trying to combine steps together in a single flow set-up. Of special interest was the reagent controlled 1,2-anitropic rearrangement, because it was not well reported under flow conditions. As an additional restriction, we attempted to build all microfluidic systems from commercially available tubing, connectors and fittings, avoiding the use of tailor-made equipment to make our approach as simple as possible. Detailed description of the experimental procedures can be found in the Chapter 5 (Experimental Details) and the spectroscopical data can be found in the *Supporting Information* of paper IV.

3.5.4.1 Vilsmeier-Haack reaction to PIV-21

The Vilsmeier reagent has been used under continuous flow conditions in several instances,²⁶⁵⁻²⁶⁷ and we set out to use a similar set-up (Figure 29). Of note, methoxy bearing benzenes were reported to provide very low yields, in contrast to free phenols.²⁶⁷ First, we investigated the formation of the iminium ion by simply mixing streams A (neat POCl₃) and B (neat DMF) at ambient temperature. When the residence time (t_r) was 5 min, we observed full conversion of POCl₃ based on ³¹P-NMR and we decided to use those conditions further. To avoid precipitation of the Vilsmeier reagent, we initially used a ratio of 3:1 DMF:POCl₃. In the next step the stream containing the electrophile was mixed with a highly concentrated solution of 1-bromo-3,5-dimethoxybenzen **PIV-20** (2.5 M in DMF). After extensive screening, we arrived at the optimized conditions of $t_r = 38$ min at 100 °C, providing 84% NMR yield of aldehyde **PIV-21** on small scale (around 100 mg). Even with such a long residence time, a high excess of the Vilsmeier reagent (6.0 eq) was needed to drive the reaction to completion.

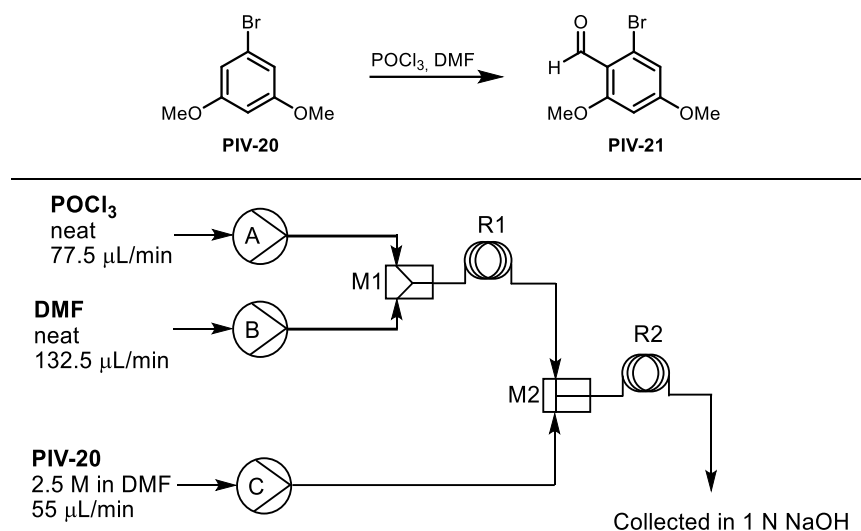


Figure 29. Schematic drawing of the flow setup for the V-H reaction. R1: $t_r = 300$ s, $T = 25$ °C and R2: $t_r = 38$ min, $T = 100$ °C.

Even though we could not decrease the amounts of reagents needed, the continuous quench of the highly reactive reaction mixture offers a distinct advantage over the classical approach. We increased the throughput to a total production rate of 6.05 mmol/h or 1.49 g/h with a somewhat diminished isolated yield of 74%. The yield for the reaction in flow were slightly lower than in the batch reaction, but little-to-no side product formation was observed.

3.5.4.2 Wolff-Kishner reaction to PIV-22

Adapting the procedures found in literature,^{268, 269} we pre-mixed the aldehyde **PIV-21** and hydrazine in triethylene glycol (TEG) to pre-form the hydrazone. Then we added KOH in ethylene glycol (EG) and the mixture was pumped with a peristaltic pump through the reaction coil at 160 °C with $t_r = 20$ min. We obtained more than 98% conversion to deoxygenated **PIV-22**. Unfortunately, the hydrazone started to precipitate from the reservoir over time, even if the latter one was heated to 50 °C. Abolishing this approach, we decided to separate the starting materials in two reservoirs (see Figure 30).

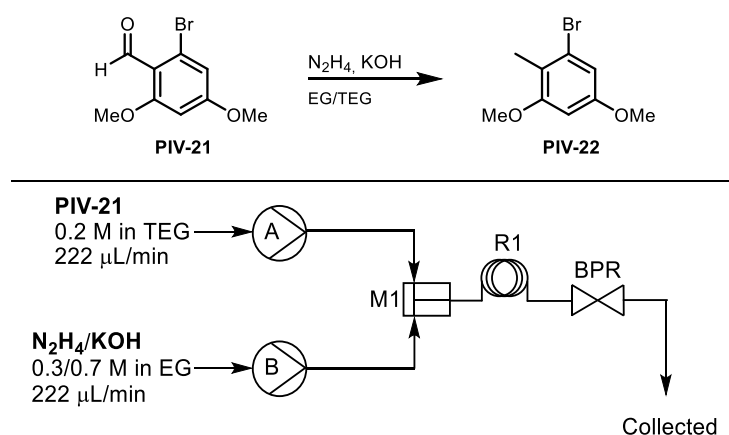
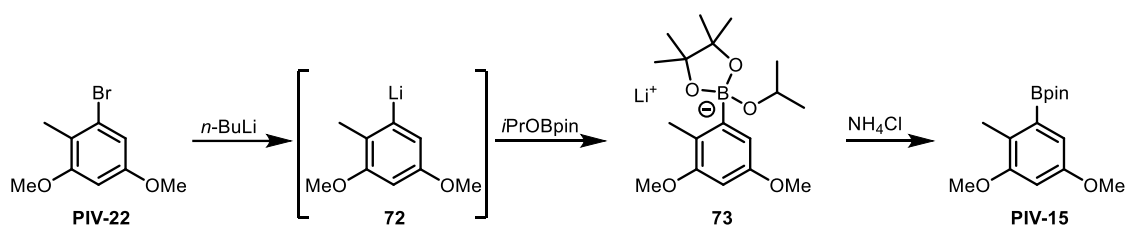


Figure 30. Schematic drawing of the flow setup for the Wolff-Kishner reaction. TEG = triethylene glycol, EG = ethylene glycol. R1: $t_r = 22.5$ min, $T = 160$ °C. Back pressure regulator (BPR) = 5.2 bar.

We used a mixture of TEG and EG to ensure solubilization of all starting materials. By mixing **PIV-21** and hydrazine just before the reaction coil and heating the hydrazone containing mixture rapidly to 160 °C, the hydrazone did not precipitate from the reaction solution. The use of a back pressure regulator (BPR = 5.2 bar) was imperative, because nitrogen gas is liberated during the reaction. If no BPR is used, the evolving gas will push the reaction mixture rapidly through the coil thus decreasing the residence time substantially. By adjusting the residence time to 22.5 min, we observed full conversion of the aldehyde and obtained deoxygenated **PIV-22** in 75% yield. We achieved a total production rate of 1.98 mmol/h or 458 mg/h. Slightly better yields were observed in the batch approach, but again the product from the batch reaction contained some impurities that were difficult to remove. As pointed out in literature,²⁶⁸ using continuous flow under pressure offers the opportunity to reduce the amount of the highly toxic hydrazine used. We could reduce the amount of hydrazine used from 2.2 eq in batch to 1.5 eq in continuous flow.

3.5.4.3 Borylation to PIV-15

In our first attempt we tried to adopt the strategy of borylation *via* an aryl-lithium intermediate **72**.²⁷⁰⁻²⁷⁶ (Scheme 15 and Figure 31).



Scheme 15. Synthesis of Ar-Bpin **PIV-15** *via* an aryl-lithium intermediate.

For the lithiation, the reported temperatures range from -60 °C to ambient temperature. In our case lowering the temperature to -78 °C and using a long residence time of 135 s (Figure 31, R1) delivered the most stable results. Carrying out the lithiation at higher temperatures also yielded quantitative conversion in most of the cases but was not always reproducible. The lithiated intermediate **72** was mixed with *i*PrOBpin (Figure 31, R2) and in-line quenched with NH₄Cl in water. During the course of the reaction a colorless solid formed, likely being boronate complex **73**,²⁷⁰ leading to blockage of the lines. Higher flow rates and sonication have been suggested to mitigate this problem,^{270, 277} and employing both strategies, we could increase the runtime of the system, though occasional blockage was still observed. Despite having good yields of up to 79% (estimated by quantitative NMR from the crudes), we usually observed some unconverted **PIV-22** and its de-brominated derivative. We therefore decided to change the strategy to a transition metal mediated coupling reaction.

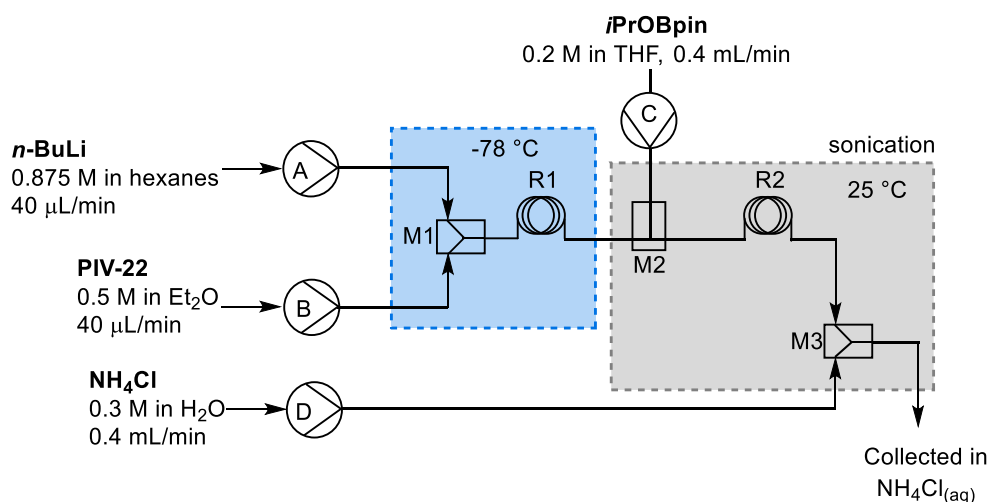


Figure 31. Schematic drawing of the flow setup for the borylation reaction. R1: $t_r = 135$ s, $T = -78$ °C. R2: $t_r = 132$ s, $T = 25$ °C.

To the best of our knowledge, the Miyaura borylation was not reported before under continuous flow conditions. However, the somewhat similar Suzuki-Miyaura coupling, often preceded by a borylation in the same flow set-up, is well established.^{270, 274, 278} Both, homogenous and heterogeneous catalysts have been used, and the homogeneous approach has been selected. By simply mixing a stream of aryl bromide **PIV-22**, B_2pin_2 (bispinacolatodiborane) and $Pd(dppf)Cl_2$ in anhydrous DMF and dried KOAc in anhydrous EG and passing it through R1 at 130 °C for 5 min we obtained **PIV-15** in 86% yield. The total production rate was 15.4 mmol/h or 1.22 g/h. The total yield was higher than in batch (75%) and less side product formation was observed.

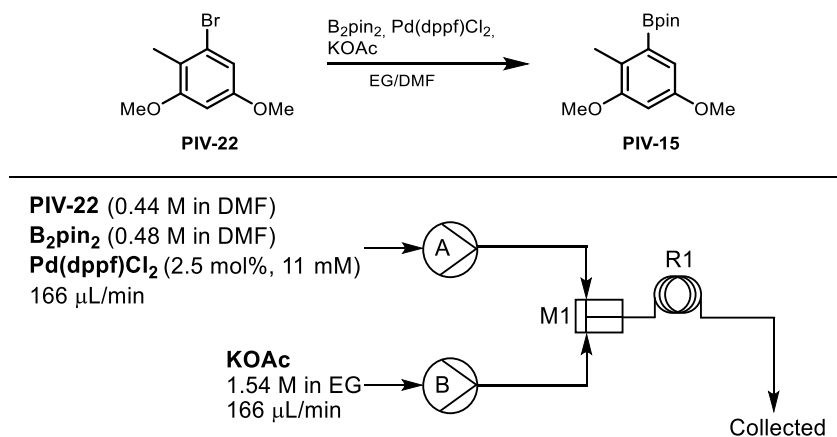


Figure 32. Schematic drawing of the flow setup for the Miyaura borylation. EG = ethylene glycol. R1: $t_r = 5$ min, $T = 130$ °C.

3.5.4.4 1,2-anitropic rearrangement to PIV-16

As pointed out before, the Matteson type 1,2-boronate rearrangement is a well described process but is not well studied under continuous flow conditions. To the best of our knowledge only three reports can be found.²⁷⁹⁻²⁸¹ While demonstrating the general feasibility of this approach, the authors were handling alkylboronic acid esters that are known to quite rapidly undergo the 1,2-shift and employed a custom made static mixer to boost the efficiency.²⁸⁰ Aryl boronic acid esters, however, are more resistant to the 1,2-shift and are worth investigating.

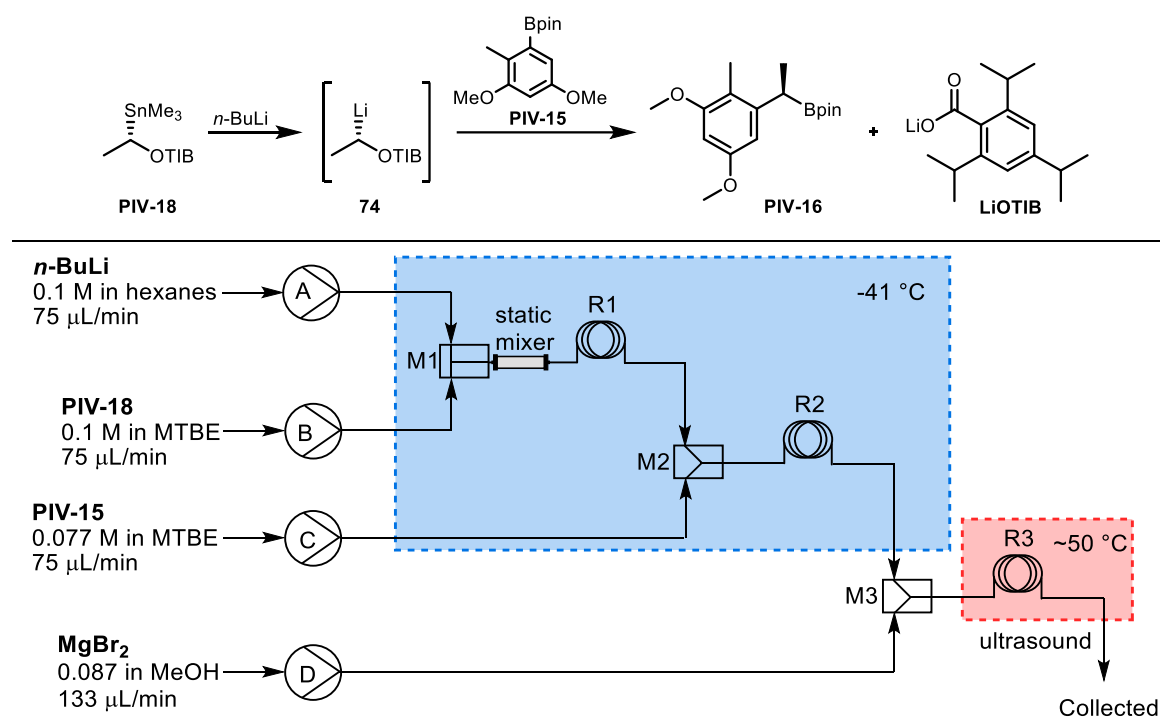


Figure 33. Schematic drawing of the flow setup for the lithiation/1,2-anitropic rearrangement. R1: $t_r = 60$ s, $T = -41$ °C, R2: $t_r = 180$ s, $T = -41$ °C, R3: $t_r = 225$ s, $T = \sim 50$ °C.

Exploring the tin-lithium exchange with stannane **PIV-18** at a variety of temperatures and residence times, we found $t_r = 60$ s at -41 °C was optimal (Figure 33). Lower temperatures hampered the exchange considerably and higher temperatures led to rapid decomposition of the secondary alkyllithium **74**. Employing a commercially available static mixer proved to be beneficial. The stream containing the lithiated benzoate **74** was then mixed with aryl boronic ester at -41 °C. We found $t_r = 180$ s to be sufficient for the formation of the ate complex **PIV-23**. The **PIV-23** containing stream exiting R2 was then combined with a stream D, containing anhydrous MgBr₂ in methanol. Initially we used a slight excess (1.1 eq) of a MgBr₂ solution (1.0 M in MeOH) and a very low flow rate of only 6.5 μ L/min. The temperature for the rearrangement was around 50 °C and the residence time (Figure 33, R3) was 6 min. Pleasingly, we obtained a ratio of 1.0:6.7 of **PIV-15**:**PIV-16** with practically no side product formation. Despite these very promising first results, the precipitation of the insoluble LiOTIB, after the

rearrangement had taken place, led to frequent blockage of reactor R3. Therefore, we decided to again utilize an ultrasound bath and in a second step increase the flow rate of stream D, while lowering the concentration of the MgBr₂ solution. The conversion dropped considerably to a ratio of 1.0:0.5 (**PIV-15:PIV-16**), most likely due to the higher dilution and the Lewis acid being less accessible for the boronate complex. Upon gradual increase of the Lewis acid to 2.0 eq, we achieved the same conversion as previously and 71% NMR yield. Blockage of the tubing was almost eliminated but could happen occasionally. To alleviate the risk of blockage even further the addition of another co-solvent just after introduction of the Lewis acid might prevent LiOTIB from precipitating, but this could not be investigated yet. The route was not developed further due to time constraints.

3.5.5 Summary of Part B

We have successfully developed an enantioselective and modifiable route towards *ent*-phenol A (**3**), an intermediate in the synthesis of aspergilone A (**2**), allowing for the formal construction of all four stereoisomers. A total of seven transformations were used with a combined yield of 5%. All steps, except for one, were good-to-high yielding and **3** could be obtained in >99% ee. The key transformations, two 1,2-anionic boronate rearrangements, allowed for complete stereocontrol of each chiral center. Furthermore, we were able to transfer the first four steps of the synthetic strategy to continuous flow, allowing for the rapid synthesis of the intermediates on multigram-scale. Even though we achieved higher yields in batch for the Vilsmeier-Haack formylation and the Wolff-Kishner reduction, the products obtained from continuous flow reactions were generally cleaner and simpler to purify. To the best of our knowledge, we were the first to show that the 1,2-anionic boronate rearrangement, using secondary alkyllithiums, is feasible under continuous flow conditions. However, more work needs to be done to overcome the problem of occasional blockage of the flow reactors.

4 Conclusion and Outlook

In this thesis we have successfully used an antimicrobial marine natural product, eusynstyelamide, as the template to design and synthesize almost 100 tetrasubstituted, amphipathic mimics, encompassing six different core structures.

All synthetic mimics of the eusynstyelamides were evaluated for their antimicrobial potency and haemolytic activity, revealing a range of promising structures with high *in vitro* activity. One derivative has been shown to have *in vivo* efficiency in a murine peritonitis model. Preliminary MoA studies suggested a membranolytic effect of our main structural classes: barbiturates and hydantoins. These findings were corroborated for one barbiturate by *in silico* molecular dynamics simulations. The counterion effect was evaluated, but no clear correlations could be identified.

We have unraveled specific SARs for combinations of *n*-alkyl linkers with amine or guanidine cationic groups. Importantly, these findings were applicable regardless of the core structure. Meanwhile, the core structure was shown to influence the overall potency and toxicity of the mimics. 4-imidazolidin-2-one exhibited the highest haemolytic activity, followed by barbituric acid and hydantoins as the least haemolytic structures.

Future works for the synthetic antimicrobials would include the thorough study of the MoA, with focus on the OM and other common intracellular targets of AMPs. Further toxicity studies are imperative to evaluate the potential of the mimics to be used as drugs.

Additionally, we have developed an enantioselective synthetic route towards *ent*-phenol A, a key intermediate in the total synthesis of the marine natural product aspergilone A and further derivatives of the citrinin-type azaphilones. We were able to design a synthetic route to access all stereoisomers of phenol A in seven steps, with only one step being low yielding. We could successfully translate the first steps of our route to continuous flow. For the first time, the 1,2-boronate rearrangement of aryl boronic acid esters was shown to be feasible under continuous flow.

Future plans include the completion of the synthesis of aspergilone A and the construction of a small library for SAR studies. Also, transferring the remaining steps towards phenol A to continuous flow systems would be a milestone.

I believe that natural products will continue to play a vital role in DDD and marine sources will be exploited increasingly. Also, synthetic mimics of AMPs are still a promising class of new potential antibiotics. The efforts of many different research groups have led to new highly promising SMAMPs, many of them exhibiting a better activity–toxicity profile and refined pharmacokinetics. These improvements may help to develop AMP mimics for systemic application.

5 Experimental Details

This chapter includes additional experimental procedures for compounds not included in manuscripts II-IV.

5.1 General methods

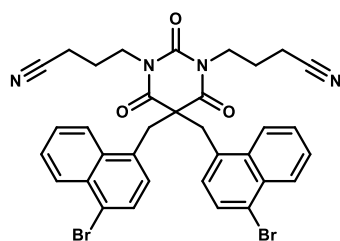
Unless otherwise noted, purchased chemicals were used as received without further purification. Solvents were dried according to standard procedures over molecular sieves of appropriate size. Normal phase flash chromatography was carried out on silica gel 60 (230–400 mesh) or on an interchim® PuriFlash XS420 flash system with the sample preloaded on a Samplet® cartridge belonging to a Biotage SP-1 system. Purification by reversed phase (RP) C18 column chromatography (H₂O with 0.1% TFA/MeCN with 0.1% TFA) was performed on an interchim® PuriFlash XS420 flash system with the sample preloaded on a Samplet® cartridge. Thin layer chromatography was carried out using Merck TLC Silica gel 60 F254 and visualized by short-wavelength ultraviolet light or by treatment with an appropriate stain.

NMR spectra were obtained on a 400 MHz Bruker Advance III HD spectrometer equipped with a 5 mm SmartProbe BB/1H (BB = 19F, 31P-15N) at 20 °C. The chemical shifts are reported in ppm relative to the solvent residual peak (CDCl₃: δH 7.26 and δC 77.16; Methanol-d₄: δH 3.31 and δC 49.00; deuterium oxide: δH 4.79; DMSO-d₆ δH 2.51 and δC 39.52). ¹³C NMR spectra were obtained with ¹H decoupling. Data are represented as follows: chemical shift, multiplicity (s = singlet, d = doublet, t = triplet, q = quartet, dt = double triplet, m = multiplet), coupling constant (*J* in Hz) and integration. The raw data was analyzed with MestReNova (Version 14.0.0-23239).

High-resolution mass spectra (HRMS) were recorded from methanol solutions on an LTQ Orbitrap XL (Thermo Scientific) either in negative or in positive electrospray ionization (ESI) mode. The data was analyzed with Thermo Scientific Xcalibur software.

The purity of all tested compounds was determined to be ≥95%. The analyses were carried out on a Waters ACQUITY UPC² system equipped with a Torus™ DEA 130Å, 1.7 μm, 2.1 mm x 50 mm column. Compounds were detected on a Waters ACQUITY PDA detector spanning wavelengths from 190 to 650 nm, coupled to a Waters ACQUITY QDA detector for low resolution mass (LRMS) detection. The derivatives were eluted with a mobile phase consisting of supercritical CO₂ and MeOH containing 0.1 % NH₃ and a linear gradient of 2 – 40 % MeOH over 2 or 4 min followed by isocratic 0.5 min of 40% MeOH. The flow rate was 1.5 mL/min.

5.1.1 PII: Attempted amidine synthesis



4,4'-(5,5-bis((4-bromonaphthalen-1-yl)methyl)-2,4,6-trioxodihydropyrimidine-1,3(2H,4H)-diyl)dibutanenitrile **52**.

5,5-disubstituted barbituric acid **PII-7a** (115 mg, 203 μmol , 1.0 eq) and K_2CO_3 (83 mg, 601 μmol , 3.0 eq) were mixed with acetone (1.5 mL).

The resulting suspension was stirred at ambient temperature for 30 min.

Then 4-bromobutanenitrile (45 μL , 453 μmol , 2.25 eq) and TBAI (8 mg, 22 μmol , 0.1 eq) were added and the suspension was stirred at 50 $^\circ\text{C}$ for 72 h. The reaction mixture was allowed to cool to ambient temperature and water and EtOAc were added. The layers were separated and the aqueous layer was extracted with EtOAc twice more. The combined organics were dried over MgSO_4 , filtered and the solvent was removed under reduced pressure. The crude was purified by automated flash chromatography on silica gel with 15-60% EtOAc in heptane as eluent to yield the *N,N*-dialkylated barbituric acid **52** (68 mg, 98 μmol , 49%) as a yellowish solid. $^1\text{H NMR}$ (400 MHz, Chloroform-*d*) δ 8.31 – 8.17 (m, 4H), 7.69 – 7.56 (m, 6H), 7.11 (d, $J = 7.8$ Hz, 2H), 4.09 (s, 4H), 3.42 (t, $J = 6.8$ Hz, 4H), 1.64 (d, $J = 14.5$ Hz, 4H), 1.20 (p, $J = 7.0$ Hz, 4H). *Note: Residual 4-bromobutanenitrile was observed.* $^{13}\text{C NMR}$ (101 MHz, Chloroform-*d*) δ 170.7, 149.4, 132.9 (2C), 132.4 (2C), 131.3 (2C), 129.3 (2C), 128.3 (2C), 128.2 (2C), 127.8 (2C), 127.3 (2C), 124.9 (2C), 123.7 (2C), 118.5 (2C), 59.6, 41.0 (2C), 40.5 (2C), 23.3 (2C), 14.5 (2C). *Note: Residual 4-bromobutanenitrile was observed.* **HRMS** (ESI): calcd for $\text{C}_{34}\text{H}_{28}\text{Br}_2\text{N}_4\text{O}_3\text{Na}^+$ [$\text{M}+\text{Na}$] $^+$ 721.0420, found 721.0444.

Unsuccessful conversion of the nitriles to the amidines:

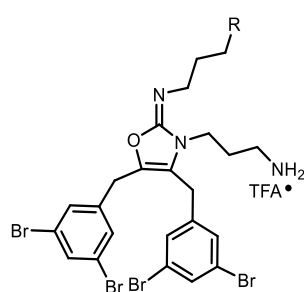
The nitrile containing barbiturate **52** (10 mg, 14 μmol , 1.0 eq) was mixed with 1,4-dioxane (dry, 500 μL) and MeOH (dry, 100 μL). The mixture was cooled to 0 $^\circ\text{C}$ and HCl (1.25 M in MeOH, 685 μL , 857 μmol , 60 eq) was added. The solution was stirred in the melting ice-water bath for 2 d. A white solid precipitated after a few minutes, which dissolved over time. The solvent was removed under reduced pressure and the resulting solids were triturated with Et_2O thrice. The solids were dried, mixed with NH_3 (7 N in MeOH) and the resulting mixture was stirred at ambient temperature for 24 h. The solvent was removed, and the crude solids triturated with Et_2O once to yield a white solid. No desired product could be identified.

The nitrile containing barbiturate **52** (10 mg, 14 μmol , 1.0 eq) was mixed with dry MeOH (500 μL) and the resulting suspension was cooled to 0 $^\circ\text{C}$. Solid NaOMe (80 μg , 1 μmol , 0.1 eq) was added and the suspension was left stirring in the melting ice-water bath. The mixture became clear after around 10 min. After a total reaction time of 48 h, NH_4Cl (1.5 mg, 29 μmol , 2.0 eq) was added and the suspension was stirred at ambient temperature for another 60 h. The suspension was filtered and the residue was washed with MeOH. The organics were collected and combined. The solvent was removed under reduced

pressure and the resulting crude solid was triturated with Et₂O twice before drying under high vacuum. A white solid was obtained. No product could be identified.

NH₄Cl (2.2 mg, 41 μmol, 3.60 eq) was suspended in dry toluene (500 μL) and cooled to 0 °C. AlMe₃ (2 M in heptane, 18.8 μL, 38 μmol, 3.30 eq) was added and the reaction was stirred at ambient temperature for 1 h. The nitrile containing barbituric acid **52** (8 mg, 11 μmol, 1.00 eq), dissolved in dry toluene (300 μL), was added dropwise. The resulting mixture was first stirred at 80 °C for 24 h and then at 105 °C for 22 h. The absence of the starting material was detected by HRMS. The mixture was allowed to cool to ambient temperature and the solvent was removed under reduced pressure. No target compound could be identified.

5.1.2 Additional compounds connected to paper III



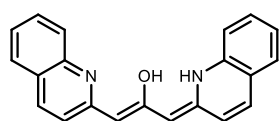
Compound **54**.

4-oxazolin-2-one **15** (100 mg, 172 μmol, 1.0 eq), tert-butyl (3-bromopropyl)carbamate **S7** (410 mg, 1.72 mmol, 10 eq) and (*n*-hexadecyl)tri-*n*-butylphosphonium bromide (88 mg, 172 μmol, 1.0 eq) were mixed with toluene (200 μL) and 10% NaHCO_{3(aq)} (200 μL). The resulting mixture was heated to 110 °C for 44 h and then allowed to cool to ambient temperature. Water and EtOAc were added and the layers were separated. The aqueous layer was extracted with EtOAc twice and the combined organics were dried over MgSO₄, filtered and the solvent was removed under reduced pressure. The crude yellow oil was purified by automated flash column chromatography on silica gel with a gradient of 5-25% EtOAc in heptane. Boc-**54** (12 mg, 13 μmol, 8%) was obtained impure as a slightly yellow solid.

Boc-**54** (12 mg, 13 μmol, 1.0 eq) was taken up in DCM (300 μL) and TFA (20 μL, 268 μmol, 20 eq) was added. The solution was stirred at ambient temperature for 20 h before removal of the solvent. The crude amine was purified by RP chromatography with a gradient of 20-60% MeCN/H₂O + 0.1% TFA to yield the di-TFA salt of **54** (10 mg, 11 μmol, 6% o2s) as a white solid.

¹H NMR (400 MHz, Methanol-d₄) δ 7.57 (t, J = 1.7 Hz, 1H), 7.52 (t, J = 1.7 Hz, 1H), 7.25 (d, J = 1.7 Hz, 2H), 7.08 (d, J = 1.7 Hz, 2H), 4.14 (s, 2H), 4.13 – 4.06 (m, 2H), 3.93 (s, 2H), 3.21 (t, J = 7.0 Hz, 2H), 3.13 (t, J = 7.2 Hz, 2H), 3.00 – 2.90 (m, 2H), 2.06 (p, J = 7.1 Hz, 2H), 1.97 – 1.85 (m, 2H). ¹³C NMR (101 MHz, Methanol-d₄) δ 144.5, 143.1, 141.6, 137.6, 133.8, 133.3, 131.4 (2C), 131.1 (2C), 129.8, 124.4 (2C), 124.1 (2C), 43.4, 39.0, 37.9, 32.6, 32.4, 29.5, 29.1, 28.5. HRMS (ESI): found: 706.8684. SFC: 97.9%.

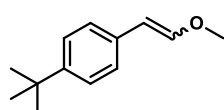
The following compound was prepared according to General Procedure A (**PIII**):



(*Z*)-3-((*Z*)-quinolin-2(1*H*)-ylidene)-1-(quinolin-2-yl)prop-1-en-2-ol **56**.

2-(Bromomethyl)quinoline (400 mg, 1.80 mmol, 2.2 eq), TosMIC (160 mg, 0.82 mmol, 1.0 eq), TBAI (60 mg, 164 μ mol, 0.2 eq), NaOH (30 wt%, 5 mL) and DCM (5 mL) were stirred for 24 h. The addition product was obtained as a dark red oil.

The addition product, HCl (37%, 350 μ L), DCM (5 mL) and THF (1 mL) were stirred at ambient temperature for 4 h. Purification by column chromatography on silica gel with 5 % EtOAc in heptane as eluent delivered **56** (35 mg, 112 μ mol, 14% o/s) as a red solid. $^1\text{H NMR}$ (400 MHz, Chloroform-*d*) δ 8.21 (dd, J = 8.7, 1.8 Hz, 2H), 8.14 (d, J = 8.5 Hz, 2H), 7.99 (d, J = 2.2 Hz, 2H), 7.89 – 7.79 (m, 4H), 7.74 (ddd, J = 8.4, 6.9, 1.5 Hz, 2H), 7.54 (ddd, J = 8.2, 6.8, 1.3 Hz, 2H). Note: Residual heptane was observed at 1.34 – 1.22 (m) and 0.88 (t, J = 4.3 Hz). $^{13}\text{C NMR}$ (101 MHz, Chloroform-*d*) δ 155.4, 148.1, 137.0, 134.7, 130.2, 129.4, 127.8, 127.7, 126.9, 119.7. Note: Residual heptane was observed at 32.0, 29.2, 22.8, 14.3. **HRMS** (ESI): calcd for $\text{C}_{21}\text{H}_{16}\text{N}_2\text{ONa}^+$ $[\text{M}+\text{Na}]^+$ 335.1155, found: 335.1154.



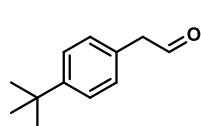
(*E*)/(*Z*)-1-(*tert*-butyl)-4-(2-methoxyvinyl)benzene **68**.

(Methoxymethyl)triphenylphosphonium chloride (9.51 g, 27.7 mmol, 1.8 eq) was taken up in dry THF (25 mL) under inert atmosphere and cooled to -78 $^{\circ}\text{C}$. NaHMDS (27.7 mL, 27.7 mmol, 1.8 eq; 1.0 M in THF) was added slowly and the resulting mixture was stirred at 0 $^{\circ}\text{C}$ for 30 min. It was re-cooled to -78 $^{\circ}\text{C}$ and 4-*tert*-butylbenzaldehyde (2.58 mL, 15.4 mmol, 1.0 eq) was slowly added. After stirring for 90 min at that temperature the mixture was stirred at ambient temperature for 40 min. Water and EtOAc were added and the layers were separated. The aqueous layer was extracted with EtOAc twice and the combined organics were dried over MgSO_4 , filtered and the solvent was removed under reduced pressure. Heptane was added to the crude solids and the suspension was sonicated for 5 min. The organic layer was collected and the procedure was repeated 3 more times. The organics were combined and the solvent was removed under reduced pressure. The crude product was purified by column chromatography on silica gel with 5-15% EtOAc in heptane to yield **68** (2.84 g, 14.9, 97%) as a yellow liquid. A 1.00:0.54 mixture of the (*E*):(*Z*) isomers was obtained.

(*Z*)-**ABML444**: $^1\text{H NMR}^{282}$ (400 MHz, Chloroform-*d*) δ 7.51 (d, J = 8.5 Hz, 2H), 7.34 – 7.30 (m, 2H), 6.11 (d, J = 7.0 Hz, 1H), 5.22 (d, J = 7.0 Hz, 1H), 3.77 (s, 3H), 1.31 (s, 9H). $^{13}\text{C NMR}$ (101 MHz, Chloroform-*d*) δ 148.8, 147.5, 133.2, 128.0 (2C), 125.2 (2C), 105.7, 60.7, 34.6, 31.5 (3C).

(*E*)-**ABML444**: $^1\text{H NMR}^{282}$ (400 MHz, Chloroform-*d*) δ 7.32 – 7.28 (m, 2H), 7.20 – 7.15 (m, 2H), 7.02 (d, J = 13.0 Hz, 1H), 5.81 (d, J = 13.0 Hz, 1H), 3.68 (s, 3H), 1.31 (s, 9H). $^{13}\text{C NMR}$ (101 MHz, Chloroform-*d*) δ 148.8, 148.5, 133.6, 125.7 (2C), 125.0 (2C), 105.0, 56.6, 34.5, 31.5 (3C).

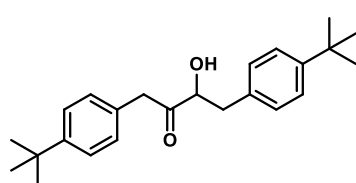
HRMS (ESI): calcd for $\text{C}_{13}\text{H}_{19}\text{O}^+$ $[\text{M}+\text{H}]^+$ 190.1358, found: *not found*.



2-(4-(*tert*-butyl)phenyl)acetaldehyde **59**.²⁸³

The mixture of (*E*):(*Z*)-**68** (2.83 g, 14.9 mmol, 1.0 eq) was mixed with chloroform (60 mL) and water (268 μ L, 14.9 mmol, 1.0 eq), EtOH (867 μ L, 14.9 mmol, 1.0 eq) and oxalyl chloride (1.30 mL, 14.9 mmol, 1.0 eq) were added under cooling to 0 °C. The suspension was stirred for 55 min at ambient temperature, before water was added. The layers were separated and the aqueous layer was extracted two more times with DCM. The combined organics were dried over MgSO₄, filtered and the solvent was removed under reduced pressure. The crude aldehyde was purified by column chromatography on silica gel with 5-10% EtOAc in heptane to yield **59** (1.92 g, 10.9 mmol, 73%) as a yellow liquid.

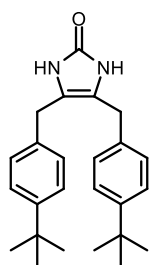
¹H NMR (400 MHz, Chloroform-*d*) δ 9.75 (t, *J* = 2.4 Hz, 1H), 7.42 – 7.38 (m, 2H), 7.19 – 7.14 (m, 2H), 3.66 (d, *J* = 2.5 Hz, 2H), 1.33 (s, 9H). ¹³C NMR (101 MHz, Chloroform-*d*) δ 199.8, 150.5, 129.5 (2C), 128.9, 126.1 (2C), 50.2, 34.7, 31.5 (3C). HRMS (ESI): calcd for C₁₂H₁₆ONa⁺ [M+Na]⁺ 199.1093, found 199.1093.



1,4-bis(4-(*tert*-butyl)phenyl)-3-hydroxybutan-2-one **60**.²⁸⁴

59 (300 mg, 1.70 mmol, 1.0 eq) and 3-benzyl-5-(2-hydroxyethyl)-4-methylthiazolium chloride (34 mg, 128 μ mol, 0.07 eq) were mixed with anhydrous PEG-400 (7 mL) under inert atmosphere. Triethylamine (119 μ L, 851 μ mol, 0.50 eq) was added and the resulting mixture was stirred at 80 °C for 5 h. The oil bath was removed, ice-water was added to the reaction mixture and stirring was continued for 1.5 h. Water and brine were added and the aqueous layer was extracted with EtOAc thrice. The combined organics were washed with water twice, dried over MgSO₄, filtered and the solvent was removed under reduced pressure. The crude product was purified by column chromatography on silica gel with 10% EtOAc in heptane to yield **60** (231 mg, 655 μ mol, 77%) as a yellow solid.

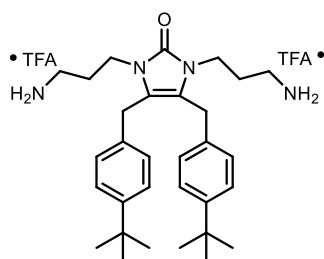
¹H NMR (400 MHz, Chloroform-*d*) δ 7.39 – 7.31 (m, 4H), 7.18 – 7.13 (m, 2H), 7.12 – 7.07 (m, 2H), 4.51 (ddd, *J* = 7.6, 5.6, 4.7 Hz, 1H), 3.80 (d, *J* = 15.8 Hz, 1H), 3.74 (d, *J* = 15.9 Hz, 1H), 3.24 (dd, *J* = 5.6, 1.3 Hz, 1H), 3.13 (dd, *J* = 14.1, 4.6 Hz, 1H), 2.87 (dd, *J* = 14.1, 7.6 Hz, 1H), 1.32 (d, *J* = 1.1 Hz, 18H). ¹³C NMR (101 MHz, Chloroform-*d*) δ 209.5, 150.4, 150.0, 133.6, 130.1, 129.3 (2C), 129.1 (2C), 125.9 (2C), 125.7 (2C), 76.8, 45.4, 39.8, 34.6 (2C), 31.5 (6C). *Note*: Residual EtOAc and heptane were observed. HRMS (ESI): calcd for C₂₄H₃₂O₂Na⁺ [M+Na]⁺ 375.2295, found 375.2298.



4,5-bis(4-(tert-butyl)benzyl)-1,3-dihydro-2H-imidazol-2-one **61**.

The acyloin **60** (610 mg, 1.73 mmol, 1.0 eq) and urea (260 mg, 4.33 mmol, 2.50 eq) were mixed with anhydrous PEG-400 (6 mL) and acetic acid (6 mL) under inert atmosphere. The mixture was heated to 130 °C for 2 h. The mixture turned red brown during the course of the reaction. After cooling to ambient temperature, the mixture was acidified to pH = 2 with 1 N HCl, upon which a precipitate formed, and stirred for 30 min at ambient temperature. The mixture was filtered and the residue was washed with water and heptane. Pure **61** (397 mg, 1.05 mmol, 61%) was obtained as a beige solid.

¹H NMR (400 MHz, Chloroform-*d*) δ 7.36 – 7.30 (m, 4H), 7.12 – 7.05 (m, 4H), 3.76 (s, 4H), 1.30 (s, 18H). **¹³C NMR** (101 MHz, Chloroform-*d*) δ 154.8, 149.7, 135.0, 128.2 (2C), 125.8 (2C), 117.3 (2C), 34.6 (2C), 31.5 (6C), 29.9 (2C). **HRMS** (ESI): calcd for C₂₅H₃₁N₂O⁻ [M-H]⁻ 375.2442, found 375.2441.

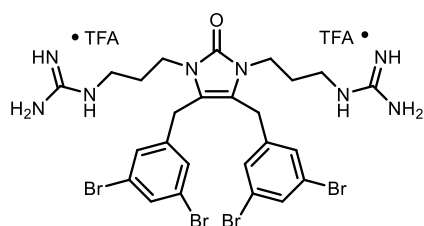


1,3-bis(3-aminopropyl)-4,5-bis(4-(tert-butyl)benzyl)-1,3-dihydro-2H-imidazol-2-one **62**.

4-imidazolidin-2-one **61** (15 mg, 40 μmol, 1.0 eq), *tert*-butyl (3-bromopropyl)carbamate (118 mg, 497 μmol, 3.0 eq) and (*n*-hexadecyl)tri-*n*-butylphosphonium bromide (4.0 mg, 8 μmol, 0.20 eq) were mixed with 10% K₂CO_{3(aq)} solution (0.5 mL) and toluene (0.5 mL) in a microwave vial. The mixture was heated to 130 °C for 2 h under μ-wave irradiation. Water and EtOAc were added and the layers were separated. The aqueous layer was extracted with EtOAc twice and the combined organics were dried over MgSO₄, filtered and the solvent was removed under reduced pressure. The crude was purified by column chromatography on silica gel with 50-85% EtOAc in heptane to yield Boc-**62** (11 mg, 16 μmol, 40%) as a clear yellow oil.

Boc-**62** was taken up in DCM (0.5 mL) and TFA (12 μL, 159 μmol, 10.0 eq) was added. The mixture was stirred at ambient temperature for 24 h. The solvent was removed and the crude was purified by RP column chromatography with 10-65% MeCN in H₂O (both containing 0.1% TFA) to yield the di-TFA salt of **62** (3 mg, 4 μmol, 26%) as a white solid.

¹H NMR (400 MHz, Methanol-*d*₄) δ 7.38 – 7.32 (m, 4H), 7.15 – 7.08 (m, 4H), 3.94 (s, 4H), 3.67 (t, J = 6.7 Hz, 4H), 2.80 (t, J = 7.0 Hz, 4H), 1.67 (p, J = 6.8 Hz, 4H), 1.30 (s, 18H). **¹³C NMR** (101 MHz, Methanol-*d*₄) δ *not recorded*. **HRMS** (ESI): calcd for C₃₁H₄₇N₄O⁺ [M+H]⁺ 491.3744, found 491.3742. **SFC**: *not recorded*.



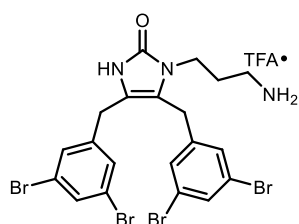
1,1'-((4,5-bis(3,5-dibromobenzyl)-2-oxo-1H-imidazole-1,3(2H)-diyl)bis(propane-3,1-diyl))diguanidine **63**.

PIII-3A (40 mg, 44 μmol , 1.0 eq) was dissolved in THF (1 mL) and DIPEA (26 μL , 152 μmol , 3.50 eq) was added. The resulting solution was stirred at ambient temperature for 10 min. *N,N'*-Di-Boc-1*H*-pyrazole-1-carboxamidine (34 mg, 109 μmol , 2.50 eq) was added and the solution was stirred at 45 °C for 2.5 h. The mixture was allowed to cool to ambient temperature and sat. $\text{NH}_4\text{Cl}_{(\text{aq})}$ solution and EtOAc were added. The layers were separated and the aqueous layer was extracted twice more with EtOAc. The combined organics were dried over Na_2SO_4 , filtered and the solvent was removed. The crude product was purified by automated flash column chromatography on silica gel with 40-80% EtOAc in heptane to yield intermediate Boc-**63** (29 mg, 25 μmol , 57%) as a clear oil.

TFA (50 μL , 651 μmol , 15.0 eq) and DCM (1 mL) were mixed with intermediate Boc-**63** and the solution was stirred at ambient temperature for 24 h. More TFA (50 μL , 651 μmol , 15.0 eq) was added and stirring was continued for another 24 h. The crude was purified by automated RP flash chromatography with a gradient of 10-50% MeCN in H_2O (both containing 0.1% TFA) to yield the di-TFA salt of **63** (19 mg, 19 μmol , 44% o2s) as a slightly yellow solid.

$^1\text{H NMR}$ (400 MHz, Methanol-*d*4) δ 7.60 (t, $J = 1.8$ Hz, 2H), 7.27 (d, $J = 1.7$ Hz, 4H), 3.99 (s, 4H), 3.65 (t, $J = 7.2$ Hz, 4H), 3.14 (t, $J = 6.9$ Hz, 4H), 1.65 (p, $J = 7.0$ Hz, 4H). $^{13}\text{C NMR}$ (101 MHz, Methanol-*d*4) δ 158.7 (2C), 155.1, 143.9 (2C), 133.7 (2C), 131.1 (4C), 124.5 (4C), 119.4 (2C), 39.9 (2C), 39.7 (2C), 29.9 (2C), 28.7 (2C). **HRMS** (ESI): calcd for $\text{C}_{25}\text{H}_{31}\text{Br}_4\text{N}_8\text{O}_1^+$ $[\text{M}+\text{H}]^+$ 774.9349, found: 774.9352. **SFC**: 97.2%.

The following compound was obtained as a side-product in the synthesis of **PIII-3A**:



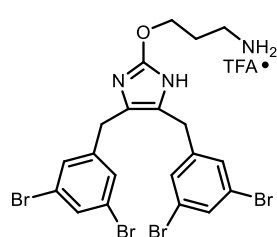
1-(3-aminopropyl)-4,5-bis(3,5-dibromobenzyl)-1,3-dihydro-2H-imidazol-2-one **64**.

ABML667 (100 mg, 172 μmol , 1.0 eq), *tert*-butyl (3-bromopropyl)carbamate (329 mg, 1.38 mmol, 8.0 eq), K_2CO_3 (135 mg, 0.98 mmol, 5.7 eq) and (*n*-hexadecyl)tri-*n*-butylphosphonium bromide (88 mg, 172 μmol , 1.0 eq) were mixed with toluene (0.5 mL) and water (0.5 mL). The resulting mixture was heated under microwave irradiation to 130 °C for 90 min and then to 150 °C for 60 min. The mixture was allowed to cool to ambient temperature. Water was added and the aqueous layer was extracted with toluene thrice. The combined organics were dried over MgSO_4 , filtered and the solvent was removed. The crude yellow solid was purified on an automated flash system equipped with a silica column and a gradient of 15-45% EtOAc in heptane (both solvents containing 2.5% MeOH). Boc-**64** was obtained as a yellow solid.

Boc-**64** was taken up in DCM (500 μ L) and TFA (75 μ L) was added. The solution was stirred at ambient temperature for 20 h, before the solvent was removed. The crude was purified by automated RP flash chromatography with a gradient of 20-55% MeCN in H₂O (both containing 0.1% TFA). **64** (11 mg, 15 μ mol, 9% o/s) was obtained as a white mono-TFA salt after lyophilization.

¹H NMR (400 MHz, Methanol-*d*₄) δ 7.59 (t, *J* = 1.7 Hz, 1H), 7.57 (t, *J* = 1.8 Hz, 1H), 7.33 (d, *J* = 1.7 Hz, 2H), 7.19 (d, *J* = 1.7 Hz, 2H), 3.96 (s, 2H), 3.79 (s, 2H), 3.61 (t, *J* = 6.7 Hz, 2H), 2.84 (t, *J* = 7.0 Hz, 2H), 1.69 (p, *J* = 6.8 Hz, 2H). ¹³C NMR (101 MHz, Methanol-*d*₄) δ 155.9, 144.2, 144.0, 133.6, 133.4, 131.4 (2C), 131.1 (2C), 124.4 (2C), 124.2 (2C), 119.3, 118.7, 38.5, 37.6, 30.0, 28.5, 28.4. HRMS (ESI): calcd for C₂₀H₂₀Br₄N₃O⁺ [M+H]⁺ 633.8334, found 633.8334. SFC: >99%.

The following compound was obtained as a side-product in the synthesis of **PIII-3A**:



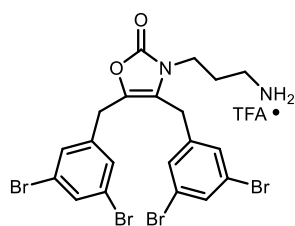
3-((4,5-bis(3,5-dibromobenzyl)oxazol-2(3H)-ylidene)amino)propan-1-amine
65.

PIII-14 (100 mg, 172 μ mol, 1.0 eq), *tert*-butyl (3-bromopropyl)carbamate (329 mg, 1.38 mmol, 8.0 eq), K₂CO₃ (135 mg, 0.98 mmol, 5.7 eq) and (*n*-hexadecyl)tri-*n*-butylphosphonium bromide (88 mg, 172 μ mol, 1.0 eq) were mixed with toluene (0.5 mL) and water (0.5 mL). The resulting mixture was heated under microwave irradiation to 130 °C for 90 min and then to 150 °C for 60 min. The mixture was allowed to cool to ambient temperature. Water was added and the aqueous layer was extracted with toluene thrice. The combined organics were dried over MgSO₄, filtered and the solvent was removed. The crude yellow solid was purified on an automated flash system equipped with a silica column and a gradient of 15-45% EtOAc in heptane (both solvents containing 2.5% MeOH). Boc-**65** was obtained as a yellow foam.

Boc-**65** was taken up in DCM (500 μ L) and TFA (75 μ L) was added. The solution was stirred at ambient temperature for 20 h, before the solvent was removed. The crude was purified by automated RP flash chromatography with a gradient of 20-55% MeCN in H₂O (both containing 0.1% TFA). **65** (10 mg, 13 μ mol, 8% o/s) was obtained as a white mono-TFA salt after lyophilization.

¹H NMR (400 MHz, Methanol-*d*₄) δ 7.57 (t, *J* = 1.8 Hz, 2H), 7.26 (d, *J* = 1.8 Hz, 4H), 4.49 (t, *J* = 5.9 Hz, 2H), 3.94 (s, 4H), 3.12 (t, *J* = 7.4 Hz, 2H), 2.24 – 2.12 (m, 2H). ¹³C NMR (101 MHz, Methanol-*d*₄) δ 152.3, 143.9 (2C), 133.5 (2C), 131.4 (4C), 124.8 (2C), 124.2 (4C), 70.3, 37.6, 30.2, 27.9. HRMS (ESI): calcd for C₂₀H₂₀Br₄N₃O⁺ [M+H]⁺ 633.8334, found 633.8331. SFC: 95.7%.

The following compound was obtained as a side-product in the synthesis of compound **54**:



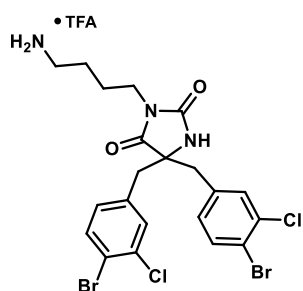
3-(4,5-bis(3,5-dibromobenzyl)-2-iminooxazol-3(2H)-yl)propan-1-amine **66**.

PIII-13 (100 mg, 172 μ mol, 1.0 eq), *tert*-butyl (3-bromopropyl)carbamate (410 mg, 1.72 mmol, 10 eq) and (*n*-hexadecyl)tri-*n*-butylphosphonium bromide (88 mg, 172 μ mol, 1.0 eq) were mixed with toluene (200 μ L) and 10% NaHCO_{3(aq)} (200 μ L). The resulting mixture was heated to 110 $^{\circ}$ C for 44 h. The mixture was allowed to cool to ambient temperature. Water and EtOAc were added and the layers were separated. The aqueous layer was extracted with EtOAc twice more and the combined organics were dried over MgSO₄, filtered and the solvent was removed. The crude yellow oil was purified on an automated flash system equipped with a silica column and a gradient gradient 5-25% EtOAc in heptane. Boc-**66** (51 mg, 69 μ mol, 40%) was obtained as a white solid.

Boc-**66** (51 mg, 69 μ mol, 1.0 eq) was taken up in DCM (300 μ L) and TFA (52 μ L, 690 μ mol, 10 eq) was added. The solution was stirred at ambient temperature for 20 h, before the solvent was removed. The crude was purified by automated RP flash chromatography with a gradient of 23-65% MeCN in H₂O (both containing 0.1% TFA). **66** (39 mg, 52 μ mol, 30% o2s) was obtained as a white mono-TFA salt after lyophilization.

¹H NMR (400 MHz, Methanol-*d*4) δ 7.66 (t, J = 1.8 Hz, 1H), 7.62 (t, J = 1.8 Hz, 1H), 7.38 (d, J = 1.7 Hz, 2H), 7.34 (d, J = 1.7 Hz, 2H), 3.96 (s, 2H), 3.85 (s, 2H), 3.56 (t, J = 6.9 Hz, 2H), 2.88 (t, J = 7.5 Hz, 2H), 1.74 (p, J = 7.1 Hz, 2H). ¹³C NMR (101 MHz, Methanol-*d*4) δ 157.6, 142.6, 142.3, 137.0, 134.1, 133.7, 131.6 (2C), 131.3 (2C), 124.6 (2C), 124.2 (2C), 122.4, 39.9, 37.9, 30.5, 28.1, 28.0. HRMS (ESI): calcd for C₂₀H₁₉Br₄N₂O₂⁺ [M+H]⁺ 634.8175, found 634.8176. SFC: >99%.

The following compound was obtained as a side-product in the synthesis of **PIII-6cA**:



3-(4-aminobutyl)-5,5-bis(4-bromo-3-chlorobenzyl)imidazolidine-2,4-dione **67**.

PIII-9c (73 mg, 144 μ mol, 1.0 eq), *tert*-butyl (4-bromobutyl)carbamate (91 mg, 360 μ mol, 2.5 eq), Cs₂CO₃ (164 mg, 504 μ mol, 3.5 eq), TBAI (5.3 mg, 14 μ mol, 0.1 eq) and acetone (2.0 mL) were stirred at 75 $^{\circ}$ C for h. Purification by column chromatography on silica with a gradient of 15-50% EtOAc in heptane delivered the impure intermediate Boc-**67** (33 mg, 49 μ mol, 34%) as a colorless oil.

TFA (37 μ L, 0.49 mmol, 10.0 eq) and DCM (0.5 mL) were added and the solution was stirred at ambient temperature for 24 h. The crude was purified by RP chromatography with a gradient of 15-55% MeCN in H₂O to yield the mono-TFA salt of **67** (10 mg, 14 μ mol, 10% o2s) as a white solid. ¹H NMR (400 MHz, Methanol-*d*4) δ 7.59 (d, J = 8.2 Hz, 2H), 7.35 (d, J = 2.1 Hz, 2H), 7.04 (dd, J = 8.3, 2.1 Hz,

2H), 3.25 (d, $J = 13.7$ Hz, 2H), 3.04 (t, $J = 6.8$ Hz, 2H), 2.97 (d, $J = 13.7$ Hz, 2H), 2.76 (t, $J = 7.3$ Hz, 2H), 1.19 – 1.00 (m, 4H). ^{13}C NMR (101 MHz, Methanol- d_4) δ 175.9, 157.6, 137.4 (2C), 135.1 (2C), 134.8 (2C), 133.2 (2C), 131.5 (2C), 122.1 (2C), 68.1, 42.5 (2C), 40.0, 37.7, 25.9, 25.2. HRMS (ESI): calcd for $\text{C}_{21}\text{H}_{22}\text{Br}_2\text{Cl}_2\text{N}_3\text{O}_2^+$ $[\text{M}+\text{H}]^+$ 575.9450, found 575.9453. SFC: 97.9%.

5.1.3 Synthesis of aspergilone A under continuous flow

All spectral data can be found in the Supporting Information of paper IV.

Vilsmeier-Haack formylation to PIV-21.

PTFE (polytetrafluoroethylene) tubing (ID = 1.0 mm) was used for all connections and as reactor coils. All reagents were pumped with either a Fusion 710 or a Fusion 100 pump from CHEMYX. POCl_3 (neat, 77.5 μL , 6.0 eq) and DMF (neat, 132.5 $\mu\text{L}/\text{min}$, 12.4 eq) were loaded into a plastic syringe. Both reagents were delivered to a Y-shaped mixer (M1, PTFE, ID = 0.8 mm, 120° contact angle) and reacted at ambient temperature for 5 min in the first reactor coil R1 ($F_R = 210$ $\mu\text{L}/\text{min}$, $V = 1.05$ mL, $l = 135$ cm). 1-Bromo-3,5-dimethoxybenzene **PIV-20** (2.5 M in DMF, 55 $\mu\text{L}/\text{min}$, 1.0 eq) was combined with the exiting stream containing the Vilsmeier-Haack reagent in a Tee mixer (M2, PTFE, 0.8 mm, 180° contact angle). The resulting mixture was passed through reactor R2 ($F_R = 265$ $\mu\text{L}/\text{min}$, $V = 10.0$ mL, $l = 12.7$ m) at 100°C (oil bath) for 38 min. The colorless solution turned gradually dark red during the course of the reaction. The exiting reaction mixture was collected into a 1 N $\text{NaOH}_{(\text{aq})}$ solution for continuous neutralization. Upon addition to the basic solution, a white solid precipitated. The system was equilibrated for 1 h to ensure steady state conditions, before collecting for 3 h and 40 min. It was ensured that the pH remained >12 and the suspension was filtered. The residue was washed with water and collected by addition of DCM. The organic layer was dried over MgSO_4 , filtered and the solvent was removed under reduced pressure to deliver an almost pure, slightly brown solid. The crude was purified by automated flash chromatography with 25-60% EtOAc in PE to yield the title product **PIV-21** (5.45 g, 22.2 mmol, 73%) as a white solid. The spectroscopical data was identical to **PIV-21** obtained from batch reactions.

Wolff-Kishner reduction to PIV-22.

PTFE tubing (ID = 1.0 mm) was used for all connections and as reactor coils. All reagents were pumped with a V-3 pump integrated in an E-Series Flow Chemistry System from Vapourtec. Both reagent streams originated from a reservoir (Schott bottle) each. The first reservoir contained aldehyde **PIV-21** (0.2 M in TEG, 1.0 eq) and the second reservoir contained a mixture of a 50-60% aqueous hydrazine solution (0.3 M in EG, 1.5 eq) and KOH (0.7 M in EG, 3.5 eq). Both streams were delivered (222 $\mu\text{L}/\text{min}$ each) to a Tee piece (M1, PTFE, ID = 1.0 mm, 180° contact angle) and the resulting mixture was heated to 160°C for 22.5 in reactor R1 ($F_R = 444$ $\mu\text{L}/\text{min}$, $V = 10.0$ mL, $l = 12.7$ m). A back pressure regulator (5.2 bar) was installed after the reaction coil. The system was equilibrated for 35 min to ensure steady state conditions, before collecting for 7 h and 7 min. The resulting hot, yellow solution was collected

and allowed to cool to ambient temperature. Water and brine were added and the aqueous layer was extracted with DCM thrice. The combined organic layers were washed once each with water and brine, dried over MgSO_4 , filtered and the solvent was removed under reduced pressure. The crude was purified by automated flash chromatography with 0-10 % EtOAc in PE to yield the title product **PIV-22** (3.72 g, 16.1 mmol, 75%) as a white solid. The spectroscopical data was identical to **PIV-22** obtained from batch reactions.

Miyaura Borylation to PIV-15.

PTFE tubing (ID = 1.0 mm) was used for all connections and as reactor coils. All reagents were pumped with a Fusion 100 pump from CHEMYX. One plastic syringe was charged with a mixture of Aryl-Br **PIV-22** (0.44 M in dry DMF, 1.0 eq), B_2pin_2 (0.48 M in dry DMF, 1.1 eq) and $\text{Pd}(\text{dppf})\text{Cl}_2$ (11 mM in DMF, 2.5 mol%). A second syringe was charged with KOAc (1.54 M in dry, freshly distilled EG). Both solutions were delivered (166 $\mu\text{L}/\text{min}$ each) to a Tee piece (M1, PEEK, ID = 1.0 mm, 180° contact angle). The resulting mixture was reacted at 130 °C for 5 min in reactor R1 ($F_R = 332 \mu\text{L}/\text{min}$, $V = 1.66\text{mL}$, $l = 211 \text{ cm}$) and then collected. The system was equilibrated for 7 min before collection for 3 h and 31 min. The collected reaction mixture was allowed to cool to ambient temperature before the addition of EtOAc and water. The layers were separated and the aqueous layer was extracted with EtOAc once. The organic layers were combined and washed five times with water. The organics were dried over MgSO_4 , filtered and the solvent was removed. The crude was purified by automated flash chromatography with 0-10% EtOAc in PE to yield the title product **PIV-15** (3.69 g, 13.3 mmol, 86%) as a white solid. The spectroscopical data was identical to **PIV-15** obtained from batch reactions.

1,2-aniotropic rearrangement to PIV-16.

PTFE tubing was used for all connections and as reactor coils. All reagents were pumped with either a Fusion 710 or a Fusion 100 pump from CHEMYX. One plastic syringe was charged with *n*-BuLi (0.1 M in hexanes, 1.3 eq) and second plastic syringe was charged with stannane **PIV-18** (0.1 M in dry MTBE, 1.3 eq). Both mixtures were delivered (75 $\mu\text{L}/\text{min}$ each) through a coiled cooling loop ($V = 150 \mu\text{L}$, $l = 30 \text{ cm}$, ID = 0.8 mm) to a Tee piece (M1, PEEK, ID = 1.0 mm, 180° contact angle) connected to a static mixer (PTFE in a plastic housing, Kenics KM type, $V = \text{unknown}$). The resulting mixture was reacted at -41 °C for 60 s in R1 ($F_R = 150 \mu\text{L}/\text{min}$, $V = 150 \mu\text{L}$, $l = 30 \text{ cm}$, ID = 0.8 mm). Aryl-Bpin **PIV-15** (0.077 M in dry MTBE, 75 $\mu\text{L}/\text{min}$, 1.0 eq), loaded in a third plastic syringe, was passed through a cooling loop ($V = 150 \mu\text{L}$, $l = 30 \text{ cm}$, ID = 0.8 mm) and then combined with the stream containing the lithiated ester in a Y-shaped mixer (M2, PTFE, ID = 1.0 mm, 120° contact angle) at -41 °C. The exiting mixture was passed through the second micro reactor R2 ($F_R = 225 \mu\text{L}/\text{min}$, $V = 675 \mu\text{L}$, $l = 134 \text{ cm}$, ID = 0.8 mm) for 180 s at -41 °C. A fourth syringe was loaded with anhydrous MgBr_2 (0.087 M in dry MeOH, 133 $\mu\text{L}/\text{min}$, 2.0 eq) and the solution was delivered with a syringe pump to a Y-shape mixer

(M3, PTFE, ID = 1.0 mm, 120° contact angle) together with the boronate containing stream. The resulting solution was directly passed through the micro reactor R3 ($F_R = 358 \mu\text{L}/\text{min}$, $V = 1.44 \text{ mL}$, $l = 177 \text{ cm}$, ID = 1.0 mm) at $\sim 50 \text{ }^\circ\text{C}$ for 225 s under ultrasound. The system was equilibrated for a total of 12 min, before collection for 7.5 min. The crude was allowed to cool to ambient temperature and was then filtered over Celite, eluting with Et_2O . The organic layer was collected, and the solvent was removed. The crude was analyzed by NMR to reveal a ratio of 1.0:6.6 s.m.:pdct and an NMR yield of 71% (standard: 5-nitro-*m*-xylene). The mixture was not analyzed further.

6 References

1. Newman, D. J.; Cragg, G. M., Natural Products as Sources of New Drugs over the Nearly Four Decades from 01/1981 to 09/2019. *J. Nat. Prod.* **2020**, *83* (3), 770-803.
2. Chassagne, F.; Cabanac, G.; Hubert, G.; David, B.; Marti, G., The landscape of natural product diversity and their pharmacological relevance from a focus on the Dictionary of Natural Products®. *Phytochem. Rev.* **2019**, *18* (3), 601-622.
3. Newman, D. J.; Cragg, G. M., Natural Products as Sources of New Drugs from 1981 to 2014. *J. Nat. Prod.* **2016**, *79* (3), 629-661.
4. Cantrell, C. L.; Dayan, F. E.; Duke, S. O., Natural Products As Sources for New Pesticides. *J. Nat. Prod.* **2012**, *75* (6), 1231-1242.
5. Embuscado, M. E., Spices and herbs: Natural sources of antioxidants – a mini review. *J. Funct. Foods* **2015**, *18*, 811-819.
6. Desam, N. R.; Al-Rajab, A. J., The Importance of Natural Products in Cosmetics. In *Bioactive Natural Products for Pharmaceutical Applications*, Pal, D.; Nayak, A. K., Eds. Springer International Publishing: Cham, 2021; pp 643-685.
7. Dias, D. A.; Urban, S.; Roessner, U., A historical overview of natural products in drug discovery. *Metabolites* **2012**, *2* (2), 303-336.
8. Murray, C. J.; Ikuta, K. S.; Sharara, F.; Swetschinski, L.; Robles Aguilar, G.; Gray, A.; Han, C.; Bisignano, C.; Rao, P.; Wool, E.; Johnson, S. C.; Browne, A. J.; Chipeta, M. G.; Fell, F.; Hackett, S.; Haines-Woodhouse, G.; Kashef Hamadani, B. H.; Kumaran, E. A. P.; McManigal, B.; Agarwal, R.; Akech, S.; Albertson, S.; Amuasi, J.; Andrews, J.; Aravkin, A.; Ashley, E.; Bailey, F.; Baker, S.; Basnyat, B.; Bekker, A.; Bender, R.; Bethou, A.; Bielicki, J.; Boonkasidecha, S.; Bukosia, J.; Carvalheiro, C.; Castañeda-Orjuela, C.; Chansamouth, V.; Chaurasia, S.; Chiurchiù, S.; Chowdhury, F.; Cook, A. J.; Cooper, B.; Cressey, T. R.; Criollo-Mora, E.; Cunningham, M.; Darboe, S.; Day, N. P. J.; De Luca, M.; Dokova, K.; Dramowski, A.; Dunachie, S. J.; Eckmanns, T.; Eibach, D.; Emami, A.; Feasey, N.; Fisher-Pearson, N.; Forrest, K.; Garrett, D.; Gastmeier, P.; Giref, A. Z.; Greer, R. C.; Gupta, V.; Haller, S.; Haselbeck, A.; Hay, S. I.; Holm, M.; Hopkins, S.; Iregbu, K. C.; Jacobs, J.; Jarovsky, D.; Javanmardi, F.; Khorana, M.; Kissoon, N.; Kobeissi, E.; Kostyanov, T.; Krapp, F.; Krumkamp, R.; Kumar, A.; Kyu, H. H.; Lim, C.; Limmathurotsakul, D.; Loftus, M. J.; Lunn, M.; Ma, J.; Mturi, N.; Munera-Huertas, T.; Musicha, P.; Mussi-Pinhata, M. M.; Nakamura, T.; Nanavati, R.; Nangia, S.; Newton, P.; Ngoun, C.; Novotney, A.; Nwakanma, D.; Obiero, C. W.; Olivás-Martínez, A.; Olliaro, P.; Ooko, E.; Ortiz-Brizuela, E.; Peleg, A. Y.; Perrone, C.; Plakkal, N.; Ponce-De-Leon, A.; Raad, M.; Ramdin, T.; Riddell, A.; Roberts, T.; Robotham, J. V.; Roca, A.; Rudd, K. E.; Russell, N.; Schnall, J.; Scott, J. A. G.; Shivamallappa, M.; Sifuentes-Osornio, J.; Steenkeste, N.; Stewardson, A. J.; Stoeva, T.; Tasak, N.; Thaiprakong, A.; Thwaites, G.; Turner, C.; Turner, P.; Van Doorn, H. R.; Velaphi, S.; Vongpradith, A.; Vu, H.; Walsh, T.; Waner, S.; Wangrangsimakul, T.; Wozniak, T.; Zheng, P.; Sartorius, B.; Lopez, A. D.; Stergachis, A.; Moore, C.; Dolecek, C.; Naghavi, M., Global burden of bacterial antimicrobial resistance in 2019: a systematic analysis. *Lancet* **2022**, *399* (10325), 629-655.
9. O'Neill, J., *Tackling drug-resistant infections globally: final report and recommendations*. Government of the United Kingdom: 2016.
10. Sung, H.; Ferlay, J.; Siegel, R. L.; Laversanne, M.; Soerjomataram, I.; Jemal, A.; Bray, F., Global Cancer Statistics 2020: GLOBOCAN Estimates of Incidence and Mortality Worldwide for 36 Cancers in 185 Countries. *CA Cancer. J. Clin.* **2021**, *71* (3), 209-249.
11. Qian, P.-Y.; Li, Z.; Xu, Y.; Li, Y.; Fusetani, N., Mini-review: Marine natural products and their synthetic analogs as antifouling compounds: 2009–2014. *Biofouling* **2015**, *31* (1), 101-122.
12. Schultz, M. P.; Bendick, J. A.; Holm, E. R.; Hertel, W. M., Economic impact of biofouling on a naval surface ship. *Biofouling* **2011**, *27* (1), 87-98.
13. Tapiolas, D. M.; Bowden, B. F.; Abou-Mansour, E.; Willis, R. H.; Doyle, J. R.; Muirhead, A. N.; Liptrot, C.; Llewellyn, L. E.; Wolff, C. W.; Wright, A. D.; Motti, C. A., Eusynstyelamides A, B, and C, nNOS inhibitors, from the ascidian *Eusynstyela latericius*. *J. Nat. Prod.* **2009**, *72* (6), 1115-1120.

14. Tadesse, M.; Tabudravu, J. N.; Jaspars, M.; Strom, M. B.; Hansen, E.; Andersen, J. H.; Kristiansen, P. E.; Haug, T., The antibacterial ent-eusynstyelamide B and eusynstyelamides D, E, and F from the Arctic bryozoan *Tegella* cf. *spitzbergensis*. *J. Nat. Prod.* **2011**, *74* (4), 837-841.
15. Som, A.; Vemparala, S.; Ivanov, I.; Tew, G. N., Synthetic mimics of antimicrobial peptides. *Pept. Sci.* **2008**, *90* (2), 83-93.
16. Strøm, M. B.; Haug, B. E.; Skar, M. L.; Stensen, W.; Stiberg, T.; Svendsen, J. S., The Pharmacophore of Short Cationic Antibacterial Peptides. *J. Med. Chem.* **2003**, *46* (9), 1567-1570.
17. Appelbaum, P. C., 2012 and beyond: potential for the start of a second pre-antibiotic era? *J. Antimicrob. Chemother.* **2012**, *67* (9), 2062-2068.
18. Shao, C.-L.; Wang, C.-Y.; Wei, M.-Y.; Gu, Y.-C.; She, Z.-G.; Qian, P.-Y.; Lin, Y.-C., Aspergilones A and B, two benzylazaphilones with an unprecedented carbon skeleton from the gorgonian-derived fungus *Aspergillus* sp. *Bioorg. Med. Chem. Lett.* **2011**, *21* (2), 690-693.
19. Warren, H. H.; Finkelstein, M.; Scola, D. A., The Synthesis and Antibacterial Activity of Analogs of Citrinin and Dihydrocitrinin. *J. Am. Chem. Soc.* **1962**, *84* (10), 1926-1928.
20. Abdel-Aziz, S. M.; Abo Elsoud, M. M.; Anise, A. A. H., Chapter 2 - Microbial Biosynthesis: A Repertory of Vital Natural Products. In *Food Biosci.*, Grumezescu, A. M.; Holban, A. M., Eds. Academic Press: 2017; pp 25-54.
21. Cragg, G. M.; Newman, D. J., Natural products: A continuing source of novel drug leads. *Biochim Biophys Acta Gen Subj* **2013**, *1830* (6), 3670-3695.
22. Tan, S. Y.; Tatsumura, Y., Alexander Fleming (1881-1955): Discoverer of penicillin. *Singapore Med J* **2015**, *56* (7), 366-367.
23. Elder, A. L., History of penicillin production. **1970**.
24. Wainwright, M., *Miracle cure: The story of penicillin and the golden age of antibiotics*. Blackwell: 1990.
25. Baker, D. D.; Chu, M.; Oza, U.; Rajgarhia, V., The value of natural products to future pharmaceutical discovery. *Nat. Prod. Rep.* **2007**, *24* (6), 1225-1244.
26. Ojima, I., Modern Natural Products Chemistry and Drug Discovery. *J. Med. Chem.* **2008**, *51* (9), 2587-2588.
27. Butler, M. S., The Role of Natural Product Chemistry in Drug Discovery. *J. Nat. Prod.* **2004**, *67* (12), 2141-2153.
28. Newman, D. J., Natural products as leads to potential drugs: an old process or the new hope for drug discovery? *J. Med. Chem.* **2008**, *51* (9), 2589-2599.
29. Rouhi, A. M., REDISCOVERING NATURAL PRODUCTS. *Chem. Eng. News* **2003**, *81* (41), 77-91.
30. Chen, Y.; de Bruyn Kops, C.; Kirchmair, J., Data Resources for the Computer-Guided Discovery of Bioactive Natural Products. *J Chem Inf Model* **2017**, *57* (9), 2099-2111.
31. Carroll, A. R.; Copp, B. R.; Davis, R. A.; Keyzers, R. A.; Prinsep, M. R., Marine natural products. *Nat. Prod. Rep.* **2022**.
32. Blunt, J. W.; Carroll, A. R.; Copp, B. R.; Davis, R. A.; Keyzers, R. A.; Prinsep, M. R., Marine natural products. *Nat. Prod. Rep.* **2018**, *35* (1), 8-53.
33. Newman, D. J.; Cragg, G. M., Drugs and Drug Candidates from Marine Sources: An Assessment of the Current "State of Play". *Planta Med.* **2016**, *82* (09/10), 775-789.
34. Dewick, P. M., *Medicinal natural products: a biosynthetic approach*. John Wiley & Sons: 2002.
35. Arcamone, F.; Cassinelli, G.; Fantini, G.; Grein, A.; Orezzi, P.; Pol, C.; Spalla, C., Adriamycin, 14-hydroxydaunomycin, a new antitumor antibiotic from *S. peuceitius* var. *caesius*. *Biotechnol. Bioeng.* **1969**, *11* (6), 1101-1110.
36. Klayman, D. L.; Lin, A. J.; Acton, N.; Scovill, J. P.; Hoch, J. M.; Milhous, W. K.; Theoharides, A. D.; Dobek, A. S., Isolation of Artemisinin (Qinghaosu) from *Artemisia annua* Growing in the United States. *J. Nat. Prod.* **1984**, *47* (4), 715-717.
37. Newman, D. J.; Cragg, G. M., Natural Products as Sources of New Drugs over the Last 25 Years. *J. Nat. Prod.* **2007**, *70* (3), 461-477.
38. Cragg, G. M.; Pezzuto, J. M., Natural Products as a Vital Source for the Discovery of Cancer Chemotherapeutic and Chemopreventive Agents. *Med Princ Pract* **2016**, *25*(suppl 2) (Suppl. 2), 41-59.

39. Wani, M. C.; Taylor, H. L.; Wall, M. E.; Coggon, P.; McPhail, A. T., Plant antitumor agents. VI. The isolation and structure of taxol, a novel antileukemic and antitumor agent from *Taxus brevifolia*. *J. Am. Chem. Soc.* **1971**, *93* (9), 2325-2327.
40. Newman, D. J.; Cragg, G. M., Marine natural products and related compounds in clinical and advanced preclinical trials. *J. Nat. Prod.* **2004**, *67* (8), 1216-1238.
41. Gerwick, William H.; Moore, Bradley S., Lessons from the Past and Charting the Future of Marine Natural Products Drug Discovery and Chemical Biology. *Chem. Biol.* **2012**, *19* (1), 85-98.
42. Olivera, B. M.; Gray, W. R.; Zeikus, R.; McIntosh, J. M.; Varga, J.; Rivier, J.; de Santos, V.; Cruz, L. J., Peptide neurotoxins from fish-hunting cone snails. *Science* **1985**, *230* (4732), 1338-1343.
43. Miljanich, G. P., Ziconotide: neuronal calcium channel blocker for treating severe chronic pain. *Curr. Med. Chem.* **2004**, *11* (23), 3029-3040.
44. McGivern, J. G., Targeting N-type and T-type calcium channels for the treatment of pain. *Drug Discov. Today* **2006**, *11* (5-6), 245-253.
45. Wang, Y. X.; Gao, D.; Pettus, M.; Phillips, C.; Bowersox, S. S., Interactions of intrathecally administered ziconotide, a selective blocker of neuronal N-type voltage-sensitive calcium channels, with morphine on nociception in rats. *Pain* **2000**, *84* (2-3), 271-281.
46. Lee, J.-Y.; Orlikova, B.; Diederich, M., Signal Transducers and Activators of Transcription (STAT) Regulatory Networks in Marine Organisms: From Physiological Observations towards Marine Drug Discovery. *Mar. Drugs* **2015**, *13* (8), 4967-4984.
47. Bergmann, W.; Feeney, R. J., THE ISOLATION OF A NEW THYMINE PENTOSIDE FROM SPONGES¹. *J. Am. Chem. Soc.* **1950**, *72* (6), 2809-2810.
48. Bergmann, W.; Feeney, R. J., CONTRIBUTIONS TO THE STUDY OF MARINE PRODUCTS. XXXII. THE NUCLEOSIDES OF SPONGES. I.¹. *J. Org. Chem.* **1951**, *16* (6), 981-987.
49. Bergmann, W.; Burke, D. C., CONTRIBUTIONS TO THE STUDY OF MARINE PRODUCTS. XXXIX. THE NUCLEOSIDES OF SPONGES. III.¹ SPONGOTHYIMIDINE AND SPONGOURIDINE². *J. Org. Chem.* **1955**, *20* (11), 1501-1507.
50. Mayer, A. M. S.; Glaser, K. B.; Cuevas, C.; Jacobs, R. S.; Kem, W.; Little, R. D.; McIntosh, J. M.; Newman, D. J.; Potts, B. C.; Shuster, D. E., The odyssey of marine pharmaceuticals: a current pipeline perspective. *Trends Pharmacol. Sci.* **2010**, *31* (6), 255-265.
51. Cimino, G.; De Rosa, S.; De Stefano, S., Antiviral agents from a gorgonian, *Eunicella cavolini*. *Experientia* **1984**, *40* (4), 339-340.
52. Wright, A. E.; Forleo, D. A.; Gunawardana, G. P.; Gunasekera, S. P.; Koehn, F. E.; McConnell, O. J., Antitumor tetrahydroisoquinoline alkaloids from the colonial ascidian *Ecteinascidia turbinata*. *J. Org. Chem.* **1990**, *55* (15), 4508-4512.
53. Rinehart, K. L.; Holt, T. G.; Fregeau, N. L.; Stroh, J. G.; Keifer, P. A.; Sun, F.; Li, L. H.; Martin, D. G., Ecteinascidins 729, 743, 745, 759A, 759B, and 770: potent antitumor agents from the Caribbean tunicate *Ecteinascidia turbinata*. *J. Org. Chem.* **1990**, *55* (15), 4512-4515.
54. Verweij, J., Soft tissue sarcoma trials: one size no longer fits all. *J Clin Oncol* **2009**, *27* (19), 3085-3087.
55. Yap, T. A.; Carden, C. P.; Kaye, S. B., Beyond chemotherapy: targeted therapies in ovarian cancer. *Nat. Rev. Cancer* **2009**, *9* (3), 167-181.
56. Cuevas, C.; Francesch, A., Development of Yondelis (trabectedin, ET-743). A semisynthetic process solves the supply problem. *Nat. Prod. Rep.* **2009**, *26* (3), 322-337.
57. Adamczyk, B.; Simon, J.; Kitunen, V.; Adamczyk, S.; Smolander, A., Tannins and Their Complex Interaction with Different Organic Nitrogen Compounds and Enzymes: Old Paradigms versus Recent Advances. *ChemistryOpen* **2017**, *6* (5), 610-614.
58. Ingkaninan, K.; von Frijtag Drabbe Künzel, J. K.; Ijzerman, A. P.; Verpoorte, R., Interference of Linoleic Acid Fraction in Some Receptor Binding Assays. *J. Nat. Prod.* **1999**, *62* (6), 912-914.
59. Colegate, S. M.; Molyneux, R. J., *Bioactive natural products: detection, isolation, and structural determination*. CRC press: 2007.
60. Cordell, G. A.; Shin, Y. G., Finding the needle in the haystack. The dereplication of natural product extracts. *Pure Appl. Chem.* **1999**, *71* (6), 1089-1094.
61. Cragg, G. M.; Newman, D. J., Biodiversity: A continuing source of novel drug leads. *Pure Appl. Chem.* **2005**, *77* (1), 7-24.

62. Laxminarayan, R.; Duse, A.; Watal, C.; Zaidi, A. K. M.; Wertheim, H. F. L.; Sumpradit, N.; Vlieghe, E.; Hara, G. L.; Gould, I. M.; Goossens, H.; Greko, C.; So, A. D.; Bigdeli, M.; Tomson, G.; Woodhouse, W.; Ombaka, E.; Peralta, A. Q.; Qamar, F. N.; Mir, F.; Kariuki, S.; Bhutta, Z. A.; Coates, A.; Bergstrom, R.; Wright, G. D.; Brown, E. D.; Cars, O., Antibiotic resistance—the need for global solutions. *Lancet Infect. Dis.* **2013**, *13* (12), 1057-1098.
63. Andersson, D. I.; Hughes, D., Microbiological effects of sublethal levels of antibiotics. *Nat. Rev. Microbiol.* **2014**, *12* (7), 465-478.
64. World Health, O., *Global action plan on antimicrobial resistance*. World Health Organization: Geneva, 2015.
65. Casapullo, A.; Finamore, E.; Minale, L.; Zollo, F., A dimeric peptide alkaloid of a completely new type, Anchinopeptolide A, from the marine sponge Anchinoe tenacior. *Tetrahedron Lett.* **1993**, *34* (39), 6297-6300.
66. Sölter, S.; Dieckmann, R.; Blumenberg, M.; Francke, W., Baretin, revisited? *Tetrahedron Lett.* **2002**, *43* (18), 3385-3386.
67. Carroll, A. R.; Avery, V. M., Leptoclinidamines A–C, Indole Alkaloids from the Australian Ascidian *Leptoclinides durus*. *J. Nat. Prod.* **2009**, *72* (4), 696-699.
68. Barykina, O. V.; Snider, B. B., Synthesis of (±)-Eusynstyelamide A. *Org. Lett.* **2010**, *12* (11), 2664-2667.
69. Steiner, H.; Hultmark, D.; Engström, Å.; Bennich, H.; Boman, H. G., Sequence and specificity of two antibacterial proteins involved in insect immunity. *Nature* **1981**, *292* (5820), 246-248.
70. Boman, H. G., Peptide antibiotics and their role in innate immunity. *Annu. Rev. Immunol.* **1995**, *13*, 61-92.
71. Zasloff, M., Antimicrobial peptides of multicellular organisms. *Nature* **2002**, *415*, 389.
72. Yeaman, M. R.; Yount, N. Y., Mechanisms of Antimicrobial Peptide Action and Resistance. *Pharmacol. Rev.* **2003**, *55* (1), 27.
73. Microbiology, D. o. P. t. A. P. D. <https://aps.unmc.edu/database/anti> (accessed 29.05.2022).
74. El Shazely, B.; Yu, G.; Johnston, P. R.; Rolff, J., Resistance Evolution Against Antimicrobial Peptides in *Staphylococcus aureus* Alters Pharmacodynamics Beyond the MIC. *Front. Microbiol.* **2020**, *11*.
75. Giuliani, A.; Pirri, G.; Nicoletto, S. F., Antimicrobial peptides: an overview of a promising class of therapeutics. *Cent. Eur. J. Biol.* **2007**, *2* (1), 1-33.
76. Huan, Y.; Kong, Q.; Mou, H.; Yi, H., Antimicrobial Peptides: Classification, Design, Application and Research Progress in Multiple Fields. *Front. Microbiol.* **2020**, *11*.
77. Hancock, R. E. W., Peptide antibiotics. *Lancet* **1997**, *349* (9049), 418-422.
78. Hancock, R. E.; Lehrer, R., Cationic peptides: a new source of antibiotics. *Trends Biotechnol.* **1998**, *16* (2), 82-88.
79. Powers, J. P.; Hancock, R. E., The relationship between peptide structure and antibacterial activity. *Peptides* **2003**, *24* (11), 1681-1691.
80. Hancock, R. E. W.; Sahl, H.-G., Antimicrobial and host-defense peptides as new anti-infective therapeutic strategies. *Nat. Biotechnol.* **2006**, *24* (12), 1551-1557.
81. Kohanski, M. A.; Dwyer, D. J.; Collins, J. J., How antibiotics kill bacteria: from targets to networks. *Nat. Rev. Microbiol.* **2010**, *8* (6), 423-435.
82. Klausen, L. H.; Fuhs, T.; Dong, M., Mapping surface charge density of lipid bilayers by quantitative surface conductivity microscopy. *Nat. Comm.* **2016**, *7* (1), 12447.
83. van Meer, G.; de Kroon, A. I., Lipid map of the mammalian cell. *J. Cell Sci.* **2011**, *124* (Pt 1), 5-8.
84. Platre, M. P.; Jaillais, Y., Anionic lipids and the maintenance of membrane electrostatics in eukaryotes. *Plant Signal. Behav.* **2017**, *12* (2), e1282022.
85. Depelteau, J. S.; Brenzinger, S.; Briegel, A., Bacterial and Archaeal Cell Structure. In *Encyclopedia of Microbiology (Fourth Edition)*, Schmidt, T. M., Ed. Academic Press: Oxford, 2019; pp 348-360.
86. Li, J.; Koh, J.-J.; Liu, S.; Lakshminarayanan, R.; Verma, C. S.; Beuerman, R. W., Membrane Active Antimicrobial Peptides: Translating Mechanistic Insights to Design. *Front. Neurosci.* **2017**, *11*.
87. Bahar, A. A.; Ren, D., Antimicrobial Peptides. *Pharmaceuticals* **2013**, *6* (12), 1543-1575.

88. Oren, Z.; Shai, Y., Mode of action of linear amphipathic alpha-helical antimicrobial peptides. *Biopolymers* **1998**, *47* (6), 451-463.
89. Uematsu, N.; Matsuzaki, K., Polar angle as a determinant of amphipathic alpha-helix-lipid interactions: a model peptide study. *Biophys. J.* **2000**, *79* (4), 2075-2083.
90. Chan, D. I.; Prenner, E. J.; Vogel, H. J., Tryptophan- and arginine-rich antimicrobial peptides: structures and mechanisms of action. *Biochim Biophys Acta* **2006**, *1758* (9), 1184-1202.
91. Boman, H. G.; Agerberth, B.; Boman, A., Mechanisms of action on Escherichia coli of cecropin P1 and PR-39, two antibacterial peptides from pig intestine. *Infect. Immun.* **1993**, *61* (7), 2978-2984.
92. Subbalakshmi, C.; Sitaram, N., Mechanism of antimicrobial action of indolicidin. *FEMS Microbiol. Lett.* **1998**, *160* (1), 91-96.
93. Park, C. B.; Yi, K.-S.; Matsuzaki, K.; Kim, M. S.; Kim, S. C., Structure-activity analysis of buforin II, a histone H2A-derived antimicrobial peptide: The proline hinge is responsible for the cell-penetrating ability of buforin II. *Proc. Natl. Acad. Sci. U.S.A.* **2000**, *97* (15), 8245-8250.
94. Cudic, M.; Otvos, L., Jr., Intracellular targets of antibacterial peptides. *Curr. Drug Targets* **2002**, *3* (2), 101-106.
95. El-Sayed Ahmed, M. A. E.-G.; Zhong, L.-L.; Shen, C.; Yang, Y.; Doi, Y.; Tian, G.-B., Colistin and its role in the Era of antibiotic resistance: an extended review (2000–2019). *Emerg. Microbes Infect.* **2020**, *9* (1), 868-885.
96. Koyama, Y., A new antibiotic 'colistin' produced by spore-forming soil bacteria. *J. Antibiot.* **1950**, *3*, 457-458.
97. Lim, L. M.; Ly, N.; Anderson, D.; Yang, J. C.; Macander, L.; Jarkowski, A., 3rd; Forrest, A.; Bulitta, J. B.; Tsuji, B. T., Resurgence of colistin: a review of resistance, toxicity, pharmacodynamics, and dosing. *Pharmacotherapy* **2010**, *30* (12), 1279-1291.
98. Bardet, L.; Okdah, L.; Le Page, S.; Baron, S. A.; Rolain, J.-M., Comparative evaluation of the UMIC Colistine kit to assess MIC of colistin of gram-negative rods. *BMC Microbiol.* **2019**, *19* (1), 60.
99. Sader, H. S.; Watters, A. A.; Fritsche, T. R.; Jones, R. N., Daptomycin antimicrobial activity tested against methicillin-resistant staphylococci and vancomycin-resistant enterococci isolated in European medical centers (2005). *BMC Infect. Dis.* **2007**, *7* (1), 29.
100. Pirri, G.; Giuliani, A.; Nicoletto, S.; Pizzuto, L.; Rinaldi, A., Lipopeptides as anti-infectives: a practical perspective. *Open Life Sci.* **2009**, *4* (3), 258-273.
101. Mojsoska, B.; Zuckermann, R. N.; Jenssen, H., Structure-Activity Relationship Study of Novel Peptoids That Mimic the Structure of Antimicrobial Peptides. *Antimicrob. Agents Chemother.* **2015**, *59* (7), 4112-4120.
102. Molchanova, N.; Hansen, P. R.; Franzyk, H., Advances in Development of Antimicrobial Peptidomimetics as Potential Drugs. *Molecules* **2017**, *22* (9).
103. Ghosh, C.; Haldar, J., Membrane-Active Small Molecules: Designs Inspired by Antimicrobial Peptides. *ChemMedChem* **2015**, *10* (10), 1606-1624.
104. Kuppusamy, R.; Willcox, M.; Black, D. S.; Kumar, N., Short Cationic Peptidomimetic Antimicrobials. *Antibiotics (Basel, Switzerland)* **2019**, *8* (2), 44.
105. Tew, G. N.; Liu, D.; Chen, B.; Doerksen, R. J.; Kaplan, J.; Carroll, P. J.; Klein, M. L.; DeGrado, W. F., *De novo* design of biomimetic antimicrobial polymers. *Proc. Natl. Acad. Sci. U.S.A.* **2002**, *99* (8), 5110-5114.
106. Liu, D.; Choi, S.; Chen, B.; Doerksen, R. J.; Clements, D. J.; Winkler, J. D.; Klein, M. L.; DeGrado, W. F., Nontoxic Membrane-Active Antimicrobial Arylamide Oligomers. *Angew. Chem. Int. Ed.* **2004**, *43* (9), 1158-1162.
107. Tang, H.; Doerksen, R. J.; Tew, G. N., Synthesis of urea oligomers and their antibacterial activity. *Chem. Commun.* **2005**, (12), 1537-1539.
108. Tang, H.; Doerksen, R. J.; Jones, T. V.; Klein, M. L.; Tew, G. N., Biomimetic Facially Amphiphilic Antibacterial Oligomers with Conformationally Stiff Backbones. *Chem. Biol.* **2006**, *13* (4), 427-435.
109. Choi, S.; Isaacs, A.; Clements, D.; Liu, D.; Kim, H.; Scott, R. W.; Winkler, J. D.; DeGrado, W. F., *De novo* design and in vivo activity of conformationally restrained antimicrobial arylamide foldamers. *Proc. Natl. Acad. Sci. U.S.A.* **2009**, *106* (17), 6968-6973.
110. Thaker, H. D.; Sgolastra, F.; Clements, D.; Scott, R. W.; Tew, G. N., Synthetic Mimics of Antimicrobial Peptides from Triaryl Scaffolds. *J. Med. Chem.* **2011**, *54* (7), 2241-2254.

111. Arnt, L.; Breitenkamp, R. B.; Tew, G. N., Facially amphiphilic phenylene ethynyls. *Polym. Adv. Technol.* **2005**, *16* (2-3), 189-194.
112. Arnt, L.; Nüsslein, K.; Tew, G. N., Nonhemolytic abiogenic polymers as antimicrobial peptide mimics. *J. Polym. Sci., Part A: Polym. Chem.* **2004**, *42* (15), 3860-3864.
113. Ishitsuka, Y.; Arnt, L.; Majewski, J.; Frey, S.; Ratajczek, M.; Kjaer, K.; Tew, G. N.; Lee, K. Y. C., Amphiphilic Poly(phenyleneethynylene)s Can Mimic Antimicrobial Peptide Membrane Disordering Effect by Membrane Insertion. *J. Am. Chem. Soc.* **2006**, *128* (40), 13123-13129.
114. Thaker, H. D.; Som, A.; Ayaz, F.; Lui, D.; Pan, W.; Scott, R. W.; Anguita, J.; Tew, G. N., Synthetic Mimics of Antimicrobial Peptides with Immunomodulatory Responses. *J. Am. Chem. Soc.* **2012**, *134* (27), 11088-11091.
115. Thaker, H. D.; Cankaya, A.; Scott, R. W.; Tew, G. N., Role of Amphiphilicity in the Design of Synthetic Mimics of Antimicrobial Peptides with Gram-Negative Activity. *ACS Med. Chem. Lett.* **2013**, *4* (5), 481-485.
116. Fu, T.-h.; Li, Y.; Thaker, H. D.; Scott, R. W.; Tew, G. N., Expedient Synthesis of SMAMPs via Click Chemistry. *ACS Med. Chem. Lett.* **2013**, *4* (9), 841-845.
117. Hickey, S. M.; Ashton, T. D.; Boer, G.; Bader, C. A.; Thomas, M.; Elliott, A. G.; Schmuck, C.; Yu, H. Y.; Li, J.; Nation, R. L.; Cooper, M. A.; Plush, S. E.; Brooks, D. A.; Pfeffer, F. M., Norbornane-based cationic antimicrobial peptidomimetics targeting the bacterial membrane. *Eur. J. Med. Chem.* **2018**, *160*, 9-22.
118. Bucki, R.; Niemirowicz, K.; Wnorowska, U.; Byfield, F. J.; Piktel, E.; Wątek, M.; Janmey, P. A.; Savage, P. B., Bactericidal Activity of Ceragenin CSA-13 in Cell Culture and in an Animal Model of Peritoneal Infection. *Antimicrob. Agents Chemother.* **2015**, *59* (10), 6274-6282.
119. Leszczyńska, K.; Namiot, A.; Cruz, K.; Byfield, F. J.; Won, E.; Mendez, G.; Sokołowski, W.; Savage, P. B.; Bucki, R.; Janmey, P. A., Potential of ceragenin CSA-13 and its mixture with pluronic F-127 as treatment of topical bacterial infections. *J. Appl. Microbiol.* **2011**, *110* (1), 229-238.
120. Saha, S.; Savage, P. B.; Bal, M., Enhancement of the efficacy of erythromycin in multiple antibiotic-resistant gram-negative bacterial pathogens. *J. Appl. Microbiol.* **2008**, *105* (3), 822-828.
121. Henderson, L. C.; Li, J.; Nation, R. L.; Velkov, T.; Pfeffer, F. M., Developing an anion host for lipid A binding and antibacterial activity. *Chem. Commun.* **2010**, *46* (18), 3197-3199.
122. Hickey, S. M.; Ashton, T. D.; White, J. M.; Li, J.; Nation, R. L.; Yu, H. Y.; Elliott, A. G.; Butler, M. S.; Huang, J. X.; Cooper, M. A.; Pfeffer, F. M., Synthesis of norbornane bisether antibiotics via silver-mediated alkylation. *RSC Advances* **2015**, *5* (36), 28582-28596.
123. Hickey, S. M.; Ashton, T. D.; Khosa, S. K.; Robson, R. N.; White, J. M.; Li, J.; Nation, R. L.; Yu, H. Y.; Elliott, A. G.; Butler, M. S.; Huang, J. X.; Cooper, M. A.; Pfeffer, F. M., Synthesis and evaluation of cationic norbornanes as peptidomimetic antibacterial agents. *Org. Biomol. Chem.* **2015**, *13* (22), 6225-6241.
124. Savage, Paul B., Design, Synthesis and Characterization of Cationic Peptide and Steroid Antibiotics. *Eur. J. Org. Chem.* **2002**, *2002* (5), 759-768.
125. Lai, X.-Z.; Feng, Y.; Pollard, J.; Chin, J. N.; Rybak, M. J.; Bucki, R.; Epan, R. F.; Epan, R. M.; Savage, P. B., Ceragenins: Cholic Acid-Based Mimics of Antimicrobial Peptides. *Acc. Chem. Res.* **2008**, *41* (10), 1233-1240.
126. Li, C.; Lewis, M. R.; Gilbert, A. B.; Noel, M. D.; Scoville, D. H.; Allman, G. W.; Savage, P. B., Antimicrobial activities of amine- and guanidine-functionalized cholic acid derivatives. *Antimicrob. Agents Chemother.* **1999**, *43* (6), 1347-1349.
127. Tew, G. N.; Scott, R. W.; Klein, M. L.; DeGrado, W. F., De Novo Design of Antimicrobial Polymers, Foldamers, and Small Molecules: From Discovery to Practical Applications. *Acc. Chem. Res.* **2010**, *43* (1), 30-39.
128. U.S. National Library of Medicine. <https://clinicaltrials.gov/ct2/results?cond=&term=brilacidin&cntry=&state=&city=&dist=> (accessed 13.06.2022).
129. Haug, B. E.; Stensen, W.; Kalaaji, M.; Rekdal, Ø.; Svendsen, J. S., Synthetic Antimicrobial Peptidomimetics with Therapeutic Potential. *J. Med. Chem.* **2008**, *51* (14), 4306-4314.
130. Laulund, A. S.; Schwartz, F. A.; Christophersen, L.; Høiby, N.; Svendsen, J. S. M.; Stensen, W.; Thomsen, K.; Cavanagh, J. P.; Moser, C., Lactoferricin-inspired peptide AMC-109 augments the

effect of ciprofloxacin against *Pseudomonas aeruginosa* biofilm in chronic murine wounds. *J. Glob. Antimicrob. Resist.* **2022**, *29*, 185-193.

131. DeGrado, W. F. L., Dahui; Scott, Richard W.; Xu, Yongjiang; Tang, Haizhong; Korczak, Bozena Synthetic Mimetics Of Host Defense And Uses Thereof. US 2010/0105703 A1, **2010**.

132. Isaksson, J.; Brandsdal, B. O.; Engqvist, M.; Flaten, G. E.; Svendsen, J. S. M.; Stensen, W., A Synthetic Antimicrobial Peptidomimetic (LTX 109): Stereochemical Impact on Membrane Disruption. *J. Med. Chem.* **2011**, *54* (16), 5786-5795.

133. Andersson, D. I.; Hughes, D.; Kubicek-Sutherland, J. Z., Mechanisms and consequences of bacterial resistance to antimicrobial peptides. *Drug Resist Updat* **2016**, *26*, 43-57.

134. Maria-Neto, S.; de Almeida, K. C.; Macedo, M. L. R.; Franco, O. L., Understanding bacterial resistance to antimicrobial peptides: From the surface to deep inside. *Biochim. Biophys. Acta* **2015**, *1848* (11, Part B), 3078-3088.

135. Devine, D. A.; Hancock, R. E., Cationic peptides: distribution and mechanisms of resistance. *Curr. Pharm. Des.* **2002**, *8* (9), 703-714.

136. Yount, N. Y.; Yeaman, M. R., Peptide antimicrobials: cell wall as a bacterial target. *Ann. N. Y. Acad. Sci.* **2013**, *1277*, 127-138.

137. Lofton, H.; Pranting, M.; Thulin, E.; Andersson, D. I., Mechanisms and Fitness Costs of Resistance to Antimicrobial Peptides LL-37, CNY100HL and Wheat Germ Histones. *PLOS ONE* **2013**, *8* (7), e68875.

138. Makarova, O.; Johnston, P.; Rodriguez-Rojas, A.; El Shazely, B.; Morales, J. M.; Rolff, J., Genomics of experimental adaptation of *Staphylococcus aureus* to a natural combination of insect antimicrobial peptides. *Sci. Rep.* **2018**, *8* (1), 15359.

139. Shin, J. M.; Gwak, J. W.; Kamarajan, P.; Fenno, J. C.; Rickard, A. H.; Kapila, Y. L., Biomedical applications of nisin. *J. Appl. Microbiol.* **2016**, *120* (6), 1449-1465.

140. Wang, K.-L.; Wu, Z.-H.; Wang, Y.; Wang, C.-Y.; Xu, Y., Mini-Review: Antifouling Natural Products from Marine Microorganisms and Their Synthetic Analogs. *Mar. Drugs* **2017**, *15* (9), 266.

141. Hakim, M. L.; Nugroho, B.; Nurrohman, M. N.; Suastika, I. K.; Utama, I. K. A. P., Investigation of fuel consumption on an operating ship due to biofouling growth and quality of anti-fouling coating. *IOP Conf. Ser. Earth Environ. Sci.* **2019**, *339* (1), 012037.

142. Shao, C.-L.; Xu, R.-F.; Wang, C.-Y.; Qian, P.-Y.; Wang, K.-L.; Wei, M.-Y., Potent Antifouling Marine Dihydroquinolin-2(1H)-one-Containing Alkaloids from the Gorgonian Coral-Derived Fungus *Scopulariopsis* sp. *Mar. Biotechnol.* **2015**, *17* (4), 408-415.

143. Schnurr, R. E. J.; Walker, T. R., Marine Transportation and Energy Use. In *Reference Module in Earth Systems and Environmental Sciences*, Elsevier: 2019.

144. Chen, C.; Tao, H.; Chen, W.; Yang, B.; Zhou, X.; Luo, X.; Liu, Y., Recent advances in the chemistry and biology of azaphilones. *RSC Advances* **2020**, *10* (17), 10197-10220.

145. Hussain, H. A.-S., Abdullah M.; Schulz, Barbara; Steinert, Michael; Khan, Ajmal; Green, Ivan R.; Ahmed, Ishtiaq, A fruitful decade for fungal polyketides from 2007 to 2016: Antimicrobial activity, chemotaxonomy and chemodiversity. *Future Med. Chem.* **2017**, *9* (14), 1631-1648.

146. Gao, J.-M.; Yang, S.-X.; Qin, J.-C., Azaphilones: Chemistry and Biology. *Chem. Rev.* **2013**, *113* (7), 4755-4811.

147. Osmanova, N.; Schultze, W.; Ayoub, N., Azaphilones: a class of fungal metabolites with diverse biological activities. *Phytochem. Rev.* **2010**, *9* (2), 315-342.

148. Stadler, M.; Anke, H.; Dekermendjian, K.; Reiss, R.; Sterner, O.; Witt, R., Novel Bioactive Azaphilones from Fruit Bodies and Mycelial Cultures of the Ascomycete *Bulgaria inquinans* (Fr.). *Nat. Prod. Lett.* **1995**, *7* (1), 7-14.

149. Wei, W.-G.; Yao, Z.-J., Synthesis Studies toward Chloroazaphilone and Vinylogous γ -Pyridones: Two Common Natural Product Core Structures. *J. Org. Chem.* **2005**, *70* (12), 4585-4590.

150. Chong, R.; King, R. R.; Whalley, W. B., The synthesis of sclerotiorin and of an analogue of rotiorin. *J. Chem. Soc. D* **1969**, (24), 1512-1513.

151. Chong, R.; King, R. R.; Whalley, W. B., The chemistry of fungi. Part LXI. The synthesis of (\pm)-sclerotiorin, of (\pm)-4,6-dimethylocta-trans-2,trans-4-dienoic acid, and of an analogue of rotiorin. *J. Chem. Soc. C* **1971**, (0), 3566-3571.

152. Suzuki, T.; Tanemura, K.; Okada, C.; Arai, T. L. K.; Awaji, A.; Shimizu, T.; Horaguchi, T., Synthesis of 7 - acetyloxy - 3,7 - dimethyl - 7,8 - dihydro - 6H - isochromene - 6,8 - dione and its analogues. *J. Heterocycl. Chem.* **2001**, *38* (6), 1409-1418.
153. Zhu, J.; Germain, A. R.; Porco Jr., J. A., Synthesis of Azaphilones and Related Molecules by Employing Cycloisomerization of o-Alkynylbenzaldehydes. *Angew. Chem. Int. Ed.* **2004**, *43* (10), 1239-1243.
154. Blanc, P. J.; Laussac, J. P.; Le Bars, J.; Le Bars, P.; Loret, M. O.; Pareilleux, A.; Prome, D.; Prome, J. C.; Santerre, A. L.; Goma, G., Characterization of monascidin A from *Monascus* as citrinin. *Int. J. Food Microbiol.* **1995**, *27* (2-3), 201-213.
155. Park, S. Y.; Kim, R.; Ryu, C. M.; Choi, S. K.; Lee, C. H.; Kim, J. G.; Park, S. H., Citrinin, a mycotoxin from *Penicillium citrinum*, plays a role in inducing motility of *Paenibacillus polymyxa*. *FEMS Microbiol. Ecol.* **2008**, *65* (2), 229-237.
156. Chai, Y.-J.; Cui, C.-B.; Li, C.-W.; Wu, C.-J.; Tian, C.-K.; Hua, W., Activation of the Dormant Secondary Metabolite Production by Introducing Gentamicin-Resistance in a Marine-Derived *Penicillium purpurogenum* G59. *Mar. Drugs* **2012**, *10* (3).
157. Guo, Z.; Cheng, F.; Zou, K.; Wang, J.; She, Z.; Lin, Y., Secondary metabolites from the mangrove endophytic fungus *Penicillium* sp. (SBE-8). *Nat Prod Commun* **2009**, *4* (11), 1481-1483.
158. Chien, M. M.; Schiff, P. L., Jr.; Slatkin, D. J.; Knapp, J. E., Metabolites of aspergilli. III. The isolation of citrinin, dihydrocitrinone and sclerin from *Aspergillus carneus*. *Lloydia* **1977**, *40* (3), 301-302.
159. Abou-Zeid, A., Review on citrinin: synthetic methods, molecular biosynthesis and effect of plant extracts. *Br. microbiol. res. j.* **2012**, *2*, 108-122.
160. Hetherington, A. C. R., H., Biochemistry of microorganisms. XIV. Production and chemical constitution of a new yellow coloring matter, citrinin, produced from dextrose by *Penicillium citrinum*. *Trans. Roy. Soc. (London)* **1931**, *B220*, 269-296.
161. Mehta, P. P.; Whalley, W. B., 704. The chemistry of fungi. Part XLII. The absolute configuration of citrinin. *J. Chem. Soc. (Resumed)* **1963**, (0), 3777-3779.
162. Hill, R. K.; Gardella, L. A., The Absolute Configuration of Citrinin. *J. Org. Chem.* **1964**, *29* (3), 766-767.
163. Kováč, Š.; Nemeč, P.; Betina, V.; Balan, J., Chemical Structure of Citrinin. *Nature* **1961**, *190* (4781), 1104-1105.
164. Rodig, O. R.; Shiro, M.; Fernando, Q., The crystal and molecular structure of citrinin. *J. Chem. Soc. D* **1971**, (23), 1553-1554.
165. Clark, B. R.; Capon, R. J.; Lacey, E.; Tennant, S.; Gill, J. H., Citrinin revisited: from monomers to dimers and beyond. *Org. Biomol. Chem.* **2006**, *4* (8), 1520-1528.
166. Tabata, S.; Iida, K.; Kimura, K.; Iwasaki, Y.; Nakazato, M.; Kamata, K.; Hirokado, M., [Investigation of ochratoxin a, B and citrinin contamination in various commercial foods]. *Shokuhin Eiseigaku Zasshi* **2008**, *49* (2), 111-115.
167. Bräse, S.; Encinas, A.; Keck, J.; Nising, C. F., Chemistry and Biology of Mycotoxins and Related Fungal Metabolites. *Chem. Rev.* **2009**, *109* (9), 3903-3990.
168. Liu, H.-C.; Du, L.; Zhu, T.-J.; Li, D.-H.; Geng, M.-Y.; Gu, Q.-Q., Two New Citrinin Dimers from a Volcano Ash-Derived Fungus, *Penicillium citrinum* HGY1-5. *Helv. Chim. Acta* **2010**, *93* (11), 2224-2230.
169. Du, L.; Li, D.; Zhang, G.; Zhu, T.; Ai, J.; Gu, Q., Novel carbon-bridged citrinin dimers from a volcano ash-derived fungus *Penicillium citrinum* and their cytotoxic and cell cycle arrest activities. *Tetrahedron* **2010**, *66* (47), 9286-9290.
170. Du, L.; Liu, H.-C.; Fu, W.; Li, D.-H.; Pan, Q.-M.; Zhu, T.-J.; Geng, M.-Y.; Gu, Q.-Q., Unprecedented Citrinin Trimer Tricitinol B Functions as a Novel Topoisomerase II α Inhibitor. *J. Med. Chem.* **2011**, *54* (16), 5796-5810.
171. Hsiao, Y.; Cheng, M.-J.; Chang, H.-S.; Wu, M.-D.; Hsieh, S.-Y.; Liu, T.-W.; Lin, C.-H.; Yuan, G.-F.; Chen, I.-S., Six new metabolites produced by *Colletotrichum aotearoa* 09F0161, an endophytic fungus isolated from *Bredia oldhamii*. *Nat. Prod. Res.* **2016**, *30* (3), 251-258.
172. Wakana, D.; Hosoe, T.; Itabashi, T.; Okada, K.; de Campos Takaki, G. M.; Yaguchi, T.; Fukushima, K.; Kawai, K.-i., New citrinin derivatives isolated from *Penicillium citrinum*. *J. Nat. Med.* **2006**, *60* (4), 279-284.

173. Xin, Z.-H.; Wang, W.-L.; Zhang, Y.-P.; Xie, H.; Gu, Q.-Q.; Zhu, W.-M., Pennicitrinone D, a new citrinin dimer from the halotolerant fungus *Penicillium notatum* B-52. *J. Antibiot. Res.* **2009**, *62* (4), 225-227.
174. Li, T.-X.; Liu, R.-H.; Wang, X.-B.; Luo, J.; Luo, J.-G.; Kong, L.-Y.; Yang, M.-H., Hypoxia-protective azaphilone adducts from *Peyronellaea glomerata*. *J. Nat. Prod.* **2018**, *81* (5), 1148-1153.
175. Abe, H.; Tango, H.; Kobayashi, T.; Ito, H., Asymmetric total synthesis and revision of absolute configurations of azaphilone derivative felinone A. *Tetrahedron Lett.* **2017**, *58* (45), 4296-4298.
176. Marsini, M. A.; Gowin, K. M.; Pettus, T. R., Total synthesis of (\pm)-mitorubrinic acid. *Org. Lett.* **2006**, *8* (16), 3481-3483.
177. Roesch, K. R.; Larock, R. C., Synthesis of Isoquinolines and Pyridines by the Palladium- and Copper-Catalyzed Coupling and Cyclization of Terminal Acetylenes. *Org. Lett.* **1999**, *1* (4), 553-556.
178. Dyker, G.; Hildebrandt, D.; Liu, J.; Merz, K., Gold(III) Chloride Catalyzed Domino Processes with Isobenzopyrylium Cation Intermediates. *Angew. Chem. Int. Ed.* **2003**, *42* (36), 4399-4402.
179. Achard, M.; Beeler, A. B.; Porco, J. A., Synthesis of Azaphilone-Based Chemical Libraries. *ACS Comb. Sci.* **2012**, *14* (3), 236-244.
180. Pysner, J. B.; Baker Dockrey, S. A.; Benítez, A. R.; Joyce, L. A.; Wiscons, R. A.; Smith, J. L.; Narayan, A. R. H., Stereodivergent, Chemoenzymatic Synthesis of Azaphilone Natural Products. *J. Am. Chem. Soc.* **2019**, *141* (46), 18551-18559.
181. Cartwright, N. J.; Robertson, A.; Whalley, W. B., A Synthesis of Citrinin. *Nature* **1949**, *163* (4133), 94-95.
182. Warren, H. H.; Dougherty, G.; Wallis, E. S., The Synthesis of Dihydrocitrinin and Citrinin. *J. Am. Chem. Soc.* **1949**, *71* (10), 3422-3423.
183. Gore, T. S.; Talavdekar, R. V.; Venkataraman, K., A new partial synthesis of citrinin. *Curr. Sci.* **1950**, *19* (1), 20-21.
184. Warren, H. H.; Dougherty, G.; Wallis, E. S., The Synthesis and Antibiotic Activity of Analogs of Citrinin and Dihydrocitrinin. *J. Am. Chem. Soc.* **1957**, *79* (14), 3812-3815.
185. Barber, J. A.; Staunton, J.; Wilkinson, M. R., A diastereoselective synthesis of the polyketide antibiotic citrinin using toluate anion chemistry. *J. Chem. Soc., Perkin Trans. 1* **1986**, (0), 2101-2109.
186. Regan, A. C.; Staunton, J., Asymmetric synthesis of (+)-citrinin using an ortho-toluato carbanion generated by a chiral base. *J. Chem. Soc., Chem. Commun.* **1987**, (7), 520-521.
187. Rödel, T.; Gerlach, H., Enantioselective synthesis of the polyketide antibiotic (3*R*,4*S*)-(-)-citrinin. *Liebigs Ann. Chem.* **1995**, *1995* (5), 885-888.
188. Byström, S.; Högberg, H.-E.; Norin, T., Chiral synthesis of (2*s*,3*s*,7*s*)-3,7-dimethylpentadecan-2-yl acetate and propionate, potential sex pheromone components of the pine saw-fly neodiprion sertifer (geoff.). *Tetrahedron* **1981**, *37* (12), 2249-2254.
189. Golding, B. T.; Hall, D. R.; Sakrikar, S., Reaction between vicinal diols and hydrogen bromide in acetic acid; synthesis of chiral propylene oxide. *J. Chem. Soc., Perkin Trans. 1* **1973**, (0), 1214-1220.
190. Ohashi, T.; Hosokawa, S., Total Syntheses of Stoloniferol B and Penicitol A, and Structural Revision of Fusaraisochromanone. *Org. Lett.* **2018**, *20* (10), 3021-3024.
191. Shafiq, N.; Arshad, U.; Zarren, G.; Parveen, S.; Javed, I.; Ashraf, A., A Comprehensive Review: Bio-Potential of Barbituric Acid and its Analogues. *Curr. Org. Chem.* **2020**, *24* (2), 129-161.
192. Shonle, H. A.; Moment, A., Some New Hypnotics of the Barbituric Acid Series. *J. Am. Chem. Soc.* **1923**, *45* (1), 243-249.
193. Nielsen, C.; Higgins, J. A.; Spruth, H. C., A Comparative Study on Hypnotics of the Barbituric Acid Series. *J. Pharmacol. Exp. Ther.* **1925**, *26* (5), 371-383.
194. Sandberg, F., Anaesthetic properties of some new N-substituted and N,N'-disubstituted derivatives of 5,5-diallylbarbituric acid. *Acta Physiol. Scand.* **1951**, *24* (1), 7-26.
195. Andrews, P. R.; Jones, G. P.; Lodge, D., Convulsant, anticonvulsant and anaesthetic barbiturates. 5-Ethyl-5-(3'-methyl-but-2'-enyl)-barbituric acid and related compounds. *Eur. J. Pharmacol.* **1979**, *55* (2), 115-120.
196. Ashour, O. M.; Naguib, F. N.; Khalifa, M. M.; Abdel-Raheem, M. H.; Panzica, R. P.; el Kouni, M. H., Enhancement of 5-fluoro-2'-deoxyuridine antitumor efficacy by the uridine phosphorylase inhibitor 5-(benzyloxybenzyl) barbituric acid acyclonucleoside. *Cancer Res.* **1995**, *55* (5), 1092-1098.

197. Kliethermes, C. L.; Metten, P.; Belknap, J. K.; Buck, K. J.; Crabbe, J. C., Selection for pentobarbital withdrawal severity: correlated differences in withdrawal from other sedative drugs. *Brain Res.* **2004**, *1009* (1), 17-25.
198. Archana; Srivastava, V. K.; Kumar, A., Synthesis of some newer derivatives of substituted quinazolinonyl-2-oxo/thiobarbituric acid as potent anticonvulsant agents. *Biorg. Med. Chem.* **2004**, *12* (5), 1257-1264.
199. Singh, P.; Kaur, M.; Verma, P., Design, synthesis and anticancer activities of hybrids of indole and barbituric acids--identification of highly promising leads. *Bioorg. Med. Chem. Lett.* **2009**, *19* (11), 3054-3058.
200. Dhorajiya, B. D.; Dholakiya, B. Z.; Mohareb, R. M., Hybrid probes of aromatic amine and barbituric acid: highly promising leads for anti-bacterial, anti-fungal and anti-cancer activities. *Med. Chem. Res.* **2014**, *23* (9), 3941-3952.
201. Wong, O.; McKeown, R. H., Substituent effects on partition coefficients of barbituric acids. *J. Pharm. Sci.* **1988**, *77* (11), 926-932.
202. Ashnagar, A.; Gharib naseri, N.; Sheeri, B., Novel Synthesis of Barbiturates. *Chin. J. Chem.* **2007**, *25* (3), 382-384.
203. Huang, H.-M.; Procter, D. J., Radical–Radical Cyclization Cascades of Barbiturates Triggered by Electron-Transfer Reduction of Amide-Type Carbonyls. *J. Am. Chem. Soc.* **2016**, *138* (24), 7770-7775.
204. Neumann, D. M.; Cammarata, A.; Backes, G.; Palmer, G. E.; Jursic, B. S., Synthesis and antifungal activity of substituted 2,4,6-pyrimidinetrione carbaldehyde hydrazones. *Biorg. Med. Chem.* **2014**, *22* (2), 813-826.
205. Bojarski, J. T.; Mokrosz, J. L.; Bartoń, H. J.; Paluchowska, M. H., Recent Progress in Barbituric Acid Chemistry. In *Adv. Heterocycl. Chem.*, Katritzky, A. R., Ed. Academic Press: 1985; Vol. 38, pp 229-297.
206. Jursic, B. S., A simple method for knoevenagel condensation of α,β -conjugated and aromatic aldehydes with barbituric acid. *J. Heterocycl. Chem.* **2001**, *38* (3), 655-657.
207. Kotha, S.; Deb, A. C.; Kumar, R. V., Spiro-annulation of barbituric acid derivatives and its analogs by ring-closing metathesis reaction. *Bioorg. Med. Chem. Lett.* **2005**, *15* (4), 1039-1043.
208. Su, M.; Xia, D.; Teng, P.; Nimmagadda, A.; Zhang, C.; Odom, T.; Cao, A.; Hu, Y.; Cai, J., Membrane-Active Hydantoin Derivatives as Antibiotic Agents. *J. Med. Chem.* **2017**, *60* (20), 8456-8465.
209. Giménez, D.; Andreu, C.; del Olmo, M.; Varea, T.; Diaz, D.; Asensio, G., The introduction of fluorine atoms or trifluoromethyl groups in short cationic peptides enhances their antimicrobial activity. *Bioorg. Med. Chem.* **2006**, *14* (20), 6971-6978.
210. Kowalski, R. P.; Romanowski, E. G.; Yates, K. A.; Mah, F. S., An Independent Evaluation of a Novel Peptide Mimetic, Brilacidin (PMX30063), for Ocular Anti-infective. *J Ocul Pharmacol Ther* **2016**, *32* (1), 23-27.
211. Teng, P.; Huo, D.; Nimmagadda, A.; Wu, J.; She, F.; Su, M.; Lin, X.; Yan, J.; Cao, A.; Xi, C.; Hu, Y.; Cai, J., Small Antimicrobial Agents Based on Acylated Reduced Amide Scaffold. *J. Med. Chem.* **2016**, *59* (17), 7877-7887.
212. Hansen, T.; Moe, M. K.; Anderssen, T.; Strøm, M. B., Metabolism of small antimicrobial β 2,2-amino acid derivatives by murine liver microsomes. *Eur. J. Drug. Metab. Pharmacokinet.* **2012**, *37* (3), 191-201.
213. Purser, S.; Moore, P. R.; Swallow, S.; Gouverneur, V., Fluorine in medicinal chemistry. *Chem. Soc. Rev.* **2008**, *37* (2), 320-330.
214. Paulsen, M. H.; Karlsen, E. A.; Ausbacher, D.; Anderssen, T.; Bayer, A.; Ochtrop, P.; Hedberg, C.; Haug, T.; Ericson Sollid, J. U.; Strøm, M. B., An amphipathic cyclic tetrapeptide scaffold containing halogenated $\beta^{2,2}$ -amino acids with activity against multiresistant bacteria. *J. Pept. Sci.* **2018**, *24* (10), e3117.
215. Paulsen, M. H.; Ausbacher, D.; Bayer, A.; Engqvist, M.; Hansen, T.; Haug, T.; Anderssen, T.; Andersen, J. H.; Sollid, J. U. E.; Strøm, M. B., Antimicrobial activity of amphipathic α,α -disubstituted β -amino amide derivatives against ESBL – CARBA producing multi-resistant bacteria; effect of halogenation, lipophilicity and cationic character. *Eur. J. Med. Chem.* **2019**, *183*, 111671.

216. Hansen, T.; Alst, T.; Havelkova, M.; Strøm, M. B., Antimicrobial Activity of Small β -Peptidomimetics Based on the Pharmacophore Model of Short Cationic Antimicrobial Peptides. *J. Med. Chem.* **2010**, *53* (2), 595-606.
217. Paulsen, M. H.; Engqvist, M.; Ausbacher, D.; Anderssen, T.; Langer, M. K.; Haug, T.; Morello, G. R.; Liikanen, L. E.; Blencke, H.-M.; Isaksson, J.; Juskewitz, E.; Bayer, A.; Strøm, M. B., Amphipathic Barbiturates as Mimics of Antimicrobial Peptides and the Marine Natural Products Eusynstyelamides with Activity against Multi-resistant Clinical Isolates. *J. Med. Chem.* **2021**.
218. Galluzzi, L.; Karp, M., Intracellular redox equilibrium and growth phase affect the performance of luciferase-based biosensors. *J. Biotechnol.* **2007**, *127* (2), 188-198.
219. Virta, M.; Åkerman, K. E. O.; Saviranta, P.; Oker-Blom, C.; Karp, M. T., Real-time measurement of cell permeabilization with low-molecular-weight membranolytic agents. *J. Antimicrob. Chemother.* **1995**, *36* (2), 303-315.
220. Pandit, K. R.; Klauda, J. B., Membrane models of E. coli containing cyclic moieties in the aliphatic lipid chain. *Biochim Biophys Acta* **2012**, *1818* (5), 1205-1210.
221. Tate, J. V.; Tinnerman II, W. N.; Jurevics, V.; Jeskey, H.; Biehl, E. R., Preparation of 5-substituted benzylbarbituric acids and investigation of the effect of the benzyl and substituted benzyl groups on the acidity of barbituric acid. *J. Heterocycl. Chem.* **1986**, *23* (1), 9-11.
222. Serajuddin, A. T. M., Salt formation to improve drug solubility. *Adv. Drug Del. Rev.* **2007**, *59* (7), 603-616.
223. Gould, P. L., Salt selection for basic drugs. *Int. J. Pharm.* **1986**, *33* (1), 201-217.
224. Pinner, A.; Klein, F., Umwandlung der Nitrile in Imide. *Ber. Dtsch. Chem. Ges.* **1877**, *10* (2), 1889-1897.
225. Pinner, A.; Klein, F., Umwandlung der Nitrile in Imide. *Ber. Dtsch. Chem. Ges.* **1878**, *11* (2), 1475-1487.
226. Pinner, A., Ueber die Umwandlung der Nitrile in Imide. *Ber. Dtsch. Chem. Ges.* **1883**, *16* (2), 1643-1655.
227. Oxley, P.; Partridge, M. W.; Short, W. F., 209. Amidines. Part VII. Preparation of amidines from cyanides, aluminium chloride, and ammonia or amines. *J. Chem. Soc. (Resumed)* **1947**, (0), 1110-1116.
228. Garigipati, R. S., An efficient conversion of nitriles to amidines. *Tetrahedron Lett.* **1990**, *31* (14), 1969-1972.
229. Kieć-Kononowicz, K.; Stadnicka, K.; Mitka, A.; Pękala, E.; Filipek, B.; Sapa, J.; Zygmunt, M., Synthesis, structure and antiarrhythmic properties evaluation of new basic derivatives of 5,5-diphenylhydantoin. *Eur. J. Med. Chem.* **2003**, *38* (6), 555-566.
230. Handzlik, J.; Bojarski, A. J.; Satała, G.; Kubacka, M.; Sadek, B.; Ashoor, A.; Siwek, A.; Więcek, M.; Kucwaj, K.; Filipek, B.; Kieć-Kononowicz, K., SAR-studies on the importance of aromatic ring topologies in search for selective 5-HT₇ receptor ligands among phenylpiperazine hydantoin derivatives. *Eur. J. Med. Chem.* **2014**, *78*, 324-339.
231. Rodgers, T. R.; LaMontagne, M. P.; Markovac, A.; Ash, A. B., Hydantoins as antitumor agents. *J. Med. Chem.* **1977**, *20* (4), 591-594.
232. El-Barbary, A. A.; Khodair, A. I.; Pedersen, E. B.; Nielsen, C., S-Glucosylated hydantoins as new antiviral agents. *J. Med. Chem.* **1994**, *37* (1), 73-77.
233. Cortes, S.; Liao, Z.-K.; Watson, D.; Kohn, H., Effect of structural modification of the hydantoin ring on anticonvulsant activity. *J. Med. Chem.* **1985**, *28* (5), 601-606.
234. Sarges, R.; Schnur, R. C.; Belletire, J. L.; Peterson, M. J., Spiro hydantoin aldose reductase inhibitors. *J. Med. Chem.* **1988**, *31* (1), 230-243.
235. Szymańska, E.; Kieć-Kononowicz, K., Antimycobacterial activity of 5-arylidene aromatic derivatives of hydantoin. *Il Farmaco* **2002**, *57* (5), 355-362.
236. Szymańska, E.; Kieć-Kononowicz, K.; Białecka, A.; Kasprowicz, A., Antimicrobial activity of 5-arylidene aromatic derivatives of hydantoin. Part 2. *Il Farmaco* **2002**, *57* (1), 39-44.
237. Handzlik, J.; Szymańska, E.; Chevalier, J.; Otrębska, E.; Kieć-Kononowicz, K.; Pagès, J.-M.; Alibert, S., Amine-alkyl derivatives of hydantoin: New tool to combat resistant bacteria. *Eur. J. Med. Chem.* **2011**, *46* (12), 5807-5816.

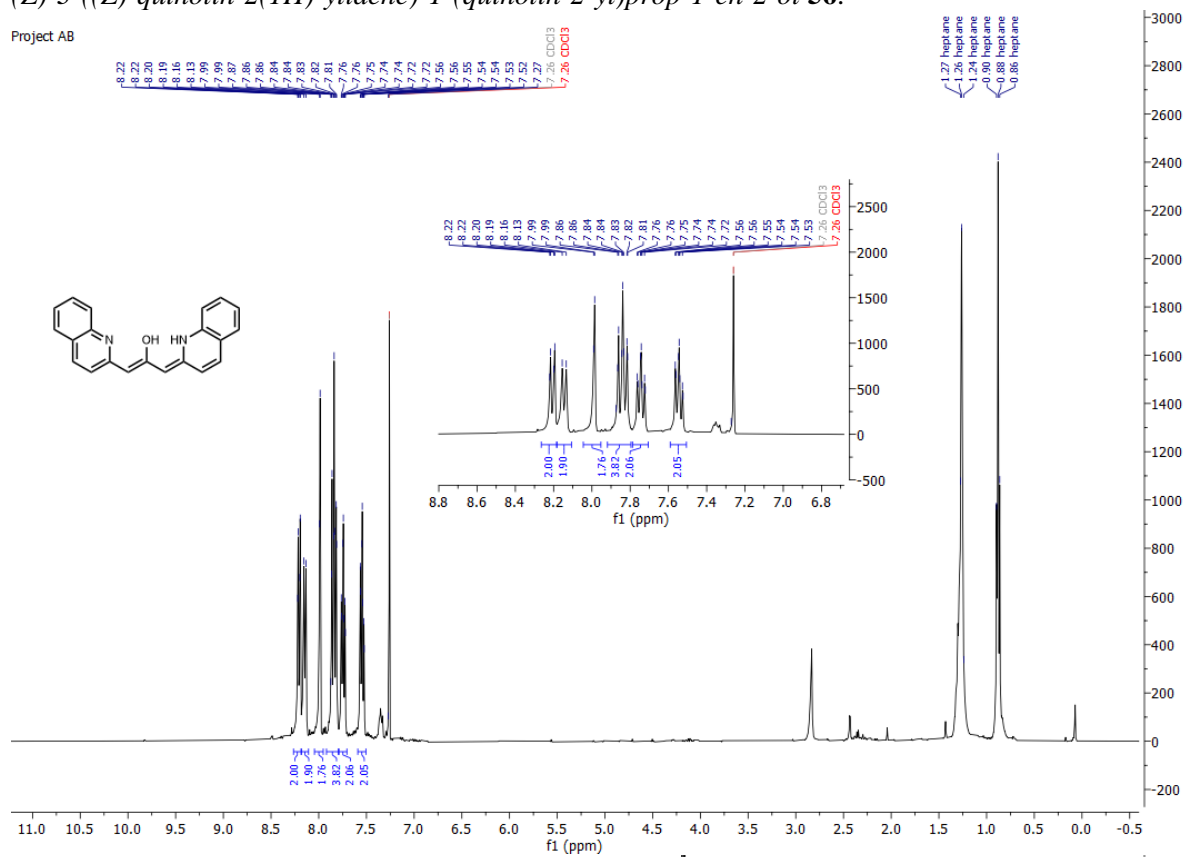
238. Muccioli, G. G.; Fazio, N.; Scriba, G. K. E.; Poppitz, W.; Cannata, F.; Poupaert, J. H.; Wouters, J.; Lambert, D. M., Substituted 2-Thioxoimidazolidin-4-ones and Imidazolidine-2,4-diones as Fatty Acid Amide Hydrolase Inhibitors Templates. *J. Med. Chem.* **2006**, *49* (1), 417-425.
239. Feng, M.; Tang, B.; Liang, S. H.; Jiang, X., Sulfur Containing Scaffolds in Drugs: Synthesis and Application in Medicinal Chemistry. *Curr. Top. Med. Chem.* **2016**, *16* (11), 1200-1216.
240. Pathania, S.; Narang, R. K.; Rawal, R. K., Role of sulphur-heterocycles in medicinal chemistry: An update. *Eur. J. Med. Chem.* **2019**, *180*, 486-508.
241. Bagley, M. C.; Dale, J. W.; Merritt, E. A.; Xiong, X., Thiopeptide Antibiotics. *Chem. Rev.* **2005**, *105* (2), 685-714.
242. Just-Baringo, X.; Albericio, F.; Álvarez, M., Thiopeptide antibiotics: retrospective and recent advances. *Mar. Drugs* **2014**, *12* (1), 317-351.
243. Neu, H. C., β -Lactam Antibiotics: Structural Relationships Affecting in Vitro Activity and Pharmacologic Properties. *Rev. Infect. Dis.* **1986**, *8*, S237-S259.
244. Thaqi, A.; McCluskey, A.; Scott, J. L., A mild Boc deprotection and the importance of a free carboxylate. *Tetrahedron Lett.* **2008**, *49* (49), 6962-6964.
245. Siro, J. G.; Martín, J.; García-Navío, J.; Remuñan, M. J.; Vaquero, J. J., Easy Microwave Assisted Deprotection of N-Boc Derivatives. *Synlett* **1998**, *1998* (02), 147-148.
246. Dandepally, S. R.; Williams, A. L., Microwave-assisted N-Boc deprotection under mild basic conditions using $K_3PO_4 \cdot H_2O$ in MeOH. *Tetrahedron Lett.* **2009**, *50* (9), 1071-1074.
247. Gawinecki, R.; Kolehmainen, E.; Dobosz, R.; Ośmiałowski, B., (1Z,3Z)-3-[Quinolin-2(1H)-ylidene]-1-(quinolin-2-yl)prop-1-en-2-ol: An unexpected most stable tautomer of 1,3-bis(quinolin-2-yl)acetone. *J. Mol. Struct.* **2009**, *930* (1), 78-82.
248. Larson, G. L. F., James L., Ionic and Organometallic-Catalyzed Organosilane Reductions. In *Org. React.*, Wiley: 2010; pp 1-737.
249. DAVIES, B. I., The importance of the geometric mean MIC. *J. Antimicrob. Chemother.* **1990**, *25* (3), 471-472.
250. D'Agostino, L. A. S., Robert Tjin Tham; Niu, Deqiang; McDonald, Joseph John; Zhu, Zhendong; Liu, Haibo; Mazdiyasi, Hormoz; Petter, Russell C.; Singh, Juswinder; Barrague, Matthieu; Gross, Alexandre; Munson, Mark; Harvey, Darren; Scholte, Andrew; Maniar, Sachin Preparation of heteroaryl compounds as inhibitors of protein kinases WO/2014/144737, **2014**.
251. Gadhwal, S.; Baruah, M.; Sandhu, J. S., Microwave Induced Synthesis of Hydrazones and Wolff-Kishner Reduction of Carbonyl Compounds. *Synlett* **1999**, *1999* (10), 1573-1574.
252. Wolfson, A. D., Christina, Glycerol as an alternative green medium for carbonyl compound reductions. *Org. Commun.* **2009**, *2* (2), 34-41.
253. Still, W. C.; Sreekumar, C., α -Alkoxyorganolithium reagents. A new class of configurationally stable carbanions for organic synthesis. *J. Am. Chem. Soc.* **1980**, *102* (3), 1201-1202.
254. Burns, M.; Essafi, S.; Bame, J. R.; Bull, S. P.; Webster, M. P.; Balieu, S.; Dale, J. W.; Butts, C. P.; Harvey, J. N.; Aggarwal, V. K., Assembly-line synthesis of organic molecules with tailored shapes. *Nature* **2014**, *513* (7517), 183-188.
255. Leonori, D.; Aggarwal, V. K., Lithiation–Borylation Methodology and Its Application in Synthesis. *Acc. Chem. Res.* **2014**, *47* (10), 3174-3183.
256. Vickery, E. H.; Pahler, L. F.; Eisenbraun, E. J., Selective O-demethylation of catechol ethers. Comparison of boron tribromide and iodotrimethylsilane. *J. Org. Chem.* **1979**, *44* (24), 4444-4446.
257. Ghiaci, M.; Asghari, J., Dealkylation of Alkyl and Aryl Ethers with $AlCl_3 - NaI$ in the Absence of Solvent. *Synth. Commun.* **1999**, *29* (6), 973-979.
258. Subbaraju, G. V. M., M.; Mohan, H. R.; Suresh, T.; Ivanisevic, I.; Andres, M.; Stephens, K. Key intermediate for the preparation of stilbenes, solid forms of pterostilbene, and methods for making the same. US20110144212A1, **2011**.
259. Hwu, J. R.; Tsay, S. C., Counterattack reagents sodium trimethylsilylanethiolate and hexamethyldisilathiane in the bis-O-demethylation of aryl methyl ethers. *J. Org. Chem.* **1990**, *55* (24), 5987-5991.
260. Johnson, D. H.; Robertson, A.; Whalley, W. B., 580. The chemistry of fungi. Part XIII. Citrinin. *J. Chem. Soc. (Resumed)* **1950**, (0), 2971-2975.
261. Plutschack, M. B.; Pieber, B.; Gilmore, K.; Seeberger, P. H., The Hitchhiker's Guide to Flow Chemistry. *Chem. Rev.* **2017**, *117* (18), 11796-11893.

262. Porta, R.; Benaglia, M.; Puglisi, A., Flow Chemistry: Recent Developments in the Synthesis of Pharmaceutical Products. *Org. Process Res. Dev.* **2016**, *20* (1), 2-25.
263. Yoshida, J.-i.; Nagaki, A.; Yamada, T., Flash Chemistry: Fast Chemical Synthesis by Using Microreactors. *Chem. Eur. J.* **2008**, *14* (25), 7450-7459.
264. Pastre, J. C.; Browne, D. L.; Ley, S. V., Flow chemistry syntheses of natural products. *Chem. Soc. Rev.* **2013**, *42* (23), 8849-8869.
265. Carrera, M.; De Coen, L.; Coppens, M.; Dermaut, W.; Stevens, C. V., A Vilsmeier Chloroformylation by Continuous Flow Chemistry. *Org. Process Res. Dev.* **2020**, *24* (10), 2260-2265.
266. Min, K.-I.; Lee, T.-H.; Park, C. P.; Wu, Z.-Y.; Girault, H. H.; Ryu, I.; Fukuyama, T.; Mukai, Y.; Kim, D.-P., Monolithic and Flexible Polyimide Film Microreactors for Organic Microchemical Applications Fabricated by Laser Ablation. *Angew. Chem. Int. Ed.* **2010**, *49* (39), 7063-7067.
267. van den Broek, S. A. M. W.; Leliveld, J. R.; Becker, R.; Delville, M. M. E.; Nieuwland, P. J.; Koch, K.; Rutjes, F. P. J. T., Continuous Flow Production of Thermally Unstable Intermediates in a Microreactor with Inline IR-Analysis: Controlled Vilsmeier–Haack Formylation of Electron-Rich Arenes. *Org. Process Res. Dev.* **2012**, *16* (5), 934-938.
268. Newman, S. G.; Gu, L.; Lesniak, C.; Victor, G.; Meschke, F.; Abahmane, L.; Jensen, K. F., Rapid Wolff–Kishner reductions in a silicon carbide microreactor. *Green Chem.* **2014**, *16* (1), 176-180.
269. Znidar, D.; O’Kearney-McMullan, A.; Munday, R.; Wiles, C.; Poehlauer, P.; Schmoelzer, C.; Dallinger, D.; Kappe, C. O., Scalable Wolff–Kishner Reductions in Extreme Process Windows Using a Silicon Carbide Flow Reactor. *Org. Process Res. Dev.* **2019**, *23* (11), 2445-2455.
270. Shu, W.; Pellegatti, L.; Oberli, M. A.; Buchwald, S. L., Continuous-Flow Synthesis of Biaryls Enabled by Multistep Solid-Handling in a Lithiation/Borylation/Suzuki–Miyaura Cross-Coupling Sequence. *Angew. Chem. Int. Ed.* **2011**, *50* (45), 10665-10669.
271. Newby, J. A.; Blaylock, D. W.; Witt, P. M.; Pastre, J. C.; Zacharova, M. K.; Ley, S. V.; Browne, D. L., Design and Application of a Low-Temperature Continuous Flow Chemistry Platform. *Org. Process Res. Dev.* **2014**, *18* (10), 1211-1220.
272. Hafner, A.; Filipponi, P.; Piccioni, L.; Meisenbach, M.; Schenkel, B.; Venturoni, F.; Sedelmeier, J., A Simple Scale-up Strategy for Organolithium Chemistry in Flow Mode: From Feasibility to Kilogram Quantities. *Org. Process Res. Dev.* **2016**, *20* (10), 1833-1837.
273. Usutani, H.; Cork, D. G., Effective Utilization of Flow Chemistry: Use of Unstable Intermediates, Inhibition of Side Reactions, and Scale-Up for Boronic Acid Synthesis. *Org. Process Res. Dev.* **2018**, *22* (6), 741-746.
274. Shu, W.; Buchwald, S. L., Enantioselective β -Arylation of Ketones Enabled by Lithiation/Borylation/1,4-Addition Sequence Under Flow Conditions. *Angew. Chem. Int. Ed.* **2012**, *51* (22), 5355-5358.
275. Newby, J. A.; Huck, L.; Blaylock, D. W.; Witt, P. M.; Ley, S. V.; Browne, D. L., Investigation of a Lithium–Halogen Exchange Flow Process for the Preparation of Boronates by Using a Cryo-Flow Reactor. *Chem. Eur. J.* **2014**, *20* (1), 263-271.
276. Hafner, A.; Meisenbach, M.; Sedelmeier, J., Flow Chemistry on Multigram Scale: Continuous Synthesis of Boronic Acids within 1 s. *Org. Lett.* **2016**, *18* (15), 3630-3633.
277. Sedelmeier, J.; Ley, S. V.; Baxendale, I. R.; Baumann, M., KMnO₄-Mediated Oxidation as a Continuous Flow Process. *Org. Lett.* **2010**, *12* (16), 3618-3621.
278. Len, C.; Bruniaux, S.; Delbecq, F.; Parmar, V. S., Palladium-Catalyzed Suzuki–Miyaura Cross-Coupling in Continuous Flow. *Catalysts* **2017**, *7* (5), 146.
279. Stueckler, C.; Hermsen, P.; Ritzen, B.; Vasiliou, M.; Poehlauer, P.; Steinhof, S.; Pelz, A.; Zinganell, C.; Felfer, U.; Boyer, S.; Goldbach, M.; de Vries, A.; Pabst, T.; Winkler, G.; LaVopa, V.; Hecker, S.; Schuster, C., Development of a Continuous Flow Process for a Matteson Reaction: From Lab Scale to Full-Scale Production of a Pharmaceutical Intermediate. *Org. Process Res. Dev.* **2019**, *23* (5), 1069-1077.
280. Kuhwald, C.; Kirschning, A., Matteson Reaction under Flow Conditions: Iterative Homologations of Terpenes. *Org. Lett.* **2021**, *23* (11), 4300-4304.
281. Desrues, T.; Legros, J.; Jubault, P.; Poisson, T., Flow synthesis of an α -amino boronic ester as a key precursor of bortezomib drug. *React. Chem. Eng.* **2022**.
282. Qiu, X.; Li, Y.; Zhou, L.; Chen, P.; Li, F.; Zhang, Y.; Ling, Y., Nickel(II)-Catalyzed Borylation of Alkenyl Methyl Ethers via C–O Bond Cleavage. *Org. Lett.* **2020**, *22* (16), 6424-6428.

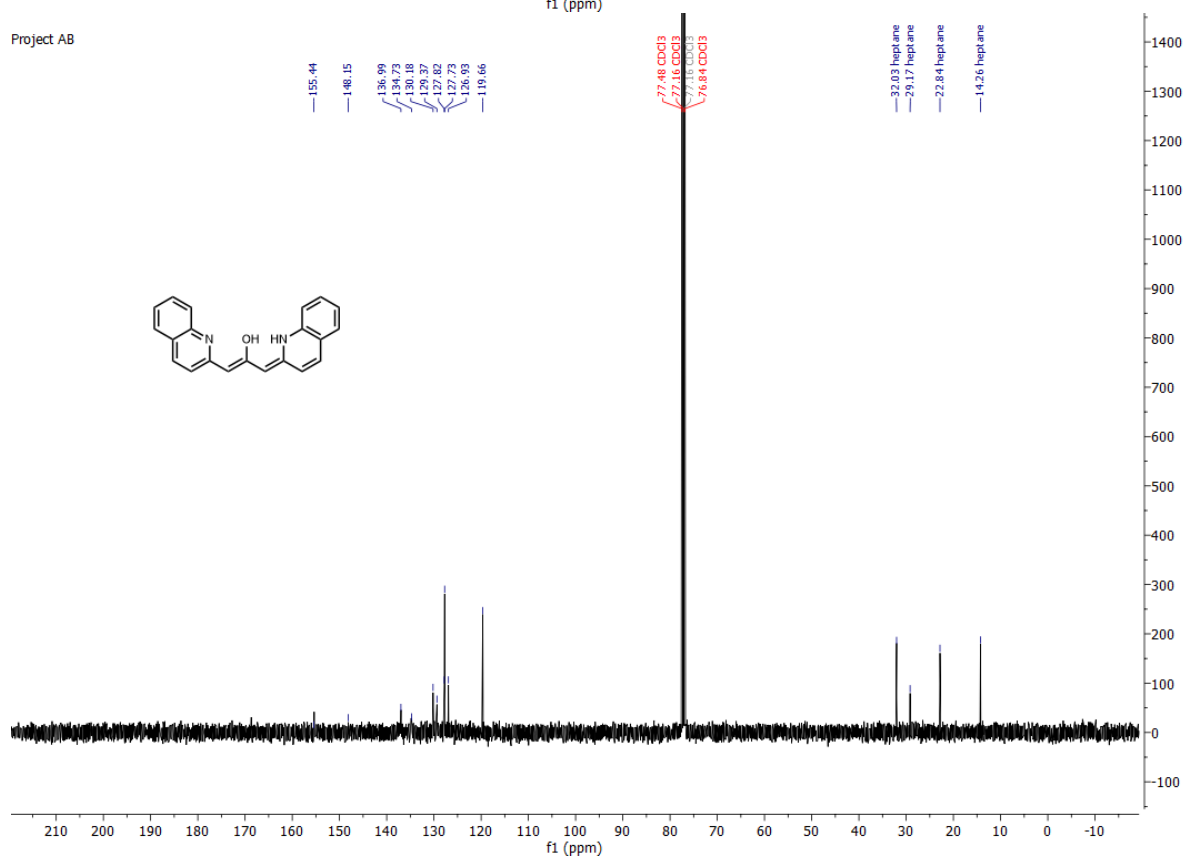
283. Sakata, R.; Soeta, T.; Ukaji, Y., One-Carbon Homologation of Pyrrole Carboxaldehyde via Wittig Reaction and Mild Hydrolysis of Vinyl Ether - Toward the Synthesis of a Sterically Locked Phytochrome Chromophore. *Heterocycles* **2015**, *91* (3), 593-603.
284. Stetter, H.; Rämisch, R. Y., Über die präparative Nutzung der 1,3-Thiazoliumsalzkatalysierten Acyloin- und Benzoin-Bildung; IV1. Herstellung von Acyloinen mit funktionellen Gruppen. *Synthesis* **1981**, *1981* (06), 477-478.

(Z)-3-((*Z*)-quinolin-2(1*H*)-ylidene)-1-(quinolin-2-yl)prop-1-en-2-ol **56**.

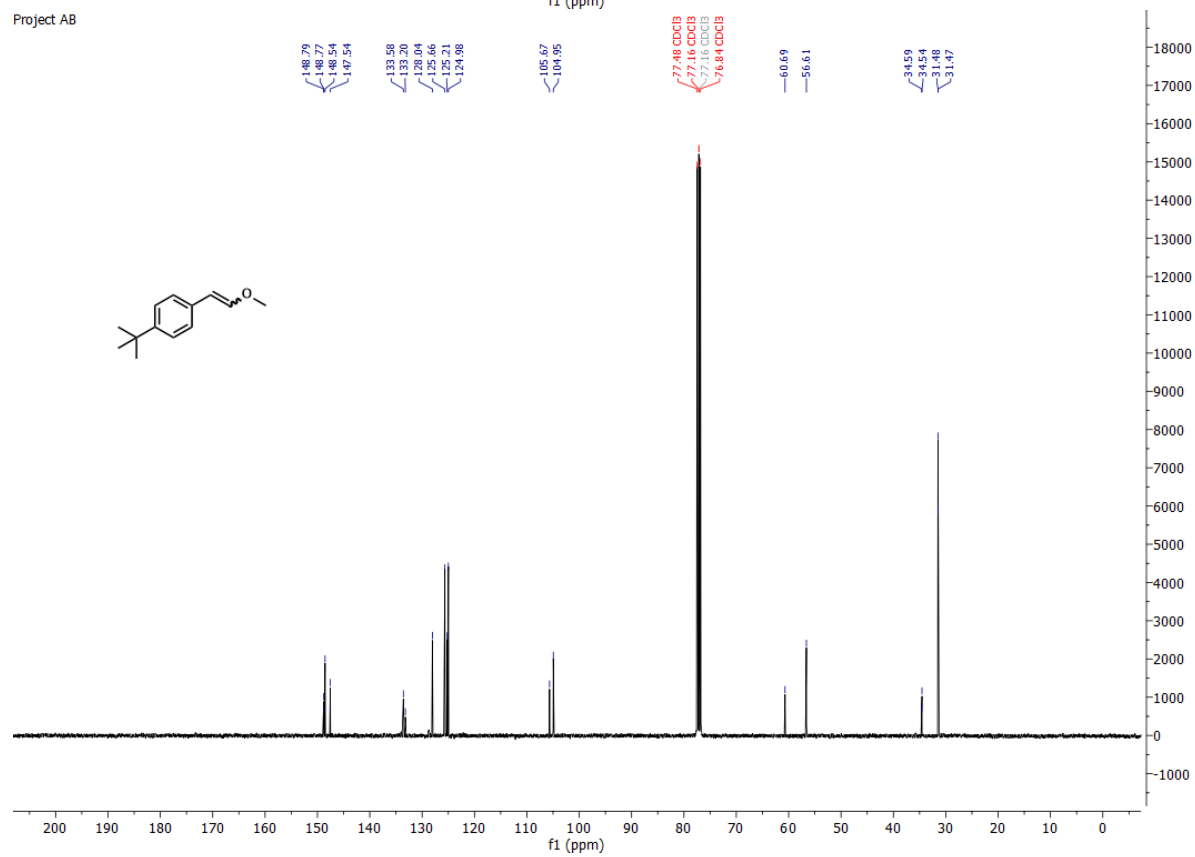
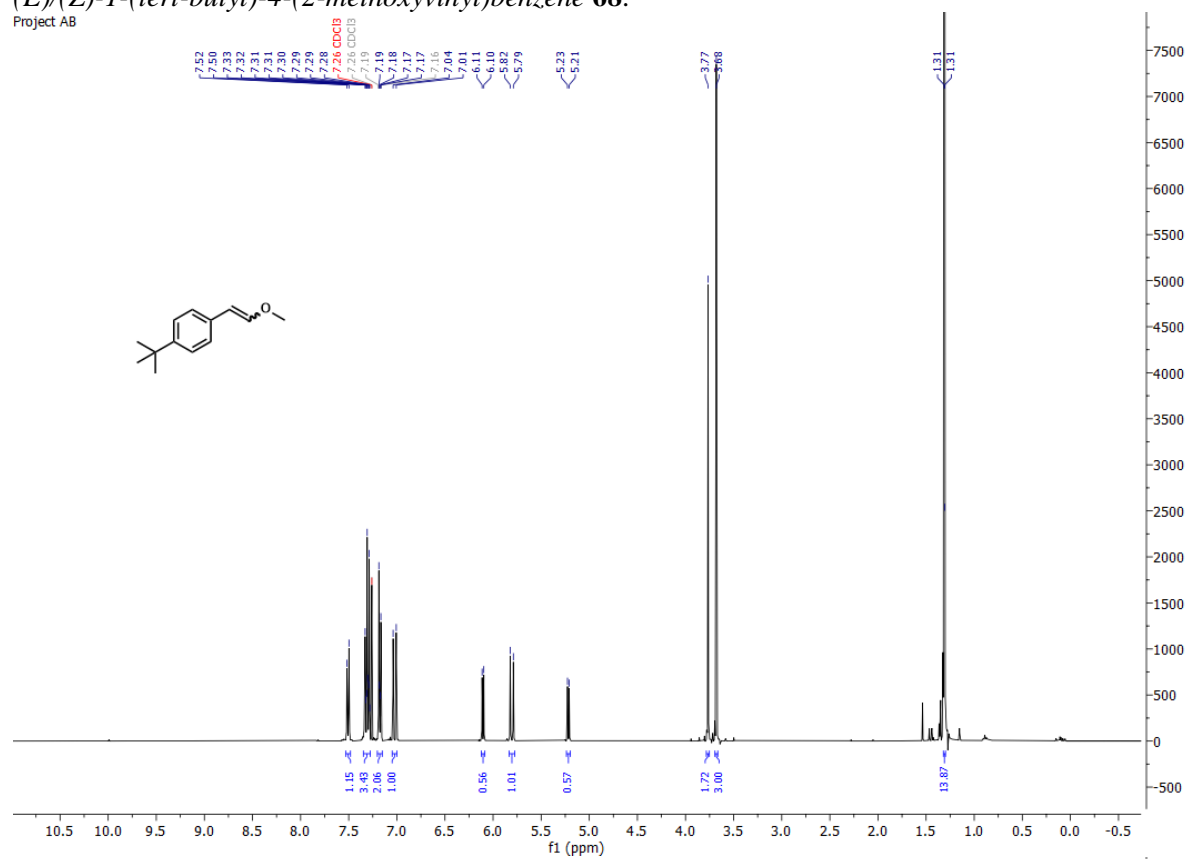
Project AB



Project AB

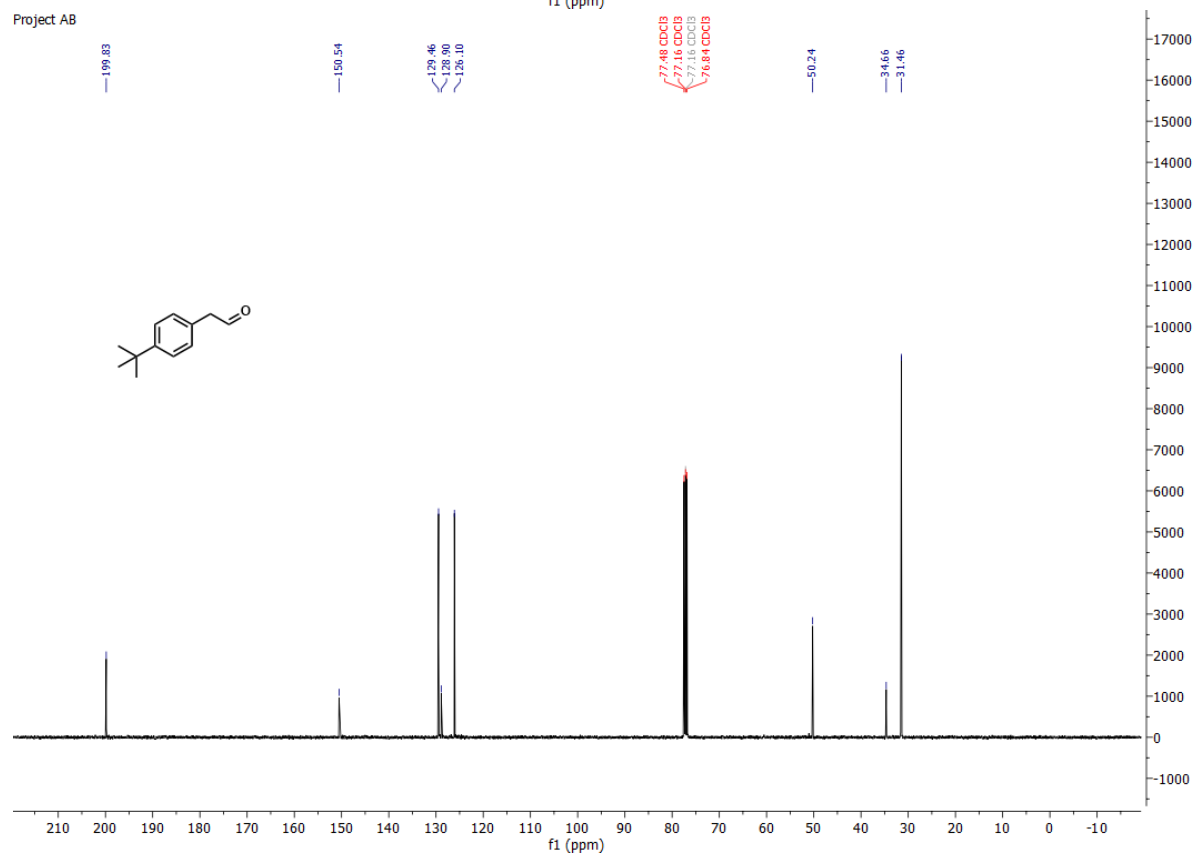
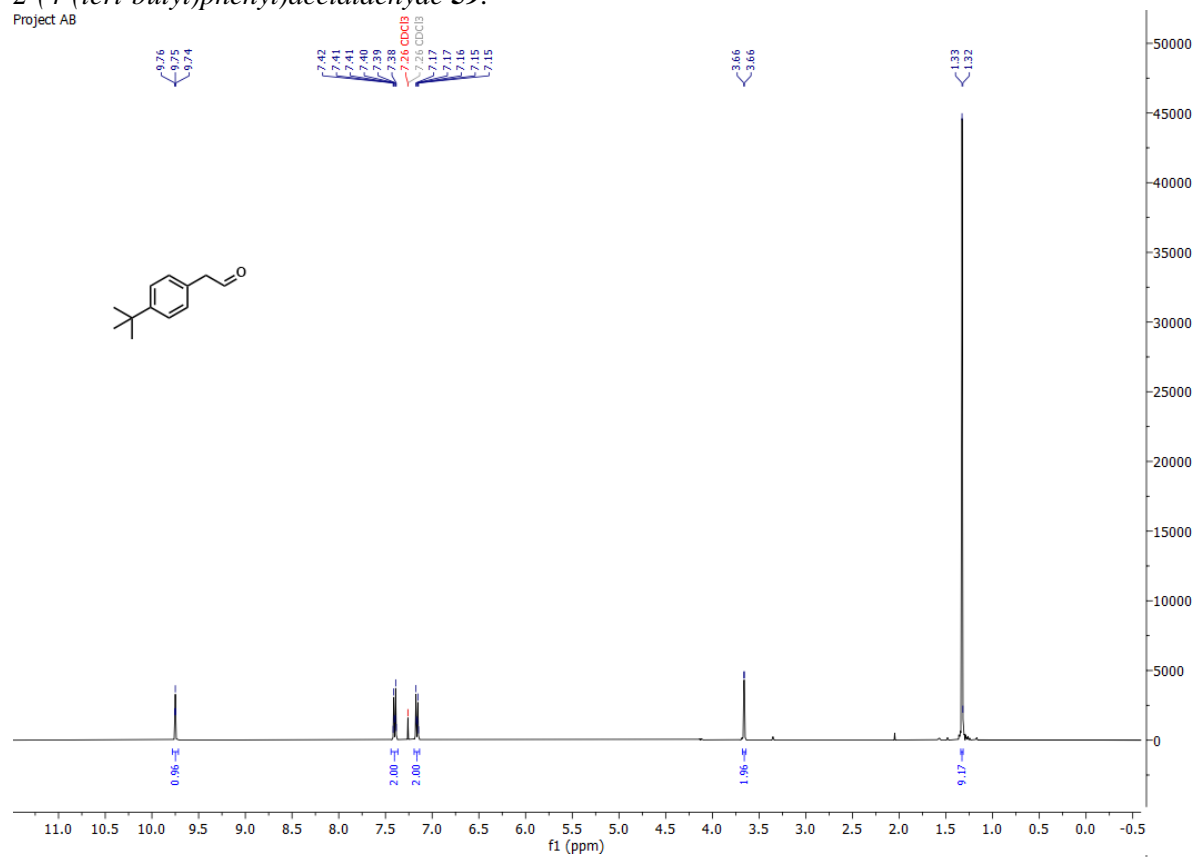


(E)/(Z)-1-(*tert*-butyl)-4-(2-methoxyvinyl)benzene **68**.
Project AB



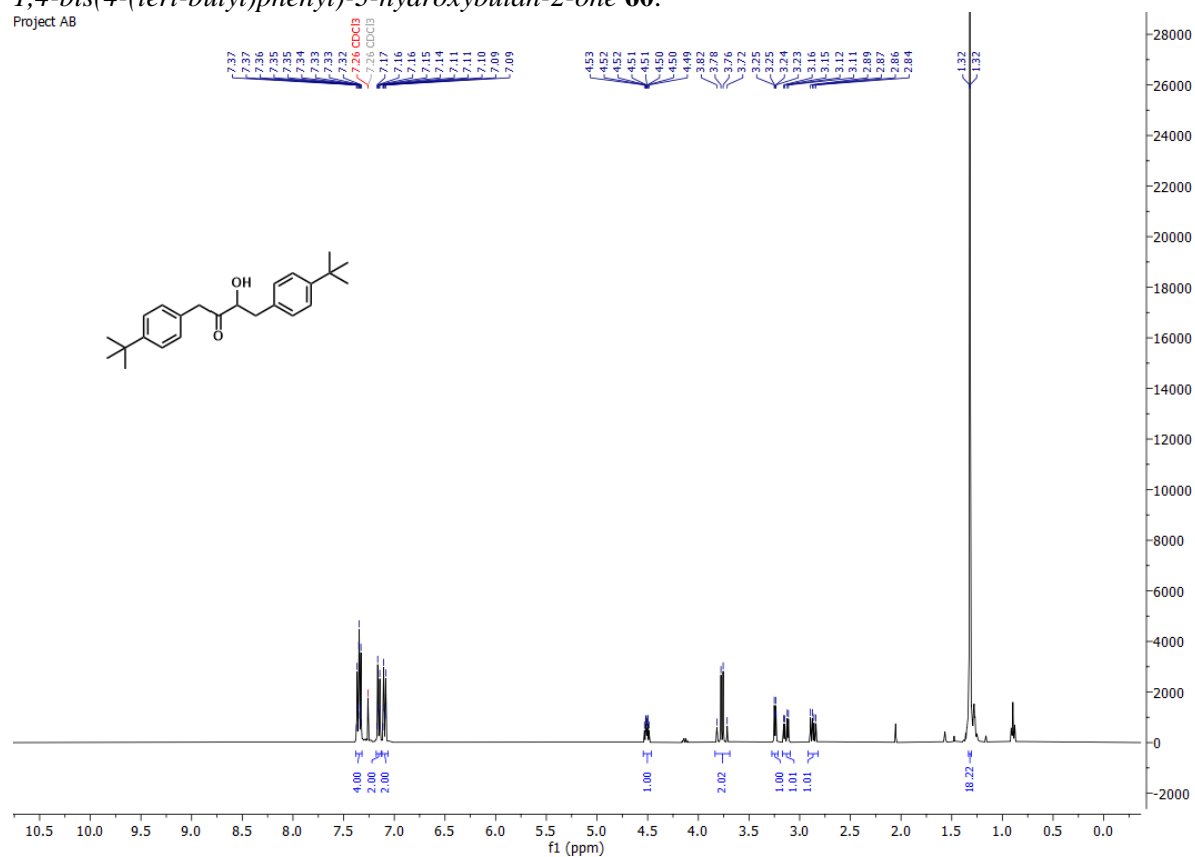
2-(4-(tert-butyl)phenyl)acetaldehyde **59**.

Project AB

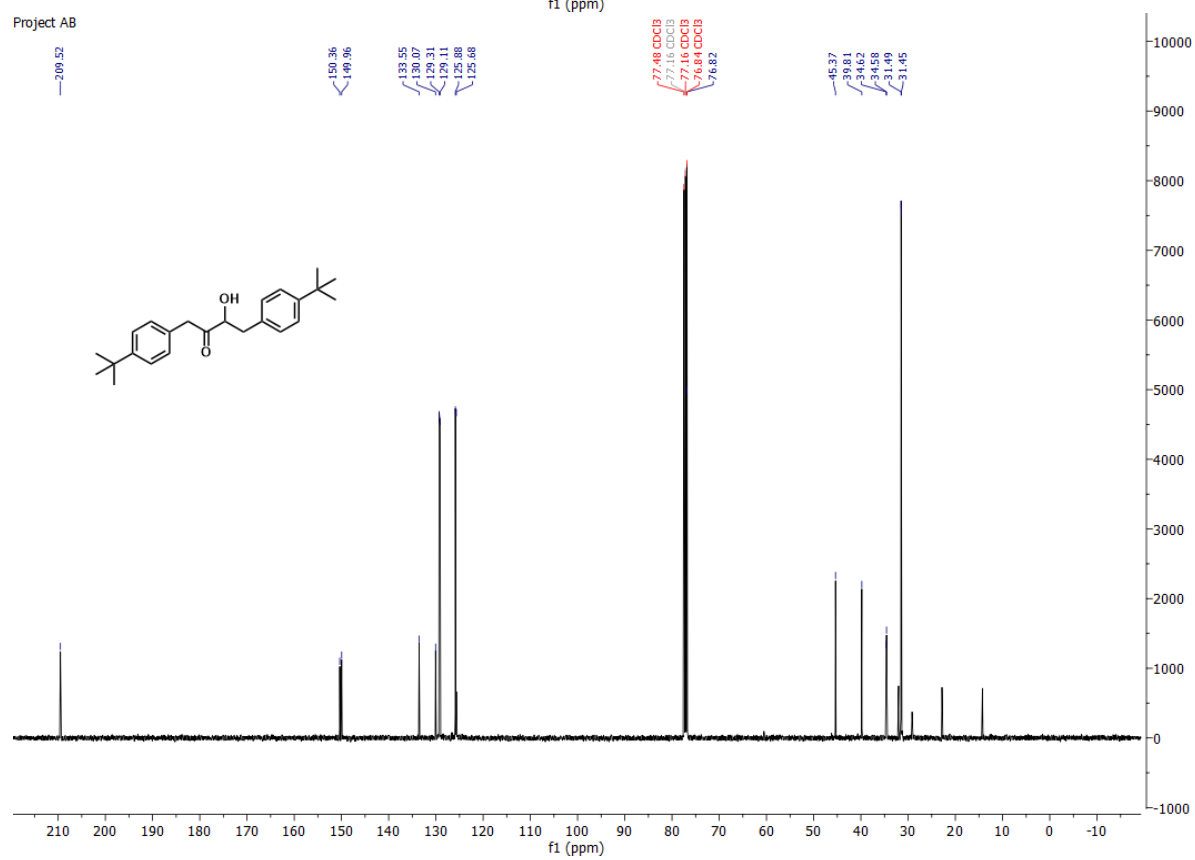


1,4-bis(4-(tert-butyl)phenyl)-3-hydroxybutan-2-one **60**.

Project AB

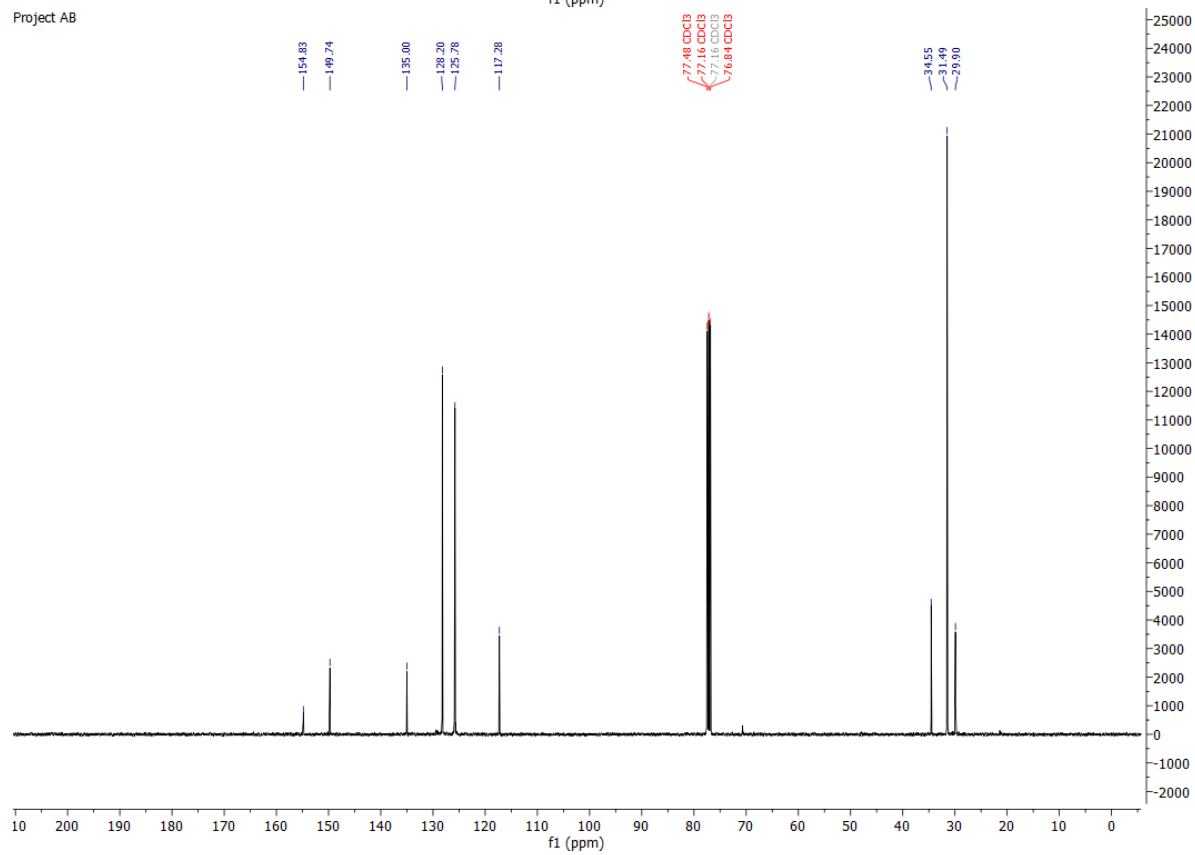
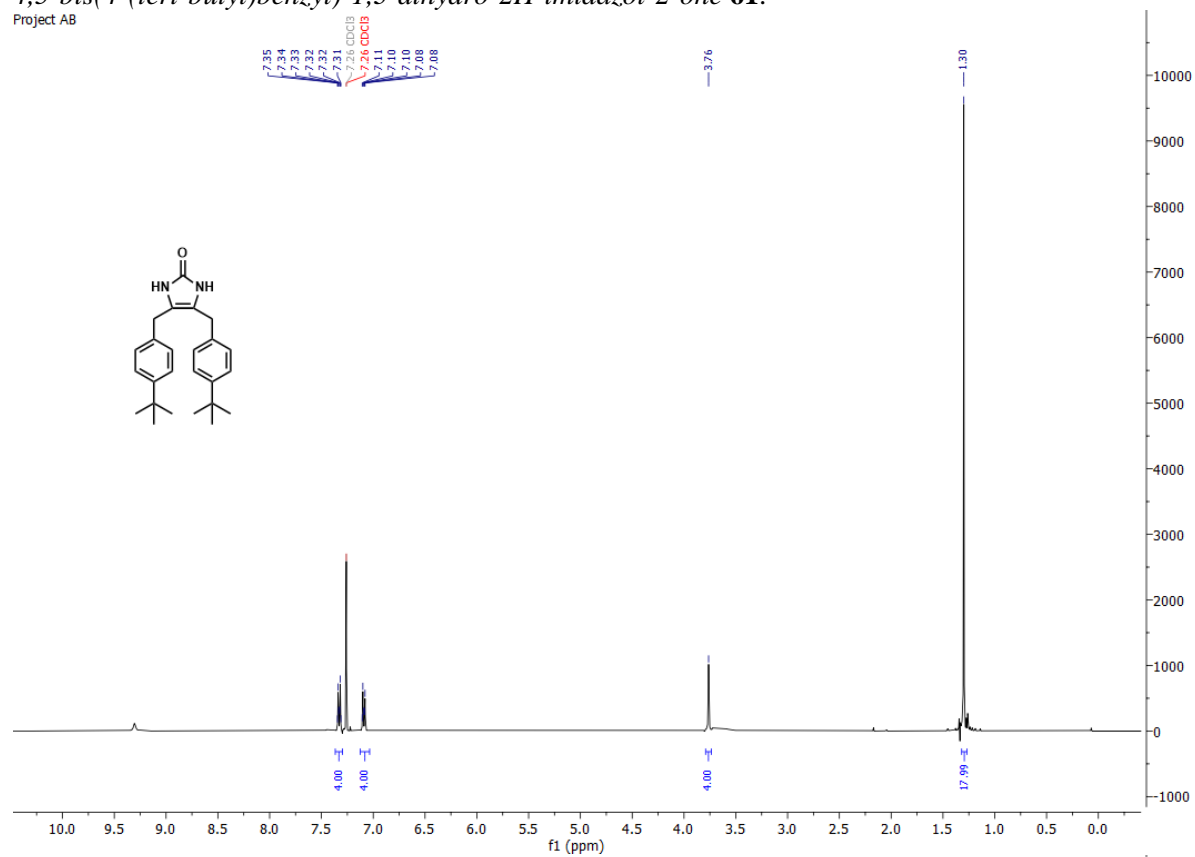


Project AB

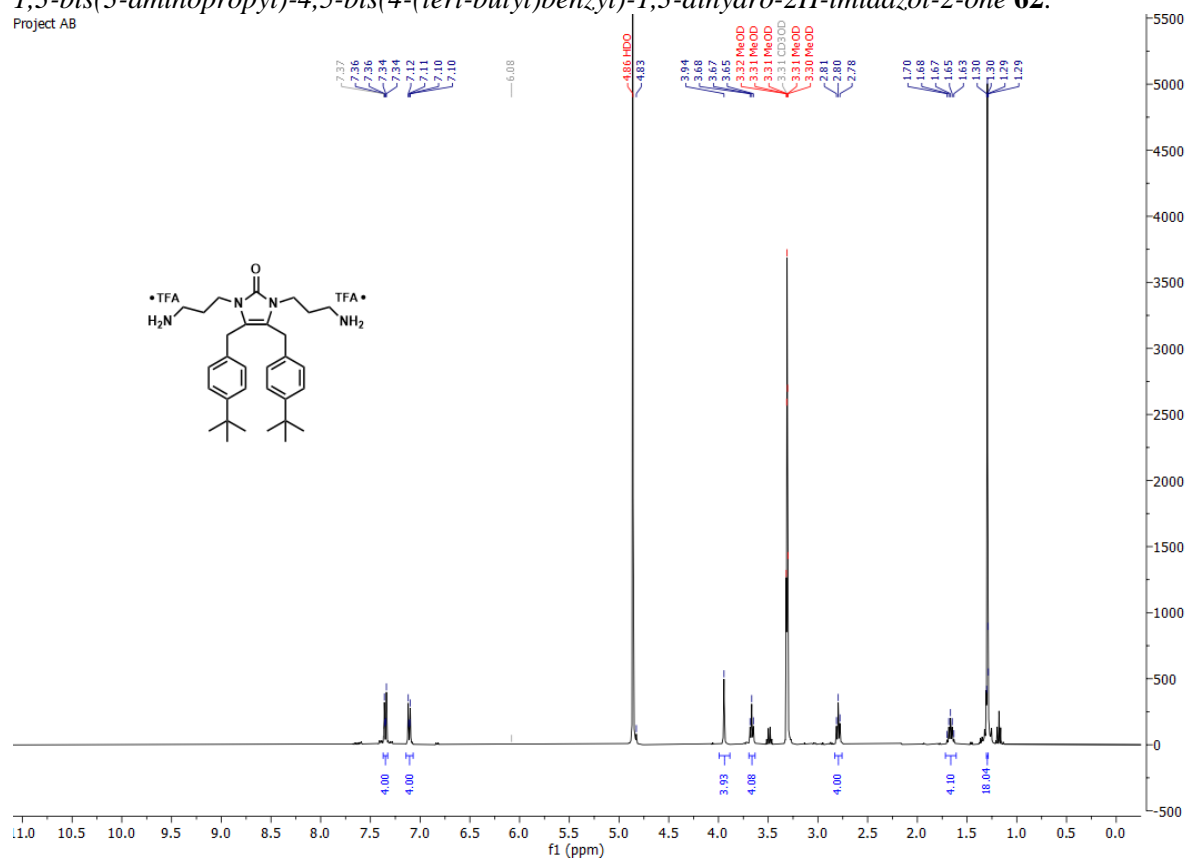


4,5-bis(4-(*tert*-butyl)benzyl)-1,3-dihydro-2H-imidazol-2-one **61**.

Project AB



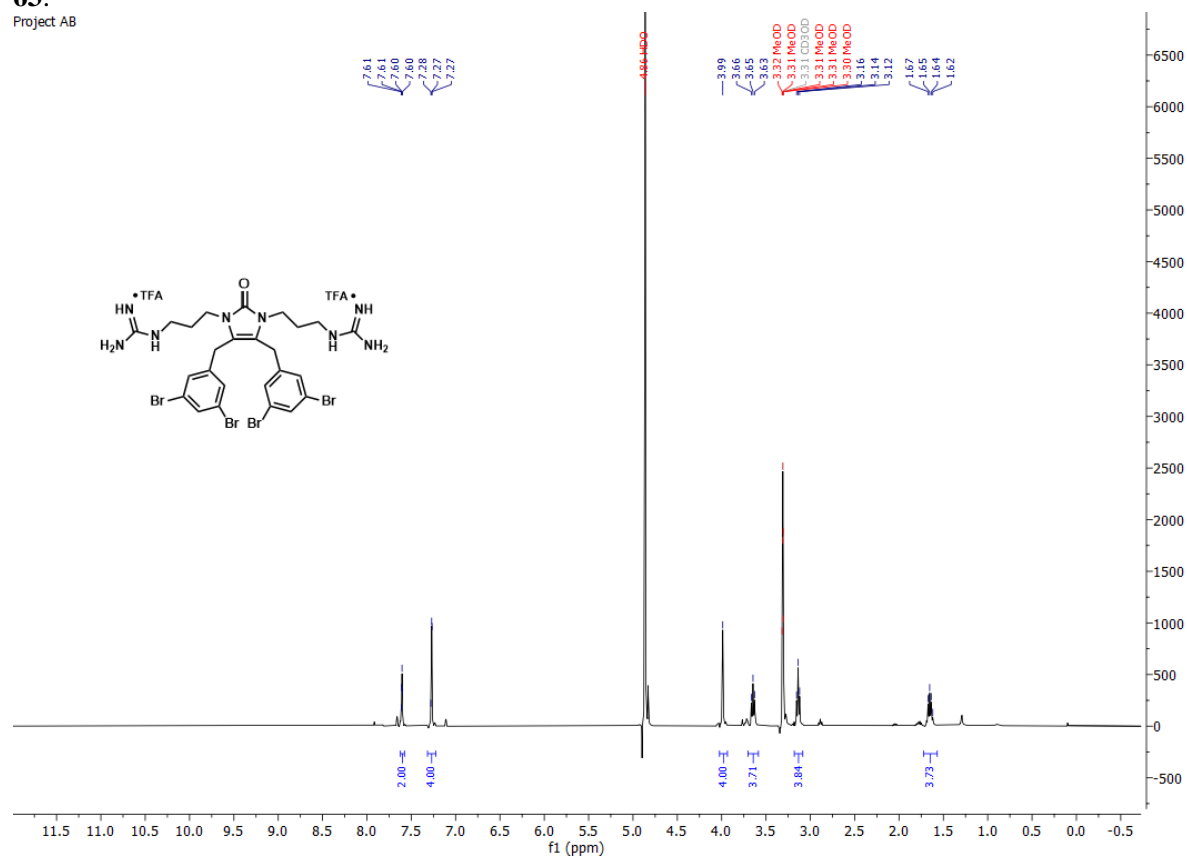
1,3-bis(3-aminopropyl)-4,5-bis(4-(tert-butyl)benzyl)-1,3-dihydro-2H-imidazol-2-one **62**.
Project AB



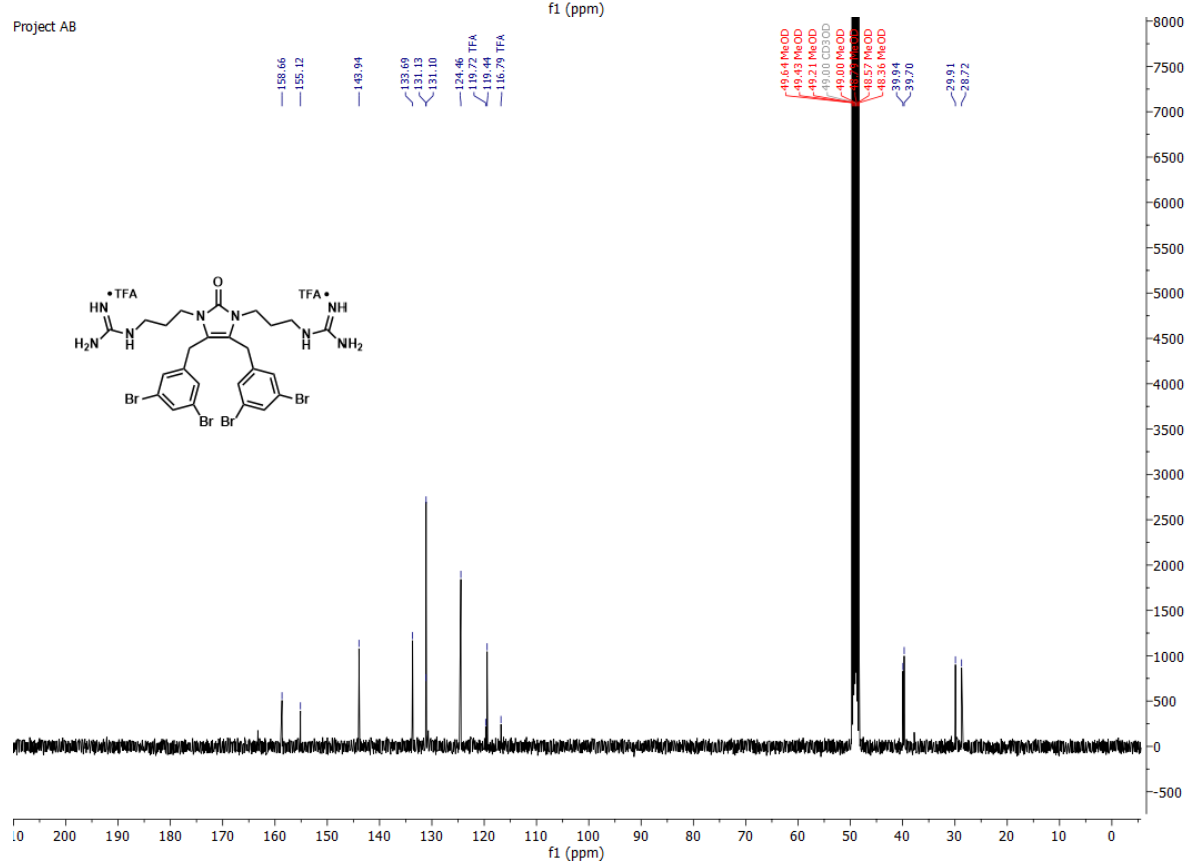
1,1'-((4,5-bis(3,5-dibromobenzyl)-2-oxo-1H-imidazole-1,3(2H)-diyl)bis(propane-3,1-diyl)diguandine

63.

Project AB

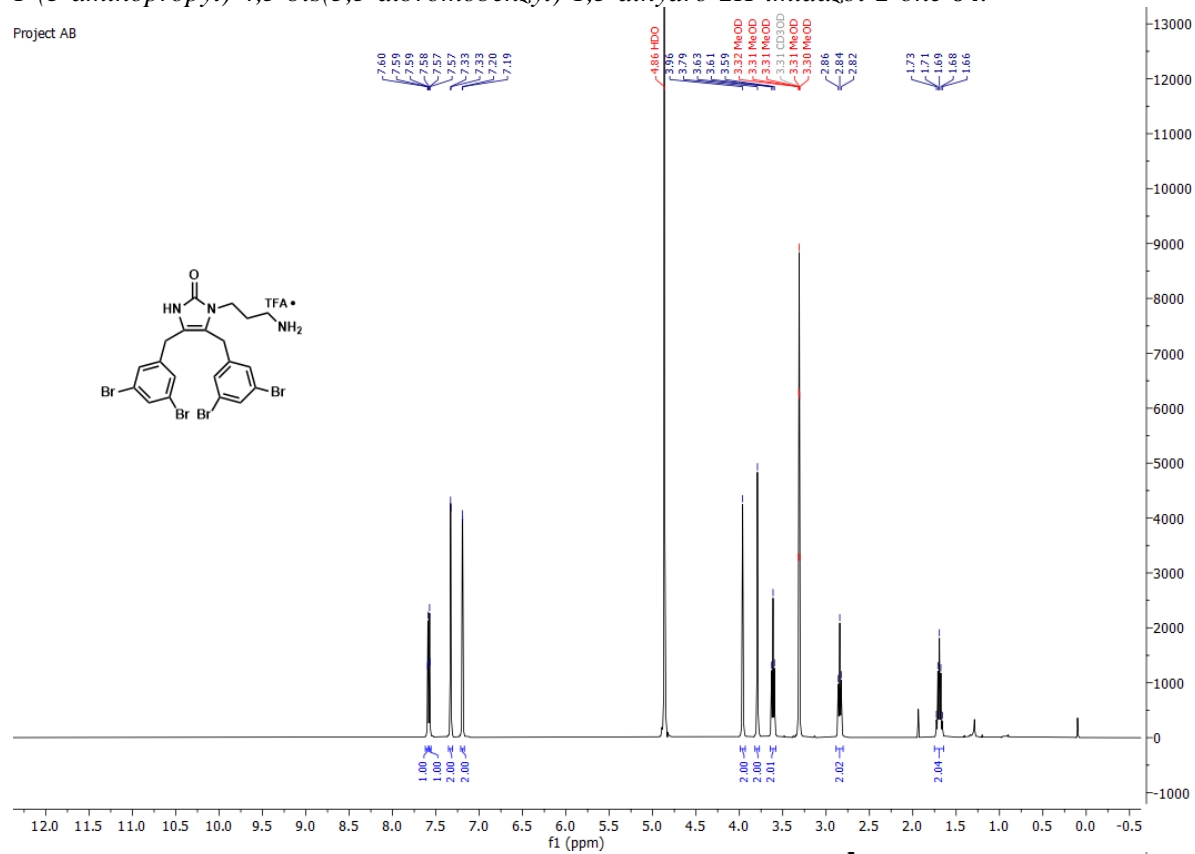


Project AB

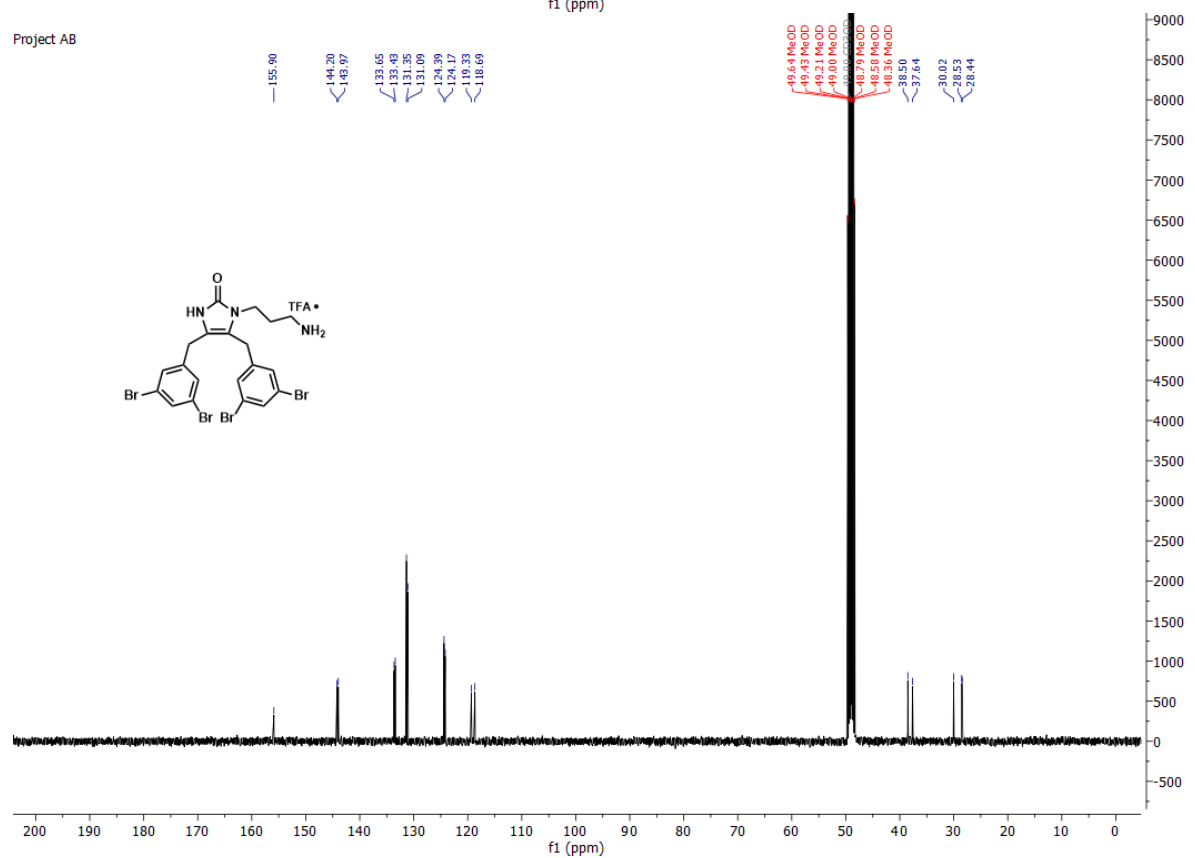


1-(3-aminopropyl)-4,5-bis(3,5-dibromobenzyl)-1,3-dihydro-2H-imidazol-2-one **64**.

Project AB

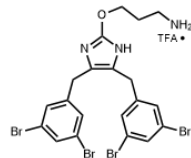
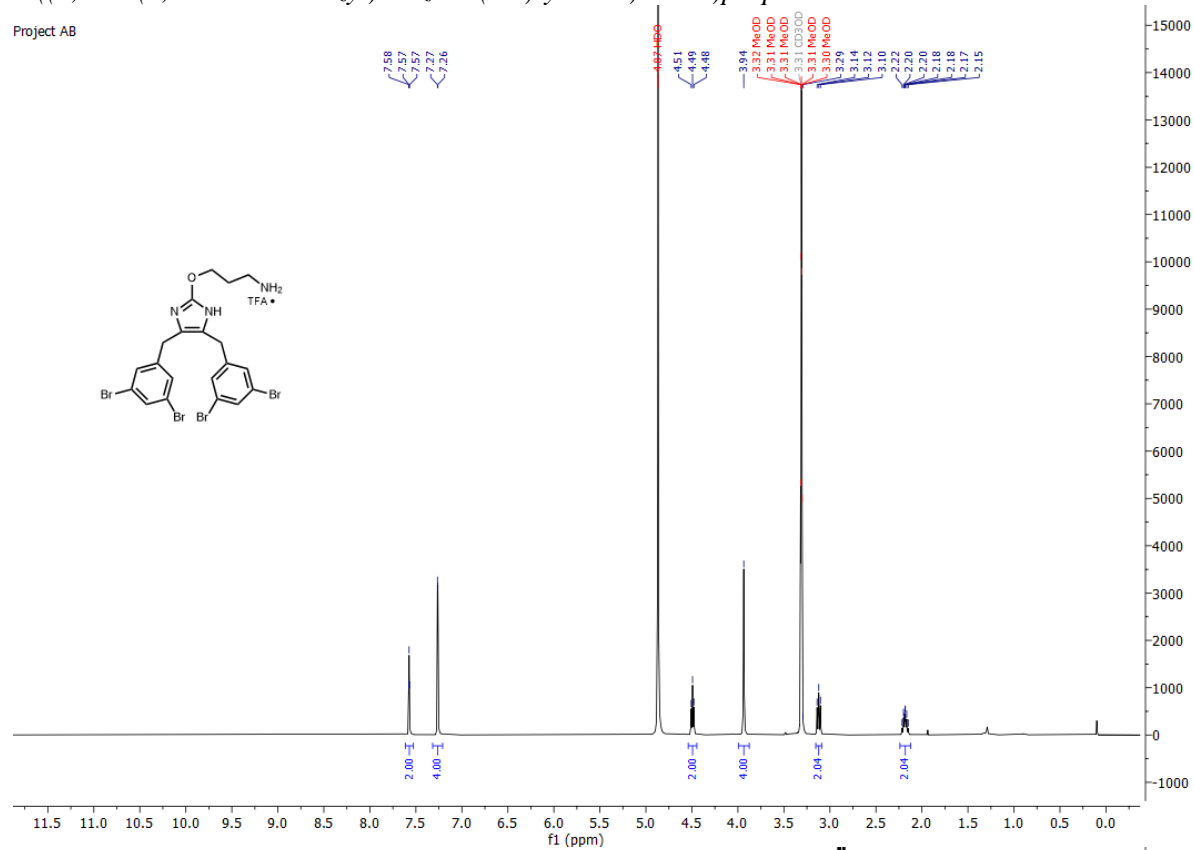


Project AB

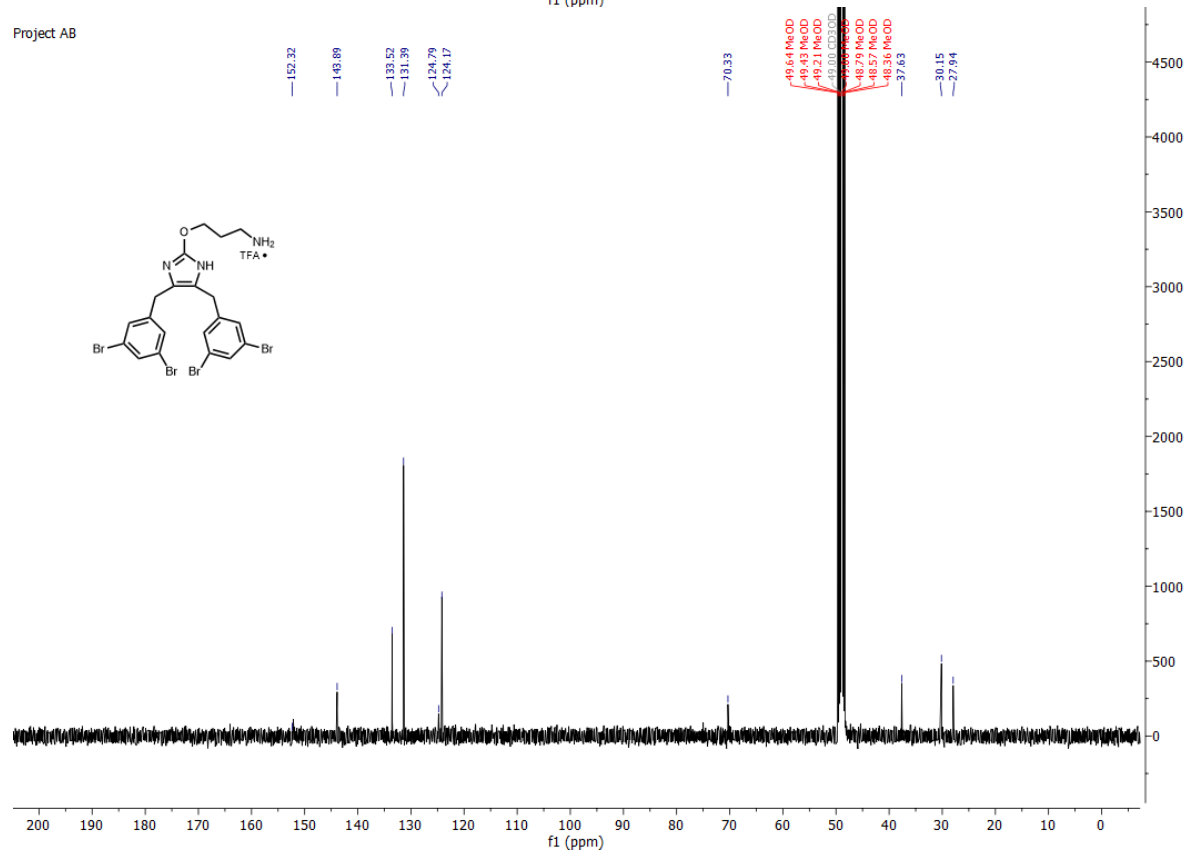


3-((4,5-bis(3,5-dibromobenzyl)oxazol-2(3H)-ylidene)amino)propan-1-amine **65**.

Project AB

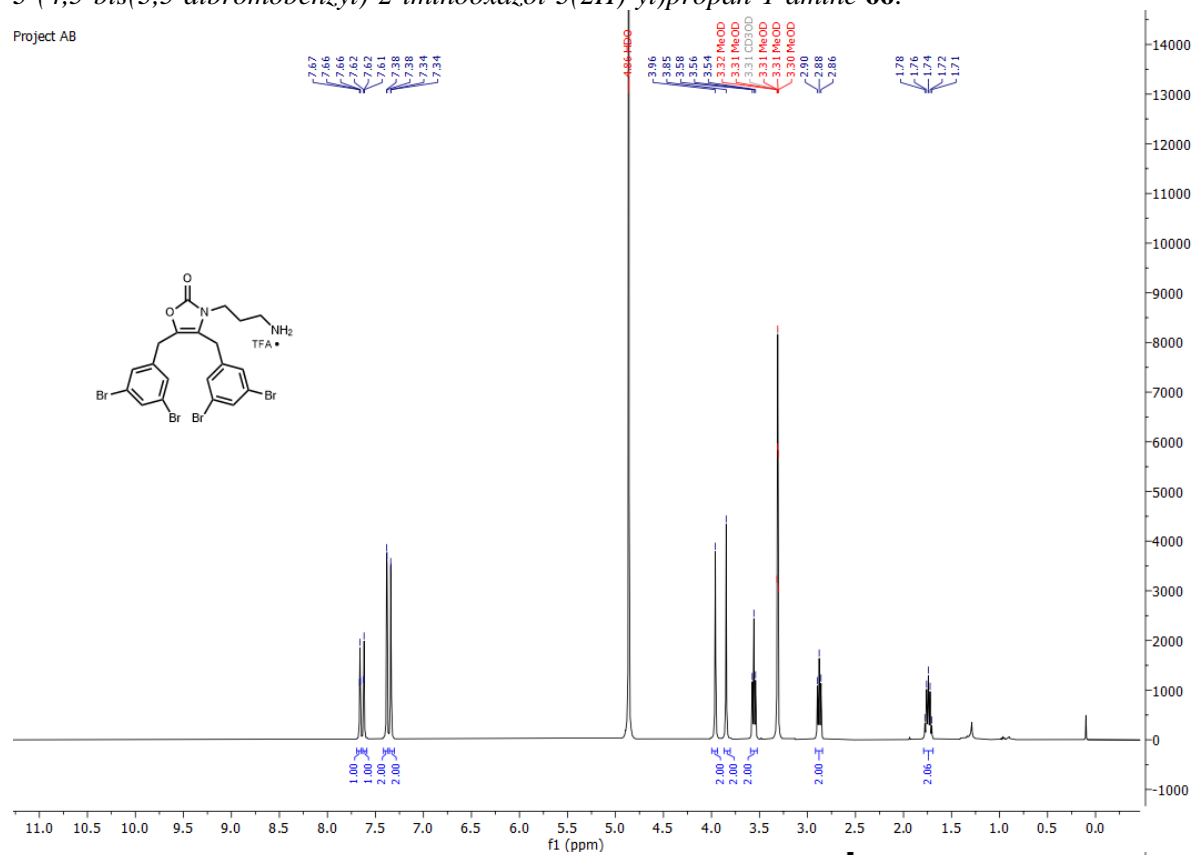


Project AB

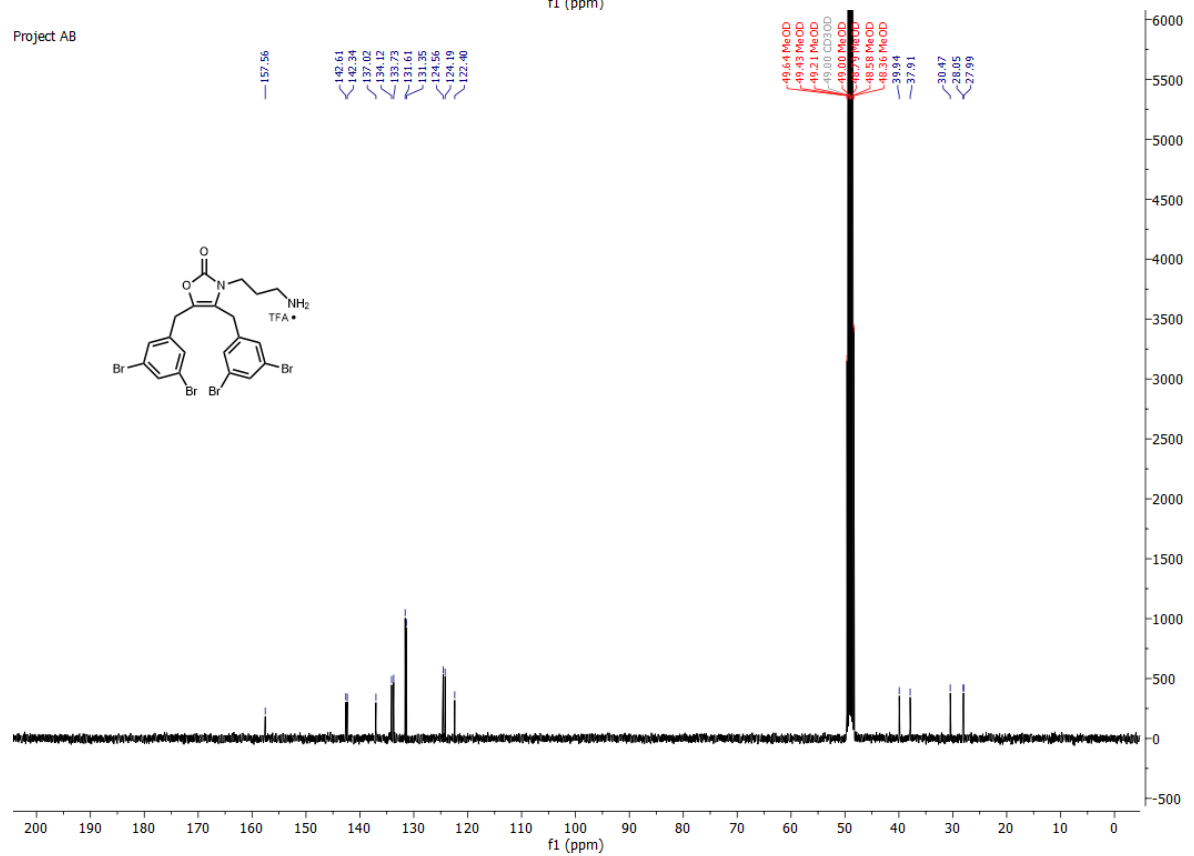


3-(4,5-bis(3,5-dibromobenzyl)-2-iminooxazol-3(2H)-yl)propan-1-amine **66**.

Project AB

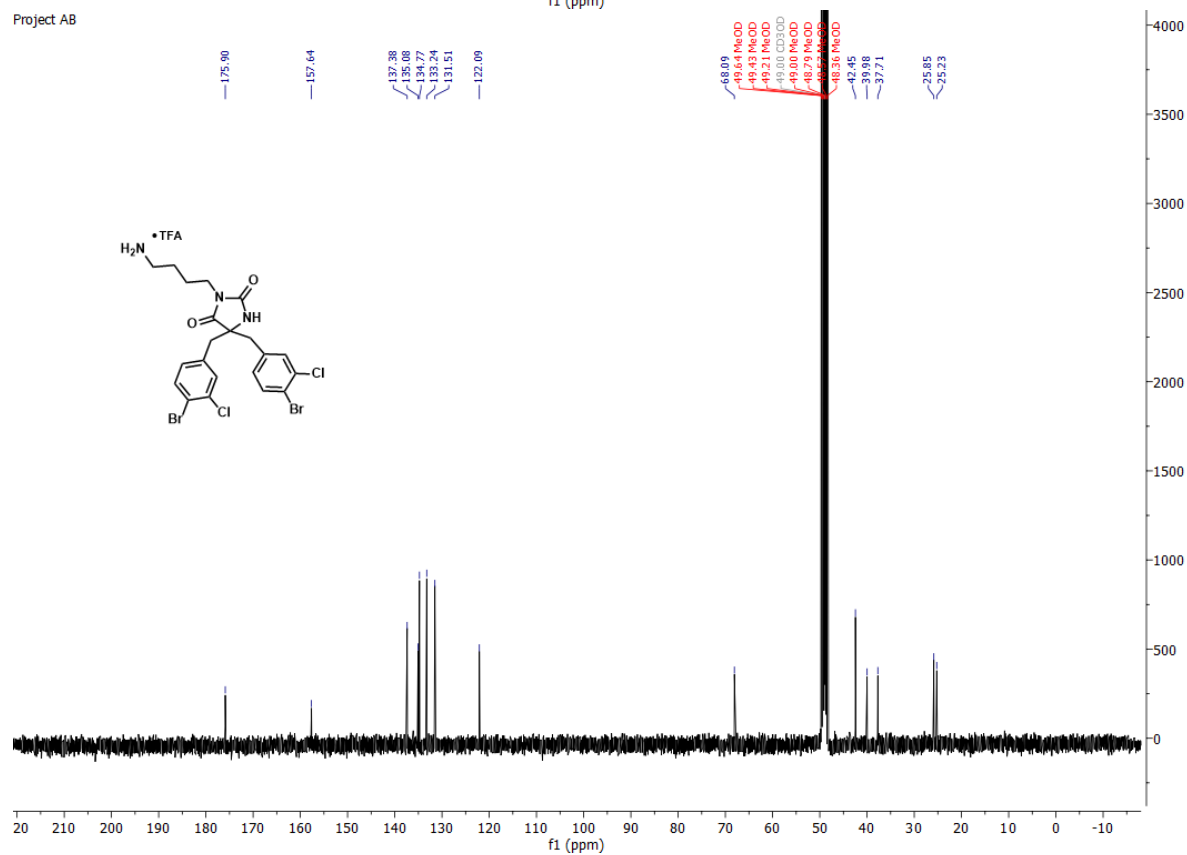
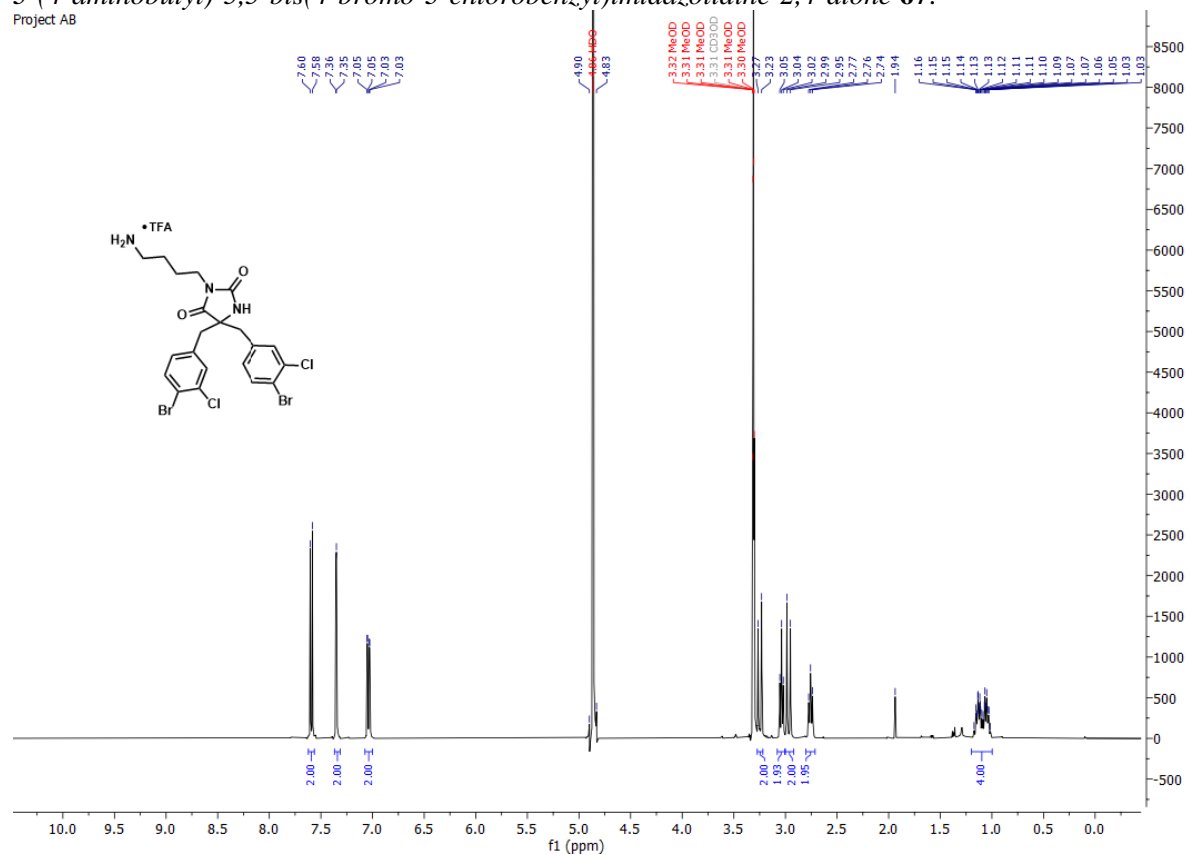


Project AB



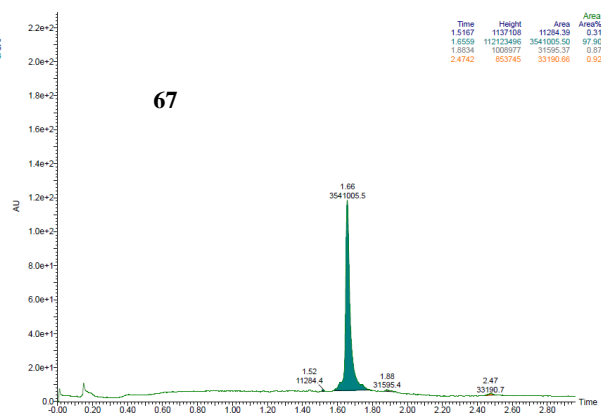
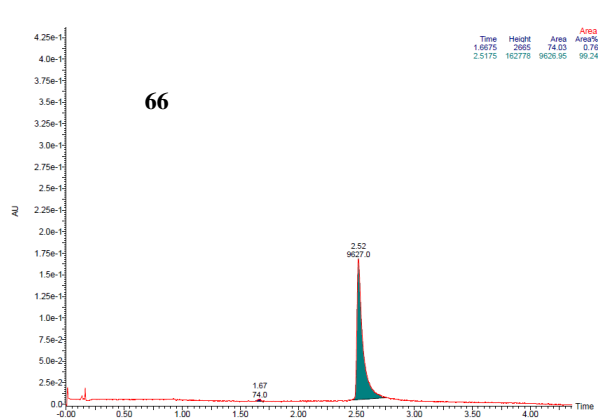
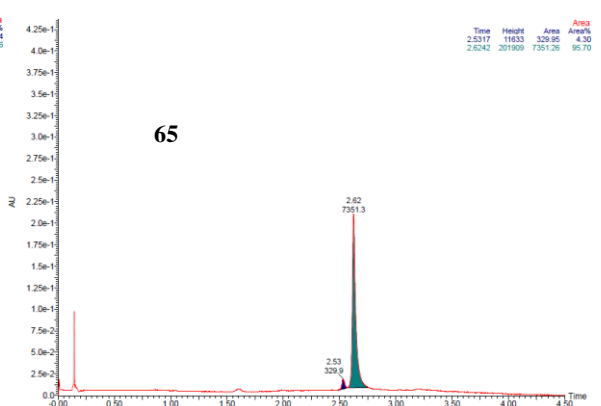
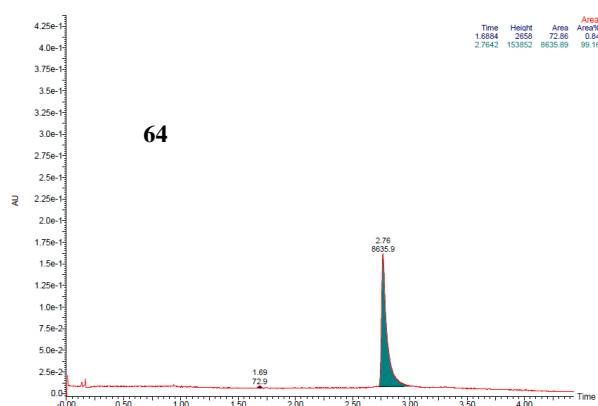
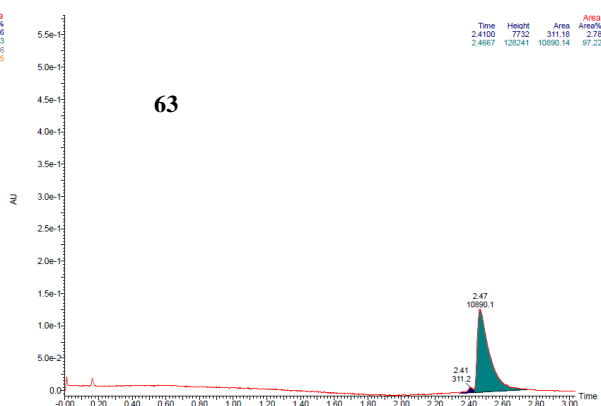
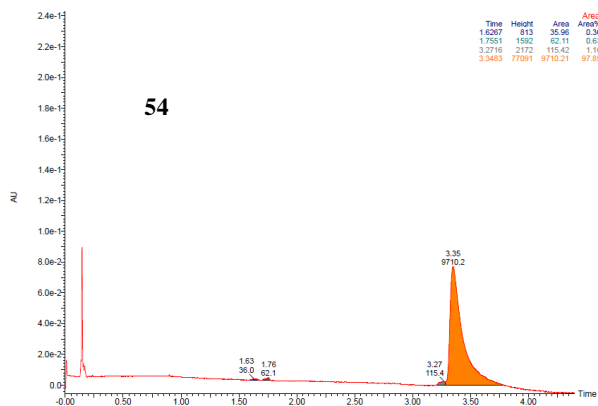
3-(4-aminobutyl)-5,5-bis(4-bromo-3-chlorobenzyl)imidazolidine-2,4-dione 67.

Project AB



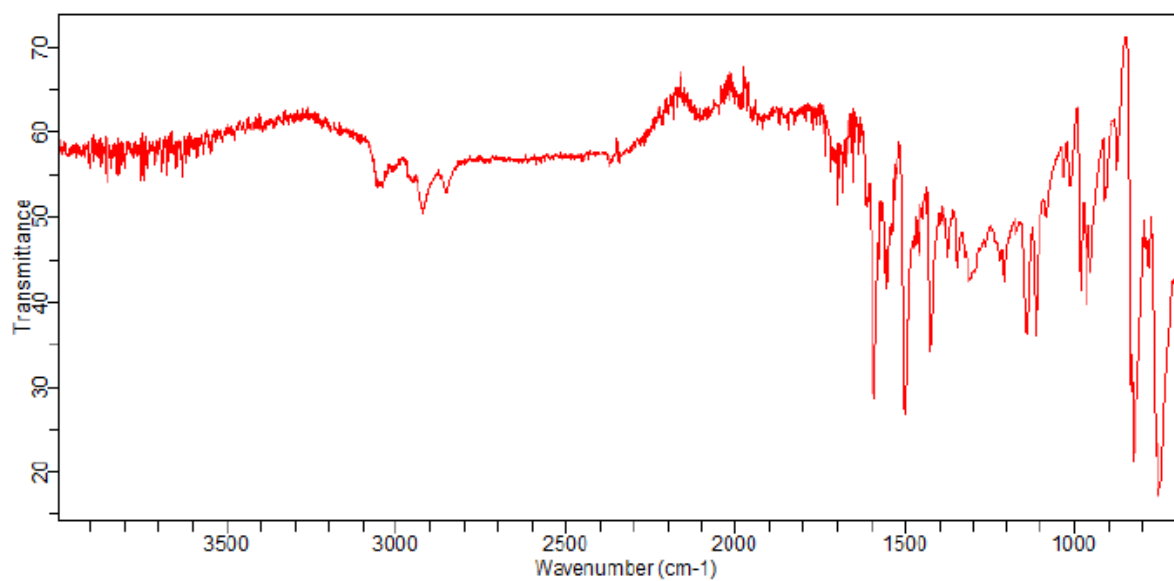
7.2 SFC traces

No SFC trace for compound **62** was obtained.

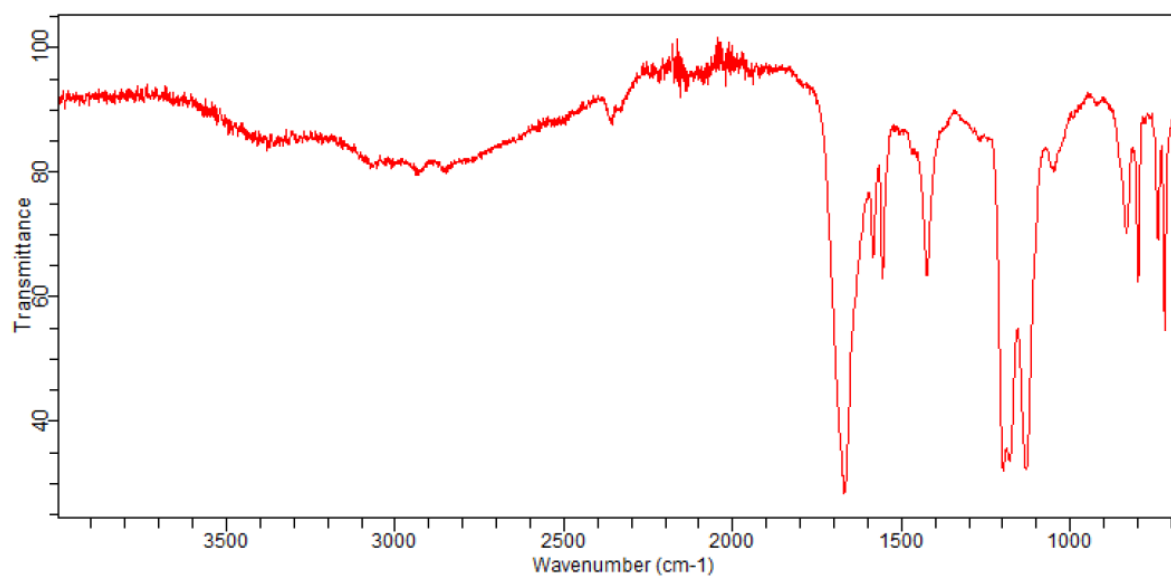


7.3 IR spectra

(Z)-3-((*Z*)-quinolin-2(1*H*)-ylidene)-1-(quinolin-2-yl)prop-1-en-2-ol **56**.



Compound 54.



Paper I

Amphipathic Barbiturates as Mimics of Antimicrobial Peptides and the Marine Natural Products Eusynstyelamides with Activity against Multi-resistant Clinical Isolates

Marianne H. Paulsen, Magnus Engqvist, Dominik Ausbacher, Trude Anderssen, **Manuel K. Langer**, Tor Haug, Glenn R. Morello, Laura E. Liikanen, Hans-Matti Blencke, Johan Isaksson, Eric Juskewitz, Annette Bayer,* and Morten B. Strøm*

J. Med. Chem. 2021, 64, 11395-11417.

DOI: <https://doi.org/10.1021/acs.jmedchem.1c00734>.

Amphipathic Barbiturates as Mimics of Antimicrobial Peptides and the Marine Natural Products Eusynstyelamides with Activity against Multi-resistant Clinical Isolates

Marianne H. Paulsen, Magnus Engqvist, Dominik Ausbacher, Trude Anderssen, Manuel K. Langer, Tor Haug, Glenn R. Morello, Laura E. Liikanen, Hans-Matti Blencke, Johan Isaksson, Eric Juskewitz, Annette Bayer,* and Morten B. Strøm*



Cite This: *J. Med. Chem.* 2021, 64, 11395–11417



Read Online

ACCESS |



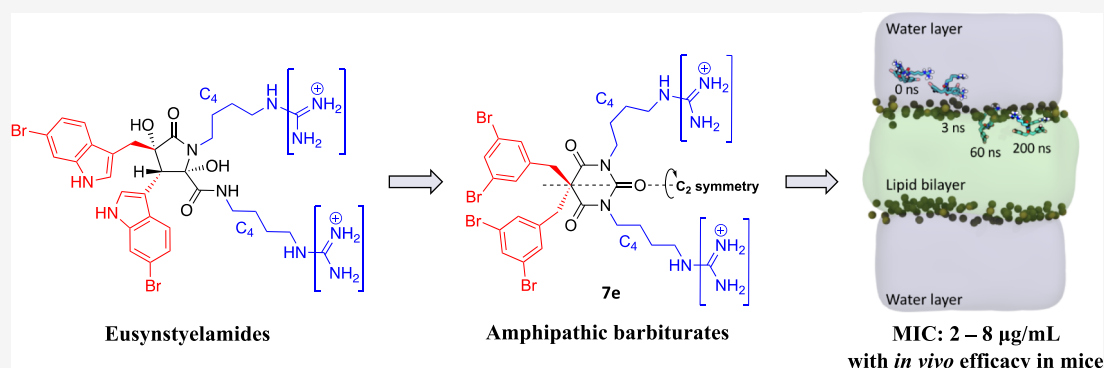
Metrics & More



Article Recommendations



Supporting Information



ABSTRACT: We report a series of synthetic cationic amphipathic barbiturates inspired by the pharmacophore model of small antimicrobial peptides (AMPs) and the marine antimicrobials eusynstyelamides. These *N,N'*-dialkylated-5,5-disubstituted barbiturates consist of an achiral barbiturate scaffold with two cationic groups and two lipophilic side chains. Minimum inhibitory concentrations of 2–8 $\mu\text{g/mL}$ were achieved against 30 multi-resistant clinical isolates of Gram-positive and Gram-negative bacteria, including isolates with extended spectrum β -lactamase–carbapenemase production. The guanidine barbiturate **7e** (3,5-di-Br) demonstrated promising *in vivo* antibiotic efficacy in mice infected with clinical isolates of *Escherichia coli* and *Klebsiella pneumoniae* using a neutropenic peritonitis model. Mode of action studies showed a strong membrane disrupting effect and was supported by nuclear magnetic resonance and molecular dynamics simulations. The results express how the pharmacophore model of small AMPs and the structure of the marine eusynstyelamides can be used to design highly potent lead peptidomimetics against multi-resistant bacteria.

INTRODUCTION

There is a desperate need for developing new antimicrobial agents to meet the worldwide emergence and spread of resistant bacteria.¹ Resistant bacteria are currently causing deaths of 33,000 European patients annually, and the worst scenarios estimate 10 million deaths by 2050 per year if no measures are effectuated.^{2,3} WHO announced in their Global action plan on antimicrobial resistance that access to and appropriate use of existing and new antimicrobial drugs are absolutely mandatory to maintain the ability to treat serious infections.⁴ Increasing antimicrobial resistance has also dramatic consequences for common medical interventions in cancer treatment, caesarean sections, and organ transplantations. Large pharmaceutical companies show nevertheless little interest in antimicrobial drug development, mainly due to economic reasons. Academia and smaller research institutions are now conceivably the most important contributors for

discovery and synthesis of new lead compounds for antimicrobial drug development.

The eusynstyelamides are in this setting a fascinating class of antimicrobials isolated from the marine Arctic bryozoan *Tegella cf. spitzbergensis* and the Australian ascidian *Eusynstyela latericius*.^{5,6} The eusynstyelamides display moderate antimicrobial activity, and a method for the synthesis of (\pm)-eusynstyelamide A is reported.^{5,7} An intriguing structural feature of the eusynstyelamides is that they consist of two cationic groups

Received: April 23, 2021

Published: July 27, 2021



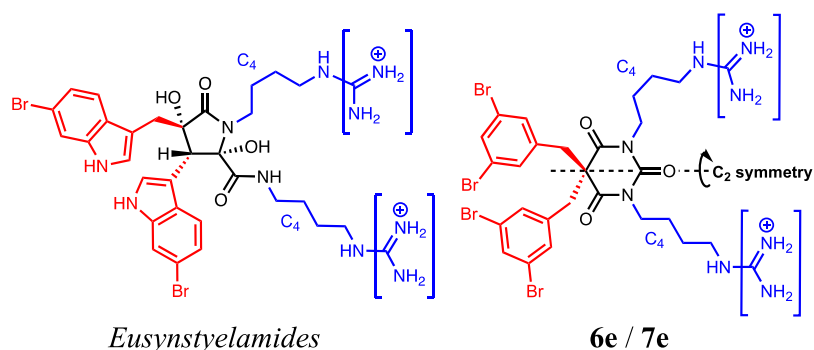
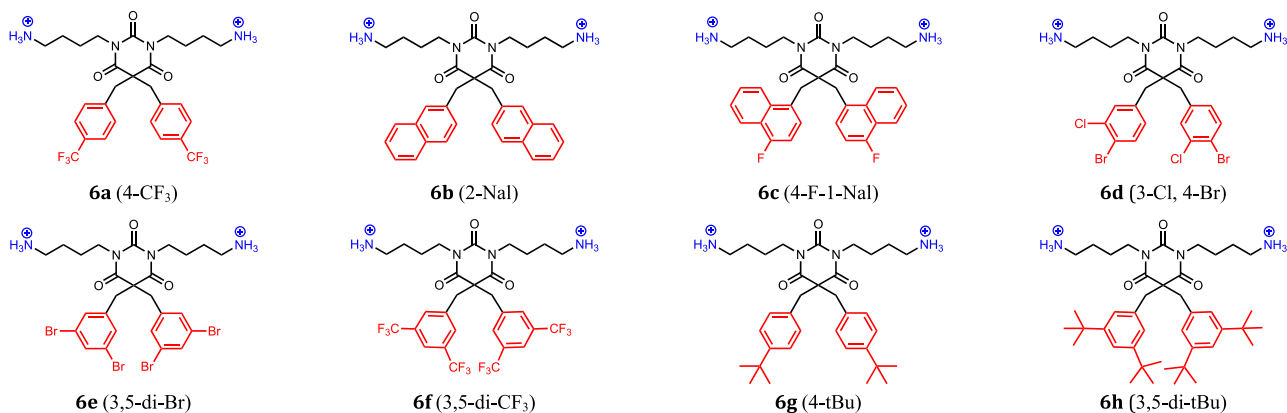


Figure 1. General structures of the marine antimicrobials eusynstyelamides (left) and the novel amphipathic barbiturates **6e** (3,5-di-Br) (amine) and **7e** (3,5-di-Br) (guanidine) (right). Brackets imply variations between cationic amine and guanidine groups. The eusynstyelamides can have different combinations of amine and guanidine groups,⁵ but in the present study, both cationic groups were identical in the synthesized amphipathic barbiturates.

Series 6: Amine barbiturates



Series 7: Guanidine barbiturates

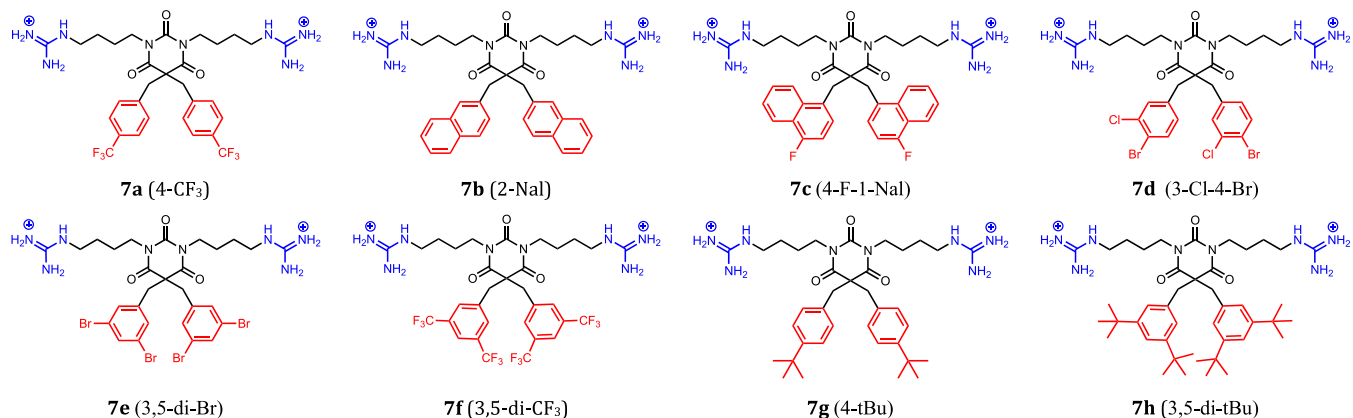
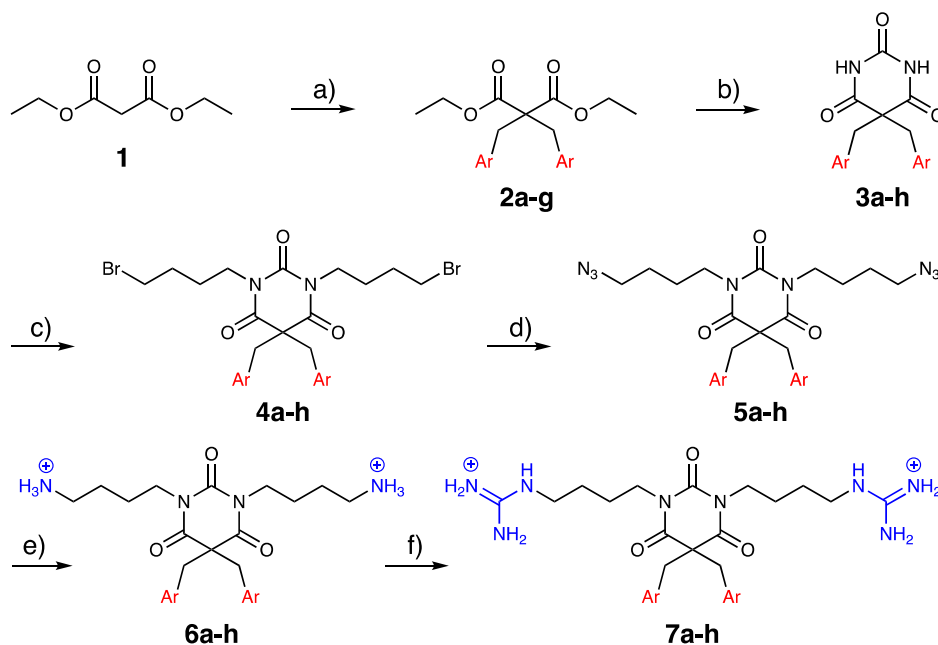


Figure 2. Structures of the synthesized amphipathic amine barbiturates (series 6) and guanidine barbiturates (series 7) investigated for antimicrobial activity. The cationic groups have TFA⁻ as the counterion.

(amine or guanidine) and two lipophilic groups attached to a five-membered dihydroxybutyrolactam ring (Figure 1). This amphipathic structural arrangement of cationic and lipophilic groups satisfies the pharmacophore model of small antimicrobial peptides (AMPs) that we and others have studied extensively by design of peptidomimetics of AMPs [also named synthetic mimics of AMPs (SMAMPs)].^{8–11} AMPs play a crucial part of innate immunity in virtually all species and constitute the first line of defense against infections by bacteria, virus, fungi, and parasites.^{12–14} Natural AMPs are

however rather large cationic peptides (+2 to +9) consisting of 12–50 amino acid residues where 20–50% are lipophilic residues. They have an amphipathic characteristic that is essential for their membrane disruptive mode of action against bacteria.^{12,15} The limitation of AMPs as drugs is related to their pharmacokinetic properties, such as low proteolytic stability, low oral bioavailability, and potential immunogenicity.¹⁶ The design of SMAMPs can offer a solution to these limitations.

Scheme 1. Successful Strategy for the Synthesis of Target Amphipathic Barbiturates^a

^aConditions: (a) ArCH₂Br, base, and DMF; (b) urea, NaH, and DMF; (c) 1,4-dibromobutane, K₂CO₃, and DMF; (d) NaN₃ and DMF; (e) (i) NaBH₄, 1,3-propanedithiol, and THF:isopropanol 1:1 and (ii) Boc₂O; (iii) CH₂Cl₂/TFA; and (f) (i) *N*-Boc-1*H*-pyrazole-1-carboxamide and THF and (ii) CH₂Cl₂/TFA. Purified using C-18 flash chromatography. The Ar groups are depicted in Figure 2.

In the present study, we report a peptidomimetic amphipathic scaffold inspired by the marine antimicrobials eusynstyelamides and fulfilling the pharmacophore model of small AMPs (Figure 1). A barbiturate ring was used as a structurally simplified mimic of the more complex dihydroxybutyrolactam ring of the eusynstyelamides, providing a scaffold without stereogenic centers. Different lipophilic and cationic groups could then be introduced on the barbiturate scaffold and provide a variety of amphipathic barbiturates (Figure 2). Selection of lipophilic side chains was based on our previous work with SMAMPs.^{17,18} The present amphipathic barbiturates were then investigated for their antimicrobial activity against bacterial reference strains and multi-resistant clinical isolates, and toxicity against human cell lines. One selected compound was investigated *in vivo* using a peritonitis model in mice to determine the efficacy against Gram-negative clinical isolates. The mode of action was studied *in vitro* using two luciferase-based membrane assays. To gain further insights into the membrane interaction of the amphipathic barbiturates, conformational analysis by nuclear magnetic resonance (NMR) in a membrane mimicking environment and molecular dynamics (MD) simulations of the interaction progression of compounds with an inner *Escherichia coli* cell membrane were performed.

RESULTS AND DISCUSSION

Synthesis. Reported methods for the synthesis of substituted barbiturates include the condensation of alkylated malonate esters with urea,^{19–21} cyclization with *N*-alkylated urea and diethyl malonate or malonic acid,^{22,23} Knoevenagel condensation of barbituric acid and aldehydes or ketones,^{20,24,25} and alkylation of barbituric acid.²⁶

We first focused on a divergent synthetic strategy to gain quick access to tetrasubstituted, amphipathic barbiturates by cyclization of *N,N'*-dialkylated ureas and disubstituted diethyl

malonates. Unfortunately, no suitable reaction conditions for the cyclization of a number of malonate derivatives with *N,N'*-dialkylated urea with a short C₂ linker to the cationic groups were found (see the Supporting Information; Section 1 for details). Depending on the reaction conditions, the dialkylated urea proved to be either unreactive, decomposed, or led to undesired side products. As this strategy did not deliver the desired results, we turned our attention to a different approach.

The condensation of dialkylated malonate esters with urea followed by *N*-alkylation became a successful strategy for the synthesis of amphipathic barbiturates (Scheme 1). Symmetrically disubstituted malonates **2a–g** were obtained from diethyl malonate **1** by dialkylation with the appropriate arylmethyl halides and were subsequently cyclized with urea by treatment with NaH in dimethylformamide (DMF) to provide the 5,5-disubstituted barbiturates **3a–h** in yields of 70–92%. Dry conditions were imperative to the yield. Cyclization of malonate **2f** (3,5-di-CF₃) gave low yields (27%) due to decarboxylation under the reaction conditions. The 5,5-disubstituted barbiturates **3a–h** were alkylated with an excess of 1,4-dibromobutane under basic conditions (K₂CO₃ in DMF) to afford *N,N'*-dialkylated barbiturates **4a–h** in 40–96% yield. These were converted to the corresponding azides **5a–h** with NaN₃ (2–3 equiv) in DMF (68–100% yield). Reduction of the azides to amines with NaBH₄ and a catalytic amount of propane-1,3-dithiol,²⁷ and subsequent Boc-protection, provided Boc-protected diamines after purification by flash chromatography. Boc-protection was important to increase the yield and ease the purification.

Deprotection with 2,2,2-trifluoroacetic acid (TFA) provided the target amine barbiturates **6a–h** [$>95\%$ purity as determined by analytical C₁₈ reversed phase (RP) HPLC]. The amine barbiturates **6a–h** were guanylated with *N*-Boc-1*H*-pyrazole-1-carboxamide in tetrahydrofuran (THF) and purified before the Boc-protecting groups were removed.

Table 1. Antimicrobial Activity (MIC in $\mu\text{g/mL}$) of Synthesized Compounds against Antibiotic Susceptible Gram-Positive and Gram-Negative Reference Strains and Hemolytic Activity (EC_{50} in $\mu\text{g/mL}$) against Human Erythrocytes (RBC)

Comp.	(side chain)	Clog P^b	M_w^c	Antimicrobial activity ^a				RBC
				S. a	C. g	E. c	P. a	tox.
6a	(4- CF_3)	3.52	814.62	64	4	128	64	>398
6b	(2-Nal)	3.82	778.75	8	1	16	16	250
6c	(4-F-1-Nal)	3.96	814.73	4	1	16	8	160
6d	(3-Cl, 4-Br)	4.08	905.31	4	1	16	32	172
6e	(3,5-di-Br)	4.37	994.21	4	1	4	8	79
6f	(3,5-di- CF_3)	4.41	950.62	16	4	16	16	177
6g	(4-tBu)	4.47	790.85	4	1	4	8	145
6h	(3,5-di-tBu)	6.29	903.06	1	0.25	2	4	<5
7a	(4- CF_3)	3.52	898.71	2	0.25	8	64	>449
7b	(2-Nal)	3.82	862.83	1	0.25	1	8	133
7c	(4-F-1-Nal)	3.96	898.81	1	0.25	1	4	90
7d	(3-Cl, 4-Br)	4.08	989.39	0.5	0.25	2	8	77
7e	(3,5-di-Br)	4.37	1078.30	1	0.25	2	4	62
7f	(3,5-di- CF_3)	4.41	1034.70	2	2	2	8	98
7g	(4-tBu)	4.47	874.93	1	<0.13	2	4	77
7h	(3,5-di-tBu)	6.29	987.14	1	0.25	4	4	<6
Oxytetracycline		460.43	0.65	0.65	2.5	20		

^aBacterial reference strains: S. a—*Staphylococcus aureus* ATCC 9144, C. g—*Corynebacterium glutamicum* ATCC 13032, E. c—*Escherichia coli* ATCC 25922, and P. a—*Pseudomonas aeruginosa* PA01, DSM 19880 (ATCC 15692). ^bSide chain Clog P was calculated for a substituted toluene, 1-methyl-Nal, or 2-methyl-Nal (ChemBioDraw Ultra v13.0.2.3020). ^cMolecular weight including 2 equiv of CF_3COO^- except for oxytetracycline.

Purification by C_{18} RP flash chromatography gave the TFA salts of the target guanylated barbiturates **7a–h** with >95% purity.

Structure–Activity Relationship Study against Reference Strains and Human Erythrocytes. Two series of amphipathic barbiturates were prepared, in which series **6** consisted of barbiturates with two cationic amino groups and series **7** encompassed barbiturates with two cationic guanidine groups (Figure 2). Note that an abbreviation for the lipophilic side chain substituents is included in parentheses to aid the discussion. The barbiturates were initially screened for antimicrobial activity against antibiotic susceptible Gram-positive and Gram-negative reference strains (Table 1). Hemolytic activity was tested against human red blood cells (RBCs) as a measurement of toxicity.

Amine Barbiturates of Series 6 against Reference Strains. For the amine barbiturates in series **6**, the minimum inhibitory concentration (MIC) values ranged from 0.25 to 64 $\mu\text{g/mL}$ against the Gram-positive strains *Staphylococcus aureus* and *Corynebacterium glutamicum* and MIC values from 2 to 128 $\mu\text{g/mL}$ against the Gram-negative bacteria *E. coli* and *Pseudomonas aeruginosa* (Table 1). Higher antimicrobial activity was thereby in general observed against Gram-positive bacteria than against Gram-negative bacteria, although the differences were marginal for the most potent amine barbiturates of series **6**. Considering a membrane-disruptive mode of action (see below), the outer cell wall of Gram-negative bacteria may provide additional protection and thereby result in higher MIC values compared to Gram-positive bacteria. For comparison, the four different eusyn-styelamides isolated from *Tegella cf. spitzbergensis* display MIC values of 6.25–12.5 $\mu\text{g/mL}$ against the Gram-positive bacteria *S. aureus* and *C. glutamicum* and 12.5–25 $\mu\text{g/mL}$ against the Gram-negative bacteria *E. coli* and *P. aeruginosa*.⁵

The most potent amine barbiturate was **6h** (3,5-di-tBu), which had two super-bulky lipophilic 3,5-di-tBu-benzylic side chains and displayed MIC values in the very low range of

0.25–4 $\mu\text{g/mL}$ against all Gram-positive and Gram-negative reference strains. The side chain Clog P of **6h** (3,5-di-tBu) (Clog P : 6.29) was the highest calculated for all the lipophilic side chains included in the study (Table 1). Derivative **6h** (3,5-di-tBu) showed, however, unacceptable high hemolytic toxicity (EC_{50} : <5 $\mu\text{g/mL}$).

The two barbiturates **6e** (3,5-di-Br) and **6g** (4-tBu) were the second most potent derivatives displaying MIC values of 1–8 $\mu\text{g/mL}$ against the bacterial reference strains and were both less hemolytic (**6e** EC_{50} : 79 $\mu\text{g/mL}$ and **6g** EC_{50} : 145 $\mu\text{g/mL}$). These had smaller lipophilic side chains and implied a correlation between side chain size or calculated side chain Clog P and antimicrobial activity.

The 3,5-di-substituted derivative **6f** (3,5-di- CF_3) was less potent and displayed MIC values of 16 $\mu\text{g/mL}$ against all strains except for the very susceptible strain *C. glutamicum* (MIC: 4 $\mu\text{g/mL}$). The *C. glutamicum* strain is a valuable strain for identifying antimicrobial agents in screenings since it is so susceptible but is otherwise not of any medical importance. Its high susceptibility resulted in that none of the barbiturates from series **6** (nor series **7**) displayed MIC values above 4 $\mu\text{g/mL}$ against *C. glutamicum*.

It is noteworthy that the calculated Clog P of **6e** (3,5-di-Br) was lower than the calculated Clog P of the less potent **6f** (3,5-di- CF_3), showing that not only the lipophilic effects of the side chains affected the antimicrobial potency but possibly also the size and electronic effects. With respect to electronic effects, a difference in electron distribution was observed both in ¹³C NMR and when calculating the electron density of the bromine and trifluoromethyl substituents of **6e** (3,5-di-Br) and **6f** (3,5-di- CF_3). The electron distribution in the side chains of **6e** (3,5-di-Br) and **6f** (3,5-di- CF_3) was different hosting an overall more negative partial charge on the CF_3 groups compared to the bromine substituents (results not shown). This may affect the electron distribution of the aromatic side chains and possibly affect the lipophilic side chains in their interaction with the bacterial membrane and especially related to

Table 2. Antimicrobial Activity (MIC in $\mu\text{g/mL}$) of Selected Amine (Series 6) and Guanidine (Series 7) Barbiturates against 30 Multi-resistant Clinical Isolates^a

Toxicity	Amine barbiturates								Guanidine barbiturates								
	6a	6b	6c	6d	6e	6f	6g	6h	7a	7b	7c	7d	7e	7f	7g	7h	
RBC EC ₅₀	>398	250	160	172	79	177	145	<5	>449	133	90	77	62	98	77	<6	
HepG2 IC ₅₀	40	7	5	6	4	9	3	2	104	59	56	15	30	19	28	15	
MRC-5 IC ₅₀	16	2	2	10	2	17	1	1	74	30	23	36	11	29	14	17	
Clinical isolates																	ESBL–CARBA ^b
<i>S. aureus</i> N315	>32	8	8	8	4	16	8	2	4	8	2	2	2	2	2	4	
<i>S. aureus</i> NCTC 10442	>32	8	8	8	4	16	8	2	4	8	2	4	2	2	2	2	
<i>S. aureus</i> strain 85/2082	>32	8	4	4	4	16	8	2	4	8	2	2	2	2	2	2	
<i>S. aureus</i> strain WIS	>32	8	8	8	4	16	8	2	4	8	2	2	2	2	2	2	
<i>S. aureus</i> IHT 99040	>32	8	8	4	4	16	8	2	8	8	2	2	2	2	2	2	
<i>E. faecium</i> 50673722	>32	16	8	16	4	8	8	2	32	16	4	4	4	2	2	2	
<i>E. faecium</i> 50901530	>32	8	4	8	4	8	4	2	8	8	4	2	2	2	4	2	
<i>E. faecium</i> K36-18	>32	16	8	16	8	16	8	2	32	16	4	4	4	4	2	2	
<i>E. faecium</i> 50758899	>32	16	8	16	4	16	8	2	>32	16	4	4	4	4	2	2	
<i>E. faecium</i> TUHSO-22	>32	8	4	4	4	8	8	2	32	8	4	2	2	2	2	2	
<i>E. coli</i> 50579417	>32	16	16	16	8	16	8	4	32	16	8	4	4	8	4	16	OXA-48
<i>E. coli</i> 50639799	>32	16	16	16	8	16	8	4	16	8	4	4	4	4	4	8	VIM-29
<i>E. coli</i> 50676002	>32	16	16	16	8	16	4	8	32	8	4	4	4	4	4	16	NDM-1
<i>E. coli</i> 50739822	>32	16	16	16	8	16	8	4	32	8	8	4	4	8	4	8	NDM-1
<i>E. coli</i> 50857972	>32	16	16	16	8	8	4	4	16	8	4	4	4	4	4	8	IMP-26
<i>P. aeruginosa</i> K34-7	>32	32	32	32	16	32	>32	8	>32	32	16	16	8	16	16	16	VIM-2
<i>P. aeruginosa</i> K34-73	>32	32	32	32	16	32	>32	16	>32	32	8	8	8	16	8	8	VIM-4
<i>P. aeruginosa</i> K44-24	>32	>32	32	32	16	32	>32	8	>32	32	16	16	8	16	16	16	IMP-14
<i>P. aeruginosa</i> 50692172	>32	32	16	32	16	32	>32	8	>32	32	16	32	8	16	16	16	NDM-1
<i>P. aeruginosa</i> 50692520	>32	32	16	32	16	32	>32	8	>32	32	16	16	16	16	16	16	VIM
<i>K. pneumoniae</i> K47-25 ^c	>32	>32	>32	32	16	>32	>32	16	>32	16	8	4	4	16	4	16	KPC-2
<i>K. pneumoniae</i> K66-45	>32	>32	32	32	16	32	32	8	>32	16	4	8	4	16	4	8	NDM-1
<i>K. pneumoniae</i> 50531633 ^c	>32	32	16	16	8	32	16	8	>32	16	8	4	4	16	4	16	NDM-1+OXA-181
<i>K. pneumoniae</i> 50625602	>32	>32	32	32	16	32	16	8	>32	16	16	4	4	8	4	16	OXA-245
<i>K. pneumoniae</i> 50667959	>32	>32	32	32	16	32	32	8	>32	16	4	8	4	16	16	8	VIM-1
<i>A. baumannii</i> K12-21	>32	32	32	32	16	16	16	4	>32	32	8	8	4	16	4	4	OXA-58
<i>A. baumannii</i> K44-35	>32	32	32	32	16	32	32	4	>32	32	8	8	4	16	8	4	OXA-23
<i>A. baumannii</i> K47-42	>32	32	32	32	16	32	16	4	>32	32	8	8	4	16	8	4	OXA-23
<i>A. baumannii</i> K55-13	>32	32	32	32	16	32	16	4	>32	32	8	8	8	16	8	4	OXA-24
<i>A. baumannii</i> K63-58 ^c	>32	16	16	32	16	32	16	4	>32	32	8	8	4	16	4	4	OXA-23

^aToxicity is displayed as the hemolytic activity against human RBCs (EC₅₀ in $\mu\text{g/mL}$ from Table 1) and cytotoxicity against HepG2 and MRC-5 cells (IC₅₀ in $\mu\text{g/mL}$). ^bESBL–CARBA: extended spectrum β -lactamase–carbapenemase producing isolates. OXA, oxacillinase; VIM, verona integron-encoded metallo- β -lactamase; NDM, New Delhi metallo- β -lactamase; IMP, imipenem-type carbapenemase; and KPC, *K. pneumoniae* carbapenemase. ^cClinical isolates resistant to the antibiotic colistin.

localization in the water–lipid interface region of the membrane. This may also explain why **6f** (3,5-di-CF₃) displayed much lower hemolytic activity (EC₅₀: 177 $\mu\text{g/mL}$) than **6e** (3,5-di-Br) (EC₅₀: 79 $\mu\text{g/mL}$).

The 3,4-disubstituted derivative **6d** (3-Cl, 4-Br) displayed high antimicrobial activity against the Gram-positive reference strains (MIC: 1–4 $\mu\text{g/mL}$) but was clearly less potent than the previous derivatives against the Gram-negative reference strains (MIC: 16–32 $\mu\text{g/mL}$). Derivative **6d** (3-Cl, 4-Br) also showed very low hemolytic activity (EC₅₀: 172 $\mu\text{g/mL}$).

The Nal-derivatives **6b** (2-Nal) and **6c** (4-F-1-Nal) showed comparable antimicrobial activities, that is, MIC: 1–8 $\mu\text{g/mL}$

against the Gram-positive reference strains and MIC: 8–16 $\mu\text{g/mL}$ against the Gram-negative strains. These Nal derivatives differed slightly in calculated side chain lipophilicity [**6b** (2-Nal): Clog *P* 3.82, and **6c** (4-F-1-Nal): Clog *P* 3.96]. An important prospect with these Nal derivatives is possible tuning of pharmacokinetic properties related to phase I hepatic oxidations *in vivo*. Our previous studies on small $\beta^{2,2}$ -amino acid-based AMP peptidomimetics have shown that 2-Nal side chains can be extensively oxidized by liver microsomes, which is a model system used to assess the potential hepatic phase I metabolism.^{17,28} This oxidation is however reduced by having electron-withdrawing aromatic fluorine substituents such as in

6c (4-F-1-Nal). Aromatic fluorine substituents are often used as “metabolic blockers” in drugs to improve the pharmacokinetic properties.²⁹ Both Nal-derivatives **6b** (2-Nal) and **6c** (4-F-1-Nal) showed very low hemolytic activity. When comparing the hemolytic results in detail, the somewhat less lipophilic derivative **6b** (2-Nal) displayed lower hemolytic activity (EC_{50} : 250 $\mu\text{g}/\text{mL}$) than **6c** (4-F-1-Nal) (EC_{50} : 160 $\mu\text{g}/\text{mL}$). In this case, a small modification by having an aromatic fluorine-substituent seemingly had an impact on RBC toxicity.

A surprisingly low antimicrobial activity was observed for the least lipophilic derivative **6a** (4- CF_3), which only had acceptable antimicrobial activity against *C. glutamicum* but very low potency against the remaining reference strains (MIC: 64–128 $\mu\text{g}/\text{mL}$). Derivative **6a** (4- CF_3) was also all together non-hemolytic within the concentration range tested (EC_{50} : >398 $\mu\text{g}/\text{mL}$).

Guanidine Barbiturates of Series 7 against the Reference Strains. Guanylation of the amine barbiturates in series **6** resulted in a striking increase in the antimicrobial activity of the resulting guanidine barbiturates in series **7** (Table 1). The highly potent guanylated barbiturates of series **7** displayed a narrow range in the MIC values of <0.13–2 $\mu\text{g}/\text{mL}$ against the Gram-positive strains *S. aureus* and *C. glutamicum* and MIC 1–8 $\mu\text{g}/\text{mL}$ against the Gram-negative bacteria *E. coli* and *P. aeruginosa*. One exception lacking increased potency against *P. aeruginosa* was **7a** (4- CF_3) (MIC: 64 $\mu\text{g}/\text{mL}$), which was the smallest guanidine derivative (in volume) and least lipophilic derivative.

Overall, the results for the guanidine series **7** followed the structural considerations discussed for the antimicrobial activity of the amine barbiturates in series **6**. Highest broad-spectrum antimicrobial activity (MIC ≤ 4 $\mu\text{g}/\text{mL}$) was displayed by **7c** (4-F-1-Nal), **7e** (3,5-di-Br), **7g** (4-tBu), and **7h** (3,5-di-tBu). The guanylated barbiturates **7b** (2-Nal), **7d** (3-Cl, 4-Br), and **7f** (3,5-di- CF_3) showed the same high potency against the Gram-positive reference strains and *E. coli* but a little lower activity against *P. aeruginosa*. Altogether, the differences in MIC values were small. The largest improvements in the antimicrobial activity following guanylation was observed for **7a** (4- CF_3) and **7f** (3,5-di- CF_3) against the Gram-positive reference strains and *E. coli*.

The guanylated barbiturates of series **7** were in comparison more hemolytic than the amine barbiturates in series **6**, and only derivatives, **7a** (4- CF_3) and **7b** (2-Nal), displayed hemolytic toxicity with EC_{50} values above 100 $\mu\text{g}/\text{mL}$. The guanylated barbiturates **7c** (4-F-1-Nal), **7d** (3-Cl, 4-Br), **7e** (3,5-di-Br), **7f** (3,5-di- CF_3), and **7g** (4-tBu) displayed hemolytic toxicity in the range EC_{50} : 62–98 $\mu\text{g}/\text{mL}$, whereas the super-bulky barbiturate **7h** (3,5-di-tBu) was highly hemolytic (EC_{50} : <6 $\mu\text{g}/\text{mL}$).

The general increase in the hemolytic activity following guanylation can be a result of the larger guanidine group forming more intricate electrostatic and hydrogen-bonding interactions than a primary amine group and thereby interact with both anionic and zwitterionic phospholipids (PLs). As we and others have reported, there is little consistency, and both increase and reduction of RBC toxicity is observed when amine groups are interchanged by guanidine groups.^{17,30–34}

Antimicrobial Activity against 30 Multi-resistant Clinical Isolates. The amine and guanidine barbiturates were screened against a panel of 30 multi-resistant clinical isolates of Gram-positive and Gram-negative bacteria (Table 2). These isolates represented different resistance mechanisms,

in which the Gram-positive isolates were methicillin-resistant *S. aureus* (MRSA) and vancomycin-resistant *Enterococcus faecium* (VRE), and the Gram-negative isolates included multi-resistant *E. coli*, *P. aeruginosa*, *Klebsiella pneumoniae*, and *Acinetobacter baumannii* with extended spectrum β -lactamase–carbapenemase (ESBL–CARBA) production. Three strains were also resistant to the last resort antibiotic colistin. Cytotoxicity was also determined against human hepatocyte carcinoma cells (HepG2) and human lung fibroblast cells (MRC-5).

Antimicrobial activity against the multi-resistant clinical isolates was high with MIC values as low as 2–4 $\mu\text{g}/\text{mL}$ for the most potent barbiturates, thereby following the same tendencies as against the antibiotic susceptible reference strains. As opposed to RBC toxicity, the guanidine barbiturates of series **7** were less cytotoxic against human HepG2 and MRC-5 cells compared to the amine barbiturates of series **6** (Table 2). The interplay between the two different cationic groups and the various lipophilic side chains thereby influenced the antimicrobial potency, hemolytic toxicity, and human cell cytotoxicity differently.

For the amine barbiturates of series **6**, highest antimicrobial potencies (MIC: 2–16 $\mu\text{g}/\text{mL}$) were achieved against the Gram-positive multi-resistant clinical isolates of *S. aureus* and *E. faecium* and the Gram-negative isolates of *E. coli*. The overall most potent amine barbiturate of series **6** was **6h** (3,5-di-tBu), closely followed by **6e** (3,5-di-Br). These amine derivatives showed high potency also against the clinical challenging isolates of *P. aeruginosa*, *K. pneumoniae*, and *A. baumannii*. The high cytotoxicity against human HepG2 and MRC-5 cells (IC_{50} : 1–17 $\mu\text{g}/\text{mL}$) displayed by the active amine barbiturates of series **6** was unsatisfactory.

The guanidine series **7** represented a major increase in the antimicrobial activity against the Gram-negative multi-resistant clinical isolates compared to the amine series **6**. The guanidine barbiturates of series **7** were also less cytotoxic against human HepG2 and MRC-5 cells compared to the amine barbiturates of series **6**. The most potent broad-spectrum guanidine barbiturates were **7c** (4-F-1-Nal), **7d** (3-Cl, 4-Br), **7e** (3,5-di-Br), **7f** (3,5-di- CF_3), **7g** (4-tBu), and **7h** (3,5-di-tBu) displaying MIC values of 2–16 $\mu\text{g}/\text{mL}$ (Table 2). The cytotoxicity of these guanidine barbiturates against human HepG2 and MRC-5 cells was in the range IC_{50} : 11–59 $\mu\text{g}/\text{mL}$ and thereby less cytotoxic than the amine barbiturates of series **6**. The broad-spectrum guanidine barbiturate **7e** (3,5-di-Br) showed overall highest antimicrobial potency against all multi-resistant clinical isolates tested and became the selected compound for the *in vivo* pilot study described below.

It should also be noted that the least lipophilic guanidine barbiturate **7a** (4- CF_3) may be a promising compound when considering specifically MRSA infections by its high potency (MIC: 4–8 $\mu\text{g}/\text{mL}$) against the clinical multi-resistant *S. aureus* isolates, low cytotoxicity against human HepG2 (IC_{50} : 104 $\mu\text{g}/\text{mL}$) and MRC-5 cells (IC_{50} : 74 $\mu\text{g}/\text{mL}$), and by being all together non-hemolytic (EC_{50} : >449 $\mu\text{g}/\text{mL}$, Table 2).

All the investigated amphipathic barbiturates displayed antimicrobial activity against the three colistin-resistant clinical isolates *K. pneumoniae* K47-25, *K. pneumoniae* S0531633, and *A. baumannii* K63-58 in the same range as against the colistin-susceptible clinical isolates. The mechanism of resistance of these clinical isolates is thought to involve altered lipopolysaccharide (LPS) outer cell wall composition and charge, changes that affect the mechanism of action of the last-resort cationic antibiotic colistin (pers. commun. prof Ø. Samuelson).

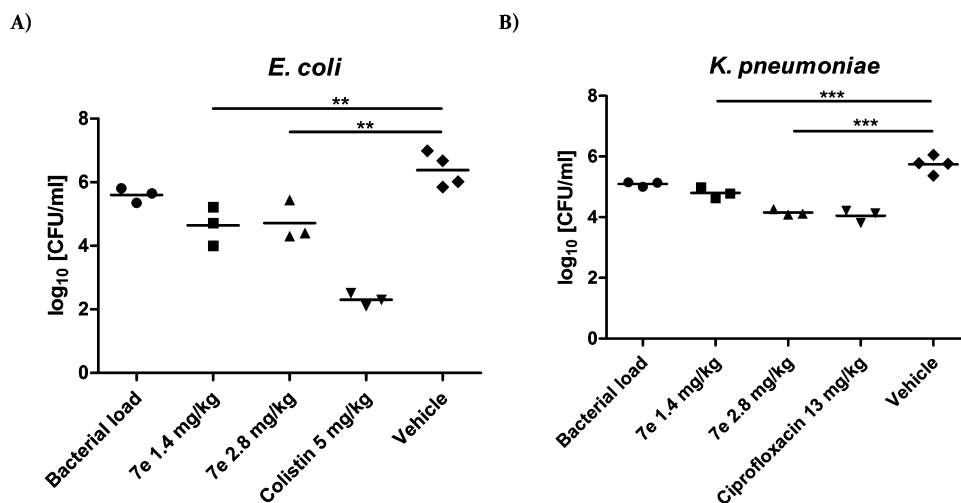


Figure 3. Reduction in the CFU of (A) *E. coli* (EC106-09) and (B) *K. pneumoniae* (KP3010) after i.p. treatment with 1.4 mg/kg (1 h post-infection) and 2.8 mg/kg (1.4 mg/kg 1 h + 3 h post-infection) of 7e (3,5-di-Br) compared to single i.p. treatment with (A) colistin (positive control, 5 mg/kg 1 h post-infection) and (B) ciprofloxacin (positive control, 13 mg/kg, 1 h post-infection) and vehicle (negative control, 1 h post-infection) was observed. The symbols (\blacktriangle , \blacklozenge , \bullet , \blacktriangledown , and \blacksquare) represent the individual mice in the experiment. The horizontal line represents the mean value of CFU counted for the parallels for the same experiment. Asterisks indicate the significant difference between vehicle control and treatment with 7e (Dunnett's test; $**p < 0.01$ and $***p < 0.001$).

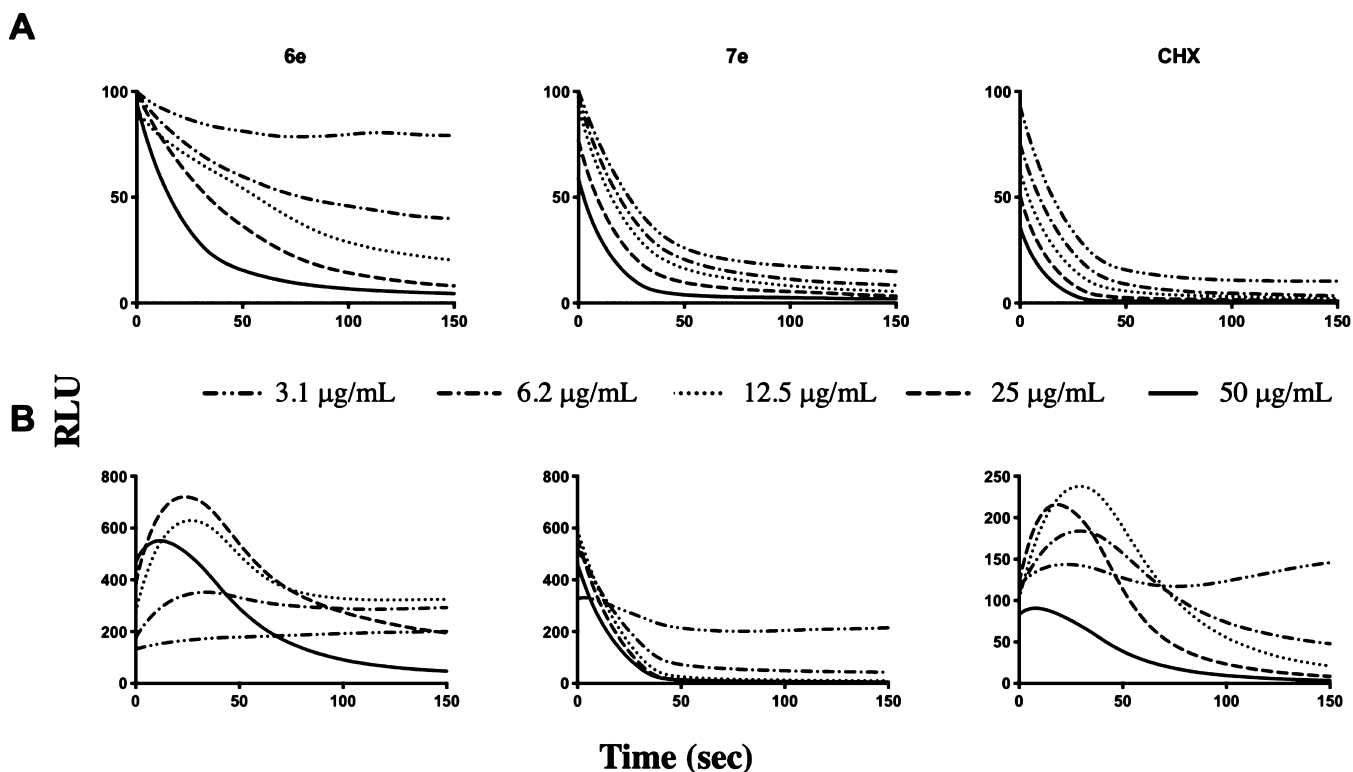


Figure 4. Comparison of the effects of 6e (3,5-di-Br), 7e (3,5-di-Br), and CHX on the kinetics of (A) viability and (B) membrane integrity in *B. subtilis*. Light emission normalized to an untreated water control (negative control) is plotted as relative light units (RLUs) over time (seconds) with untreated luminescence set to 100 RLU. After addition of the bacterial cell suspension (with 1 mM D-luciferin for the membrane integrity assay) to the analytes in each well, the light emission was measured each second for 150 s. Each line represents the kinetics of 150 subsequent data points of the analyte concentration. Each analysis was repeated at least three times independently. The figure shows a representative data set.

The altered LPS structure seemed not to have any major impact on the binding and activity of the most potent amphipathic barbiturates.

In Vivo Efficacy of 7e (3,5-di-Br) in a Murine Neutropenic Peritonitis Model. The overall most potent guanidine barbiturate 7e (3,5-di-Br) was investigated *in vivo*

using an established murine peritonitis model at Statens Serum Institut (SSI, Denmark).³⁵ Our aim was to determine the efficacy of 7e (3,5-di-Br) in mice infected with clinical isolates of *E. coli* (EC106-09) and *K. pneumoniae* (KP3010). Initially, the MIC of 7e (3,5-di-Br) was determined to be 4 $\mu\text{g}/\text{mL}$ against both strains, which was in coherence with our previous

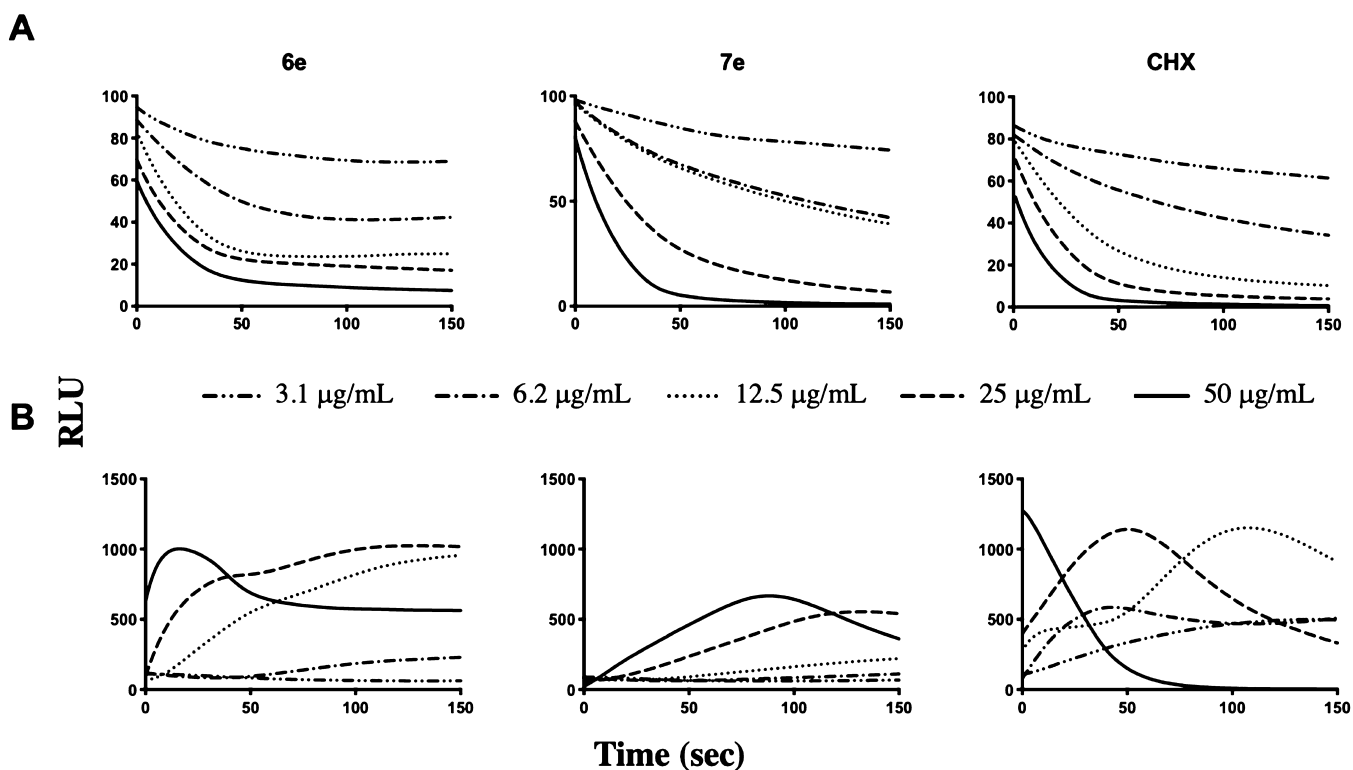


Figure 5. Comparison of the effects of **6e** (3,5-di-Br), **7e** (3,5-di-Br), and CHX on the kinetics of (A) viability and (B) membrane integrity in *E. coli*. Light emission normalized to the untreated water control (negative control) is plotted as RLU over time (seconds) with untreated luminescence set to 100 RLU. After addition of the bacterial cell suspension (with 1 mM D-luciferin for the membrane assay) to the analytes in each well, the light emission was measured each second for 150 s. Each line represents the kinetics of 150 subsequent data points of the analyte concentration. Each analysis was repeated at least three times independently. The figure shows a representative data set.

screening results. A maximal tolerated dose (MTD) was determined prior to evaluation of *in vivo* efficacy. In brief, the MTD was determined by intraperitoneal (i.p.) injection of escalating doses of derivative **7e** (3,5-di-Br). Derivative **7e** (3,5-di-Br) was well tolerated up to 2.8 mg/kg after i.p. injection with no or mild clinical signs of discomfort. At 3.6 mg/kg, moderate signs of discomfort were observed, but the mice recovered within a few hours. The MTD was determined to be 7 mg/kg.

In our vehicle controls, a log colony-forming unit per mL (CFU/mL) of 6.4 was determined for *E. coli*, indicating a 0.8 log CFU increase at the end of the experiment. A log CFU/mL of 5.7 was determined for *K. pneumoniae* corresponding to an approximately 0.6 CFU/mL increase at the end of the experiment. In contrast, treatment with **7e** (3,5-di-Br) caused a 1.7-log (98%) reduction of the bacterial loads of *E. coli* already at a concentration of 1.4 mg/mL (Figure 3A). Treatment with 1.4 mg/kg of **7e** (3,5-di-Br) against *K. pneumoniae* resulted in a 1 log CFU/mL reduction (90%) compared to treatment with vehicle (Figure 3B). A repeated injection after 3 h with **7e** (3,5-di-Br) resulted in a 1.6 log CFU/mL (97%) reduction of the bacterial load. Despite limitations regarding the MTD, our results demonstrated that **7e** (3,5-di-Br) could significantly reduce the number of viable bacterial cells in this *in vivo* model. We can conclude that the complex environment of the peritoneal cavity and the peritoneal fluid did not lead to a rapid inactivation of **7e** (3,5-di-Br). However, at this point, we can only speculate about the time range **7e** (3,5-di-Br) is present in sufficient concentrations for effective bacterial killing. Pharmacokinetic

studies as well as different routes of administration have to be undertaken in order to fully reveal the potential of this type of compound *in vivo*.

Mode of Action Studies. The amphipathic amine barbiturate **6e** (3,5-di-Br) and guanidine barbiturate **7e** (3,5-di-Br) were compared in a mode of action study using two luciferase-based biosensor assays in *Bacillus subtilis* 168 and *E. coli* HB101 (Figures 4 and 5).^{36,37} The two different biosensor systems evaluate the effects on bacterial viability and membrane integrity, respectively, which are closely linked functionalities in bacterial cells (see the Supporting Information; Section S9 for detailed information regarding the assays). The bacteriolytic agent chlorhexidine (CHX), known for its membrane-disruptive properties, was analyzed for comparison.³⁸

The overall results demonstrated a strong and immediate membrane disrupting activity for both compounds. A more rapid membranolytic effect was observed against the Gram-positive *B. subtilis* compared to Gram-negative *E. coli*. We also observed the differences in the rate of membrane lysis related to the test concentrations, in which concentrations higher than the MIC value led to a more rapid lysis, that is, a concentration-dependent killing effect.

The observed effects in the viability assay corresponded well with the respective MICs [**6e** (3,5-di-Br): 6.3 µg/mL and **7e** (3,5-di-Br): 3.1 µg/mL against both *B. subtilis* and *E. coli* biosensor strains], in spite of an initial 1000-fold higher concentration of bacteria in the inoculum compared to the MIC assay. The decrease in light emission was rapid, dose-dependent, and similar to the CHX control, suggesting a

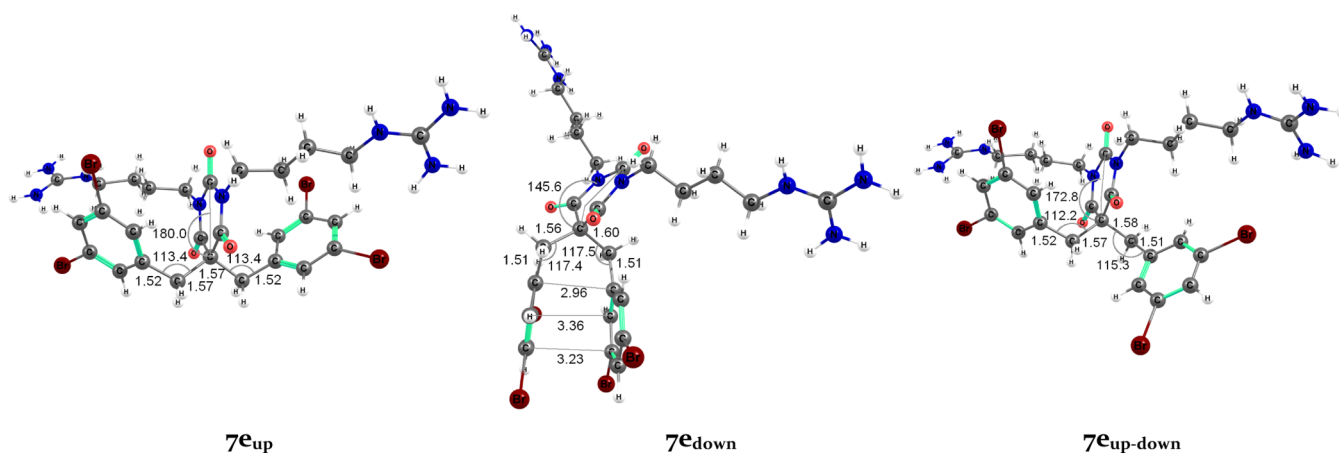


Figure 6. Optimized geometries from DFT calculations of $7e_{up}$ (left, also described as the W-shaped conformation), $7e_{down}$ (middle), and $7e_{up-down}$ (right). The bond distances are reported in Å and the bond angles are given in degrees.

membrane-related mode of action against both strains (Figures 4A and 5A). In order to confirm that the rapid decrease in bacterial viability was due to membrane damage, the membrane integrity assay was performed. Also, in this assay, a dose-dependent effect was observed against both strains (Figures 4B and 5B). The effects (rapid peak emission due to the influx of D-luciferin into the cells) were for the most part coinciding with the respective MIC values, indicating that membrane damage was indeed a major effect. The well-by-well measurements allowed for catching the actual light peaks, apart from measurements with $7e$ (3,5-di-Br) in *B. subtilis*, which seemed to act substantially faster than $6e$ (3,5-di-Br) and CHX and therefore only showed a decrease in light emission from a level substantially higher than the control (Figure 4B).

When comparing the results obtained from the viability assay (Figure 4A) and the membrane integrity assay (Figure 4B) in *B. subtilis* for compounds $6e$ (3,5-di-Br), $7e$ (3,5-di-Br), and CHX, the patterns appeared somewhat similar, indicating a rapid membranolytic activity for all compounds. However, in the membrane integrity assay in *B. subtilis*, we were not able to determine a peak in light emission for any concentration above MIC for $7e$ (3,5-di-Br) (Figure 4B). Light emission declined immediately, indicating that peak emission already had occurred before the first measurement, that is, within 2 s after analyte addition. At MIC (3.1 $\mu\text{g/mL}$), a small peak in light emission was observed after approximately 5 s, but the emission did neither decrease nor increase substantially within the measurement window. Altogether, the effect of $7e$ (3,5-di-Br) on *B. subtilis* shown in the viability assay seemed to be immediate (Figure 4A) and corresponded to the membranolytic effect shown in the membrane integrity assay (Figure 4B).

In *E. coli*, the observed overall picture was somewhat different. A rise or peak of light emission in the membrane integrity assay for $6e$ (3,5-di-Br) coincided with an immediate decrease of light emission in the viability assay (similar to the results in *B. subtilis*) (Figure 5). However, an emission peak was not reached for the lowest (1–4 \times MIC) concentrations of $7e$ (3,5-di-Br) within the 150 s test window in the membrane integrity assay (Figure 5B). On the other hand, the concentration-dependent reduction in viability observed with the guanidine barbiturate $7e$ (3,5-di-Br) resembled the results of the guanidine-containing CHX (Figure 5A), but the decrease in viability was substantially slower than for similar concentrations in *B. subtilis* (Figure 4B). In general, the

membrane integrity effects of all tested compounds seemed to occur at a slightly slower rate in the Gram-negative *E. coli* compared to the Gram-positive *B. subtilis*. It is tempting to speculate that especially for $7e$ (3,5-di-Br), the outer membrane of *E. coli* acted as a barrier, causing a delayed action in the membrane integrity assay. This would however not explain the presence of light production at a time point where the viability assay emits almost no light at all and accordingly indicates complete metabolic shutdown. This effect, even though less pronounced, was also observable for $6e$ (3,5-di-Br) and the CHX control. Although ATP is necessary for replenishment of the fatty aldehyde pool, this might indicate that reduction equivalents were the limiting factor for light emission of the viability sensor assay and that ATP under these conditions was not a limiting factor after treatment with $6e$ (3,5-di-Br), and especially, $7e$ (3,5-di-Br) until after the measurement window ended. Alternatively, there were different subpopulations of bacterial cells present, with different susceptibility to the analytes, resulting in an average light emission, which does not represent any of the subpopulations.

While the main mode of action against *B. subtilis* for both $6e$ (3,5-di-Br) and $7e$ (3,5-di-Br) seemed to be disruption of membrane integrity, our results did not exclude the possibility that especially $7e$ (3,5-di-Br) might have additional targets than the bacterial cytoplasmic membrane. Further work is needed to elucidate if $7e$ (3,5-di-Br) possibly targets other components of the cell and if there is a dual mode of action.

Conformational Analysis and Membrane Interaction Simulations. To gain insights into the interactions of the amphipathic barbiturates with a PL membrane surface, we determined the most stable conformations of the barbiturates, followed by a membrane interaction simulation. Density functional theory (DFT)-based geometry optimizations of amine $6e$ (3,5-di-Br) and guanidine $7e$ (3,5-di-Br) gave similar distortions and energy differences and indicated three low-energy conformations mainly differing in the orientation of the benzylic side chains (Figure 6). In the up ($7e_{up}$), down ($7e_{down}$), and up-down ($7e_{up-down}$) conformations, the benzylic side chains were either directed upward in a W-shape, downward, or having one side chain pointing up and the other pointing down. The $7e_{up}$ conformation was lowest in energy, whereas $7e_{up-down}$ and $7e_{down}$ were 4.9 and 9.8 kcal/mol higher in energy, respectively (see Supporting Information

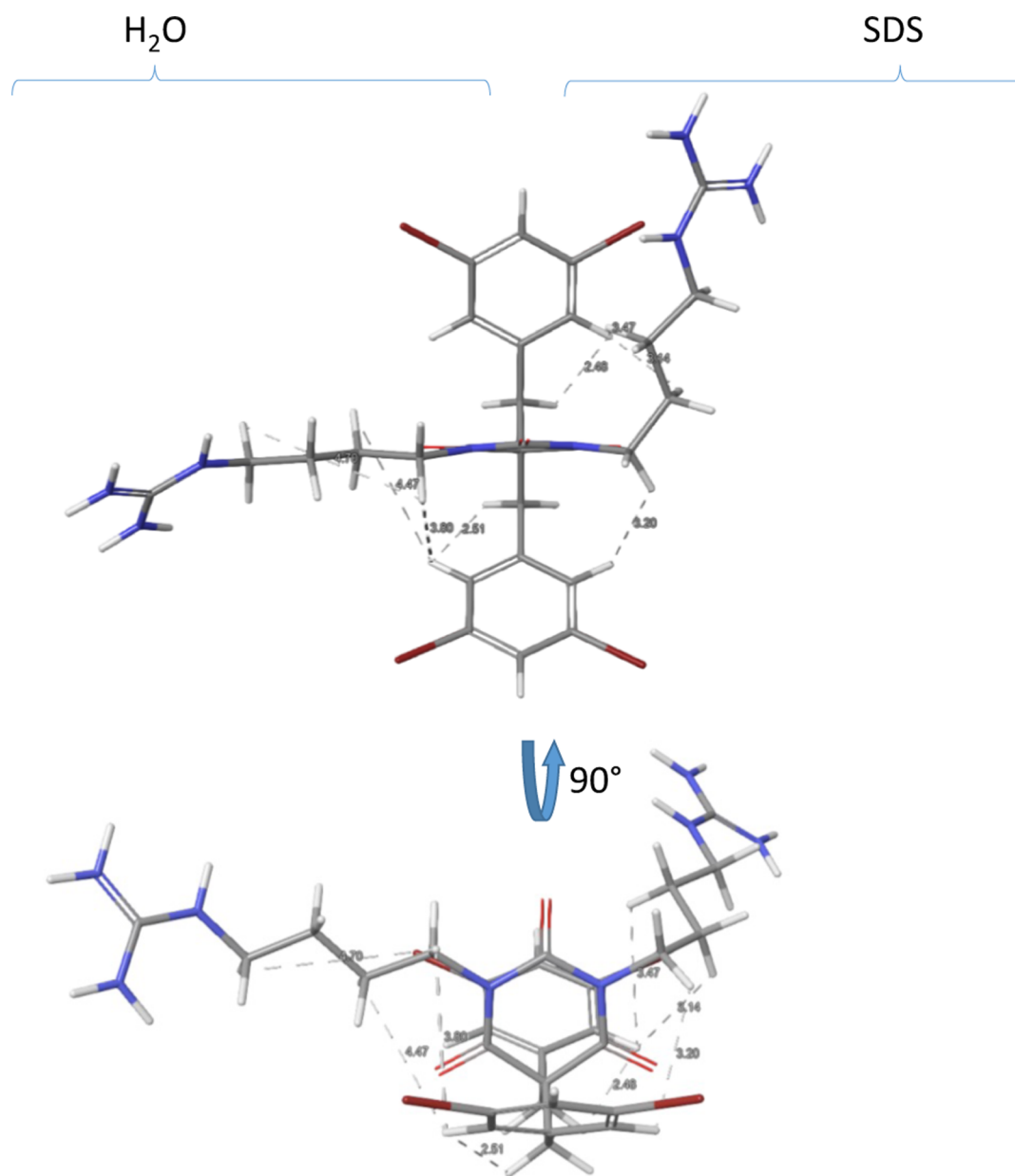


Figure 7. Schematic visualization of the observed ROESY correlations for **7e** (3,5-di-Br) in water (left side) and in SDS (right side) using sculpted structures.

Section S10 for more details of the conformational analysis). An X-ray structure of **7b** (2-Nal) supported the low energy conformation suggested by DFT calculations (see [Supporting Information](#) Section S11 for details).

The ROESY spectra acquired in water and micelle [sodium dodecyl sulfate (SDS)] solutions of the guanidine barbiturate **7e** (3,5-di-Br) were used to qualitatively assess the conformation experimentally (see [Supporting Information](#) Section 12 for details of the NMR conformational analysis). The structural NMR data in water ([Figure 7](#), left side) supported the orientations of the benzylic side chains described by the DFT calculations. It was evident from the ROESY detectable correlations between H7 and H10–H12 (5–10% of the reference volume) that the benzylic side chains and the barbiturate ring adopted the W-shape (similar to the **7e_{up}** conformation in [Figure 6](#)). There were no dramatic conformational changes in SDS, but there was a shift of

populations that made the guanidine side chains spend more time closer to the 3,5-dibromophenyl rings ([Figure 7](#), right side). This was reflected in the volumes of the H7/H11,12 cross-peaks that increased from ~10 to ~40% of the reference volume.

MD simulations were used to elucidate details on the membrane interactions of **7e** (3,5-di-Br) with an *E. coli* inner membrane model ([Figure 8](#)).³⁹ Similar MD simulations of **6a** (4-CF₃), **6e** (3,5-di-Br), **6g** (4-tBu), and **7g** (4-tBu) are included in the [Supporting Information](#) (Table S3 and Figures S6–S10), and a possible explanation to the low potency of **6a** (4-CF₃) is included below. For each compound, three parallel simulations were performed.

The course of the membrane insertion was tracked by following the location of the sp³ carbon opposite from the carbonyl carbon (C₅), as noted by the *z*-coordinate position in the simulation box ([Figure 8B](#)). The lipid bilayer surface (black

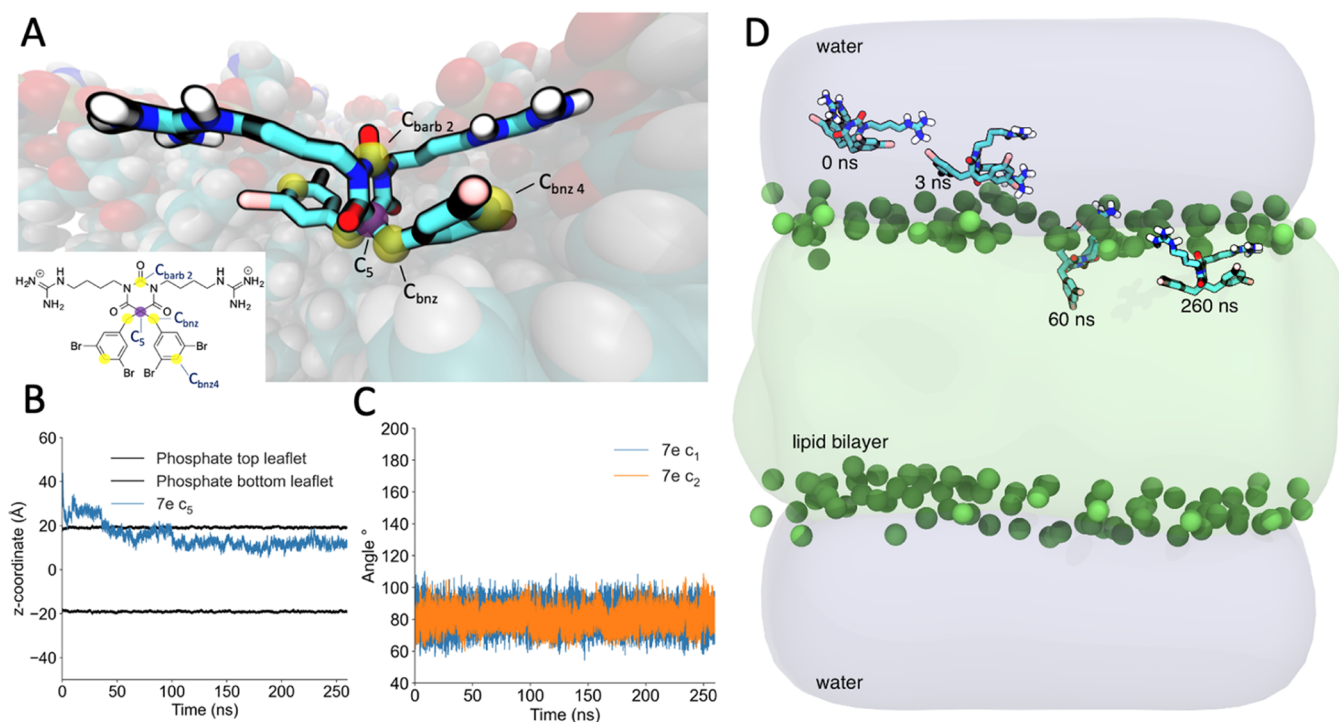


Figure 8. MD simulations of the interactions and conformations of **7e** (3,5-di-Br) in an *E. coli* inner membrane model. (A) **7e** (3,5-di-Br) in the membrane environment after 260 ns and the naming of atoms used for tracking of the compound. The purple sphere highlights carbon C_5 , which was the atom used for tracking the position of **7e** (3,5-di-Br) with respect to the PL headgroups (z -coordinate). The yellow spheres highlight atoms $C_{\text{barb}2}$, C_{bnz} , and $C_{\text{bnz}4}$, which formed the tracked angles c_1 or c_2 representing the conformation of two benzylic side chains. (B) Time evolution for location of the C_5 carbon (blue line) of **7e** (3,5-di-Br) in the simulation box. The lipid bilayer surface (black line) is shown as the average position of the phosphorous atoms (z -coordinate, -20 and 20 Å) of the PL headgroups. (C) Tracking of the two angles c_1 (in blue) and c_2 (in orange), which revealed if the compound remained in the up conformation or changed to the up–down conformation. Since both the blue and orange lines in the shown parallel oscillated around 80° , the compound was in the up conformation. When one of the lines also oscillated around 140° (not shown), the compound adopted the up–down conformation. (D) Simplified side view of the MD simulation system. Light gray pads represent water, light green pad in the middle is the PL bilayer, green spheres at the upper and lower borders of the PL bilayer are phosphorous atoms of the lipid headgroups, and the repeated copies of a small molecule in the upper half of the image is the **7e** (3,5-di-Br) compound. The time evolution of **7e** (3,5-di-Br) is shown as snapshots from the simulation and spanning from left to right; 0, 3, 60, and 260 ns. Explicit water molecules, PL tails and headgroups, ions, and non-polar hydrogen atoms in **7e** (3,5-di-Br) are omitted for clarity.

lines) is shown as the average position of the phosphorous atoms of the PL headgroups (z -coordinate, -20 and 20 Å). The blue line shows the time evolution for location of the C_5 carbon of **7e** (3,5-di-Br). The MD simulations for compounds **6e** (3,5-di-Br), **6g** (4-tBu), **7e** (3,5-di-Br), and **7g** (4-tBu) revealed a rapid membrane insertion between 7 and 35 ns, which was as expected due to the electrostatic interaction between the negatively charged membrane surface and the positively charged compounds.

The starting conformation of **7e** (3,5-di-Br) in the MD simulations was up. In the shown simulation parallel in Figure 8C, tracking of the two angles c_1 (blue) and c_2 (orange), representing the two benzylic side chains, revealed that **7e** (3,5-di-Br) remained in the up conformation throughout this simulation. This is shown by the blue and orange lines both oscillating around 80° , as opposed to if one of the lines was also oscillating around 140° , indicating an up–down conformation (Figure 8C). As shown in the Supporting Information, however, the conformations of all modeled compounds varied between the up and up–down conformations in at least one of the three parallels, and the changes from up to the up–down conformation occurred sometime between 60 and 255 ns (Table S3 and Figures S6–S10). In most parallels of the MD simulation, the compounds remained incorporated in the membrane throughout the duration of the

simulation. Except for **6a** (4-CF₃) as described below, if a molecule left the membrane, it was only for a few nanoseconds before it returned to the membrane environment, as can be seen from the time evolution of the C_5 z -coordinate for the other modeled compounds.

A simplified side view of the MD simulation system is presented in Figure 8D, which shows the interaction of **7e** (3,5-di-Br) with an *E. coli* inner membrane model. This includes a water pad over and under the PL bilayer, a PL bilayer in the middle, the phosphorous atoms of the lipid headgroups, and the location and time evolution of **7e** (3,5-di-Br) when interacting with the model membrane.

A reference set of simulations were also run with **6a** (4-CF₃) to investigate the selectivity of the membrane model. As described above, compound **6a** (4-CF₃) was much less potent against *E. coli* (MIC: 128 $\mu\text{g}/\text{mL}$) compared to the other modeled compounds. The simulations also showed that **6a** (4-CF₃) had less affinity to remain in the model membrane environment compared to the other compounds (Table S3 and Figure S6). In all the three parallels of MD simulations of **6a** (4-CF₃), it entered and left the membrane environment several times. This contrasted with the behavior seen in the simulations of **6e** (3,5-di-Br), **6g** (4-tBu), **7e** (3,5-di-Br), and **7g** (4-tBu) where once incorporated, the compounds remained in the membrane environment. The conformation of **6a** (4-

CF₃) varied between up and up–down, but there was an increase in events where **6a** (4-CF₃) returned from up–down to the up conformation (Figure S6). This behavior was not observed for other compounds in the MD simulations where only the shift from up to up–down was observed. As can be seen from Figure S6, **6a** (4-CF₃) also traveled out from the top of the simulation box and appeared at the bottom side of the simulation box and did this several times during the 260 ns simulation (Table S3). The periodic boundary conditions in the MD simulations allowed the free flow of molecules in and out of the simulation box. The behavior of **6a** (4-CF₃) compared to the other modeled compounds suggested that **6a** (4-CF₃) did not find favorable interactions in the membrane environment, and this may in part explain its low antimicrobial potency against *E. coli*.

CONCLUSIONS

In order to succeed transforming AMPs with non-optimal pharmacokinetic properties into clinical useful antimicrobials, an innovative strategy is to develop SMAMPs with imperative functional side chains embodied on a peptidomimetic scaffold. We have in the present study developed a novel peptidomimetic scaffold that fulfills the pharmacophore model of small AMPs and that was inspired by the marine antimicrobials eusynstyelamides. Compared to the structure of the eusynstyelamides, this novel series of cationic amphipathic barbiturates is achiral and easy to modify synthetically with respect to variation in cationic and lipophilic groups for optimization studies. The relative ease of synthesis has important implications for reducing future production costs and enabling large-scale production, which is an argument often raised against several classes of AMPs. We achieved improved antimicrobial activity compared with the eusynstyelamides, and several of the barbiturates displayed high antimicrobial activity against a panel of 30 multi-resistant clinical isolates of Gram-positive and Gram-negative bacteria. This included high activity against Gram-negative ESBL–CARBA isolates and strains resistant to the last resort antibiotic colistin. A pilot *in vivo* study using a murine neutropenic peritonitis model demonstrated that the overall most potent lead peptidomimetic **7e** (3,5-di-Br) significantly reduced the number of viable bacterial cells of clinical isolates of *E. coli* and *K. pneumoniae*. Although further structural optimizations are required to improve the MTD in mice, as well as pharmacokinetic studies including exploration of different routes of administration, demonstration of *in vivo* efficacy gives hope to the drug potential of this class of SMAMPs for treatment of serious infections.

EXPERIMENTAL SECTION

Chemicals and Equipment. All reagents and solvents were purchased from commercial sources and used as supplied with the exception of the starting material 1-(bromomethyl)-4-fluoronaphthalene, which was synthesized from the 4-fluoro-1-naphthoic acid according to the literature procedures.⁴⁰ Anhydrous DMF was prepared by storage over 4 Å molecular sieves. The reactions were monitored by thin-layer chromatography (TLC) with Merck pre-coated silica gel plates (60 F₂₅₄). Visualization was accomplished with either UV light or by immersion in potassium permanganate or phosphomolybdic acid (PMA), followed by light heating with a heating gun. Purifications using normal phase flash chromatography were either done by normal column chromatography using Normal Sil 60, 40–63 mm silica gel, or by automated normal phase flash chromatography (heptane/EtOAc) with the sample preloaded on a

Samplet cartridge belonging to a Biotage SP-1. Purification of reactions by RP C₁₈ column chromatography (water with 0.1% TFA/ acetonitrile with 0.1% TFA) was also executed on an automated purification module with the sample preloaded on a Samplet cartridge. All samples used for biological testing were determined to be of >95% purity. The analyses were carried out on a Waters ACQUITY UPC² system equipped with a Torus DEA 130 Å, 1.7 μm, 2.1 mm × 50 mm column coupled to a Waters ACQUITY PDA detector spanning from wavelengths 190–650 nm. The derivatives were eluted with a mobile phase consisting of supercritical CO₂ and MeOH containing 0.1% NH₃ and a linear gradient of 2–40% MeOH over 2 or 4 min, followed by isocratic 0.5 min of 40% MeOH. The flow rate was 1.5 mL/min. NMR spectra were obtained on a 400 MHz Bruker Avance III HD equipped with a 5 mm SmartProbe BB⁺H (BB = ¹⁹F, ³¹P–¹⁵N). Data are represented as follows: chemical shift, multiplicity (s = singlet, d = doublet, t = triplet, q = quartet, p = pentet, h = heptet, and m = multiplet), coupling constant (J, Hz), and integration. Chemical shifts (δ) are reported in ppm relative to the residual solvent peak (CDCl₃: δ_H 7.26 and δ_C 77.16; CD₃OD: δ_H 3.31 and δ_C 49.00). Positive and negative ion electrospray ionization mass spectrometry (ESI-MS) was conducted on a Thermo electron LTQ Orbitrap XL spectrometer.

Synthesis. Dialkylated Malonate Ester (2a–g). General Procedure. To a stirred solution of diethyl malonate in DMF (≈100 mg/mL) and base was added arylmethyl halide (≈2 equiv). The reaction was continuously stirred at room temperature overnight. The reaction mixture was diluted with EtOAc (30 mL) and washed with water (25 mL), aqueous 5% LiCl solution (3 × 25 mL), and brine (25 mL). The organic phase was dried over Na₂SO₄, filtered, and concentrated. The crude product was dissolved in CH₂Cl₂ (20 mL) and adsorbed on Celite. The product was purified on a silica column using 1–5% EtOAc in pentane as the mobile phase.

Diethyl 2,2-Bis(4-(trifluoromethyl)benzyl)malonate (2a). According to the general procedure, to a stirred solution of diethyl malonate (3.26 g, 20.4 mmol) in DMF (25 mL) over K₂CO₃ (8.5 g, 61.2 mmol) was added 1-(bromomethyl)-4-(trifluoromethyl)benzene (10 g, 41.8 mmol). The reaction was stirred at room temperature overnight. The reaction mixture was diluted with EtOAc (75 mL) and washed with water (5 × 50 mL), aqueous 5% LiCl solution (30 mL), and brine (40 mL). The organic phase was dried over Na₂SO₄, filtered, and concentrated. The crude product (9.97 g) was dissolved in CH₂Cl₂ (50 mL) and adsorbed on Celite. The product was purified on a silica column using 1–5% EtOAc in pentane as the mobile phase to afford **2a** (8.64 g, 89%) as a white solid. ¹H NMR (400 MHz, CDCl₃): δ 7.54 (d, J = 8.1 Hz, 4H), 7.28 (d, J = 8.1 Hz, 4H), 4.10 (q, J = 7.2 Hz, 4H), 3.27 (s, 4H), 1.13 (t, J = 7.1 Hz, 6H). ¹³C NMR (101 MHz, CDCl₃): δ 170.5, 140.4 (d, ⁴J_{C,F} = 1.8 Hz), 130.6, 129.6 (q, ²J_{C,F} = 32.5 Hz), 125.3 (q, ³J_{C,F} = 3.8 Hz), 124.3 (q, ¹J_{C,F} = 271.9 Hz), 61.7, 60.1, 39.8, 13.9. HRMS-ESI: C₂₃H₂₂F₆NaO₄⁺ [M + Na]⁺ calcd, 499.1315; found, 499.1298.

Diethyl 2,2-Bis(naphthalen-2-yl-methyl)malonate (2b). To a stirred solution of diethyl malonate (3.44 g, 21.5 mmol) in 15 mL of CH₂Cl₂ at 0 °C was added DBU (3.3 mL, 22.6 mmol). The reaction mixture was stirred for 5 min before adding 2-(bromomethyl)naphthalene (5.0 g, 22.6 mmol). The reaction was allowed to reach room temperature and stirred overnight. The reaction was concentrated, and the crude product isolated as a brown oil. The oil was dissolved in EtOAc (30 mL) and washed with water (2 × 30 mL), 10% citric acid (30 mL), 10% NaHCO₃ soln (30 mL), and brine (30 mL). The organic phase was dried over Na₂SO₄, filtered, and concentrated affording 4.83 g of almost pure monoalkylated diethyl malonate. To a suspension of NaH (774 mg, 32.2 mmol) in dry THF (15 mL) at 0 °C was added diethyl 2-(naphthalen-2-ylmethyl)malonate (4.8 g) dropwise as a solution in THF (15 mL). The resulting mixture was stirred for 10 min before adding 2-naphthyl methyl bromide (5 g, 22.6 mmol). The reaction was allowed to reach room temperature and stirred overnight. The reaction mixture was cooled in an ice bath, unreacted NaH was quenched with 10% citric acid solution, and the reaction mixture was concentrated. The crude product was then dissolved in EtOAc and washed with 10% citric acid soln (3 × 30 mL), 10% NaHCO₃ soln (2

× 30 mL), and brine (30 mL). The organic phase was dried over Na_2SO_4 , filtered, and concentrated to afford crude **2b** (7.35 g, 78%). $^1\text{H NMR}$ (400 MHz, CDCl_3): δ 7.85–7.80 (m, 2H), 7.77 (d, J = 8.1 Hz, 4H), 7.65 (d, J = 1.7 Hz, 2H), 7.49–7.43 (m, 4H), 7.32 (dd, J = 8.5, 1.7 Hz, 2H), 4.14 (q, J = 7.1 Hz, 4H), 3.45 (s, 4H), 1.14 (t, J = 7.1 Hz, 6H). $^{13}\text{C NMR}$ not determined. HRMS-ESI: $\text{C}_{29}\text{H}_{29}\text{O}_4^+ [\text{M} + \text{H}]^+$ calcd, 441.2060; found, 441.2059.

Diethyl 2,2-Bis(4-fluoronaphthalene-1-yl)methylmalonate (2c). According to the general procedure, to a stirred solution of diethyl malonate (1.3 g, 8.16 mmol) in DMF (10 mL) over K_2CO_3 (3.36 g, 24.3 mmol) was added 1-(bromomethyl)-4-fluoronaphthalene (4 g, 16.7 mmol). The reaction was continuously stirred at room temperature overnight. The reaction mixture was diluted with EtOAc (30 mL) and washed with water (3 × 20 mL), aqueous 5% LiCl solution (20 mL), and brine (20 mL). The organic phase was dried over Na_2SO_4 , filtered, and concentrated. In a round-bottomed flask, the brown solid crude product was dissolved in warm EtOH, capped with alumina foil, and left for 4 days at room temperature. Upon standing for an hour, the product **2c** crashed out of the brown solution as a white solid (1.6 g, 41%). $^1\text{H NMR}$ (400 MHz, CDCl_3): δ 8.18–8.08 (m, 2H), 8.05–7.95 (m, 2H), 7.57–7.46 (m, 4H), 7.36 (dd, J = 8.0, 5.5 Hz, 2H), 7.04 (dd, J = 10.2, 8.0 Hz, 2H), 3.81 (s, 4H), 3.75 (q, J = 7.2 Hz, 4H), 0.85 (t, J = 7.1 Hz, 6H). $^{13}\text{C NMR}$ (101 MHz, CDCl_3): δ 171.3, 158.1 (d, $J_{\text{C,F}}$ = 251.4 Hz), 134.2 (d, $J_{\text{C,F}}$ = 4.2 Hz), 128.9 (d, $J_{\text{C,F}}$ = 4.6 Hz), 127.6 (d, $J_{\text{C,F}}$ = 8.2 Hz), 126.8, 125.9 (d, $J_{\text{C,F}}$ = 2.1 Hz), 124.1–123.9 (m), 121.2 (d, $J_{\text{C,F}}$ = 6.0 Hz), 108.9 (d, $J_{\text{C,F}}$ = 19.7 Hz), 61.5, 59.8, 35.5, 13.6. HRMS-ESI: $\text{C}_{29}\text{H}_{26}\text{F}_2\text{NaO}_4^+ [\text{M} + \text{Na}]^+$ calcd, 499.1691; found, 499.1689.

Diethyl 2,2-Bis(4-bromo-3-chlorobenzyl)malonate (2d). According to the general procedure, to a stirred solution of diethyl malonate (313 mg, 1.95 mmol) in DMF (6 mL) over Cs_2CO_3 (1.91 g, 5.86 mmol) was added 1-bromo-4-(bromomethyl)-2-chlorobenzene (1.14 g, 4.01 mmol). The reaction was continuously stirred at 40 °C for 22 h. The reaction mixture was diluted with EtOAc (20 mL) and washed with aqueous 5% LiCl solution (3 × 20 mL). The organic phase was dried over MgSO_4 , filtered, and concentrated. The crude product was dissolved in CH_2Cl_2 (20 mL) and adsorbed on Celite. The product was purified on a silica column using 5% EtOAc in heptane as the mobile phase to afford **2d** (1.04 g, 94%) as a white solid. $^1\text{H NMR}$ (400 MHz, CDCl_3): δ 7.50 (d, J = 8.3 Hz, 2H), 7.24 (d, J = 2.1 Hz, 2H), 6.91 (dd, J = 8.3, 2.1 Hz, 2H), 4.13 (q, J = 7.1 Hz, 4H), 3.12 (s, 4H), 1.18 (t, J = 7.1 Hz, 6H). $^{13}\text{C NMR}$ (101 MHz, CDCl_3): δ 170.3, 137.1, 134.4, 133.6, 132.1, 129.8, 121.2, 61.9, 59.9, 39.1, 14.0. HRMS-ESI: $\text{C}_{21}\text{H}_{20}\text{Br}_2\text{Cl}_2\text{O}_4^+ [\text{M} + \text{Na}]^+$ calcd, 586.8998; found, 586.9005.

Diethyl 2,2-Bis(3,5-dibromobenzyl)malonate (2e). According to the general procedure, to a stirred solution of diethyl malonate (460 mg, 2.9 mmol) in DMF (5 mL) over Cs_2CO_3 (2.0 g, 6.37 mmol) was added 1,3-dibromo-5-(bromomethyl)benzene (2.0 g, 6.0 mmol). The reaction was continuously stirred at room temperature overnight. The reaction mixture was diluted with EtOAc (30 mL) and washed with water (25 mL), aqueous 5% LiCl solution (3 × 25 mL), and brine (25 mL). The organic phase was dried over Na_2SO_4 , filtered, and concentrated. The crude product was dissolved in CH_2Cl_2 (20 mL) and adsorbed on Celite. The product was purified on a silica column using 1–5% EtOAc in pentane as the mobile phase to afford **2e** (1.17 g, 61%) as a white solid. $^1\text{H NMR}$ (400 MHz, CDCl_3): δ 7.56 (t, J = 1.8 Hz, 2H), 7.24 (d, J = 1.8 Hz, 4H), 4.15 (q, J = 7.1 Hz, 4H), 3.11 (s, 4H), 1.20 (t, J = 7.2 Hz, 6H). $^{13}\text{C NMR}$ (101 MHz, CDCl_3): δ 170.0, 139.9, 132.8, 132.0, 122.7, 61.9, 60.0, 39.3, 13.9. HRMS-ESI: $\text{C}_{21}\text{H}_{20}\text{Br}_4\text{NaO}_4^+ [\text{M} + \text{Na}]^+$ calcd, 674.7987; found, 674.7961.

Diethyl 2,2-Bis(3,5-bis(trifluoromethyl)benzyl)malonate (2f). According to the general procedure, to a stirred solution of diethyl malonate (490 mg, 3.1 mmol) in DMF (5 mL) over Cs_2CO_3 (2.2 g, 6.83 mmol) was added 1-(bromomethyl)-3,5-bis(trifluoromethyl)benzene (2 g, 6.51 mmol). The reaction was continuously stirred at room temperature overnight. The reaction mixture was diluted with EtOAc (30 mL) and washed with water (25 mL), aqueous 5% LiCl solution (3 × 25 mL), and brine (25 mL). The organic phase was dried over Na_2SO_4 , filtered, and concentrated. The crude product was dissolved in CH_2Cl_2 (20 mL) and adsorbed on Celite. The product

was purified on a silica column using 1–5% EtOAc in pentane as the mobile phase to afford **2f** (0.89 g, 63%) as a white solid. $^1\text{H NMR}$ (400 MHz, CDCl_3): δ 7.79 (s, 2H), 7.71–7.54 (m, 4H), 4.10 (q, J = 7.1 Hz, 4H), 3.32 (s, 4H), 1.13 (t, J = 7.1 Hz, 6H). $^{13}\text{C NMR}$ (101 MHz, CDCl_3): δ 169.8, 138.5, 131.8 (q, $^2J_{\text{C,F}}$ = 33.3 Hz), 130.9–130.2 (m), 123.3 (q, $^1J_{\text{C,F}}$ = 272.7 Hz), 121.5 (p, $^3J_{\text{C,F}}$ = 3.9 Hz), 62.2, 60.3, 40.3, 13.8. HRMS-ESI: $\text{C}_{25}\text{H}_{19}\text{F}_{12}\text{O}_4^- [\text{M} - \text{H}]^-$ calcd, 611.1098; found, 611.1097.

Diethyl 2,2-Bis(4-tert-butylbenzyl)malonate (2g). According to the general procedure, to a stirred solution of diethyl malonate (3.43 g, 21.4 mmol) in DMF (25 mL) over K_2CO_3 (8.8 g, 64.2 mmol) was added 1-(bromomethyl)-4-tert-butylbenzene (10 g, 44 mmol). The reaction was continuously stirred at room temperature overnight. The reaction mixture was diluted with EtOAc (80 mL) and washed with water (3 × 50 mL), aqueous 5% LiCl solution (50 mL), and brine (50 mL). The organic phase was dried over Na_2SO_4 , filtered, and concentrated. The crude product was dissolved in CH_2Cl_2 (20 mL) and adsorbed on Celite. The product was purified on a silica column using 1–5% EtOAc in pentane as the mobile phase to afford **2g** (8.80 g, 90%) as a white solid. $^1\text{H NMR}$ (400 MHz, CDCl_3): δ 7.28 (d, J = 8.3 Hz, 4H), 7.11 (d, J = 8.4 Hz, 4H), 4.10 (q, J = 7.1 Hz, 4H), 3.19 (s, 4H), 1.30 (s, 18H), 1.14 (t, J = 7.1 Hz, 6H). $^{13}\text{C NMR}$ (101 MHz, CDCl_3): δ 171.2, 149.7, 133.4, 129.9, 125.2, 61.2, 60.4, 38.6, 34.5, 31.5, 14.0. HRMS-ESI: $\text{C}_{29}\text{H}_{40}\text{NaO}_4^+ [\text{M} + \text{Na}]^+$ calcd, 475.2818; found, 475.2795.

Condensation of Malonates (2) with Urea to Barbiturates (3).
5,5-Bis(4-trifluoromethylbenzyl)pyrimidine-2,4,6-(1H,3H,5H)-trione (3a). To a solution of urea (3.15 g, 52.5 mmol) in anhydrous DMF (15 mL) was added NaH (315 mg, 13.1 mmol). The reaction mixture was stirred 5 min before adding a solution of **2a** (2.5 g, 5.22 mmol) in anhydrous DMF (10 mL) dropwise. The reaction mixture was left under stirring overnight until TLC showed full conversion using 5% EtOAc in CHCl_3 as the mobile phase [R_f (product) 0.38, R_f (starting material) 0.89]. The reaction was diluted with 100 mL of EtOAc and washed with 10% citric acid soln (3 × 50 mL), 10% NaHCO_3 soln (2 × 50 mL), and brine (2 × 50 mL). The organic phase was dried over Na_2SO_4 , filtered, and concentrated, yielding the crude product (2.39 g). The crude was dissolved in CH_2Cl_2 and adsorbed onto Celite before being purified on a silica column using 5% EtOAc in CHCl_3 as the mobile phase to afford **3a** (1.63 g, 70%) as a white solid. $^1\text{H NMR}$ (400 MHz, CDCl_3): δ 7.53 (d, J = 8.1 Hz, 4H), 7.26* (d, 4H), 3.50 (s, 4H). $^{13}\text{C NMR}$ (101 MHz, CDCl_3): δ 170.4, 146.4, 138.1, 130.6 (q, $^2J_{\text{C,F}}$ = 32.7 Hz), 130.2, 126.0 (q, $^3J_{\text{C,F}}$ = 3.7 Hz), 124.0 (q, $^1J_{\text{C,F}}$ = 272.2 Hz), 60.3, 44.3. *Overlap with solvent. HRMS-ESI: $\text{C}_{20}\text{H}_{13}\text{F}_6\text{N}_2\text{O}_3^- [\text{M} - \text{H}]^-$ calcd, 443.0836; found, 443.0826.

5,5-Bis(naphthalen-2-yl)methylpyrimidine-2,4,6-(1H,3H,5H)-trione (3b). NaH (9 mg, 0.37 mmol) was added to a stirred solution of urea (91 mg, 1.49 mmol) in anhydrous DMF (3 mL) at room temperature. The reaction mixture was left to stir for 10 min before adding **2b** (66 mg, 0.15 mmol) slowly, and the reaction was left to stir overnight. The reaction mixture was diluted with EtOAc (20 mL) and washed with water (4 × 20 mL), followed by brine (20 mL). The organic phase was dried over Na_2SO_4 , filtered, and concentrated. The crude product was dissolved in CHCl_3 and adsorbed onto Celite before purification on a silica column using 0–5% EtOAc in CHCl_3 as the mobile phase to afford **3b** (50 mg, 82%). $^1\text{H NMR}$ (400 MHz, CD_3OD): δ 7.76–7.70 (m, 4H), 7.69 (d, J = 8.6 Hz, 2H), 7.62 (s, 2H), 7.44–7.36 (m, 4H), 7.26 (dd, J = 8.4, 1.7 Hz, 2H), 3.60 (s, 4H). $^{13}\text{C NMR}$ (101 MHz, CD_3OD): δ 173.2, 149.5, 133.8, 133.1, 132.8, 129.1, 128.7, 128.1, 127.9, 127.8, 126.6, 126.4, 60.8, 45.1. HRMS-ESI: $\text{C}_{26}\text{H}_{19}\text{N}_2\text{O}_3^- [\text{M} - \text{H}]^-$ calcd, 407.1417; found, 407.1416.

5,5-Bis(4-fluoronaphthalene-1-yl)methylpyrimidine-2,4,6-(1H,3H,5H)-trione (3c). To a stirred solution of urea (630 mg, 10.49 mmol) in anhydrous DMF (4 mL) was added NaH (76 mg, 3.16 mmol), and the resulting solution was stirred for 10 min before adding **2c** (500 mg, 1.05 mmol) slowly. The resulting mixture was stirred overnight. The reaction mixture was diluted with 25 mL of EtOAc and washed with 4 × 50 mL of water, followed by 20 mL of brine. The organic phase was dried over Na_2SO_4 , filtered, and concentrated. The crude product was dissolved in CHCl_3 and

adsorbed onto Celite before purification on a silica column using 0–5% EtOAc in CHCl₃ as the mobile phase to afford **3c** (430 mg, 92%). ¹H NMR (400 MHz, CDCl₃): δ 8.23 (d, *J* = 8.5 Hz, 2H), 8.14–8.04 (m, 2H), 7.64–7.49 (m, 4H), 7.46 (s, 2H), 7.29–7.26* (m, 2H), 7.00 (dd, *J* = 9.9, 8.1 Hz, 2H), 4.05 (s, 4H). ¹³C NMR (101 MHz, CDCl₃): δ 171.4, 158.7 (d, *J*_{C,F} = 253.3 Hz), 146.8, 133.3 (d, *J*_{C,F} = 4.5 Hz), 128.0 (d, *J*_{C,F} = 8.7 Hz), 127.4, 126.7 (d, *J* = 4.7 Hz), 126.5 (d, *J* = 1.9 Hz), 124.4–124.1 (m), 121.3 (d, *J* = 6.2 Hz), 109.1 (d, *J* = 20.1 Hz), 59.8, 40.0. *Overlap with solvent. HRMS-ESI: C₂₆H₃₁F₂N₂O₃[−] [M − H][−] calcd, 443.1213; found, 443.1181.

5,5-Bis(4-bromo-3-chlorobenzyl)pyrimidine-2,4,6-(1H,3H,5H)-trione (3d). To a stirred solution of urea (621 mg, 10.3 mmol) in anhydrous DMF (8 mL) was added NaH (124 mg, 3.1 mmol, 60% in mineral oil), and the resulting solution was stirred for 20 min before slowly adding **2d** (586 mg, 1.03 mmol), dissolved in 2 mL of anhydrous DMF. The resulting mixture was stirred for 20 h. The reaction mixture was diluted with 20 mL of EtOAc and washed with 4 × 20 mL of aq 5% LiCl. The organic phase was dried over MgSO₄, filtered, and concentrated. The crude product was adsorbed onto Celite before purification on a silica column using 20% EtOAc in heptane as the mobile phase to afford **3d** (364 mg, 66%). ¹H NMR (400 MHz, DMSO-*d*₆): δ 11.51 (NH, s, 2H), 7.71 (d, *J* = 8.2 Hz, 2H), 7.24 (d, *J* = 2.1 Hz, 2H), 6.93 (dd, *J* = 8.3, 2.1 Hz, 2H), 3.26 (s, 4H). ¹³C NMR (101 MHz, DMSO-*d*₆): δ 171.4, 148.8, 136.7, 134.0, 133.0, 131.3, 129.8, 120.6, 58.2, 41.9. HRMS-ESI: C₁₈H₁₁Br₂Cl₂N₂O₃[−] [M − H][−] calcd, 530.8519; found, 530.8520.

5,5-Bis(3,5-dibromobenzyl)pyrimidine-2,4,6-(1H,3H,5H)-trione (3e). To a stirred solution of urea (1.83 g, 2.79 mmol) in anhydrous DMF (15 mL) was added NaH (183 mg, 7.6 mmol), and the resulting solution was stirred for 10 min before adding **2e** (2.0 g, 3.05 mmol). The resulting mixture was stirred overnight. The reaction was diluted with EtOAc (50 mL) and washed with 10% citric acid soln (3 × 25 mL), 10% NaHCO₃ soln (2 × 30 mL), and brine (30 mL). The organic phase was dried over Na₂SO₄, filtered, and concentrated. The white solid was dissolved in CHCl₃ (25 mL), concentrated again, and purified by flash chromatography to afford **3e** (1.52 g, 88%). ¹H NMR (400 MHz, CDCl₃): δ 7.82 (NH, s, 2H), 7.58 (t, *J* = 1.8 Hz, 2H), 7.21 (d, *J* = 1.5 Hz, 4H), 3.32 (s, 4H). ¹³C NMR (101 MHz, CDCl₃): δ 170.0, 146.4, 137.7, 134.2, 131.5, 123.6, 59.9, 43.4. HRMS-ESI: C₁₈H₁₁⁷⁹Br₂N₂O₃[−] [M − H][−] calcd, 618.7509; found, 618.7501.

5,5-Bis(3,5-bis(trifluoromethyl)benzyl)pyrimidine-2,4,6-(1H,3H,5H)-trione (3f). To a solution of urea (1.3 g, 21.6 mmol) in 20 mL of anhydrous DMF was added NaH (128 mg, 5.3 mmol), and the resulting solution was stirred for 10 min before adding **2f** (1.0 g, 1.7 mmol). The resulting mixture was stirred overnight. The reaction was diluted with EtOAc (50 mL) and washed with 10% citric acid soln (3 × 30 mL), 10% NaHCO₃ soln (2 × 20 mL), and brine (30 mL). The organic phase was dried over Na₂SO₄, filtered, and concentrated. The crude was purified by automated flash chromatography to afford **3f** (0.27 g, 27%) as a white powder. ¹H NMR (400 MHz, CDCl₃): δ 7.82 (NH, s, 2H), 7.73 (s, 2H), 7.62–7.57 (m, 4H), 3.57 (s, 4H). ¹³C NMR (101 MHz, CDCl₃): δ 169.8, 146.1, 136.3, 132.6 (q, ²*J*_{C,F} = 33.6 Hz), 130.4–129.7 (m), 122.0 (q, ¹*J*_{C,F} = 272.8 Hz), 122.9–122.2 (m), 59.9, 43.5. HRMS-ESI: C₂₂H₁₁F₁₂N₂O₃[−] [M − H][−] calcd, 579.0584; found, 579.0583.

5,5-Bis(4-tert-butylbenzyl)pyrimidin-2,4,6-(1H,3H,5H)-trione (3g). To a stirred solution of urea (6.63 g, 110 mmol) at room temperature in anhydrous DMF (20 mL) was added NaH (660 mg, 27.5 mmol), and the reaction was stirred for 5 min. A solution of **2g** (5 g, 11 mmol) in anhydrous DMF (20 mL) was added dropwise to the reaction mixture, and the reaction was stirred overnight. The reaction mixture was diluted with EtOAc (20 mL) and washed with 10% citric acid (100 mL), 10% NaHCO₃ soln (50 mL), brine (50 mL), water (20 mL), and brine (2 × 50 mL). The organic phase was dried over Na₂SO₄, filtered, and concentrated. The crude product was purified by automated flash chromatography (heptane/EtOAc) affording 4.09 g (88%) of **3g** as a white powder. ¹H NMR (400 MHz, CD₃OD): δ 7.26 (d, *J* = 7.7 Hz, 2H), 7.05 (d, *J* = 7.6 Hz, 2H), 3.31 (s, 4H, overlap CD₃OD), 1.24 (s, 18H). ¹³C NMR (101 MHz, CD₃OD): δ 174.2, 151.5*, 133.5, 130.4, 126.4, 61.4, 45.0, 35.3, 31.7. *Assumed overlap

of two signals. HRMS-ESI: C₂₆H₃₁N₂O₃[−] [M − H][−] calcd, 419.2340; found, 419.2335.

5,5-Bis(3,5-di-tert-butylbenzyl)pyrimidine-2,4,6-(1H,3H,5H)-trione (3h). Compound **3h** was provided to us by Elizaveta M. Igumnova. ¹H NMR (400 MHz, CDCl₃): δ 7.25–7.24 (m, 2H), 6.96 (d, *J* = 1.8 Hz, 4H), 3.45 (s, 4H), 1.26 (s, 36H). ¹³C NMR (101 MHz, CDCl₃): δ 171.5, 151.3, 133.7, 123.9, 121.3, 61.7, 45.4, 34.9, 31.5. HRMS-ESI: C₃₄H₄₇N₂O₃[−] [M − H][−] calcd, 531.3592; found, 531.3592.

N-Alkylation of Barbiturates (3) with 1,4-Dibromobutane. 1,3-Bis(4-bromobutyl)-5,5-bis(4-trifluoromethylbenzyl)pyrimidine-2,4,6-(1H,3H,5H)-trione (4a). To a stirred solution of **3a** (1.59 g, 3.58 mmol) at room temperature in DMF (15 mL) were added K₂CO₃ (2.00 g, 14.47 mmol) and 1,4-dibromobutane (4.24 mL, 35.8 mmol). The reaction mixture was stirred for 48 h, diluted with EtOAc (50 mL), and washed with 10% citric acid soln (3 × 25 mL), 10% NaHCO₃ soln (2 × 25 mL), and brine (25 mL). The organic phase was dried over Na₂SO₄, filtered, and concentrated. The crude product was purified using automated flash chromatography affording **4a** (2.47 g, 96%) as a white powder. ¹H NMR (400 MHz, CDCl₃): δ 7.50 (d, *J* = 7.8 Hz, 4H), 7.20 (d, *J* = 8.0 Hz, 4H), 3.61 (t, *J* = 7.3 Hz, 4H), 3.51 (s, 4H), 3.31 (t, *J* = 6.5 Hz, 4H), 1.67–1.49 (m, 4H), 1.39 (p, *J* = 7.1 Hz, 4H). ¹³C NMR (101 MHz, CDCl₃): δ 170.2, 149.3, 138.8, 130.4 (q, ²*J*_{C,F} = 32.7 Hz), 130.1, 125.8 (q, ³*J*_{C,F} = 3.7 Hz), 123.9 (q, ¹*J*_{C,F} = 272.2 Hz), 60.0, 45.2, 41.1, 32.7, 29.5, 26.4. HRMS-ESI: C₂₈H₂₈⁷⁹Br₂F₆KN₂O₃⁺ [M + K]⁺ calcd, 751.0002; found, 751.0006.

1,3-Bis(4-bromobutyl)-5,5-bis(naphthalen-2-yl-methyl)pyrimidine-2,4,6-(1H,3H,5H)-trione (4b). To a stirred suspension of **3b** (200 mg, 0.49 mmol) and K₂CO₃ (273 mg, 1.95 mmol) in DMF (4 mL) was added 1,4-dibromobutane (0.57 mL, 4.9 mmol). The reaction was stirred for 18–48 h until completion was indicated by TLC (5% EtOAc in CHCl₃). The reaction mixture was diluted with EtOAc (25 mL), and K₂CO₃ was filtered off. The organic phase was washed with 10% citric acid solution (30 mL), 10% NaHCO₃ soln (30 mL), water (3 × 30 mL), and brine (30 mL); dried with Na₂SO₄, filtered; and concentrated. The crude product was dissolved in CHCl₃ (30 mL) and adsorbed onto Celite before purification on a silica column using 0–5% EtOAc in CHCl₃ to afford **4b** (347 mg, 80%) as a white powder. ¹H NMR (400 MHz, CDCl₃): δ 7.75 (dd, *J* = 9.4, 6.4 Hz, 4H), 7.70 (d, *J* = 8.4 Hz, 2H), 7.57 (s, 2H), 7.48–7.42 (m, 4H), 7.18 (dd, *J* = 8.5, 1.7 Hz, 2H), 3.68 (s, 4H), 3.53 (t, *J* = 6.7 Hz, 4H), 2.99 (t, *J* = 6.2 Hz, 4H), 1.35–1.19 (m, 8H). ¹³C NMR (101 MHz, CDCl₃): δ 170.9, 149.6, 133.3, 132.7, 132.5, 128.8, 128.5, 127.8, 127.7, 127.2, 126.6, 126.3, 60.8, 45.8, 40.9, 32.8, 29.5, 26.3. HRMS-ESI: C₃₄H₃₄⁷⁹Br₂N₂NaO₃⁺ [M + Na]⁺ calcd, 699.0827; found, 699.0839.

1,3-Bis(4-bromobutyl)-5,5-bis(4-F-naphthalene-1-yl-methyl)pyrimidine-2,4,6-(1H,3H,5H)-trione (4c). To a stirred suspension of **3c** (242 mg, 0.54 mmol) and K₂CO₃ (300 mg, 2.17 mmol) in DMF (5 mL) was added 1,4-dibromobutane (0.64 mL, 5.4 mmol). The reaction was stirred for 18–48 h until completion was indicated by TLC (CHCl₃, R_f product: 0.74, R_f starting material: 0.11). The reaction mixture was diluted with EtOAc (25 mL), and K₂CO₃ filtered off. The organic phase was washed with 10% citric acid soln (30 mL), 10% NaHCO₃ soln (30 mL), water (3 × 30 mL), and brine (30 mL); dried with Na₂SO₄, filtered; and concentrated, yielding the crude as an oil. The crude product was dissolved in CHCl₃ (30 mL) and adsorbed onto Celite before purification on a silica column using CHCl₃ as the mobile phase to afford **4c** (237 mg, 61%) as a white solid. ¹H NMR (400 MHz, CDCl₃): δ 8.23 (d, *J* = 8.6 Hz, 2H), 8.08 (d, *J* = 8.3 Hz, 2H), 7.63 (t, *J* = 7.7 Hz, 2H), 7.54 (t, *J* = 7.6 Hz, 2H), 7.23 (dd, *J* = 8.0, 5.5 Hz, 2H), 7.00 (dd, *J* = 9.8, 8.1 Hz, 2H), 4.06 (s, 4H), 3.33 (t, *J* = 7.2 Hz, 4H), 3.05 (t, *J* = 6.6 Hz, 4H), 1.34–1.12 (m, 4H), 1.08–0.90 (m, 4H). ¹³C NMR (101 MHz, CDCl₃): δ 178.0 (d, *J*_{C,F} = 8.4 Hz), 158.5 (d, ¹*J*_{C,F} = 253.3 Hz), 149.4, 133.2 (d, *J*_{C,F} = 4.4 Hz), 129.0 (d, *J*_{C,F} = 8.4 Hz), 127.4 (d, *J*_{C,F} = 4.7 Hz), 127.2, 126.4 (d, *J*_{C,F} = 2.1 Hz), 124.8 (d, *J*_{C,F} = 2.7 Hz), 124.1 (d, *J*_{C,F} = 15.7 Hz), 121.1 (d, *J*_{C,F} = 6.0 Hz), 108.9 (d, *J*_{C,F} = 20.0 Hz), 60.0, 40.9, 40.7, 32.7, 29.3, 25.9. HRMS-ESI: C₃₄H₃₂⁷⁹Br₂F₂N₂NaO₃⁺ [M + Na]⁺ calcd, 735.0639; found, 735.0622.

5,5-Bis(4-bromo-3-chlorobenzyl)-1,3-bis(4-bromobutyl)-pyrimidine-2,4,6-(1H,3H,5H)-trione (4d). To a stirred suspension of **3d** (1.748 g, 3.267 mmol) and K_2CO_3 (1.806 g, 13.07 mmol) in DMF (15 mL) was added 1,4-dibromobutane (4.46 mL, 37.3 mmol). The reaction was stirred for 14 days. The organic phase was washed with 10% citric acid soln (30 mL), 10% $NaHCO_3$ soln (30 mL), water (3 × 30 mL), and brine (30 mL); dried with Na_2SO_4 ; filtered; and concentrated, yielding the crude as an oil. The crude product was purified on an automated flash system silica column using DCM/MeOH as the mobile phase to afford **4d** (1.78 mg, 68%) as a white solid. 1H NMR (400 MHz, $CDCl_3$): δ 7.47 (d, J = 8.2 Hz, 2H), 7.15 (d, J = 2.1 Hz, 2H), 6.80 (dd, J = 8.2, 2.1 Hz, 2H), 3.64 (t, J = 7.3 Hz, 4H), 3.41–3.28 (m, 8H), 1.65–1.55 (m, 4H), 1.51–1.40 (m, 4H). ^{13}C NMR (101 MHz, $CDCl_3$): δ 170.1, 149.2, 135.5, 134.9, 134.1, 131.4, 129.1, 122.2, 59.7, 44.3, 41.2, 32.7, 29.7, 26.5. HRMS-ESI: $C_{26}H_{26}^{79}Br_4Cl_2N_2NaO_3^+$ [M + Na] $^+$ calcd, 822.7946; found, 822.7960.

1,3-Bis(4-bromobutyl)-5,5-bis(3,5-dibromobenzyl)pyrimidine-2,4,6-(1H,3H,5H)-trione (4e). To a stirred solution of **3e** (300 mg, 0.48 mmol) in DMF (6 mL) was added K_2CO_3 (265 mg, 1.92 mmol) and 1,4-dibromobutane (0.57 mL, 4.81 mmol). The reaction was stirred for 18–48 h until completion was indicated by TLC (5% EtOAc in $CHCl_3$). The reaction mixture was diluted with EtOAc (25 mL), and K_2CO_3 was filtered off. The organic phase was washed with 10% citric acid soln (30 mL), 10% $NaHCO_3$ soln (30 mL), water (3 × 30 mL), and brine (30 mL); dried with Na_2SO_4 ; filtered; and concentrated, resulting in an oil that slowly turned into white crystals. The crude product was dissolved in $CHCl_3$ (30 mL) and adsorbed onto Celite before purification on a silica column using pentane: CH_2Cl_2 (7:3 to 1:1) to afford **4e** (347 mg, 80%) as a white powder. 1H NMR (400 MHz, $CDCl_3$): δ 7.54 (d, J = 1.8 Hz, 2H), 7.14 (d, J = 1.7 Hz, 4H), 3.65 (t, J = 7.4 Hz, 4H), 3.38 (t, J = 6.7 Hz, 4H), 3.33 (s, 4H), 1.77–1.61 (m, 4H), 1.58–1.43 (m, 4H). ^{13}C NMR (101 MHz, $CDCl_3$): δ 169.9, 149.1, 138.4, 133.9, 131.3, 123.4, 59.9, 44.2, 41.3, 32.7, 30.0, 26.7. HRMS-ESI: $C_{26}H_{26}^{79}Br_3^{81}Br_3ClN_2O_3^-$ [M + Cl] $^-$ calcd, 928.6671; found, 928.6669.

1,3-Bis(4-bromobutyl)-5,5-bis(3,5-bis(trifluoromethyl)benzyl)pyrimidine-2,4,6-(1H,3H,5H)-trione (4f). To a stirred solution of **3f** (0.864 g, 1.57 mmol) in DMF (20 mL) were added K_2CO_3 (1.233 g, 8.93 mmol) and 1,4-dibromobutane (1.76 mL, 14.9 mmol). The reaction mixture was stirred for 48 h, diluted with EtOAc (30 mL), and washed with water (3 × 20 mL), 5% LiCl soln (3 × 20), and brine (20 mL). The crude product was purified by automated flash chromatography to afford **4f** (0.64 g, 50%) as a white powder. 1H NMR (400 MHz, $CDCl_3$): δ 7.79 (s, 2H), 7.53 (s, 4H), 3.59 (s, 4H), 3.57–3.51 (m, 4H), 3.26 (t, J = 6.8 Hz, 4H), 1.67–1.55 (m, 4H), 1.43–1.29 (m, 4H). ^{13}C NMR (101 MHz, $CDCl_3$): δ 169.4, 148.4, 136.9, 132.2 (q, $^2J_{C,F}$ = 33.6 Hz), 130.0–129.4 (m), 122.9 (q, $^1J_{C,F}$ = 272.9 Hz), 122.1 (p, $^3J_{C,F}$ = 3.8 Hz), 59.7, 44.3, 41.1, 31.7, 29.6, 26.1. HRMS-ESI: $C_{30}H_{26}^{79}Br_3F_{12}N_2O_3^-$ [M + Br] $^-$ calcd, 926.9308; found, 926.9308.

1,3-Bis(4-bromobutyl)-5,5-bis(4-tert-butylbenzyl)pyrimidine-2,4,6-(1H,3H,5H)-trione (4g). To a stirred solution of **3g** (3.88 g, 9.23 mmol) at room temperature in DMF (50 mL) were added K_2CO_3 (5.12 g, 37 mmol) and 1,4-dibromobutane (10.9 mL, 92.5 mmol). The reaction mixture was stirred overnight. The reaction mixture was diluted with EtOAc (100 mL) and washed with water (100 mL). The crude product was purified by automated flash chromatography, affording the product **4g** (2.60 g, 40%) as a white powder. 1H NMR (400 MHz, $CDCl_3$): δ 7.22 (d, J = 7.8 Hz, 4H), 6.98 (d, J = 7.9 Hz, 4H), 3.60 (t, J = 6.9 Hz, 4H), 3.41 (s, 4H), 3.33 (t, J = 6.4 Hz, 4H), 1.56 (p, J = 7.3 Hz, 4H), 1.42 (p, J = 7.7 Hz, 4H), 1.25 (s, 18H). ^{13}C NMR (101 MHz, $CDCl_3$): δ 170.9, 150.7, 149.9, 131.9, 129.2, 125.5, 60.7, 45.0, 40.7, 34.5, 32.9, 31.4, 29.5, 26.2. HRMS-ESI: $C_{34}H_{46}^{79}Br_2N_2NaO_3^+$ [M + Na] $^+$ calcd, 711.1774; found, 711.1773.

1,3-Bis(4-bromobutyl)-5,5-bis(3,5-di-tert-butylbenzyl)pyrimidine-2,4,6-(1H,3H,5H)-trione (4h). To a stirred solution of **3h** (0.86 g, 1.62 mmol) in DMF was added K_2CO_3 (1.2 g, 8.9 mmol). The reaction mixture was stirred for 5 min before addition of 1,4-

dibromobutane (1.76 mL, 14.8 mmol). The reaction was stirred for 18–48 h until completion was indicated by TLC (5% EtOAc in $CHCl_3$). The reaction mixture was diluted with EtOAc (15 mL), and K_2CO_3 was filtered off. The organic phase was washed with 10% citric acid soln (30 mL), 10% $NaHCO_3$ soln (30 mL), water (3 × 30 mL), and brine (30 mL); dried with Na_2SO_4 ; filtered; and concentrated. The crude was purified by automated flash chromatography to afford **4h** (0.64 g, 74%). 1H NMR (400 MHz, $CDCl_3$): δ 7.26 (t, J = 1.9 Hz, 2H), 6.89 (d, J = 1.8 Hz, 4H), 3.59* (t, J = 7.5 Hz, 4H), 3.46 (s, 4H), 3.23 (t, J = 6.7 Hz, 4H), 1.51 (p, J = 6.8 Hz, 4H), 1.35–1.23 (m, 40H). ^{13}C NMR (101 MHz, $CDCl_3$): δ 171.0, 151.1, 150.0, 134.4, 123.7, 121.5, 60.5, 46.5, 40.9, 34.8, 32.4, 31.6, 29.7, 26.5. *Distorted triplet. HRMS-ESI: $C_{42}H_{62}^{79}Br_2KN_2O_3^+$ [M + K] $^+$ calcd, 839.2759; found, 839.2755.

Transformation to Azides (5). **1,3-Bis(4-azidobutyl)-5,5-bis(4-trifluoromethylbenzyl)pyrimidine-2,4,6-(1H,3H,5H)-trione (5a).** To a stirred solution of **4a** (2.40 g, 3.35 mmol) in 5 mL of DMF was added NaN_3 (762 mg, 11.7 mmol) and stirred for 18 h. The reaction mixture was diluted with EtOAc (30 mL) and washed with water (3 × 50 mL). The organic phase was dried over Na_2SO_4 , filtered, and concentrated to afford the crude product **5a** as white crystals (1.91 g, 89%). 1H NMR (400 MHz, $CDCl_3$): δ 7.49 (d, J = 7.8 Hz, 4H), 7.19 (d, J = 7.8 Hz, 4H), 3.67–3.58 (m, 4H), 3.51 (s, 4H), 3.27–3.15 (m, 4H), 1.38–1.23 (m, 8H). ^{13}C NMR (101 MHz, $CDCl_3$): δ 170.2, 149.3, 138.8, 130.4 (q, $^2J_{C,F}$ = 32.7 Hz), 130.1, 126.0–125.6 (m), 123.9 (q, $^1J_{C,F}$ = 272.2 Hz), 59.9, 50.8, 45.1, 41.4, 26.0, 24.9. HRMS-ESI: $C_{28}H_{28}F_6N_8O_3Na^+$ [M + Na] $^+$ calcd, 661.2079; found, 661.2074.

1,3-Bis(4-azidobutyl)-5,5-bis(naphthalen-2-yl)pyrimidine-2,4,6-(1H,3H,5H)-trione (5b). To a stirred solution of **4b** (509 mg, 0.75 mmol) in DMF (3 mL) was added NaN_3 (146 mg, 2.25 mmol). The reaction was stirred overnight until completion was indicated by TLC (5% EtOAc in $CHCl_3$). The reaction mixture was diluted with EtOAc (20 mL) and washed with water (3 × 20 mL). The organic phase was dried over Na_2SO_4 , filtered, and concentrated. The crude product was dissolved in $CHCl_3$ and adsorbed onto Celite before purification on a silica column using 0–5% EtOAc in $CHCl_3$ to afford **5b** (194 mg, 91%). 1H NMR (400 MHz, $CDCl_3$): δ 7.80–7.71 (m, 4H), 7.68 (d, J = 8.4 Hz, 2H), 7.57 (s, 2H), 7.51–7.41 (m, 4H), 7.17 (d, J = 8.4 Hz, 2H), 3.68 (s, 4H), 3.52 (t, J = 7.0 Hz, 4H), 2.85 (t, J = 6.6 Hz, 4H), 1.14 (p, J = 7.4 Hz, 4H), 1.02 (p, J = 7.0 Hz, 4H). ^{13}C NMR (101 MHz, $CDCl_3$): δ 170.9, 149.6, 133.4, 132.7, 132.5, 128.8, 128.5, 127.8, 127.7, 127.2, 126.6, 126.3, 60.8, 50.7, 45.8, 41.2, 25.8, 24.9. HRMS-ESI: $C_{34}H_{34}N_8NaO_3^+$ [M + Na] $^+$ calcd, 625.2646; found, 625.2647.

1,3-Bis(4-azidobutyl)-5,5-bis(4-fluoronaphthalen-1-yl)methyl)pyrimidine-2,4,6-(1H,3H,5H)-trione (5c). To a stirred solution of **4c** (166 mg, 0.23 mmol) in DMF (3 mL) was added NaN_3 (45 mg, 0.69 mmol). The reaction was stirred overnight until completion was indicated by TLC ($CHCl_3$). Then, the reaction mixture was diluted with EtOAc (20 mL) and washed with water (3 × 30 mL) and brine (30 mL). The organic phase was dried over Na_2SO_4 , filtered, and concentrated to afford **5c** (142 mg, 95%). 1H NMR (400 MHz, $CDCl_3$): δ 8.23 (d, J = 8.6 Hz, 2H), 8.08 (d, J = 8.3 Hz, 2H), 7.62 (t, J = 7.6 Hz, 2H), 7.54 (t, J = 7.5 Hz, 2H), 7.22 (t, J = 6.6 Hz, 2H), 6.98 (t, J = 9.0 Hz, 2H), 4.06 (s, 4H), 3.33 (t, J = 6.8 Hz, 4H), 2.94 (t, J = 6.4 Hz, 4H), 1.10–0.74 (m, 8H). ^{13}C NMR (101 MHz, $CDCl_3$): δ 170.9, 158.5 (d, $^1J_{C,F}$ = 253.4 Hz), 149.4, 133.2 (d, $J_{C,F}$ = 4.4 Hz), 127.9 (d, $J_{C,F}$ = 8.5 Hz), 127.4 (d, $J_{C,F}$ = 4.6 Hz), 127.2, 126.4 (d, $J_{C,F}$ = 1.9 Hz), 124.8 (d, $J_{C,F}$ = 2.6 Hz), 124.1 (d, $J_{C,F}$ = 15.7 Hz), 121.1 (d, $J_{C,F}$ = 6.1 Hz), 108.8 (d, $J_{C,F}$ = 20.0 Hz), 60.0, 50.7, 41.1, 40.7, 25.6, 24.4. HRMS-ESI: $C_{34}H_{32}ClF_2N_8O_3^-$ [M + Cl] $^-$ calcd, 673.2259; found, 673.2259.

1,3-Bis(4-azidobutyl)-5,5-bis(4-bromo-3-chlorobenzyl)pyrimidine-2,4,6-(1H,3H,5H)-trione (5d). To a stirred solution of **4d** (1.28 g, 1.58 mmol) in DMF (20 mL) was added NaN_3 (0.29 g, 4.75 mmol). The reaction was stirred overnight until completion was indicated by TLC (5% EtOAc in $CHCl_3$). Then, the reaction mixture was diluted with EtOAc (25 mL) and washed with water (2 × 20 mL). The organic phase was dried over Na_2SO_4 , filtered, and concentrated to yield the crude product **5d** (1.153 g, 98%). The crude

product was used without further purification. ^1H NMR (400 MHz, CDCl_3): δ 7.46 (d, $J = 8.2$ Hz, 2H), 7.15 (d, $J = 2.0$ Hz, 2H), 6.80 (dd, $J = 8.2, 2.1$ Hz, 2H), 3.63 (t, $J = 6.7$ Hz, 4H), 3.35 (s, 4H), 3.30–3.21 (m, 4H), 1.36 (h, $J = 3.2$ Hz, 8H). ^{13}C NMR (101 MHz, CDCl_3): δ 170.1, 149.2, 135.5, 134.9, 134.1, 131.4, 129.1, 122.2, 59.7, 50.9, 44.3, 41.5, 26.1, 25.1. HRMS-ESI: $\text{C}_{26}\text{H}_{26}^{79}\text{Br}_2\text{Cl}_2\text{N}_8\text{NaO}_3^+ [\text{M} + \text{Na}]^+$ calcd, 748.9764; found, 748.9777.

1,3-Bis(4-azidobutyl)-5,5-bis(3,5-dibromobenzyl)pyrimidine-2,4,6-(1H,3H,5H)-trione (5e). To a stirred solution of **4e** (239 mg, 0.26 mmol) in DMF (3 mL) was added NaN_3 (52 mg, 0.8 mmol). The reaction was stirred overnight until completion was indicated by TLC (5% EtOAc in CHCl_3). Then, the reaction mixture was diluted with EtOAc (15 mL) and washed with water (2 \times 20 mL). The organic phase was dried over Na_2SO_4 , filtered, and concentrated. The crude product was dissolved in CHCl_3 and adsorbed onto Celite before purification on a silica column using 0–5% EtOAc in CHCl_3 to afford **5e** (194 mg, 91%). ^1H NMR (400 MHz, CDCl_3): δ 7.54 (s, 2H), 7.14 (s, 4H), 3.73–3.58 (m, 4H), 3.33 (s, 4H), 3.31–3.22 (m, 4H), 1.58–1.29 (m, 8H). ^{13}C NMR (101 MHz, CDCl_3): δ 169.9, 149.1, 138.4, 133.8, 131.4, 123.3, 59.9, 50.9, 44.2, 41.6, 26.1, 25.3. HRMS-ESI: $\text{C}_{26}\text{H}_{26}^{79}\text{Br}_4\text{ClN}_8\text{O}_3^- [\text{M} + \text{Cl}]^-$ calcd, 848.8555; found, 848.8564.

1,3-Bis(4-azidobutyl)-5,5-bis(3,5-bis(trifluoromethyl)benzyl)pyrimidine-2,4,6-(1H,3H,5H)-trione (5f). To a stirred solution of **4f** (101 mg, 0.12 mmol) in DMF (1 mL) was added NaN_3 (23 mg, 0.35 mmol). The reaction was stirred overnight. When full conversion was reached according to MS analysis, the reaction mixture was diluted with EtOAc (15 mL) and washed with water (3 \times 20 mL). The organic phase was dried over Na_2SO_4 , filtered, and concentrated to afford the crude of **5f** (63 mg, 68%) as a white powder. ^1H NMR (400 MHz, CDCl_3): δ 7.78 (s, 2H), 7.53 (s, 4H), 3.59 (s, 4H), 3.57–3.48 (m, 4H), 3.19 (t, $J = 6.7$ Hz, 4H), 1.42–1.31 (m, 4H), 1.31–1.20 (m, 4H). ^{13}C NMR (101 MHz, CDCl_3): δ 169.6, 148.6, 137.0, 132.3 (q, $^2J_{\text{C,F}} = 33.6$ Hz), 129.9, 123.0 (q, $^3J_{\text{C,F}} = 272.9$ Hz), 122.8–121.9 (m), 59.8, 50.6, 44.5, 41.6, 26.0, 24.9. HRMS-ESI: $\text{C}_{30}\text{H}_{26}\text{ClF}_{12}\text{N}_8\text{O}_3^- [\text{M} + \text{Cl}]^-$ calcd, 809.1630; found, 809.1622.

1,3-Bis(4-azidobutyl)-5,5-bis(4-tert-butylbenzyl)pyrimidine-2,4,6-(1H,3H,5H)-trione (5g). To a stirred solution of bromide **4g** (2.40 g, 3.47 mmol) in DMF (15 mL) was added NaN_3 (678 mg, 10.4 mmol) and stirred for 18 h. The reaction mixture was diluted with EtOAc (50 mL) and washed with water (4 \times 50 mL). The organic phase was dried over Na_2SO_4 , filtered, and concentrated. The crude product **5g** was isolated as a clear oil (2.16 g, 100%). ^1H NMR (400 MHz, CDCl_3): δ 7.20 (d, $J = 7.7$ Hz, 4H), 6.97 (d, $J = 7.8$ Hz, 4H), 3.59 (s, 4H), 3.40 (s, 4H), 3.21 (s, 4H), 1.37–1.28 (m, 8H), 1.24 (s, 18H). ^{13}C NMR (101 MHz, CDCl_3): δ 171.0, 150.8, 150.0, 132.0, 129.3, 125.5, 60.7, 50.9, 45.1, 41.1, 34.6, 31.4, 26.0, 24.8. HRMS-ESI: $\text{C}_{34}\text{H}_{46}\text{N}_8\text{O}_3\text{Na}^+ [\text{M} + \text{Na}]^+$ calcd, 637.3577; found, 637.3583.

1,3-Bis(4-azidobutyl)-5,5-bis(4-tert-butylbenzyl)pyrimidine-2,4,6-(1H,3H,5H)-trione (5h). To a stirred solution of **4h** (630 mg, 0.78 mmol) in DMF (10 mL) was added NaN_3 (140 mg, 2.15 mmol). The reaction was stirred overnight. When full conversion was reached according to MS analysis, the reaction mixture was diluted with EtOAc (50 mL) and washed with water 4 \times 50 mL. The organic phase was dried over Na_2SO_4 , filtered, and concentrated, affording the crude product **5h** (463 mg, 80%). ^1H NMR (400 MHz, CDCl_3): δ 7.25 (t, $J = 1.9$ Hz, 2H), 6.87 (d, $J = 1.7$ Hz, 4H), 3.56 (t, $J = 7.2$ Hz, 4H), 3.45 (s, 4H), 3.14 (t, $J = 6.5$ Hz, 4H), 1.25 (s, 44H). ^{13}C NMR (101 MHz, CDCl_3): δ 171.1, 151.1, 150.0, 134.4, 123.8, 121.6, 60.6, 50.8, 46.5, 41.3, 34.8, 31.6, 25.9, 25.1. HRMS-ESI: $\text{C}_{42}\text{H}_{62}\text{N}_8\text{NaO}_3^+ [\text{M} + \text{Na}]^+$ calcd, 749.4838; found, 749.4838.

Reduction of Azides (5) to Amines (6). **1,3-Bis(4-aminobutyl)-5,5-bis(4-(trifluoromethyl)benzyl)pyrimidin-2,4,6-(1H,3H,5H)-trione (6a).** To a stirred solution of **5a** (1.86 g, 2.90 mmol) and Et_3N (0.96 mL, 6.89 mmol) in *i*-PrOH/THF (1:1, 10 mL) was added 1,3-propanedithiol (0.1 mL, 0.99 mmol). The mixture was stirred for 5 min before addition of NaBH_4 (316 mg, 8.35 mmol). After a 48 h reaction time, Boc_2O (1.75 g, 8.02 mmol) and K_2CO_3 (1.91 g, 13.8 mmol) were added, and the reaction was stirred for 18 h and evaporated before adding EtOAc (20 mL) and water (15 mL) and

stirring for 1 h. The organic phase was washed with water (3 \times 15 mL) and brine (15 mL) and concentrated. The resulting crude was purified by automated flash chromatography and evaporated. The Boc-protected intermediate was deprotected with TFA (2 mL, 26 mmol) in CH_2Cl_2 (5 mL) for 18 h. The reaction mixture was concentrated, and the crude product was purified by RP automated flash chromatography and lyophilized to afford **6a** (160 mg, 7%) as the TFA salt. ^1H NMR (400 MHz, CD_3OD): δ 7.58 (d, $J = 8.1$ Hz, 4H), 7.28 (d, $J = 8.1$ Hz, 4H), 3.71–3.58 (m, 4H), 3.57 (s, 4H), 2.96–2.75 (m, 4H), 1.42 (p, $J = 7.3$ Hz, 4H), 1.30 (p, $J = 7.3$ Hz, 4H). ^{13}C NMR (101 MHz, CD_3OD): δ 171.4, 162.9 (q, $^2J_{\text{C,F}} = 34.7$ Hz, TFA), 150.7, 140.9, 131.5, 131.0 (q, $^2J_{\text{C,F}} = 32.6$ Hz), 126.6 (q, $^1J_{\text{C,F}} = 3.8$ Hz), 125.5 (q, $^3J_{\text{C,F}} = 272.3$ Hz), 118.2 (q, $^1J_{\text{C,F}} = 292.5$ Hz, TFA), 61.1, 45.8, 42.0, 40.0, 25.6 (overlap, two carbons). HRMS-ESI: $\text{C}_{28}\text{H}_{33}\text{F}_6\text{N}_4\text{O}_3^+ [\text{M} + \text{H}]^+$ calcd, 587.2452; found, 587.2460.

1,3-Bis(4-aminobutyl)-5,5-bis(naphthalen-2-yl-methyl)pyrimidin-2,4,6-(1H,3H,5H)-trione (6b). To a stirred solution of **5b** (438 mg, 0.73 mmol) and Et_3N (0.22 mL, 1.59 mmol) in *i*-PrOH/THF (1:1, 4 mL) was added 1,3-propanedithiol (0.1 mL, 0.99 mmol). The mixture was stirred for 5 min before addition of NaBH_4 (68 mg, 1.81 mmol). After a 72 h reaction time, Boc_2O (333 mg, 1.53 mmol) and NaHCO_3 (244 mg, 2.90 mmol) were added, and the reaction was stirred for 18 h before being filtered through a pad of Celite and concentrated. The resulting crude was purified by automated flash chromatography and evaporated. The Boc-protected intermediate (305 mg) was deprotected with TFA (2 mL, 26.1 mmol) in CH_2Cl_2 (5 mL) overnight. When MS analysis showed full deprotection, the reaction mixture was concentrated, and the crude product was purified by RP automated flash chromatography and lyophilized to afford **6b** (287 mg, 90%) as the TFA salt. ^1H NMR (400 MHz, CD_3OD): δ 7.90–7.68 (m, 6H), 7.60 (s, 2H), 7.52–7.43 (m, 4H), 7.19 (d, $J = 8.3$ Hz, 2H), 3.70 (s, 4H), 3.59–3.50 (m, 4H), 2.56–2.37 (m, 4H), 1.30–0.96 (m, 8H). ^{13}C NMR (101 MHz, CD_3OD): δ 172.2, 162.8 (q, $J = 35.2$ Hz, TFA), 151.0, 134.7, 134.1, 134.0, 129.9, 129.4, 128.8, 128.7, 128.2, 127.6, 127.3, 118.1 (d, $J = 292.3$ Hz, TFA), 62.0, 46.6, 41.7, 39.8, 25.6, 25.5. HRMS-ESI: $\text{C}_{34}\text{H}_{39}\text{N}_4\text{O}_3^+ [\text{M} + \text{H}]^+$ calcd, 551.3017; found, 551.3020.

1,3-Bis(4-aminobutyl)-5,5-bis((4-fluoronaphthalen-1-yl)methyl)pyrimidin-2,4,6-(1H,3H,5H)-trione (6c). To a stirred solution of **5c** (67 mg, 0.105 mmol) and Et_3N (0.03 mL, 0.21 mmol) in *i*-PrOH/THF (1:1, 4 mL) was added 1,3-propanedithiol (0.1 mL, 0.99 mmol). The mixture was stirred for 5 min before addition of NaBH_4 (8 mg, 0.21 mmol). After a 72 h reaction time, Boc_2O (48 mg, 0.22 mmol) and NaHCO_3 (35 mg, 0.42 mmol) were added, and the reaction was stirred for 18 h before being filtered through a pad of Celite and concentrated. The resulting crude was purified by automated flash chromatography and evaporated. The Boc-protected intermediate (72 mg) was deprotected with TFA (0.2 mL, 2.61 mmol) in CH_2Cl_2 (5 mL) overnight. When MS analysis showed full deprotection, the reaction mixture was concentrated, and the crude product was purified by RP automated flash chromatography and lyophilized to yield **6c** (82 mg, 89%) as the TFA salt. ^1H NMR (400 MHz, CD_3OD): δ 8.34 (d, $J = 7.9$ Hz, 2H), 8.07 (d, $J = 7.7$ Hz, 2H), 7.74–7.53 (m, 4H), 7.38–7.19 (m, 2H), 7.08 (t, $J = 8.9$ Hz, 2H), 4.13 (s, 4H), 3.39–3.33 (m, 4H), 2.60 (t, $J = 6.8$ Hz, 4H), 1.20–1.00 (m, 4H), 0.94–0.71 (m, 4H). ^{13}C NMR (101 MHz, CDCl_3): δ 172.2, 163.11 (q, $^2J_{\text{C,F}} = 34.1$ Hz, TFA), 159.6 (d, $^1J_{\text{C,F}} = 251.5$ Hz), 150.8, 134.5 (d, $J_{\text{C,F}} = 4.4$ Hz), 129.3 (d, $J_{\text{C,F}} = 4.5$ Hz), 128.4 (d, $J_{\text{C,F}} = 8.5$ Hz), 128.2, 127.6 (d, $J_{\text{C,F}} = 1.1$ Hz), 126.3 (d, $J_{\text{C,F}} = 2.4$ Hz), 125.2 (d, $J_{\text{C,F}} = 15.6$ Hz), 121.5 (d, $J_{\text{C,F}} = 6.2$ Hz), 118.23 (q, $^1J_{\text{C,F}} = 292.8$ Hz, TFA), 109.76 (d, $J_{\text{C,F}} = 20.2$ Hz), 61.0, 41.7, 41.3, 39.9, 25.3, 25.1. HRMS-ESI: $\text{C}_{34}\text{H}_{37}\text{F}_2\text{N}_4\text{O}_3^+ [\text{M} + \text{H}]^+$ calcd, 587.2828; found, 587.2828.

1,3-Bis(4-aminobutyl)-5,5-bis(4-bromo-3-chlorobenzyl)pyrimidine-2,4,6-(1H,3H,5H)-trione (6d). To a stirred solution of **5d** (588 mg, 0.81 mmol) and Et_3N (0.23 mL, 1.69 mmol) in *i*-PrOH/THF (1:1, 10 mL) was added 1,3-propanedithiol (0.164 mL, 1.76 mmol). After a 48 h reaction time, Boc_2O (528 mg, 2.42 mmol) was added, and the reaction mixture was stirred for 18 h and evaporated. To the crude mixture was added EtOAc (20 mL) and water (15 mL)

and stirred for 30 min. The organic phase was washed with water (3 × 15 mL) and brine (15 mL) and concentrated. The resulting crude was purified by automated flash chromatography (EtOAc/heptane) and evaporated. The Boc-protected intermediate was deprotected with TFA (2 mL, 26 mmol) in CH₂Cl₂ (5 mL) for 18 h. The reaction mixture was concentrated, and the crude product was purified by RP automated flash chromatography and lyophilized to afford **6d** (0.542 mg, 77%) as the TFA salt. ¹H NMR (400 MHz, CD₃OD): δ 7.59 (d, *J* = 8.2 Hz, 2H), 7.24 (d, *J* = 2.1 Hz, 2H), 6.92 (dd, *J* = 8.3, 2.1 Hz, 2H), 3.73–3.59 (m, 4H), 3.43 (s, 4H), 3.01–2.76 (m, 4H), 1.59–1.43 (m, 4H), 1.36 (t, *J* = 9.3, 6.0 Hz, 4H). ¹³C NMR (101 MHz, CD₃OD): δ 171.4, 150.7, 137.7, 135.5, 135.3, 132.7, 130.7, 122.6, 61.0, 44.9, 42.1, 40.2, 26.0, 25.8. HRMS-ESI: C₂₆H₃₁⁷⁹Br₂Cl₂N₄O₃⁺ [M + H]⁺ calcd, 675.0134; found, 675.0145.

1,3-Bis(4-aminobutyl)-5,5-bis(3,5-dibromobenzyl)pyrimidin-2,4,6-(1H,3H,5H)-trione (6e). To a stirred solution of **5e** (810 mg, 0.99 mmol) and Et₃N (0.32 mL, 2.29 mmol) in *i*-PrOH/THF (1:1, 5 mL) was added 1,3-propanedithiol (0.20 mL, 1.99 mmol). The mixture was stirred for 5 min before addition of NaBH₄ (90 mg, 2.37 mmol). After a 48 h reaction time, Boc₂O (650 mg, 2.97 mmol) was added, and the reaction mixture was stirred for 18 h and evaporated. To the crude mixture were added EtOAc (15 mL) and water (15 mL) and stirred for 30 min. The organic phase was washed with water (3 × 15 mL) and brine (15 mL) and concentrated. The resulting crude was purified by automated flash chromatography and evaporated. The Boc-protected intermediate was deprotected with TFA (2 mL, 26 mmol) in CH₂Cl₂ (5 mL) for 18 h. The reaction mixture was concentrated, and the crude product was purified by RP automated flash chromatography and lyophilized to afford **6e** (374 mg, 38%) as the TFA salt. ¹H NMR (400 MHz, CD₃OD): δ 7.66 (s, 2H), 7.23 (s, 4H), 3.68 (t, *J* = 7.7 Hz, 4H), 3.43 (s, 4H), 3.08–2.82 (m, 4H), 1.76–1.48 (m, 4H), 1.49–1.32 (m, 4H). ¹³C NMR (101 MHz, CD₃OD): δ 171.2, 163.01 (q, *J* = 34.4 Hz, TFA), 150.4, 140.5, 134.5, 132.7, 124.1, 118.2 (q, *J* = 293.3 Hz, TFA), 61.2, 44.8, 42.2, 40.3, 26.3, 25.8. HRMS-ESI: C₂₆H₃₁⁷⁹Br₂N₄O₃⁺ [M + H]⁺ calcd, 762.9124; found, 762.9124.

1,3-Bis(4-aminobutyl)-5,5-bis(3,5-bis(trifluoromethyl)benzyl)pyrimidin-2,4,6-(1H,3H,5H)-trione (6f). To a stirred solution of **5f** (63 mg, 0.81 mmol) and Et₃N (0.034 mL, 0.24 mmol) in *i*-PrOH/THF (1:1, 2 mL) was added 1,3-propanedithiol (0.10 mL, 0.99 mmol). The mixture was stirred for 5 min before addition of NaBH₄ (92 mg, 0.24 mmol). After a 48 h reaction time, Boc₂O (70 mg, 0.32 mmol) and K₂CO₃ (45 mg, 0.33 mmol) were added, and the reaction was stirred for another night, before being diluted with EtOAc (10 mL) and water (10 mL) and stirred for 1 h. The organic phase was washed with water (3 × 15 mL) and brine (15 mL) and concentrated. The resulting crude was purified by automated flash chromatography and evaporated. The Boc-protected intermediate was deprotected with TFA (2 mL, 26 mmol) in CH₂Cl₂ (5 mL) for 18 h. The reaction mixture was concentrated, and the crude product was purified by RP automated flash chromatography and lyophilized to afford **6f** (12 mg, 16%) as the TFA salt. ¹H NMR (400 MHz, CD₃OD): δ 7.93 (s, 2H), 7.68 (s, 4H), 3.71 (s, 4H), 3.61–3.54 (m, 4H), 2.87–2.80 (m, 4H), 1.57–1.46 (m, 4H), 1.33–1.22 (m, 4H). ¹³C NMR (101 MHz, CD₃OD): δ 170.9, 150.1, 139.4, 133.0 (q, ²*J*_{C,F} = 33.4 Hz), 131.6–131.1 (m), 124.6 (q, ¹*J*_{C,F} = 272.1 Hz), 123.0, 61.1, 44.8, 42.3, 40.0, 25.9, 25.7. HRMS-ESI: C₃₀H₃₁F₁₂N₄O₃⁺ [M + H]⁺ calcd, 723.2197; found, 723.2161.

1,3-Bis(4-aminobutyl)-5,5-bis(4-tert-butylbenzyl)pyrimidin-2,4,6-(1H,3H,5H)-trione (6g). To a stirred solution of **5g** (2.16 g, 3.52 mmol) and Et₃N (0.98 mL, 7.05 mmol) in *i*-PrOH/THF (1:1, 10 mL) was added 1,3-propanedithiol (0.1 mL, 0.99 mmol). The mixture was stirred for 5 min before addition of NaBH₄ (270 mg, 7.14 mmol). After a 72 h reaction time, Boc₂O (1.69 g, 7.74 mmol) and K₂CO₃ (1.94 g, 14.0 mmol) were added, and the reaction was stirred for 18 h and evaporated before adding EtOAc (20 mL) and water (15 mL) and stirring for 30 min. The organic phase was washed with water (3 × 15 mL) and brine (15 mL) and concentrated. The resulting crude was purified by automated flash chromatography and evaporated. The Boc-protected intermediate was deprotected with TFA (2.2 mL, 28.7

mmol) in CH₂Cl₂ (10 mL) for 18 h. The reaction mixture was concentrated, and the crude product was purified by RP automated flash chromatography and lyophilized to afford **6g** (367 mg, 85%) as the TFA salt. ¹H NMR (400 MHz, CD₃OD): δ 7.25 (d, *J* = 7.1 Hz, 4H), 6.98 (d, *J* = 7.2 Hz, 4H), 3.62–3.53 (m, 4H), 3.39 (s, 4H), 2.87 (t, *J* = 7.4 Hz, 4H), 1.55–1.36 (m, 4H), 1.36–1.15 (m, 22H). ¹³C NMR (101 MHz, CD₃OD): δ 172.3, 163.0 (q, *J* = 34.4 Hz, TFA), 151.9, 151.0, 133.5, 130.3, 126.5, 118.2 (q, *J* = 292.8 Hz, TFA), 61.9, 45.9, 41.7, 40.0, 35.3, 31.7, 25.6, 25.5. HRMS-ESI: C₃₄H₅₁N₄O₃⁺ [M + H]⁺ calcd, 563.3956; found, 563.3934.

1,3-Bis(4-aminobutyl)-5,5-bis(3,5-di-tert-butylbenzyl)pyrimidin-2,4,6-(1H,3H,5H)-trione (6h). To a stirred solution of **5h** (405 mg, 0.55 mol) and Et₃N (0.16 mL, 1.15 mmol) in *i*-PrOH/THF (1:1, 6 mL) was added 1,3-propanedithiol (0.12 mL, 1.15 mmol). The mixture was stirred for 5 min before addition of NaBH₄ (44 mg, 1.16 mmol). After a 72 h reaction time, Boc₂O (490 mg, 2.25 mmol) was added, and the reaction was stirred for another night before being diluted with EtOAc (10 mL) and water (10 mL) and stirred for 1 h. The organic phase was washed with water (3 × 15 mL) and brine (15 mL) and concentrated. The resulting crude was purified by automated flash chromatography and evaporated. The Boc-protected intermediate was deprotected with TFA (1.7 mL, 22.2 mmol) in CH₂Cl₂ (5 mL) for 6 h. The reaction mixture was concentrated, and the crude product was purified by RP automated flash chromatography and lyophilized to afford **6h** (154 mg, 31%) as the TFA salt. ¹H NMR (400 MHz, CD₃OD): δ 7.31 (t, *J* = 1.5 Hz, 2H), 6.89 (d, *J* = 1.6 Hz, 4H), 3.59 (t*, 4H), 3.44 (s, 4H), 2.78 (t*, 4H), 1.40 (p, *J* = 7.7 Hz, 4H), 1.26 (s, 36H), 1.17 (p, *J* = 7.6 Hz, 4H). ¹³C NMR (101 MHz, CD₃OD): δ 172.3, 162.8 (q, *J* = 34.7 Hz, TFA), 152.3, 151.1, 135.8, 124.7, 122.6, 118.1 (q, *J* = 292.5 Hz, TFA), 61.8, 47.3, 42.0, 39.9, 35.6, 31.9, 25.9, 25.5. *Distorted triplets. HRMS-ESI: C₄₂H₆₇N₄O₃⁺ [M + H]⁺ calcd, 675.5211; found, 675.5211.

Guanylation of Amines (6) to Guanidines (7). **1,1'-(2,4,6-Trioxo-5,5-bis(4-(trifluoromethyl)benzyl)dihydropyrimidine-1,3(2H,4H)-diyl)bis(butane-4,1-diyl)diguandine (7a).** To a stirred solution of the TFA salt of **6a** (33 mg, 0.41 μmol) in THF (3 mL) were added NaHCO₃ (27 mg, 0.31 mmol) and *N,N'*-bis-Boc-1-guanylpiperazine (27 mg, 0.86 mmol). The reaction was stirred at room temperature for 48 h until TLC (CH₂Cl₂) showed full guanylation of the diamine. The reaction mixture was concentrated, and the crude product was then dissolved in EtOAc (10 mL) and washed with 10% citric acid soln (2 × 10 mL), 10% NaHCO₃ soln (10 mL), and brine (10 mL). The organic phase was dried over Na₂SO₄, filtered, and concentrated. The crude product was purified by automated flash chromatography, and the resulting Boc-protected intermediate was deprotected with TFA (0.2 mL, 2.61 mmol) in CH₂Cl₂ (2 mL) for 18 h. The reaction mixture was concentrated, and the crude was purified by RP automated flash chromatography and lyophilized to afford **7a** (24 mg, 65%) as a white powder. ¹H NMR (400 MHz, CD₃OD): δ 7.56 (d, *J* = 8.1 Hz, 4H), 7.28 (d, *J* = 8.0 Hz, 4H), 3.62 (t, *J* = 6.7 Hz, 4H), 3.57 (s, 4H), 3.11 (t, *J* = 6.5 Hz, 4H), 1.37–1.28 (m, 8H). ¹³C NMR (101 MHz, CD₃OD): δ 171.5, 162.4 (q, ²*J*_{C,F} = 35.5 Hz, TFA), 158.7, 150.8, 140.9, 131.5, 131.1 (q, ²*J*_{C,F} = 32.4 Hz), 126.7–126.4 (m), 125.46 (q, ¹*J*_{C,F} = 271.3 Hz), 117.9 (q, ¹*J*_{C,F} = 291.1 Hz, TFA), 61.1, 45.9, 42.3, 41.8, 26.9, 25.8. HRMS-ESI: C₃₀H₃₇F₆N₈O₃⁺ [M + H]⁺ calcd, 671.2887; found, 671.2836.

1,1'-(5,5-Bis(naphthalen-2-ylmethyl)-2,4,6-trioxodihydropyrimidine-1,3(2H,4H)-diyl)bis(butane-4,1-diyl)diguandine (7b). To a stirred solution of the TFA salt of **6b** (54 mg, 0.069 mmol) in THF (4 mL) were added *N,N'*-bis-Boc-1-guanylpiperazine (63 mg, 0.20 mmol) and NaHCO₃ (41 mg, 0.48 mmol) and stirred at room temperature for 48 h until TLC (CHCl₃) showed full conversion. The reaction mixture was diluted with EtOAc (5 mL), washed with 10% citric acid soln (2 × 10 mL) and brine (10 mL), dried over Na₂SO₄, filtered, and concentrated. The Boc-protected intermediate was dissolved in CHCl₃ and adsorbed onto Celite before purification on a silica column using CHCl₃ as the mobile phase. The Boc-protected intermediate (64 mg of a total of 104 mg, 0.057 mmol) was deprotected with TFA (0.2 mL) in CH₂Cl₂ (4 mL) overnight. The reaction mixture was concentrated and purified by RP automated flash

chromatography and lyophilized to afford **7b** (60 mg, 99%) as a white powder. ^1H NMR (400 MHz, CD_3OD): δ 7.85–7.69 (m, 6H), 7.59 (s, 2H), 7.53–7.40 (m, 4H), 7.20 (dd, $J = 8.4, 1.8$ Hz, 2H), 3.69 (s, 4H), 3.54 (t, $J = 7.1$ Hz, 4H), 2.80 (t, $J = 7.1$ Hz, 4H), 1.21–1.08 (m, 4H), 1.08–0.98 (m, 4H). ^{13}C NMR (101 MHz, CD_3OD): δ 172.3, 163.1 (q, $J = 34.3$ Hz, TFA), 158.5, 151.0, 134.7, 134.1, 134.0, 129.8, 129.4, 128.7, 128.6, 128.3, 127.6, 127.3, 118.2 (q, $J = 293.0$ Hz, TFA), 62.0, 46.6, 42.1, 41.8, 26.6, 25.9. HRMS-ESI: $\text{C}_{36}\text{H}_{43}\text{N}_8\text{O}_3^+$ [$\text{M} + \text{H}$] $^+$ calcd, 635.3450; found, 635.3448.

1,1'-(5,5-Bis(4-fluoronaphthalen-1-yl)methyl)-2,4,6-trioxodihydropyrimidine-1,3(2H,4H)-diyl)bis(butane-4,1-diyl)diguandine (7c). To a stirred solution of the TFA salt of **6c** (35 mg, 43 μmol) in THF (3 mL) were added N,N' -bis-Boc-1-guanylpyrazole (38 mg, 122 μmol) and NaHCO_3 (25 mg, 0.29 mmol) and stirred at room temperature for 48 h until TLC (CHCl_3) showed full conversion. The reaction mixture was diluted with EtOAc (5 mL), washed with 10% citric acid soln and brine, dried over Na_2SO_4 , filtered, and concentrated. The Boc-protected intermediate was dissolved in CHCl_3 and adsorbed onto Celite before purification on a silica column using CHCl_3 as the mobile phase. The Boc-protected intermediate (41 mg of a total of 95 mg, 0.038 mmol) was deprotected with TFA (0.1 mL) in CH_2Cl_2 (4 mL) overnight. The reaction mixture was concentrated and purified by RP automated flash chromatography and lyophilized to afford **7c** (20 mg, 52%) as a white powder. ^1H NMR (400 MHz, CD_3OD): δ 8.32 (d, $J = 8.6$ Hz, 2H), 8.06 (d, $J = 7.9$ Hz, 2H), 7.71–7.55 (m, 4H), 7.25 (dd, $J = 8.0, 5.5$ Hz, 2H), 7.06 (dd, $J = 10.2, 8.1$ Hz, 2H), 4.12 (s, 4H), 3.35 (t, $J = 7.2$ Hz, 4H), 2.87 (t, $J = 7.1$ Hz, 4H), 1.00 (p, $J = 7.2$ Hz, 4H), 0.86 (p, $J = 7.4, 6.8$ Hz, 4H). ^{13}C NMR (101 MHz, CD_3OD): δ 172.2, 163.1 (q, $^2J_{\text{C,F}} = 34.1$ Hz, TFA), 159.6 (d, $^1J_{\text{C,F}} = 251.6$ Hz), 158.5, 150.9, 134.5 (d, $^3J_{\text{C,F}} = 4.3$ Hz), 129.2 (d, $J_{\text{C,F}} = 4.6$ Hz), 128.9 (d, $J_{\text{C,F}} = 8.5$ Hz), 128.2, 127.6 (d, $J_{\text{C,F}} = 1.6$ Hz), 126.2 (d, $J_{\text{C,F}} = 2.5$ Hz), 125.2 (d, $J_{\text{C,F}} = 15.8$ Hz), 121.5 (d, $J_{\text{C,F}} = 6.2$ Hz), 118.2 (q, $J_{\text{C,F}} = 292.8$ Hz, TFA), 109.7 (d, $J_{\text{C,F}} = 20.2$ Hz), 60.9, 42.1, 41.8, 41.4, 26.5, 25.4. HRMS-ESI: $\text{C}_{36}\text{H}_{41}\text{F}_2\text{N}_8\text{O}_3^+$ [$\text{M} + \text{H}$] $^+$ calcd, 671.3264; found, 671.3244.

1,1'-(5,5-Bis(4-bromo-3-chlorobenzyl)-2,4,6-trioxodihydropyrimidine-1,3(2H,4H)-diyl)bis(butane-4,1-diyl)diguandine (7d). To a stirred solution of the TFA salt of **6d** (203 mg, 0.299 mmol) in THF (20 mL) were added NaHCO_3 (155 mg, 1.12 mmol) and N,N' -bis-Boc-1-guanylpyrazole (350 mg, 1.1 mmol) and stirred at room temperature for 48 h until MS analysis showed full guanylation. The reaction mixture was filtered and concentrated. The crude product was dissolved in EtOAc (15 mL) and washed with brine (2×15 mL). The organic phase was dried over Na_2SO_4 , filtered, and concentrated. The crude product was purified by automated flash chromatography, and the resulting Boc-protected intermediate was deprotected with TFA (2 mL) in CH_2Cl_2 (2 mL) for 18 h. The reaction mixture was concentrated, and the crude was purified by RP automated flash chromatography and lyophilized to afford **7d** as a white powder. The yield was not determined. ^1H NMR (400 MHz, CD_3OD): δ 7.57 (d, $J = 8.2$ Hz, 2H), 7.22 (d, $J = 2.1$ Hz, 2H), 6.92 (dd, $J = 8.3, 2.1$ Hz, 2H), 3.74–3.61 (m, 4H), 3.43 (s, 4H), 3.23–3.12 (m, 4H), 1.47–1.29 (m, 8H). ^{13}C NMR (101 MHz, CD_3OD): δ 171.5, 158.6, 150.7, 137.7, 135.5, 135.3, 132.6, 130.7, 122.6, 61.0, 45.0, 42.5, 42.0, 26.9, 26.1. HRMS-ESI: $\text{C}_{28}\text{H}_{35}^{79}\text{Br}_2\text{Cl}_2\text{N}_8\text{O}_3^+$ [$\text{M} + \text{H}$] $^+$ calcd, 759.0570; found, 759.0578.

1,1'-(5,5-Bis(3,5-dibromobenzyl)-2,4,6-trioxodihydropyrimidine-1,3(2H,4H)-diyl)bis(butane-4,1-diyl)diguandine (7e). To a stirred solution of the TFA salt of **6e** (360 mg, 0.362 mmol) in THF (5 mL) were added NaHCO_3 (240 mg, 2.86 mmol) and N,N' -bis-Boc-1-guanylpyrazole (564 mg, 1.82 mmol) and stirred at room temperature for 48 h until MS analysis showed full guanylation. The reaction mixture was filtered and concentrated. The crude product was dissolved in EtOAc (20 mL) and washed with brine (2×20 mL). The organic phase was dried over Na_2SO_4 , filtered, and concentrated. The crude product was purified by automated flash chromatography, and the resulting Boc-protected intermediate was deprotected with TFA (0.2 mL) in CH_2Cl_2 (2 mL) for 18 h. The reaction mixture was concentrated, and the crude was purified by RP automated flash chromatography and lyophilized to afford **7e** (44 mg, 11%) as a white

powder. ^1H NMR (400 MHz, CD_3OD): δ 7.65 (t, $J = 1.8$ Hz, 2H), 7.22 (d, $J = 1.7$ Hz, 4H), 3.67 (t, $J = 7.2$ Hz, 4H), 3.42 (s, 4H), 3.20 (t, $J = 6.7$ Hz, 4H), 1.52–1.36 (m, 8H). ^{13}C NMR (101 MHz, CD_3OD): δ 171.3, 163.0 (q, $J = 34.6$ Hz, TFA), 158.6, 150.5, 140.5, 134.5, 132.6, 124.1, 118.2 (q, $J = 292.7$ Hz, TFA), 61.2, 44.9, 42.6, 42.1, 27.0, 26.4. HRMS-ESI: $\text{C}_{28}\text{H}_{35}^{79}\text{Br}_2^{81}\text{Br}_2\text{N}_8\text{O}_3^+$ [$\text{M} + \text{H}$] $^+$ calcd, 850.9525; found, 850.9532.

1,1'-(5,5-Bis(3,5-bis(trifluoromethyl)benzyl)-2,4,6-trioxodihydropyrimidine-1,3(2H,4H)-diyl)bis(butane-4,1-diyl)diguandine (7f). To a stirred solution of the TFA salt of **6f** (21 mg, 0.02 mmol) in THF (1 mL) were added DIPEA (15.4 μL , 0.09 mmol) and N,N' -bis-Boc-1-guanylpyrazole (17 mg, 0.06 mmol). The reaction was stirred at 45 $^\circ\text{C}$ for 2 h. The reaction mixture was concentrated, and the crude product was dissolved in EtOAc (10 mL) and washed with 10% citric acid soln (2×10 mL), 10% NaHCO_3 soln (10 mL), and brine (10 mL). The organic phase was dried over MgSO_4 , filtered, and concentrated. The crude product was purified by automated flash chromatography, and the resulting Boc-protected intermediate was deprotected with TFA (25 μL) in CH_2Cl_2 for 18 h. The reaction mixture was concentrated, and the crude was purified by RP automated flash chromatography and lyophilized to afford **7f** (4 mg, 17%) as a white powder. ^1H NMR (400 MHz, CD_3OD): δ 7.91 (s, 2H), 7.67 (d, $J = 1.7$ Hz, 4H), 3.71 (s, 4H), 3.63–3.53 (m, 4H), 3.10 (t, $J = 7.1$ Hz, 4H), 1.40 (tt, $J = 7.7, 4.0$ Hz, 4H), 1.36–1.24 (m, 4H). ^{13}C NMR (101 MHz, CD_3OD): δ 171.0, 158.7, 150.2, 139.4, 133.1 (q, $^2J_{\text{C,F}} = 33.4$ Hz, 4C), 131.4–131.2 (m, 4C), 124.54 (q, $^1J_{\text{C,F}} = 272.1$ Hz, 4C), 123.0–122.8 (m, 2C), 61.1, 44.9, 42.5, 41.7, 26.8, 26.0. HRMS-ESI: $\text{C}_{30}\text{H}_{31}\text{F}_{12}\text{N}_4\text{O}_3^+$ [$\text{M} + \text{H}$] $^+$ calcd 807.2635; found, 807.2632.

1,1'-(5,5-Bis(4-tert-butylbenzyl)-2,4,6-trioxodihydropyrimidine-1,3(2H,4H)-diyl)bis(butane-4,1-diyl)diguandine (7g). To a stirred solution of the TFA salt of **6g** (129 mg, 0.16 mmol) in THF (2 mL) were added NaHCO_3 (68 mg, 0.81 mmol) and N,N' -bis-Boc-1-guanylpyrazole (200 mg, 0.64 mmol). The reaction was stirred at room temperature for 48 h. The reaction mixture was concentrated, and the crude product was dissolved in EtOAc (20 mL) and washed with 10% citric acid soln (2×20 mL), 10% NaHCO_3 soln (20 mL), and brine (20 mL). The organic phase was dried over Na_2SO_4 , filtered, and concentrated. The crude product was purified by automated flash chromatography, and the resulting Boc-protected intermediate was deprotected with TFA (1 mL) in CH_2Cl_2 for 18 h. The reaction mixture was concentrated, and the crude was purified by RP automated flash chromatography and lyophilized to afford **7g** (16 mg, 11%) as a white powder. ^1H NMR (400 MHz, CD_3OD): δ 7.24 (d, $J = 8.3$ Hz, 4H), 6.98 (d, $J = 8.3$ Hz, 4H), 3.58 (t, $J = 6.7$ Hz, 4H), 3.39 (s, 4H), 3.13 (t, $J = 6.6$ Hz, 4H), 1.39–1.29 (m, 8H), 1.24 (s, 18H). ^{13}C NMR (101 MHz, CD_3OD): δ 172.4, 162.4 (q, $J = 35.6$ Hz, TFA), 158.7, 151.9, 151.2, 133.4, 130.3, 126.4, 117.9 (q, $J = 291.5$ Hz, TFA), 61.9, 45.9, 42.0, 41.9, 35.3, 31.7, 26.8, 25.8. HRMS-ESI: $\text{C}_{36}\text{H}_{55}\text{N}_8\text{O}_3^+$ [$\text{M} + \text{H}$] $^+$ calcd, 647.4393; found, 647.4378.

1,1'-(5,5-Bis(3,5-di-tert-butylbenzyl)-2,4,6-trioxodihydropyrimidine-1,3(2H,4H)-diyl)bis(butane-4,1-diyl)diguandine (7h). To a stirred solution of the TFA salt of **6h** (118 mg, 0.13 mmol) in THF (3 mL) were added N,N' -bis-Boc-1-guanylpyrazole (245 mg, 0.79 mmol) and NaHCO_3 (49 mg, 0.59 mmol) and stirred at room temperature for 48 h until TLC (CHCl_3) showed full conversion. The reaction mixture was diluted with EtOAc (5 mL), washed with 10% citric acid soln and brine, dried over Na_2SO_4 , filtered, and concentrated. The crude was purified by automated flash chromatography, and the resulting Boc-protected intermediate was deprotected with TFA (1.5 mL) in CH_2Cl_2 (1.5 mL) for 4 h. The reaction mixture was concentrated, and the crude was purified by RP automated flash chromatography and lyophilized to afford **7h** (44 mg, 34%) as a white powder. ^1H NMR (400 MHz, CD_3OD): δ 7.30 (t, $J = 1.8$ Hz, 2H), 6.89 (d, $J = 1.8$ Hz, 4H), 3.58* (t, $J = 7.5$ Hz, 4H), 3.44 (s, 4H), 3.06 (t, $J = 7.0$ Hz, 4H), 1.38–1.14 (m, 44H). ^{13}C NMR (101 MHz, CD_3OD): δ 172.4, 162.8 (q, $J = 35.2$ Hz, TFA), 158.6, 152.3, 151.3, 135.8, 124.6, 122.6, 118.0 (q, $J = 292.3$ Hz, TFA), 61.7, 47.3, 42.4, 41.8, 35.6, 31.9, 26.7, 26.2. *Distorted triplet. HRMS-ESI: $\text{C}_{44}\text{H}_{71}\text{N}_8\text{O}_3^+$ [$\text{M} + \text{H}$] $^+$ calcd, 759.5644; found, 759.5637.

Biological Test Methods. The bacterial reference strains are displayed in Table 1 for the first antimicrobial screening. The Norwegian National Advisory Unit on Detection of Antimicrobial Resistance (K-res), University Hospital of Northern-Norway (UNN), provided the collection of 30 multi-drug-resistant isolates in Table 2. All isolates were deposited at the Norwegian Organization for Surveillance of Resistant Microorganisms (NORM) in the period of 2012–2014.

MIC Assay. The working solutions of the test derivatives were prepared with up to 100% dimethyl sulfoxide (DMSO) and stored at $-20\text{ }^{\circ}\text{C}$. If necessary, the solutions were heated to $40\text{--}80\text{ }^{\circ}\text{C}$ before testing to facilitate complete dissolution. Double-distilled water was used in all dilutions prepared. The final concentration of DMSO in the test series was $\leq 1\%$ and did not affect the assay results. A microdilution susceptibility test was used for MIC determination according to CLSI M07-A9⁴¹ with modifications as described by Igumnova *et al.*⁴² Briefly, the bacterial inoculum was adjusted to approximately $2.5\text{--}3 \times 10^4$ cells/mL in the Mueller–Hinton broth (MHB, Difco Laboratories, USA) and incubated in a ratio of 1:1 with test derivatives in polystyrene 96-well flat-bottomed microplates (NUNC, Roskilde, Denmark). The positive growth control (without test derivatives) and negative control (without bacteria) were included. The reference antibiotic was oxytetracycline hydrochloride (Sigma-Aldrich, Saint Louis, MO, USA). The microplates were incubated in an EnVision microplate reader (PerkinElmer, Turku, Finland) placed in an incubator set to $35\text{ }^{\circ}\text{C}$ for 48 h. The MIC value was defined as the lowest concentration of the derivative resulting in no bacterial growth as determined by OD_{600} measurement. All derivatives were tested in three parallels.

Antimicrobial Screening against Clinical Isolates. The MIC assay was performed as explained above with some exceptions; the working solutions of the test derivatives were prepared from the concentrated DMSO stocks stored at room temperature, the density of the bacterial inoculum was increased $40 \times$ to $1\text{--}1.2 \times 10^6$ cells/mL, enterococci were incubated in the Brain Heart Infusion broth (BHIB, Difco Laboratories, USA), the polypropylene microplates (Greiner Bio-One, Frickenhausen, Germany) were incubated for 24 h, and the derivatives were tested in four parallels.

Determination of Hemolytic Activity. The protocol was adapted from Paulsen *et al.*¹⁷ Hemolysis was determined using a heparinized fraction (10 IU/mL) of freshly drawn blood. The blood collected in ethylenediaminetetraacetic acid-containing test tubes (Vacutest, KIMA, Arzergande, Italy) was used for the determination of the hematocrit (hct). The heparinized blood was washed $3 \times$ with pre-warmed phosphate-buffered saline (PBS) and adjusted to a final hct of 4%. Derivatives in DMSO (50 mM) were added to a 96-well polypropylene V-bottom plate (NUNC, Fisher Scientific, Oslo, Norway) and serially diluted. The test concentration range was $500\text{--}4\text{ }\mu\text{M}$ with DMSO contents $\leq 1\%$. A solution of 1% triton X-100 was used as a positive control for 100% hemolysis. As a negative control, a solution of 1% DMSO in PBS was included. No signs of DMSO toxicity were detected. RBCs (1% v/v final concentration) were added to the well plate and incubated at $37\text{ }^{\circ}\text{C}$ and 800 rpm for 1 h. After centrifugation (5 min, 3000g), 100 μL of each well was transferred to a 96-well flat-bottomed microtiter plate, and absorbance was measured at 545 nm with a microplate reader (VersaMaxTM, Molecular Devices, Sunnyvale, CA, USA). The percentage of hemolysis was calculated as the ratio of the absorbance in the derivative-treated and surfactant-treated samples, corrected for the PBS background. Three independent experiments were performed, and EC_{50} values are presented as averages.

Determination of Toxicity against MRC5 and HepG2. Adherent, non-malignant lung fibroblasts MRC5 (ATCC CCL-171TM) and human hepatocellular carcinoma cells HepG2 (ATCC HB-8065) were used as toxicity control. MRC5 cells, suspended in Eagle's minimal essential medium (MEM) with 10% fetal bovine serum, 2 mM stable glutamine, 1% non-essential amino acids, 1% sodium pyruvate, 2% NaHCO_3 , and 10 $\mu\text{g}/\text{mL}$ gentamicin, were seeded in 96-well microtiter plates at 15,000 cells/well. HepG2 cells, suspended in Eagle's MEM with 10% fetal bovine serum, 1 mM stable

glutamine, 1% non-essential amino acids, 1% sodium pyruvate, and 10 $\mu\text{g}/\text{mL}$ gentamicin, were seeded in 96-well microtiter plates at 20,000 cells/well (adherent cell lines). The adherent cell lines were incubated for 24 h before adding compounds 6a–h and 7a–h and were then incubated for 4 h. The cell viability was determined by a colorimetric 3-(4,5-dimethylthiazol-2-yl)-5-(3-carboxymethoxyphenyl)-2-(4-sulphophenyl)-2H-tetrazolium assay. At the end of the exposure time, 10 μL of Cell Titer 96 Aqueous One Solution Reagent (Promega, Madison, WI, USA) was added to each well, and the plates were incubated for 1 h before absorbance was measured using a DTX 880 multimode detector (Beckman Coulter, CA, USA) at 485 nm. Cells in their respective growth medium were used as negative control, and cells treated with 10% DMSO were used as positive control. Growth inhibition was determined by using the measured optical density (OD) and was calculated as follows: cell survival (%) = $(\text{OD treated well} - \text{OD positive control well}) / (\text{OD negative control well} - \text{OD positive control well}) \times 100$.

In Vivo Murine Neutropenic Peritonitis Model. The MIC of 7e (3,5-di-Br) against *E. coli* (EC106-09) and *K. pneumoniae* (KP3010) was determined according to the CLSI guidelines. The concentration range used was $0.032\text{--}32\text{ }\mu\text{g}/\text{mL}$. Colistin was included as a comparator and quality control (QC), and *E. coli* (ATCC 25922) was included as a QC strain. The MIC of colistin against *E. coli* (ATCC 25922) was within the CLSI QC range $0.25\text{--}2\text{ }\mu\text{g}/\text{mL}$, indicating a correct procedure. Derivative 7e (3,5-di-Br) was dissolved in PEG400 to 10 mg/mL and further diluted in 0.0015 M Tris buffer to concentrations of 1 and 0.2 mg/mL. The *in vivo* efficacy of compound 7e (3,5-di-Br) against *E. coli* (EC106-09) and *K. pneumoniae* (KP3010) in 32 female neutropenic NMRI mice (weight 28–32 g) was investigated after i.p. injection of 1.4 and 2.8 mg/kg given 1 and 3 h post-infection at Statens Serum Institute (SSI) in Denmark.³⁵ Mice were first rendered neutropenic with injections of cyclophosphamide (day-4 and day-1) and on day 0 inoculated with *E. coli* (EC106-09) or *K. pneumoniae* (KP3010) before being treated with 7e (3,5-di-Br) and the control antibiotics colistin (5 mg/kg), ciprofloxacin (13 mg/kg), or vehicle 1 h post-infection. Mice were observed for clinical signs of infection for 4 h after injection. The bacterial loads in the peritoneum were thereafter determined by sampling peritoneal fluid for the determination of CFU 4 h after treatment. The colony counts in peritoneal fluid were determined 5 h post-inoculation. All animal experiments were conducted in compliance with the institutional guidelines of SSI.

Bacterial Membrane Integrity Assay. The real-time membrane integrity assay was modified from Virta *et al.*³⁷ The test strains were *B. subtilis* 168 (ATCC 23857) and *E. coli* HB101 carrying the plasmid pCSS962. Overnight cultures were grown in MHB with chloramphenicol (5 $\mu\text{g}/\text{mL}$ *B. subtilis* and 20 $\mu\text{g}/\text{mL}$ *E. coli*, Merck KGaA, Darmstadt, Germany). The bacteria were pelleted by centrifugation for 5 min at 4000g before they were resuspended in MHB to obtain an OD_{600} of 0.1. D-Luciferin potassium salt (pH 7.4, SynChem Inc, IL, USA) was added to a final concentration of 1 mM, and the background luminescence was measured. Black round-bottomed 96-well microplates (Nunc, Roskilde, Denmark), containing dilutions of the test compounds (5 μL per well), were loaded into a Synergy H1 Hybrid Reader (BioTek, Winooski, VT, USA). The amine barbiturate 6e (3,5-di-Br) and the guanidine barbiturate 7e (3,5-di-Br) were screened for membrane activity by injecting 95 μL of inoculum with D-luciferin successively (well by well) to the test wells by an automatic injector with tracking of the luminescence emission every second for 150 s at room temperature. CHX acetate (Fresenius Kabi, Halden, Norway) was used as a positive control.

Bacterial Viability Assay. The compounds 6e (3,5-di-Br) and 7e (3,5-di-Br) were also selected for the viability assay. The test strains were *B. subtilis* 168 and *E. coli* HB101 carrying a constitutively expressed *lux* operon as a chromosomal integration of the *lux* operon in the *sacA* locus (PliaG) or the plasmid pCGLS-1, respectively.^{43,44} The bacterial suspension for the real-time viability assay was prepared as described for the membrane integrity assay with the exception that no external substrate was added and that 100 $\mu\text{g}/\text{mL}$ of ampicillin was used for selection of *E. coli* carrying the plasmid pCGLS-11. The assay

was performed using the same type of microplates and procedure as described in the membrane integrity assay.

Structural Investigations. Electronic Structure Calculations. Quantum electronic structure calculations were performed at the DFT level of theory with the Gaussian 16 package,⁴⁵ employing the B3LYP functional^{46,47} with empirical dispersion corrections as formulated by Grimme⁴⁸ (B3LYP-GD3). Ground-state optimizations used the 6-31g basis set with additional diffuse (+) and polarization functions (d,p) for accurate description of neutral and charged species, 6-31 + g(d,p).^{49,50} Solvent effects were included in all calculations *via* the polarized continuum method, with water as the solvent.^{51,52} Additional single-point energy calculations were performed with the larger 6-311 ++ g(2d,2p) basis set. The larger basis set is expected to provide more accurate energies compared to the smaller 6-31 + g(d,p) by providing more flexibility to the electron density, especially in the case of charged groups. Calculated energy Hessians confirmed stationary points as minima (zero imaginary frequencies). The reported electronic energies are given in kcal/mol.

Nuclear Magnetic Resonance. All spectra were acquired on a Bruker Avance III HD spectrometer operating at 600 MHz for protons and equipped with an inverse TCI probe with cryogenic enhancement for ¹H, ²H, and ¹³C. NMR samples were prepared by dissolving 1 mg of **7e** in 500 μ L of H₂O/D₂O 9:1 in a 5 mm NMR tube. SDS was subsequently added to this sample in a 20:1 M ratio, resulting in a clear solution. Experiments were acquired using TopSpin 3.2, with gradient selection, adiabatic pulses, and excitation sculpting where applicable.

MD Simulation. An *E. coli* inner membrane model was adapted from Pandit and Klauda (2012) with a 4:1 PE/PG ratio.³⁹ Systems for MD simulations of the membrane and for each molecule **6a** (4-CF₃), **6e** (3,5-di-Br), **6g** (4-tBu), **7e** (3,5-di-Br), and **7g** (4-tBu) were prepared in VMD.⁵³ Each molecule was placed approximately 8 Å from the membrane surface and oriented such that the direct interactions of the guanidine and lysine groups with the membrane surface were not favored. All membrane systems were solvated in a rectangular simulation box with a 0.15 mol/L KCl concentration. In addition to membrane simulations, each of the molecules **6a** (4-CF₃), **6e** (3,5-di-Br), **6g** (4-tBu), **7e** (3,5-di-Br), and **7g** (4-tBu) were prepared for water simulations in rectangular simulation boxes. Cl⁻ ions were added for counterions.

Molecules **6a** (4-CF₃), **6e** (3,5-di-Br), **6g** (4-tBu), **7e** (3,5-di-Br), and **7g** (4-tBu) were built in PyMol.⁵⁴ Each of the compounds was given a starting structure where both phenyl groups are oriented in the up conformation. A simple minimization was performed in the builder tool of PyMol to clean the structures. Each molecule was assigned atom types, parameters, and charges with the CGenff online program.^{55,56}

Three parallels of all-atom MD simulations were performed for all systems with the molecular modeling software NAMD and the CHARMM36 force field.^{57,58} A 10,000 step conjugate gradient and line search minimization was performed to ensure a stable starting structure for the MD simulations. Each membrane system parallel was run for 260 ns, and each water system parallel was run for 100 ns. All simulations were run at 310.15 K with a 2 fs time step and periodic boundary conditions.

Particle Mesh Ewald was used for calculating the electrostatic interactions.⁵⁹ For non-bonded interactions, the scaled 1–4 principle was used for exclusion and 1.0 was used for scaling coefficient. A smoothing function was applied to the non-bonded forces with a cutoff of 12.0 Å and a switching distance of 10.0 Å. A pair list for the calculation of non-bonded interactions was updated every 20 steps, called one cycle, and the maximum distance for inclusion in the pair list for a pair of atoms was set to 16.0 Å. The pair list was regenerated twice every cycle. Bond lengths for hydrogen atoms were constrained with the SHAKE algorithm.⁶⁰ Both full electrostatic forces and the non-bonded forces were evaluated at every time step. The NPT ensemble was used for all simulations. Pressure control for the simulations was performed with Nosé-Hoover Langevin piston with a target pressure of 1 atm.^{61,62} A flexible simulation cell was used for the membrane system. Langevin dynamics were used for temperature

control. Trajectory files were written every 1000 steps and energies were recorded every 125 steps.

Analysis of the MD trajectories was performed with the VMD GUI and VMD scripts. Figures were made with VMD and PyMol, and all graphs were generated with pandas, seaborn, and Matplotlib.^{63–65}

X-ray Crystallography. A rod-like specimen of **7b** (2-Nal) was used for X-ray crystallographic analysis. The X-ray intensity data were measured with the Cu source ($\lambda = 1.54178$ Å) of an in-house Bruker D8 Venture system. Frames were integrated using the Bruker SAINT software package, and the structure was solved and refined using the Bruker SHELXTL software package. The structure factors of **7b** have been deposited with the Cambridge Crystallographic Data Centre with deposition number 2026641. The integration of the data using a monoclinic unit cell yielded a total of 21874 reflections to a maximum θ angle of 66.75° (0.84 Å resolution), of which 6692 were independent (average redundancy 3.269, completeness = 99.6%, $R_{int} = 3.12\%$, and $R_{sig} = 2.71\%$) and 5846 (87.36%) were greater than $2\sigma(F_2)$. The final cell constants were 17.6014(15), 15.4212(12), and 16.0233(17) Å with $\beta = 106.833(4)^\circ$. The final anisotropic refinement converged with an R_1/wR_2 of 6.8/21% with a GoF of 1.04. The structure of the asymmetric unit of **7b** (2-Nal) with thermal ellipsoids is shown in Figure S2.

■ ASSOCIATED CONTENT

Supporting Information

The Supporting Information is available free of charge at <https://pubs.acs.org/doi/10.1021/acs.jmedchem.1c00734>.

(PDF)

¹H and ¹³C NMR spectra and SFC analysis data of the synthesized compounds; detailed description of the biosensor assays; comprehensive discussion of the conformational analysis; and molecular formula strings and MIC and toxicity data for compounds **6a–h** and **7a–h** (CSV)

■ AUTHOR INFORMATION

Corresponding Authors

Annette Bayer – Department of Chemistry, UiT The Arctic University of Norway, NO-9037 Tromsø, Norway;

orcid.org/0000-0003-3481-200X;

Email: annette.bayer@uit.no

Morten B. Strøm – Department of Pharmacy, Faculty of Health Sciences, UiT The Arctic University of Norway, NO-9037 Tromsø, Norway; orcid.org/0000-0003-1973-0778; Email: morten.strom@uit.no

Authors

Marianne H. Paulsen – Department of Pharmacy, Faculty of Health Sciences, UiT The Arctic University of Norway, NO-9037 Tromsø, Norway

Magnus Engqvist – Department of Chemistry, UiT The Arctic University of Norway, NO-9037 Tromsø, Norway

Dominik Ausbacher – Department of Pharmacy, Faculty of Health Sciences, UiT The Arctic University of Norway, NO-9037 Tromsø, Norway

Trude Anderssen – Department of Pharmacy, Faculty of Health Sciences, UiT The Arctic University of Norway, NO-9037 Tromsø, Norway

Manuel K. Langer – Department of Chemistry, UiT The Arctic University of Norway, NO-9037 Tromsø, Norway

Tor Haug – The Norwegian College of Fishery Science, Faculty of Biosciences, Fisheries and Economics, UiT The Arctic University of Norway, NO-9037 Tromsø, Norway;

orcid.org/0000-0003-1104-5813

Glenn R. Morello – Department of Chemistry, UiT The Arctic University of Norway, NO-9037 Tromsø, Norway; Department of Science, Valley City State University, Valley City 58072 North Dakota, United States

Laura E. Liikanen – Department of Chemistry, UiT The Arctic University of Norway, NO-9037 Tromsø, Norway

Hans-Matti Blencke – The Norwegian College of Fishery Science, Faculty of Biosciences, Fisheries and Economics, UiT The Arctic University of Norway, NO-9037 Tromsø, Norway

Johan Isaksson – Department of Chemistry, UiT The Arctic University of Norway, NO-9037 Tromsø, Norway;

orcid.org/0000-0001-6287-7594

Eric Juskewitz – Department of Medical Biology, Faculty of Health Sciences, UiT The Arctic University of Norway, NO-9037 Tromsø, Norway

Complete contact information is available at:

<https://pubs.acs.org/10.1021/acs.jmedchem.1c00734>

Notes

The authors declare no competing financial interest.

ACKNOWLEDGMENTS

This study was funded by the Research Council of Norway (RCN) (grant nos. 214493/F20 and 224790/O30), UiT—The Arctic University of Norway (project nos. A23260 and 235560), pre-seed grant from Novo Nordisk Fonden (grant no. NNF17OC0030098), and the MABIT programme (grant no. BS0079). The computational work has furthermore received funding from the RCN (grant no. 231706/F20), the Norwegian supercomputing program NOTUR (grant nos. NN4654K and NN9330K), and assistance of computational resources at the Center for Computationally Assisted Science and Technology (CCAST) at North Dakota State University, US. The authors thank professor Ørjan Samuelsen (K-Res/UNN) for giving us access to multi-drug-resistant clinical isolates. We also thank engineers Alena Didriksen (UNN) and Hege Devold (UiT) for their technical assistance with MIC screening, engineer Elizaveta M. Igumnova (UNN/UiT) for providing compound **3h**, Dr. Bjarte Aarmo Lund (UiT) for X-ray crystallographic analysis, *in vivo* studies at Statens Serum Institute (SSI, DK), and MIC studies at the Advanced Microscopy Core Facility (AMCF, UiT).

ABBREVIATIONS

A. baumannii, *Acinetobacter baumannii*; *B. subtilis*, *Bacillus subtilis*; *C. glutamicum*, *Corynebacterium glutamicum*; *E. coli*, *Escherichia coli*; *E. faecium*, *Enterococcus faecium*; *K. pneumoniae*, *Klebsiella pneumoniae*; MRSA, methicillin-resistant *S. aureus*; *P. aeruginosa*, *Pseudomonas aeruginosa*; *S. aureus*, *Staphylococcus aureus*; VRE, vancomycin-resistant *Enterococcus*; AMPs, antimicrobial peptides; Boc₂O, di-*tert*-butyl dicarbonate; CFU, colony-forming units; CHX, chlorhexidine; DBU, 1,8-diazabicyclo[5.4.0]undec-7-ene; DFT, density functional theory; DMF, dimethylformamide; DMSO, dimethyl sulfoxide; ESBL–CARBA, extended spectrum β -lactamase–carbapenemase; HCTU, (2-(6-chloro-1H-benzotriazol-1-yl)-1,1,3,3-tetramethylammonium-hexafluorophosphate); i.p., intraperitoneal; LPS, lipopolysaccharide; MD, molecular dynamics; MIC, minimum inhibitory concentration; MTD, maximal tolerated dose; NMR, nuclear magnetic resonance; PL, phospholipid; PMA, phosphomolybdic acid; RBCs, red blood cells; RLU,

relative light units; SMAMPs, synthetic mimics of antimicrobial peptides; TFA, trifluoroacetic acid; THF, tetrahydrofuran

REFERENCES

- (1) World Health Organization. *2019 Antibacterial Agents in Clinical Development: An Analysis of the Antibacterial Clinical Development Pipeline*; World Health Organization: Geneva, 2019.
- (2) O'Neill, J. *Tackling Drug-Resistant Infections Globally: Final Report and Recommendations*; www.amr-reveiw.org, 2016.report
- (3) Cassini, A.; Högberg, L. D.; Plachouras, D.; Quattrocchi, A.; Hoxha, A.; Simonsen, G. S.; Colomb-Cotinat, M.; Kretzschmar, M. E.; Devleeschauwer, B.; Cecchini, M.; Ouakrim, D. A.; Oliveira, T. C.; Struelens, M. J.; Suetens, C.; Monnet, D. L.; Strauss, R.; Mertens, K.; Struyf, T.; Catry, B.; Latour, K.; Ivanov, I. N.; Dobrea, E. G.; Tambic Andrašević, A.; Soprek, S.; Budimir, A.; Paphitou, N.; Zemlicková, H.; Schytte Olsen, S.; Wolff Sönksen, U.; Martin, P.; Ivanova, M.; Lyytikäinen, O.; Jalava, J.; Coignard, B.; Eckmanns, T.; Abu Sin, M.; Haller, S.; Daikos, G. L.; Gikas, A.; Tsiodras, S.; Kontopidou, F.; Tóth, A.; Hajdu, A.; Guólaugsson, O.; Kristinsson, K. G.; Murchan, S.; Burns, K.; Pezzotti, P.; Gagliotti, C.; Dumpis, U.; Liuimiene, A.; Perrin, M.; Borg, M. A.; de Greeff, S. C.; Monen, J. C.; Koek, M. B.; Elström, P.; Zabicka, D.; Deptula, A.; Hryniewicz, W.; Caniça, M.; Nogueira, P. J.; Fernandes, P. A.; Manageiro, V.; Popescu, G. A.; Serban, R. I.; Schréterová, E.; Litvová, S.; Stefkovicová, M.; Kolman, J.; Klavs, I.; Korošec, A.; Aracil, B.; Asensio, A.; Pérez-Vázquez, M.; Billström, H.; Larsson, S.; Reilly, J. S.; Johnson, A.; Hopkins, S. Attributable deaths and disability-adjusted life-years caused by infections with antibiotic-resistant bacteria in the EU and the European Economic Area in 2015: a population-level modelling analysis. *Lancet Infect. Dis.* **2019**, *19*, 56–66.
- (4) World Health Organization. *Global Action Plan on Antimicrobial Resistance* (accessed 04 02 2017).
- (5) Tadesse, M.; Tabudravu, J. N.; Jaspars, M.; Strøm, M. B.; Hansen, E.; Andersen, J. H.; Kristiansen, P. E.; Haug, T. The antibacterial ent-eusynstyelamide B and eusynstyelamides D, E, and F from the Arctic bryozoan *tegella cf. spitzbergensis*. *J. Nat. Prod.* **2011**, *74*, 837–841.
- (6) Tapiolas, D. M.; Bowden, B. F.; Abou-Mansour, E.; Willis, R. H.; Doyle, J. R.; Muirhead, A. N.; Liprot, C.; Llewellyn, L. E.; Wolff, C. W. W.; Wright, A. D.; Motti, C. A. Eusynstyelamides A, B, and C, nNOS Inhibitors, from the Ascidian *Eusynstyla latericus*. *J. Nat. Prod.* **2009**, *72*, 1115–1120.
- (7) Barykina, O. V.; Snider, B. B. Synthesis of (+/-)-eusynstyelamide A. *Org. Lett.* **2010**, *12*, 2664–2667.
- (8) Strøm, M. B.; Haug, B. E.; Skar, M. L.; Stensen, W.; Stiberg, T.; Svendsen, J. S. The pharmacophore of short cationic antibacterial peptides. *J. Med. Chem.* **2003**, *46*, 1567–1570.
- (9) Ghosh, C.; Haldar, J. Membrane-active small molecules: designs inspired by antimicrobial peptides. *ChemMedChem* **2015**, *10*, 1606–1624.
- (10) Gunasekaran, P.; Rajasekaran, G.; Han, E. H.; Chung, Y.-H.; Choi, Y.-J.; Yang, Y. J.; Lee, J. E.; Kim, H. N.; Lee, K.; Kim, J.-S.; Lee, H.-J.; Choi, E.-J.; Kim, E.-K.; Shin, S. Y.; Bang, J. K. Cationic amphipathic triazines with potent anti-bacterial, anti-inflammatory and anti-atopic dermatitis properties. *Sci. Rep.* **2019**, *9*, 1292.
- (11) Jiang, Y.; Chen, Y.; Song, Z.; Tan, Z.; Cheng, J. Recent advances in design of antimicrobial peptides and polypeptides toward clinical translation. *Adv. Drug Deliv. Rev.* **2021**, *170*, 261–280.
- (12) Giuliani, A.; Pirri, G.; Nicoletto, S. Antimicrobial peptides: an overview of a promising class of therapeutics. *Cent. Eur. J. Biol.* **2007**, *2*, 1–33.
- (13) Zasloff, M. Antimicrobial peptides of multicellular organisms. *Nature* **2002**, *415*, 389–395.
- (14) Hancock, R. E. W.; Haney, E. F.; Gill, E. E. The immunology of host defence peptides: beyond antimicrobial activity. *Nat. Rev. Immunol.* **2016**, *16*, 321–334.
- (15) Powers, J.-P. S.; Hancock, R. E. W. The relationship between peptide structure and antibacterial activity. *Peptides* **2003**, *24*, 1681–1691.

- (16) Latham, P. W. Therapeutic peptides revisited. *Nat. Biotechnol.* **1999**, *17*, 755–757.
- (17) Paulsen, M. H.; Ausbacher, D.; Bayer, A.; Engqvist, M.; Hansen, T.; Haug, T.; Anderssen, T.; Andersen, J. H.; Sollid, J. U. E.; Strøm, M. B. Antimicrobial activity of amphipathic α,α -disubstituted β -amino amide derivatives against ESBL - CARBA producing multi-resistant bacteria; effect of halogenation, lipophilicity and cationic character. *Eur. J. Med. Chem.* **2019**, *183*, 111671.
- (18) Hansen, T.; Ausbacher, D.; Flaten, G. E.; Havelkova, M.; Strøm, M. B. Synthesis of cationic antimicrobial $\beta(2,2)$ -amino acid derivatives with potential for oral administration. *J. Med. Chem.* **2011**, *54*, 858–868.
- (19) Wong, O.; McKeown, R. H. Substituent effects on partition coefficients of barbituric acids. *J. Pharm. Sci.* **1988**, *77*, 926–932.
- (20) Ashnagar, A.; Naseri, N. G.; Sheeri, B. Novel synthesis of barbiturates. *Chin. J. Chem.* **2007**, *25*, 382–384.
- (21) Huang, H.-M.; Procter, D. J. Radical-radical cyclization cascades of barbiturates triggered by electron-transfer reduction of amide-type carbonyls. *J. Am. Chem. Soc.* **2016**, *138*, 7770–7775.
- (22) Neumann, D. M.; Cammarata, A.; Backes, G.; Palmer, G. E.; Jursic, B. S. Synthesis and antifungal activity of substituted 2,4,6-pyrimidinetrione carbaldehyde hydrazones. *Bioorg. Med. Chem.* **2014**, *22*, 813–826.
- (23) Gunasekaran, P.; Yim, M. S.; Ahn, M.; Soung, N.-K.; Park, J.-E.; Kim, J.; Bang, G.; Shin, S. C.; Choi, J.; Kim, M.; Kim, H. N.; Lee, Y.-H.; Chung, Y.-H.; Lee, K.; EunKyeong Kim, E.; Jeon, Y.-H.; Kim, M. J.; Lee, K.-R.; Kim, B.-Y.; Lee, K. S.; Ryu, E. K.; Bang, J. K. Development of a polo-like kinase-1 polo-box domain inhibitor as a tumor growth suppressor in mice models. *J. Med. Chem.* **2020**, *63*, 14905–14920.
- (24) Jursic, B. S. A simple method for Knoevenagel condensation of α,β -conjugated and aromatic aldehydes with barbituric acid. *J. Heterocycl. Chem.* **2001**, *38*, 655–657.
- (25) Jursic, B. S.; Neumann, D. M. Reductive C-alkylation of barbituric acid derivatives with carbonyl compounds in the presence of platinum and palladium catalysts. *Tetrahedron Lett.* **2001**, *42*, 4103–4107.
- (26) Kotha, S.; Deb, A. C.; Kumar, R. V. Spiro-annulation of barbituric acid derivatives and its analogs by ring-closing metathesis reaction. *Bioorg. Med. Chem. Lett.* **2005**, *15*, 1039–1043.
- (27) Pei, Y.; Wickham, B. O. S. Regioselective syntheses of 3-aminomethyl-5-substituted isoxazoles: A facile and chemoselective reduction of azide to amine by sodium borohydride using 1,3-propanedithiol as a catalyst. *Tetrahedron Lett.* **1993**, *34*, 7509–7512.
- (28) Hansen, T.; Moe, M. K.; Anderssen, T.; Strøm, M. B. Metabolism of small antimicrobial $\beta(2,2)$ -amino acid derivatives by murine liver microsomes. *Eur. J. Drug Metab. Pharmacokinet.* **2012**, *37*, 191–201.
- (29) Gillis, E. P.; Eastman, K. J.; Hill, M. D.; Donnelly, D. J.; Meanwell, N. A. Applications of fluorine in medicinal chemistry. *J. Med. Chem.* **2015**, *58*, 8315–8359.
- (30) Kim, S.-H.; Semanya, D.; Castagnolo, D. Antimicrobial drugs bearing guanidine moieties: A review. *Eur. J. Med. Chem.* **2021**, *216*, 113293.
- (31) Andreev, K.; Bianchi, C.; Laursen, J. S.; Citterio, L.; Hein-Kristensen, L.; Gram, L.; Kuzmenko, I.; Olsen, C. A.; Gidalevitz, D. Guanidino groups greatly enhance the action of antimicrobial peptidomimetics against bacterial cytoplasmic membranes. *Biochim. Biophys. Acta* **2014**, *1838*, 2492–2502.
- (32) Gabriel, G. J.; Madkour, A. E.; Dabkowski, J. M.; Nelson, C. F.; Nüsslein, K.; Tew, G. N. Synthetic mimic of antimicrobial peptide with nonmembrane-disrupting antibacterial properties. *Biomacromolecules* **2008**, *9*, 2980–2983.
- (33) Locock, K. E. S.; Michl, T. D.; Valentin, J. D. P.; Vasilev, K.; Hayball, J. D.; Qu, Y.; Traven, A.; Griesser, H. J.; Meagher, L.; Haeussler, M. Guanlylated polymethacrylates: a class of potent antimicrobial polymers with low hemolytic activity. *Biomacromolecules* **2013**, *14*, 4021–4031.
- (34) Yang, S.-T.; Shin, S. Y.; Lee, C. W.; Kim, Y.-C.; Hahm, K.-S.; Kim, J. I. Selective cytotoxicity following Arg-to-Lys substitution in tritrypticin adopting a unique amphipathic turn structure. *FEBS Lett.* **2003**, *540*, 229–233.
- (35) SSI Novel Polymyxin Derivatives Effective in Treating Experimental Peritoneal E. coli Infection in Mice. <https://en.ssi.dk/-/media/arkiv/uk/products-and-services/contract-research-organization/antimicrobial-evaluation/poster---efficacy-study-in-the-peritonitis-model.pdf?la=en> (accessed 18 02 2021).
- (36) Galluzzi, L.; Karp, M. Intracellular redox equilibrium and growth phase affect the performance of luciferase-based biosensors. *J. Biotechnol.* **2007**, *127*, 188–198.
- (37) Virta, M.; Åkerman, K. E. O.; Saviranta, P.; Oker-Blom, C.; Karp, M. T. Real-time measurement of cell permeabilization with low-molecular-weight membranolytic agents. *J. Antimicrob. Chemother.* **1995**, *36*, 303–315.
- (38) Kuyyakonond, T.; Quesnel, L. B. The mechanism of action of chlorhexidine. *FEMS Microbiol. Lett.* **1992**, *100*, 211–215.
- (39) Pandit, K. R.; Klauda, J. B. Membrane models of E. coli containing cyclic moieties in the aliphatic lipid chain. *Biochim. Biophys. Acta* **2012**, *1818*, 1205–1210.
- (40) Dixon, E. A.; Fischer, A.; Robinson, F. P. Preparation of a series of substituted fluoromethylnaphthalenes. *Can. J. Chem.* **1981**, *59*, 2629–2641.
- (41) Clinical and Laboratory Standards Institute. *Methods for Dilution Antimicrobial Susceptibility Tests for Bacteria that Grow Aerobically*. Approved Standard, M07-A9, 9; CLSI: Wayne, PA, 2012.
- (42) Igumnova, E. M.; Mishchenko, E.; Haug, T.; Blencke, H.-M.; Sollid, J. U. E.; Fredheim, E. G. A.; Lauksund, S.; Stensvåg, K.; Strøm, M. B. Synthesis and antimicrobial activity of small cationic amphipathic aminobenzamide marine natural product mimics and evaluation of relevance against clinical isolates including ESBL-CARBA producing multi-resistant bacteria. *Bioorg. Med. Chem.* **2016**, *24*, 5884–5894.
- (43) Radeck, J.; Kraft, K.; Bartels, J.; Cikovic, T.; Dürr, F.; Emenegger, J.; Kelterborn, S.; Sauer, C.; Fritz, G.; Gebhard, S.; Mascher, T. The Bacillus BioBrick Box: generation and evaluation of essential genetic building blocks for standardized work with *Bacillus subtilis*. *J. Biol. Eng.* **2013**, *7*, 29.
- (44) Frackman, S.; Anhalt, M.; Neelson, K. H. Cloning, organization, and expression of the bioluminescence genes of *Xenorhabdus luminescens*. *J. Bacteriol.* **1990**, *172*, 5767–5773.
- (45) Frisch, M. J.; Trucks, G. W.; Schlegel, H. B.; Scuseria, G. E.; Robb, M. A.; Cheeseman, J. R.; Scalmani, G.; Barone, V.; Mennucci, B.; Petersson, G. A.; Nakatsuji, H.; Caricato, M.; Li, X.; Hratchian, H. A.; Izmaylov, A. F.; Bloino, G. Z.; Sonnenberg, J. L.; Hada, M.; Ehara, M.; Toyota, K.; Fukuda, R.; Hasegawa, J.; Ishida, M.; Nakajima, T.; Honda, Y.; Kitao, O.; Nakai, H.; Vreven, T.; Montgomery, J.; Peralta, J. E.; Ogliaro, F.; Bearpark, M.; Heyd, J. J.; Brothers, E.; Kudin, K. N.; Staroverov, V. N.; Keith, T.; Kobayashi, R.; Normand, J.; Raghavachari, K.; Rendell, A.; Burant, J. C.; Iyengar, S. S.; Tomasi, J.; Cossi, M.; Rega, N.; Millam, J. M.; Klene, M.; Knox, J. E.; Cross, J. B.; Bakken, V.; Adamo, C.; Jaramillo, J.; Gomperts, R.; Stratmann, R. E.; Yazyev, O.; Austin, A. J.; Cammi, R.; Pomelli, C.; Ochterski, J. W.; Martin, R. L.; Morokuma, K.; Zakrzewski, V. G.; Voth, G. A.; Salvador, P.; Dannenberg, J. J.; Dapprich, S.; Daniels, A. D.; Farkas, O.; Foresman, J. B.; Ortiz, J. V.; Cioslowski, J.; Fox, D. J. *Gaussian 09*, Revision D.01; Gaussian Inc.: Wallingford, CT, 2013.
- (46) Becke, A. D. A new mixing of Hartree-Fock and local density-functional theories. *J. Chem. Phys.* **1993**, *98*, 1372–1377.
- (47) Lee, C.; Yang, W.; Parr, R. G. Development of the Colle-Salvetti correlation-energy formula into a functional of the electron density. *Phys. Rev. B: Condens. Matter Mater. Phys.* **1988**, *37*, 785–789.
- (48) Grimme, S.; Antony, J.; Ehrlich, S.; Krieg, H. A consistent and accurate ab initio parametrization of density functional dispersion correction (DFT-D) for the 94 elements H-Pu. *J. Chem. Phys.* **2010**, *132*, 154104.

(49) McLean, A. D.; Chandler, G. S. Contracted Gaussian basis sets for molecular calculations. I. Second row atoms, Z=11-18. *J. Chem. Phys.* **1980**, *72*, 5639–5648.

(50) Krishnan, R.; Binkley, J. S.; Seeger, R.; Pople, J. A. Self-consistent molecular orbital methods. XX. A basis set for correlated wave functions. *J. Chem. Phys.* **1980**, *72*, 650–654.

(51) Tomasi, J.; Mennucci, B.; Cancès, E. The IEF version of the PCM solvation method: an overview of a new method addressed to study molecular solutes at the QM ab initio level. *J. Mol. Struct.* **1999**, *464*, 211–226.

(52) Cancès, E.; Mennucci, B.; Tomasi, J. A new integral equation formalism for the polarizable continuum model: Theoretical background and applications to isotropic and anisotropic dielectrics. *Chem. Phys.* **1997**, *107*, 3032–3041.

(53) Humphrey, W.; Dalke, A.; Schulten, K. VMD: visual molecular dynamics. *J. Mol. Graph.* **1996**, *14*, 33–38.

(54) *The PyMOL Molecular Graphics System, Version 2.0*; Schrödinger, LLC.

(55) Vanommeslaeghe, K.; MacKerell, A. D., Jr. Automation of the CHARMM General Force Field (CGenFF) I: bond perception and atom typing. *J. Chem. Inf. Model.* **2012**, *52*, 3144–3154.

(56) Vanommeslaeghe, K.; Raman, E. P.; MacKerell, A. D., Jr. Automation of the CHARMM General Force Field (CGenFF) II: assignment of bonded parameters and partial atomic charges. *J. Chem. Inf. Model.* **2012**, *52*, 3155–3168.

(57) Phillips, J. C.; Braun, R.; Wang, W.; Gumbart, J.; Tajkhorshid, E.; Villa, E.; Chipot, C.; Skeel, R. D.; Kalé, L.; Schulten, K. Scalable molecular dynamics with NAMD. *J. Comput. Chem.* **2005**, *26*, 1781–1802.

(58) Klauda, J. B.; Venable, R. M.; Freites, J. A.; O'Connor, J. W.; Tobias, D. J.; Mondragon-Ramirez, C.; Vorobyov, I.; MacKerell, A. D., Jr.; Pastor, R. W. Update of the CHARMM all-atom additive force field for lipids: validation on six lipid types. *J. Phys. Chem. B* **2010**, *114*, 7830–7843.

(59) Darden, T.; York, D.; Pedersen, L. Particle mesh Ewald: an N-log(N) method for Ewald sums in large systems. *J. Chem. Phys.* **1993**, *98*, 10089–10092.

(60) Ryckaert, J.-P.; Ciccotti, G.; Berendsen, H. J. C. Numerical integration of the cartesian equations of motion of a system with constraints: molecular dynamics of n-alkanes. *J. Comput. Phys.* **1977**, *23*, 327–341.

(61) Feller, S. E.; Zhang, Y.; Pastor, R. W.; Brooks, B. R. Constant pressure molecular dynamics simulation: the Langevin piston method. *J. Chem. Phys.* **1995**, *103*, 4613–4621.

(62) Martyna, G. J.; Tobias, D. J.; Klein, M. L. Constant pressure molecular dynamics algorithms. *J. Chem. Phys.* **1994**, *101*, 4177–4189.

(63) McKinney, W. In *Data structures for statistical computing in python. Proceedings of the 9th Python in Science Conference*: Austin, TX, 2010; pp 51–56.

(64) Michael, W.; The Seaborn Development Team. *Mwaskom/Seaborn, 0.11.0*; Zenodo, 2020.

(65) Hunter, J. D. Matplotlib: A 2D graphics environment. *Comput. Sci. Eng.* **2007**, *9*, 90–95.

Supporting Information for

Amphipathic Barbiturates as Mimics of Antimicrobial Peptides and the Marine Natural Products Eusynstyelamides with Activity Against Multi-Resistant Clinical Isolates

Marianne H. Paulsen^a, Magnus Engqvist^b, Dominik Ausbacher^a, Trude Anderssen^a, Manuel K. Langer^b, Tor Haug^c, Glenn R. Morello^{b,d}, Laura E. Liikanen^b, Hans-Matti Blencke^c, Johan Isaksson^b, Eric Juskewitz^e, Annette Bayer^{b*}, Morten B. Strøm^{a*}

^a Department of Pharmacy, Faculty of Health Sciences, UiT – The Arctic University of Norway, NO-9037 Tromsø, NORWAY.

^b Department of Chemistry, UiT – The Arctic University of Norway, NO-9037 Tromsø, NORWAY.

^c The Norwegian College of Fishery Science, Faculty of Biosciences, Fisheries and Economics, UiT – The Arctic University of Norway, NO-9037 Tromsø, NORWAY.

^d Department of Science, Valley City State University, 58072, Valley City, North Dakota, USA.

^e Department of Medical Biology, Faculty of Health Sciences, UiT – The Arctic University of Norway, NO-9037 Tromsø, NORWAY.

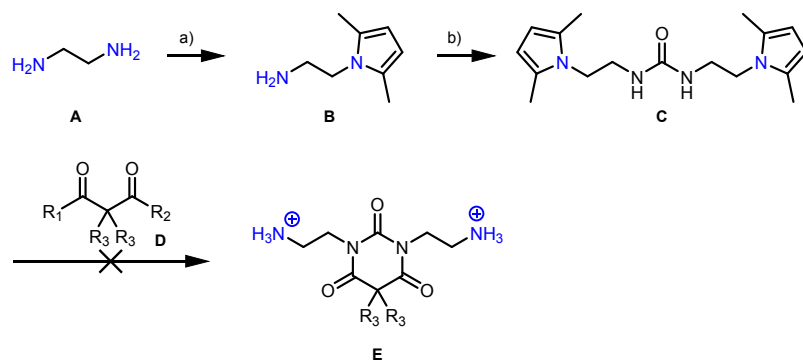
* Shared senior authorship and corresponding authors. E-mail: annette.bayer@uit.no and morten.strom@uit.no.

Table of content

1.	Attempted cyclisation of <i>N,N'</i> -dialkylated ureas with disubstituted diethyl malonates.....	2
2.	¹ H and ¹³ C NMR spectra of disubstituted malonate esters (2)	13
3.	¹ H and ¹³ C NMR spectra of C-dialkylated barbiturates (3)	20
4.	¹ H and ¹³ C NMR spectra of <i>N</i> -alkylated bromo barbiturates (4).....	28
5.	¹ H and ¹³ C NMR spectra of <i>N</i> -alkylated azide barbiturates 5	36
6.	¹ H and ¹³ C NMR spectra of amine barbiturates (6).....	44
7.	¹ H and ¹³ C NMR spectra of guanidine barbiturates (7).....	53
8.	SFC analysis of final compounds.....	61
9.	Mode of action studies	64
10.	Theoretical calculations - geometry optimisation of conformations.....	64
11.	X-Ray crystallography of 7b	65
12.	NMR conformational analysis of 7e	66
13.	Molecular modeling.....	70

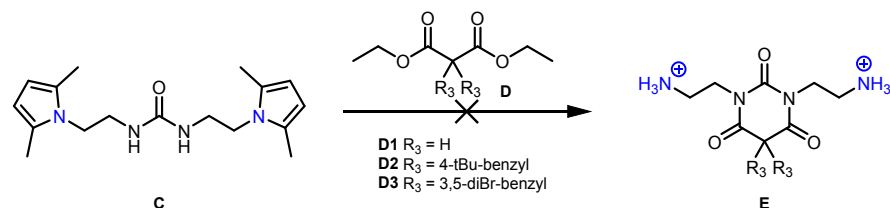
1. Attempted cyclisation of *N,N'*-dialkylated ureas with disubstituted diethyl malonates

The cyclisation of *N,N'*-dialkylated ureas and disubstituted diethyl malonates as shown in **Scheme S1** was envisioned as a synthetic route that could provide quick access to the desired 1,3,5,5-tetrasubstituted barbituric acid derivatives from a library of substituted malonic acid esters and a second library of alkylated urea. Our studies towards the corresponding cyclisation are described in the following.



Scheme S1. Schematic approach towards the synthesis of 1,3,5,5-tetrasubstituted barbituric acid derivatives. Conditions: a) hexane-2,5-dione, chloramine-T, MeCN, r.t., 1 h; b) CDI, DIPEA, DCM, r.t., 18h.

1.1 Attempted cyclisation of dialkyl urea C with diethyl malonic acid esters



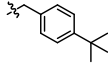
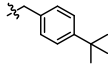
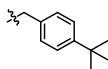
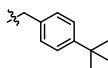
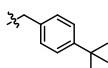
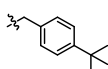
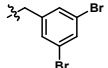
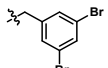
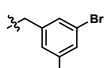
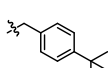
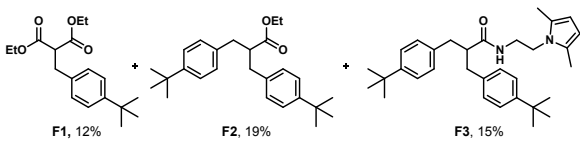
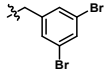
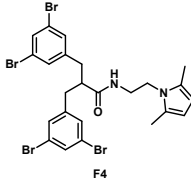
Scheme S2. General synthetic approach towards tetrasubstituted barbiturate E.

We initiated our studies with an attempt to cyclize disubstituted urea **C** with malonate esters **D1-D3** (**Scheme S2**). Several approaches were investigated (**Table S1**):

- The cyclisation of **C** with unsubstituted diethyl malonic acid ester **D1** under Lewis acid (entry 1) and strong basic conditions (entry 2 and 3). No conversion was observed, even at elevated temperatures.
- The cyclisation of **C** with disubstituted diethyl malonic acid ester **D2** employing a range of different bases and Lewis acids (entry 4-9) led to degradation of the starting materials. No conversion or unidentifiable products were obtained.
- The cyclisation of **C** with disubstituted diethyl malonic acid ester **D3** employing microwave irradiation. Starting off with a weak base (entry 10-11) no conversion was obtained, even at high temperatures. Lowering the temperature and increasing the base strength (entry 12) did not improve the conversion, but led to partial degradation of the starting material. Raising the temperature under strong basic conditions (entry 13) gave low yields of three different products. Debonylation delivered compound **F1**, decarboxylation compound **F2** and mono-coupling and subsequent decarboxylation and urea cleavage resulted in compound **F3**. Subsequently, the temperature was reduced (entry 14), but only small amounts of the corresponding amide derivative **F4** were obtained.

As the cyclisation of **C** with malonate esters was not successful, we abandoned this approach.

Table S1. Coupling conditions for disubstituted diethyl malonate esters with *N,N'*-dialkylated ureas.

Entry	R ₃	additive	conditions	Result
1	H	Al(Me) ₃ (6.0 eq)	anhydr. DCM, 0 to 25 °C, 16 h	No conversion
2	H	NaH (2.2 eq)	anhydr. DMF, 60 °C, 16 h	No conversion
3	H	NaH (2.2 eq)	anhydr. DMF, 140 °C, 40 h	No conversion
4		NaH (2.2 eq)	anhydr. DMF, r.t. to 55 °C, 48 h	No conversion
5		Na (2.0 eq)	anhydr. MeOH, r.t. to 100 °C, 48 h	Degradation
6		TiCl ₄ (6.0 eq)	anhydr. DCM, 0 to 25 °C, 2.5 h	No conversion
7		AlMe ₃ (6.0 eq)	anhydr. DCM, 0 to 25 °C, 16h	No conversion
8		Ti(OiPr) ₄ (6.0 eq)	anhydr. toluene, 0 to 75 °C, 18h	Partial conversion to an unidentifiable product
9		BF ₃ ·OEt ₂ (6.0 eq)	anhydr. toluene, 0 to 75 °C, 18h	No conversion
10		K ₂ CO ₃ (3.0 eq)	anhydr. DMF, μ-wave, 150 °C, 7 min	No conversion
11		K ₂ CO ₃ (3.0 eq)	anhydr. DMF, μ-wave, 210 °C, 10 min	No conversion
12		KOtBu (2.0 eq)	anhydr. DMF, μ-wave, 130 °C, 5 min	No conversion, sm. partially degraded
13		NaH (2.2 eq)	anhydr. DMF, μ-wave, 190 °C, 10 min	 <p>F1, 12% F2, 19% F3, 15%</p>
14		NaH (2.2 eq)	anhydr. DMF, μ-wave, 150 °C, 5 min	Addition and urea cleavage  <p>F4</p>

General procedures for the attempted cyclisation of disubstituted ureas **C** with malonate esters **D1-D3**.

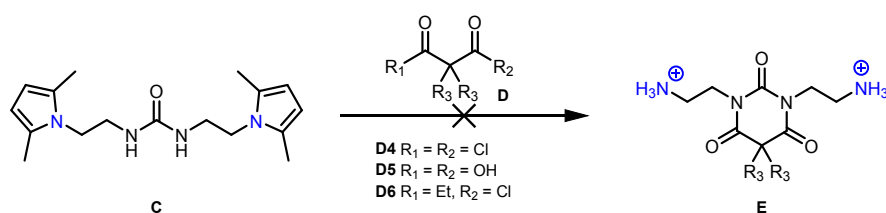
Procedure A – Conventional heating:

1,3-Bis(2-(2,5-dimethyl-1H-pyrrol-1-yl)ethyl)urea (2.0 eq) was taken up in degassed, anhydrous solvent. The mixture was cooled to 0 °C and Lewis acid (6.0 eq) or base (2.0 – 2.2 eq) were added. The solution was stirred at 0 °C for 5 min, the ice-bath was removed for 20 min and then re-cooled to 0 °C. Diethyl 2,2-bis(4-(tert-butyl)benzyl)malonate (1.0 eq), dissolved in 0.5 mL of degassed, anhydrous solvent was added dropwise. The reaction was stirred at the indicated temperature. After the time indicated, water was added and the phases were separated. The aqueous phase was extracted with DCM (x2) and the combined organic phases were washed with water and brine. The organic phase was dried over Na₂SO₄, filtered and the solvent removed under reduced pressure. The crude product was analyzed by NMR.

Procedure B – μ -wave irradiation:

N,N'-Dialkylated urea (1.0 eq) was taken up in anhydrous DMF under inert atmosphere. K₂CO₃ (3.0 eq) was added and the mixture was stirred for 10 min at ambient temperature. Then di-substituted malonate ethyl ester (1.0 eq) was added and the mixture was heated under microwave irradiation for 5-10 min. After cooling to ambient temperature, EtOAc was added and the organic phase was washed with 5% LiCl_(aq) solution (x4), dried over Na₂SO₄, filtered and the solvent removed under reduced pressure. If NMR indicated conversion, the crude product was purified by column chromatography on silica gel with EtOAc:heptane as mobile phase.

1.2 Attempted cyclisation of dialkyl urea **C** with activated diethyl malonic acid

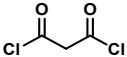
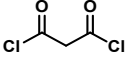
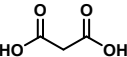
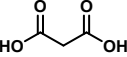
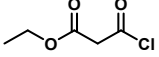
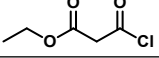


Scheme S3. Attempted cyclisation of dialkyl urea **C** with activated diethyl malonic acid.

As the cyclisation with malonate esters was unsuccessful, we investigated the use of more reactive, activated malonate derivatives such as acid chlorides or active esters formed in situ from malonic acid. (Scheme S3). The following approaches were investigated (**Table S2**):

- Using malonyl chloride (entry 1 and 2) lead to the formation of insoluble products, which were most likely polymers due to the high reactivity of the acid chloride. Slow addition of the highly diluted acid chloride (entry 2) at -78 °C did not improve the result.
- Attempts to activate malonic acid with DCC or DIC provided no conversion (entry 3 and 4) indicating that the provided species were not reactive enough.
- We envisioned that the use of a mono-activated malonate species could lead to the formation of the first amide bond and that the resulting intermediate could cyclize upon subsequent heating to form the barbituric acid core. When ethyl malonyl chloride was employed, two-fold addition to the urea derivative was observed at 0 °C (entry 5). Only by reducing the temperature to -78 °C (entry 6) partial mono addition could be achieved. Since the controlled mono addition of malonyl chloride and subsequent cyclization was not possible this strategy was discarded.

Table S2. Synthesis of *N,N'*-disubstituted barbituric acid by activated malonic acid derivatives

Entry	Acid derivative (1.0 eq)	Conditions	Result
1		Urea (1.1 eq), Et ₃ N (1.0 eq), DCM, 25 °C, 3 h	Polymer formation
2	 (diluted in DCM)	Urea (1.1 eq), Et ₃ N (1.0 eq), DCM, 0.012 M, -78 °C to r.t., 14 h	Polymer formation
3		Urea (1.0 eq), DCC (5.0 eq), 4-DMAP (0.2 eq), DCM, 0 to 45 °C, 24 h	No conversion
4		Urea (1.0 eq), DIC (3.0 eq), 4-DMAP (0.2 eq), DCM 0 to 45 °C, 24 h	No conversion
5 ^{1,2}		Urea (1.0 eq), DCM, 0 to 25 °C, 18 h	Double addition
6 ²		Urea (1.0 eq), DCM, -78 °C, 1 h	Mixture of mono and di-substituted

¹HRMS showed the presence of the mono-amide formation and the cyclized product, but those could not be isolated. ²Dropwise addition of the acid chloride.

General procedures for the attempted cyclisation of disubstituted ureas **C** with malonate esters **D4-D6**.

Starting from malonyl dichloride:

1,3-Bis(2-(2,5-dimethyl-1*H*-pyrrol-1-yl)ethyl)urea (47 mg, 1.1 eq, 0.16 mmol) was dissolved in anhydrous DCM (1 mL) and the mixture was cooled to 0 °C. Malonyl dichloride (20 mg, 14 μL, 1 eq, 0.14 mmol) and triethylamine (16 mg, 22 μL, 1.1 eq, 0.16 mmol) were added dropwise via a syringe. The mixture turned red upon addition of malonyl chloride and was left stirring in the melting ice/water bath. A red solid formed during the course of the reaction. After 3h water was added and the phases were separated. The aqueous phase was extracted with DCM (x2) and the combined organics washed with water (x1) and brine (x1). The organic phase was dried over Na₂SO₄, filtered and the solvent removed under reduced pressure to yield a crude orange solid. The insolubility of the solids indicated polymer formation. No target molecule was obtained.

For Table S2, entry 2 same amount of reagents but 9 mL of DCM and malonyl chloride was diluted with 3 mL DCM prior to addition. No target molecule was obtained.

Starting from malonic acid:

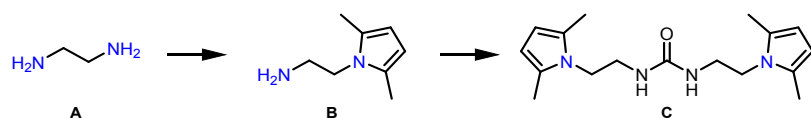
1,3-Bis(2-(2,5-dimethyl-1*H*-pyrrol-1-yl)ethyl)urea (30.0 mg, 1.0 eq, 0.099 mmol) was taken up in anhydrous DCM (1 mL) under inert atmosphere and cooled to 0 °C. Malonic acid (10.3 mg, 1.0 eq, 0.99 mmol), DCC (61.3 mg, 3.0 eq, 0.30 mmol) or DIC (46 μL, 3.0 eq, 0.30 mmol) and 4-DMAP (2.42 mg, 0.2 eq, 20 μmol) were added successively. The mixture was left stirring in the melting ice/water bath overnight. A precipitate formed in the yellow mixture after 1 h. Subsequently, it was warmed to 45 °C for further 22h. Water was added and the phases were separated. The organic phase was washed with sat. NH₄Cl_(aq) solution (x1) and brine (x1). It was dried over Na₂SO₄, filtered and the solvent removed under reduced pressure to yield an orange crude solid. No conversion was observed.

Starting from ethyl malonyl chloride:

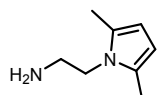
1,3-Bis(2-(2,5-dimethyl-1*H*-pyrrol-1-yl)ethyl)urea (25 mg, 1.0 eq, 83 μmol) was taken up in anhydrous DCM (0.7 mL) under inert gas and cooled to the temperature indicated. Ethyl 3-chloro-3-oxopropanoate (11 μL, 1.0 eq, 83 μmol) was added dropwise and the mixture was left stirring at the temperature indicated. After the time indicated 10% NaHCO_{3(aq)} solution was added, the phases were separated and

the organic phase was washed with 10% NaHCO_{3(aq)} solution. The organic phase was dried over Na₂SO₄, filtered and the solvent removed under reduced pressure. A red solid was obtained that could not be identified.

1.3 Synthesis of substituted urea C



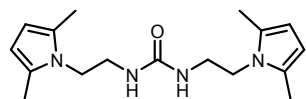
2-(2,5-dimethyl-1H-pyrrol-1-yl)ethan-1-amine⁴ (B)



To a solution of ethane-1,2-diamine (1.11 mL, 1 eq, 16.64 mmol) and hexane-2,5-dione (1.95 mL, 1.0 eq, 16.64 mmol) in acetonitril (25 mL) was added chloramine-T (204.4 mg, 0.05 eq, 0.83 mmol) at room temperature. The mixture was stirred for 60 min until TLC indicated completion of the reaction. The solvent was removed under reduced pressure, DCM was added and the catalyst was removed by filtration. The solvent was removed under reduced pressure and the crude red-brown oil was purified by column chromatography on silica gel with DCM:MeOH:Et₃N (96:3:1) as eluent. 2-(2,5-dimethyl-1H-pyrrol-1-yl)ethan-1-amine (2.145 g, 15.52 mmol, 93%) was obtained as a yellow liquid.

R_f = 0.63 (DCM:MeOH:Et₃N, 97:2:1); **HRMS** (ESI): calcd. for C₈H₁₅N₂⁺ [M+H]⁺ 139.1230, found 139.1228. **¹H NMR** (400.18 MHz, CDCl₃) δ 5.80 (s, 2H), 3.83 (t, *J* = 6.8 Hz, 2H), 2.94 (t, *J* = 6.8 Hz, 2H), 2.26 (s, 6H), 1.34 (s, 2H). **¹³C NMR** (100.64 MHz, CDCl₃) δ 127.6, 105.4, 46.4, 42.5, 12.7.

1,3-bis(2-(2,5-dimethyl-1H-pyrrol-1-yl)ethyl)urea⁵ (C)



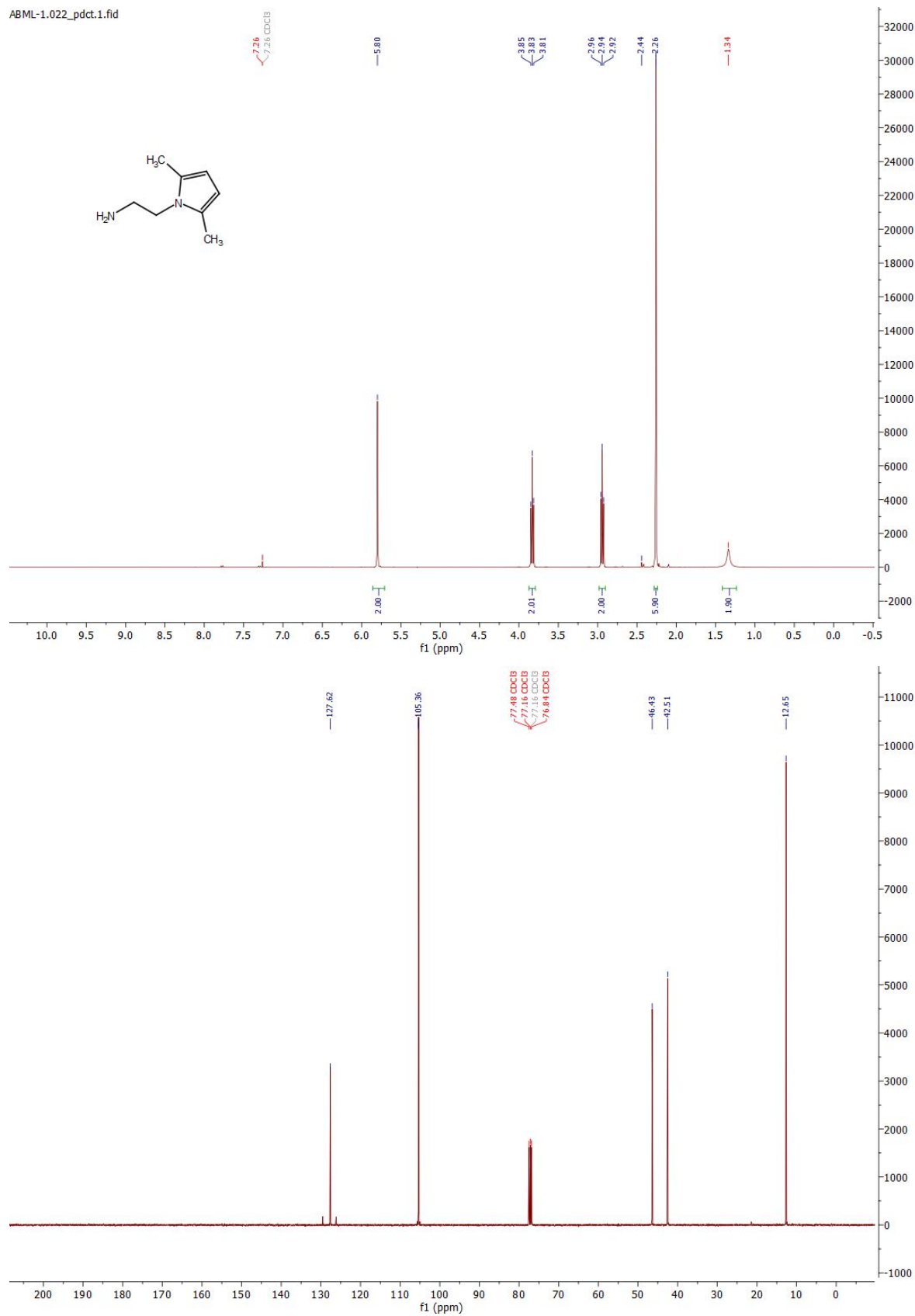
To a stirred solution of di(1H-imidazol-1-yl)methanone (1.24 g, 1.05 eq, 7.66 mmol) in DCM (35 mL) was added 2-(2,5-dimethyl-1H-pyrrol-1-yl)ethan-1-amine (2.02 g, 2.0 eq, 14.59 mmol) and DIPEA (2.50 mL, 2.0 eq, 14.59 mmol) at ambient temperature. After stirring for 18 h the solvent was removed under reduced pressure and the crude product was adsorbed on silica. The crude product was purified by column chromatography on silica with heptane:EtOAc 1:1 + 2.5% MeOH as eluent. 1,3-Bis(2-(2,5-dimethyl-1H-pyrrol-1-yl)ethyl)urea (1.72 g, 5.69 mmol, 78%) was obtained as slightly orange solid.

R_f = 0.50 (35% EtOAc in heptane + 2.5% MeOH); **HRMS** (ESI): calcd. for C₁₇H₂₇ON₄⁺ [M+H]⁺ 303.2179, found 303.2179. **¹H NMR** (400.18 MHz, CD₃OD) δ 5.65 (s, 1H), 3.84 (t, *J* = 6.7 Hz, 1H), 3.27 (t, *J* = 6.7 Hz, 1H), 2.19 (s, 3H). **¹³C NMR** (100.64 MHz, CD₃OD) δ 160.8, 128.5, 106.3, 44.3, 41.5, 12.6.

1.4 ¹H and ¹³C NMR spectra

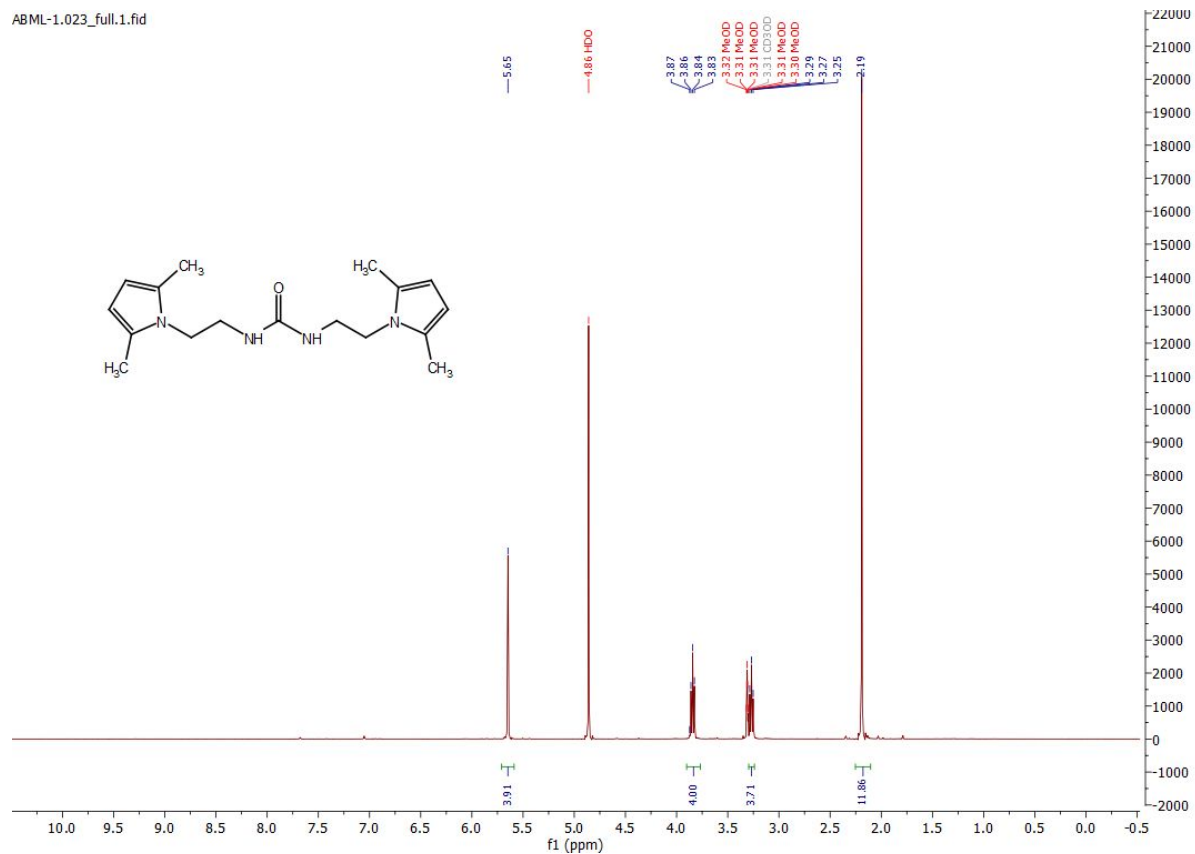
Compound B

ABML-1.022_pdct.1.fid

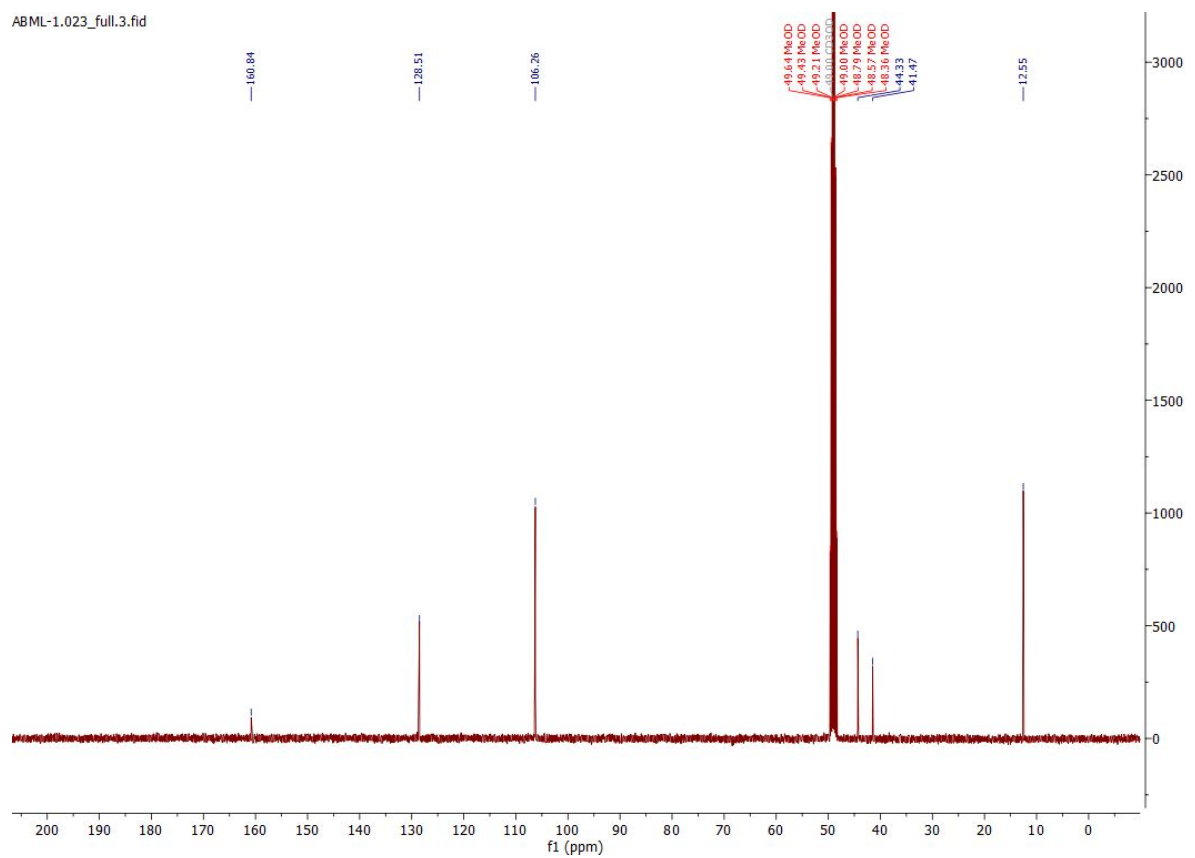


Compound C

ABML-1.023_full.1.fid

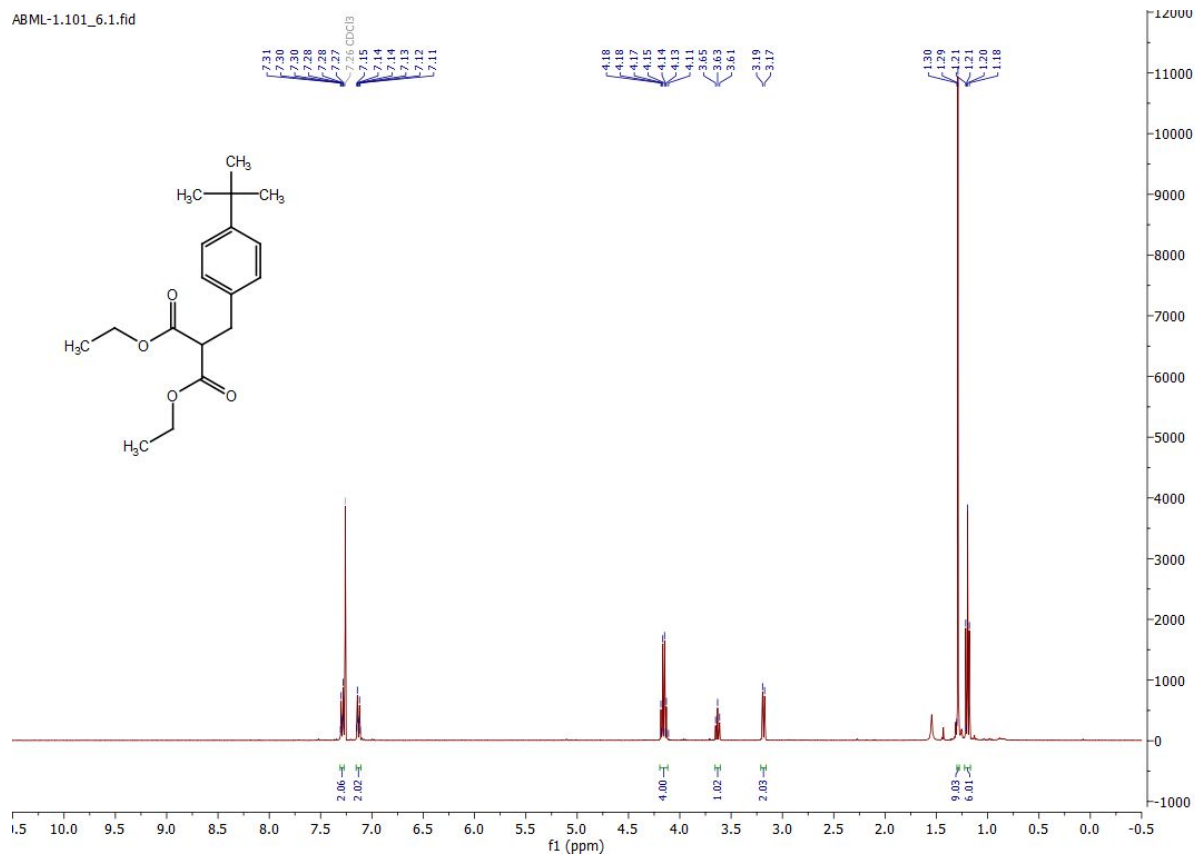


ABML-1.023_full.3.fid

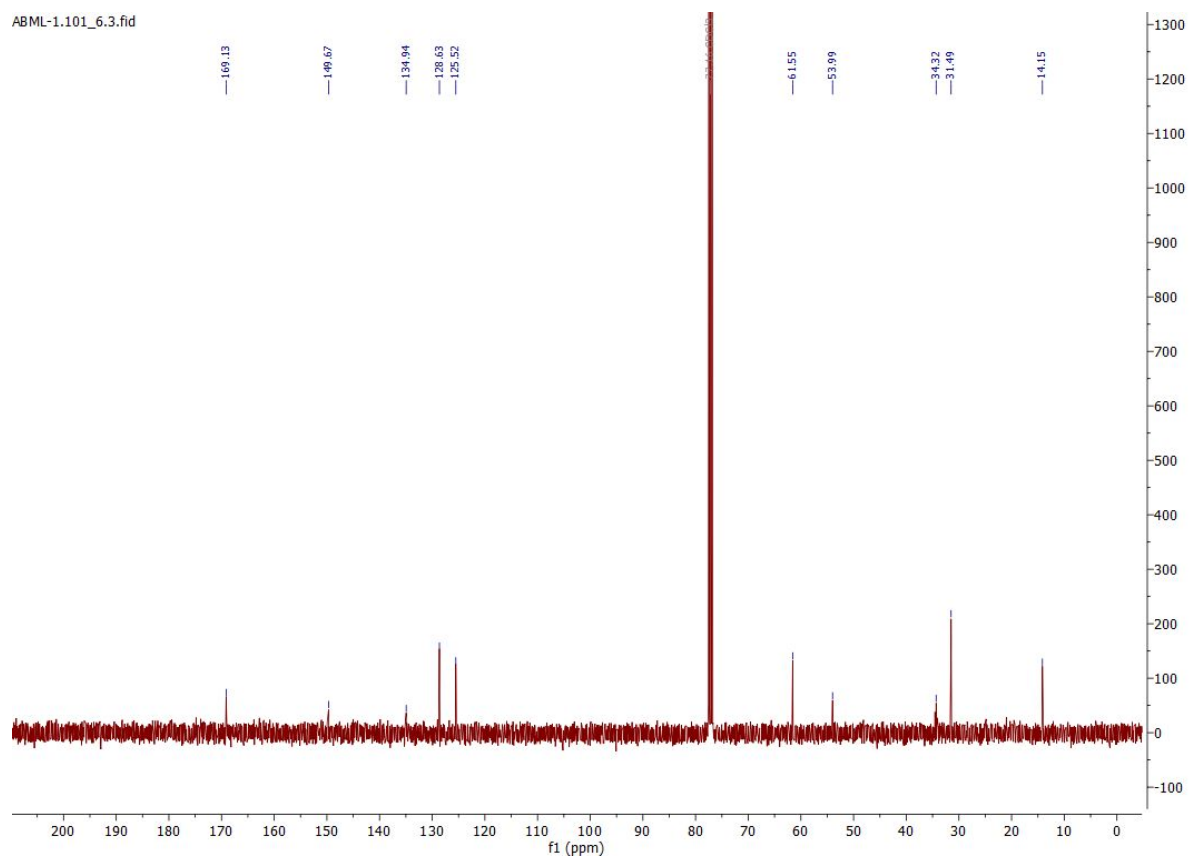


Compound F1

ABML-1.101_6.1.fid

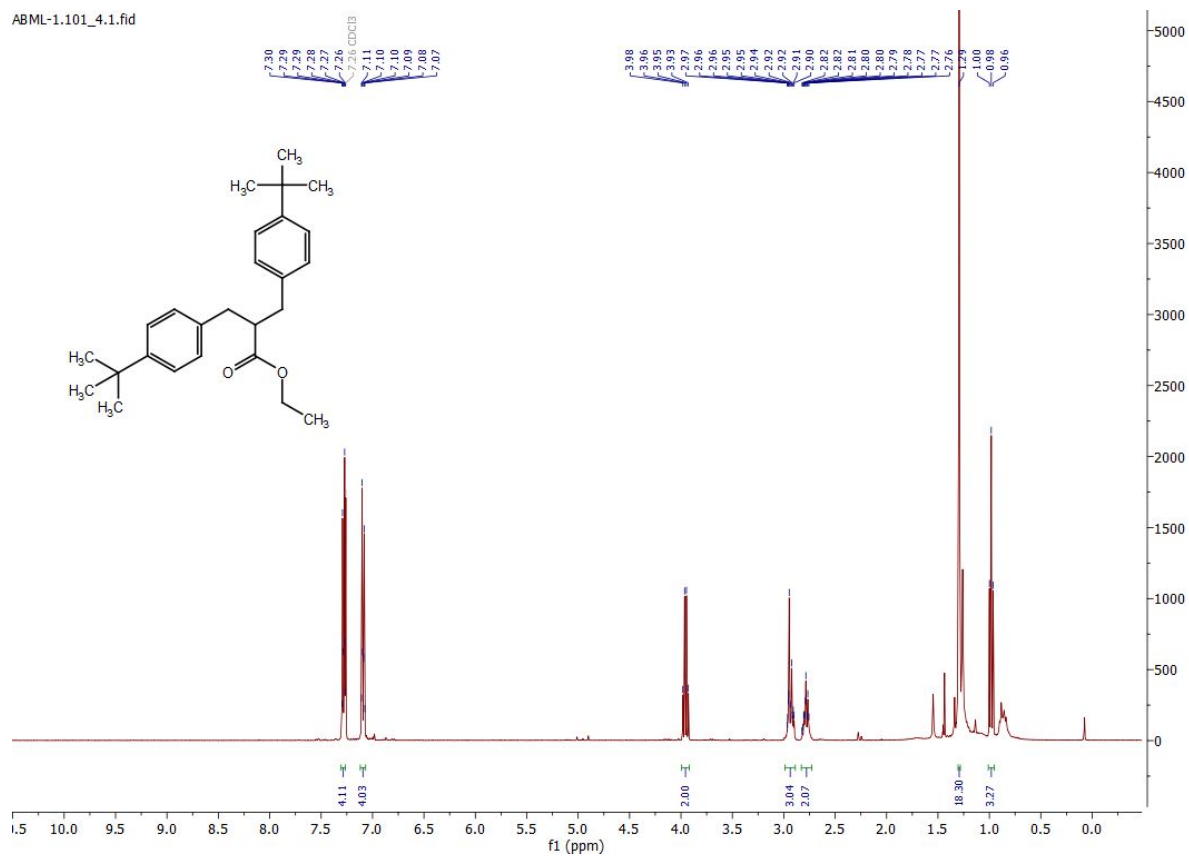


ABML-1.101_6.3.fid

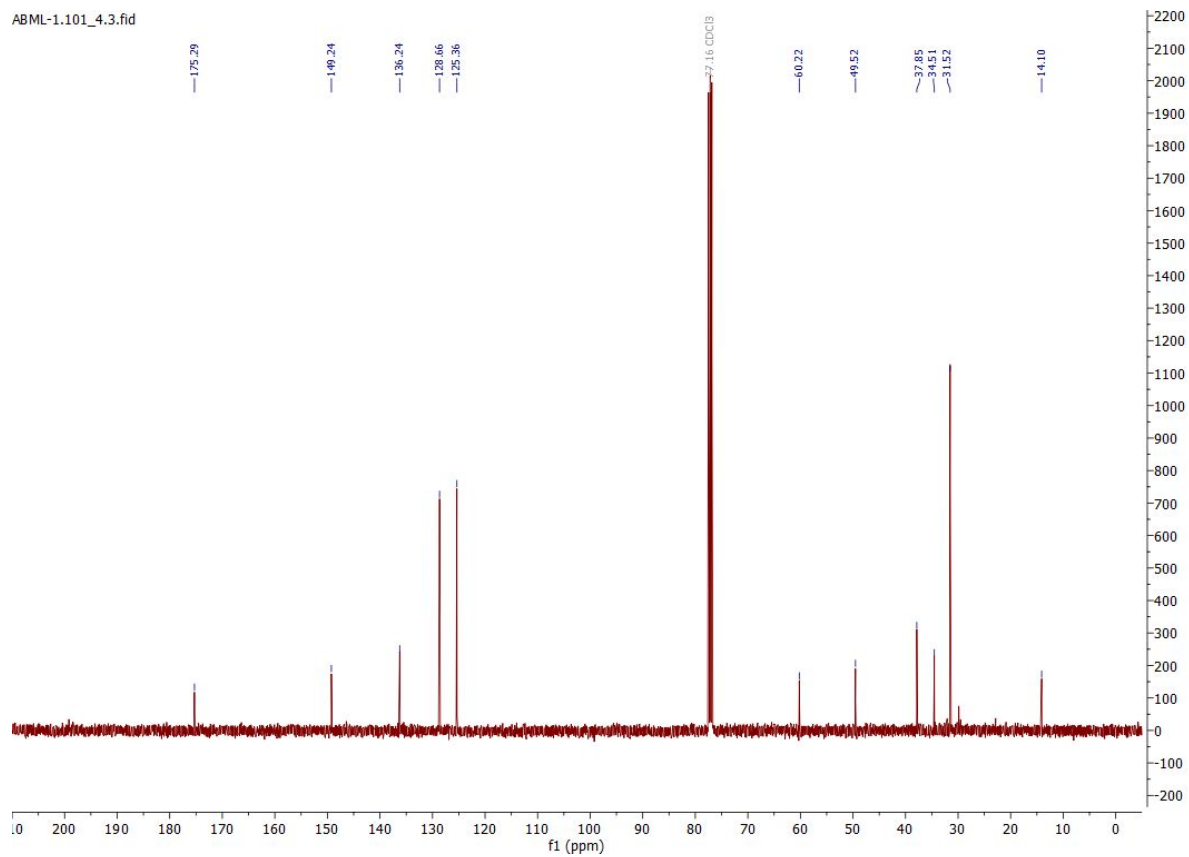


Compound F2

ABML-1.101_4.1.fid



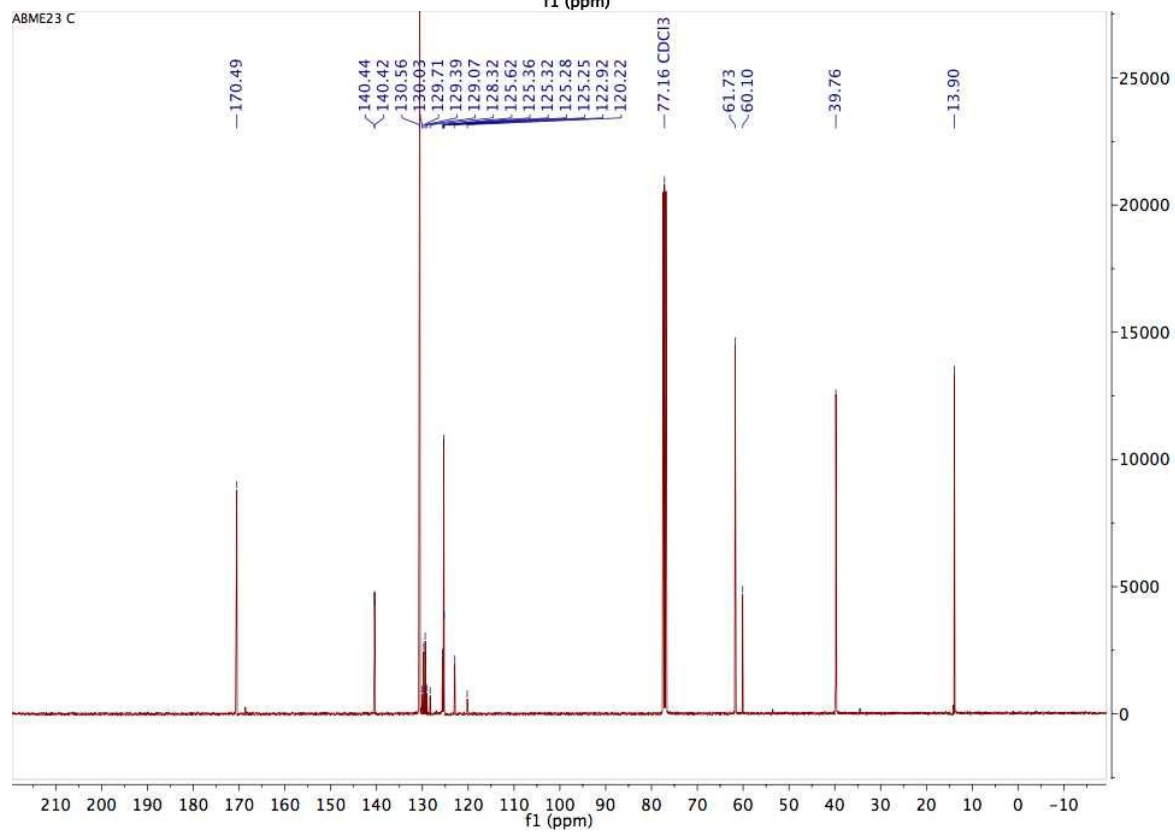
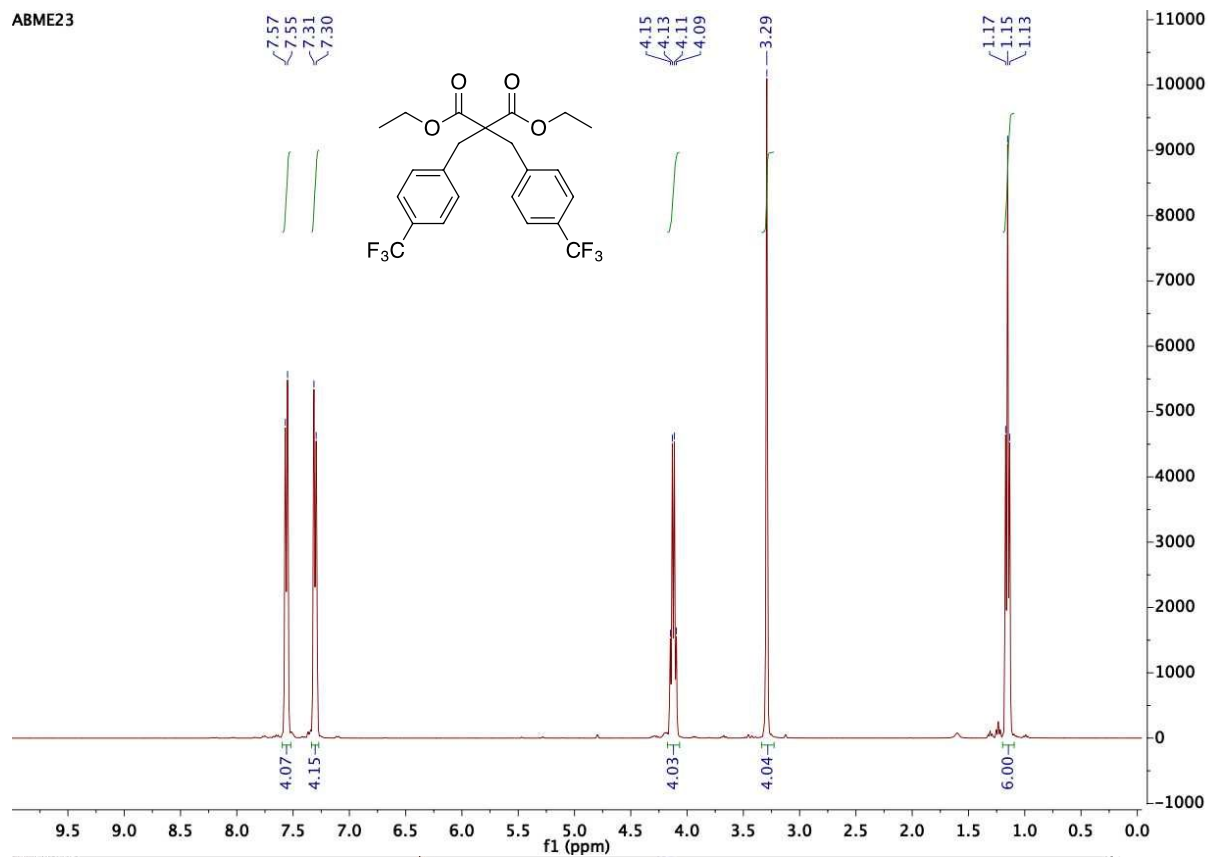
ABML-1.101_4.3.fid



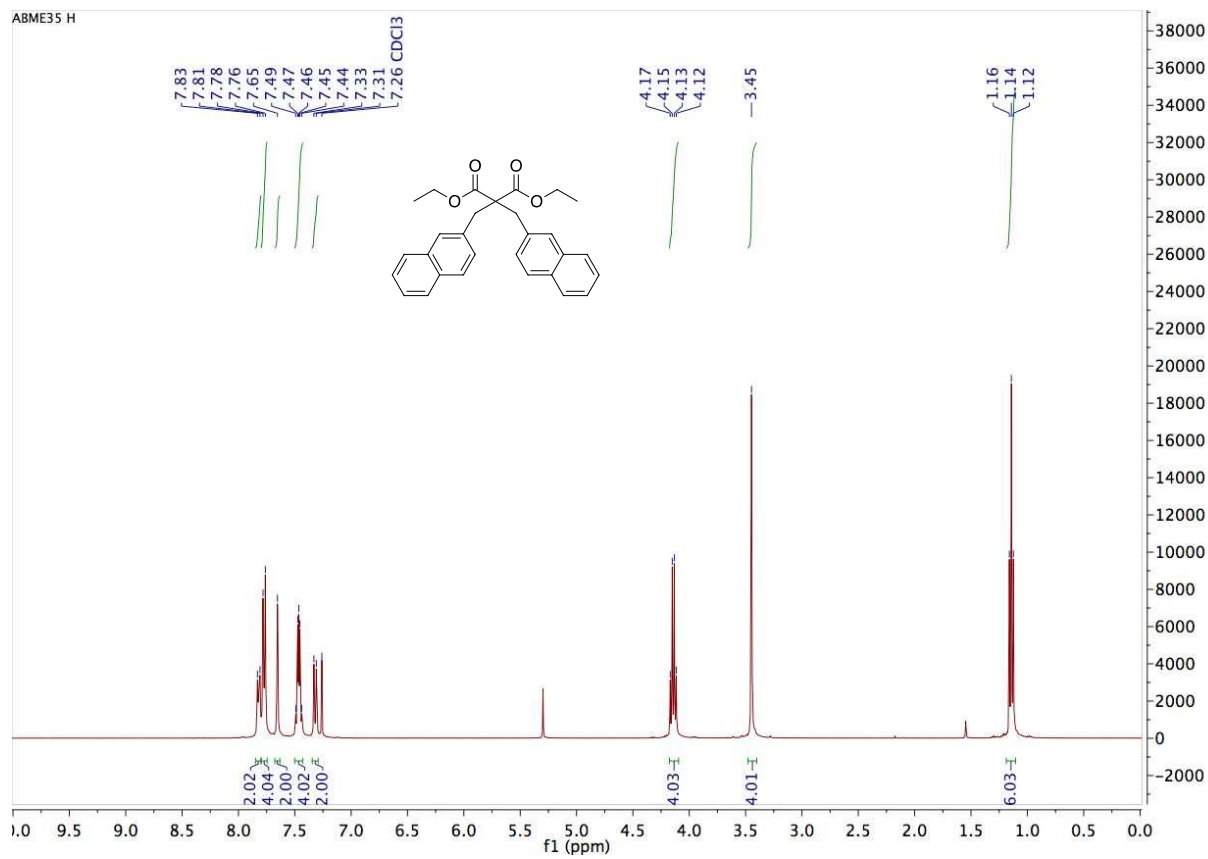
2. ¹H and ¹³C NMR spectra of disubstituted malonate esters (2)

2.1 Compound 2a

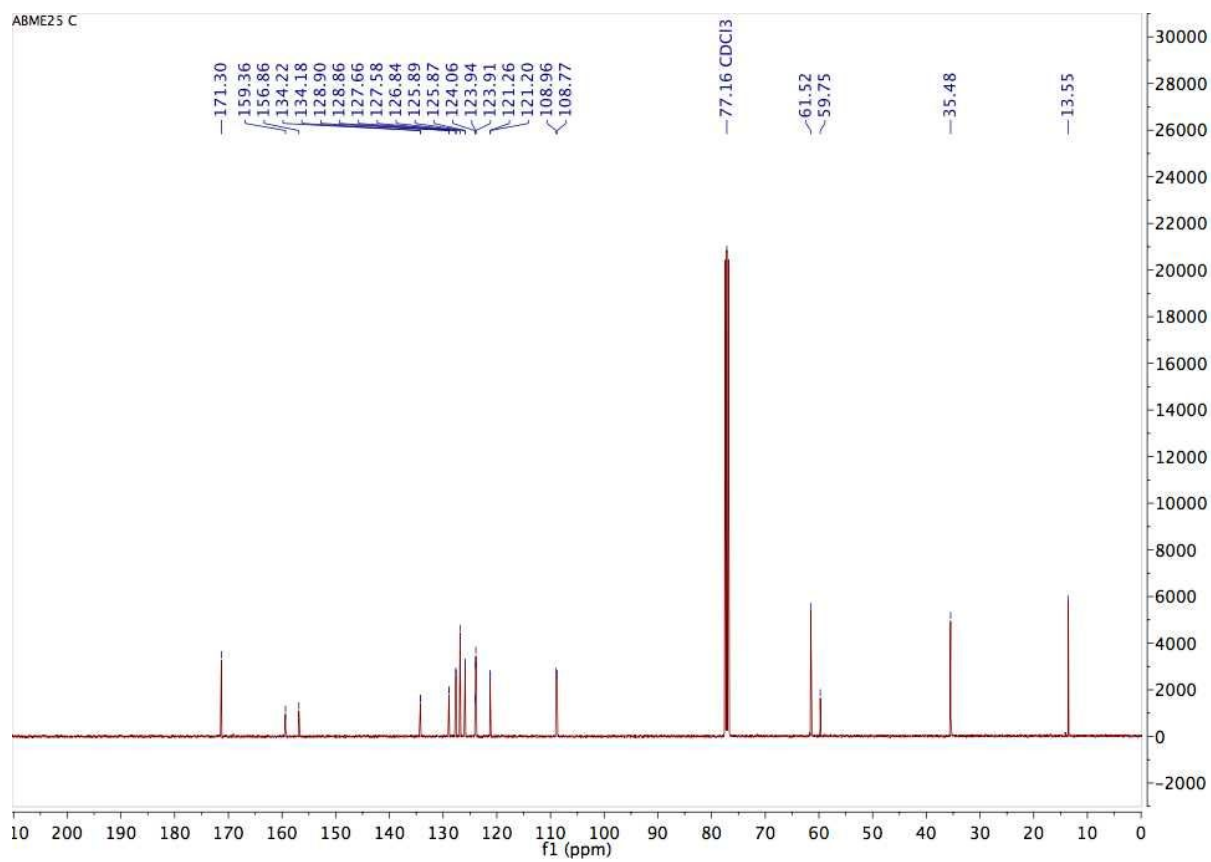
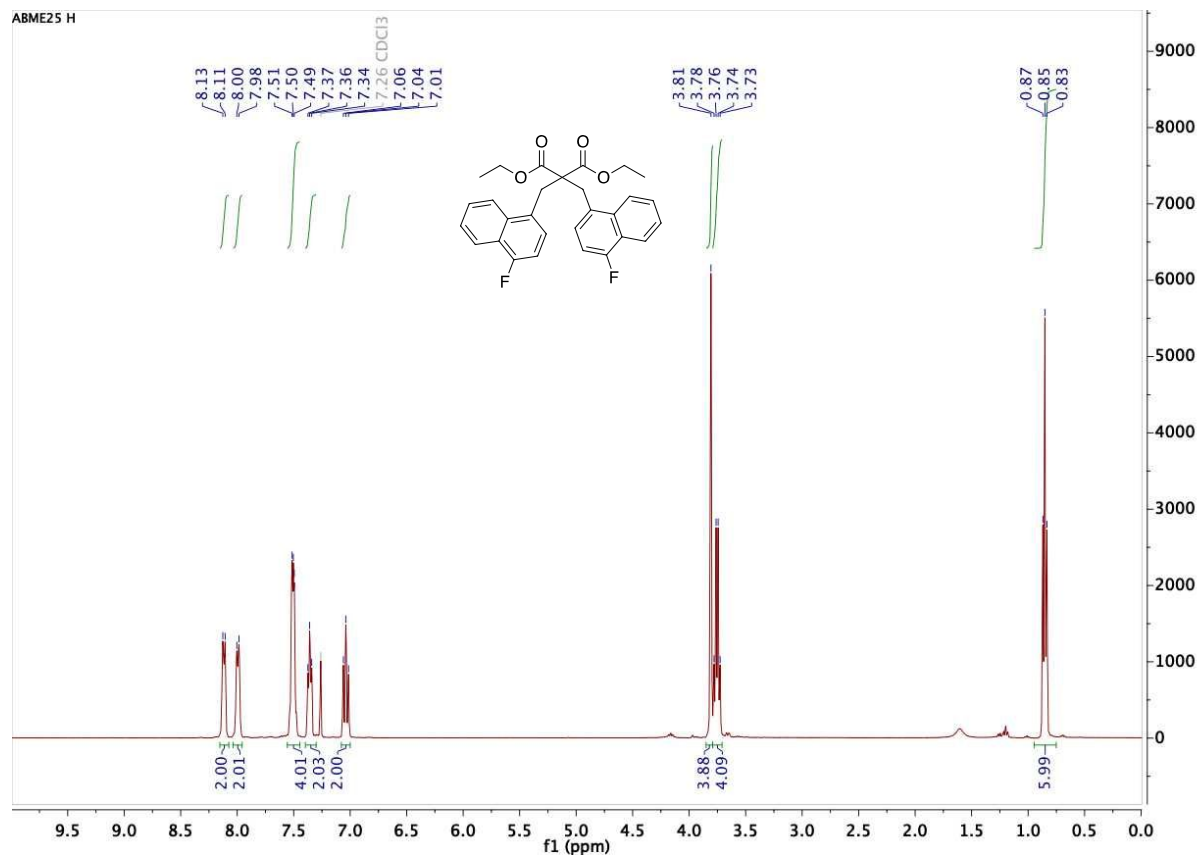
ABME23



2.2 Compound 2b

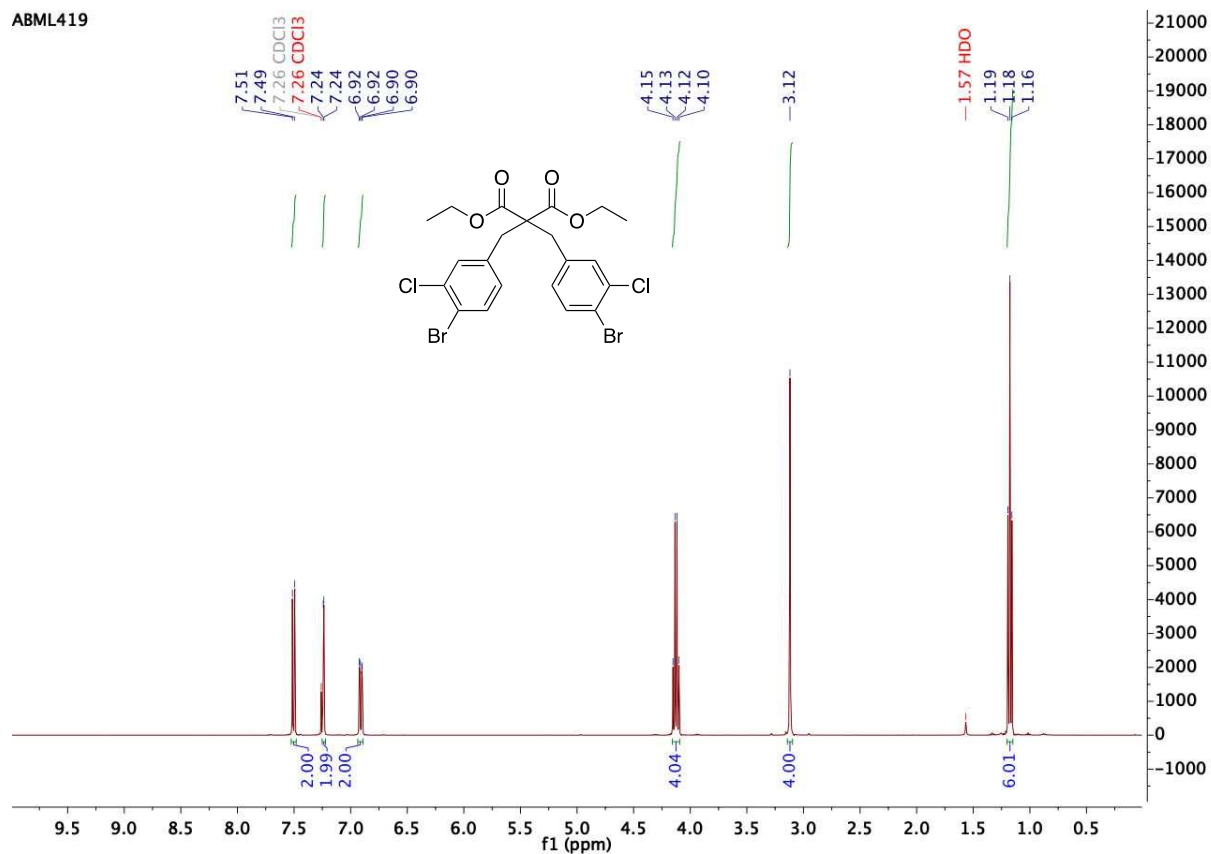


2.3 Compound 2c

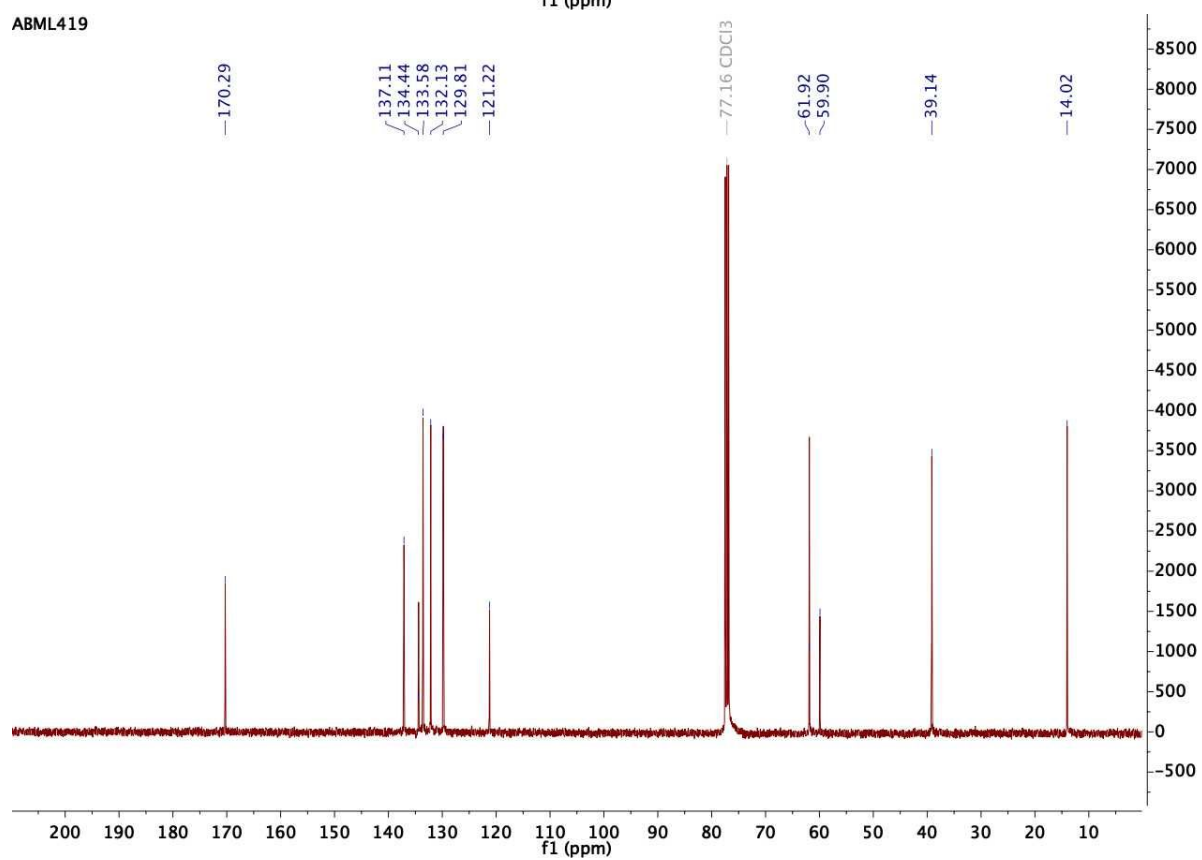


2.4 Compound 2d

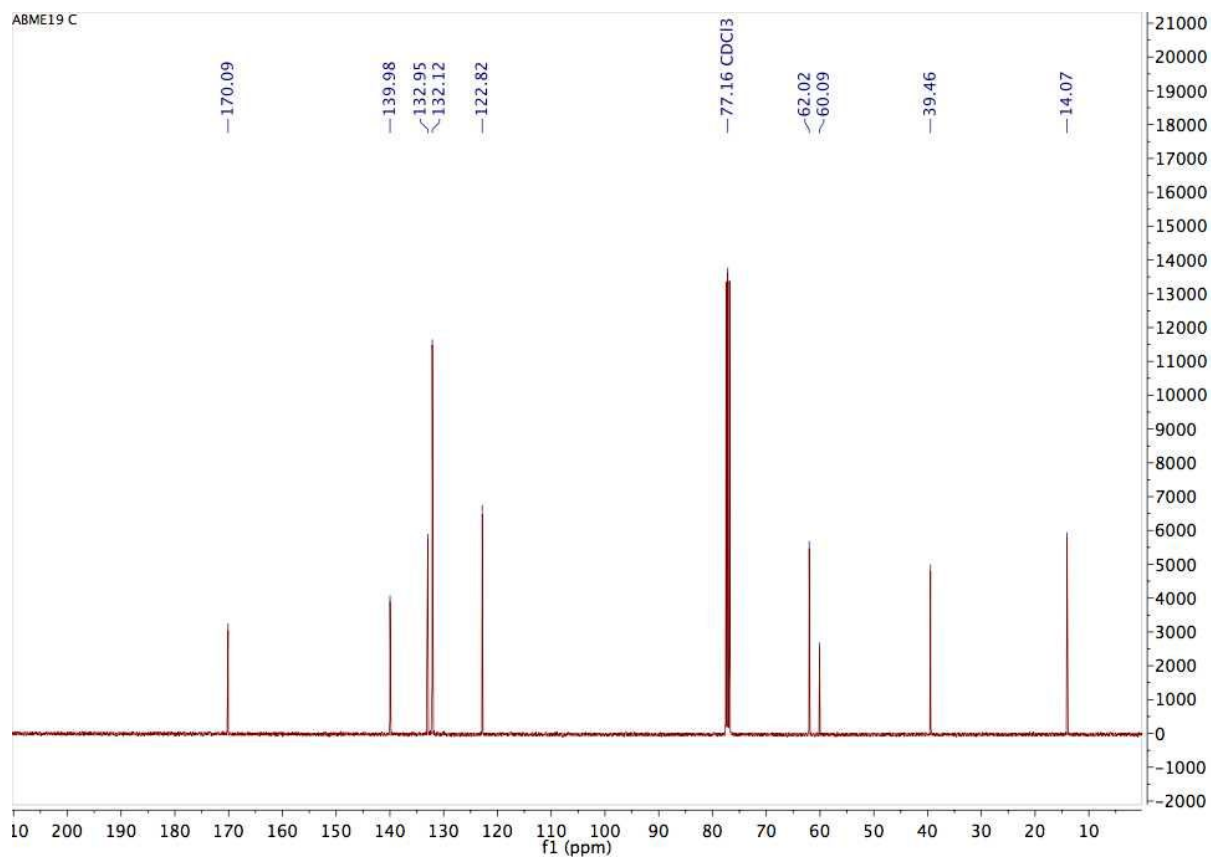
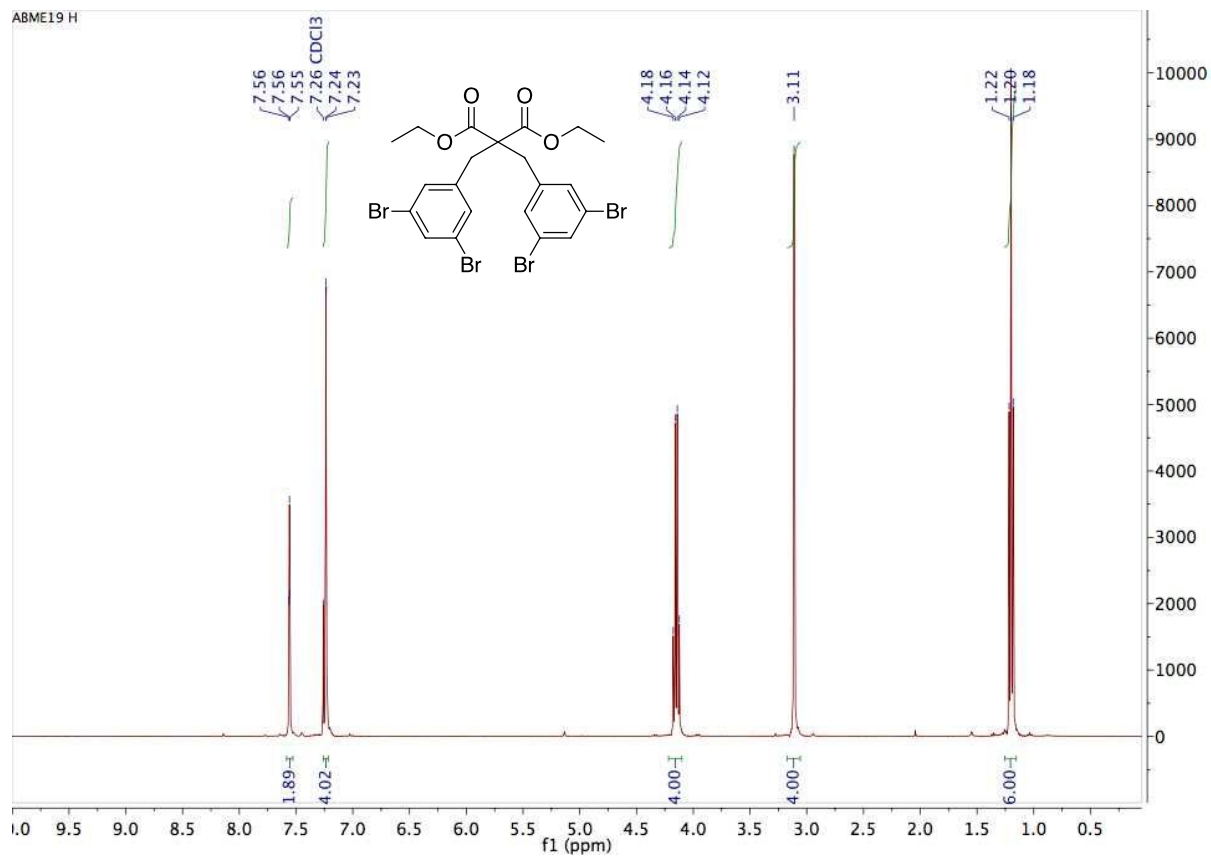
ABML419



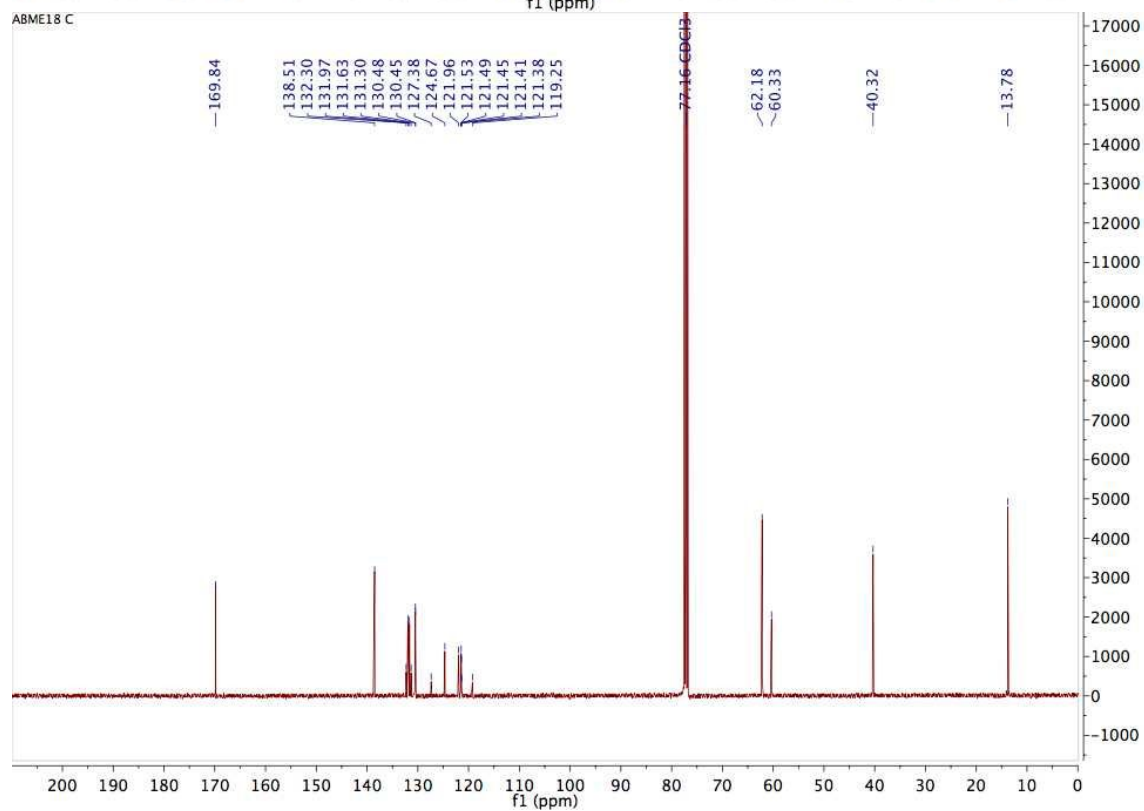
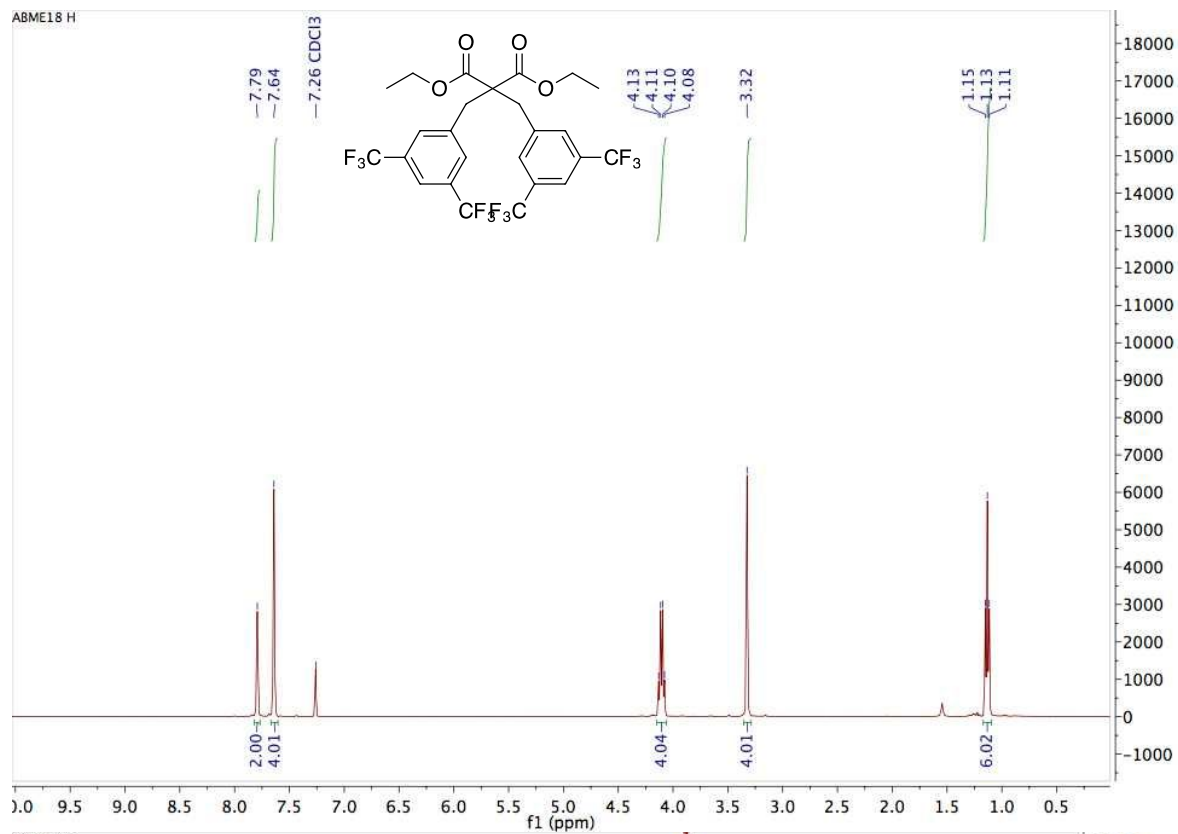
ABML419



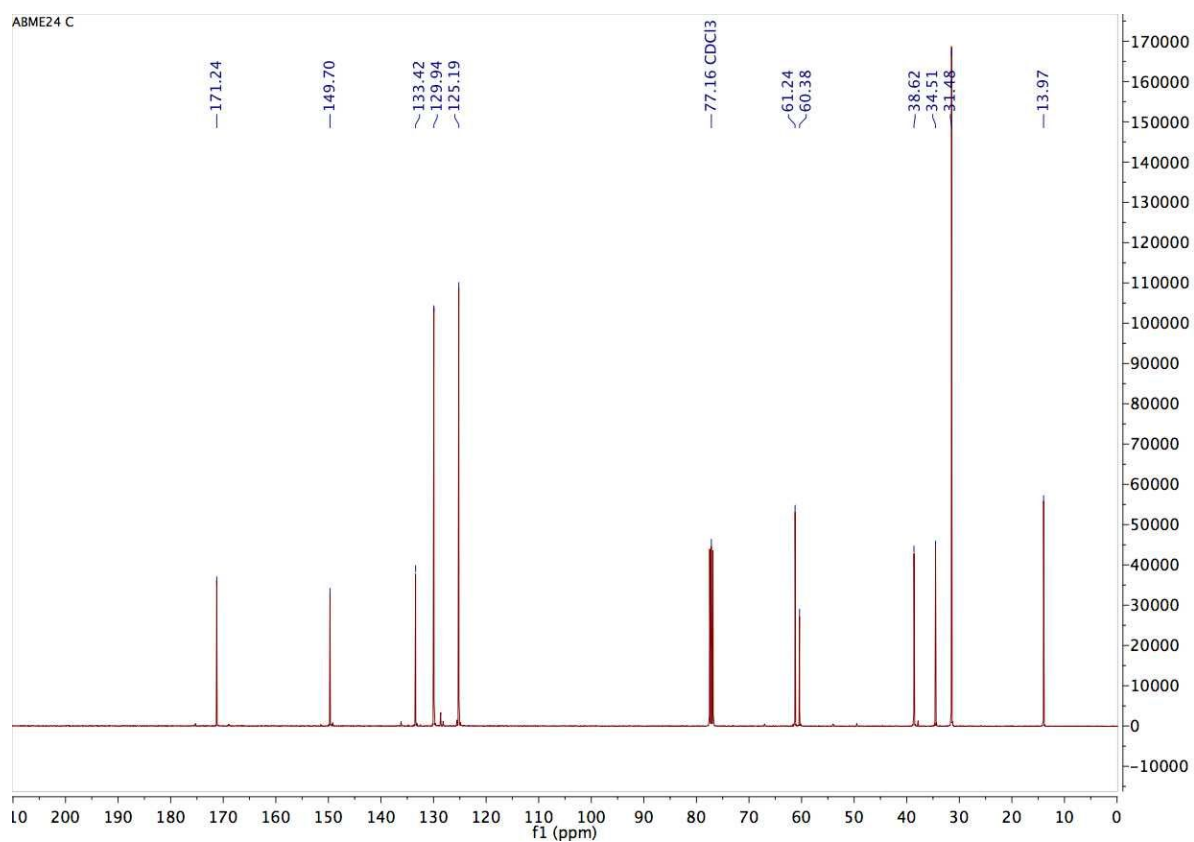
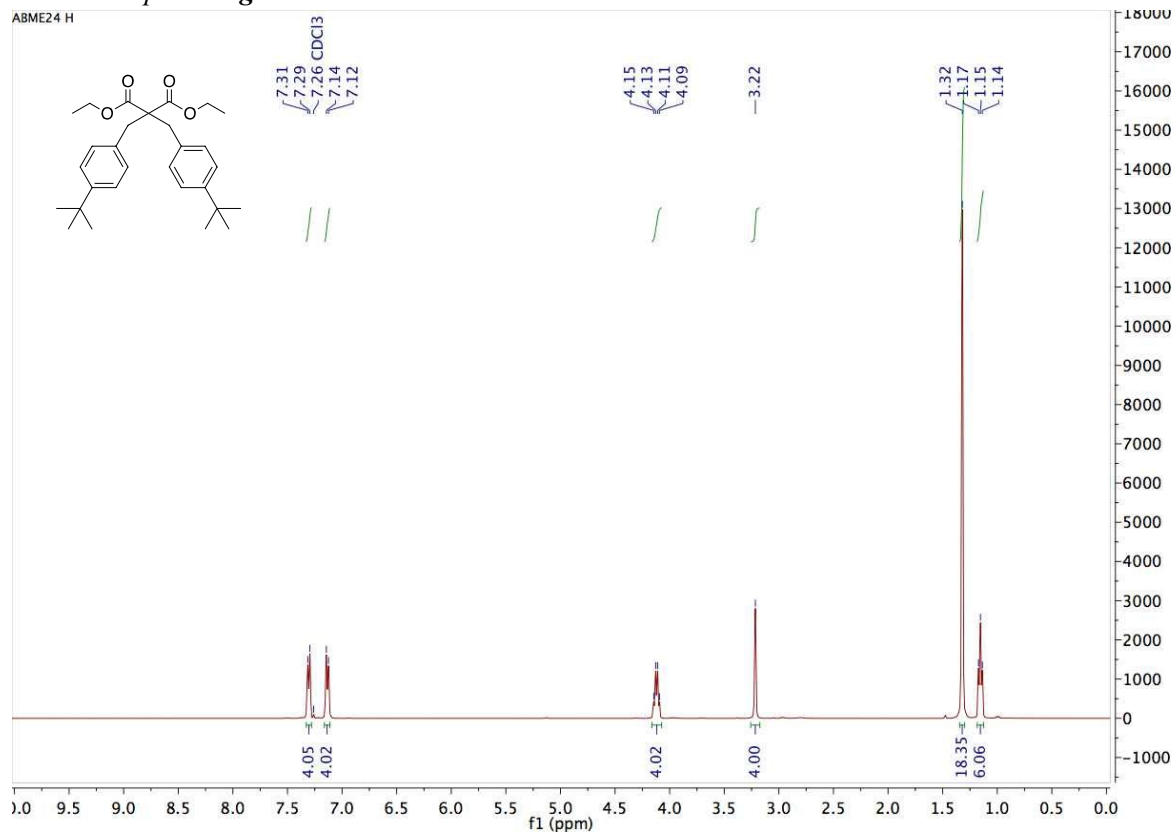
2.5 Compound 2e



2.6 Compound **2f**

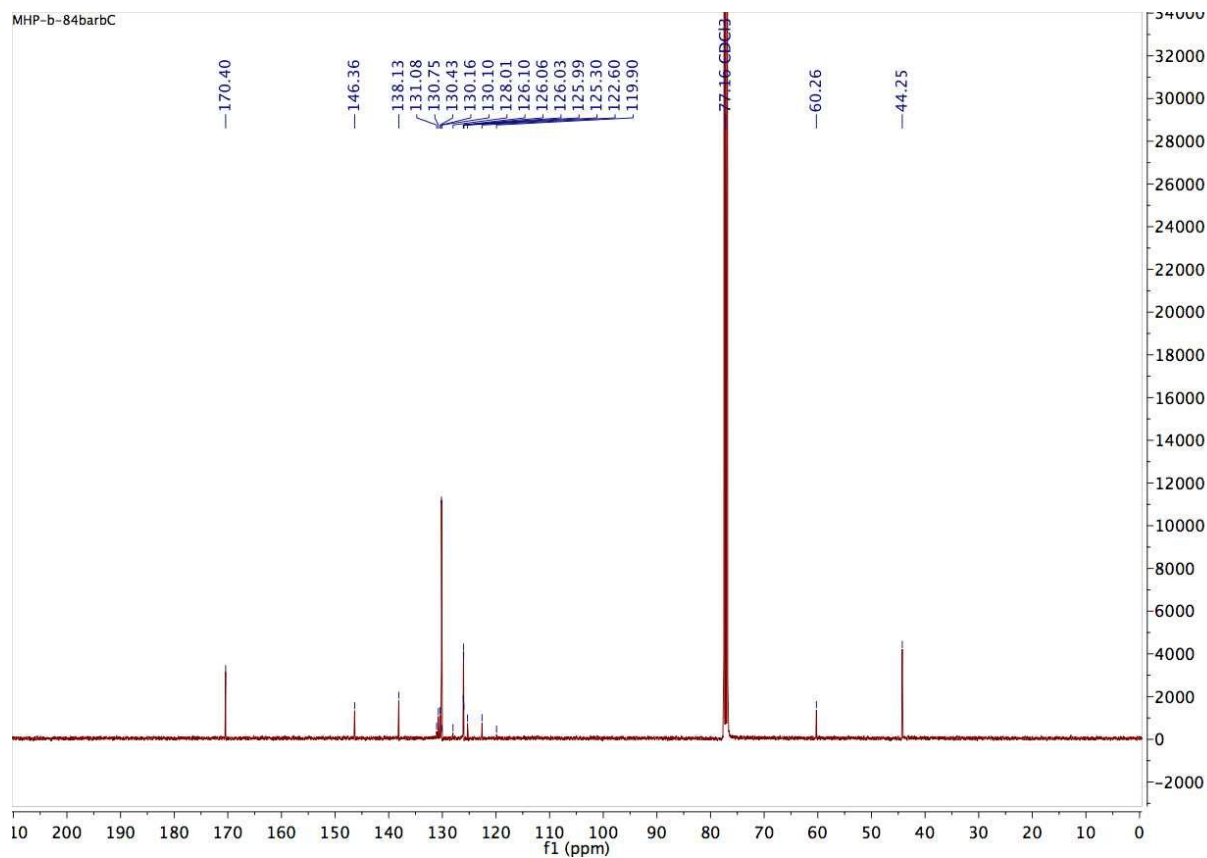
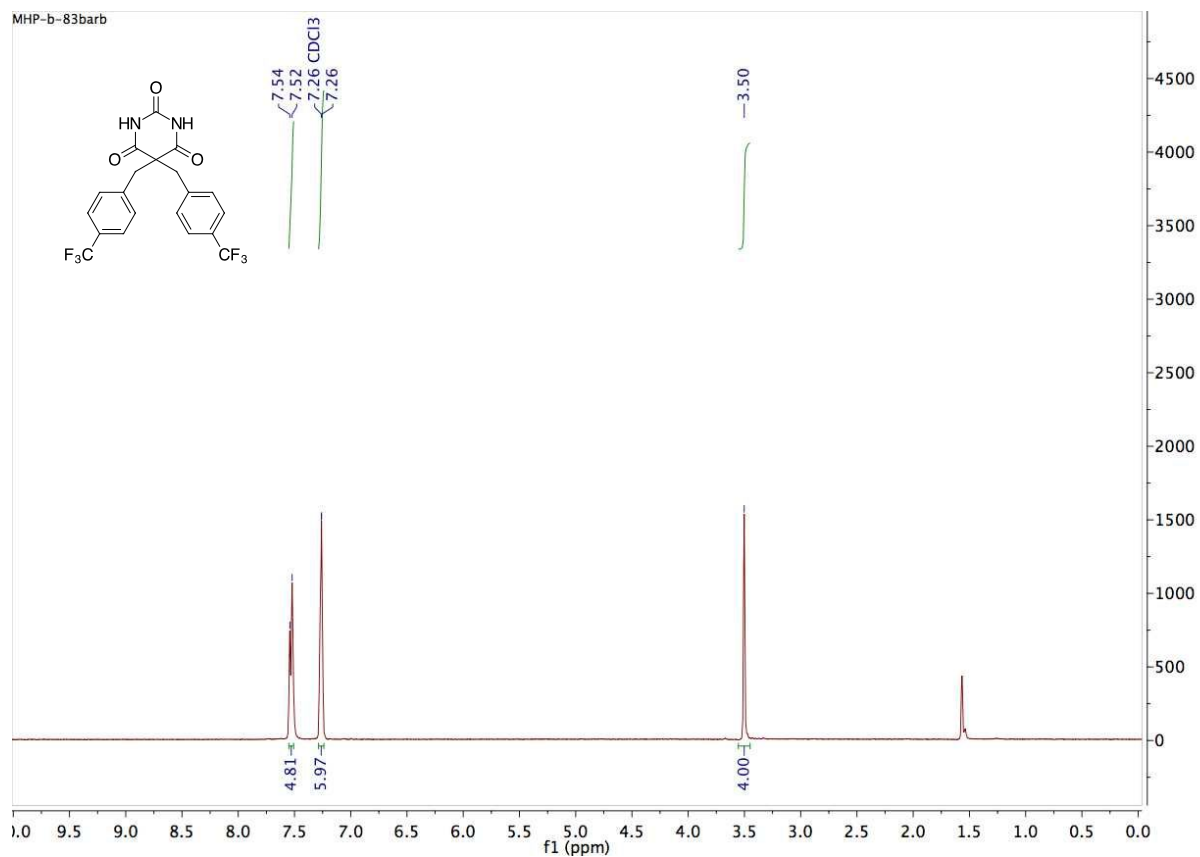


2.7 Compound 2g

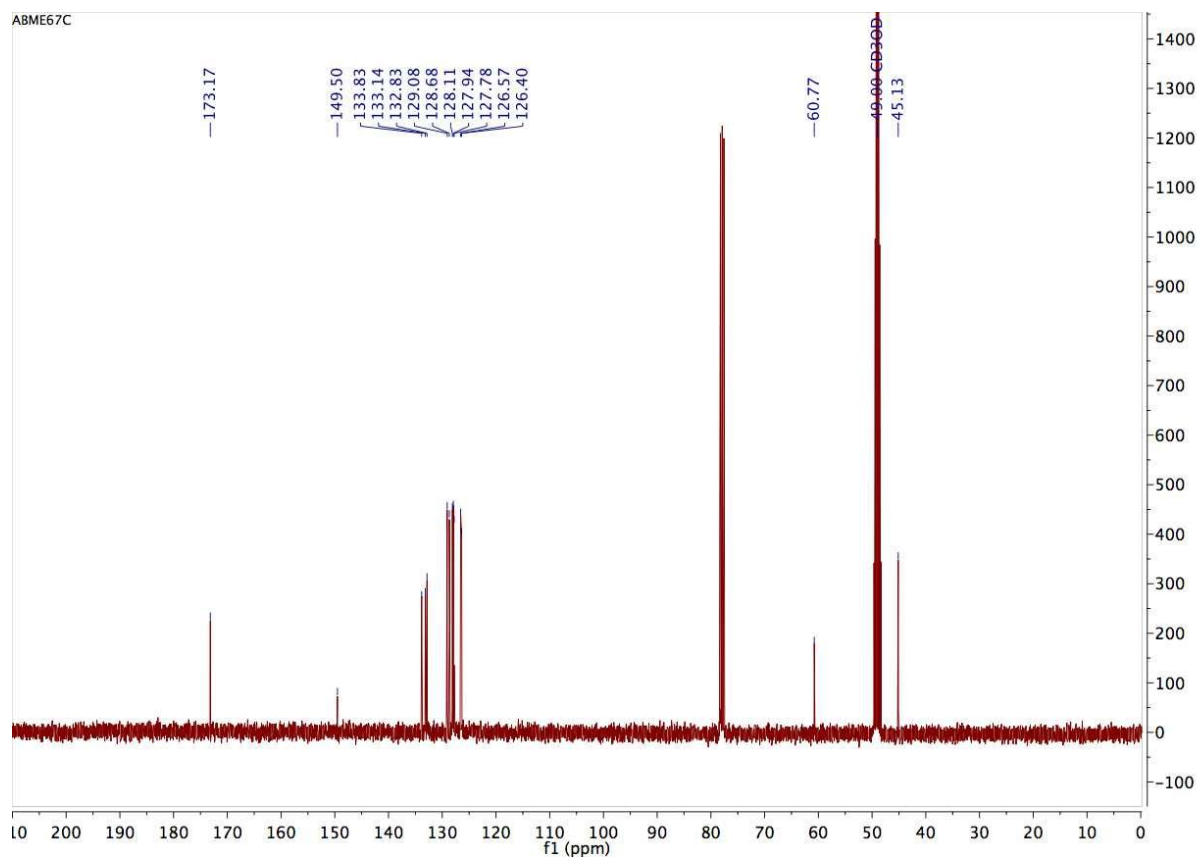
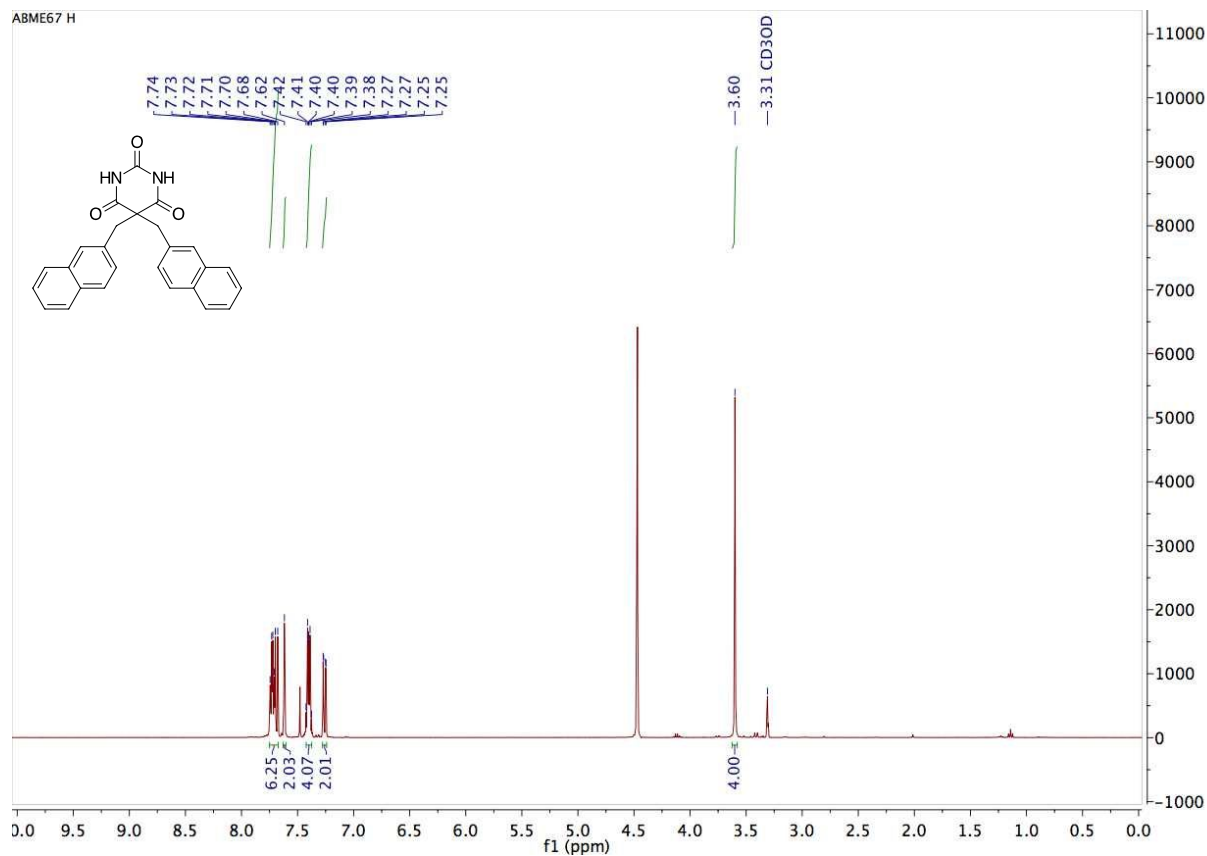


3. ^1H and ^{13}C NMR spectra of C-dialkylated barbiturates (3)

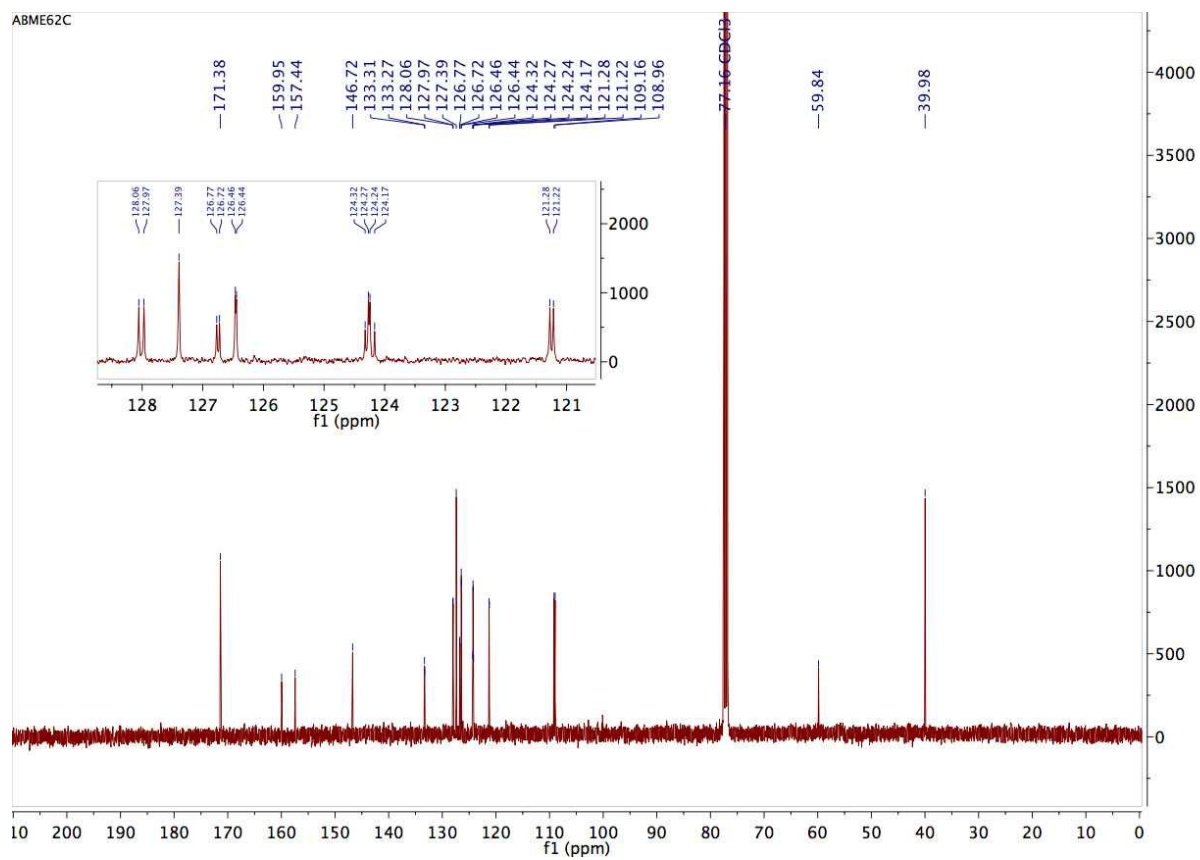
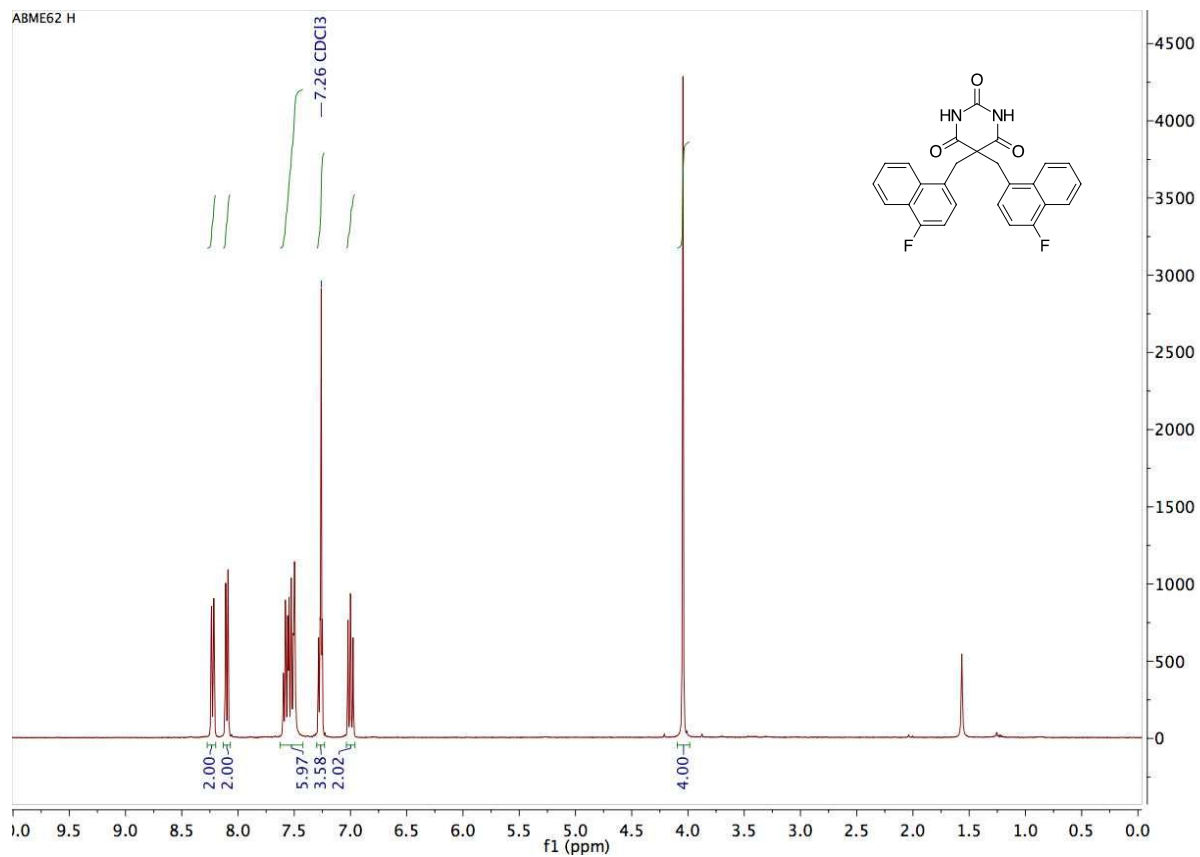
3.1 Compound 3a



3.2 Compound 3b

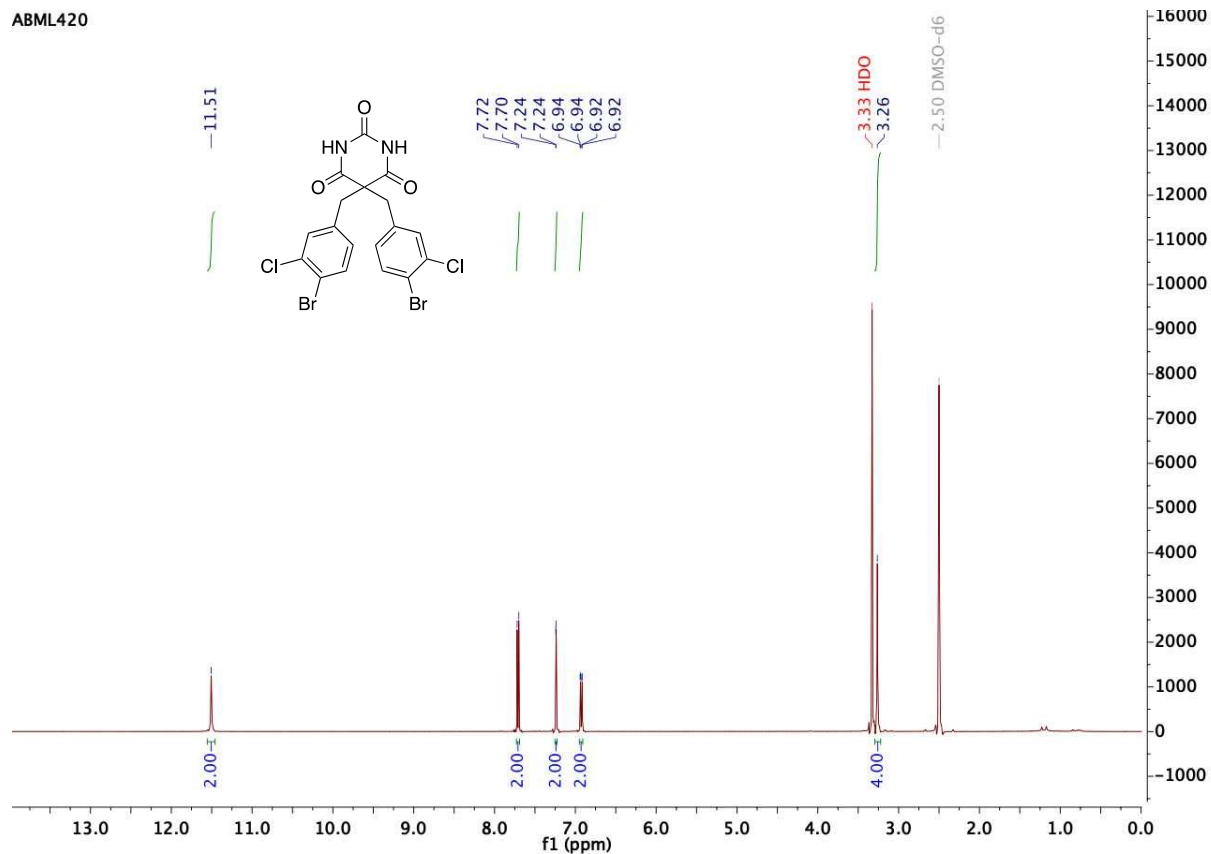


3.3 Compound 3c

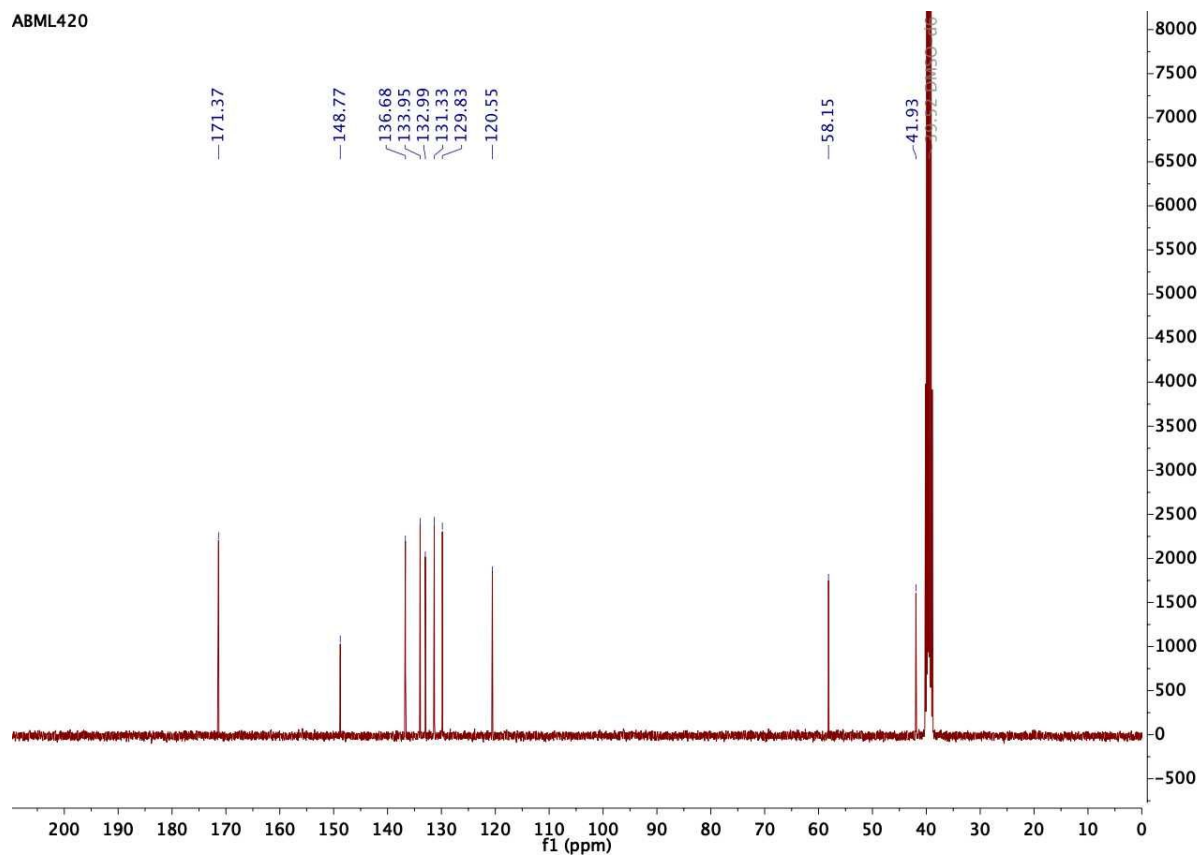


3.4 Compound 3d

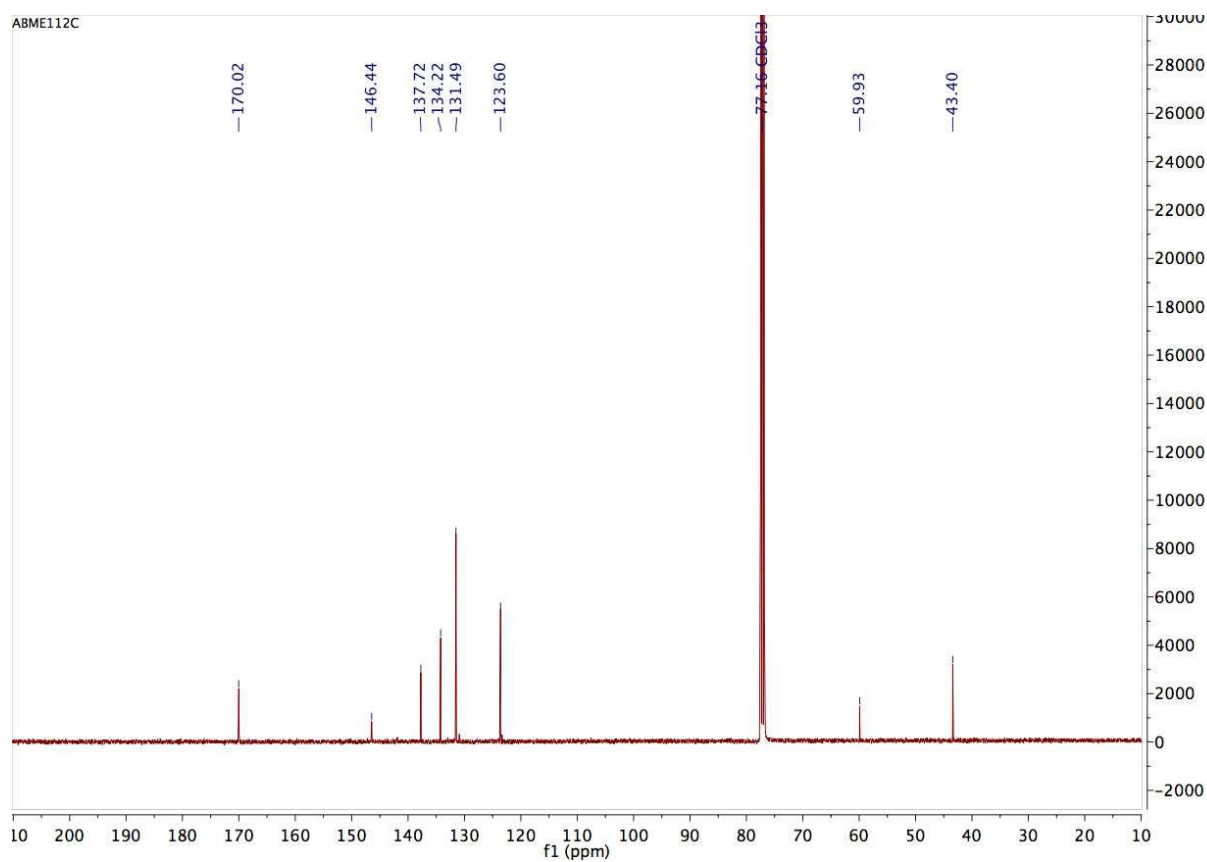
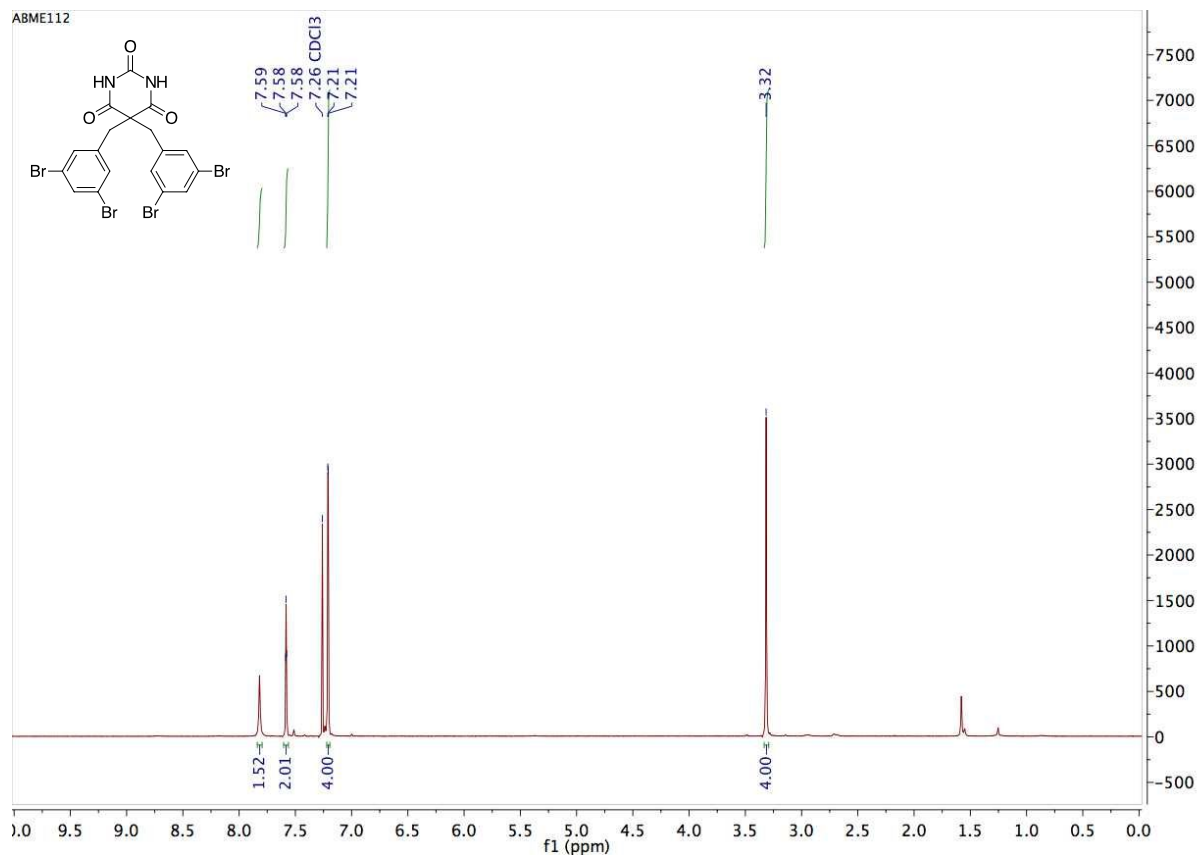
ABML420



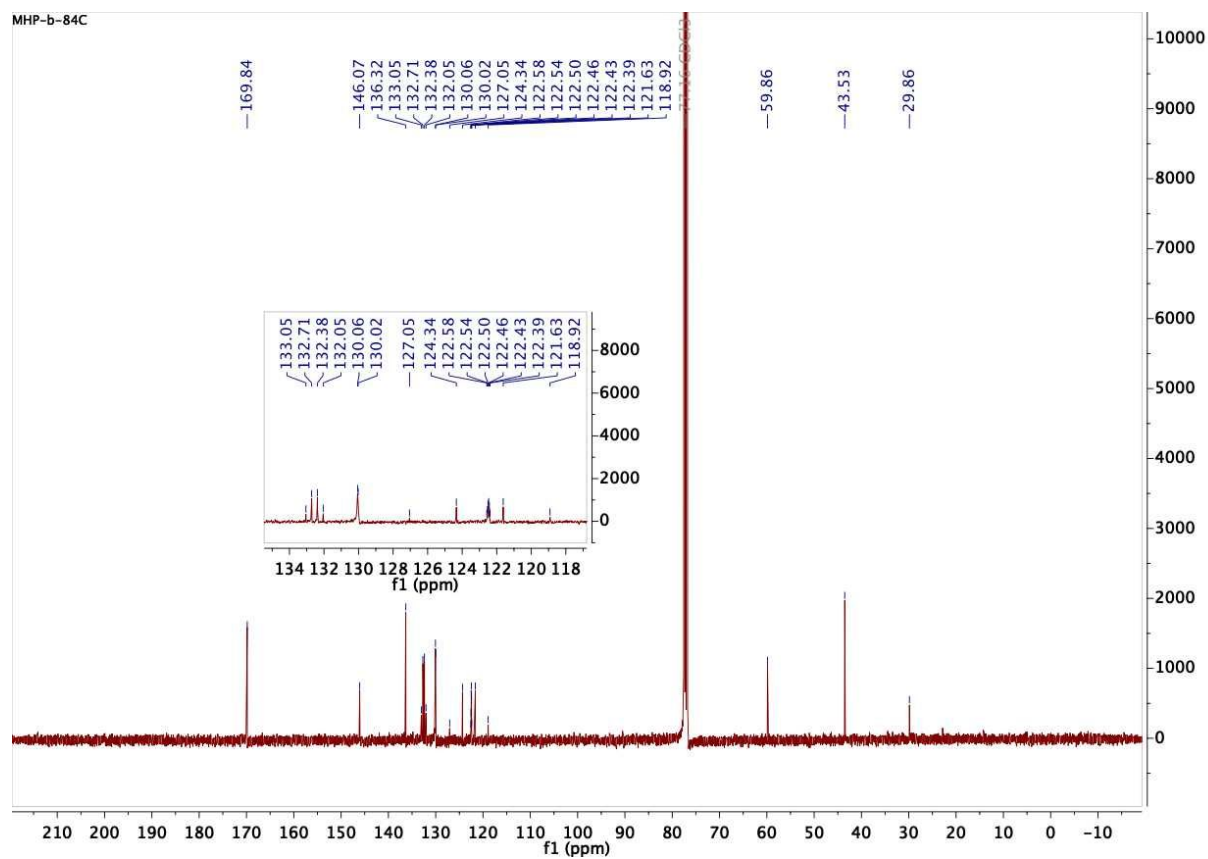
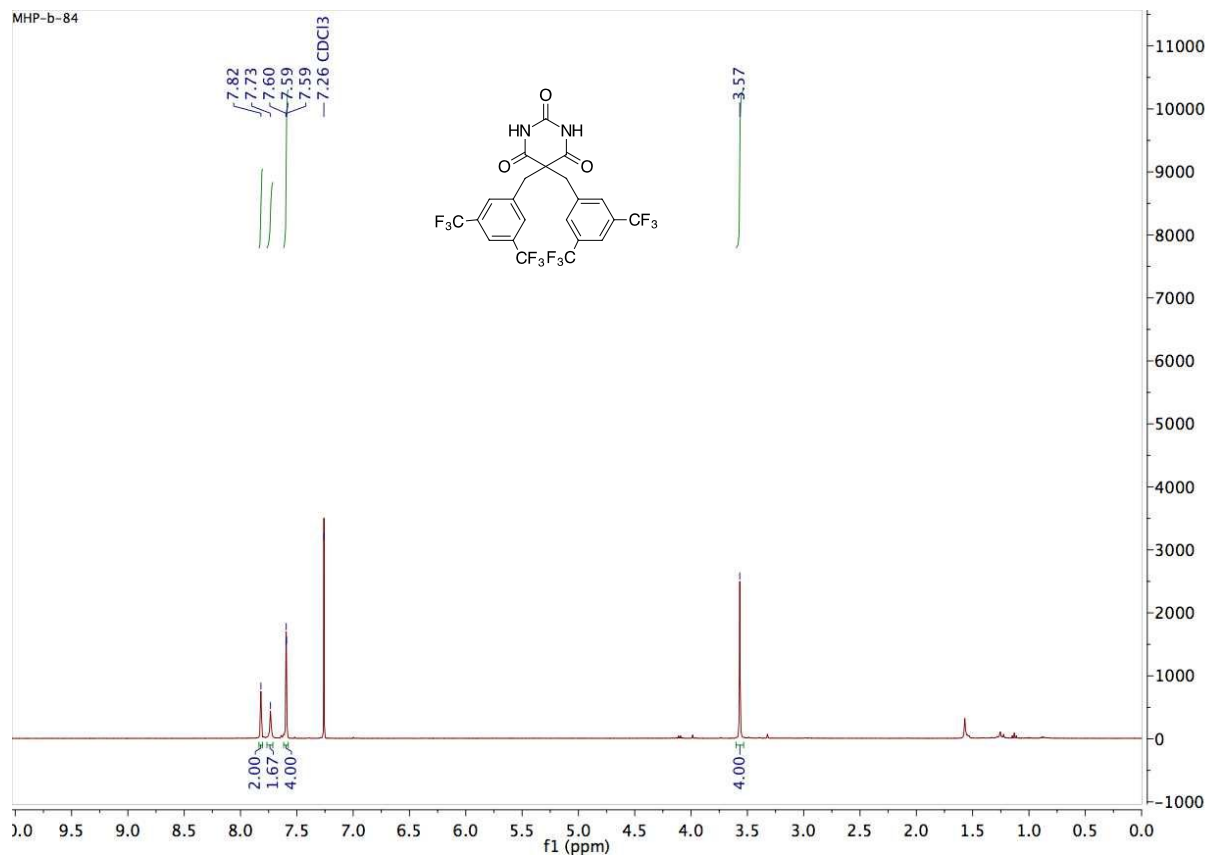
ABML420



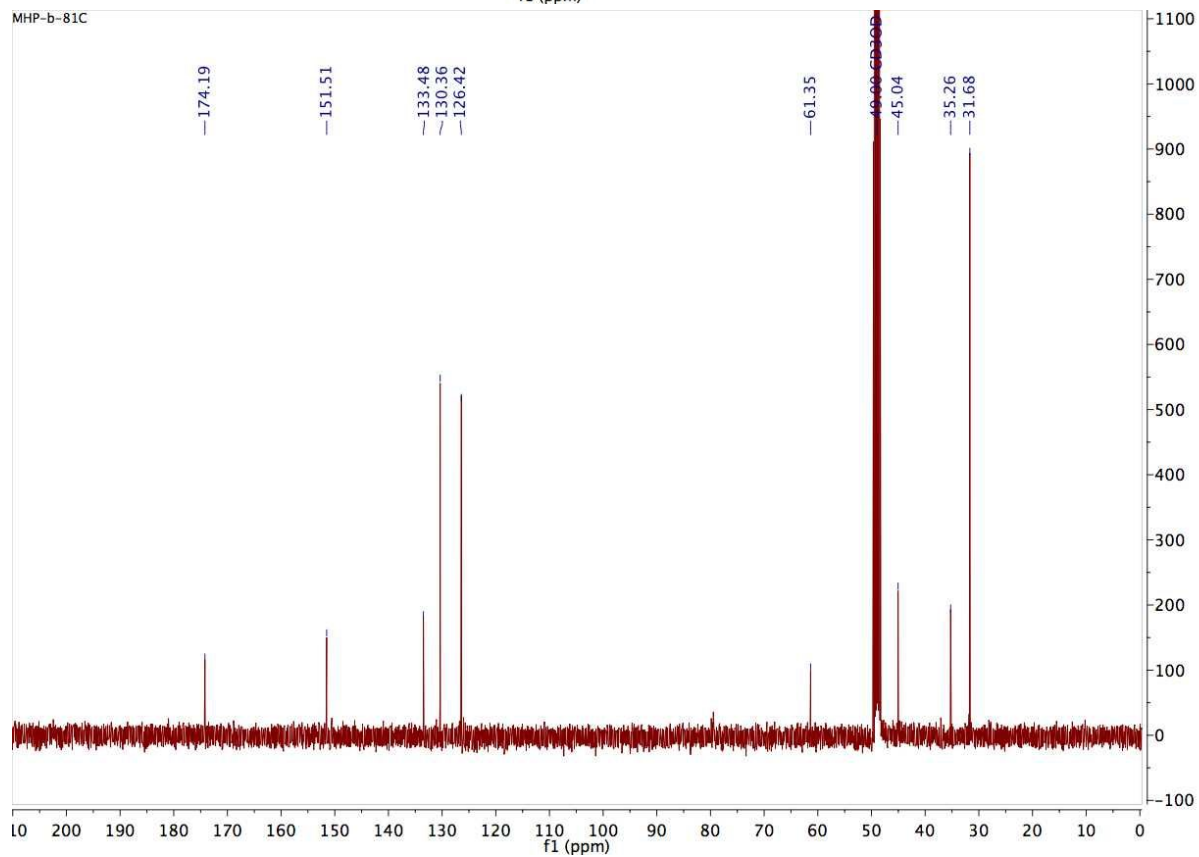
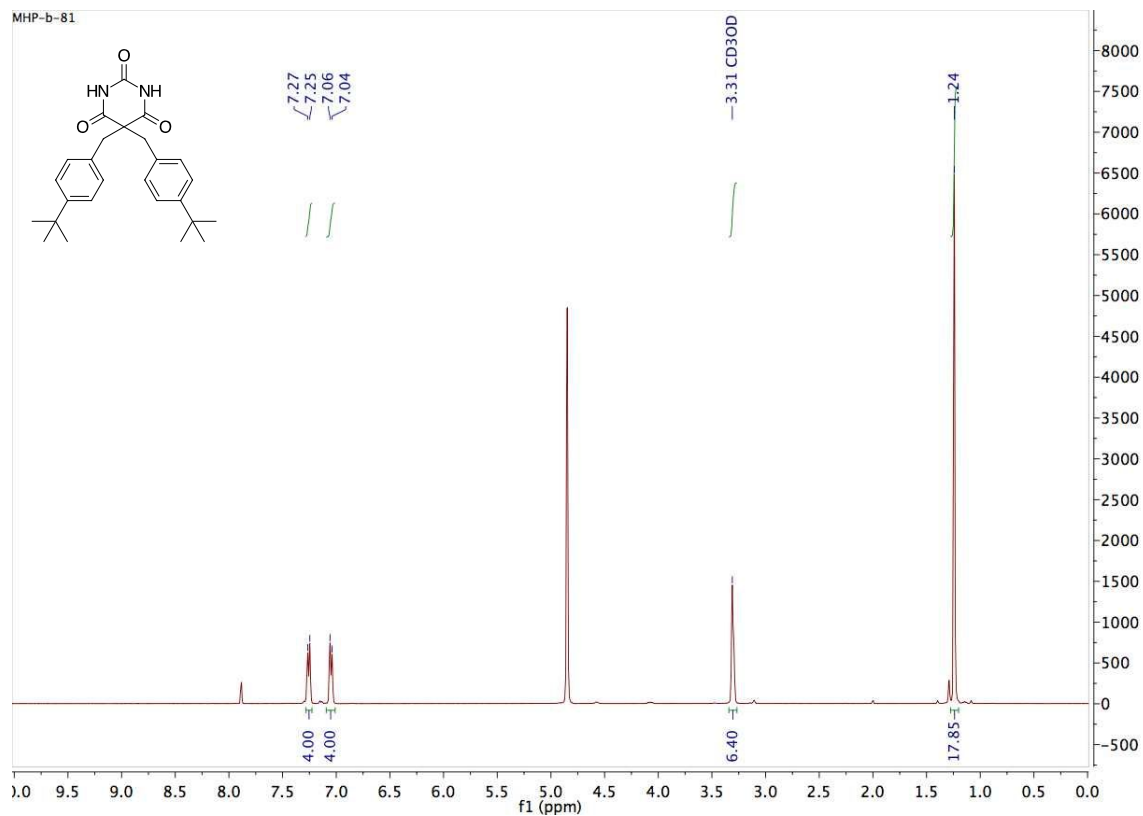
3.5 Compound 3e



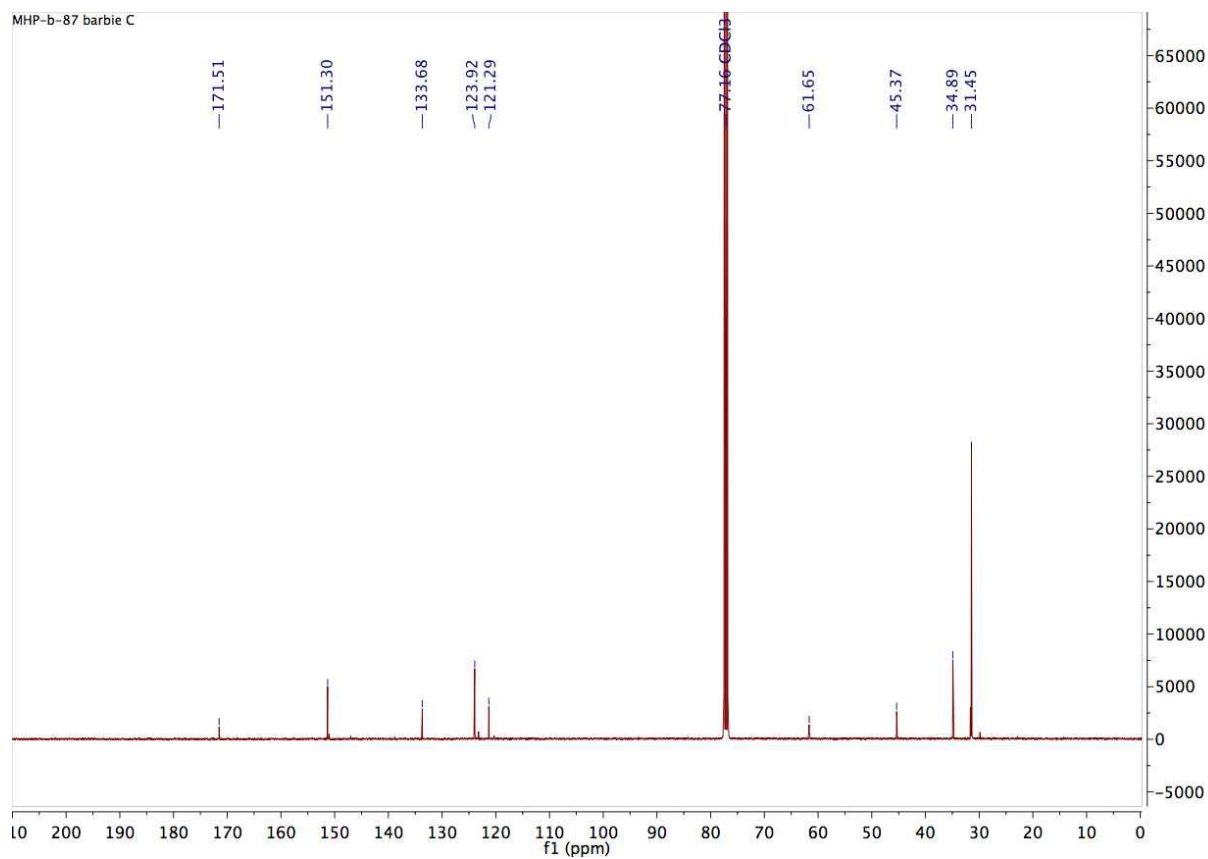
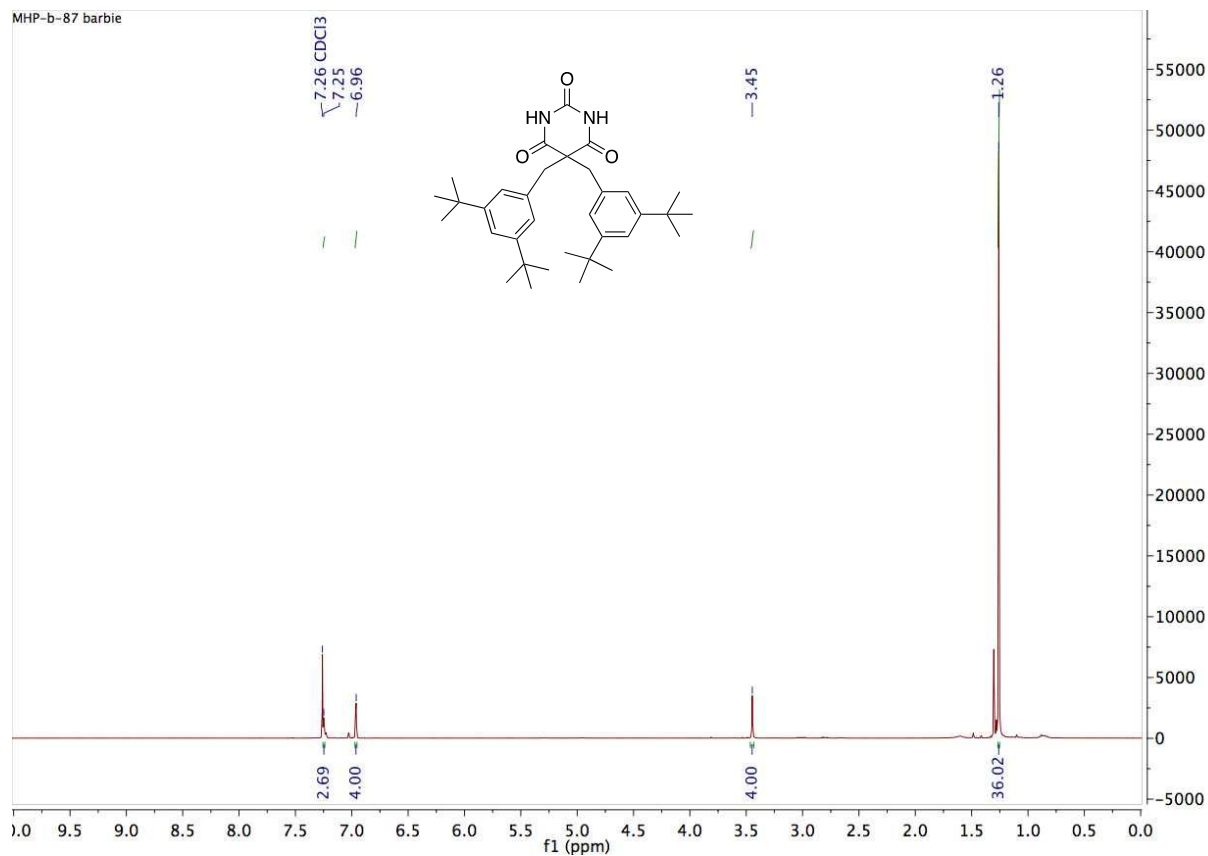
3.6 Compound 3f



3.7 Compound 3g

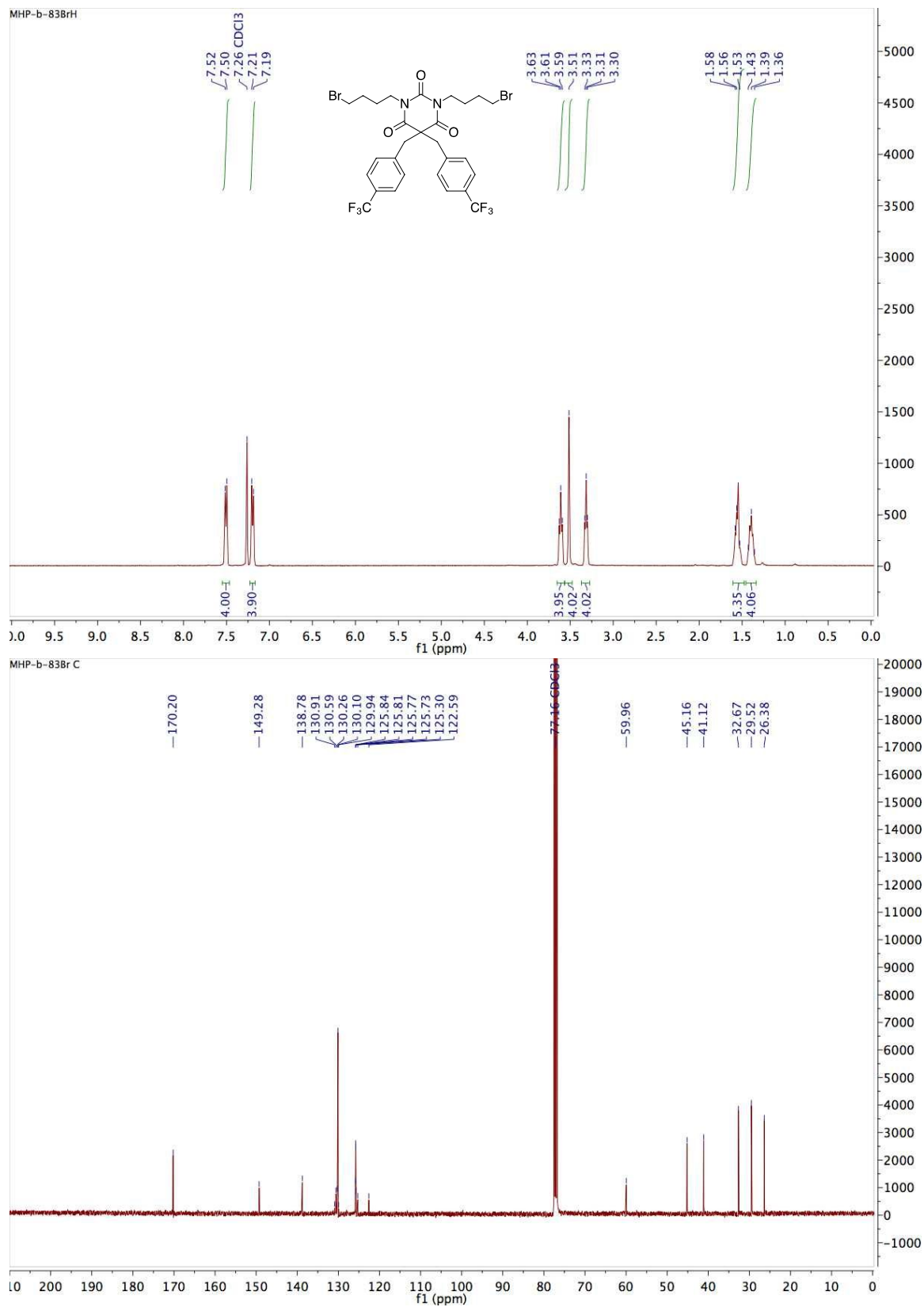


3.8 Compound 3h

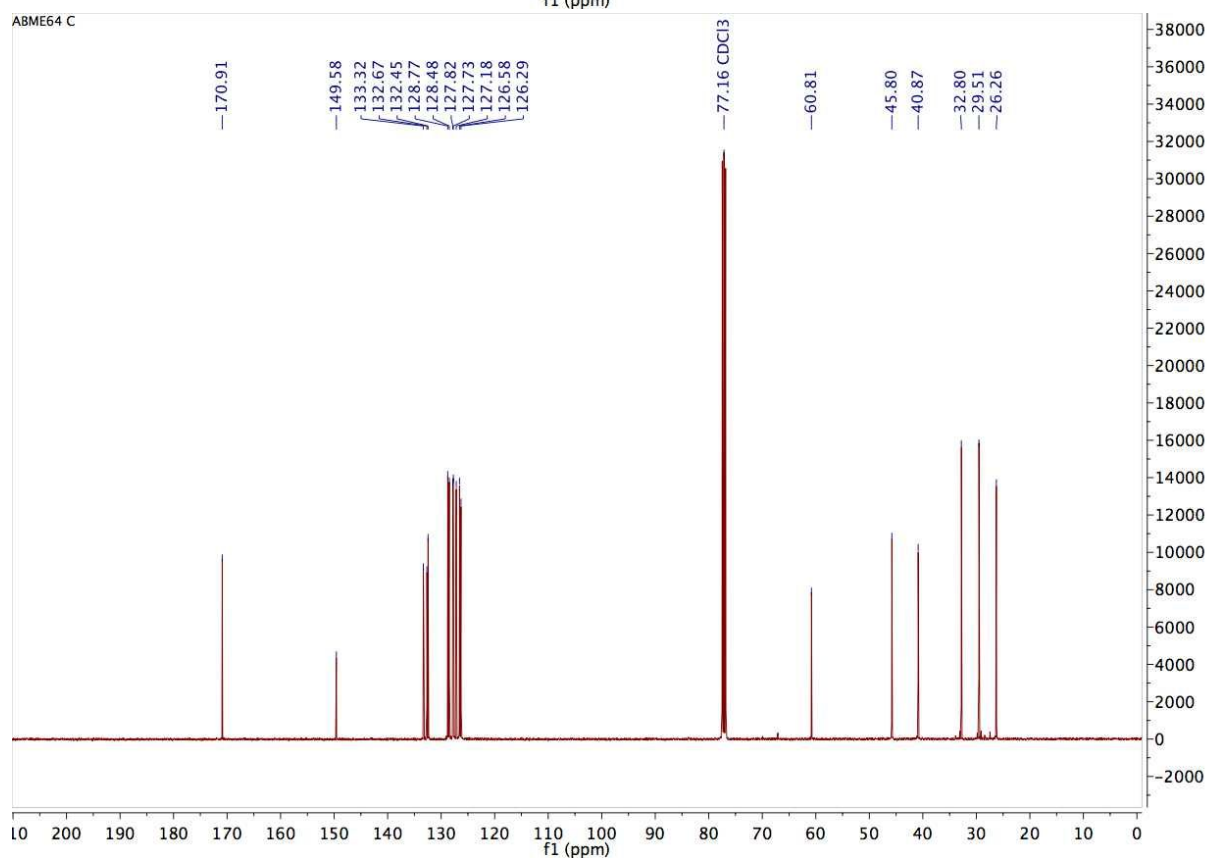
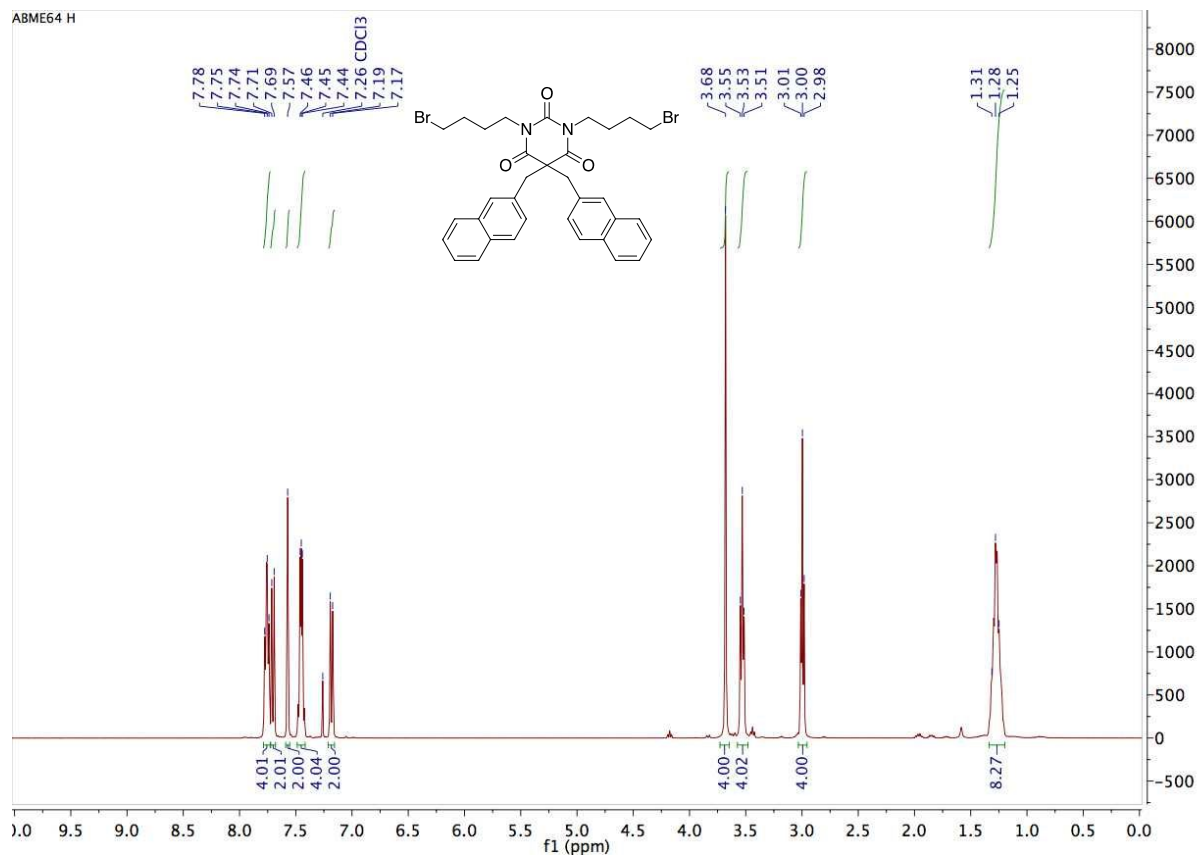


4. ^1H and ^{13}C NMR spectra of *N*-alkylated bromo barbiturates (4)

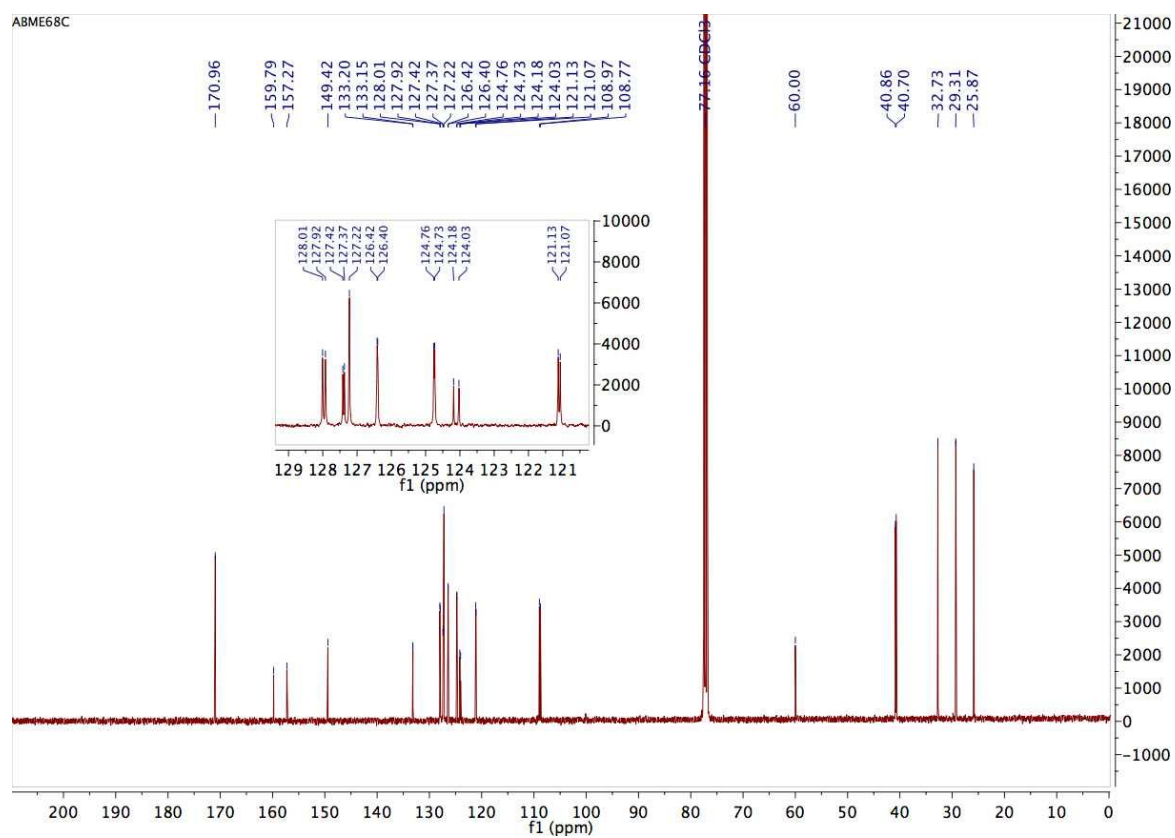
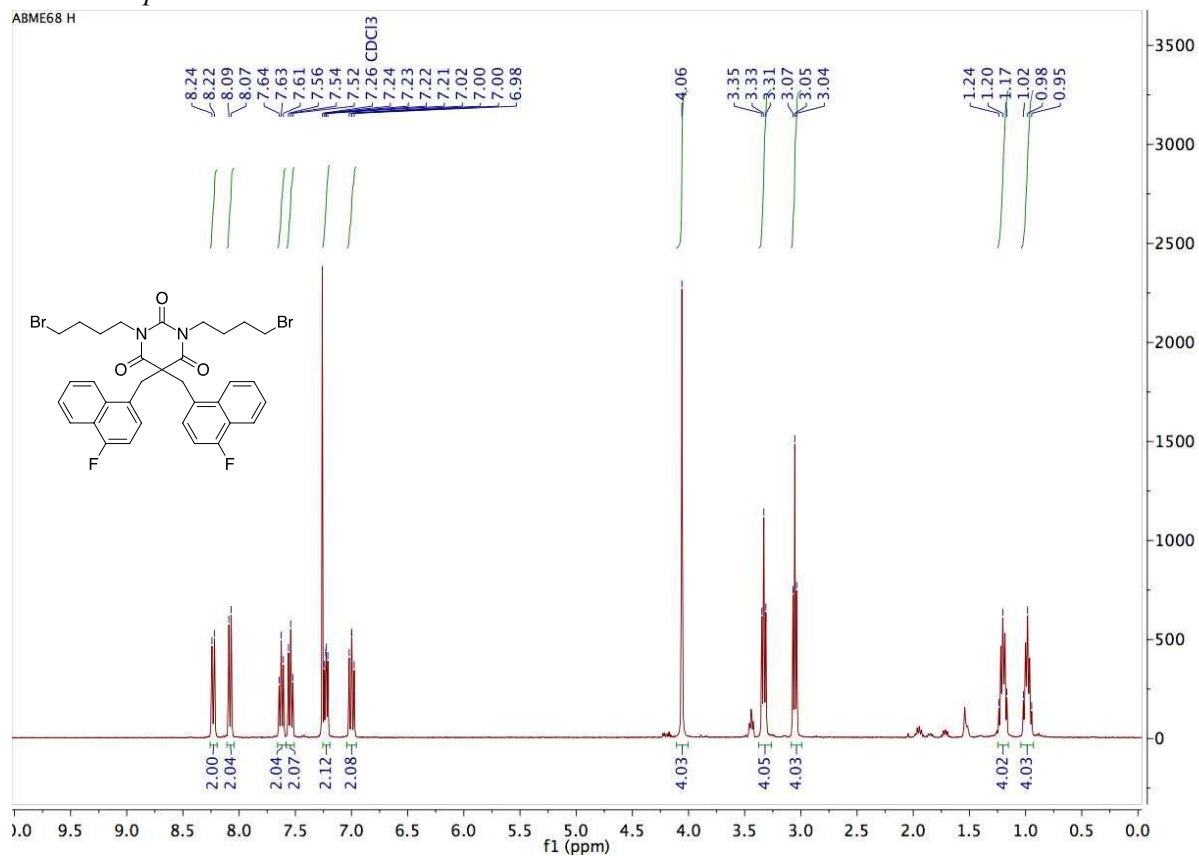
4.1 Compound 4a



4.2 Compound 4b

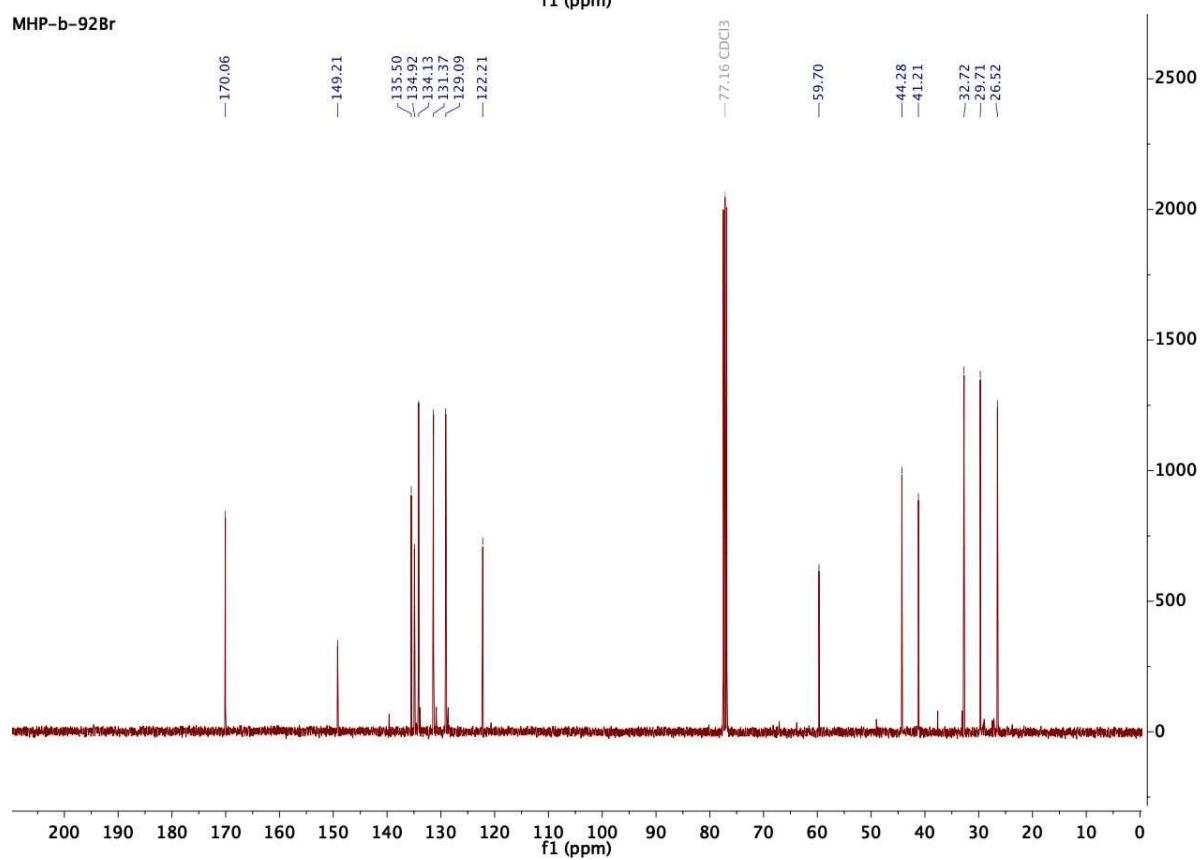
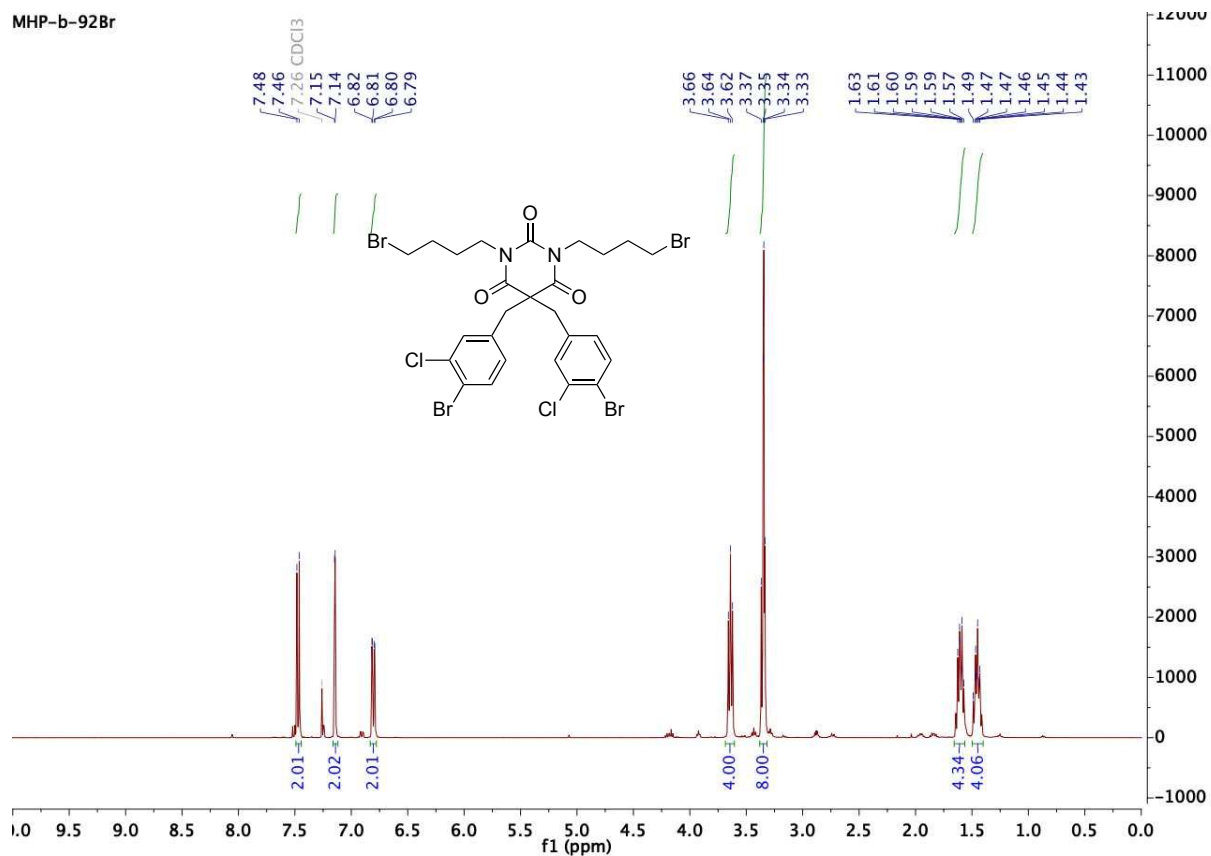


4.3 Compound 4c

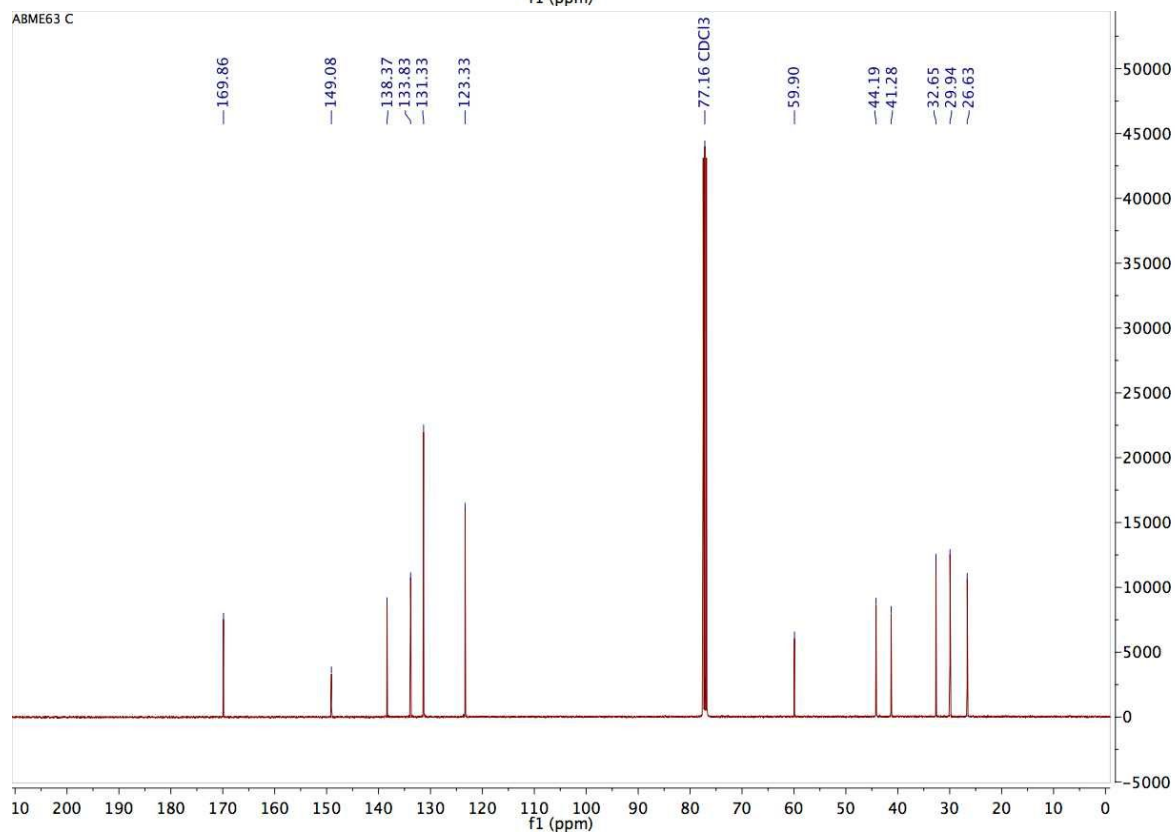
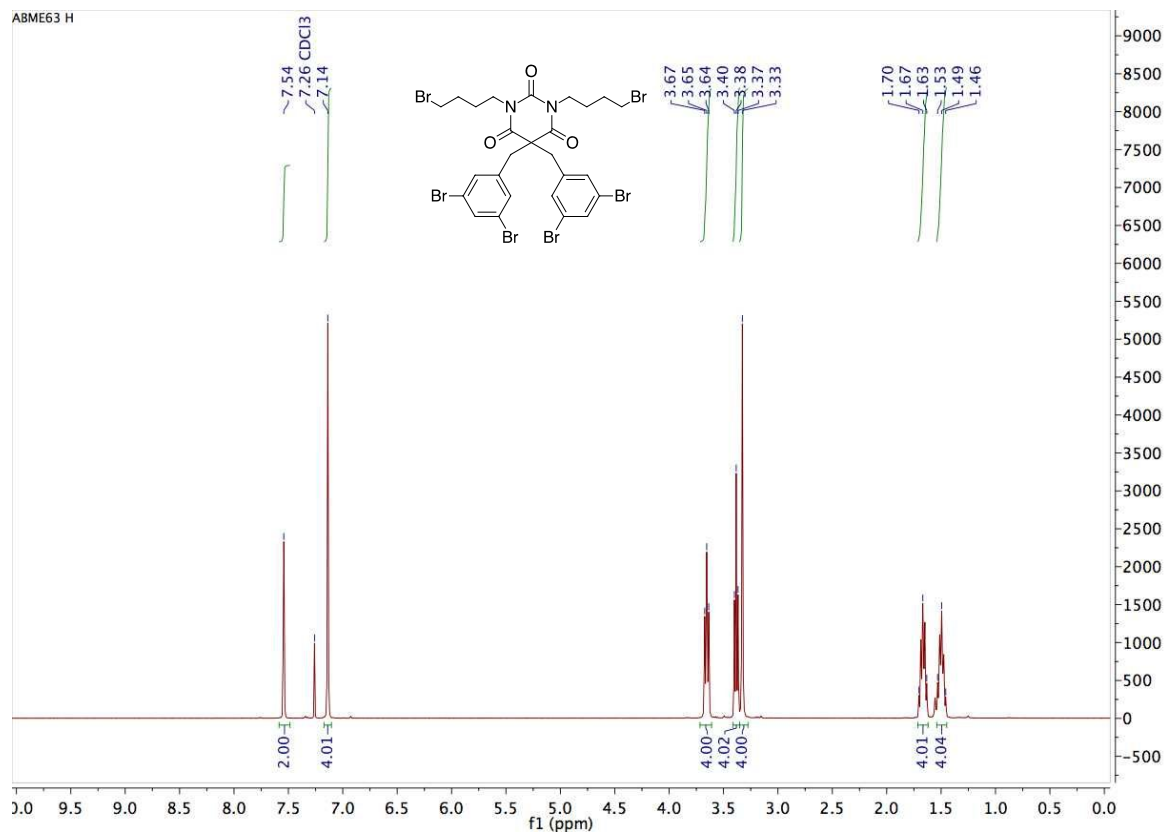


4.4 Compound 4d

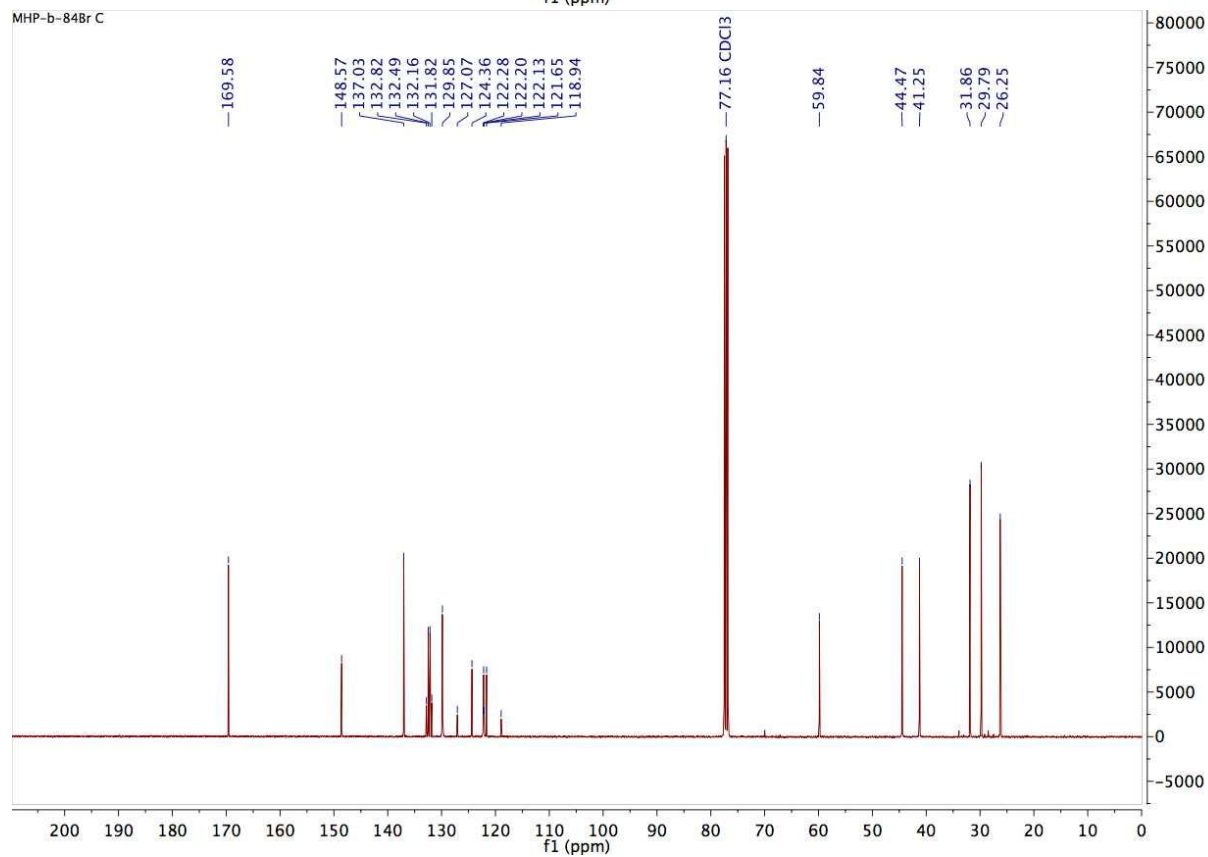
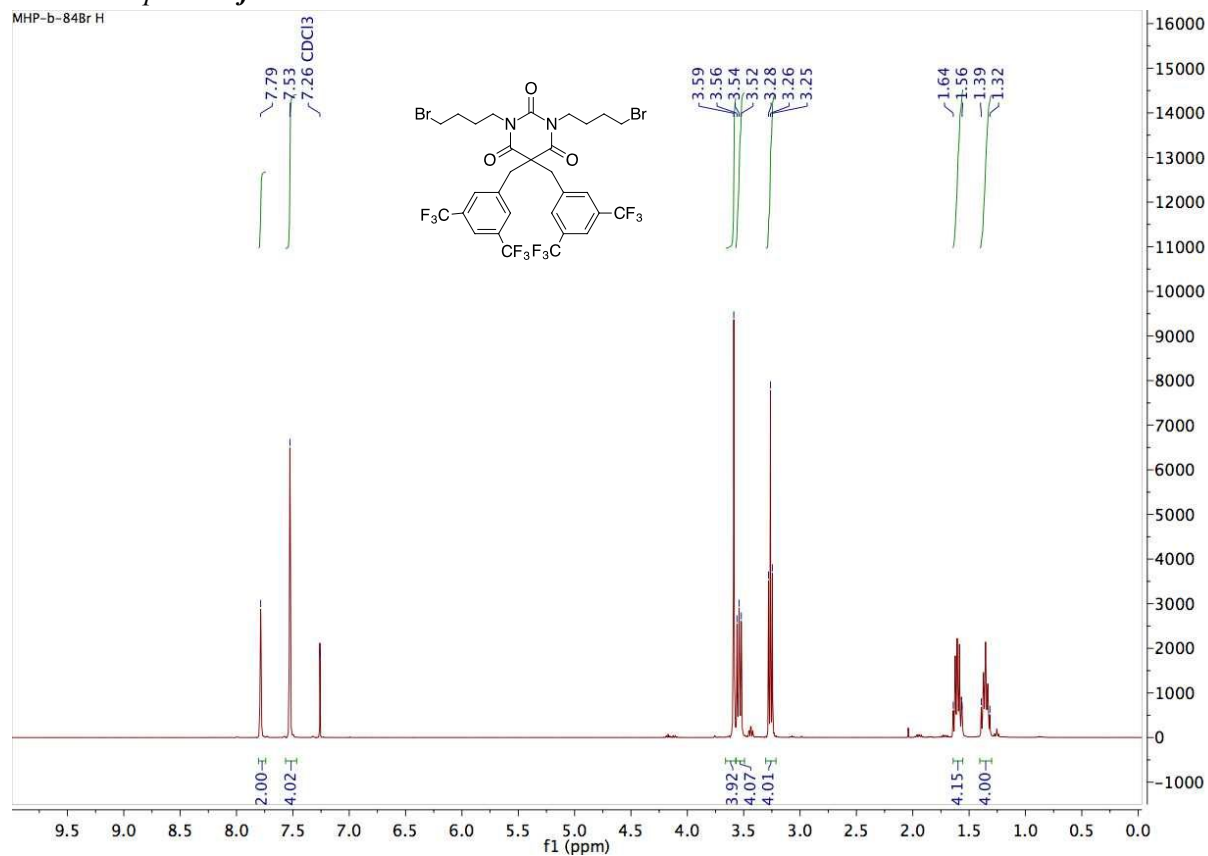
MHP-b-92Br



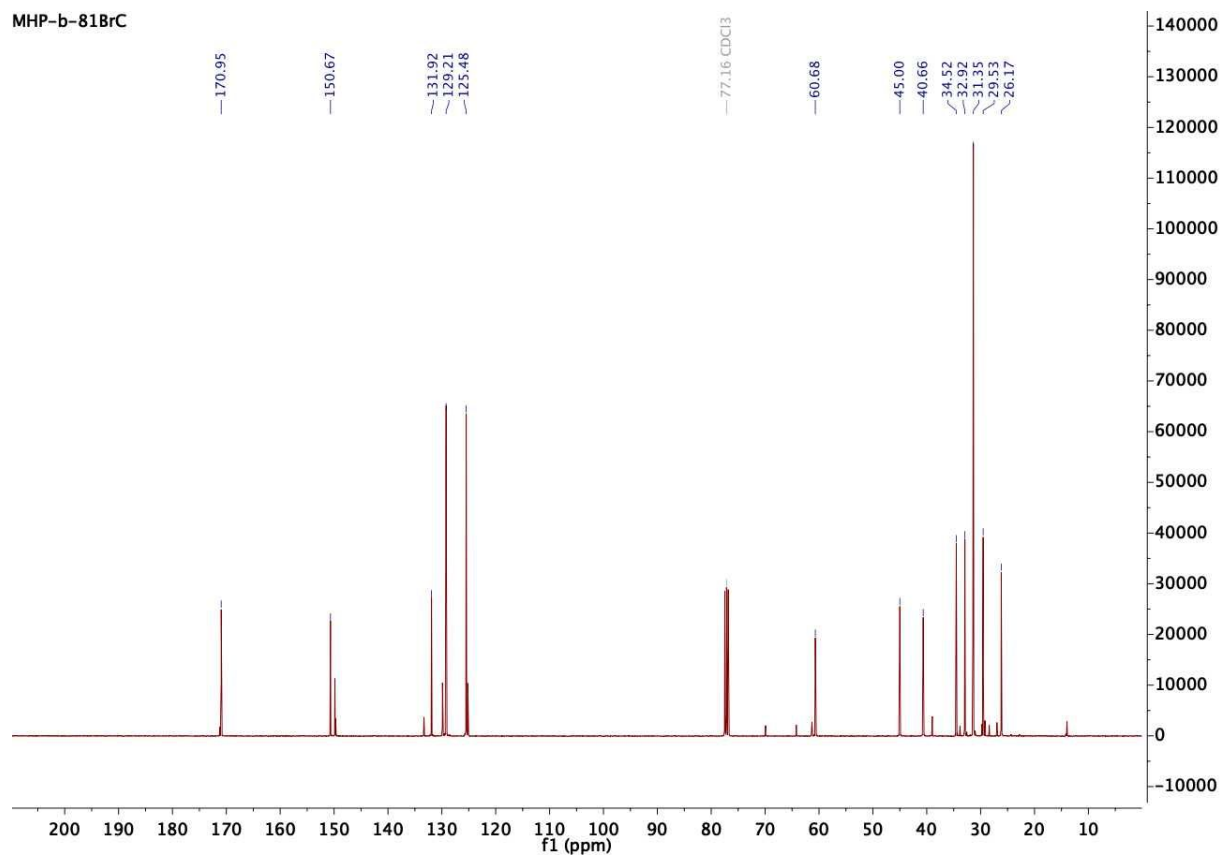
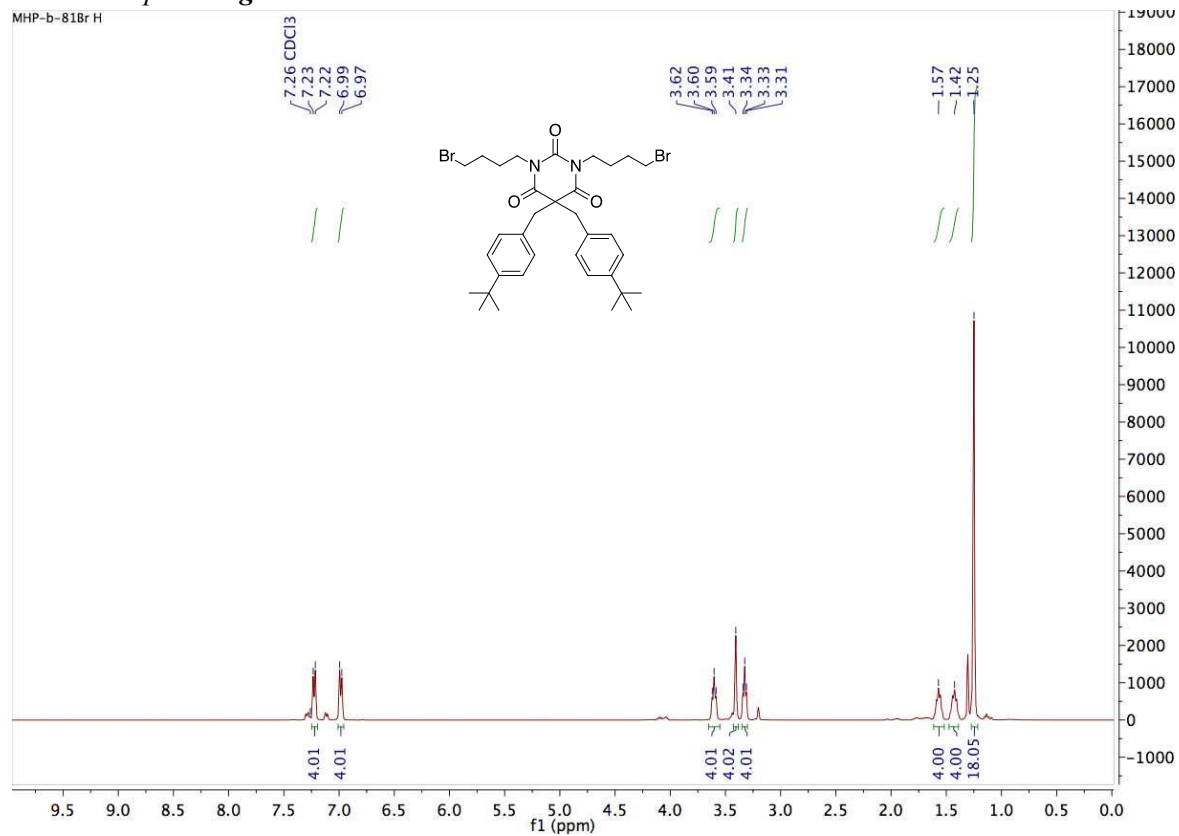
4.5 Compound 4e



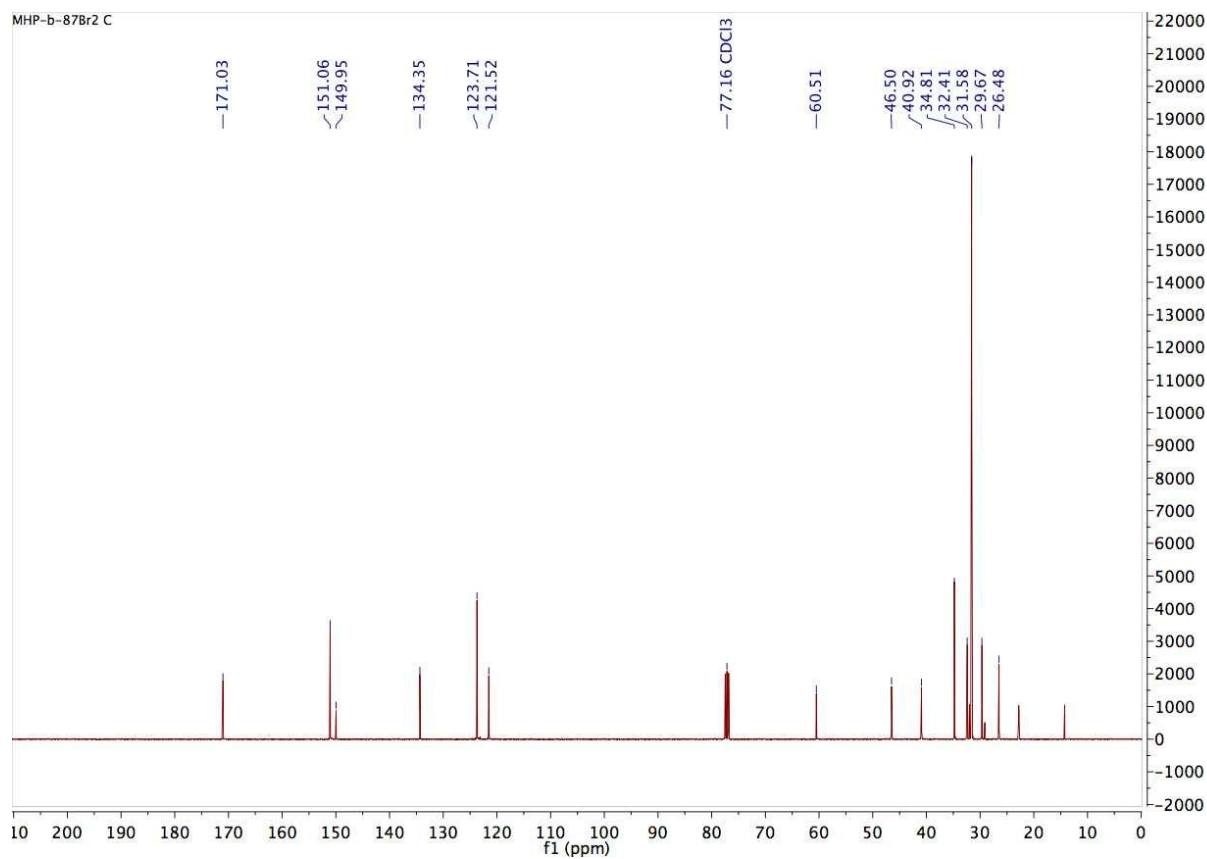
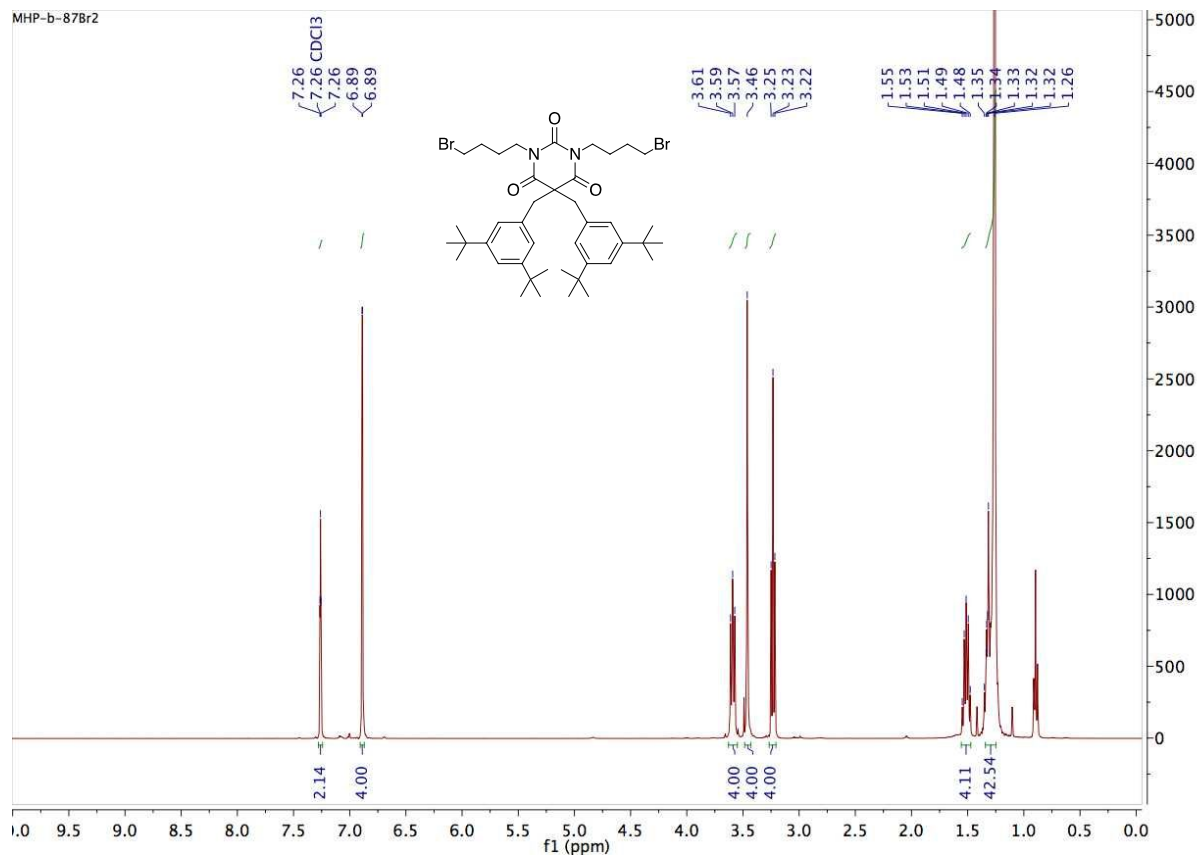
4.6 Compound 4f



4.7 Compound 4g

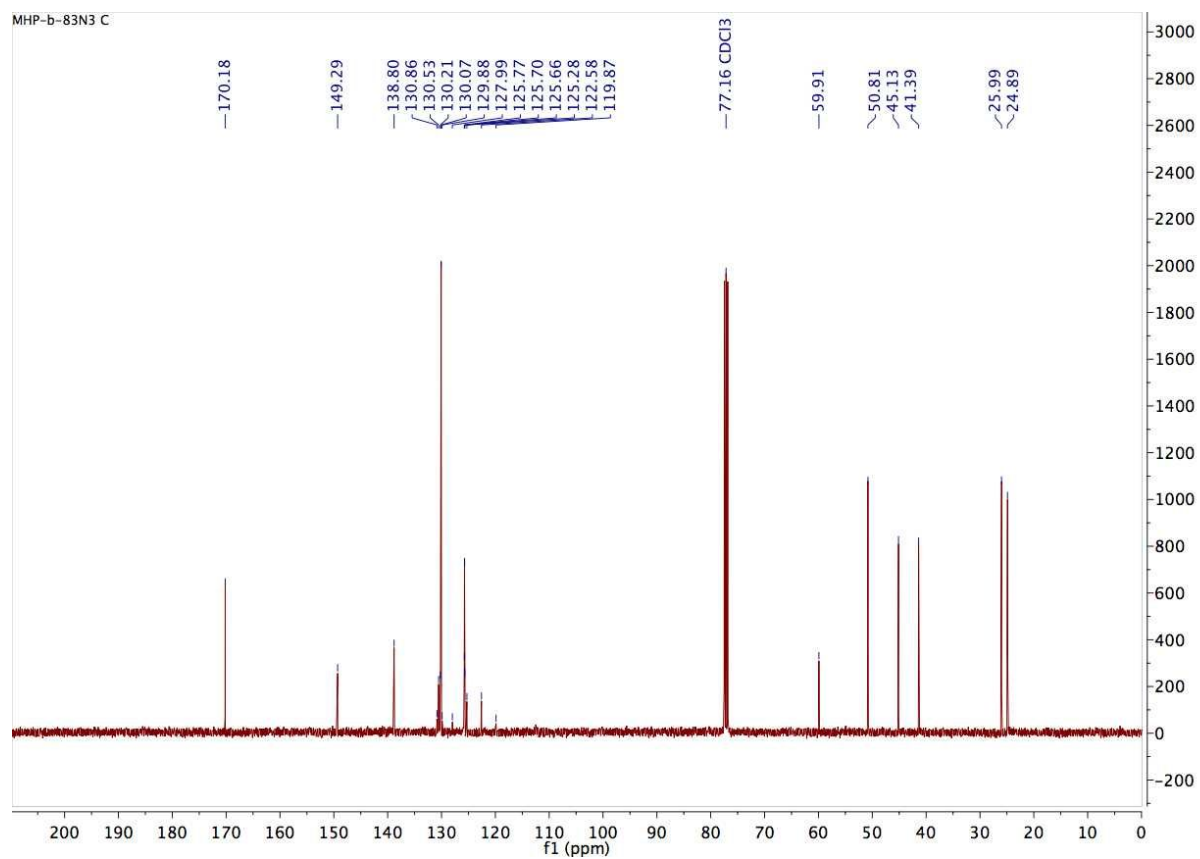
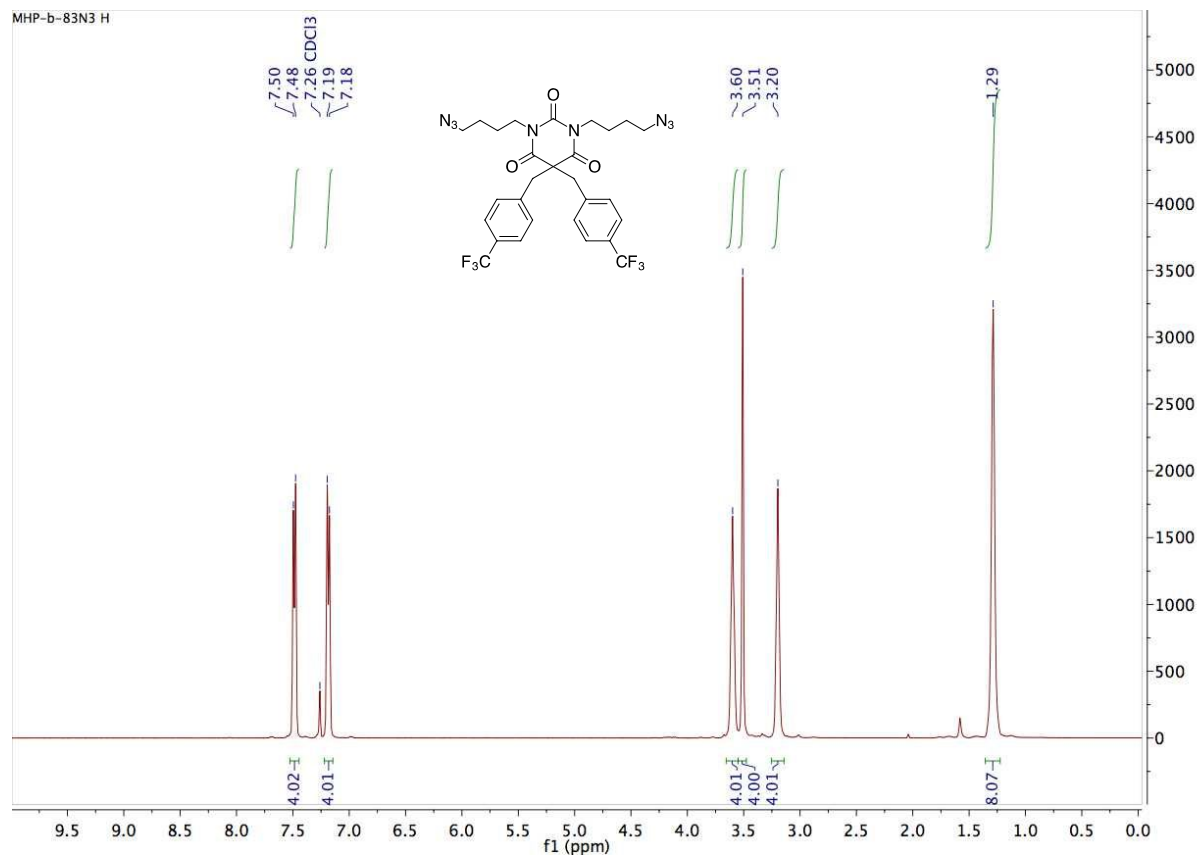


4.8 Compound 4h

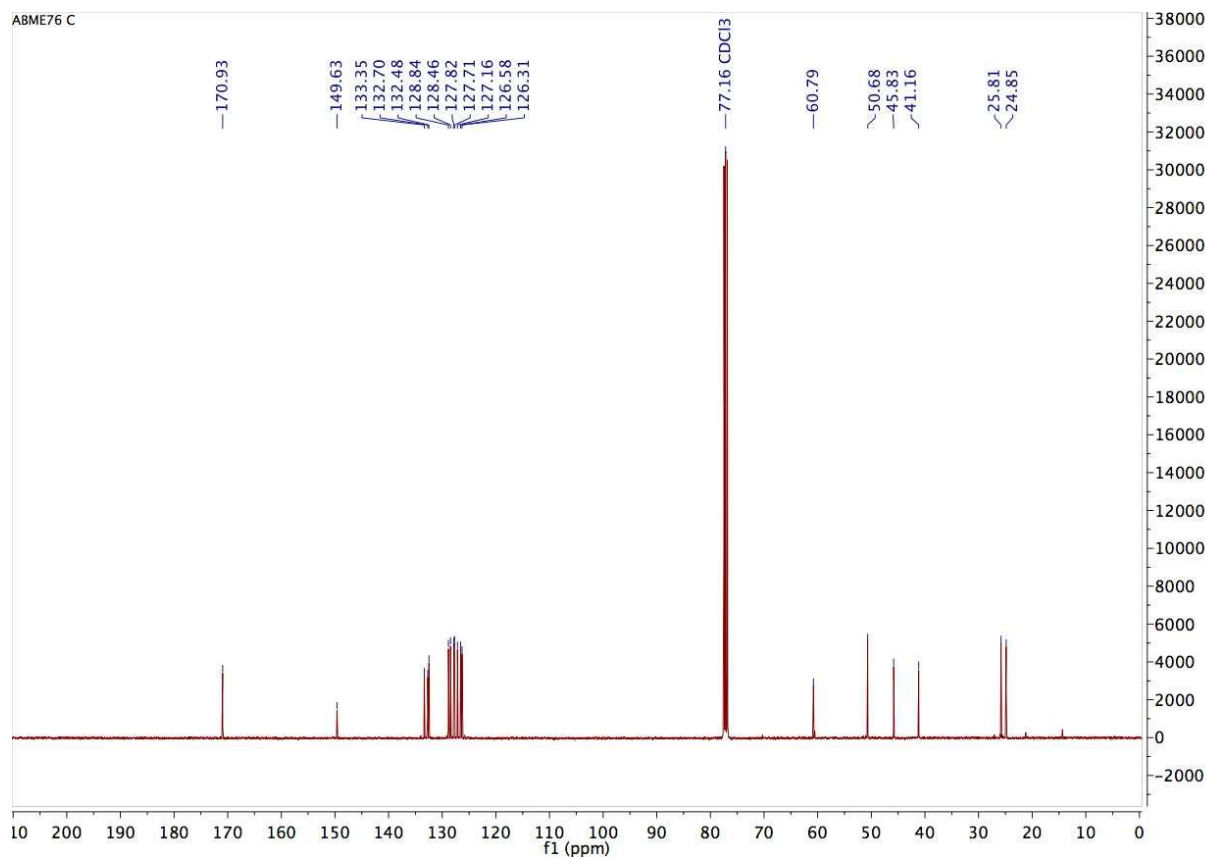
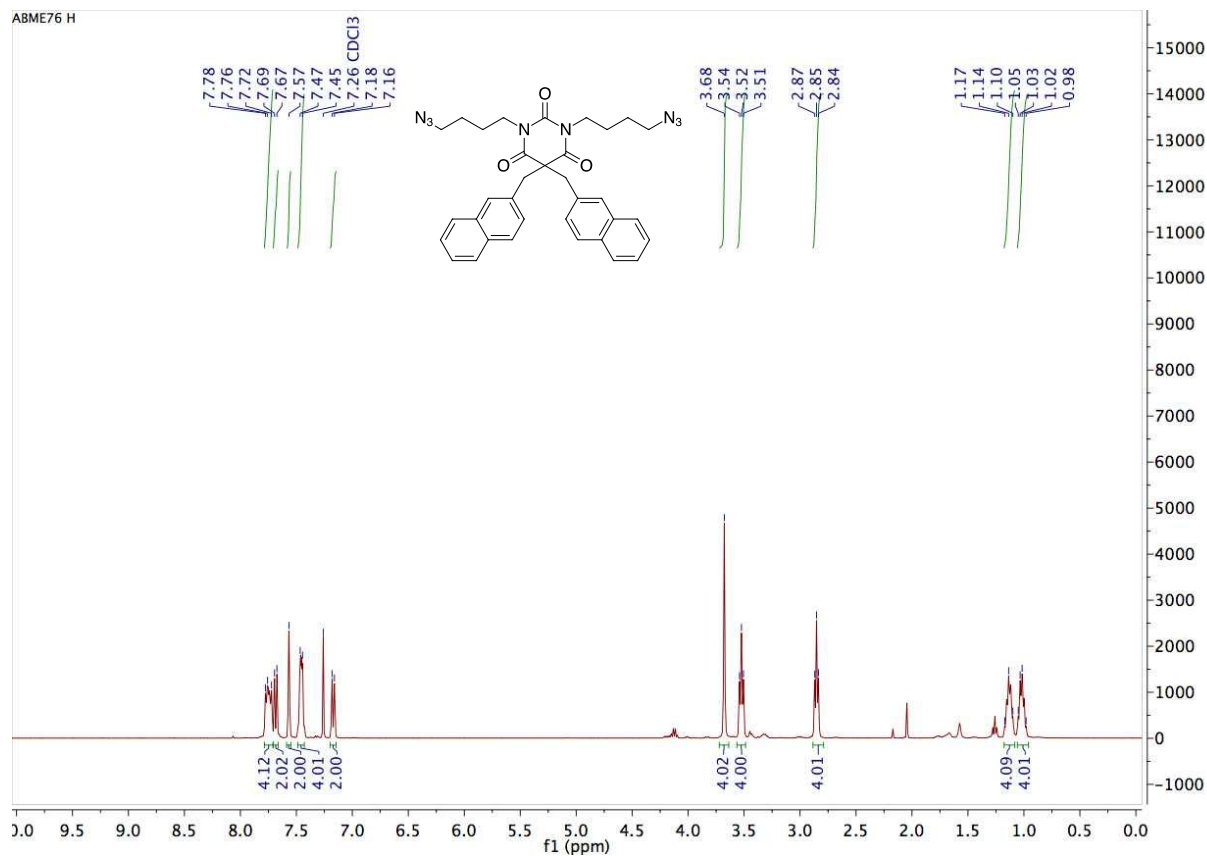


5. ^1H and ^{13}C NMR spectra of *N*-alkylated azide barbiturates 5

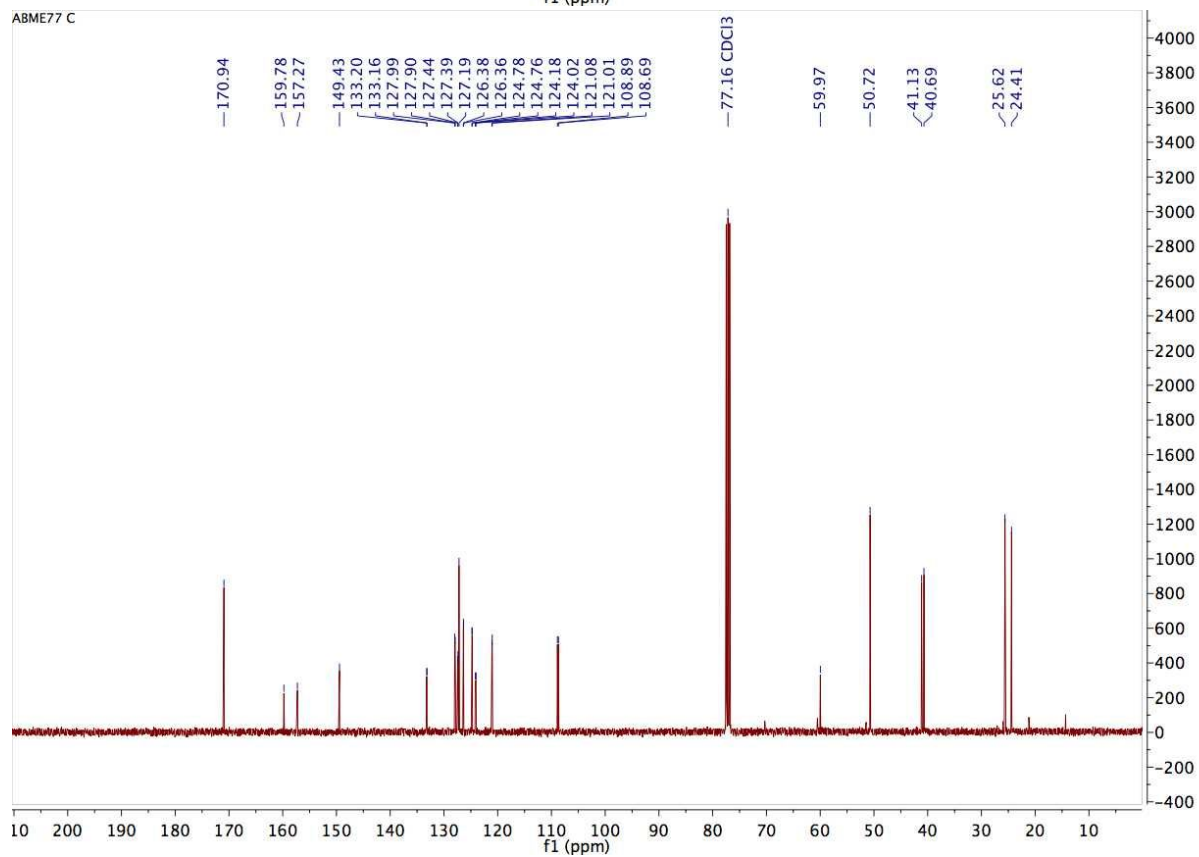
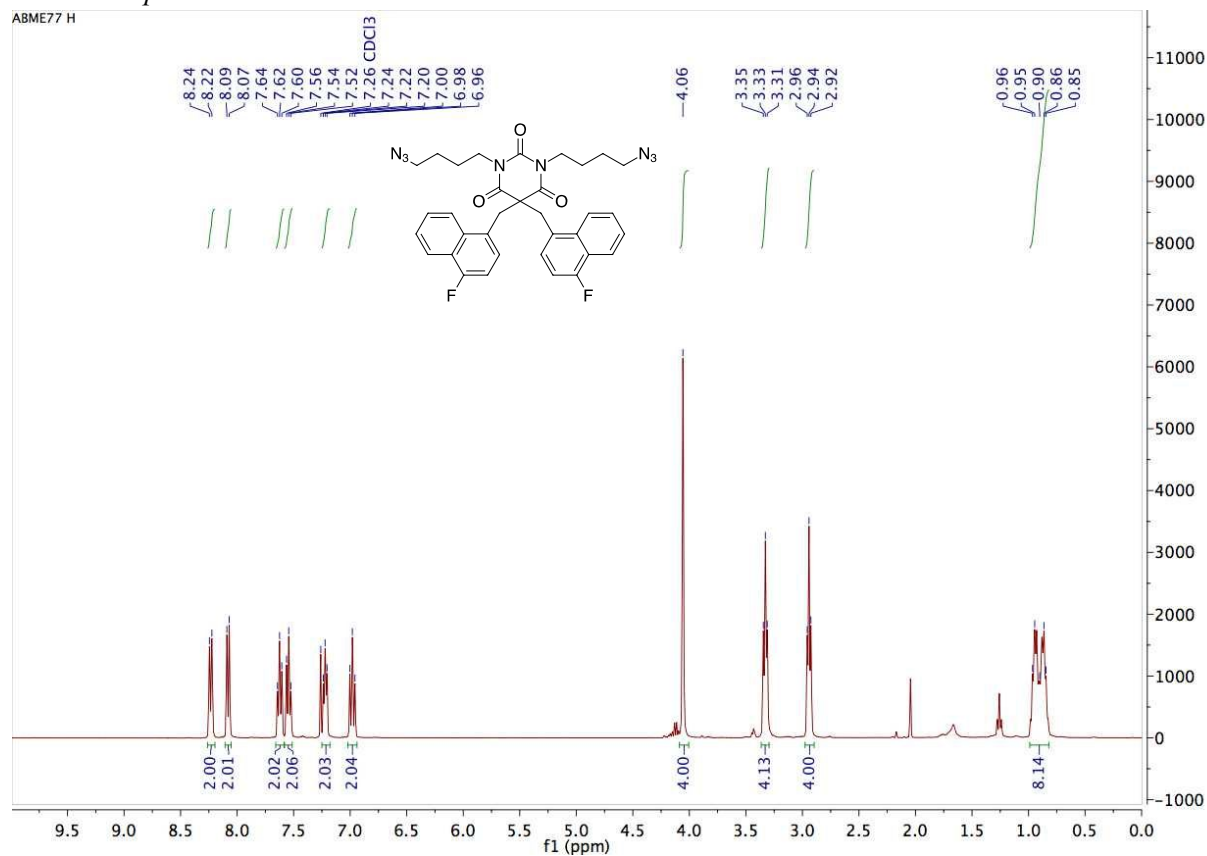
5.1 Compound 5a



5.2 Compound 5b

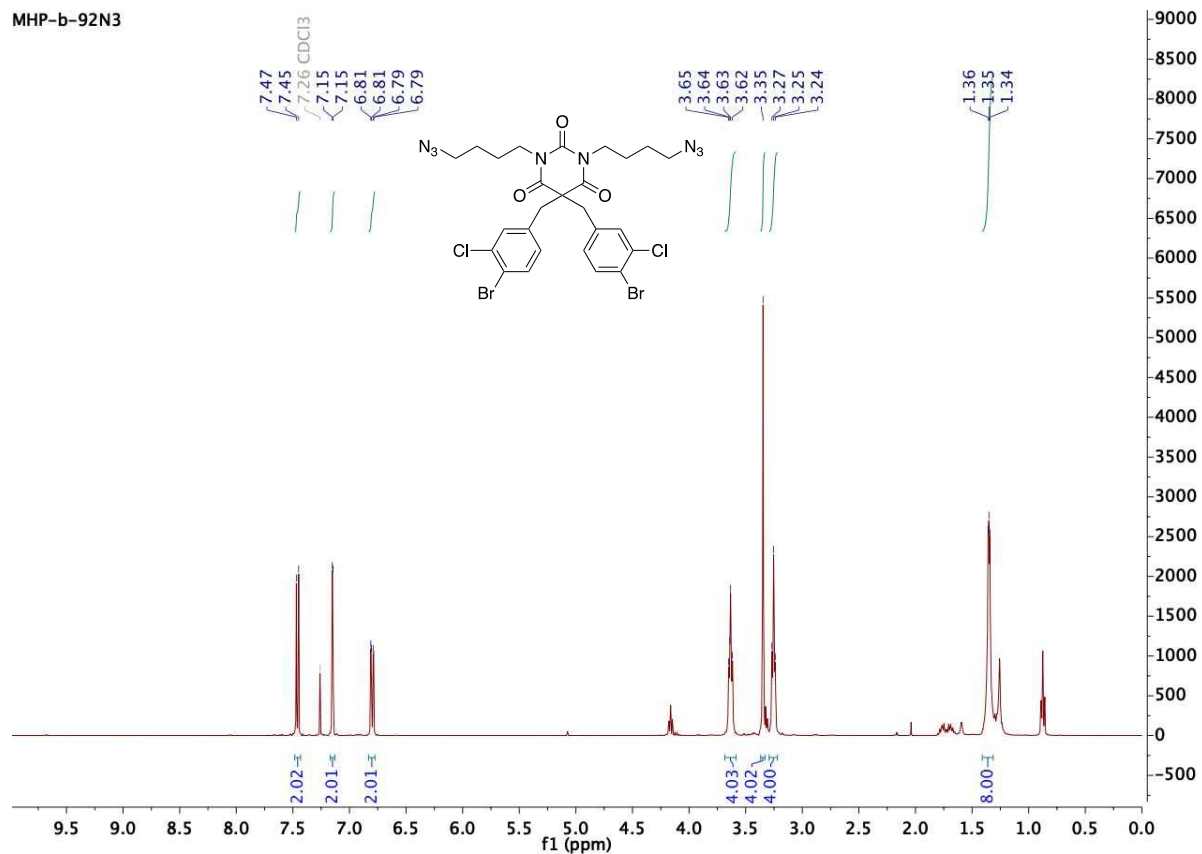


5.3 Compound 5c

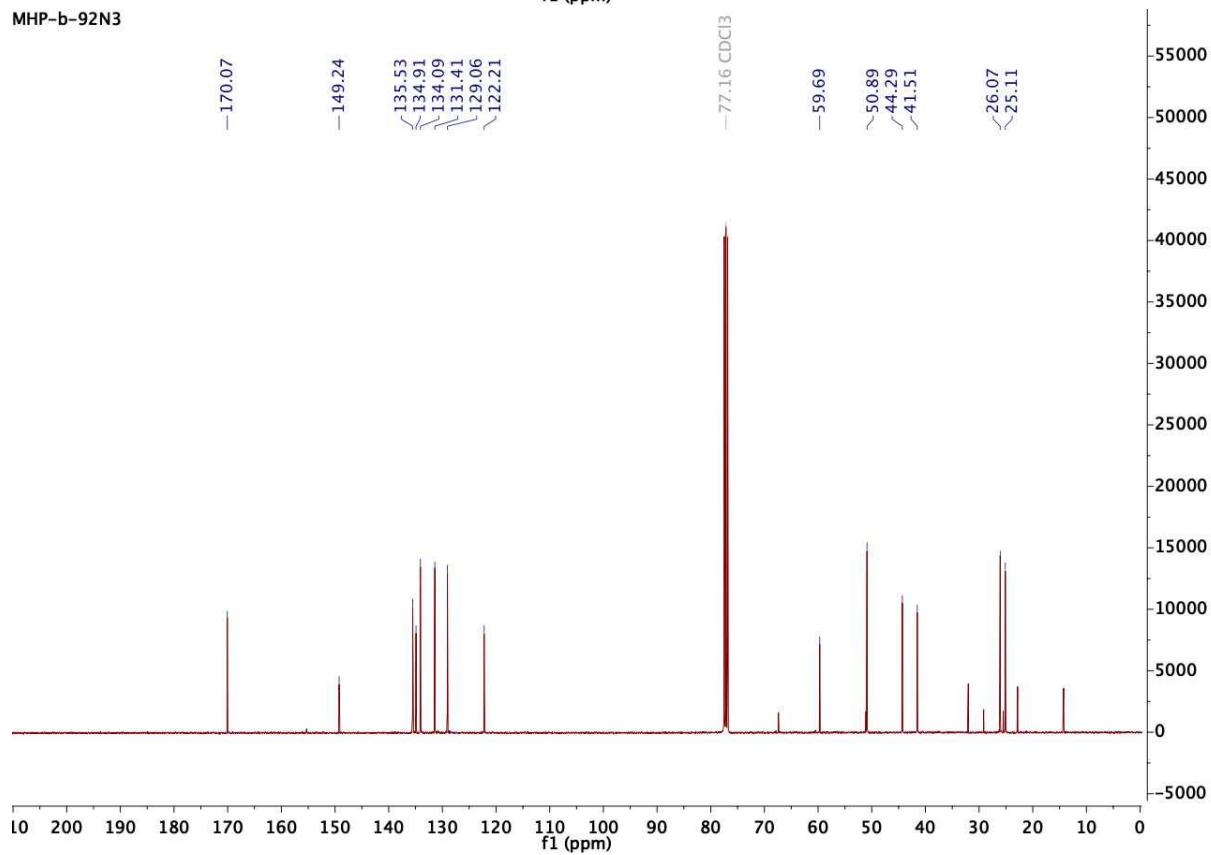


5.4 Compound 5d

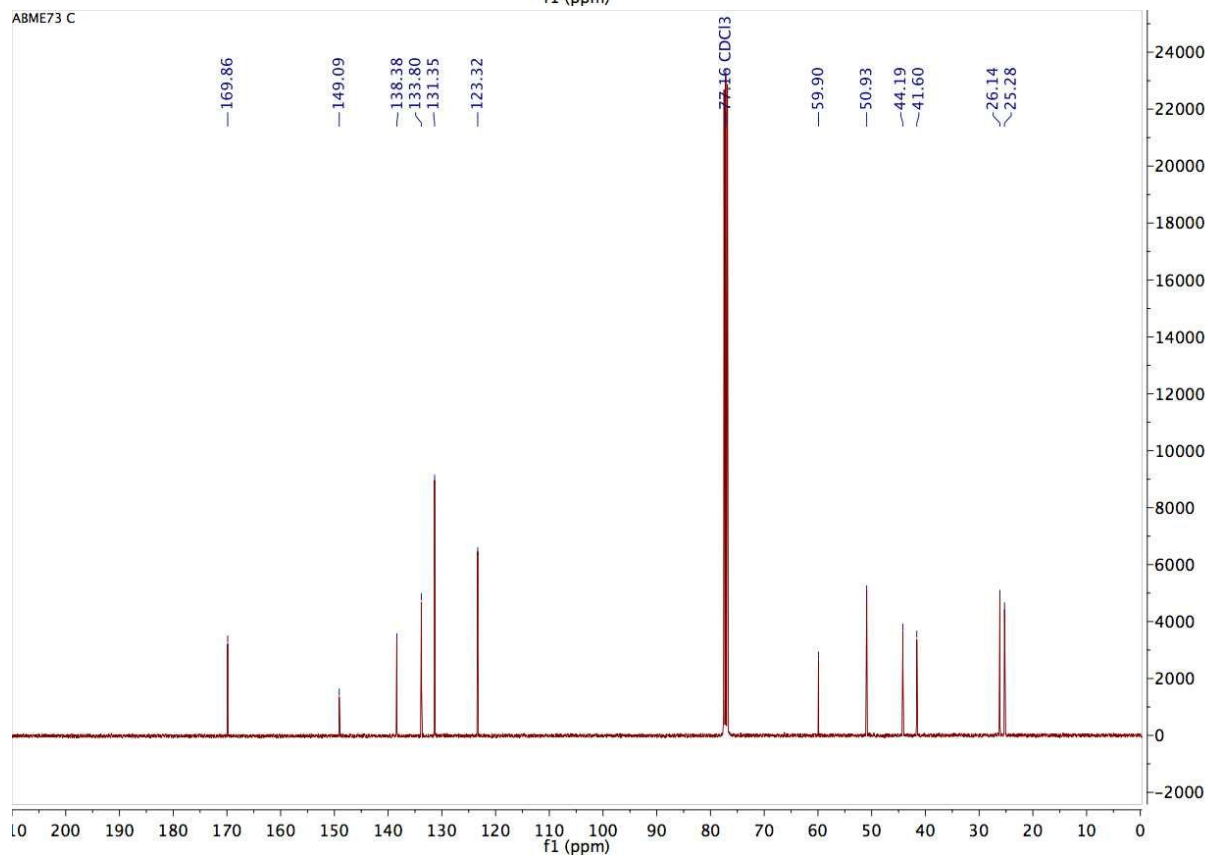
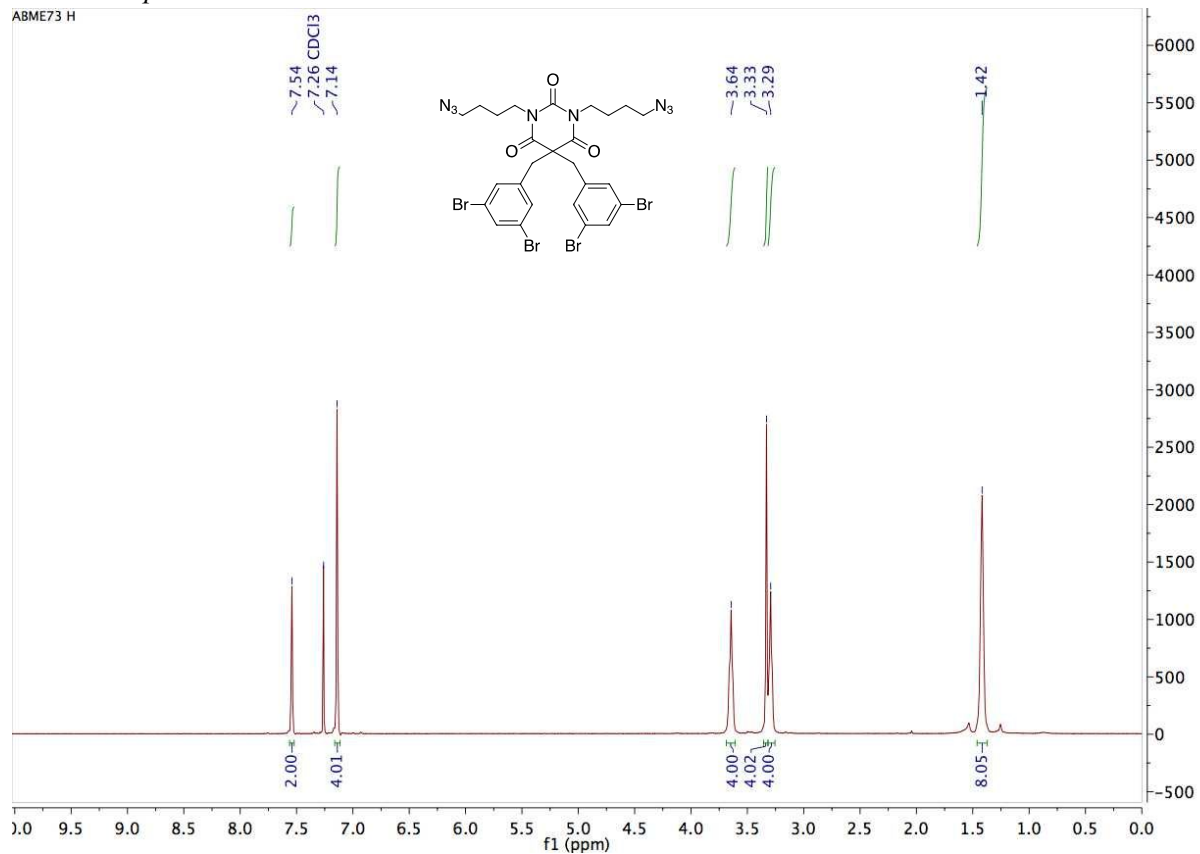
MHP-b-92N3



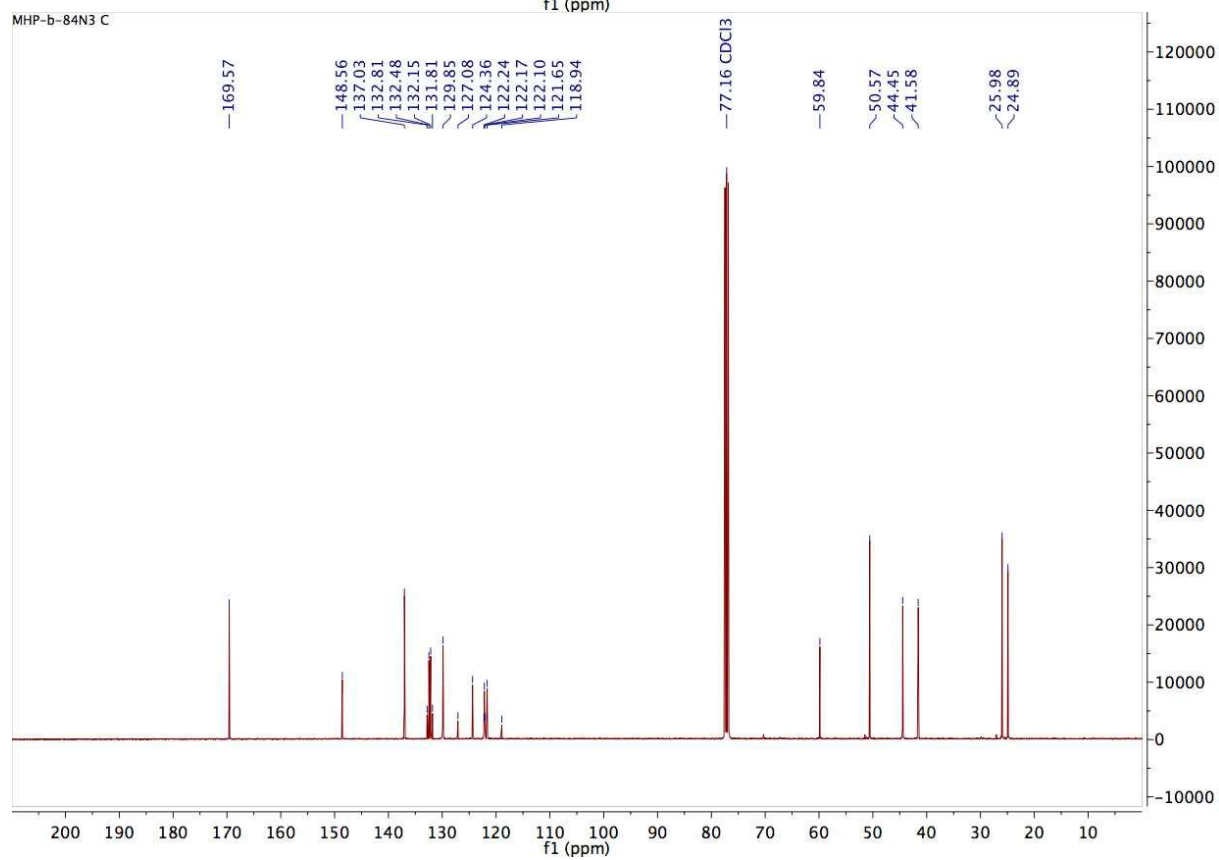
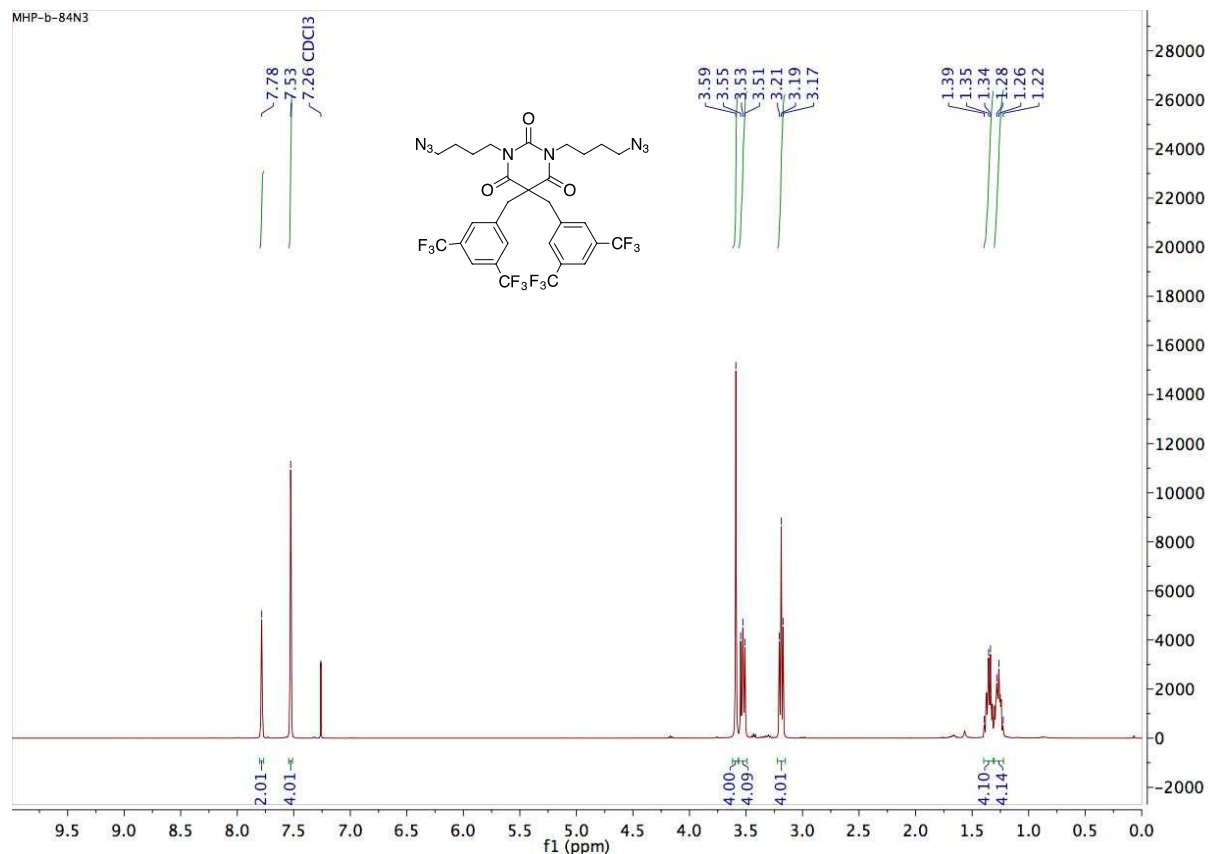
MHP-b-92N3



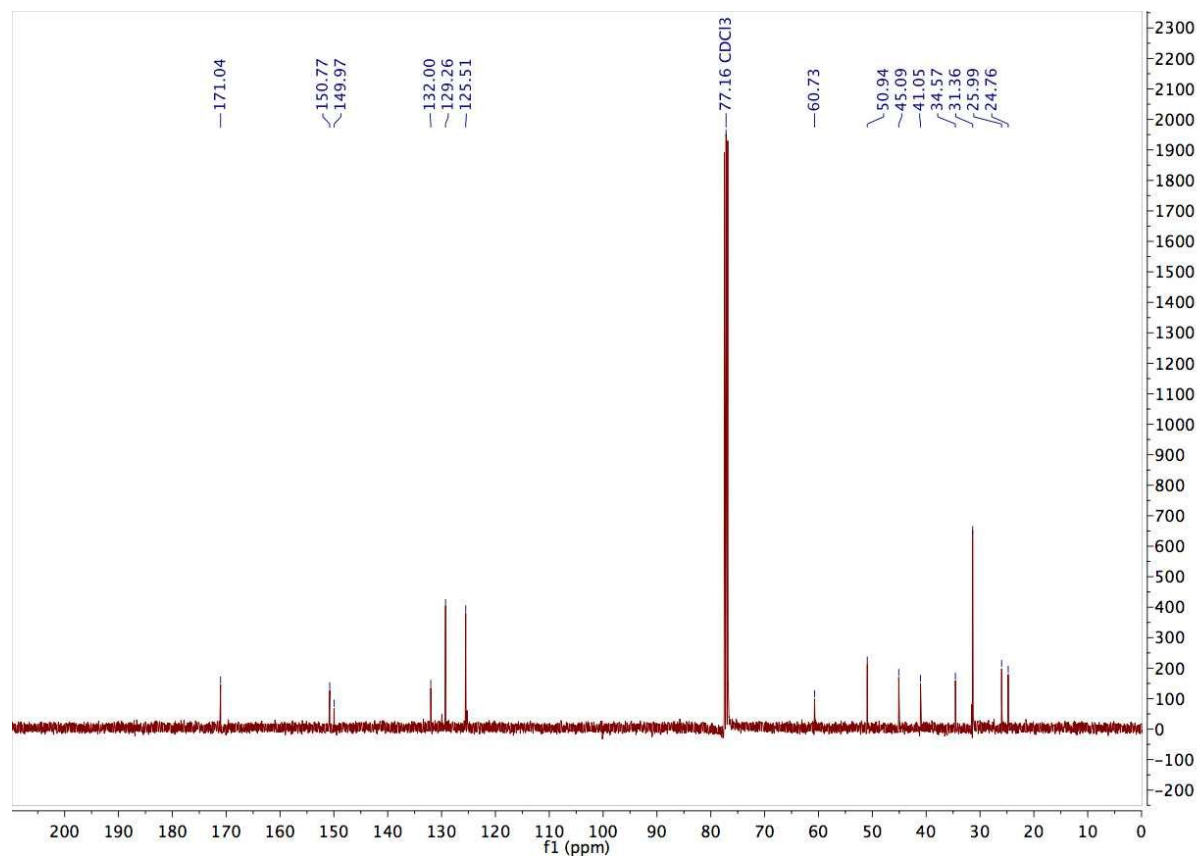
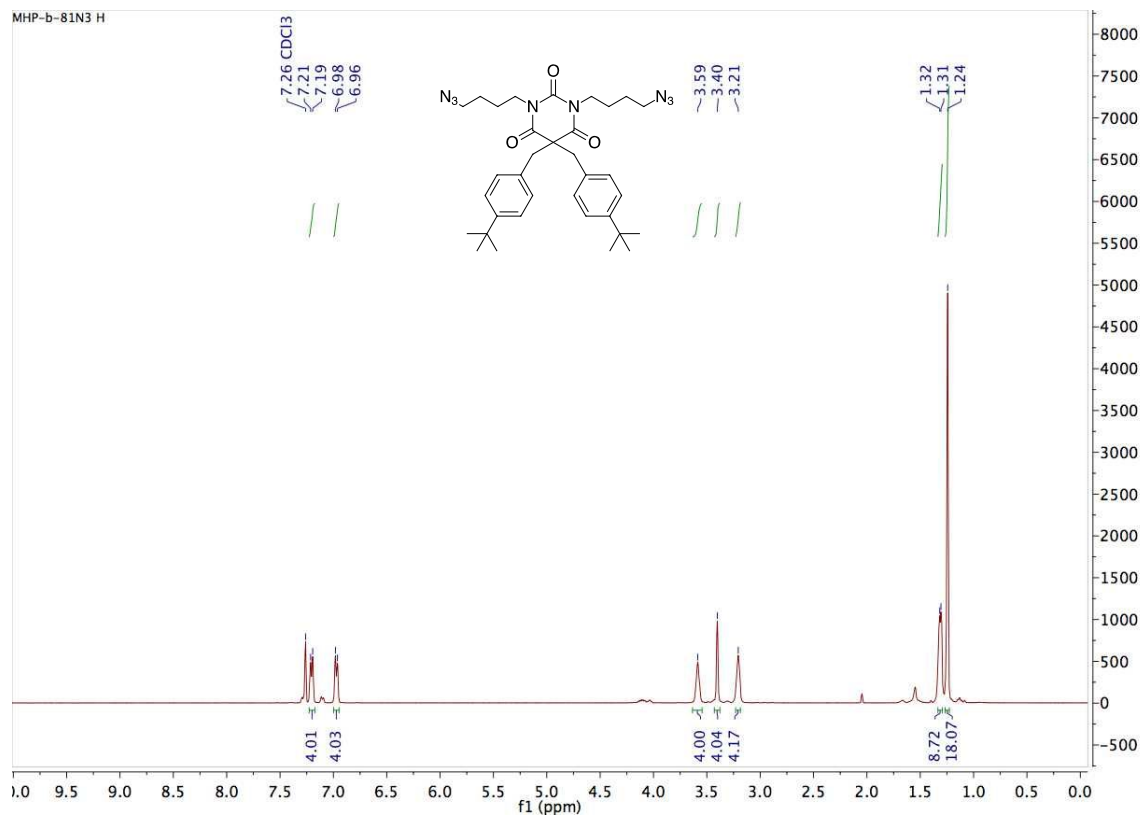
5.5 Compound 5e



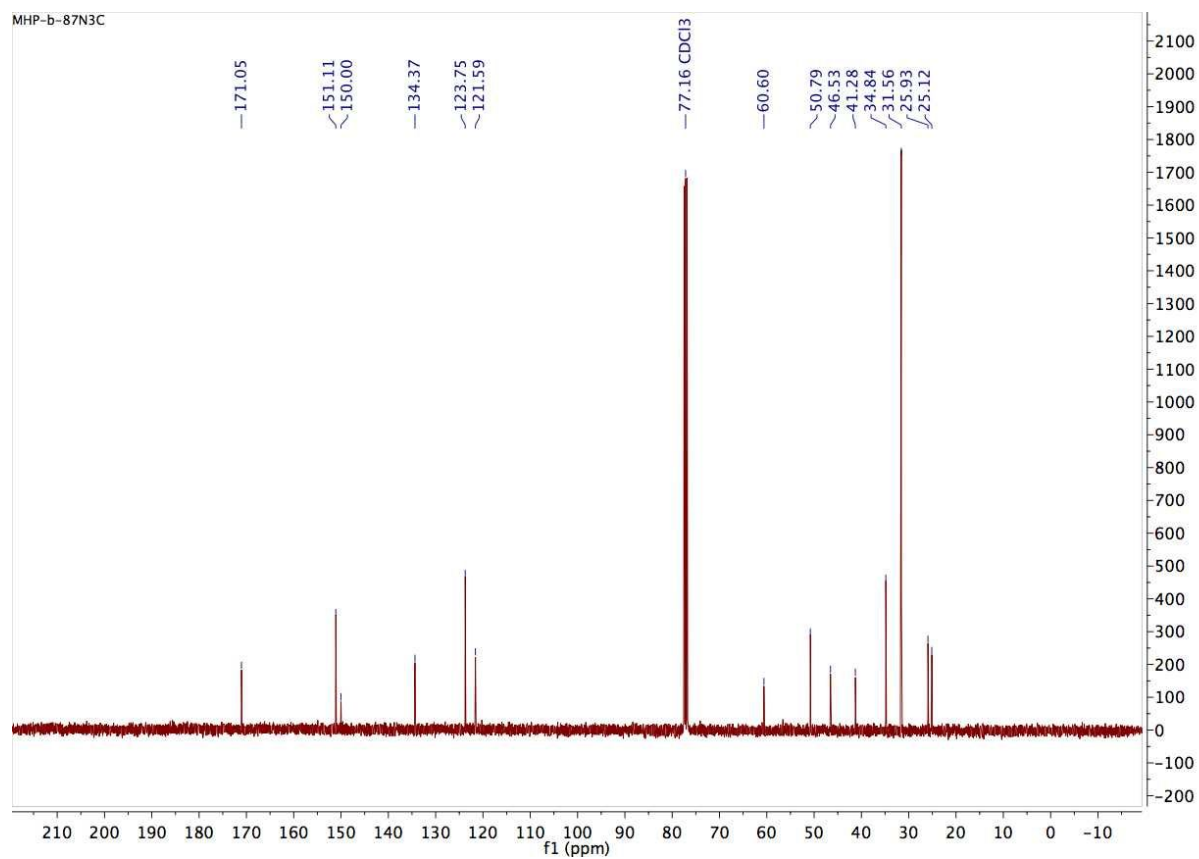
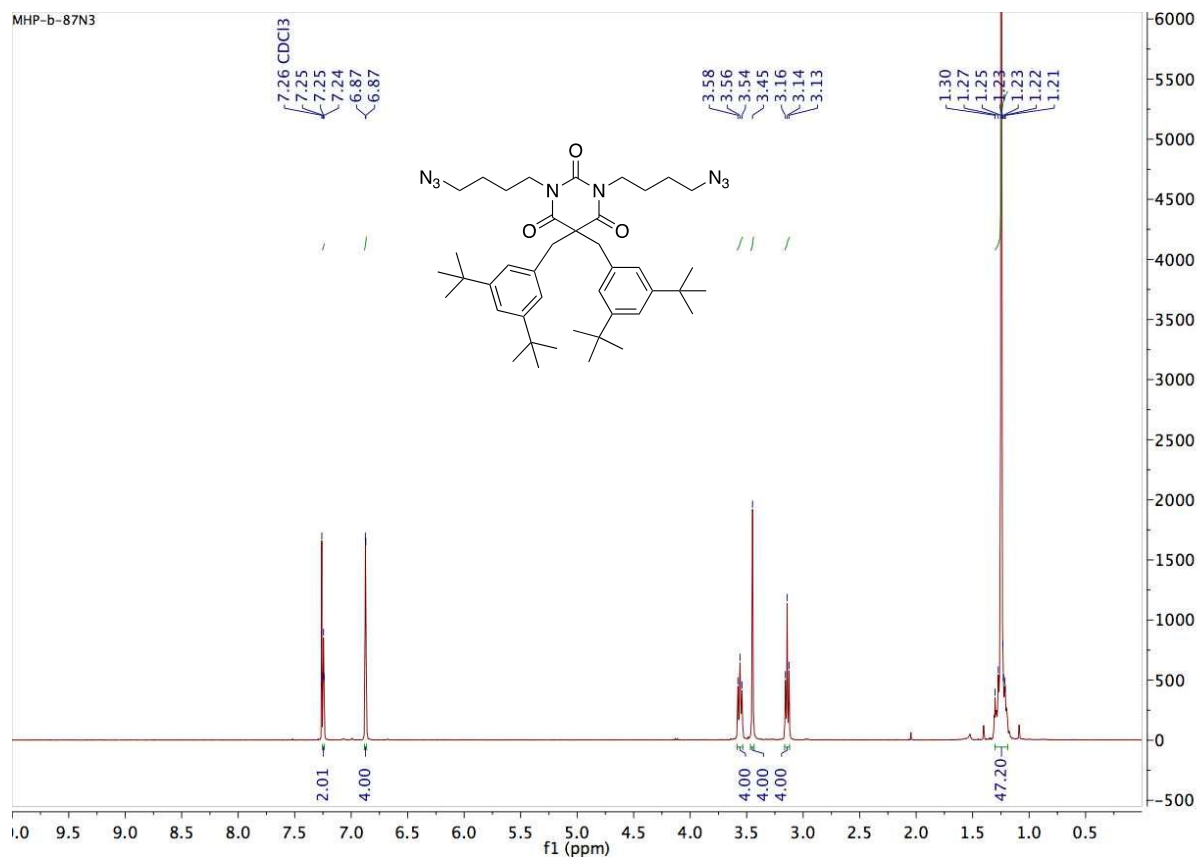
5.6 Compound 5f



5.7 Compound 5g

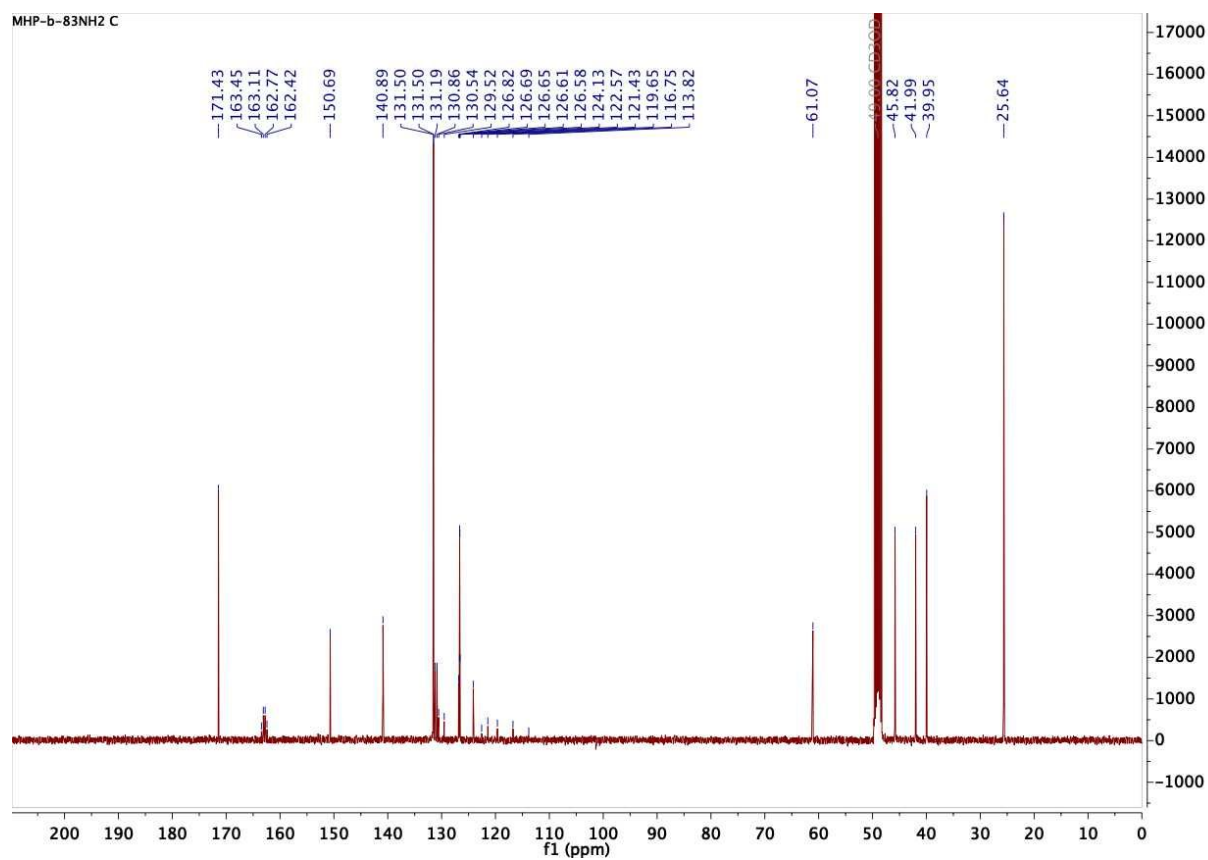
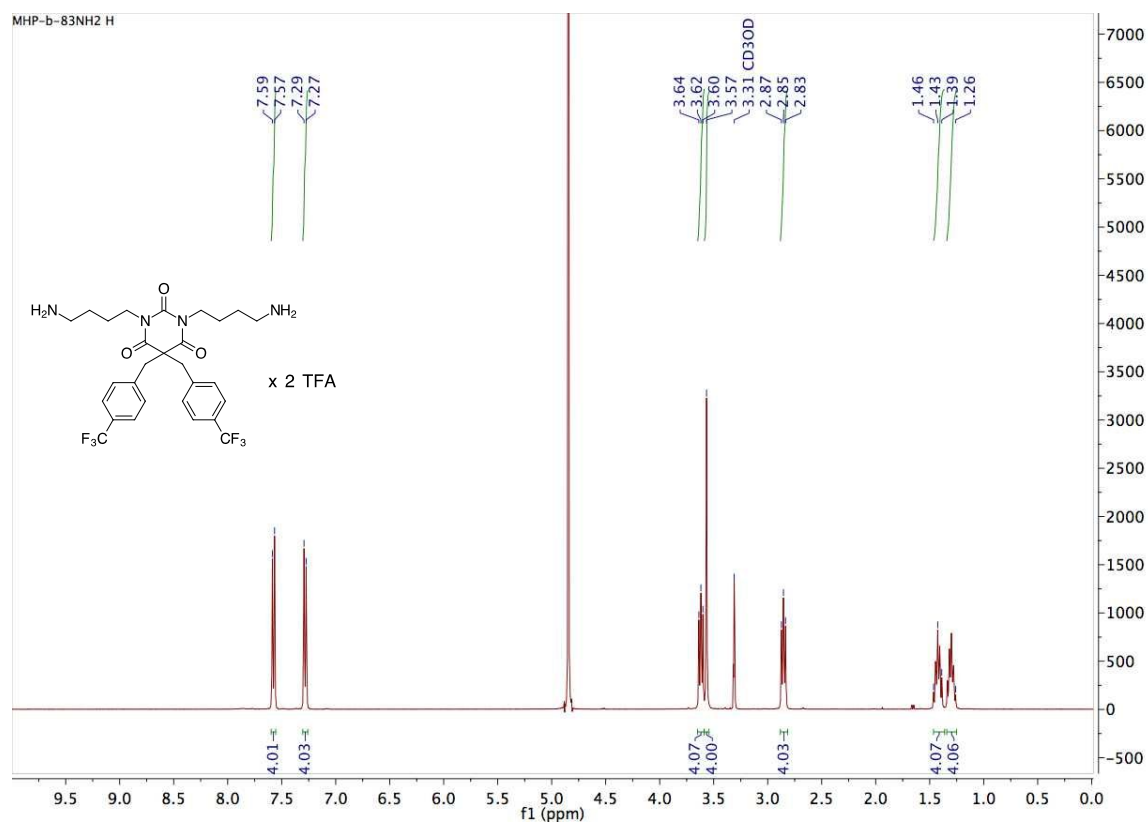


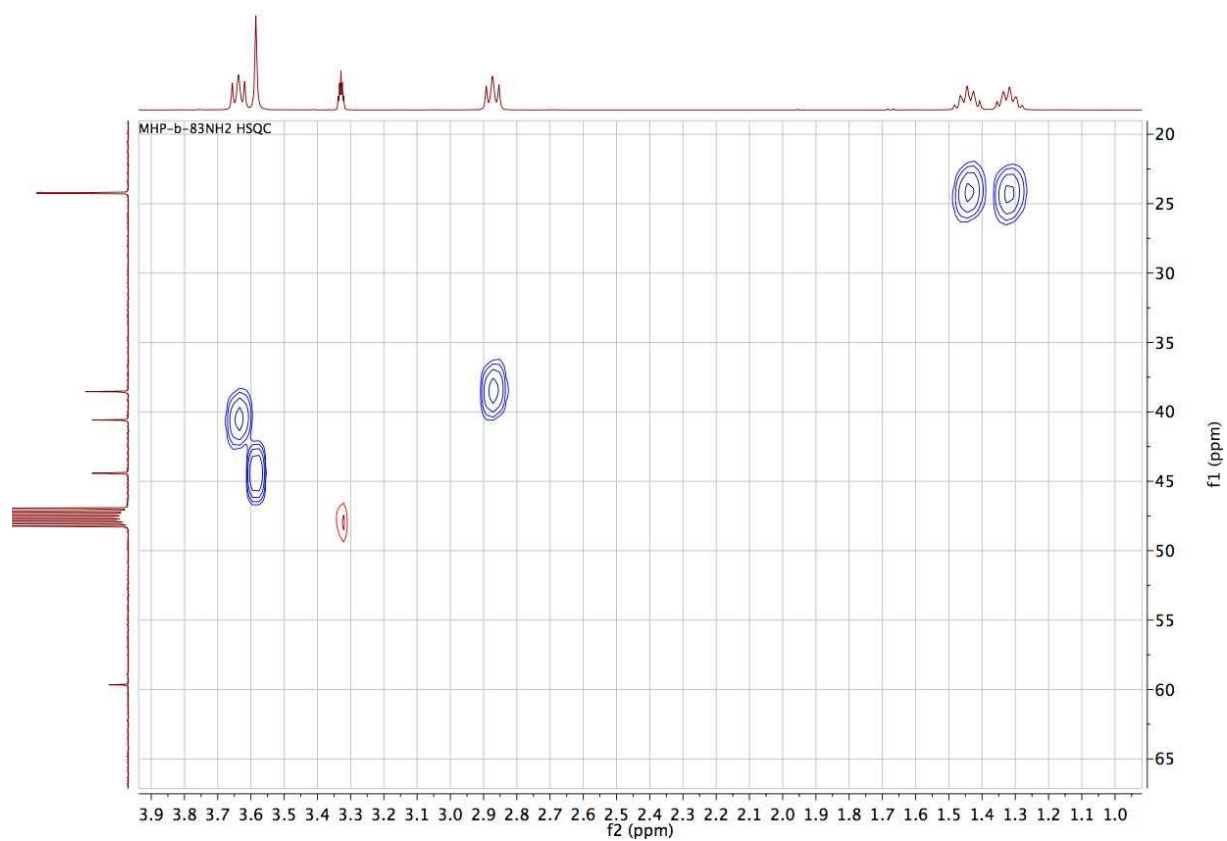
5.8 Compound 5h



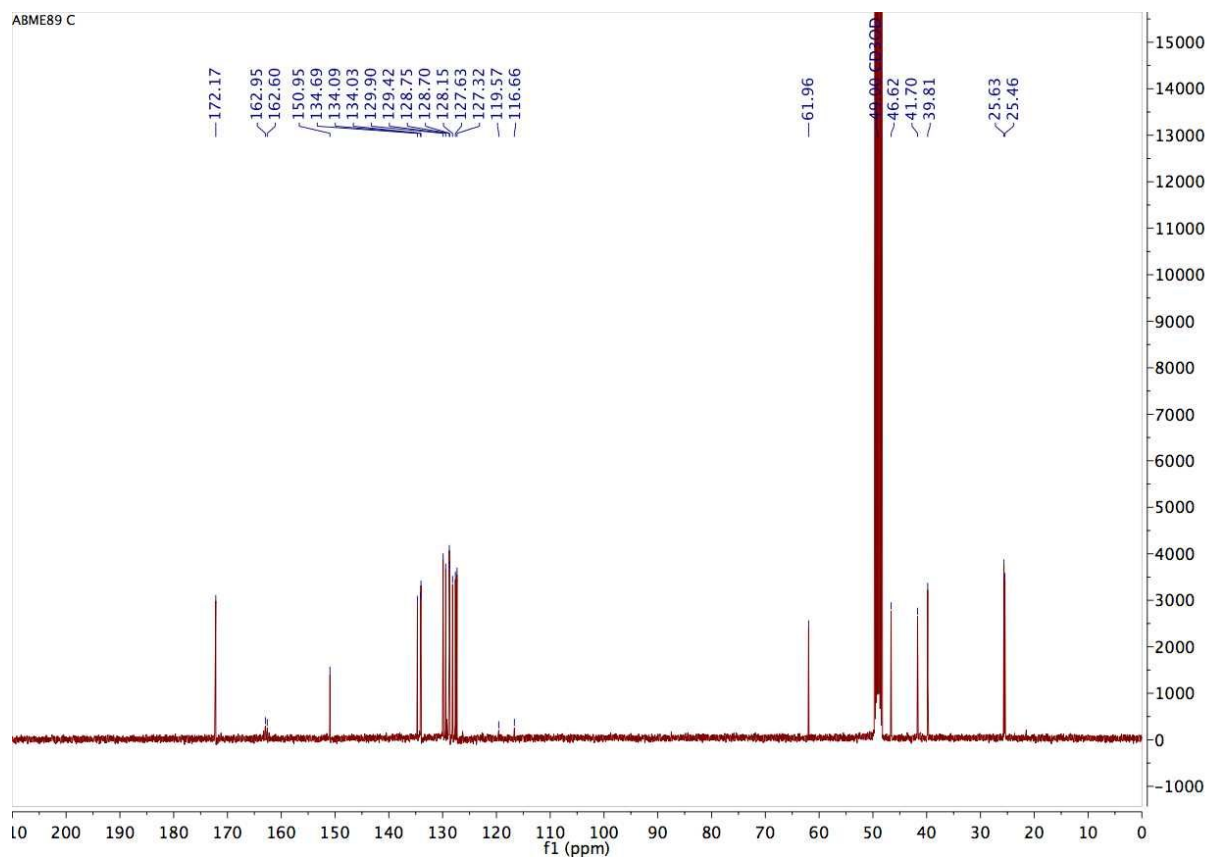
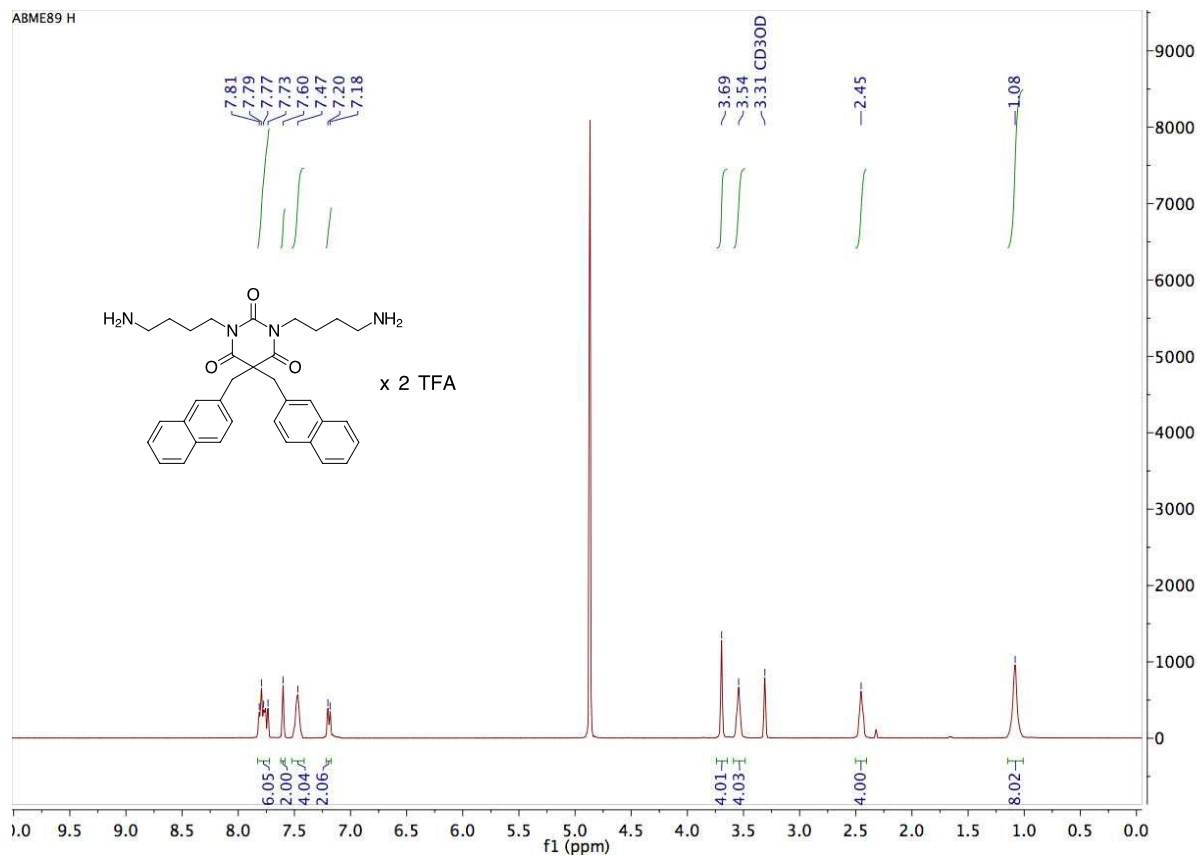
6. ^1H and ^{13}C NMR spectra of amine barbiturates (6)

6.1 Compound 6a

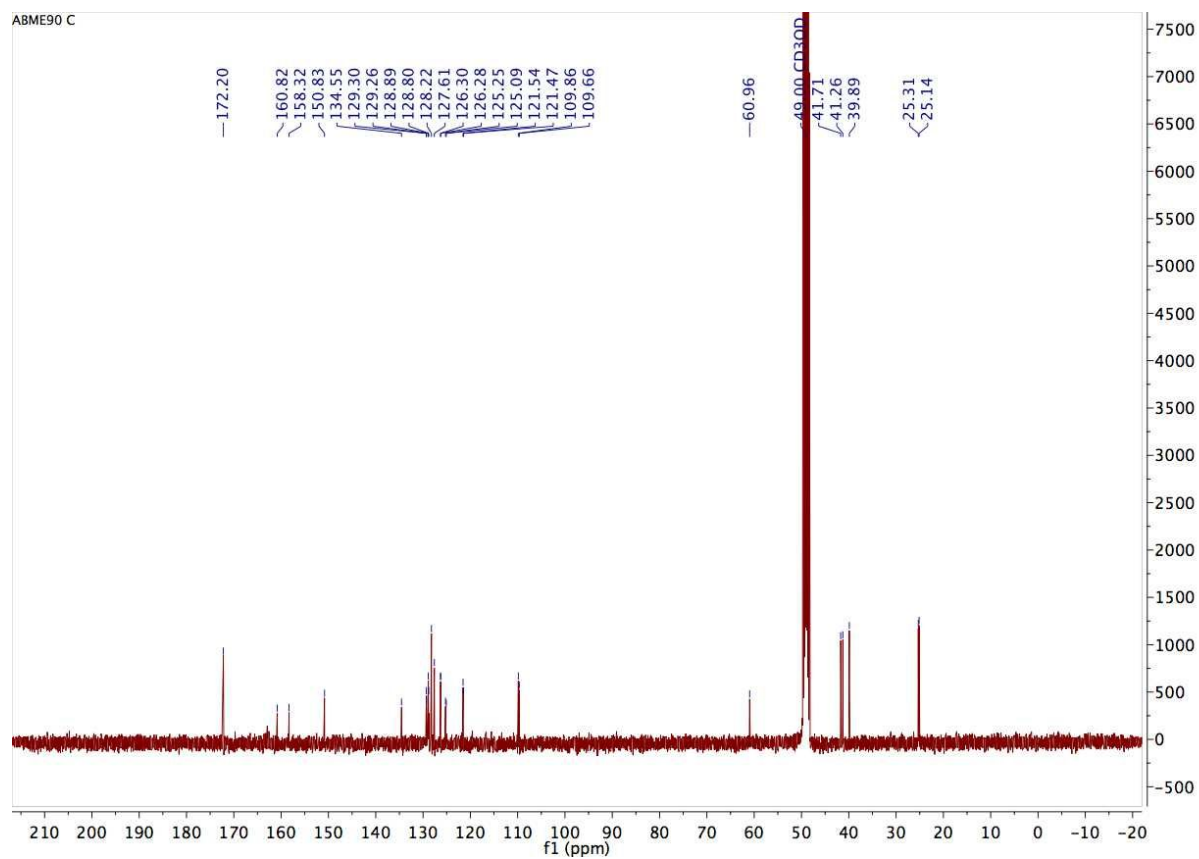
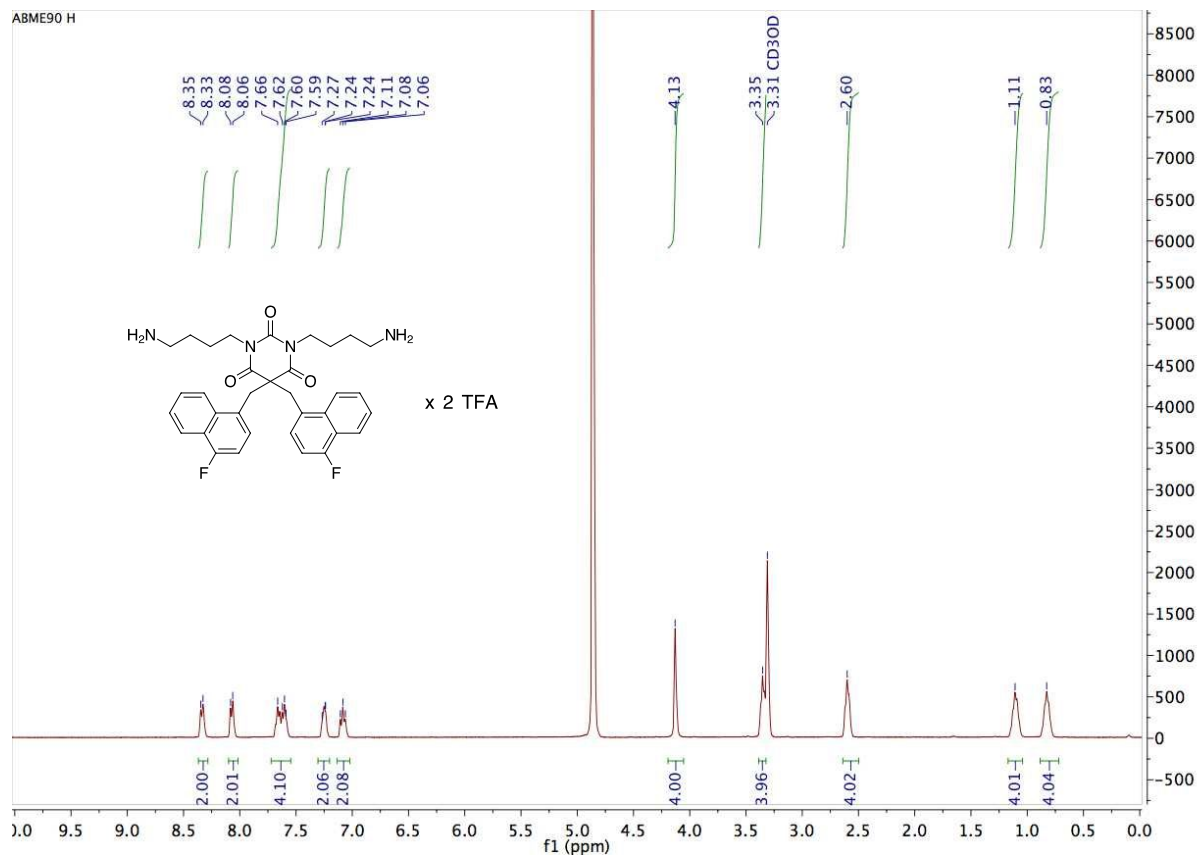




6.2 Compound 6b

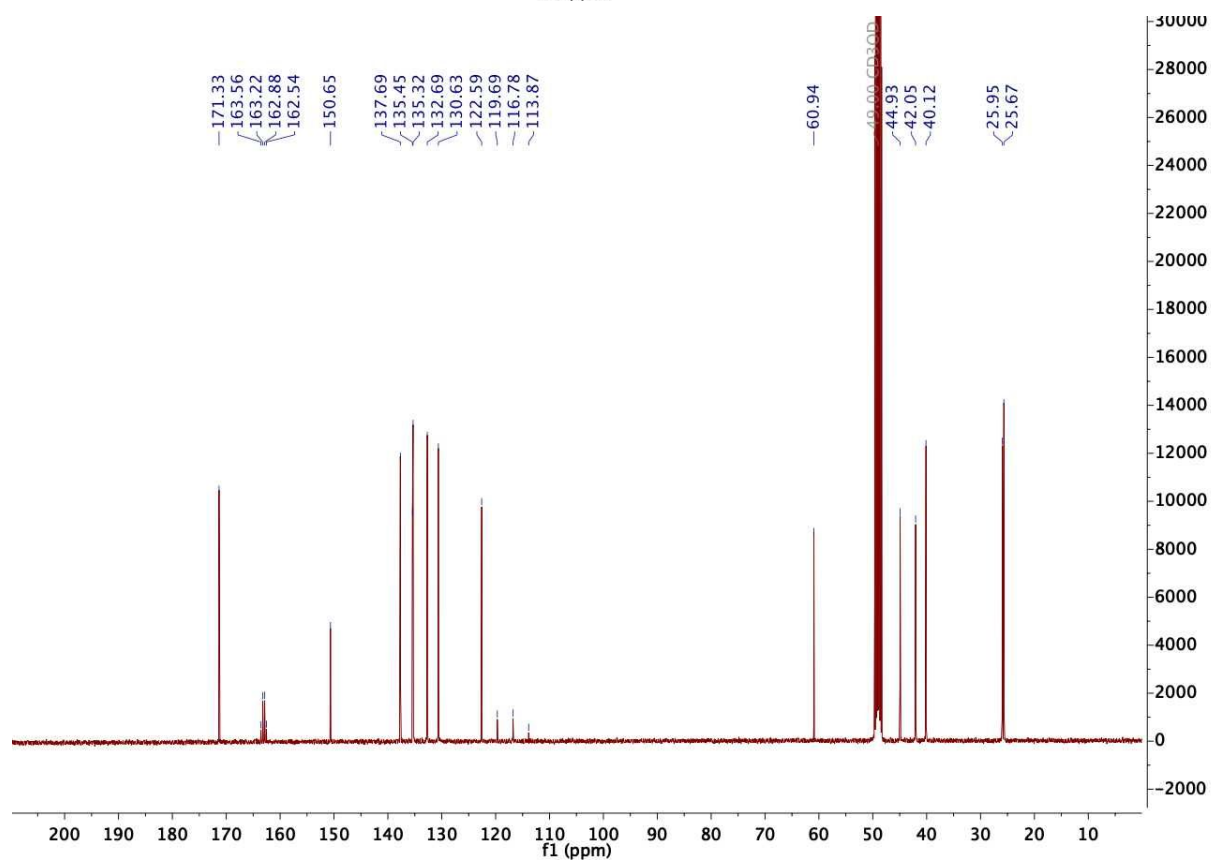
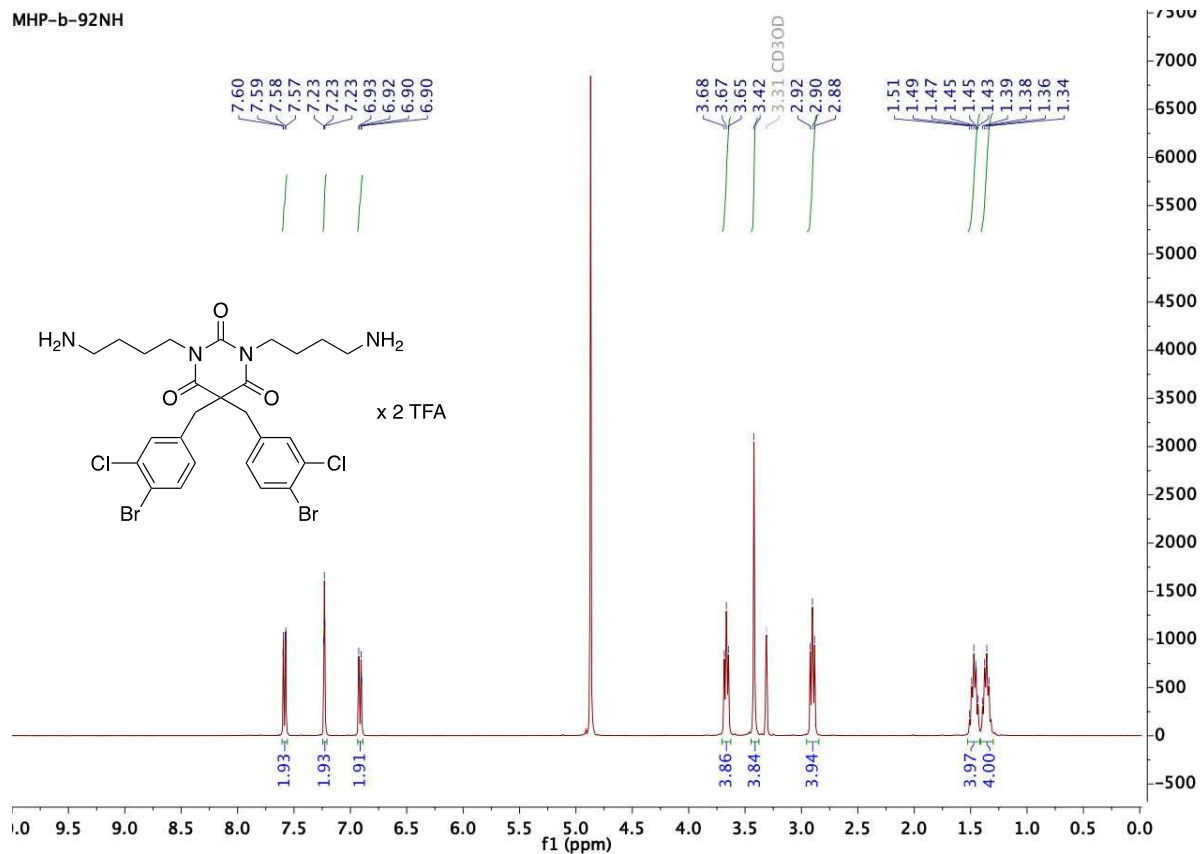


6.3 Compound 6c

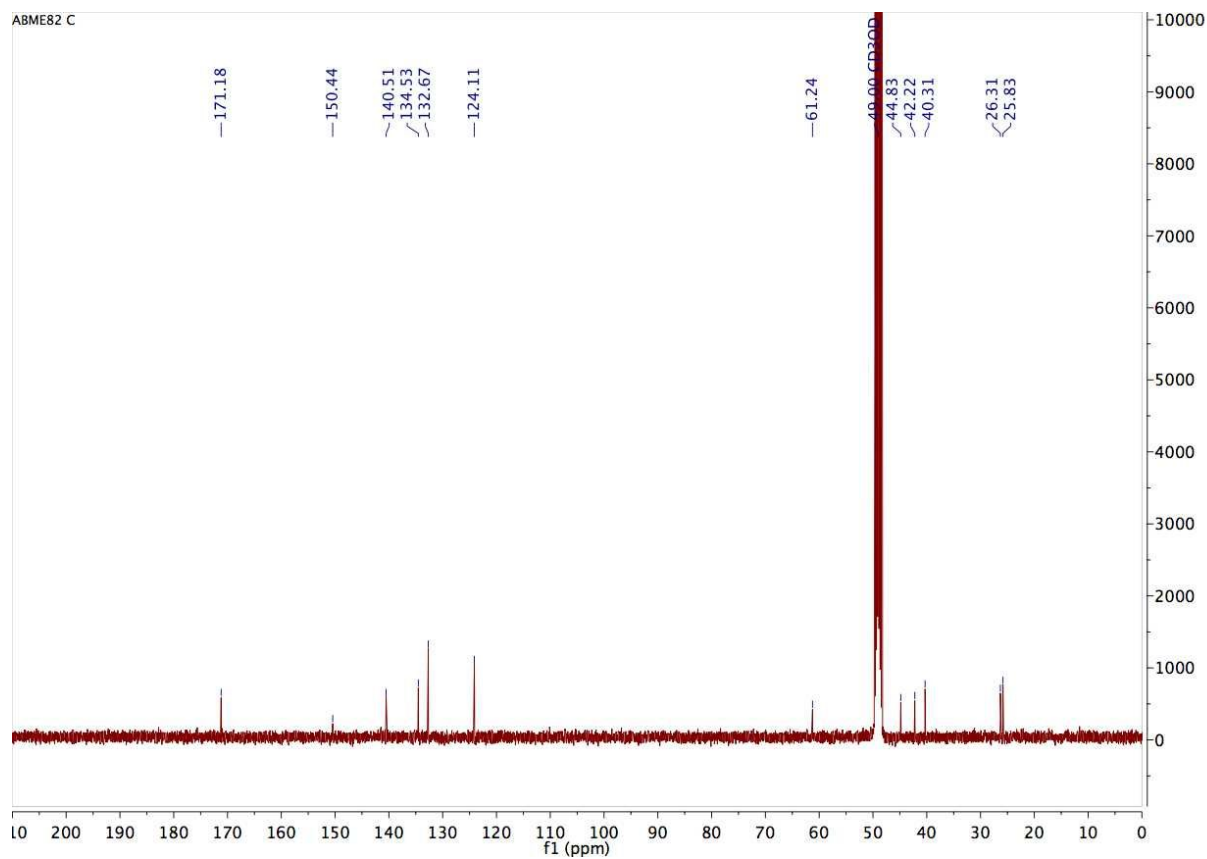
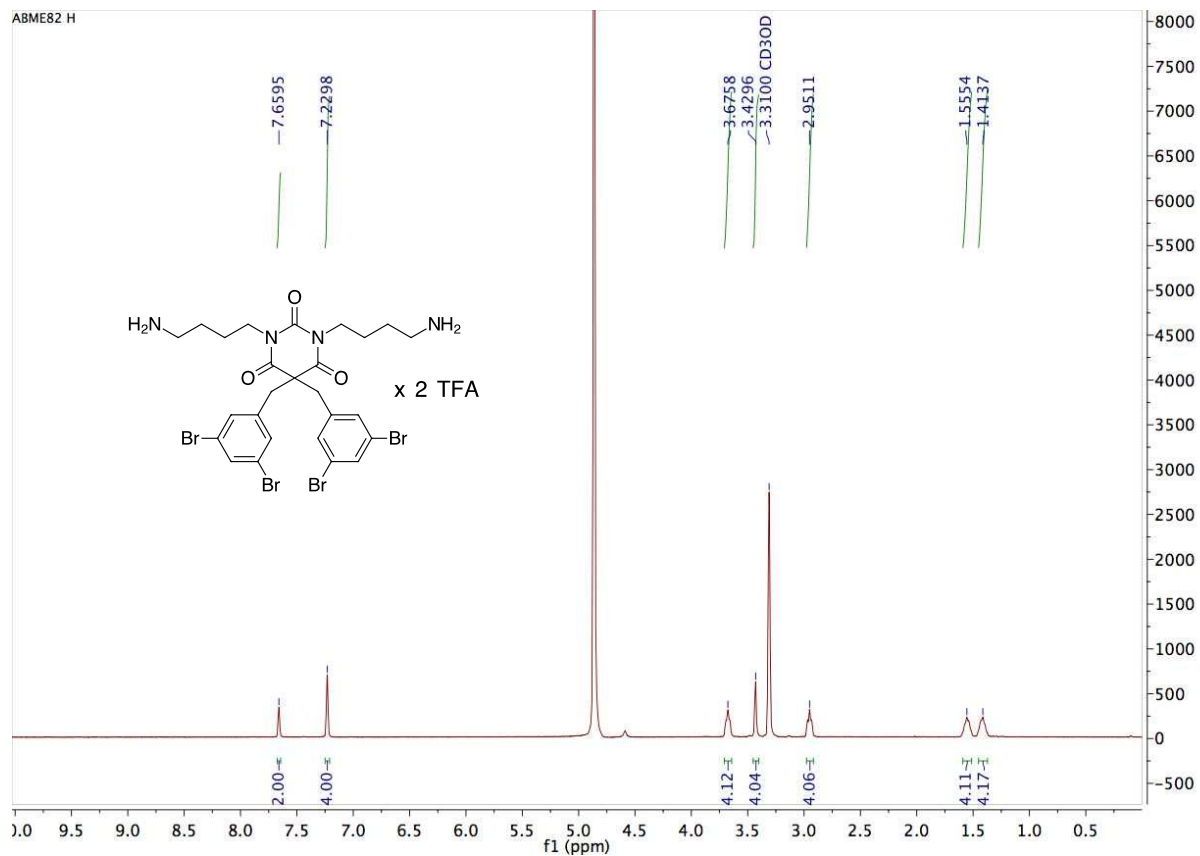


6.4 Compound 6d

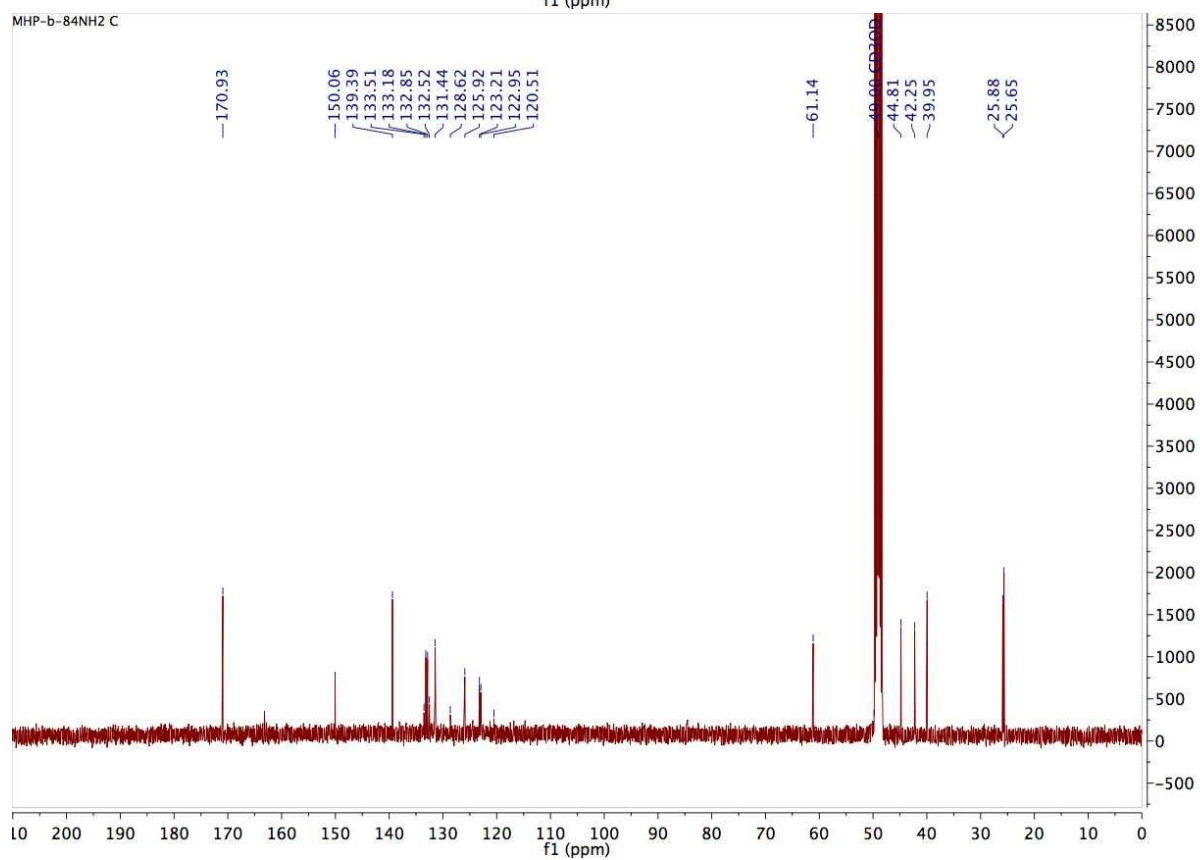
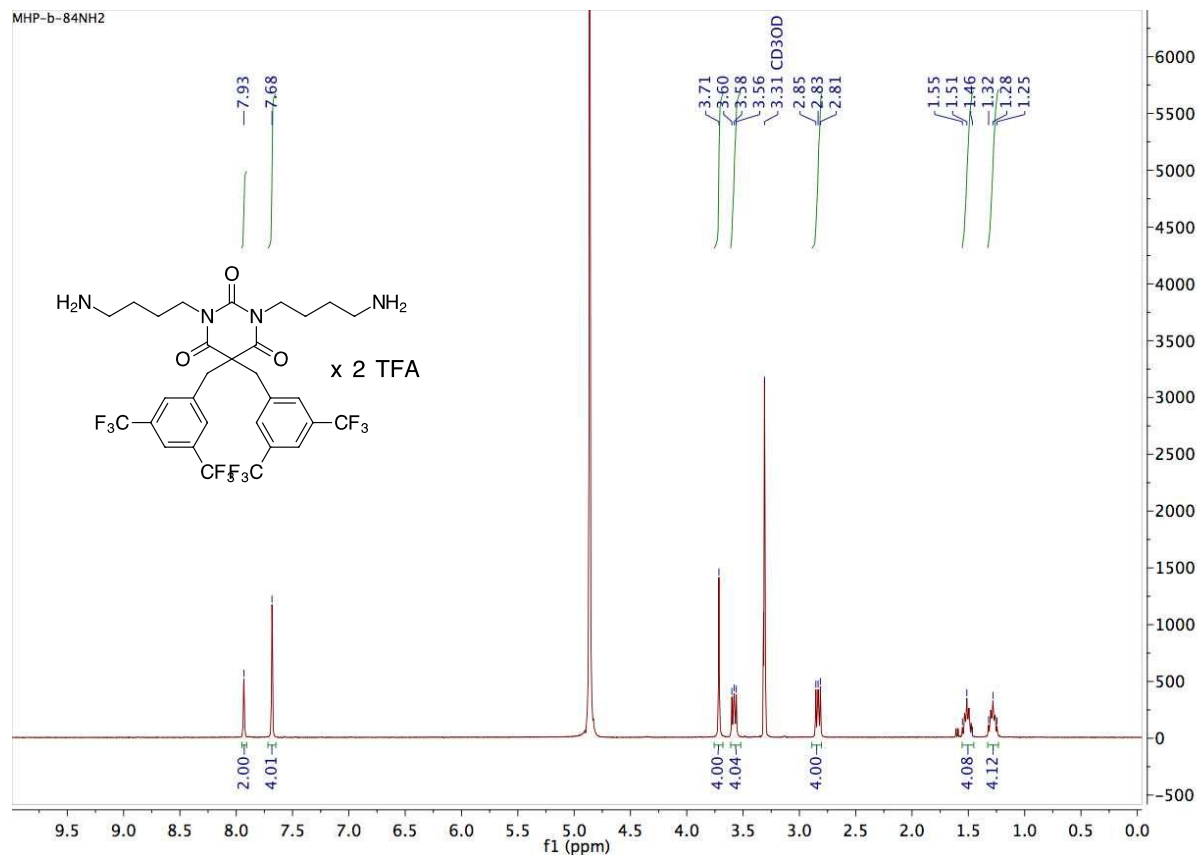
MHP-b-92NH



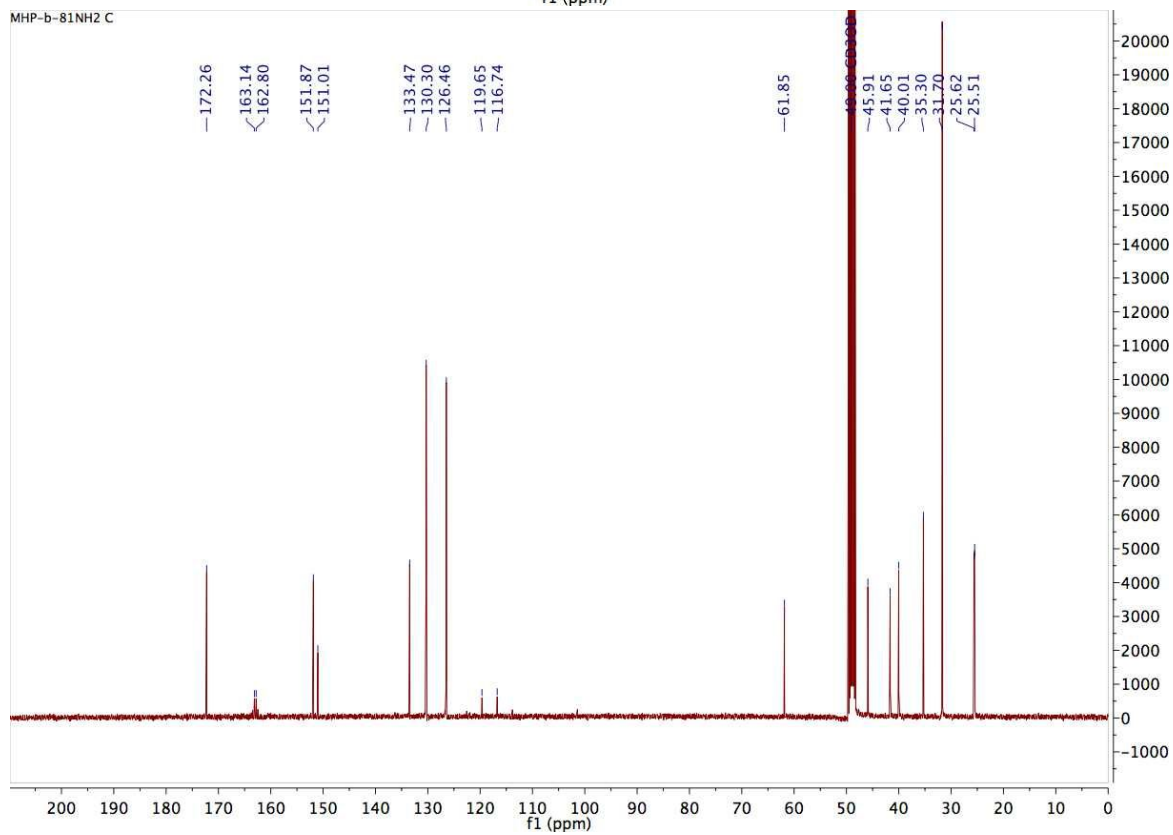
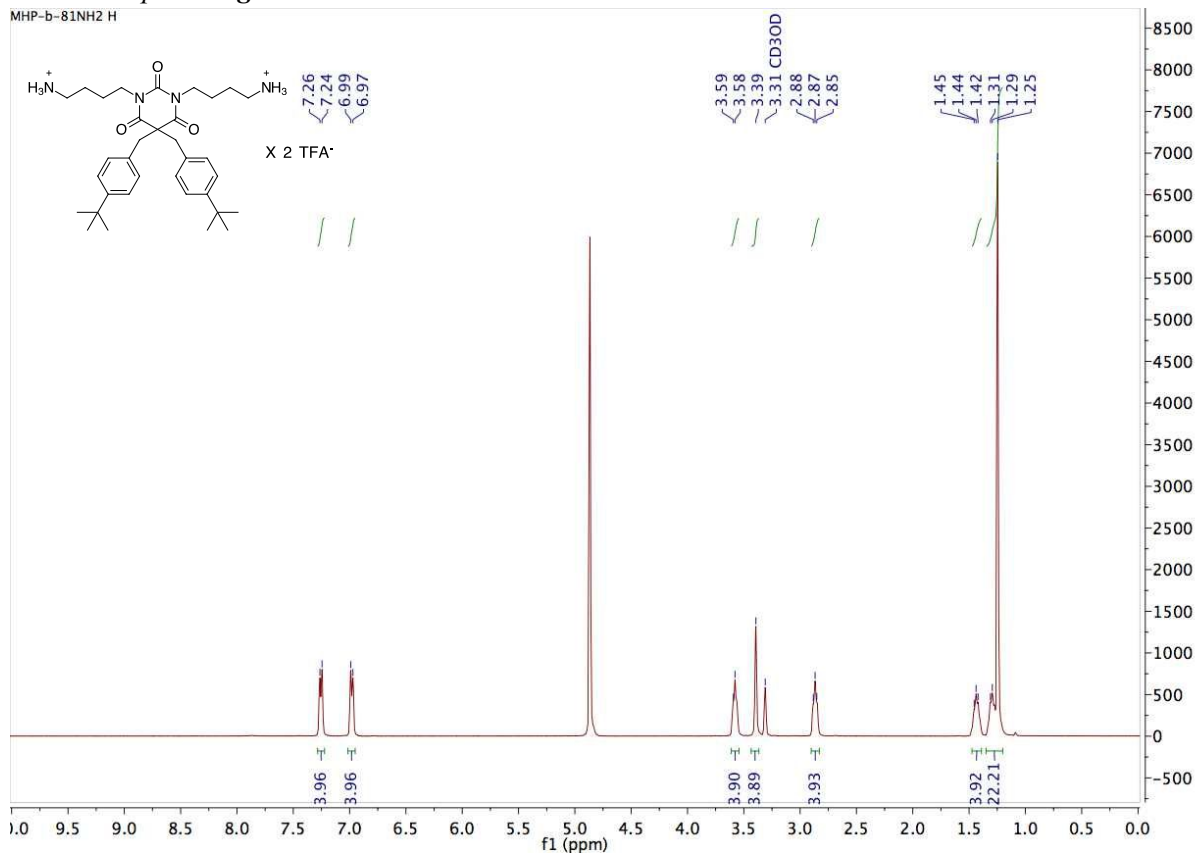
6.5 Compound 6e



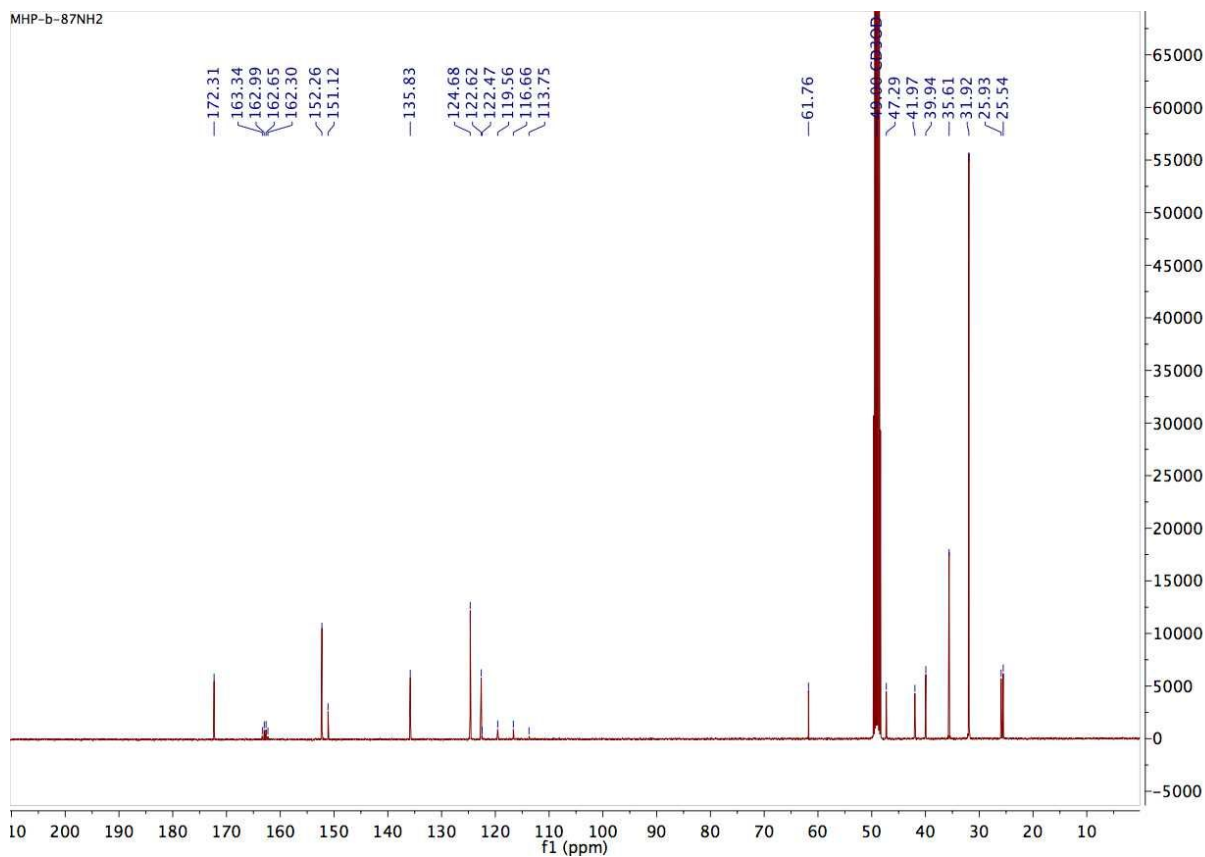
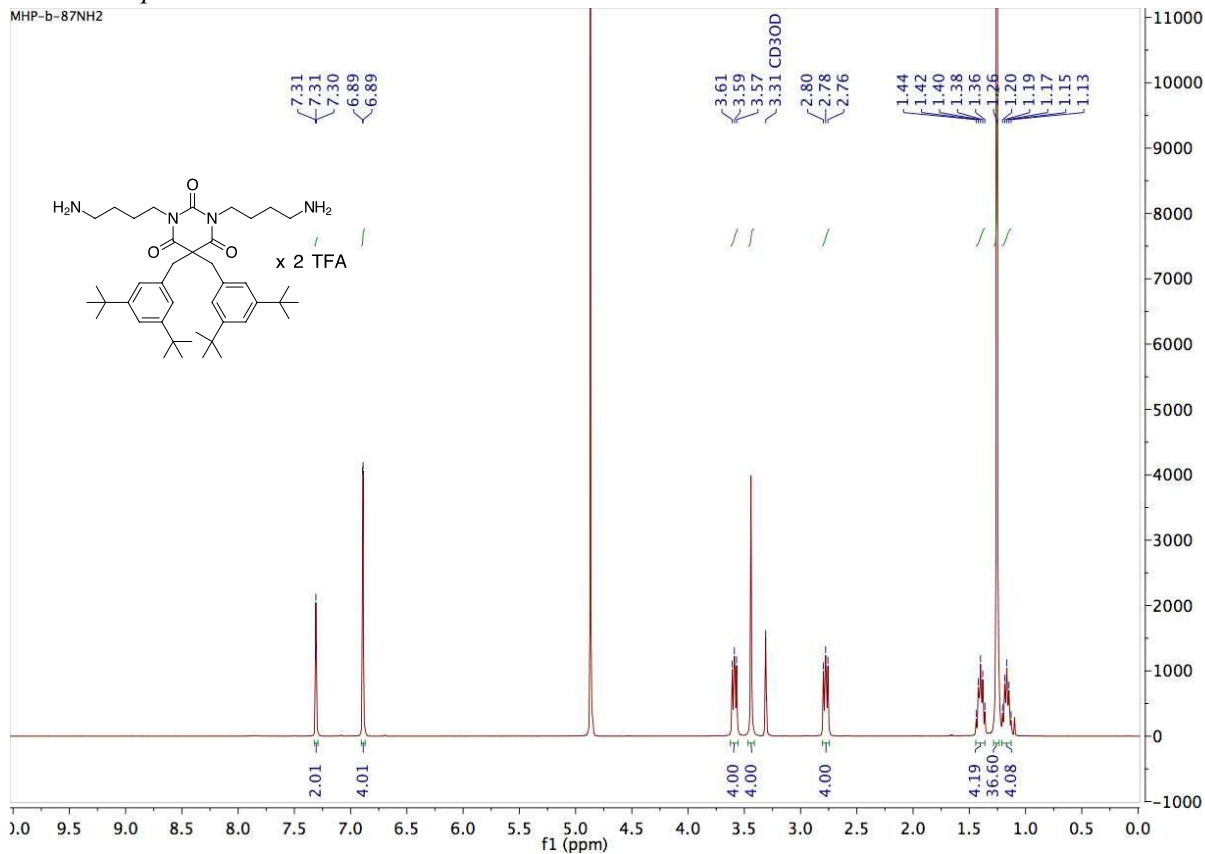
6.6 Compound 6f



6.7 Compound 6g

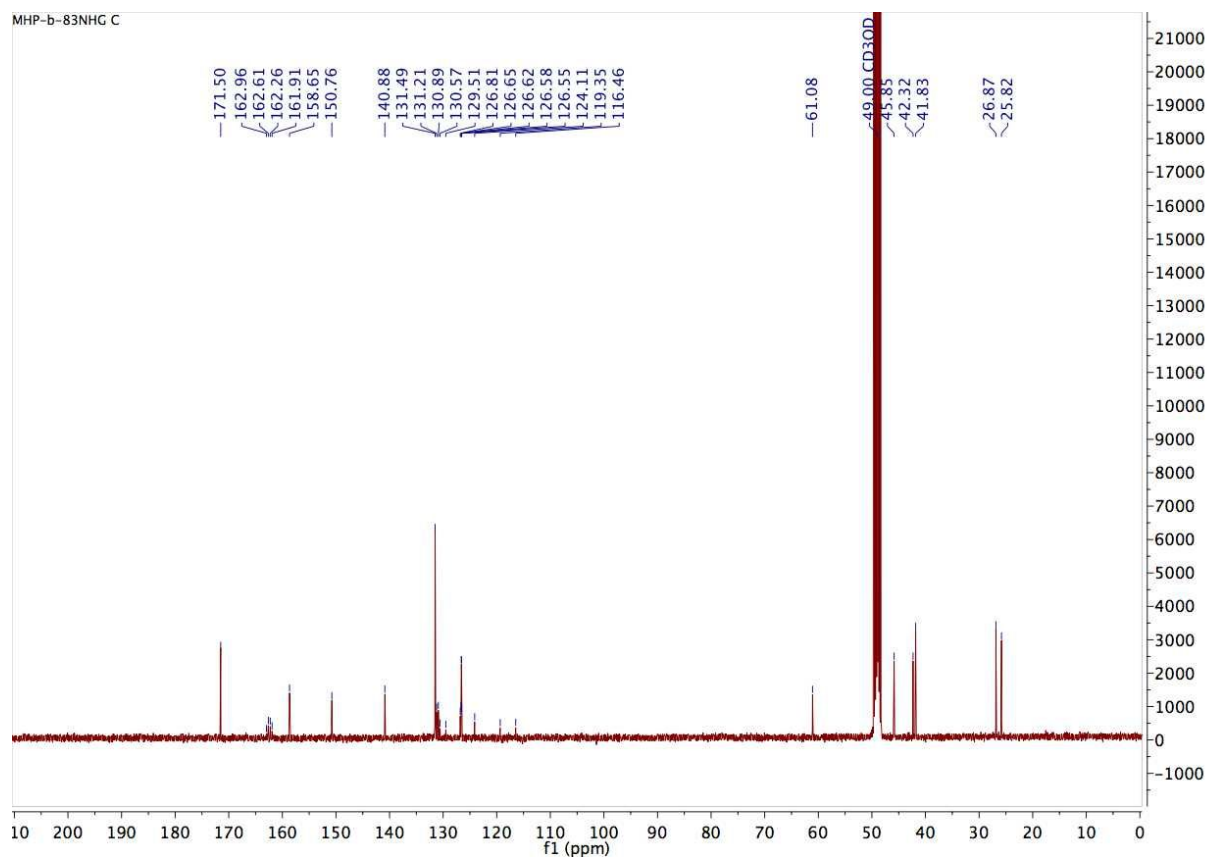
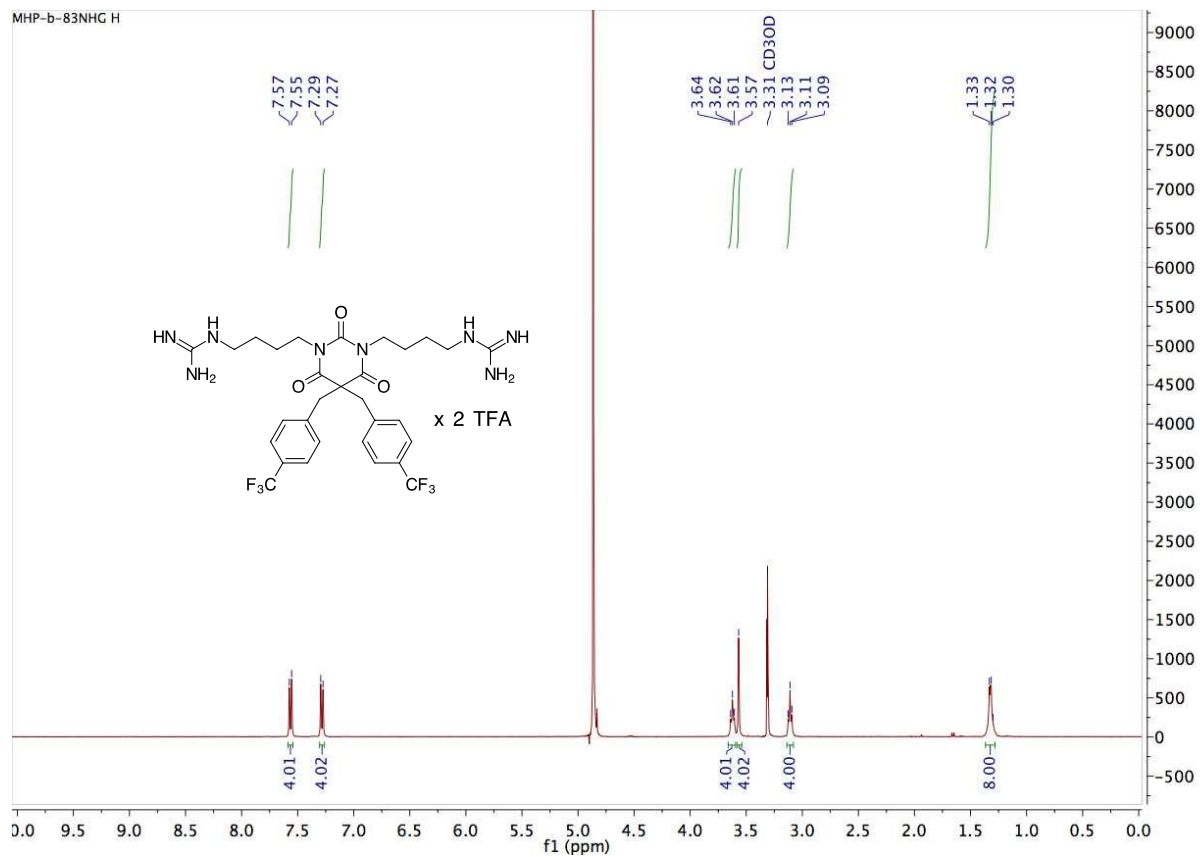


6.8 Compound 6h

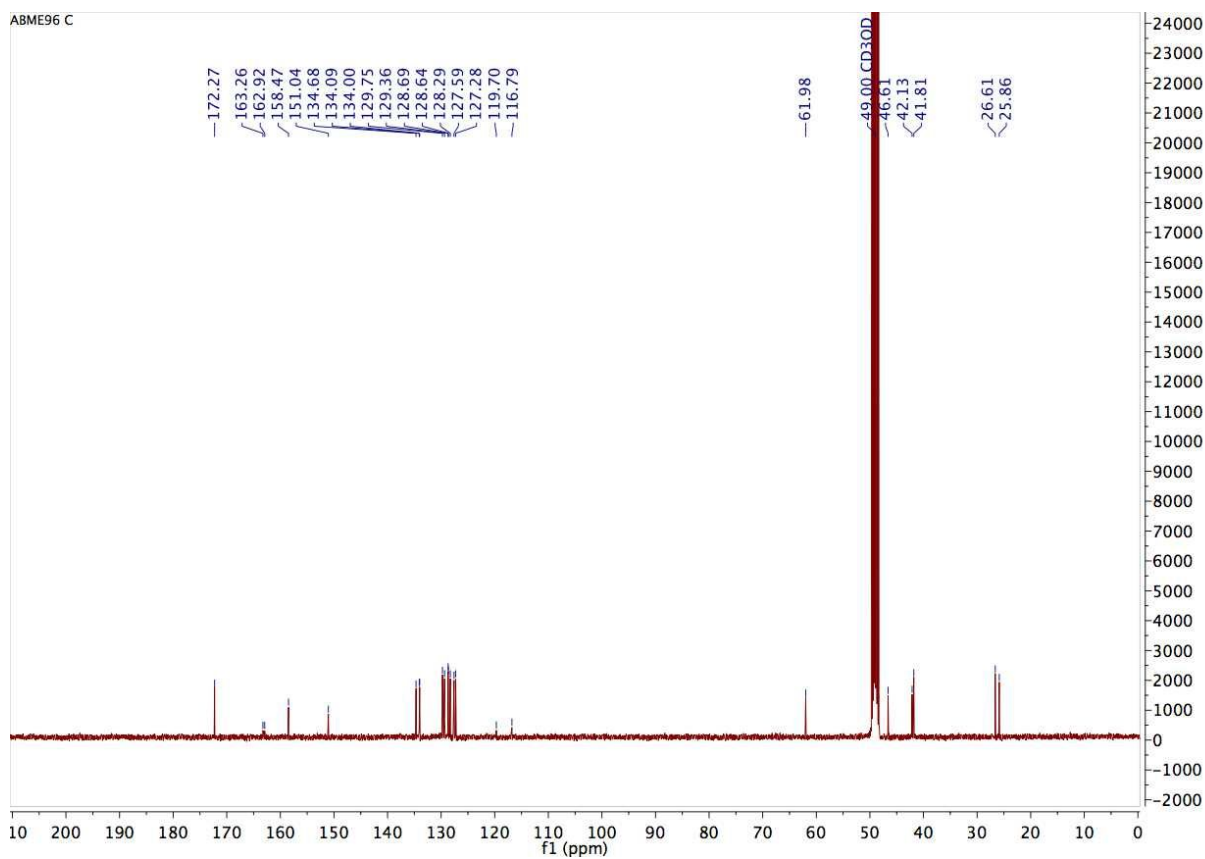
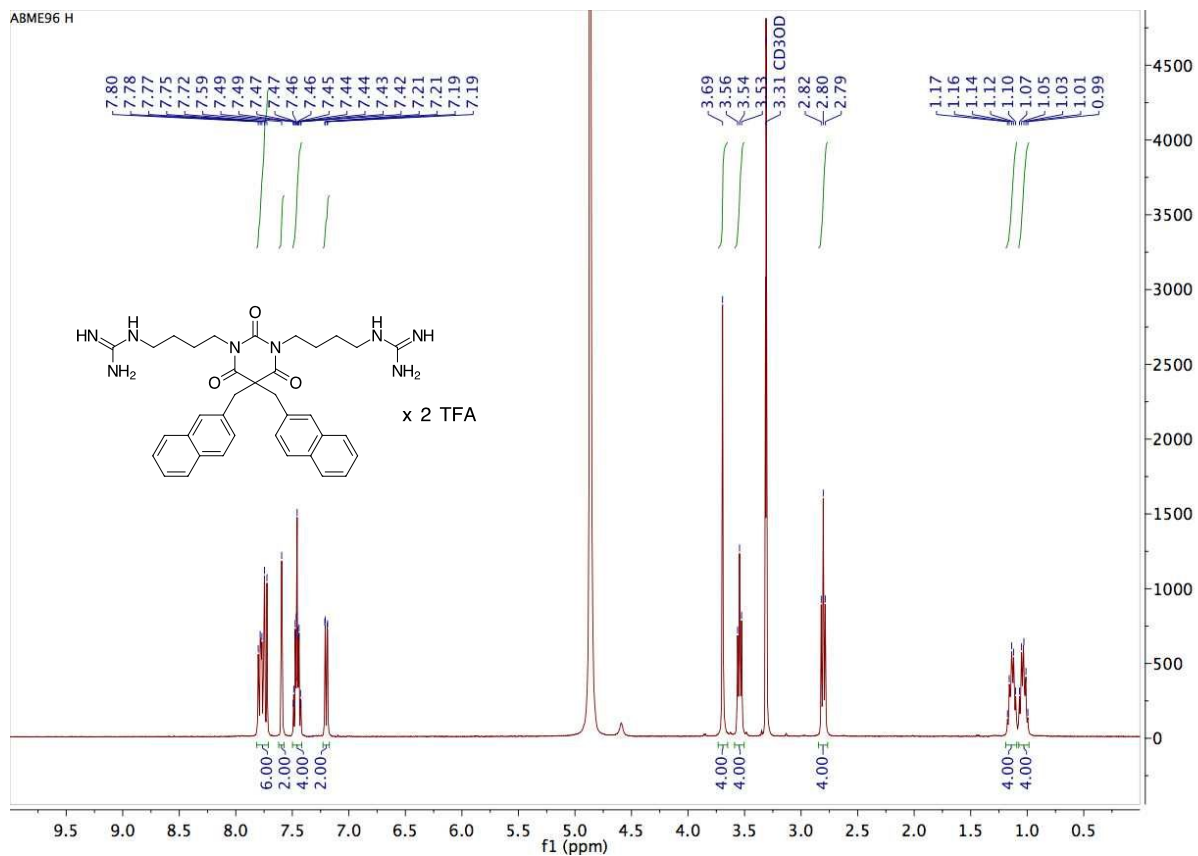


7. ^1H and ^{13}C NMR spectra of guanidine barbiturates (7)

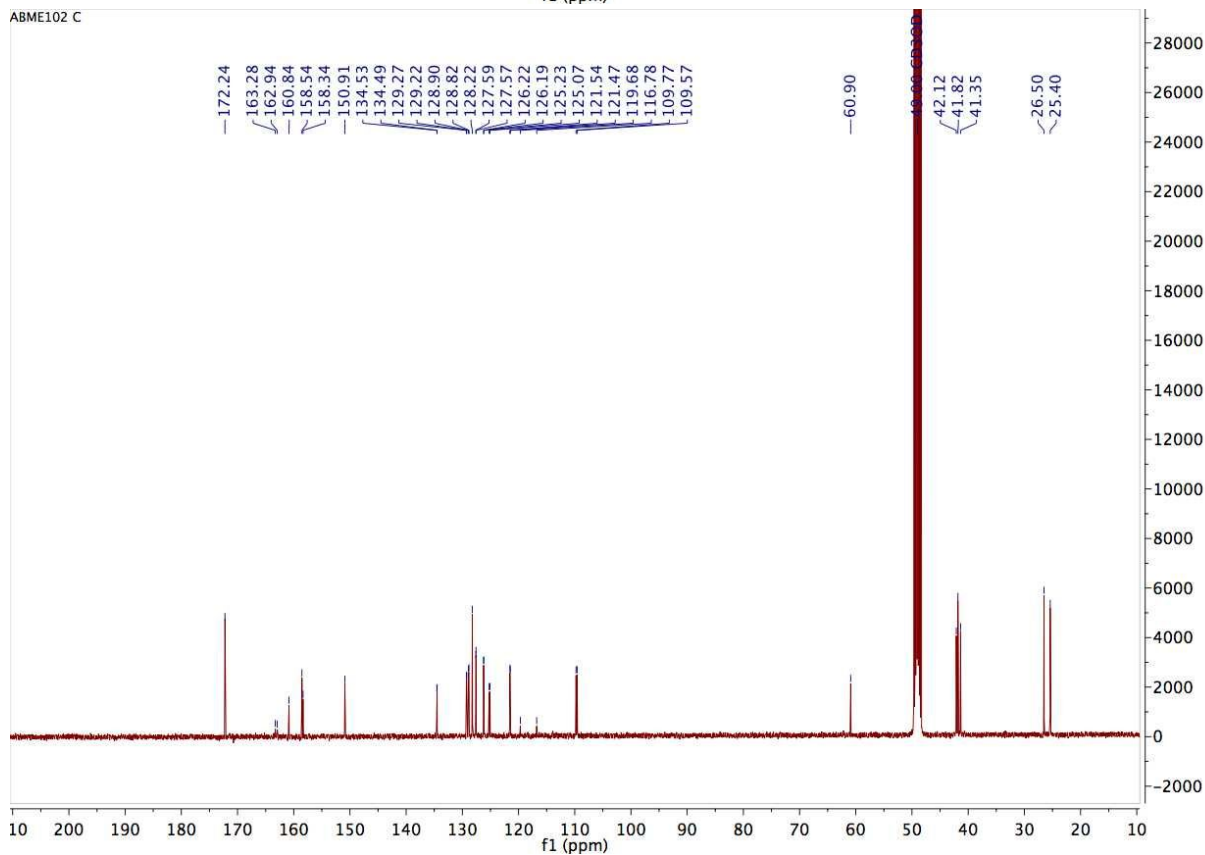
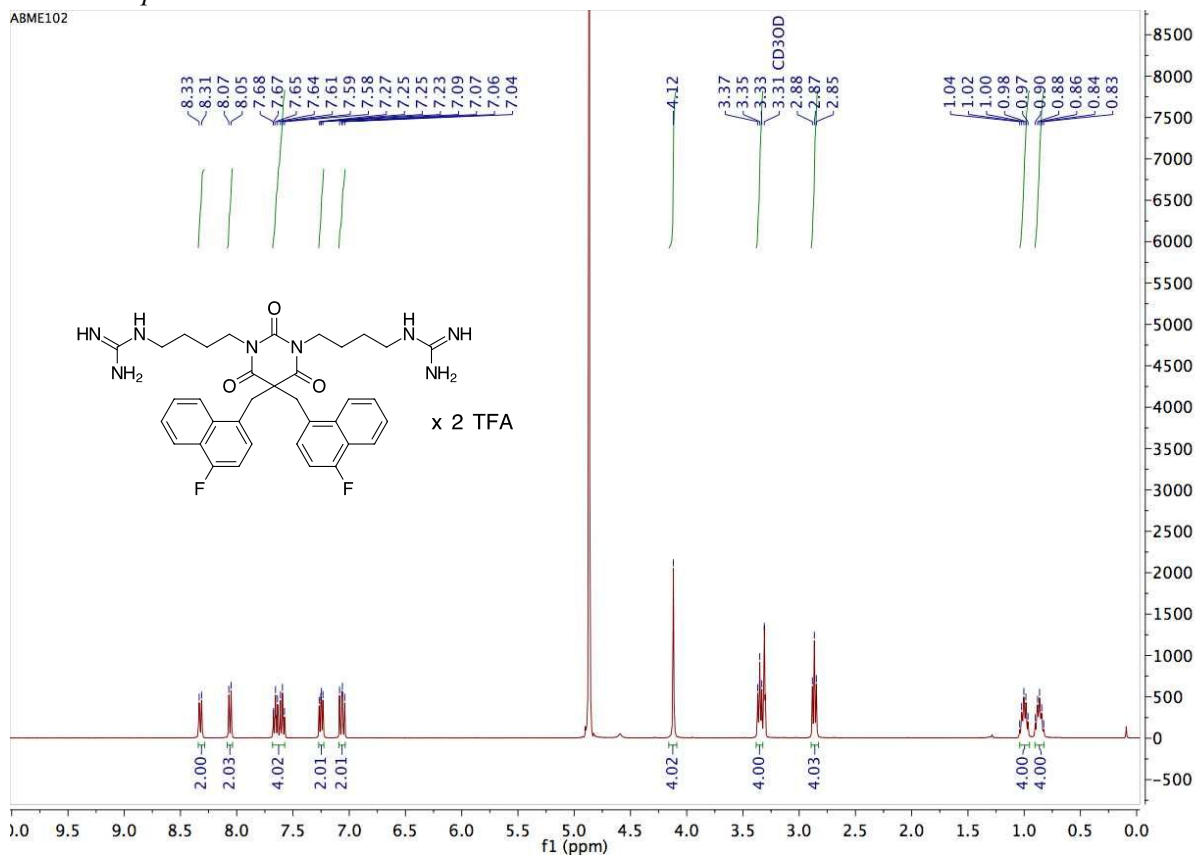
7.1 Compound 7a



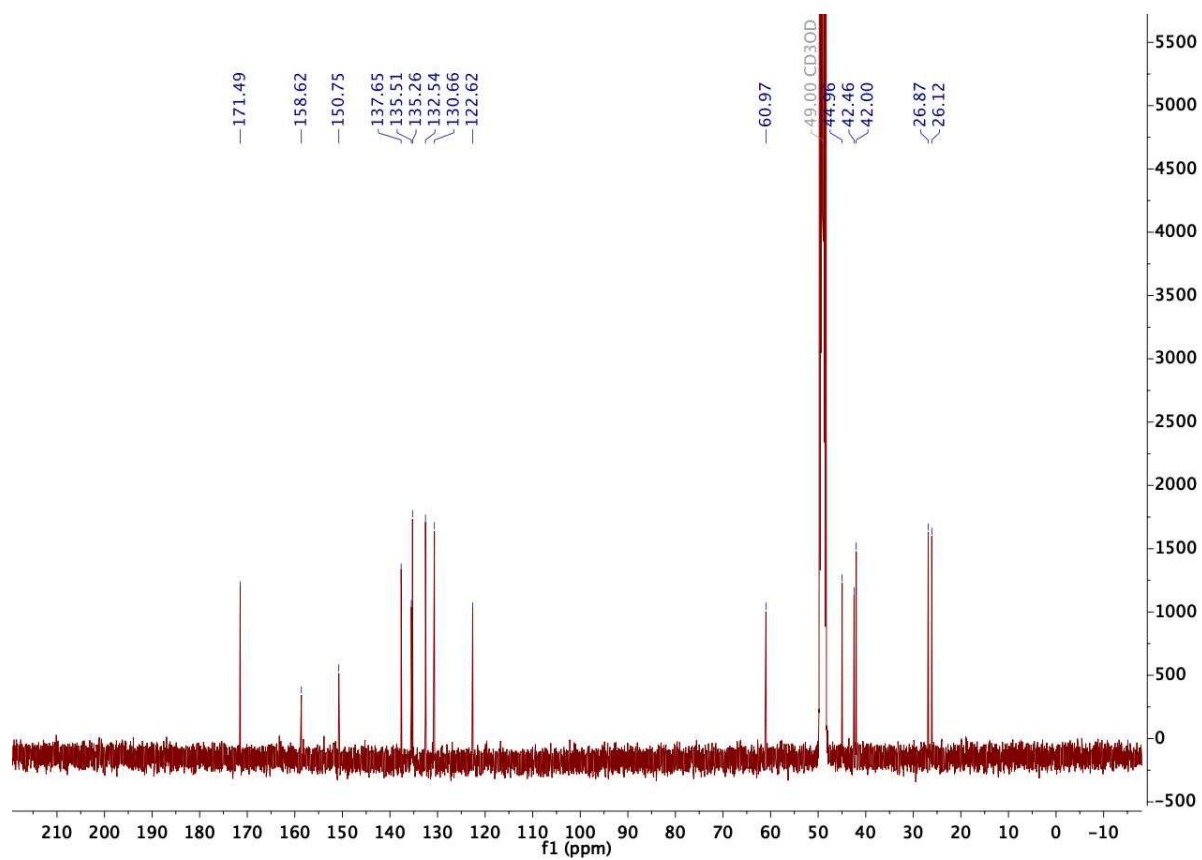
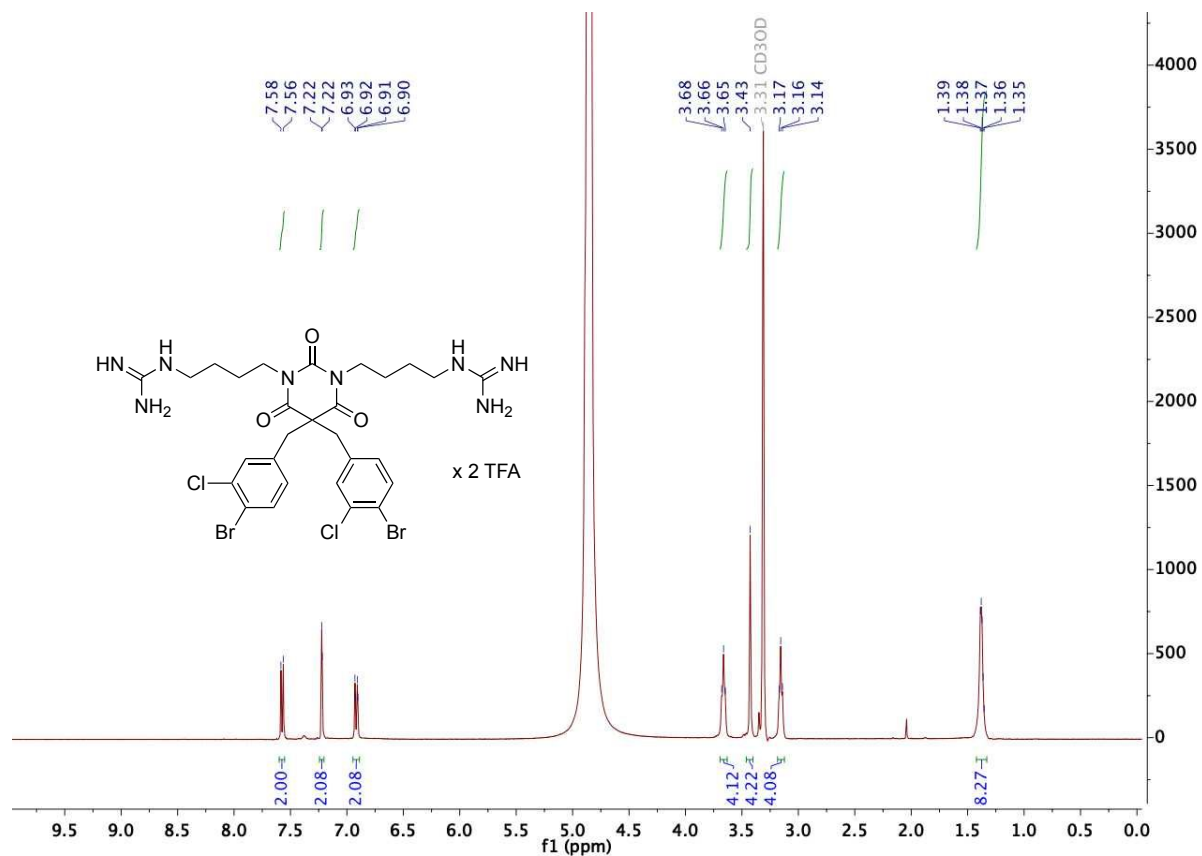
7.2 Compound 7b



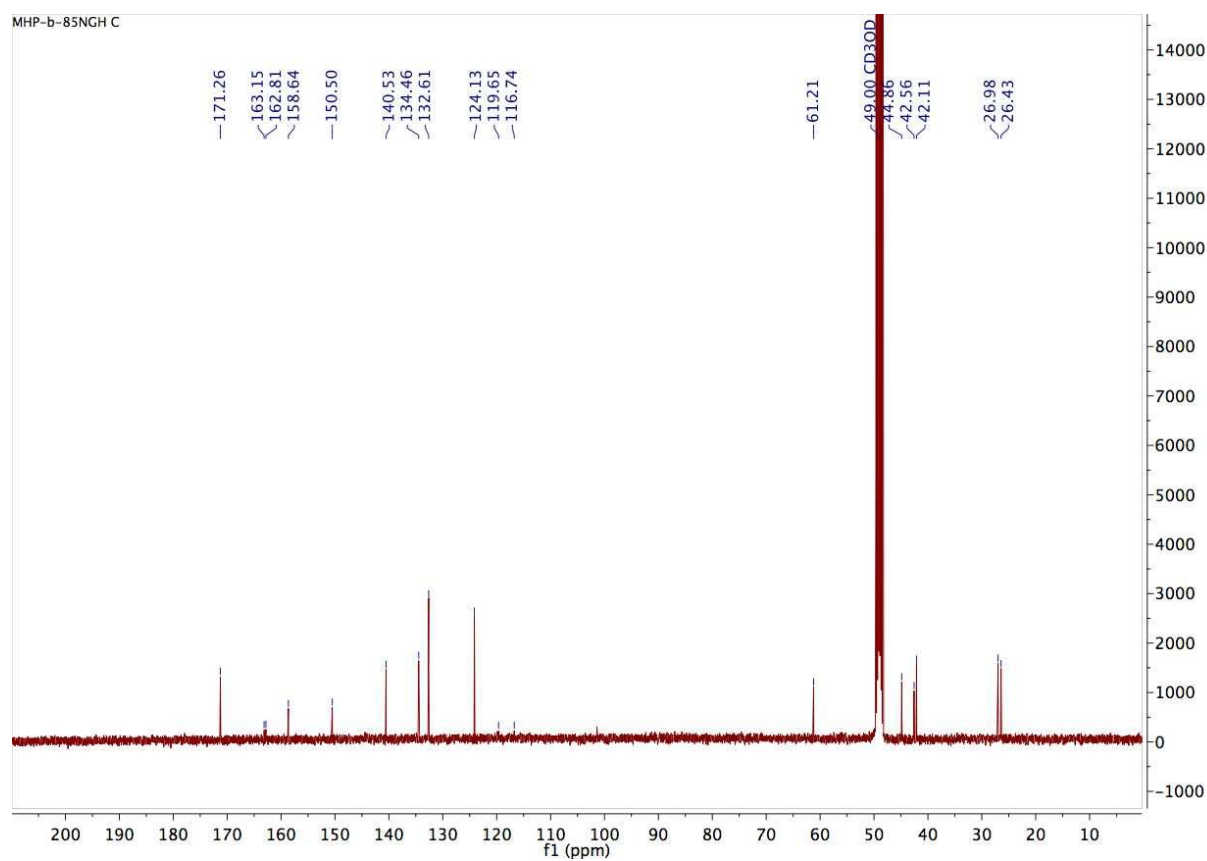
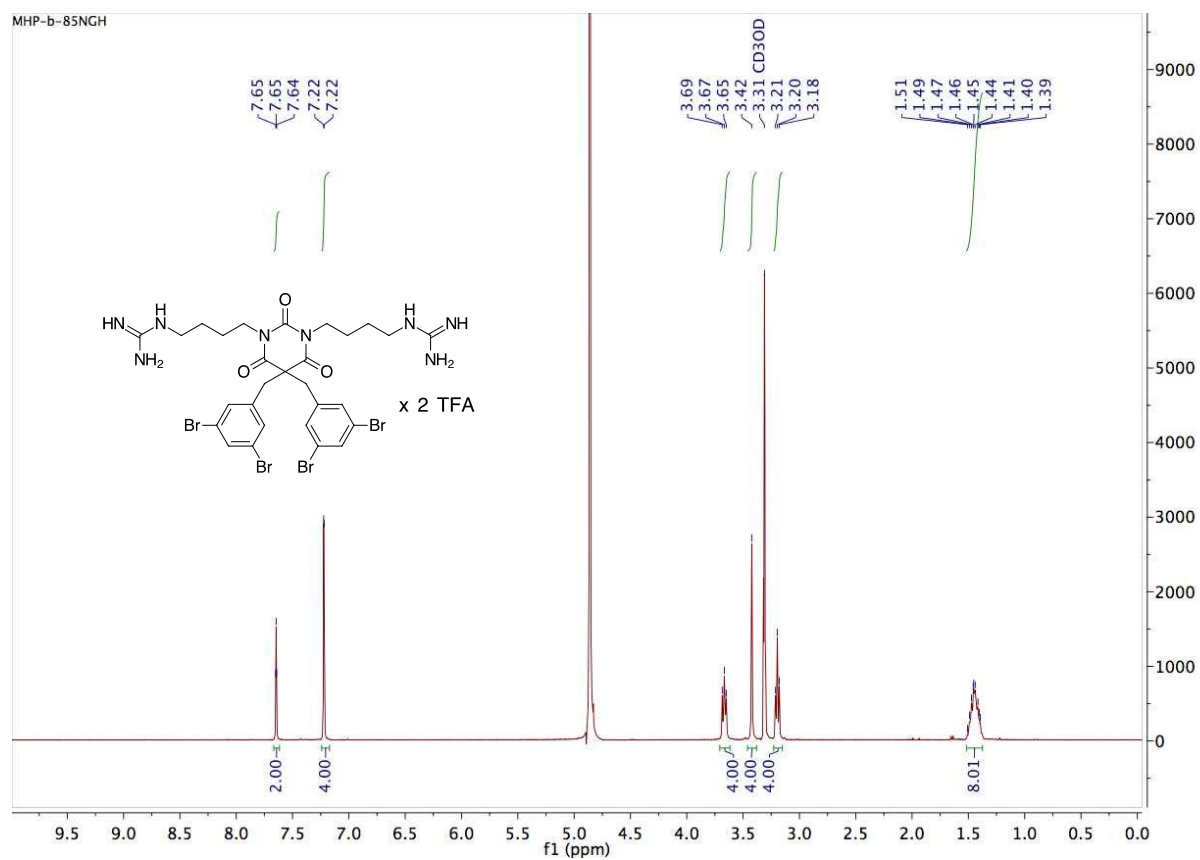
7.3 Compound 7c



7.4 Compound 7d

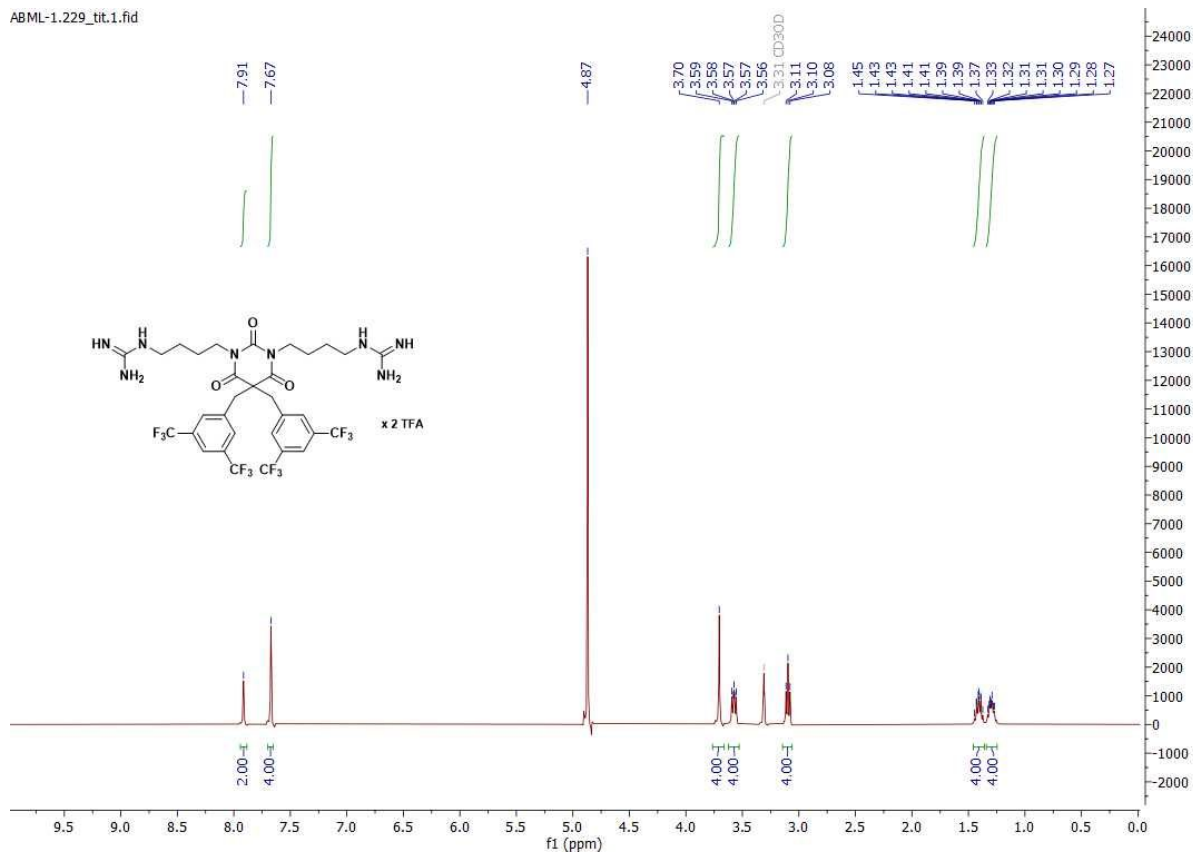


7.5 Compound 7e

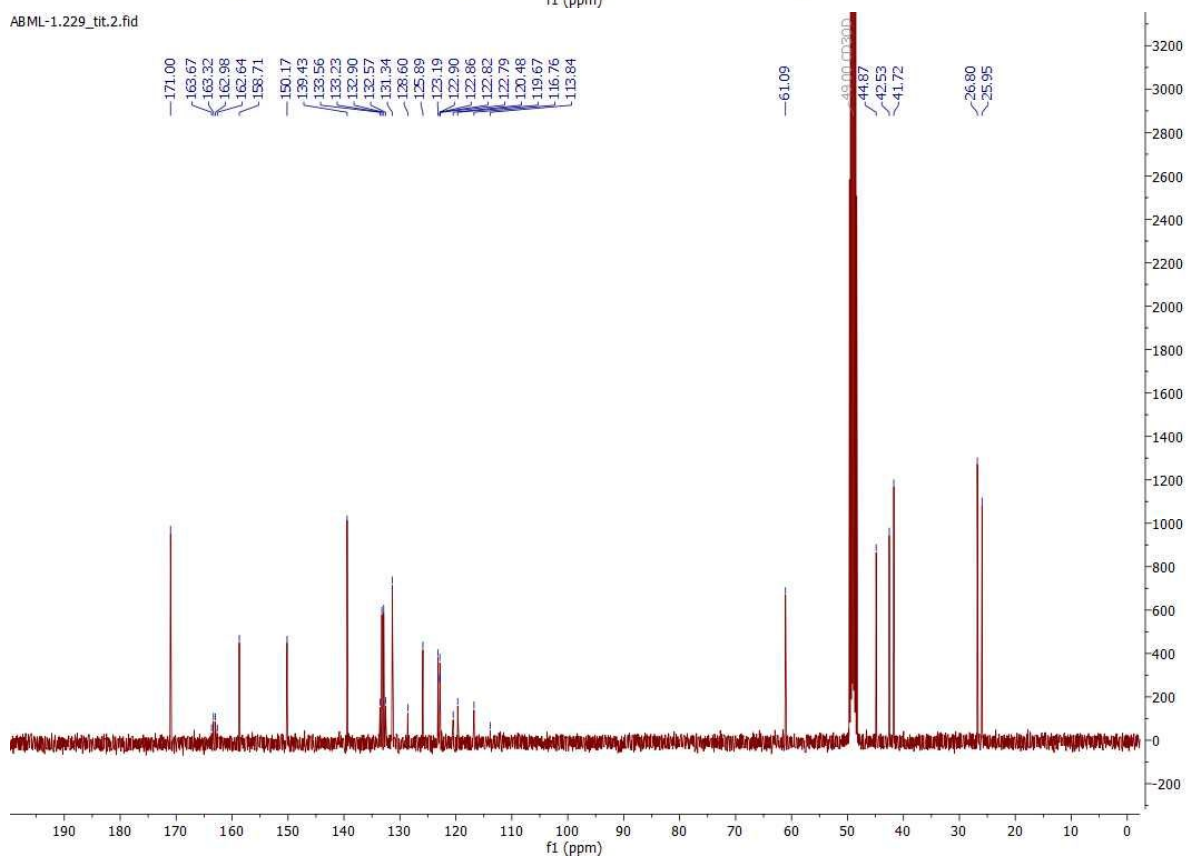


7.7 Compound 7f

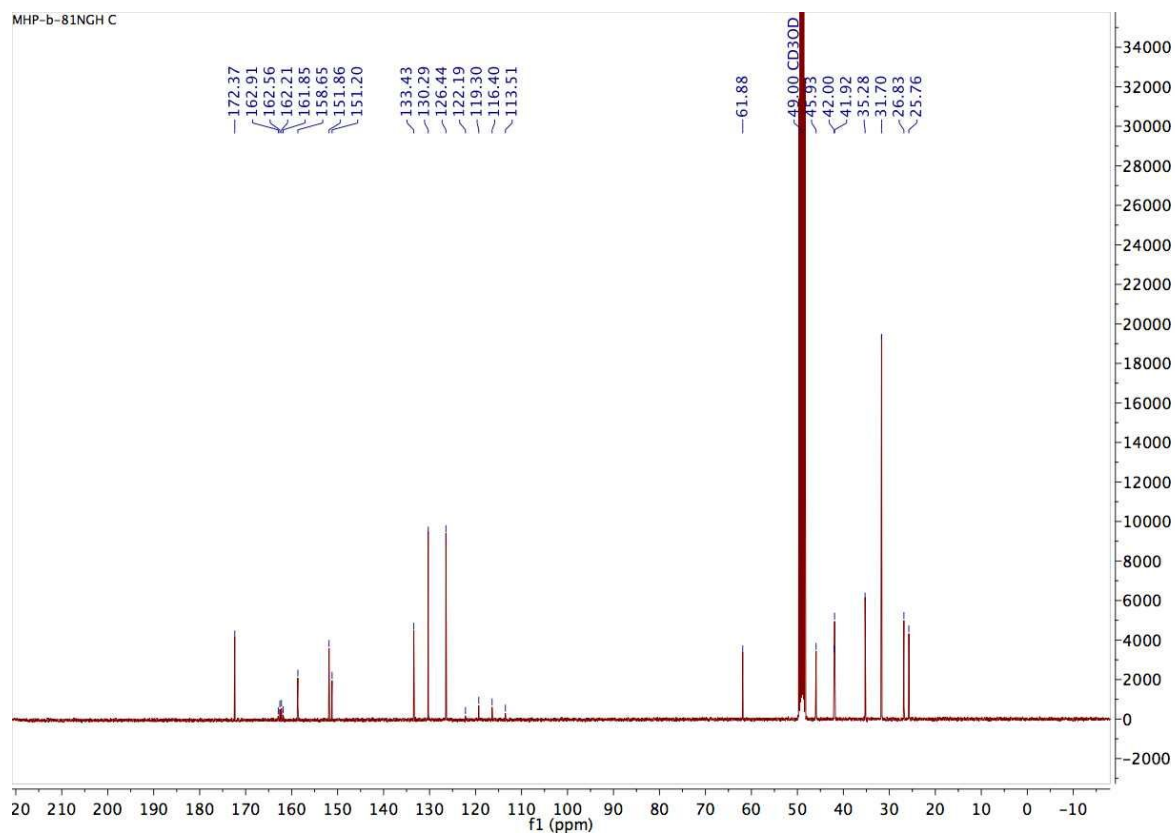
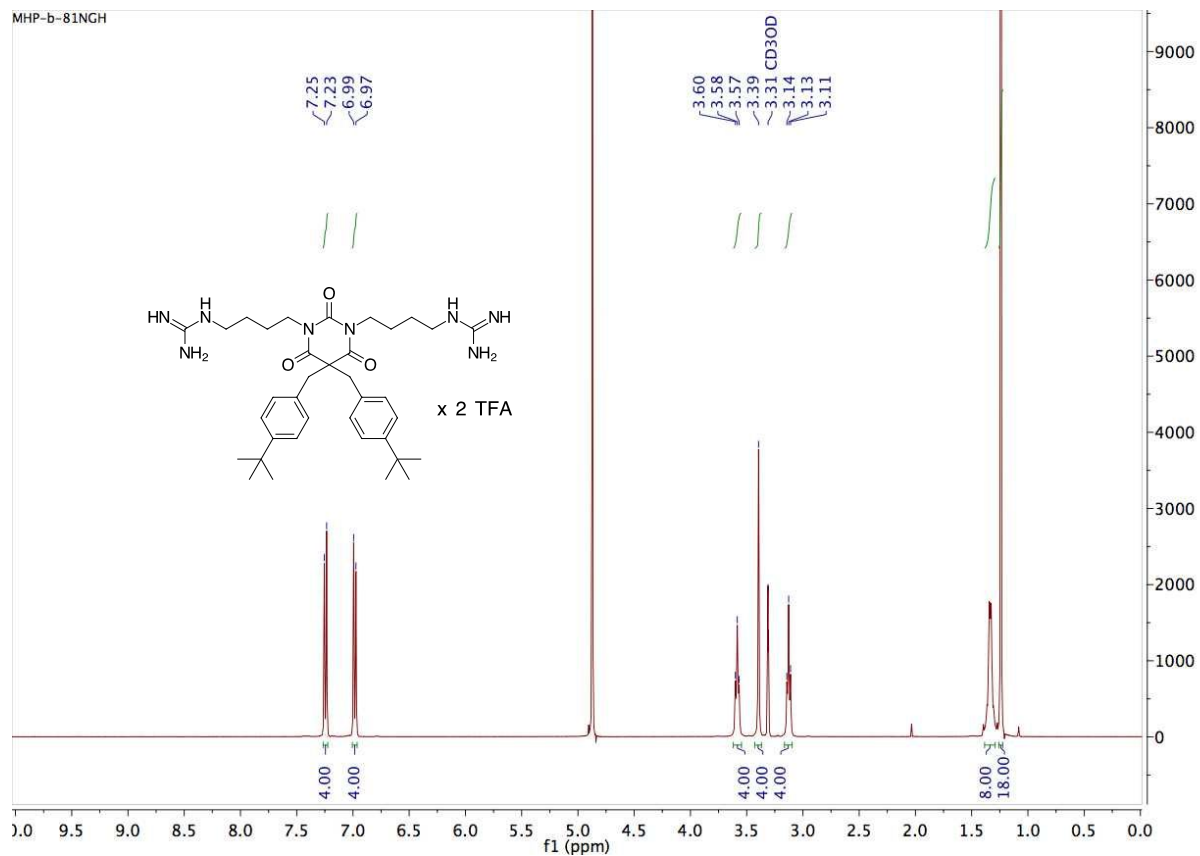
ABML-1.229_tit.1.fid



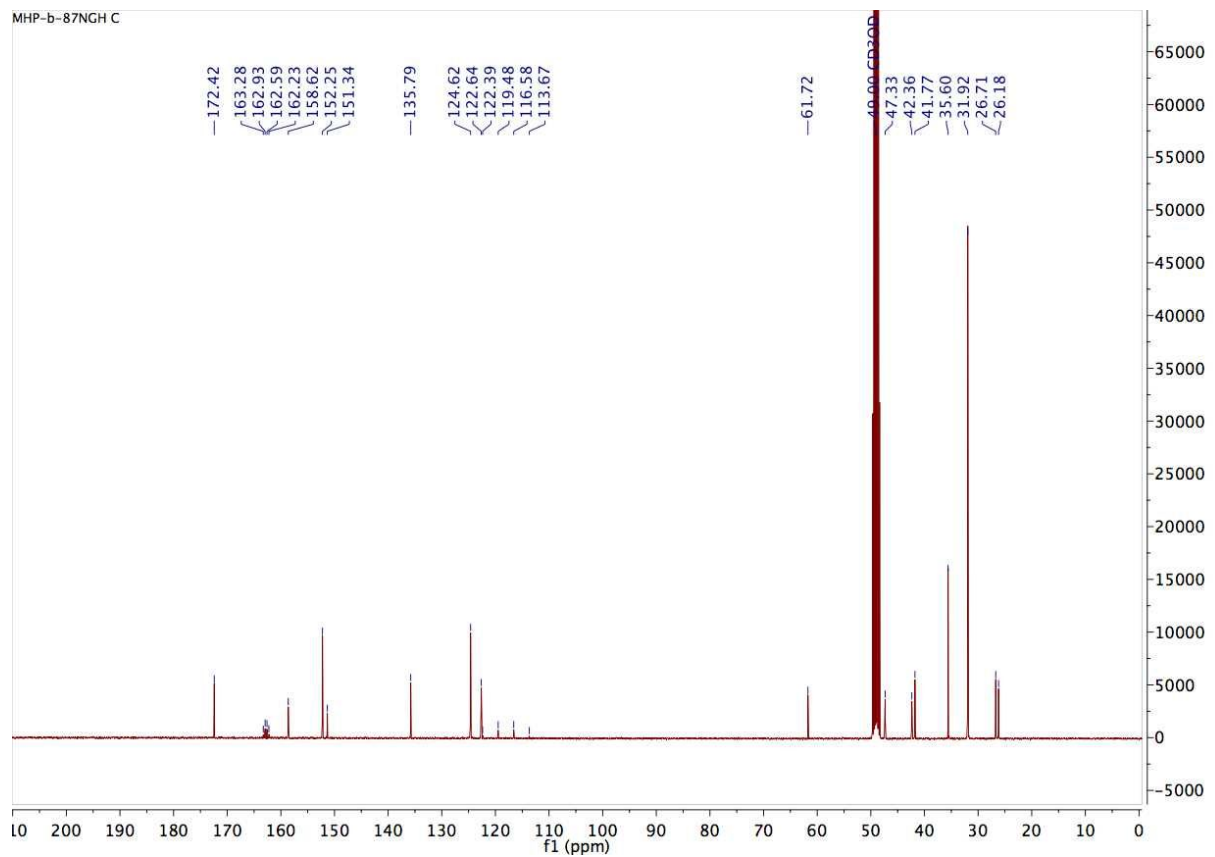
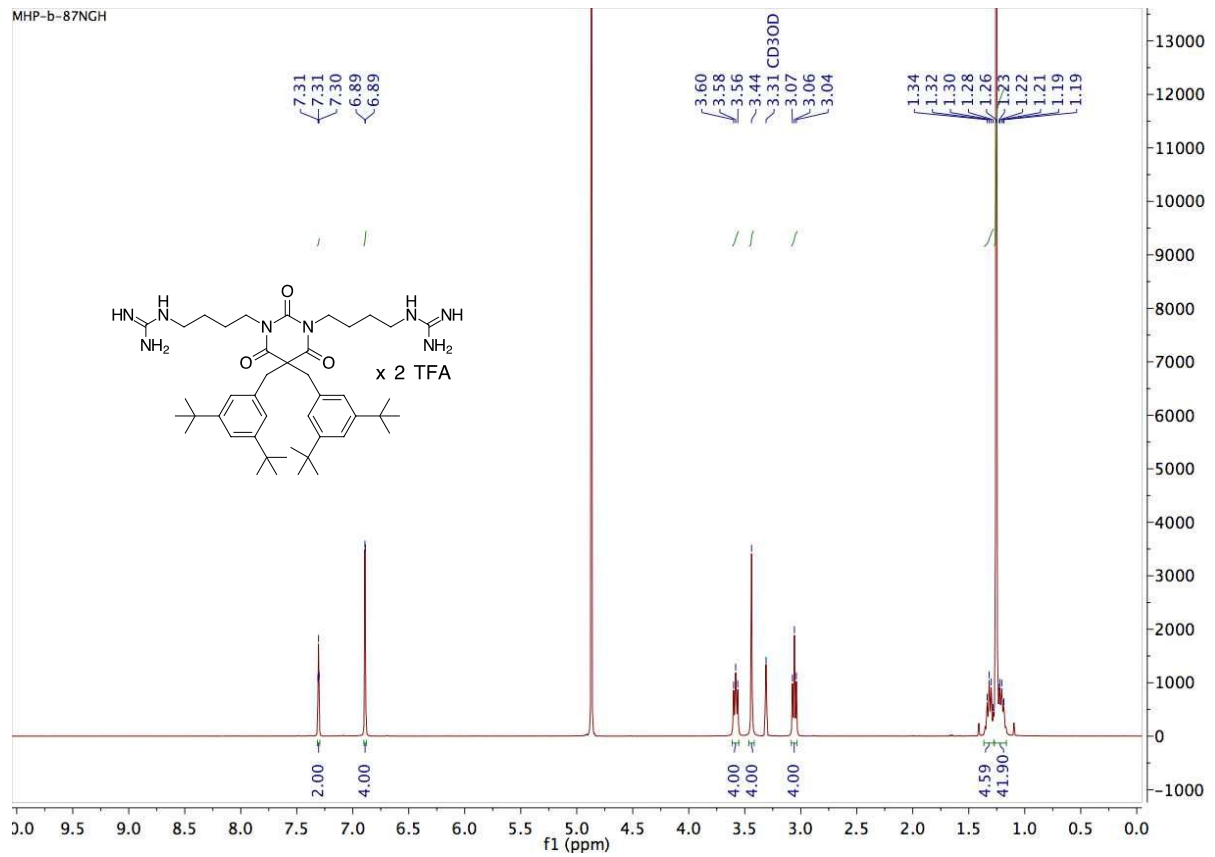
ABML-1.229_tit.2.fid



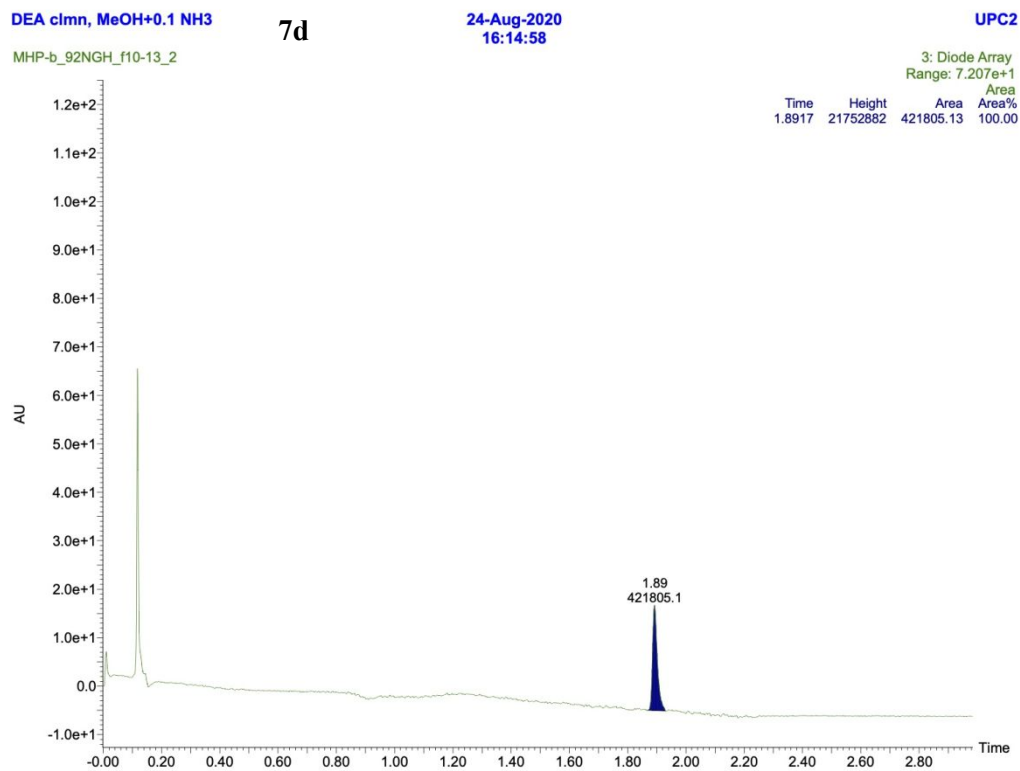
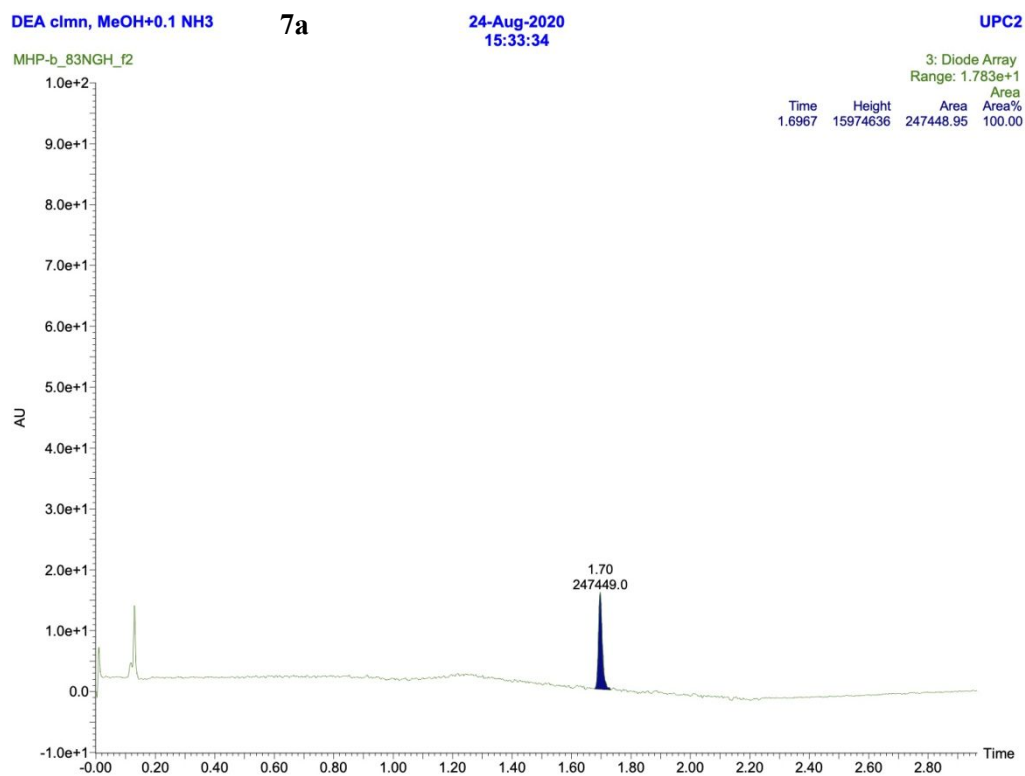
7.8 Compound 7g



7.9 Compound 7h



8. SFC analysis of final compounds



DEA clmn

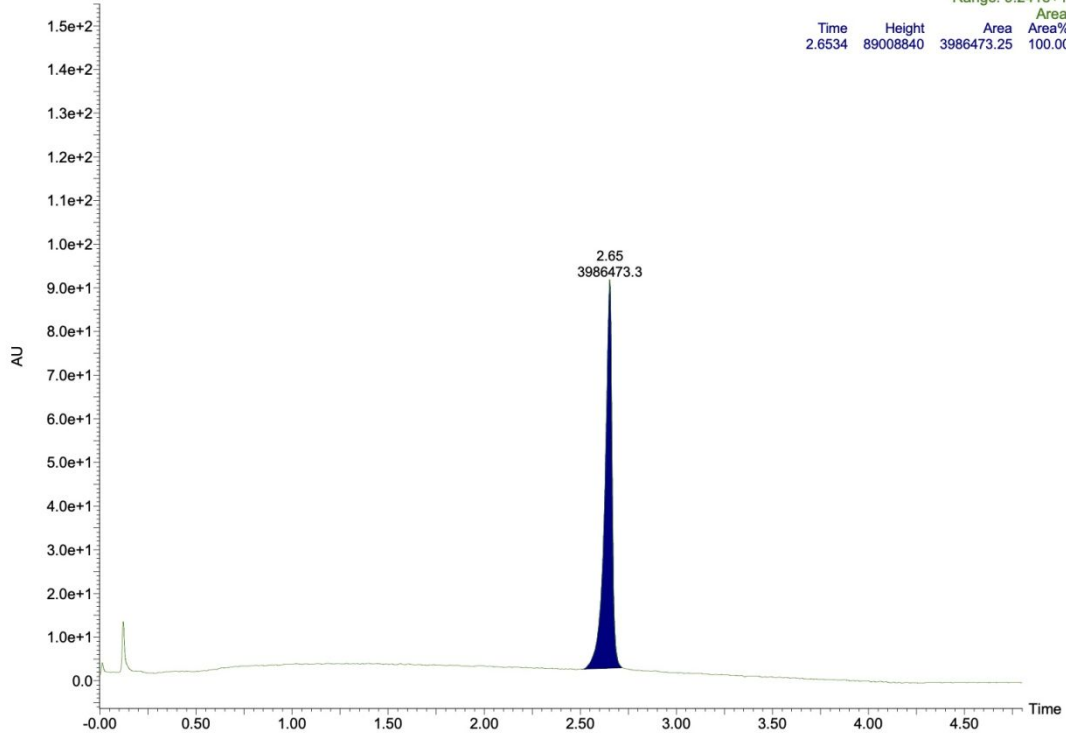
7e

17-Jan-2020
13:11:30

UPC2

ABML218 Sm (Mn, 4x4)

3: Diode Array
Range: 9.241e+1



DEA clmn

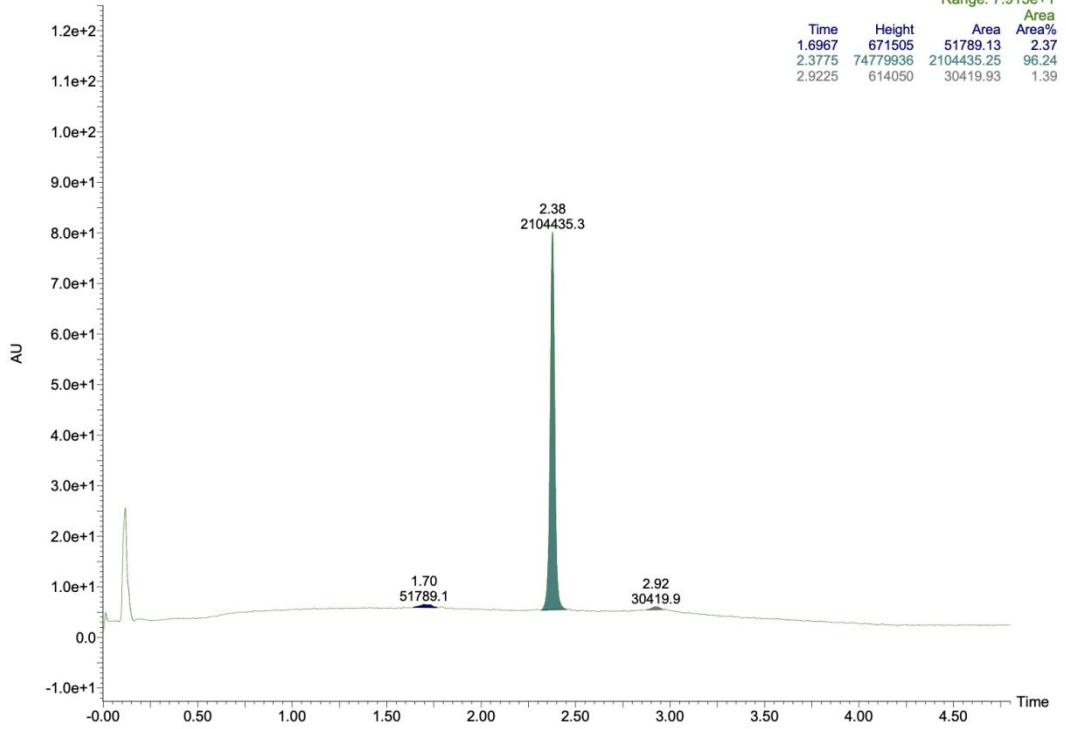
7f

23-Sep-2019
20:00:28

UPC2

ABML229_2 Sm (Mn, 4x4)

3: Diode Array
Range: 7.915e+1



DEA clmn, MeOH+0.1 NH3

7g

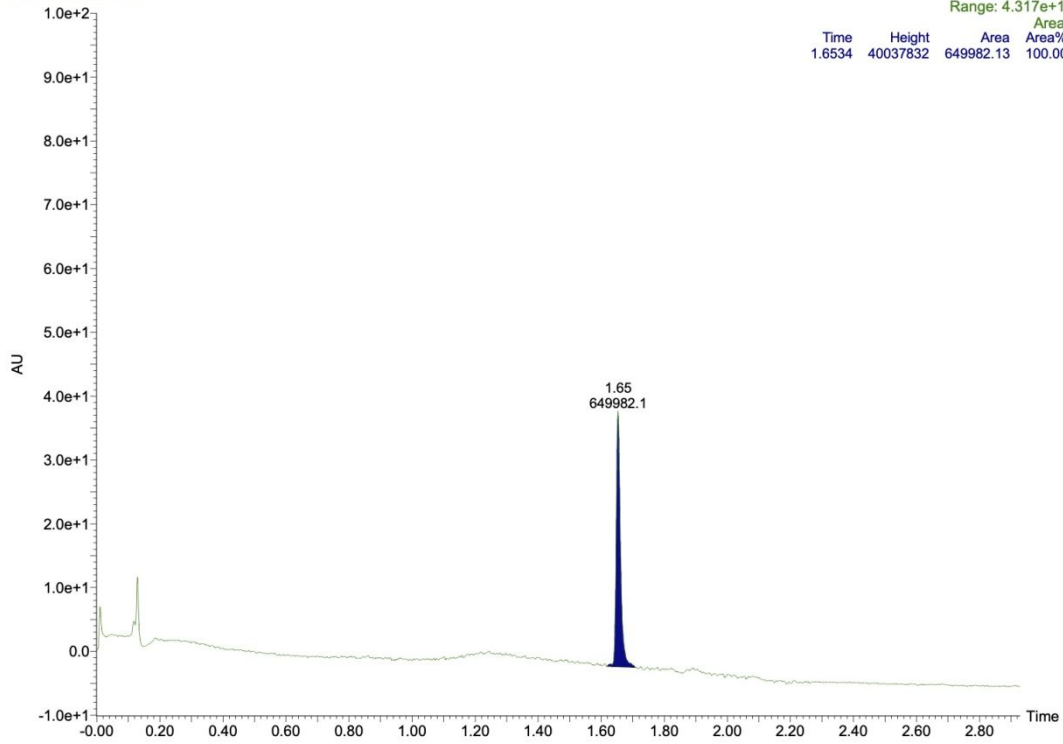
24-Aug-2020
15:38:04

UPC2

MHP-b_81NGH_f16

3: Diode Array
Range: 4.317e+1

Time	Height	Area	Area%
1.6534	40037832	649982.13	100.00



DEA clmn, MeOH+0.1 NH3

7h

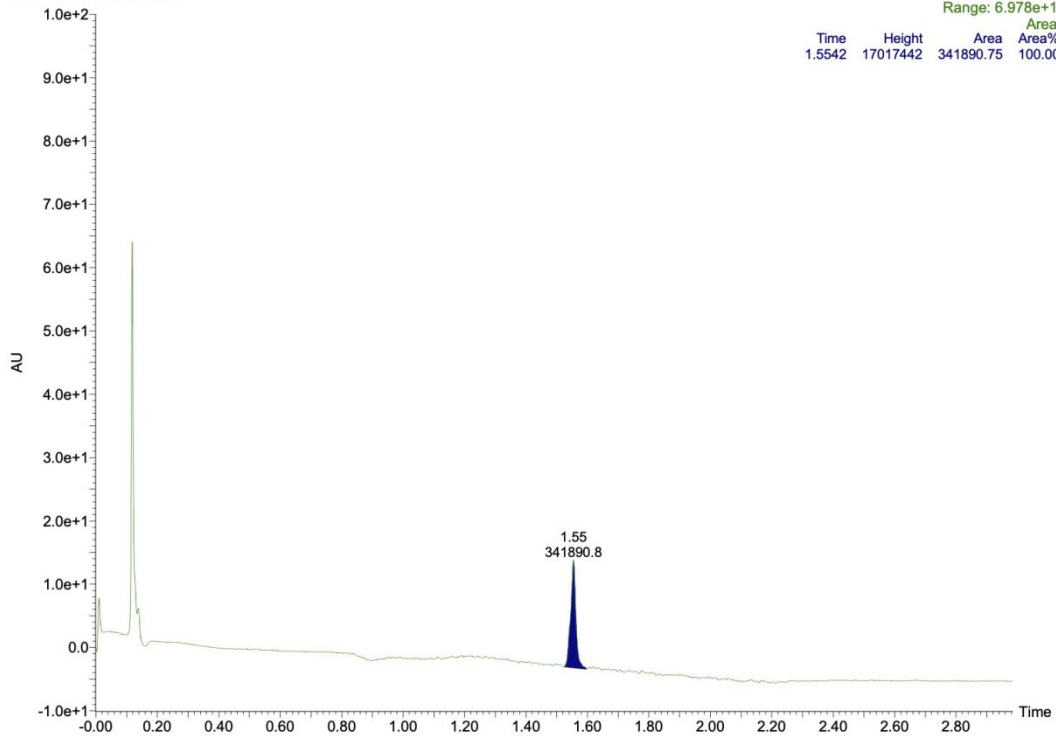
25-Aug-2020
17:05:20

UPC2

MHP-b_87NGH_f8HCl_2

3: Diode Array
Range: 6.978e+1

Time	Height	Area	Area%
1.5542	17017442	341890.75	100.00



9. Mode of action studies

The *viability assay* measures bacterial viability in terms of light production by recombinantly expressed bacterial luciferase originating from the *Photobacterium luminescens lux* operon.¹ Light production by the bacterial *lux* operon is independent of external addition of substrates but is dependent on the pool of reduced flavin mononucleotide (FMN) and long-chain aliphatic aldehydes provided by the bacterium itself. NADH, NADPH and ATP are however necessary to constantly replenish the pool of substrates, which makes the bacterial luciferase a good real time sensor for several metabolic processes and hence bacterial viability.¹

The *membrane integrity assay* is based on the luciferase (*luxI* gene) from the luminous click beetle *Pyrophorus plagiophthalmus*.² In contrast to bacterial luciferase, the light reaction of *luxI* is strictly dependent on the externally added substrate D-luciferin, which at neutral pH diffuses very slowly across biological membranes.² The luciferase-expressing strains will therefore emit a luminescence peak only if their membranes are disrupted. Increased influx of D-luciferin results in an initial increase in light production, in which the curve *peaks* rapidly, followed by a decrease in light production as the ATP of dying cells is consumed.

Both assays were performed in a well-by-well format where the bacterial inoculum was injected directly to a well with an aliquot of the analyte. Using this setup, light emission could be recorded immediately (ca. 1.5 s) after injection and in 1 s intervals for 150 s.

The two different biosensor systems evaluate the effects on bacterial viability and membrane integrity, respectively, which are closely linked functionalities in bacterial cells. The *viability assay* measures bacterial viability in terms of light production by recombinantly expressed bacterial luciferase originating from the *Photobacterium luminescens lux* operon.¹ Light production by the bacterial *lux* operon is independent of external addition of substrates but is dependent on the pool of reduced flavin mononucleotide (FMN) and long-chain aliphatic aldehydes provided by the bacterium itself. NADH, NADPH and ATP are however necessary to constantly replenish the pool of substrates, which makes the bacterial luciferase a good real time sensor for several metabolic processes and hence bacterial viability.¹ The *membrane integrity assay* is based on the luciferase (*luxI* gene) from the luminous click beetle *Pyrophorus plagiophthalmus*.² In contrast to bacterial luciferase, the light reaction of *luxI* is strictly dependent on the externally added substrate D-luciferin, which at neutral pH diffuses very slowly across biological membranes.² The luciferase-expressing strains will therefore emit a luminescence peak only if their membranes are disrupted. Increased influx of D-luciferin results in an initial increase in light production, in which the curve *peaks* rapidly, followed by a decrease in light production as the ATP of dying cells is consumed. Both assays were performed in a well-by-well format where the bacterial inoculum was injected directly to a well with an aliquot of the analyte. Using this setup, light emission could be recorded immediately (ca. 1.5 s) after injection and in 1 s intervals for 150 s. The bacteriolytic agent chlorhexidine, known for its membrane-disruptive properties, was analysed for comparison.³

10. Theoretical calculations - geometry optimisation of conformations

Geometry optimizations of **6e** (3,5-di-Br) and **7e** (3,5-di-Br) were performed to explore the most stable conformations of the molecules and to better understand their interaction with a phospholipid membrane surface. The amine **6e** (3,5-di-Br) and the guanidine **7e** (3,5-di-Br) gave similar energy differences and distortions between the different conformations and the results for **7e** (3,5-di-Br) are shown in Figure 6. Three low-energy conformations were determined mainly differing in the orientation of the benzylic sidechains. In the *up* (**7e_{up}**), *down* (**7e_{down}**) and *up-down* (**7e_{up-down}**) conformations, the benzylic sidechains were either directed upwards in a W-shape, downwards, or having one sidechain pointing up

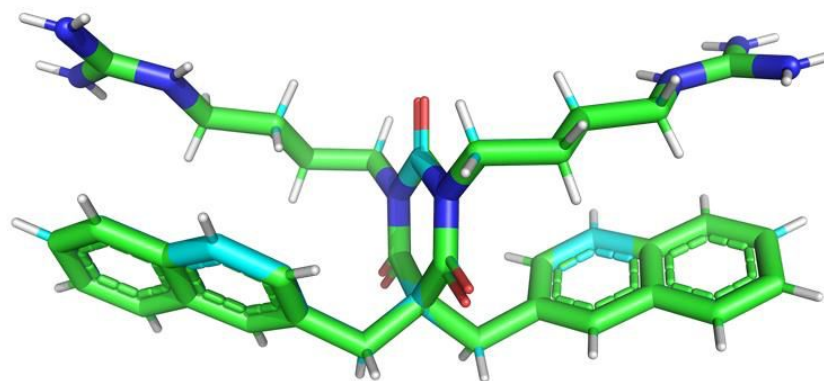
and the other pointing down. The $7e_{up}$ conformation was lowest in energy, whereas $7e_{up-down}$ was 4.9 kcal/mol higher and $7e_{down}$ was 9.8 kcal/mol higher in energy than $7e_{up}$.

In the $7e_{down}$ conformation the distance between the closest two carbon atoms of the benzylic sidechains was 2.96 Å (**Figure 6**). In contrast, in the $7e_{up}$ conformation the upwards orientation of the benzylic sidechains allowed a more tetrahedral geometry at the benzylic CH₂ carbon and prevented unfavourable interactions between the benzylic sidechains, and thereby lowering the overall energy of the molecule. In the $7e_{up}$ conformation, the barbiturate ring was also planar as measured from the top carbonyl carbon, through the plane of the ring, and to the sp³ carbon opposite from the carbonyl carbon (180.0°), whereas the angle was decreased to 145.6° in the $7e_{down}$ conformation. No other lower energy conformations were found with any favourable Br---NH_x group interactions in neither **6e** (3,5-di-Br) nor **7e** (3,5-di-Br). Therefore, stabilization of the $7e_{up}$ conformation resulted from the elimination of the unfavourable steric interactions between the benzylic sidechains in the $7e_{down}$ conformation. Energy comparisons placed the $7e_{up-down}$ conformation between the $7e_{up}$ and $7e_{down}$ as one might expect based on a steric argument.

The higher potency of **6e** (3,5-di-Br) and **7e** (3,5-di-Br) may be rationalized by evaluating their low energy conformations with respect to interactions with a phospholipid membrane surface. Molecules with a larger surface are expected to interact with a larger area of the phospholipid membrane surface. The larger distance between the sidechains in the *up* conformation caused the molecules to have a larger surface area which seemed important, as opposed to when both sidechains were pointing downwards and potentially could have penetrated deeper into the acyl chain region of the phospholipid membrane. The *up-down* geometry is expected to have a surface area somewhere between the *up* and *down* conformations, and we anticipate the *up-down* conformation to contribute less to the molecule's activity.

11. X-Ray crystallography of **7b**

Crystals for X-ray analysis could only be obtained for **7b** (2-Nal). The X-ray structure of **7b** (2-Nal) supported the conformations suggested by DFT calculations and NMR structure analysis. As depicted in **Figure S1** the crystal structure of **7b** (2-Nal) adopted a similar W-shaped conformation as seen for $7e_{up}$ (3,5-di-Br) in **Figure 6**. Structure of the asymmetric unit of **7b** (2-Nal) with thermal ellipsoids can be seen in **Figure S2**.



*Figure S1. X-ray structure of **7b** (2-Nal) showing a similar up or W-shaped conformation as demonstrated for **7e** (3,5-di-Br) by DFT calculations and NMR.*

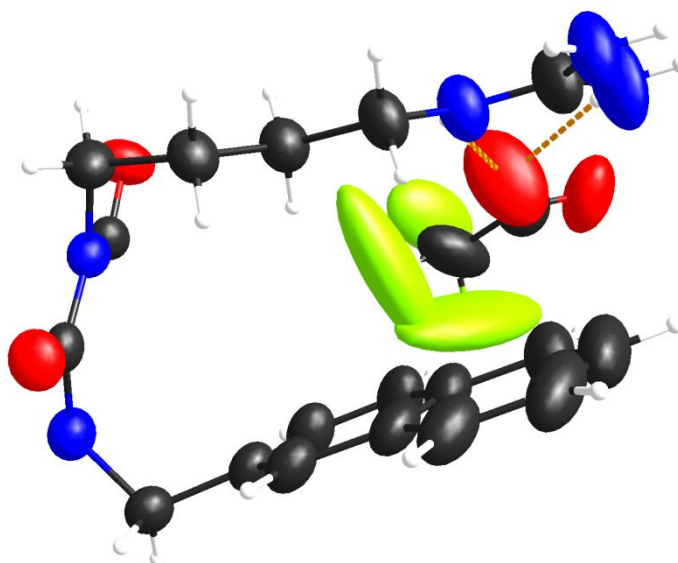


Figure S2. Structure of the asymmetric unit of 7b with thermal ellipsoids to visualize atomic disorder showing half of the molecule, the rest remainder can be shown by expanding the symmetry operations.

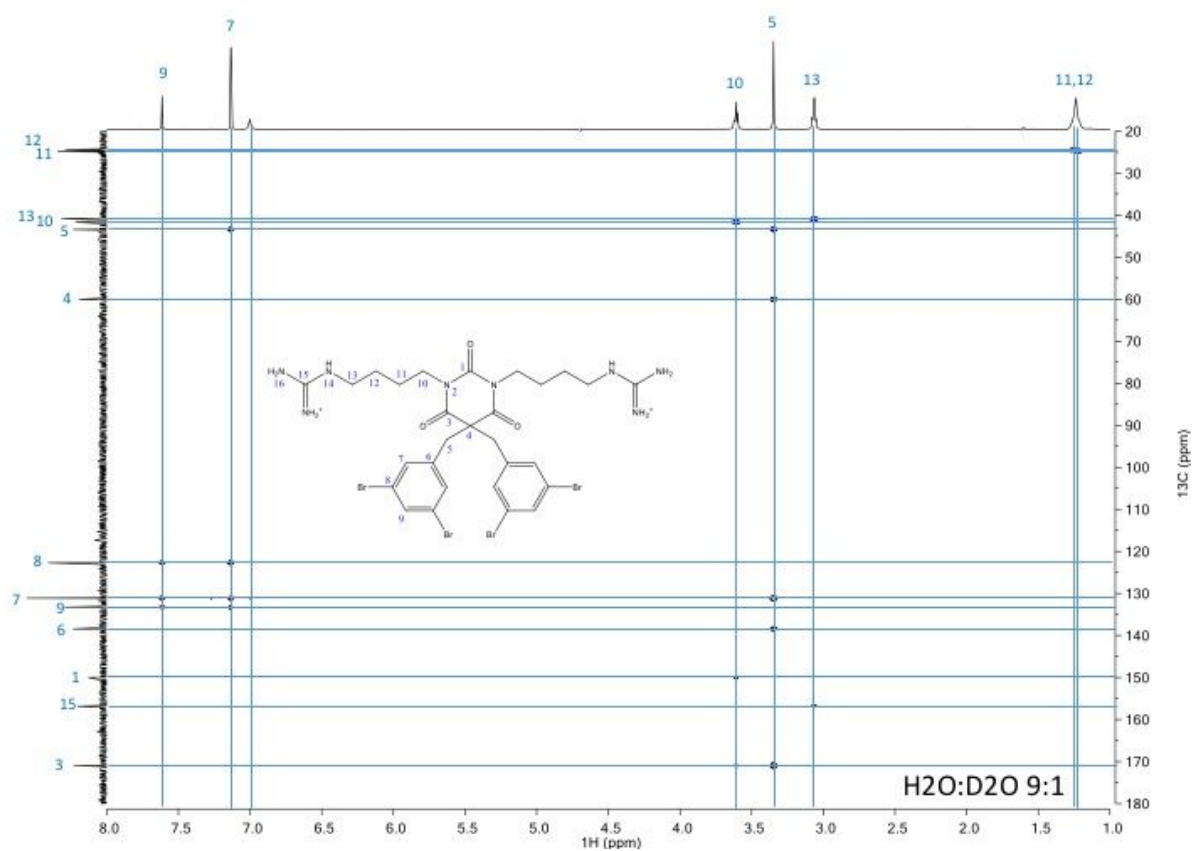
12. NMR conformational analysis of 7e

ROESY spectra acquired in water and micelle (SDS – sodium dodecyl sulphate) solutions of the guanidine barbiturate **7e** (3,5-di-Br) were used to qualitatively assess the conformation experimentally (**Figure S3 -Figure S5**). NOESY would normally have been preferred for conformational analysis since ROESY is prone to TOCSY contributions, but the intermediate size of the molecule resulted in very weak NOE build-up in water.

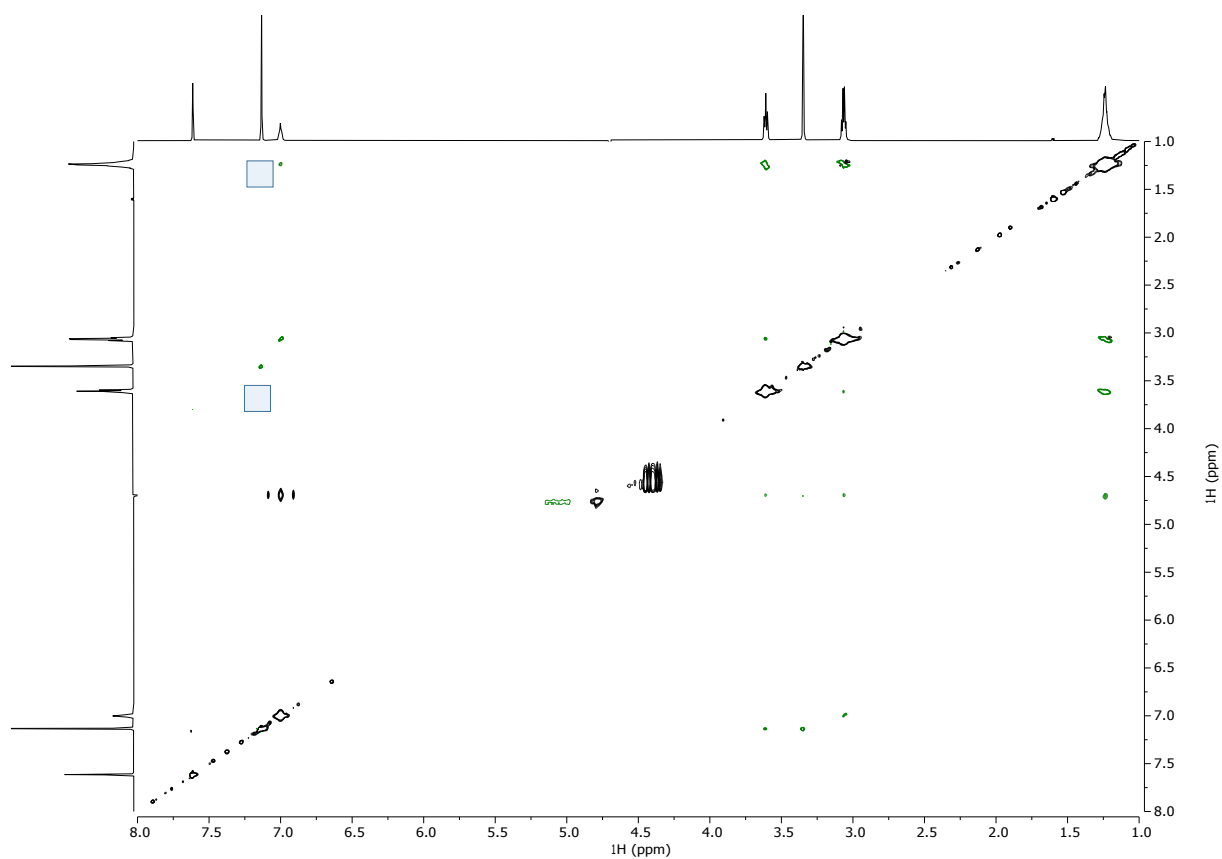
The guanidine barbiturate **7e** (3,5-di-Br) displayed only one set of signals for every set of protons, indicating that the conformational time average had a two-fold symmetry. It is assumed that there are very fast rotations around all bonds in the guanidine sidechains due to isochronous geminal protons, and that the 3,5-dibromo benzylic sidechains were relatively free to rotate. The normalized 300 ms ROESY volumes were used to estimate the conformational preferences in solution, using the H7 to H5 correlation as an internal reference (**Figure S4**). Because the molecule is highly flexible, we refrain from discussing distances, but rather make qualitative observations based on ROE build-up. All ROESY correlations relevant to the conformation are shown schematically in **Figure S4**.

The structural NMR data in water supported the orientations of the benzylic sidechains described by DFT calculations above. It was evident from the ROESY detectable correlations between H7 and H10 – H12 (5-10% of the reference volume) that the benzylic sidechains and the barbiturate ring adopted the W-shape (similar to the **7e_{up}** conformation in **Figure 6**) and interacted with the guanidine sidechains rather than stacking with each other. This was also supported by H7 and H9 having chemical shifts in the expected region for aromatic ring protons, i.e., no significant anisotropic shielding (face-face stacking) or deshielding (face-edge stacking) was observed. The guanidine sidechain protons showed only weak correlations to the H7 proton, and there were no detectable correlations to H9, suggesting that the aliphatic chain on average was pointing away from the ring surfaces (see **left** side of **Figure S5**). There were no dramatic conformational changes in SDS, but there was a shift of populations that made the guanidine sidechains spend more time closer to the 3,5-dibromophenyl rings (see **right** side of **Figure S5**). This was reflected in the volumes of the H7/H11,12 cross peaks, that increased from

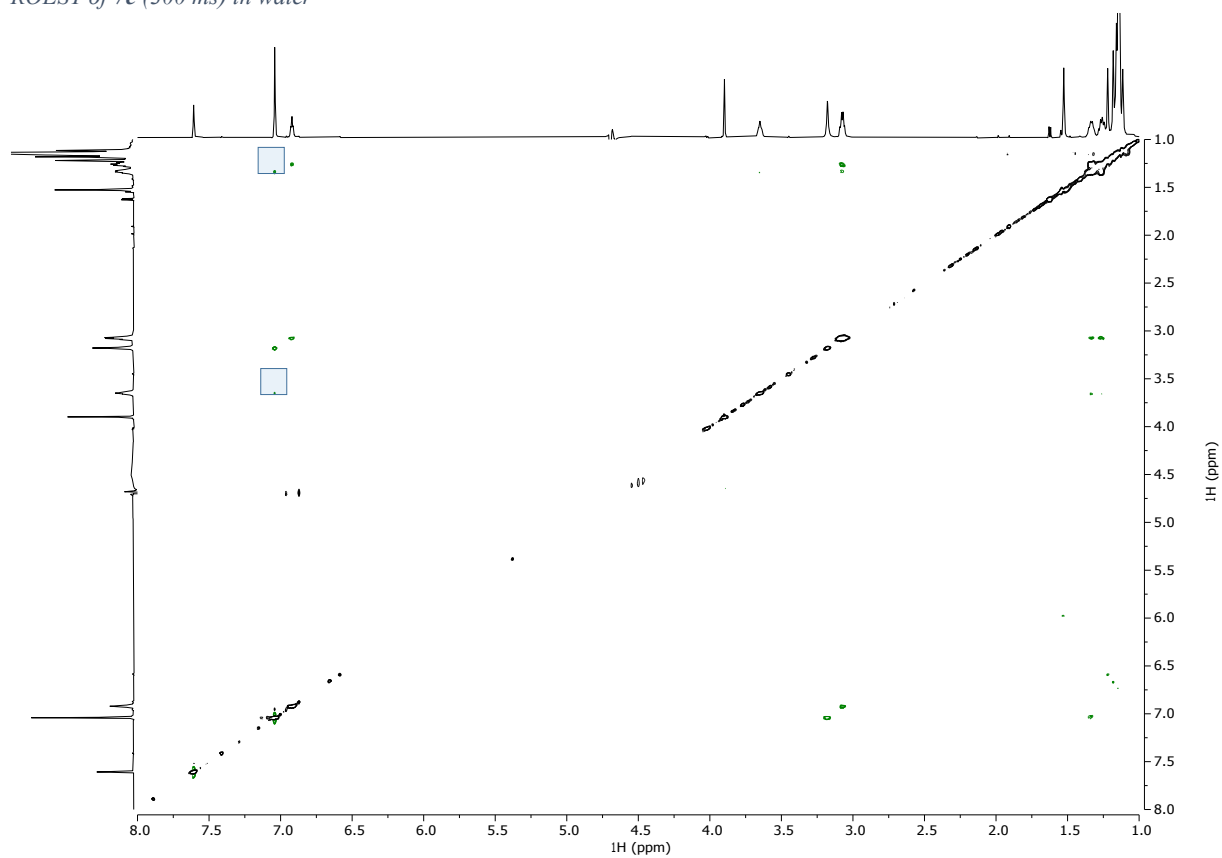
~10% to ~40% of the reference volume. In no case were there any detectable correlations involving the para-proton H9. There was also a small net deshielding effect in SDS of the guanidinium sidechain protons, as well as a shielding effect on the H7 and H5 protons, supporting a shift in conformational populations of the 3,5-dibromophenyl ring positions in SDS.



HMBC + HSQC of 7e in H₂O:D₂O (9:1).



ROESY of **7e** (300 ms) in water



ROESY of **7e** (300 ms) in SDS

Figure S3. Top: HMBC + HSQC of **7e** in H₂O:D₂O (9:1). Middle: ROESY of **7e** (300 ms) in water. Bottom: ROESY of **7e** (300 ms) in SDS. The boxes in the middle and bottom spectra highlights the correlations/peaks in Figure S2.

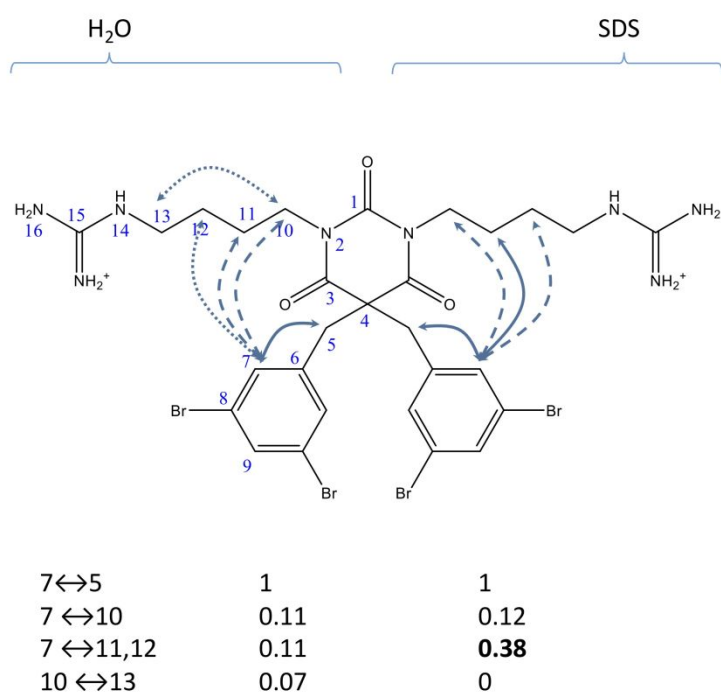


Figure S4. Schematic representation of relevant ROESY contacts for **7e** (3,5-di-Br) observed in water (left side) and in SDS (right side). Relatively stronger correlations are colour coded in green and relatively weaker in red, and the reference volume in blue.

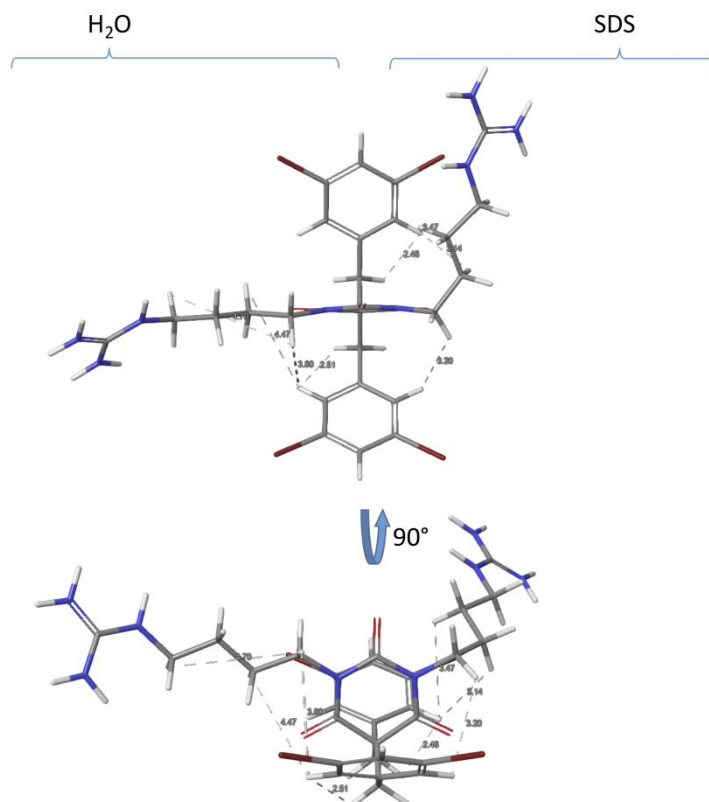


Figure S5. Schematic visualization of the observed ROESY correlations for **7e** (3,5-di-Br) in water (left side) and in SDS (right side), using sculpted structures.

13. Molecular modeling

*Table S3. A summary of data from MD simulations of compounds 6a, 6e, 6g, 7e and 7g. Third column: the percentage of the 260 ns membrane simulation when the compound is in the **up** conformation. Fourth column: the percentage of the 100 ns water simulation when the compound is in the **up** conformation. Fifth column: the occurrences of membrane insertion in the MD simulation given in ns.*

Compound	Parallel	% up in membrane system	% up in water system	Membrane insertion ns
6a	1	47	100	80 (120), 135 ^a
	2	75	100	25 (135) ^a
	3	100	100	25 (163), 175 (230) ^a
6e	1	23	100	10
	2	98	3	7
	3	100	52	25
6g	1	76	100	20
	2	100	100	7
	3	37	100	15
7e	1	100	100	35
	2	59	98	25
	3	100	50 ^c	25
7g	1	100	100	12
	2	69	100	20
	3	100	100	25 ^b

^a Compound inserts into membrane several times. Values in parentheses indicate when the compound exits the membrane environment.

^b Molecule travels briefly through the top of the simulation box and appears at the bottom.

^c Switches back and forth between **up** and **up-down**.

Time evolution of the C₅ z-coordinate and the two conformations of 6a in a membrane model system:

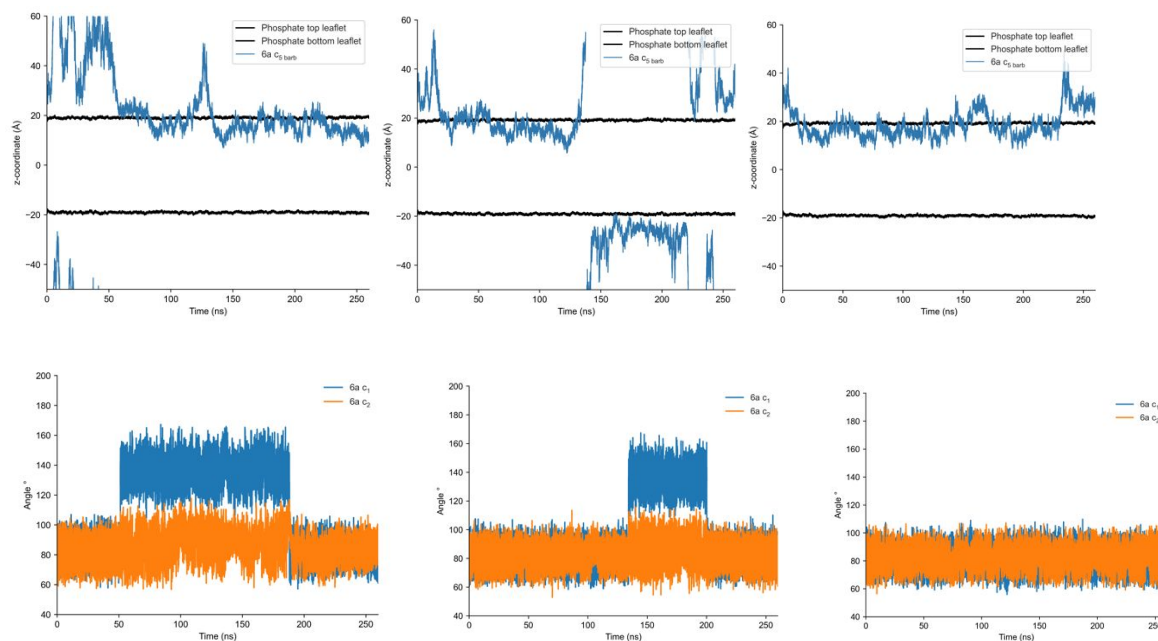


Figure S6. Compound 6a z-coordinate and conformation tracking in MD simulations. Top row: z-coordinate tracking of atom C₅. Bottom row: angle C_{barb 2}, C_{benz} and C_{benz 4} tracking. From left to right: parallel 1, 2 and 3.

Time evolution of the C₅ z-coordinate and the two conformations of 6e in a membrane model system:

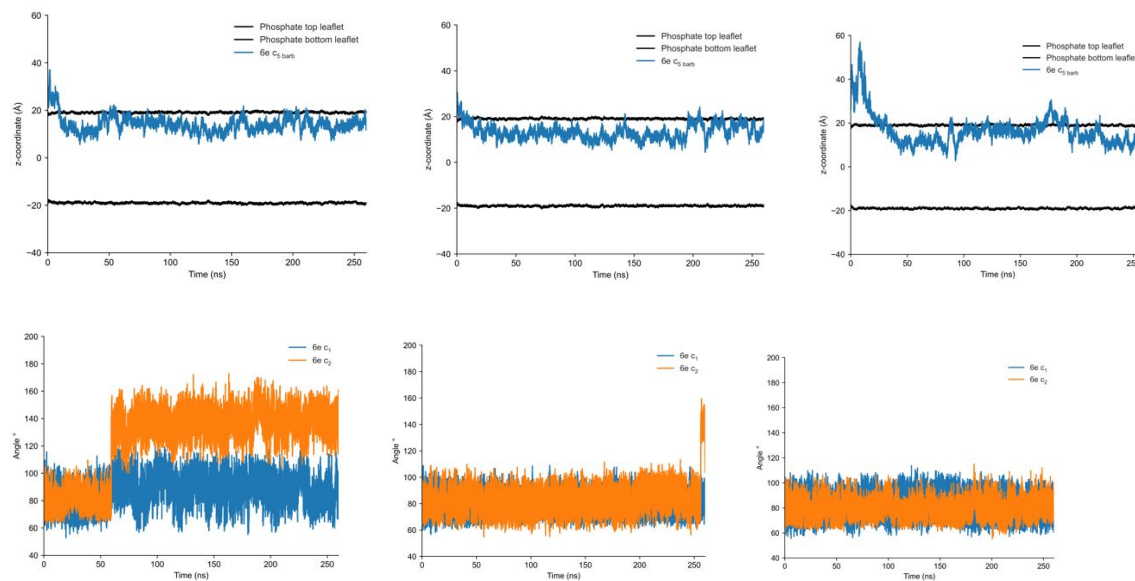


Figure S7. Compound 6e z-coordinate and conformation tracking in MD simulations. Top row: z-coordinate tracking of atom C₅. Bottom row: angle C_{barb 2}, C_{benz} and C_{benz 4} tracking. From left to right: parallel 1, 2 and 3.

Time evolution of the C_5 z-coordinate and the two conformations of **6g** in a membrane model system:

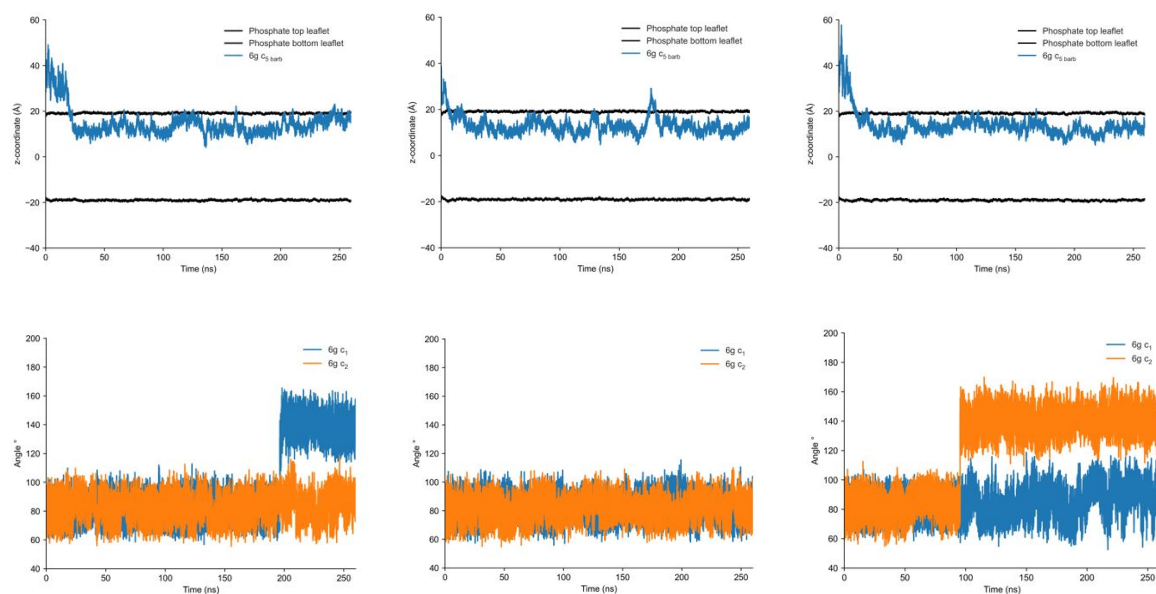


Figure S8. Compound **6g** z-coordinate and conformation tracking in MD simulations. Top row: z-coordinate tracking of atom C_5 . Bottom row: angle $C_{barb\ 2}$, C_{benz} and $C_{benz\ 4}$ tracking. From left to right: parallel 1, 2 and 3.

Time evolution of the C_5 z-coordinate and the two conformations of **7e** in a membrane model system:

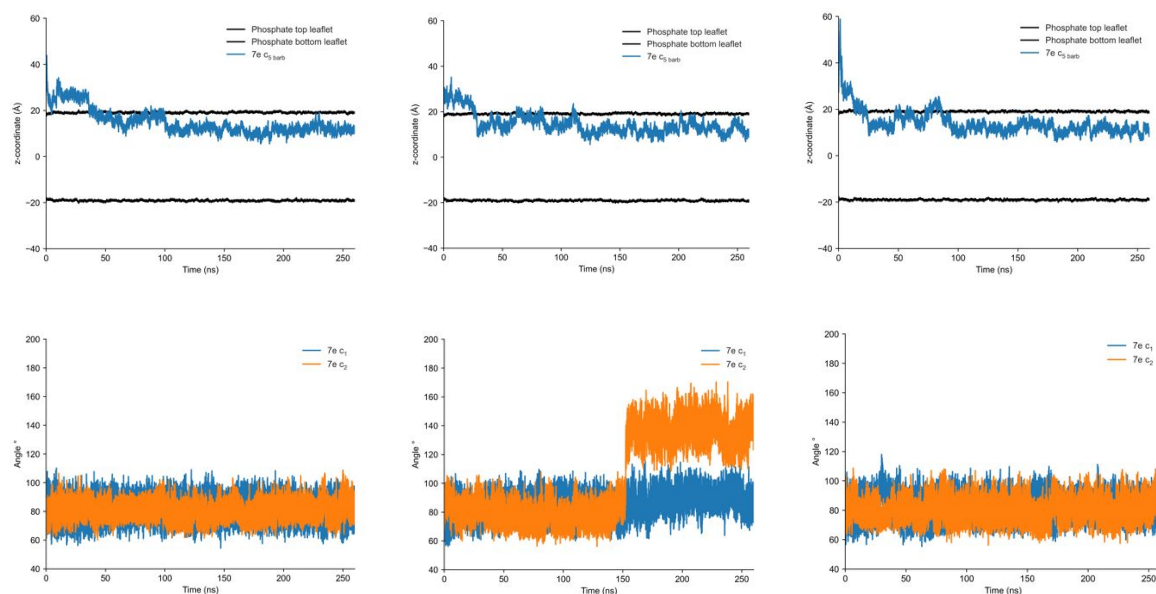


Figure S9. Compound **7e** z-coordinate and conformation tracking in MD simulations. Top row: z-coordinate tracking of atom C_5 . Bottom row: angle $C_{barb\ 2}$, C_{benz} and $C_{benz\ 4}$ tracking. From left to right: parallel 1, 2 and 3.

Time evolution of the C₅ z-coordinate and the two conformations of 7g in a membrane model system:

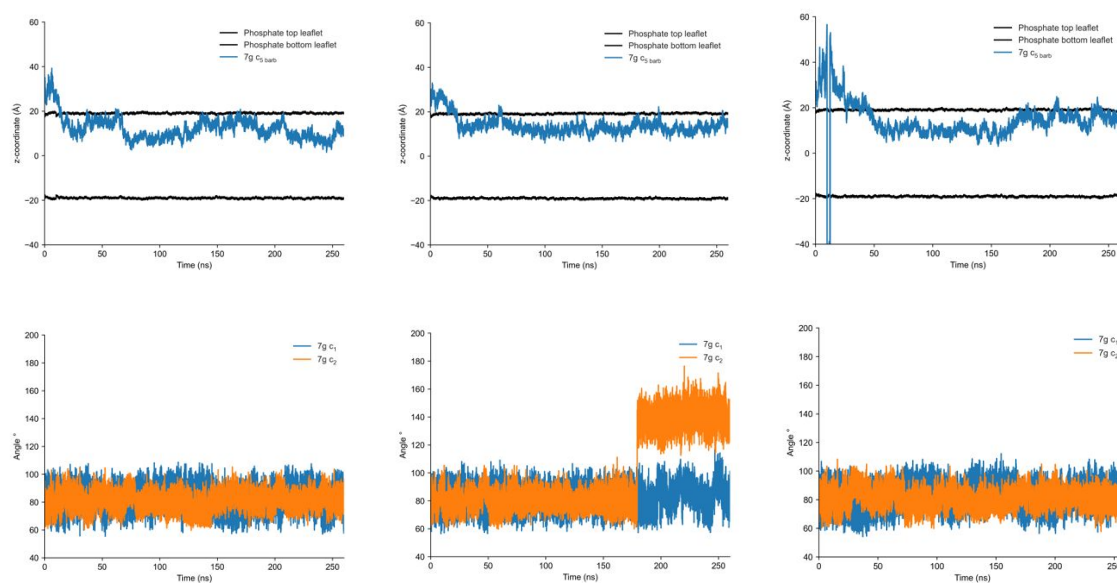


Figure S10. Compound 7g z-coordinate and conformation tracking in MD simulations. Top row: z-coordinate tracking of atom C₅. Bottom row: angle C_{carb 2}, C_{benz 3} and C_{benz 4} tracking. From left to right: parallel 1, 2 and 3.

REFERENCES

1. Galluzzi, L.; Karp, M., Intracellular redox equilibrium and growth phase affect the performance of luciferase-based biosensors. *J Biotechnol* **2007**, *127* (2), 188-198.
2. Virta, M.; Akerman, K. E.; Saviranta, P.; Oker-Blom, C.; Karp, M. T., Real-time measurement of cell permeabilization with low-molecular-weight membranolytic agents. *J Antimicrob Chemother* **1995**, *36* (2), 303-315.
3. Kuyyakanond, T.; Quesnel, L. B., The mechanism of action of chlorhexidine. *FEMS Microbiol Lett* **1992**, *100* (1-3), 211-215.

Paper II

A concise SAR-analysis of antimicrobial cationic amphipathic barbiturates for an improved activity-toxicity profile

Manuel K. Langer, Ataur Rahman, Hymonti Dey, Trude Anderssen, Francesco Zilioli, Tor Haug, Hans-Matti Blencke, Klara Stensvåg, Morten B. Strøm, Annette Bayer

Submitted to Eur. J. Med. Chem. (20.05.2022)

A concise SAR-analysis of antimicrobial cationic amphipathic barbiturates for an improved activity-toxicity profile

Manuel K. Langer^{a#}, Ataur Rahman^{b#}, Hymonti Dey^b, Trude Anderssen^c, Francesco Zilioli^a, Tor Haug^b, Hans-Matti Blencke^b, Klara Stensvåg^b, Morten B. Strøm^{c*}, Annette Bayer^{a*}

^a Department of Chemistry, UiT The Arctic University of Norway, NO-9037 Tromsø, NORWAY.

^b The Norwegian College of Fishery Science, Faculty of Biosciences, Fisheries and Economics, UiT The Arctic University of Norway, NO-9037 Tromsø, NORWAY.

^c Department of Pharmacy, Faculty of Health Sciences, UiT The Arctic University of Norway, NO-9037 Tromsø, NORWAY.

Authors contributed equally to this work; * Corresponding authors. E-mail: Annette.bayer@uit.no; Morten.strom@uit.no.

MANUSCRIPT INFO

ABSTRACT

Article history:

Received

Received in revised form

Accepted

Available online

Keywords:

Antibacterial

Barbiturates

Peptidomimetics

SMAMPs – synthetic mimics of antimicrobial peptides

An amphipathic barbiturate mimic of the marine eusynstyelamides is reported as a promising class of antimicrobial agents. We hereby report a detailed analysis of the structure-activity relationship for cationic amphipathic *N,N*-dialkylated-5,5-disubstituted barbiturates. The influence of various cationic groups, hydrocarbon linkers and lipophilic side chains on the compounds' antimicrobial potency and haemolytic activity was studied. A comprehensive library of 58 compounds was prepared using a concise synthetic strategy. We found cationic amine and guanidyl groups to yield the highest broad-spectrum activity and cationic trimethylated quaternary amine groups to exert narrow-spectrum activity against Gram-positive bacteria. *n*-Propyl hydrocarbon linkers proved to be the best compromise between potency and haemolytic activity. The combination of two different lipophilic side chains allowed for further fine-tuning of the biological properties. Using these insights, we were able to prepare both potent narrow-spectrum barbiturate **1c** and the broad-spectrum barbiturates **3bG** and **5eA**, all having low or no haemolytic activity. The guanidine derivative **3bG** demonstrated a strong membrane disrupting effect in luciferin-based assays. We believe that these results may be valuable in further development of antimicrobial lead structures.

1. Introduction

Since the golden age of antibiotics, the developing rate of new agents has decreased notably, while antimicrobial resistance (AMR) has been rising to a global threat.¹ The prominence of this problem is well demonstrated by the World Health Organization (WHO) enacting a global action plan on fighting antimicrobial resistance.² While the action plan is focusing on a framework at many different levels, the need for potent antimicrobials stays. As the antibiotics employed for decades start to lose activity against resistant bacteria, several alternative approaches have been investigated. Among these are combination therapy^{3, 4}, bacteriophage therapy,⁵ photodynamic therapy,⁶ antibacterial antibodies,⁷ phytochemicals,⁵ nanoparticles⁸ and antimicrobial peptides.^{9, 10}

From the above stated list, the short, cationic antimicrobial peptides (AMPs) are an intriguing class of compounds. They constitute the first line of host defense in virtually all eukaryotic species including plants, mammals, insects, etc.¹¹ They generally feature between 20-50% hydrophobic residues and have an overall positive charge (+2 to +9) at neutral pH.¹²⁻¹⁴ Their amphipathic nature is the basis of their most common mode of action, to permeabilize bacterial membranes. AMPs attach to the negatively charged cytoplasmic membrane by electrostatic interactions and subsequently disrupt the apolar bilayer with their hydrophobic part.¹⁵ It is believed that due to these non-specific interactions, bacterial resistance is less likely to be induced.¹⁶ This makes AMPs a promising group of

compounds despite their generally lower activity compared to marketed antibiotics.¹⁷

Despite these promising properties, the clinical application of peptide based drugs is often limited by their poor oral uptake and proteolytic instability.¹⁸ Therefore, considerable efforts towards the development of synthetic AMP analogues have been made, cumulating in the development of a variety of different groups of analogues.¹⁹⁻²⁷ Focusing on small molecules, we have recently reported substituted barbituric acid derivatives,²⁸ inspired by a family of marine natural products, the *eusynstyelamides*,^{29, 30} as peptidomimetics of AMPs. The lead structure **1eG** (Figure 1) from our previous study²⁸ demonstrated good *in vitro* and *in vivo* activity as a proof of principle.

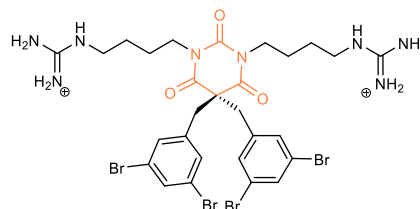


Figure 1. Lead structure **1eG** from our previous study²⁸ with the barbituric acid core highlighted in orange.

Encouraged by the *in vivo* activity of **1eG** we herein describe an in-depth SAR investigation to improve the potency and selectivity of these peptidomimetics. Several series of amphipathic barbiturates with systematically varying substituents were designed and synthesized. Our

aim was to assess the qualitative influence of each structural component aside from the barbituric acid on the antimicrobial and haemolytic activity. Once the impact of each component is identified, improved narrow- and broad-spectrum compounds may be prepared. All new compounds were screened for activity against a panel of antibiotic susceptible strains to determine their minimal inhibitory concentration (MIC) values. Cytotoxicity was assessed by determining the EC₅₀ values for the lysis of human red blood cells (RBC). Promising candidates were investigated for their antibacterial mode of action (MoA), using three luciferase-based assays of the viability and integrity of the cytoplasmic inner and outer membrane of bacterial cells.

2. Results and Discussion

2.1. Design of the study

To systematically study the influence of structural components of **1eG**²⁸ (**Figure 1**) on the antibacterial and haemolytic activity, we devised several series of compounds based on the general structure shown in **Figure 2**. All structures consisted of a central barbituric acid core, which was kept constant. Three structural parts were varied in the design of the compound library: (i) the cationic head groups (blue placeholder in **Figure 2**) attached to the nitrogen atoms of the barbiturate core by (ii) a hydrocarbon linker chain (green placeholder) and (iii) the two lipophilic side chains (red placeholders) connected to the barbiturate C-5 carbon.

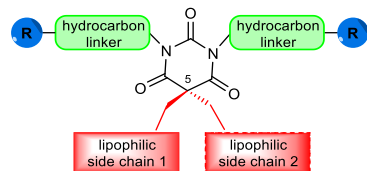


Figure 2. General structure of the tetrasubstituted barbituric acids used in this study. R = cationic group. The individual parts were evaluated in five series, namely screening of the cationic moieties (series 1), lipophilic side chains (series 2 side chain 1 = side chain 2 and series 3 side chain 1 ≠ side chain 2), hydrocarbon linker chains (series 4) and optimized structures (series 5).

The influence of the cationic head groups (R; **Figure 2**) was investigated by including 1° amines, methylated 2°, 3° and 4° amines and imine derivatives containing guanidino or pyridinium groups in the library design. The cationic groups were chosen based on the prospect of varying the interactions with bacterial membranes and their ability to cross the latter and accumulate in Gram-negative *Escherichia coli* (*E. coli*).^{31, 32} Compounds with varying cationic groups are found in compound series 1.

The lipophilic side chains (**Figure 2**) were hypothesized to influence the compounds' ability to insert into the hydrophobic lipid bilayer of the bacteria. In our library design haloaryls, hetero-aryls, and linear and cyclic hydrocarbons were chosen as lipophilic side chains. The selection was based on results from our previous study²⁸ and commercial availability. Two different compound series were included in the study; in series 2 the two lipophilic side chains were identical,

while in series 3 two different lipophilic side chains were combined resulting in derivatives with mixed side chains.

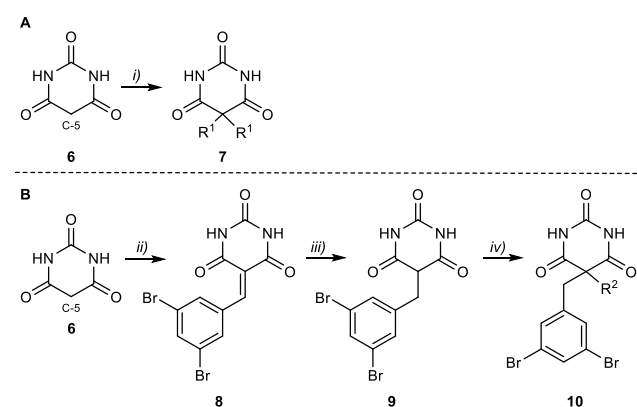
The hydrocarbon linkers (**Figure 2**) were chosen on the premises of investigating the influence of the flexibility and distance of the cationic groups relative to the barbiturate core. Linear hydrocarbon chains of 2 – 6 carbons length gave flexible linkers, while cyclic hydrocarbon linkers (cyclobutyl and cyclohexyl) gave more restricted analogues. Compounds with varying linkers are included in series 4.

Based on the results from series 4 we prepared a range of compounds included in series 5, having *n*-propyl linkers.

2.2. Synthesis

Our previously reported synthesis of 5,5-dialkylated barbiturates provided amine and guanidine analogues in six or eight synthetic steps, respectively.²⁸ In the present study, the demand for a large library of compounds prompted us to develop a shorter synthetic approach. Both amines and guanidines were successfully obtained in three steps from barbituric acid.

The synthetic strategy started with the preparation of symmetrical (**7**) or unsymmetrical (**10**) 5,5-dialkylated barbituric acid (**Scheme 1**). For the preparation of identically dialkylated compounds, barbituric acid **6** could be di-substituted at the C-5 carbon using organohalides to give **7** in 5-92% yield in the presence of NaHCO₃ in PEG-400 (**Scheme 1A**). Low yields (5-35%) were obtained for primary alkyl halides and heteroaryls, whereas haloaryls were delivered in good to excellent yields (70-92%). PEG-400 served as a green solvent alternative and phase transfer catalyst.³³ Commonly applied conditions³⁴ employing an inorganic base such as K₂CO₃ and benzyltriethylammonium chloride (BTEAC) in CHCl₃ performed worse. Weak electrophiles, such as alkyl halides posed an inherent problem. Harsher conditions were needed, which inevitably led to additional *N*-alkylation due to the acidity of the *N*-H protons (pK_a = 7-9^{35, 36} compared to the pK_a (H-C5) = 3-4^{36, 37}).



Scheme 1. Synthesis of core structures **7** and **10**. **A:** Reaction conditions: *i*) Alkylating agent, NaHCO₃, PEG-400, 45–100 °C, 5–92%. **B:** Reaction conditions: *ii*) 3,5-dibromobenzaldehyde, H₂O/EtOH (3:1), 105 °C, 58%; *iii*) NaBH₄, EtOH, 70 °C, 80%; *iv*) Alkyl bromide, NaHCO₃, PEG-400, 50–100 °C, 5–61%.

To obtain unsymmetrically 5,5-dialkylated barbituric acids a different approach was needed, since mono-alkylation enhances the nucleophilicity of the barbiturate

C-5 carbon leading to inevitable dialkylation.³⁷ We investigated several reported methods for selective monoalkylation and *in situ* reductions,³⁷⁻³⁹ which did not work well in our hands. We therefore decided to use a step-wise approach as shown in **Scheme 1B**. Barbituric acid **6** and 3,5-dibromobenzaldehyde were condensed⁴⁰ to give compound **8** and subsequent reduction with NaBH₄ in EtOH⁴¹ gave the C-5 mono-substituted derivative **9** in 80% yield. We found **9** being an approximate 2:1 mixture of the keto and enol form. This mixture was alkylated a second time using the conditions employed for 5,5-dialkylation of barbituric acid to deliver intermediates **10**. Yields ranged from 5-61%, depending on the reactivity of the employed electrophiles.

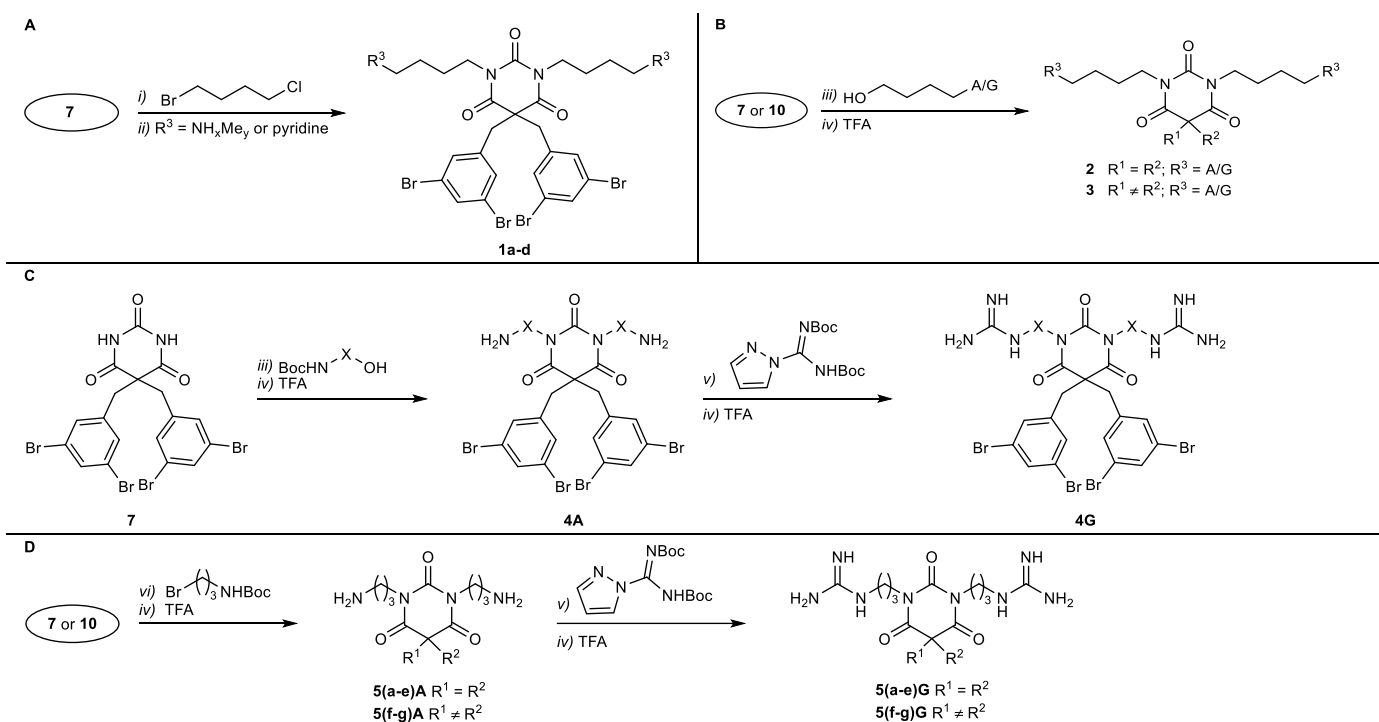
Starting from intermediates **7** or **10**, a wide range of *N,N'*-dialkylated barbituric acid derivatives were prepared, employing a range of methods for *N*-alkylation depending on the availability of reactants (**Scheme 2**).

All compounds synthesized are summarized in **Tables 1-5**. Compounds denoted with capital **A** have an amine as a cationic group and those denoted with capital **G** have cationic guanidino groups, correspondingly. The compounds are grouped into five series (series **1 - 5**) based on their structural variations.

Series **1** (**Table 1**) encompasses compounds with varying cationic groups, while the C-5 substituents (3,5-dibromobenzyl) and hydrocarbon linker (*n*-butyl) were kept unchanged. To obtain the methylated amines and pyridinium containing compounds **1a-d**, 5,5-bis(3,5-dibromobenzyl)barbituric acid **7a** (R¹ = 3,5-Br₂PhCH₂) was *N,N'*-dialkylated with either 1-bromo-4-chlorobutane or 1,4-dibromobutane and Cs₂CO₃ in

acetone (**Scheme 2A**). Subsequent S_N2 substitution of the terminal halo substituent with methylated ammonia or pyridine in acetonitrile at elevated temperature led to compounds **1a-d** in 33-88% yield. Having a bromide as leaving group proved to be necessary for substitution with methylamine and dimethylamine. Substitutions were only successful with organic solutions of the amines, while hydrohalo salts of the amines could not be used. An optimized method for preparation of the previously reported 1° amine **1eA** and guanidine **1eG**²⁸ is described in the next paragraph.

Compound series **2** (**Table 2**) contained identically 5,5-disubstituted barbiturates and series **3** (**Table 3**) contained unsymmetrically 5,5-disubstituted barbiturates, while the hydrocarbon linker for both series was a *n*-butyl chain. As cationic groups, both amino (**A**) or guanidino (**G**) groups were explored. Compounds were synthesized from the barbituric acid derivatives **7(e-j)** or **10(a-g)** by *N,N'*-dialkylation with *N*-Boc protected 4-aminobutanol (**A**) or *N,N'*-di-Boc protected 1-(4-hydroxybutyl)guanidine (**G**) (**Scheme 2B**). Due to the low pK_a value of the imidic hydrogens⁴² a Mitsunobu protocol using diisopropylazodicarboxylate (DIAD) and PPh₃ could be employed. Removal of the Boc protection mediated by TFA:DCM and subsequent reversed phase (RP) chromatography gave target series **2** (R¹ = R²) and **3** (R¹ ≠ R²) as di-TFA salts in 20-89% yield. In some cases the TFA salts were contaminated with reduced DIAD, which could largely be removed by trituration with Et₂O. Interestingly, employment of the more reactive coupling system 1,1'-(azodicarbonyl)dipiperidine ADDP/P(*n*-Bu)₃ and *N,N,N',N'*-tetramethyldicarboxamide TMAD/P(*n*-Bu)₃⁴² led to lower yields and mono-alkylation.



Scheme 2 Synthetic approach to target series **1 - 5**, where **A** denotes amine head groups and **G** the guanidine derivatives. **A** R³ = NH₂Me, NHMe₂, NMe₃, pyridinyl; Reaction conditions: i) Cs₂CO₃, acetone, 55 °C, 85%; ii) MeCN, 70-90 °C, 33-88%. **B** Reaction conditions: iii) DIAD, PPh₃, anhydrous DCM or THF, 0 to r.t., iv) TFA, DCM, r.t., 20-89% o2s. **C** X = ethyl, *n*-propyl, (cyclo)-butyl, *n*-pentyl, (cyclo)-hexyl; Reaction conditions: iii) DIAD, PPh₃, anhydrous DCM or THF, 0 to r.t., iv) TFA, DCM, r.t., 23-73% o2s, v) DIPEA or DBU, THF, 45 °C, 14-92% o2s (after TFA deprotection). **D** Reaction conditions: vi) base, TBAI, acetone, 50-70 °C, then TFA, DCM, r.t., 34-76% o2s (after TFA deprotection); v) DIPEA or DBU, THF, 45 °C, then TFA, DCM, r.t., 20-91% o2s (after TFA deprotection).

Series 4 (Table 4) contained compounds with varying linkers, such as aliphatic chains with 2 – 6 carbons length as well as cyclic hydrocarbons. The C-5 substituents were set to 3,5-dibromobenzyl and the cationic groups were either amino (A) or guanidino (G) groups. As the relevant linkers were commercially available as *N*-Boc-amino alcohols, we decided to explore the above Mitsunobu protocol in a stepwise synthetic approach (Scheme 2C). The 5,5-bis(3,5-dibromobenzyl)barbituric acid 7 was *N,N'*-dialkylated with the appropriate Boc-protected amino alcohol using the Mitsunobu conditions followed by TFA:DCM treatment to obtain series 4(a-h)A in 23 – 73% over 2 steps. Treatment of the amines 4(a-h)A with *N,N'*-Di-Boc-1*H*-pyrazole-1-carboxamide and DIPEA or DBU, followed by Boc removal with TFA in DCM delivered the guanidines 4(a-h)G in 14 – 92% yield. Employing the well-known and cheaper alternative *N,N'*-bis(*tert*-butoxycarbonyl)-*S*-methylisothio-urea^{43, 44} led to an inseparable mixture of Boc protected amine and Boc protected guanyl compounds.

Based on the bioactivities observed for series 1 – 4, a fifth collection of compounds (series 5, Table 5), exploring the effect of an *n*-propyl linker more broadly, was prepared. Series 5 contained selected identically (series 2) or unsymmetrically (series 3) 5-substituted barbiturates with both 1-propyl-3-amino (A) or 1-propyl-3-guanidino groups (G) as *N,N'*-substituents. Starting from compounds 7 or 10, *N,N'*-alkylation with *N*-Boc *n*-propylbromide, followed by TFA mediated Boc removal and purification by RP chromatography gave identically 5(a-e)A or unsymmetrically 5(f-g)A substituted primary amines in 34-76% yield (Scheme 2D). The Mitsunobu protocol was evaluated but discarded due to difficulties with purification of some compounds. Treatment of the primary amines with *N,N'*-di-Boc-1*H*-pyrazole-1-carboxamide and DIPEA, followed by TFA facilitated Boc removal and RP flash chromatography purification yielded the respective guanidines 5(a-h)G in 20-91% yield.

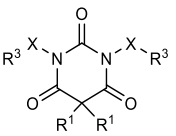
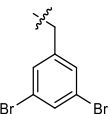
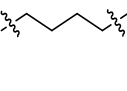
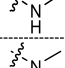
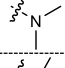
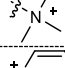
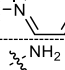
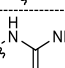
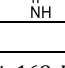
2.3. SAR analysis

All compounds were screened for antimicrobial activity against antibiotic susceptible Gram-positive and Gram-negative reference strains (Table 1-5). Haemolytic activity against human red blood cells (RBCs), expressed by the EC₅₀ value, was used as a measurement of cytotoxicity. We have earlier reported compounds 1eA and 1eG,²⁸ which here are used as reference compounds together with the known antibiotic ciprofloxacin as a positive control. The descriptors for amine derivatives (A) and guanidine derivatives (G) are omitted for derivatives with other cationic groups.

2.3.1. Compound Series 1: Exploring the cationic head group (R³)

First, we set out to investigate the influence of the effective charge of the cationic groups (Table 1, R³ group and Figure 2, blue space holders). Upon *N*-methylation the electron density at the nitrogen increases, as does its basicity, but the polarity decreases. Successive introduction of one (1a), two (1b) or three (1c) methyl groups had no noteworthy influence on the activity against the Gram-positive strains (MIC: 4 – 8 µg/mL), but the activity against the Gram-negative strains dropped considerably for compound 1c (MIC: 128 – 256 µg/mL). It is suggested that, among other factors, the electrostatic interaction between these compounds and bacterial membrane plays an important role in the compound's activity.⁴⁵ Successive introduction of methyl groups lowers the effective charge of the amine head groups, thus reducing their interaction with the lower charge per area membrane of Gram-negative bacteria compared to Gram-positive strains.⁴⁶ Additionally, quaternary ammonium compounds (quats or QACs) are known for their impaired ability to cross the outer membrane of Gram-negative *Pseudomonas aeruginosa* (*P. aeruginosa*).⁴⁷ Recent studies showed generally impaired uptake of compounds containing methylated primary amines in *E. coli*.³¹ Despite that presumably lower uptake, secondary (1a) and tertiary amines (1b) were still active against *E. coli* (MIC: 8 µg/mL).

Table 1. Antimicrobial activity (MIC in µg/mL) against bacterial reference strains and haemolytic activity against human RBC (EC₅₀ in µg/mL) for compounds in series 1.

Core structure	Comp. ID	R ¹	X	R ³	CLogP ^a	Antimicrobial activity				EC ₅₀ ^b
						S. a	B. s	E. c	P. a	
	1a				-0.66	8	4	8	16	73
	1b				-0.52	8	4	8	64	157
	1c				0.42	4	8	128	256	>539
	1d				0.72	2	4	8	128	>559
	1eA ^c				-1.20	4	2	4	8	79
	1eG ^d				-2.39	2	2	2	8	62
	Ciprofloxacin								0.06	<0.03

Bacterial reference strains: S. a – *Staphylococcus aureus* ATCC 9144, B. s – *Bacillus subtilis* 168, E. c – *Escherichia coli* ATCC 25922, and P. a – *Pseudomonas aeruginosa* ATCC 27853. ^a CLogP values were calculated for the respective non protonated cationic group (calculated with ChemBioDraw Ultra v19.0.0.1.28). ^b Values given as *greater than* correspond to the highest concentration (500 µM) tested in the RBC assay. ^c Values were taken from reference ²⁸. ^d We have reported this compound previously having the following MIC values: S. a: 1 µg/mL, B. s: 2 µg/mL, E. c: 2 µg/mL, P. a: 4 µg/mL.²⁸

Table 2. Antimicrobial activity (MIC in $\mu\text{g/mL}$) against bacterial reference strains and haemolytic activity against human RBC (EC_{50} in $\mu\text{g/mL}$) for compounds in Series 2.

Core structure	Comp. ID	R ¹	X	R ³	CLogP ^a	Antimicrobial activity				EC ₅₀ ^b
						S. a	B. s	E. c	P. a	
	2aA				2.53	256	64	>256	>256	>390
	2aG				2.53	8	16	128	>256	>432
	2bA				3.39	16	4	256	256	>469
	2bG				3.39	2	4	16	128	461
	2cA				3.87	16	8	32	64	>333
	2cG				3.87	2	2	4	16	143
	2dA				4.68	2	2	4	4	27
	2dG				4.68	4	4	4	8	36
	2eA				5.03	4	4	8	8	27
	2eG				5.03	4	4	4	8	32
	2fA				5.03	2	2	4	4	30
	2fG				5.03	2	1	4	4	30

Bacterial reference strains: S. a – *Staphylococcus aureus* ATCC 9144, B.s – *Bacillus subtilis* 168, E. c – *Escherichia coli* ATCC 25922, and P. a – *Pseudomonas aeruginosa* ATCC 27853. ^a CLogP values were calculated for the respective lipophilic side chains (calculated with ChemBioDraw Ultra v19.0.0.1.28). ^b Values given as *greater than* correspond to the highest concentration (500 μM) tested in the RBC assay.

By replacing the quaternary trimethylated ammonium (**1c**) with a pyridinium group (**1d**), the activity against the Gram-positive strains improved (MIC: 2 – 4 $\mu\text{g/mL}$) and the activity against *E. coli* was restored (MIC: 8 $\mu\text{g/mL}$), probably due to increased accumulation.³² Tertiary (**1b**, EC_{50} : 157 $\mu\text{g/mL}$) and quaternary amines (**1c** and **1d**; both EC_{50} : >500 $\mu\text{g/mL}$) displayed lower haemolytic activity compared to the primary (**1eA**, EC_{50} : 79 $\mu\text{g/mL}$) and secondary (**1a**, EC_{50} : 73 $\mu\text{g/mL}$) amines.

The quaternary ammonium compound **1c** exhibited narrow-spectrum antimicrobial activity against Gram-positive strains and was non-haemolytic. Compared to the above investigated head groups, the recently reported amine (**1eA**) and guanidine derivatives (**1eG**) appeared to be the most effective against the Gram-negative strains, thus rendering them suitable for broad-spectrum applications. The consecutively developed compounds were therefore synthesized with either amino or guanidino groups.

2.3.2. Compound Series 2: Exploring new lipophilic side chains (R¹)

In series 2, the influence of heterocyclic, aliphatic and highly brominated lipophilic side chains (**Table 2**, R¹ groups and **Figure 2**, red space holders) on the biological activity was examined. Both side chains employed were identical

The antimicrobial activity for the amine barbiturates **2(a-f)A** ranged from MIC: 2 – 256 $\mu\text{g/mL}$ and for the guanidine barbiturates **2(a-f)G** from MIC: 1 – 16 $\mu\text{g/mL}$ against the Gram-positive strains *Staphylococcus aureus* (*S. aureus*) and *Bacillus subtilis* (*B. subtilis*). Against the Gram-negative strains *E. coli* and *P. aeruginosa* both, the amine and guanidine derivatives showed MIC values of 4- >256 $\mu\text{g/mL}$. We included quinoline and 6-bromoquinoline as heterocyclic alternatives. The amine derivative **2aA** (R¹ = 2-methylquinolinyl) was neither antibacterial (MIC: ≥ 64 $\mu\text{g/mL}$) nor haemolytic, whereas the guanidine derivative **2aG** (R¹ = 2-methylquinolinyl) exhibited some activity against the Gram-positive strains (MIC: 8 – 16 $\mu\text{g/mL}$).

Upon inserting a bromine in the 6-position for **2bA** (R¹ = 6-Br-2-methylquinolinyl) the CLogP rose considerably, and the amine derivative became active against the Gram-positive bacteria (MIC: 4 – 16 $\mu\text{g/mL}$). The respective guanidine **2bG** (R¹ = 6-Br-2-quinolinyl) was found to be active against both the Gram-positive strains and *E. coli* (MIC: 2 – 16 $\mu\text{g/mL}$), while being non haemolytic. The bromine substituent seemed to be essential for good antimicrobial activity against Gram-positive strains and *E. coli*.

In the next step we replaced the aromatic side chains by alkyl chains as found in antimicrobial quaternary ammonium compounds (quats).^{48, 49} We decided to incorporate two hexyl chains, which mimic the single long alkyl chain commonly found in quats.⁵⁰ The amine

derivative **2cA** ($R^1 = n$ -hexyl) showed weak activity against all bacterial strains (MIC: 8 – 64 $\mu\text{g/mL}$), whereas the guanidine derivative **2cG** ($R^1 = n$ -hexyl) showed high antibacterial activity with MIC values of 2 – 4 $\mu\text{g/mL}$ against all strains except for *P. aeruginosa*. Haemolysis was still moderate, with EC_{50} : 143 $\mu\text{g/mL}$. Interestingly, the shorter hexyl chains perform just as good as the longer alkyl chains in quats,⁴⁸ suggesting that the overall hydrophobic bulk is more important than the actual chain length.

Compounds **2d** ($R^1 = 4$ -Br-1-Nal) were prepared based on the previously reported 4-F-1-naphtyl barbituric acid.²⁸ Introduction of electron withdrawing fluorine into molecules is known to hamper *in vivo* oxidation of aromatic side chains during Phase I metabolism.^{51, 52} Replacing the fluorine for a bromine increases the hydrophobic bulk, while having similar electronic effects.⁵³ Surprisingly, the amine derivative **2dA** ($R^1 = 4$ -Br-1-Nal) was equally potent as the guanidine **2dG** ($R^1 = 4$ -Br-1-Nal) with MIC values of 2 – 8 $\mu\text{g/mL}$ against all reference strains. However, both **2dA** and **2dG** were also highly haemolytic (EC_{50} : 27 – 36 $\mu\text{g/mL}$).

Previously, we have found bromo substituents on the phenyl ring having a positive effect on the biological activity, with 3,5-dibromophenyl providing the highest activity.²⁶ We therefore prepared derivatives **2eA** and **2eG** ($R^1 = 2,4,5$ -tri-BrBn) and **2fA** and **2fG** ($R = 2,4,6$ -tri-

BrBn) being at the far end of the hydrophobicity scale. They all displayed potent antibacterial activity, with MIC values $\leq 8 \mu\text{g/mL}$ against all strains. However, haemolytic activity also increased for all these compounds (EC_{50} : 27 – 32 $\mu\text{g/mL}$). The positioning of the bromines on the phenyl ring had a minor influence on antibacterial activity, with **2fA** and **2fG** ($R^1 = 2,4,6$ -tri-BrBn) being most potent.

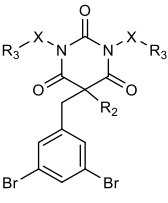
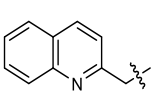
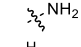
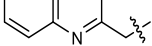
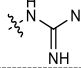
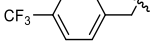
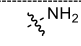
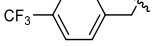
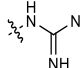
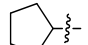
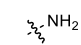
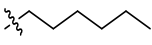
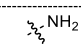
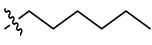
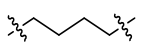
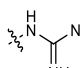

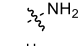

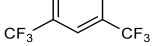
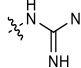
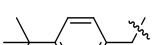
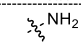
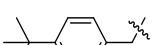
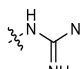
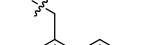
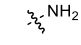
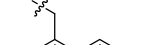
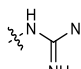
In summary, halogenated heterocycles are promising side chains for narrow-spectrum application. The hydrophobicity of the C-5 substituents had the greatest influence, while the structure being secondary. When exceeding $CLogP \approx 4.50$, the structures mostly became too haemolytic to be of interest for further studies.

2.3.3. Compound Series 3: Exploring mixed lipophilic groups ($R^1 \neq R^2$)

A series of compounds containing two different side chains were prepared to tune lipophilicity and side chain structure with respect to antimicrobial activity and haemolytic activity. We intended to pair the potent 3,5-dibromobenzyl side chain ($R^1 = 3,5$ -di-BrBn) with side chains (R^2) of different varying lipophilicity (**Table 3**; R^2 group; **Figure 2**, red space holders).

First, we chose to incorporate previously documented non potent side chains (see series **2** and previously reported^{26, 28}) in compounds **3a** ($R^2 =$ quinolone) and **3b** ($R^2 = 4$ -CF₃Bn).

Table 3. Antimicrobial activity (MIC in $\mu\text{g/mL}$) against bacterial reference strains and haemolytic activity against human RBC (EC_{50} in $\mu\text{g/mL}$) for compounds in Series 3.

Core structure	Comp. ID	R ₂	X	R ₃	CLogP ^a	Antimicrobial activity				EC ₅₀ ^b
						S. a	B. s	E. c	P. a	
	3aA				3.45	32	8	128	256	>444
	3aG				3.45	2	4	32	32	450
	3bA				3.95	16	8	32	64	342
	3bG				3.95	2	4	2	16	161
	3cA				3.58	16	8	64	64	>407
	3dA				4.12	4	4	16	16	144
	3dG				4.12	2	4	4	8	58
	3eA				4.39	8	2	8	8	93
	3eG				4.39	2	2	2	4	36
	3fA				4.42	4	4	8	8	82
	3fG				4.42	2	2	2	4	39
	3gA				4.52	4	4	4	8	47
	3gG				4.52	1	4	4	8	58

Bacterial reference strains: S. a – *Staphylococcus aureus* ATCC 9144, B. s – *Bacillus subtilis* 168, E. c – *Escherichia coli* ATCC 25922, and P. a – *Pseudomonas aeruginosa* ATCC 27853. Guanidyl barbiturate **3cG** could not be obtained. ^a CLogP values were calculated for the respective lipophilic side chains and are presented as the average for the two substituents. (calculated with ChemBioDraw Ultra v19.0.0.1.28). ^b Values given as *greater than* correspond to the highest concentration (500 μM) tested in the RBC assay.

The amine derivatives **3aA** and **3bA** displayed weak activity, mainly against *B. subtilis* (MIC: 8 µg/mL) but can be considered non-haemolytic. The guanidine derivatives **3aG** and **3bG** were still almost non-haemolytic (EC₅₀: up to 161 µg/mL) and displayed potent activity against the Gram-positive strains (MIC: 2 – 4 µg/mL). The derivative **3bG** showed additionally good activity against the Gram-negative *E. coli* (MIC: 4 µg/mL). The superior performance of **3bG** over **3aG** may be attributed to the higher average CLogP value of the lipophilic side chain of **3bG**. The polar nitrogen atom in the quinolinyl side chain (**3bG**) might also reduce the compounds' activity.

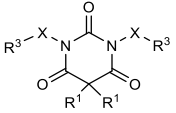
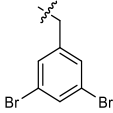
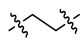
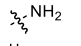
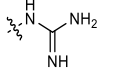
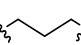
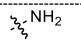
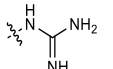
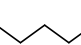
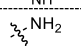
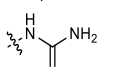
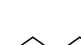
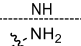
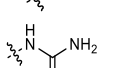

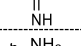
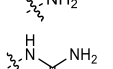

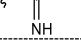
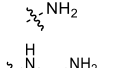
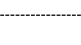
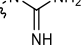
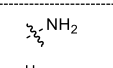

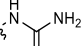
Next, we tested two hydrocarbon analogues **3c** (R² = cyclopentyl) and **3d** (R² = *n*-hexyl), with comparable average hydrophobicity to **3a** and **3b**, respectively. Compound **3cA** was potent against both Gram-positive strains and non-haemolytic. The amine derivative **3dA** was mainly acting against the Gram-positive strains (MIC: 4 µg/mL) but showed 3-fold higher haemolytic activity compared to **3bA**. The guanyl derivative **3dG** exhibited potent antibacterial activity, with MIC-values of 2 – 8 µg/mL against all strains tested. Even though its average CLogP was only marginally higher than **3bG**, its haemolytic activity was pronouncedly higher (EC₅₀ = 58 µg/mL). Both compounds, **3c** (R² = cyclopentyl) and **3d** (R² = *n*-hexyl) indicated that a

combination of an aromatic and a hydrocarbon lipophilic side chains leads to higher haemolytic activity, compared to two aromatic side chains.

To study the influence of the structure of the lipophilic side chains we prepared structurally different, but of similar lipophilicity, compounds **3e** (R² = 3,5-di-CF₃Bn), **3f** (R² = 4-*tert*-butylBn), and **3g** (R² = 4-Br-1-Nal). All their amine derivatives displayed low MIC values of 2 – 8 µg/mL against all reference strains and **3eA** was least haemolytic (EC₅₀: 93 µg/mL). Upon guanylation, a further improvement in antimicrobial activity was achieved, but haemolytic activity was also increased. Thus, **3eG** and **3fG** became twice as potent and haemolytic (EC₅₀: 36– 39 µg/mL), rendering them unfavorable for systemic *in vivo* treatment. The bromo-naphthyl containing **3gG** became more potent against *S. aureus* (MIC: 1 µg/mL), yet haemolytic activity (EC₅₀: 58 µg/mL) was still unfavorably high. No clear trend for the antimicrobial activity could be deduced, based on the structure of the lipophilic side chains.

Taken all together **3aG** (R² = quinoline) displays promising narrow-spectrum activity and absence of haemolytic activity. Compounds **3eG** (R² = 3,5-di-CF₃Bn) and **3fG** (R² = 4-*tert*-butylBn) are highly potent derivatives but displayed high haemolytic activity.

Table 4. Antimicrobial activity (MIC in µg/mL) against bacterial reference strains and haemolytic activity against human RBC (EC₅₀ in µg/mL) for compounds in Series 4.

Core structure	Comp. ID	R ¹	X	R ³	CLogP ^a	Antimicrobial activity				EC ₅₀ ^b
						S. a	B. s	E. c	P. a	
	4aA				1.75	4	4	4	8	39
	4aG			1.75	2	2	4	16	164	
	4bA				2.28	4	4	8	8	99
	4bG			2.28	2	2	4	8	187	
	4cA				3.34	4	4	8	8	24
	4cG			3.34	4	4	4	8	29 ^b	
	4dA				3.87	4	4	4	16	30
	4dG			3.87	4	4	4	32	57 ^b	
	4eA				2.24	8	4	4	8	50
	4eG			2.24	2	2	4	8	75	
	4fA				2.24	4	4	4	8	93
	4fG			2.24	2	4	4	8	62	
	4gA				3.35	4	4	4	8	15
	4gG			3.35	2	1	4	4	30	
4hA			3.35	2	2	2	4	16		

Bacterial reference strains: S. a – *Staphylococcus aureus* ATCC 9144, B. s – *Bacillus subtilis* 168, E. c – *Escherichia coli* ATCC 25922, and P. a – *Pseudomonas aeruginosa* ATCC 27853. ^a CLogP values were calculated for the respective hydrocarbon linkers (calculated with ChemBioDraw Ultra v19.0.0.1.28). ^b Values given as *greater than* correspond to the highest concentration (500 µM) tested in the RBC assay. ^c Precipitation in the RBC assay observed.

2.3.4. Compound Series 4: Exploring the hydrocarbon linker chain (X)

We incorporated various linear and cyclic hydrocarbon linkers (**Table 4**, X group; **Figure 2**, green space holder) between the central scaffold and the cationic residue. 3,5-Dibromobenzyl was kept fixed as the lipophilic side chain and the previously reported compounds **1eA** and **1eG** (both X = *n*-butyl) served as reference substances for comparison. Shortening or elongating the alkyl chains to 2,3,5 or 6 methylene groups (**4(a-d)A**) led to no significant change in antibacterial activity (MIC: 4 – 16 µg/mL against all strains). The haemolytic activity increased slightly compared to **1eA** (X = *n*-butyl), except for **4bA** (X = *n*-propyl), which became slightly less haemolytic. So far, guanidine derivatives tended to have a higher haemolytic activity (*vide supra*) compared to amine derivatives. In contrast, **4bG** (X = *n*-propyl) and **4aG** (X = ethyl) were observed to exhibit 2-fold and 4-fold decreased haemolytic activity, respectively, compared to their amine counterparts. The activity against the Gram-positive strains was slightly improved, whereas the potencies against the Gram-negative *P. aeruginosa* were retained or a little diminished. The derivatives **4cA** and **4cG** (X = *n*-pentyl) displayed virtually the same MIC and EC₅₀ values, whereas **4dG** (X = *n*-hexyl) was less potent against *P.*

aeruginosa (MIC: 32 µg/mL) compared to **4dA** (X = *n*-hexyl) (MIC: 16 µg/mL). Both guanylated compounds were less potent than the previously investigated derivative **1eG** (X = *n*-butyl) and their haemolytic levels were comparably high (EC₅₀: 29 – 57 µg/mL). Compounds **4cG** (X = *n*-pentyl) and **4dG** (X = *n*-hexyl) led also to precipitation in the RBC assay upon sample preparation, possibly due to their higher overall hydrophobicity, demonstrating an unfavorable solubility profile

To investigate if the conformational freedom of the linker influenced the compounds potency, 1,3-cyclobutyl and 1,4-cyclohexyl were used as surrogates for the *n*-propyl and *n*-butyl chains, taking advantage of their restricted spatial arrangement. Compounds **4eA** (X = *cis*-1,3-cyclobutyl) and **4fA** (X = *trans*-1,3-cyclobutyl) displayed the same MIC values (4 – 8 µg/mL) as **4bA** (X = *n*-propyl) against all strains, but **4eA** (*cis*) was almost twice as haemolytic as **4bA** (X = *n*-propyl) and **4fA** (*trans*). Their guanylated counterparts **4eG** (*cis*) and **4fG** (*trans*), were more potent against the Gram-positive strains, but no change in MIC was observed against the Gram-negative strains. Both derivatives exhibited considerably higher haemolytic activity compared to **4bG** (X = *n*-propyl).

Table 5. Antimicrobial activity (MIC in µg/mL) against bacterial reference strains and haemolytic activity against human RBC (EC₅₀ in µg/mL) for compounds in Series 5.

Core structure	Comp ID	R ¹	R ²	R ₃	CLogP ^a	Antimicrobial activity				EC ₅₀ ^b
						S. a	B. s	E. c	P. a	
	5aA				3.39	32	8	64	256	>455
	5aG				3.39	8	4	64	>128	>497
	5bA				3.87	64	16	64	128	>393
	5bG				3.87	8	4	128	256	>435
	5cA				4.08	8	4	8	16	323
	5cG				4.08	2	2	8	32	348
	5dA				4.68	2	2	4	4	23
	5dG				4.68	2	2	4	8	61
	5eA				5.03	8	4	8	8	176
	5eG				5.03	4	2	8	16	445
	5fA				3.95	32	8	16	32	>438
	5fG				3.95	4	4	16	64	>480
	5gA				4.42	4	2	8	8	47
	5gG				4.42	1	1	2	16	169

Bacterial reference strains: S. a – *Staphylococcus aureus* ATCC 9144, B. s – *Bacillus subtilis* 168, E. c – *Escherichia coli* ATCC 25922, and P. a – *Pseudomonas aeruginosa* ATCC 27853. ^a CLogP values were calculated for the respective lipophilic side chains. For non-identical side chains, the value stated is the average of both individual side chains. Values were calculated for substituted benzyl groups (calculated with ChemBioDraw Ultra v19.0.0.1.28). ^b Values given as *greater than* correspond to the highest concentration (500 µM) tested in the RBC assay.

While being equally haemolytic (EC_{50} : 15 $\mu\text{g}/\text{mL}$) and 5-times more haemolytic than **6eA** ($X = n\text{-butyl}$), **4hA** ($X = \text{trans-1,4-cyclohexyl}$) was twice as potent as **4gA** ($X = \text{cis-1,4-cyclohexyl}$). The guanidine derivatives **4hG** (*trans*) and **4gG** (*cis*) were both highly potent (MIC: 2 – 4 $\mu\text{g}/\text{mL}$) against all bacterial strains, but their haemolytic activity was also too high to be of therapeutic value for systemic application. Of note, the guanylated derivative (**4gG**) was nevertheless less haemolytic than the amine derivative (**4aA**).

In summary, compounds with rigid cyclic linkers showed similar or slightly higher potency compared to their linear analogues, but they tended to be more haemolytic. Furthermore, compounds with pentyl and hexyl linkers showed furthermore decreased water solubility. The amine derivatives having ethyl, propyl or butyl linkers displayed similar antibacterial bioactivity profiles, whereas the equivalent guanidine derivatives displayed descending antimicrobial activity as follows: *n*-butyl > *n*-propyl > ethyl. The best balance between high antimicrobial activity and low haemolytic activity was presented by compounds having *n*-propyl hydrocarbon linker chains.

2.3.5. Compound Series 5: Investigating compounds with a *n*-propyl hydrocarbon linker

In series **5** (Table 5), we studied the effect of the *n*-propyl linker more closely due to the promising balance between high antimicrobial activity and low haemolytic activity seen in series **4**. We selected the lipophilic side chains (R^1/R^2) based on our previous findings. We reasoned that compounds **5a**, **5b** and **5f** would mainly act against Gram-positive strains, whereas compounds **5c-e** and **5g** should provide a higher broad-spectrum activity. Amines **5aA** ($R^1/R^2 = 6\text{-Br-2-methylquinolinyl}$) and **5bA** ($R^1/R^2 = 4\text{-CF}_3\text{Bn}$) displayed generally low antibacterial activity against all strains (MIC: 8 – 256 $\mu\text{g}/\text{mL}$). However, the guanyl equivalents **5aG** and **5bG** exhibited fair activity and selectivity for Gram-positive

strains (MIC: 4 – 8 $\mu\text{g}/\text{mL}$) and weak activity towards Gram-negative strain (MIC: ≥ 64 $\mu\text{g}/\text{mL}$). None of the four compounds was haemolytic.

Compound **5cA** ($R^1/R^2 = 4\text{-Br, 3-ClBn}$) displayed good activity against all strains (MIC: 4 – 8 $\mu\text{g}/\text{mL}$) except for the Gram-negative *P. aeruginosa* (MIC: 16 $\mu\text{g}/\text{mL}$). The guanyl derivative **5cG** ($R^1/R^2 = 4\text{-Br, 3-ClBn}$) displayed further improved activity against the Gram-positive strains (MIC: 2 $\mu\text{g}/\text{mL}$), but the activity against *P. aeruginosa* was lost. Noteworthy, the amine **5cA** and guanidine **5cG** derivatives were non-haemolytic (EC_{50} : >300 $\mu\text{g}/\text{mL}$), despite the relatively high CLogP values of their lipophilic side chains.

Derivatives **5dA** and **5dG** contained the bulky bromonaphthyl ($R^1/R^2 = 4\text{-Br-1-Nal}$) group. The amine derivative **5dA** was highly potent (MIC: 2 – 4 $\mu\text{g}/\text{mL}$) against all strains, but too haemolytic to be of practical use (EC_{50} : 23 $\mu\text{g}/\text{mL}$). Upon guanylation, **5dG** still had good activity against all strains (MIC: 2 – 8 $\mu\text{g}/\text{mL}$) and an almost three-fold decrease in haemolytic activity (EC_{50} : 61 $\mu\text{g}/\text{mL}$) was observed. The relatively high haemolytic activity is still unfavorable, but the positive

effect of exchanging *n*-butyl linkers (**2dG**) for *n*-propyl linkers (**5dG**) is well demonstrated.

The amine derivative **5eA**, featuring 3,5-di(trifluoromethyl)benzyl side chains ($R^1/R^2 = 3,5\text{-di-CF}_3\text{Bn}$), was potent against all strains (MIC: 4 – 8 $\mu\text{g}/\text{mL}$) and displayed low haemolytic activity (EC_{50} : 176 $\mu\text{g}/\text{mL}$). The guanyl analogue **5eG** was twice as potent against the Gram-positive strains, while the activity against *P. aeruginosa* was reduced (MIC: 16 $\mu\text{g}/\text{mL}$). Pleasingly, the guanylation rendered the compound non-haemolytic.

The unsymmetrically C-5 substituted amine **5fA** ($R^1 = 3,5\text{-di-BrBn}$, $R^2 = 4\text{-CF}_3\text{Bn}$) displayed acceptable activity only against *B. subtilis* (MIC: 8 $\mu\text{g}/\text{mL}$). The guanyl derivative **5fG** exhibited good activity against both Gram-positive strains (MIC: 4 $\mu\text{g}/\text{mL}$), but its intermediate activity against Gram-negative *E. coli* (MIC: 16 $\mu\text{g}/\text{mL}$) limits its narrow-spectrum application against Gram-positive bacteria.

The unsymmetrically substituted amine **5gA** ($R^1 = 3,5\text{-di-BrBn}$, $R^2 = 4\text{-tert-butylBn}$) was potent against all strains tested (MIC: 2-8 $\mu\text{g}/\text{mL}$) but was quite haemolytic (EC_{50} : 47 $\mu\text{g}/\text{mL}$). The guanyl derivative **5gG** became more potent against all strains but *P. aeruginosa* (MIC: 16 $\mu\text{g}/\text{mL}$), accompanied by an almost 4-fold decrease in haemolytic activity (EC_{50} : 169 $\mu\text{g}/\text{mL}$), rendering it a very promising candidate for further studies.

Using *n*-propyl linkers clearly had a positive effect and led to development of the potent derivatives **5cA**, **5eA**, **5eG**, **5fG** and **5gG** with broad-spectrum activity. All five derivatives displayed low haemolytic activity, making them promising candidates for further evaluation.

2.3.6. Summary of SAR analysis

The general trends of our SAR analysis are summarized in Figure 3. When assessing the potency of the lipophilic side chains and the hydrocarbon linkers, amine and guanidine derivatives were not distinguished, as they generally follow the same trends.

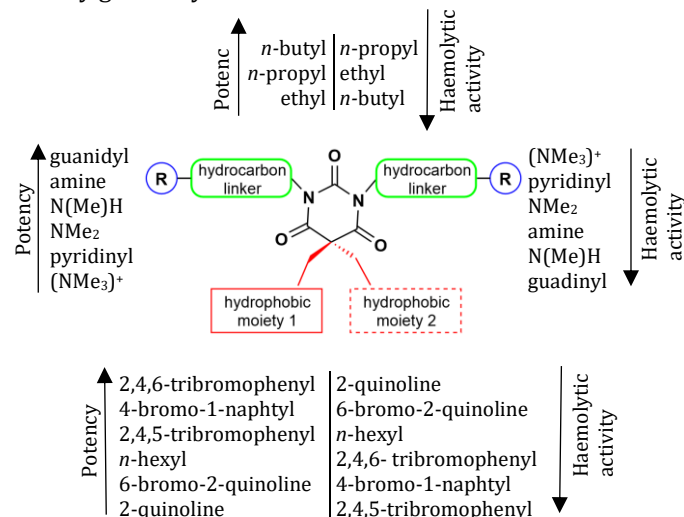


Figure 3. Overview over the general trends observed during the SAR investigation. The trends for haemolytic activity were assessed for the average between the respective amines and guanidines.

We found that the antimicrobial activity decreased along the line of *n*-butyl > *n*-propyl > ethyl and haemolytic activity increased as follows: *n*-propyl < ethyl < *n*-butyl.

The cyclic hydrocarbons, *n*-pentyl and *n*-hexyl displayed varying MIC values, but where all too haemolytic to be of any practical use and were therefore excluded from the list. Guanyl compounds with *n*-butyl linkers were more haemolytic than their amine counterparts.

Interestingly, for ethyl and *n*-propyl linkers this trend was reversed (see Figure S1 in the SI). Based on this, *n*-propyl seemed to be the best compromise to achieve high antimicrobial activity and moderate haemolytic activity.

In line with our previous findings, the compounds potency and haemolytic activity increased with higher CLogP values of the lipophilic side chains for both, amines and guanidines. Bromines proved to be a good modulator of the hydrophobicity of aryl groups. The structure of the side chains seemed thereby to be secondary. The most potent compounds proved to be too haemolytic for future therapeutic considerations. By combining two lipophilic side chains of different structure and hydrophobicity (**3aG** and **3bG**), antimicrobial potency and haemolytic activity of the compounds could be fine-tuned.

To achieve good broad-spectrum activity, amine or guanidine groups proved to be necessary. Methylated primary amines showed reduced activity against Gram-negative *P. aeruginosa* alongside reduced haemolytic activity. The least haemolytic cationic groups were the quaternary ammonium compounds in **1c** and **1d**. Due to its lack of haemolytic activity and high activity against Gram-positive bacterial strains, **1c** could prove valuable for narrow-spectrum applications against Gram-positive bacteria.

2.4. Selectivity index

A common measurement for the efficiency of antimicrobial agents is the selectivity index (SI) given by the ratio EC₅₀/MIC (for all values see Table S1). Our efforts led to promising candidates for narrow as well as broad-spectrum applications. We have grouped them into three groups (Table 6) based on their activity and SI against Gram-positive strains (entries 1-4), Gram-positive strains and *E. coli* (entries 5-7) and all strains tested (entries 8-11), respectively. Compounds were considered active if the MIC values were ≤16 µg/mL.

The first group, **1c**, **3aG**, **5aG** and **5bG** (Table 6, entries 1-4), comprises compounds that had a SI ≥54 for the Gram-positive strains, while showing no activity against Gram-negative strains and human red blood cells. These properties make them ideal candidates for narrow-spectrum application against Gram-positive bacteria.

Compounds in the second group had SI ≥40 (Table 6, entries 5-7) against the Gram-positive strains and the Gram-negative *E. coli* and a medium SI (<20) against Gram-negative *P. aeruginosa*. Of the three compounds **1d**, **3bG** and **5gG**, only pyridinyl derivative **1d** (entry 5) did not show measurable haemolytic activity. But despite having moderate EC₅₀ values (161 and 169 µg/mL), guanyl derivatives **3bG** and **5gG** had a high SI. The third group comprises molecules with a SI ≥20 (Table 6, entries 8-11) against all four strains. Compounds **4bG** and **5eA** (entries 8-9) displayed a good overall SI and had

also good activity against the Gram-negative *P. aeruginosa* (MIC: 8 µg/mL).

Table 6. Selectivity index (SI) of the most promising wide and narrow-spectrum antimicrobials. EC₅₀ values are given in [µg/mL].

entry	Comp. ID	SI (EC ₅₀ /MIC) ^a				EC ₅₀ ^b
		S. a	B. s	E. c	P. a	
1	1c	>135	>67	-	-	>539
2	3aG	225	113	-	-	450
3	5aG	>62	>124	-	-	>497
4	5bG	>54	>109	-	-	>435
5	1d	>280	>140	>70	-	>559
6	3bG	81	40	81	10	161
7	5gG	169	169	85	11	169
8	4bG	93	93	47	23	187
9	5eA	23	46	23	23	176
10	5eG	111	222	56	28	445
11	5cA	40	81	40	20	323
12	1eA	20	40	20	10	79
13	1eG	31	31	31	8	62

Bacterial reference strains: S. a – *Staphylococcus aureus* ATCC 9144, B. s – *Bacillus subtilis* 168, E. c – *Escherichia coli* ATCC 25922, and P. a – *Pseudomonas aeruginosa* ATCC 27853. ^a –: No SI was calculated if the MIC was >16 µg/mL. ^b Values given as *greater than* correspond to the highest concentration (500 µM) tested in the RBC assay.

Compounds **5eG** and **5cA** (entries 10-11) were mildly potent against *P. aeruginosa* (MIC: 16 µg/mL), but due to their low haemolytic activity they still display promising SI values. Their absence of cytotoxicity makes them promising candidates, despite their mild activity against Gram-negative *P. aeruginosa*, keeping in mind that most naturally occurring AMPs display low activity against this Gram-negative strain as well.¹⁷ Additionally, group 3 compounds generally matched or outperformed our reference compounds **1eA** and **1eG** (entries 12-13).

2.5. Effect of the counterion on solubility and activity

The counterion of acidic and basic drugs is known to greatly influence their overall physicochemical properties such as solubility, membrane permeability and stability.^{54, 55} From the long list of physiological anions for basic active pharmaceutical ingredients (APIs), hydrochloride salts are predominant⁵⁵ and known to improve water solubility.⁵⁶

We found that the water solubility of the TFA salts decreased noticeably when the CLogP values of the lipophilic side chains rose beyond 4. To study if we could counteract this trend, we converted selected compounds to HCl salts. Additionally, we wanted to investigate if the counterion affected the biological activity. Table 7 summarizes the re-evaluated MIC and EC₅₀ values of selected compounds as hydrochloride salts. Water solubility was assessed qualitatively by setting the threshold at 1 mg/mL. Entries 1-3 show that previously not soluble (-) TFA salts became soluble (+). Compound **5cG** (entry 4) and several others (data not shown) remained poorly soluble in water, especially if several bromine substituents were present in the lipophilic side chain.

Hydrochloride salts of the amine derivatives **5eA** and **5cA** exhibited no change in their MIC values and showed only slightly differing EC₅₀ values (entries 1-2).

Table 7. MIC and EC₅₀ values in µg/mL of selected di-trifluoroacetic acid (TFA, first value) and di-hydrochloride (HCl, second value) salts. Improved values are highlighted in green.

entry	code	MIC		EC ₅₀ [µg/mL]	Solubility ^b
		S. a	E. c		
1	5eA	8/8	8/8	176/224	-/+
2	5cA	8/8	8/8	323/271 ^c	-/+
3	5eG	4/2	8/8	445/118	-/+
4	5cG	2/0.5	8/8	348/291 ^d	-/-

^a Bacterial reference strains: S. a – *Staphylococcus aureus* ATCC 9144 and E. c – *Escherichia coli* ATCC 25922. ^b If solubility in pure water is equal or greater than 1 mg/mL it is denoted with (+), if lower (-). ^cEC₅₀ = 368/375 µM (TFA/HCl). ^dEC₅₀ = 362/362 µM (TFA/HCl).

No clear trend could be observed whether hydrochloride salts tended to be more or less haemolytic than TFA salts. Surprisingly, the HCl salts of guanyl derivatives **5eG** and **5cG** displayed improved MIC values against *S. aureus* (Entries 3-4), while the activity against *E. coli* remained unchanged. Compound **5eG** was the only HCl salt being considerably more haemolytic than its TFA counterpart (Entry 3), for yet undetermined reasons. The deceptively higher haemolytic activity of derivatives **5cA** and **5cG** as HCl salts (Entry 2 and 4) can be attributed to the lower molecular weight of the HCl salts.

2.6. Mode of action studies

Luciferase-based biosensor assays (viability and membrane integrity) were performed to explore the mode-of-action of promising compounds on *B. subtilis* 168 and *E. coli* K12.⁵⁷ The biosensor-based viability assay measures bacterial viability as light production through recombinantly expressed bacterial luciferase originating from the *Photobacterium luminescens lux* operon. The addition of external substrates does not affect the production of light by the bacterial *lux* operon. The bacterium itself provides the pool of reduced flavin mononucleotide (FMN_{H2}) and long-chain aliphatic aldehydes, which are the substrates responsible for light production. Bacterial luciferase is an excellent real-time sensor for bacterial viability, as NADH, NADPH, and ATP are necessary to constantly top up the substrates' pool.

The biosensor-based membrane integrity assay depends on the luciferase (*lucGR* gene) originating from the luminous click beetle *Pyrophorus plagiophthalmus*. In contrast to bacterial luciferase, the light reaction of *lucGR* is stringently reliant on the substrate D-luciferin, which is added externally. D-luciferin is inadequately crossing intact biological membranes at neutral pH. After the addition of antimicrobial substances, the uptake is explored to determine if the membrane becomes.

permeable to the substrate D-luciferin. An increase in light production occurs when D-luciferin enters (increased influx) through a compromised membrane. Light production peaks rapidly if membrane integrity is compromised and, thereafter, usually decreases while the ATP from dying cells is consumed. Based on structural modifications, MIC values, haemolytic activity, and selectivity index, 17 compounds were selected for

mode of action studies against *B. subtilis* 168 (see supporting information, **Table S2**) as they were mainly potent against Gram-positive bacteria. Furthermore, based on their broad-spectrum activity, 14 additional compounds were tested against both, the Gram-positive *B. subtilis* 168 and the Gram-negative *E. coli* K12 biosensor strain (see the SI, **Tables S2** and **S3**). In general, most of the compounds tested affected viability and showed strong membrane disrupting activity against both bacterial strains. However, some of the compounds showed a more pronounced effect on viability and a faster membranolytic effect against *B. subtilis* compared to *E. coli*. For most compounds, both viability and membrane integrity were affected when the concentration of the compounds was higher than the MIC value. Additionally, increasing concentrations affected viability and membranolytic activity in increasing rates, indicating a concentration-dependent killing effect.

We selected the broad-spectrum barbiturate **3bG** to exemplify the results of the viability and membrane integrity assay in detail (**Figure 4** and **Figure 5**). Barbiturate **3bG** clearly affected the viability of *B. subtilis* (**Figure 4A**, left). The membrane integrity assay was performed on the *B. subtilis* biosensor strain to confirm that the rapid decrease in bacterial viability was caused by membrane damage. Derivative **3bG** showed a membrane-related mode of action as light emission decreased rapidly in a dose-dependent manner (**Figure 4B**, left), similar to chlorhexidine (CHX) (**Figure 4B**, right). The reference control CHX is a bactericidal agent recognized for its cell wall and membrane disruptive properties,⁵⁸ with MIC values of 1.5 µg/mL against both, *B. subtilis* 168 and *E. coli* K12. The disruptive membrane effect of barbiturate **3bG** on *B. subtilis* was shown at a concentration as low as 6.4 µg/mL, which is approximately 1.6 times higher than its MIC (4 µg/mL) (**Figure 4B**, left). The lowest concentration (3.2 µg/mL), which is slightly lower than its MIC value, showed a limited membrane disruption effect and the peak emission did not decline during the assay period. The bacterial concentration for these experiments was approximately 1000 times higher than the concentration used in the MIC assay, which could explain why slightly higher concentrations of barbiturate **3bG** were needed to affect the viability and membrane integrity.

When it comes to the effects of barbiturate **3bG** on the viability and membrane integrity in the Gram-negative *E. coli*, the picture is somewhat different from that of the Gram-positive *B. subtilis*. The broad-spectrum derivative **3bG** affected the viability of the *E. coli* strain and showed a concentration-dependent killing effect like CHX (**Figure 5A**). Although **3bG** affected the viability, a much less prominent inner membrane disruptive effect was observed as only the two highest concentrations (6.4 – 12.8x MIC) gave a rise in light emission (and did not decline during the test period) (**Figure 5B**, left). The delayed and reduced action of **3bG** on the membrane integrity might be due to the outer membrane of *E. coli*, which probably acts as an additional barrier.

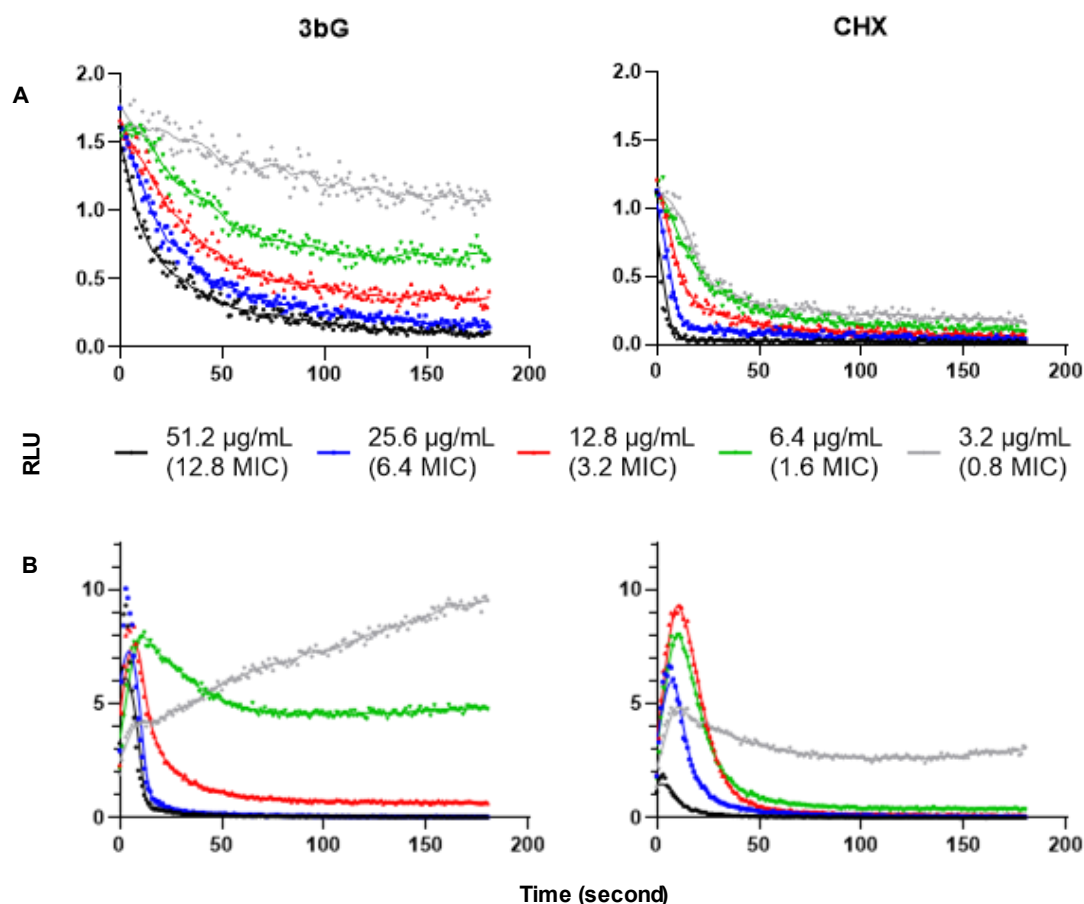


Figure 4. The effects of **3bG** (broad-spectrum) and CHX (positive control) on the kinetics of (A) viability and (B) membrane integrity in *B. subtilis* 168. Normalized light emission (normalized with a negative, untreated water control) is plotted as relative light units (RLU) over time (seconds). Light emission was measured each second for 180 s after adding the bacterial cell suspension (with 1 mM D-luciferin for the membrane integrity assay) to the analytes in separate wells. The multiples of the MIC values given in parentheses refers only to compound **3bG**. The figure shows a representative data set from at least three independent experiments.

To confirm the assumption about the outer membrane barrier in *E. coli*, we used the 1-*N*-phenyl naphthylamine (NPN) fluorescent probe to determine whether compound **3bG** can affect the outer membrane to become more permeable. The small molecule NPN (219 Da) is weakly fluorescent in an aqueous solution, but when bound to phospholipids, it gives strong fluorescence.⁵⁹ The hydrophobic NPN cannot efficiently cross the outer membrane of intact *E. coli* cells, yielding low fluorescence, but if the outer membrane is compromised, NPN can reach the periplasmic space and bind phospholipids of the inner and outer membranes, thus producing increased fluorescence.

In this assay, low concentrations (3.2 µg/mL) of barbiturate **3bG** led to higher fluorescence levels (Figure 5C, left), but did not initially give any increase in luminescence in the inner membrane integrity assay (Figure 5B, left). This phenomenon suggests that most of the cells are intact and viable without having significantly compromised integrity of the inner membrane but have increased permeability of the outer membrane. Upon increasing the concentration of barbiturate **3bG**, the fluorescence levels were lower (Figure 5C, left) indicating either an intact outer membrane or rapid

membrane disintegration before the start of the measurement. At the same time the viability of the bacterial cells was clearly reduced (Figure 5A, left) and the inner membrane integrity was impaired (Figure 5B, left). When the 10 µL sample of the NPN assay was spotted on an agar plate after the test period, the viability of the bacterial cells was clearly reduced for concentrations of 25.6 to 51.2 µg/mL (6.4 – 12.8x MIC) (see Figure S4), confirming the bactericidal effect of barbiturate **3bG**. Those results strongly suggest that barbiturate **3bG** disrupts both the outer and the inner membrane at the same rate when the concentration is high enough. However, it cannot be excluded that higher concentrations of **3bG** induce a different mode of action, resulting in the compound crossing the outer membrane without disrupting it. Our results indicate that the primary mode of action for most of the compounds, including the broad-spectrum barbiturate **3bG**, against both the Gram-positive *B. subtilis* and the Gram-negative *E. coli*, is the disruption of the membrane integrity in a concentration-dependent manner. However, there might also be other targets than the bacterial cytoplasmic membrane, and more work is required to conclude if there is any dual mode of action present or not.

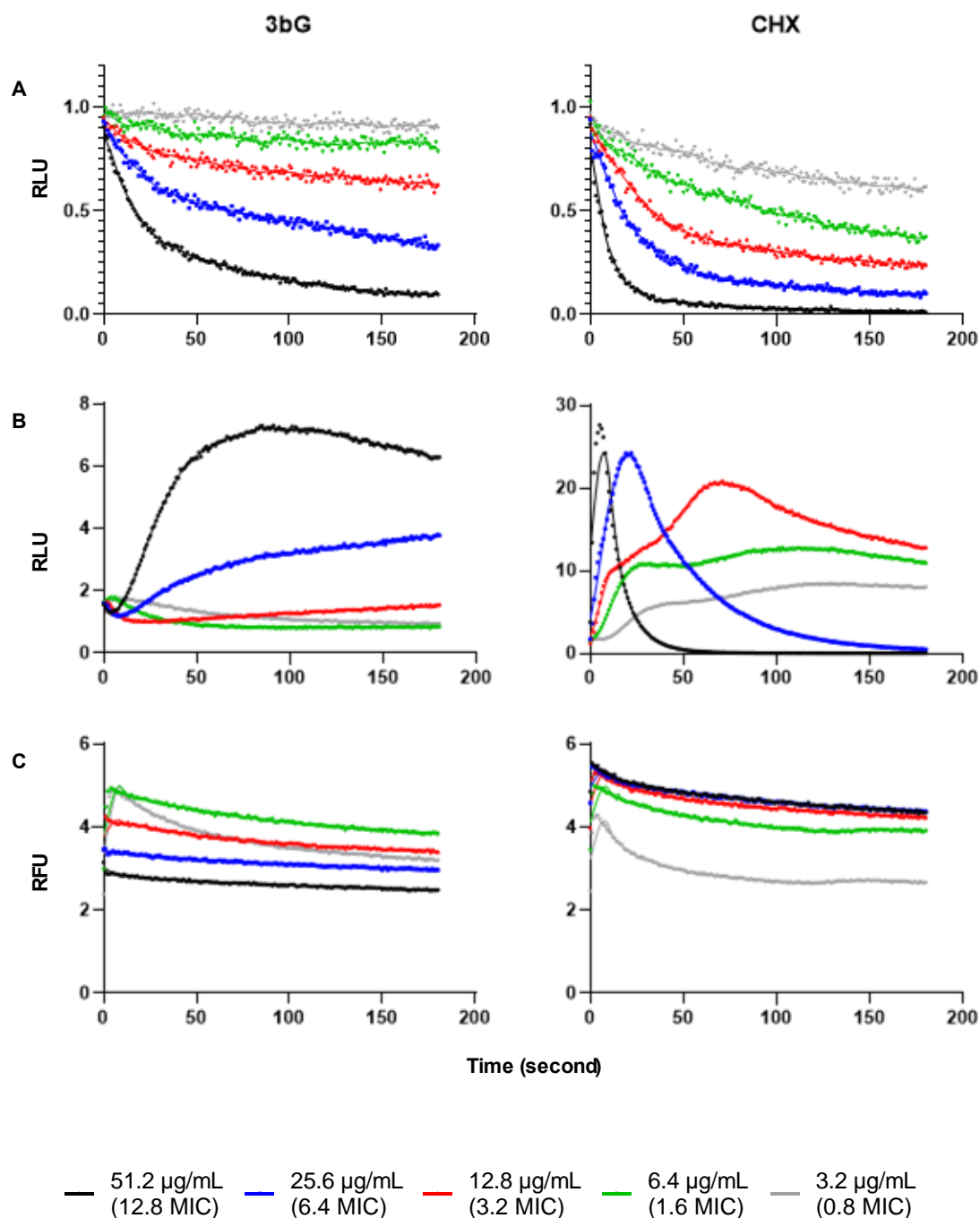


Figure 5. The effects of **3bG** (broad-spectrum) and a CHX (positive control) on the kinetics of (A) viability and (B) inner membrane integrity (C) outer membrane integrity in *E. coli* K12. Normalized light emission (normalized with a negative, untreated water control) is plotted as relative light units (RLU) over time (seconds) for A and B. For C, normalized fluorescence (normalized with a negative, untreated water control) is plotted as relative fluorescence units (RFU) over time (seconds). Light emission/fluorescence was measured each second for 180 s after adding the bacterial cell suspension (with 1 mM D-luciferin for the inner membrane integrity assay and 20 µM 1-*N*-phenylnaphthylamine for outer membrane integrity assay) to the analytes in separate wells. The multiples of the MIC values given in parentheses refers only to compound **3bG**. The figure shows a representative data set from at least three independent experiments.

3. Conclusion

In the present study, we have investigated the qualitative influence of the individual structural components of *N,N*-dialkylated-5,5-disubstituted amphipathic barbiturates on their bioactivity. We found

that *n*-propyl linkers provide the best balance between antibacterial potency and haemolytic activity and *n*-butyl linkers provide the highest potency. Guanidyl head-groups led to the highest antimicrobial potency, whereas trimethylated amines proved to be attractive for narrow-spectrum application. By choosing the individual components carefully, we were able to prepare several

compounds having SI values ≥ 20 and being active towards two (**1c**, **3aG**, **5aG**, **5bG**), three (**1d**, **3bG**, **5gG**) or all four (**4bG**, **5cA**, **5eA**, **5eG**) strains of our test panel. The best compounds (**4bG** and **5eA**) had an improved selectivity index compared to the initial starting point (**1eG**).

Studies on the integrity of the membranes and the viability of bacterial cells suggest that our compounds exert their bactericidal activity by disrupting the bacterial cell wall of Gram-positive *B. subtilis* in a concentration-dependent manner as exemplified by barbiturate **3bG**. In Gram-negative *E. coli* both, the inner and outer membrane, were supposedly rapidly disrupted at higher compound concentration, but a second mechanism of action might be present in addition.

We believe that our detailed analysis can help to devise new amphipathic cationic mimics of antimicrobial peptides.

4. Experimental Section

For a detailed description of all chemical and biological experimental procedures, chemical analysis, and supporting results, see the Supporting Information. Additional raw data is available through the DataverseNO repository, link: <https://doi.org/10.18710/GNTWOG>.

Author contributions

M.K.L, A.B. and M.B.S. designed the compound library; M.K.L and F.Z. performed the compound synthesis and analysis; A.R., H.D., H.-M.B., T.H. and K.S. determined the biological assays; A.R., H.D., T.A. performed the biological assays and M.K.L, A.R., H.D., H.-M.B., T.H., K.S., A.B. and M.B.S. analysed and interpreted the data. The manuscript was written through contributions of all authors. All authors have given approval to the final version of the manuscript.

Acknowledgements

MKL, AR and HD thank for a PhD fellowship provided by UiT as part of the AntifoMar and LeadScAMR grants.

Declaration of competing interest

The authors declare no conflict of interests.

References

1. Hutchings, M. I.; Truman, A. W.; Wilkinson, B., Antibiotics: past, present and future. *Curr. Opin. Microbiol.* **2019**, *51*, 72-80.
2. Global action plan on antimicrobial resistance. World Health Organization: Geneva, 2015.
3. Tamma, P. D.; Cosgrove, S. E.; Maragakis, L. L., Combination Therapy for Treatment of Infections with Gram-Negative Bacteria. *Clin. Microbiol. Rev.* **2012**, *25* (3), 450-470.
4. Laws, M.; Shaaban, A.; Rahman, K. M., Antibiotic resistance breakers: current approaches and future directions. *FEMS Microbiol Rev* **2019**, *43* (5), 490-516.
5. Mandal, S. M.; Roy, A.; Ghosh, A. K.; Hazra, T. K.; Basak, A.; Franco, O. L., Challenges and future prospects

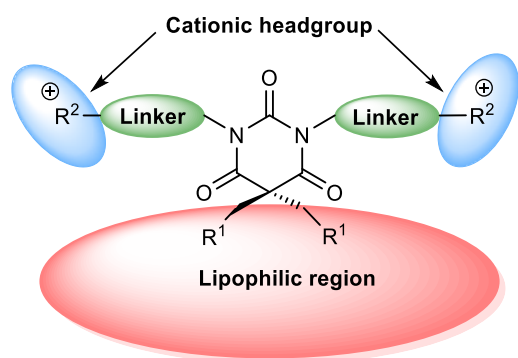
of antibiotic therapy: from peptides to phages utilization. *Front. Pharmacol.* **2014**, *5* (105).

6. Hamblin, M. R.; Hasan, T., Photodynamic therapy: a new antimicrobial approach to infectious disease? *Photochem Photobiol Sci* **2004**, *3* (5), 436-450.
7. DiGiandomenico, A.; Sellman, B. R., Antibacterial monoclonal antibodies: the next generation? *Curr. Opin. Microbiol.* **2015**, *27*, 78-85.
8. Beyth, N.; Hourri-Haddad, Y.; Domb, A.; Khan, W.; Hazan, R., Alternative Antimicrobial Approach: Nano-Antimicrobial Materials. *Evid.-Based Complementary Altern. Med.* **2015**, *2015*, 246012.
9. Mulani, M. S.; Kamble, E. E.; Kumkar, S. N.; Tawre, M. S.; Pardesi, K. R., Emerging Strategies to Combat ESKAPE Pathogens in the Era of Antimicrobial Resistance: A Review. *Front. Microbiol.* **2019**, *10* (539).
10. Hancock, R. E.; Patrzykat, A., Clinical development of cationic antimicrobial peptides: from natural to novel antibiotics. *Curr. Drug Targets Infect. Disord.* **2002**, *2* (1), 79-83.
11. Mahlapuu, M.; Håkansson, J.; Ringstad, L.; Björn, C., Antimicrobial Peptides: An Emerging Category of Therapeutic Agents. *Front. Cell. Infect. Microbiol.* **2016**, *6* (194).
12. Hancock, R. E. W.; Sahl, H.-G., Antimicrobial and host-defense peptides as new anti-infective therapeutic strategies. *Nat. Biotechnol.* **2006**, *24* (12), 1551-1557.
13. Pasupuleti, M.; Schmidtchen, A.; Malmsten, M., Antimicrobial peptides: key components of the innate immune system. *Crit. Rev. Biotechnol.* **2012**, *32* (2), 143-171.
14. Yeaman, M. R.; Yount, N. Y., Mechanisms of Antimicrobial Peptide Action and Resistance. *Pharmacol. Rev.* **2003**, *55* (1), 27.
15. Hancock, R. E. W., Peptide antibiotics. *Lancet* **1997**, *349* (9049), 418-422.
16. Brown, K. L.; Hancock, R. E. W., Cationic host defense (antimicrobial) peptides. *Curr. Opin. Immunol.* **2006**, *18* (1), 24-30.
17. Ebbensgaard, A.; Mordhorst, H.; Overgaard, M. T.; Nielsen, C. G.; Aarestrup, F. M.; Hansen, E. B., Comparative Evaluation of the Antimicrobial Activity of Different Antimicrobial Peptides against a Range of Pathogenic Bacteria. *PLoS one* **2015**, *10* (12), e0144611-e0144611.
18. Fosgerau, K.; Hoffmann, T., Peptide therapeutics: current status and future directions. *Drug Discov. Today* **2015**, *20* (1), 122-128.
19. Yang, Y.; Cai, Z.; Huang, Z.; Tang, X.; Zhang, X., Antimicrobial cationic polymers: from structural design to functional control. *Polym. J.* **2018**, *50* (1), 33-44.
20. Strassburg, A.; Kracke, F.; Wenners, J.; Jemeljanova, A.; Kuepper, J.; Petersen, H.; Tiller, J. C., Nontoxic, Hydrophilic Cationic Polymers—Identified as Class of Antimicrobial Polymers. *Macromol. Biosci.* **2015**, *15* (12), 1710-1723.
21. Liu, D.; DeGrado, W. F., De Novo Design, Synthesis, and Characterization of Antimicrobial β -Peptides. *J. Am. Chem. Soc.* **2001**, *123* (31), 7553-7559.
22. Sang, P.; Shi, Y.; Teng, P.; Cao, A.; Xu, H.; Li, Q.; Cai, J., Antimicrobial A-peptides. *Curr Top Med Chem* **2017**, *17* (11), 1266-1279.

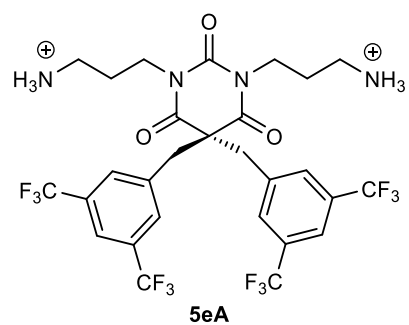
23. Hansen, T.; Alst, T.; Havelkova, M.; Strøm, M. B., Antimicrobial Activity of Small β -Peptidomimetics Based on the Pharmacophore Model of Short Cationic Antimicrobial Peptides. *J. Med. Chem.* **2010**, *53* (2), 595-606.
24. Teng, P.; Nimmagadda, A.; Su, M.; Hong, Y.; Shen, N.; Li, C.; Tsai, L.-Y.; Cao, J.; Li, Q.; Cai, J., Novel bis-cyclic guanidines as potent membrane-active antibacterial agents with therapeutic potential. *Chem. Commun.* **2017**, *53* (87), 11948-11951.
25. Paulsen, M. H.; Karlsen, E. A.; Ausbacher, D.; Anderssen, T.; Bayer, A.; Ochtrop, P.; Hedberg, C.; Haug, T.; Ericson Sollid, J. U.; Strøm, M. B., An amphipathic cyclic tetrapeptide scaffold containing halogenated β 2,2-amino acids with activity against multiresistant bacteria. *J. Pept. Sci.* **2018**, *24* (10), e3117.
26. Paulsen, M. H.; Ausbacher, D.; Bayer, A.; Engqvist, M.; Hansen, T.; Haug, T.; Anderssen, T.; Andersen, J. H.; Sollid, J. U. E.; Strøm, M. B., Antimicrobial activity of amphipathic α,α -disubstituted β -amino amide derivatives against ESBL – CARBA producing multi-resistant bacteria; effect of halogenation, lipophilicity and cationic character. *Eur. J. Med. Chem.* **2019**, *183*, 111671.
27. Wang, M.; Feng, X.; Gao, R.; Sang, P.; Pan, X.; Wei, L.; Lu, C.; Wu, C.; Cai, J., Modular Design of Membrane-Active Antibiotics: From Macromolecular Antimicrobials to Small Scorpionlike Peptidomimetics. *J. Med. Chem.* **2021**, *64* (14), 9894-9905.
28. Paulsen, M. H.; Engqvist, M.; Ausbacher, D.; Anderssen, T.; Langer, M. K.; Haug, T.; Morello, G. R.; Liikanen, L. E.; Blencke, H.-M.; Isaksson, J.; Juskewitz, E.; Bayer, A.; Strøm, M. B., Amphipathic Barbiturates as Mimics of Antimicrobial Peptides and the Marine Natural Products Eusynstyelamides with Activity against Multi-resistant Clinical Isolates. *J. Med. Chem.* **2021**.
29. Tapiolas, D. M.; Bowden, B. F.; Abou-Mansour, E.; Willis, R. H.; Doyle, J. R.; Muirhead, A. N.; Liptrot, C.; Llewellyn, L. E.; Wolff, C. W.; Wright, A. D.; Motti, C. A., Eusynstyelamides A, B, and C, nNOS inhibitors, from the ascidian *Eusynstyela latericius*. *Journal of natural products* **2009**, *72* (6), 1115-1120.
30. Tadesse, M.; Tabudravu, J. N.; Jaspars, M.; Strom, M. B.; Hansen, E.; Andersen, J. H.; Kristiansen, P. E.; Haug, T., The antibacterial ent-eusynstyelamide B and eusynstyelamides D, E, and F from the Arctic bryozoan *Tegella cf. spitzbergensis*. *Journal of natural products* **2011**, *74* (4), 837-841.
31. Richter, M. F.; Drown, B. S.; Riley, A. P.; Garcia, A.; Shirai, T.; Svec, R. L.; Hergenrother, P. J., Predictive compound accumulation rules yield a broad-spectrum antibiotic. *Nature* **2017**, *545* (7654), 299-304.
32. Perlmutter, S. J.; Geddes, E. J.; Drown, B. S.; Motika, S. E.; Lee, M. R.; Hergenrother, P. J., Compound Uptake into *E. coli* Can Be Facilitated by N-Alkyl Guanidiniums and Pyridiniums. *ACS Infect. Dis.* **2021**, *7* (1), 162-173.
33. Zhang, S.; Shi, Z.; Cao, W.; Gao, T.; Deng, H., Synthesis of a series of perfluoroalkyl containing spiro cyclic barbituric acid derivatives. *J. Chem. Res.* **2009**, *2009* (6), 381-383.
34. Kotha, S.; Deb, A. C.; Kumar, R. V., Spiroannulation of barbituric acid derivatives and its analogs by ring-closing metathesis reaction. *Bioorg. Med. Chem. Lett.* **2005**, *15* (4), 1039-1043.
35. Mahmudov, K. T.; Kopylovich, M. N.; Maharramov, A. M.; Kurbanova, M. M.; Gurbanov, A. V.; Pombeiro, A. J. L., Barbituric acids as a useful tool for the construction of coordination and supramolecular compounds. *Coord. Chem. Rev.* **2014**, *265*, 1-37.
36. Bojarski, J. T.; Mokrosz, J. L.; Bartoń, H. J.; Paluchowska, M. H., Recent Progress in Barbituric Acid Chemistry. In *Adv. Heterocycl. Chem.*, Katritzky, A. R., Ed. Academic Press: 1985; Vol. 38, pp 229-297.
37. Tate, J. V.; Tinnerman II, W. N.; Jurevics, V.; Jeskey, H.; Biehl, E. R., Preparation of 5-substituted benzylbarbituric acids and investigation of the effect of the benzyl and substituted benzyl groups on the acidity of barbituric acid. *J. Heterocycl. Chem.* **1986**, *23* (1), 9-11.
38. Ramachary, D. B.; Kishor, M.; Reddy, Y. V., Development of Pharmaceutical Drugs, Drug Intermediates and Ingredients by Using Direct Organoclick Reactions. *Eur. J. Org. Chem.* **2008**, *2008* (6), 975-993.
39. Kalita, S. J.; Deka, D. C., 2-Phenyl-2,3-dihydrobenzo[d]thiazole: A Mild, Efficient, and Highly Active in situ Generated Chemoselective Reducing Agent for the One-Pot Synthesis of 5-Monoalkylbarbiturates in Water. *Synlett* **2018**, *29* (04), 477-482.
40. Figueroa-Villar, J. D.; Cruz, E. R.; Lucia dos Santos, N., Synthesis of Oxadezaflavines from Barbituric Acid and Aromatic Aldehydes. *Synth. Commun.* **1992**, *22* (8), 1159-1164.
41. Vieira, A. A.; Marinho, B. G.; de Souza, L. G.; Fernandes, P. D.; Figueroa-Villar, J. D., Design, synthesis and in vivo evaluation of sodium 2-benzylchloromalonates as new central nervous system depressants. *MedChemComm* **2015**, *6* (8), 1427-1437.
42. Fletcher, S., The Mitsunobu reaction in the 21st century. *Org. Chem. Front.* **2015**, *2* (6), 739-752.
43. Katritzky, A. R.; Rogovoy, B. V., Recent developments in guanylation agents. *Arkivoc* **2005**, (iv), 49-87.
44. Gers, T.; Kunce, D.; Markowski, P.; Izdebski, J., Reagents for Efficient Conversion of Amines to Protected Guanidines. *Synthesis* **2004**, *2004* (01), 37-42.
45. Midura-Nowaczek, K.; Markowska, A., Antimicrobial peptides and their analogs: searching for new potential therapeutics. *Perspect Medicin Chem* **2014**, *6*, 73-80.
46. Dickson, J. S.; Koohmaraie, M., Cell surface charge characteristics and their relationship to bacterial attachment to meat surfaces. *Appl Environ Microbiol* **1989**, *55* (4), 832-836.
47. Bruinsma, G. M.; Rustema-Abbing, M.; van der Mei, H. C.; Lakkis, C.; Busscher, H. J., Resistance to a polyquaternium-1 lens care solution and isoelectric points of *Pseudomonas aeruginosa* strains. *J. Antimicrob. Chemother.* **2006**, *57* (4), 764-766.
48. Skrzypczak, A.; Brycki, B.; Mirska, I.; Pernak, J., Synthesis and antimicrobial activities of new quats. *Eur. J. Med. Chem.* **1997**, *32* (7), 661-668.

49. Devínsky, F.; Lacko, I.; Bittererová, F.; Mlynarčík, D., Quaternary ammonium-salts. 18. Preparation and relationship between structure, IR spectral characteristics, and antimicrobial activity of some new bis-quaternary isomers of 1,5-pentanediammonium dibromides. *Chem. Pap.* **1987**, *6* (41), 803-814.
50. Gilbert, P.; Moore, L. E., Cationic antiseptics: diversity of action under a common epithet. *J. Appl. Microbiol.* **2005**, *99* (4), 703-715.
51. Hansen, T.; Moe, M. K.; Anderssen, T.; Strøm, M. B., Metabolism of small antimicrobial β ,2-amino acid derivatives by murine liver microsomes. *Eur. J. Drug Metab. Pharmacokinet.* **2012**, *37* (3), 191-201.
52. Gillis, E. P.; Eastman, K. J.; Hill, M. D.; Donnelly, D. J.; Meanwell, N. A., Applications of Fluorine in Medicinal Chemistry. *J. Med. Chem.* **2015**, *58* (21), 8315-8359.
53. McDaniel, D. H.; Brown, H. C., An Extended Table of Hammett Substituent Constants Based on the Ionization of Substituted Benzoic Acids. *J. Org. Chem.* **1958**, *23* (3), 420-427.
54. Gupta, D.; Bhatia, D.; Dave, V.; Sutariya, V.; Varghese Gupta, S., Salts of Therapeutic Agents: Chemical, Physicochemical, and Biological Considerations. *Molecules* **2018**, *23* (7), 1719.
55. Serajuddin, A. T. M., Salt formation to improve drug solubility. *Adv. Drug Deliv. Rev.* **2007**, *59* (7), 603-616.
56. Gould, P. L., Salt selection for basic drugs. *Int. J. Pharm.* **1986**, *33* (1), 201-217.
57. Virta, M.; Åkerman, K. E. O.; Saviranta, P.; Oker-Blom, C.; Karp, M. T., Real-time measurement of cell permeabilization with low-molecular-weight membranolytic agents. *J. Antimicrob. Chemother.* **1995**, *36* (2), 303-315.
58. Kuyyakanond, T.; Quesnel, L. B., The mechanism of action of chlorhexidine. *FEMS Microbiol. Lett.* **1992**, *100* (1-3), 211-215.
59. Loh, B.; Grant, C.; Hancock, R. E., Use of the fluorescent probe 1-N-phenylnaphthylamine to study the interactions of aminoglycoside antibiotics with the outer membrane of *Pseudomonas aeruginosa*. *Antimicrob. Agents Chemother.* **1984**, *26* (4), 546-551.

Graphical Abstract



58 examples



broad-spectrum potency (MIC: 4 – 8 µg/mL)
low haemolytic activity (EC50: 176 µg/mL)
membranolytic

Supporting Information

for

A concise SAR-analysis of antimicrobial cationic amphipathic barbiturates for an improved activity-toxicity profile

Manuel K. Langer^{a#}, Ataur Rahman^{b#}, Hymonti Dey^b, Trude Anderssen^c, Francesco Zilioli^a, Tor Haug^b, Hans-Matti Blencke^b, Klara Stensvåg^b, Morten B. Strøm^{c*}, Annette Bayer^{a*}

^a Department of Chemistry, UiT – The Arctic University of Norway, NO-9037 Tromsø, NORWAY.

^b The Norwegian College of Fishery Science, Faculty of Biosciences, Fisheries and Economics, UiT – The Arctic University of Norway, NO-9037 Tromsø, NORWAY.

^c Department of Pharmacy, Faculty of Health Sciences, UiT – The Arctic University of Norway, NO-9037 Tromsø, NORWAY.

Authors contributed equally; * Corresponding authors.

Table of Contents

1	Trends in haemolytic activity	2
1.1	Comparison of amines vs. guanidines by linker length.....	2
1.2	Comparison of <i>n</i> -propyl vs. <i>n</i> -butyl linkers by cationic group.....	3
2	Experimental procedures	5
2.1	General methods.....	5
2.2	Synthesis of starting materials.....	5
2.3	General procedures.....	5
2.4	Synthesis of barbiturates with identical lipophilic side chains 7	7
2.5	Synthesis of barbiturates with mixed hydrophobic residues 10	10
2.6	Synthesis of series 1	12
2.7	Synthesis of series 2	13
2.8	Synthesis of series 3	17
2.9	Synthesis of series 4	22
2.10	Synthesis of series 5	27
3	¹ H and ¹³ C NMR spectra of final compounds	33
3.1	¹ H and ¹³ C NMR spectra of compounds in series 1	33
3.2	¹ H and ¹³ C NMR spectra of compounds in series 2	37
3.3	¹ H and ¹³ C NMR spectra of compounds in series 3	49
3.4	¹ H and ¹³ C NMR spectra of compounds in series 4	62
3.5	¹ H and ¹³ C NMR spectra of compounds in series 5	77
4	SFC analysis of final compounds	91
5	Full selectivity index table.....	99
6	Biological methods.....	100
6.1	Minimum inhibitory concentration (MIC) assay.....	100
6.2	Membrane integrity assays.....	100
6.3	Viability assay	101
6.4	Red Blood Cell Haemolysis Assay.....	101
7	Membrane integrity and viability assay	102
8	Literature	104

1 Trends in haemolytic activity

When comparing the haemolytic activity of amine and guanidine derivatives for a given linker length, we could see a distinguishable difference between the *n*-propyl and *n*-butyl linkers. We have grouped selected compounds into four scaffold groups for this comparison (**Figure S1**). Each group consisted of compounds with six different hydrophobic side chain combinations **S1-S6** for a given scaffold: *n*-propyl linkers and amine head groups (**3CA**), *n*-propyl linkers and guanidine head groups (**3CG**), *n*-butyl linkers and amine head groups (**4CA**) and *n*-butyl linkers and guanidine head groups (**4CG**). The comparison is visualized in **Figure S2** and **Figure S3**. Compounds having two 6-bromo-2-quinolyl (**2bA**, **2bG**, **5aA** and **5aG**) or two 4-trifluoromethylbenzyl (**5bA** and **5bG**) side chains are excluded due to their lack of haemolytic activity. RBC values for compounds containing *n*-butyl linkers and hydrophobic moieties 4-bromo-3-chlorobenzyl **S3** and 3,5-di(trifluoromethyl)benzyl **S4** were obtained in our previous study.^[1]

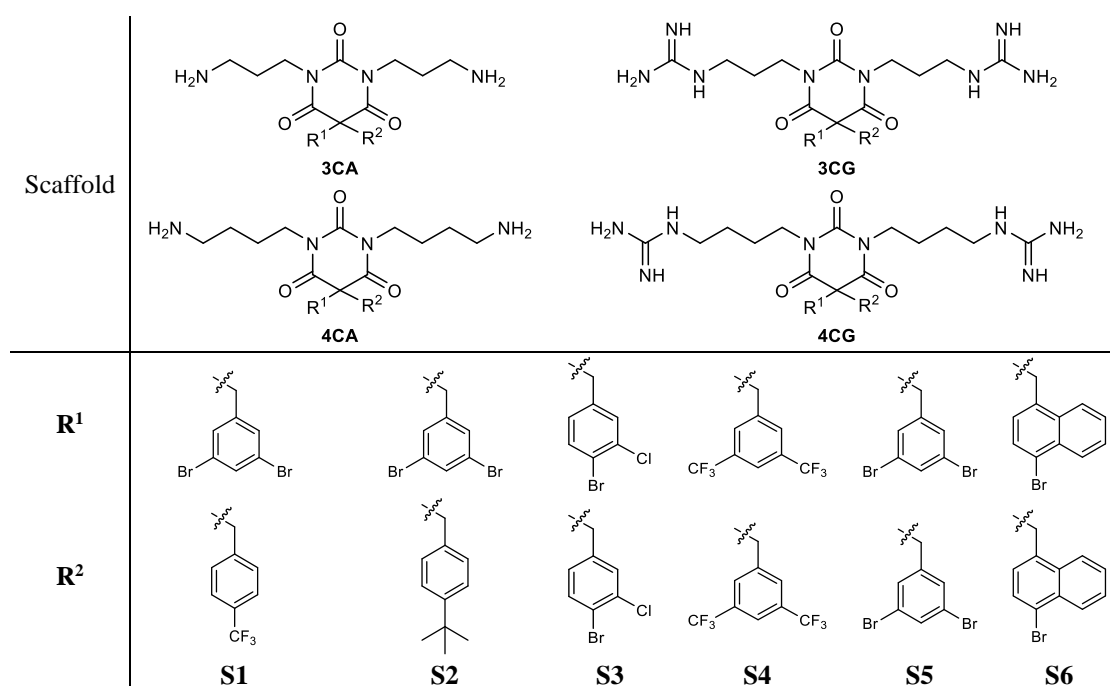


Figure S1. Overview of the scaffolds **3CA**, **3CG**, **4CA** and **4CG** and the linker combinations **S1-S6**.

1.1 Comparison of amines vs. guanidines by linker length

Figure S2 shows the comparison of haemolytic activity for amine and guanidine derivatives by linker length. For each compound series with a specific linker length (*n*-propyl **3C** or *n*-butyl **4C**) and hydrophobic side chain combination **S1-S6**, we subtracted the RBC values, given in $\mu\text{g/mL}$, for the amine derivative (**A**) from the guanidyl derivative (**G**). For a negative value the guanidine derivative was more and for a positive value less haemolytic than its amine counterpart.

For *n*-butyl linkers (**Figure S2**, grey bars) the guanidyl derivatives were more haemolytic than their amine counterparts, when side chain combinations **S1-S5** were employed. The difference ranged from a mere $17 \mu\text{g/mL}$ for di-3,5-dibromobenzyl **S5** to a significant $181 \mu\text{g/mL}$ for combination **S1**. Only when 4-bromo-1-methylnaphtyl **S6** was incorporated, the amine derivative was slightly more haemolytic. No clear correlation between structure and hydrophobicity could be found.

For *n*-propyl linkers (**Figure S2**, yellow bars), the effect was reversed. When side chain combination **S1** was incorporated both, amine and guanidine derivatives were non haemolytic leading to a difference of zero. For all other side chain combinations **S2-S6** the guanidyl derivatives were slightly (**S3**, $25 \mu\text{g/mL}$) to considerably (**S4**, $269 \mu\text{g/mL}$) less haemolytic than their amine counterparts. Again, this trend could not be correlated to any structural features.

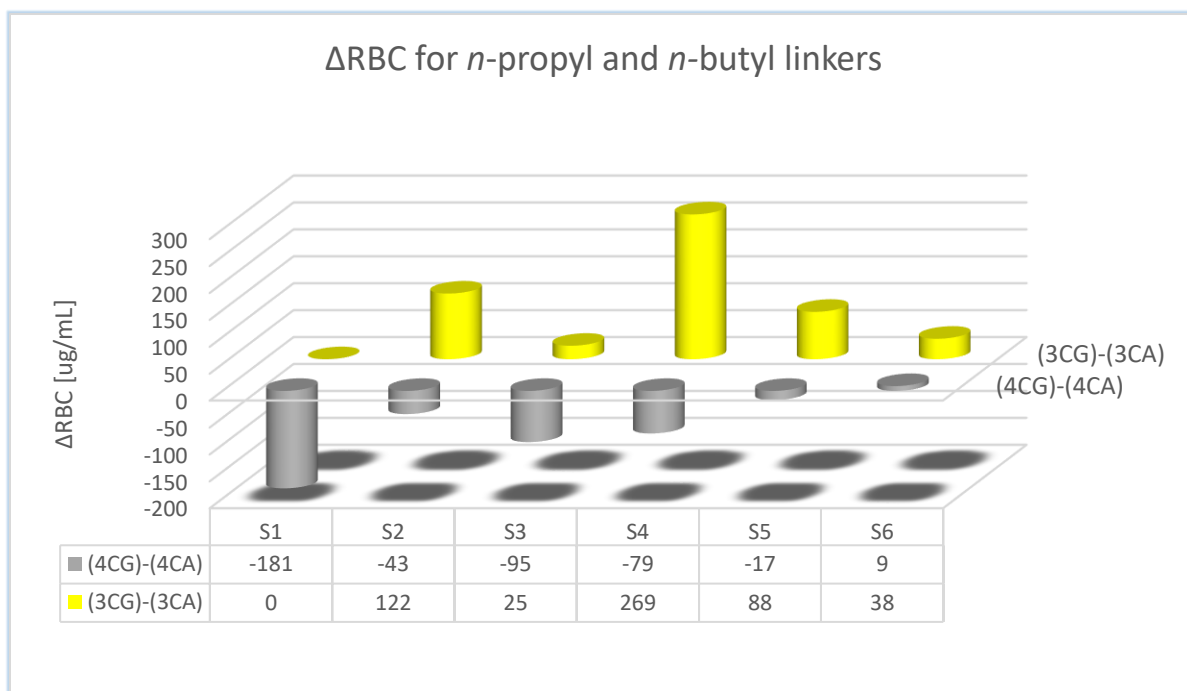


Figure S2. Comparison of the difference in haemolytic activity (RBC values in $\mu\text{g/mL}$) between the amine and guanidine derivatives for two linker series. For a given hydrophobic side chain combination (**S1-S6**) and hydrophobic linker (*n*-propyl **3C** or *n*-butyl **4C**), the RBC value of the amine derivative (**A**) was subtracted from the RBC value of the guanidyl derivatives (**G**), stated as (**3CG**)-(3CA) and (**4CG**)-(4CA). For negative values the guanidine derivative was more haemolytic than the amine. For positive values the guanidine derivative was less haemolytic than the amine. X-axis: hydrophobic moieties **S1-S6**, Y-axis: Δ RBC values in ($\mu\text{g/mL}$), z-axis: linker series. Grey: Comparison of derivatives with a *n*-butyl linker. Yellow: Comparison of derivatives with a *n*-propyl.

1.2 Comparison of *n*-propyl vs. *n*-butyl linkers by cationic group

Using the same grouping (**Figure S1**) we looked at the difference of the haemolytic activity between amine derivatives (**A**) having either a *n*-butyl (**4CA**) or *n*-propyl linker (**3CA**). The same comparison was composed for the guanidine derivatives (**3CG** and **4CG**) (both **Figure S3**). For each compound series with a specific cationic group (amine **A** or guanidine **G**) and hydrophobic side chain combination **S1-S6**, we subtracted the RBC values, given in $\mu\text{g/mL}$, for the *n*-butyl linker derivative (**4C**) from the *n*-propyl linker derivative (**3C**). For positive values the *n*-propyl derivatives were less and for negative values more haemolytic than their *n*-butyl containing counterparts.

For side chain combinations **S2** and **S4-S6** the amines were of comparable haemolytic activity regardless of the linker (**Figure S3**, grey bars) and displayed no obvious trend. For combinations **S1** and **S3** the *n*-propyl containing derivatives were considerably less haemolytic than their *n*-butyl counterparts by values of 158 and 151 $\mu\text{g/mL}$, respectively.

Unsurprisingly, a far more pronounced effect was observed, when comparing the linker series for the guanidyl derivatives (**G**) (**Figure S3**, yellow bars). As guanidyl derivatives (**G**) bearing *n*-propyl linkers (**3C**) are less haemolytic and ones bearing *n*-butyl linkers (**4C**) are more haemolytic than their amine (**A**) counterparts, one would expect a big difference in the absolute values for **3CG** and **4CG**. Indeed, all side chain combinations **S1-S6** together with a guanidyl group led to reduced haemolytic activity when going from *n*-butyl (**4C**) to *n*-propyl linkers (**3C**). The difference ranged from 25 – 347 $\mu\text{g/mL}$, with combination **S4** (di-3,5-(trifluoromethyl)benzyl) displaying the greatest reduction in haemolytic activity. As the structural changes are minor, no obvious SAR could be deduced. We are currently working on understanding this effect.

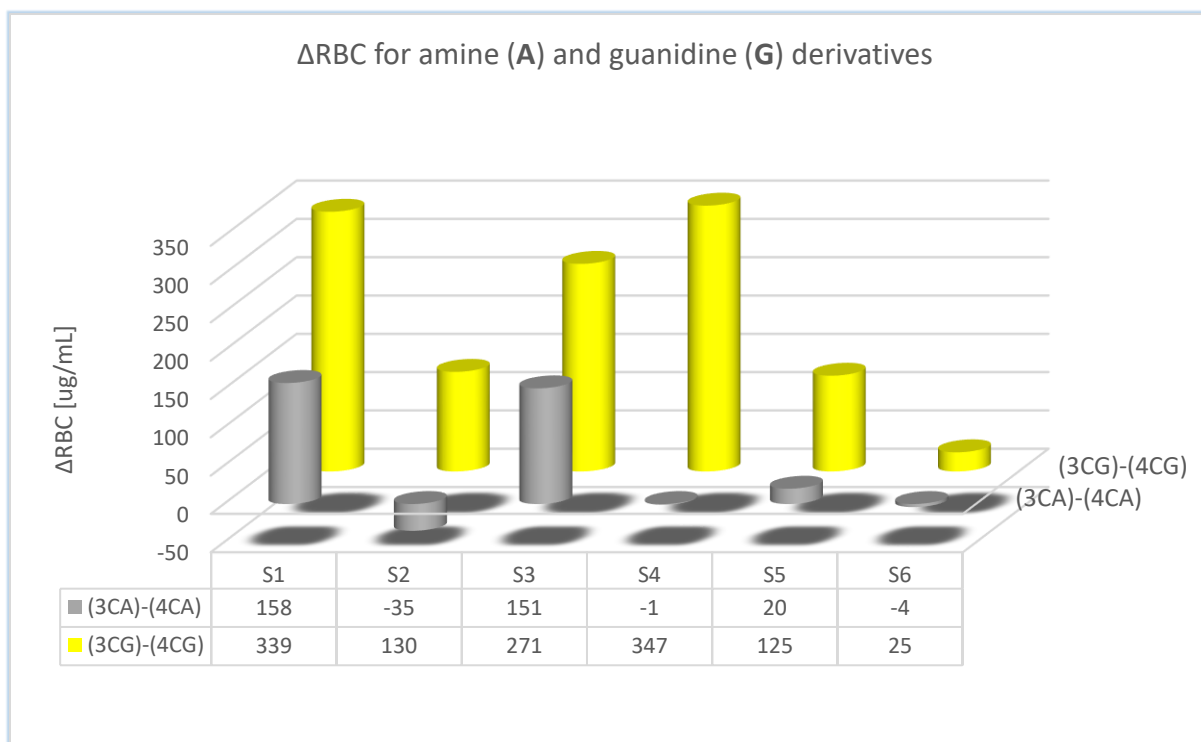


Figure S3. Comparison of the difference in haemolytic activity (RBC values in $\mu\text{g/mL}$) between the *n*-propyl and *n*-butyl derivatives for the amine and guanidine series. For a given hydrophobic side chain (**S1-S6**) and cationic group (amine **A** or guanidine **G**), the RBC value of the *n*-butyl (**4C**) was subtracted from the RBC value of the *n*-propyl (**3C**) derivative, stated as (**3CG**)-(4CG) and (**3CA**)-(4CA). For a positive value the *n*-propyl (**3C**) containing derivatives were less and for a negative value they were more haemolytic than the *n*-butyl derivatives. X-axis: hydrophobic moieties **S1-S6**, Y-axis: Δ RBC values in ($\mu\text{g/mL}$), z-axis: cationic group series. Grey: Comparison of derivatives with an amine group (**A**). Yellow: Comparison of derivatives with a guanidine group (**G**).

2 Experimental procedures

2.1 General methods

Unless otherwise noted, purchased chemicals were used as received without further purification. Solvents were dried according to standard procedures over molecular sieves of appropriate size. Normal phase flash chromatography was carried out on silica gel 60 (230–400 mesh) or on an interchim® PuriFlash XS420 flash system with the sample preloaded on a Samplet® cartridge belonging to a Biotage SP-1 system. Purification by reversed phase (RP) C18 column chromatography (H₂O with 0.1 % TFA/MeCN with 0.1 % TFA) was performed on an interchim® PuriFlash XS420 flash system with the sample preloaded on a Samplet® cartridge. Thin layer chromatography was carried out using Merck TLC Silica gel 60 F254 and visualized by short-wavelength ultraviolet light or by treatment with an appropriate stain.

NMR spectra were obtained on a 400 MHz Bruker Advance III HD spectrometer equipped with a 5 mm SmartProbe BB/1H (BB = 19F, 31P-15N) at 20 °C. The chemical shifts are reported in ppm relative to the solvent residual peak (CDCl₃: δH 7.26 and δC 77.16; Methanol-d₄: δH 3.31 and δC 49.00; deuterium oxide: δH 4.79; DMSO-d₆ δH 2.51 and δC 39.52). ¹³C NMR spectra were obtained with ¹H decoupling. Data are represented as follows: chemical shift, multiplicity (s = singlet, d = doublet, t = triplet, q = quartet, p = pentet, h = heptet, dt = doublet of triplet, tt = triplet of triplet, m = multiplet), coupling constant (*J* in Hz) and integration. The raw data was analyzed with MestReNova (Version 14.0.0-23239).

High-resolution mass spectra (HRMS) were recorded from methanol solutions on an LTQ Orbitrap XL (Thermo Scientific) either in negative or in positive electrospray ionization (ESI) mode. The data was analyzed with Thermo Scientific Xcalibur software.

The purity of all tested compounds was determined to be ≥95%. The analyses were carried out on a Waters ACQUITY UPC² system equipped with a Torus™ DEA 130Å, 1.7 μm, 2.1 mm x 50 mm column or a Torus™ 2-PIC 130Å, 1.7 μm, 2.1 mm x 50 mm column. Compounds were detected on a Waters ACQUITY PDA detector spanning wavelengths from 190 to 650 nm, coupled to a Waters ACQUITY QDA detector for low resolution mass (LRMS) detection. The derivatives were eluted with a mobile phase consisting of supercritical CO₂ and MeOH containing 0.1 % NH₃ and a linear gradient of 2 – 40 % MeOH over 2 or 4 min followed by isocratic 0.5 min of 40% MeOH. The flow rate was 1.5 mL/min.

2.2 Synthesis of starting materials

1-bromo-4-(bromomethyl)naphthalene^[2], 2-(bromomethyl)quinoline^[2-3], 6-bromo-2-(bromomethyl)quinoline^[3], *tert*-butyl (2-bromoethyl)carbamate, *tert*-butyl (3-bromopropyl)carbamate^[4], *tert*-butyl (2-hydroxyethyl)carbamate^[5], *tert*-butyl (4-hydroxybutyl)carbamate^[6], *N,N'*-di(*tert*-butoxycarbonyl)-guanidinybutanol^[7] were prepared as described in literature. *tert*-butyl (5-hydroxypentyl)carbamate and *tert*-butyl (6-hydroxyhexyl)carbamate were purchased from commercial sources. Compounds **1eA** and **1eG** were synthesized as described in literature.^[1]

Note: All final compounds were obtained as di-TFA salts. TFA is typically observed at δ 162.1 (q, J = 35.7 Hz) and δ 117.7 (q, J = 290.3 Hz) in ¹³C-NMR and is not reported for each compound individually.

2.3 General procedures

General procedure A: Synthesis of identically 5,5-disubstituted barbituric acids **7**

Barbituric acid was taken up in PEG-400 and sodium bicarbonate was added. The reaction mixture was stirred for 5 min before the respective benzyl bromide or alkyl halide was added in one portion. The suspension was stirred at elevated temperature until full conversion was achieved (TLC) and was then allowed to cool to ambient temperature. Upon addition of 10% NaHCO_{3(aq)} solution a white solid precipitated, which was filtered off and washed with 10% NaHCO_{3(aq)} solution, water, and heptane. The obtained solid was collected, mixed with water, and the suspension was heated to reflux for 15 min. After the suspension had cooled to ambient temperature, the solid was collected by filtration and lyophilized for 24 h. MeOH was added, and the resulting suspension was sonicated for 5 min. The suspension was filtered, and the residue was collected and dried to yield the 5,5-disubstituted barbituric acids.

If no precipitate was obtained upon addition of 10% NaHCO_{3(aq)} solution, the aqueous layer was extracted with a suitable solvent three times. The combined organics were dried over Na₂SO₄, filtered and the solvent was removed. The crude was purified by column chromatography on silica gel with EtOAc in heptane as eluent.

General procedure B: N-alkylation with alkyl halides and subsequent Boc deprotection

The 5,5-disubstituted barbituric acid **7** or **10** was mixed with acetone and an inorganic base. The reaction mixture was stirred at ambient temperature for 10 min before *tert*-butyl-(3-bromopropyl)carbamate and TBAI were added. The suspension was heated until TLC indicated full conversion. The mixture was allowed to cool to ambient temperature and EtOAc and 10% NaHCO₃ (aq) solution were added. The layers were separated, and the organic layer was washed twice with 10 % NaHCO₃ (aq) solution. The organic layer was dried over MgSO₄, filtered and the solvent was removed under reduced pressure. The crude was purified on an automated flash system equipped with a silica column and EtOAc in heptane as eluent, to deliver the *N*-Boc-protected amines.

To the *N*-Boc-protected amine in DCM, was added TFA and the mixture was stirred at ambient temperature until HRMS indicated full conversion. The solvent was removed, and the crude product was purified on an automated flash system equipped with a C18 column and MeCN/H₂O containing 0.1% TFA as solvents. The product containing fractions were collected, the solvent was removed, and the product lyophilized for 48 h. The amines were obtained as di-TFA salts.

General procedure C: Guanidine formation

The di-TFA salts of the amines were mixed with THF and DIPEA and stirred at ambient temperature for 10 min. *N,N*-Di-Boc-1*H*-pyrazole-1-carboximidine was added and the solution was stirred at elevated temperatures until TLC indicated full conversion. The mixture was allowed to cool to ambient temperature and sat. NH₄Cl_(aq) solution and EtOAc were added. The layers were separated, and the aqueous layer was extracted twice with EtOAc. The combined organics were dried over Na₂SO₄, filtered and the solvent was removed. The crude products were purified on an automated flash system equipped with a silica column and EtOAc/heptane as eluent to yield the *N,N'*-di-Boc-protected guanidines.

The *N,N'*-di-Boc-protected guanidines were stirred with TFA in DCM at ambient temperature until HRMS indicated full conversion. In some cases, multiple additions of TFA were needed. The solvent was removed, and the crude product was purified on an automated flash system equipped with a C18 column and MeCN/H₂O containing 0.1% TFA as eluent. The product-containing fractions were collected, the solvent was removed, and the product was lyophilized for 48 h. The guanidines were obtained as di-TFA salts.

General Procedure D: N-alkylation via the Mitsunobu reaction

The respective 5,5-disubstituted barbituric acid **7** or **10**, *tert*-butyl (4-hydroxybutyl)carbamate or *N,N'*-di(*tert*-butoxycarbonyl)-guanidinybutanol and PPh₃ were mixed with anhydrous DCM in a heat dried vial under argon atmosphere. The mixture was cooled to 0 °C and upon dropwise addition of DIAD a clear yellow solution was obtained. The mixture was left stirring in the melting ice-water bath until TLC indicated full conversion. Then 10% NaHCO_{3(aq)} solution and EtOAc were added, and the layers were separated. The aqueous layer was extracted twice with EtOAc and the combined organics were dried over Na₂SO₄, filtered and the solvent was removed under reduced pressure. The crude product was purified by column chromatography on silica gel with EtOAc/heptane as eluent to yield the *N,N*-alkylated barbituric acids.

To the di-*N*-Boc amines or di-*N,N'*-di-Boc protected guanidines, dissolved in DCM, was added TFA and the mixture was stirred at ambient temperature until HRMS indicated full conversion. Sometimes multiple TFA additions were needed. The solvent was removed, and the crude product was purified on an automated flash system equipped with a C18 column and MeCN/H₂O containing 0.1% TFA as eluent. The product containing fractions were collected, the solvent was removed, and the product was lyophilized for 24 h. The obtained solids were triturated three times with Et₂O or heptane. The solids were dissolved in MeOH, and water was added. The mixture was lyophilized for 48 h to yield the desired amines or guanidines as di-TFA salts.

General Procedure E: Introduction of alkylated amines

1,3-bis(4-chlorobutyl)-5,5-bis(3,5-dibromobenzyl)pyrimidine-2,4,6(1*H*,3*H*,5*H*)-trione **S7** was mixed with MeCN and methylamine, dimethylamine or trimethylamine were added. The mixture was heated until HRMS indicated full conversion. It was allowed to cool to ambient temperature and the solvent was removed. The crude product was purified by automated RP chromatography with MeCN/H₂O containing 0.1% TFA as solvent. The product containing fractions were collected, the solvent was removed, and the product was lyophilized for 48 h. The amines were obtained as di-TFA salts.

General Procedure F: Synthesis of 5,5-disubstituted barbituric acids **10** with mixed substituents

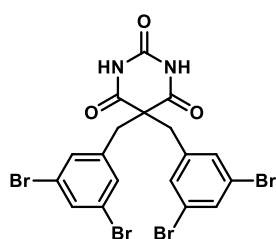
Mono-alkylated barbituric acid **9** was taken up in PEG-400, NaHCO₃ was added, and the suspension was stirred at ambient temperature. After 10 min the alkylating agent was added, and the mixture was stirred at elevated temperature until HRMS indicated full conversion. The mixture was allowed to cool to ambient temperature and Et₂O and 10% NaHCO_{3(aq)} solution were added. The layers were separated, and the aqueous layer was extracted once with Et₂O and EtOAc each. The combined organics were dried over Na₂SO₄, filtered and the solvent was removed under reduced pressure. The crude products were purified by column chromatography on silica with EtOAc/heptane as eluent to yield the desired barbituric acids **10**.

General Procedure G: Preparation of di-hydrochloric (HCl) salts

The previously obtained di-TFA salts of the amines and guanidines were taken up in MeOH and HCl in MeOH (1.25 M, 10.0 eq) was added. The solution was stirred for 5 min, before removal of the solvent under a nitrogen stream. The resulting residue was lyophilized for 24 h. The procedure was repeated twice more to yield the respective di-HCl salts. The absence of fluorine was confirmed by ¹⁹F NMR (not included).

2.4 Synthesis of barbiturates with identical lipophilic side chains **7**

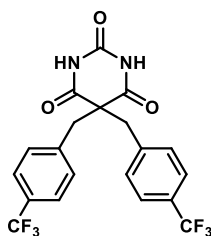
All compounds were synthesized according to General Procedure A



5,5-bis(3,5-dibromobenzyl)pyrimidine-2,4,6(1*H*,3*H*,5*H*)-trione **7a**.

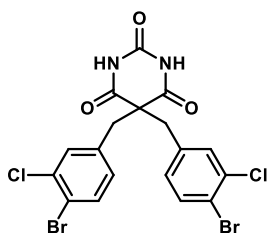
Barbituric acid (500 mg, 3.90 mmol, 1.0 eq), PEG-400 (15 mL), NaHCO₃ (656 mg, 7.81 mmol, 2.0 eq), 1,3-dibromo-5-(bromomethyl)benzene (2.05 g, 6.25 mmol, 1.6 eq). The mixture was stirred at 45 °C for 20 h. The title compound **7a** (1.62 g, 3.12 mmol, 83%) was obtained as a white solid. ¹H NMR (400 MHz, DMSO-*d*₆) δ 11.60 (s, 2H), 7.76 (t, *J* = 1.8 Hz, 2H), 7.22 (d, *J* = 1.8 Hz, 4H), 3.26 (s, 4H). ¹³C NMR (101 MHz, DMSO-*d*₆) δ 171.3 (2C), 148.9, 139.6 (2C), 132.6 (2C), 131.5 (4C), 122.4 (4C), 58.1, 41.7 (2C).

HRMS (ESI): calcd for C₁₈H₁₁Br₄N₂O₃⁻ [M-H]⁻ 618.7509, found 618.7514.



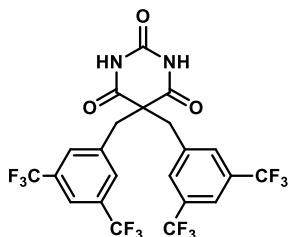
5,5-bis(4-(trifluoromethyl)benzyl)pyrimidine-2,4,6(1*H*,3*H*,5*H*)-trione **7b**.

Barbituric acid (1.25 g, 9.76 mmol, 1.0 eq), PEG-400 (50 mL), NaHCO₃ (1.64 g, 19.52 mmol, 2.0 eq), 1-(bromomethyl)-4-(trifluoromethyl)benzene (4.20 g, 17.59 mmol, 1.8 eq). The mixture was stirred at 45 °C for 45 h. The title compound **7b** (1.62 g, 3.12 mmol, 84%) was obtained as a white solid. ¹H NMR (400 MHz, DMSO-*d*₆) δ 11.40 (s, 2H), 7.68 (d, *J* = 8.0 Hz, 4H), 7.27 (d, *J* = 8.0 Hz, 4H), 3.40 (s, 4H). ¹³C NMR (101 MHz, DMSO-*d*₆) δ 171.4 (2C), 148.8, 139.8 (2C), 130.3 (4C), 128.1 (q, *J* = 31.7 Hz, 2C), 125.5 – 125.3 (m, 4C), 124.15 (q, *J* = 272.1 Hz, 2C), 58.4, 43.0 (2C). HRMS (ESI): calcd for C₂₀H₁₃F₆N₂O₃⁻ [M-H]⁻ 443.0836, found 443.0831.



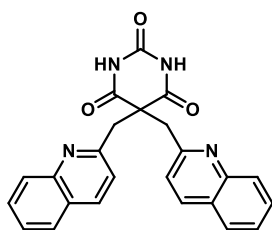
5,5-bis(4-bromo-3-chlorobenzyl)pyrimidine-2,4,6(1H,3H,5H)-trione 7c.

Barbituric acid (324 mg, 2.53 mmol, 1.0 eq), PEG-400 (30 mL), NaHCO₃ (489 mg, 5.82 mmol, 2.3 eq), 1-bromo-4-(bromomethyl)-2-chlorobenzene (1.37 g, 4.81 mmol, 1.9 eq). The mixture was stirred at 45 °C for 15 h and then at 65 °C for 22 h. The crude compound was purified by column chromatography on silica with 15% EtOAc/hepante containing 2.5% MeOH as eluent. The title compound **7c** (752 mg, 1.41 mmol, 56%) was obtained as a white solid. ¹H NMR (400 MHz, DMSO-*d*₆) δ 11.51 (s, 2H), 7.71 (d, *J* = 8.2 Hz, 2H), 7.24 (d, *J* = 2.1 Hz, 2H), 6.93 (dd, *J* = 8.3, 2.1 Hz, 2H), 3.26 (s, 4H). ¹³C NMR (101 MHz, DMSO-*d*₆) δ 171.4 (2C), 148.8, 136.7 (2C), 134.0 (2C), 133.0 (2C), 131.3 (2C), 129.8 (2C), 120.6 (2C), 58.2, 41.9 (2C). HRMS (ESI): calcd for C₁₈H₁₁Br₂Cl₂N₂O₃⁻ [M-H]⁻ 530.8519, found 530.8520.



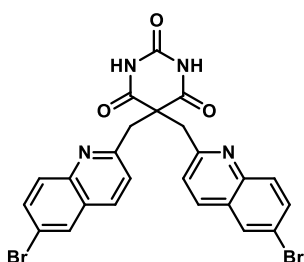
5,5-bis(3,5-bis(trifluoromethyl)benzyl)pyrimidine-2,4,6(1H,3H,5H)-trione 7d.

Barbituric acid (650 mg, 5.07 mmol, 1.0 eq), PEG-400 (35 mL), NaHCO₃ (853 mg, 10.15 mmol, 2.0 eq), 1-(bromomethyl)-3,5-bis(trifluoromethyl)benzene (2.73 g, 1.63 mL, 8.88 mmol, 1.75 eq). The mixture was stirred at 45 °C for 22 h. The title compound **7d** (2.33 g, 4.01 mmol, 79%) was obtained as a white solid. ¹H NMR (400 MHz, DMSO-*d*₆) δ 11.64 (s, 2H), 8.04 (s, 2H), 7.71 (d, *J* = 1.7 Hz, 4H), 3.53 (s, 4H). ¹³C NMR (101 MHz, DMSO-*d*₆) δ 171.2 (2C), 148.6, 138.3 (2C), 130.7 – 130.5 (m, 4C), 130.2 (q, *J* = 32.9 Hz, 4C), 123.2 (q, *J* = 274 Hz), 121.5 – 121.3 (m, 2C), 57.9, 41.3 (2C). HRMS (ESI): calcd for C₂₂H₁₁F₁₂N₂O₃⁻ [M-H]⁻ 579.0584, found 579.0566.



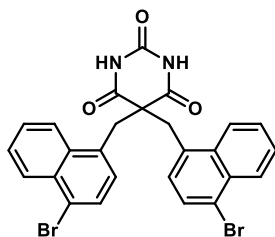
5,5-bis(quinolin-2-ylmethyl)pyrimidine-2,4,6(1H,3H,5H)-trione 7e.

Barbituric acid (600 mg, 4.68 mmol, 1.0 eq), PEG-400 (30 mL), NaHCO₃ (786 mg, 9.36 mmol, 2.0 eq), 2-(bromomethyl)quinoline (1.71 g, 7.94 mmol, 1.70 eq). The mixture was stirred at 45 °C for 16 h and then at 60 °C for 24 h. The title compound **7e** (981 mg, 2.39 mmol, 56%) was obtained as a white solid. ¹H NMR (400 MHz, DMSO-*d*₆) δ 10.86 (s, 2H), 8.27 (d, *J* = 8.5 Hz, 2H), 7.93 (dd, *J* = 8.1, 1.3 Hz, 2H), 7.77 (dd, *J* = 8.5, 1.4 Hz, 2H), 7.72 (ddd, *J* = 8.3, 6.6, 1.4 Hz, 2H), 7.56 (ddd, *J* = 8.1, 6.6, 1.5 Hz, 2H), 7.40 (d, *J* = 8.5 Hz, 2H), 3.71 (s, 4H). ¹³C NMR (101 MHz, DMSO-*d*₆) δ 173.7 (2C), 156.8 (2C), 151.3, 146.4 (2C), 136.4 (2C), 129.6 (2C), 128.0 (2C), 127.8 (2C), 126.5 (2C), 126.3 (2C), 121.5 (2C), 52.2, 45.7 (2C). HRMS (ESI): calcd for C₂₄H₁₇N₄O₃⁻ [M-H]⁻ 409.1306, found 409.1304.



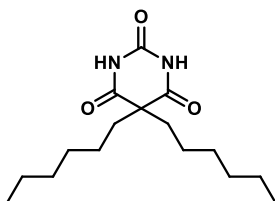
5,5-bis((6-bromoquinolin-2-yl)methyl)pyrimidine-2,4,6(1H,3H,5H)-trione 7f.

Barbituric acid (90 mg, 0.70 mmol, 1.0 eq), PEG-400 (10 mL), NaHCO₃ (112 mg, 1.34 mmol, 1.90 eq), 6-bromo-2-(bromomethyl)quinoline (402 mg, 1.34 mmol, 1.90 eq). The mixture was stirred at 60 °C for 20 h and then at 60 °C for 24 h. The title compound **7f** (109 mg, 0.19 mmol, 27%) was obtained as an off-white solid. ¹H NMR (400 MHz, DMSO-*d*₆) δ 11.17 (s, 2H), 8.29 (d, *J* = 8.5 Hz, 2H), 8.26 (d, *J* = 2.2 Hz, 2H), 7.90 (dd, *J* = 8.9, 2.3 Hz, 2H), 7.66 (d, *J* = 8.9 Hz, 2H), 7.48 (d, *J* = 8.6 Hz, 2H), 3.75 (s, 4H). ¹³C NMR (101 MHz, DMSO-*d*₆) δ 173.5 (2C), 157.6 (2C), 151.2, 145.0 (2C), 135.3 (2C), 132.8 (2C), 130.1 (2C), 129.9 (2C), 127.8 (2C), 122.5 (2C), 119.1 (2C), 52.01, 45.6 (2C). HRMS (ESI): calcd for C₂₄H₁₅Br₂N₄O₃⁻ [M-H]⁻ 564.9516, found 564.9517.



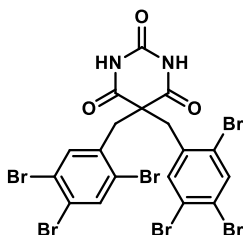
5,5-bis((4-bromonaphthalen-1-yl)methyl)pyrimidine-2,4,6(1H,3H,5H)-trione **7g**.

Barbituric acid (650 mg, 5.07 mmol, 1.0 eq), PEG-400 (15 mL), NaHCO₃ (853 mg, 10.15 mmol, 2.0 eq), 1-bromo-4-(bromomethyl)naphthalene (1.71 g, 8.65 mmol, 1.71 eq). The mixture was stirred at 45 °C for 24 h. The title compound **7g** (2.25 g, 3.98 mmol, 92%) was obtained as a white solid. ¹H NMR (400 MHz, DMSO-*d*₆) δ 10.44 (s, 2H), 7.57 – 7.46 (m, 2H), 7.38 – 7.30 (m, 2H), 7.00 (d, *J* = 7.8 Hz, 2H), 6.87 (dq, *J* = 12.8, 6.6 Hz, 4H), 6.30 (d, *J* = 7.8 Hz, 2H), 3.16 (s, 4H). ¹³C NMR (101 MHz, DMSO-*d*₆) δ 172.2 (2C), 149.1, 133.1 (2C), 132.5 (2C), 131.2 (2C), 129.5 (2C), 127.8 (2C), 127.5 (2C), 127.1 (2C), 126.9 (2C), 125.1 (2C), 121.6 (2C), 69.8, 57.5 (2C). HRMS (ESI): calcd for C₂₆H₁₇Br₂N₂O₃⁻ [M-H]⁻ 562.9611, found 562.9612.



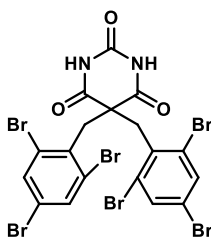
5,5-dihexylpyrimidine-2,4,6(1H,3H,5H)-trione **7h**.

Barbituric acid (445 mg, 3.47 mmol, 1.0 eq), PEG-400 (6 mL), NaHCO₃ (730 mg, 8.69 mmol, 2.50 eq), 1-iodohexane (1.33 g, 0.92 mL, 6.25 mmol, 1.80 eq). The mixture was stirred at 100 °C for 48 h and then allowed to cool to ambient temperature and 10% NaHCO_{3(aq)} was added. The aqueous layer was extracted with THF (2x) and MTBE (1x), the combined organics dried over Na₂SO₄, filtered and the solvent was removed under reduced pressure. The crude product was purified by column chromatography on silica with 25% EtOAc in heptane. The title compound **7h** (42 mg, 0.18 mmol, 5%) was obtained as a yellow solid. ¹H NMR (400 MHz, DMSO-*d*₆) δ 11.51 (s, 2H), 1.81 – 1.73 (m, 4H), 1.29 – 1.13 (m, 12H), 1.12 – 0.99 (m, 4H), 0.87 – 0.77 (m, 6H). ¹³C NMR (101 MHz, DMSO-*d*₆) δ 173.2 (2C), 149.8, 55.0, 38.3 (2C), 30.7 (2C), 28.5 (2C), 24.3 (2C), 21.8 (2C), 13.8 (2C). HRMS (ESI): calcd for C₁₆H₂₇N₂O₃⁻ [M-H]⁻ 295.2027, found 295.2024.



5,5-bis(2,4,5-tribromobenzyl)pyrimidine-2,4,6(1H,3H,5H)-trione **7i**.

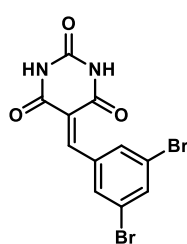
Barbituric acid (350 mg, 2.73 mmol, 1.0 eq), PEG-400 (13 mL), NaHCO₃ (377 mg, 4.49 mmol, 1.65 eq), 1,2,4-tribromo-5-(bromomethyl)benzene (1.51 g, 3.71 mmol, 1.36 eq). The mixture was stirred at 45 °C for 4.5 d. Instead of sonicating the solids were boiled in MeOH for 30 min, cooled to ambient temperature and filtered. The title compound **7i** (1.07 g, 1.37 mmol, 74%) was obtained as a white solid. ¹H NMR (400 MHz, DMSO-*d*₆) δ 11.81 (s, 1H), 8.07 (s, 1H), 7.35 (s, 1H), 3.45 (s, 2H). ¹³C NMR (101 MHz, DMSO-*d*₆) δ 170.7 (2C), 149.1, 136.7 (2C), 136.4 (2C), 134.5 (2C), 124.7 (2C), 123.7 (2C), 123.1 (2C), 70.2, 55.3 (2C). HRMS (ESI): calcd for C₁₈H₉Br₆N₂O₃⁻ [M-H]⁻ 774.5719, found 774.5727.



5,5-bis(2,4,6-tribromobenzyl)pyrimidine-2,4,6(1H,3H,5H)-trione **7j**.

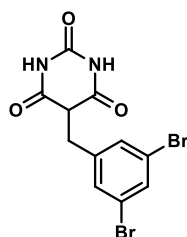
Barbituric acid (300 mg, 2.34 mmol, 1.0 eq), PEG-400 (20 mL), NaHCO₃ (374 mg, 4.45 mmol, 1.90 eq), 1,3,5-tribromo-2-(bromomethyl)benzene (1.51 g, 3.71 mmol, 1.59 eq). The mixture was stirred at 45 °C for 66 h. Instead of sonicating, the solids were boiled in MeOH for 30 min, cooled to ambient temperature and filtered. The title compound **7j** (1.13 g, 1.37 mmol, 78%) was obtained as a white solid. ¹H NMR (400 MHz, DMSO-*d*₆) δ 11.47 (s, 2H), 7.90 (s, 4H), 3.83 (s, 4H). ¹³C NMR (101 MHz, DMSO-*d*₆) δ 170.7 (2C), 149.7, 135.7 (2C), 134.4 (4C), 127.3 (4C), 121.4 (2C), 54.6, 43.0 (2C). HRMS (ESI): calcd for C₁₈H₉Br₆N₂O₃⁻ [M-H]⁻ 774.5719, found 774.5718.

2.5 Synthesis of barbiturates with mixed hydrophobic residues **10**



5-(3,5-dibromobenzylidene)pyrimidine-2,4,6(1H,3H,5H)-trione **8**.

Barbituric acid (485 mg, 3.79 mmol, 1.0 eq) was taken up in water (15 mL) and heated to 105 °C until the compound dissolved. 3,5-dibromobenzaldehyde (1.00 g, 3.79 mmol, 1.0 eq) was dissolved in EtOH (5 mL) and added to the aqueous solution. A fine white precipitate formed which dissolved again after 1 min. After a few minutes a yellow precipitate formed. The mixture was stirred for a total of 25 min. After cooling to ambient temperature, it was filtered and the residue was washed with water and EtOAc. The solids were collected and dried to yield pure **8** (817 mg, 2.19 mmol, 58%) as a yellow solid. **¹H NMR** (400 MHz, DMSO-*d*₆) δ 11.46 (s, 1H), 11.30 (s, 1H), 8.17 (s, 1H), 8.12 (d, *J* = 1.8 Hz, 2H), 7.94 (t, *J* = 2.0 Hz, 1H). **¹³C NMR** (101 MHz, DMSO-*d*₆) δ 162.7, 161.3, 150.4, 150.2, 137.1, 135.3, 133.0 (2C), 121.9, 121.7 (2C). **HRMS** (ESI): calcd for C₁₁H₅Br₂N₂O₃⁻ [M-H]⁻ 370.8672, found 370.8672.



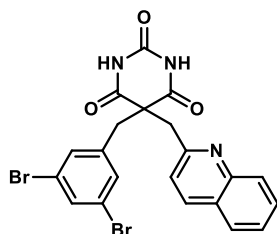
5-(3,5-dibromobenzyl)pyrimidine-2,4,6(1H,3H,5H)-trione **9**.

Compound **8** (1.00 g, 2.67 mmol, 1.0 eq) was taken up in EtOH (22 mL) and NaBH₄ (202 mg, 5.35 mmol, 2.0 eq) was added in one portion. After stirring at 70 °C for 5 min the yellow solid turned white. The mixture was allowed to cool to ambient temperature and the mixture was acidified to pH = 1 with 1 N HCl. The solid was collected by filtration to yield **9** (805 mg, 2.14 mmol, 80%) as a white solid. A 2:1 mixture of the Keto and Enol-form was obtained. The mixture was used without further purification.

Keto-9: **¹H NMR** (400 MHz, DMSO-*d*₆) δ 11.25 (s, 2H), 7.67 (s, 1H), 7.36 (d, *J* = 1.8 Hz, 2H), 4.08 (t, *J* = 5.3 Hz, 1H), 3.22 (d, *J* = 5.3 Hz, 1H). **¹³C NMR** (101 MHz, DMSO-*d*₆) δ 169.6, 150.7, 143.3, 131.6, 131.0 (2C), 122.2 (2C), 49.2, 31.5.

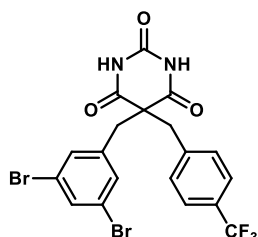
Enol-9: **¹H NMR** (400 MHz, DMSO-*d*₆) δ 10.72 (s, 2H), 7.60 (t, *J* = 1.8 Hz, 1H), 7.36 (d, *J* = 1.8 Hz, 2H), 3.55 (s, 1H). **¹³C NMR** (101 MHz, DMSO-*d*₆) δ 150.4, 146.7, 131.1, 130.4 (2C), 122.6 (2C), 88.2, 27.1. **HRMS** (ESI): calcd for C₁₁H₇Br₂N₂O₃⁻ [M-H]⁻ 372.8829, found. 372.8828.

The following compounds were synthesized according to *General Procedure F*:



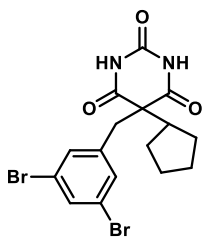
5-(3,5-dibromobenzyl)-5-(quinolin-2-ylmethyl)pyrimidine-2,4,6(1H,3H,5H)-trione **10a**.

Compound **9** (200 mg, 532 μmol, 1.0 eq), 2-(bromomethyl)quinoline (118 mg, 532 μmol, 1.0 eq), NaHCO₃ (67 mg, 798 μmol, 1.50 eq) and PEG-400 (3 mL) were stirred at 60 °C for 41 h. The crude was purified with 20-35% EtOAc in heptane to yield **10a** (110 mg, 213 μmol, 40%) as a white solid. **¹H NMR** (400 MHz, Methanol-*d*₄) δ 8.15 (d, *J* = 8.1 Hz, 1H), 7.81 (dd, *J* = 7.6, 1.2 Hz, 1H), 7.70 – 7.64 (m, 2H), 7.61 (ddd, *J* = 8.4, 6.7, 1.5 Hz, 1H), 7.48 (ddd, *J* = 8.1, 5.4, 1.4 Hz, 1H), 7.36 (d, *J* = 8.7 Hz, 1H), 7.33 (d, *J* = 1.7 Hz, 2H), 3.92 (s, 2H), 3.28 (s, 2H). **¹³C NMR** (101 MHz, Methanol-*d*₄) δ 175.1, 158.2, 152.2, 148.0, 140.1, 137.8, 134.4, 132.8, 130.6, 129.1, 128.8, 128.2, 127.4, 123.9, 121.7, 56.4, 45.3, 45.0. **HRMS** (ESI): calcd for C₂₁H₁₄Br₂N₃O₃⁻ [M-H]⁻ 513.9407, found.: 513.9406.



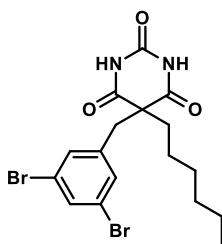
5-(3,5-dibromobenzyl)-5-(4-(trifluoromethyl)benzyl)pyrimidine-2,4,6(1H,3H,5H)-trione **10b**.

Compound **9** (200 mg, 532 μmol, 1.0 eq), 1-(bromomethyl)-4-(trifluoromethyl)benzene (82 μL, 532 μmol, 1.0 eq), NaHCO₃ (67 mg, 798 μmol, 1.50 eq) and PEG-400 (3 mL) were stirred at 50 °C for 18h. The crude was purified with 15% EtOAc in heptane to yield **10b** (83 mg, 155 μmol, 29%) as a white solid. **¹H NMR** (400 MHz, Methanol-*d*₄) δ 16.82 (t, *J* = 1.8 Hz, 1H), 6.76 (d, *J* = 8.1 Hz, 2H), 6.52 (d, *J* = 8.1 Hz, 2H), 6.49 (d, *J* = 1.7 Hz, 2H), 2.63 (s, 2H), 2.56 (s, 2H). **¹³C NMR** (101 MHz, Methanol-*d*₄) δ 163.6, 140.6, 131.3 (2C), 124.9, 123.3, 122.0, 121.5 (q, *J* = 32.4 Hz), 117.0 (t, *J* = 3.9 Hz), 116.1 (q, *J* = 273.0 Hz), 114.5, 51.2, 35.4, 34.4. **HRMS** (ESI): calcd for C₂₂H₁₄Br₂N₃O₃⁻ [M-H]⁻ 590.8560, found.: 590.8565.



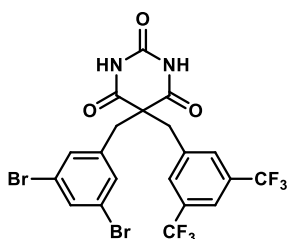
5-cyclopentyl-5-(3,5-dibromobenzyl)pyrimidine-2,4,6(1H,3H,5H)-trione 10c.

Compound **9** (158 mg, 420 μmol , 1.0 eq), bromocyclopentane (43 μL , 399 μmol , 0.95 eq), NaHCO_3 (34 mg, 399 μmol , 0.95 eq), TBAI (23 mg, 63 μmol , 0.15 eq) and PEG-400 (2 mL) were stirred at 100 $^\circ\text{C}$ for 48 h and then at 140 $^\circ\text{C}$ for 72 h. The crude was purified with 15% EtOAc in heptane to yield impure **10c** (9 mg, 20 μmol , 5%) as a yellow solid. **NMR** no suitable data was obtained. **HRMS** (ESI): calcd for $\text{C}_{16}\text{H}_{15}\text{Br}_2\text{N}_2\text{O}_3^-$ $[\text{M}-\text{H}]^-$ 440.9455, found: 440.9464.



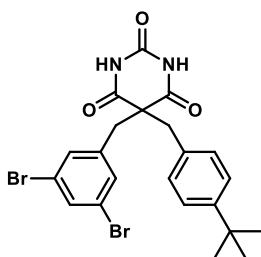
5-(3,5-dibromobenzyl)-5-hexylpyrimidine-2,4,6(1H,3H,5H)-trione 10d.

Compound **9** (200 mg, 532 μmol , 1.0 eq), 1-iodohexane (75 μL , 506 μmol , 0.95 eq), NaHCO_3 (45 mg, 532 μmol , 1.00 eq) and PEG-400 (2 mL) were stirred at 100 $^\circ\text{C}$ for 5 d. The crude was purified with 0-45% EtOAc in heptane to yield **10d** (129 mg, 280 μmol , 53%) as a colorless foam. **^1H NMR** (400 MHz, Methanol-*d*₄) δ 7.61 (t, J = 1.8 Hz, 1H), 7.24 (d, J = 1.8 Hz, 2H), 3.16 (s, 2H), 2.09 – 2.00 (m, 2H), 1.38 – 1.16 (m, 8H), 0.94 – 0.84 (m, 3H). **^{13}C NMR** (101 MHz, Methanol-*d*₄) δ 174.0, 150.7, 141.1, 134.2, 132.6, 123.9, 59.0, 44.2, 40.1, 32.4, 30.2, 25.9, 23.5, 14.3. **HRMS** (ESI): calcd for $\text{C}_{17}\text{H}_{19}\text{Br}_2\text{N}_2\text{O}_3^-$ $[\text{M}-\text{H}]^-$ 456.9768, found.: 456.9767.



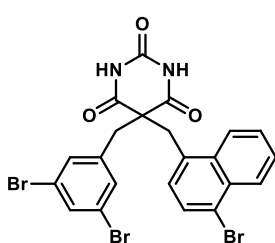
5-(3,5-bis(trifluoromethyl)benzyl)-5-(3,5-dibromobenzyl)pyrimidine-2,4,6(1H,3H,5H)-trione 10e.

Compound **9** (294 mg, 782 μmol , 1.0 eq), 1-(bromomethyl)-3,5-bis(trifluoromethyl)benzene (143 μL , 798 μmol , 1.00 eq), NaHCO_3 (99 mg, 1.17 mmol, 1.50 eq), and PEG-400 (20 mL) were stirred at 50 $^\circ\text{C}$ for 7 d. 10% NaHCO_3 (aq) solution was added, the aqueous layer was extracted with DCM (3x) and the combined organic layers dried over MgSO_4 . The crude was purified with 30% EtOAc in heptane to yield **10e** (471 mg, 327 μmol , 42%) as a white solid. **^1H NMR** (400 MHz, DMSO-*d*₆) δ 11.63 (s, 2H), 8.05 (s, 1H), 7.77 (d, J = 1.8 Hz, 1H), 7.70 (s, 2H), 7.23 (d, J = 1.8 Hz, 2H), 3.50 (s, 2H), 3.30 (s, 2H). **^{13}C NMR** (101 MHz, DMSO-*d*₆) δ 171.3 (2C), 148.7, 139.5, 138.4, 132.6, 131.6 (2C), 130.6 – 130.4 (m, 2C), 130.2 (q, J = 32.8 Hz, 2C), 123.2 (q, J = 273.9 Hz, 2C), 122.4 (2C), 121.6 – 121.4 (m, 1C) 58.1, 41.6, 41.5. **HRMS** (ESI): calcd for $\text{C}_{20}\text{H}_{11}\text{Br}_2\text{F}_6\text{N}_2\text{O}_3^-$ $[\text{M}-\text{H}]^-$ 598.9046, found: 598.9040.



5-(4-(tert-butyl)benzyl)-5-(3,5-dibromobenzyl)pyrimidine-2,4,6(1H,3H,5H)-trione 10f.

Compound **9** (200 mg, 532 μmol , 1.0 eq), 1-(bromomethyl)-4-(tert-butyl)benzene (147 μL , 798 μmol , 1.50 eq), NaHCO_3 (67 mg, 798 μmol , 1.50 eq), and PEG-400 (6 mL) were stirred at 100 $^\circ\text{C}$ for 21 h. The crude was purified with 10-15% EtOAc in heptane to yield **10f** (169 mg, 324 μmol , 61%) as a white solid. **^1H NMR** (400 MHz, DMSO-*d*₆) δ 11.40 (s, 2H), 7.75 (t, J = 1.8 Hz, 1H), 7.33 – 7.25 (m, 2H), 7.22 (d, J = 1.8 Hz, 2H), 7.00 – 6.93 (m, 2H), 3.28 (s, 2H), 3.21 (s, 2H), 1.22 (s, 9H). **^{13}C NMR** (101 MHz, DMSO-*d*₆) δ 171.6, 149.7, 148.8, 134.0, 132.5, 131.7, 131.4, 129.0, 125.2, 122.4, 58.5, 43.3, 42.0, 34.2, 31.0. **HRMS** (ESI): calcd for $\text{C}_{22}\text{H}_{21}\text{Br}_2\text{N}_2\text{O}_3^-$ $[\text{M}-\text{H}]^-$ 518.9924, found: 518.9924.

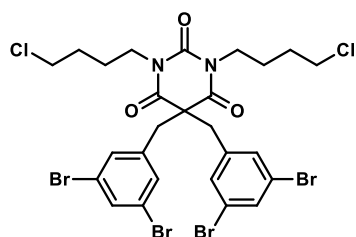


5-((4-bromonaphthalen-1-yl)methyl)-5-(3,5-dibromobenzyl)pyrimidine-2,4,6(1H,3H,5H)-trione 10g.

Compound **9** (75 mg, 200 μmol , 1.0 eq), 1-bromo-4-(bromomethyl)naphthalene (60 mg, 200 μmol , 1.0 eq), NaHCO_3 (25 mg, 300 μmol , 1.50 eq) and PEG-400 (1 mL) were stirred at 50 $^\circ\text{C}$ for 14h. The crude was purified with 20% EtOAc in heptane to yield **10g** (66 mg, 111 μmol , 56%) as a white solid. **^1H NMR** (400 MHz, DMSO-*d*₆) δ 1.40 (s, 2H), 8.22 (d, J = 7.8 Hz, 1H), 8.16 (dd, J = 8.4, 1.4 Hz, 1H), 7.84 (d, J = 7.8 Hz, 1H), 7.75 (t, J = 1.8 Hz, 1H), 7.70 (ddd, J = 8.3, 6.8, 1.2 Hz, 1H), 7.64 (ddd, J = 8.3, 6.8, 1.5 Hz, 1H), 7.27 (d, J = 1.8 Hz, 2H), 7.13

(d, $J = 7.8$ Hz, 1H), 3.81 (s, 2H), 3.45 (s, 2H). ^{13}C NMR (101 MHz, DMSO- d_6) δ 171.6, 148.7, 140.0, 132.9, 132.5, 132.0, 131.6, 131.2, 129.4, 128.0, 127.8, 127.1, 126.9, 125.0, 122.3, 121.8, 57.9, 41.5. HRMS (ESI): calcd for $\text{C}_{22}\text{H}_{14}\text{Br}_3\text{N}_2\text{O}_3^-$ [M-H] $^-$ 590.8560, found.: 590.8565.

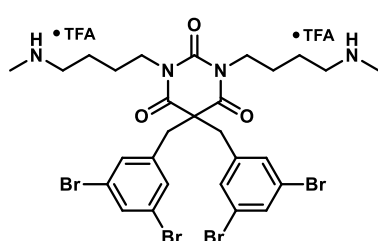
2.6 Synthesis of series 1



1,3-bis(4-chlorobutyl)-5,5-bis(3,5-dibromobenzyl)pyrimidine-2,4,6(1H,3H,5H)-trione S7.

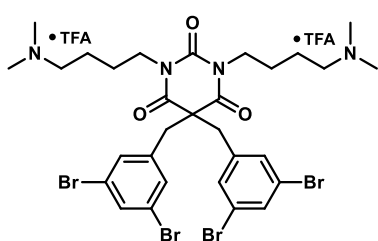
5,5-bis(3,5-dibromobenzyl)pyrimidine-2,4,6(1H,3H,5H)-trione **7a** (250 mg, 400 μmol , 1.0 eq) and Cs_2CO_3 (326 mg, 1.00 mmol, 2.50 eq) were stirred in acetone (5 mL) at ambient temperature for 10 min. 1-bromo-4-chlorobutane (208 μL , 1.80 mmol, 4.50 eq) was added and the mixture was heated to 50 $^\circ\text{C}$ for 72 h. EtOAc and 10% $\text{NaHCO}_3(\text{aq})$ solution were added, the layers were separated and the organic layer was washed with 10% $\text{NaHCO}_3(\text{aq})$ solution twice. The organic layer was dried over Na_2SO_4 , filtered and the solvent was removed. The crude product was purified on an automated flash system equipped with a silica column and gradient 0-30 % EtOAc/heptane. **S7** (273 mg, 339 μmol , 85%) was obtained as a colorless oil. ^1H NMR (400 MHz, Chloroform- d) δ 7.53 (dq, $J = 3.2, 1.8$ Hz, 2H), 7.13 (q, $J = 2.2$ Hz, 4H), 3.65 (td, $J = 7.1, 2.5$ Hz, 4H), 3.51 (td, $J = 6.4, 2.8$ Hz, 4H), 3.36 – 3.25 (m, 4H), 1.62 – 1.53 (m, 4H), 1.53 – 1.43 (m, 4H). ^{13}C NMR (101 MHz, Chloroform- d) δ 169.9 (2C), 149.1, 138.4 (2C), 133.8 (2C), 131.3 (4C), 123.3 (4C), 59.9, 44.2 (2C), 41.4 (2C), 29.8 (2C), 25.4 (2C). HRMS (ESI): *not found*.

The following compounds were synthesized according to General Procedure E



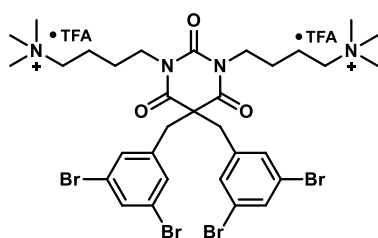
5,5-bis(3,5-dibromobenzyl)-1,3-bis(4-(methylamino)butyl)pyrimidine-2,4,6(1H,3H,5H)-trione 1a.

S7 (40 mg, 45 μmol , 1.0 eq), methylamine (2M in THF, 179 μL , 358 μmol , 8.0 eq) and MeCN (1 mL) were stirred at 70 $^\circ\text{C}$ for 40 h. The crude was purified by automated RP column chromatography with gradient 15-53% MeCN/ H_2O + 0.1% TFA to yield the di-TFA salt of **1a** (15 mg, 15 μmol , 33%) as a slightly yellow solid. ^1H NMR (400 MHz, Methanol- d_4) δ 7.65 (t, $J = 1.6$ Hz, 2H), 7.22 (d, $J = 1.8$ Hz, 4H), 3.68 (t, $J = 7.6$ Hz, 4H), 3.42 (s, 4H), 3.11 – 2.96 (m, 4H), 2.69 (s, 6H), 1.58 (p, $J = 7.7$ Hz, 4H), 1.41 (p, $J = 7.8$ Hz, 4H). ^{13}C NMR (101 MHz, Methanol- d_4) δ 171.2 (2C), 150.5, 140.5 (2C), 134.5 (2C), 132.7 (4C), 124.1 (4C), 61.2, 49.7 (2C), 44.8 (2C), 42.2 (2C), 33.5 (2C), 26.3 (2C), 24.3 (2C). HRMS (ESI): calcd for $\text{C}_{28}\text{H}_{35}\text{Br}_4\text{N}_4\text{O}_3^+$ [M+H] $^+$ 790.9437, found 790.9436. SFC: 98.0%.



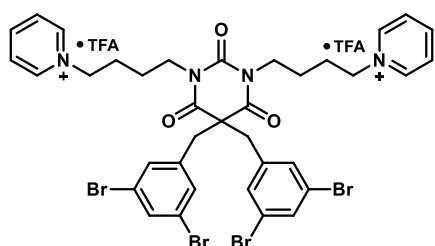
5,5-bis(3,5-dibromobenzyl)-1,3-bis(4-(dimethylamino)butyl)pyrimidine-2,4,6(1H,3H,5H)-trione 1b.

S7 (40 mg, 45 μmol , 1.0 eq), dimethylamine (2M in THF, 179 μL , 358 μmol , 8.0 eq) and MeCN (1 mL) were stirred at 70 $^\circ\text{C}$ for 24 h. The crude was purified by automated RP column chromatography with gradient 15-53% MeCN/ H_2O + 0.1% TFA to yield the di-TFA salt of **1b** (35 mg, 33 μmol , 75%) as a slightly yellow solid. ^1H NMR (400 MHz, Methanol- d_4) δ 7.66 (t, $J = 1.6$ Hz, 2H), 7.22 (d, $J = 1.8$ Hz, 4H), 3.69 (t, $J = 7.7$ Hz, 4H), 3.42 (s, 4H), 3.20 – 3.09 (m, 4H), 2.88 (d, $J = 1.6$ Hz, 12H), 1.70 – 1.55 (m, 4H), 1.40 (p, $J = 7.7$ Hz, 4H). ^{13}C NMR (101 MHz, Methanol- d_4) δ 171.2 (2C), 150.5, 140.5 (2C), 134.5 (2C), 132.6 (4C), 124.1 (4C), 61.2, 58.4 (2C), 44.8 (2C), 43.4 (4C), 42.1 (2C), 26.2 (2C), 22.8 (2C). HRMS (ESI): calcd for $\text{C}_{30}\text{H}_{39}\text{Br}_4\text{N}_4\text{O}_3^+$ [M+H] $^+$ 818.9750, found 818.9744. SFC: 96.4%.



4,4'-(5,5-bis(3,5-dibromobenzyl)-2,4,6-trioxodihydropyrimidine-1,3(2H,4H)-diyl)bis(*N,N,N*-trimethylbutan-1-aminium) **1c**.

S7 (45 mg, 56 μmol , 1.0 eq), trimethylamine (1M in THF, 783 μL , 783 μmol , 14.0 eq), NaI (15 mg, 100 μmol , 1.8 eq) and MeCN (1 mL) were stirred at 70 °C for 96 h. The crude was purified by automated RP column chromatography with gradient 15-55% MeCN/H₂O + 0.1% TFA to yield the di-TFA salt of **1c** (53 mg, 49 μmol , 88%) as a slightly yellow solid. ¹H NMR (400 MHz, Methanol-*d*₄) δ 7.66 (t, *J* = 1.8 Hz, 2H), 7.22 (d, *J* = 1.8 Hz, 4H), 3.78 – 3.66 (m, 4H), 3.43 (s, 4H), 3.41 – 3.34 (m, 4H), 3.13 (s, 18H), 1.82 – 1.68 (m, 4H), 1.39 (tt, *J* = 10.6, 6.4 Hz, 4H). ¹³C NMR (101 MHz, Methanol-*d*₄) δ 171.2 (2C), 150.4, 139.8 (2C), 134.5 (2C), 132.6 (4C), 124.2 (4C), 67.1 (t, *J* = 3.0 Hz, 2C), 61.1, 53.6 (t, *J* = 4.0 Hz 6C), 44.8 (2C), 42.2 (2C), 26.0 (2C), 21.3 (2C). HRMS (ESI): calcd for C₃₂H₄₄Br₄N₄O₃²⁺ [M]²⁺ 424.0068, found 424.0068. SFC: 97.7%.

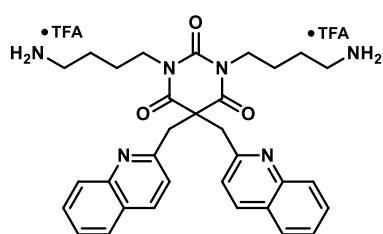


1,1'-((5,5-bis(3,5-dibromobenzyl)-2,4,6-trioxodihydropyrimidine-1,3(2H,4H)-diyl)bis(butane-4,1-diyl))bis(pyridin-1-ium) **1d**.

S7 (28 mg, 35 μmol , 1.0 eq), pyridine (500 μL), NaI (2.6 mg, 17 μmol , 0.5 eq) and MeCN (0.5 mL) were stirred at 90 °C for 64 h. The crude was purified by automated RP column chromatography with gradient 10-70% MeCN/H₂O + 0.1% TFA to yield the di-TFA salt of **1d** (21 mg, 19 μmol , 54%) as a slightly yellow solid. ¹H NMR (400 MHz, Methanol-*d*₄) δ 9.10 – 8.99 (m, 4H), 8.64 (tt, *J* = 7.8, 1.3 Hz, 2H), 8.23 – 8.12 (m, 4H), 7.62 (t, *J* = 1.8 Hz, 2H), 7.20 (d, *J* = 1.8 Hz, 4H), 4.75 – 4.65 (m, 4H), 3.80 – 3.68 (m, 4H), 3.44 (s, 4H), 1.95 (p, *J* = 7.5 Hz, 4H), 1.45 (tt, *J* = 9.7, 6.6 Hz, 4H). ¹³C NMR (101 MHz, Methanol-*d*₄) δ 171.3 (2C), 150.5, 147.2 (2C), 146.0 (4C), 140.5 (2C), 134.5 (2C), 132.6 (4C), 129.7 (4C), 124.1 (4C), 62.1 (2C), 61.2, 44.8 (2C), 42.0 (2C), 29.4 (2C), 25.6 (2C). HRMS (ESI): calcd for C₃₆H₃₆Br₄N₄O₃²⁺ [M]²⁺ 443.9755, found. 443.9757 SFC: >99.5%.

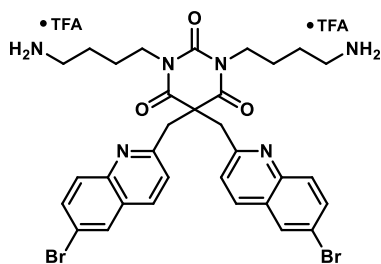
2.7 Synthesis of series 2

The compounds were prepared according to General Procedure D.



1,3-bis(4-aminobutyl)-5,5-bis(quinolin-2-ylmethyl)pyrimidine-2,4,6(1H,3H,5H)-trione **2aA**.

Barbiturate **7e** (145 mg, 350 μmol , 1.0 eq), *tert*-butyl (4-hydroxybutyl)carbamate (166 mg, 875 μmol , 2.5 eq), PPh₃ (273 mg, 1.05 mmol, 3.0 eq) and DIAD (206 μL , 1.05 mmol, 3.0 eq) were stirred in DCM (2.0 mL) for 25 h. The crude was purified with 0-70% EtOAc in heptane to yield boc-**2aA** (84 mg, 112 μmol , 32%) as a slightly yellow solid. TFA (130 μL , 1.70 mmol, 15.5 eq) and DCM (1.5 mL) were added, and the mixture was stirred at ambient temperature for 18 h. The crude was purified by automated RP column chromatography with a gradient of 0-70% MeCN/H₂O + 0.1% TFA to yield the di-TFA salt of **2aA** (61 mg, 78 μmol , 22% o2s) as a white solid, m.p. 85-95 °C. ¹H NMR (400 MHz, Methanol-*d*₄) δ 8.31 (d, *J* = 8.5 Hz, 2H), 7.93 (d, *J* = 8.2 Hz, 2H), 7.76 (d, *J* = 3.5 Hz, 4H), 7.59 (dt, *J* = 8.1, 4.0 Hz, 2H), 7.45 (d, *J* = 8.6 Hz, 2H), 3.98 (s, 4H), 3.82 (t, *J* = 6.9 Hz, 4H), 2.60 (t, *J* = 7.4 Hz, 4H), 1.51 – 1.30 (m, 8H). ¹³C NMR (101 MHz, Methanol-*d*₄) δ 174.1 (2C), 158.2 (2C), 153.4, 148.2 (2C), 138.2 (2C), 131.0 (2C), 129.2 (2C), 129.1 (2C), 128.5 (2C), 127.7 (2C), 122.6 (2C), 54.8, 42.0 (2C), 39.9 (2C), 25.9 (2C), 25.7 (2C). One carbon signal was not observed. HRMS (ESI): calcd for C₃₂H₃₇N₆O₃⁺ [M+H]⁺ 553.2922, found 553, 2920. SFC: >99.5%.

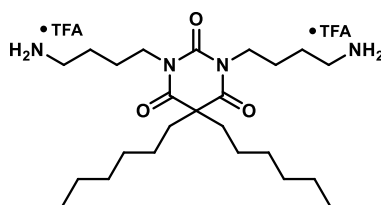


1,3-bis(4-aminobutyl)-5,5-bis((6-bromoquinolin-2-yl)methyl)pyrimidine-2,4,6(1H,3H,5H)-trione 2bA.

Barbiturate **7f** (39 mg, 69 μ mol, 1.0 eq), *tert*-butyl (4-hydroxybutyl)carbamate (32 mg, 172 μ mol, 2.5 eq), PPh₃ (54 mg, 206 μ mol, 3.0 eq) and DIAD (43 μ L, 206 μ mol, 3.0 eq) were stirred in DCM (1.0 mL) for 20 h. The crude was purified with 20-62% EtOAc in heptane to yield boc-**2bA** (40 mg, 44 μ mol, 64%) as a white solid.

TFA (79 μ L, 1.03 mmol, 15.0 eq) and DCM (0.7 mL) were added, and the mixture was stirred at ambient temperature for 17 h. The

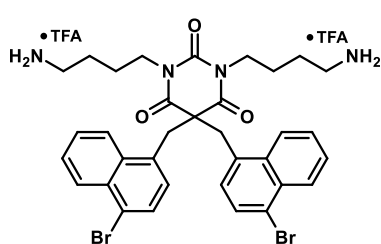
crude was purified by automated RP column chromatography with a gradient of 10-60% MeCN/H₂O + 0.1% TFA to yield the di-TFA salt of **2bA** (40 mg, 43 μ mol, 62% o2s) as a white solid. ¹H NMR (400 MHz, Methanol-*d*₄) δ 8.22 – 8.15 (m, 2H), 8.10 (d, *J* = 2.2 Hz, 2H), 7.81 (dd, *J* = 8.9, 2.2 Hz, 2H), 7.61 (d, *J* = 9.0 Hz, 2H), 7.41 (d, *J* = 8.5 Hz, 2H), 3.93 (s, 4H), 3.79 (t, *J* = 6.8 Hz, 4H), 2.66 (t, *J* = 7.2 Hz, 4H), 1.49 – 1.34 (m, 8H). ¹³C NMR (101 MHz, Methanol-*d*₄) δ 173.8 (2C), 158.9 (2C), 153.3, 146.7 (2C), 137.2 (2C), 134.3 (2C), 131.3 (2C), 131.0 (2C), 129.6 (2C), 123.6 (2C), 121.2 (2C), 54.5, 48.2 (2C), 42.0 (2C), 39.9 (2C), 25.9 (2C), 25.7 (2C). HRMS (ESI): calcd for C₃₂H₃₅Br₂N₆O₃⁺ [M+H]⁺ 709.1132, found 709.1129. SFC: 99.2%.



1,3-bis(4-aminobutyl)-5,5-dihexylpyrimidine-2,4,6(1H,3H,5H)-trione 2cA.

Barbiturate **7h** (37 mg, 125 μ mol, 1.0 eq), *tert*-butyl (4-hydroxybutyl)carbamate (59 mg, 312 μ mol, 2.5 eq), PPh₃ (98 mg, 375 μ mol, 3.0 eq) and DIAD (78 μ L, 374 μ mol, 3.0 eq) were stirred in DCM (1.0 mL) for 20 h. The crude was purified with 10-40% EtOAc in heptane to yield boc-**2cA** (66 mg, 103 μ mol, 83%) as a white solid.

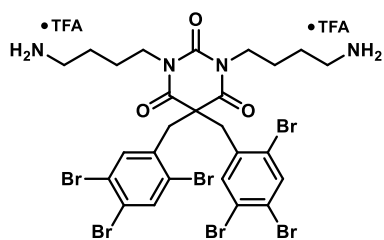
TFA (96 μ L, 1.25 mmol, 10.0 eq) and DCM (1.0 mL) were added, and the mixture was stirred at ambient temperature for 22 h. The crude was purified by automated RP column chromatography with a gradient of 10-60% MeCN/H₂O + 0.1% TFA to yield the di-TFA salt of **2cA** (58 mg, 87 μ mol, 70% o2s) as a white powder. ¹H NMR (400 MHz, Methanol-*d*₄) δ 4.00 – 3.86 (m, 4H), 3.06 – 2.93 (m, 4H), 1.99 – 1.89 (m, 4H), 1.70 (h, *J* = 3.8 Hz, 8H), 1.32 – 1.18 (m, 12H), 1.09 (dt, *J* = 9.5, 4.6 Hz, 4H), 0.87 (t, *J* = 6.8 Hz, 6H). ¹³C NMR (101 MHz, Methanol-*d*₄) δ 173.2 (2C), 151.9, 57.8, 42.2 (2C), 41.0 (2C), 40.2 (2C), 32.3 (2C), 30.2 (2C), 26.0 (2C), 25.9 (4C), 23.5 (2C), 14.3 (2C). HRMS (ESI): calcd for C₂₄H₄₇N₄O₃⁺ [M+H]⁺ 439.3643, found 439.3642. SFC: 96.5%.



1,3-bis(4-aminobutyl)-5,5-bis((4-bromonaphthalen-1-yl)methyl)pyrimidine-2,4,6(1H,3H,5H)-trione 2dA.

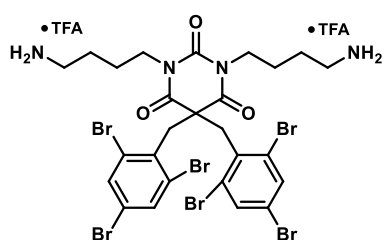
Barbiturate **7g** (201 mg, 350 μ mol, 1.0 eq), *tert*-butyl (4-hydroxybutyl)carbamate (166 mg, 880 μ mol, 2.5 eq), PPh₃ (277 mg, 1.06 mmol, 3.0 eq) and DIAD (205 μ L, 1.04 mmol, 3.0 eq) were stirred in DCM (2.0 mL) for 24 h. The crude was purified with 0-70% EtOAc in heptane to yield boc-**2dA** (315 mg, 346 μ mol, 99%) as a white solid.

TFA (0.42 mL, 5.48 mmol, 15.8 eq) and DCM (2.0 mL) were added, and the mixture was stirred at ambient temperature for 18 h. The crude was purified by automated RP column chromatography with a gradient of 0-70% MeCN/H₂O + 0.1% TFA to yield the di-TFA salt of **2dA** (153 mg, 163 μ mol, 47% o2s) as a white solid, m.p. 105-110°C. ¹H NMR (400 MHz, Methanol-*d*₄) δ 8.35 – 8.27 (m, 2H), 8.25 – 8.18 (m, 2H), 7.75 – 7.57 (m, 6H), 7.13 (d, *J* = 7.8 Hz, 2H), 4.10 (s, 4H), 3.35 (t, 4H), 2.60 (t, *J* = 7.7 Hz, 4H), 1.06 (p, 4H), 0.78 (p, *J* = 15.0, 7.6 Hz, 4H). ¹³C NMR (101 MHz, Methanol-*d*₄) δ 172.0 (2C), 150.7, 134.4 (2C), 133.5 (2C), 133.4 (2C), 130.5 (2C), 129.3 (2C), 128.7 (2C), 128.5 (2C), 128.1 (2C), 126.6 (2C), 123.8 (2C), 60.4, 41.7 (2C), 41.5 (2C), 40.0 (2C), 25.2 (2C), 25.1 (2C). HRMS (ESI): calcd for C₃₄H₃₇Br₂N₄O₃⁺ [M+H]⁺ 707.1227, found 707.1230. SFC: 95.3%.



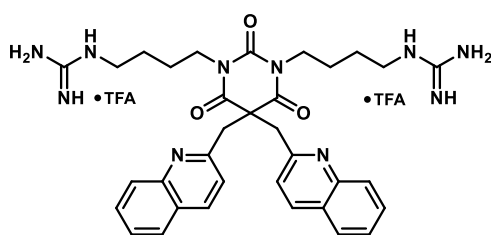
1,3-bis(4-aminobutyl)-5,5-bis(2,4,5-tribromobenzyl)pyrimidine-2,4,6(1H,3H,5H)-trione 2eA.

Barbiturate **7i** (80 mg, 102 μmol , 1.0 eq), *tert*-butyl (4-hydroxybutyl)carbamate (58 mg, 307 μmol , 3.0 eq), PPh_3 (81 mg, 307 μmol , 3.0 eq) and DIAD (64 μL , 307 μmol , 3.0 eq) were stirred in DCM (0.5 mL) for 12 h. The crude was purified with 0-40% EtOAc in heptane to yield boc-**2eA** (97 mg, 86 μmol , 84%) as a slightly yellow oil. TFA (66 μL , 0.86 mmol, 10.0 eq) and DCM (1.0 mL) were added, and the mixture was stirred at ambient temperature for 18 h. The crude was purified by automated RP column chromatography with a gradient of 20-45% MeCN/ H_2O + 0.1% TFA to yield the di-TFA salt of **2eA** (57 mg, 50 μmol , 49% o2s) as a white powder. $^1\text{H NMR}$ (400 MHz, Methanol-*d*4) δ 7.95 (s, 2H), 7.34 (s, 2H), 3.81 (t, $J = 7.0$ Hz, 4H), 3.64 (s, 4H), 2.92 (t, $J = 7.4$ Hz, 4H), 1.61 – 1.44 (m, 8H). $^{13}\text{C NMR}$ (101 MHz, Methanol-*d*4) δ 170.6 (2C), 150.9, 138.6 (2C), 137.6 (2C), 136.0 (2C), 125.7 (2C), 125.5 (2C), 124.6 (2C), 58.1, 43.5 (2C), 42.7 (2C), 40.2 (2C), 26.0 (2C), 25.8 (2C). **HRMS** (ESI): calcd for $\text{C}_{26}\text{H}_{29}\text{Br}_6\text{N}_4\text{O}_3^+$ $[\text{M}+\text{H}]^+$ 918.7334, found: 918.7343. **SFC**: 98.8%.



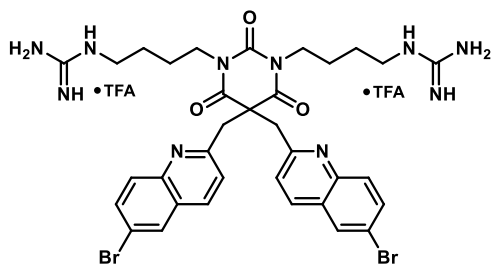
1,3-bis(4-aminobutyl)-5,5-bis(2,4,6-tribromobenzyl)pyrimidine-2,4,6(1H,3H,5H)-trione 2fA.

Barbiturate **7j** (70 mg, 90 μmol , 1.0 eq), *tert*-butyl (4-hydroxybutyl)carbamate (42 mg, 224 μmol , 2.5 eq), PPh_3 (70 mg, 269 μmol , 3.0 eq) and DIAD (56 μL , 269 μmol , 3.0 eq) were stirred in anhydrous DMPU:dimethylcarbonate (1:1, 4.0 mL) for 24 h. The crude was purified with 10-40% EtOAc in heptane to yield impure boc-**2fA** (101 mg, 90 μmol , 100%) as a colorless viscous oil. TFA (69 μL , 0.90 mmol, 10.0 eq) and DCM (1.0 mL) were added, and the mixture was stirred at ambient temperature for 18 h. The crude was purified by automated RP column chromatography with a gradient of 15-50% MeCN/ H_2O + 0.1% TFA to yield the di-TFA salt of **2fA** (26 mg, 23 μmol , 25% o2s) as a white powder. $^1\text{H NMR}$ (400 MHz, Methanol-*d*4) δ 7.81 (s, 2H), 4.03 (s, 2H), 3.77 (t, $J = 7.3$ Hz, 2H), 2.94 – 2.83 (m, 2H), 1.55 (p, $J = 7.7$ Hz, 2H), 1.43 – 1.32 (m, 2H). $^{13}\text{C NMR}$ (101 MHz, Methanol-*d*4) δ 170.6 (2C), 151.7, 137.0 (2C), 136.1 (4C), 128.6 (4C), 123.0 (2C), 57.3, 45.7 (2C), 42.6 (2C), 40.2 (2C), 25.9 (2C), 25.6 (2C). *TFA signals were observed but are not reported.* **HRMS** (ESI): calcd for $\text{C}_{26}\text{H}_{29}\text{Br}_6\text{N}_4\text{O}_3^+$ $[\text{M}+\text{H}]^+$ 918.7334, found: 918.7332. **SFC**: 96.5%.



1,1'-((2,4,6-trioxo-5,5-bis(quinolin-2-ylmethyl)dihydropyrimidine-1,3(2H,4H)-diyl)bis(butane-4,1-diyl))diguanidine 2aG.

Barbiturate **7e** (49 mg, 120 μmol , 1.0 eq), *N,N'*-di(*tert*-butoxycarbonyl)-guanidinybutanol (80 mg, 240 μmol , 2.5 eq), PPh_3 (273 mg, 1.05 mmol, 3.0 eq) and DIAD (75 μL , 360 μmol , 3.0 eq) were stirred in DCM (1.0 mL) for 16 h. The crude was purified with 10-70% EtOAc in heptane to yield boc-**2aG** (85 mg, 82 μmol , 68%) as a slightly yellow highly viscous oil. TFA (138 μL , 1.80 mmol, 15.0 eq) and DCM (1.0 mL) were added, and the mixture was stirred at ambient temperature for 17 h. The crude was purified by automated RP column chromatography with a gradient of 0-70% MeCN/ H_2O + 0.1% TFA to yield the di-TFA salt of **2aG** (39 mg, 45 μmol , 38% o2s) as a slightly brown solid. $^1\text{H NMR}$ (400 MHz, Methanol-*d*4) δ 8.22 (d, $J = 8.5$ Hz, 2H), 7.93 – 7.82 (m, 2H), 7.75 – 7.66 (m, 4H), 7.55 (dq, $J = 8.1, 4.5, 4.0$ Hz, 2H), 7.37 (d, $J = 8.5$ Hz, 2H), 3.94 (s, 4H), 3.81 (t, $J = 7.0$ Hz, 4H), 2.82 (t, $J = 7.4$ Hz, 4H), 1.40 (p, $J = 7.1$ Hz, 4H), 1.22 – 1.11 (m, 4H). $^{13}\text{C NMR}$ (101 MHz, Methanol-*d*4) δ 172.9 (2C), 156.9 (2C), 156.7 (2C), 152.1, 146.8 (2C), 136.7 (2C), 129.6 (2C), 127.7 (4C), 127.1 (2C), 126.3 (2C), 121.1 (2C), 53.5, 47.0 (2C), 40.9 (2C), 40.4 (2C), 25.5 (2C), 24.8 (2C). **HRMS** (ESI): calcd for $\text{C}_{34}\text{H}_{41}\text{N}_{10}\text{O}_3^+$ $[\text{M}+\text{H}]^+$ 637.3358, found 637.3353. **SFC**: 99.3%.

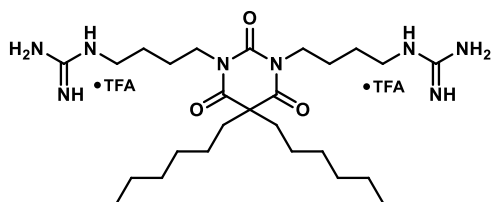


*1,1'-((5,5-bis((6-bromoquinolin-2-yl)methyl)-2,4,6-trioxodihydropyrimidine-1,3(2H,4H)-diyl)bis(butane-4,1-diyl))diguanidine **2bG**.*

Barbiturate **7f** (35 mg, 62 μ mol, 1.0 eq), *N,N'*-di(tert-butoxycarbonyl)-guanidinybutanol (51 mg, 154 μ mol, 2.5 eq), PPh_3 (48 mg, 185 μ mol, 3.0 eq) and DIAD (39 μ L, 185 μ mol, 3.0 eq) were stirred in DCM (1.0 mL) for 20 h. The crude was purified with 30-70% EtOAc in heptane to

yield boc-**2bG** (72 mg, 60 μ mol, 98%) as a yellow highly viscous oil.

TFA (71 μ L, 0.92 mmol, 15.0 eq) and DCM (1.0 mL) were added, and the mixture was stirred at ambient temperature for 22 h. The crude was purified by automated RP column chromatography with a gradient of 10-60% MeCN/ H_2O + 0.1% TFA to yield the di-TFA salt of **2bG** (41 mg, 40 μ mol, 65% o2s) as a white powder. $^1\text{H NMR}$ (400 MHz, Methanol-*d*4) δ 8.17 (d, J = 8.5 Hz, 2H), 8.09 (d, J = 2.2 Hz, 2H), 7.80 (dd, J = 9.0, 2.2 Hz, 2H), 7.60 (d, J = 9.0 Hz, 2H), 7.41 (d, J = 8.5 Hz, 2H), 3.92 (s, 4H), 3.82 (t, J = 7.0 Hz, 4H), 2.85 (t, J = 7.4 Hz, 4H), 1.41 (p, J = 7.1 Hz, 4H), 1.19 (qd, J = 7.1, 5.9, 3.9 Hz, 4H). $^{13}\text{C NMR}$ (101 MHz, Methanol-*d*4) δ 174.0 (2C), 158.9 (2C), 158.3 (2C), 153.4, 146.7 (2C), 137.3 (2C), 134.3 (2C), 131.3 (2C), 131.0 (2C), 129.6 (2C), 123.5 (2C), 121.2 (2C), 54.5, 48.3 (2C), 42.3 (2C), 41.8 (2C), 26.8 (2C), 26.2 (2C). **HRMS** (ESI): calcd for $\text{C}_{34}\text{H}_{39}\text{Br}_2\text{N}_{10}\text{O}_3^+$ [$\text{M}+\text{H}$] $^+$ 793.1568, found 793.1575. **SFC**: >99.5%.

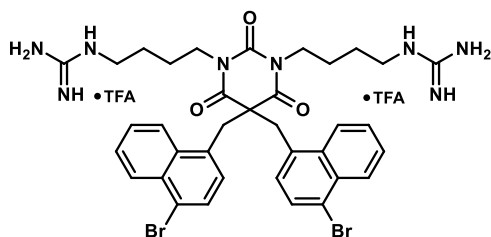


*1,1'-((5,5-dihexyl-2,4,6-trioxodihydropyrimidine-1,3(2H,4H)-diyl)bis(butane-4,1-diyl))diguanidine **2cG**.*

Barbiturate **7h** (22 mg, 74 μ mol, 1.0 eq), *N,N'*-di(tert-butoxycarbonyl)-guanidinybutanol (62 mg, 186 μ mol, 2.5 eq), PPh_3 (58 mg, 223 μ mol, 3.0 eq) and DIAD (48 μ L, 223 μ mol, 3.0 eq) were stirred in DCM (1.0 mL) for 20 h.

The crude was purified with 10-40% EtOAc in heptane to yield boc-**2cG** (66 mg, 72 μ mol, 96%) as a yellow oil.

TFA (85 μ L, 1.11 mmol, 15.0 eq) and DCM (1.0 mL) were added, and the mixture was stirred at ambient temperature for 22 h. The crude was purified by automated RP column chromatography with a gradient of 10-60% MeCN/ H_2O + 0.1% TFA to yield the di-TFA salt of **2cG** (48 mg, 64 μ mol, 86% o2s) as a white powder. $^1\text{H NMR}$ (400 MHz, Methanol-*d*4) δ 3.94 (t, J = 6.9 Hz, 4H), 3.23 (t, J = 6.8 Hz, 4H), 2.00 – 1.91 (m, 4H), 1.74 – 1.57 (m, 8H), 1.33 – 1.17 (m, 12H), 1.08 (dd, J = 10.4, 6.4 Hz, 4H), 0.87 (t, J = 6.9 Hz, 6H). $^{13}\text{C NMR}$ (101 MHz, Methanol-*d*4) δ 173.3 (2C), 158.9 (2C), 152.0, 57.8, 42.4 (2C), 42.0 (2C), 41.1 (2C), 32.4 (2C), 30.1 (2C), 27.2 (2C), 26.2 (2C), 26.0 (2C), 23.5 (2C), 14.3 (2C). **HRMS** (ESI): calcd for $\text{C}_{26}\text{H}_{51}\text{N}_8\text{O}_3^+$ [$\text{M}+\text{H}$] $^+$ 523.4079, found 523.4078. **SFC**: >99.5%.



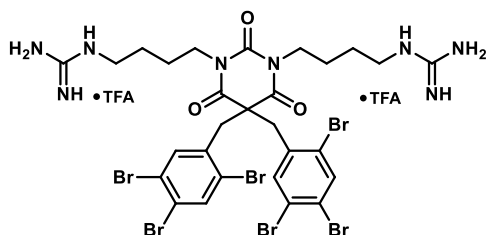
*1,1'-((5,5-bis((4-bromonaphthalen-1-yl)methyl)-2,4,6-trioxodihydropyrimidine-1,3(2H,4H)-diyl)bis(butane-4,1-diyl))diguanidine **2dG**.*

Barbiturate **7g** (71 mg, 125 μ mol, 1.0 eq), *N,N'*-di(tert-butoxycarbonyl)-guanidinybutanol (83 mg, 250 μ mol, 2.0 eq), PPh_3 (98 mg, 375 μ mol, 3.0 eq) and DIAD (79 μ L, 275 μ mol, 3.0 eq) were stirred in DCM (1.5 mL) for 16 h.

The crude was purified with 10-60% EtOAc in heptane to yield boc-**2dG** (124 mg, 104 μ mol, 83%) as a colorless oil.

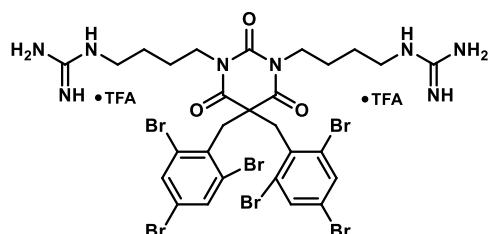
TFA (287 μ L, 3.76 mmol, 30.0 eq) and DCM (1.5 mL) were added, and the mixture was stirred at ambient temperature for 36 h. The crude was purified by automated RP column chromatography with a gradient of 0-70% MeCN/ H_2O + 0.1% TFA to yield the di-TFA salt of **2dG** (85 mg, 83 μ mol, 67% o2s) as a white solid. $^1\text{H NMR}$ (400 MHz, Methanol-*d*4) δ 8.38 – 8.29 (m, 2H), 8.22 (dt, J = 7.8, 2.7 Hz, 2H), 7.68 (d, J = 7.8 Hz, 2H), 7.66 – 7.61 (m, 4H), 7.15 (d, J = 7.8 Hz, 2H), 4.13 (s, 4H), 3.36 (t, J = 7.2 Hz, 4H), 2.87 (t, J = 7.1 Hz, 4H), 0.97 (ddd, J = 14.3, 7.5, 4.0 Hz, 4H), 0.84 (tt, J = 8.4, 6.2 Hz, 4H). $^{13}\text{C NMR}$ (101 MHz, Methanol-*d*4) δ 172.0 (2C), 158.5 (2C), 150.9, 134.4 (2C), 133.5 (2C), 133.4 (2C), 130.4 (2C), 129.4 (2C), 128.7 (2C), 128.5 (2C), 128.1 (2C), 126.2 (2C), 123.8 (2C), 60.4, 42.1 (2C),

41.8 (2C), 41.6 (2C), 26.5 (2C), 25.4 (2C). **HRMS** (ESI): calcd for $C_{36}H_{41}Br_2N_8O_3^+$ $[M+H]^+$ 791.1663, found 791,1665. **SFC**: >99.5%.



1,1'-((2,4,6-trioxo-5,5-bis(2,4,5-tribromobenzyl)dihydropyrimidine-1,3(2H,4H)-diyl)bis(butane-4,1-diyl))diguanidine **2eG**.

7i (80 mg, 102 μ mol, 1.0 eq), *N,N'*-di(tert-butoxycarbonyl)-guanidinybutanol (58 mg, 307 μ mol, 3.0 eq), PPh_3 (81 mg, 307 μ mol, 3.0 eq) and DIAD (64 μ L, 307 μ mol, 3.0 eq) were stirred in DCM (0.5 mL) for 12 h. The crude was purified with 0-40% EtOAc in heptane to yield boc-**2eG** (98 mg, 70 μ mol, 68%) as a slightly yellow oil. TFA (80 μ L, 1.04 mmol, 15.0 eq) and DCM (1.0 mL) were added, and the mixture was stirred at ambient temperature for 18 h. The crude was purified by automated RP column chromatography with a gradient of 20-45% MeCN/H₂O + 0.1% TFA to yield the di-TFA salt of **2eG** (43 mg, 35 μ mol, 34% o2s) as a white powder. **¹H NMR** (400 MHz, Methanol-*d*₄) δ 7.95 (s, 2H), 7.31 (s, 2H), 3.81 (t, *J* = 6.9 Hz, 4H), 3.64 (s, 4H), 3.16 (t, *J* = 6.6 Hz, 4H), 1.57 – 1.41 (m, 8H). **¹³C NMR** (101 MHz, Methanol-*d*₄) δ 170.7 (2C), 158.6 (2C), 150.9, 138.6 (2C), 137.6 (2C), 135.8 (2C), 125.7 (2C), 125.5 (2C), 124.7 (2C), 58.0, 43.5 (2C), 43.0 (2C), 42.0 (2C), 27.0 (2C), 26.2 (2C). **HRMS** (ESI): calcd for $C_{28}H_{33}Br_6N_8O_3^+$ $[M+H]^+$ 1002.7770, found: 1002.7768. **SFC**: 98.5%.

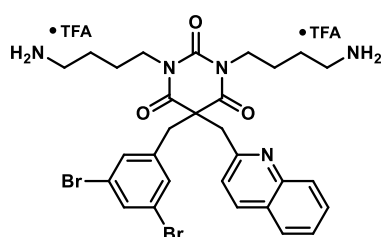


1,1'-((2,4,6-trioxo-5,5-bis(2,4,6-tribromobenzyl)dihydropyrimidine-1,3(2H,4H)-diyl)bis(butane-4,1-diyl))diguanidine **2fG**.

Barbiturate **7j** (70 mg, 90 μ mol, 1.0 eq), *N,N'*-di(tert-butoxycarbonyl)-guanidinybutanol (74 mg, 224 μ mol, 2.5 eq), PPh_3 (70 mg, 269 μ mol, 3.0 eq) and DIAD (56 μ L, 269 μ mol, 3.0 eq) were stirred in anhydrous DMPU:dimethylcarbonate (1:1, 4.0 mL) for 24 h. The crude was purified with 10-40% EtOAc in heptane to yield boc-**2fG** (79 mg, 56 μ mol, 63%) as a colorless oil. TFA (206 μ L, 2.68 mmol, 30.0 eq) and DCM (1.0 mL) were added, and the mixture was stirred at ambient temperature for 43 h. The crude was purified by automated RP column chromatography with a gradient of 20-55% MeCN/H₂O + 0.1% TFA to yield the di-TFA salt of **2fG** (37 mg, 30 μ mol, 33% o2s) as a white powder. **¹H NMR** (400 MHz, Methanol-*d*₄) δ 7.80 (s, 4H), 4.02 (s, 4H), 3.77 (t, *J* = 7.1 Hz, 4H), 3.13 (t, *J* = 7.0 Hz, 4H), 1.52 – 1.31 (m, 8H). **¹³C NMR** (101 MHz, Methanol-*d*₄) δ 170.6 (2C), 158.7 (2C), 151.7, 137.0 (2C), 136.1 (4C), 128.5 (4C), 123.0 (2C), 57.3, 45.8 (2C), 42.9 (2C), 42.0 (2C), 27.2 (2C), 25.8 (2C). **HRMS** (ESI): calcd for $C_{28}H_{34}Br_6N_8O_3$ for $[M+2H]^{2+}$ 501.8922, found: 501.8917. **SFC**: 98.1%.

2.8 Synthesis of series 3

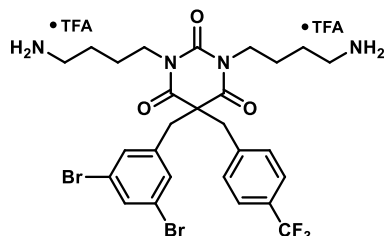
The following products were synthesized according to General Procedure D:



1,3-bis(4-aminobutyl)-5-(3,5-dibromobenzyl)-5-(quinolin-2-ylmethyl)pyrimidine-2,4,6(1H,3H,5H)-trione **3aA**.

Barbiturate **10a** (55 mg, 107 μ mol, 1.0 eq), *tert*-butyl (4-hydroxybutyl)carbamate (50 mg, 266 μ mol, 2.5 eq), PPh_3 (84 mg, 319 μ mol, 3.0 eq) and DIAD (67 μ L, 319 μ mol, 3.0 eq) were stirred in DCM (0.5 mL) for 16 h. The crude was purified with 10-50% EtOAc in heptane to yield impure boc-**3aA** (145 mg, 169 μ mol, 159%) as a colorless oil. TFA (81 μ L, 1.06 mmol, 10.00 eq) and DCM (0.7 mL) were added, and the mixture was stirred at ambient temperature for 21 h. The crude was purified by automated RP column chromatography with a gradient of 15-53% MeCN/H₂O + 0.1% TFA to yield the di-TFA salt of **3aA** (70 mg, 81 μ mol, 76% o2s) as a white solid. **¹H NMR** (400 MHz, Methanol-*d*₄) δ 8.21 (d, *J* = 8.5 Hz, 1H), 7.86 (dd, *J* = 8.1, 1.5 Hz, 1H), 7.72 (t, *J* = 1.7 Hz, 1H), 7.65 (ddd, *J* = 8.4, 6.9, 1.5 Hz, 1H), 7.51 (ddd, *J* = 8.2, 6.9, 1.2

Hz, 1H), 7.48 – 7.44 (m, 1H), 7.41 (d, $J = 8.5$ Hz, 1H), 7.25 (d, $J = 1.8$ Hz, 2H), 4.03 (s, 2H), 3.87 – 3.69 (m, 4H), 3.36 (s, 2H), 2.87 – 2.71 (m, 4H), 1.67 – 1.38 (m, 8H). $^{13}\text{C NMR}$ (101 MHz, Methanol- d_4) δ 173.2 (2C), 158.6, 152.4, 147.8, 140.1, 138.11, 134.6, 132.7 (2C), 130.9, 129.2, 128.6, 128.4, 127.5, 124.0 (2C), 122.0, 56.8, 46.4, 45.9, 42.2 (2C), 40.1 (2C), 26.3 (2C), 25.9 (2C). **HRMS** (ESI): calcd for $\text{C}_{29}\text{H}_{34}\text{Br}_2\text{N}_5\text{O}_3^+$ $[\text{M}+\text{H}]^+$ 658.1023, found 658.1027. **SFC**: >99.5%.

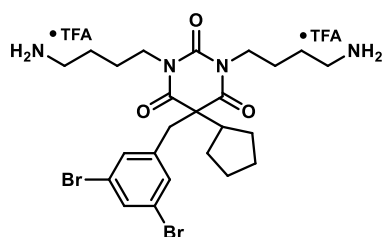


1,3-bis(4-aminobutyl)-5-(3,5-dibromobenzyl)-5-(4-(trifluoromethyl)benzyl)pyrimidine-2,4,6(1H,3H,5H)-trione 3bA.

Barbiturate **10b** (36 mg, 67 μmol , 1.0 eq), *tert*-butyl (4-hydroxybutyl)carbamate (32 mg, 169 μmol , 2.5 eq), PPh_3 (53 mg, 202 μmol , 3.0 eq) and DIAD (42 μL , 202 μmol , 3.0 eq) were stirred in DCM (0.5 mL) for 16 h. The crude was purified with 10-40% EtOAc in heptane to yield boc-**3bA** (55 mg, 63 μmol , 93%) as a colorless oil.

TFA (41 μL , 539 μmol , 8.00 eq) and DCM (0.7 mL) were added, and the mixture was stirred at ambient temperature for 17 h. The crude

was purified by automated RP column chromatography with a gradient of 15-60% MeCN/ H_2O + 0.1% TFA to yield the di-TFA salt of **3bA** (41 mg, 47 μmol , 69% o2s) as a white powder. $^1\text{H NMR}$ (400 MHz, Methanol- d_4) δ 7.66 (t, $J = 1.8$ Hz, 1H), 7.57 (d, $J = 8.1$ Hz, 2H), 7.27 (d, $J = 8.1$ Hz, 2H), 7.24 (d, $J = 1.8$ Hz, 2H), 3.70 (ddd, $J = 13.0, 9.3, 5.7$ Hz, 2H), 3.59 (ddd, $J = 13.0, 9.0, 5.9$ Hz, 2H), 3.53 (s, 2H), 3.46 (s, 2H), 2.97 – 2.86 (m, 4H), 1.56 – 1.45 (m, 4H), 1.45 – 1.24 (m, 4H). $^{13}\text{C NMR}$ (101 MHz, Methanol- d_4) δ 171.3 (2C), 150.6, 140.8 – 140.7 (m, 2C), 140.7, 134.5, 132.8 (2C), 131.4 (2C), 131.08 (q, $J = 32.4$ Hz), 126.7 (q, $J = 3.5$ Hz, 2C), 124.1 (2C), 61.1, 45.6, 45.1, 42.1 (2C), 40.2 (2C), 26.0 (2C), 25.7 (2C). CF_3 carbon was not observed, due to too low intensity. **HRMS** (ESI): calcd for $\text{C}_{27}\text{H}_{32}\text{Br}_4\text{F}_3\text{N}_4\text{O}_3^+$ $[\text{M}+\text{H}]^+$ 675.0788, found 675.0793. **SFC**: 95.3%.

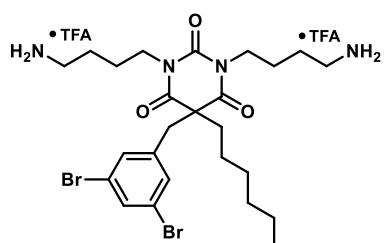


1,3-bis(4-aminobutyl)-5-cyclopentyl-5-(3,5-dibromobenzyl)pyrimidine-2,4,6(1H,3H,5H)-trione 3cA.

Barbiturate **10c** (45 mg, 101 μmol , 1.0 eq), *tert*-butyl (4-hydroxybutyl)carbamate (48 mg, 253 μmol , 2.5 eq), PPh_3 (81 mg, 304 μmol , 3.0 eq) and DIAD (64 μL , 304 μmol , 3.0 eq) were stirred in DCM (1.0 mL) for 16 h. The crude was purified with 10-50% EtOAc in heptane to yield boc-**3cA** (63 mg, 80 μmol , 79%) as a yellow oil.

TFA (116 μL , 1.52 mmol, 15.00 eq) and DCM (1.0 mL) were added,

and the mixture was stirred at ambient temperature for 17 h. The crude was purified by automated RP column chromatography with a gradient of 15-60% MeCN/ H_2O + 0.1% TFA to yield the di-TFA salt of **3cA** (21 mg, 26 μmol , 25% o2s) as a white powder. $^1\text{H NMR}$ (400 MHz, Methanol- d_4) δ 7.61 (t, $J = 1.8$ Hz, 1H), 7.23 (d, $J = 1.8$ Hz, 2H), 3.83 (t, $J = 7.3$ Hz, 4H), 3.37 (s, 2H), 3.03 – 2.90 (m, 4H), 2.60 (h, $J = 8.1$ Hz, 1H), 1.78 (d, $J = 8.9$ Hz, 2H), 1.69 – 1.45 (m, 14H). $^{13}\text{C NMR}$ (101 MHz, Methanol- d_4) δ 171.6 (2C), 151.4, 141.9, 134.0, 133.1 (2C), 123.8 (2C), 61.3, 51.8, 42.2 (2C), 42.0, 40.3 (2C), 28.4, 26.2 (2C), 25.9, 25.5 (2C). **HRMS** (ESI): calcd for $\text{C}_{24}\text{H}_{35}\text{Br}_2\text{N}_4\text{O}_3^+$ $[\text{M}+\text{H}]^+$ 585.1070, found 585.1068. **SFC**: >99.5%.



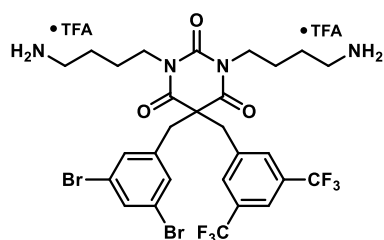
1,3-bis(4-aminobutyl)-5-(3,5-dibromobenzyl)-5-hexylpyrimidine-2,4,6(1H,3H,5H)-trione 3dA.

Barbiturate **10d** (52 mg, 113 μmol , 1.0 eq), *tert*-butyl (4-hydroxybutyl)carbamate (54 mg, 283 μmol , 2.5 eq), PPh_3 (89 mg, 339 μmol , 3.0 eq) and DIAD (71 μL , 339 μmol , 3.0 eq) were stirred in DCM (1.0 mL) for 20 h. The crude was purified with 10-50% EtOAc in heptane to yield boc-**3dA** (86 mg, 107 μmol , 95%) as a colorless oil.

TFA (87 μL , 1.13 mmol, 10.0 eq) and DCM (1.0 mL) were added,

and the mixture was stirred at ambient temperature for 22 h. The crude was purified by automated RP column chromatography with a gradient of 15-60% MeCN/ H_2O + 0.1% TFA to yield the di-TFA salt of **3dA** (68 mg, 82 μmol , 73% o2s) as a white powder. $^1\text{H NMR}$ (400 MHz, Methanol- d_4) δ 7.64 (t, $J = 1.8$ Hz, 1H), 7.17 (d, $J = 1.8$ Hz, 2H), 3.80 (tdd, $J = 13.0, 8.8, 7.3$ Hz, 4H), 3.23 (s, 2H), 2.97 (td, $J = 7.2, 3.0$ Hz, 4H), 2.17 – 2.08 (m, 2H), 1.70 – 1.54 (m, 6H), 1.47 (qt, $J = 10.6, 3.3$ Hz, 2H), 1.34 –

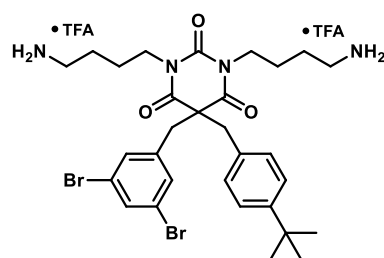
1.20 (m, 6H), 1.11 (tt, $J = 11.7, 6.6$ Hz, 2H), 0.93 – 0.84 (m, 3H). ^{13}C NMR (101 MHz, Methanol- d_4) δ 172.1 (2C), 151.1, 140.9, 134.3, 132.6 (2C), 124.0 (2C), 59.4, 45.7, 42.3 (2C), 40.7, 40.3 (2C), 32.3, 30.1, 26.2 (2C), 25.9, 25.8 (2C), 23.5, 14.23. HRMS (ESI): calcd for $\text{C}_{25}\text{H}_{39}\text{Br}_2\text{N}_4\text{O}_3^+$ $[\text{M}+\text{H}]^+$ 601.1383, found 601.1384. SFC: 95.2%.



1,3-bis(4-aminobutyl)-5-(3,5-bis(trifluoromethyl)benzyl)-5-(3,5-dibromobenzyl)pyrimidine-2,4,6(1H,3H,5H)-trione 3eA.

Barbiturate **10e** (90 mg, 150 μmol , 1.0 eq), *tert*-butyl (4-hydroxybutyl)carbamate (85 mg, 449 μmol , 3.0 eq), PPh_3 (118 mg, 449 μmol , 3.0 eq) and DIAD (94 μL , 449 μmol , 3.0 eq) were stirred in anhydrous THF (1.0 mL) for 12 h. The crude was purified with 0-40% EtOAc in heptane to yield boc-**3eA** (110 mg, 117 μmol , 78%) as a pale-yellow oil.

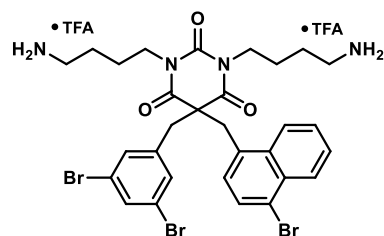
TFA (90 μL , 1.17 mmol, 10.0 eq) and DCM (1.0 mL) were added, and the mixture was stirred at ambient temperature for 18 h. The crude was purified by automated RP column chromatography with a gradient of 20-45% MeCN/ H_2O + 0.1% TFA to yield the di-TFA salt of **3eA** (82 mg, 84 μmol , 56% o2s) as a white foam. ^1H NMR (400 MHz, Methanol- d_4) δ 7.90 (s, 1H), 7.68 – 7.64 (m, 3H), 7.24 (d, $J = 1.7$ Hz, 2H), 3.71 – 3.53 (m, 4H), 3.65 (s, 2H), 3.47 (s, 2H), 2.90 (dd, $J = 9.1, 6.6$ Hz, 4H), 1.59 – 1.48 (m, 4H), 1.46 – 1.26 (m, 4H). ^{13}C NMR (101 MHz, Methanol- d_4) δ 171.1 (2C), 150.3, 140.3, 139.6, 134.7, 133.0 (q, $J = 33.3$ Hz, 2C) 132.7 (2C), 131.4 (q, $J = 2.7$ Hz, 2C), 124.6 (q, $J = 272.2$ Hz, 2C), 124.2 (2C), 122.9 – 122.7 (m, 1C), 61.2, 45.3, 44.4, 42.2 (2C), 40.1 (2C), 26.1 (2C), 25.7 (2C). HRMS (ESI): calcd for $\text{C}_{28}\text{H}_{31}\text{Br}_2\text{F}_6\text{N}_4\text{O}_3^+$ $[\text{M}+\text{H}]^+$ 743.0662, found 743.0670. SFC: 97.4%.



1,3-bis(4-aminobutyl)-5-(4-(tert-butyl)benzyl)-5-(3,5-dibromobenzyl)pyrimidine-2,4,6(1H,3H,5H)-trione 3fA.

Barbiturate **10f** (56 mg, 107 μmol , 1.0 eq), *tert*-butyl (4-hydroxybutyl)carbamate (51 mg, 268 μmol , 2.5 eq), PPh_3 (85 mg, 322 μmol , 3.0 eq) and DIAD (67 μL , 322 μmol , 3.0 eq) were stirred in DCM (1.0 mL) for 6 h. The crude was purified with 0-45% EtOAc in heptane to yield impure boc-**3fA** (101 mg, 117 μmol , 109%) as a yellow solid.

TFA (82 μL , 1.07 mmol, 10.00 eq) and DCM (1.0 mL) were added, and the mixture was stirred at ambient temperature for 17 h. The crude was purified by automated RP column chromatography with a gradient of 10-65% MeCN/ H_2O + 0.1% TFA to yield the di-TFA salt of **3fA** (85 mg, 95 μmol , 89% o2s) as a white powder. ^1H NMR (400 MHz, Methanol- d_4) δ 7.63 (t, $J = 1.8$ Hz, 1H), 7.30 – 7.25 (m, 2H), 7.24 (d, $J = 1.7$ Hz, 2H), 7.00 – 6.93 (m, 2H), 3.68 (ddd, $J = 13.0, 8.8, 6.0$ Hz, 2H), 3.56 (ddd, $J = 13.0, 8.7, 6.2$ Hz, 2H), 3.44 (s, 2H), 3.38 (s, 2H), 2.91 (td, $J = 7.2, 1.9$ Hz, 4H), 1.57 – 1.44 (m, 4H), 1.44 – 1.30 (m, 4H), 1.25 (s, 9H). ^{13}C NMR (101 MHz, Methanol- d_4) δ 171.7 (2C), 152.2, 150.70, 141.21, 134.2, 132.8 (2C), 130.2 (2C), 126.6 (2C), 124.0 (2C), 61.6, 46.5, 44.2, 41.9 (2C), 40.17 (2C), 35.3, 31.7 (3C), 26.0 (2C), 25.7 (2C). HRMS (ESI): calcd for $\text{C}_{30}\text{H}_{41}\text{Br}_2\text{N}_4\text{O}_3^+$ $[\text{M}+\text{H}]^+$ 663.1540, found 663.1545. SFC: 98.8%.

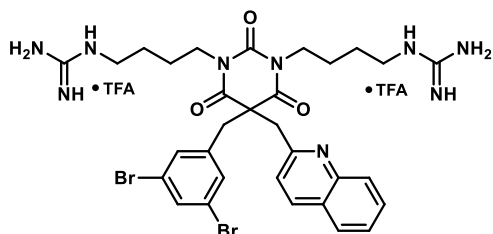


1,3-bis(4-aminobutyl)-5-((4-bromonaphthalen-1-yl)methyl)-5-(3,5-dibromobenzyl)pyrimidine-2,4,6(1H,3H,5H)-trione 3gA.

Barbiturate **10g** (55 mg, 92 μmol , 1.0 eq), *tert*-butyl (4-hydroxybutyl)carbamate (44 mg, 231 μmol , 2.5 eq), PPh_3 (73 mg, 277 μmol , 3.0 eq) and DIAD (58 μL , 277 μmol , 3.0 eq) were stirred in DCM (0.5 mL) for 16 h. The crude was purified with 10-65% EtOAc in heptane to yield boc-**3gA** (85 mg, 91 μmol , 98%) as a colorless oil.

TFA (57 μL , 740 μmol , 8.00 eq) and DCM (0.7 mL) were added, and the mixture was stirred at ambient temperature for 17 h. The crude was purified by automated RP column chromatography with a gradient of 15-60% MeCN/ H_2O + 0.1% TFA to yield the di-TFA salt of **3gA** (62 mg, 66 μmol , 71% o2s) as a white powder. ^1H NMR (400 MHz, Methanol- d_4) δ 8.30 – 8.22 (m, 1H), 8.17 (dt, $J = 7.9, 2.6$ Hz, 1H), 7.72 (d, $J = 7.7$ Hz, 1H), 7.68 – 7.60 (m, 3H), 7.28 (d, $J = 1.8$ Hz, 2H), 7.15 (d, $J = 7.8$ Hz, 1H), 3.96 (s, 2H), 3.62 (s, 2H), 3.50 (ddd, $J = 13.1, 8.9, 6.0$ Hz, 2H), 3.39 (ddd,

$J = 13.1, 8.9, 5.9$ Hz, 2H), 2.88 – 2.73 (m, 4H), 1.31 (h, $J = 7.4$ Hz, 4H), 1.21 – 0.99 (m, 4H). ^{13}C NMR (101 MHz, Methanol- d_4) δ 171.5 (2C), 150.5, 141.2, 134.3, 134.2, 133.4, 133.1 (2C), 132.8, 130.6, 128.8, 128.7, 128.3, 126.2, 124.0, 123.9 (2C), 61.1, 44.0, 42.4, 42.0 (2C), 40.2 (2C), 25.7 (2C), 25.6 (2C). **HRMS** (ESI): calcd for $\text{C}_{30}\text{H}_{34}\text{Br}_3\text{N}_4\text{O}_3^+$ $[\text{M}+\text{H}]^+$ 735.0176, found 735.0181. **SFC**: 96.1%.

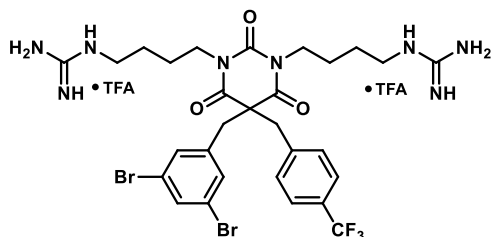


1,1'-((5-(3,5-dibromobenzyl)-2,4,6-trioxo-5-(quinolin-2-ylmethyl)dihydropyrimidine-1,3(2H,4H)-diyl)bis(butane-4,1-diyl)diguanidine 3aG.

Barbiturate **10a** (42 mg, 81 μmol , 1.0 eq), *N,N'*-di(*tert*-butoxycarbonyl)-guanidinybutanol (67 mg, 203 μmol , 2.5 eq), PPh_3 (64 mg, 244 μmol , 3.0 eq) and DIAD (51 μL , 245 μmol , 3.0 eq) were stirred in DCM (1.0 mL) for 20 h. The crude was purified with 10-45% EtOAc in heptane to

yield impure boc-**3aG** (149 mg, 130 μmol , 160%) as a white solid.

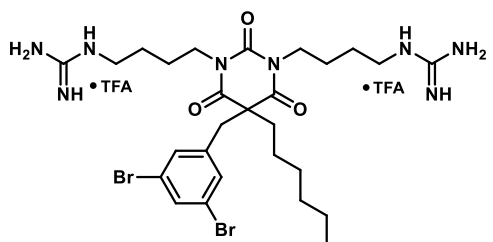
TFA (187 μL , 2.44 mmol, 30.00 eq) and DCM (0.7 mL) were added, and the mixture was stirred at ambient temperature for 48 h. The crude was purified by automated RP column chromatography with a gradient of 15-53% MeCN/ H_2O + 0.1% TFA to yield the di-TFA salt of **3aG** (32 mg, 33 μmol , 41% o2s) as a white powder. ^1H NMR (400 MHz, Methanol- d_4) δ 8.20 (d, $J = 8.5$ Hz, 1H), 7.89 – 7.82 (m, 1H), 7.70 (t, $J = 1.8$ Hz, 1H), 7.64 (ddd, $J = 8.4, 7.0, 1.4$ Hz, 1H), 7.50 (ddd, $J = 8.1, 7.0, 1.2$ Hz, 1H), 7.47 (d, $J = 8.4$ Hz, 1H), 7.41 (d, $J = 8.5$ Hz, 1H), 7.24 (d, $J = 1.7$ Hz, 2H), 4.02 (s, 2H), 3.88 – 3.68 (m, 4H), 3.35 (d, $J = 2.0$ Hz, 2H), 3.11 – 2.91 (m, 5H), 1.67 – 1.33 (m, 8H). ^{13}C NMR (101 MHz, Methanol- d_4) δ 173.2 (2C), 158.6 (2C), 158.4, 152.4, 147.8, 140.1, 138.1, 134.5, 132.6 (2C), 130.9, 129.2, 128.6, 128.3, 127.5, 124.0 (2C), 122.0, 56.8, 46.4, 45.9, 42.5 (2C), 42.0 (2C), 27.0 (2C), 26.4 (2C). **HRMS** (ESI): calcd for $\text{C}_{27}\text{H}_{43}\text{Br}_2\text{N}_8\text{O}_3^+$ $[\text{M}+\text{H}]^+$ 742.1459, found 742.1456. **SFC**: >99.5%.



(4-(5-(3,5-dibromobenzyl)-3-(4-guanidinobutyl)-2,4,6-trioxo-5-(4-(trifluoromethyl)benzyl)tetrahydropyrimidin-1(2H)-yl)butyl)-1,2-azanecarboximidamide 3bG.

Barbiturate **10b** (43 mg, 81 μmol , 1.0 eq), *N,N'*-di(*tert*-butoxycarbonyl)-guanidinybutanol (67 mg, 201 μmol , 2.5 eq), PPh_3 (63 mg, 242 μmol , 3.0 eq) and DIAD (51 μL , 242 μmol , 3.0 eq) were stirred in DCM (1.0 mL) for 20 h. The crude was purified with 10-35% EtOAc in heptane to yield boc-**3bG** (82 mg, 71 μmol , 88%) as a white solid.

TFA (185 μL , 2.42 mmol, 30.00 eq) and DCM (0.7 mL) were added, and the mixture was stirred at ambient temperature for 48 h. The crude was purified by automated RP column chromatography with a gradient of 15-60% MeCN/ H_2O + 0.1% TFA to yield the di-TFA salt of **3bG** (55 mg, 56 μmol , 69% o2s) as a white powder. ^1H NMR (400 MHz, Methanol- d_4) δ 7.64 (t, $J = 1.8$ Hz, 1H), 7.59 – 7.53 (m, 2H), 7.26 (d, $J = 8.7$ Hz, 2H), 7.23 (d, $J = 1.8$ Hz, 2H), 3.75 – 3.64 (m, 2H), 3.64 – 3.55 (m, 2H), 3.52 (s, 2H), 3.45 (s, 2H), 3.16 (t, $J = 6.6$ Hz, 4H), 1.48 – 1.28 (m, 8H). ^{13}C NMR (101 MHz, Methanol- d_4) δ 171.4 (2C), 158.7 (2C), 150.6, 140.7 (2C), 134.4, 132.9 (2C), 131.4 (2C), 131.1 (q, $J = 32.4$ Hz), 126.6 (q, $J = 3.8$ Hz, 2C), 125.4 (q, $J = 272.7$ Hz), 124.1 (2C), 61.1, 45.7, 45.0, 42.4 (2), 41.9 (2C), 26.9 (2C), 26.1 (2C). **HRMS** (ESI): calcd for $\text{C}_{29}\text{H}_{36}\text{Br}_2\text{F}_3\text{N}_8\text{O}_3^+$ $[\text{M}+\text{H}]^+$ 759.1224, found 759.1221. **SFC**: 98.5%.



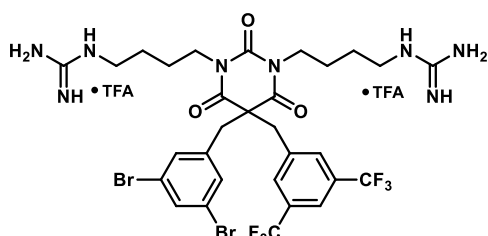
1,1'-((5-(3,5-dibromobenzyl)-5-hexyl-2,4,6-trioxodihydropyrimidine-1,3(2H,4H)-diyl)bis(butane-4,1-diyl)diguanidine 3dG.

Barbiturate **10d** (32 mg, 70 μmol , 1.0 eq), *N,N'*-di(*tert*-butoxycarbonyl)-guanidinybutanol (58 mg, 174 μmol , 2.5 eq), PPh_3 (55 mg, 209 μmol , 3.0 eq) and DIAD (44 μL , 209 μmol , 3.0 eq) were stirred in DCM (1.0 mL) for 20 h. The crude was purified with 10-42% EtOAc in heptane to

yield impure boc-**3dG** (81 mg, 75 μmol , 107%) as a white solid.

TFA (80 μL , 1.04 mmol, 15.00 eq) and DCM (1.0 mL) were added, and the mixture was stirred at ambient temperature for 22 h. The crude was purified by automated RP column chromatography with a

gradient of 10-55% MeCN/H₂O + 0.1% TFA to yield the di-TFA salt of **3dG** (54 mg, 59 μmol, 85% o2s) as a white powder. ¹H NMR (400 MHz, Methanol-*d*₄) δ 7.63 (t, *J* = 1.8 Hz, 1H), 7.17 (d, *J* = 1.7 Hz, 2H), 3.88 – 3.73 (m, 4H), 3.28 – 3.17 (m, 6H), 2.17 – 2.08 (m, 2H), 1.66 – 1.39 (m, 8H), 1.34 – 1.19 (m, 7H), 1.11 (dd, *J* = 10.6, 5.9 Hz, 2H), 0.93 – 0.85 (m, 3H). ¹³C NMR (101 MHz, Methanol-*d*₄) δ 172.2 (2C), 158.7, 151.2, 140.9, 134.3, 132.5 (2C), 124.1 (2C), 59.4, 45.6, 42.5 (2C), 42.0 (2C), 40.9, 32.3, 30.1, 27.1 (2C), 26.4 (2C), 26.0, 23.5, 14.3. HRMS (ESI): calcd for C₂₇H₄₃Br₂N₈O₃⁺ [M+H]⁺ 685.1819, found 685.1821. SFC: 99.1%.

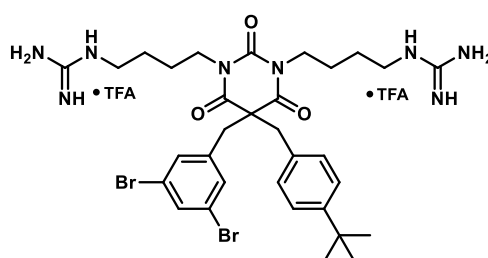


1,1'-((5-(3,5-bis(trifluoromethyl)benzyl)-5-(3,5-dibromo-benzyl)-2,4,6-trioxodihydropyrimidine-1,3(2H,4H)-diyl)bis(butane-4,1-diyl))diguanidine **3eG**.

Barbiturate **10e** (90 mg, 150 μmol, 1.0 eq), *N,N*-di(*tert*-butoxycarbonyl)-guanidinybutanol (149 mg, 449 μmol, 3.0 eq), PPh₃ (118 mg, 449 μmol, 3.0 eq) and DIAD (94 μL, 449 μmol, 3.0 eq) were stirred in anhydrous THF (1.0 mL) for 12 h. The crude was purified with 0-40% EtOAc in heptane to yield boc-**3eG** (64 mg, 52 μmol, 35%) as a pale-yellow oil.

TFA (60 μL, 781 μmol, 15.0 eq) and DCM (1.0 mL) were added, and the mixture was stirred at ambient temperature for 18 h. The crude was purified by automated RP column chromatography with a gradient of 20-45% MeCN/H₂O + 0.1% TFA to yield the di-TFA salt of **3eG** (31 mg, 29 μmol, 20% o2s) as a white foam.

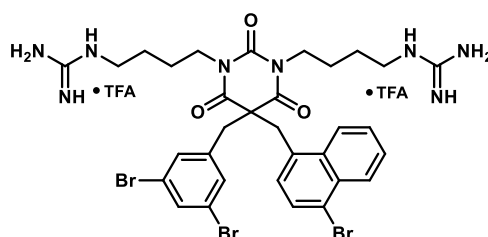
¹H NMR (400 MHz, Methanol-*d*₄) δ 7.90 (d, *J* = 1.8 Hz, 1H), 7.65 (t, *J* = 1.8 Hz, 1H), 7.64 (d, *J* = 1.5 Hz, 2H), 7.23 (d, *J* = 1.7 Hz, 2H), 3.65 (s, 2H), 3.71 – 3.53 (m, 4H), 3.47 (s, 2H), 3.15 (t, *J* = 6.8 Hz, 4H), 1.50 – 1.26 (m, 8H). ¹³C NMR (101 MHz, Methanol-*d*₄) δ 171.1 (2C), 158.7 (2C), 150.3, 140.3, 139.6, 134.7, 133.0 (q, *J* = 33.4 Hz, 2C), 132.7 (2C), 131.3 (q, *J* = 2.5 Hz, 2C), 124.5 (q, *J* = 272.1 Hz, 2C), 124.2 (2C), 122.8 – 122.6 (m, 1C), 61.2, 45.2, 44.6, 42.5 (2C), 41.9 (2C), 26.9 (2C), 26.2 (2C). HRMS (ESI): calcd for C₃₀H₃₅Br₂F₆N₈O₃⁺ M+H]⁺ 827.1098, found: 827.1106. SFC: 98.0%.



(4-(5-(4-(*tert*-butyl)benzyl)-5-(3,5-dibromobenzyl)-3-(4-guanidinobutyl)-2,4,6-trioxotetrahydropyrimidin-1(2H)-yl)butyl)-1,2-azanecarboximidamide **3fG**.

Barbiturate **10f** (58 mg, 111 μmol, 1.0 eq), *N,N*-di(*tert*-butoxycarbonyl)-guanidinybutanol (92 mg, 278 μmol, 2.5 eq), PPh₃ (88 mg, 333 μmol, 3.0 eq) and DIAD (70 μL, 333 μmol, 3.0 eq) were stirred in DCM (1.0 mL) for 48 h. The crude was purified with 0-40% EtOAc in heptane to yield boc-**3fG** (110 mg, 96 μmol, 86%) as a yellow oil.

TFA (128 μL, 166 μmol, 15.0 eq) and DCM (1.0 mL) were added, and the mixture was stirred at ambient temperature for 17 h. The crude was purified by automated RP column chromatography with a gradient of 10-65% MeCN/H₂O + 0.1% TFA to yield the di-TFA salt of **3fG** (82 mg, 84 μmol, 76% o2s) as a white powder. ¹H NMR (400 MHz, Methanol-*d*₄) δ 7.61 (t, *J* = 1.8 Hz, 1H), 7.29 – 7.24 (m, 2H), 7.24 (d, *J* = 1.8 Hz, 2H), 7.01 – 6.90 (m, 2H), 3.73 – 3.62 (m, 1H), 3.56 (ddd, *J* = 12.9, 8.0, 5.2 Hz, 2H), 3.43 (s, 2H), 3.37 (s, 2H), 3.16 (t, *J* = 6.6 Hz, 4H), 1.48 – 1.31 (m, 8H), 1.24 (s, 9H). ¹³C NMR (101 MHz, Methanol-*d*₄) δ 171.8 (2C), 158.7 (2C), 152.2, 150.8, 141.2, 134.2, 132.8, 132.7 (2C), 130.2 (2C), 126.6 (2C), 124.0 (2C), 61.6, 46.6, 44.3, 42.3 (2C), 42.0 (2C), 35.3, 31.7 (3C), 26.9 (2C), 26.1 (2C). HRMS (ESI): calcd for C₃₂H₄₅Br₂N₈O₃⁺ [M+H]⁺ 747.1976, found: 747.1981. SFC: 95.4%.



1,1'-((5-((4-bromonaphthalen-1-yl)methyl)-5-(3,5-dibromobenzyl)-2,4,6-trioxodihydropyrimidine-1,3(2H,4H)-diyl)bis(butane-4,1-diyl))diguanidine **3gG**.

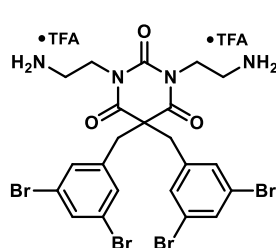
Barbiturate **10g** (103 mg, 173 μmol, 1.0 eq), *N,N*-di(*tert*-butoxycarbonyl)-guanidinybutanol (143 mg, 434 μmol, 2.5 eq), PPh₃ (136 mg, 519 μmol, 3.0 eq) and DIAD (109 μL, 519 μmol, 3.0 eq) were stirred in DCM (1.0 mL) for 20 h. The crude was purified with 10-38% EtOAc in heptane

to yield impure boc-**3gG** (216 mg, 177 μmol, 102%) as a white solid.

TFA (398 μL , 5.20 mmol, 30.00 eq) and DCM (0.7 mL) were added, and the mixture was stirred at ambient temperature for 48 h. The crude was purified by automated RP column chromatography with a gradient of 10-65% MeCN/H₂O + 0.1% TFA to yield the di-TFA salt of **3gG** (133 mg, 128 μmol , 74% o2s) as a white powder. ¹H NMR (400 MHz, Methanol-*d*₄) δ 8.28 – 8.20 (m, 1H), 8.20 – 8.13 (m, 1H), 7.71 (d, *J* = 7.7 Hz, 1H), 7.68 – 7.62 (m, 2H), 7.61 (t, *J* = 1.8 Hz, 1H), 7.28 (d, *J* = 1.7 Hz, 2H), 7.15 (d, *J* = 7.8 Hz, 1H), 3.95 (s, 2H), 3.62 (s, 2H), 3.50 (ddd, *J* = 12.9, 8.6, 6.0 Hz, 2H), 3.38 (ddd, *J* = 13.3, 8.4, 5.8 Hz, 2H), 3.04 (t, *J* = 7.0 Hz, 4H), 1.35 – 1.00 (m, 8H). ¹³C NMR (101 MHz, Methanol-*d*₄) δ 171.6 (2C), 158.6 (2C), 150.6, 141.2, 134.2, 133.4, 133.0 (2C), 132.8, 130.5, 129.7, 128.8, 128.7, 128.3, 126.2, 124.1, 124.0 (2C), 61.1, 44.0, 42.5, 42.3 (2C), 42.0 (2C), 26.7 (2C), 25.9 (2C). HRMS (ESI): calcd for C₃₂H₃₈Br₃N₈O₃⁺ [M+H]⁺ 819.0612, found 819.0610. SFC: 96.3%.

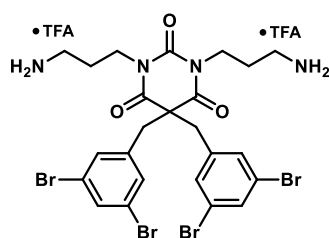
2.9 Synthesis of series 4

2.9.1 Amine derivatives



1,3-bis(2-aminoethyl)-5,5-bis(3,5-dibromobenzyl)pyrimidine-2,4,6(1H,3H,5H)-trione 4aA.

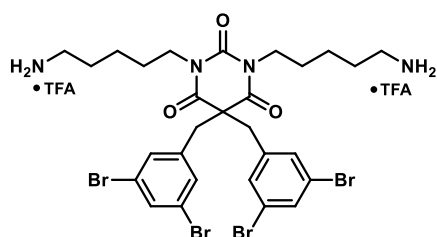
The compound was synthesized according to General Procedure D. Barbiturate **7a** (80 mg, 128 μmol , 1.0 eq), *tert*-butyl (2-hydroxyethyl)carbamate (52 mg, 321 μmol , 2.5 eq), PPh₃ (101 mg, 385 μmol , 3.0 eq) and DIAD (81 μL , 385 μmol , 3.0 eq) were stirred in DCM (1.0 mL) for 20 h. The crude was purified with 10-50% EtOAc in heptane to yield boc-**4aA** (97 mg, 107 μmol , 83%) as a colorless oil. TFA (98 μL , 1.28 mmol, 10.0 eq) and DCM (1.0 mL) were added, and the mixture was stirred at ambient temperature for 22 h. The crude was purified by automated RP column chromatography with a gradient of 10-60% MeCN/H₂O + 0.1% TFA to yield the di-TFA salt of **4aA** (83 mg, 89 μmol , 69% o2s) as a white powder. ¹H NMR (400 MHz, Methanol-*d*₄) δ 7.64 (t, *J* = 1.8 Hz, 2H), 7.29 (d, *J* = 1.8 Hz, 4H), 4.00 (t, *J* = 6.6 Hz, 4H), 3.39 (s, 4H), 3.02 (t, *J* = 6.6 Hz, 4H). ¹³C NMR (101 MHz, Methanol-*d*₄) δ 171.3 (2C), 151.1, 140.3 (2C), 134.6 (2C), 133.0 (4C), 124.0 (4C), 60.7, 44.0 (2C), 40.4 (2C), 38.6 (2C). HRMS (ESI): calcd for C₂₂H₂₃Br₄N₄O₃⁺ [M+H]⁺ 706.8498, found 706.8502. SFC: 96.7%.



1,3-bis(3-aminopropyl)-5,5-bis(3,5-dibromobenzyl)pyrimidine-2,4,6(1H,3H,5H)-trione 4bA.

The compound was synthesized according to General Procedure B. Barbiturate **7a** (468 mg, 0.75 mmol, 1.0 eq), *tert*-butyl (3-bromopropyl)carbamate (366 mg, 1.53 mmol, 2.05 eq), K₂CO₃ (311 mg, 2.25 mmol, 3.0 eq), TBAI (28 mg, 75 μmol , 0.1 eq) and acetone (7 mL) were stirred at 50 °C for 20 h. Boc-**4bA** (600 mg, 0.64 mmol, 85%) was obtained as a yellow solid. TFA (0.75 mL, 9.78 mmol, 15.0 eq) and DCM (2.5 mL) were added, and the mixture was stirred at ambient temperature for 17 h. The crude was purified by automated RP column chromatography with a gradient of 0-70% MeCN/H₂O + 0.1% TFA to yield the di-TFA salt of **4bA** (495 mg, 0.42 mmol, 56% o2s) as a white powder, m.p. 208-212 °C. ¹H NMR (400 MHz, Methanol-*d*₄) δ 7.67 (s, 2H), 7.25 (d, *J* = 1.8 Hz, 4H), 3.78 (t, 4H), 3.45 (s, 4H), 2.85 (t, *J* = 7.1 Hz, 4H), 1.77 (p, *J* = 7.1 Hz, 4H). ¹³C NMR (101 MHz, Methanol-*d*₄) δ 171.3 (2C), 150.8, 140.4 (2C), 134.7 (2C), 132.6 (4C), 124.2 (4C), 61.4, 44.8 (2C), 40.2 (2C), 38.2 (2C), 27.3 (2C). HRMS (ESI): calcd for C₂₄H₂₇Br₄N₄O₃⁺ [M+H]⁺ 734.8811, found 734.8806. SFC: >99.5%.

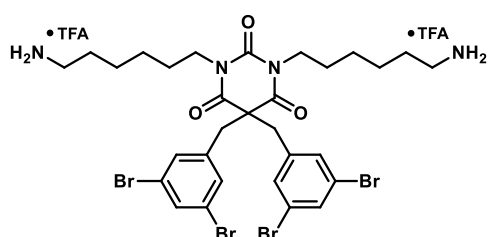
The following compounds were synthesized according to General Procedure D.



1,3-bis(5-aminopentyl)-5,5-bis(3,5-dibromobenzyl)pyrimidine-2,4,6(1H,3H,5H)-trione 4cA.

Barbiturate **7a** (82 mg, 131 μmol , 1.0 eq), *tert*-butyl (5-hydroxypentyl)carbamate **1** (67 mg, 329 μmol , 2.5 eq), PPh₃ (103 mg, 394 μmol , 3.0 eq) and DIAD (83 μL , 394 μmol , 3.0 eq) were stirred in DCM (1.0 mL) for 20 h. The crude was purified with 10-50% EtOAc in heptane to yield boc-**4cA** (104 mg, 105 μmol ,

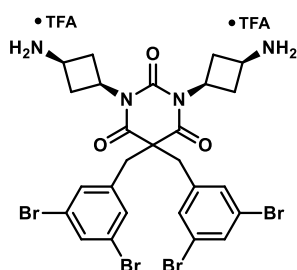
80%) as a slightly yellow solid. TFA (101 μ L, 1.31 mmol, 10.0 eq) and DCM (1.0 mL) were added, and the mixture was stirred at ambient temperature for 22 h. The crude was purified by automated RP column chromatography with a gradient of 10-60% MeCN/H₂O + 0.1% TFA to yield the di-TFA salt of **4cA** (92 mg, 69 μ mol, 69% o2s) as a white powder. ¹H NMR (400 MHz, Methanol-*d*₄) δ 7.63 (t, *J* = 1.8 Hz, 2H), 7.20 (d, *J* = 1.7 Hz, 4H), 3.71 – 3.58 (m, 4H), 3.40 (s, 4H), 2.97 – 2.86 (m, 4H), 1.75 – 1.63 (m, 4H), 1.42 – 1.31 (m, 4H), 1.31 – 1.21 (m, 4H). ¹³C NMR (101 MHz, Methanol-*d*₄) δ 171.1 (2C), 150.3, 140.5 (2C), 134.4 (2C), 132.6 (4C), 124.1 (4C), 61.1, 44.8 (2C), 42.6 (2C), 40.5 (2C), 28.6 (2C), 28.2 (2C), 24.6 (2C). HRMS (ESI): calcd for C₂₈H₃₅Br₄N₄O₃⁺ [M+H]⁺ 790.9437, found 790.9443. SFC: >99.5%.



1,3-bis(6-aminohexyl)-5,5-bis(3,5-dibromobenzyl)pyrimidine-2,4,6(1H,3H,5H)-trione 4dA.

Barbiturate **7a** (80 mg, 128 μ mol, 1.0 eq), *tert*-butyl (6-hydroxyhexyl)carbamate **2** (70 mg, 321 μ mol, 2.5 eq), PPh₃ (101 mg, 385 μ mol, 3.0 eq) and DIAD (81 μ L, 385 μ mol, 3.0 eq) were stirred in DCM (1.0 mL) for 20 h. The crude was purified with 10-40% EtOAc in heptane to yield boc-**4dA** (105 mg, 103 μ mol, 80%) as a colorless oil.

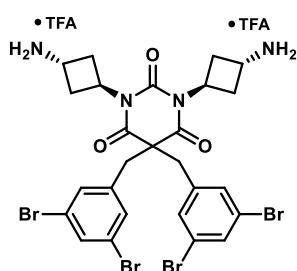
TFA (98 μ L, 1.28 mmol, 10.0 eq) and DCM (1.0 mL) were added, and the mixture was stirred at ambient temperature for 22 h. The crude was purified by automated RP column chromatography with a gradient of 10-60% MeCN/H₂O + 0.1% TFA to yield the di-TFA salt of **4dA** (98 mg, 93 μ mol, 73% o2s) as a white powder. ¹H NMR (400 MHz, Methanol-*d*₄) δ 7.63 (t, *J* = 1.7 Hz, 2H), 7.20 (d, *J* = 1.8 Hz, 4H), 3.72 – 3.56 (m, 4H), 3.39 (s, 4H), 2.97 – 2.86 (m, 4H), 1.71 – 1.57 (m, 4H), 1.38 (dp, *J* = 22.6, 8.1, 7.7 Hz, 8H), 1.25 – 1.13 (m, 4H). ¹³C NMR (101 MHz, Methanol-*d*₄) δ 171.1 (2C), 150.4, 140.5 (2C), 134.4 (2C), 132.6 (4C), 124.1 (4C), 61.0, 44.9 (2C), 42.8 (2C), 40.6 (2C), 28.9 (2C), 28.5 (2C), 27.2 (2C), 27.0 (2C). HRMS (ESI): calcd for C₃₀H₃₉Br₄N₄O₃⁺ [M+H]⁺ 818.9750, found 818.9756. SFC: 98.5%.



1,3-bis((1s,3S)-3-aminocyclobutyl)-5,5-bis(3,5-dibromobenzyl)pyrimidine-2,4,6(1H,3H,5H)-trione 4eA.

Barbiturate **7a** (300 mg, 481 μ mol, 1.0 eq), *tert*-butyl trans-(3-hydroxycyclobutyl)carbamate (225 mg, 1.20 mmol, 2.5 eq), PPh₃ (378 mg, 1.44 mmol, 3.0 eq) and DIAD (302 μ L, 1.44 mmol, 3.0 eq) were stirred in anhydrous DCM (1.5 mL) at ambient temperature for 24 h. The crude was purified with 0-40% EtOAc in heptane to yield boc-**4eA** (404 mg, 420 μ mol, 87%) as a colorless oil. Boc-**4eA** (404 mg, 420 μ mol, 1.0 eq), TFA (161 μ L, 2.10 mmol, 5.0 eq) and DCM (3.0 mL) were combined, and the mixture was

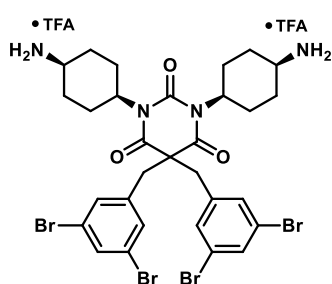
stirred at ambient temperature until HRMS indicated full conversion. The crude was purified by automated RP column chromatography with a gradient of 15-45% MeCN/H₂O + 0.1% TFA to yield the di-TFA salt of **4eA** (306 mg, 309 μ mol, 64% o2s) as a white solid. ¹H NMR (400 MHz, Methanol-*d*₄) δ 7.64 (t, *J* = 1.8 Hz, 2H), 7.25 (d, *J* = 1.8 Hz, 4H), 4.89 (p, *J* = 8.8 Hz, 2H), 3.56 (p, *J* = 7.8 Hz, 2H), 3.43 (s, 4H), 2.82 (tdd, *J* = 10.5, 9.4, 5.7, 1.8 Hz, 4H), 2.70 – 2.60 (m, 4H). *Partial overlap of a methylene signals with residual water.* ¹³C NMR (101 MHz, Methanol-*d*₄) δ 171.5 (2C), 150.4, 140.4 (2C), 134.6 (2C), 132.7 (4C), 124.2 (4C), 61.6, 44.7 (2C), 43.5 (2C), 40.7 (2C), 33.8 (4C). HRMS (ESI): calcd for C₂₆H₂₇Br₄N₄O₃⁺ [M+H]⁺ 758.8811, found: 758.8810. SFC: >99.5%



1,3-bis((1r,3R)-3-aminocyclobutyl)-5,5-bis(3,5-dibromobenzyl)pyrimidine-2,4,6(1H,3H,5H)-trione 4fA.

Barbiturate **7a** (300 mg, 481 μ mol, 1.0 eq), *tert*-butyl trans-(3-hydroxycyclobutyl)carbamate (225 mg, 1.20 mmol, 2.5 eq), PPh₃ (378 mg, 1.44 mmol, 3.0 eq) and DIAD (302 μ L, 1.44 mmol, 3.0 eq) were stirred in anhydrous THF (2.5 mL) at ambient temperature for 24 h. The crude was purified with 0-40% EtOAc in heptane to yield boc-**4fA** (262 mg, 272 μ mol, 67%) as a colorless oil.

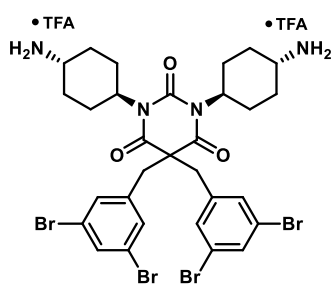
Boc-**4fA** (262 mg, 272 μmol , 1.0 eq), TFA (125 μL , 1.63 mmol, 6.0 eq) and DCM (2.0 mL) were combined, and the mixture was stirred at ambient temperature for 38 h. The crude was purified by automated RP column chromatography with a gradient of 15-45% MeCN/H₂O + 0.1% TFA to yield the di-TFA salt of **4fA** (125 mg, 126 μmol , 26% o2s) as a white solid. ¹H NMR (400 MHz, Methanol-*d*₄) δ 7.66 (t, *J* = 1.8 Hz, 2H), 7.24 (d, *J* = 1.8 Hz, 4H), 5.41 (tt, *J* = 10.1, 7.2, 1.0 Hz, 2H), 4.07 (tdd, *J* = 9.1, 4.4, 3.4 Hz, 2H), 3.44 (s, 4H), 2.90 – 2.74 (m, 4H), 2.54 – 2.41 (m, 4H). ¹³C NMR (101 MHz, Methanol-*d*₄) δ 171.3 (2C), 150.0, 140.5 (2C), 134.5 (2C), 132.6 (4C), 124.2 (4C), 61.5 (2C), 45.3 (2C), 44.8 (2C), 43.5 (2C), 32.7 (4C). HRMS (ESI): calcd for C₂₆H₂₇Br₄N₄O₃⁺ [M+H]⁺ 758.8811, found: 758.8813. SFC: >99.5%



1,3-bis((1S,4S)-4-aminocyclohexyl)-5,5-bis(3,5-dibromobenzyl)pyrimidine-2,4,6(1H,3H,5H)-trione **4gA**.

Barbiturate **7a** (200 mg, 321 μmol , 1.0 eq), *tert*-butyl (*trans*-4-hydroxycyclohexyl)carbamate (173 mg, 801 μmol , 2.5 eq), PPh₃ (252 mg, 962 μmol , 3.0 eq) and DIAD (201 μL , 962 μmol , 3.0 eq) were stirred in DCM (1.0 mL) for 18 h. The crude was purified with 0-40% EtOAc in heptane to yield boc-**4gA** (179 mg, 176 μmol , 55%) as a colorless oil.

Boc-**4gA** (160 mg, 157 μmol , 1.0 eq), TFA (98 μL , 1.28 mmol, 10.0 eq) and DCM (1.0 mL) were combined, and the mixture was stirred at ambient temperature for 22 h. The crude was purified by automated RP column chromatography with a gradient of 15-50% MeCN/H₂O + 0.1% TFA to yield the di-TFA salt of **4gA** (138 mg, 132 μmol , 46% o2s) as a white powder. ¹H NMR (400 MHz, Methanol-*d*₄) δ 7.66 (t, *J* = 1.8 Hz, 2H), 7.24 (d, *J* = 1.8 Hz, 4H), 4.61 – 4.41 (m, 2H), 3.54 – 3.47 (m, 2H), 3.43 (s, 4H), 2.54 – 2.21 (m, 4H), 2.06 – 1.94 (m, 4H), 1.94 – 1.78 (m, 4H), 1.29 – 1.17 (m, 4H). ¹³C NMR (101 MHz, Methanol-*d*₄) δ 171.6 (2C), 149.9, 140.5 (2C), 134.5 (2C), 132.7 (4C), 124.3 (4C), 61.3, 55.2 (2C), 46.8 (2C), 45.0 (2C), 29.2 (4C), 24.1 (4C). HRMS (ESI): calcd for C₃₀H₃₅Br₄N₄O₃⁺ [M+H]⁺ 814.9437, found 814.9444. SFC: >99.5%



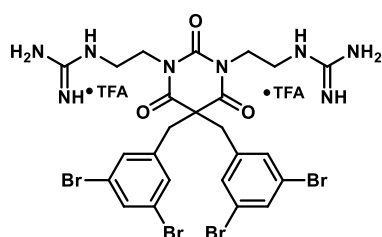
1,3-bis((1R,4R)-4-aminocyclohexyl)-5,5-bis(3,5-dibromobenzyl)pyrimidine-2,4,6(1H,3H,5H)-trione **4hA**.

Barbiturate **7a** (300 mg, 481 μmol , 1.0 eq), *tert*-Butyl (*cis*-4-hydroxycyclohexyl)carbamate (259 mg, 1.20 mmol, 2.5 eq), PPh₃ (378 mg, 1.44 mmol, 3.0 eq) and DIAD (302 μL , 1.44 mmol, 3.0 eq) were stirred in anhydrous THF (2.5 mL) at 45 °C for 72 h. The crude was purified with 0-40% EtOAc in heptane to yield boc-**4hA** (169 mg, 166 μmol , 35%) as a colorless oil.

Boc-**4hA** (169 mg, 166 μmol , 1.0 eq), TFA (127 μL , 1.66 mmol, 10.0 eq) and DCM (2.0 mL) were combined, and the mixture was stirred at ambient temperature until HRMS indicated full conversion. The crude was purified by automated RP column chromatography with a gradient of 15-45% MeCN/H₂O + 0.1% TFA to yield the di-TFA salt of **4hA** (116 mg, 111 μmol , 23% o2s) as a white solid. ¹H NMR (400 MHz, Dimethylsulfoxide-*d*₆) δ 7.94 (s, 6H), 7.80 (t, *J* = 1.7 Hz, 2H), 7.13 (d, *J* = 1.8 Hz, 4H), 4.36 – 4.17 (m, 2H), 3.08 – 2.92 (m, 2H), 2.21 – 2.04 (m, 4H), 2.03 – 1.91 (m, 4H), 1.47 – 1.29 (m, 4H), 1.28 – 1.13 (m, 4H). ¹³C NMR (101 MHz, Dimethylsulfoxide-*d*₆) δ 169.7 (2C), 148.4, 139.0 (2C), 132.8 (2C), 131.3 (4C), 122.8 (4C), 59.5, 53.6 (2C), 48.0 (2C), 43.2 (2C), 29.6 (4C), 26.2 (4C). HRMS (ESI): calcd for C₃₀H₃₅Br₄N₄O₃⁺ [M+H]⁺ 814.9437, found: 814.9441. SFC: 91.0%

2.9.2 Guanidine derivatives

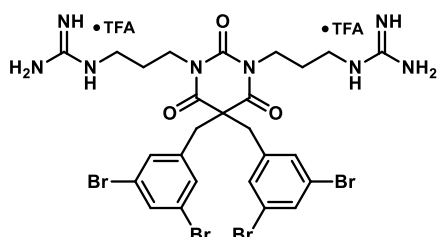
The compounds were synthesized according to General Procedure C.



1,1'-((5,5-bis(3,5-dibromobenzyl)-2,4,6-trioxodihydropyrimidine-1,3(2H,4H)-diyl)bis(ethane-2,1-diyl))diguanidine 4aG.

Barbiturate **4aA** (18 mg, 19 μmol , 1.0 eq), *N,N'*-Di-Boc-1*H*-pyrazole-1-carboxamidine (18 mg, 58 μmol , 3.0 eq), DIPEA (10 μL , 57 μmol , 3.00 eq) and THF (1 mL) were stirred at 45 $^{\circ}\text{C}$ for 3.0 h. The crude was purified with 10-45% EtOAc in heptane to yield impure boc-**4aG** (30 mg, 25 μmol , 131%) as a colorless oil.

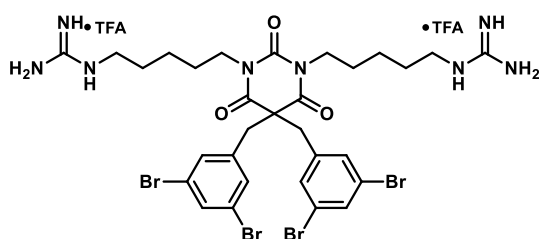
TFA (22 μL , 287 μmol , 15.0 eq) and DCM (1 mL) were added, and the mixture was stirred at ambient temperature for 40 h. The crude was purified by automated RP column chromatography with a gradient of 25-65% MeCN/H₂O + 0.1% TFA to yield the di-TFA salt of **4aG** (18 mg, 18 μmol , 92% o2s) as a white solid. ¹H NMR (400 MHz, Methanol-*d*₄) δ 7.67 (t, *J* = 1.6 Hz, 2H), 7.29 (d, *J* = 1.8 Hz, 4H), 3.88 (t, *J* = 6.5 Hz, 4H), 3.43 (s, 4H), 3.25 (t, *J* = 6.6 Hz, 4H). ¹³C NMR (101 MHz, Methanol-*d*₄) δ 171.4 (2C), 158.9 (2C), 151.1 (2C), 140.3 (2C), 134.7 (2C), 132.9 (4C), 124.1 (4C), 61.1, 44.4 (2C), 41.6 (2C), 40.5 (2C). HRMS (ESI): calcd for C₂₄H₂₈Br₄N₈O₃²⁺ [M+2H]²⁺ 395.9503, found 395.9511. SFC: 98.2%.



1,1'-((5,5-bis(3,5-dibromobenzyl)-2,4,6-trioxodihydropyrimidine-1,3(2H,4H)-diyl)bis(propane-3,1-diyl))diguanidine 4bG.

Barbiturate **4bA** (70 mg, 73 μmol , 1.0 eq), *N,N'*-Di-Boc-1*H*-pyrazole-1-carboxamidine (56 mg, 181 μmol , 2.50 eq), DIPEA (51 μL , 290 μmol , 4.00 eq) and THF (1 mL) were stirred at 45 $^{\circ}\text{C}$ for 2.5 h. The crude was purified with 20% EtOAc in heptane to yield boc-**ABML261** (54 mg, 44 μmol , 61%) as a white foam.

TFA (83 μL , 1.09 mmol, 15.0 eq) and DCM (1 mL) were added, and the mixture was stirred at ambient temperature for 40 h. The crude was purified by automated RP column chromatography with a gradient of 10-60% MeCN/H₂O + 0.1% TFA to yield the di-TFA salt of **4bG** (43 mg, 41 μmol , 57% o2s) as a white powder. ¹H NMR (400 MHz, Methanol-*d*₄) δ 7.65 (t, *J* = 1.8 Hz, 2H), 7.23 (d, *J* = 1.8 Hz, 4H), 3.77 – 3.67 (m, 4H), 3.44 (s, 4H), 3.08 (t, *J* = 7.0 Hz, 4H), 1.62 (dq, *J* = 9.2, 7.1 Hz, 4H). ¹³C NMR (101 MHz, Methanol-*d*₄) δ 171.3 (2C), 158.7 (2C), 150.5, 140.5 (2C), 134.58 (2C), 132.6 (4C), 124.2 (4C), 61.4, 44.8 (2C), 40.4 (2C), 39.6 (2C), 28.9 (2C). HRMS (ESI): calcd for C₂₆H₃₁Br₄N₈O₃⁺ [M+H]⁺ 818.9247, found 818.9250. SFC: >99.5%.

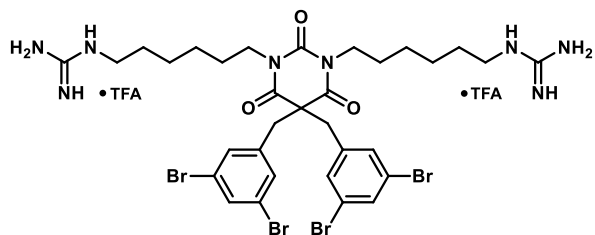


1,1'-((5,5-bis(3,5-dibromobenzyl)-2,4,6-trioxodihydropyrimidine-1,3(2H,4H)-diyl)bis(pentane-5,1-diyl))diguanidine 4cG.

Barbiturate **4cA** (13 mg, 13 μmol , 1.0 eq), *N,N'*-Di-Boc-1*H*-pyrazole-1-carboxamidine (12 mg, 38 μmol , 3.0 eq), DIPEA (7 μL , 38 μmol , 3.00 eq) and THF (1 mL) were stirred at 45 $^{\circ}\text{C}$ for 3.0 h. The crude was purified with 10-45% EtOAc in heptane to yield boc-

4cG (15 mg, 12 μmol , 92%) as a yellow oil.

TFA (15 μL , 191 μmol , 15.0 eq) and DCM (1 mL) were added, and the mixture was stirred at ambient temperature for 20 h. The crude was purified by automated RP column chromatography with a gradient of 25-65% MeCN/H₂O + 0.1% TFA to yield the di-TFA salt of **4cG** (12 mg, 11 μmol , 85% o2s) as a white solid. ¹H NMR (400 MHz, Methanol-*d*₄) δ 7.64 (t, *J* = 1.6 Hz, 2H), 7.21 (d, *J* = 1.7 Hz, 4H), 3.63 (t, *J* = 7.6 Hz, 4H), 3.41 (s, 4H), 3.16 (t, *J* = 7.2 Hz, 4H), 1.62 (p, *J* = 7.3 Hz, 4H), 1.42 – 1.30 (m, 4H), 1.25 (p, *J* = 7.6 Hz, 4H). ¹³C NMR (101 MHz, Methanol-*d*₄) δ 171.2 (2C), 158.7 (2C), 150.4, 140.6 (2C), 134.4 (2C), 132.6 (4C), 124.1 (4C), 61.1, 44.9 (2C), 42.8 (2C), 42.3 (2C), 29.5 (2C), 28.8 (2C), 24.8 (2C). HRMS (ESI): calcd for C₃₀H₄₀Br₄N₈O₃²⁺ [M+2H]²⁺ 437.9973, found 437.9978. SFC: 98.4%.

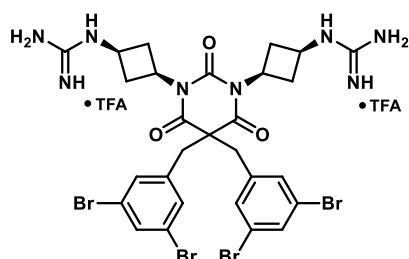


1,1'-((5,5-bis(3,5-dibromobenzyl)-2,4,6-trioxodihydropyrimidine-1,3(2H,4H)-diyl)bis(hexane-6,1-diyl))diguanidine 4dG.

Barbiturate **4dA** (38 mg, 36 μ mol, 1.0 eq), *N,N'*-Di-Boc-1*H*-pyrazole-1-carboxamide (34 mg, 109 μ mol, 3.0 eq), DBU (22 μ L, 148 μ mol, 4.00 eq) and THF (1 mL) were stirred at 45 $^{\circ}$ C for 3.5 h. The organic layer was washed with 10% citric acid_(aq) solution instead of 10% NaHCO_{3(aq)} solution. Partial cleavage of the Boc groups was observed. Boc-**4dG** was used without further purification.

4M HCl in Dioxane (452 μ L, 1.81 mmol, 50.0 eq) was added and the mixture was stirred at ambient temperature for 24 h. The crude was purified by RP chromatography with a gradient of 10-70% MeCN/H₂O + 0.1% TFA to yield the di-TFA salt of **4dG** (30 mg, 26 μ mol, 73% o2s) as a white solid.

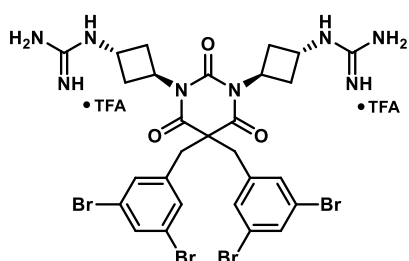
¹H NMR (400 MHz, Methanol-*d*₄) δ 7.63 (t, *J* = 1.8 Hz, 2H), 7.20 (d, *J* = 1.7 Hz, 4H), 3.68 – 3.57 (m, 4H), 3.40 (s, 4H), 3.17 (t, *J* = 7.1 Hz, 4H), 1.57 (p, *J* = 7.3 Hz, 4H), 1.47 – 1.27 (m, 8H), 1.20 (p, *J* = 7.7 Hz, 4H). ¹³C NMR (101 MHz, Methanol-*d*₄) δ 171.2 (2C), 158.6 (2C), 150.5, 140.6 (2C), 134.4 (2C), 132.6 (4C), 124.1 (4C), 61.1, 44.9 (2C), 42.9 (2C), 42.4 (2C), 29.8 (2C), 29.0 (2C), 27.3 (2C), 27.3 (2C). HRMS (ESI): calcd for C₃₂H₄₄Br₄N₈O₃²⁺ [M+2H]²⁺ 452.0129, found 452.0137. SFC: 98.1%.



1,1'-((1S,1'S,3s,3'S)-(5,5-bis(3,5-dibromobenzyl)-2,4,6-trioxodihydropyrimidine-1,3(2H,4H)-diyl)bis(cyclobutane-3,1-diyl))diguanidine 4eG.

Barbiturate **4eA** (200 mg, 202 μ mol, 1.0 eq), *N,N'*-Di-Boc-1*H*-pyrazole-1-carboxamide (157 mg, 505 μ mol, 2.5 eq), DIPEA (140 μ L, 808 μ mol, 4.0 eq) and THF (4.0 mL) were stirred at 45 $^{\circ}$ C for 3 h. The crude was purified with 10-45% EtOAc in heptane to yield boc-**4eG** (134 mg, 108 μ mol, 53%) as a colorless oil.

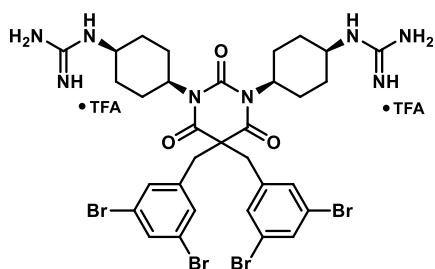
TFA (124 μ L, 1.61 mmol, 15.0 eq) and DCM (0.5 mL) were added, and the mixture was stirred at ambient temperature until HRMS indicated full conversion. The crude was purified by automated RP column chromatography with a gradient of 18-45% MeCN/H₂O + 0.1% TFA to yield the di-TFA salt of **4eG** (52 mg, 48 μ mol, 24% o2s) as a white solid. ¹H NMR (400 MHz, Methanol-*d*₄) δ 7.65 (t, *J* = 1.8 Hz, 2H), 7.23 (d, *J* = 1.8 Hz, 4H), 4.67 (tt, *J* = 9.3, 8.1 Hz, 2H), 3.80 – 3.69 (m, 2H), 2.79 – 2.67 (m, 4H), 2.63 – 2.51 (m, 4H). ¹³C NMR (101 MHz, Methanol-*d*₄) δ 171.6 (2C), 157.7 (2C), 150.3, 140.4 (2C), 134.5 (2C), 132.6 (4C), 124.2 (4C), 61.5, 44.8 (2C), 43.8 (2C), 41.4 (2C), 36.3 (4C). HRMS (ESI): calcd for C₂₈H₃₁Br₄N₈O₃⁺ [M+H]⁺ 842.9247, found 842.9238. SFC: 98.6%.



1,1'-((1R,1'R,3r,3'r)-(5,5-bis(3,5-dibromobenzyl)-2,4,6-trioxodihydropyrimidine-1,3(2H,4H)-diyl)bis(cyclobutane-3,1-diyl))diguanidine 4fG.

Barbiturate **4fA** (87 mg, 88 μ mol, 1.0 eq), *N,N'*-Di-Boc-1*H*-pyrazole-1-carboxamide (68 mg, 220 μ mol, 2.5 eq), DIPEA (61 μ L, 351 μ mol, 4.0 eq) and THF (4.0 mL) were stirred at 45 $^{\circ}$ C for 3 h. The crude was purified with 10-45% EtOAc in heptane to yield impure boc-**4fG** (116 mg, 93 μ mol, 106%) as a colorless oil.

TFA (107 μ L, 1.39 mmol, 15.0 eq) and DCM (0.5 mL) were added, and the mixture was stirred at ambient temperature until HRMS indicated full conversion. The crude was purified by automated RP column chromatography with a gradient of 15-45% MeCN/H₂O + 0.1% TFA to yield the di-TFA salt of **4fG** (31 mg, 29 μ mol, 32% o2s) as a white solid. ¹H NMR (400 MHz, Methanol-*d*₄) δ 7.64 (t, *J* = 1.7 Hz, 2H), 7.23 (d, *J* = 1.7 Hz, 4H), 5.32 – 5.20 (m, 2H), 4.26 – 4.17 (m, 2H), 3.42 (s, 4H), 2.97 – 2.85 (m, 4H), 2.36 – 2.25 (m, 4H). ¹³C NMR (101 MHz, Methanol-*d*₄) δ 171.4 (2C), 158.3 (2C), 150.0, 140.5 (2C), 134.5 (2C), 132.6 (4C), 124.2 (4C), 61.5, 46.5 (2C), 44.8 (2C), 43.9 (2C), 35.2 (4C). HRMS (ESI): calcd for C₂₈H₃₁Br₄N₈O₃⁺ [M+H]⁺ 842.9247, found 842.9254. SFC: 92.1%.



*1,1'-((1*S*,1'*S*,4*s*,4'*s*)-(5,5-bis(3,5-dibromobenzyl)-2,4,6-trioxodihydropyrimidine-1,3(2*H*,4*H*)-diyl)bis(cyclohexane-4,1-diyl))diguanidine **4gG**.*

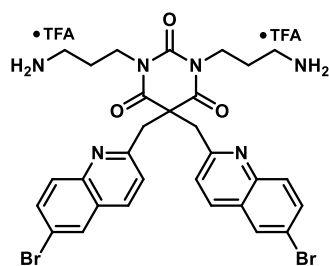
Barbiturate **4gA** (125 mg, 120 μ mol, 1.0 eq), *N,N'*-Di-Boc-1*H*-pyrazole-1-carboxamide (93 mg, 299 μ mol, 2.5 eq), DIPEA (83 μ L, 478 μ mol, 4.0 eq) and THF (0.5 mL) were stirred at 45 $^{\circ}$ C for 17 h. The crude was purified with 45% EtOAc in heptane to yield boc-**4gG** (106 mg, 81 μ mol, 68%) as a colorless oil. TFA (94 μ L, 1.22 mmol, 15.0 eq) and DCM (0.5 mL) were

added, and the mixture was stirred at ambient temperature until HRMS indicated full conversion. The crude was purified by automated RP column chromatography with a gradient of 15-45% MeCN/H₂O + 0.1% TFA to yield the di-TFA salt of **4gG** (19 mg, 17 μ mol, 14% o2s) as a white solid. ¹H NMR (400 MHz, Methanol-*d*₄) δ 7.64 (t, *J* = 1.8 Hz, 2H), 7.22 (d, *J* = 1.7 Hz, 4H), 4.60 – 4.32 (m, 2H), 3.80 – 3.70 (m, 2H), 3.40 (s, 4H), 2.55 – 2.18 (m, 4H), 1.93 (d, *J* = 14.0 Hz, 4H), 1.78 – 1.62 (m, 4H), 1.25 – 1.11 (m, 4H). ¹³C NMR (101 MHz, Methanol-*d*₄) δ 171.6 (2C), 158.0 (2C), 150.0, 140.6 (2C), 134.4 (2C), 132.7 (4C), 124.3 (4C), 61.2, 55.6 (2C), 46.6 (2C), 45.0 (2C), 30.6 (4C), 24.5 (4C). HRMS (ESI): calcd for C₃₂H₃₉Br₄N₈O₃⁺ [M+H]⁺ 898.9873, found 898.9880. SFC: 97.2%.

2.10 Synthesis of series 5

2.10.1 Amine derivatives

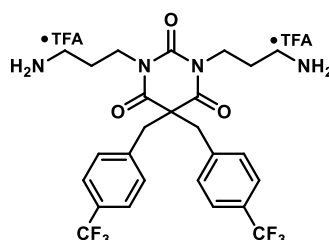
All compounds were synthesized according to General procedure B:



*1,3-bis(3-aminopropyl)-5,5-bis((6-bromoquinolin-2-yl)methyl)pyrimidine-2,4,6(1*H*,3*H*,5*H*)-trione **5aA**.*

Barbiturate **7f** (54 mg, 95 μ mol, 1.0 eq), *tert*-butyl (3-bromopropyl)carbamate (57 mg, 0.24 mmol, 2.50 eq), Cs₂CO₃ (77 mg, 0.24 mmol, 2.50 eq), TBAI (7 mg, 19 μ mol, 0.2 eq) and acetone (1.5 mL) were stirred at 60 $^{\circ}$ C for 40 h. The crude was purified with 10-70% EtOAc in heptane to yield boc-**5aA** (29 mg, 33 μ mol, 35%) as a colorless oil.

TFA (73 μ L, 0.95 mmol, 10.0 eq) and DCM (0.7 mL) were added, and the mixture was stirred at ambient temperature for 22 h. The crude was purified by automated RP column chromatography with a gradient of 10-60% MeCN/H₂O + 0.1% TFA to yield the di-TFA salt of **5aA** (29 mg, 32 μ mol, 34% o2s) as a white powder. ¹H NMR (400 MHz, Methanol-*d*₄) δ 8.25 – 8.18 (m, 2H), 8.13 (d, *J* = 2.2 Hz, 2H), 7.83 (dd, *J* = 8.9, 2.2 Hz, 2H), 7.61 (d, *J* = 9.0 Hz, 2H), 7.44 (d, *J* = 8.5 Hz, 2H), 3.97 (s, 4H), 3.89 (t, *J* = 6.9 Hz, 4H), 2.62 (t, *J* = 7.0 Hz, 4H), 1.82 (p, *J* = 7.0 Hz, 4H). ¹³C NMR (101 MHz, Methanol-*d*₄) δ 174.3 (2C), 158.9 (2C), 153.2, 146.7 (2C), 137.5 (2C), 134.7 (2C), 131.4 (2C), 130.7 (2C), 129.6 (2C), 123.5 (2C), 121.3 (2C), 54.5, 48.2 (2C), 39.9 (2C), 38.1 (2C), 27.0 (2C). HRMS (ESI): calcd for C₃₀H₃₁Br₂N₆O₃⁺ [M+H]⁺ 681.0819, found 681.0823. SFC: >99.5%.

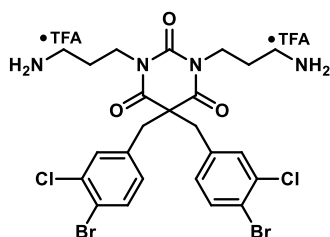


*1,3-bis(3-aminopropyl)-5,5-bis(4-(trifluoromethyl)benzyl)pyrimidine-2,4,6(1*H*,3*H*,5*H*)-trione **5bA**.*

Barbiturate **7b** (332 mg, 0.75 mmol, 1.0 eq), *tert*-butyl (3-bromopropyl)carbamate (368 mg, 1.55 mmol, 2.07 eq), K₂CO₃ (315 mg, 2.28 mmol, 3.0 eq), TBAI (28 mg, 75 μ mol, 0.1 eq) and acetone (8 mL) were stirred at 50 $^{\circ}$ C for 21 h. Boc-**5bA** (469 mg, 0.62 mmol, 83%) was obtained as a yellow solid and used without further purification.

TFA (0.72 mL, 9.38 mmol, 15.1 eq) and DCM (2.5 mL) were added, and the mixture was stirred at ambient temperature for 17 h. The crude was purified by automated RP column chromatography with a gradient of 0-70% MeCN/H₂O + 0.1% TFA to yield the di-TFA salt of **5bA** (448 mg, 0.57 mmol, 76% o2s) as a white powder, m.p. 180-184 $^{\circ}$ C. ¹H NMR (400 MHz, Methanol-*d*₄) δ 7.60 (d, *J* = 8.1 Hz, 4H), 7.30 (d, *J* = 8.0 Hz, 4H), 3.70 (t, 4H), 3.58 (s, 4H), 2.72 (t, *J* = 7.3 Hz, 4H), 1.69 (p, *J* = 7.3 Hz, 4H). ¹³C NMR (101 MHz, Methanol-*d*₄) δ 171.5 (2C), 150.9, 140.6 (2C), 131.4 (4C), 131.2 (q, *J* = 32.4 Hz, 2C), 126.7 (q, *J* = 3.7 Hz, 4C), 125.4 (q, *J* = 271.0 Hz, 2C), 61.3, 45.7

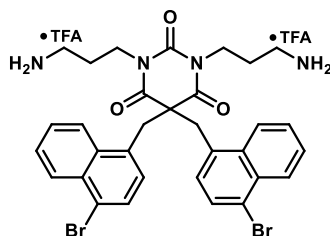
(2C), 40.0 (2C), 38.0 (2C), 26.7 (2C). **HRMS** (ESI): calcd for $C_{26}H_{29}F_6N_4O_3^+$ $[M+H]^+$ 559.2138, found 559.2145. **SFC**: 95.6%.



1,3-bis(3-aminopropyl)-5,5-bis(4-bromo-3-chlorobenzyl)pyrimidine-2,4,6(1H,3H,5H)-trione 5cA.

Barbiturate **7c** (401 mg, 0.75 mmol, 1.0 eq), *tert*-butyl (3-bromopropyl)carbamate (366 mg, 1.54 mmol, 2.05 eq), K_2CO_3 (314 mg, 2.27 mmol, 3.0 eq), TBAI (28 mg, 75 μ mol, 0.1 eq) and acetone (7 mL) were stirred at 50 °C for 21 h. Boc-**5cA** (564 mg, 0.68 mmol, 91%) was obtained as a beige highly viscous oil and used without further purification.

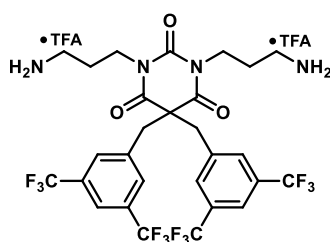
TFA (0.78 mL, 10.2 mmol, 15.0 eq) and DCM (2.5 mL) were added, and the mixture was stirred at ambient temperature for 18 h. The crude was purified by automated RP column chromatography with a gradient of 0-70% MeCN/H₂O + 0.1% TFA to yield the di-TFA salt of **5cA** (365 mg, 0.42 mmol, 55% o2s) as a white powder, m.p. 213-216 °C. **¹H NMR** (400 MHz, Methanol-*d*₄) δ 7.61 (d, *J* = 8.2 Hz, 2H), 7.24 (d, *J* = 2.1 Hz, 2H), 6.94 (dd, *J* = 8.3, 2.1 Hz, 2H), 3.74 (t, 4H), 3.44 (s, 4H), 2.80 (t, *J* = 7.2 Hz, 4H), 1.74 (p, *J* = 7.2 Hz, 4H). **¹³C NMR** (101 MHz, Methanol-*d*₄) δ 171.5 (2C), 150.9, 137.6 (2C), 135.6 (2C), 135.4 (2C), 132.5 (2C), 130.7 (2C), 122.8 (2C), 61.2, 44.8 (2C), 40.1 (2C), 38.1 (2C), 27.0 (2C). **HRMS** (ESI): calcd for $C_{24}H_{27}Br_2Cl_2N_4O_3^+$ $[M+H]^+$ 646.9821, found 646.9832. **SFC**: 95.2%.



1,3-bis(3-aminopropyl)-5,5-bis((4-bromonaphthalen-1-yl)methyl)pyrimidine-2,4,6(1H,3H,5H)-trione 5dA.

Barbiturate **7g** (428 mg, 0.75 mmol, 1.0 eq), *tert*-butyl (3-bromopropyl)carbamate (369 mg, 1.55 mmol, 2.07 eq), K_2CO_3 (313 mg, 2.26 mmol, 3.0 eq), TBAI (28 mg, 75 μ mol, 0.1 eq) and acetone (7 mL) were stirred at 50 °C for 21 h. The crude was purified with 15-60% EtOAc in heptane to yield boc-**5dA** (379 mg, 0.43 mmol, 57%) as a white solid. TFA (0.49 mL, 6.40 mmol, 15.0 eq) and DCM (2.0 mL) were added, and

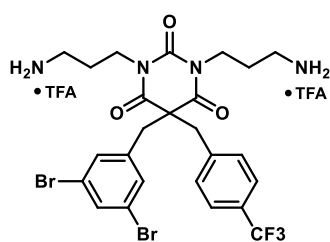
the mixture was stirred at ambient temperature for 18 h. The crude was purified by automated RP column chromatography with a gradient of 0-70% MeCN/H₂O + 0.1% TFA to yield the di-TFA salt of **5dA** (355 mg, 0.39 mmol, 52% o2s) as a white powder. m.p.: 204-207 °C. **¹H NMR** (400 MHz, Methanol-*d*₄) δ 8.40 – 8.11 (m, 4H), 7.73 (dd, *J* = 7.8, 2.3 Hz, 2H), 7.70 – 7.59 (m, 4H), 7.26 – 7.03 (m, 2H), 4.15 (s, 4H), 3.41 (t, *J* = 7.0 Hz, 4H), 2.44 (t, *J* = 6.5, 5.4 Hz, 4H), 1.38 (p, *J* = 7.1 Hz, 4H). **¹³C NMR** (101 MHz, Methanol-*d*₄) δ 172.2 (2C), 151.2, 134.4 (2C), 133.4 (2C), 133.3 (2C), 130.5 (2C), 129.1 (2C), 128.8 (2C), 128.7 (2C), 128.4 (2C), 126.3 (2C), 124.0 (2C), 60.2, 41.7 (2C), 39.9 (2C), 37.8 (2C), 26.6 (2C). **HRMS** (ESI): calcd for $C_{32}H_{33}Br_2N_4O_3^+$ $[M+H]^+$ 679.0914, found 679.0903. **SFC**: 96.5%.



1,3-bis(3-aminopropyl)-5,5-bis(3,5-bis(trifluoromethyl)benzyl)pyrimidine-2,4,6(1H,3H,5H)-trione 5eA.

Barbiturate **7d** (261 mg, 0.45 mmol, 1.0 eq), *tert*-butyl (3-bromopropyl)carbamate (214 mg, 0.90 mmol, 2.00 eq), Cs_2CO_3 (323 mg, 0.99 mmol, 2.2 eq), TBAI (17 mg, 45 μ mol, 0.1 eq) and acetone (2.5 mL) were stirred at 70 °C for 3.5 d. The crude was purified with 0-70% EtOAc in heptane to yield boc-**5eA** (265 mg, 0.30 mmol, 66%) as a white solid. TFA (0.28 mL, 3.60 mmol, 8.0 eq) and DCM (2.0 mL) were added, and

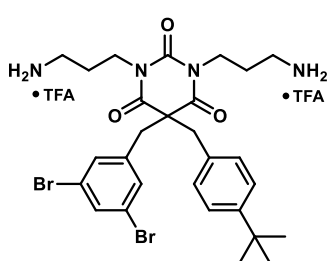
the mixture was stirred at ambient temperature for 12 h. The crude was purified by automated RP column chromatography with a gradient of 0-70% MeCN/H₂O + 0.1% TFA to yield the di-TFA salt of **5eA** (251 mg, 0.27 mmol, 61% o2s) as a white powder. **¹H NMR** (400 MHz, Methanol-*d*₄) δ 7.93 (s, 2H), 7.73 – 7.68 (m, 4H), 3.76 – 3.68 (m, 8H), 2.80 (t, *J* = 7.1 Hz, 4H), 1.67 (dq, *J* = 9.0, 7.2 Hz, 4H). **¹³C NMR** (101 MHz, Methanol-*d*₄) δ 171.1 (2C), 150.6, 139.3 (2C), 133.1 (q, *J* = 33.4 Hz, 4C), 131.6 – 131.4 (m, 4C), 124.6 (q, *J* = 272 Hz, 4C), 123.1 – 122.8 (m, 2C), 61.0, 44.6 (2C), 40.3 (2C), 38.0 (2C), 26.9 (2C). **HRMS** (ESI): calcd for $C_{28}H_{27}F_{12}N_4O_3^+$ $[M+H]^+$ 695.1886, found 695.1884. **SFC**: 95.2%.



1,3-bis(3-aminopropyl)-5-(3,5-dibromobenzyl)-5-(4-(trifluoromethyl)benzyl)pyrimidine-2,4,6(1H,3H,5H)-trione 5fA.

Barbiturate **10b** (479 mg, 0.90 mmol, 1.0 eq), *tert*-butyl (3-bromopropyl)carbamate (470 mg, 1.97 mmol, 2.2 eq), K_2CO_3 (372 mg, 2.69 mmol, 3.0 eq), TBAI (33 mg, 90 μ mol, 0.1 eq) and acetone (15 mL) were stirred at 50 °C for 18 h. The crude was purified by column chromatography on silica gel with EtOAc in heptane to yield boc-**5fA** (340 mg, 0.40 mmol, 45%) as a pale-yellow oil.

TFA (0.30 mL, 3.88 mmol, 10.0 eq) and DCM (3.0 mL) were added, and the mixture was stirred at ambient temperature for 17 h. The crude was purified by automated RP column chromatography with a gradient of 15-50% MeCN/H₂O + 0.1% TFA to yield the di-TFA salt of **5fA** (334 mg, 0.39 mmol, 44% o2s) as a white powder. ¹H NMR (400 MHz, Methanol-*d*₄) δ 7.67 (t, *J* = 1.8 Hz, 1H), 7.60 (d, *J* = 8.0 Hz, 2H), 7.29 (d, *J* = 8.0 Hz, 2H), 7.26 (d, *J* = 1.8 Hz, 2H), 3.81 – 3.67 (m, 4H), 3.56 (s, 2H), 3.48 (s, 2H), 2.89 – 2.71 (m, 4H), 1.82 – 1.62 (m, 4H). ¹³C NMR (101 MHz, Methanol-*d*₄) δ 171.4 (2C), 150.9, 140.7 – 140.6 (m, 1C), 140.5, 134.6, 132.6 (2C), 131.5, 131.2 (q, *J* = 32.5 Hz, 1C), 126.8 (q, *J* = 3.9 Hz, 2C), 125.4 (q, *J* = 271.9 Hz, 1C), 124.2 (2C), 61.4, 45.4, 45.0, 40.1 (2C), 38.1 (2C), 27.0 (2C). HRMS (ESI): calcd for C₂₅H₂₈Br₂F₃N₄O₃⁺ [M+H]⁺ 647.0475, found 647.0473. SFC: 97.3%.



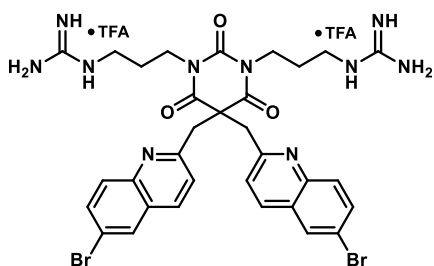
1,3-bis(3-aminopropyl)-5-(4-(tert-butyl)benzyl)-5-(3,5-dibromobenzyl)pyrimidine-2,4,6(1H,3H,5H)-trione 5gA.

Barbiturate **10f** (100 mg, 192 μ mol, 1.0 eq), *tert*-butyl (3-hydroxypropyl)carbamate (84 mg, 479 μ mol, 2.5 eq), PPh₃ (151 mg, 575 μ mol, 3.0 eq) and DIAD (120 μ L, 574 μ mol, 3.0 eq) were stirred in anhydrous DCM (0.5 mL) for 16 h. The crude was purified with 0-40% EtOAc in heptane to yield impure boc-**5gA** (161 mg, 192 μ mol, 101%) as a colorless oil.

TFA (129 μ L, 1.67 mmol, 10.0 eq) and DCM (1.0 mL) were added, and the mixture was stirred at ambient temperature for 18 h. The crude was purified by automated RP column chromatography with a gradient of 15-50% MeCN/H₂O + 0.1% TFA to yield the di-TFA salt of **5gA** (118 mg, 137 μ mol, 71% o2s) as a white powder. ¹H NMR (400 MHz, Methanol-*d*₄) δ 7.64 (t, *J* = 1.7 Hz, 1H), 7.31 (d, *J* = 8.3 Hz, 2H), 7.26 (d, *J* = 1.7 Hz, 2H), 6.99 (d, *J* = 8.3 Hz, 2H), 3.79 – 3.64 (m, 4H), 3.46 (s, 2H), 3.41 (s, 2H), 2.76 (oct, *J* = 7.1 Hz, 4H), 1.83 – 1.62 (m, 4H). ¹³C NMR (101 MHz, Methanol-*d*₄) δ 171.9 (2C), 152.5, 151.1, 141.1, 134.4, 132.7, 132.6 (2C), 130.2 (2C), 126.7 (2C), 124.1 (2C), 61.9, 46.5, 44.2, 40.0 (2C), 38.2 (2C), 35.4, 31.7 (3C), 27.0 (2C). HRMS (ESI): calcd for C₂₈H₃₇Br₂N₄O₃⁺ [M+H]⁺ 635.1227, found: 635.1232. SFC: 97.0%.

2.10.2 Guanidine derivatives

All compounds were synthesized according to General Procedure C:

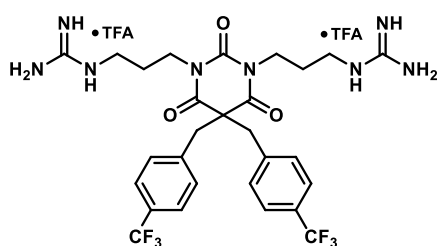


1,1'-((5,5-bis((6-bromoquinolin-2-yl)methyl)-2,4,6-trioxodihydropyrimidine-1,3(2H,4H)-diyl)bis(propane-3,1-diyl))diguandine 5aG.

Barbiturate **5aA** (11 mg, 12.1 μ mol, 1.0 eq), *N,N'*-Di-Boc-1H-pyrazole-1-carboxamidine (9.4 mg, 30.2 μ mol, 2.50 eq), DIPEA (5.3 μ L, 30.2 μ mol, 2.50 eq) and THF (0.5 mL) were stirred at 45 °C for 2.5 h. The crude was purified with 20-60% EtOAc in heptane to yield boc-**5aG** (13 mg, 11.1 μ mol, 92%) as a white foam.

TFA (28 μ L, 181 μ mol, 30.0 eq) and DCM (0.5 mL) were added, and the mixture was stirred at ambient temperature for 24 h. The crude was purified by automated RP column chromatography with a gradient of 20-60% MeCN/H₂O + 0.1% TFA to yield the di-TFA salt of **5aG** (11 mg, 11 μ mol, 91% o2s) as a white powder. ¹H NMR (400 MHz, Methanol-*d*₄) δ 8.20 (d, *J* = 8.5 Hz, 2H), 8.11 (d, *J* = 2.2 Hz, 2H), 7.81 (dd, *J* = 8.9, 2.2 Hz, 2H), 7.58 (d, *J* = 9.0 Hz, 2H), 7.44 (d, *J* = 8.6 Hz, 2H), 3.97 (s, 4H), 3.86 (t, *J* = 6.8 Hz, 4H), 2.80 (t, *J* = 6.9 Hz, 4H), 1.64 (p, *J* = 6.9 Hz, 4H). ¹³C NMR (101 MHz, Methanol-*d*₄) δ

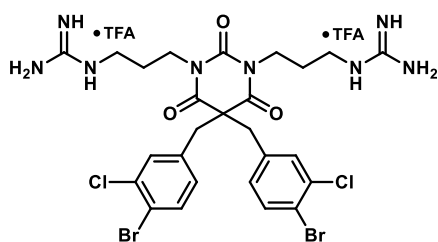
174.2 (2C), 159.0 (2C), 158.4, 153.4 (2C), 146.7 (2C), 137.4 (2C), 134.5 (2C), 131.4 (2C), 130.8 (2C), 129.6 (2C), 123.5 (2C), 121.3 (2C), 54.5, 48.3 (2C), 40.2 (2C), 39.7 (2C), 28.5 (2C). **HRMS** (ESI): calcd for $C_{32}H_{35}Br_2N_{10}O_3^+$ $[M+H]^+$ 765.1255, found 765.1259. **SFC**: 97.4%



1,1'-((2,4,6-triisopropoxy-5,5-bis(4-(trifluoromethyl)benzyl)di)hydropyrimidine-1,3(2H,4H)-diyl)bis(propane-3,1-diyl)diguandine
5bG.

Barbiturate **5bA** (70 mg, 89 μ mol, 1.0 eq), *N,N'*-Di-Boc-1*H*-pyrazole-1-carboxamidine (69 mg, 223 μ mol, 2.50 eq), DIPEA (62 μ L, 356 μ mol, 4.00 eq) and THF (1 mL) were stirred at 45 $^{\circ}$ C for 2.5 h. The crude was purified with 15% EtOAc in heptane to yield boc-**5bG** (73 mg, 70 μ mol, 79%) as a white foam.

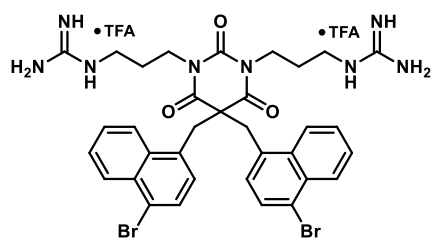
TFA (102 μ L, 1.33 mmol, 15.0 eq) and DCM (1 mL) were added, and the mixture was stirred at ambient temperature for 40 h. The crude was purified by automated RP column chromatography with a gradient of 10-60% MeCN/H₂O + 0.1% TFA to yield the di-TFA salt of **5bG** (61 mg, 70 μ mol, 79% o2s) as a white powder. **¹H NMR** (400 MHz, Methanol-*d*₄) δ 7.57 (d, *J* = 8.0 Hz, 4H), 7.29 (d, *J* = 8.0 Hz, 4H), 3.72 – 3.63 (m, 4H), 3.58 (s, 4H), 2.93 (t, *J* = 6.8 Hz, 4H), 1.53 (dq, *J* = 8.8, 7.0 Hz, 4H). **¹³C NMR** (101 MHz, Methanol-*d*₄) δ 171.5 (2C), 158.7 (2C), 150.8, 140.8 (2C), 131.5 (4C), 131.2 (q, *J* = 32.5 Hz, 2C), 126.7 (q, *J* = 3.7 Hz, 4C), 125.4 (d, *J* = 271 Hz, 4C), 61.2, 45.8 (2C), 40.3 (2C), 39.6 (2C), 28.2 (2C). **HRMS** (ESI): calcd for $C_{28}H_{33}F_6N_8O_3^+$ $[M+H]^+$ 643.2574, found 643.2579. **SFC**: 98.6%.



1,1'-((5,5-bis(4-bromo-3-chlorobenzyl)di)hydropyrimidine-1,3(2H,4H)-diyl)bis(propane-3,1-diyl)diguandine
5cG.

Barbiturate **5cA** (70 mg, 80 μ mol, 1.0 eq), *N,N'*-Di-Boc-1*H*-pyrazole-1-carboxamidine (62 mg, 200 μ mol, 2.50 eq), DIPEA (56 μ L, 319 μ mol, 4.00 eq) and THF (1 mL) were stirred at 45 $^{\circ}$ C for 2.5 h. The crude was purified with 20% EtOAc in heptane to yield boc-**5cG** (81 mg, 71 μ mol, 90%) as a clear solid.

TFA (92 μ L, 1.20 mmol, 15.0 eq) and DCM (1 mL) were added, and the mixture was stirred at ambient temperature for 40 h. The crude was purified by automated RP column chromatography with a gradient of 10-60% MeCN/H₂O + 0.1% TFA to yield the di-TFA salt of **5cG** (61 mg, 64 μ mol, 80% o2s) as a white powder. **¹H NMR** (400 MHz, Methanol-*d*₄) δ 7.57 (d, *J* = 8.3 Hz, 2H), 7.22 (d, *J* = 2.1 Hz, 2H), 6.91 (dd, *J* = 8.3, 2.1 Hz, 2H), 3.75 – 3.67 (m, 4H), 3.42 (s, 4H), 3.00 (t, *J* = 6.9 Hz, 4H), 1.64 – 1.52 (m, 4H). **¹³C NMR** (101 MHz, Methanol-*d*₄) δ 171.4 (2C), 158.7 (2C), 150.7, 137.6 (2C), 135.6 (2C), 135.3 (2C), 132.5 (2C), 130.6 (2C), 122.7 (2C), 61.1, 44.9 (2C), 40.3 (2C), 39.6 (2C), 28.5 (2C). **HRMS** (ESI): calcd for $C_{26}H_{31}Br_2Cl_2N_8O_3^+$ $[M+H]^+$ 731.0257, found 731.0263. **SFC**: >99.5%.

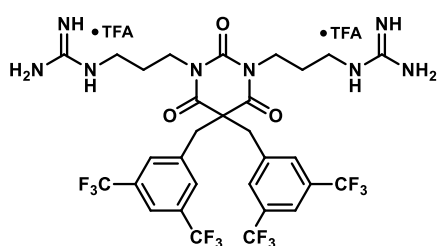


1,1'-((5,5-bis((4-bromonaphthalen-1-yl)methyl)di)hydropyrimidine-1,3(2H,4H)-diyl)bis(propane-3,1-diyl)diguandine
5dG.

Barbiturate **5dA** (70 mg, 77 μ mol, 1.0 eq), *N,N'*-Di-Boc-1*H*-pyrazole-1-carboxamidine (60 mg, 193 μ mol, 2.50 eq), DIPEA (54 μ L, 308 μ mol, 4.00 eq) and THF (1 mL) were stirred at 45 $^{\circ}$ C for 2.5 h. The crude was purified with 15% EtOAc in heptane to

yield boc-**5dG** (83 mg, 71 μ mol, 93%) as a white foam.

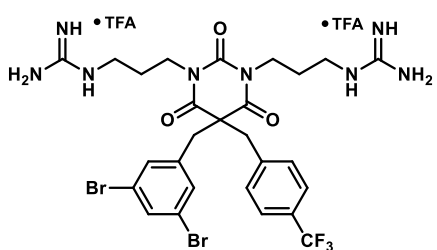
TFA (89 μ L, 1.16 mmol, 15.0 eq) and DCM (1 mL) were added, and the mixture was stirred at ambient temperature for 40 h. The crude was purified by automated RP column chromatography with a gradient of 10-60% MeCN/H₂O + 0.1% TFA to yield the di-TFA salt of **5dG** (67 mg, 68 μ mol, 88% o2s) as a white powder. **¹H NMR** (400 MHz, Methanol-*d*₄) δ 8.39 – 8.30 (m, 2H), 8.29 – 8.19 (m, 2H), 7.70 (d, *J* = 7.8 Hz, 2H), 7.65 (td, *J* = 7.0, 6.6, 3.6 Hz, 4H), 7.16 (d, *J* = 7.8 Hz, 2H), 4.17 (s, 4H), 3.45 – 3.35 (m, 4H), 2.57 (t, *J* = 6.9 Hz, 4H), 1.09 (p, *J* = 7.0 Hz, 4H). **¹³C NMR** (101 MHz, Methanol-*d*₄) δ 172.2 (2C), 158.4 (2C), 150.9, 134.4 (2C), 133.4 (2C), 130.4 (2C), 129.3 (2C), 128.8 (2C), 128.6 (2C), 128.2 (2C), 126.5 (2C), 123.9 (2C), 60.6, 41.5 (2C), 40.1 (2C), 39.2 (2C), 27.8 (2C). **HRMS** (ESI): calcd for $C_{34}H_{37}Br_2N_8O_3^+$ $[M+H]^+$ 763.1350, found 763.1356. **SFC**: >99.5%.



1,1'-((5,5-bis(3,5-bis(trifluoromethyl)benzyl)-2,4,6-trioxodihydropyrimidine-1,3(2H,4H)-diyl)bis(propane-3,1-diyl)diguani dine 5eG.

Barbiturate **5eA** (50 mg, 54 μ mol, 1.0 eq), *N,N'*-Di-Boc-1*H*-pyrazole-1-carboxamidine (42 mg, 136 μ mol, 2.50 eq), DIPEA (38 μ L, 217 μ mol, 4.00 eq) and THF (1 mL) were stirred at 45 $^{\circ}$ C for 2.5 h. The crude was purified with 15% EtOAc in heptane to yield boc-**5eG** (49 mg, 42 μ mol, 77%) as a white foam.

TFA (62 μ L, 0.81 mmol, 15.0 eq) and DCM (1 mL) were added, and the mixture was stirred at ambient temperature for 40 h. The crude was purified by automated RP column chromatography with a gradient of 10–60% MeCN/H₂O + 0.1% TFA to yield the di-TFA salt of **5eG** (42 mg, 42 μ mol, 77% o2s) as a white powder. ¹H NMR (400 MHz, Methanol-*d*4) δ 7.93 (s, 2H), 7.69 (d, *J* = 1.6 Hz, 4H), 3.72 (s, 4H), 3.69 – 3.60 (m, 4H), 3.03 (t, *J* = 6.9 Hz, 4H), 1.49 (dq, *J* = 9.4, 7.0 Hz, 4H). ¹³C NMR (101 MHz, Methanol-*d*4) δ 171.1 (2C), 158.7 (2C), 150.2, 139.4 (2C), 133.10 (q, *J* = 33.4 Hz, 4C), 131.5 – 131.3 (m, 4C), 124.5 (q, *J* = 272 Hz, 4C) 123.1 – 122.8 (m, 2C), 61.2, 44.8 (2C), 40.5 (2C), 39.5 (2C), 28.5 (2C). HRMS (ESI): calcd for C₃₀H₃₁F₁₂N₈O₃⁺ [M+H]⁺ 779.2322, found 779.2324. SFC: >99.5%.

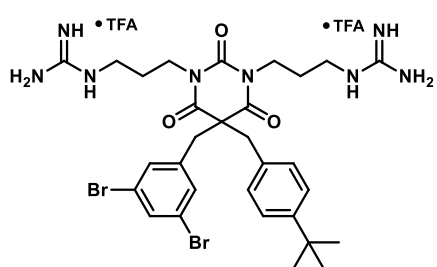


1,1'-((5-(3,5-dibromobenzyl)-2,4,6-trioxo-5-(4-(trifluoromethyl)benzyl)dihydropyrimidine-1,3(2H,4H)-diyl)bis(propane-3,1-diyl)diguani dine 5fG.

Barbiturate **5fA** (150 mg, 171 μ mol, 1.0 eq), *N,N'*-Di-Boc-1*H*-pyrazole-1-carboxamidine (90 mg, 291 μ mol, 1.7 eq), DIPEA (119 μ L, 685 μ mol, 4.0 eq) and THF (0.5 mL) were stirred at 45 $^{\circ}$ C for 2.5 h. The crude was purified with 10–45% EtOAc in heptane to yield boc-**5fG** (121 mg, 107 μ mol, 62%) as a white

foam.

TFA (246 μ L, 3.20 mmol, 30.0 eq) and DCM (1.5 mL) were added, and the mixture was stirred at ambient temperature for 36 h. The crude was purified by automated RP column chromatography with a gradient of 15–45% MeCN/H₂O + 0.1% TFA to yield the di-TFA salt of **5fG** (11 mg, 11 μ mol, 20% o2s) as a white powder. ¹H NMR (400 MHz, Methanol-*d*4) δ 7.64 (t, *J* = 1.8 Hz, 1H), 7.57 (d, *J* = 8.0 Hz, 2H), 7.27 (d, *J* = 8.0 Hz, 2H), 7.24 (d, *J* = 1.7 Hz, 2H), 3.74 (ddd, *J* = 13.3, 8.6, 6.2 Hz, 2H), 3.65 (ddd, *J* = 13.2, 8.6, 6.0 Hz, 2H), 3.54 (s, 2H), 3.47 (s, 2H), 1.58 (dddd, *J* = 22.8, 13.3, 6.9, 2.0 Hz, 4H). ¹³C NMR (101 MHz, Methanol-*d*4) δ 171.4 (2C), 158.7 (2C), 150.7, 140.6 (2C), 134.5, 132.7 (2C), 131.4, 131.2 (q, *J* = 32.6 Hz, 1C), 126.7 (q, *J* = 3.8 Hz, 2C), 125.4 (q, *J* = 271.1 Hz, 1C) 124.2 (2C), 61.3, 45.7, 44.9, 40.3 (2C), 39.6 (2C), 28.6 (2C). HRMS (ESI): calcd for C₂₇H₃₂Br₂F₃N₈O₃⁺ [M+H]⁺ 731.0911, found: 731.0919 SFC: 97.8%.



1,1'-((5-(4-(tert-butyl)benzyl)-5-(3,5-dibromobenzyl)-2,4,6-trioxodihydropyrimidine-1,3(2H,4H)-diyl)bis(propane-3,1-diyl)diguani dine 5gG.

Barbiturate **5gA** (60 mg, 69 μ mol, 1.0 eq), *N,N'*-Di-Boc-1*H*-pyrazole-1-carboxamidine (54 mg, 174 μ mol, 2.5 eq), DIPEA (30 μ L, 174 μ mol, 2.5 eq) and THF (1.5 mL) were stirred at 50 $^{\circ}$ C for 2.5 h. The crude was purified with 10–50% EtOAc in heptane to yield impure boc-**5gG** (86 mg, 77 μ mol, 111%) as a white solid.

TFA (80 μ L, 1.04 mmol, 15.0 eq) and DCM (1.5 mL) were added, and the mixture was stirred at ambient temperature for 24 h. The crude was purified by automated RP column chromatography with a gradient of 10–45% MeCN/H₂O + 0.1% TFA to yield the di-TFA salt of **5gG** (39 mg, 41 μ mol, 59% o2s) as a white powder. ¹H NMR (400 MHz, Methanol-*d*4) δ 7.62 (t, *J* = 1.8 Hz, 1H), 7.30 – 7.26 (m, 2H), 7.25 (d, *J* = 1.8 Hz, 2H), 7.00 – 6.94 (m, 2H), 3.72 (ddd, *J* = 13.2, 8.1, 6.7 Hz, 2H), 3.63 (ddd, *J* = 13.5, 8.0, 6.2 Hz, 2H), 3.45 (s, 2H), 3.39 (s, 2H), 2.98 (td, *J* = 6.9, 5.1 Hz, 4H), 1.65 – 1.49 (m, 4H), 1.25 (s, 9H). ¹³C NMR (101 MHz, Methanol-*d*4) δ 171.9 (2C), 158.7 (2C), 152.4, 150.9, 141.2, 134.3, 132.7, 130.2

(2C), 126.7 (2C), 124.1 (2C), 61.8, 46.7, 44.1, 40.2 (2C), 39.6 (2C), 35.3, 31.6 (3C), 28.5 (2C). **HRMS**
(ESI): calcd for $C_{30}H_{41}Br_2N_8O_3^+$ $[M+H]^+$ 719.1663, found: 719.1664. **SFC**: 98.6%

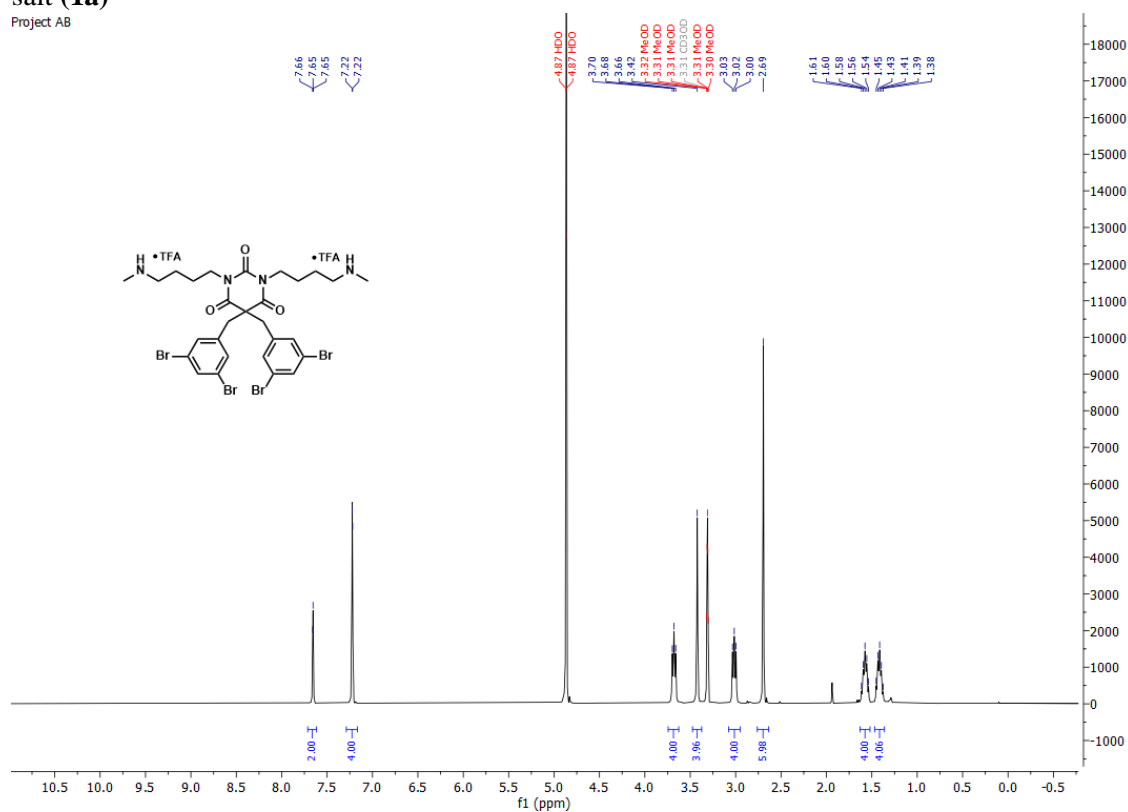
3 ^1H and ^{13}C NMR spectra of final compounds

NMR raw data of all intermediates can be found here: <https://doi.org/10.18710/GNTWOG>.

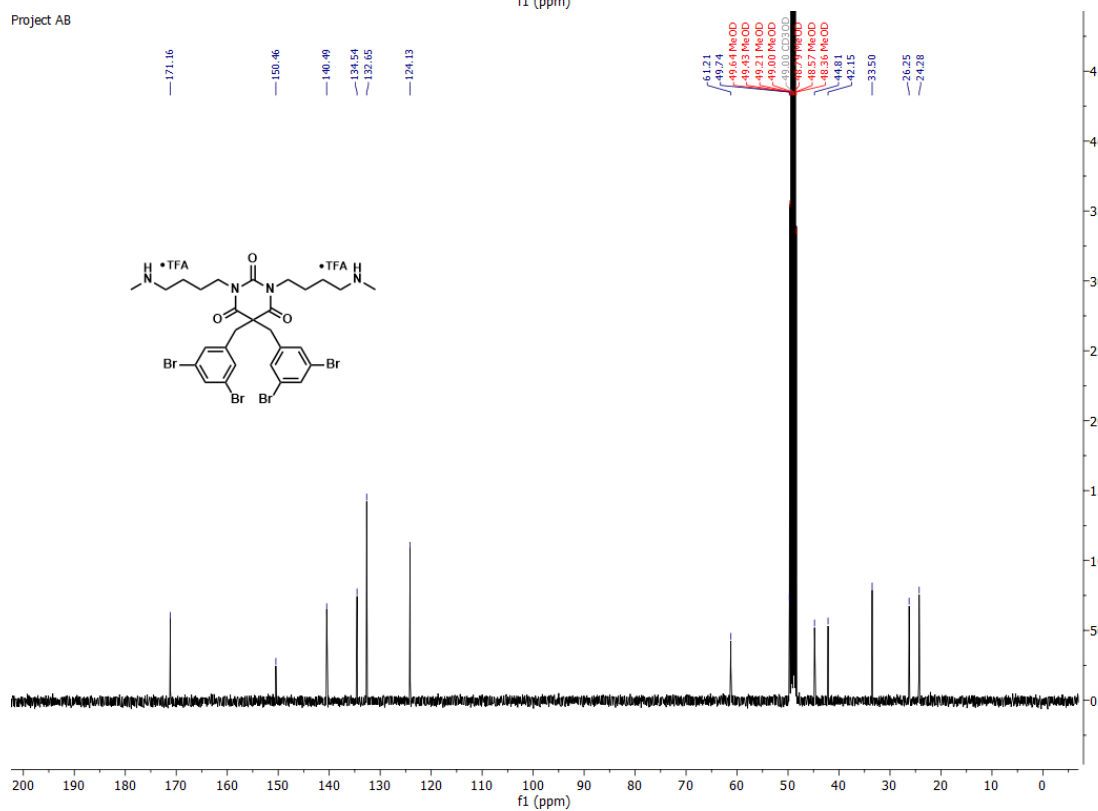
3.1 ^1H and ^{13}C NMR spectra of compounds in series 1

5,5-bis(3,5-dibromobenzyl)-1,3-bis(4-(methylamino)butyl)pyrimidine-2,4,6(1*H*,3*H*,5*H*)-trione di-TFA salt (**1a**)

Project AB

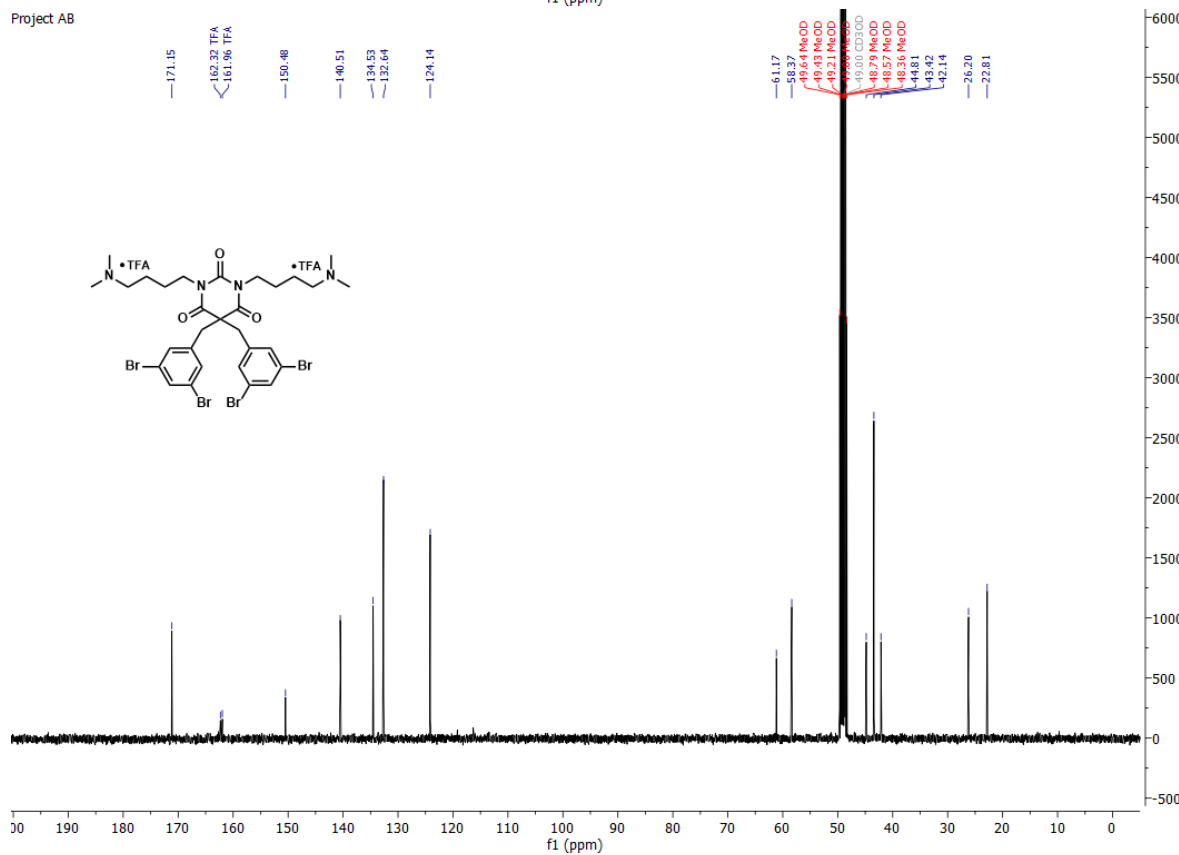
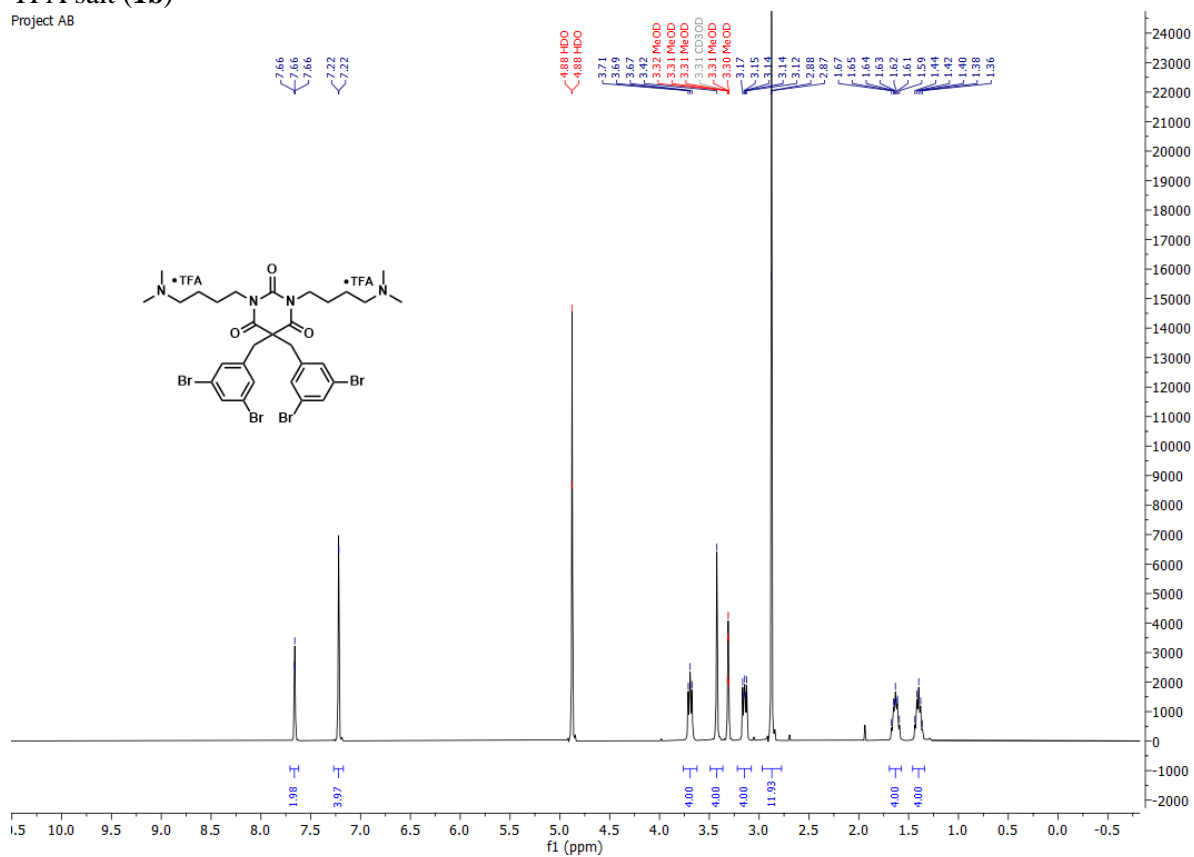


Project AB



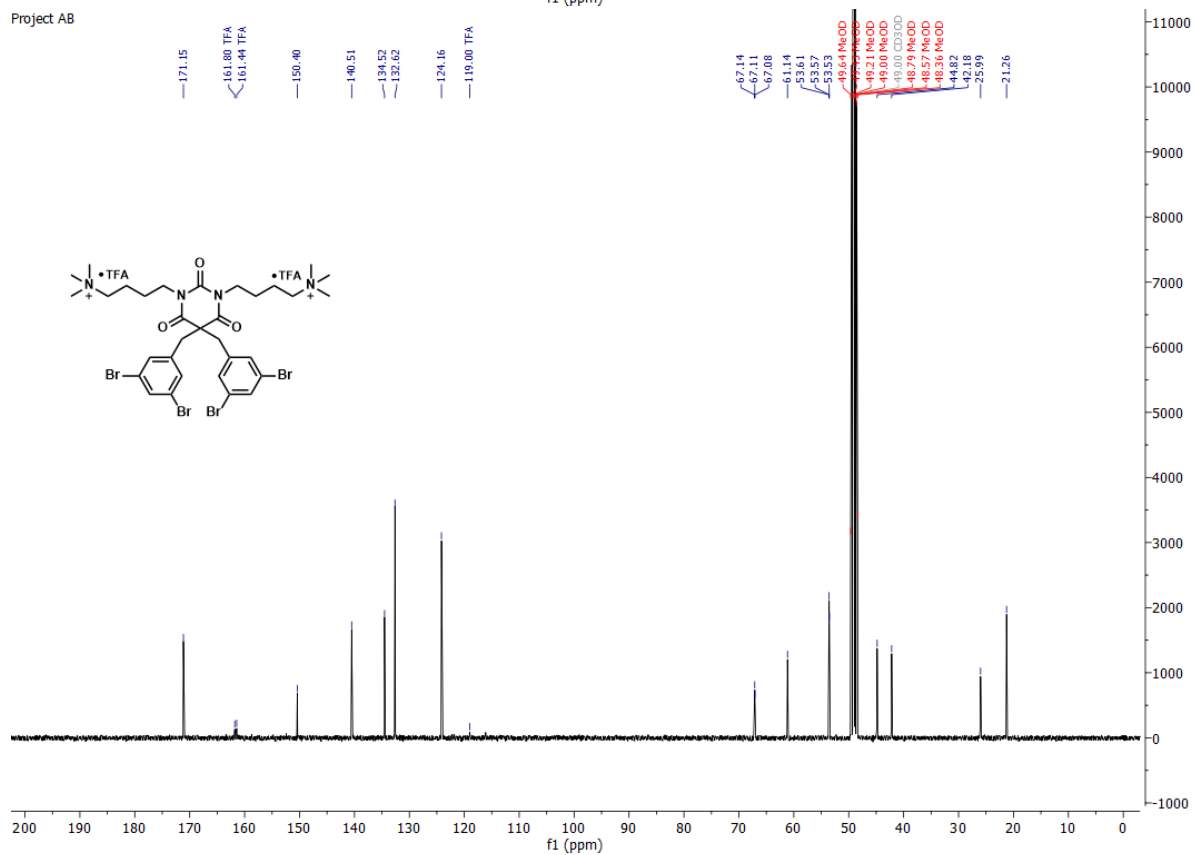
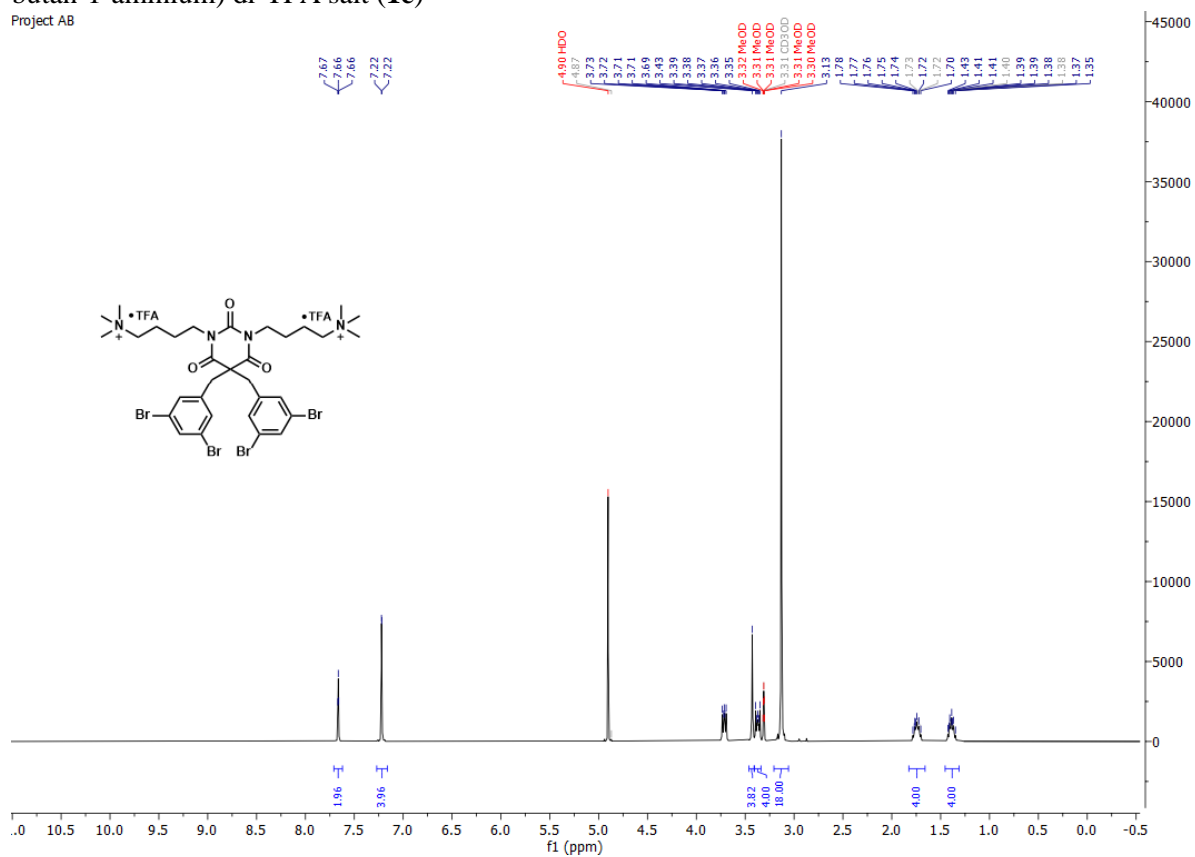
5,5-bis(3,5-dibromobenzyl)-1,3-bis(4-(dimethylamino)butyl)pyrimidine-2,4,6(1*H*,3*H*,5*H*)-trione di-TFA salt (**1b**)

Project AB



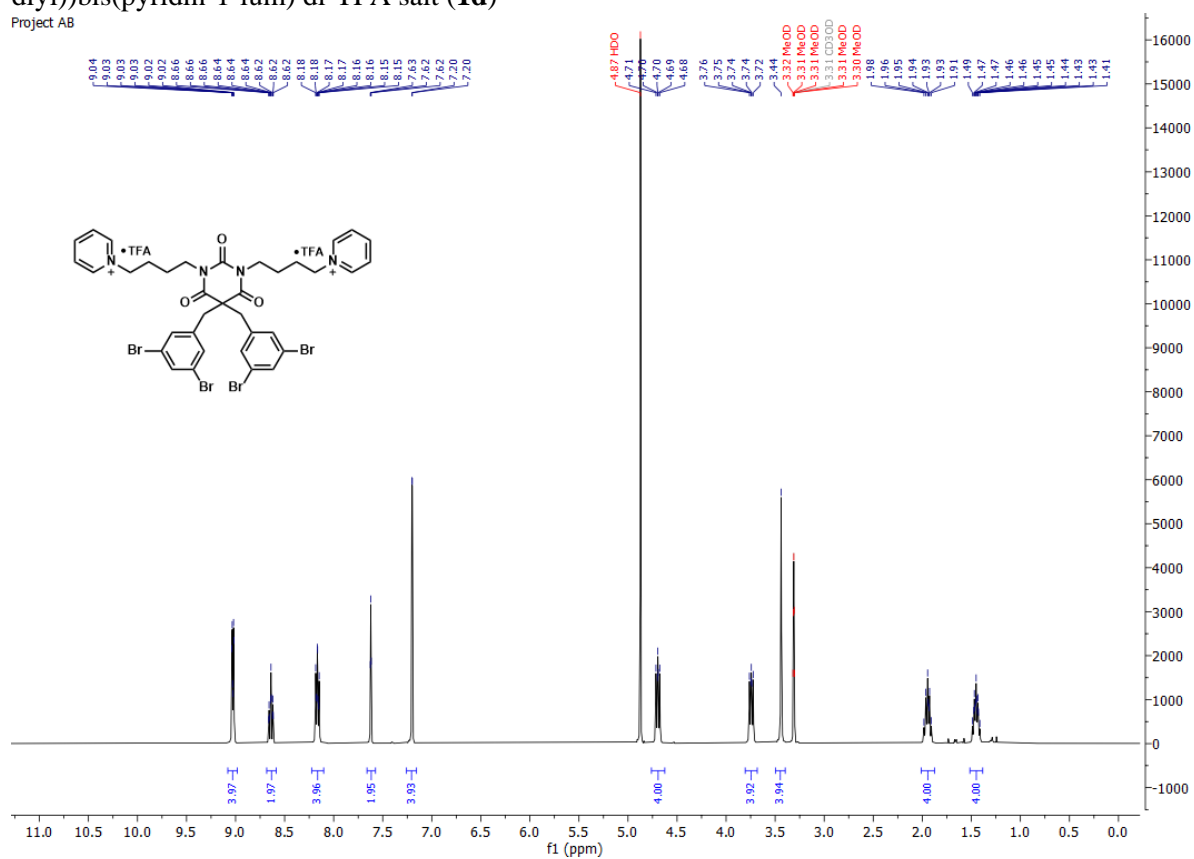
4,4'-(5,5-bis(3,5-dibromobenzyl)-2,4,6-trioxodihydropyrimidine-1,3(2*H*,4*H*)-diyl)bis(*N,N,N*-trimethylbutan-1-aminium) di-TFA salt (**1c**)

Project AB

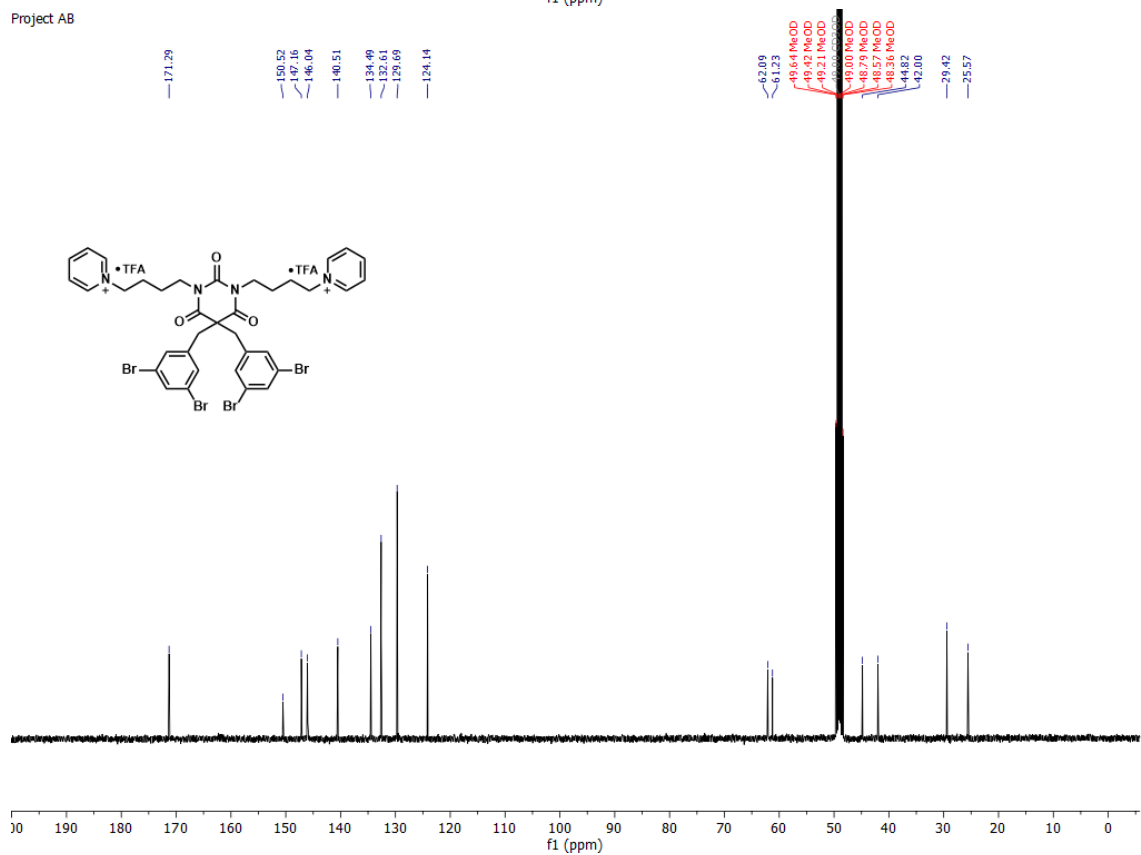


1,1'-((5,5-bis(3,5-dibromobenzyl)-2,4,6-trioxodihydropyrimidine-1,3(2H,4H)-diyl)bis(butane-4,1-diyl))bis(pyridin-1-ium) di-TFA salt (**1d**)

Project AB



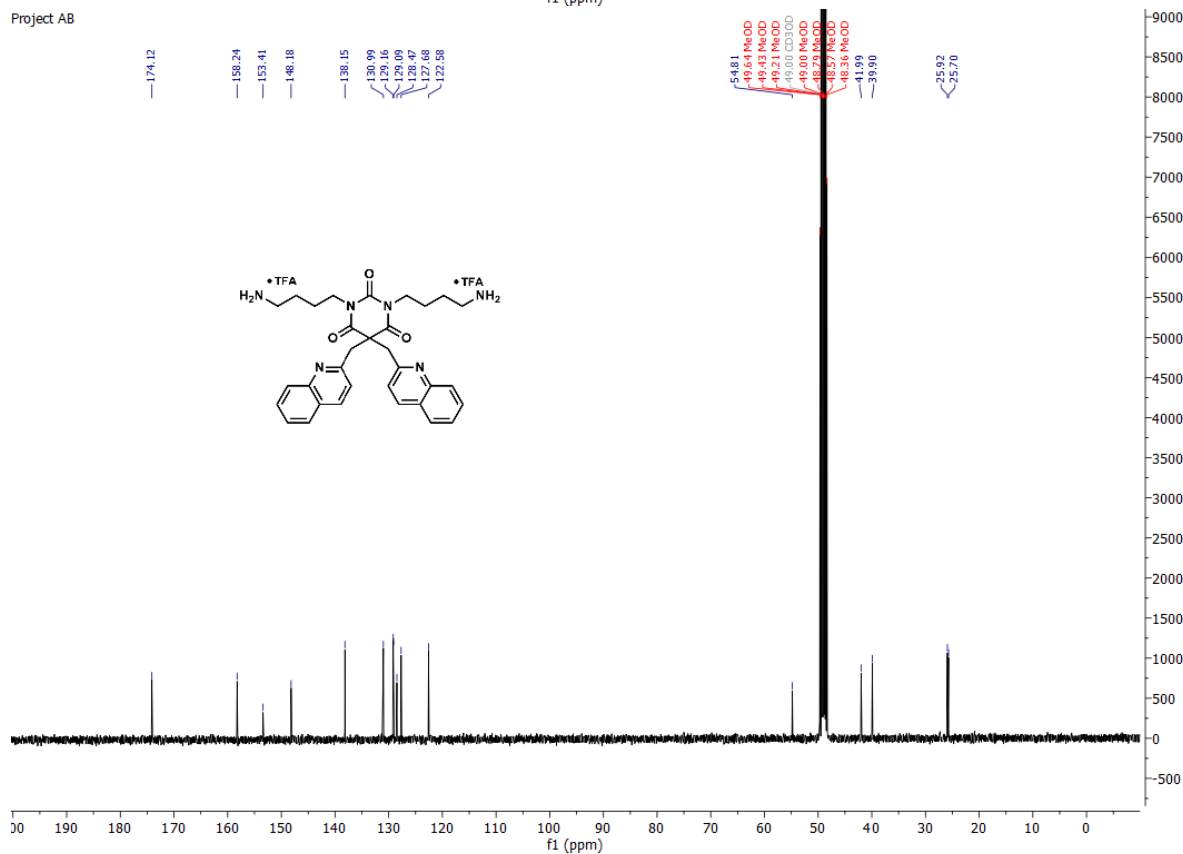
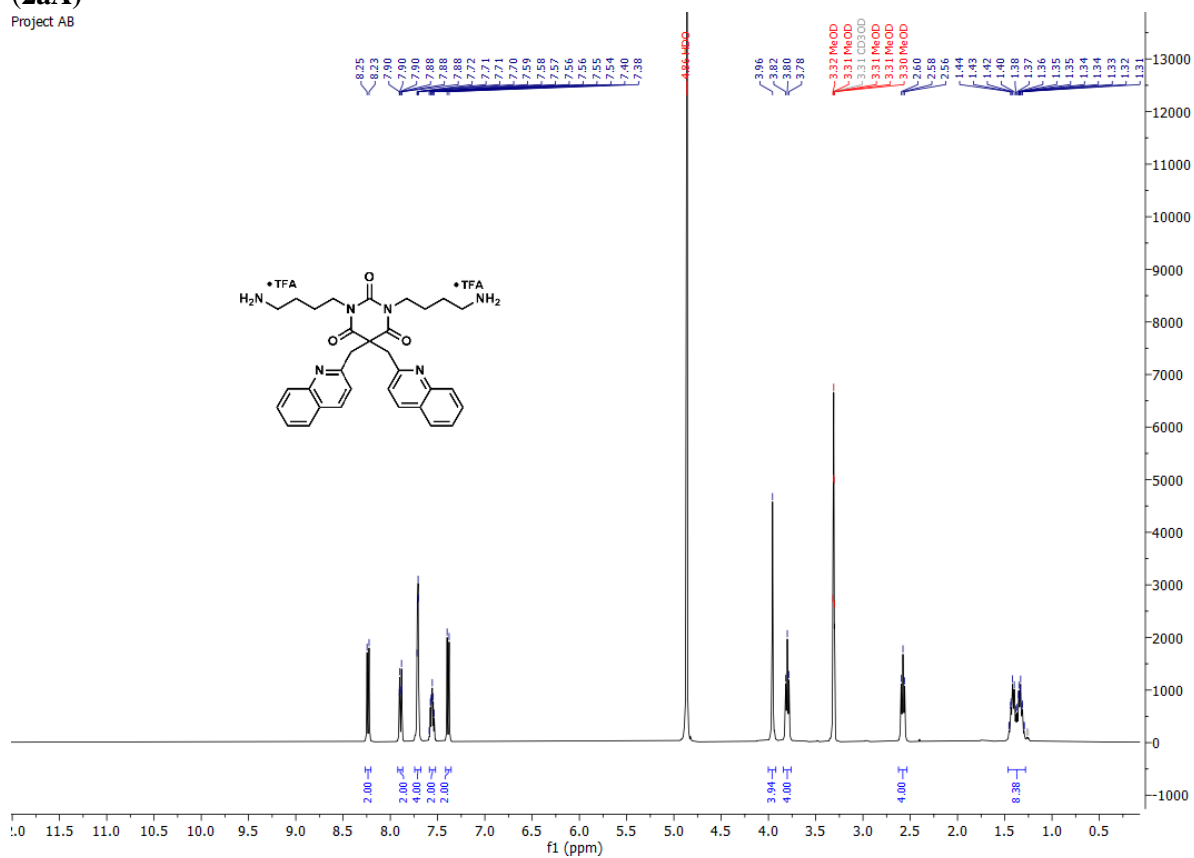
Project AB



3.2 ^1H and ^{13}C NMR spectra of compounds in series 2

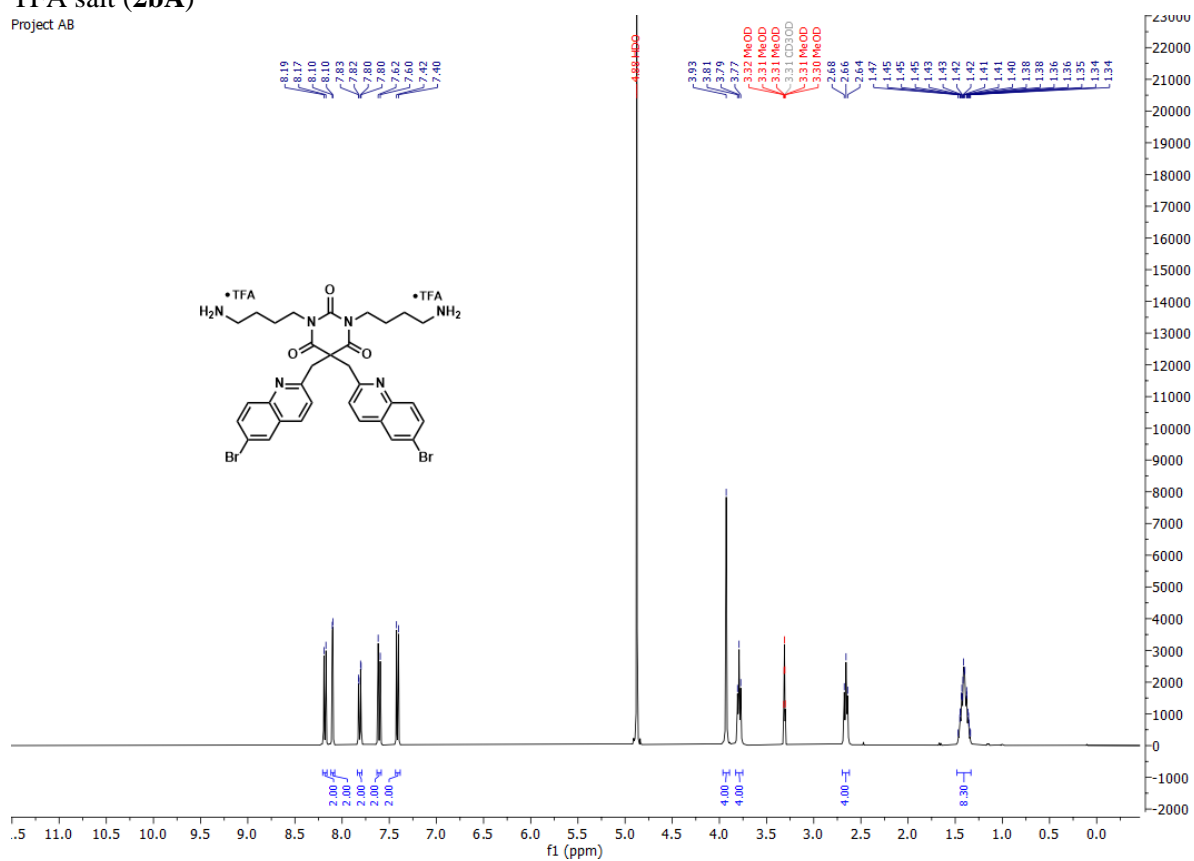
1,3-bis(4-aminobutyl)-5,5-bis(quinolin-2-ylmethyl)pyrimidine-2,4,6(1*H*,3*H*,5*H*)-trione di-TFA salt (**2aA**)

Project AB

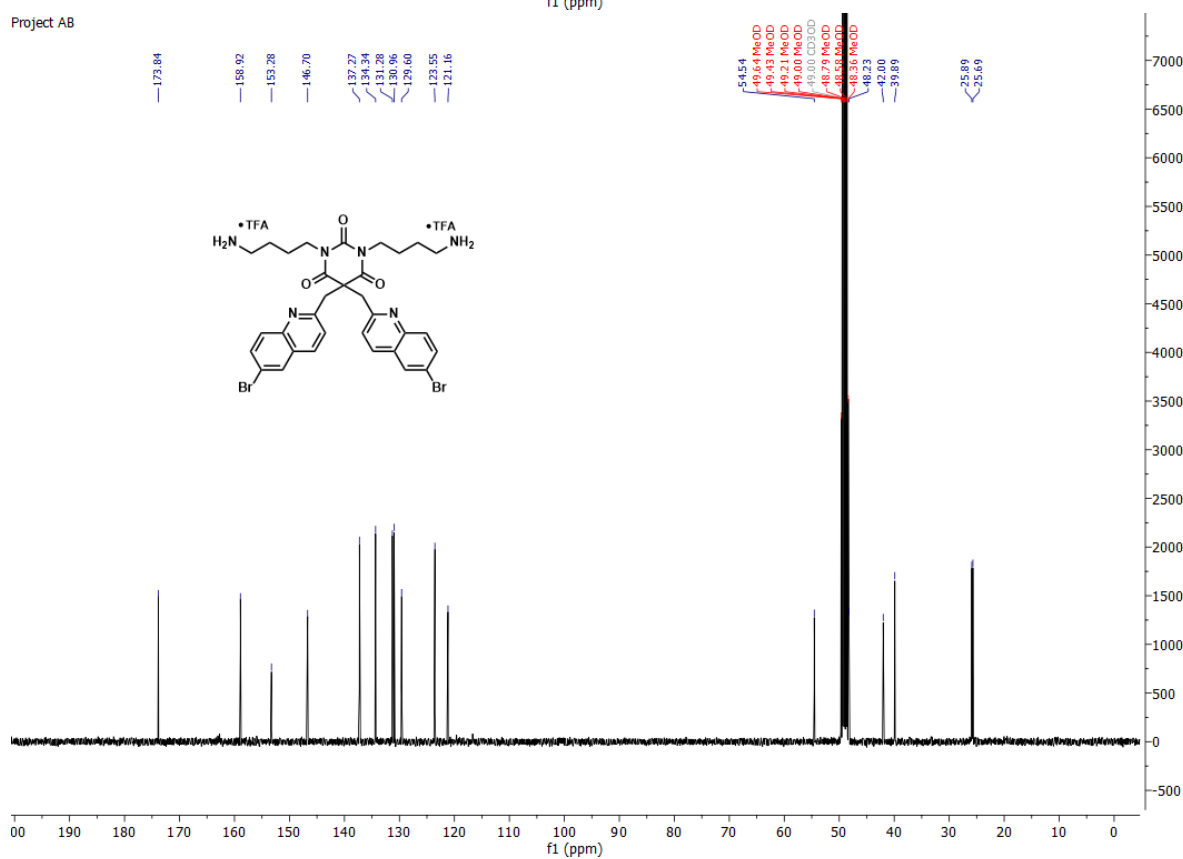


1,3-bis(4-aminobutyl)-5,5-bis((6-bromoquinolin-2-yl)methyl)pyrimidine-2,4,6(1*H*,3*H*,5*H*)-trione di-TFA salt (**2bA**)

Project AB

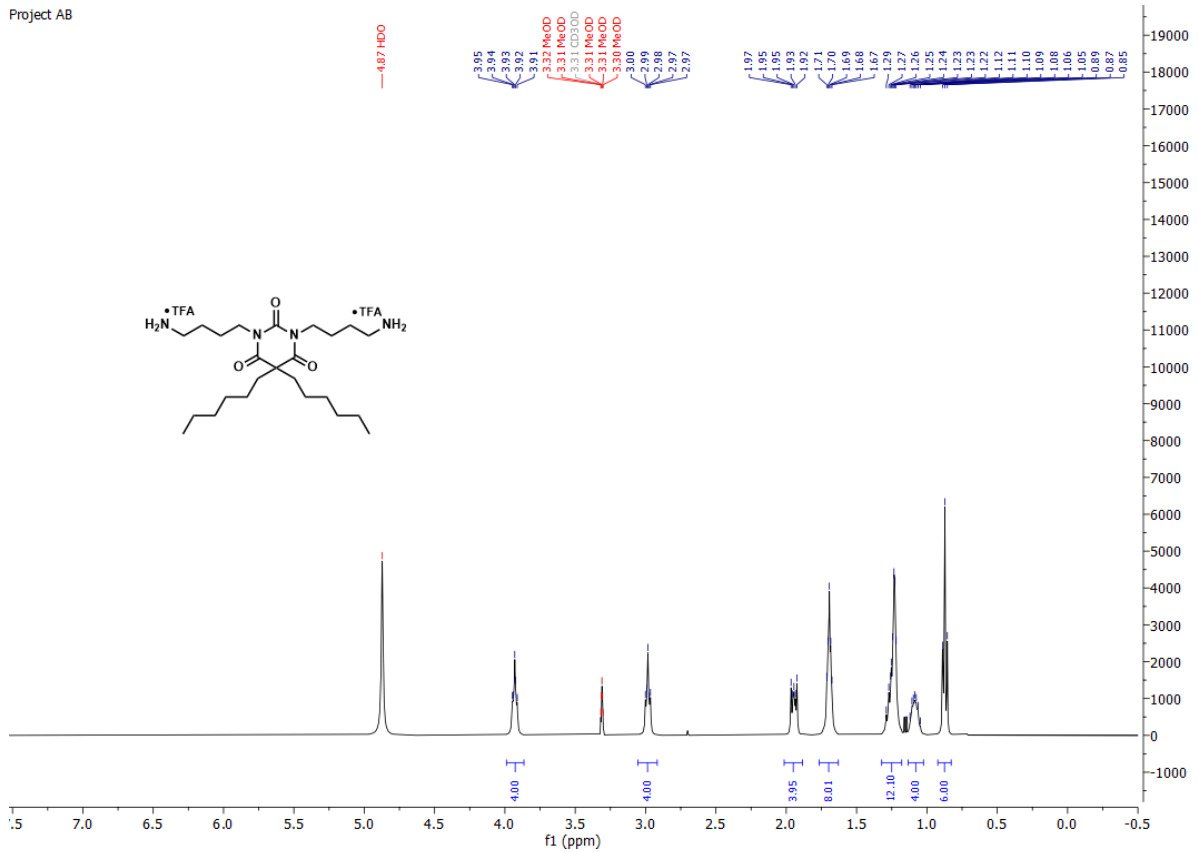


Project AB

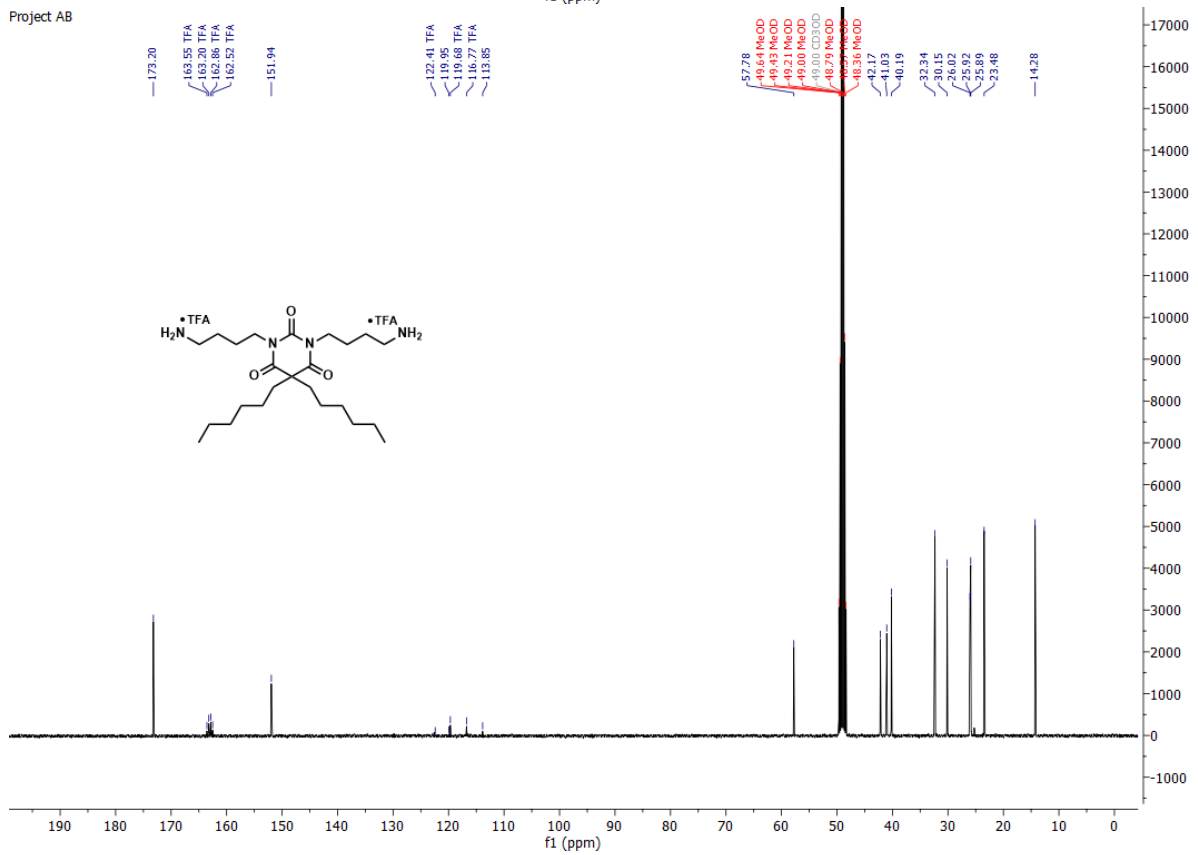


1,3-bis(4-aminobutyl)-5,5-dihexylpyrimidine-2,4,6(1*H*,3*H*,5*H*)-trione di-TFA salt (**2cA**)

Project AB

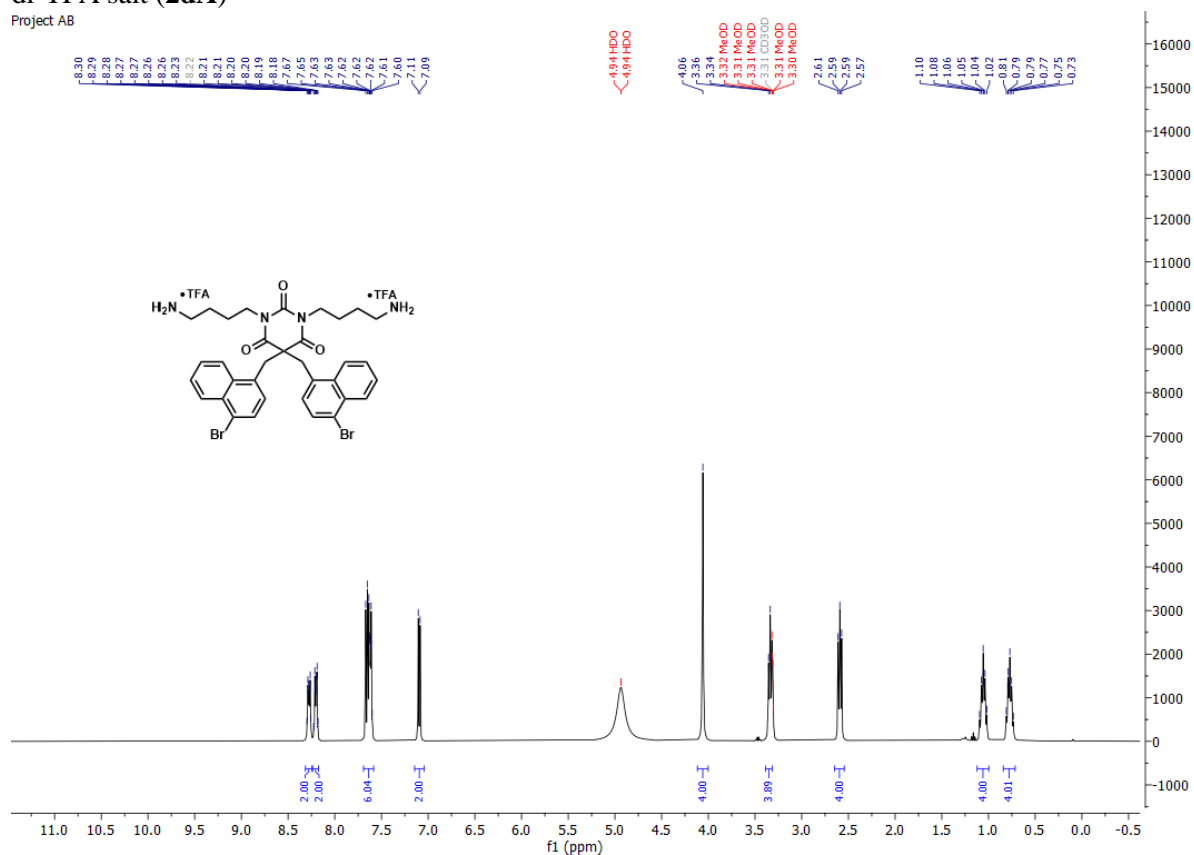


Project AB

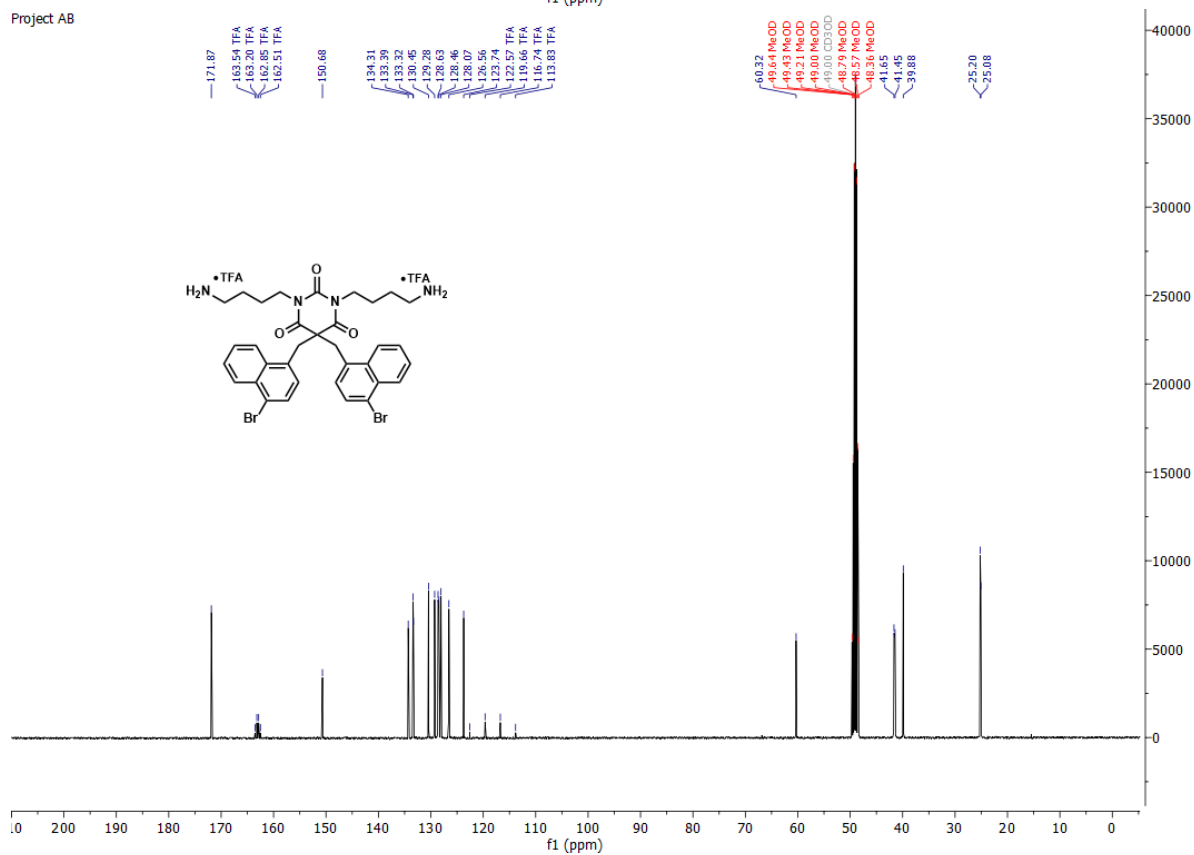


1,3-bis(4-aminobutyl)-5,5-bis((4-bromonaphthalen-1-yl)methyl)pyrimidine-2,4,6(1*H*,3*H*,5*H*)-trione di-TFA salt (**2dA**)

Project AB

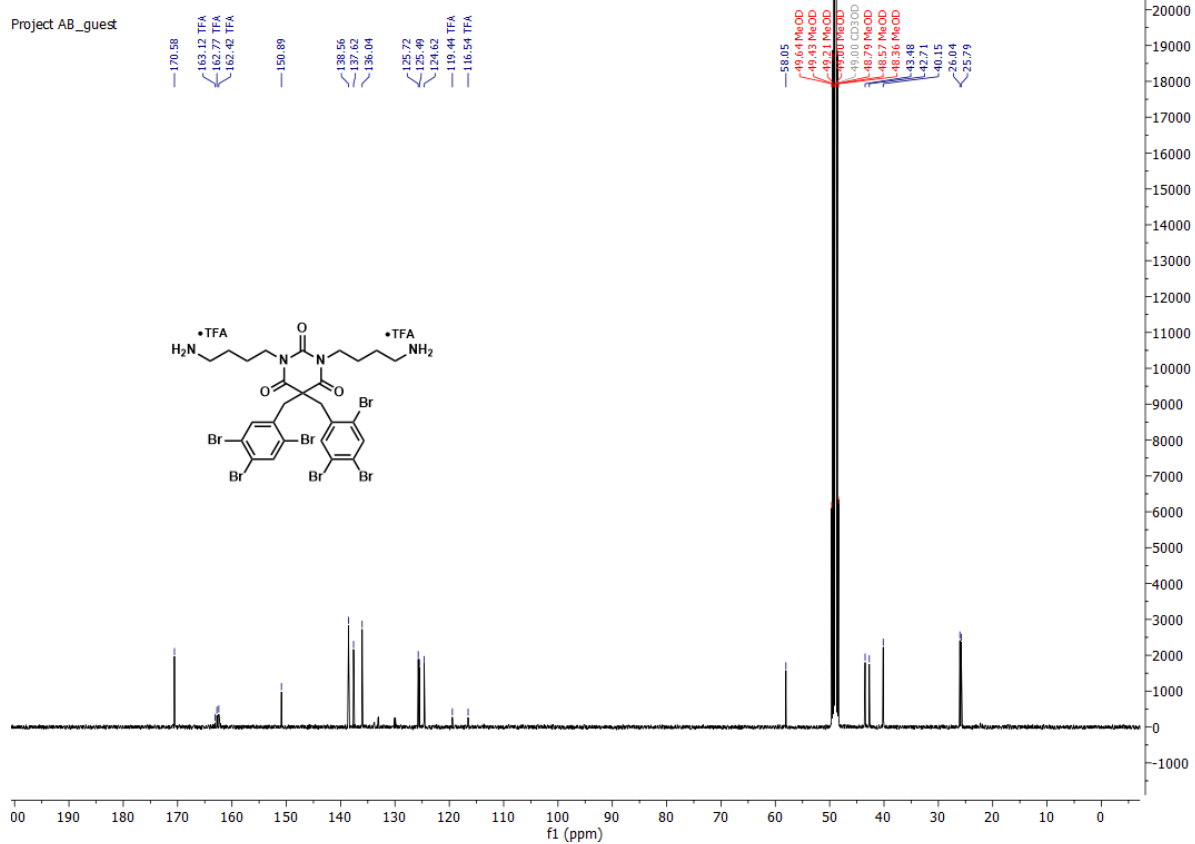
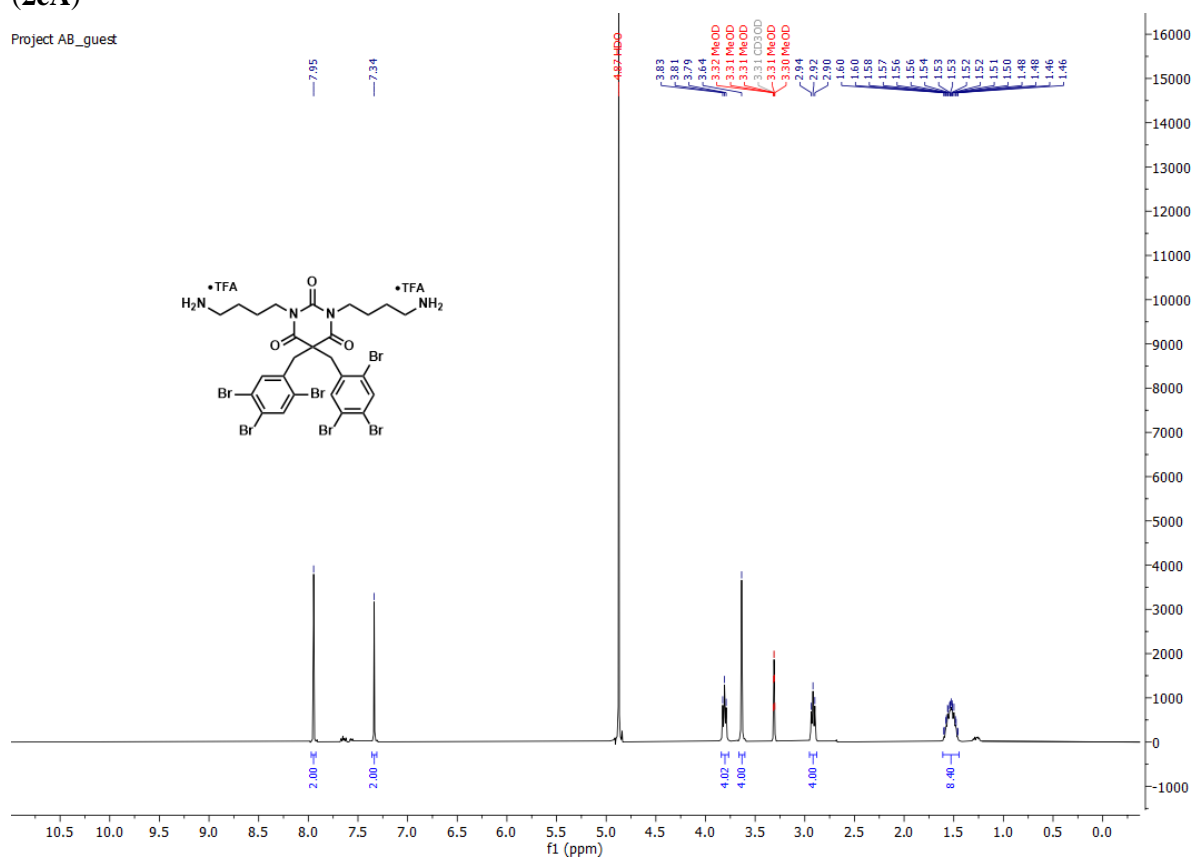


Project AB



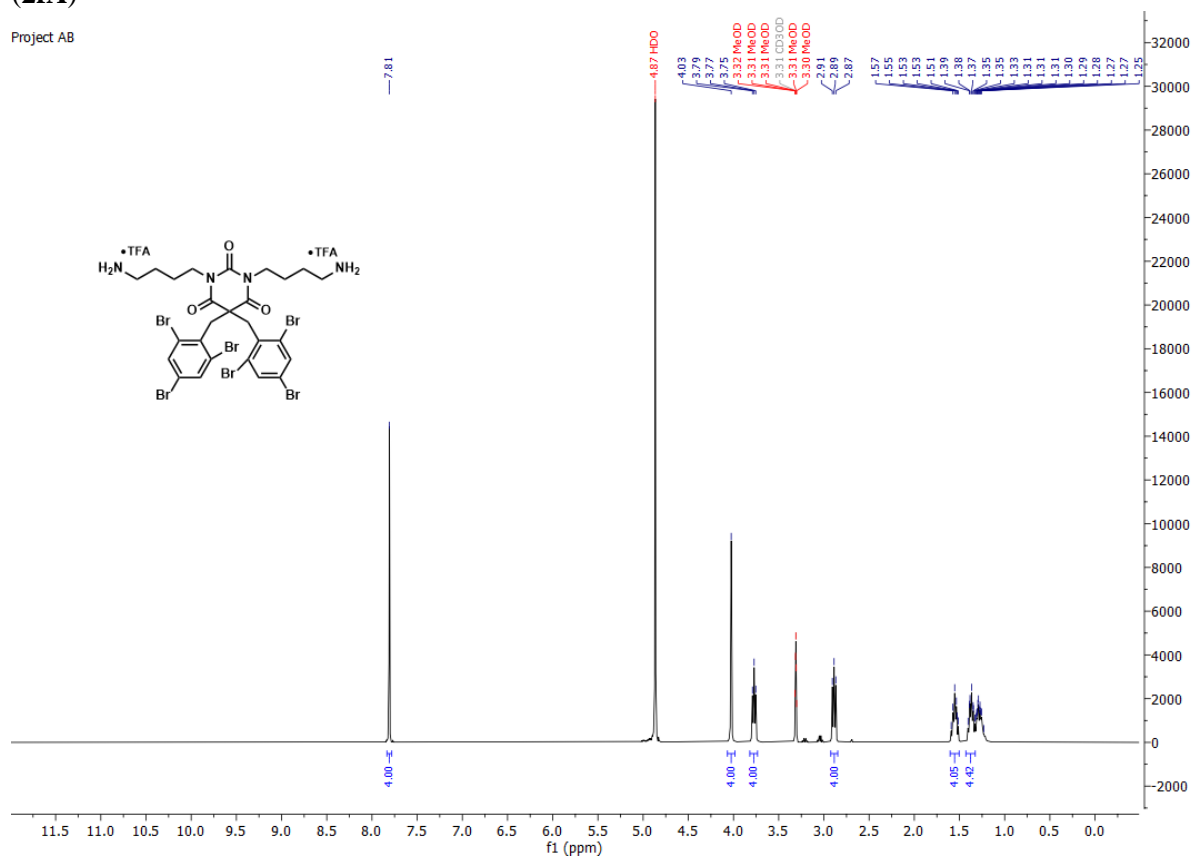
1,3-bis(4-aminobutyl)-5,5-bis(2,4,5-tribromobenzyl)pyrimidine-2,4,6(1*H*,3*H*,5*H*)-trione di-TFA salt (**2eA**)

Project AB_guest

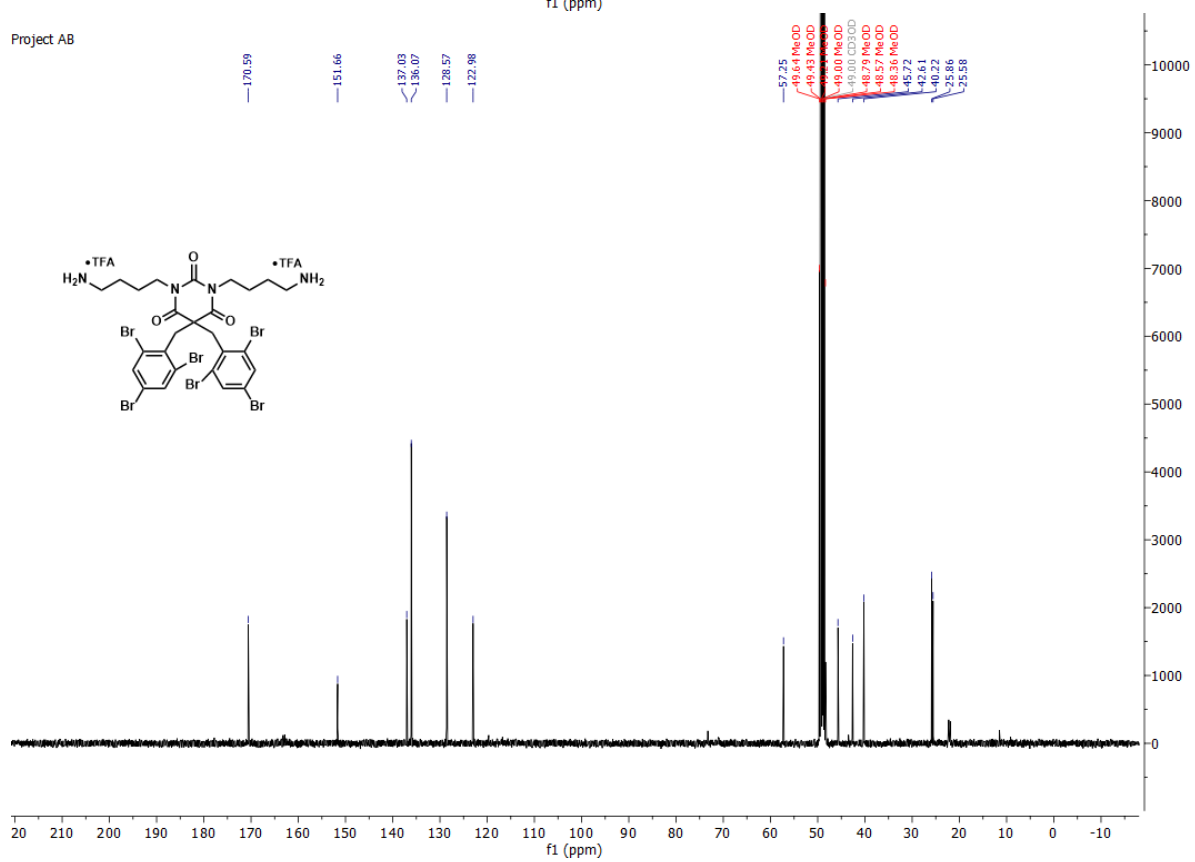


1,3-bis(4-aminobutyl)-5,5-bis(2,4,6-tribromobenzyl)pyrimidine-2,4,6(1*H*,3*H*,5*H*)-trione di-TFA salt (**2fA**)

Project AB

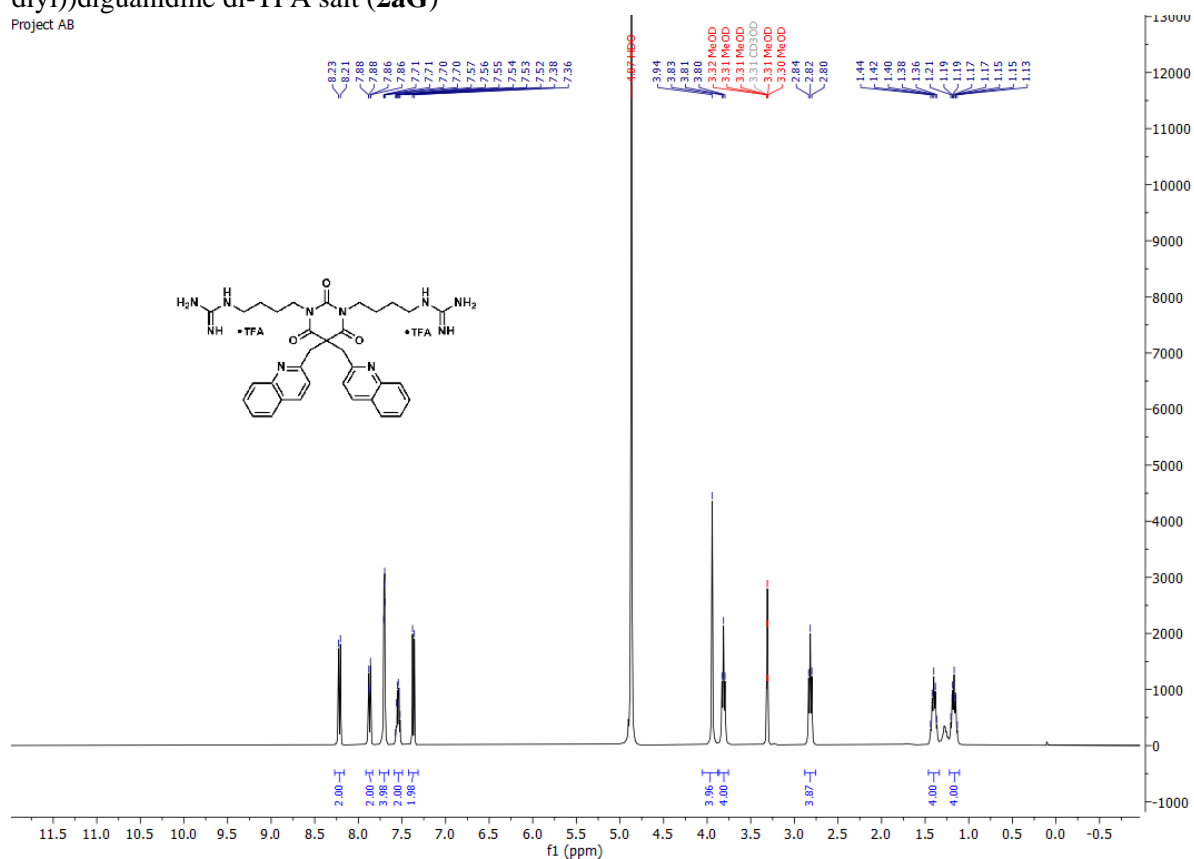


Project AB

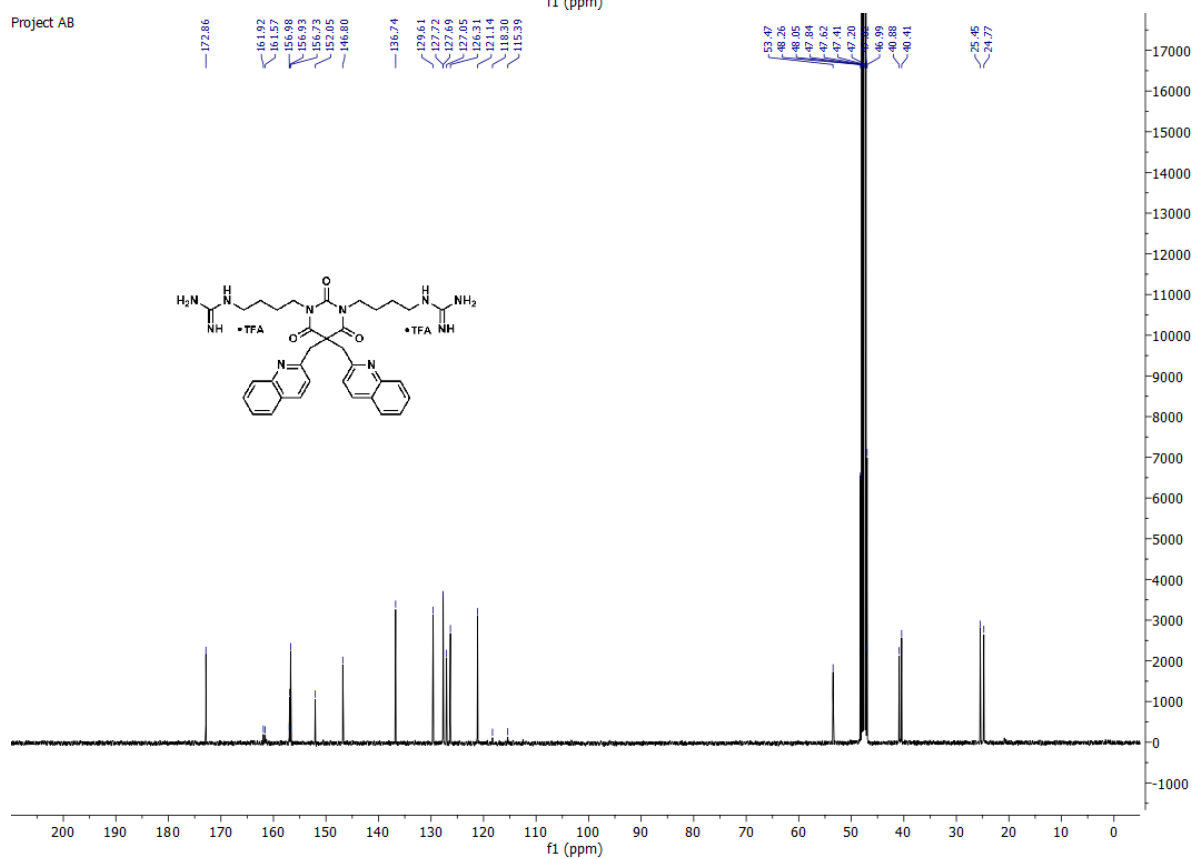


1,1'-((2,4,6-trioxo-5,5-bis(quinolin-2-ylmethyl)dihydropyrimidine-1,3(2*H*,4*H*)-diyl)bis(butane-4,1-diyl))diguanidine di-TFA salt (**2aG**)

Project AB

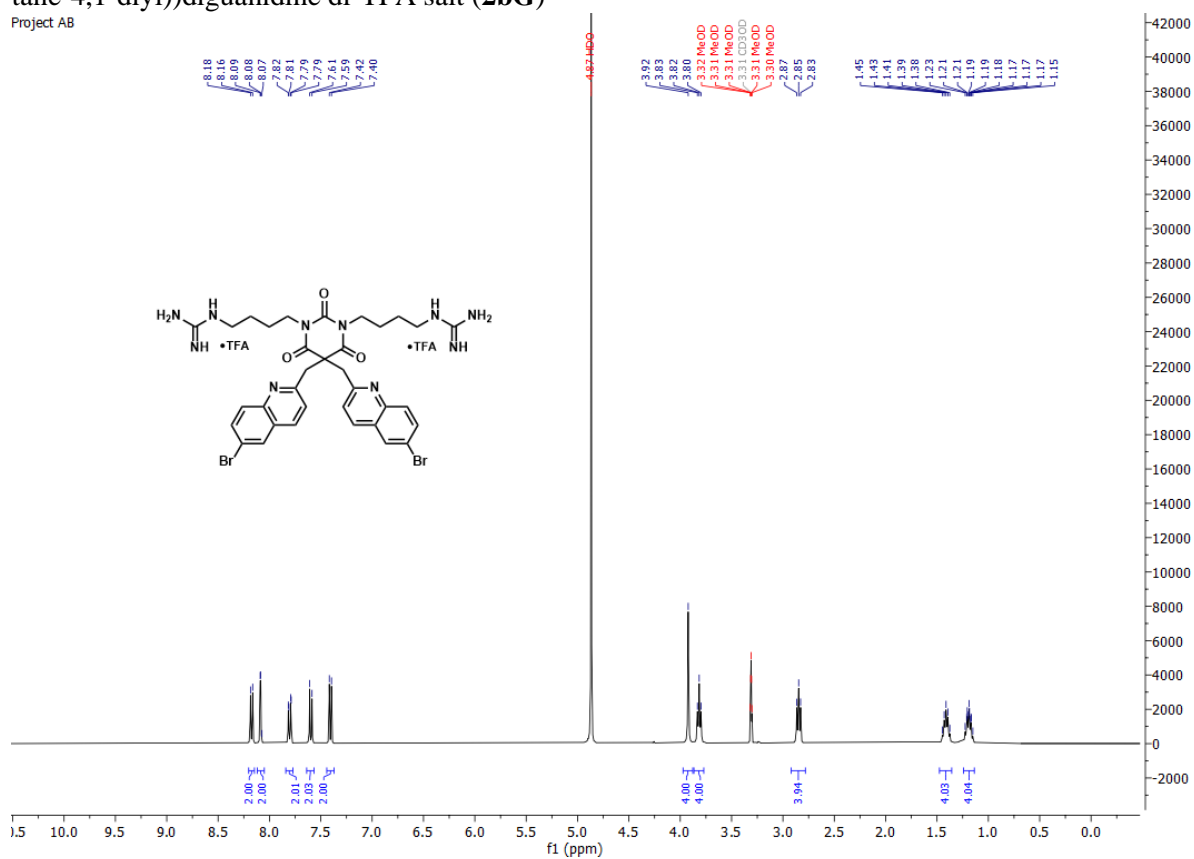


Project AB

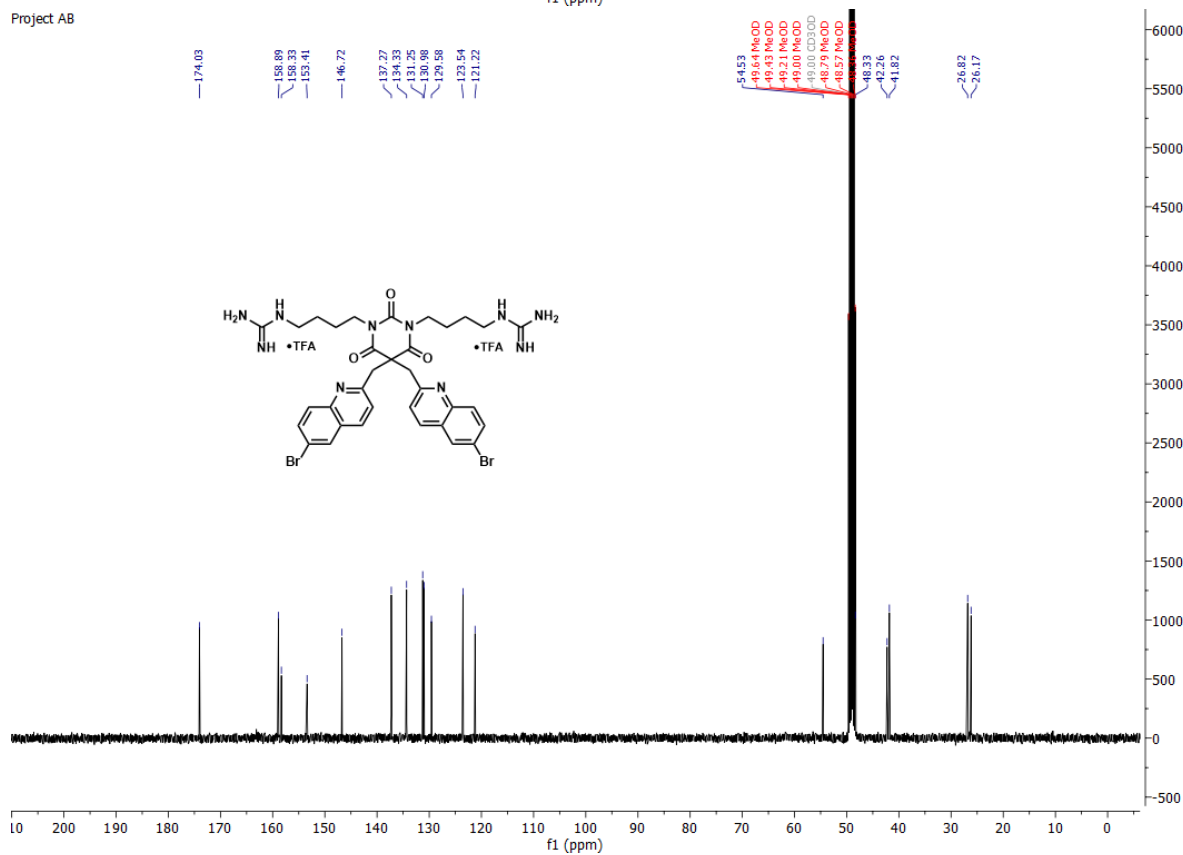


1,1'-((5,5-bis((6-bromoquinolin-2-yl)methyl)-2,4,6-trioxodihydropyrimidine-1,3(2*H*,4*H*)-diyl)bis(butane-4,1-diyl))diguandine di-TFA salt (**2bG**)

Project AB

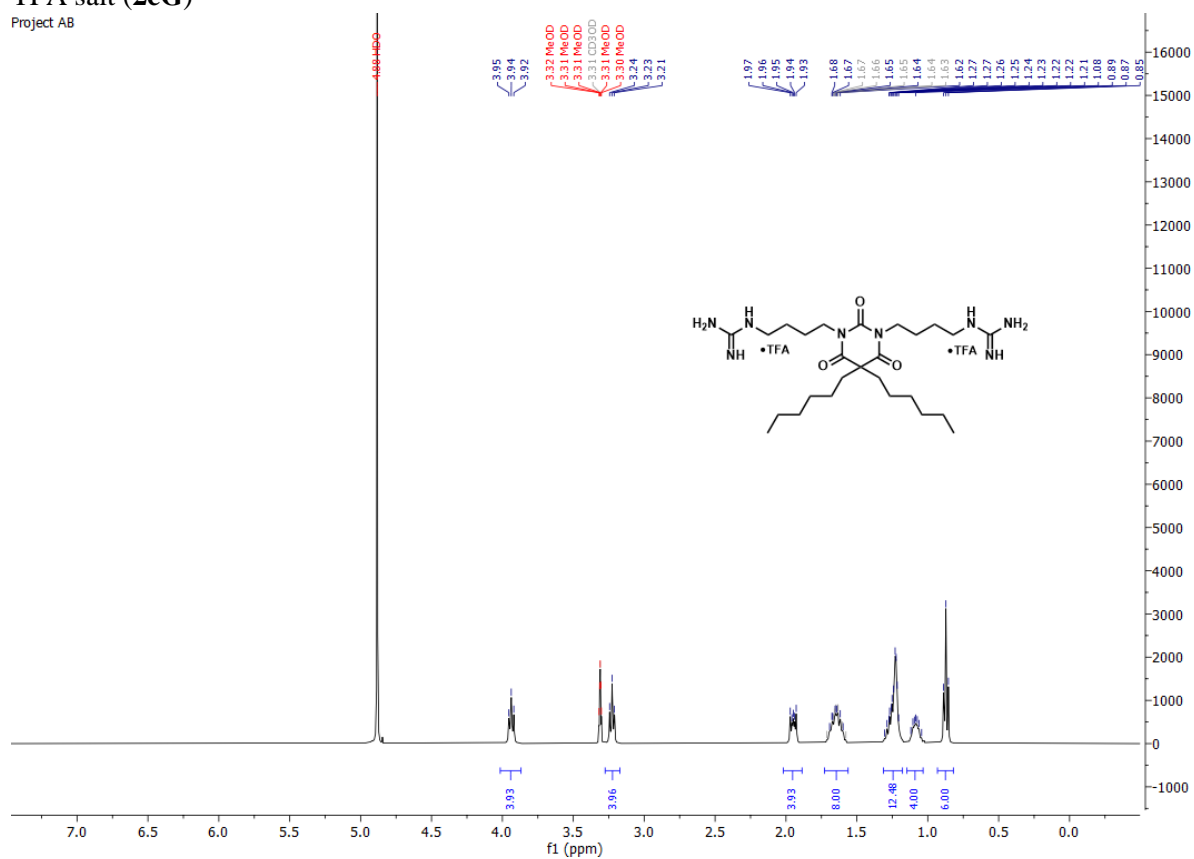


Project AB

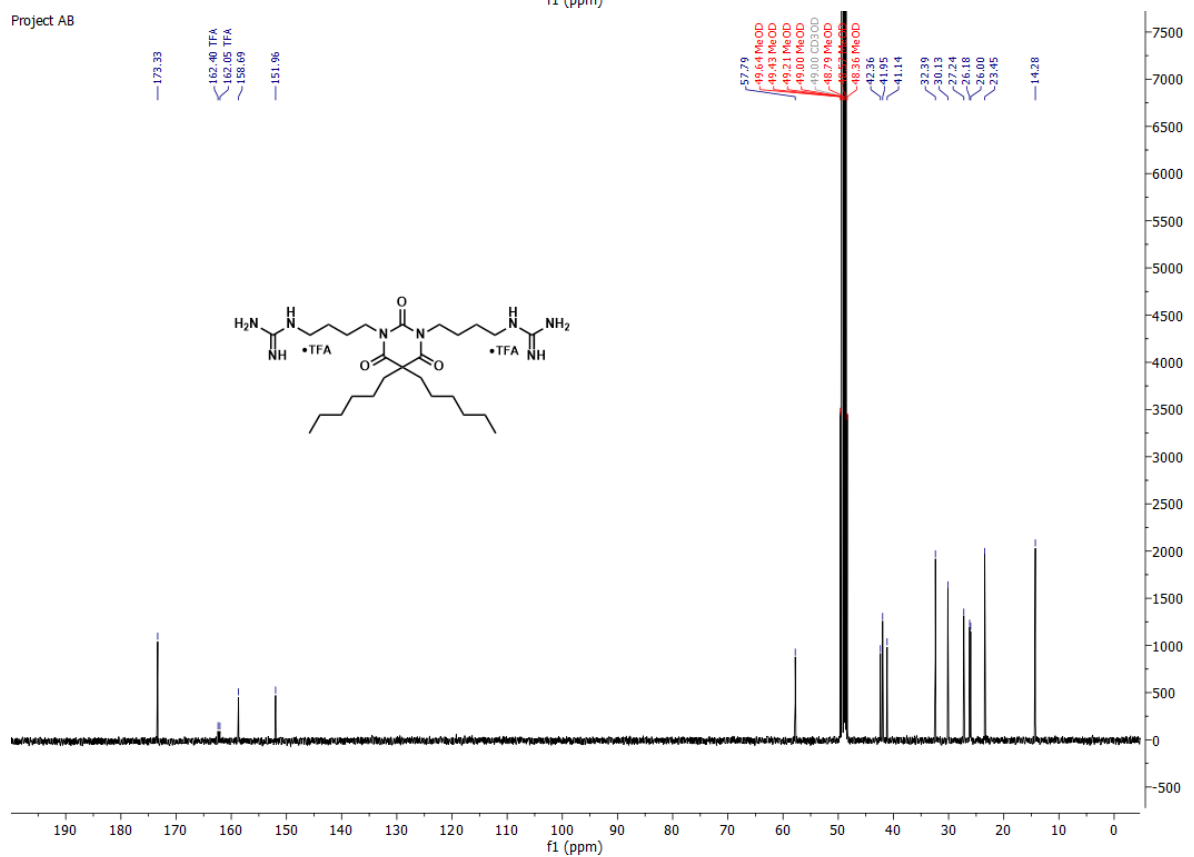


1,1'-((5,5-dihexyl-2,4,6-trioxodihydropyrimidine-1,3(2*H*,4*H*)-diyl)bis(butane-4,1-diyl)diguanidine di-TFA salt (**2cG**)

Project AB

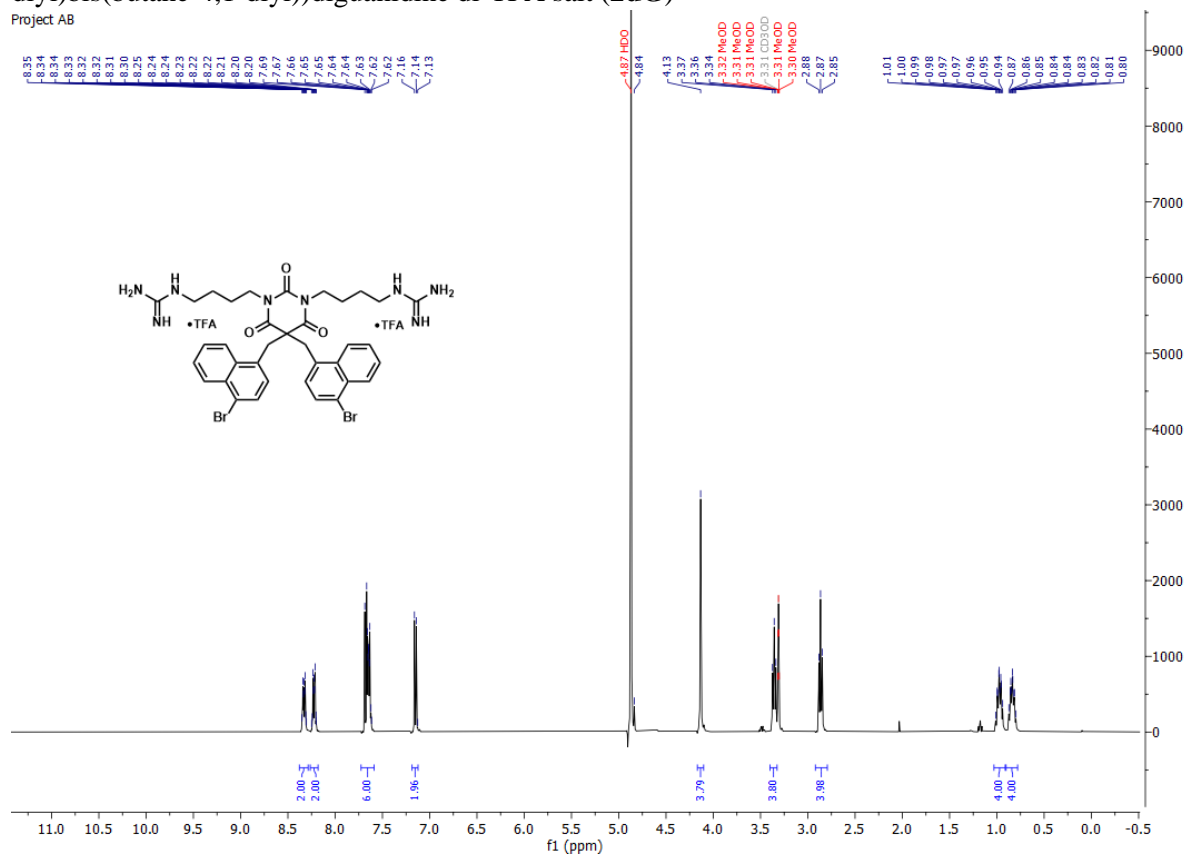


Project AB

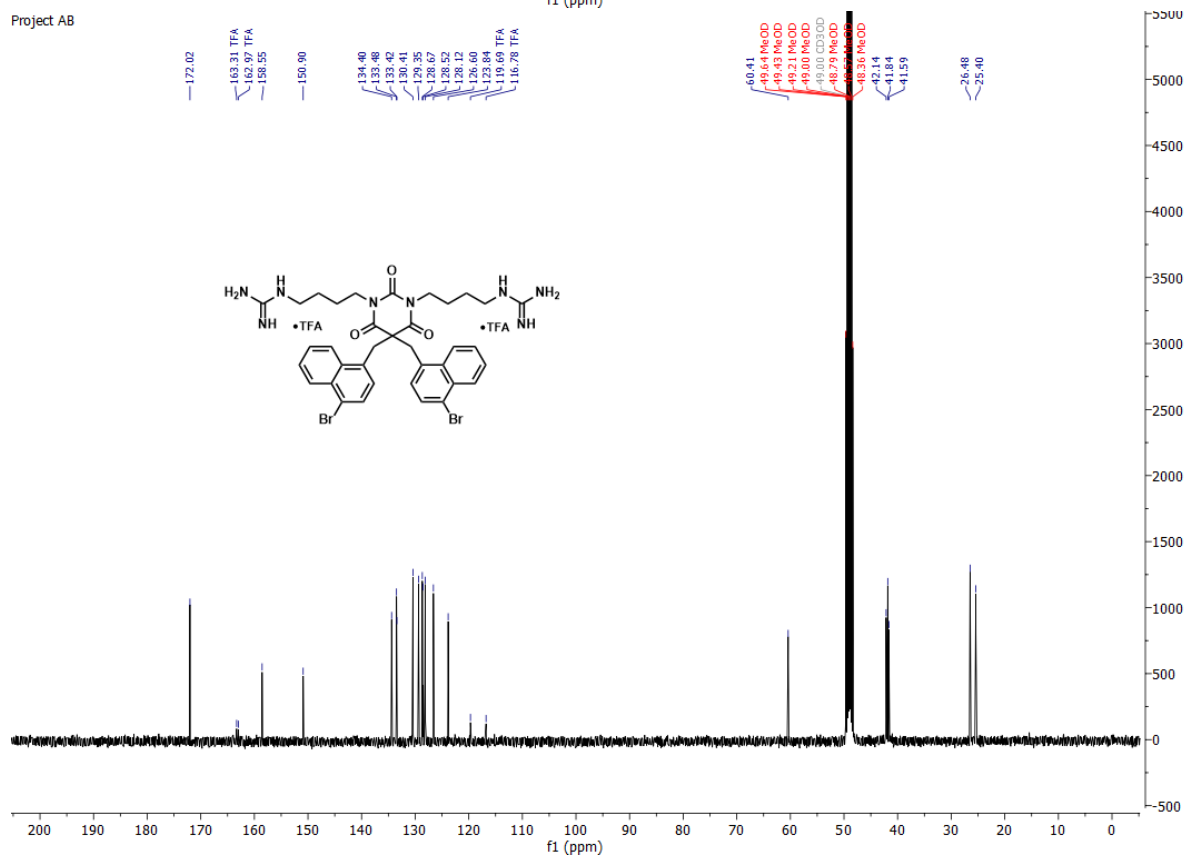


1,1'-((5,5-bis((4-bromonaphthalen-1-yl)methyl)-2,4,6-trioxodihydropyrimidine-1,3(2*H*,4*H*)-diyl)bis(butane-4,1-diyl)diguandine di-TFA salt (**2dG**)

Project AB

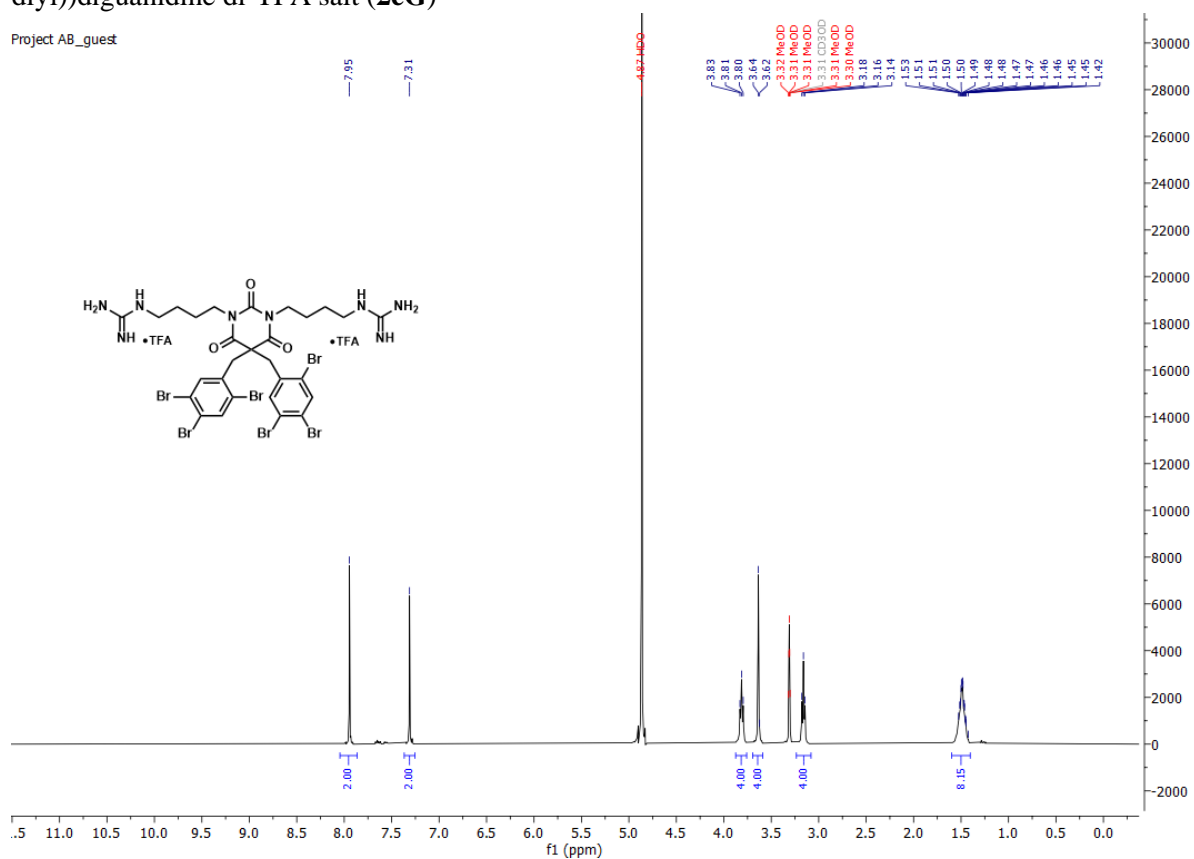


Project AB

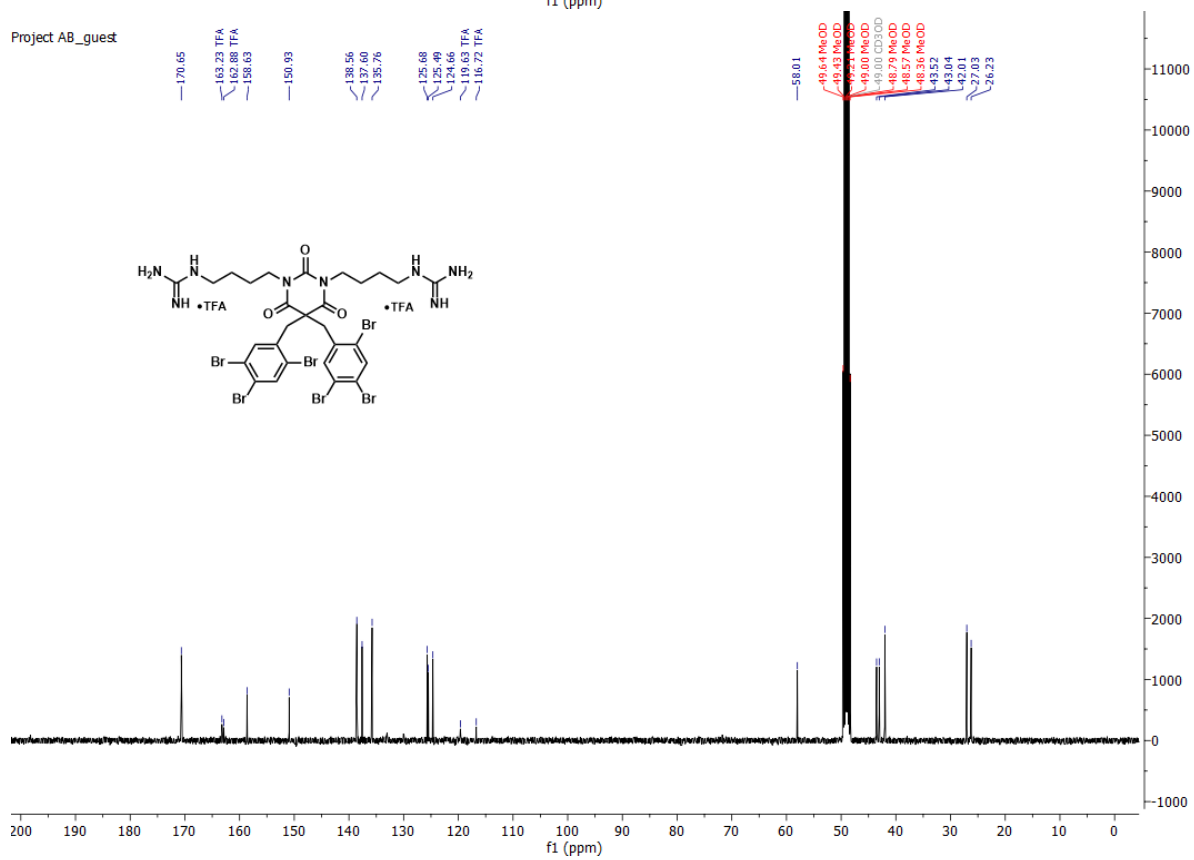


1,1'-((2,4,6-trioxo-5,5-bis(2,4,5-tribromobenzyl)dihydropyrimidine-1,3(2*H*,4*H*)-diyl)bis(butane-4,1-diyl))diguanidine di-TFA salt (**2eG**)

Project AB_guest

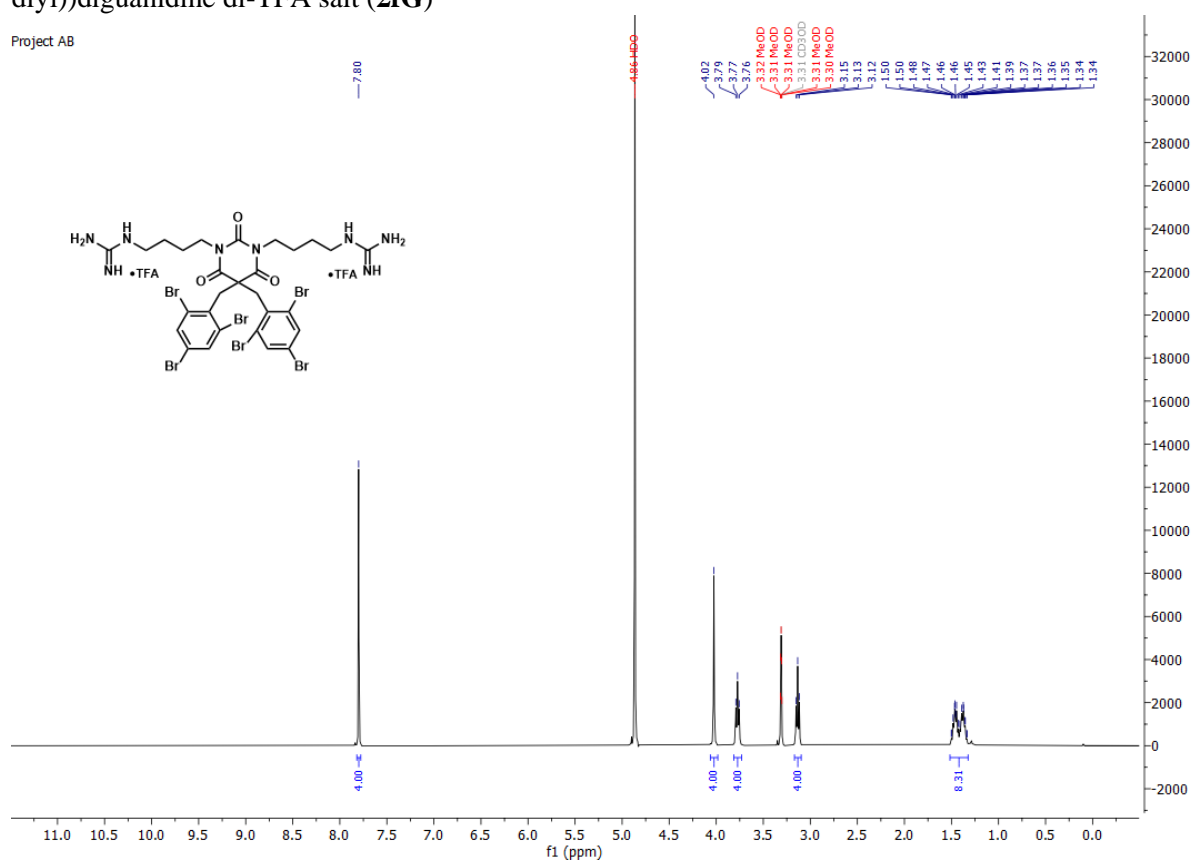


Project AB_guest

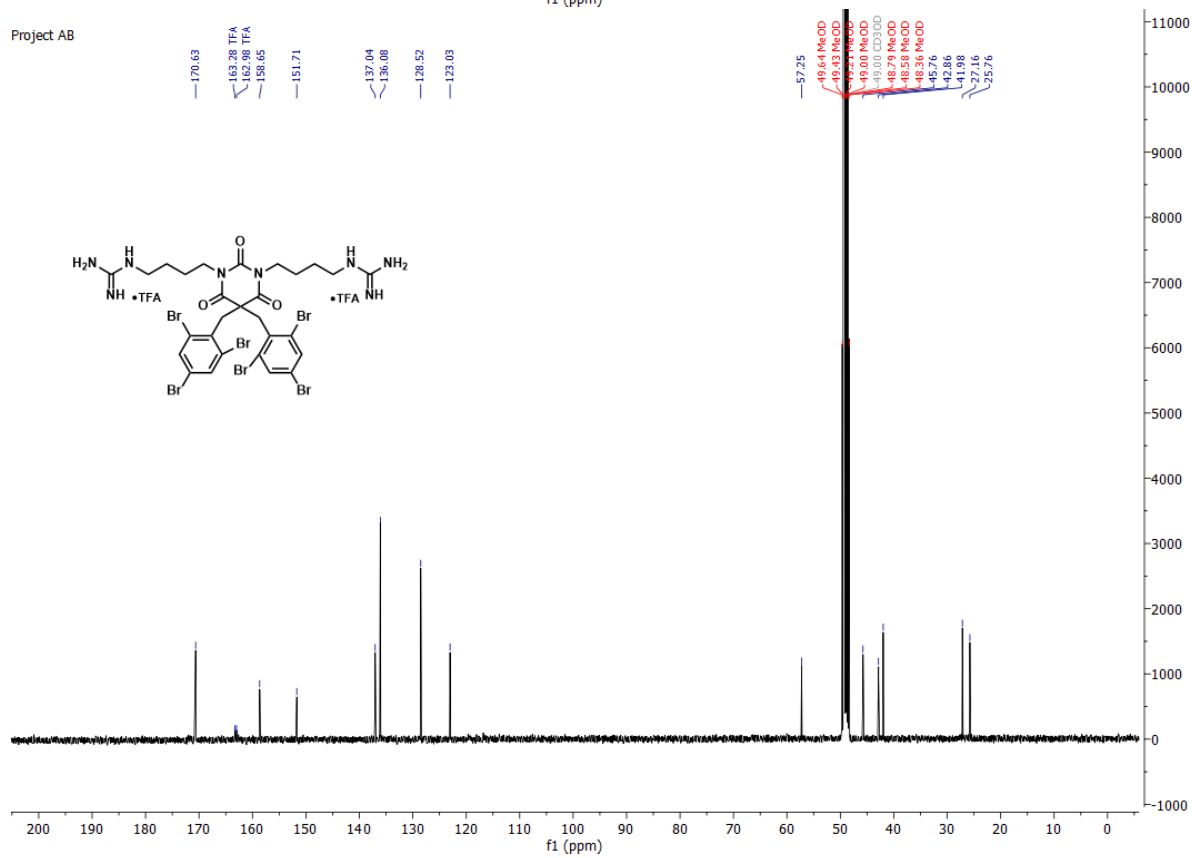


1,1'-((2,4,6-trioxo-5,5-bis(2,4,6-tribromobenzyl)dihydropyrimidine-1,3(2*H*,4*H*)-diyl)bis(butane-4,1-diyl))diguanidine di-TFA salt (**2fG**)

Project AB

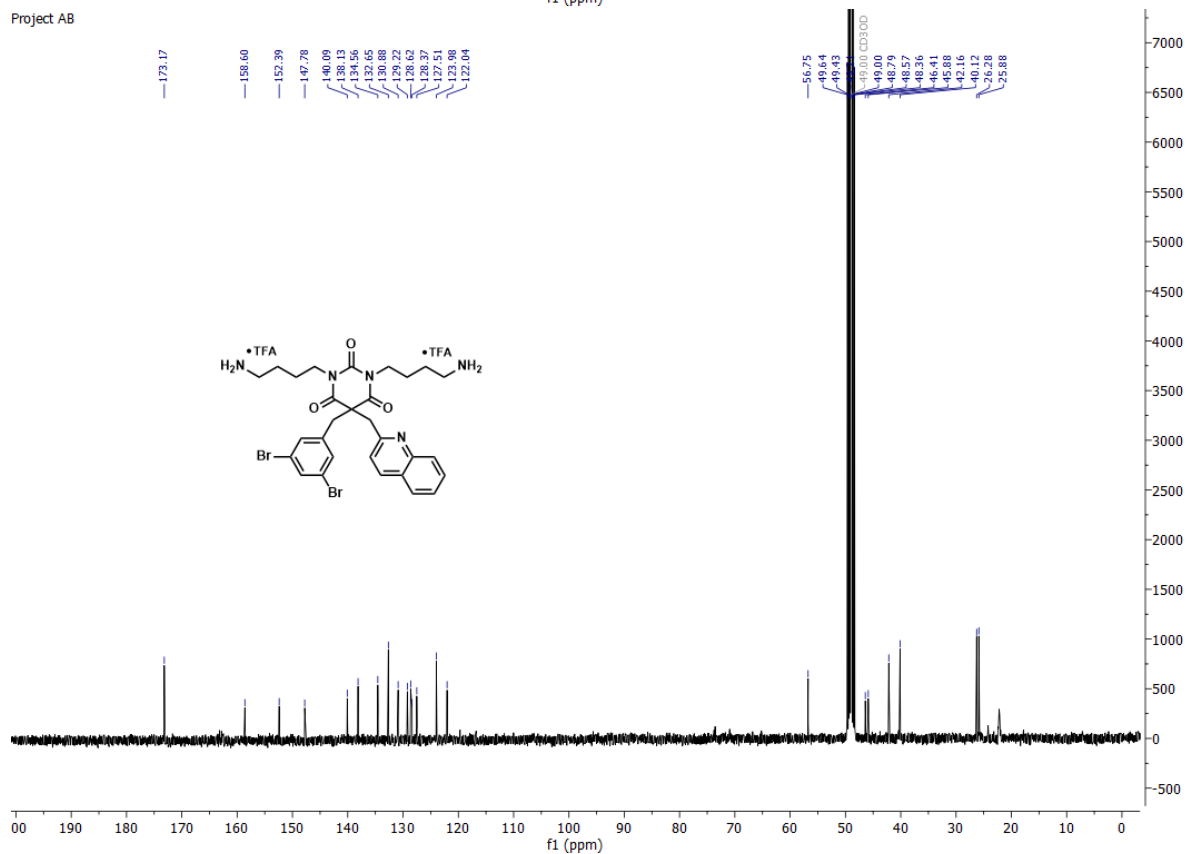
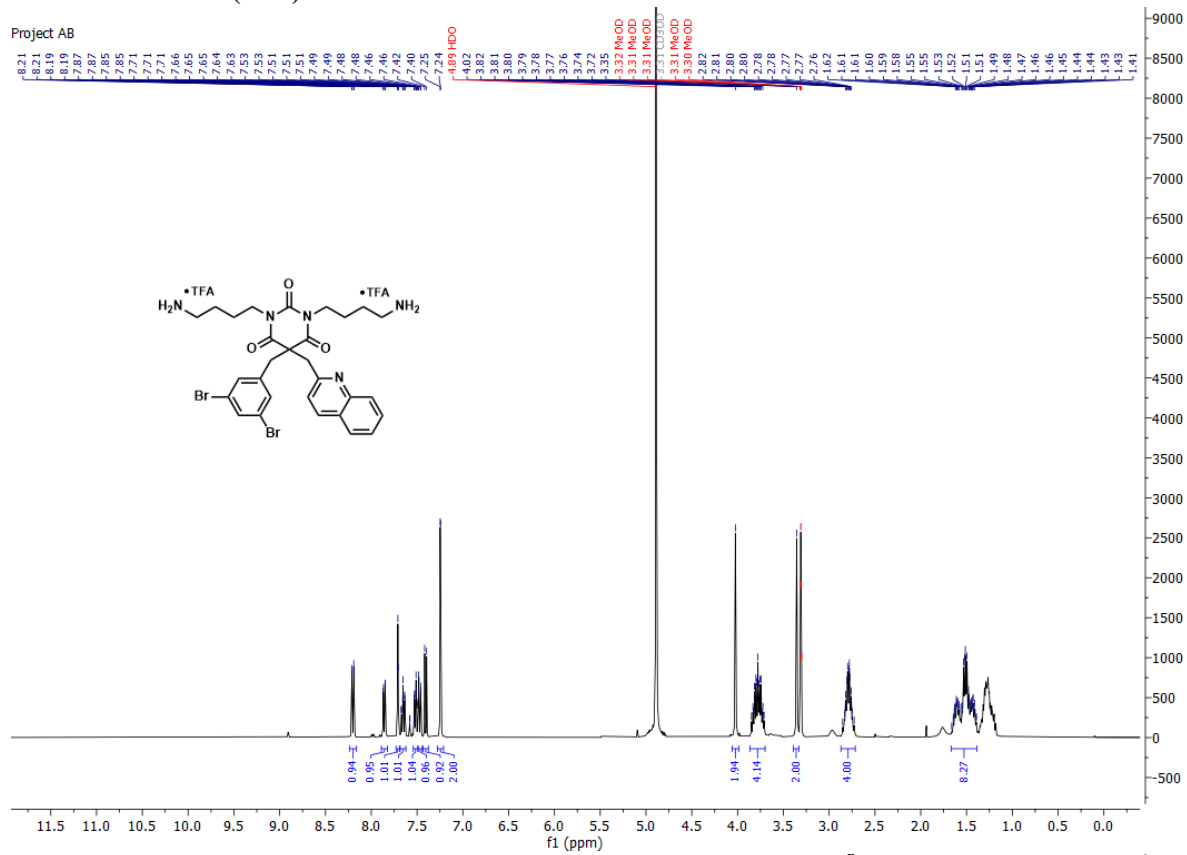


Project AB



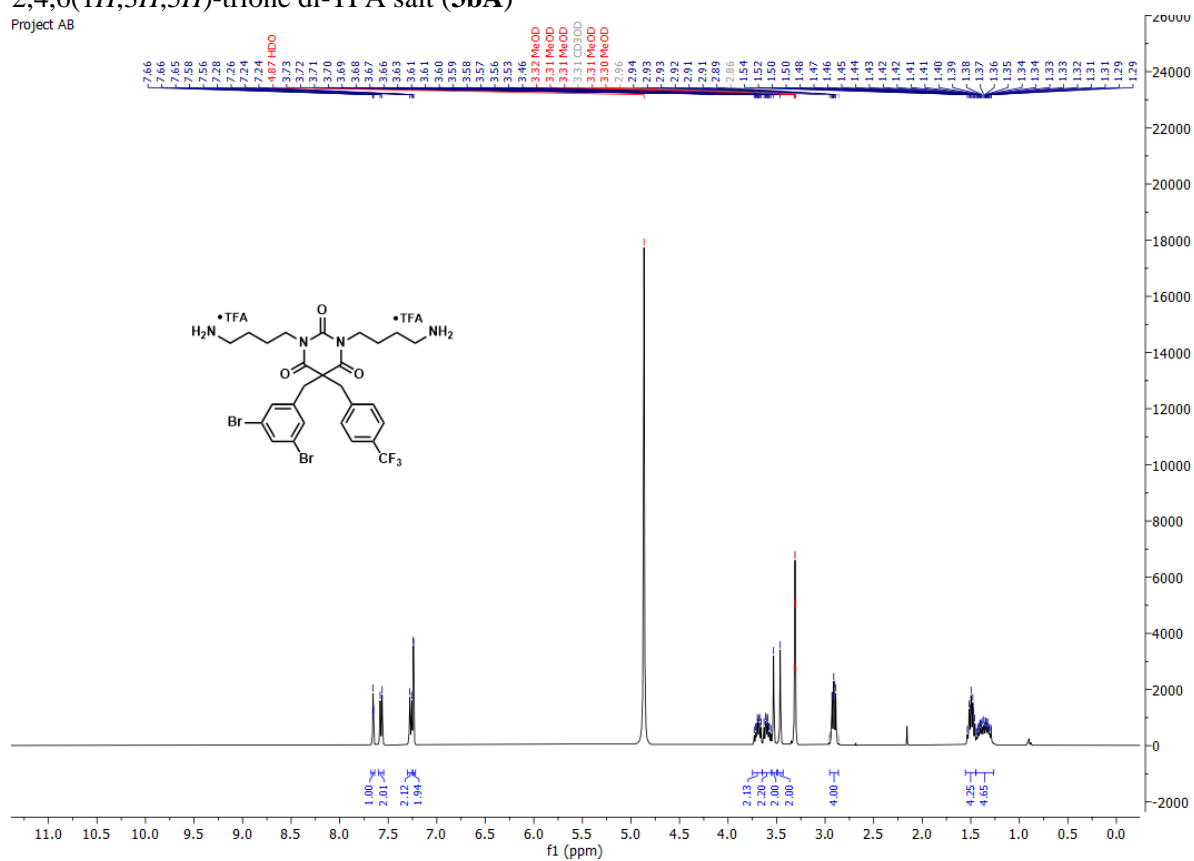
3.3 ^1H and ^{13}C NMR spectra of compounds in series 3

1,3-bis(4-aminobutyl)-5-(3,5-dibromobenzyl)-5-(quinolin-2-ylmethyl)pyrimidine-2,4,6(1*H*,3*H*,5*H*)-trione di-TFA salt (**3aA**)

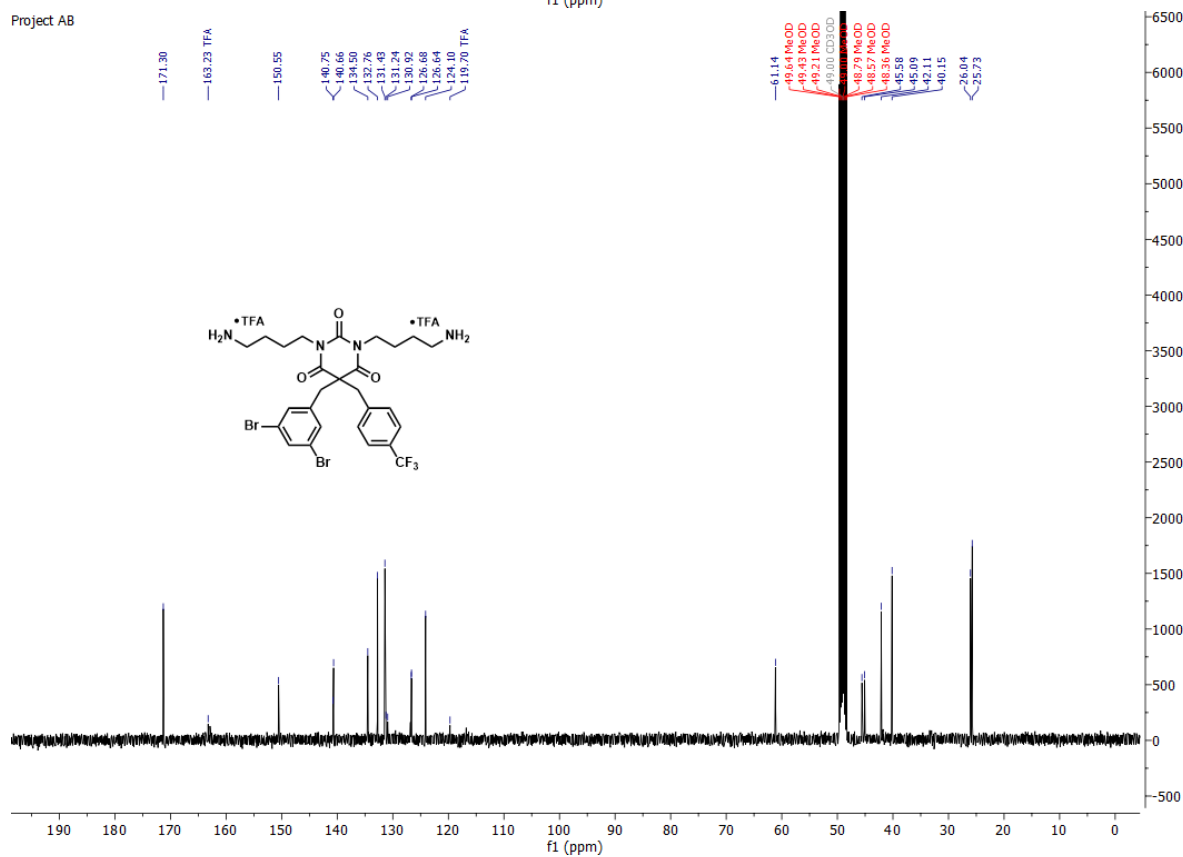


1,3-bis(4-aminobutyl)-5-(3,5-dibromobenzyl)-5-(4-(trifluoromethyl)benzyl)pyrimidine-2,4,6(1*H*,3*H*,5*H*)-trione di-TFA salt (**3bA**)

Project AB

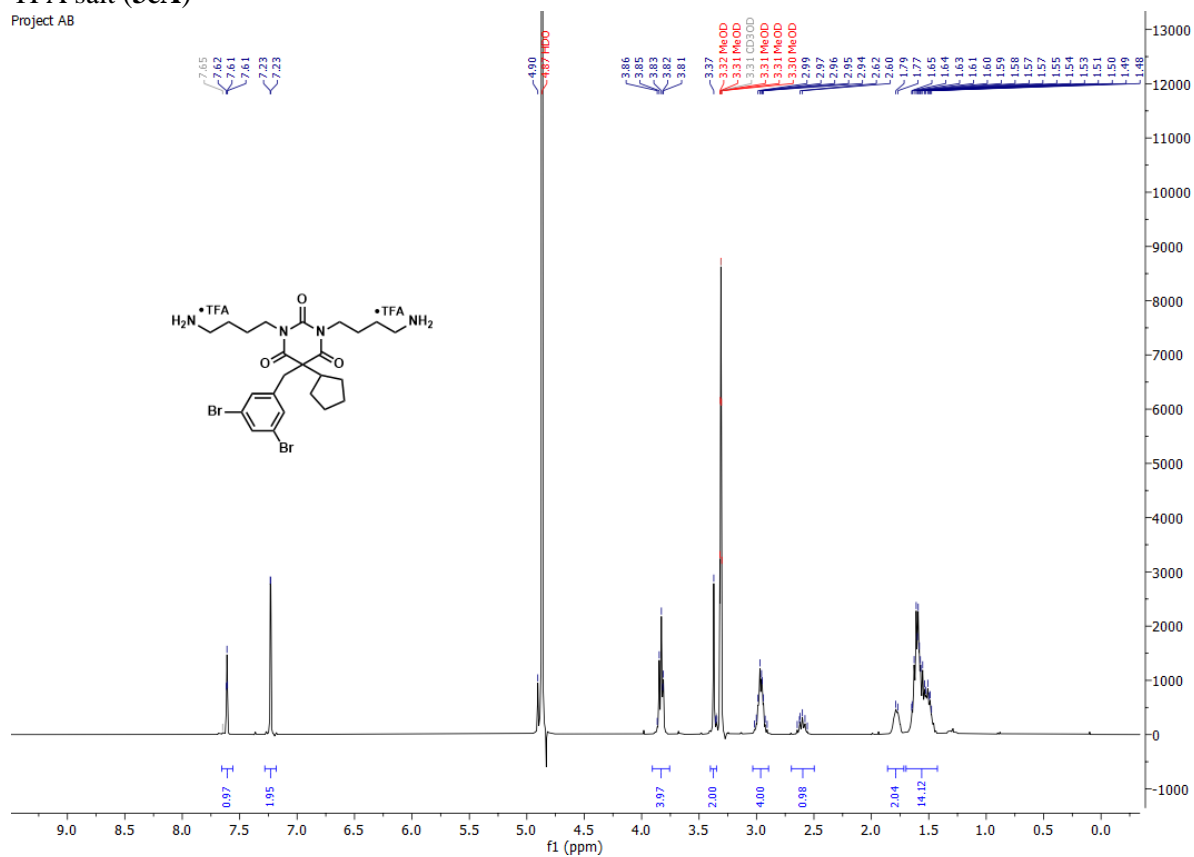


Project AB

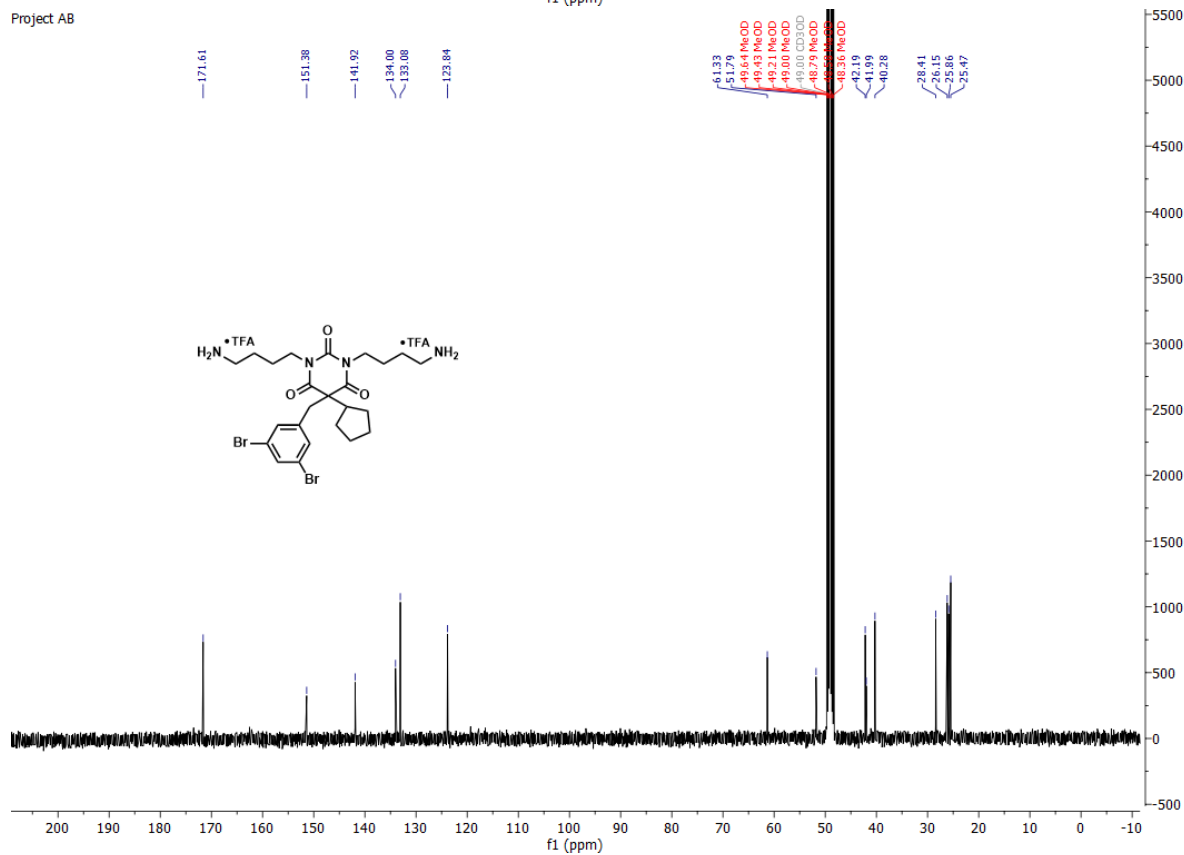


1,3-bis(4-aminobutyl)-5-cyclopentyl-5-(3,5-dibromobenzyl)pyrimidine-2,4,6(1*H*,3*H*,5*H*)-trione di-TFA salt (**3cA**)

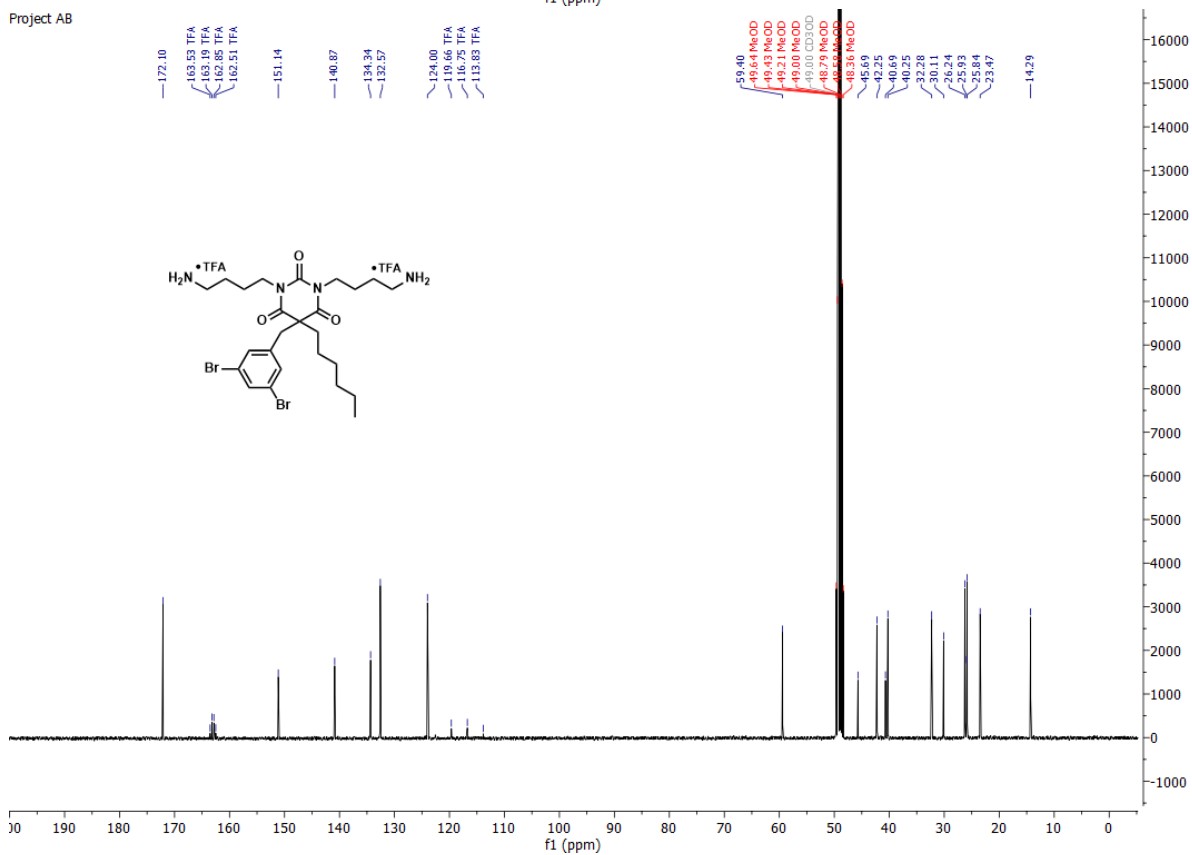
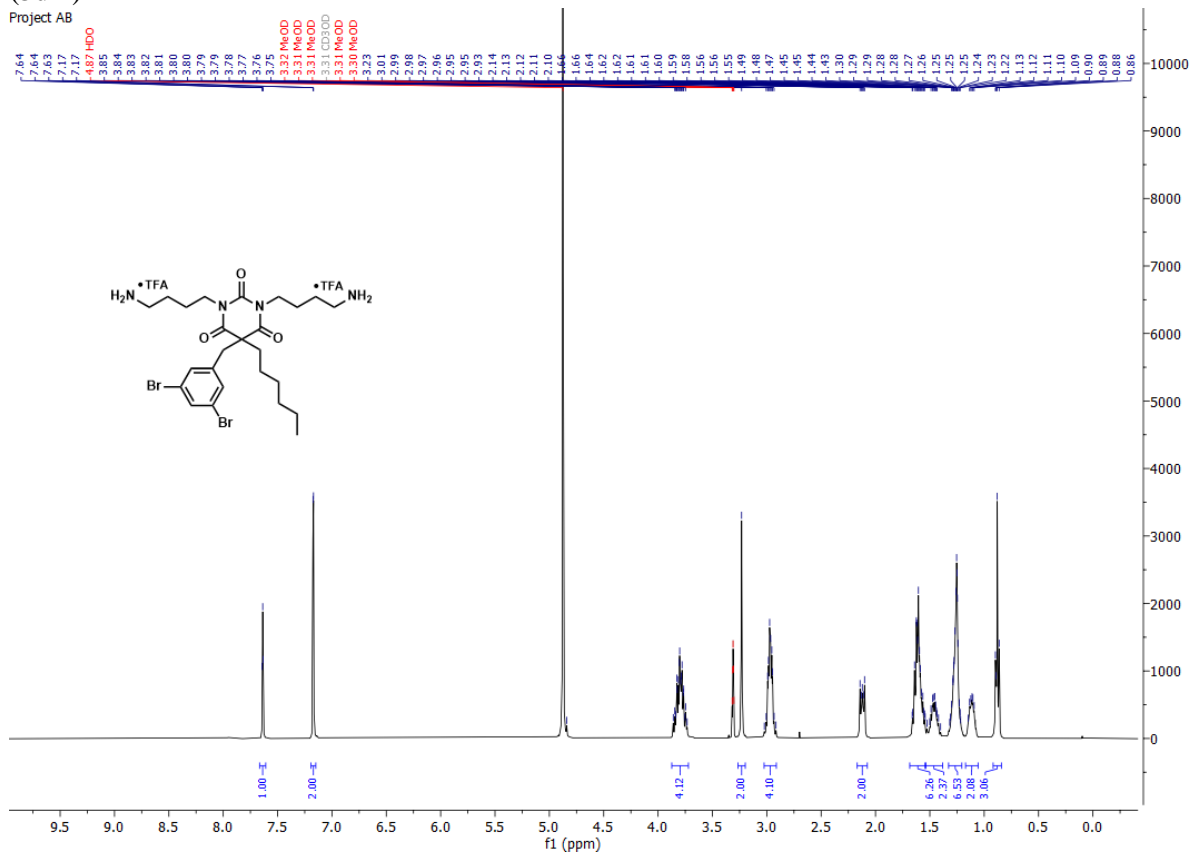
Project AB



Project AB

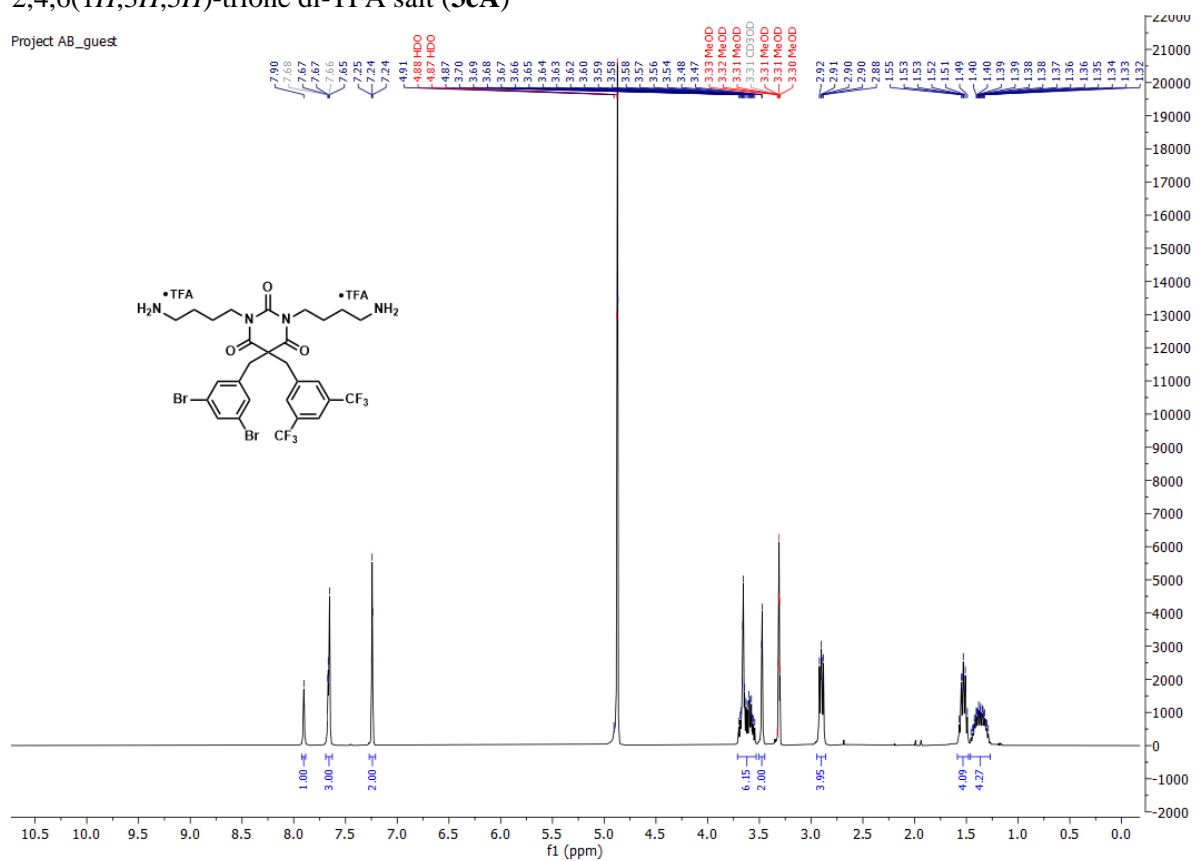


1,3-bis(4-aminobutyl)-5-(3,5-dibromobenzyl)-5-hexylpyrimidine-2,4,6(1*H*,3*H*,5*H*)-trione di-TFA salt
(3dA)

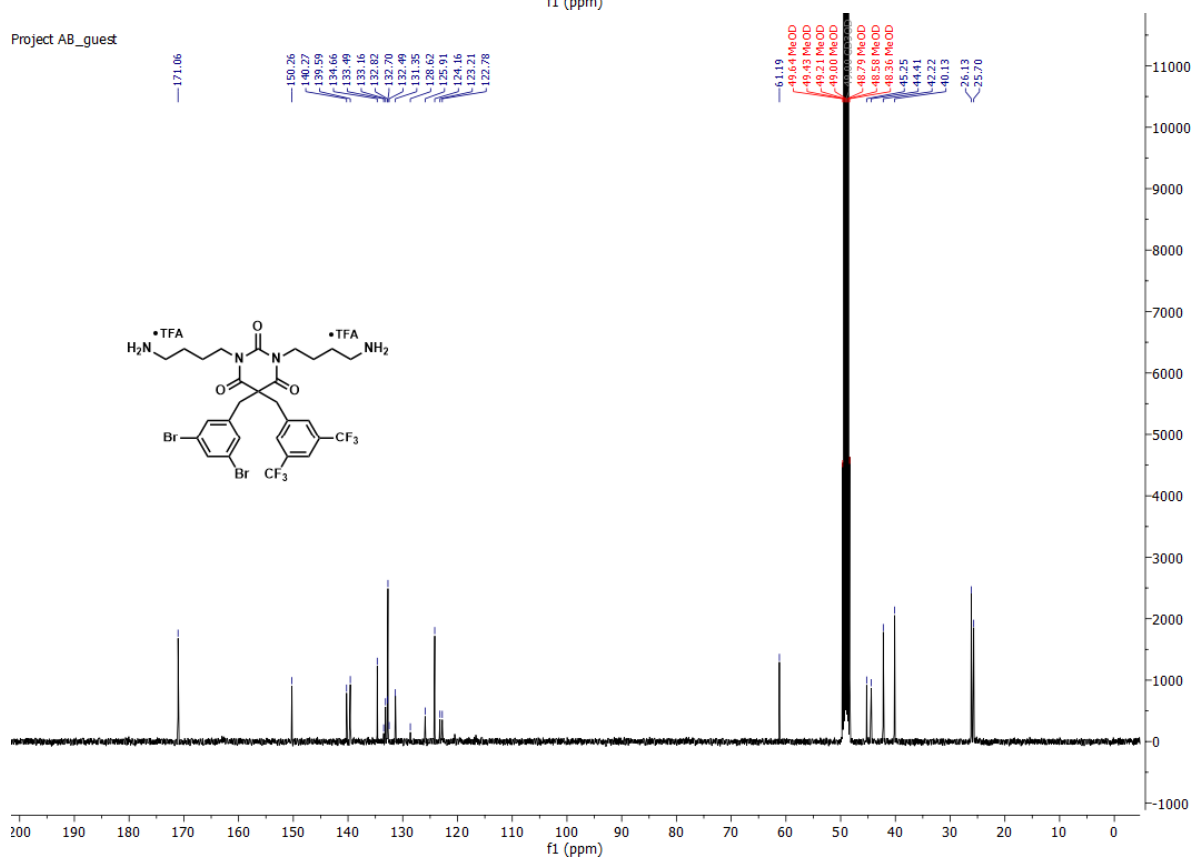


1,3-bis(4-aminobutyl)-5-(3,5-bis(trifluoromethyl)benzyl)-5-(3,5-dibromobenzyl)pyrimidine-2,4,6(1*H*,3*H*,5*H*)-trione di-TFA salt (**3eA**)

Project AB_guest

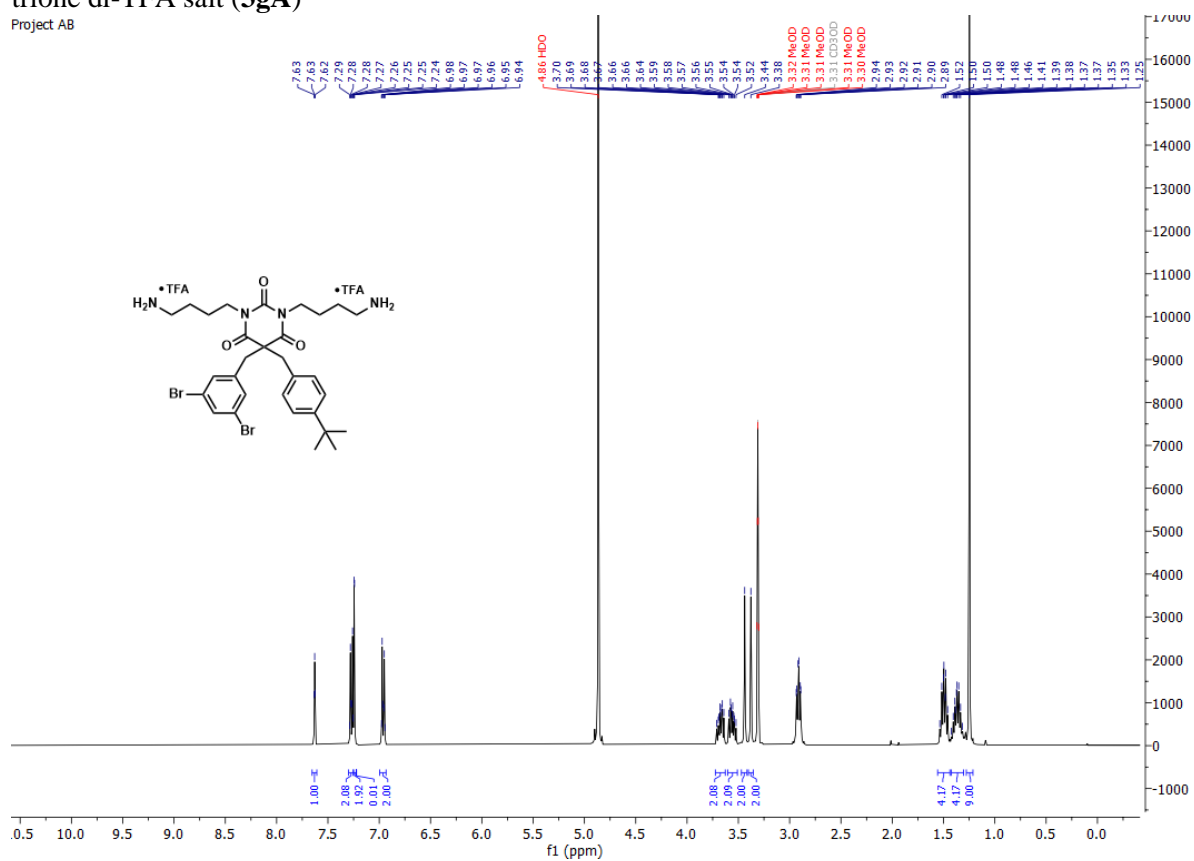


Project AB_guest

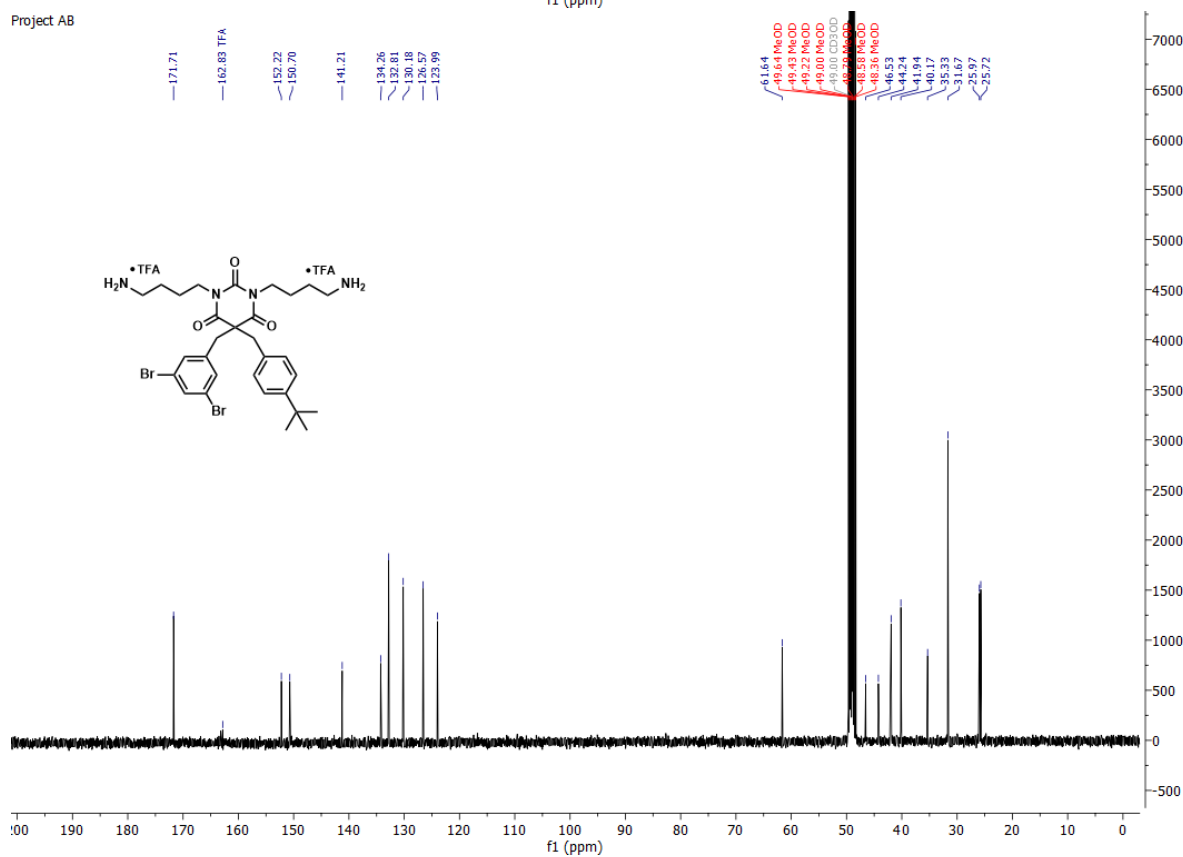


1,3-bis(4-aminobutyl)-5-(4-(*tert*-butyl)benzyl)-5-(3,5-dibromobenzyl)pyrimidine-2,4,6(1*H*,3*H*,5*H*)-trione di-TFA salt (**3gA**)

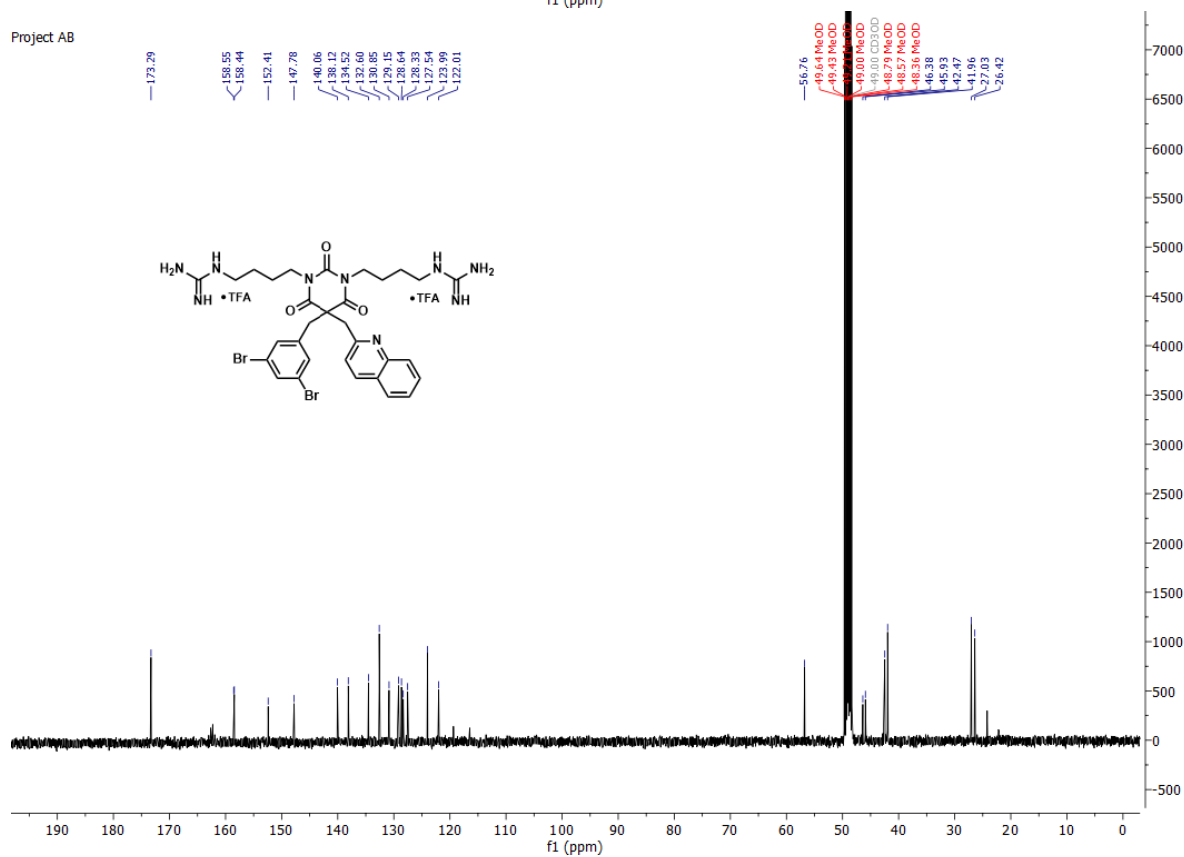
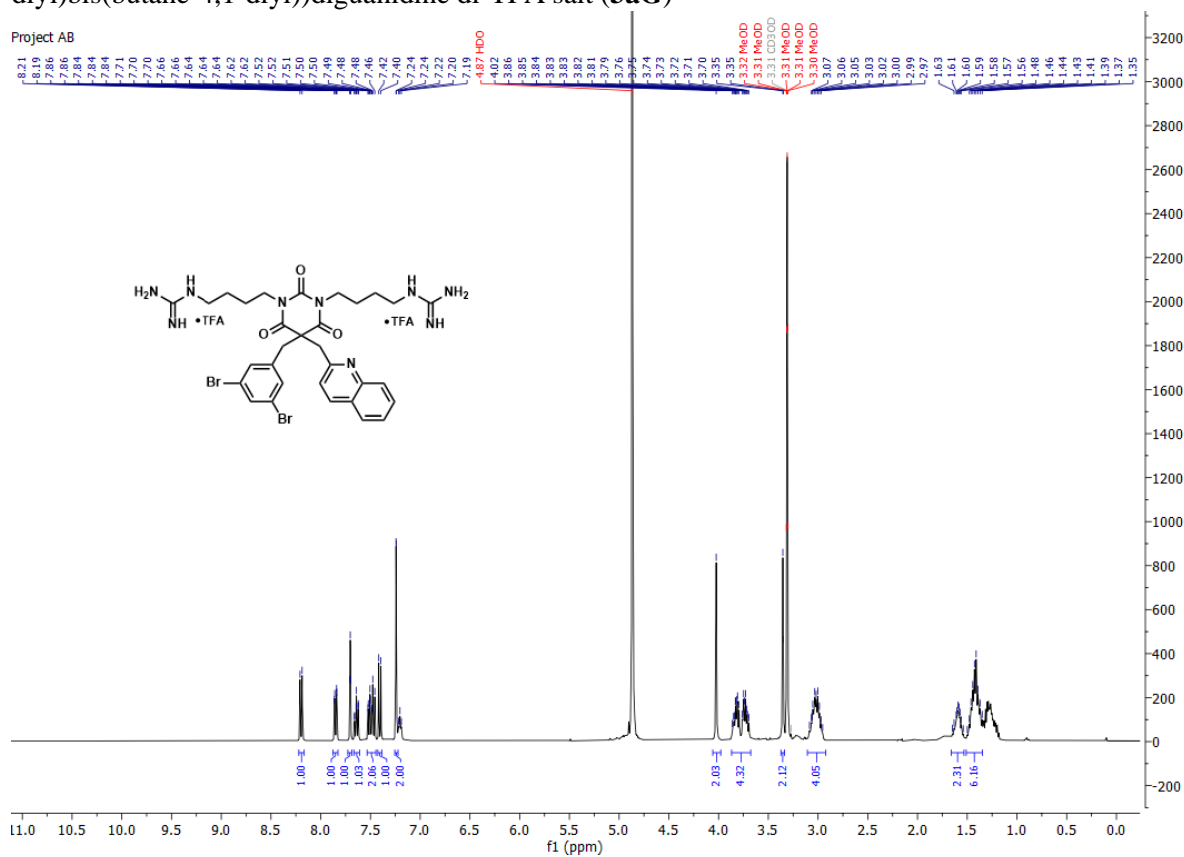
Project AB



Project AB

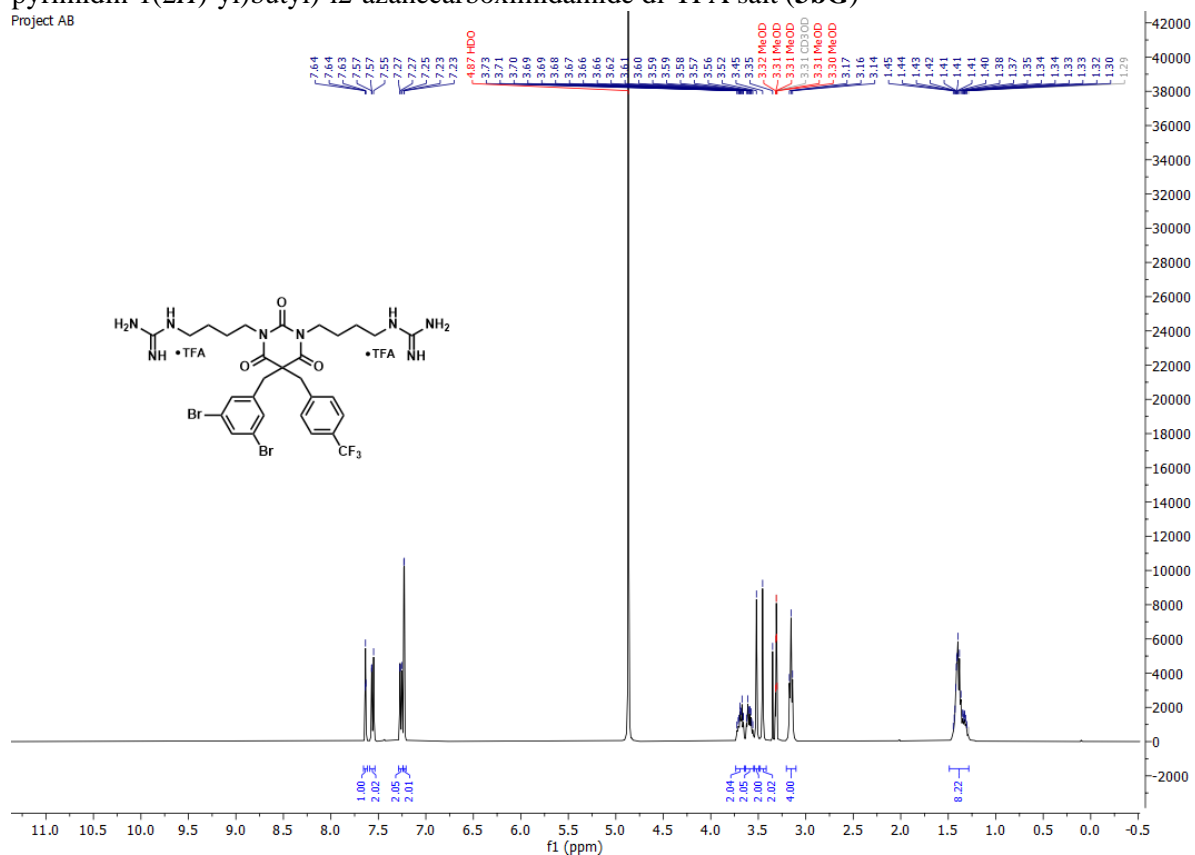


1,1'-((5-(3,5-dibromobenzyl)-2,4,6-trioxo-5-(quinolin-2-ylmethyl) dihydropyrimidine-1,3(2H,4H)-diyl)bis(butane-4,1-diyl)diguandine di-TFA salt (**3aG**)

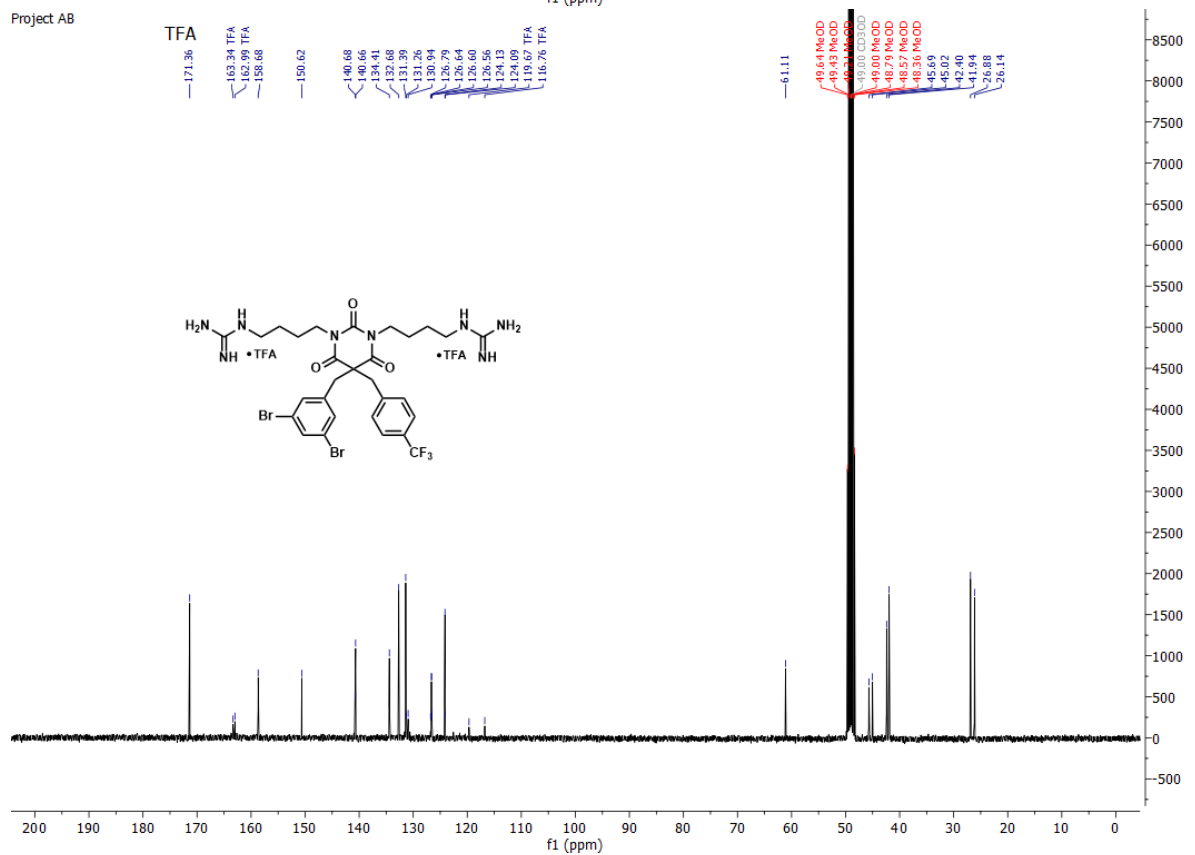


(4-(5-(3,5-dibromobenzyl)-3-(4-guanidinobutyl)-2,4,6-trioxo-5-(4-(trifluoromethyl)benzyl)tetrahydro-pyrimidin-1(2H)-yl)butyl)-1,2-azancarboximidamide di-TFA salt (**3bG**)

Project AB

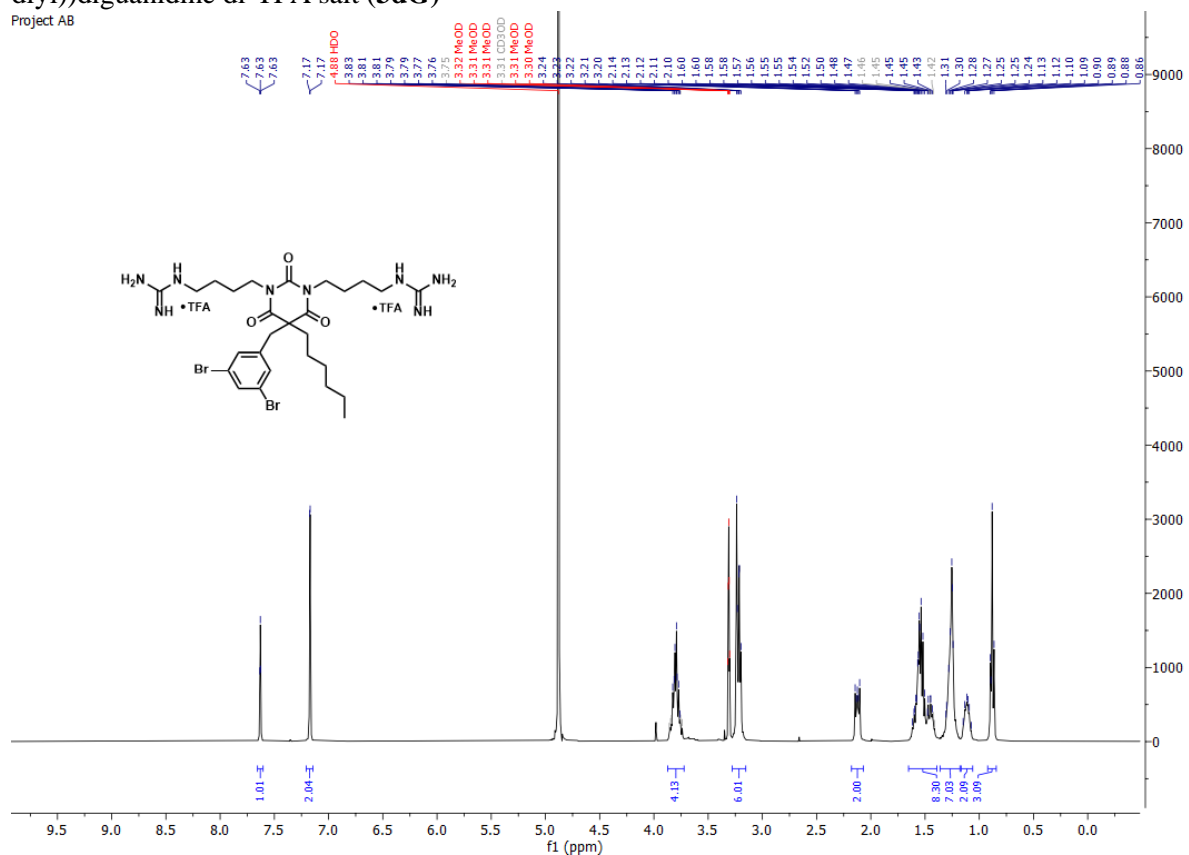


Project AB

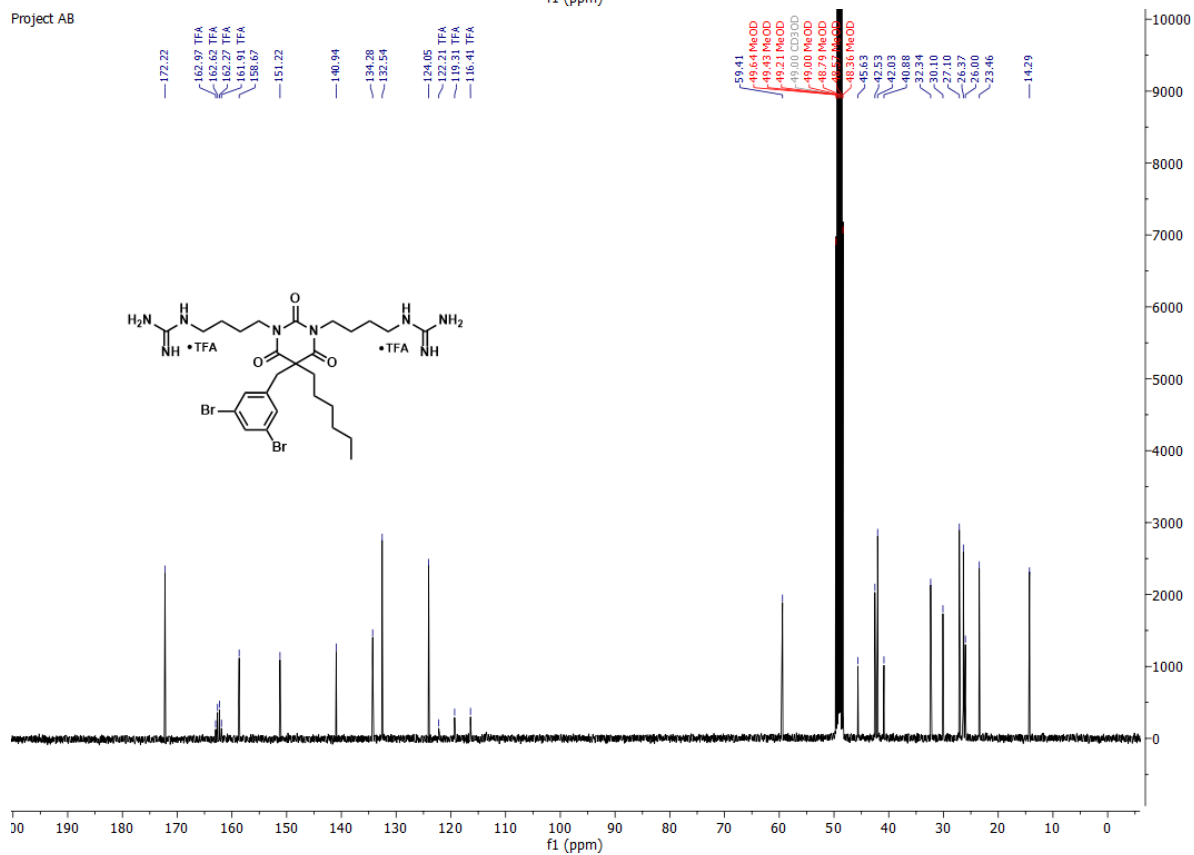


1,1'-((5-(3,5-dibromobenzyl)-5-hexyl-2,4,6-trioxodihydropyrimidine-1,3(2H,4H)-diyl)bis(butane-4,1-diy))diguanidine di-TFA salt (**3dG**)

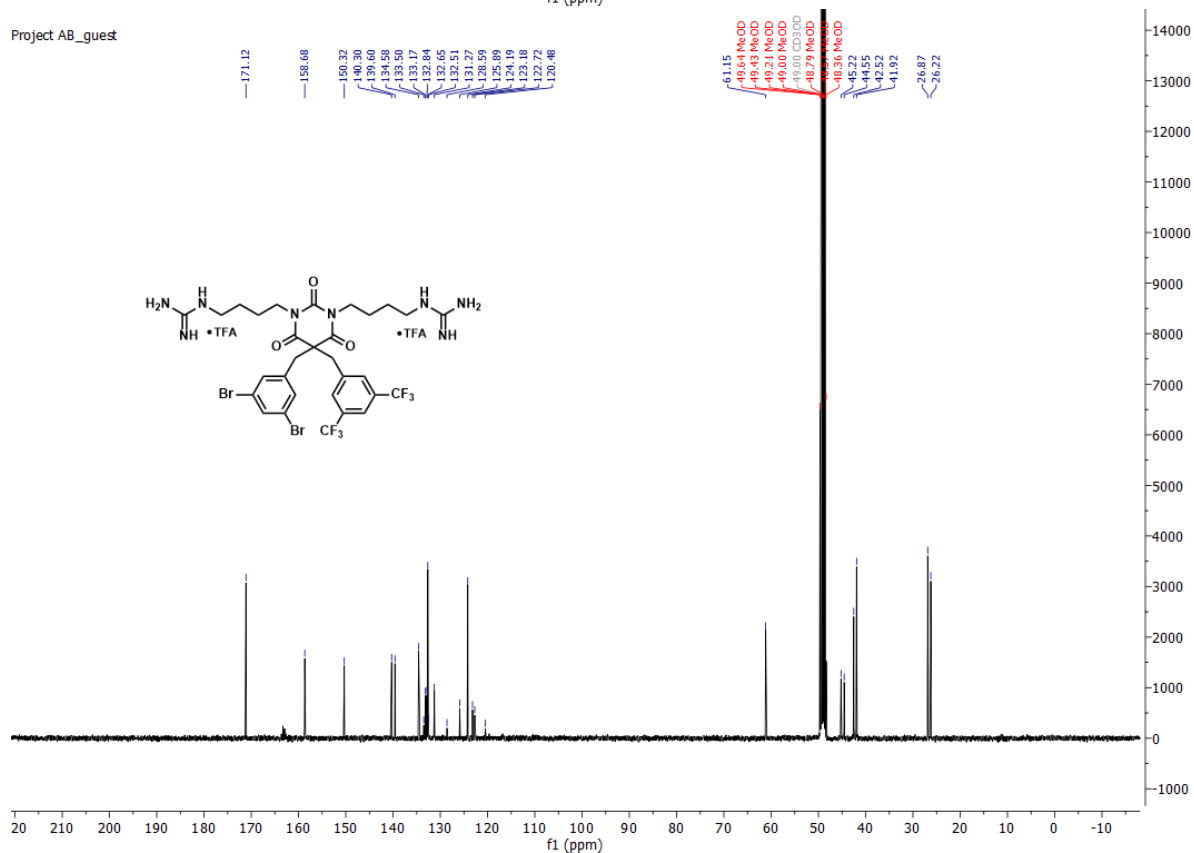
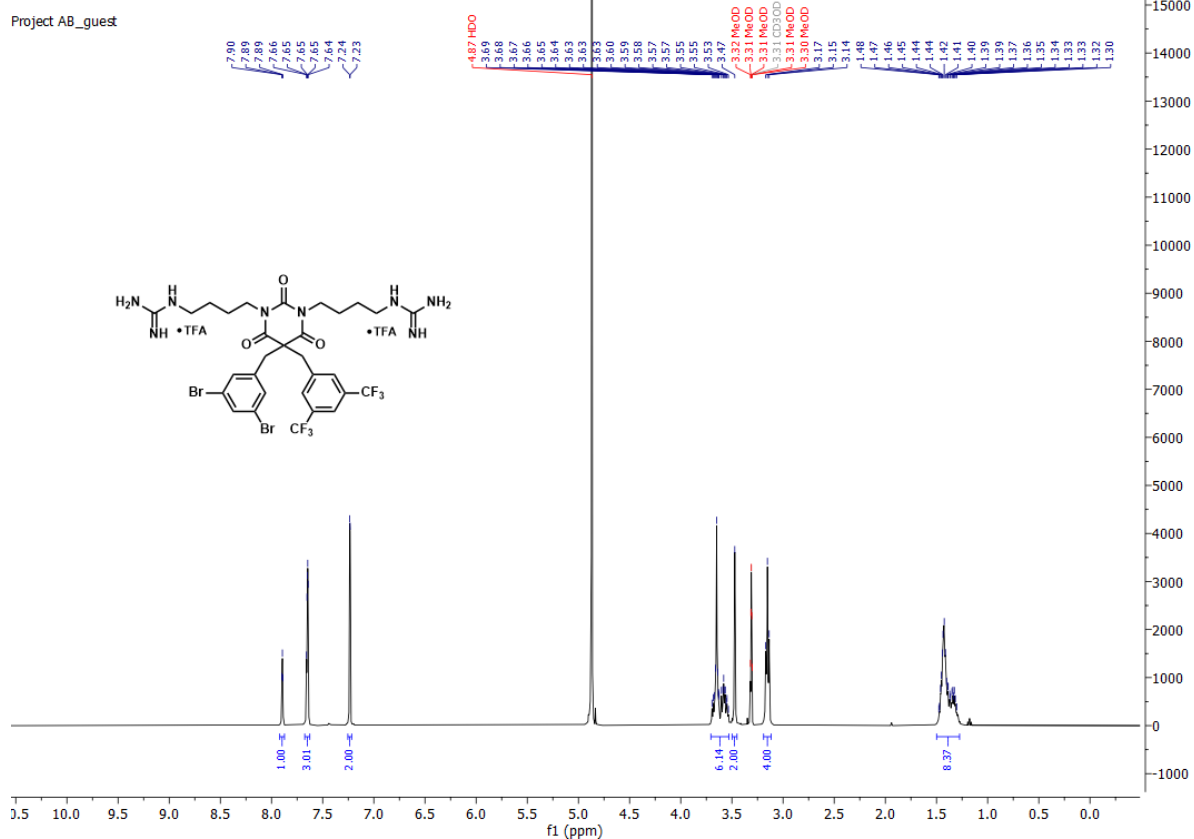
Project AB



Project AB

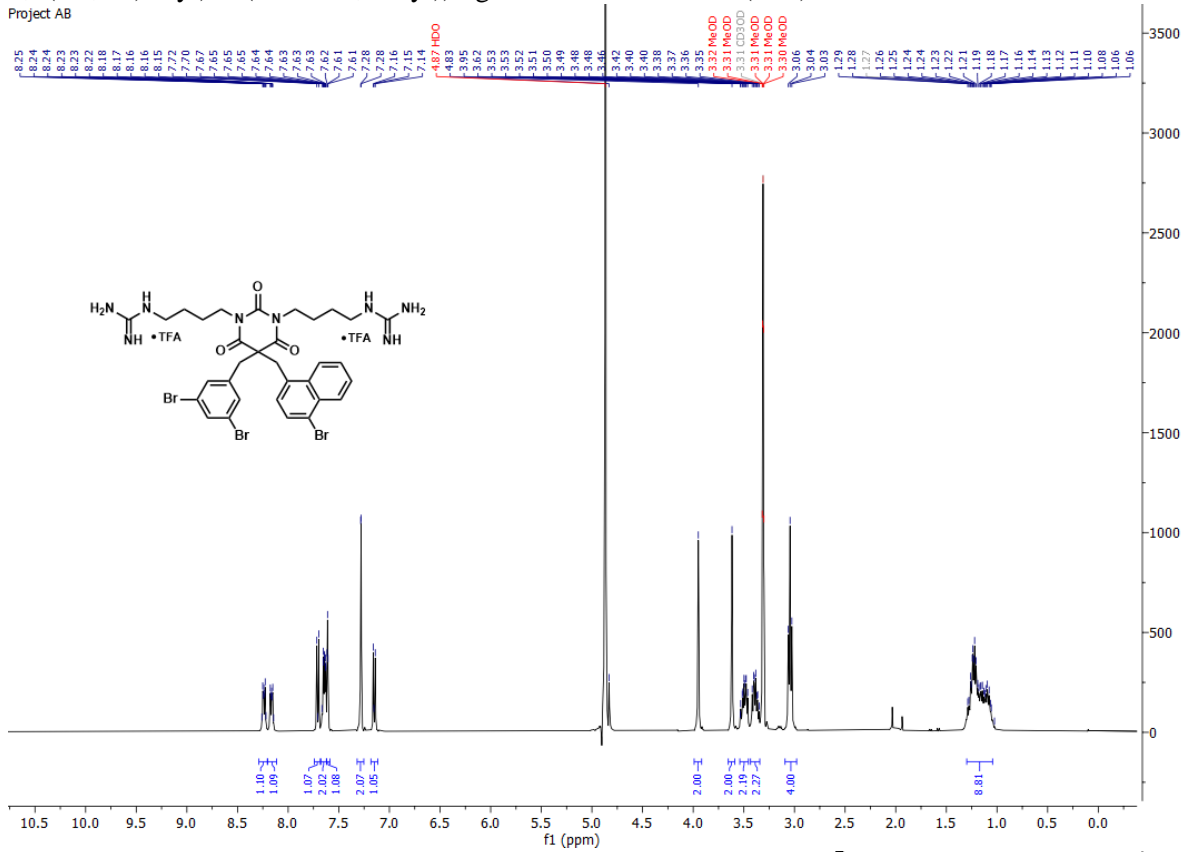


1,1'-((5-(3,5-bis(trifluoromethyl)benzyl)-5-(3,5-dibromobenzyl)-2,4,6-trioxodihydropyrimidine-1,3(2*H*,4*H*)-diyl)bis(butane-4,1-diyl)diguanidine di-TFA salt (**3eG**)



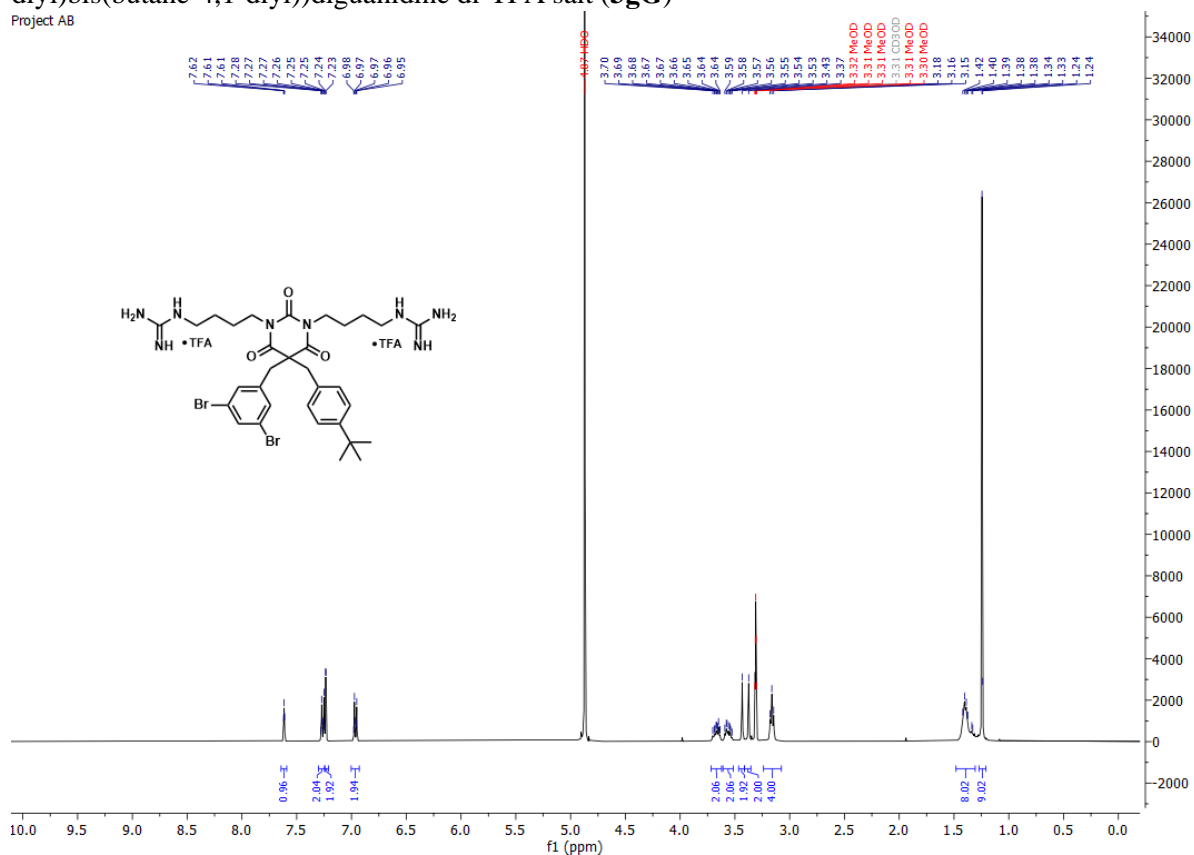
1,1'-((5-((4-bromonaphthalen-1-yl)methyl)-5-(3,5-dibromobenzyl)-2,4,6-trioxodihydropyrimidine-1,3(2*H*,4*H*)-diyl)bis(butane-4,1-diyl)diguandine di-TFA salt (**3fG**)

Project AB

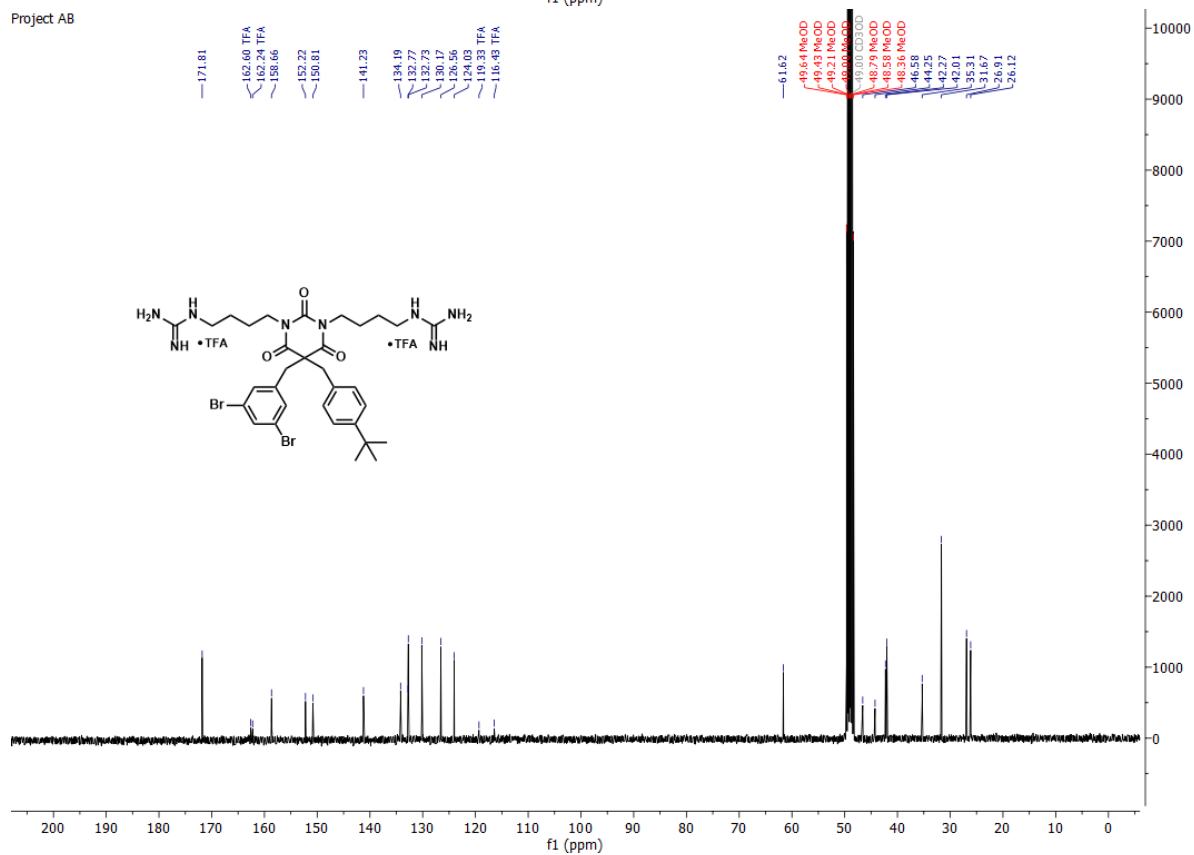


1,1'-((5-(4-*tert*-butylbenzyl)-5-(3,5-dibromobenzyl)-2,4,6-trioxodihydropyrimidine-1,3(2*H*,4*H*)-diyl)bis(butane-4,1-diyl)diguandine di-TFA salt (**3gG**)

Project AB



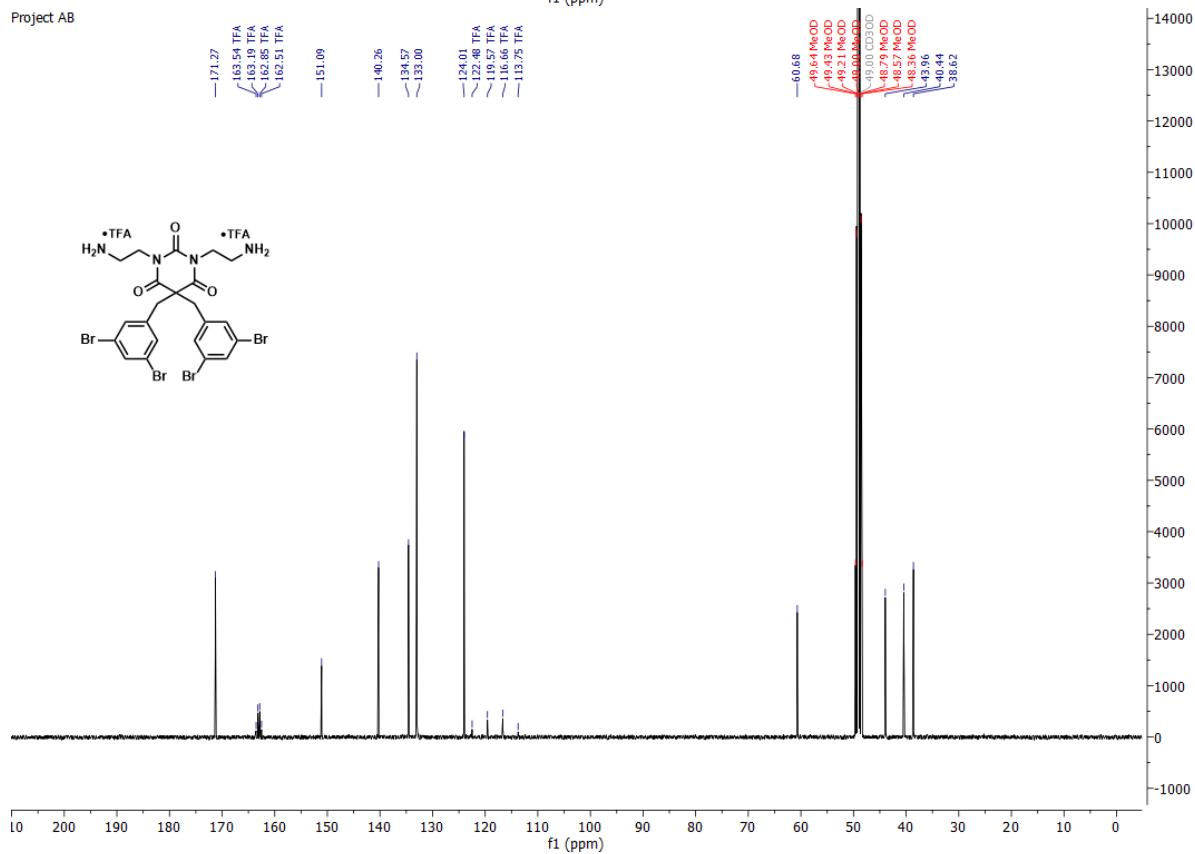
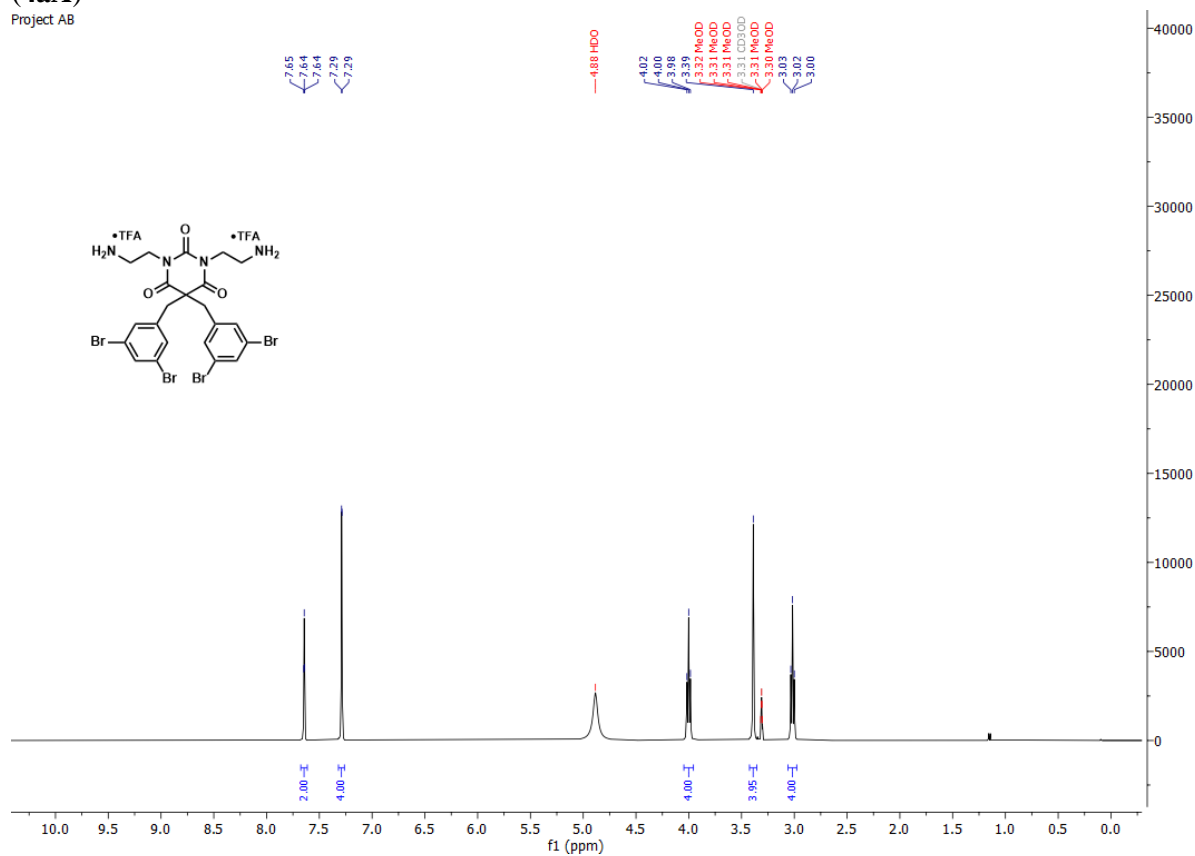
Project AB



3.4 ^1H and ^{13}C NMR spectra of compounds in series 4

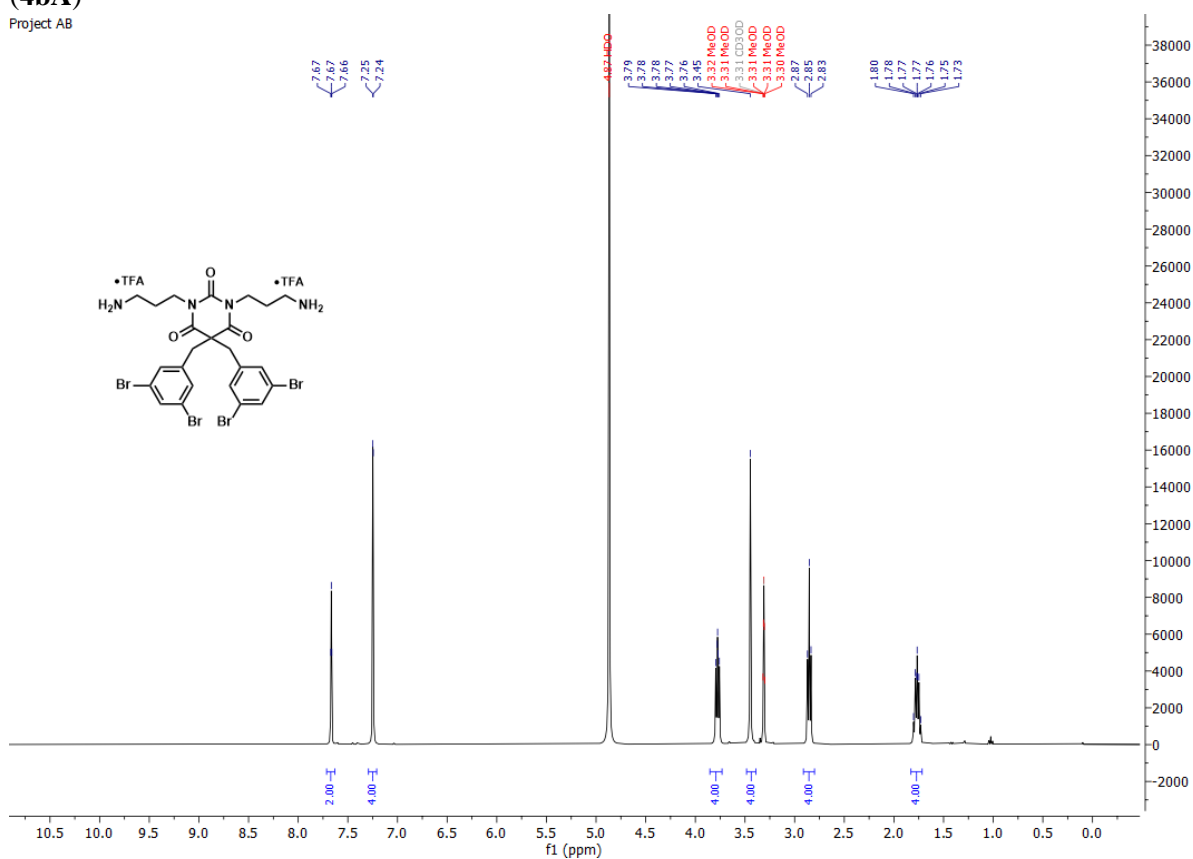
1,3-bis(2-aminoethyl)-5,5-bis(3,5-dibromobenzyl)pyrimidine-2,4,6(1*H*,3*H*,5*H*)-trione di-TFA salt (**4aA**)

Project AB

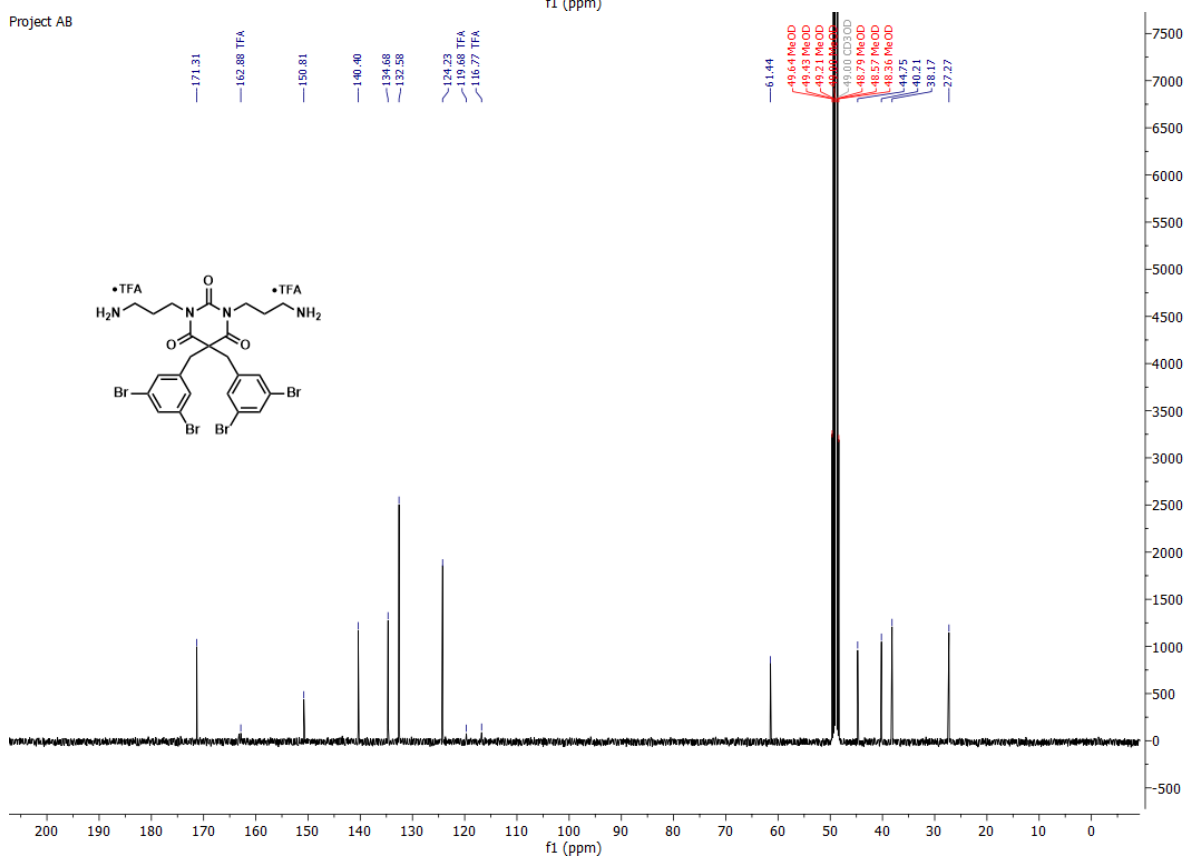


1,3-bis(3-aminopropyl)-5,5-bis(3,5-dibromobenzyl)pyrimidine-2,4,6(1*H*,3*H*,5*H*)-trione di-TFA salt
(4bA)

Project AB

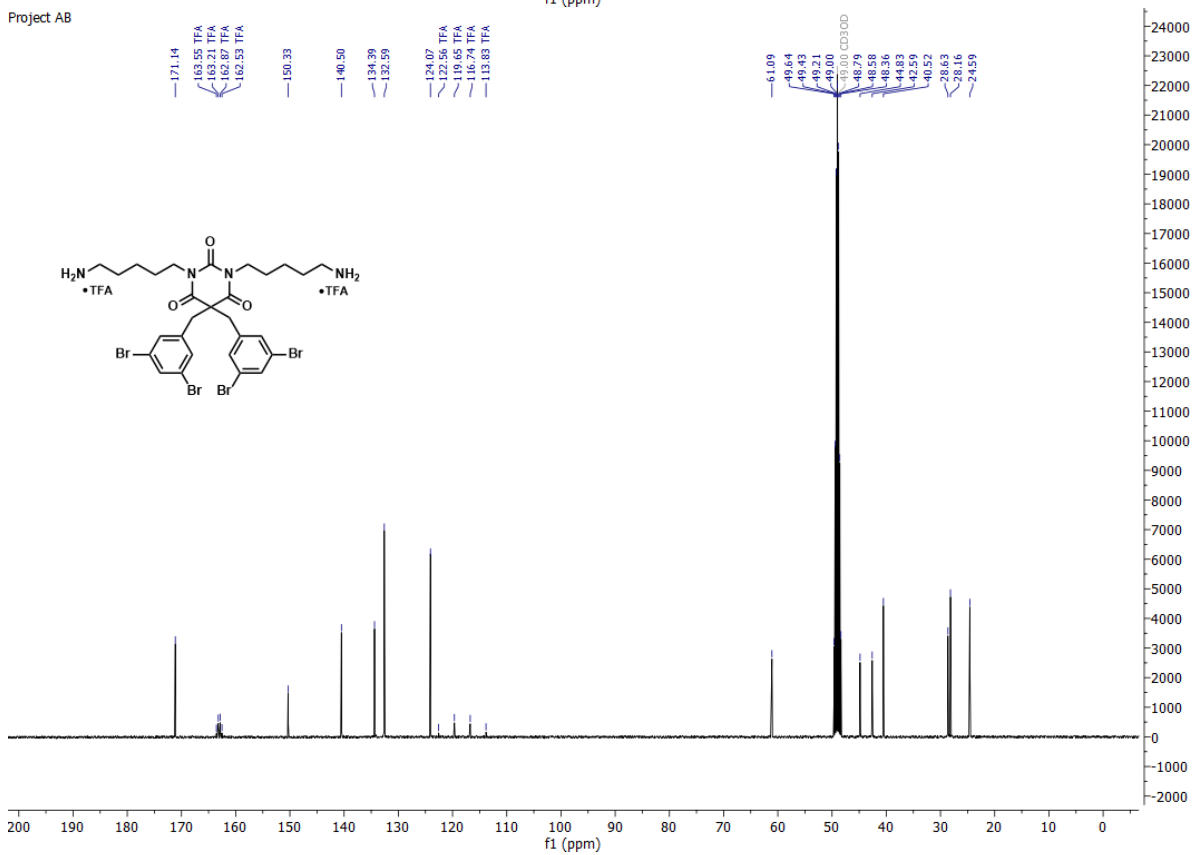
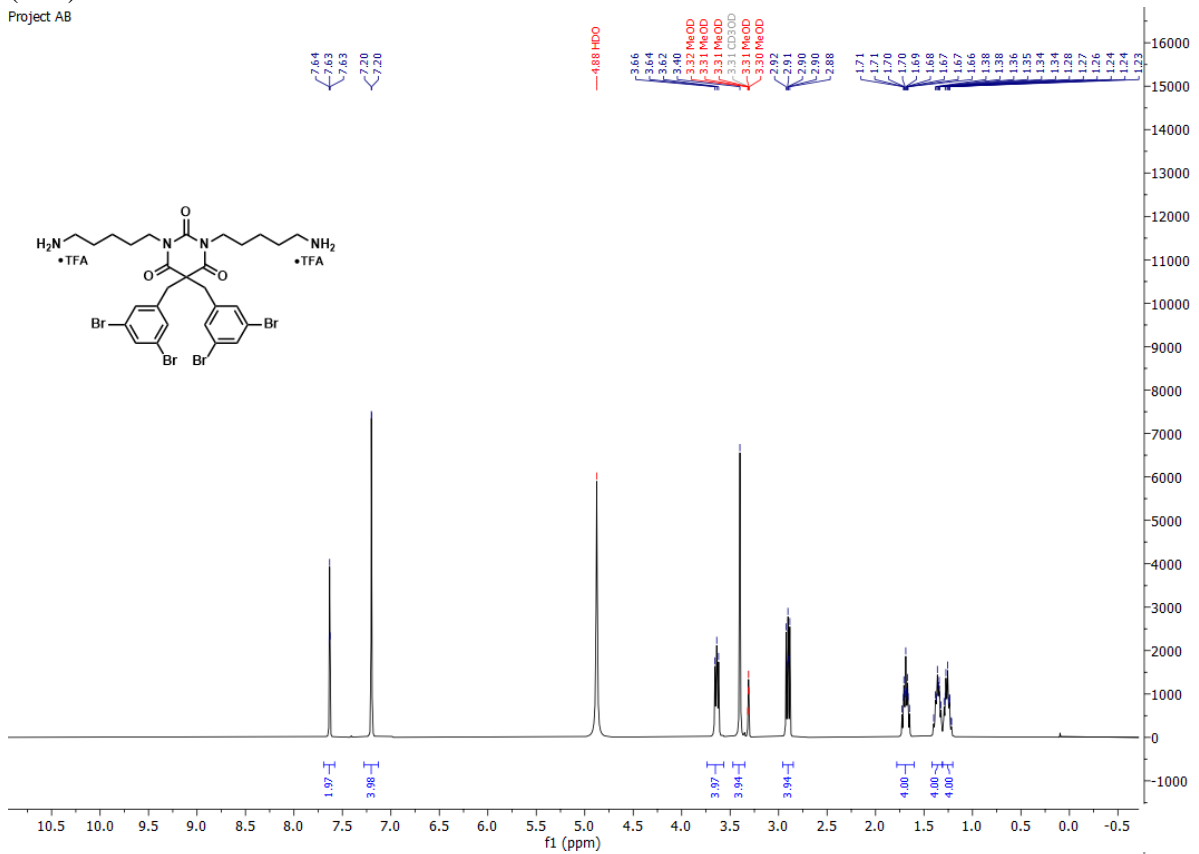


Project AB



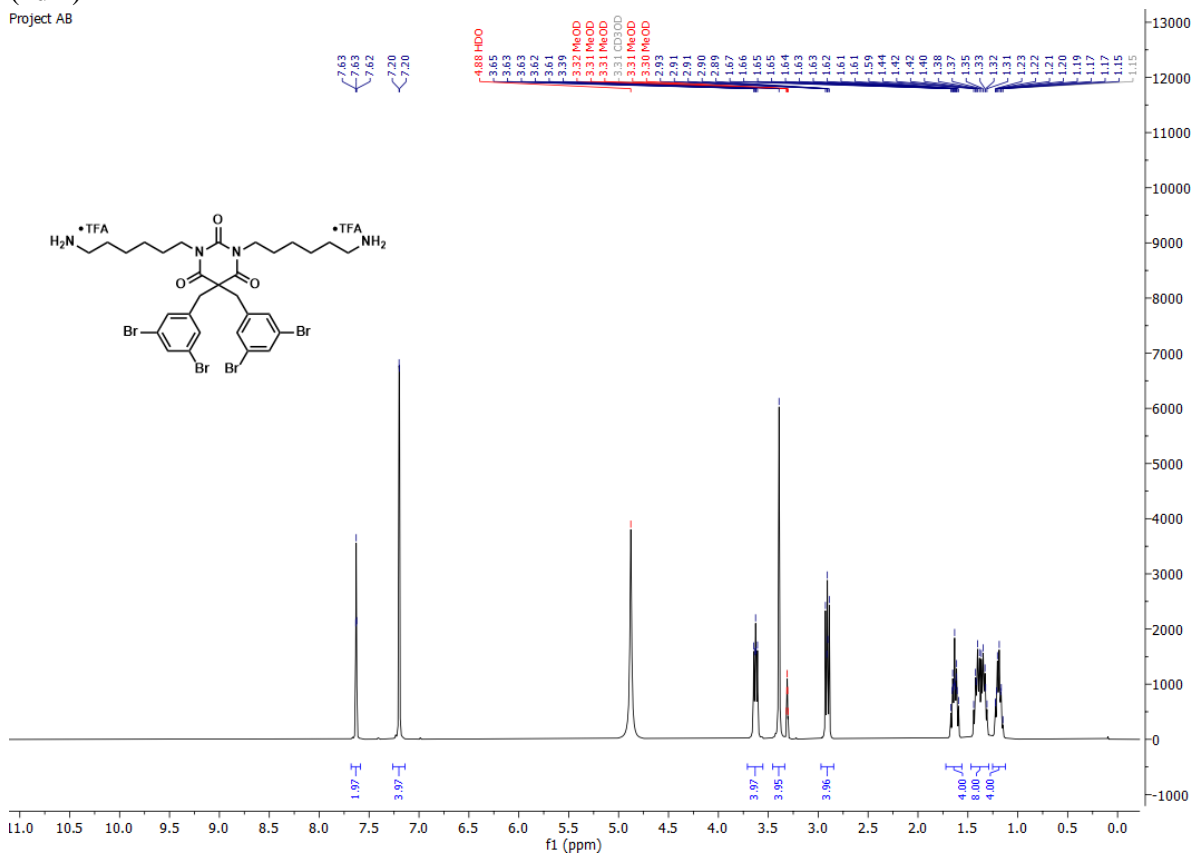
1,3-bis(5-aminopentyl)-5,5-bis(3,5-dibromobenzyl)pyrimidine-2,4,6(1*H*,3*H*,5*H*)-trione di-TFA salt
(4cA)

Project AB

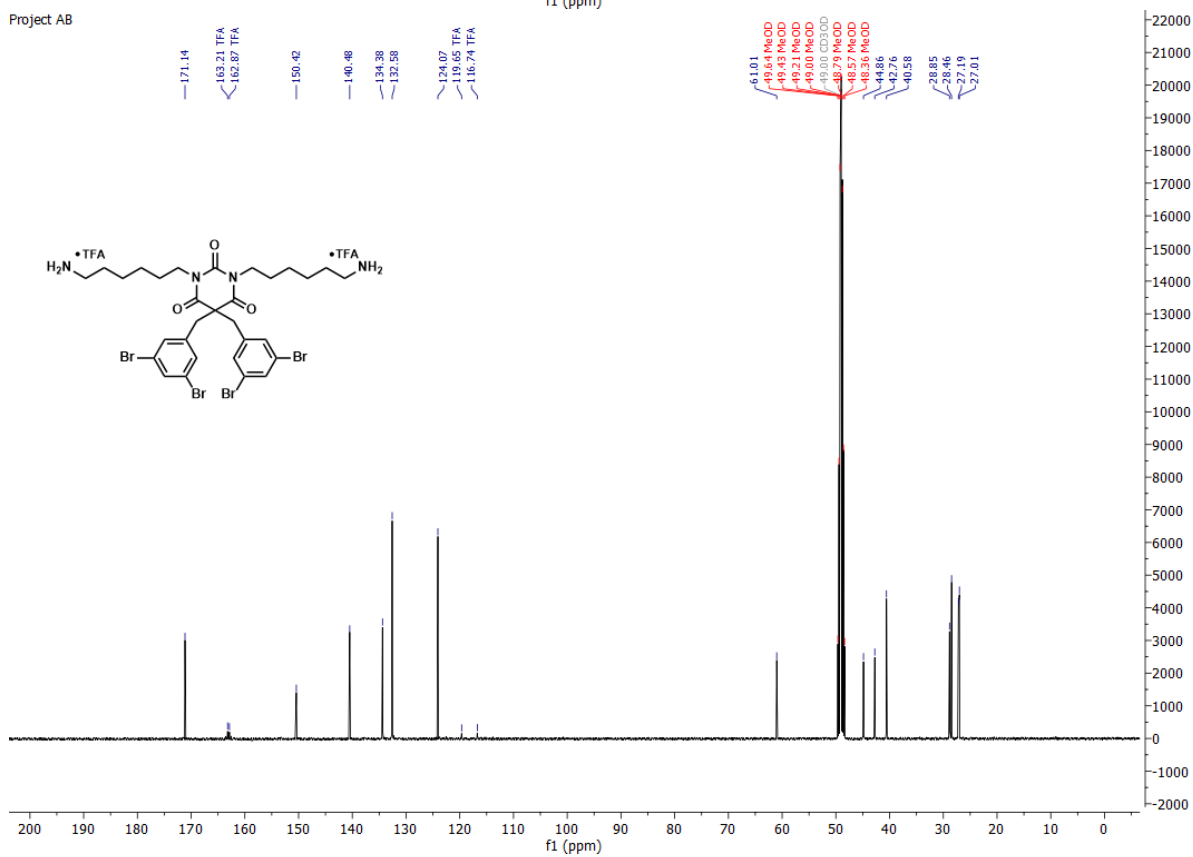


1,3-bis(6-aminohexyl)-5,5-bis(3,5-dibromobenzyl)pyrimidine-2,4,6(1*H*,3*H*,5*H*)-trione di-TFA salt
(4dA)

Project AB

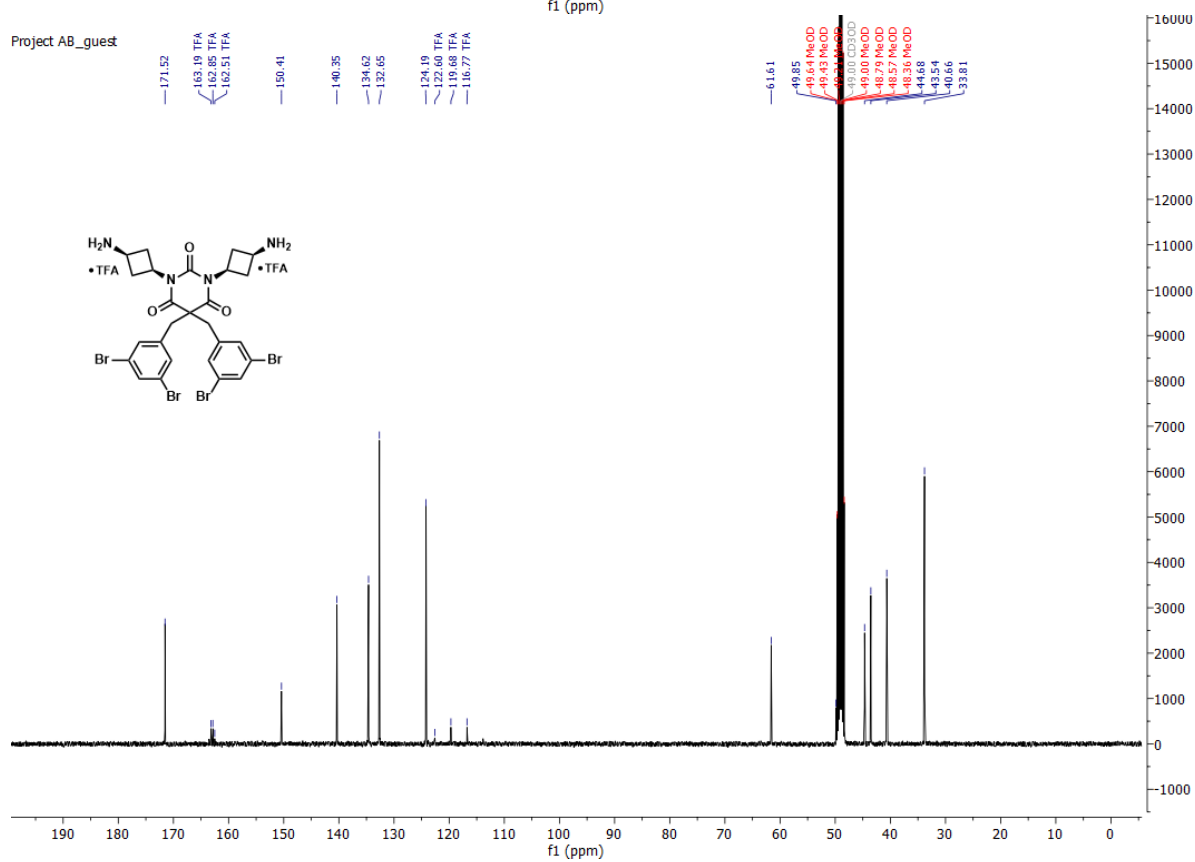
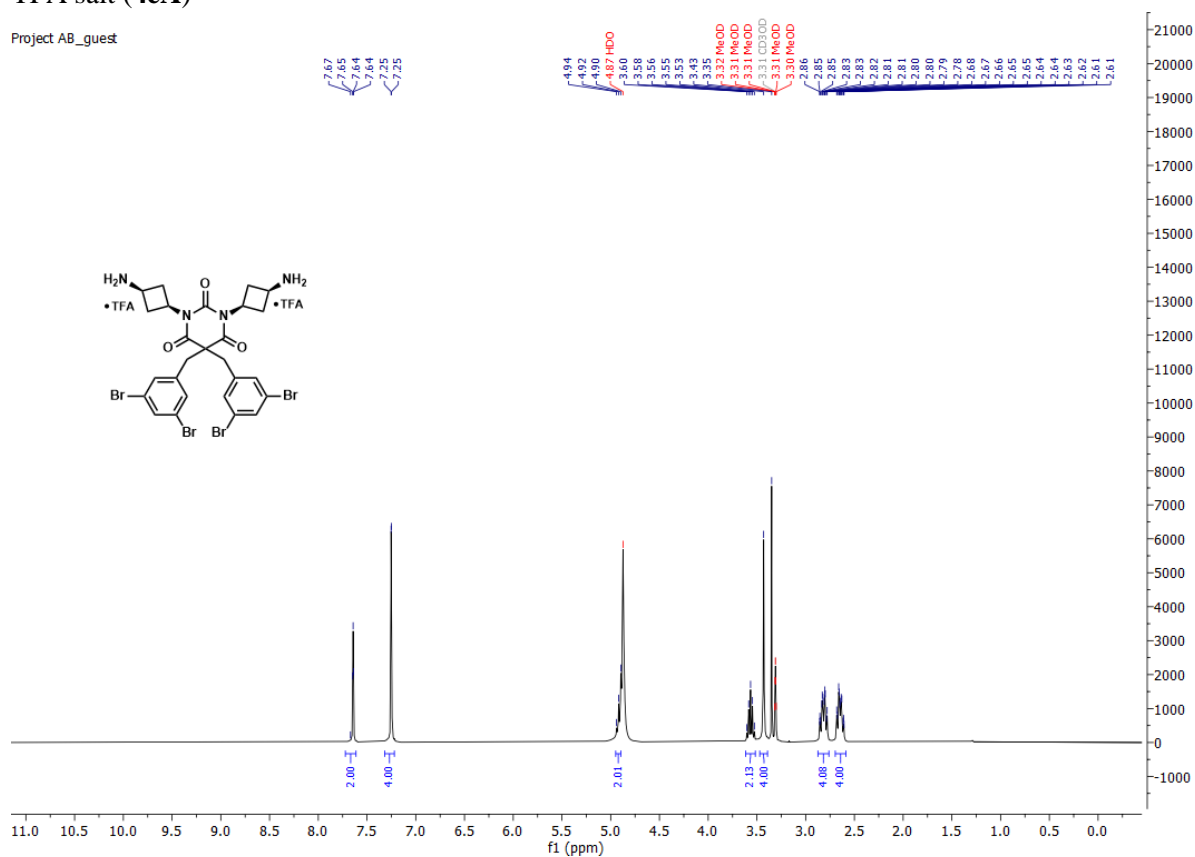


Project AB



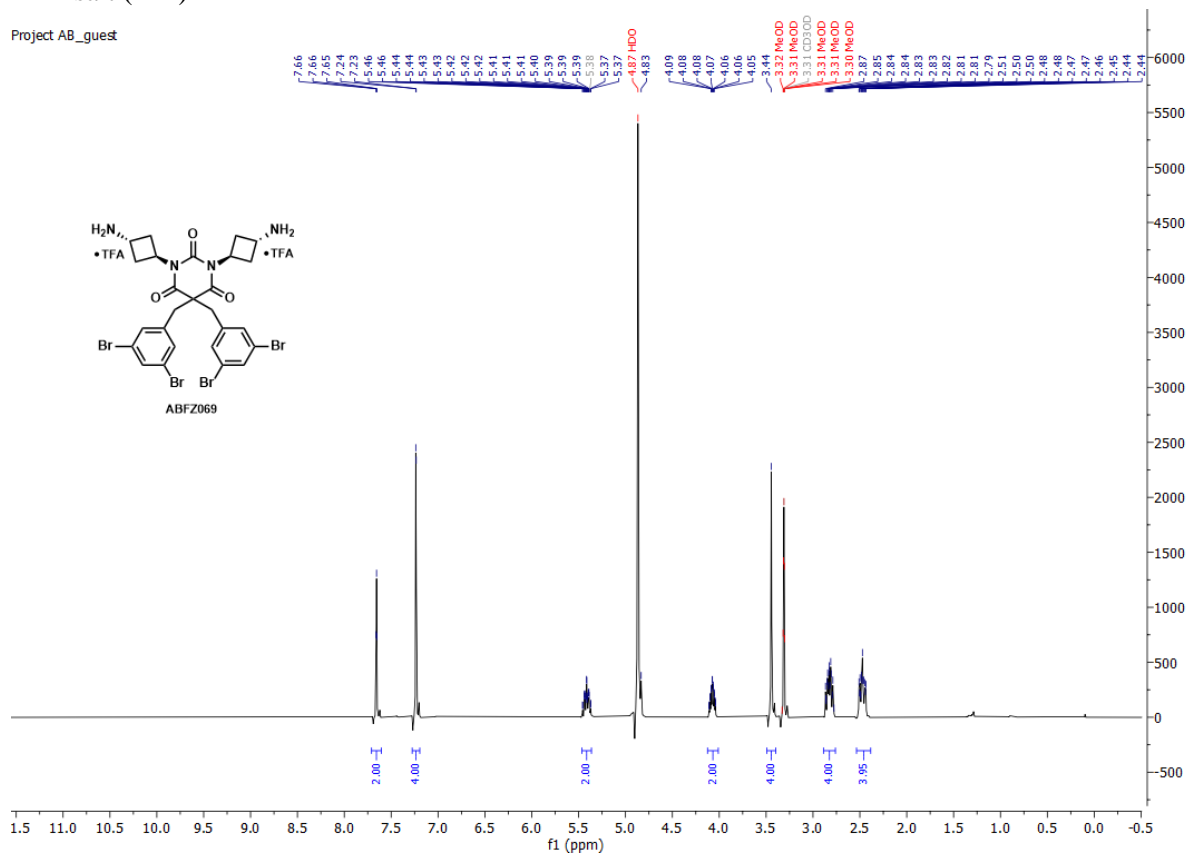
1,3-bis((1*s*,3*S*)-3-aminocyclobutyl)-5,5-bis(3,5-dibromobenzyl)pyrimidine-2,4,6(1*H*,3*H*,5*H*)-trione di-TFA salt (**4eA**)

Project AB_guest

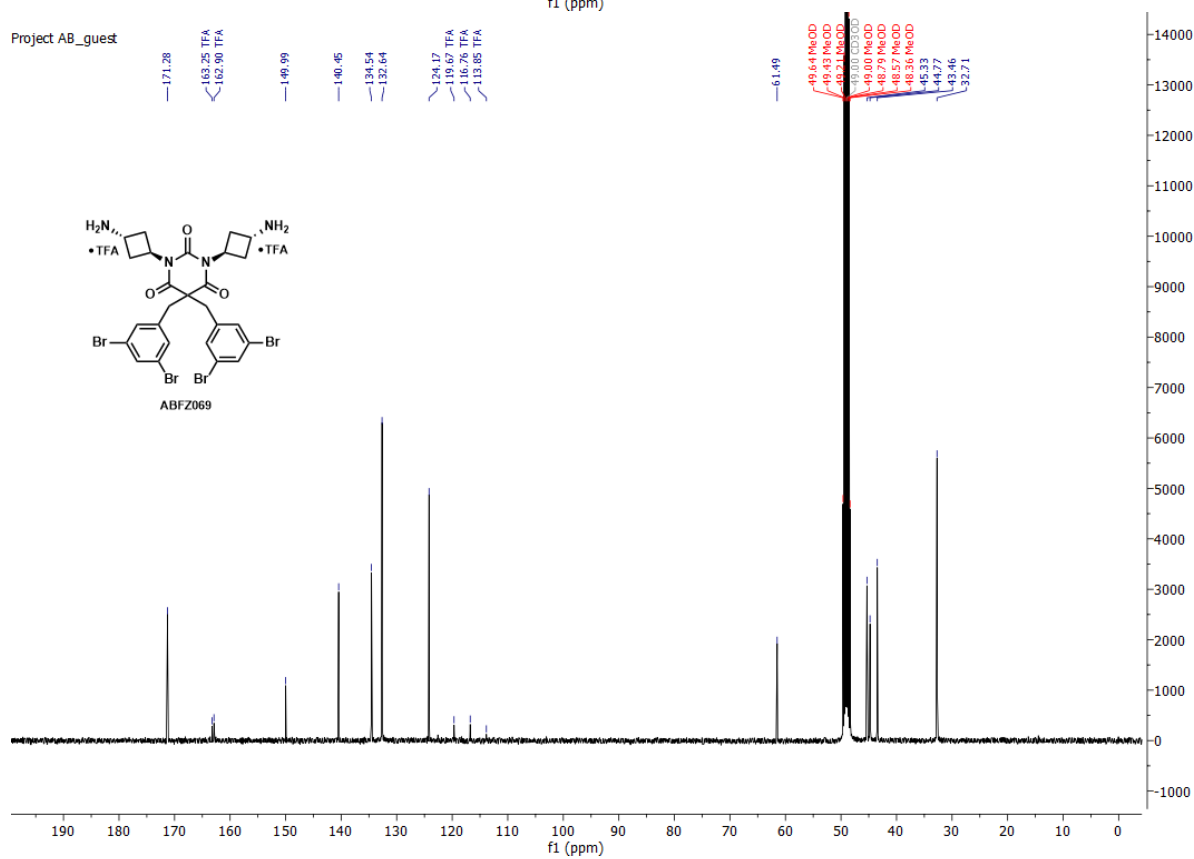


1,3-bis((1*r*,3*R*)-3-aminocyclobutyl)-5,5-bis(3,5-dibromobenzyl)pyrimidine-2,4,6(1*H*,3*H*,5*H*)-trione di-TFA salt (**4fA**)

Project AB_guest

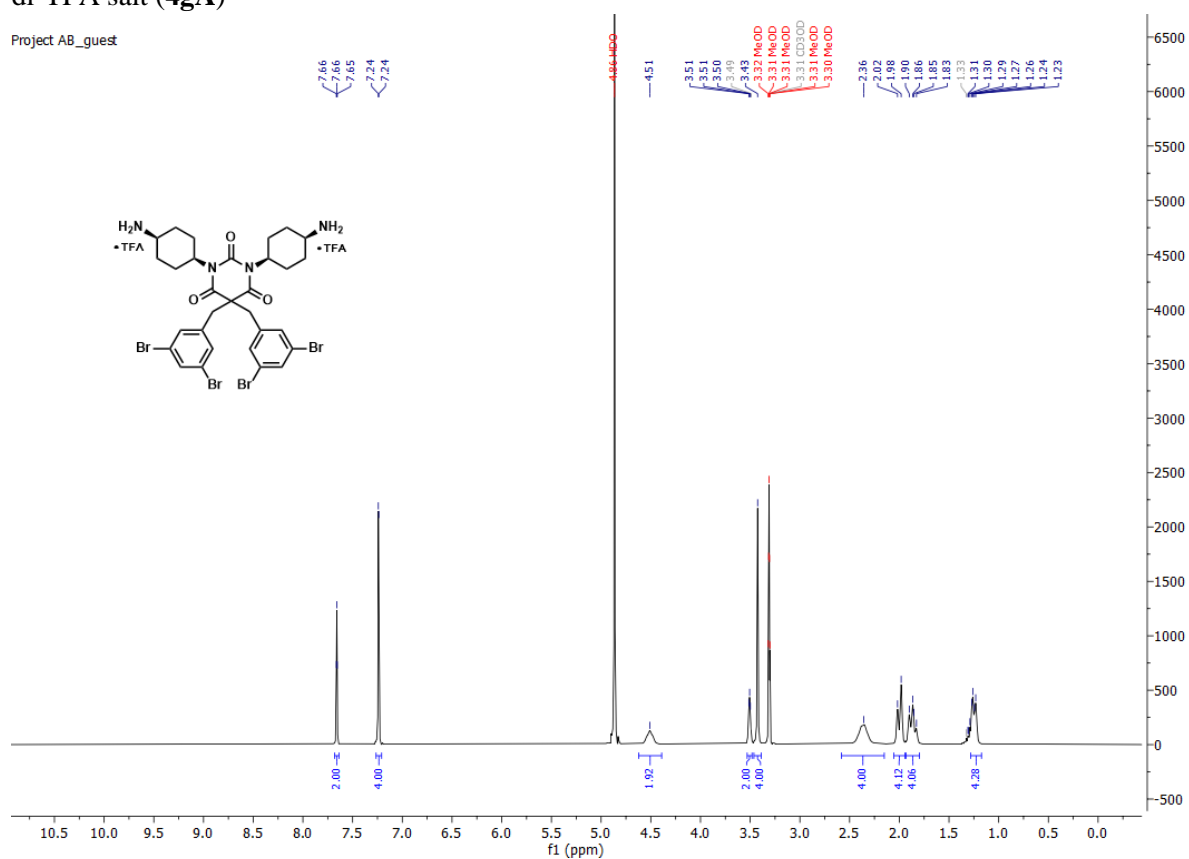


Project AB_guest

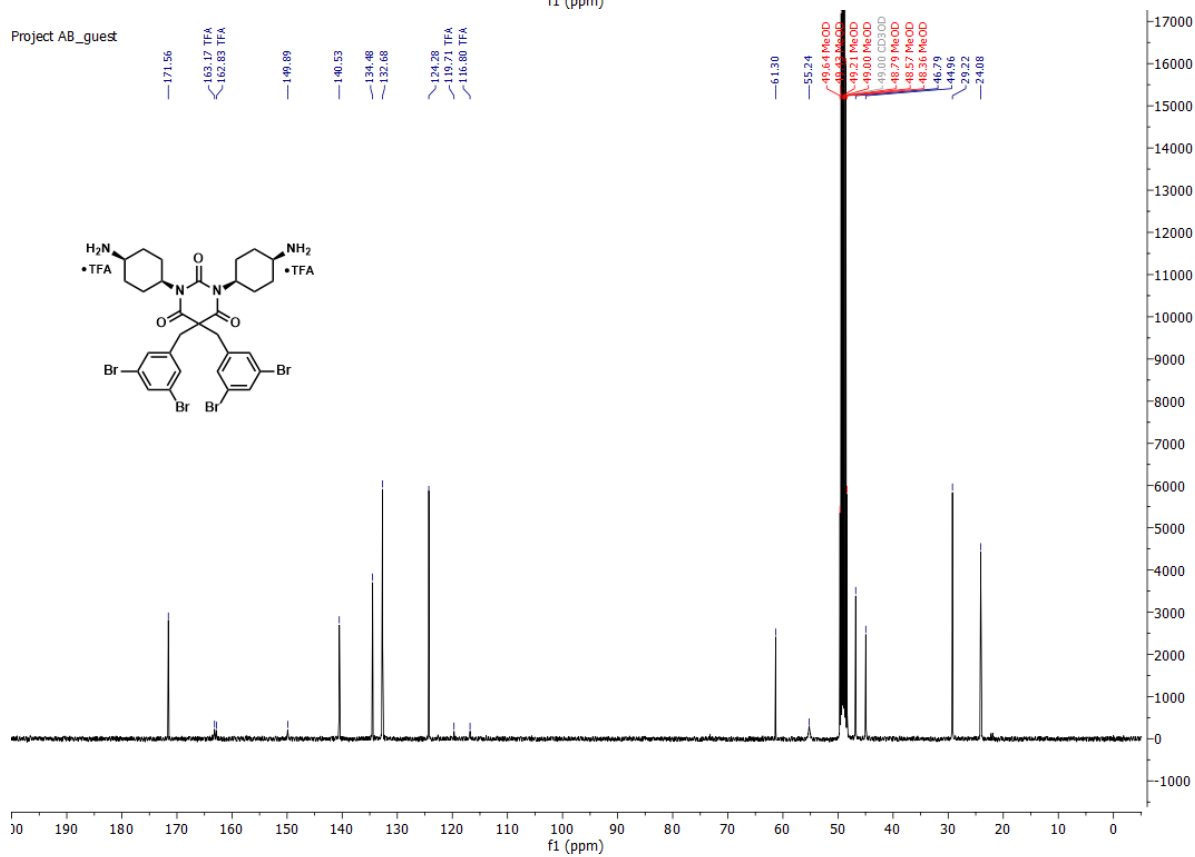


1,3-bis((1*s*,4*S*)-4-aminocyclohexyl)-5,5-bis(3,5-dibromobenzyl)pyrimidine-2,4,6(1*H*,3*H*,5*H*)-trione di-TFA salt (**4gA**)

Project AB_guest

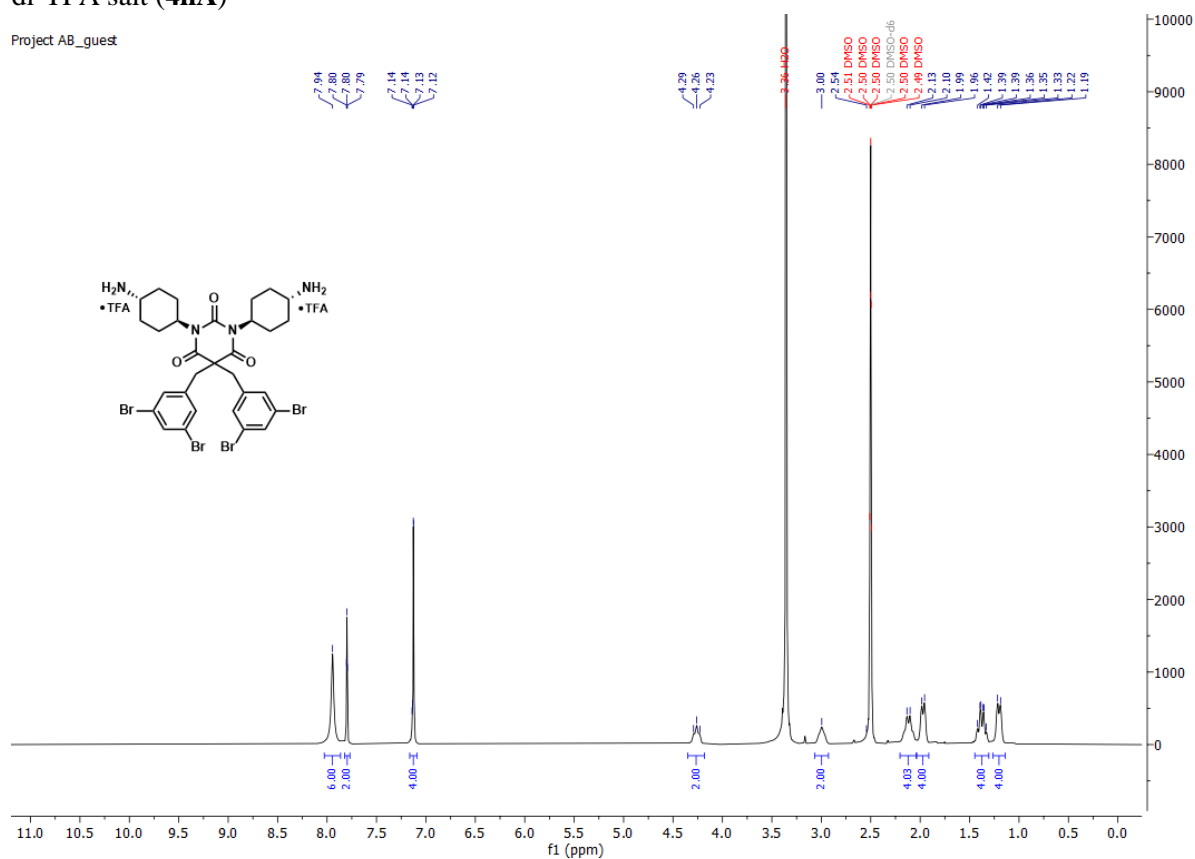


Project AB_guest

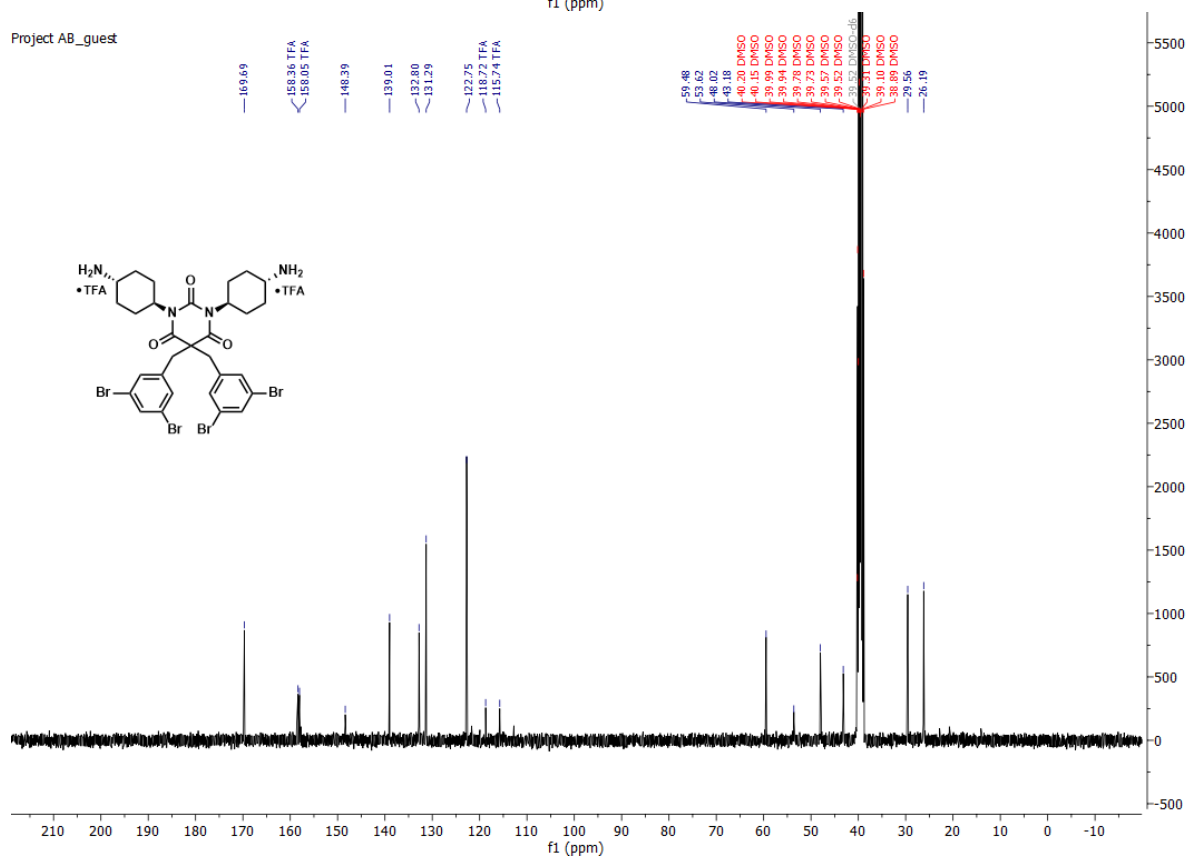


1,3-bis((1*r*,4*R*)-4-aminocyclohexyl)-5,5-bis(3,5-dibromobenzyl)pyrimidine-2,4,6(1*H*,3*H*,5*H*)-trione di-TFA salt (**4hA**)

Project AB_guest

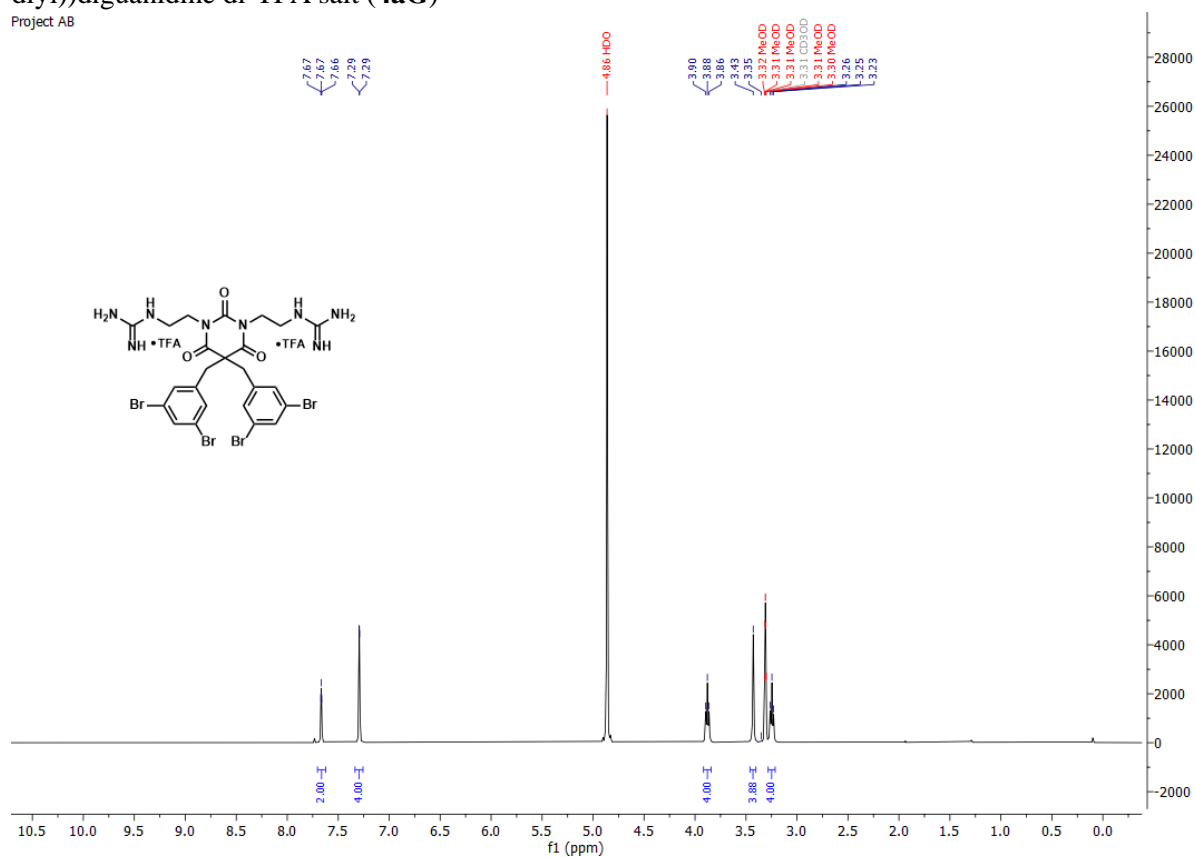


Project AB_guest

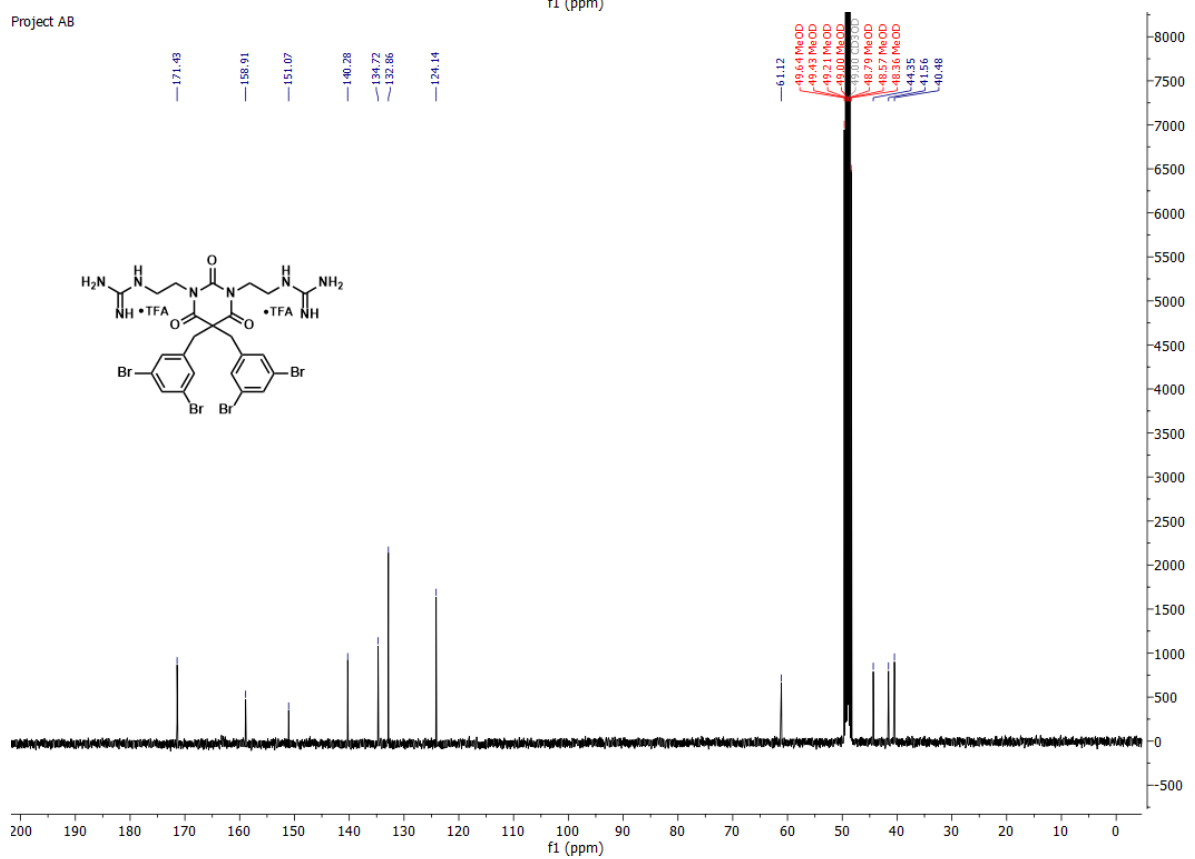


1,1'-((5,5-bis(3,5-dibromobenzyl)-2,4,6-trioxodihydropyrimidine-1,3(2*H*,4*H*)-diyl)bis(ethane-2,1-diyl))diguanidine di-TFA salt (**4aG**)

Project AB

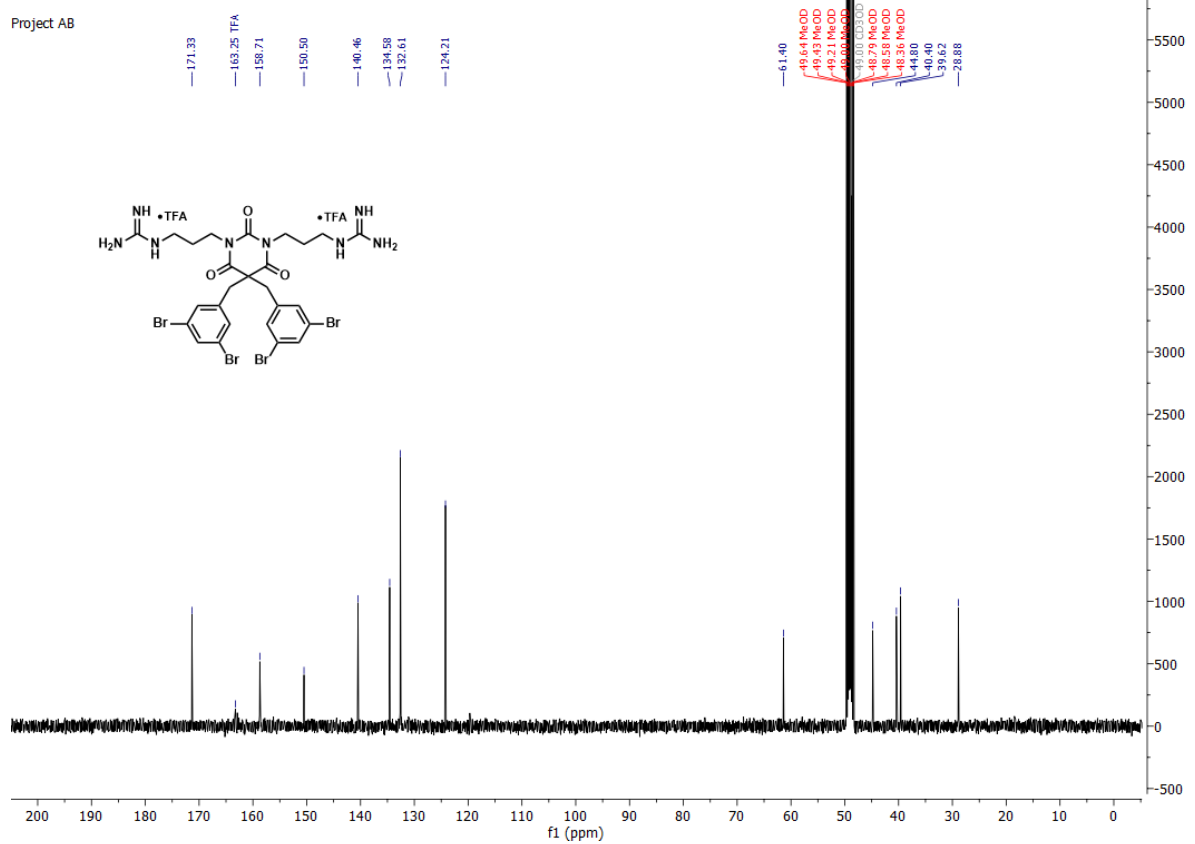
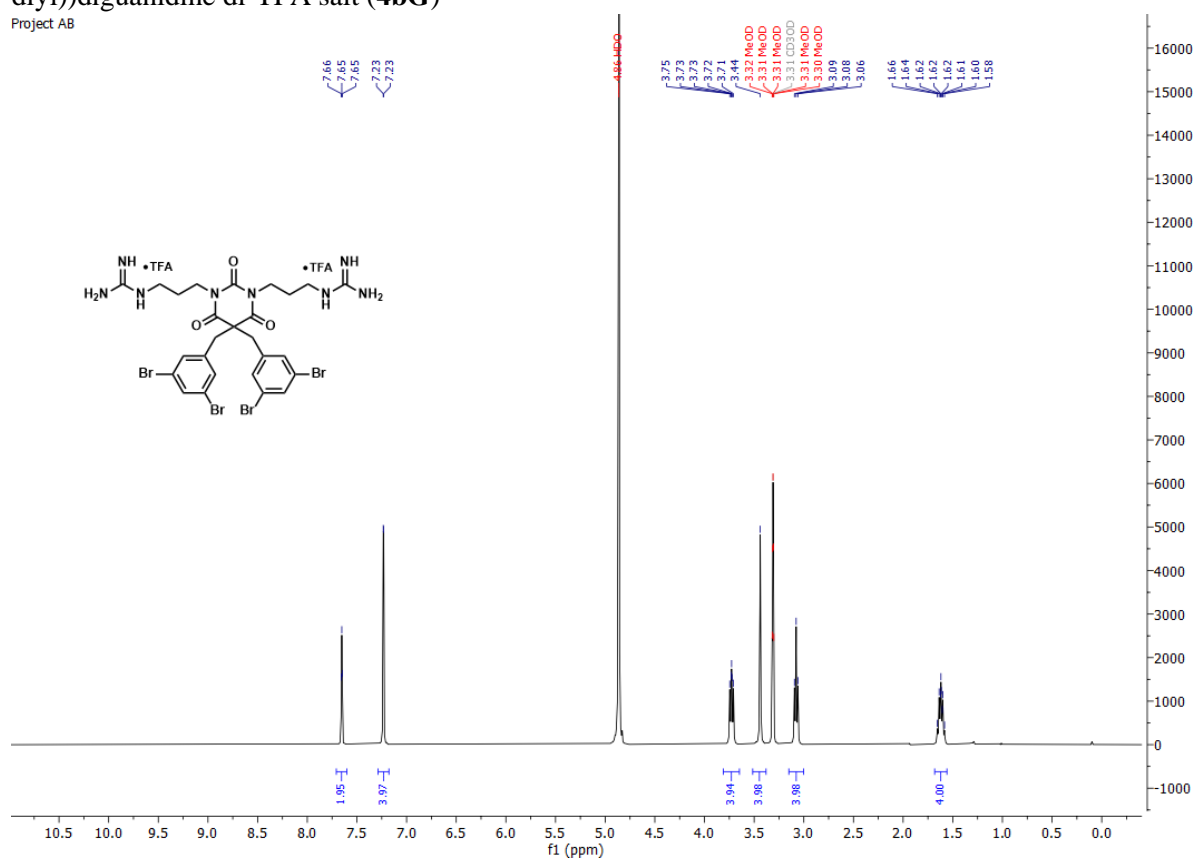


Project AB



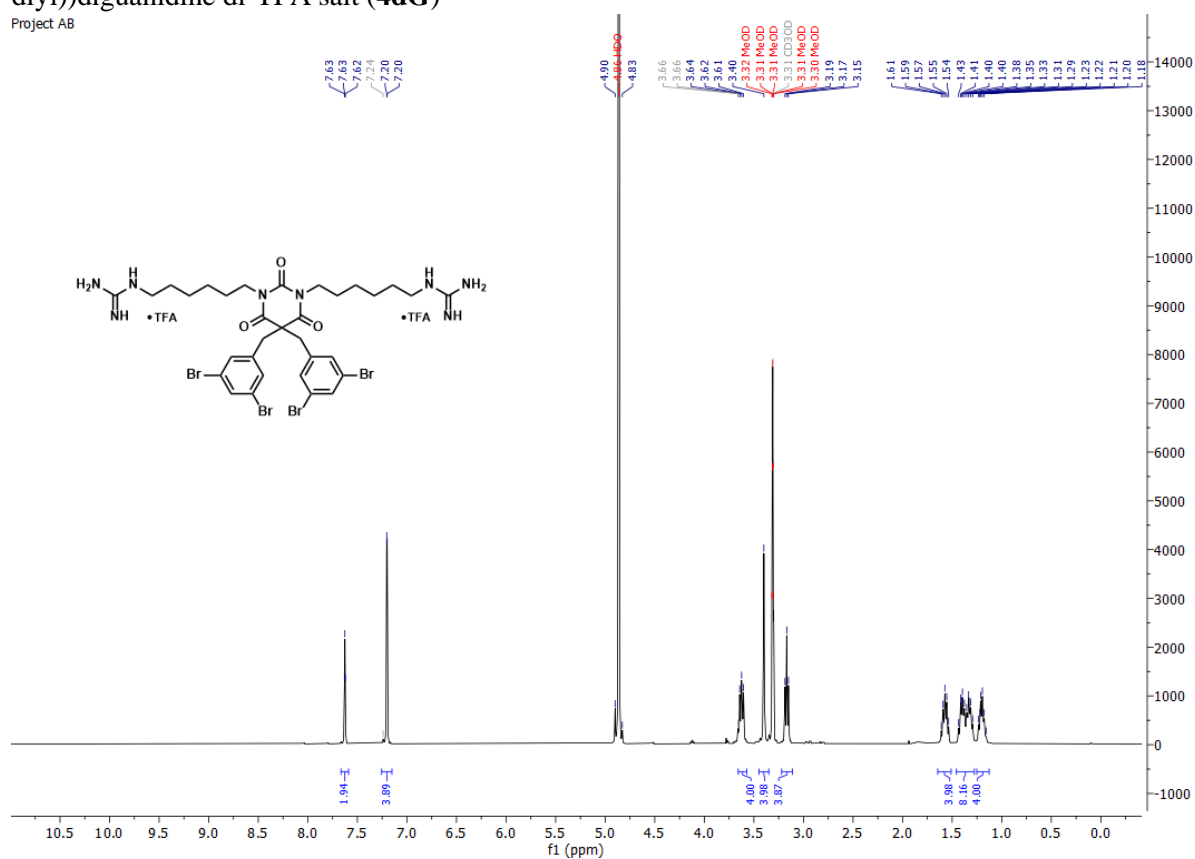
1,1'-((5,5-bis(3,5-dibromobenzyl)-2,4,6-trioxodihydropyrimidine-1,3(2*H*,4*H*)-diyl)bis(propane-3,1-diyl))diguanidine di-TFA salt (**4bG**)

Project AB

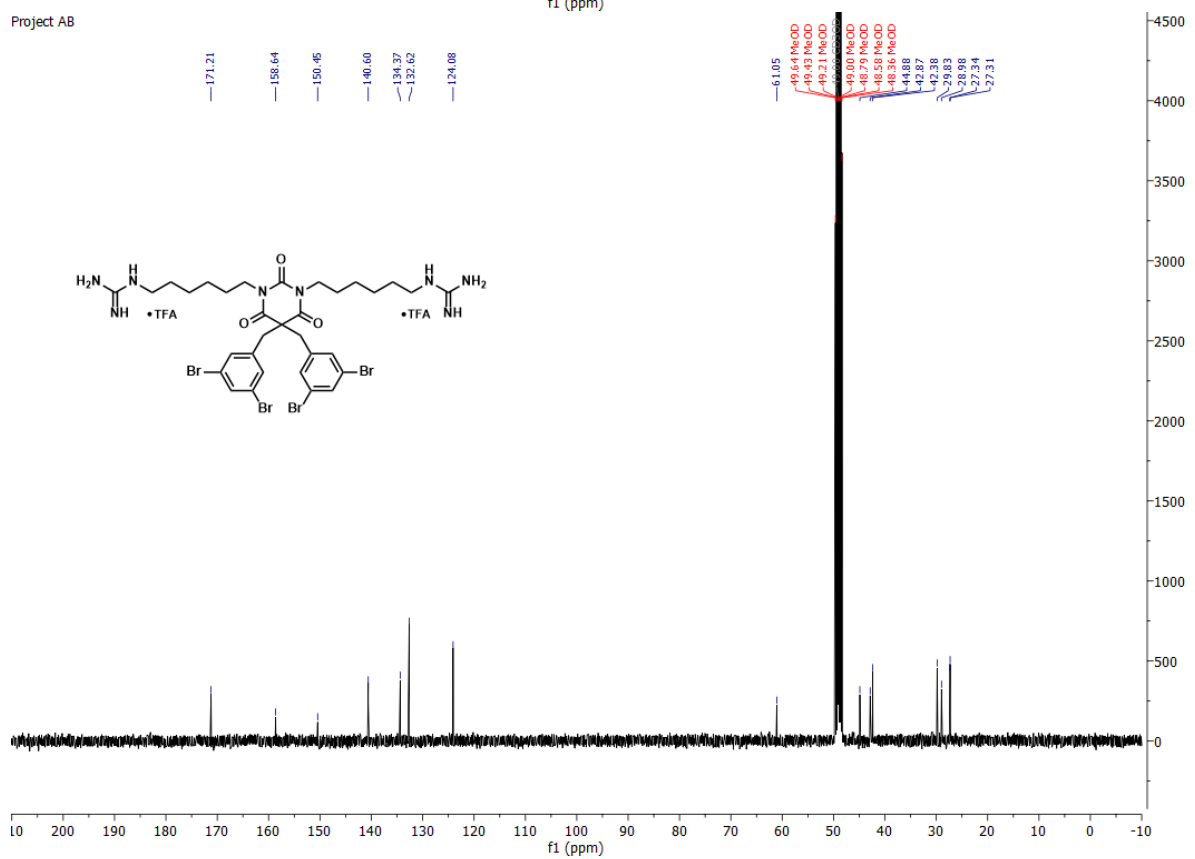


1,1'-((5,5-bis(3,5-dibromobenzyl)-2,4,6-trioxodihydropyrimidine-1,3(2H,4H)-diyl)bis(hexane-6,1-diy))diguanidine di-TFA salt (**4dG**)

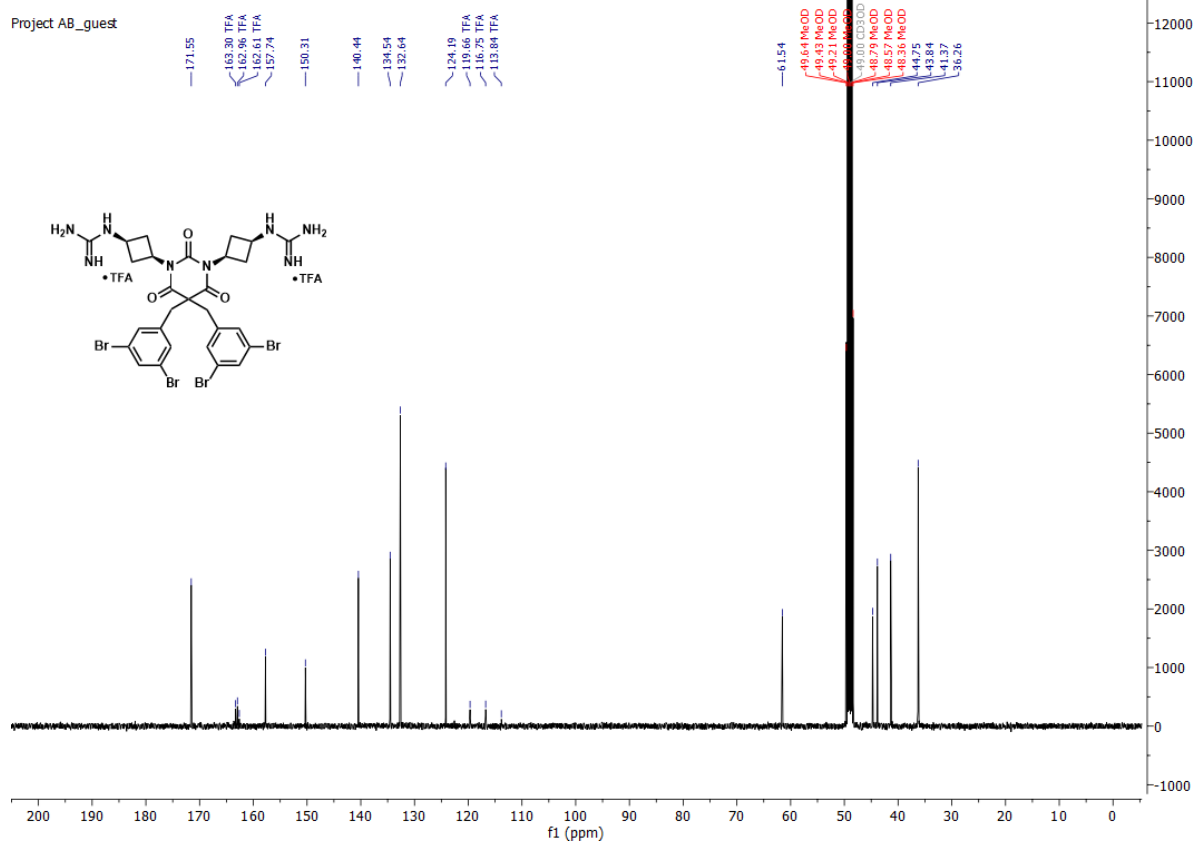
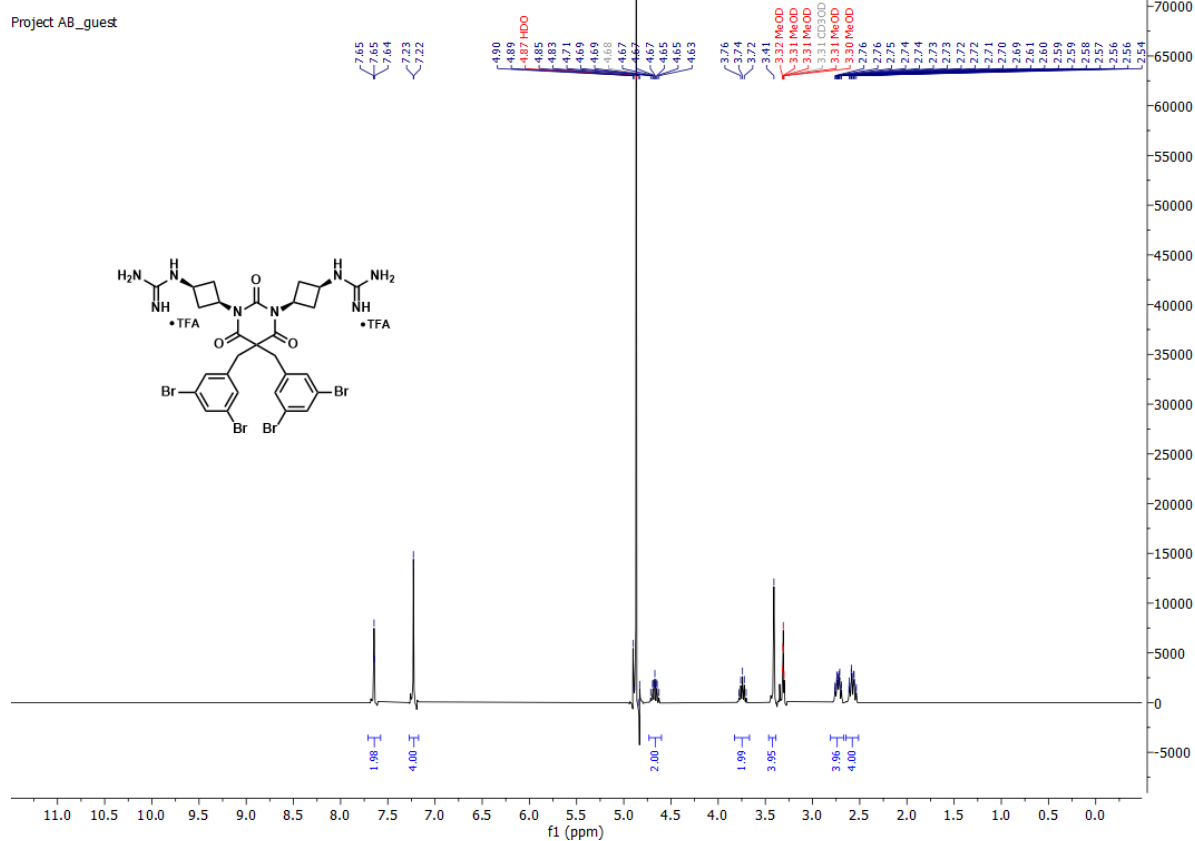
Project AB



Project AB

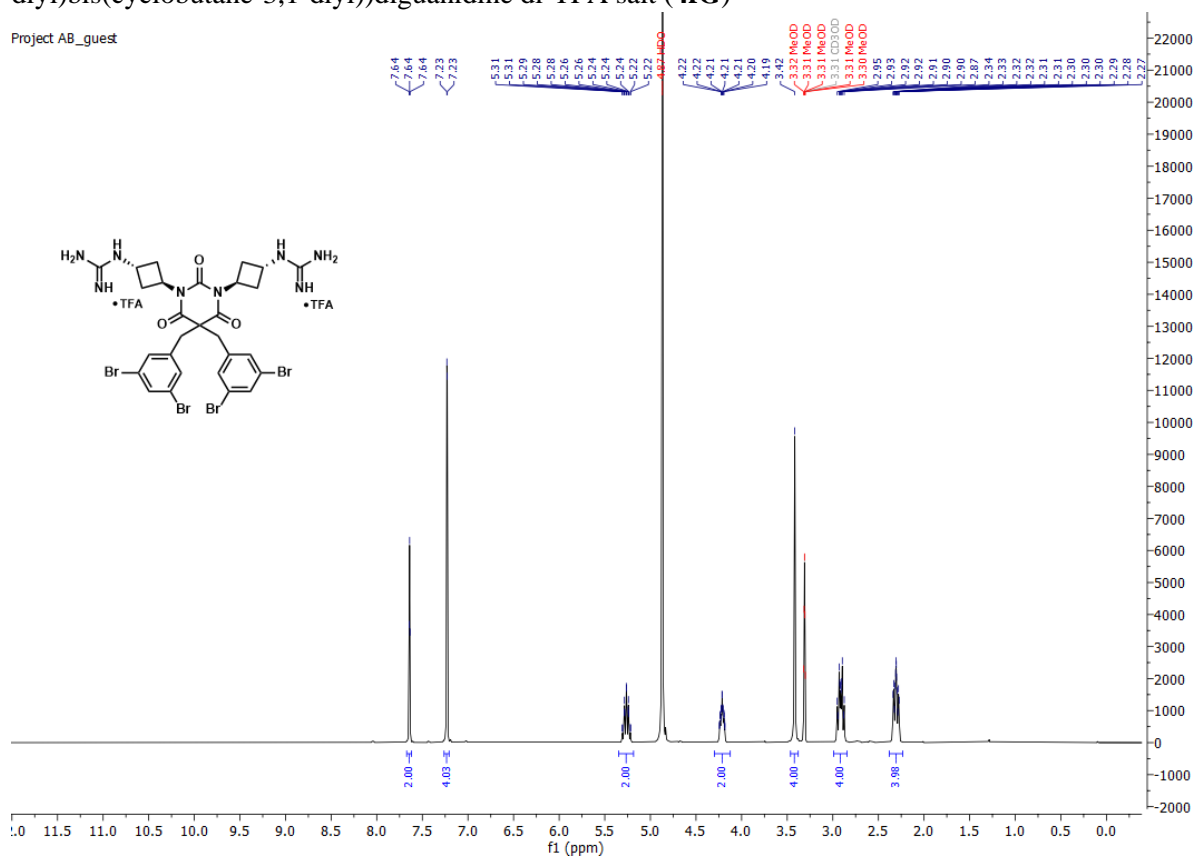


1,1'-((1*S*,1'*S*,3*s*,3'*s*)-(5,5-bis(3,5-dibromobenzyl)-2,4,6-trioxodihydropyrimidine-1,3(2*H*,4*H*)-diyl)bis(cyclobutane-3,1-diyl))diguanidine di-TFA salt (**4eG**)

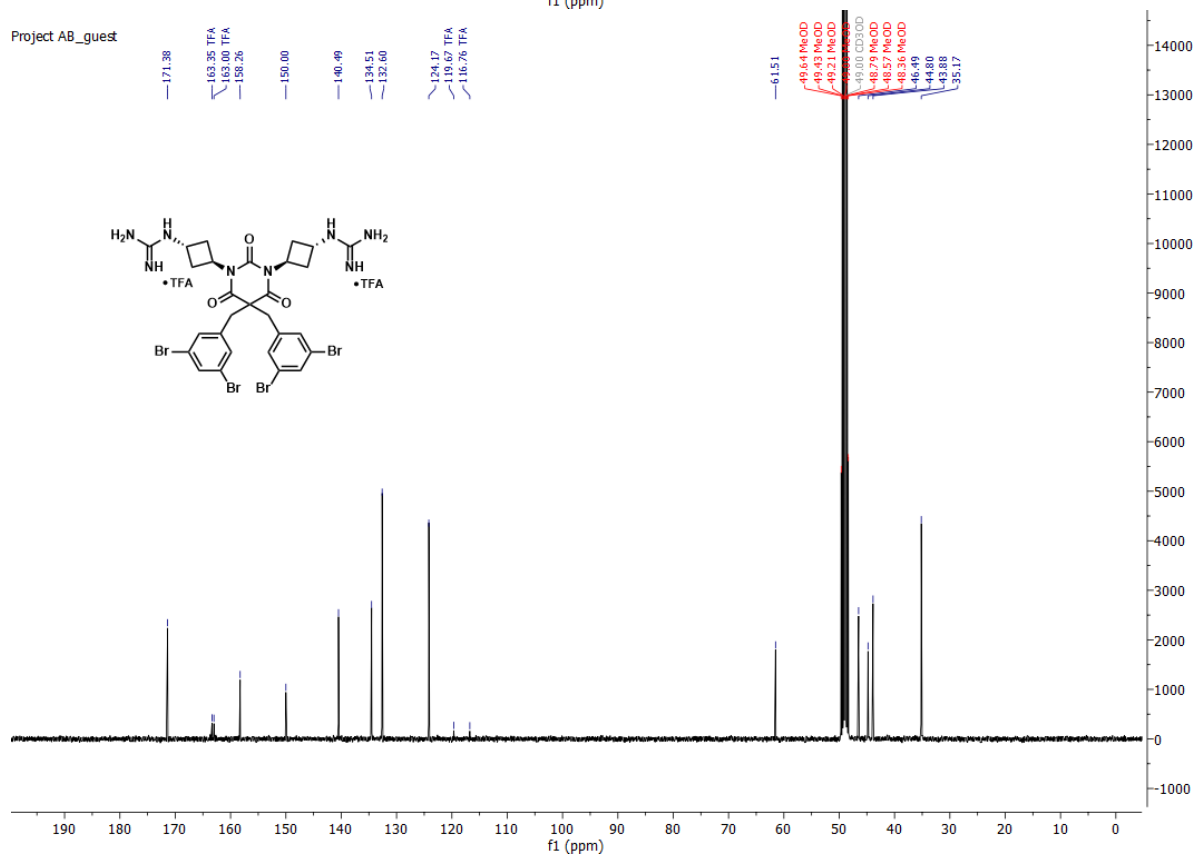


1,1'-((1*R*,1'*R*,3*r*,3'*r*)-(5,5-bis(3,5-dibromobenzyl)-2,4,6-trioxodihydropyrimidine-1,3(2*H*,4*H*)-diyl)bis(cyclobutane-3,1-diyl))diguanidine di-TFA salt (**4fG**)

Project AB_guest

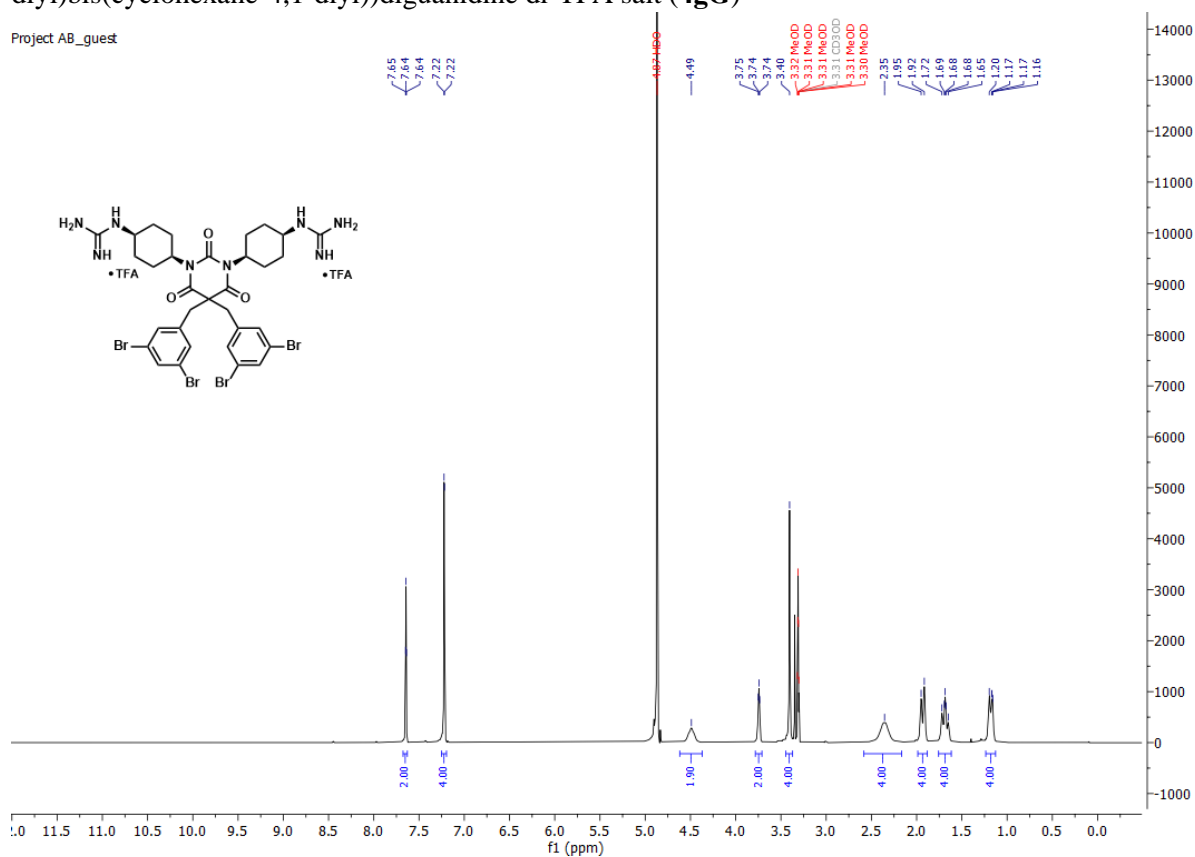


Project AB_guest

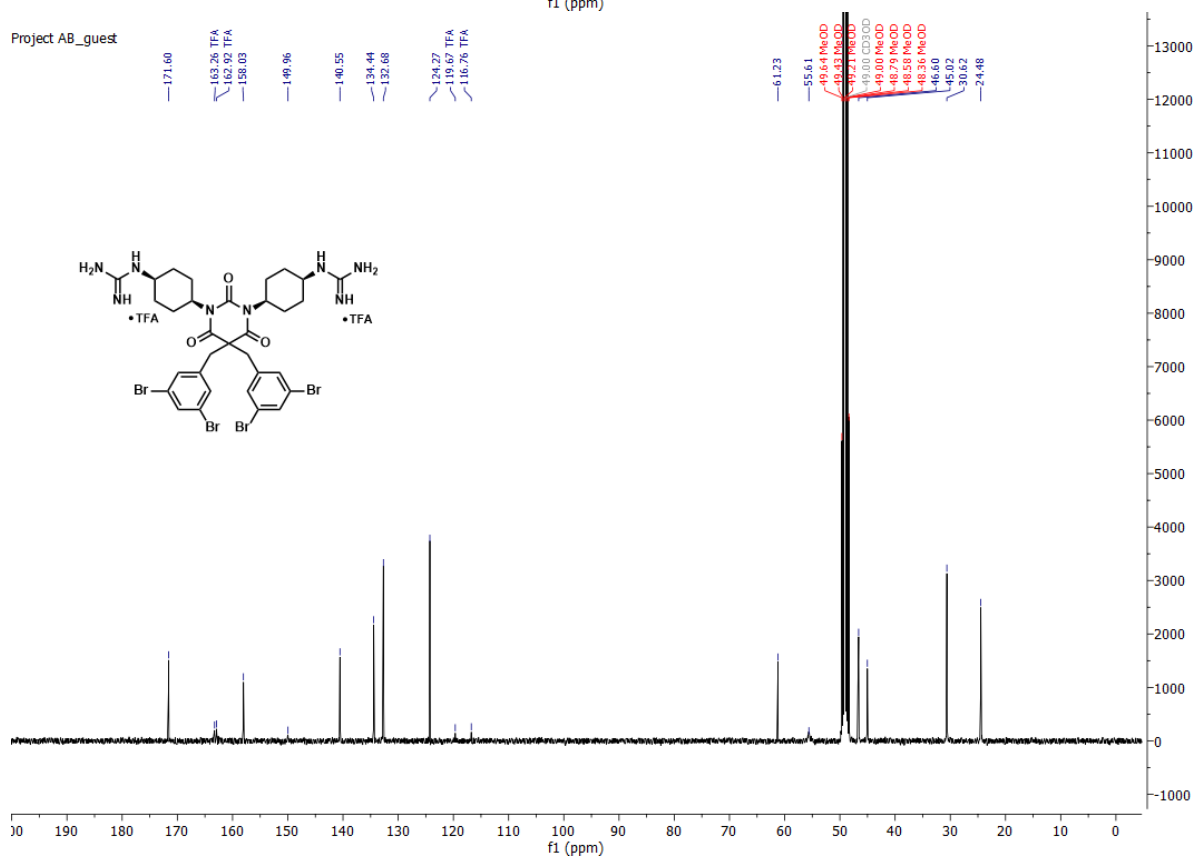


1,1'-((1*S*,1'*S*,4*s*,4'*s*)-(5,5-bis(3,5-dibromobenzyl)-2,4,6-trioxodihydropyrimidine-1,3(2*H*,4*H*)-diyl)bis(cyclohexane-4,1-diyl))diguanidine di-TFA salt (**4gG**)

Project AB_guest



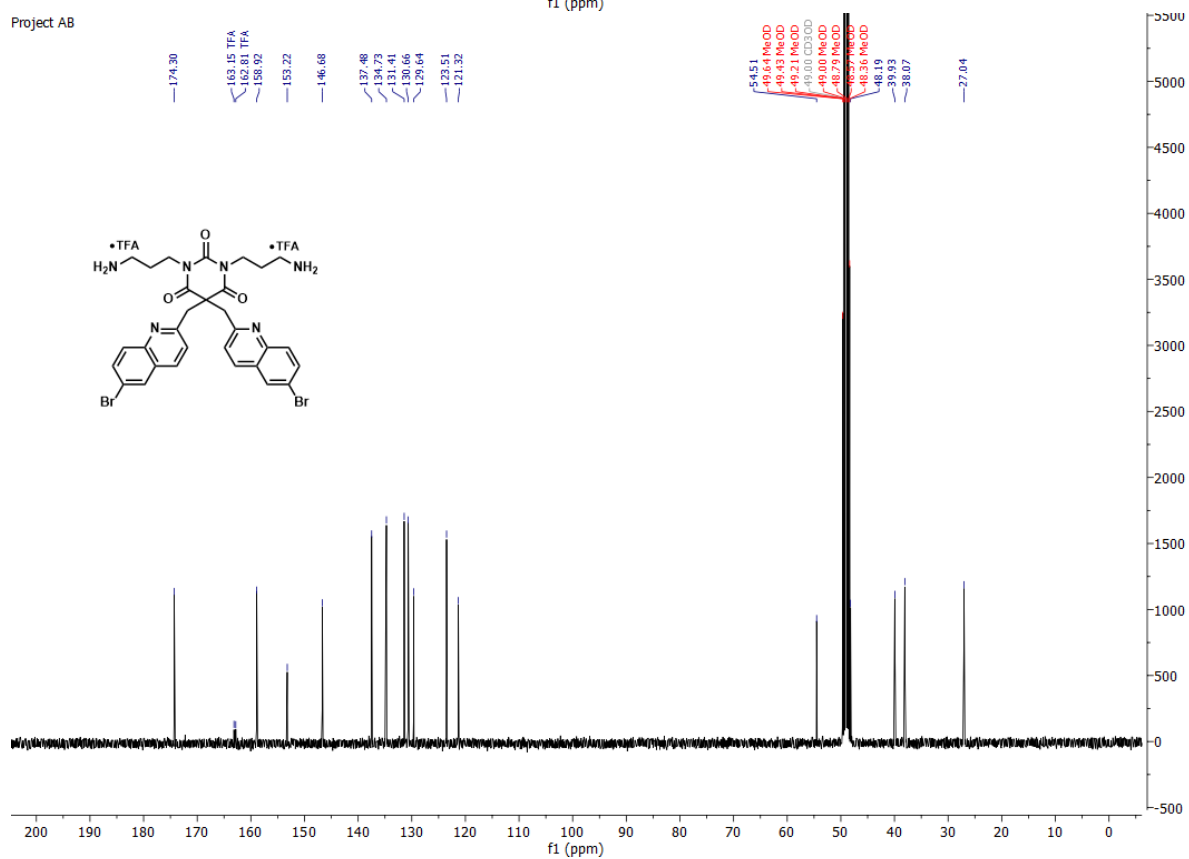
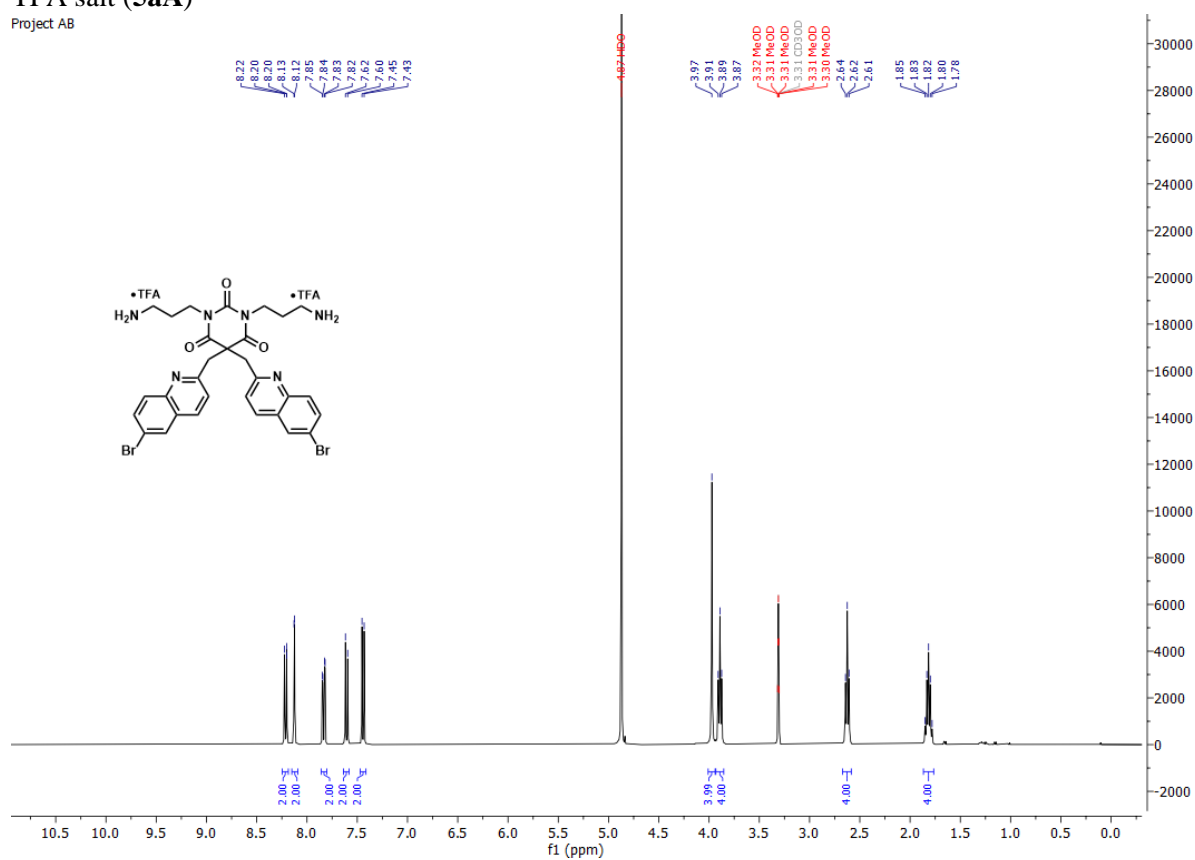
Project AB_guest



3.5 ¹H and ¹³C NMR spectra of compounds in series 5

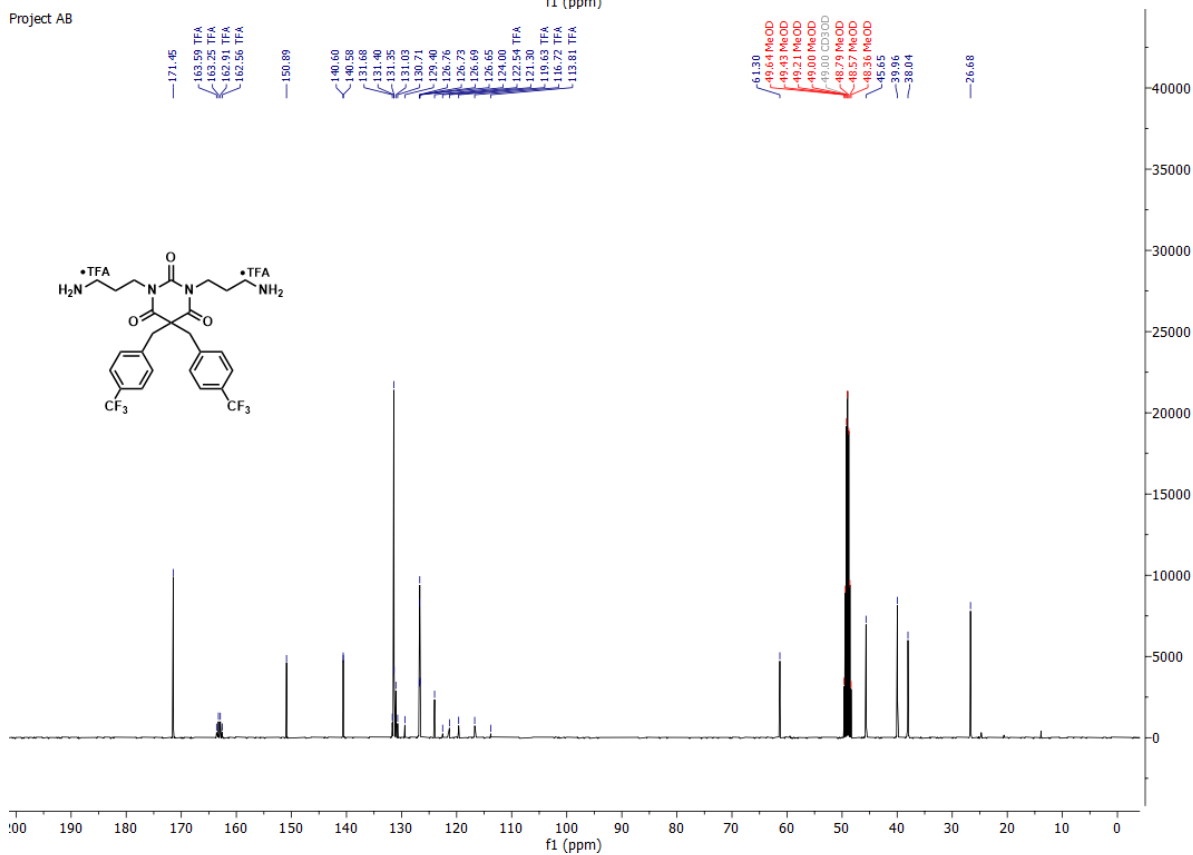
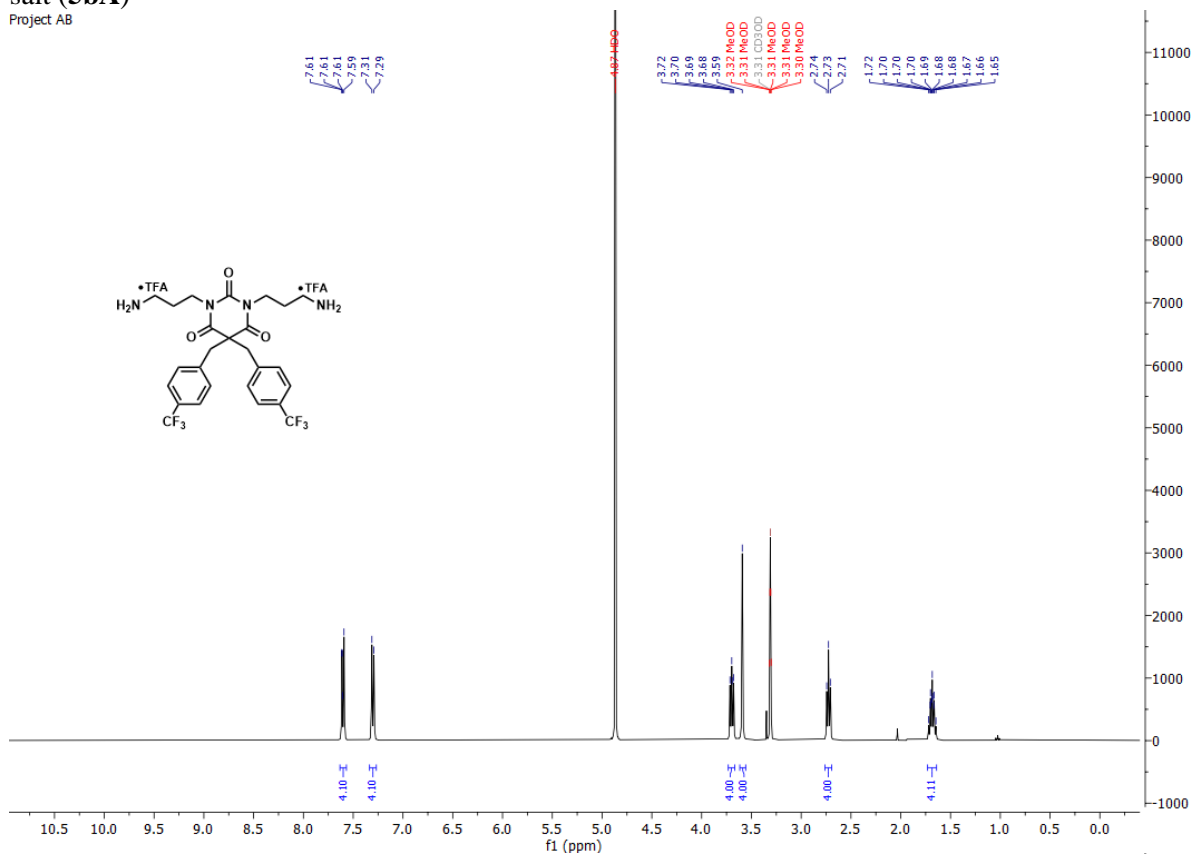
1,3-bis(3-aminopropyl)-5,5-bis((6-bromoquinolin-2-yl)methyl)pyrimidine-2,4,6(1*H*,3*H*,5*H*)-trione di-TFA salt (**5aA**)

Project AB



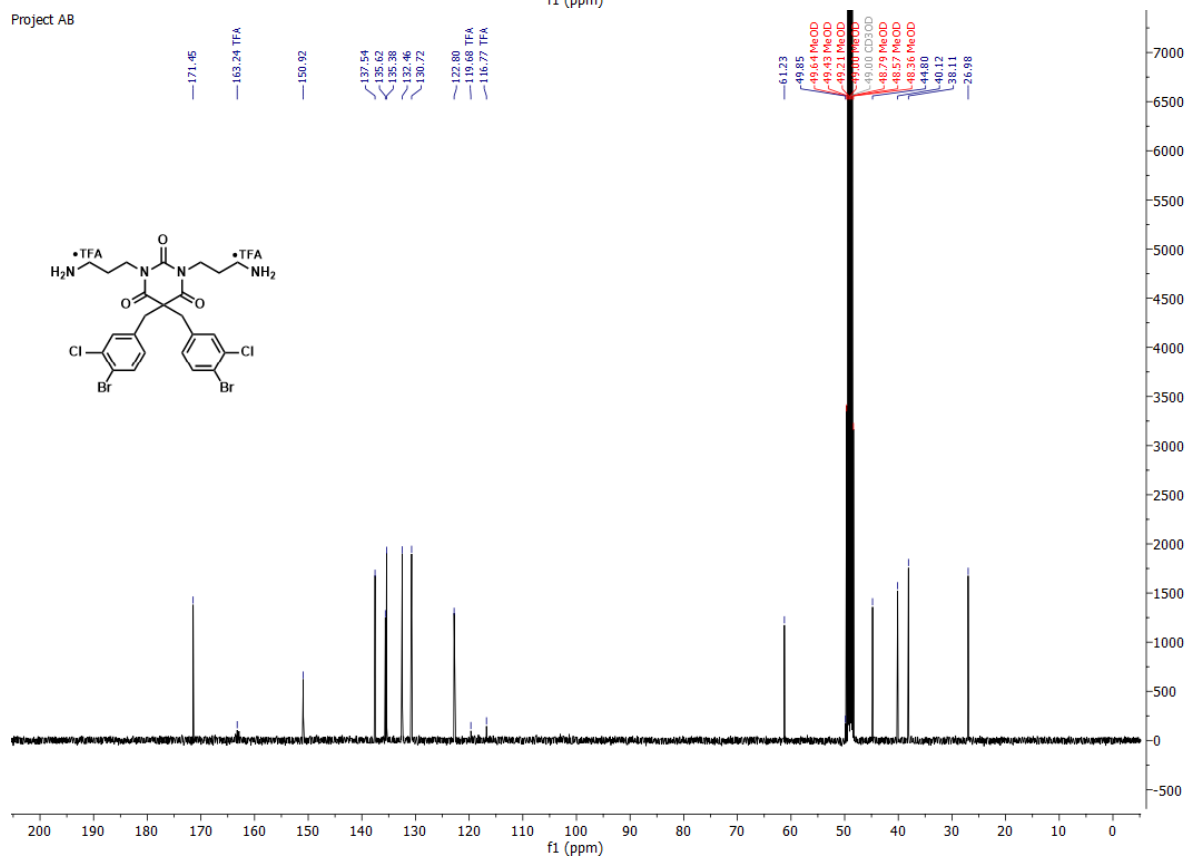
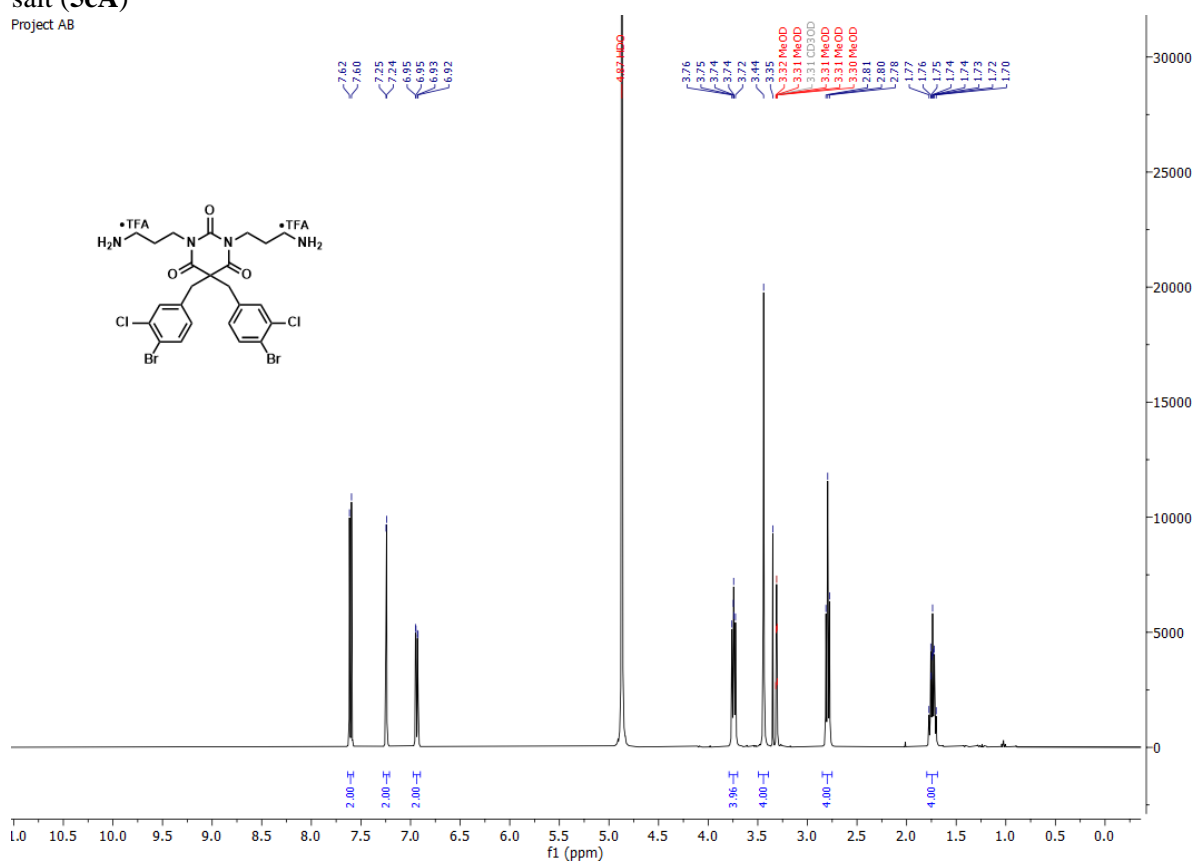
1,3-bis(3-aminopropyl)-5,5-bis(4-(trifluoromethyl)benzyl)pyrimidine-2,4,6(1*H*,3*H*,5*H*)-trione di-TFA salt (**SbA**)

Project AB



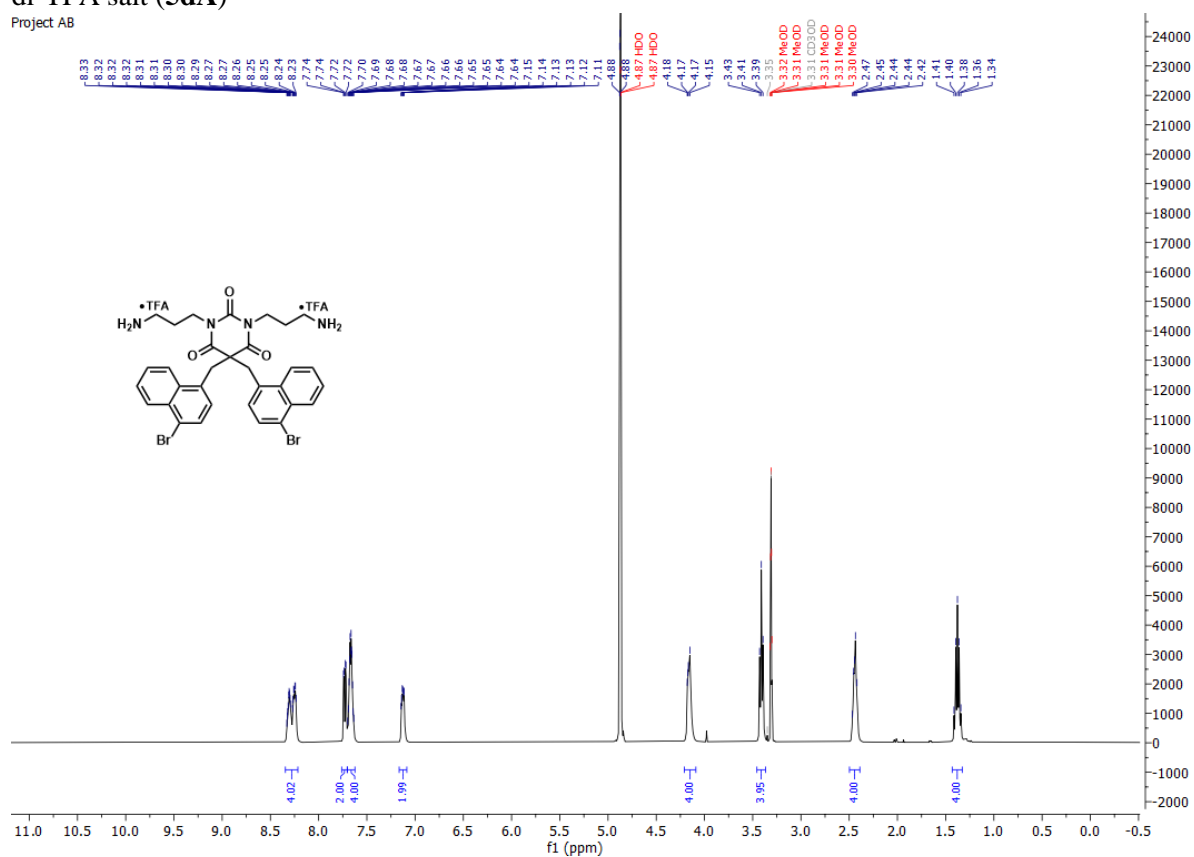
1,3-bis(3-aminopropyl)-5,5-bis(4-bromo-3-chlorobenzyl)pyrimidine-2,4,6(1*H*,3*H*,5*H*)-trione di-TFA salt (**5cA**)

Project AB

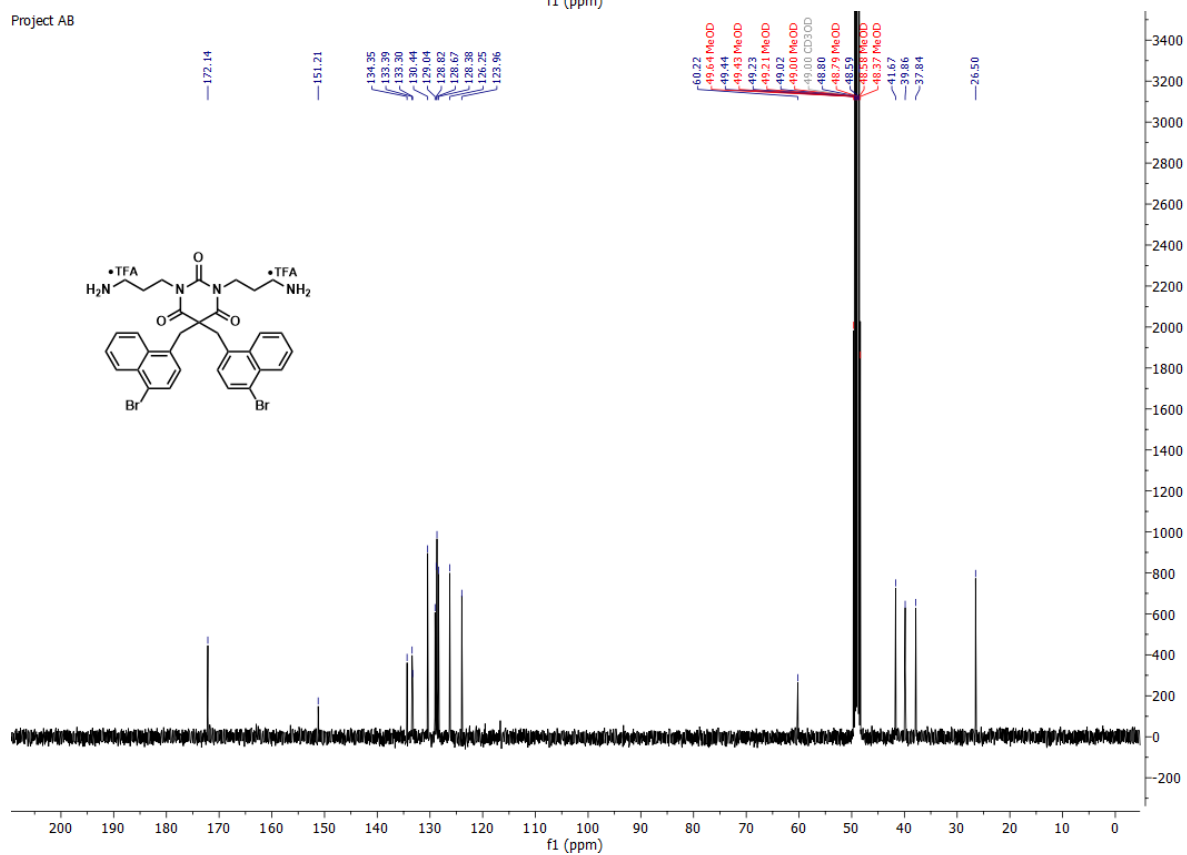


1,3-bis(3-aminopropyl)-5,5-bis((4-bromonaphthalen-1-yl)methyl)pyrimidine-2,4,6(1*H*,3*H*,5*H*)-trione di-TFA salt (**5dA**)

Project AB

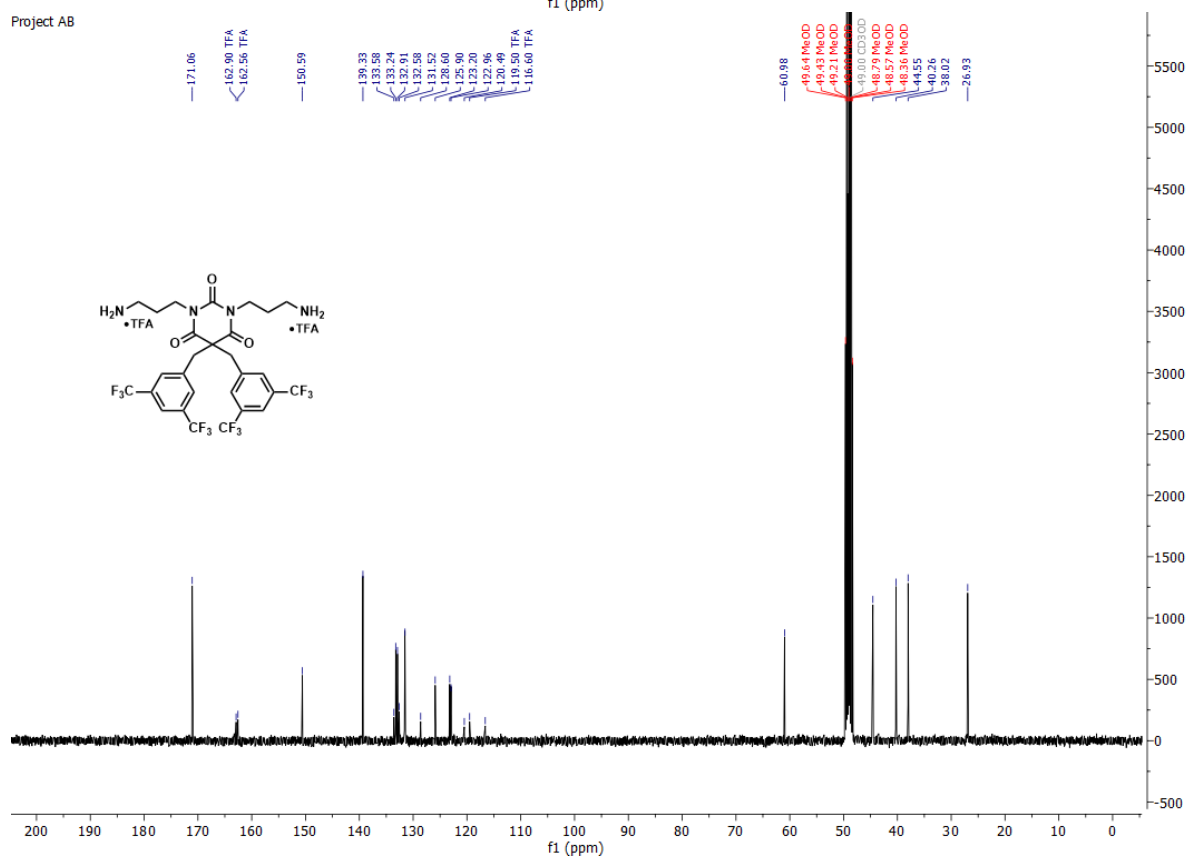
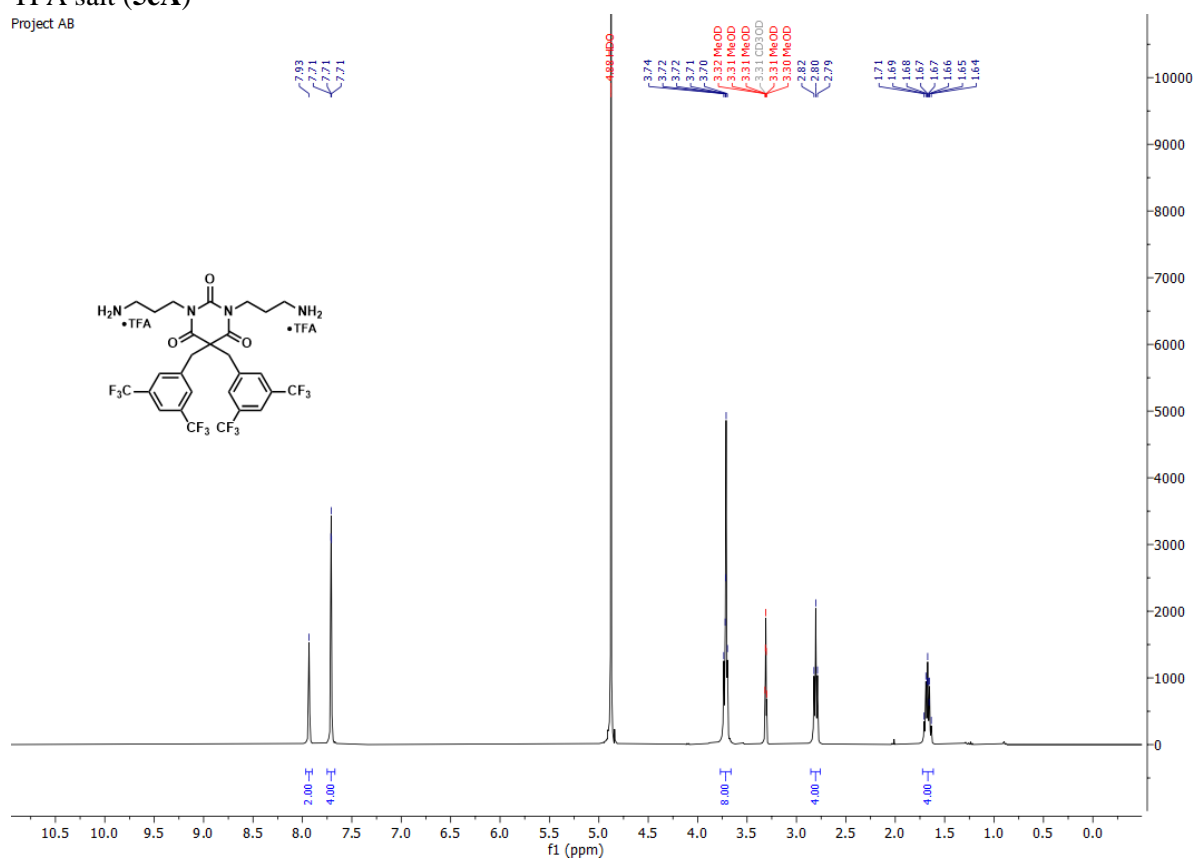


Project AB



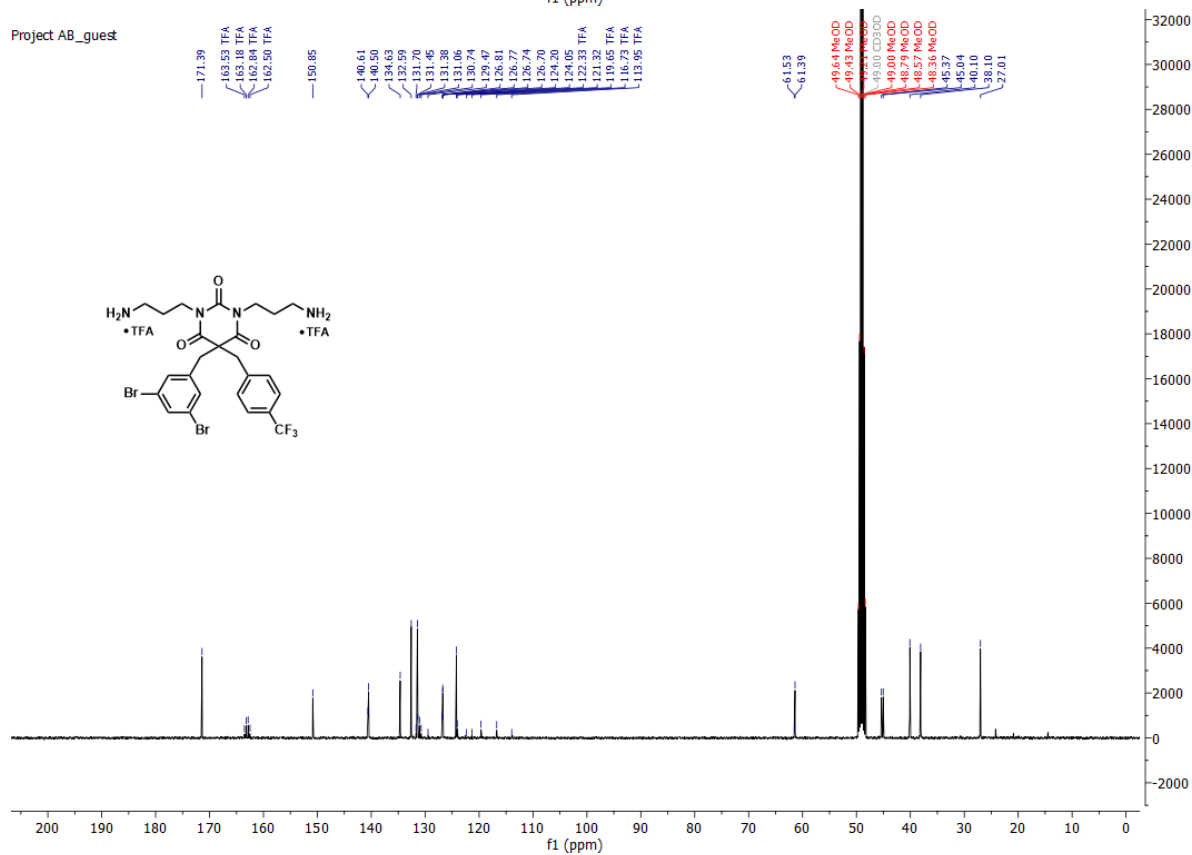
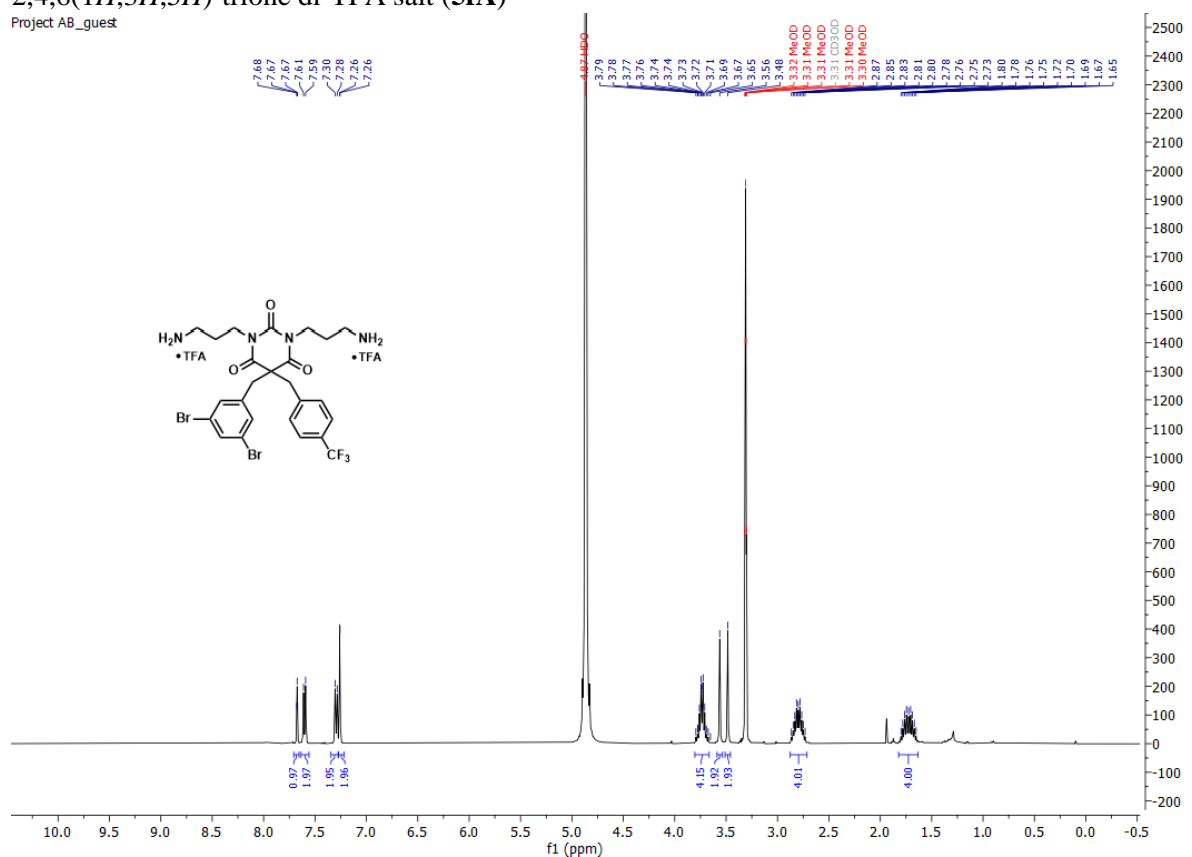
1,3-bis(3-aminopropyl)-5,5-bis(3,5-bis(trifluoromethyl)benzyl)pyrimidine-2,4,6(1*H*,3*H*,5*H*)-trione di-TFA salt (**5eA**)

Project AB



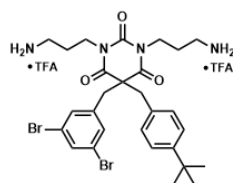
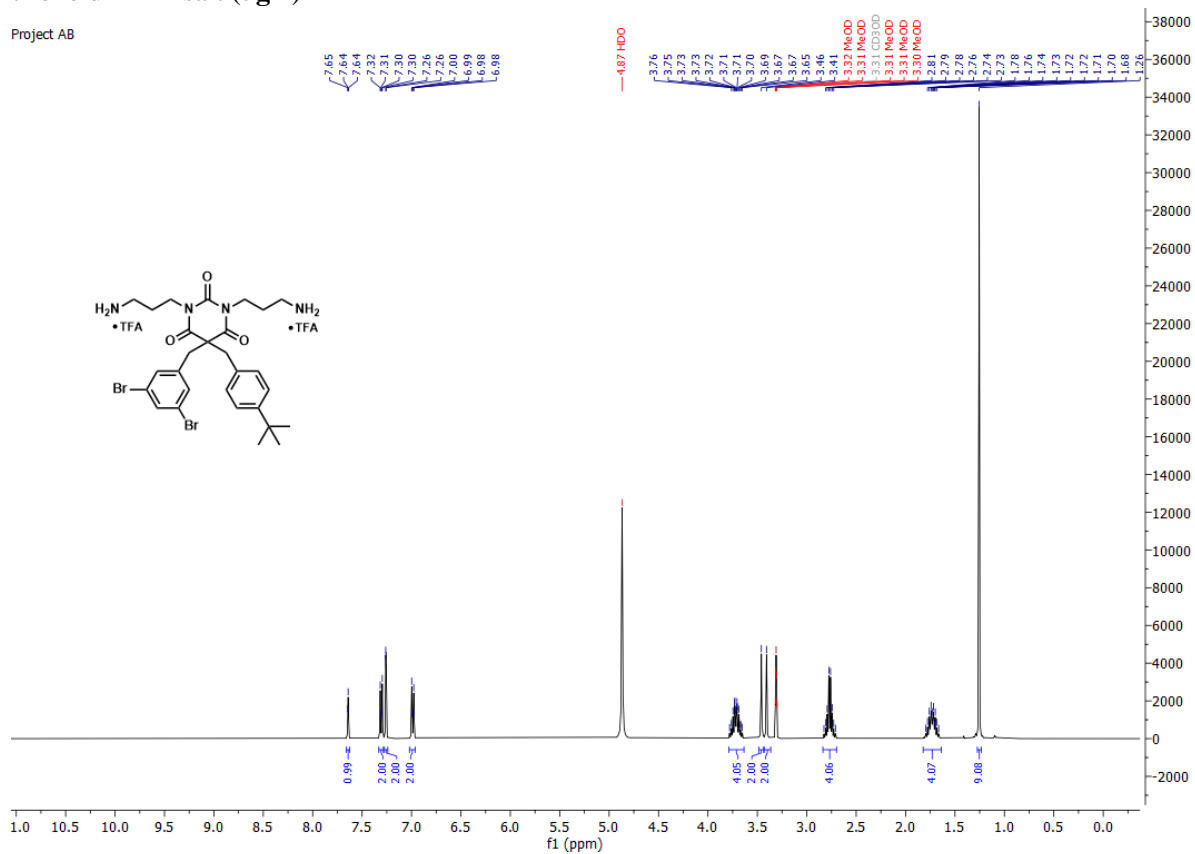
1,3-bis(3-aminopropyl)-5-(3,5-dibromobenzyl)-5-(4-(trifluoromethyl)benzyl)pyrimidine-2,4,6(1*H*,3*H*,5*H*)-trione di-TFA salt (**5fA**)

Project AB_guest

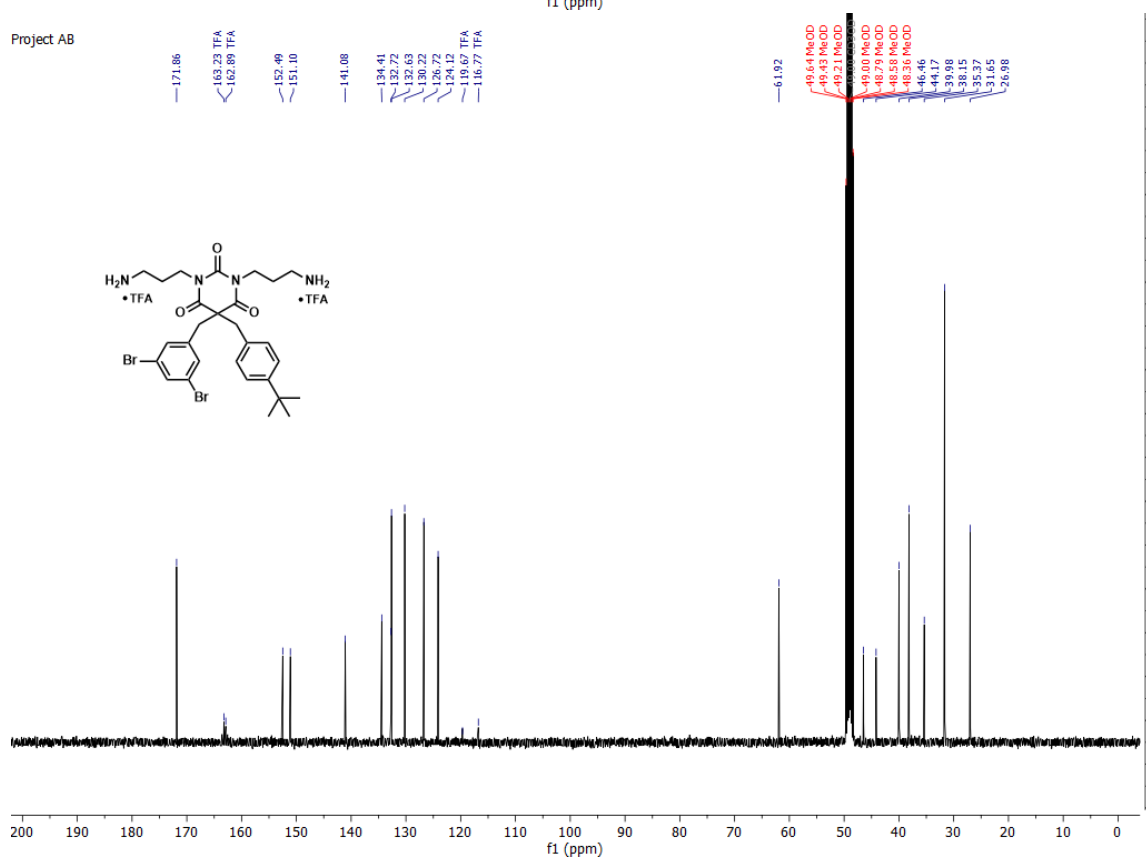


1,3-bis(3-aminopropyl)-5-(4-(*tert*-butyl)benzyl)-5-(3,5-dibromobenzyl)pyrimidine-2,4,6(1*H*,3*H*,5*H*)-trione di-TFA salt (**5gA**)

Project AB

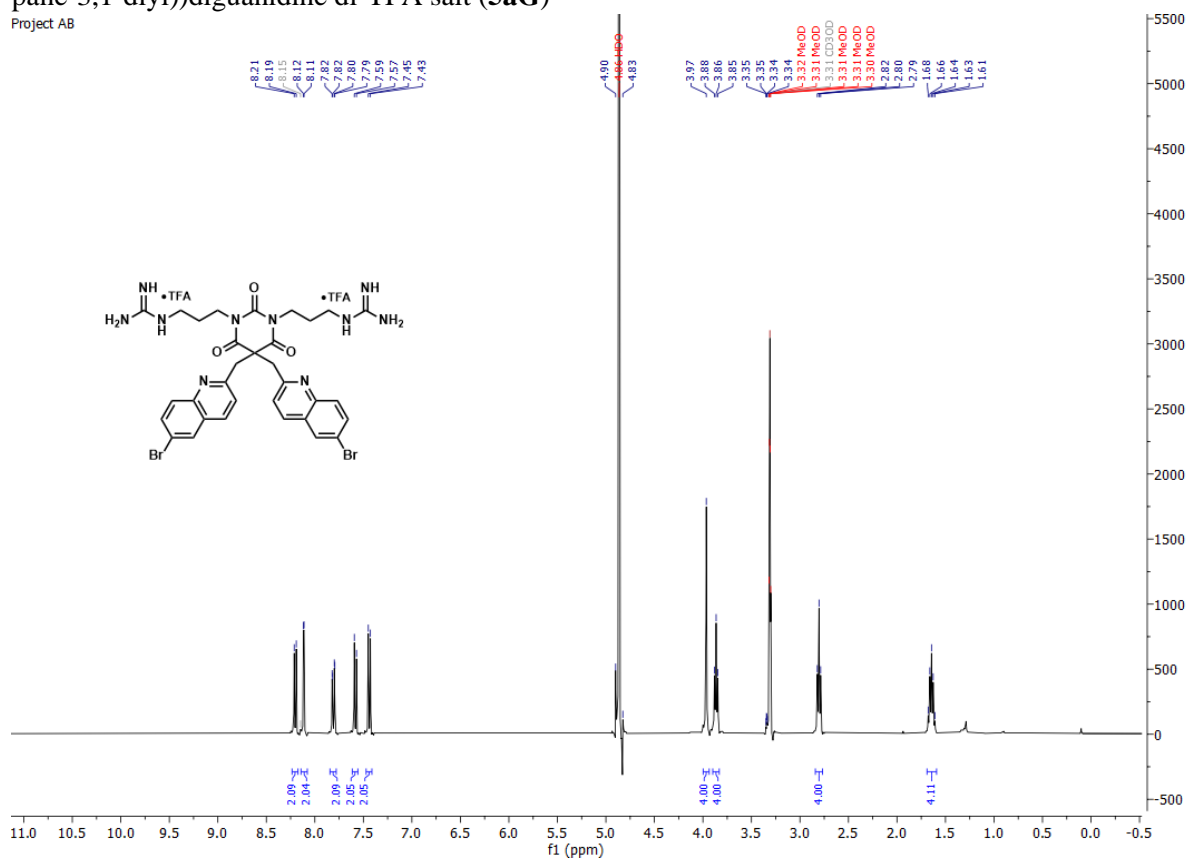


Project AB

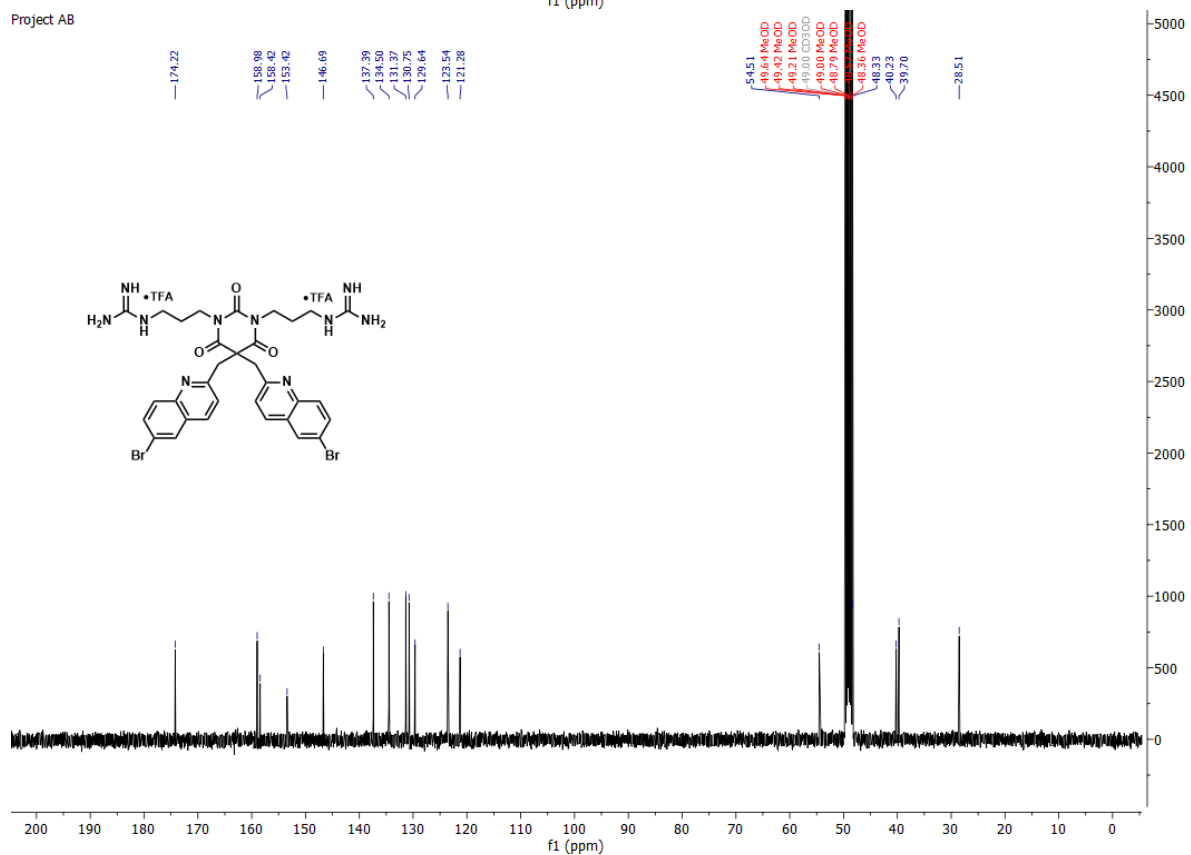


1,1'-((5,5-bis((6-bromoquinolin-2-yl)methyl)-2,4,6-trioxodihydropyrimidine-1,3(2*H*,4*H*)-diyl)bis(propane-3,1-diyl))diguanidine di-TFA salt (**5aG**)

Project AB

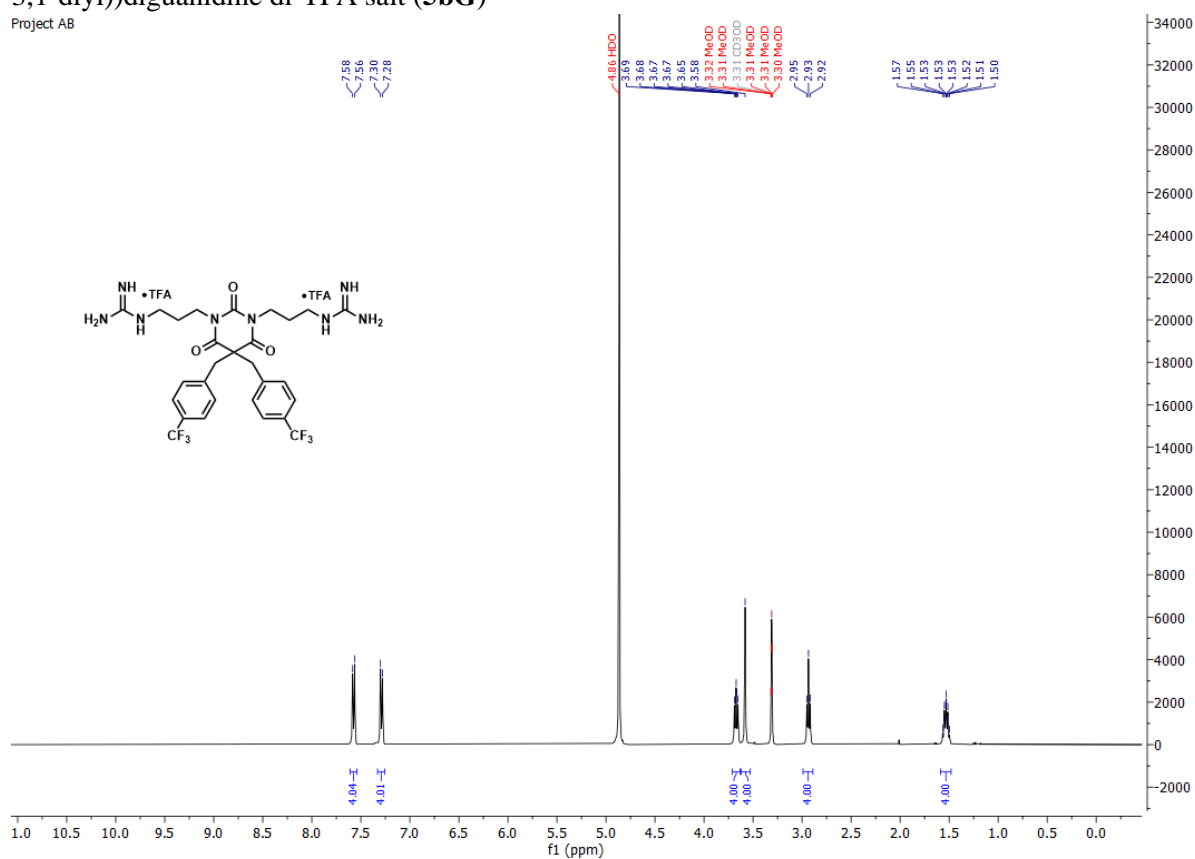


Project AB

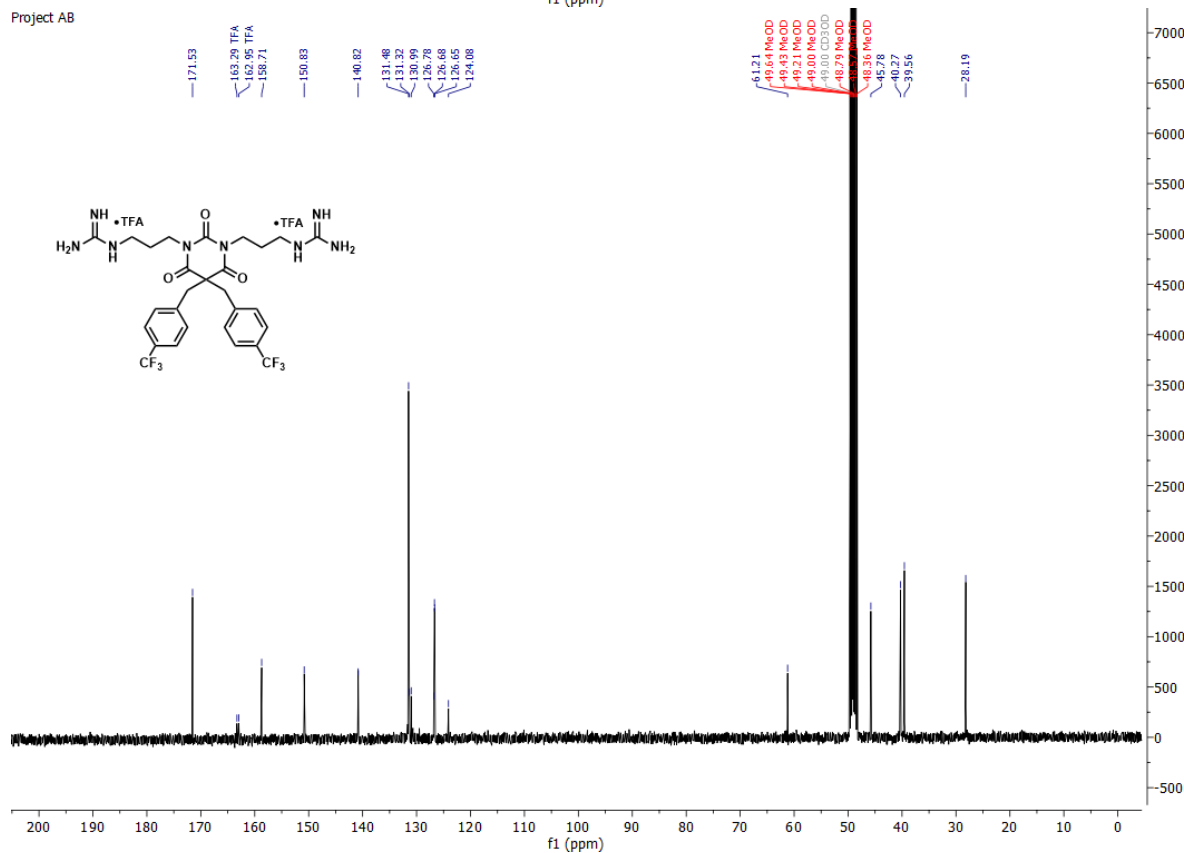


1,1'-((2,4,6-trioxo-5,5-bis(4-(trifluoromethyl)benzyl)dihydropyrimidine-1,3(2*H*,4*H*)-diyl)bis(propane-3,1-diyl))diguanidine di-TFA salt (**5bG**)

Project AB

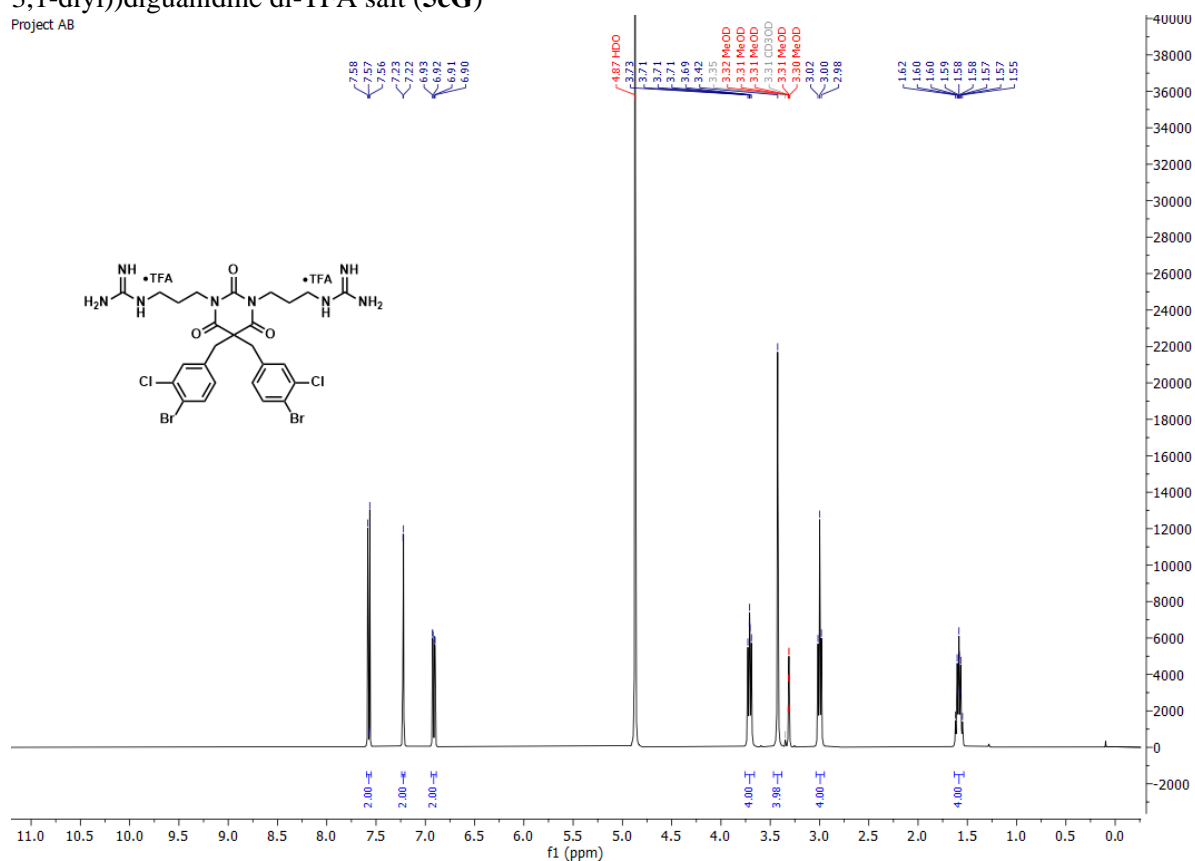


Project AB

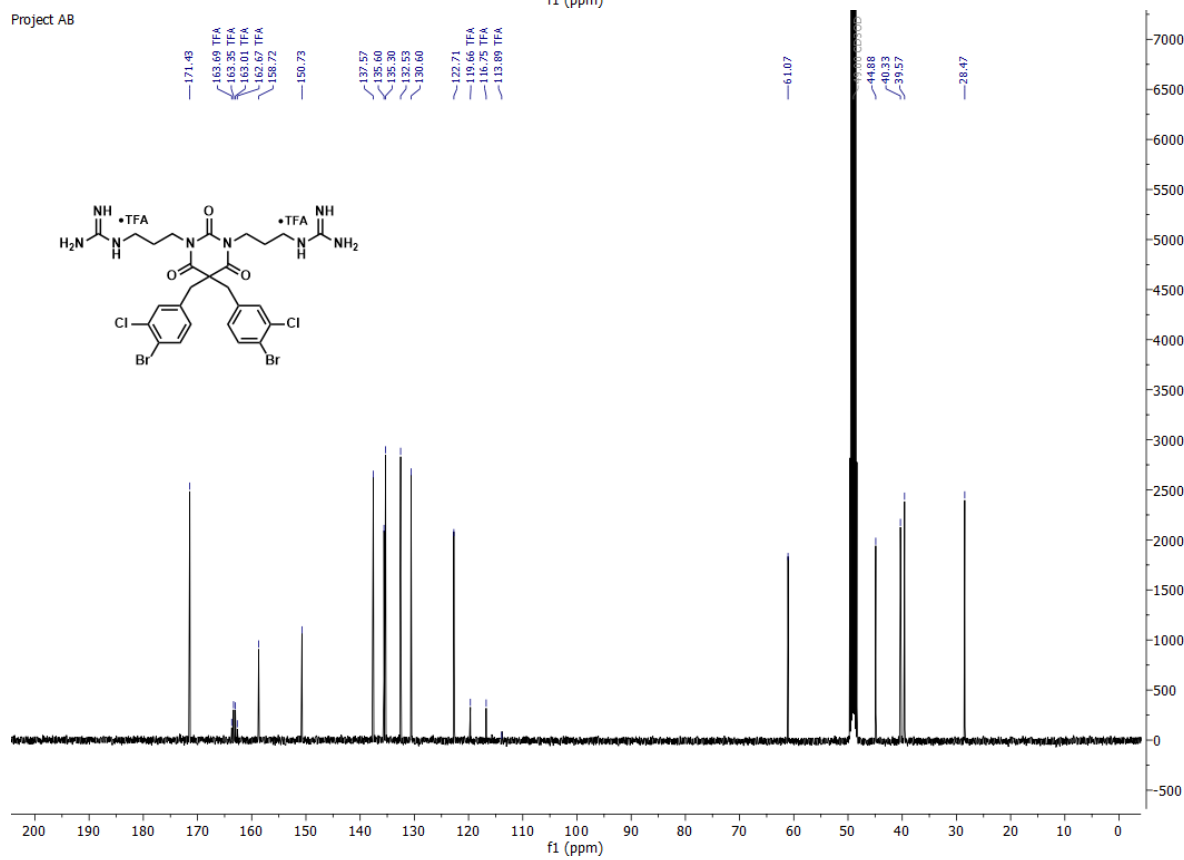


1,1'-((5,5-bis(4-bromo-3-chlorobenzyl)-2,4,6-trioxodihydropyrimidine-1,3(2*H*,4*H*)-diyl)bis(propane-3,1-diyl))diguanidine di-TFA salt (**5cG**)

Project AB

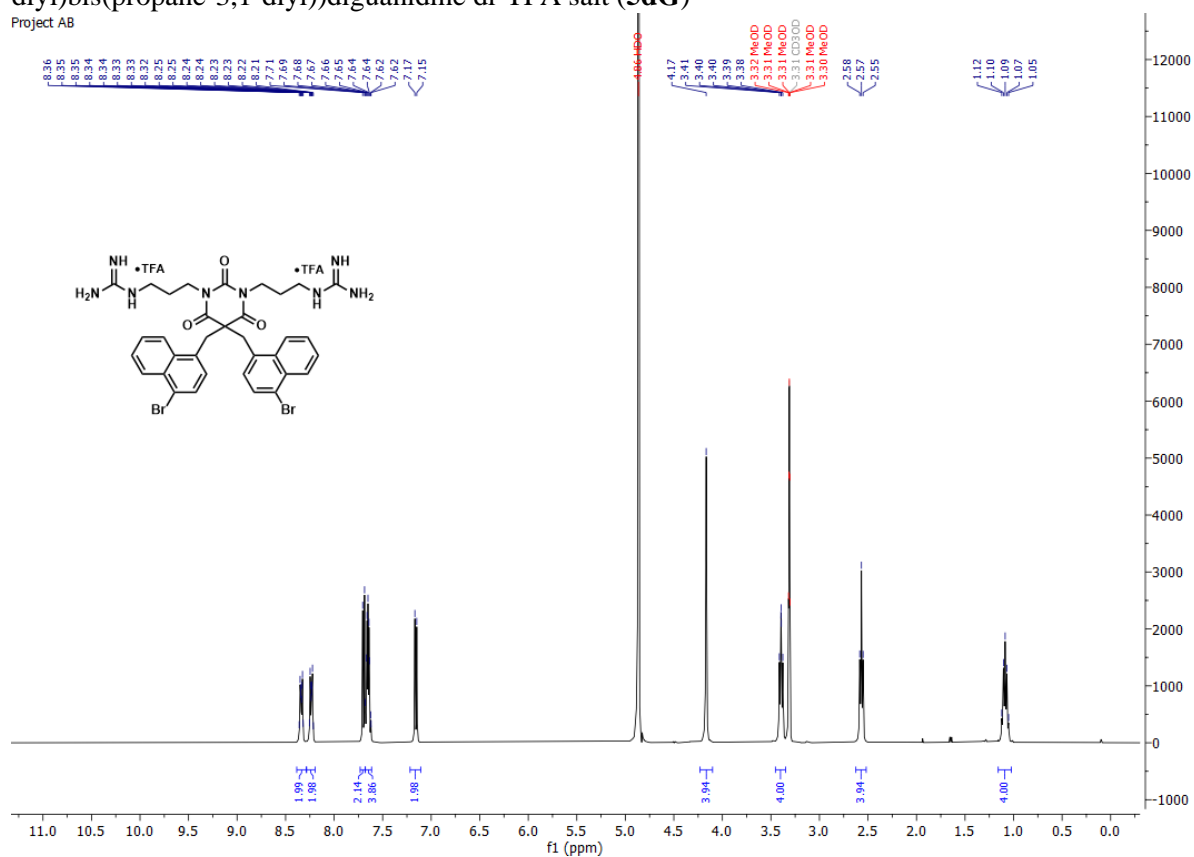


Project AB

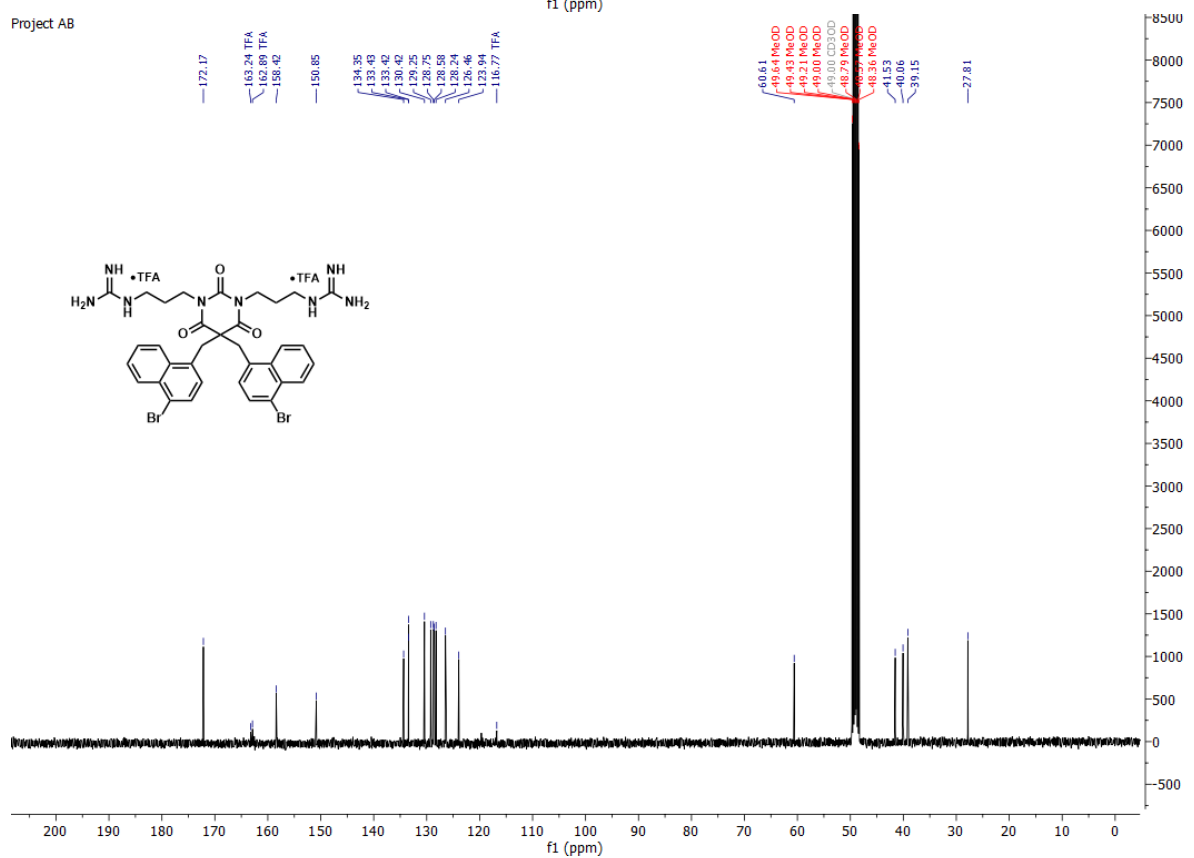


1,1'-((5,5-bis((4-bromonaphthalen-1-yl)methyl)-2,4,6-trioxodihydropyrimidine-1,3(2*H*,4*H*)-diyl)bis(propane-3,1-diyl)diguanidine di-TFA salt (**5dG**)

Project AB

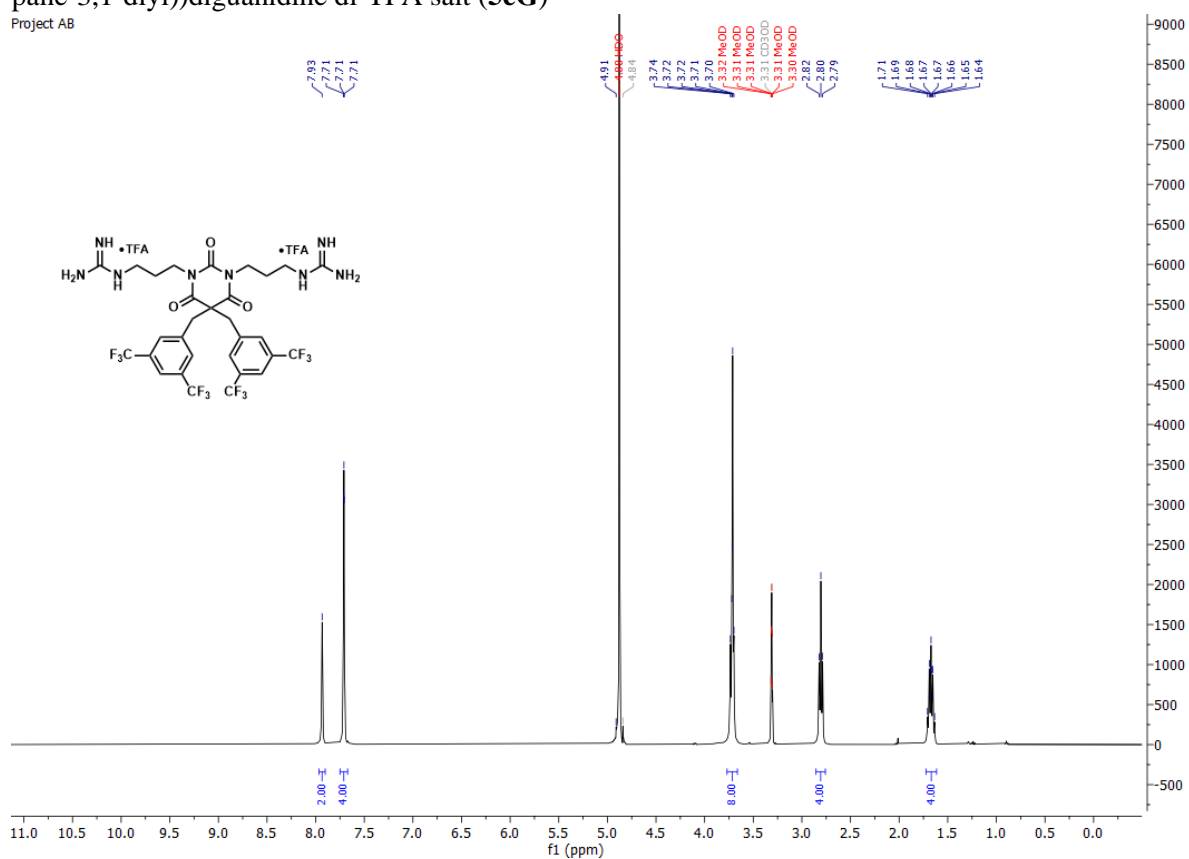


Project AB

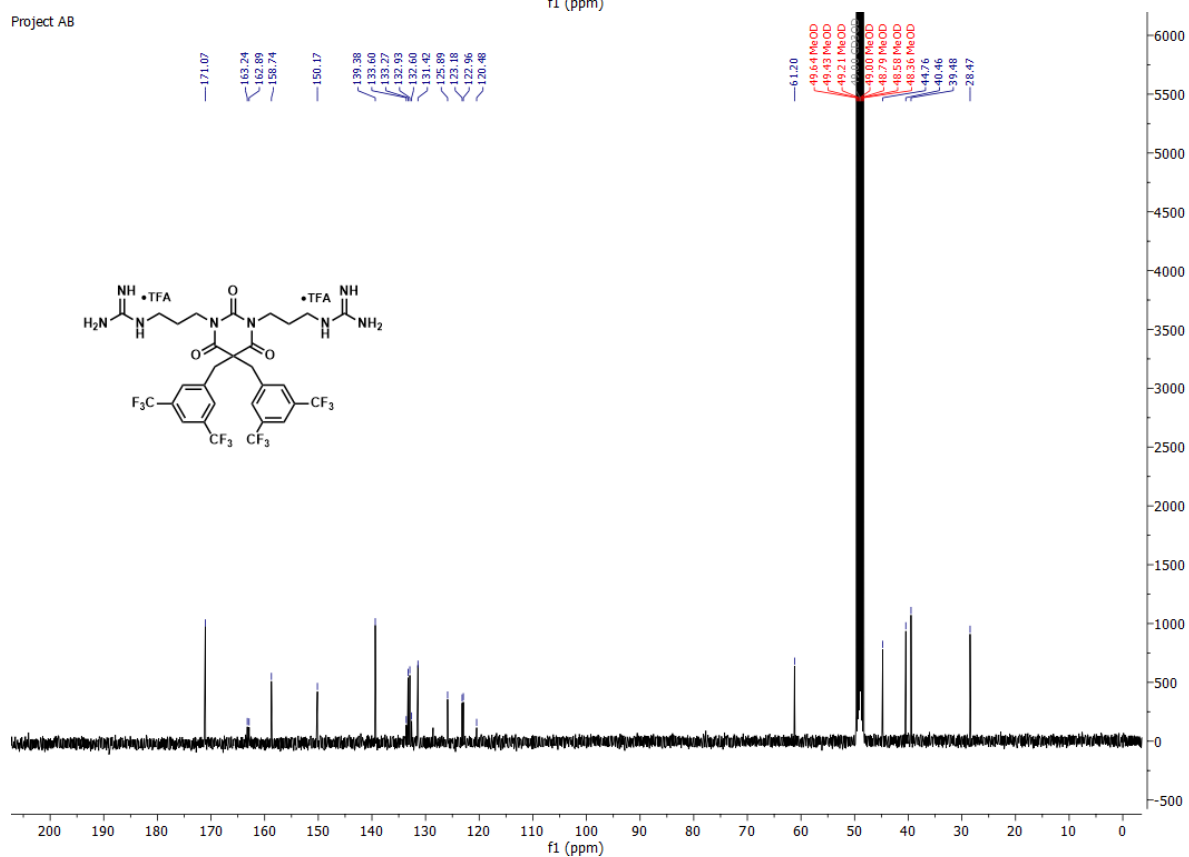


1,1'-((5,5-bis(3,5-bis(trifluoromethyl)benzyl)-2,4,6-trioxodihydropyrimidine-1,3(2H,4H)-diyl)bis(propane-3,1-diyl))diguanidine di-TFA salt (**5eG**)

Project AB

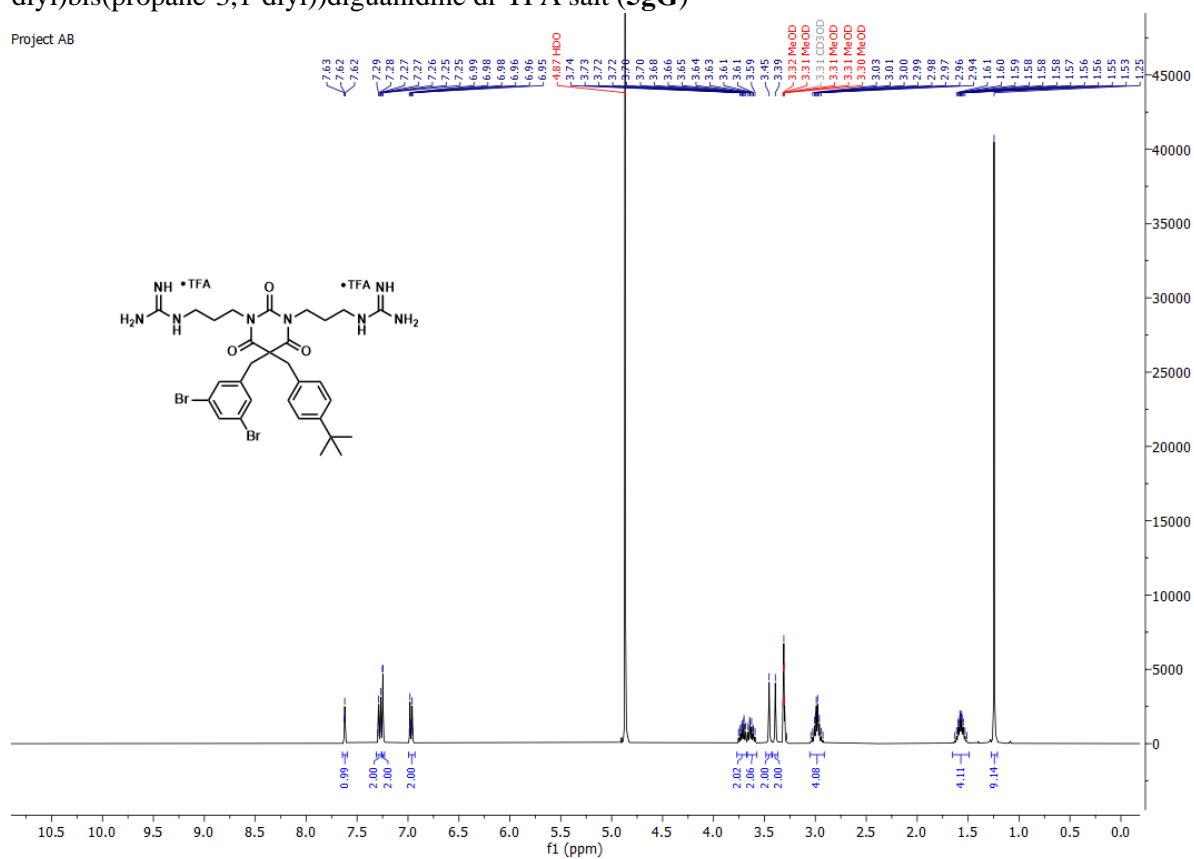


Project AB

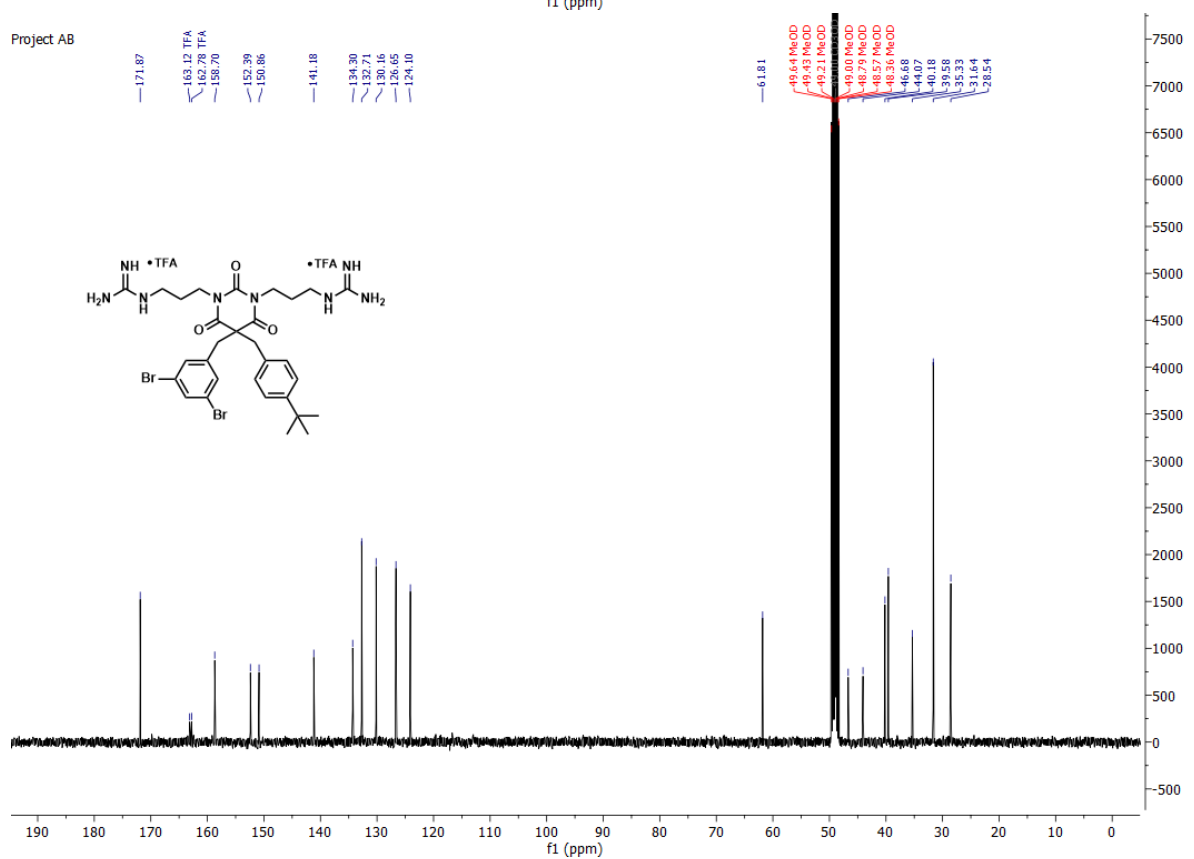


1,1'-((5-(4-(*tert*-butyl)benzyl)-5-(3,5-dibromobenzyl)-2,4,6-trioxodihydropyrimidine-1,3(2*H*,4*H*)-diyl)bis(propane-3,1-diyl)diguanidine di-TFA salt (**5gG**)

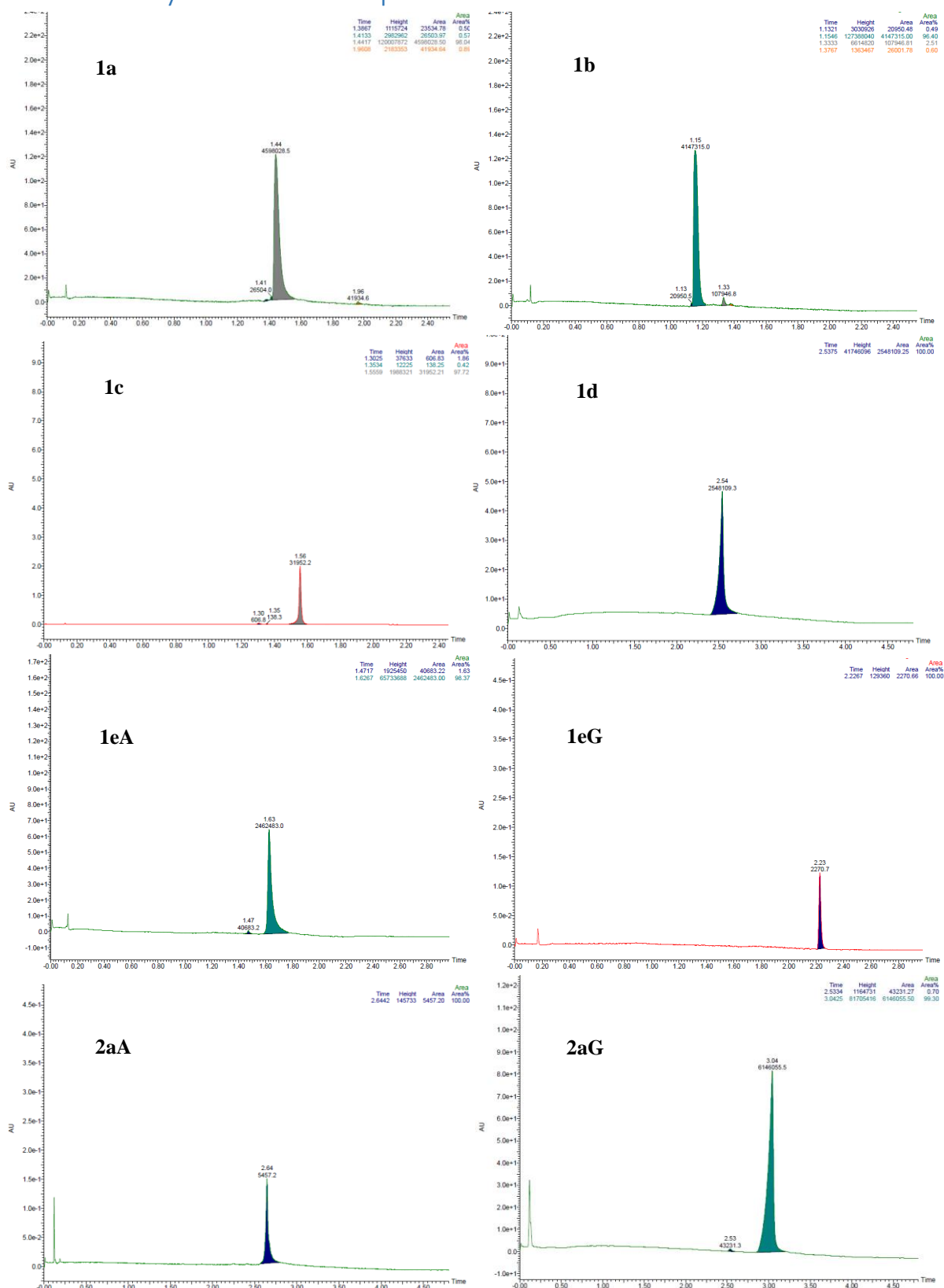
Project AB

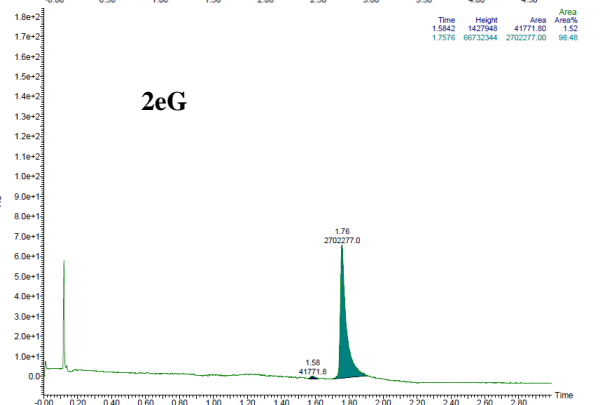
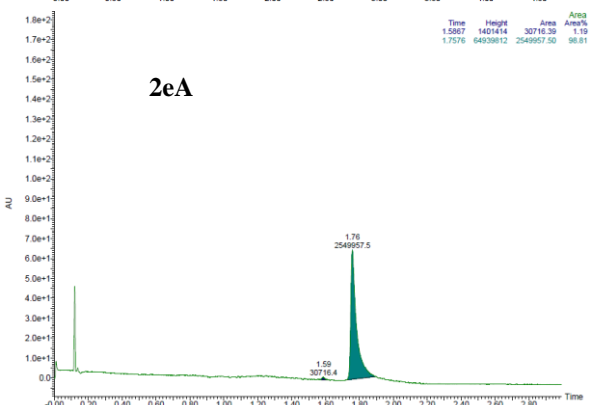
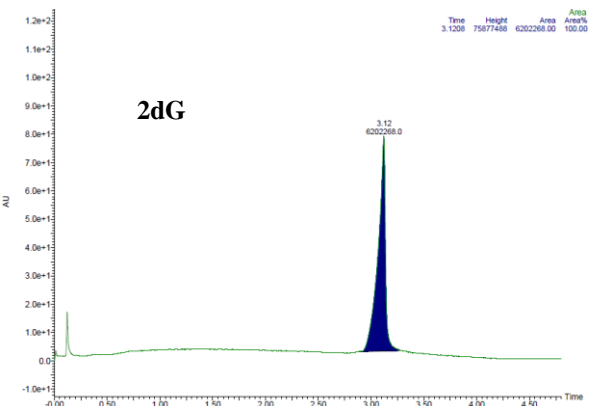
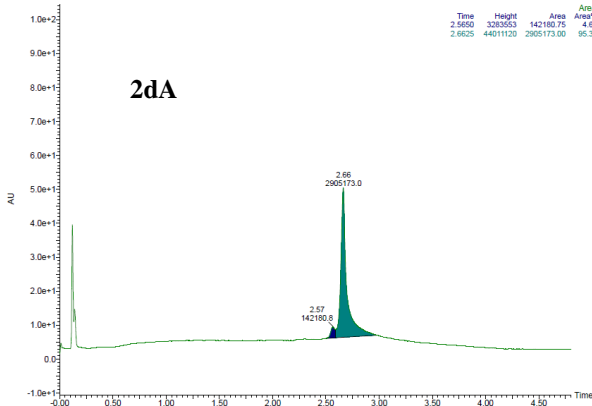
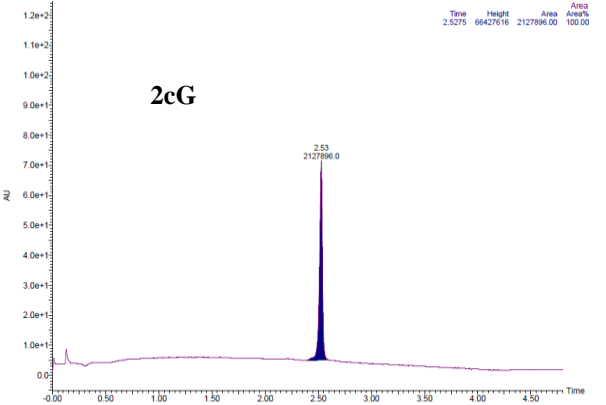
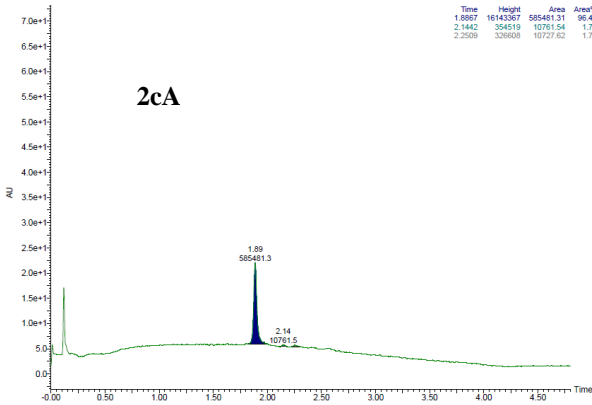
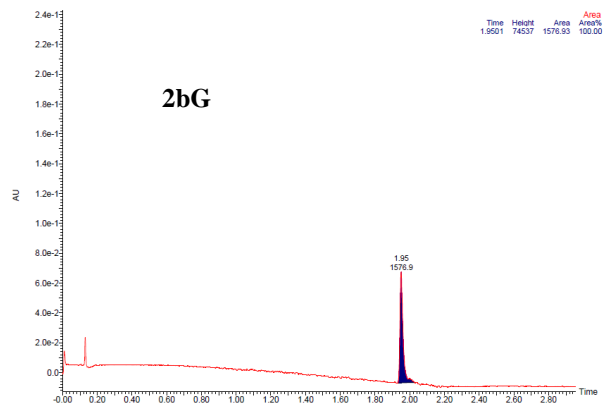
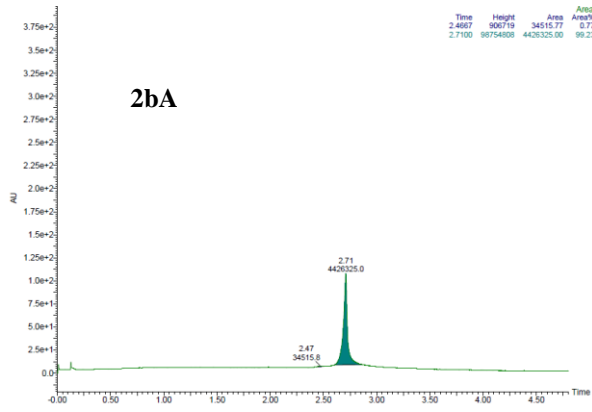


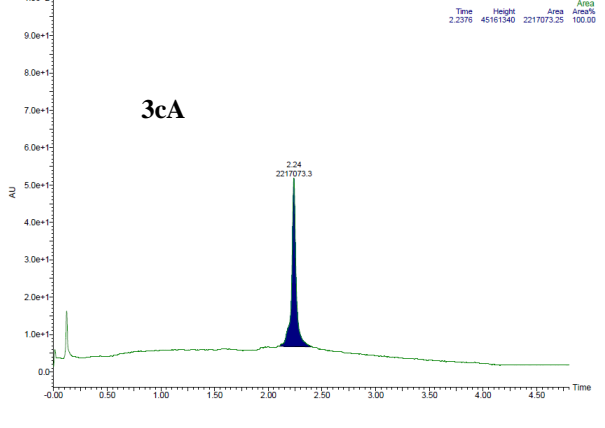
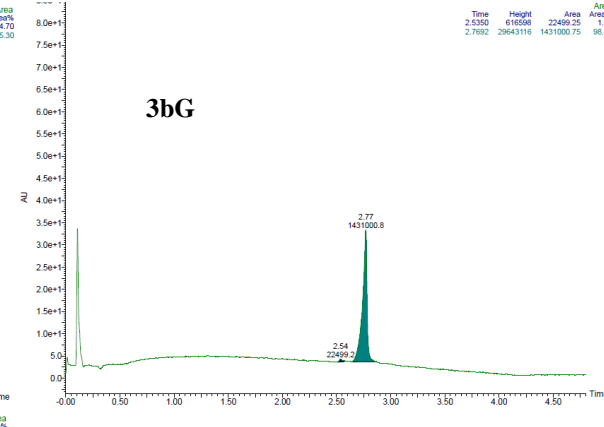
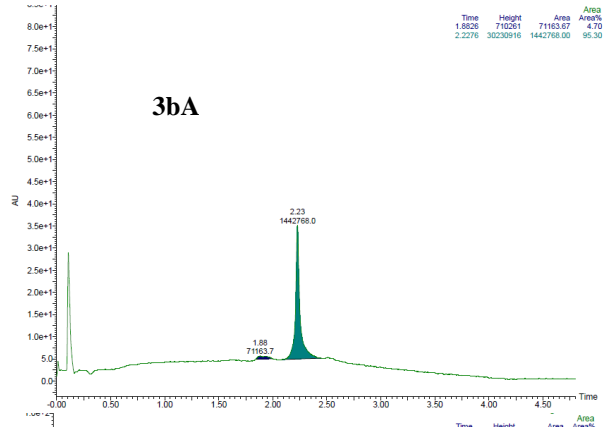
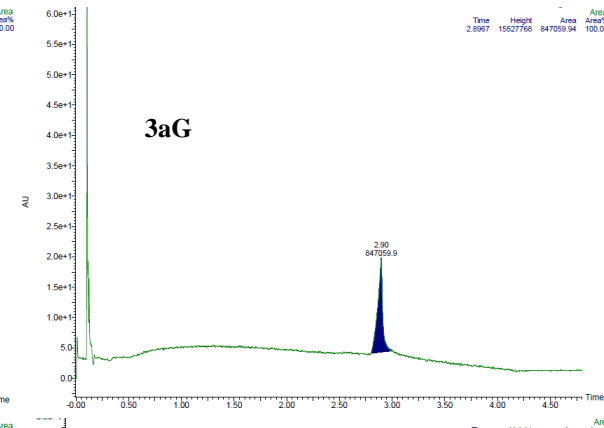
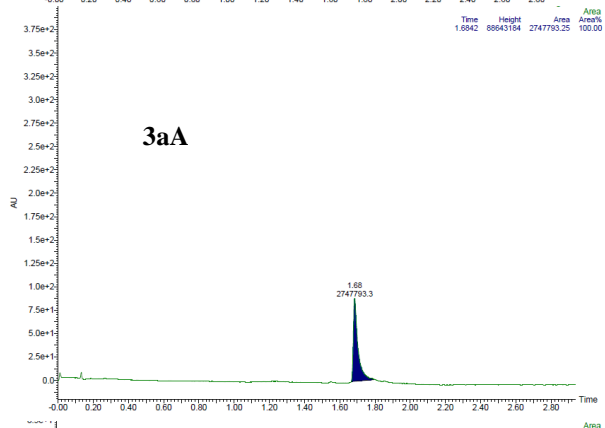
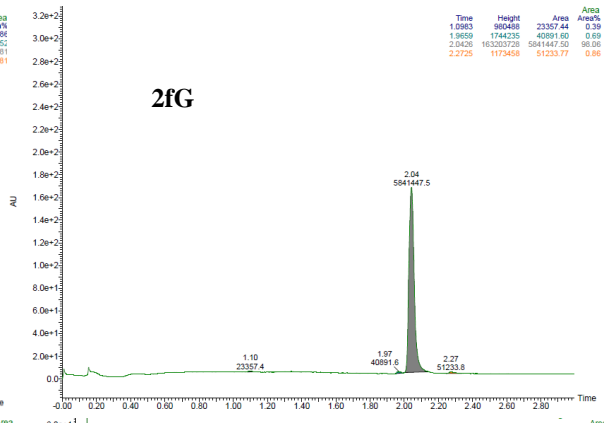
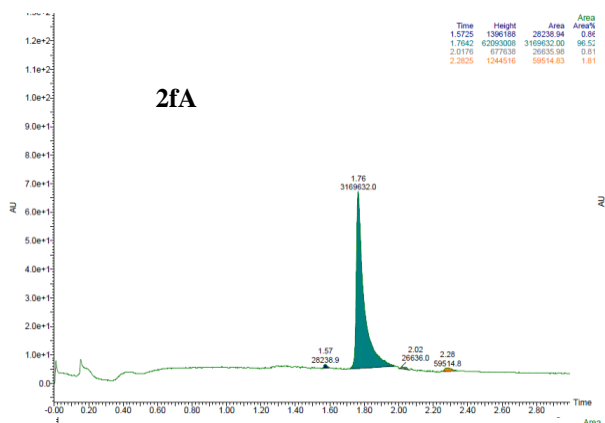
Project AB

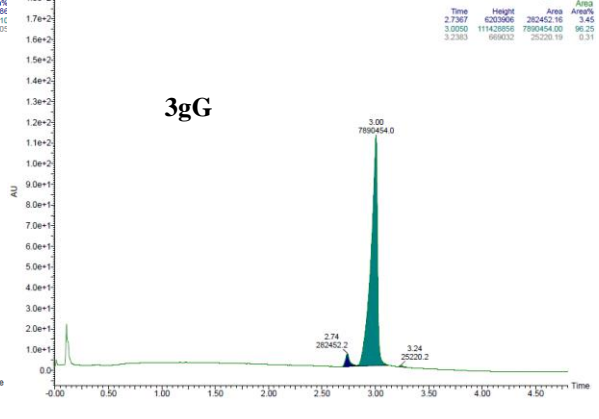
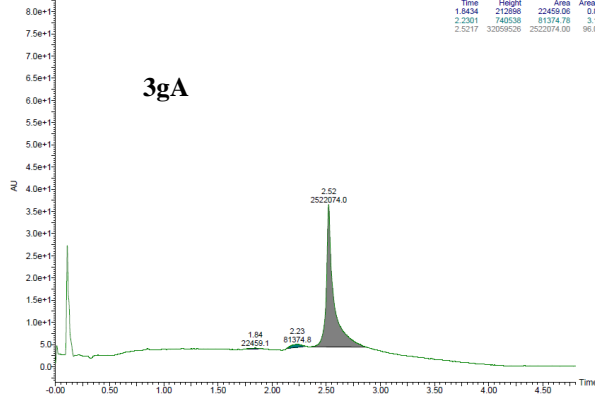
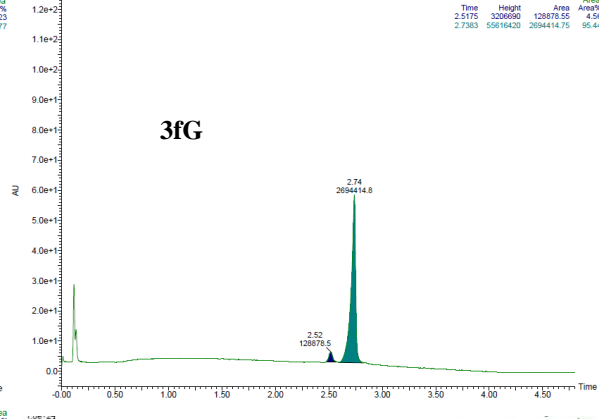
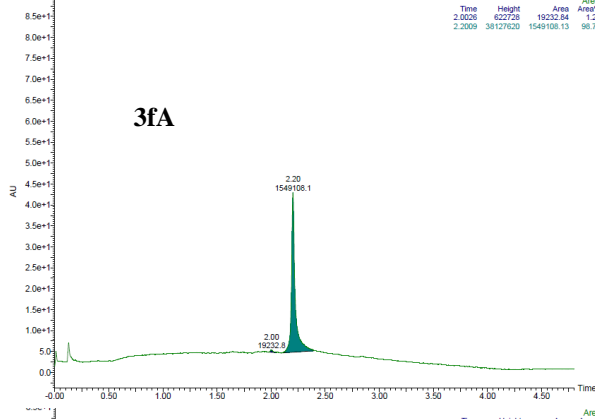
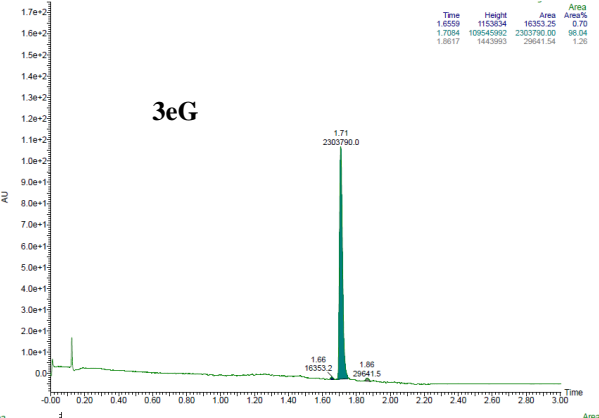
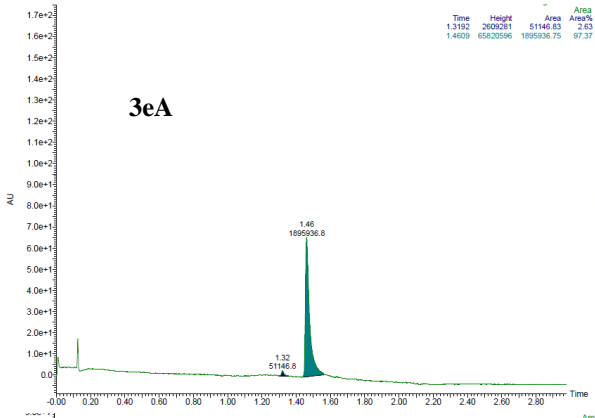
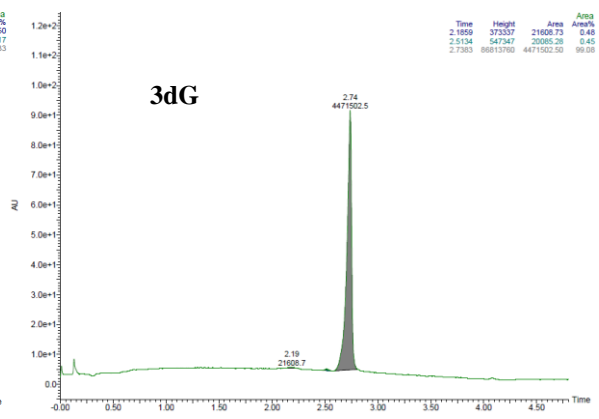
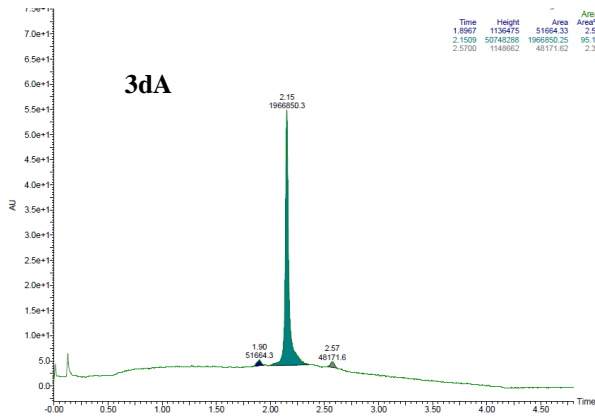


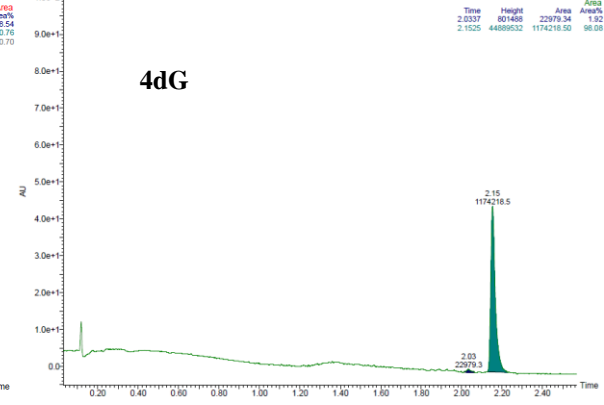
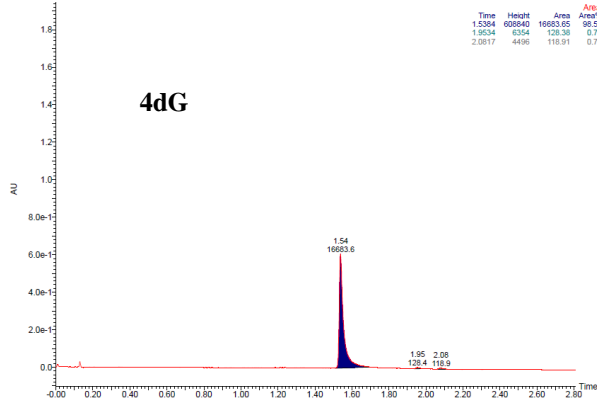
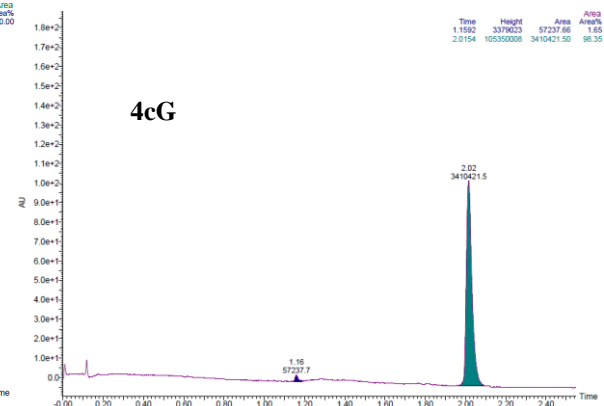
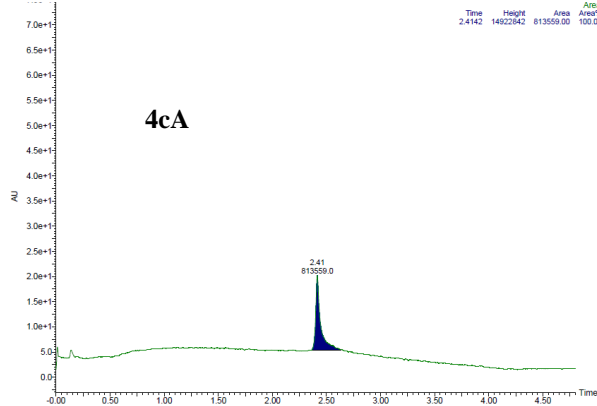
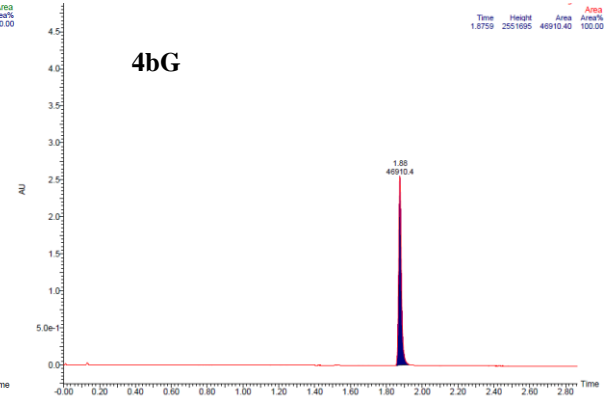
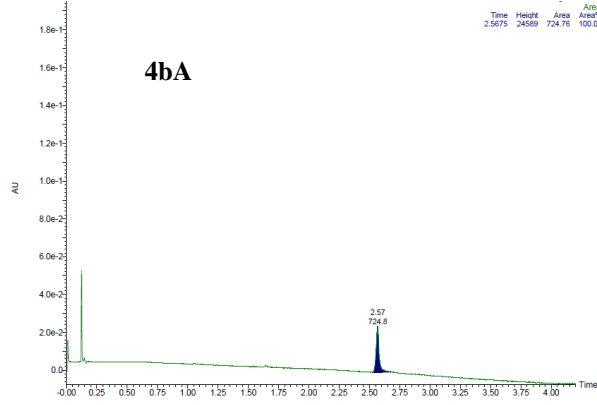
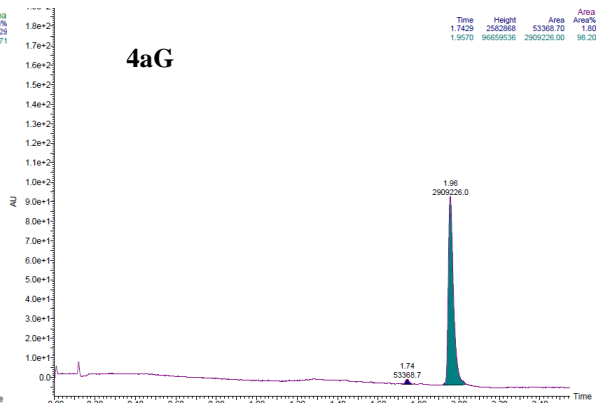
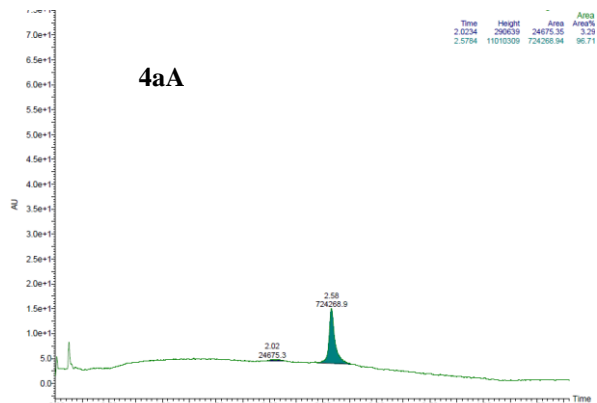
4 SFC analysis of final compounds

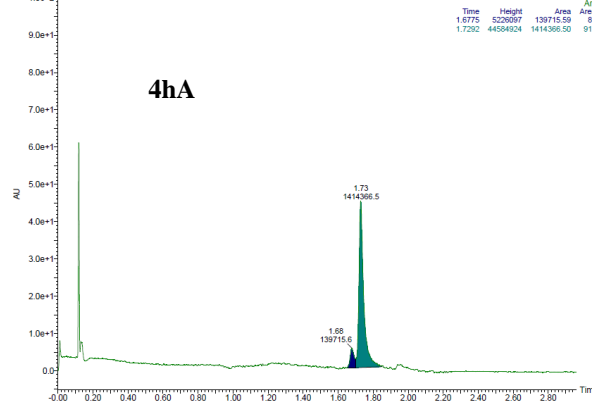
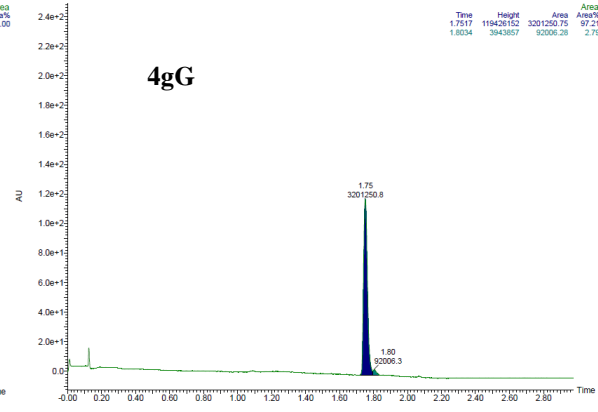
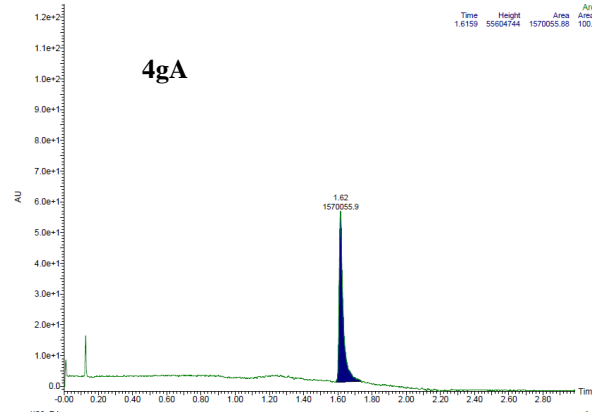
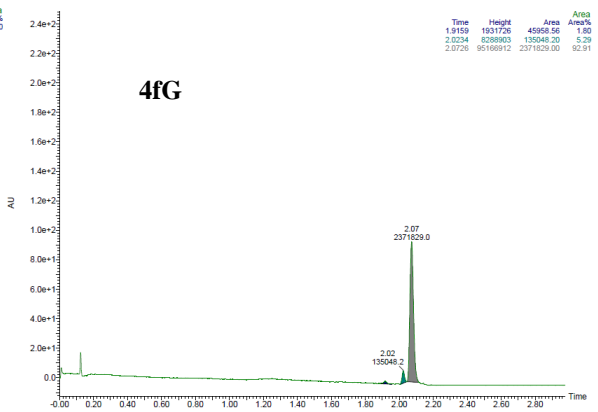
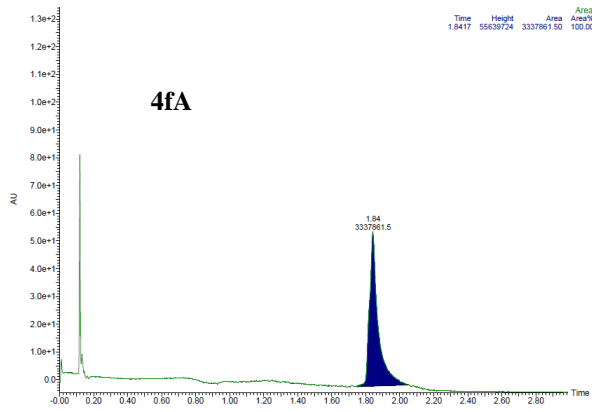
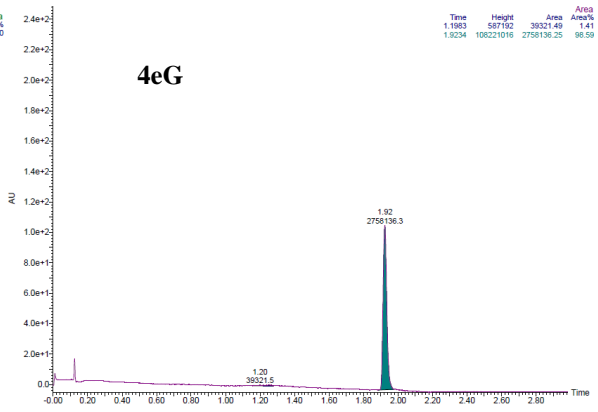
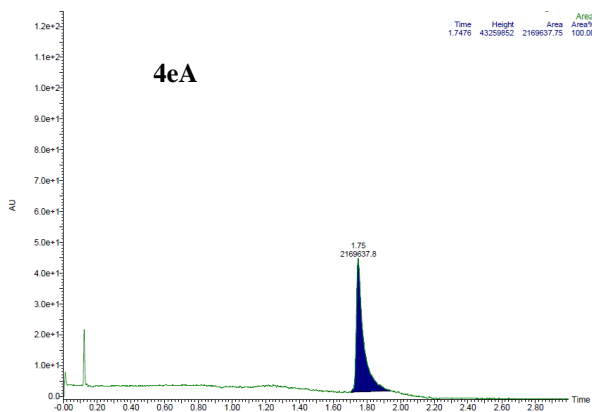


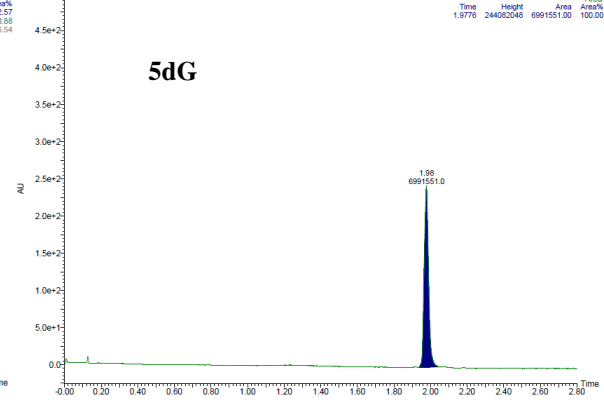
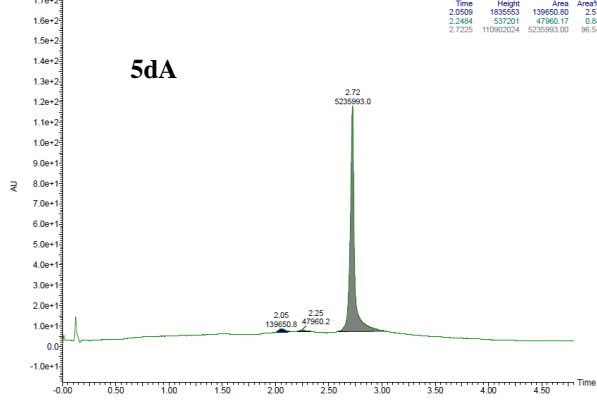
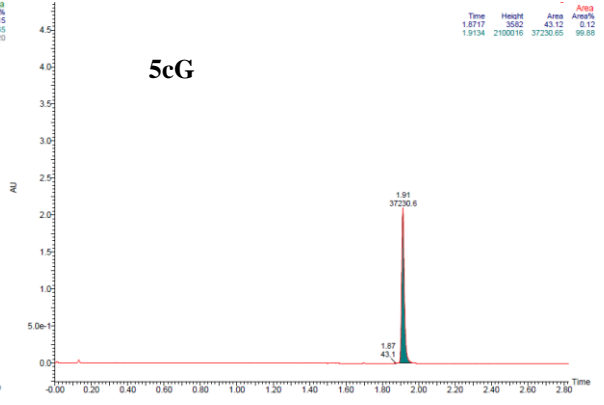
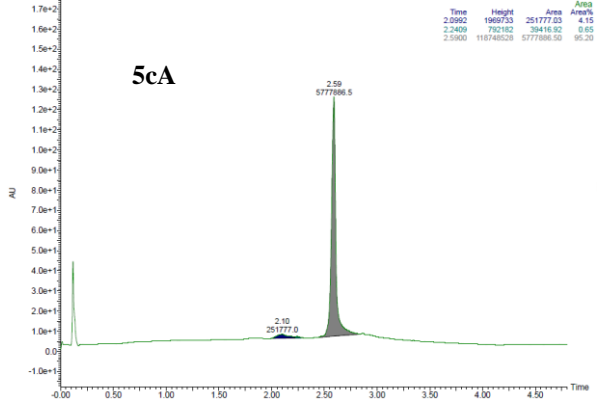
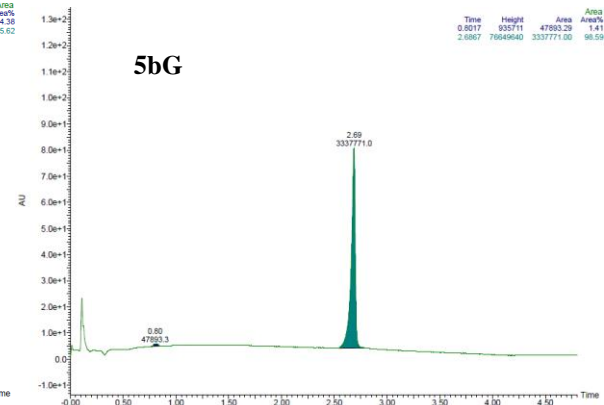
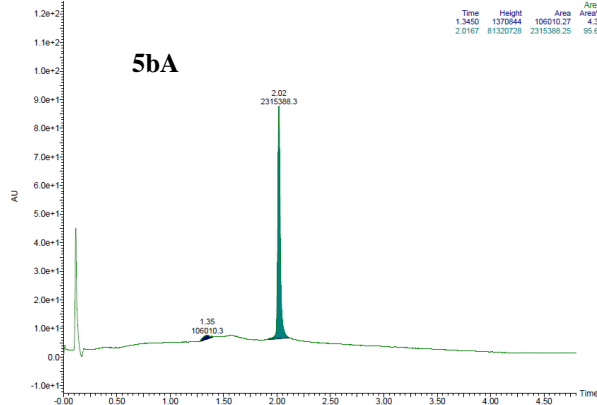
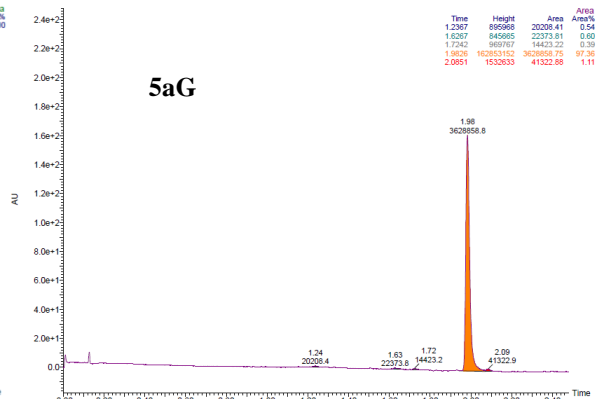
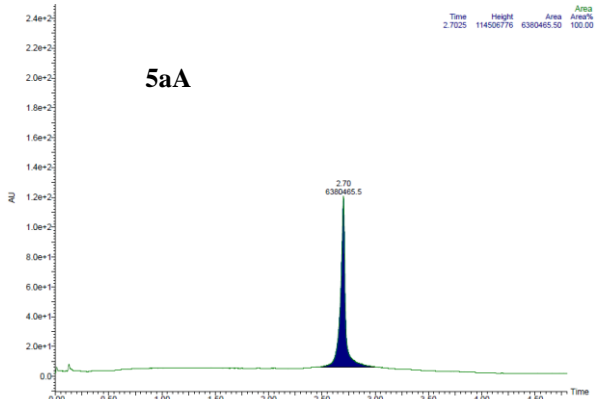


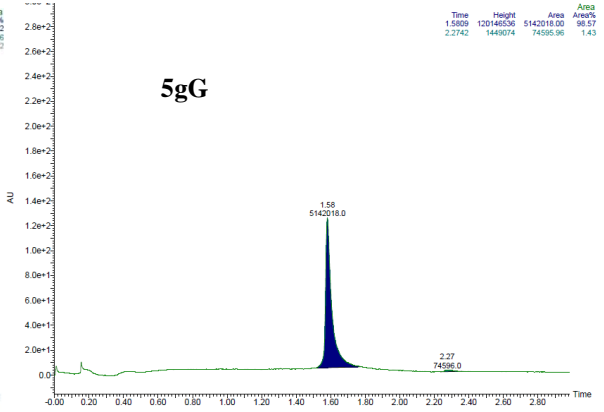
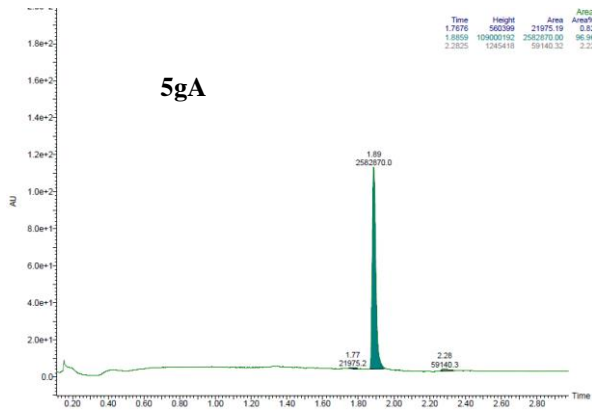
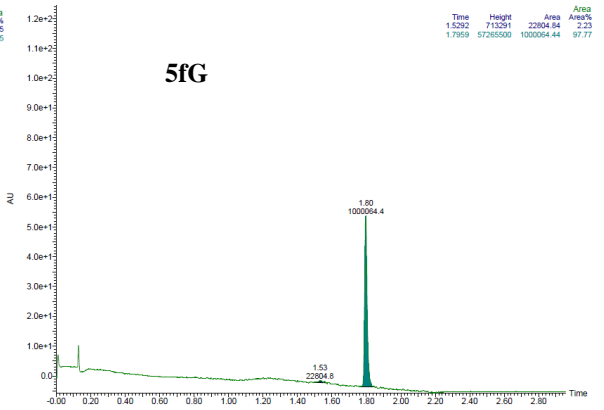
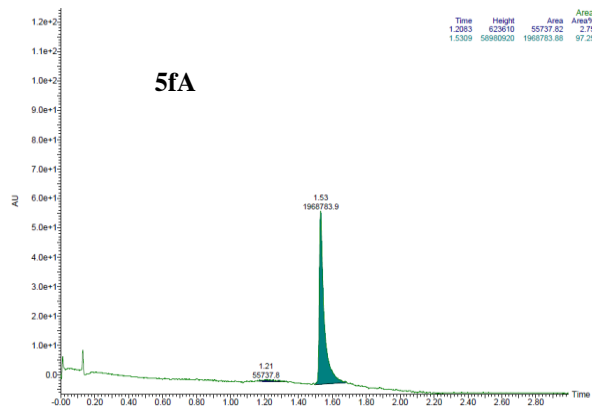
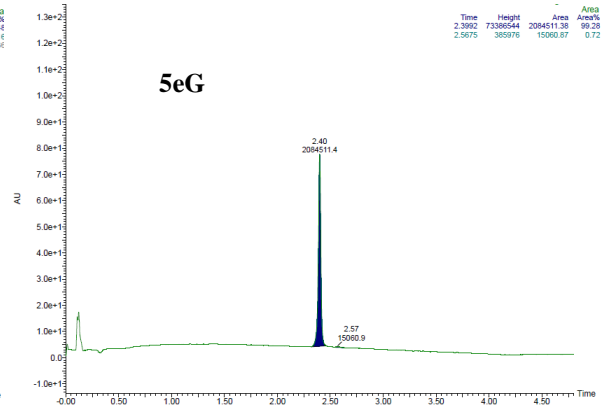
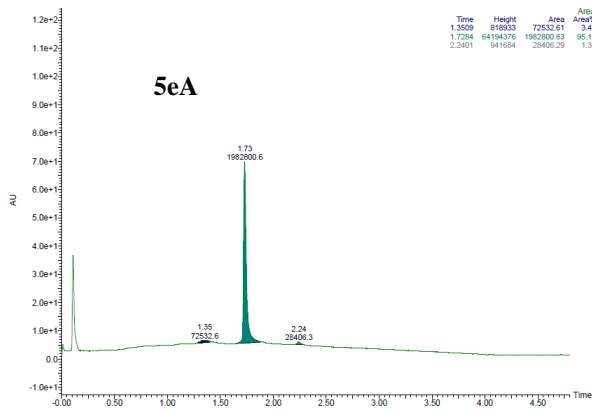












5 Full selectivity index table

Table S1 Selectivity index (SI) of all compounds towards all bacterial strains tested. EC₅₀ values are given in [μg/mL].

Code	Basic group	X	SI (MIC/EC ₅₀) ^a				
			S. a	B. s	E. c	P. a	EC ₅₀
1a	(N(Me)H)	<i>n</i> -butyl	9	18	9	5	73
1b	(NMe ₂)	<i>n</i> -butyl	20	39	20	–	157
1c	(NMe ₃)	<i>n</i> -butyl	>135	>67	–	–	>539
1d	(pyridinyl)	<i>n</i> -butyl	>280	>140	>70	–	>559
1eA	NH ₂	<i>n</i> -butyl	20	40	20	10	79
1eG	guanidyl	<i>n</i> -butyl	31	31	31	8	62

Code	R ¹	X	SI (MIC/EC ₅₀) ^a					Code	SI (MIC/EC ₅₀) ^a				
			S. a	B. s	E. c	P. a	EC ₅₀		S. a	B. s	E. c	P. a	EC ₅₀
2aA	(2-methylquinoline)	<i>n</i> -butyl	–	–	–	–	>390	2aG	>54	>27	–	–	>432
2bA	(6-Br-2-methylquinoline)	<i>n</i> -butyl	>29	>117	–	–	>469	2bG	230	115	29	–	461
2cA	(<i>n</i> -hexyl)	<i>n</i> -butyl	>21	>42	–	–	>333	2cG	72	72	36	9	143
2dA	(4-Br-1-Me-Nal)	<i>n</i> -butyl	14	14	7	7	27	2dG	9	9	9	5	36
2eA	(2,4,5-tri-BrBn)	<i>n</i> -butyl	7	7	3	3	27	2eG	8	8	8	4	32
2fA	(2,4,6-tri-BrBn)	<i>n</i> -butyl	15	15	8	8	30	2fG	15	15	8	8	30

Code	Basic group	X	SI (MIC/EC ₅₀) ^a					Code	SI (MIC/EC ₅₀) ^a				
			S. a	B. s	E. c	P. a	EC ₅₀		S. a	B. s	E. c	P. a	EC ₅₀
3aA	(2-methylquinoline)	<i>n</i> -butyl	–	>56	–	–	>444	3aG	225	113	–	–	450
3bA	(4-CF ₃ Bn)	<i>n</i> -butyl	21	43	–	–	342	3bG	81	40	81	10	161
3cA	(cyclopentyl)	<i>n</i> -butyl	25	51	–	–	>407						
3dA	(<i>n</i> -hexyl)	<i>n</i> -butyl	36	36	9	9	144	3dG	29	15	15	7	58
3eA	(3,5-di-CF ₃ Bn)	<i>n</i> -butyl	12	46	12	12	93	3eG	18	18	18	9	36
3fA	(4- <i>tert</i> -butylBn)	<i>n</i> -butyl	12	12	12	6	47	3fG	20	20	20	10	39
3gA	(4-Br-1-Me-Nal)	<i>n</i> -butyl	21	21	10	10	82	3fG	15	15	15	7	58

Code	R ¹	X	SI (MIC/EC ₅₀) ^a					Code	SI (MIC/EC ₅₀) ^a				
			S. a	B. s	E. c	P. a	EC ₅₀		S. a	B. s	E. c	P. a	EC ₅₀
4aA	(3,5-di-BrBn)	(C ₂ H ₄)	10	10	10	5	39	4aG	82	82	41	10	164
4bA	(3,5-di-BrBn)	(C ₃ H ₆)	25	25	12	12	99	4bG	93	93	47	23	187
4cA	(3,5-di-BrBn)	(C ₅ H ₁₀)	6	6	3	3	24	4cG	5	5	5	4	29 ^b
4dA	(3,5-di-BrBn)	(C ₆ H ₁₂)	8	8	8	2	30	4dG	14	14	14	2	57 ^b
4eA	(3,5-di-BrBn)	(<i>cis</i> -cyclobutane)	6	13	13	6	50	4eG	37	37	19	9	75
4fA	(3,5-di-BrBn)	(<i>trans</i> -cyclobutane)	23	23	23	12	93	4fG	31	16	16	8	62
4gA	(3,5-di-BrBn)	(<i>cis</i> -cyclohexyl)	4	4	4	2	15	4gG	15	>30	8	8	30
4hA	(3,5-di-BrBn)	(<i>trans</i> -cyclohexyl)	8	8	8	4	16						

Code	R ¹	X	SI (MIC/EC ₅₀) ^a					Code	SI (MIC/EC ₅₀) ^a				
			S. a	B. s	E. c	P. a	EC ₅₀		S. a	B. s	E. c	P. a	EC ₅₀
5aA	(6-Br-2-methylquinoline)	<i>n</i> -propyl	–	>57	–	–	>455	5aG	>62	>124	–	–	>497
5bA	(4-CF ₃ Bn)	<i>n</i> -propyl	–	>25	–	–	>393	5bG	>54	>109	–	–	>435
5cA	(3-Cl, 4-BrBn)	<i>n</i> -propyl	40	81	40	20	323	5cG	174	174	44	–	348
5dA	(4-Br-1-Nal)	<i>n</i> -propyl	11	11	6	6	23	5dG	31	31	15	8	61
5eA	(3,5-di-CF ₃ Bn)	<i>n</i> -propyl	23	46	23	23	176	5eG	111	222	56	28	445
5fA^c	R ² = (4-CF ₃ Bn)	<i>n</i> -propyl	–	>55	>27	–	>438	5fG	>120	>120	>30	–	>480
5gA^c	R ² = (4- <i>tert</i> -butylBn)	<i>n</i> -propyl	11	11	6	6	23	5gG	169	169	85	11	169

Bacterial reference strains: S. a – *Staphylococcus aureus* ATCC 9144, B. s – *Bacillus subtilis* 168, E. c – *Escherichia coli* ATCC 25922, and P. a – *Pseudomonas aeruginosa* ATCC 27853;^aNo SI was calculated if MIC > 16 μg/mL; –: not calculated. ^b Precipitation in the RBC assay. ^c Mixed lipophilic side chain, 3,5-dibromobenzyl and R₂.

6 Biological methods

6.1 Minimum inhibitory concentration (MIC) assay

Stock solutions of the water-soluble compounds were prepared by dissolving them in ultrapure water (Milli-Q H₂O, Millipore, MA, USA). The less water-soluble compounds were first dissolved in 25 - 50 μ L 100% DMSO before further dilution with ultrapure water. The DMSO concentration was always less than 1% in the working concentration of each compound. A modified broth microdilution susceptibility test^[8], based on the CLSI M07-A9 protocol,^[9] was used to determine minimal inhibitory concentrations (MIC). Briefly, the test compounds were two-fold diluted with ultrapure water in polystyrene 96-well flat-bottom microplates (NUNC, Roskilde, Denmark). The bacterial inoculum was diluted to $2.5 - 3 \times 10^4$ cells/mL in Mueller-Hinton broth (MHB, Difco Laboratories, USA) and added to the different diluted compounds in a ratio of 1:1. Positive control (ciprofloxacin, Sigma-Aldrich, USA), negative control (bacteria + water), and media control (media + water) were included in each experiment. The microplates were incubated for 48 h at 35 °C in an EnVision microplate reader (Perkin-Elmer, Turku, Finland). The lowest concentration of compounds that caused no bacterial growth, as determined by optical density (OD₆₀₀) measurements, was defined as the MIC value. All compounds were tested in 3 technical replicates.

6.2 Membrane integrity assays

6.2.1 Inner membrane

The inner membrane integrity assay was performed in a real-time manner using *Bacillus subtilis* 168 (ATCC 23857) and *Escherichia coli* K12 (ATCC MC1061) as test strains, both transformed with the reporter plasmid pCSS962 containing the gene encoding eukaryotic luciferase (*lucGR* gene).^[10] Externally added D-luciferin was used as a substrate for the luciferase to detect light emission. *B. subtilis* and *E. coli* colonies were suspended in MH media supplemented with 5 μ g/mL chloramphenicol (Merck KGaA, Darmstadt, Germany) and a mixture of 20 μ g/mL chloramphenicol and 100 μ g/mL ampicillin (Sigma-Aldrich, USA), respectively, and grown overnight at RT. Overnight cultures were further diluted and grown at RT for 2-3 hrs until they reached OD₆₀₀ = 0.1. D-luciferin potassium salt (Synchem Inc., Elk Grove Village, IL, USA) was added to the bacterial cultures at a final concentration of 1 mM, and the background luminescence was measured before the actual assay. Black round-bottom 96-well microtiter plates (Nunc, Roskilde, Denmark) were prepared with two-fold dilution series of the compounds (10 μ L per well) at final concentrations ranging from 50 to 1.56 μ g/mL. Chlorhexidine acetate (Frese-nius Kabi, Halden, Norway) and MQ-H₂O were used as positive and negative control, respectively. A Synergy H1 Hybrid Reader (BioTek, Winooski, VT, USA) was primed with bacterial suspension before the assay plate was loaded into the plate reader. Aliquots of 90 μ L bacterial inoculum with D-luciferin were successively (well by well) injected into the test wells by an automated injector. The light (luminescence) emission, as a result of bacterial membrane disruption, was monitored every second for 3 minutes. Each study was performed at least three times independently, and the figures show a representative dataset.

6.2.2 Outer membrane

The outer membrane integrity assay was performed in a real-time manner using *E. coli*, the same strain as used in the inner membrane integrity assay. Externally added 1-*N*-phenyl-naphthylamine (NPN) was used as a substrate for the fluorescence to detect light emission. *E. coli* colonies were suspended in MH media and grown overnight at RT. Overnight cultures were further diluted and grown at RT for 2-3 hrs until they reached OD₆₀₀ = 0.1. NPN (Sigma-Aldrich, USA) was added to the bacterial cultures at a final concentration of 20 μ M in glucose hepes buffer (5mM), and the background fluorescence was measured before the actual assay. Black round-bottom 96-well microtiter plates were prepared with two-fold dilution series of the compounds (10 μ L per well) at final concentrations ranging from 50 to 1.56 μ g/mL. Chlorhexidine acetate and MQ-H₂O were used as positive and negative control. A Synergy H1 Hybrid Reader was primed with bacterial suspension before the assay plate was loaded into the plate reader. Aliquots of 90 μ L bacterial inoculum with NPN were successively (well by well) injected into the test

wells by an automated injector. The light (fluorescence) emission, as a result of bacterial outer membrane disruption, was monitored every second for 3 minutes. Each study was performed at least three times independently, and the figures show a representative dataset.

6.3 Viability assay

The real-time measurement of bacterial viability was performed by using *B. subtilis* 168 and *E. coli* K12, the same strains as used in the inner membrane integrity assay. However, in this assay *B. subtilis* 168 is carrying a constitutively expressed lux operon as a chromosomal integration in the *sacA* locus (Pli_aG) and *E. coli* K12 was transformed with the reporter plasmid pCGLS-1.^[11] *B. subtilis* and *E. coli* cultures were prepared the same way as the membrane integrity assay in MH media supplemented with 5 µg/mL chloramphenicol and a mixture of 20 µg/mL chloramphenicol and 100 µg/mL ampicillin, respectively. The continuous light production by these biosensors was monitored in the Synergy H1 Hybrid Reader, and the respective injector was primed with bacterial suspension. Black round-bottom 96-well microtiter plates were prepared with 10 µL of each compound at the final concentration ranging from 50 to 1.56 µg/mL (two-fold dilutions), including Chlorhexidine as a positive control and MQ-H₂O as a negative control. An aliquot of 90 µL bacterial suspension was subsequently added by the automated injector. As a result of changes in bacterial viability, the decrease in light emission was monitored every second for 3 minutes. Each study was performed at least three times independently, and the figures show a representative dataset.

6.4 Red Blood Cell Haemolysis Assay

The protocol was adapted from Paulsen *et al.*^[1] Haemolysis was determined using a heparinized fraction (10 IU/mL) of freshly drawn blood. The blood collected in ethylenediaminetetraacetic acid-containing test tubes (Vacutest, KIMA, Arzergrande, Italy) was used for the determination of the hematocrit (hct). The heparinized blood was washed 3× with pre-warmed phosphate-buffered saline (PBS) and adjusted to a final hct of 4%. Derivatives in DMSO (50 mM) were added to a 96-well polypropylene V-bottom plate (NUNC, Fisher Scientific, Oslo, Norway) and serially diluted. The test concentration range was 500–4 µM with DMSO contents ≤1%. A solution of 1% triton X-100 was used as a positive control for 100% haemolysis. As a negative control, a solution of 1% DMSO in PBS was included. No signs of DMSO toxicity were detected. RBCs (1% v/v final concentration) were added to the well plate and incubated at 37 °C and 800 rpm for 1 h. After centrifugation (5 min, 3000g), 100 µL of each well was transferred to a 96-well flat-bottomed microtiter plate, and absorbance was measured at 545 nm with a microplate reader (VersaMax™, Molecular Devices, Sunnyvale, CA, USA). The percentage of haemolysis was calculated as the ratio of the absorbance in the derivative-treated and surfactant-treated samples, corrected for the PBS background. Three independent experiments were performed, and EC₅₀ values are presented as averages.

7 Membrane integrity and viability assay

Table S2 Summary of the membrane integrity and viability assay against *B. subtilis* 168.

Code	MIC ¹ (µg/ml, 24h)		MIA (activity and speed) ²	VA (effects) ³
	B. s	E. c		
1b	4	64	+++	+
1c	8	128	–	-
1d	4	16	+	+
2bA	4	256	++	+
2bG	4	16	++	++
2cG	2	4	++++	++
3aG	4	32	+++	++
3bA	8	32	+++	+
3bG	4	2	++++	++
3dA	4	16	+++	+
3dG	4	4	++++	++
3eA	2	8	++++	++
3eG	2	2	++++	+++
3fA	2	8	++++	++
3fG	2	2	++++	+++
4aA	4	4	+++	++
4aG	2	4	++++	+++
4bA	4	8	+++	+++
4bG	2	4	++++	+++
4eG	2	4	++	+++
4fA	4	4	++	++
5aG	4	64	++	+
5bG	4	128	–	+
5cA	4	8	+++	+
5cG	2	8	+++	+
5dG	2	4	+++	+++
5eA	4	8	++	+
5eG	2	8	++++	++
5fG	4	16	++++	++
5gA	2	8	+++	++
5gG	1	2	++++	+++

B. s: *Bacillus subtilis*, E. c: *Escherichia coli*

¹MIC assay was also performed in biosensor assay, and the value was similar.

²For membrane integrity assay: High active, fast speed (++++) Medium active, Intermediate speed (+++), Medium active, Slow speed (++) , Low active, Slow speed (+) and Not active (–).

³For viability assay: High effect (+++), Medium effect (++) , Low effect (+) and No effect (-). The highest concentration (51.2 µg/mL) was used to compare and evaluate the membrane integrity and viability assay results.

Table S3 Summary of the membrane integrity and viability assay against *E. coli* K12.

Code	MIC ¹ (µg/mL, 24h)		MIA (activity and speed) ²	VA (effects) ³
	B. s	E. c		
2cG	2	4	+++	++
3bG	2	2	++	++
3dG	4	4	+++	++
3eA	2	8	++	++
3eG	2	2	++	++
3fG	2	2	++	++
4aA	4	4	++++	++
4bA	4	8	++	+
4bG	2	4	+++	++
4eG	2	4	+	++
4fA	4	4	++	++
5dG	2	4	+	++
5eA	4	8	++	++
5eG	2	8	+++	++

B. s: *Bacillus subtilis*, E. c: *Escherichia coli*

¹MIC assay was also performed in biosensor assay, and the value was similar.

²For membrane integrity assay: High active, fast speed (++++), Medium active, Intermediate speed (+++), Medium active, Slow speed (++), Low active, Slow speed (+) and Not active (-).

³For viability assay: High effect (+++), Medium effect (++), Low effect (+) and No effect (-). The highest concentration (51.2 µg/mL) was used to compare and evaluate the membrane integrity and viability assay results.

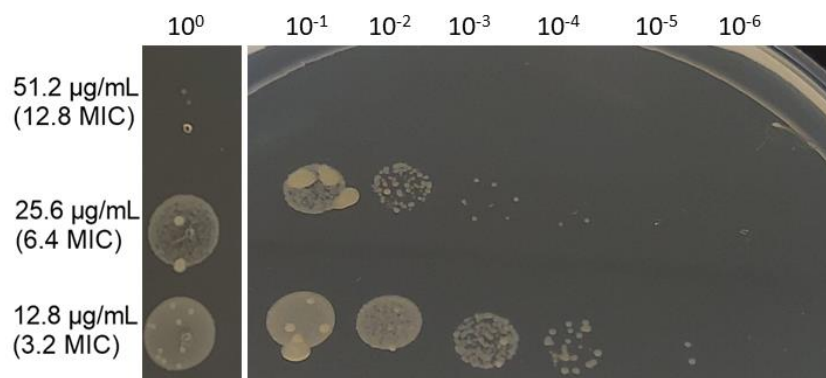


Figure S4. Bactericidal effect of barbiturate **3bG** against *E. coli* after the outer membrane study with NPN. Horizontal: Dilution of the bacterial load.

8 Literature

- [1] M. H. Paulsen, M. Engqvist, D. Ausbacher, T. Anderssen, M. K. Langer, T. Haug, G. R. Morello, L. E. Liikanen, H.-M. Blencke, J. Isaksson, E. Juskewitz, A. Bayer, M. B. Strøm, *J. Med. Chem.* **2021**.
- [2] C. Huixiong, L. Jean-Philippe, G. Nohad, G. Christiane, *Eur. J. Org. Chem.* **2006**, 2006, 2329-2335.
- [3] W. Z. Bi, C. Qu, X. L. Chen, S. K. Wei, L. B. Qu, S. Y. Liu, K. Sun, Y. F. Zhao, *Tetrahedron* **2018**, 74, 1908-1917.
- [4] M. Donnier-Maréchal, P. Carato, P.-E. Larchanché, S. Ravez, R. Boulahjar, A. Barczyk, B. Oxombre, P. Vermersch, P. Melnyk, *Eur. J. Med. Chem.* **2017**, 138, 964-978.
- [5] M. Delor, J. Dai, T. D. Roberts, J. R. Rogers, S. M. Hamed, J. B. Neaton, P. L. Geissler, M. B. Francis, N. S. Ginsberg, *J. Am. Chem. Soc.* **2018**, 140, 6278-6287.
- [6] P. H. Huy, J. C. Westphal, A. M. P. Koskinen, *Beilstein J. Org. Chem.* **2014**, 10, 369-383.
- [7] M. Botta, F. Corelli, G. Maga, F. Manetti, M. Renzulli, S. Spadari, *Tetrahedron* **2001**, 57, 8357-8367.
- [8] E. M. Igumnova, E. Mishchenko, T. Haug, H.-M. Blencke, J. U. E. Sollid, E. G. A. Fredheim, S. Lauksund, K. Stensvåg, M. B. Strøm, *Biorg. Med. Chem.* **2016**, 24, 5884-5894.
- [9] F. R. Cockerill, 9th ed. (Ed.: C. a. L. S. Institut), Wayne, Pa : Clinical and Laboratory Standards Institut, **2012**.
- [10] M. Virta, K. E. O. Åkerman, P. Saviranta, C. Oker-Blom, M. T. Karp, *J. Antimicrob. Chemother.* **1995**, 36, 303-315.
- [11] aJ. Radeck, K. Kraft, J. Bartels, T. Cikovic, F. Dürr, J. Emenegger, S. Kelterborn, C. Sauer, G. Fritz, S. Gebhard, T. Mascher, *J. Biol. Eng.* **2013**, 7, 29; bS. Frackman, M. Anhalt, K. H. Nealson, *J. Bacteriol.* **1990**, 172, 5767-5773.

Paper III

Hydantoins as a Promising Platform for the Development of Tetrasubstituted, Amphipathic Antimicrobials with Membranolytic Properties

Manuel K. Langer, Ataur Rahman, Hymonti Dey, Trude Anderssen, Hans-Matti Blencke, Tor Haug,
Klara Stensvåg, Morten B. Strøm, Annette Bayer

Manuscript

Hydantoins as a Promising Platform for the Development of Tetrasubstituted, Amphipathic Antimicrobials with Membranolytic Properties

Manuel K. Langer^a, Ataur Rahman^b, Hymonti Dey^b, Trude Anderssen^c, Hans-Matti Blencke^b, Tor Haug^b, Klara Stensvåg^b, Morten B. Strøm^{a*}, Annette Bayer^{b*}

^a Department of Chemistry, UiT – The Arctic University of Norway, NO-9037 Tromsø, NORWAY.

^b The Norwegian College of Fishery Science, Faculty of Biosciences, Fisheries and Economics, UiT – The Arctic University of Norway, NO-9037 Tromsø, NORWAY.

^c Department of Pharmacy, Faculty of Health Sciences, UiT – The Arctic University of Norway, NO-9037 Tromsø, NORWAY.

* Corresponding authors.

MANUSCRIPT INFO	ABSTRACT
<p><i>Article history:</i></p> <p>Received: Received in revised form Accepted</p> <p><i>Available online</i></p> <p><i>Keywords:</i> Antimicrobial peptides (AMP) Small synthetic analogues of AMPs (SMAMPs) Hydantoin</p>	<p>Mimics of antimicrobial peptides (AMPs) have been proposed as a promising class of antimicrobial agents. We report the analysis of five tetrasubstituted, cationic, amphipathic heterocycles as potential AMP mimics. The analysis showed that the heterocyclic scaffold had a strong influence on the haemolytic activity of the compounds, and the hydantoin scaffold was identified as a promising platform. Subsequently, a total of 20 hydantoin derivatives were studied for their antimicrobial potency and haemolytic activity. We found 19 of those derivatives to have very low haemolytic toxicity and could identify three lead structures, 2dA, 6cG and 6dG with potential broad-spectrum potency and MIC values of 1–16 µg/mL. Initial mode of action studies performed on amine derivative 2dA, utilizing a luciferin-based assay, suggested a strong membrane disrupting effect for the inner and outer membrane in <i>E. coli</i>. Our findings show that the physical properties and structural arrangement induced by the heterocyclic scaffolds are an important factor in the design of AMP mimics.</p>

1. Introduction

Antimicrobial resistance is now considered to have a similar impact on humans as global climate change.¹ Despite that, only around 30-40 new antimicrobial agents are currently in clinical trials and are mainly derivatives of already marketed compound classes.² To combat the rising resistance, new and underdeveloped classes have to be utilized.

One promising group of antibiotic agents are the naturally occurring cationic antimicrobial peptides (AMPs), found in practically all higher forms of life.³ Their amphipathic nature allows them to associate with the negatively charged bacterial membrane and the lipophilic residues can insert and disrupt the membrane.³ It is believed that due to the lack of a specific target, AMPs are less likely to induce resistance.⁴ But proteolytic instability,⁵ sometimes tedious synthetic procedures⁶ and moderate activity⁴ are among the drawbacks AMPs have been facing, thus retarding their development. To address these issues a range of synthetic analogues have been reported including peptoids,^{7, 8} oligoureas,⁹ γ -AApeptides^{10, 11} and small molecules.^{6, 12, 13}

In recent years, we have focussed on the development of synthetic analogues of AMPs that fulfil and operate at the limit of the pharmacophore model for AMPs. That is, the presence of two cationic and two lipophilic groups of sufficient bulk to exert broad-spectrum activity.¹⁴ Among these were β -amino amides,^{15, 16} cyclic tetrapeptides,¹⁶ barbiturates¹⁷ and others.^{18, 19} The barbituric acid framework **1** has proven to be a valuable scaffold for the preparation of highly active antimicrobials,^{17, 20} and we were curious if our results would translate to other template structures.

In this work we started by investigating five heterocyclic scaffolds **2-5** and **15** (**Figure 1**), that would

allow for the same substitution pattern of two lipophilic side chains and two cationic chains as utilized for barbituric acid **1**. To achieve segregation of the cationic and lipophilic part we intended to attach the lipophilic side chains (Ar) at the bottom side of the heterocycles, bound to carbon atoms (**Figure 1**). The *n*-alkyl linkers bearing the cationic head group (R¹) were incorporated onto the top side, bound to the nitrogen atoms (**Figure 1**). We then constructed a small library based on the most promising scaffold, the hydantoin **2**, and evaluated the effect of different lipophilic and cationic side chains. For the best analogues, their membranolytic behaviour was studied.

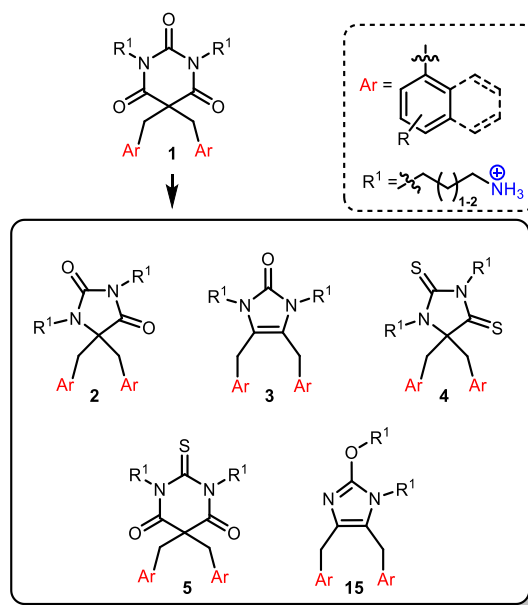


Figure 1. Previously utilized barbituric acid **1** and core structures **2-5** and **15** used in this study. Ar = lipophilic side chain, R¹ = *n*-alkyl linker with a cationic head group. Red: lipophilic part, blue: cationic part.

2. Results and Discussion

2.1 Design of the study

We planned three sets of compounds. In the first set all core structures (**2-5** and **15**) shown in **Figure 1** were synthesized with a combination of substituents (**Figure 2**, left) that we had evaluated in a previous study of amphipathic, antimicrobial barbituric acid.²⁰

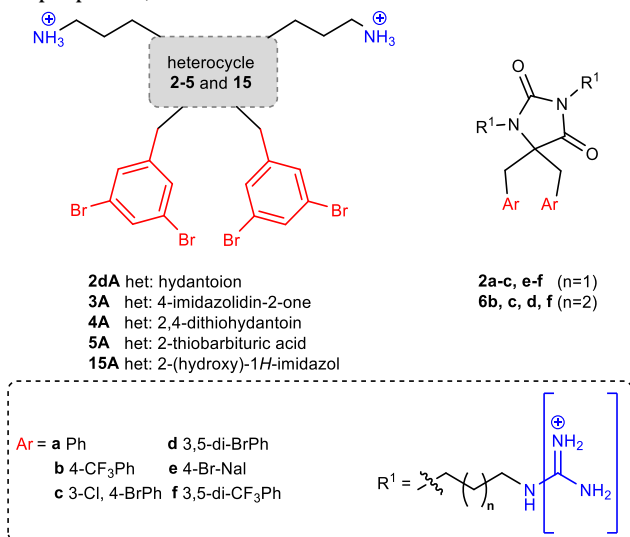


Figure 2. Illustration of the three sets of compounds investigated. Brackets imply variations between cationic amine and guanidine groups.

Lipophilic 3,5-dibromobenzyl (3,5-di-Br) side chains were found earlier to be beneficial for the antimicrobial potency.^{16, 17} Aliphatic *n*-propyl linkers exhibited a good balance between antimicrobial potency and haemolytic activity²⁰ and amine groups were most accessible. It should be noted here that we did not account for 2-(hydroxy)-1H-imidazol **15A** in the initial plan, but **15A** was obtained as a side product during synthesis. The second set was comprised of tetrasubstituted hydantoins **2** (**Figure 2**, right) with different lipophilic side chains, *n*-propyl linkers, and amines and guanidines as cationic head groups. The lipophilic side chains and cationic groups were chosen based on their performance in previous studies^{16, 17, 20, 21} For the third set we used promising lipophilic side chains from the second set and incorporated *n*-butyl linkers to deliver hydantoins **6** (**Figure 2**, right). The *n*-butyl linkers have previously demonstrated to yield more potent derivatives.^{17, 20}

Imidazolidine-2,4-dione **2**, commonly known as hydantoin, is a very well-known scaffold in medicinal chemistry, found in drugs against various indications.²²⁻²⁷ However, it is only rarely seen in antimicrobial agents.^{6, 28-30} In the related 4-imidazolidin-2-one **3**, the lipophilic side chains were attached to two vicinal sp² hybridized carbons, providing more spatial separation and altered dihedral angle between the side chains. Additionally, removal of the amidic oxygen from hydantoin **2** led to a slight change in polarity. The changes in structure and physical properties may affect the compounds' ability to interact with the bacterial membrane. Lastly, we thought to investigate the effect of sulphur on the biological

activity. Thioamides are often utilized in peptide synthesis³¹ and are known to hamper enzymatic degradation of peptides.³² Sulphur is also found in a variety of different drugs,^{33, 34} including some antimicrobial thio-peptides^{35, 36} and β -lactam antibiotics such as penicillins and cephalosporins.³⁷ In those structures the sulphur atom usually is part of a heterocyclic ring or a (di)sulfide, but not a thioamide or a related motif. Therefore, we were interested in joining those two areas by replacing some oxygens for sulphur atoms in the hydantoin and barbituric acid¹⁷ core structure. The resulting structures were 2,4-dithiohydantoin **4** and 2-thiobarbituric acid **5**.

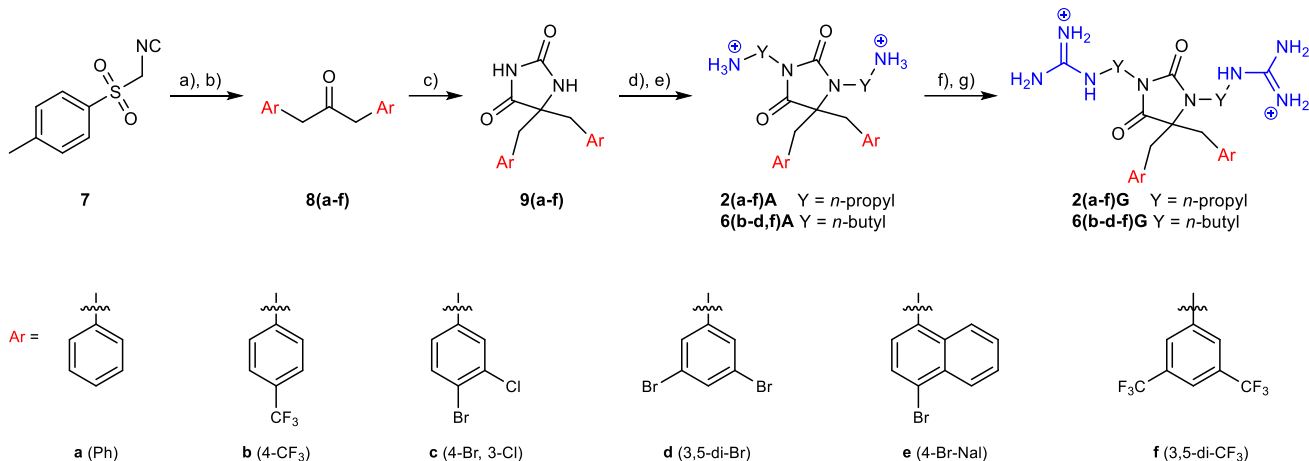
2.2 Synthesis

Hydantoins **2** and **6**

The hydantoin structure can be accessed from a range of different reactions³⁸⁻⁴¹, including the Read⁴², Bucherer-Bergs⁴³ and Biltz⁴⁴ syntheses. To achieve higher substitution patterns, modern strategies have been developed such as multicomponent reactions (MCRs) for the facile access of compound libraries.^{45, 46}

Based on the required substitution pattern and the nature of substituents, we decided to utilize the Bucherer-Bergs reaction as the key step in our synthetic strategy towards hydantoins **2A** and **6A** (**Scheme 1**). To that end, we prepared symmetric ketones **6** from *p*-toluenesulfonylmethyl isocyanate (TosMIC) **7**.⁴⁷ TosMIC was α -dialkylated using phase-transfer catalysis (PTC) in DCM and aqueous NaOH solution with the benzyl bromide of choice. The crude products were hydrolysed by treatment with concentrated HCl⁴⁷ to yield symmetric ketones **8(a-f)** in 53-69% yield over two steps (o2s). The Bucherer-Bergs reaction is commonly performed in a mixture of EtOH/H₂O,⁴³ with precipitation of the resulting hydantoins as the main driving force. Unfortunately, only the unsubstituted diphenylpropan-2-one (R₂ = Ph) could be prepared following this protocol. The other derivatives proved to be insoluble and the solvent needed to be changed to DMSO. Interestingly, an additional base, potassium acetate, was needed to obtain the hydantoins **9(a-f)** in moderate to high yields of 45-85%. For *N,N'*-dialkylation, the hydantoins **9** were treated with *N*-Boc-3-bromopropylamine or *N*-Boc-4-bromobutylamine, caesium carbonate (Cs₂CO₃) and tetrabutylammonium iodide (TBAI) in acetone at elevated temperature.

Subsequent TFA/DCM induced Boc removal delivered the target hydantoins **2A** and **6A** in 45-85% over two steps. Conversion of the amine-modified hydantoins **2A** and **6A** to their guanidyl counterparts was achieved with *N,N'*-di-Boc-1H-pyrazole-1-carboxamide and *N,N'*-diisopropylethylamine (DIPEA) in THF. Ensuing Boc removal with TFA/DCM delivered guanidyl hydantoins **2G** and **6G** in 33-91% yield over two steps.

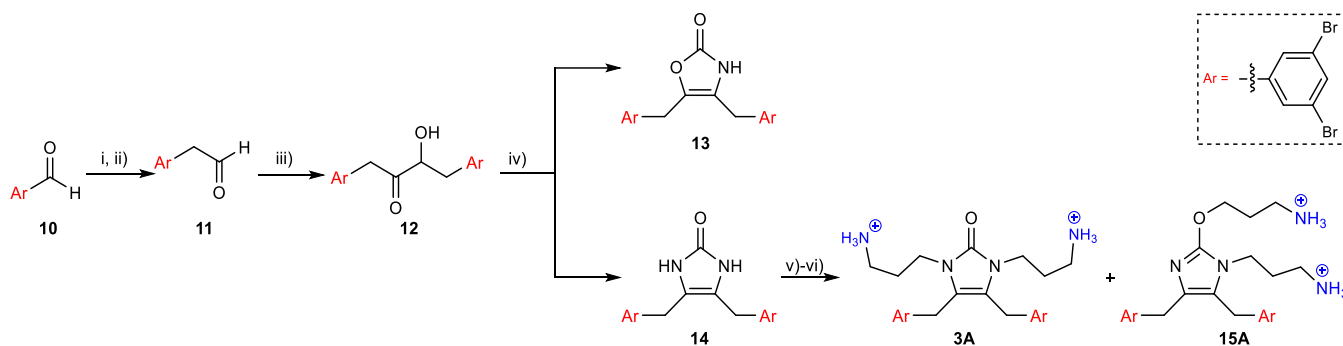


Scheme 1. Synthetic strategy towards target hydantoin **2** and **6**. Reaction conditions: a) ArCH₂Br, TBAB or TBAI, DCM, NaOH_(aq) (20-35 wt%), r.t.; b) HCl_(conc), DCM/THF, r.t., 53–69% o2s; c) KCN, NH₄CO₃, KOAc, DMSO or KCN, NH₄CO₃, EtOH/H₂O, 60-75 °C, 45–85%; d) *N*-Boc-3-bromopropylamine or *N*-Boc-4-bromobutylamine, Cs₂CO₃, TBAI, acetone, 65 °C then e) TFA, DCM, r.t., 45–85% o2s; f) *N,N'*-Di-Boc-1*H*-pyrazole-1-carboxamide, DIPEA, THF, 45 °C then g) TFA, DCM, r.t., 33-91% o2s.

4-imidazolidin-2-one **3A** and 2-(hydroxy)-1*H*-imidazol **15A**

We first set out to obtain the 4-imidazolidin-2-one derivative **3A** by a two-step process from the Boc protected hydantoin **2dA** (Ar = 3,5-di-BrPh) (see Scheme S1 in the Supporting Information). Even though the transformation was feasible, **3A** could not be purified satisfyingly. Therefore, we changed the synthetic strategy as shown in **Scheme 2**. Starting from 3,5-dibromobenzaldehyde **10**, we employed a Wittig reaction with Ph₃PCH₂(OMe)Cl to generate the corresponding vinyl ether in 91% yield as a mixture of the *E*- and *Z*-isomer (*E/Z* = 1.5 : 1.0). Treatment of the vinyl ether with hydrochloric acid in THF and formic acid or TFA in DCM delivered complex mixtures. Using *in-situ* generated HCl by combining oxalyl chloride, EtOH and H₂O⁴⁸ led to quick and full conversion to the desired aldehyde, but the results were not always reproducible. The most reliable results were finally achieved by using trimethylsilyl chloride (TMS-Cl) and sodium iodide in dry MeCN with high dilution.⁴⁹ The homologated aldehyde **11** was obtained in 60% yield. Aldehyde **11** was subsequently converted in a benzoin-type condensation

to the α-hydroxy ketone **12** by treatment with Et₃N and catalytic amounts of 3-benzyl-5-(2-hydroxyethyl)-4-methylthiazolium chloride in dry PEG-400.⁵⁰ We used PEG-400 instead of the more commonly employed EtOH⁵⁰, due to the low solubility of aldehyde **11**. Based on literature,⁵¹ we condensed the α-hydroxy ketone **12** with urea in the presence of glacial acetic acid in anhydrous PEG-400. We obtained 4-imidazolidin-2-one **14** in 39% yield as the major product and found unexpectedly 4-oxazolidin-2-one **13** in 18% yield. In previous reports, the side product was only observed when the benzoin reagent had electron donating substituents (4,4'-dimethoxybenzoin) or heterocyclic nitrogen (2,2'-pyridoin).⁵¹ The authors were reasoning that the electron donating para-methoxy substituents would render the hydroxyl group of the intermediate more nucleophilic as does the basic pyridinyl nitrogen by intramolecular hydrogen bonding. One possible explanation could be the bromine atom acting as a Lewis base, forming a hydrogen bond to the hydroxyl hydrogen. This interaction would be comparable to the basic pyridinyl hydrogen and would facilitate an intramolecular attack of the urea oxygen, leading to compound **13**.



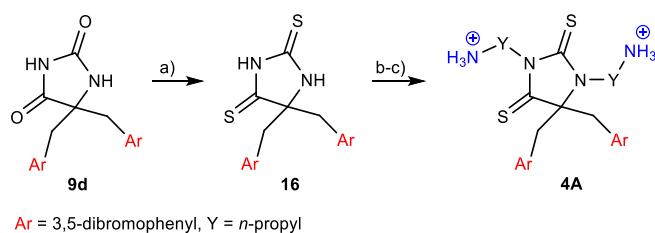
Scheme 2. Synthetic strategy towards tetrasubstituted 4-imidazolidin-2-one **3A** and its constitutional isomer **15A**. Ar = 3,5-dibromophenyl. Reaction conditions: i) Ph₃PCH₂OMeCl, NaHMDS, THF (dry), -78 °C to r.t., 91%; *E/Z* = 1.5/1.0; ii) TMSCl, NaI, MeCN (dry), r.t., 60%; iii) 3-benzyl-5-(2-hydroxyethyl)-4-methylthiazolium chloride, Et₃N, PEG-400 (dry), 80 °C, 39%; iv) urea, AcOH, PEG-400 (dry), 130 °C, 18% for **13** and 39% for **14**; v) *N*-Boc-3-bromopropylamine, K₂CO₃, (*n*-hexadecyl)tri-*n*-butylphosphonium bromide, toluene:water, μ-wave, 130-150 °C then vi) TFA, DCM, r.t., 6-19% o2s.

We then alkylated 4-oxazolin-2-one **13** and 4-imidazolidin-2-one **14**, respectively, with *N*-*boc*-3-bromopropylamine using (*n*-hexadecyl)tri-*n*-butylphosphonium bromide as phase transfer catalyst and potassium carbonate as a base in a biphasic mixture of water and toluene under μ -wave irradiation. Subsequently, the di-alkylated products were deprotected with TFA/DCM. 4-Oxazolin-2-one **13** delivered a di-alkylated compound with an unresolved structure and was not further investigated.

Compound **14** delivered the desired *N,N'*-dialkylated 4-imidazolidin-2-one **3A** in low yields (19% o2s). Surprisingly, *N,O*-dialkylated 2-(hydroxy)-1*H*-imidazol **15A** (17% o2s) was obtained from the same reaction mixture. The mono alkylated derivatives of structures **3A** and **15A** were obtained as well, partially explaining the low yields.

2,4-Dithiohydantoin **4A**

By employing *in situ* generated NH_4CN and CS_2 ⁵² we intended to obtain 2,4-thiohydantoin **4A** from ketone **8d** (Ar = 3,5-di-BrPh), but no conversion was observed. Instead hydantoin **9d** (3,5-di-Br) was treated with Lawesson's reagent at elevated temperature⁵³ to deliver 2,4-thiohydantoin **16** (3,5-di-Br) in 82% yield (**Scheme 3**). *N,N'*-Dialkylation of **16** with *N*-*Boc*-3-bromopropylamine afforded 2,4-dithiohydantoin **4A** in 56% yield.



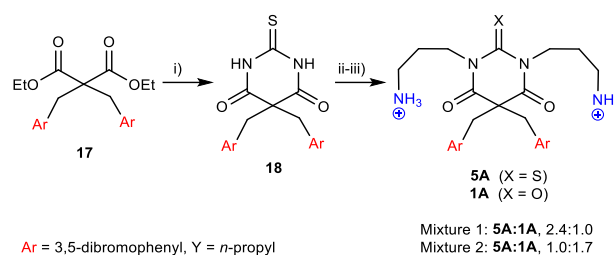
Scheme 3. Synthetic strategy towards 2,4-dithiohydantoin **4A**. Reaction conditions: a) Lawesson's reagent, 1,4-Dioxane, 115 °C, 82%; b) *N*-*Boc*-3-bromopropylamine, Cs_2CO_3 , TBAI, acetone, 65 °C then c) TFA, DCM, r.t., 56%

2-Thiobarbituric acid **5A**

In a first approach we tried to thiolate 5,5-bis(3,5-dibromobenzyl) barbituric acid with the Lawesson's reagent under the same conditions as used to obtain 2,4-dithiohydantoin (*vide supra*).

Unfortunately, we obtained an inseparable mixture of the mono-, di- and tri-thiolated barbituric acid. Therefore, we decided to adapt our previously reported procedure¹⁷ by replacing urea with thiourea. Treatment of di-benzylated diethyl malonate **17** and thiourea with NaH in a mixture of anhydrous THF and DMF yielded the 5,5-dibenzylated-2-thiobarbituric acid **18** in low yields (**Scheme 4**). *N*-alkylation with *N*-*Boc*-3-bromopropylamine, Cs_2CO_3 and TBAI in acetone at elevated temperature, followed by TFA/DCM mediated Boc removal delivered the tetrasubstituted barbiturates **5A** and **1A** in very low yields (9%). Partial desulfurization had taken place, delivering two mixtures of tetrasubstituted 2-thiobarbituric acid **5A** (X = S) and

barbituric acid **1A** (X = O). Mixture 1 (Mix 1) constituted a ratio of 2.4:1.0 (**5A:1A**) and mixture 2 (Mix 2) constituted a ratio of 1.0:1.7 (**5A:1A**). The mixtures were inseparable but stable in solid state and were tested as such. Only when the mixture was in solution and under prolonged light exposure, we could see slow desulfurization take place.



Scheme 4. Synthetic strategy towards 2-thiobarbituric acid **5A**. Mixtures of 2-thiobarbituric acid **5A** (X = S) and barbituric acid **1A** (X = O) were obtained. Ar = 3,5-dibromophenyl. Reaction conditions: i) Thiourea, NaH, anhydrous THF:DMF, 65 °C, 24%; ii) *tert*-butyl (3-bromopropyl)carbamate, Cs_2CO_3 , TBAI, acetone, 70 °C, then iii) TFA, DCM, r.t., 9% o2s.

2.3 SAR Analysis

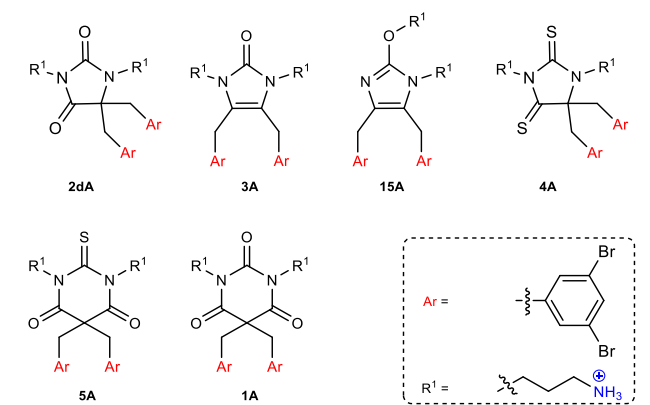
All compounds were screened for their antimicrobial activity against antibiotic susceptible Gram-positive and Gram-negative reference strains. Haemolytic activity against human red blood cells (RBCs), expressed by the EC_{50} value, was used as a measurement of cytotoxicity. As a reference we used the already reported barbiturate **1A**²⁰ (**Table 1**, Entry 8). The commercially available antibiotic ciprofloxacin served as a positive control. Capital A in the compound codes denotes cationic amine derivatives and capital G guanidine derivatives. For Series 2 and 3 the substituents on the phenyl groups are given in brackets for each compound to aid the discussion. The hydrophilicity of each core structure, bearing four substituents, was estimated with the ChemBioDraw Ultra software.

2.3.1 Exploring new scaffolds

We started our investigation by comparing the different scaffolds **2dA**, **3A**, **4A**, **5A** and **15A** to identify the most promising candidate (**Table 1**). All scaffolds were decorated with the same lipophilic (Ar = 3,5-dibromophenyl) and cationic group ($\text{R}^1 = 3$ -aminoprop-1-yl). The five membered hydantoin **2dA** (entry 1) was marginally less potent (MIC: 4 – 16 $\mu\text{g}/\text{mL}$) than the barbituric acid **1A** (entry 7), although it was estimated to be slightly more hydrophilic. Interestingly, hydantoin **2dA** was almost 3.5 times less haemolytic (EC_{50} : 344 $\mu\text{g}/\text{mL}$) than **1A**. The 4-imidazolidin-2-one core **3A** (entry 2) was one order of magnitude more lipophilic than the hydantoin core. **3A** demonstrated a 4-fold increase in antimicrobial potency (MIC: 2 – 4 $\mu\text{g}/\text{mL}$) against all strains except for Gram-negative *P. aeruginosa*, but also a 7-8-fold increase in haemolytic activity (EC_{50} : 52 $\mu\text{g}/\text{mL}$). The constitutional isomer 4-oxazolin-2-one **15A** (entry 3) gave a similar result (MIC: 2 – 4 $\mu\text{g}/\text{mL}$, EC_{50} : 44 $\mu\text{g}/\text{mL}$). Despite being very potent, the systemic application of these compounds is

limited by their high haemolytic activity. It did not become clear why those core structures were so distinctively more haemolytic than hydantoin **2dA**. The 2,4-dithiohydantoin **4A** (entry 4) was inactive against Gram-negative *P. aeruginosa* (MIC: 32 $\mu\text{g/mL}$). Dithio-derivative **4A** was only marginally less haemolytic (EC_{50} : 385 $\mu\text{g/mL}$) than its dioxo counterpart (EC_{50} : 344 $\mu\text{g/mL}$).

Table 1 Antimicrobial activity (MIC in $\mu\text{g/mL}$) against bacterial reference strains and haemolytic activity against human RBC (EC_{50} in $\mu\text{g/mL}$) for compounds with different core structures.



Entry	Comp. ID	CLogP ^a	Antimicrobial activity				EC_{50}
			S. a	B. s	E. c	P. a	
1	2dA	-1.69	8	4	16	8	344
2	3A	-0.47	2	1	4	8	52
3	15A	0.26	2	2	4	4	44
4	4A	-1.22	8	8	16	32	385
5	Mixture 1 ^b	n.d.	8	4	4	16	305
6	Mixture 2 ^c	n.d.	8	4	8	8	182
7 ²⁰	1A	-1.44	4	4	8	8	99
8	Ciprofloxacin		0.06	<0.03	<0.03	0.25	

Bacterial reference strains: S. a – *Staphylococcus aureus* ATCC 9144, B.s – *Bacillus subtilis* 168, E. c – *Escherichia coli* ATCC 25922, and P. a – *Pseudomonas aeruginosa* ATCC 27853. ^a ClogP values were calculated for the respective tetrasubstituted core structures (calculated with ChemBioDraw Ultra v19.0.0.1.28). n.d.: not determined. ^b Mixture of 2.4:1.0 (**5A:1A**). ^c Mixture of 1.0:1.7 (**5A:1A**).

Mixture 1 (entry 5), being enriched with 2-thiobarbituric acid **5A**, exhibited reduced potency against Gram-negative *P. aeruginosa* (MIC: 16 $\mu\text{g/mL}$) and the haemolytic activity decreased by a factor of three (EC_{50} : 305 $\mu\text{g/mL}$). By reduction of the amount of **5A** in mixture 2 (entry 6), antimicrobial activity (MIC: 4 – 8 $\mu\text{g/mL}$) and more pronouncedly the haemolytic activity (EC_{50} : 182 $\mu\text{g/mL}$) approached the values found for **1A** (entry 7). In conclusion, sulfur containing derivatives were less haemolytic and less active against Gram-negative *P. aeruginosa*. Combined with the synthetic challenges and the chemical instability, thionylated derivatives were not worthwhile to investigate further. Clearly the hydantoin scaffold was the most promising core structure to study further derivatives.

2.3.2 Hydantoins with *n*-propyl linkers (**2**)

A series of hydantoins **2** (**Table 2**) with *n*-propyl linkers connecting the cationic amino (**A**) or guanidino

(**G**) groups to the core were constructed to screen different lipophilic side chains (**a-c** and **e-f**) for their impact on the compounds' potency and haemolytic toxicity. We have chosen (pseudo)halogenated benzyl groups, based on their beneficial properties shown in previous studies.^{16, 17, 21} The compounds are ranged according to increasing lipophilicity.

Generally, the compounds in amine series **2(a-e)A** (**Table 2**, entry 1-6) exhibited improved biological potency and increased haemolytic activity with higher CLogP values of the lipophilic side chains, except for hydantoin **2fA** (3,5-di- CF_3). Derivatives **2aA** (Ph) and **2bA** (4- CF_3) were practically inactive against all strains (MIC: 16 – >256 $\mu\text{g/mL}$). Hydantoin **2cA** (3-Cl, 4-Br) was only active against the Gram-positive strains (MIC: 4 – 8 $\mu\text{g/mL}$), whereas amines **2(d-f)A** (entries 4-6) were potent against all strains tested (MIC: 4 – 16 $\mu\text{g/mL}$). The most active amine derivative was **2eA** (4-Br-1-Nal), showing good broad-spectrum potency (MIC: 4 – 8 $\mu\text{g/mL}$). Interestingly, it was at least 5-times more haemolytic (EC_{50} : 69 $\mu\text{g/mL}$) than any of the other amine derivatives (**2A**). Hydantoin **2fA** (3,5-di- CF_3) was more lipophilic than **2eA** (4-Br-1-Nal) but less potent (MIC: 8 – 16 $\mu\text{g/mL}$) than the latter one by a factor of two to four.

The electron withdrawing trifluoromethyl groups may lead to a slight polarisation of the aromatic ring, thus reducing its ability to interact with the lipid membrane. The most promising amine derivative was **2dA** (3,5-di-Br), having good broad-spectrum activity (MIC: 4 – 16 $\mu\text{g/mL}$) and negligible haemolytic activity (EC_{50} : 344 $\mu\text{g/mL}$). Surprisingly, it demonstrated higher activity against Gram-negative *P. aeruginosa* than *E. coli*. The guanidyl series **2(a-e)G** (**Table 2**, entry 7-13) exhibited the same general trend for potency and haemolytic activity as in the amine series, which derivative **2fG** (3,5-di- CF_3) again did not follow. The guanidyl derivatives were generally more potent against the Gram-positive strains than their amine counterparts by a factor of two to four. Guanidyl hydantoins **2(b-g)G** (entries 8-12) exhibited good to very good potency (MIC: 2 – 16 $\mu\text{g/mL}$) against the Gram-positive strains. The potency against Gram-negative *E. coli* was virtually unchanged compared to their amine correlates.

For Gram-negative *P. aeruginosa* the activity dropped two-fold for **2cG** (3-Cl, 4-Br) and **2fG** (3,5-di- CF_3) and four-fold for **2dG** (3,5-di-Br) and **2eG** (4-Br-1-Nal), correspondingly. All guanidyl derivatives were pronouncedly less haemolytic than their amine equivalents. The most promising guanidine derivative was **2eG** (4-Br-1-Nal), which demonstrated good potency against all strains (MIC: 2 – 8 $\mu\text{g/mL}$) except for Gram-negative *P. aeruginosa* and had low haemolytic toxicity (EC_{50} : 206 $\mu\text{g/mL}$). The combination of *n*-propyl linkers and guanidyl head groups having improved potency against Gram-positive strains and reduced potency against Gram-negative *P. aeruginosa*, as well as reduced haemolytic activity had also been observed earlier for amphipathic barbiturates.²⁰

In summary, guanidyl derivatives **2(c-f)G** showed good potency against Gram-positive strains (MIC:

Table 2 Antimicrobial activity (MIC in $\mu\text{g/mL}$) against bacterial reference strains and haemolytic activity against human RBC (EC_{50} in $\mu\text{g/mL}$) for tetrasubstituted hydantoin **2** and **6**.

2A Y = *n*-propyl
6A Y = *n*-butyl

2G Y = *n*-propyl
6G Y = *n*-butyl

a (Ph) **b** (4- CF_3) **c** (4-Br, 3-Cl) **d** (3,5-di-Br) **e** (4-Br-1-Nal) **f** (3,5-di- CF_3)

Entry	Comp. ID	R^1	Y	CLogP	Antimicrobial activity				
					S. a	B. s	E. c	P. a	EC_{50}
1	2aA	(Ph)	<i>n</i> -propyl	2.64	>256	256	>256	>256	>311
2	2bA	(4- CF_3)	<i>n</i> -propyl	3.52	64	16	256	>256	>379
3	2cA	(4-Br, 3-Cl)	<i>n</i> -propyl	4.08	8	4	32	32	368
4	2dA	(3,5-di-Br)	<i>n</i> -propyl	4.38	8	4	16	8	344
5	2eA	(4-Br-1-Nal)	<i>n</i> -propyl	4.68	4	4	8	8	69
6	2fA	(3,5-di- CF_3)	<i>n</i> -propyl	5.03	16	8	16	16	399
7	2aG	(Ph)	<i>n</i> -propyl	2.64	64	128	>256	>256	>353
8	2bG	(4- CF_3)	<i>n</i> -propyl	3.52	16	8	128	>256	>421
9	2cG	(4-Br, 3-Cl)	<i>n</i> -propyl	4.08	2	2	32	64	>467
10	2dG	(3,5-di-Br)	<i>n</i> -propyl	4.38	2	4	16	32	486
11	2eG	(4-Br-1-Nal)	<i>n</i> -propyl	4.68	2	2	8	32	206
12	2fG	(3,5-di- CF_3)	<i>n</i> -propyl	5.03	4	2	32	32	>489
13	6bA	(4- CF_3)	<i>n</i> -butyl	3.52	64	16	>128	>128	>393
14	6cA	(4-Br, 3-Cl)	<i>n</i> -butyl	4.08	8	4	64	64	>439
15	6dA	(3,5-di-Br)	<i>n</i> -butyl	4.38	8	2	32	32	364
16	6fA	(3,5-di- CF_3)	<i>n</i> -butyl	5.03	16	4	64	64	>461
17	6bG	(4- CF_3)	<i>n</i> -butyl	3.52	4	4	64	>128	>503
18	6cG	(4-Br, 3-Cl)	<i>n</i> -butyl	4.08	4	2	16	8	347
19	6dG	(3,5-di-Br)	<i>n</i> -butyl	4.38	1	1	4	16	206
20	6fG	(3,5-di- CF_3)	<i>n</i> -butyl	5.03	2	2	8	32	384
21		Ciprofloxacin			0.06	<0.03	<0.03	0.25	

Bacterial reference strains: S. a – *Staphylococcus aureus* ATCC 9144, B. s – *Bacillus subtilis* 168, E. c – *Escherichia coli* ATCC 25922, and P. a – *Pseudomonas aeruginosa* ATCC 27853. ^a ClogP values were calculated for substituted benzyl groups (calculated with ChemBioDraw Ultra v19.0.0.1.28).

2 – 4 $\mu\text{g/mL}$), but none of the guanidyl derivatives **2G** was potent against *P. aeruginosa*. Amines **2dA** (3,5-di-Br) and **2eA** (4-Br-1-Nal) were the most potent derivatives of hydantoin **2**, with **2dA** (3,5-di-Br) being non haemolytic.

2.3.3 Hydantoin with *n*-butyl linkers (**6**)

In our previous study on tetrasubstituted barbiturates, a combination of guanidyl head groups and *n*-butyl linkers achieved the highest broad-spectrum activity. Due to the structural similarity, we reasoned that *n*-butyl linkers would boost the hydantoin's potency. We chose the most promising side chains **b** (4- CF_3), **c** (3-Cl, 4-Br), **d** (3,5-di-Br) and **f** (3,5-di- CF_3) from hydantoin derivatives **2**.

Amine hydantoin **6A** displayed the same potency against Gram-positive strains as derivatives **2A** but had reduced activity against the Gram-negative strains by a

factor for two to four (**Table 2**). None of the derivatives was haemolytic (EC_{50} : >364 $\mu\text{g/mL}$).

Upon guanylation, all compounds **6G** became highly active against the Gram-positive strains as derivatives **2A** (MIC: <1 – 4 $\mu\text{g/mL}$). Despite all hydantoin **6G** becoming more active than their amine analogues **6A**, no outstanding results were obtained. Guanidino hydantoin **6cG** (3-Cl, 4-Br) demonstrated the best broad-spectrum activity (MIC: 2 – 16 $\mu\text{g/mL}$) with no noteworthy haemolytic activity (EC_{50} : 347 $\mu\text{g/mL}$). Hydantoin **6dG** (3,5-di-Br) had excellent activity against Gram-positive strains (MIC <1 $\mu\text{g/mL}$) and good to moderate activity against the Gram-negative strains (MIC: 4 – 16 $\mu\text{g/mL}$).

In summary, we did observe increased potency and haemolytic activity for the guanidyl compounds **6G** compared to their amine counterparts **6A** (*vide supra*). While being non-haemolytic, the potency of the amine derivatives was rather unsatisfying. The guanidyl compounds **6cG** (3-Cl, 4-Br) and **6dG** (3,5-di-Br),

however, displayed promising potency and moderate to low haemolytic activity.

2.4 Selectivity index and counterion effect

The selectivity index (SI) is a simple descriptor given by the ratio of EC₅₀/MIC for the efficiency of antimicrobial agents. We have summarized the most promising compounds in **Table 3**. Compounds were only considered active if the MIC value was ≤16 µg/mL.

Table 3. Selectivity index (SI) of the most promising wide and narrow-spectrum antimicrobials. EC₅₀ values are given in [µg/mL].

Entry	Comp. ID	SI (EC ₅₀ /MIC) ^a				EC ₅₀
		S. a	B. s	E. c	P. a	
1	2cG	>234	>234	-	-	>467
2	2fG	>122	>245	-	-	>489
3	6cA	>55	>110	-	-	>439
4	2dG	243	122	30	-	486
5	2eG	103	103	26	-	206
6	6fG	192	192	48	-	384
7	2dA	43	86	22	43	344
8	2fA	25	50	25	25	399
9	6cG	87	172	22	44	347
10	6dG	206	206	52	13	206

Bacterial reference strains: S. a – *Staphylococcus aureus* ATCC 9144, B. s – *Bacillus subtilis* 168, E. c – *Escherichia coli* ATCC 25922, and P. a – *Pseudomonas aeruginosa* ATCC 27853. ^a -: No SI was calculated if MIC was >16 µg/mL.

Compounds **2cG** (3-Cl, 4-Br), **2fG** (3,5-di-CF₃), **6cA** (3-Cl, 4-Br), **2dG** (3,5-di-Br), **2eG** (4-Br-1-Nal) and **6fG** (3,5-di-CF₃) demonstrated excellent selectivity for the Gram-positive strains (entries 1-6). Hydantoin **2dG**, **2eG** and **6fG** (entries 4-6) had additionally good selectivity (SI: >20) for *E. coli*. All six derivatives showed low to no haemolytic toxicity. Derivatives **2dA**, **2fA**, **6cG** and **6dG** (entries 7-10) had good SI values for all strains tested. Most promising hydantoin **2dA** (3,5-di-Br) and **6cG** (3-Cl, 4-Br) had SI values >40 against Gram-negative *P. aeruginosa*, which can be considered very good.

All compounds tested were obtained as di-trifluoroacetate (di-TFA) salts, which are non-physiological. Therefore, we converted **2cA**, **2cG**, **2dA** and **2dG** to physiological di-hydrochloride (di-HCl) salts, to assess if the biological behaviour would be altered (see Supporting Information for details). We did not observe any major changes in the MIC or EC₅₀ values for any of the four derivatives. Minor improvements for the antimicrobial potency could be observed for **2cA** (4-Br, 3-Cl) and **2cG** (4-Br, 3-Cl), but no clear trend became apparent. Also, the haemolytic activity was only influenced to a small extend and could often be correlated to the lower molecular weight of the di-HCl salts compared to the di-TFA salts.

2.5 Mode of Action (MoA) studies

Seven compounds were chosen based on structural changes, MIC values, haemolytic activity, and selective indexes for mode of action studies against *B. subtilis* 168 (see Supporting Information, **Table S4**), as they were primarily potent against Gram-positive bacteria.

Furthermore, six additional compounds have been tested against *B. subtilis* 168 and *E. coli* K12 biosensors strains with broad-spectrum activity (see SI, **Tables S4** and **S5**).⁵⁴

To explore the modes of action of promising compounds in *B. subtilis* 168 and *E. coli* K12, we conducted luciferase-based biosensor tests (viability and membrane integrity). The biosensor-based viability test measures the viability of bacterial cells as light production by recombinant expressed bacterial luciferase derived from *Photobacterium luminescens* lux operation. External substrates do not affect light production by bacterial lux operons. Bacteria themselves provide a reduced flavin mononucleotide (FMN_{H2}) and a long-chain aldehyde pool, which is the substrate for light production. Bacterial luciferase is a very efficient real-time sensor of bacterial viability because NADH, NADPH, and ATP are required to constantly fill the substrate pool.

The biosensor-based membrane integrity test is based on the lucGR gene (luciferase) of *Pyrophorus plagiophthalmus*, which is a luminous click beetle. Unlike bacterial luciferase, the light reaction is closely dependent on externally added D-luciferin substrates. D-luciferin is inadequate to cross the intact biological membrane at neutral pH. The uptake of D-luciferin is explored after the addition of antimicrobial substances to determine whether the membrane becomes permeable or not. When D-luciferin enters through damaged membranes, light production increases. Light production peaks quickly if the integrity of the membrane is compromised and then usually decreases during the consumption of dying cells' ATP.

In general, most of the compounds tested influenced survival (viability) and showed strong membrane disrupting activity against *B. subtilis*, but some of them were active against both bacterial species. However, some compounds had more prominent effects on survival and faster membranolytic effects on *B. subtilis* than *E. coli*. If the concentration of the compounds exceeded the MIC value, both the viability and the integrity of the membrane were affected for most compounds. Furthermore, the increase in concentrations affected viability and membranolytic activity at an increasing rate, indicating a concentration-dependent killing effect. Compound **2dA** (3,5-di-Br) was chosen as a broad-spectrum hydantoin to illustrate the results with regard to viability and membrane integrity in detail (**Figure 3** and **Figure 4**). Hydantoin **2dA** had a minor influence on the survival of *B. subtilis* (**Figure 3A**, left). In the *B. subtilis* biosensor strain, membrane integrity tests were conducted to confirm that rapid decrease in bacterial viability was caused by membrane damage. The derivative **2dA** showed membrane-related action because light emittance decreased rapidly and dose-dependently (**Figure 3B**, left), similar to chlorohexidine (CHX) (**Figure 3B**, right). The CHX reference control is a bactericidal agent that affects the cell walls and membranes of both *B. subtilis* 168 and *E. coli* K12.⁵⁵ The MIC value for CHX is 1.6 µg/mL against both *B. subtilis* 168 and *E. coli* K12. The disruptive membrane effect of hydantoin **2dA** on *B. subtilis* was shown to be at a

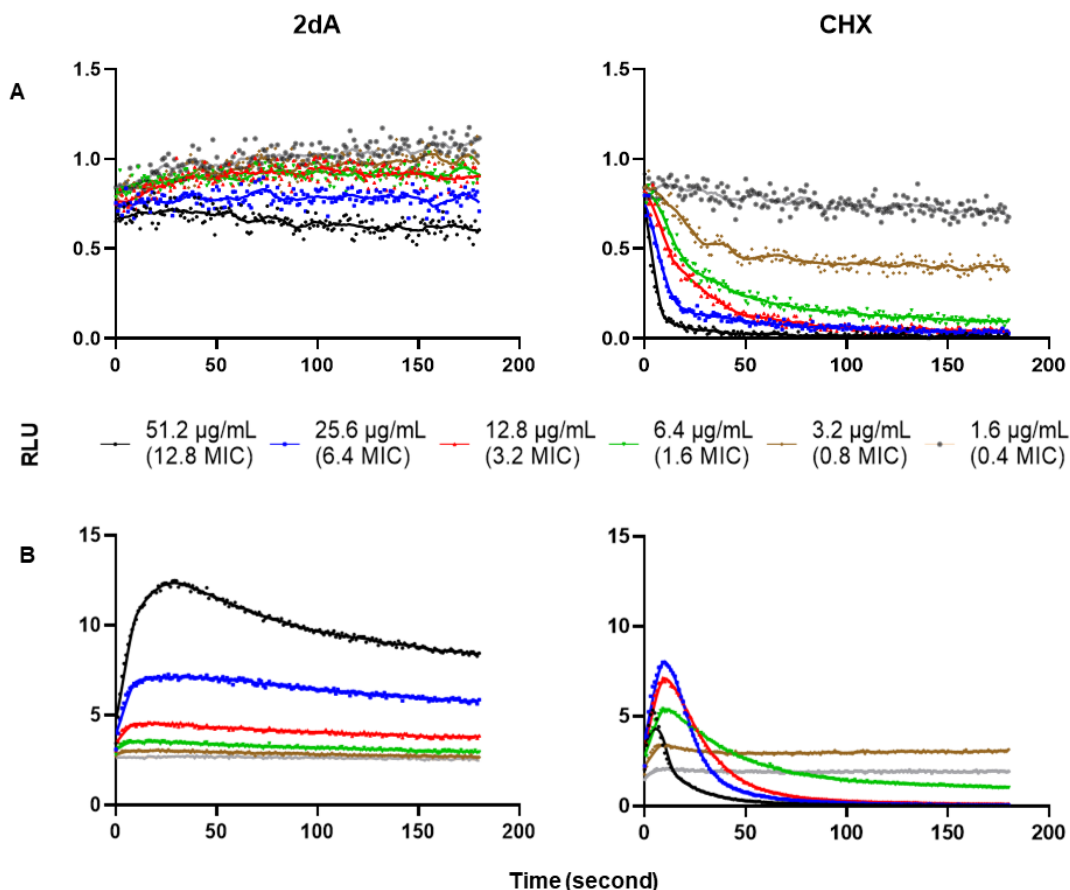


Figure 3. The effects of **2dA** (broad spectrum) and CHX (positive control) on the kinetics of (A) viability and (B) membrane integrity in *B. subtilis* 168. Normalized light emission (normalized with a negative, untreated water control) is plotted as relative light units (RLU) over time (seconds). Light emission was measured each second for 180 s after adding the bacterial cell suspension (with 1 mM D-luciferin for the membrane integrity assay) to the analytes in separate wells. The multiples of the MIC values given in parentheses refer only to compound **2dA**. The figure shows a representative data set from at least three independent experiments.

concentration of 25.6 µg/mL (black line, **Figure 3B**, left), which was 6.4 times higher than its MIC (4 µg/mL). Concentrations below 25.6 µg/mL showed a limited membrane disruption effect, with peak emissions not decreasing during the measurement period. The bacterial concentration in these experiments was approximately 100 times higher than that used in MIC testing, and this could explain why a slightly higher concentration of **2dA** hydantoin was required to affect the viability and integrity of the membrane.

The effect of hydantoin **2dA** on the viability and membrane integrity of Gram-negative *E. coli* differs somewhat from that of Gram-positive *B. subtilis*. The broad-spectrum derivative **2dA** influenced the viability of *E. coli* and showed a concentration-dependent killing effect such as CHX (**Figure 4A**). Although **2dA** affected viability, only the two highest concentrations (6.4 – 12.8x MIC) increased light emissions in the inner membrane assay and did not decline during the test period (less notable impact on the disruptive effect of the inner membrane) (**Figure 4B**, left). The delay and reduction in **2dA**'s effect on membrane integrity could be caused by the outer membrane of *E. coli*, which may act as an additional barrier.

We used 1-*N*-phenyl-naphthylamine (NPN) fluorescent probes to determine whether **2dA** compounds affected outer membrane permeability to confirm the speculation

of the effect of the *E. coli* outer membrane barrier. Small NPN molecules (219 Da) have low fluorescence in water solutions, but if bound to phospholipids, they produce high fluorescence. Hydrophobic NPN cannot effectively pass through the outer membrane of intact *E. coli* cells, resulting in low fluorescence; however, if the outer membrane is damaged, NPN can reach the periplasmic space, bind to the phospholipids of the inner and outer membrane, and produce enhanced fluorescence.⁵⁶ In this test, low concentrations (6.4 µg/mL) of hydantoin **2dA** produced higher fluorescence levels (**Figure 4C**, left), whereas no increase in fluorescence in the inner membrane integrity test was observed (**Figure 4B**, left). This trend indicates that most cells are intact and viable without significantly compromising the integrity of the inner membrane but have increased the permeability of the outer membrane. When the concentration of **2dA** increased, the fluorescence level was lower (**Figure 4C**, left), indicating an intact outer membrane or rapid membrane disruption before the measurement began. At the same time, bacterial cell survival was significantly reduced (**Figure 4A**, left) and inner membrane integrity was altered (**Figure 4B**, left).

The viability of the bacterial cells was markedly reduced for concentrations of 25.6 to 51.2 µg/mL (6.4 – 12.8x MIC) (see **Figure S1**) when the 10 µL sample of the NPN assay was spotted on an agar plate after the test

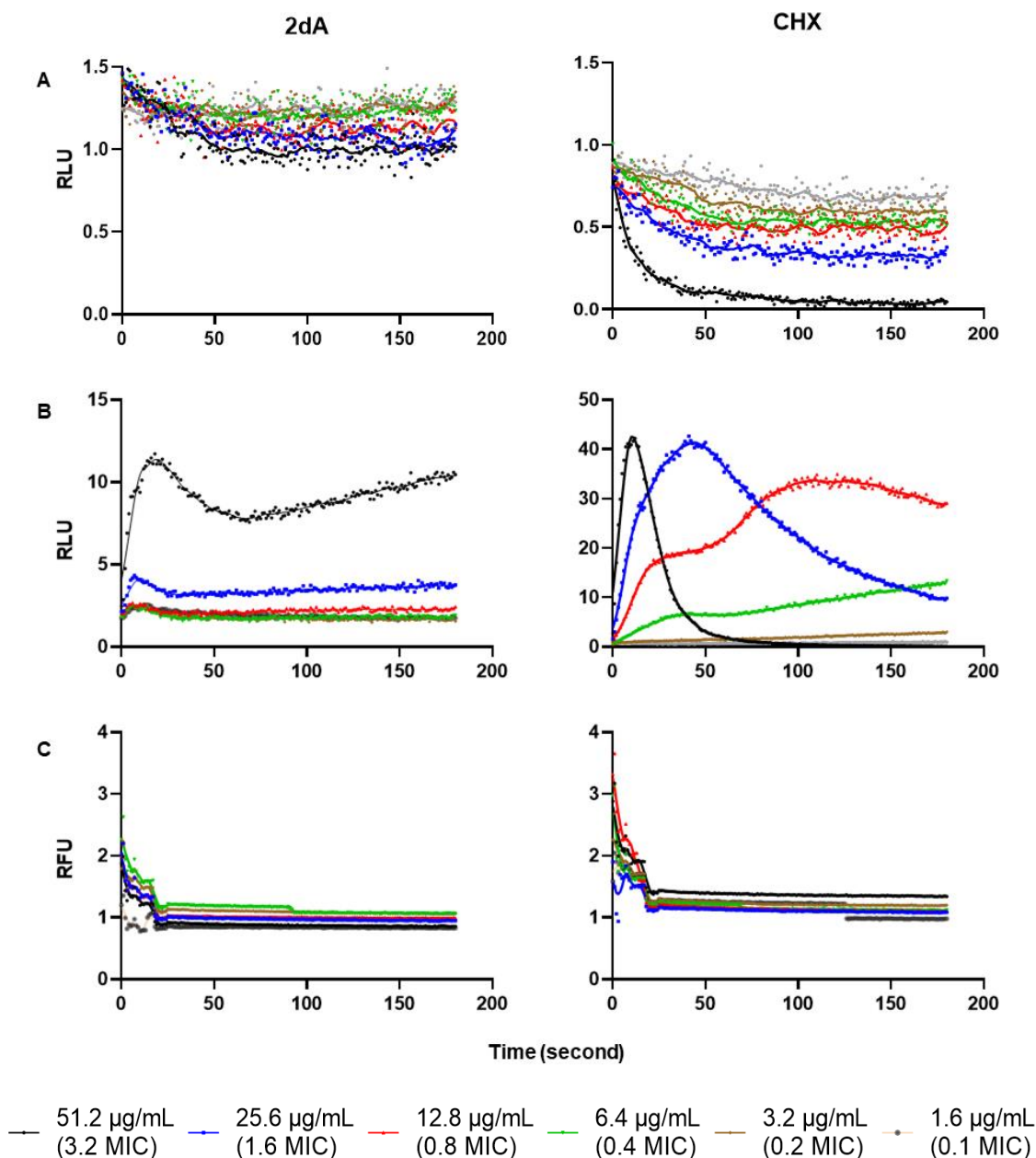


Figure 4. The effects of **2dA** (broad spectrum) and a CHX (positive control) on the kinetics of (A) viability and (B) inner membrane integrity (C) outer membrane integrity in *E. coli* K12. Normalized light emission (normalized with a negative, untreated water control) is plotted as relative light units (RLU) over time (seconds) for A and B. For C, normalized fluorescence (normalized with a negative, untreated water control) is plotted as relative fluorescence units (RFU) over time (seconds). Light emission/fluorescence was measured each second for 180 s after adding the bacterial cell suspension (with 1 mM D-luciferin for the inner membrane integrity assay and 20 µM 1-*N*-phenyl-naphthylamine for outer membrane integrity assay) to the analytes in separate wells. The multiples of the MIC values given in parentheses refer only to compound **2dA**. The figure shows a representative data set from at least three independent experiments.

period, proving the bactericidal effect of **2dA**. These results strongly suggest that when concentrations are high enough, hydantoin **2dA** disrupts the outer membranes and inner membranes at the same speed. However, it cannot be excluded that higher concentrations of **2dA** cause a different mode of action, leading the compound to cross the outer membrane without affecting the latter.

Our results indicate that the main mode of action of most compounds is to interrupt the integrity of the membrane in a concentration-dependent manner, including broad-spectrum hydantoin **2dA**, against both Gram-positive *B. subtilis* and Gram-negative *E. coli*.

However, other targets may exist in addition to bacterial cytoplasmic membranes, so further studies are needed to determine whether there are other types of mode of action.

3. Conclusion

We investigated five scaffolds for their suitability to construct tetrasubstituted, amphipathic antimicrobials, revealing the hydantoin as a promising template. By screening different combinations of lipophilic side chains, *n*-alkyl linkers and cationic groups we identified **2dA** (3,5-di-Br), **6cG** (3-Cl, 4-Br) and **6dG** (3,5-di-Br) as very promising lead structures. The results from viability

and membrane integrity assays, suggested a rapid membranolytic effect for hydantoin **2dA** (3,5-di-Br) in *B. subtilis* and *E. coli*. Interestingly, both, the inner and the outer membrane in *E. coli* seemed to be disrupted at a similar speed. We believe that our findings on the qualitative contribution of the scaffold structures can help the development of further small molecule analogues of AMPs.

4. Experimental Section

For a detailed description of all chemical and biological experimental procedures, chemical analysis and further discussions see the Supporting Information.

Author contributions

M.K.L, A.B. and M.B.S. designed the compound library; M.K.L performed the compound synthesis and analysis; A.R., H.D., H.-M.B., T.H. and K.S. determined the biological assays; A.R., H.D., T.A. performed the biological assays and M.K.L, A.R., H.D., H.-M.B., T.H., K.S., A.B. and M.B.S. analysed and interpreted the data. The manuscript was written through contributions of all authors. All authors have given approval to the final version of the manuscript.

Acknowledgements

MKL, AR and HD thank for a PhD fellowship provided by UiT as part of the AntifoMar and LeadScAMR grants. We thank Senior Engineer Jostein Johansen for help with the HRMS and Prof. Máté Erdélyi for sharing his knowledge.

Declaration of competing interest

The authors declare no conflict of interests.

References

1. Nolte, O., Antimicrobial resistance in the 21st century: a multifaceted challenge. *Protein Pept Lett* **2014**, *21* (4), 330-335.
2. Miethke, M.; Pieroni, M.; Weber, T.; Brönstrup, M.; Hammann, P.; Halby, L.; Arimondo, P. B.; Glaser, P.; Aigle, B.; Bode, H. B.; Moreira, R.; Li, Y.; Luzhetskyy, A.; Medema, M. H.; Pernodet, J.-L.; Stadler, M.; Tormo, J. R.; Genilloud, O.; Truman, A. W.; Weissman, K. J.; Takano, E.; Sabatini, S.; Stegmann, E.; Brötz-Oesterhelt, H.; Wohlleben, W.; Seemann, M.; Empting, M.; Hirsch, A. K. H.; Loretz, B.; Lehr, C.-M.; Titz, A.; Herrmann, J.; Jaeger, T.; Alt, S.; Hesterkamp, T.; Winterhalter, M.; Schiefer, A.; Pfarr, K.; Hoerauf, A.; Graz, H.; Graz, M.; Lindvall, M.; Ramurthy, S.; Karlén, A.; van Dongen, M.; Petkovic, H.; Keller, A.; Peyrane, F.; Donadio, S.; Fraisse, L.; Piddock, L. J. V.; Gilbert, I. H.; Moser, H. E.; Müller, R., Towards the sustainable discovery and development of new antibiotics. *Nat. Rev. Chem.* **2021**, *5* (10), 726-749.
3. Pasupuleti, M.; Schmidtchen, A.; Malmsten, M., Antimicrobial peptides: key components of the innate immune system. *Crit. Rev. Biotechnol.* **2012**, *32* (2), 143-171.
4. Fjell, C. D.; Hiss, J. A.; Hancock, R. E.; Schneider, G., Designing antimicrobial peptides: form follows function. *Nat. Rev. Drug Discov.* **2011**, *11* (1), 37-51.

5. Carmona, G.; Rodriguez, A.; Juarez, D.; Corzo, G.; Villegas, E., Improved protease stability of the antimicrobial peptide Pin2 substituted with D-amino acids. *Protein J.* **2013**, *32* (6), 456-466.
6. Su, M.; Xia, D.; Teng, P.; Nimmagadda, A.; Zhang, C.; Odom, T.; Cao, A.; Hu, Y.; Cai, J., Membrane-Active Hydantoin Derivatives as Antibiotic Agents. *J. Med. Chem.* **2017**, *60* (20), 8456-8465.
7. Kapoor, R.; Eimerman, P. R.; Hardy, J. W.; Cirillo, J. D.; Contag, C. H.; Barron, A. E., Efficacy of antimicrobial peptoids against *Mycobacterium tuberculosis*. *Antimicrob Agents Chemother* **2011**, *55* (6), 3058-3062.
8. Ghosh, C.; Manjunath, G. B.; Akkapeddi, P.; Yarlaga, V.; Hoque, J.; Uppu, D. S.; Konai, M. M.; Haldar, J., Small molecular antibacterial peptoid mimics: the simpler the better! *J. Med. Chem.* **2014**, *57* (4), 1428-1436.
9. Violette, A.; Fournel, S.; Lamour, K.; Chaloin, O.; Frisch, B.; Briand, J. P.; Monteil, H.; Guichard, G., Mimicking helical antibacterial peptides with nonpeptidic folding oligomers. *Chem. Biol.* **2006**, *13* (5), 531-538.
10. Teng, P.; Shi, Y.; Sang, P.; Cai, J., γ -AApeptides as a New Class of Peptidomimetics. *Chem. Eur. J.* **2016**, *22* (16), 5458-5466.
11. Shi, Y.; Teng, P.; Sang, P.; She, F.; Wei, L.; Cai, J., γ -AApeptides: Design, Structure, and Applications. *Acc. Chem. Res.* **2016**, *49* (3), 428-441.
12. Teng, P.; Nimmagadda, A.; Su, M.; Hong, Y.; Shen, N.; Li, C.; Tsai, L.-Y.; Cao, J.; Li, Q.; Cai, J., Novel bis-cyclic guanidines as potent membrane-active antibacterial agents with therapeutic potential. *Chem. Commun.* **2017**, *53* (87), 11948-11951.
13. Wang, M.; Gao, R.; Zheng, M.; Sang, P.; Li, C.; Zhang, E.; Li, Q.; Cai, J., Development of Bis-cyclic Imidazolidine-4-one Derivatives as Potent Antibacterial Agents. *J. Med. Chem.* **2020**, *63* (24), 15591-15602.
14. Strøm, M. B.; Haug, B. E.; Skar, M. L.; Stensen, W.; Stiberg, T.; Svendsen, J. S., The Pharmacophore of Short Cationic Antibacterial Peptides. *J. Med. Chem.* **2003**, *46* (9), 1567-1570.
15. Hansen, T.; Alst, T.; Havelkova, M.; Strøm, M. B., Antimicrobial Activity of Small β -Peptidomimetics Based on the Pharmacophore Model of Short Cationic Antibacterial Peptides. *J. Med. Chem.* **2010**, *53* (2), 595-606.
16. Paulsen, M. H.; Ausbacher, D.; Bayer, A.; Engqvist, M.; Hansen, T.; Haug, T.; Anderssen, T.; Andersen, J. H.; Sollid, J. U. E.; Strøm, M. B., Antimicrobial activity of amphipathic α,α -disubstituted β -amino amide derivatives against ESBL - CARBA producing multi-resistant bacteria; effect of halogenation, lipophilicity and cationic character. *Eur. J. Med. Chem.* **2019**, *183*, 111671.
17. Paulsen, M. H.; Engqvist, M.; Ausbacher, D.; Anderssen, T.; Langer, M. K.; Haug, T.; Morello, G. R.; Liikanen, L. E.; Blencke, H.-M.; Isaksson, J.; Juskevitz, E.; Bayer, A.; Strøm, M. B., Amphipathic Barbiturates as Mimics of Antimicrobial Peptides and the Marine Natural Products Eusynstyelamides with Activity against Multi-resistant Clinical Isolates. *J. Med. Chem.* **2021**.

18. Igumnova, E. M.; Mishchenko, E.; Haug, T.; Blencke, H.-M.; Sollid, J. U. E.; Fredheim, E. G. A.; Lauksund, S.; Stensvåg, K.; Strøm, M. B., Synthesis and antimicrobial activity of small cationic amphipathic aminobenzamide marine natural product mimics and evaluation of relevance against clinical isolates including ESBL-CARBA producing multi-resistant bacteria. *Bioorg. Med. Chem.* **2016**, *24* (22), 5884-5894.
19. Bakka, T. A.; Strøm, M. B.; Andersen, J. H.; Gautun, O. R., Synthesis and antimicrobial evaluation of cationic low molecular weight amphipathic 1,2,3-triazoles. *Bioorg. Med. Chem. Lett.* **2017**, *27* (5), 1119-1123.
20. Langer, M. K.; Rahman, A.; Dey, H.; Anderssen, T.; Zilioli, F.; Haug, T.; Blencke, H.-M.; Stensvåg, K.; Strøm, M. B.; Bayer, A., A concise SAR-analysis of antimicrobial cationic amphipathic barbiturates for an improved activity-toxicity profile. (*submitted Manuscript*) **2022**.
21. Paulsen, M. H.; Karlsen, E. A.; Ausbacher, D.; Anderssen, T.; Bayer, A.; Ochtrop, P.; Hedberg, C.; Haug, T.; Ericson Sollid, J. U.; Strøm, M. B., An amphipathic cyclic tetrapeptide scaffold containing halogenated $\beta^{2,2}$ -amino acids with activity against multiresistant bacteria. *J. Pept. Sci.* **2018**, *24* (10), e3117.
22. Kieć-Kononowicz, K.; Stadnicka, K.; Mitka, A.; Pękala, E.; Filipek, B.; Sapa, J.; Zygmunt, M., Synthesis, structure and antiarrhythmic properties evaluation of new basic derivatives of 5,5-diphenylhydantoin. *Eur. J. Med. Chem.* **2003**, *38* (6), 555-566.
23. Handzlik, J.; Bojarski, A. J.; Satała, G.; Kubacka, M.; Sadek, B.; Ashoor, A.; Siwek, A.; Więcek, M.; Kucwaj, K.; Filipek, B.; Kieć-Kononowicz, K., SAR-studies on the importance of aromatic ring topologies in search for selective 5-HT₇ receptor ligands among phenylpiperazine hydantoin derivatives. *Eur. J. Med. Chem.* **2014**, *78*, 324-339.
24. Rodgers, T. R.; LaMontagne, M. P.; Markovac, A.; Ash, A. B., Hydantoins as antitumor agents. *J. Med. Chem.* **1977**, *20* (4), 591-594.
25. El-Barbary, A. A.; Khodair, A. I.; Pedersen, E. B.; Nielsen, C., S-Glucosylated hydantoins as new antiviral agents. *J. Med. Chem.* **1994**, *37* (1), 73-77.
26. Cortes, S.; Liao, Z.-K.; Watson, D.; Kohn, H., Effect of structural modification of the hydantoin ring on anticonvulsant activity. *J. Med. Chem.* **1985**, *28* (5), 601-606.
27. Sarges, R.; Schnur, R. C.; Belletire, J. L.; Peterson, M. J., Spiro hydantoin aldose reductase inhibitors. *J. Med. Chem.* **1988**, *31* (1), 230-243.
28. Szymańska, E.; Kieć-Kononowicz, K., Antimycobacterial activity of 5-arylidene aromatic derivatives of hydantoin. *Il Farmaco* **2002**, *57* (5), 355-362.
29. Szymańska, E.; Kieć-Kononowicz, K.; Białecka, A.; Kasprowicz, A., Antimicrobial activity of 5-arylidene aromatic derivatives of hydantoin. Part 2. *Il Farmaco* **2002**, *57* (1), 39-44.
30. Handzlik, J.; Szymańska, E.; Chevalier, J.; Otrębska, E.; Kieć-Kononowicz, K.; Pagès, J.-M.; Alibert, S., Amine-alkyl derivatives of hydantoin: New tool to combat resistant bacteria. *Eur. J. Med. Chem.* **2011**, *46* (12), 5807-5816.
31. White, C. J.; Yudin, A. K., Contemporary strategies for peptide macrocyclization. *Nat. Chem.* **2011**, *3* (7), 509-524.
32. Chen, X.; Mietlicki-Baase, E. G.; Barrett, T. M.; McGrath, L. E.; Koch-Laskowski, K.; Ferrie, J. J.; Hayes, M. R.; Petersson, E. J., Thioamide Substitution Selectively Modulates Proteolysis and Receptor Activity of Therapeutic Peptide Hormones. *J. Am. Chem. Soc.* **2017**, *139* (46), 16688-16695.
33. Feng, M.; Tang, B.; Liang, S. H.; Jiang, X., Sulfur Containing Scaffolds in Drugs: Synthesis and Application in Medicinal Chemistry. *Curr. Top. Med. Chem.* **2016**, *16* (11), 1200-1216.
34. Pathania, S.; Narang, R. K.; Rawal, R. K., Role of sulphur-heterocycles in medicinal chemistry: An update. *Eur. J. Med. Chem.* **2019**, *180*, 486-508.
35. Bagley, M. C.; Dale, J. W.; Merritt, E. A.; Xiong, X., Thiopeptide Antibiotics. *Chem. Rev.* **2005**, *105* (2), 685-714.
36. Just-Baringo, X.; Albericio, F.; Álvarez, M., Thiopeptide antibiotics: retrospective and recent advances. *Mar. Drugs* **2014**, *12* (1), 317-351.
37. Neu, H. C., β -Lactam Antibiotics: Structural Relationships Affecting in Vitro Activity and Pharmacologic Properties. *Rev. Infect. Dis.* **1986**, *8*, S237-S259.
38. Ware, E., The Chemistry of the Hydantoins. *Chem. Rev.* **1950**, *46* (3), 403-470.
39. Meusel, M.; Gütschow, M., Recent Developments in Hydantoin Chemistry. A Review. *Org. Prep. Proced. Int.* **2004**, *36* (5), 391-443.
40. López, C. A.; Trigo, G. G., The Chemistry of Hydantoins. In *Adv. Heterocycl. Chem.*, Katritzky, A. R., Ed. Academic Press: 1985; Vol. 38, pp 177-228.
41. Konnert, L.; Lamaty, F.; Martinez, J.; Colacino, E., Recent Advances in the Synthesis of Hydantoins: The State of the Art of a Valuable Scaffold. *Chem. Rev.* **2017**, *117* (23), 13757-13809.
42. Read, W. T., Researches on Hydantoins. Synthesis of the soporific, 4,4-phenylethyl-hydantoin (Nirvanol). *J. Am. Chem. Soc.* **1922**, *44* (8), 1746-1755.
43. Bucherer, H. T. L., V.A., Syntheses of hydantoins. II. Formation of substituted hydantoins from aldehydes and ketones. *J. Prakt. Chem* **1934**, *141*, 5-43.
44. Biltz, H., Constitution of the Products of the Interaction of Substituted Carbamides on Benzil and Certain New Methods for the Preparation of 5,5-Diphenylhydantoin. *Ber. Dtsch. Chem. Ges.* **1908**, *41*, 1379-1393.
45. Hulme, C.; Ma, L.; Romano, J. J.; Morton, G.; Tang, S.-Y.; Cherrier, M.-P.; Choi, S.; Salvino, J.; Labaudiniere, R., Novel applications of carbon dioxide/MeOH for the synthesis of hydantoins and cyclic ureas via the Ugi reaction. *Tetrahedron Lett.* **2000**, *41* (12), 1889-1893.
46. Hulme, C.; Bienaymé, H.; Nixey, T.; Chenera, B.; Jones, W.; Tempest, P.; Smith, A. L., Library Generation via Postcondensation Modifications of Isocyanide-Based Multicomponent Reactions. In *Methods in Enzymology*, Academic Press: 2003; Vol. 369, pp 469-496.
47. Leusen, D. V.; Leusen, A. M. V., Synthetic Uses of Tosylmethyl Isocyanide (TosMIC). In *Organic Reactions*, pp 417-666.

48. Sakata, R.; Soeta, T.; Ukaji, Y., One-Carbon Homologation of Pyrrole Carboxaldehyde via Wittig Reaction and Mild Hydrolysis of Vinyl Ether - Toward the Synthesis of a Sterically Locked Phytochrome Chromophore. *Heterocycles* **2015**, *91* (3), 593-603.
49. Kosarych, Z.; Cohen, T., Rapid, high-yield cleavage of enol and dienol methyl ethers under mild conditions using chlorotrimethylsilane/sodium iodide. *Tetrahedron Lett.* **1980**, *21* (41), 3959-3962.
50. Stetter, H.; Rämisch, R. Y., Über die präparative Nutzung der 1,3-Thiazoliumsalzkatalysierten Acyloin- und Benzoin-Bildung; IV1. Herstellung von Acyloinen mit funktionellen Gruppen. *Synthesis* **1981**, *1981* (06), 477-478.
51. Kim, Y. B.; Kim, C. S.; Lee, C. K., Condensation reactions of aryl acyloins with ureas in ethylene glycol. *J. Heterocycl. Chem.* **1994**, *31* (6), 1653-1656.
52. Carrington, H. C., 131. Thiohydantoins. Part I. Preparation of 5 : 5-disubstituted 2 : 4-dithiohydantoins from the corresponding ketones. *J. Chem. Soc. (Resumed)* **1947**, (0), 681-683.
53. Marinov, M.; Minchev, S.; Stoyanov, N.; Ivanova, G.; Spassova, M.; Enchev, V., Synthesis, Spectroscopic Characterization and ab initio Investigation of Thioanalogues of Spirohydantoins. *Croat. Chem. Acta* **2005**, *78*, 9-16.
54. Virta, M.; Åkerman, K. E. O.; Saviranta, P.; Oker-Blom, C.; Karp, M. T., Real-time measurement of cell permeabilization with low-molecular-weight membranolytic agents. *J. Antimicrob. Chemother.* **1995**, *36* (2), 303-315.
55. Kuyyakanond, T.; Quesnel, L. B., The mechanism of action of chlorhexidine. *FEMS Microbiol. Lett.* **1992**, *100* (1-3), 211-215.
56. Loh, B.; Grant, C.; Hancock, R. E., Use of the fluorescent probe 1-N-phenyl-naphthylamine to study the interactions of aminoglycoside antibiotics with the outer membrane of *Pseudomonas aeruginosa*. *Antimicrob Agents Chemother* **1984**, *26* (4), 546-551.

Supporting Information

for

Hydantoins as a Promising Platform for the Development of Tetrasubstituted, Amphipathic Antimicrobials with Membranolytic Properties

Manuel K. Langer^a, Aatur Rahman^b, Hymonti Dey^b, Trude Anderssen^c, Hans-Matti Blencke^b, Tor Haug^b, Klara Stensvåg^b, Morten B. Strøm^{a*}, Annette Bayer^{b*}

^a Department of Chemistry, UiT – The Arctic University of Norway, NO-9037 Tromsø, NORWAY.

^b The Norwegian College of Fishery Science, Faculty of Biosciences, Fisheries and Economics, UiT – The Arctic University of Norway, NO-9037 Tromsø, NORWAY.

^c Department of Pharmacy, Faculty of Health Sciences, UiT – The Arctic University of Norway, NO-9037 Tromsø, NORWAY.

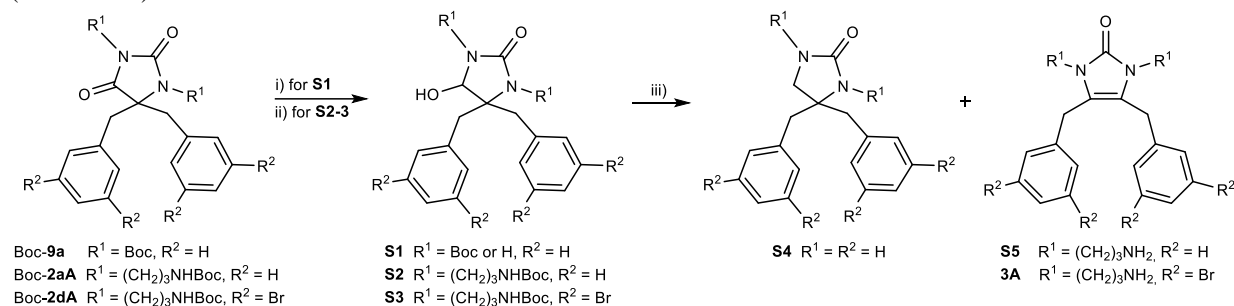
* Shared senior authorship and corresponding authors.

Table of Contents

1.	4-imidazolidin-2-ones <i>via</i> <i>N</i> -acyliminium ion rearrangement	2
2.	Counterion effect	3
3.	Experimental Details	4
1.1	General methods	4
1.2	Synthesis of building blocks	4
1.3	General procedures	4
1.4	Experimental procedures for the synthesis of hydantoins	5
1.5	Synthesis of different core structures 3-5 and 15	14
2.	NMR spectra	20
2.1	Symmetrical ketones 8	20
2.2	Hydantoins 9	26
2.3	<i>N,N</i> -dialkylated hydantoins 2A	32
2.4	<i>N,N</i> -dialkylated hydantoins 2G	38
2.5	<i>N,N</i> -dialkylated hydantoins 6A	44
2.6	<i>N,N</i> -dialkylated hydantoins 6G	48
2.7	2,4-Dithiohydantoin core	52
2.8	2-Thiobarbituric acid core	54
2.9	4-imidazolidin-2-one and its constitutional isomers	56
2.10	4-imidazolidin-2-one <i>via</i> <i>N</i> -acyliminium ion rearrangement	63
3.	SFC traces	68
3.1	Scaffolds 3A , 4A , 5A and 15A	68
3.2	Hydantoins 2A and 2G	68
3.3	Hydantoins 6A and 6G	70
4.	Full selectivity index table	71
5.	Biological Methods	72
5.1	Minimum inhibitory concentration (MIC) assay	72
5.2	Membrane integrity assay	72
5.3	Viability assay	72
5.4	Red Blood Cell Haemolysis Assay	73
6.	Membrane integrity and viability assay	74
7.	Literature	76

1. 4-imidazolidin-2-ones *via* *N*-acyliminium ion rearrangement

Based on the pioneering work of Speckamp and co-workers^[1] *N*-acyliminium intermediates have been used in a variety of cationic cyclisations.^[2] Far less explored are the *N*-acyliminium ion triggered rearrangements, predominantly Cope-type, which are mostly reported as the underlying mechanism for certain cyclisations.^[3] But when Kohn et al. studied the preparation of annulated imidazolidinones from 4-hydroxy-5,5-dimethylimidazolidin-2-one, they also observed a 1,2-methylshift to the corresponding 4-imidazolin-2-one.^[4] As the 4-hydroxy-imidazolidinones can be accessed by reducing the corresponding hydantoin, we envisioned a similar sequence, starting from the di-Boc protected hydantoin Boc-**9a** and the previously prepared hydantoin Boc-**2aA** and Boc-**2dA** (Scheme S1).



Scheme S1. Synthetic strategy towards **3A** *via* a cationic rearrangement from an *in situ* generated *N*-acyliminium ion. Reaction conditions: i) NaBH₄, EtOH, r.t., 16 h, no yield determined; ii) DIBAL, DCM (dry), -78 to 0 °C, 3 h, 56-70%; iii) see **Table S1**.

Using Boc-**9a** was appealing, because a later introduction of the alkyl linkers would be advantageous for building libraries. NaBH₄ mediated reduction of the amidic carbonyl of Boc-**9a** delivered intermediate **S1**. Upon sequential treatment of the latter one with catalytic amounts of *para*-toluenesulfonic acid (*p*-TsOH) at 120 °C followed by TFA in DCM (Table S1, Entry 1) deoxygenated imidazolidine **S4** was obtained. Consequently, we decided to employ **2aA** and **2dA** instead. Both tetrasubstituted hydantoin could be reduced by DIBAL in DCM to yield 4-hydroxy-imidazolidinones **S2** and **S3** in 56% and 70%, respectively. Refluxing intermediate **S2** with a catalytic amount of *p*-TsOH in anhydrous toluene^[4] (Table S1, Entry 2) led to quantitative conversion. During this process we observed partial degradation of the Boc groups and decided to treat the crude with TFA in DCM and obtained fully deprotected 4-imidazolidin-2-one **S5** in a yield of 74%. Both TFA alone and with additional trifluoro acetic acid anhydride (TFAA) (Entry 3 and 4) effectively promoted the rearrangement. Using formic acid (Entry 4) led to a mixture of the desired product alongside unreacted starting material with zero to two Boc-groups being intact. When treating halo-aryl containing derivative **S3** with TFA (Entry 5), we observed only partial rearrangement to **3A**. Presumably, partial Boc removal takes place prior to the *N*-acyliminium ion formation, leading to a positively net charged compound and thus raising the barrier for the dehydration and subsequent introduction of another positive charge. Even though we could demonstrate the practical value of this strategy towards 4-imidazolidin-2-ones, the final products **S5** and **3A** were difficult to purify, supposedly due to partial fragmentation of the intermediate *N*-acyliminium ion. We decided therefore to abolish this strategy.

Table S1. Reaction conditions for the cationic rearrangement and subsequent Boc-deprotection

Entry	Reactant	Acid (eq)	Solvent ^a	Temperature [°C]	Time [h]	Product (Yield [%])
1	S1	1. <i>p</i> -TsOH (0.20) 2. TFA (20.0 eq)	1. Toluene 2. DCM	1. 120 2. 25	1. 24 2. 18	S4 (34)
2 ^b	S2	1. <i>p</i> -TsOH (0.20) 2. TFA (20.0)	1. Toluene 2. DCM	1. 120 2. 25	1. 5.5 2. 18	S5 (74)
3	S2	TFA (20.0 eq)	DCM	25	18	S5 (82)
4	S2	TFAA (1.30)	TFA:DCM (2:1)	50	18	S5 (83)
5	S2	Formic acid (1.05)	DCM	50	4	n.d. ^c
6	S3	TFA (15.0)	DCM	25	22	S17A (43%)

^a Anhydrous solvents were used. ^b Upon completion of the rearrangement toluene was removed and replaced by DCM. ^c A mixture of reactant, Boc-deprotected reactant and the rearranged product was obtained.

2. Counterion effect

Physicochemical properties like adsorption, solubility and membrane permeability of basic and acidic drugs can be greatly influenced by their counterions.^[5] We converted the di-trifluoroacetate (di-TFA) salts of hydantoins **2c** (3-Cl, 4-Br) and **2d** (3,5-di-Br) into their di-hydrochloride (di-HCl) salts to improve their water solubility^[6] and to evaluate the impact of counterions on their biological activity (**Table S2**).

Table S2. MIC and EC₅₀ values in [µg/mL] of selected di-trifluoroacetate (TFA) and di-hydrochloride (HCl) salts. Improved values are shown in green.

Comp. ID	Side chain	MIC (TFA)				EC ₅₀ (TFA)	MIC (HCl)				EC ₅₀ (HCl)	Solubility ^a
		S. a	B. s	E. c	P. a		S. a	B. s	E. c	P. a		
2cA	(3-Cl, 4-Br)	8	4	32	32	368	8	2	16	32	>400	+/+
2dA	(3,5-di-Br)	8	4	16	8	344	8	2	16	4	289	+/+
2cG	(3-Cl, 4-Br)	2	2	32	8	>467	<1	2	16	64	342	-/-
2dG	(3,5-di-Br)	2	1	16	16	486	2	2	16	32	303	-/-

S. a – *Staphylococcus aureus* ATCC 9144, B.s – *Bacillus subtilis* 168, E. c – *Escherichia coli* ATCC 25922, and P. a – *Pseudomonas aeruginosa* ATCC 27853. ^a If solubility in pure water is equal or greater than 1 mg/mL it is denoted with (+), if lower (–).

Water solubility was assessed qualitatively, by setting the threshold at 1 mg/mL. Di-TFA and di-HCl salts of the amine derivatives **2A** were water soluble, but neither of the salt forms of **2G** were water soluble according to the established criteria. The amine derivatives **2A** demonstrated a minor increase in antimicrobial potency against individual strains by a factor of two. The guanidyl derivatives **2G** did not follow a clear trend, except for Gram-negative *P. aeruginosa*. The di-HCl salts of both guanidyl hydantoins were less potent against *P. aeruginosa*, especially **2cG** showed an 8-fold decrease in potency for undetermined reasons. The haemolytic activity of the amine derivatives **2A** was comparable for both salt forms, but the di-HCl salts of the guanidyl analogues seemed to be more haemolytic than the di-TFA salts. The effect was less pronounced when EC₅₀ values given in µM were compared, but it was still observable. In summary, the di-HCl salts of the amine derivatives **2A** showed slightly improved biological properties, whereas for the guanidyl derivatives **2G** no clear conclusion could be drawn.

3. Experimental Details

1.1 General methods

Unless otherwise noted, purchased chemicals were used as received without further purification. Solvents were dried according to standard procedures over molecular sieves of appropriate size.

Normal phase flash chromatography was carried out on silica gel 60 (230–400 mesh) or on an interchim® PuriFlash XS420 flash system with the sample preloaded on a Samplet® cartridge belonging to a Biotage SP-1 system. Purification by reversed phase (RP) C18 column chromatography (H₂O with 0.1 % TFA/MeCN with 0.1 % TFA) was performed on an interchim® PuriFlash XS420 flash system with the sample preloaded on a Samplet® cartridge.

Thin layer chromatography was carried out using Merck TLC Silica gel 60 F254 and visualized by short-wavelength ultraviolet light or by treatment with an appropriate stain.

NMR spectra were obtained on a 400 MHz Bruker Advance III HD spectrometer equipped with a 5 mm SmartProbe BB/1H (BB = 19F, 31P-15N) at 20 °C. The chemical shifts are reported in ppm relative to the solvent residual peak (CDCl₃: δH 7.26 and δC 77.16; Methanol-d₄: δH 3.31 and δC 49.00; deuterium oxide: δH 4.79; DMSO-d₆ δH 2.51 and δC 39.52). ¹³C NMR spectra were obtained with ¹H decoupling. Data are represented as follows: chemical shift, multiplicity (s = singlet, d = doublet, t = triplet, q = quartet, p = pentet, dt = doublet of triplet, m = multiplet), coupling constant (*J* in Hz) and integration. The raw data was analyzed with MestReNova (Version 14.0.0-23239).

High-resolution mass spectra (HRMS) were recorded from methanol solutions on an LTQ Orbitrap XL (Thermo Scientific) either in negative or in positive electrospray ionization (ESI) mode. The data was analyzed with Thermo Scientific Xcalibur software.

All final products were lyophilized for 48 h to yield their di-TFA salts.

The purity of all tested compounds was determined to be ≥ 95%. The analyses were carried out on a Waters ACQUITY UPC² system equipped with a Torus™ DEA 130Å, 1.7 μm, 2.1 mm x 50 mm column. Compounds were detected on a Waters ACQUITY PDA detector spanning wavelengths from 190 to 650 nm, coupled to a Waters ACQUITY QDA detector for low resolution mass (LRMS) detection. The derivatives were eluted with a mobile phase consisting of supercritical CO₂ and MeOH containing 0.1 % NH₃ and a linear gradient of 2 – 40 % MeOH over 2 or 4 min followed by isocratic 0.5 min of 40% MeOH. The flow rate was 1.5 mL/min.

1.2 Synthesis of building blocks

1-bromo-4-(bromomethyl)naphthalene **S6**^[7], *tert*-butyl (3-bromopropyl)carbamate **S7**^[8], and *tert*-butyl (4-bromobutyl)carbamate **S8**^[9] were prepared as described in literature.

Note: All compounds were obtained as di-TFA salts. TFA is typically observed at 162.1 (q, J = 35.7 Hz) and 117.7 (q, J = 290.3 Hz) in ¹³C-NMR and is not reported for each compound individually.

1.3 General procedures

General Procedure A: Synthesis of symmetrical ketones 8

Substituted benzyl bromide, TosMiC and TBAB or TBAI were mixed with DCM and a NaOH_(aq) solution was added. The mixture was stirred vigorously until TLC indicated full conversion. The layers were separated, and the organic layer was washed with water twice. The organic layer was dried over Na₂SO₄, filtered and the solvent was removed under reduced pressure. The disubstituted TosMiC derivative was obtained as a viscous oil.

The crude oil was taken up in a suitable solvent and HCl_(conc.) was added. The solution was stirred at room temperature until TLC indicated full conversion. Water was added and the pH was adjusted to 8–9 with a 2 N NaOH_(aq) solution. The aqueous layer was extracted with DCM (3x) and the combined organics were washed with a 10% NaHCO_{3(aq)} solution (2x), dried over Na₂SO₄, filtered and the solvent was removed under reduced pressure. The crude product was purified by column chromatography on silica gel with EtOAc/heptane as eluent. Some of the ketones were not obtained pure but used for the next synthetic step.

General Procedure B: Synthesis of Hydantoins 9 by the Bucherer-Bergs reaction

The symmetrical ketone **8** was taken up in DMSO and NH_4CO_3 , KOAc and KCN were added. The solution was stirred at 60 °C until all starting material had been consumed. Water was added and the pH was adjusted to 1-2 by dropwise addition of 1 N $\text{HCl}_{(\text{aq})}$, upon which a white solid precipitated. The mixture was stirred for 30 min at ambient temperature and then filtered. The residue was washed with water and chloroform extensively. The solids were collected and lyophilized for 24 h to yield the desired hydantoins.

General Procedure C: *N,N'*-dialkylation and subsequent Boc-removal

Hydantoin **9**, *tert*-butyl (3-bromopropyl)carbamate **S7** or *tert*-butyl (4-bromobutyl)carbamate **S8**, Cs_2CO_3 and TBAI were mixed with acetone and stirred at 65–75 °C until no more starting material and mono-alkylated compound could be observed (HRMS). The reaction mixture was allowed to cool to ambient temperature before water and EtOAc were added. The layers were separated and the aqueous layer was extracted twice more with EtOAc. The combined organics were dried over MgSO_4 , filtered and the solvent was removed under reduced pressure. The crude products were purified by automated column chromatography on silica gel with EtOAc in heptane as eluent to deliver the Boc protected *N,N'*-dialkylated intermediates Boc-**2A** and Boc-**6A**.

The Boc protected *N,N'*-dialkylated intermediates were dissolved in DCM and TFA was added. The resulting mixture was stirred at ambient temperature until HRMS indicated the cleavage of all Boc groups. The solvent was removed and the crude products were purified by automated RP column chromatography with a gradient of MeCN in H_2O (both containing 0.1% TFA). Fractions containing the target compound were collected, most of the solvent was removed under reduced pressure and the residual solution lyophilized for 48 h. The desired hydantoins **2A** and **6A** were obtained as di-TFA salts.

General procedure D: Guanidine formation

The d-TFA salts of **2A** or **6A** were mixed with THF and DIPEA and stirred at ambient temperature for 10 min. *N,N'*-Di-Boc-1*H*-pyrazole-1-carboximidine was added and the solution was stirred at elevated temperatures until TLC indicated full conversion. The mixture was allowed to cool to ambient temperature and sat. $\text{NH}_4\text{Cl}_{(\text{aq})}$ solution and EtOAc were added. The layers were separated and the aqueous layer was extracted twice more with EtOAc. The combined organics were dried over Na_2SO_4 , filtered and the solvent was removed. The crude products were purified by automated flash column chromatography on silica gel and EtOAc in heptane as eluent to yield the Boc-protected guanidine containing hydantoins Boc-**2G** or Boc-**6G**.

The Boc-protected guanidines were stirred with TFA in DCM at ambient temperature until HRMS indicated full conversion. The solvent was removed and the crude products were purified by automated RP column chromatography with a gradient of MeCN in H_2O (both containing 0.1% TFA). Fractions containing the product were collected, most of the solvent was removed and the residual solution was lyophilized for 48 h. The desired guanylated hydantoins **2G** and **6G** were obtained as di-TFA salts.

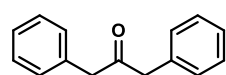
General Procedure E: Preparation of hydrochloric (HCl) salts

The previously obtained TFA salts were taken up in MeOH and HCl in MeOH (1.25 M, 10.0 eq) was added. The solvent was removed and the residue was lyophilized for 24 h. The procedure was repeated twice more to yield the respective HCl salts in $\geq 95\%$ purity. The absence of fluorine was confirmed by ^{19}F NMR (not included).

1.4 Experimental procedures for the synthesis of hydantoins

1.4.1 Synthesis of symmetric ketones **8**

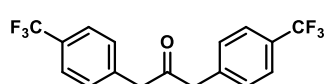
The following compounds were synthesized according to General Procedure A:



1,3-diphenylpropan-2-one **8a**.

Bromomethyl benzene (1.75 g, 10.24 mmol, 2.0 eq), TosMIC (1.00 g, 5.12 mmol, 1.0 eq), TBAB (661 mg, 2.05 mmol, 0.4 eq), NaOH (35 wt%, 35 mL) and DCM (70 mL) were stirred for 14 h. The addition product was obtained as a brown oil.

The addition product, HCl (37%, 2.0 mL), DCM (30 mL) and THF (7 mL) were stirred at ambient temperature for 17 h. Purification by column chromatography on silica gel with 5 % EtOAc in heptane as eluent delivered **8a** (857 mg, 1.78 mmol, 53% o2s) as a colorless liquid. ^1H NMR (400 MHz, Chloroform-*d*) δ 7.45 – 7.33 (m, 6H), 7.29 – 7.22 (m, 4H), 3.80 (s, 4H). ^{13}C NMR (101 MHz, Chloroform-*d*) δ 205.4, 134.0 (2C), 129.4 (4C), 128.6 (4C), 126.9 (2C), 48.9 (2C). HRMS (ESI): calcd for $\text{C}_{15}\text{H}_{14}\text{ONa}^+$ $[\text{M}+\text{Na}]^+$ 233.0937, found: 233.0938.

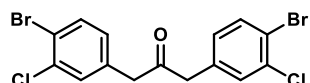


1,3-bis(4-(trifluoromethyl)phenyl)propan-2-one **8b**.

4-(trifluoromethyl)benzyl bromide (4.90 g, 20.50 mmol, 2.0 eq), TosMIC (2.00 g, 10.24 mmol, 1.0 eq), TBAB (1.65 g, 5.12 mmol, 0.5 eq), NaOH (20 wt%, 50 mL)

and DCM (100 mL) were stirred for 24 h. The addition product was obtained as a brown oil.

The addition product, HCl (37%, 8 mL), DCM (33 mL) and THF (7 mL) were stirred at ambient temperature for 17 h. Purification by column chromatography on silica gel with 15% EtOAc in heptane as eluent delivered impure **8b** (2.43 g, 7.02 mmol, 69% o2s) as an off-white solid. ¹H NMR (400 MHz, Methanol-*d*₄) δ 7.59 (d, *J* = 8.1 Hz, 4H), 7.36 (d, *J* = 8.0 Hz, 4H), 3.98 (s, 4H). ¹³C NMR (101 MHz, Methanol-*d*₄) δ 206.1, 140.2 (2C), 131.5 (4C), 130.2 (q, *J* = 32 Hz, 2C), 126.28 (q, *J* = 3.9, 4C), 125.8 (q, *J* = 271.0 Hz, 2C), 49.5 (2C). HRMS (ESI): calcd for C₁₇H₁₁F₆O⁻ [M-H]⁻ 345.0720, found: 345.0717.

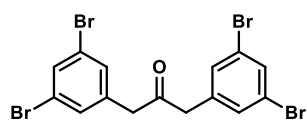


1,3-bis(4-bromo-3-chlorophenyl)propan-2-one **8c**.

1-bromo-4-(bromomethyl)-2-chlorobenzene (1.75 g, 6.15 mmol, 2.0 eq), TosMIC (600 mg, 3.07 mmol, 1.0 eq), TBAB (396 mg, 1.23 mmol, 0.4 eq), NaOH (20 wt%, 12 mL) and DCM (25 mL) were stirred for 24 h. The addition product was obtained

as a brown oil.

The addition product, HCl (37%, 1.5 mL), DCM (20 mL) and THF (5 mL) were stirred at ambient temperature for 6.5 h. Purification by column chromatography on silica gel with 12% EtOAc in heptane as eluent delivered impure **8c** (0.96 g, 3.97 mmol, 59% o2s) as an off-white solid. ¹H NMR (400 MHz, Chloroform-*d*) δ 7.56 (d, *J* = 8.2 Hz, 2H), 7.24 (d, *J* = 2.1 Hz, 2H), 6.90 (dd, *J* = 8.2, 2.1 Hz, 2H), 3.69 (s, 4H). ¹³C NMR (101 MHz, Chloroform-*d*) δ 203.0, 134.9, 134.3, 134.1, 131.9, 129.2, 122.2, 48.3 (2C). HRMS (ESI): calcd for C₁₅H₉Br₂Cl₂O⁻ [M-H]⁻ 432.8403, found: 432.8404.

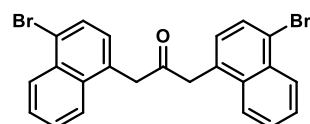


1,3-bis(3,5-dibromophenyl)propan-2-one **8d**.^[10]

1,3-dibromo-5-(bromomethyl)benzene (4.04 g, 12.30 mmol, 2.0 eq), TosMIC (1.20 g, 6.15 mmol, 1.0 eq), TBAB (793 mg, 2.55 mmol, 0.4 eq), NaOH (20 wt%, 60 mL) and DCM (125 mL) were stirred for 14 h. The addition product was obtained

as a brown oil.

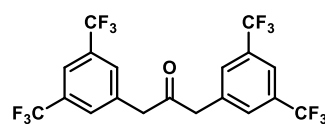
The addition product, HCl (37%, 5 mL), DCM (40 mL) and THF (7 mL) were stirred at ambient temperature for 5 h. The title compound was precipitated from DCM by addition of EtOH. The solids were collected and washed with H₂O and EtOH to yield pure **8d** (1.94 g, 3.68 mmol, 60 % o2s) as a white solid. ¹H NMR (400 MHz, DMSO-*d*₆) δ 7.71 (t, *J* = 1.8 Hz, 2H), 7.44 (d, *J* = 1.8 Hz, 4H), 3.94 (s, 4H). ¹³C NMR (101 MHz, DMSO-*d*₆) δ 203.7, 139.8 (2C), 132.0 (4C), 131.5 (4C), 122.6 (2C), 47.2 (2C). HRMS (ESI): calcd for C₁₅H₉Br₄O⁻ [M-H]⁻ 520.7392, found: 520.7393.



1,3-bis(4-bromonaphthalen-1-yl)propan-2-one **8e**.

1-bromo-4-(bromomethyl)naphthalene **S6** (1.84 g, 6.15 mmol, 2.0 eq), TosMIC (600 mg, 3.07 mmol, 1.0 eq), TBAB (396 mg, 1.23 mmol, 0.4 eq), NaOH (20 wt%, 30 mL) and DCM (65 mL) were stirred for 14 h. The addition product was obtained as a brown oil.

The addition product, HCl (37%, 6.0 mL), DCM (30 mL) and THF (7 mL) were stirred at ambient temperature for 17 h. Upon addition of water and EtOH a white solid precipitated. The solids were collected and washed with water to deliver **8e** (820 mg, 3.07 mmol, 57% o2s) as a white solid. ¹H NMR (400 MHz, Chloroform-*d*) δ 8.31 – 8.24 (m, 2H), 7.70 (d, *J* = 7.6 Hz, 2H), 7.63 (dt, *J* = 8.5, 0.8 Hz, 2H), 7.58 (ddd, *J* = 8.2, 6.9, 1.2 Hz, 2H), 7.43 (ddd, *J* = 8.3, 6.8, 1.3 Hz, 2H), 7.10 (d, *J* = 7.6 Hz, 2H), 4.10 (s, 4H). ¹³C NMR (101 MHz, Chloroform-*d*) δ 205.4, 133.4, 132.3, 130.8, 129.7, 128.9, 128.2, 127.5, 127.4, 124.4, 123.0, 47.2. HRMS (ESI): calcd for C₂₃H₁₆Br₂O⁻Na⁺ [M+Na]⁺ 488.9460, found: 488.9458.



1,3-bis(3,5-bis(trifluoromethyl)phenyl)propan-2-one **8f**.

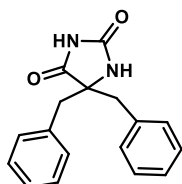
3,5-bis(trifluoromethyl)benzyl bromide (2.25 g, 7.32 mmol, 2.2 eq), TosMIC (650 mg, 3.33 mmol, 1.0 eq), TBAI (246 mg, 0.67 mmol, 0.2 eq), NaOH (30 wt%, 12 mL) and DCM (12 mL) were stirred for 24 h. The addition product was obtained as a brown oil.

The addition product, HCl (37%, 4.2 mL), DCM (20 mL) and THF (4 mL) were stirred at ambient temperature for 17 h. Purification by column chromatography on silica gel with 10% EtOAc in heptane as eluent delivered **8f** (857 mg, 1.78 mmol, 53% o2s) as an off-white solid. ¹H NMR (400 MHz, Methanol-*d*₄) δ 7.84 (s, 2H), 7.82 (s, 4H), 4.18 (s, 4H). ¹³C NMR (101 MHz, Methanol-*d*₄) δ 203.2, 137.4, 131.2 (q, *J* = 32.9 Hz, 2C), 130.3 – 130.1

(m, 2C), 123.5 (q, $J = 272.0$ Hz, 2C), 120.3 – 120.1 (m, 1C). Methylene-carbons were not observed, due to overlap with the deuterated solvent. **HRMS** (ESI): calcd for $C_{19}H_9F_{12}O^-$ [$M-H$] $^-$ 481.0467, found: 481.0461.

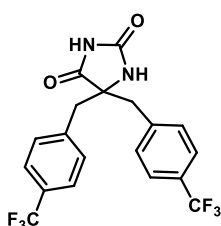
1.4.2 Synthesis of hydantoin 9

The following compounds were prepared according to general procedure B:



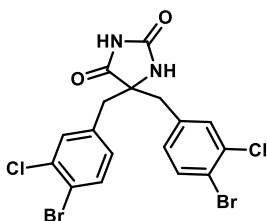
5,5-dibenzylimidazolidine-2,4-dione **9a**.

8a (36 mg, 0.17 mmol, 1.0 eq), KCN (22 mg, 0.34 mmol, 2.0 eq), NH_4CO_3 (82 mg, 0.86 mmol, 5.0 eq), water (0.5 mL) and EtOH (0.5 mL) were stirred at 75 °C for 24 h. Pure **9a** (35 mg, 125 μ mol, 73%) was obtained as a white solid. **1H NMR** (400 MHz, DMSO- d_6) δ 9.97 (s, 1H), 8.00 (s, 1H), 7.33 – 7.12 (m, 10H), 3.10 (d, $J = 13.4$ Hz, 2H), 2.86 (d, $J = 13.4$ Hz, 2H). **^{13}C NMR** (101 MHz, Methanol- d_4) δ 179.1, 158.6, 136.1 (2C), 131.4 (4C), 129.2 (4C), 128.2 (2C), 70.3, 43.9 (2C). **HRMS** (ESI): calcd for $C_{17}H_{16}N_2O_2^-$ [$M-H$] $^-$ 279.1139, found: 279.1137.



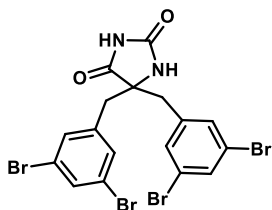
5,5-bis(4-(trifluoromethyl)benzyl)imidazolidine-2,4-dione **9b**.

8b (1.76 g, 5.07 mmol, 1.0 eq), KCN (826 mg, 12.69 mmol, 2.5 eq), NH_4CO_3 (1.95 g, 20.30 mmol, 4.0 eq), KOAc (996 mg, 10.15 mmol, 2.0 eq) and DMSO (15 mL) were stirred at 60 °C for 21 h. Pure **9b** (1.76 g, 4.23 mmol, 83%) was obtained as a slightly brown solid. **1H NMR** (400 MHz, DMSO- d_6) δ 10.01 (s, 1H), 8.16 (s, 1H), 7.67 (d, $J = 8.0$ Hz, 4H), 7.40 (d, $J = 7.9$ Hz, 4H), 3.23 (d, $J = 13.3$ Hz, 2H), 3.00 (d, $J = 13.3$ Hz, 2H). **^{13}C NMR** (101 MHz, DMSO- d_6) δ 174.7, 155.6, 139.9 (2C), 131.0 (4C), 127.6 (q, $J = 31.6$ Hz, 4C), 124.9 (q, $J = 3.8$ Hz, 4C), 124.3 (q, $J = 274$ Hz, 2C), 66.0, 41.8 (2C). **HRMS** (ESI): calcd for $C_{19}H_{13}F_6N_2O_2^-$ [$M-H$] $^-$ 415.0887, found: 415.0882.



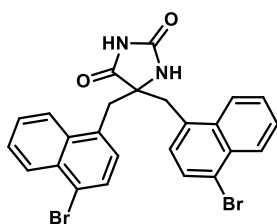
5,5-bis(4-bromo-3-chlorobenzyl)imidazolidine-2,4-dione **9c**.

8c (737 mg, 1.69 mmol, 1.0 eq), KCN (275 mg, 4.22 mmol, 2.5 eq), NH_4CO_3 (648 mg, 6.75 mmol, 4.0 eq), KOAc (331 mg, 3.37 mmol, 2.0 eq) and DMSO (7 mL) were stirred at 60 °C for 16 h. Pure **9c** (387 mg, 0.76 mmol, 45%) was obtained as an off-white solid. **1H NMR** (400 MHz, DMSO- d_6) δ 10.30 (s, 1H), 8.14 (s, 1H), 7.70 (d, $J = 8.2$ Hz, 2H), 7.39 (d, $J = 2.0$ Hz, 2H), 7.06 (dd, $J = 8.2, 2.0$ Hz, 2H), 3.09 (d, $J = 13.4$ Hz, 2H), 2.85 (d, $J = 13.5$ Hz, 2H). **^{13}C NMR** (101 MHz, DMSO- d_6) δ 175.7, 156.4, 136.7, 133.4, 132.5, 132.0, 130.7, 120.0, 66.6, 40.8 (2C). **HRMS** (ESI): calcd for $C_{17}H_{11}Br_2Cl_2N_2O_2^-$ [$M-H$] $^-$ 502.8570, found: 502.8570.



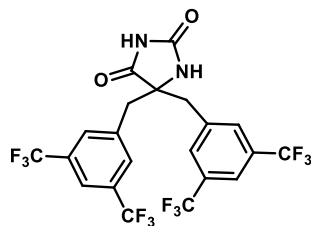
5,5-bis(3,5-dibromobenzyl)imidazolidine-2,4-dione **9d**.

8d (1.21 g, 2.30 mmol, 1.0 eq), KCN (374 mg, 5.75 mmol, 2.5 eq), NH_4CO_3 (884 mg, 9.20 mmol, 4.0 eq), KOAc (451 mg, 4.60 mmol, 2.0 eq) and DMSO (9 mL) were stirred at 60 °C for 16 h. Pure **9d** (1.17 g, 1.96 mmol, 85%) was obtained as a grey solid. **1H NMR** (400 MHz, DMSO- d_6) δ 10.42 (s, 1H), 8.22 (s, 1H), 7.73 (t, $J = 1.8$ Hz, 2H), 7.37 (d, $J = 1.9$ Hz, 4H), 3.09 (d, $J = 13.4$ Hz, 2H), 2.84 (d, $J = 13.4$ Hz, 2H). **^{13}C NMR** (101 MHz, DMSO- d_6) δ 175.7, 154.7, 139.6 (2C), 132.8 (4C), 132.0 (4C), 122.0 (2C), 67.0, 40.77 (2C). **HRMS** (ESI): calcd for $C_{17}H_{11}Br_4N_2O_2^-$ [$M-H$] $^-$ 590.7560, found: 590.7562.



5,5-bis((4-bromonaphthalen-1-yl)methyl)imidazolidine-2,4-dione **9e**.

8e (842 mg, 1.80 mmol, 1.0 eq), KCN (410 mg, 6.29 mmol, 3.5 eq), NH_4CO_3 (1.21 g, 12.59 mmol, 7.0 eq), KOAc (410 mg, 4.18 mmol, 2.0 eq) and DMSO (7 mL) were stirred at 75 °C for 90 h. Pure **9e** (627 mg, 1.16 mmol, 65%) was obtained as a red solid. **1H NMR** (400 MHz, DMSO- d_6) δ 9.91 (s, 1H), 8.41 (dt, $J = 8.0, 2.8$ Hz, 2H), 8.21 – 8.11 (m, 2H), 8.06 (d, $J = 1.7$ Hz, 1H), 7.83 (d, $J = 7.8$ Hz, 2H), 7.73 – 7.63 (m, 4H), 7.42 (d, $J = 7.8$ Hz, 2H), 3.86 (d, $J = 14.2$ Hz, 2H), 3.54 (d, $J = 14.2$ Hz, 2H). **^{13}C NMR** (101 MHz, DMSO- d_6) δ 176.8, 155.6, 133.6, 132.4, 131.1, 129.5, 129.3, 127.4, 126.7, 126.6, 126.0, 121.4, 68.0, 37.7. **HRMS** (ESI): calcd for $C_{25}H_{17}Br_2N_2O_2^-$ [$M-H$] $^-$ 534.9662, found: 534.9660.

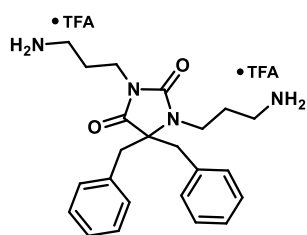


5,5-bis(3,5-bis(trifluoromethyl)benzyl)imidazolidine-2,4-dione **9f**.

8f (806 mg, 1.67 mmol, 1.0 eq), KCN (272 mg, 4.18 mmol, 2.5 eq), NH_4CO_3 (642 mg, 6.69 mmol, 4.0 eq), KOAc (410 mg, 4.18 mmol, 2.50eq) and DMSO (15 mL) were stirred at 60 °C for 20 h. Pure **9f** (470 mg, 0.85 mmol, 51%) was obtained as a white solid. $^1\text{H NMR}$ (400 MHz, DMSO-*d*₆) δ 10.38 (s, 1H), 8.34 (s, 1H), 8.02 (s, 2H), 7.84 (s, 4H), 3.40 (d, J = 13.3 Hz, 2H), 3.12 (d, J = 13.4 Hz, 2H). $^{13}\text{C NMR}$ (101 MHz, DMSO-*d*₆) δ 175.6, 155.5, 138.2 (2C), 131.0 – 130.8 (m, 4C), 129.9 (q, J = 32.7 Hz, 4C), 123.3 (q, J = 272.8 Hz, 4C), 121.1 – 120.8 (m, 2C), 68.1, 40.9 (2C). **HRMS** (ESI): calcd for $\text{C}_{21}\text{H}_{11}\text{F}_{12}\text{N}_2\text{O}_2^-$ [M-H]⁻ 551.0634, found: 551.0628

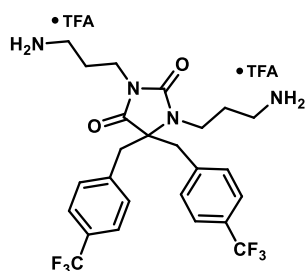
1.4.3 Synthesis of *N,N'*-dialkylated hydantoins **2A**

The following compound were prepared according to General Procedure C:



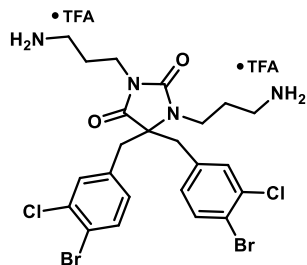
1,3-bis(3-aminopropyl)-5,5-dibenzylimidazolidine-2,4-dione **2aA**.

9a (168 mg, 0.60 mmol, 1.0 eq), *tert*-butyl (3-bromopropyl)carbamate **S7** (429 mg, 1.8 mmol, 3.0 eq), Cs_2CO_3 (586 mg, 1.8 mmol, 3.0 eq), TBAI (44 mg, 120 μmol , 0.2 eq) and acetone (8.0 mL) were stirred at 65 °C for 72 h. Purification by column chromatography on silica gel with a gradient of 0-70% EtOAc in heptane delivered the intermediate Boc-**2aA** (302 mg, 508 μmol , 85%) as a white solid. TFA (460 μL , 6.00 mmol, 10.0 eq) and DCM (3.0 mL) were added and the solution was stirred at ambient temperature for 3.5 h. The crude was purified by RP chromatography with a gradient of 0-70% MeCN/ H_2O + 0.1% TFA to yield the di-TFA salt of **2aA** (272 mg, 437 μmol , 73% o2s) as a white solid. $^1\text{H NMR}$ (400 MHz, Methanol-*d*₄) δ 7.33 – 7.22 (m, 6H), 7.21 – 7.15 (m, 4H), 3.65 – 3.58 (m, 2H), 3.35 (d, J = 14.5 Hz, 2H), 3.26 (d, J = 14.5 Hz, 2H), 3.25 (t, J = 6.7 Hz, 2H), 2.86 (t, J = 7.3 Hz, 2H), 2.27 (t, J = 7.3 Hz, 2H), 2.02 (p, J = 7.4 Hz, 2H), 1.47 (p, J = 7.4 Hz, 2H). $^{13}\text{C NMR}$ (101 MHz, Methanol-*d*₄) δ 175.9, 158.6, 135.9 (2C), 131.0 (4C), 129.7 (4C), 128.7 (2C), 73.6, 41.7 (2C), 39.5, 38.4, 37.7, 35.9, 28.2, 26.8. **HRMS** (ESI): calcd for $\text{C}_{23}\text{H}_{31}\text{N}_4\text{O}_2^+$ [M+H]⁺ 395.2442, found 395.2445. **SFC**: 93.2%.



1,3-bis(3-aminopropyl)-5,5-bis(4-(trifluoromethyl)benzyl)imidazolidine-2,4-dione **2bA**.

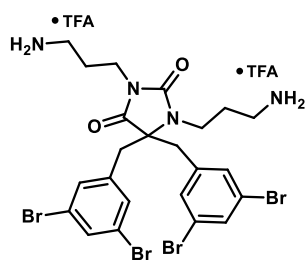
9b (250 mg, 0.60 mmol, 1.0 eq), *tert*-butyl (3-bromopropyl)carbamate **S7** (429 mg, 1.80 mmol, 3.0 eq), Cs_2CO_3 (586 mg, 1.8 mmol, 3.0 eq), TBAI (44 mg, 120 μmol , 0.2 eq) and acetone (8 mL) were stirred at 65 °C for 72 h. Purification by column chromatography on silica gel with a gradient of 0-70% EtOAc in heptane delivered the intermediate Boc-**2bA** (434 mg, 594 μmol , 99%) as a white solid. TFA (551 μL , 7.20 mmol, 12.0 eq) and DCM (2.5 mL) were added and the solution was stirred at ambient temperature for 16 h. The crude was purified by RP chromatography with a gradient of 0-70% MeCN/ H_2O + 0.1% TFA to yield the di-TFA salt of **2bA** (388 mg, 512 μmol , 85% o2s) as a white solid. $^1\text{H NMR}$ (400 MHz, Methanol-*d*₄) δ 7.60 (d, J = 8.1 Hz, 4H), 7.40 (d, J = 8.0 Hz, 4H), 3.69 – 3.62 (m, 2H), 3.41 (s, 4H), 3.27 (t, J = 6.9 Hz, 2H), 2.99 (t, J = 7.3 Hz, 2H), 2.44 (t, J = 7.0 Hz, 2H), 2.08 (p, J = 7.4 Hz, 2H), 1.50 (p, J = 6.9 Hz, 2H). $^{13}\text{C NMR}$ (101 MHz, Methanol-*d*₄) δ 175.2, 158.2, 140.3 (2C), 131.9 (4C), 130.9 (q, J = 32.5 Hz, 2C), 126.4 (q, J = 3.8 Hz, 4C), 125.5 (q, J = 271.3 Hz, 4C), 72.9, 41.2 (2C), 39.5, 38.4, 37.7, 35.9, 28.3, 26.8. **HRMS** (ESI): calcd for $\text{C}_{25}\text{H}_{29}\text{F}_6\text{N}_4\text{O}_2^+$ [M+H]⁺ 531.2189, found 531.2186. **SFC**: >99.0%.



1,3-bis(3-aminopropyl)-5,5-bis(4-bromo-3-chlorobenzyl)imidazolidine-2,4-dione **2cA**.

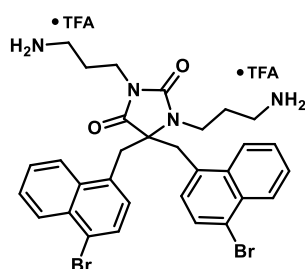
9c (127 mg, 0.25 mmol, 1.0 eq), *tert*-butyl (3-bromopropyl)carbamate **S7** (179 mg, 0.75 mmol, 3.0 eq), Cs_2CO_3 (244 mg, 0.75 mmol, 3.0 eq), TBAI (18 mg, 50 μmol , 0.2 eq) and acetone (1.5 mL) were stirred at 65 °C for 70 h. Purification by column chromatography on silica gel with a gradient of 0-55% EtOAc in heptane delivered the slightly impure intermediate Boc-**2cA** (201 mg, 245 μmol , 98%) as a white foam. TFA (230 μL , 3.00 mmol, 12.0 eq) and DCM (1.5 mL) were added and the solution was stirred at ambient temperature for 16 h. The crude was purified by RP chromatography with a gradient of 0-70% MeCN/ H_2O + 0.1% TFA to yield the di-TFA salt of **2cA** (170 mg, 203 μmol , 81% o2s) as a white solid. $^1\text{H NMR}$ (400 MHz, Methanol-*d*₄) δ 7.62 (d, J = 8.3 Hz, 2H), 7.34 (d, J = 2.1 Hz, 2H), 7.05 (dd, J = 8.3, 2.1 Hz, 2H), 3.64 – 3.55 (m, 2H), 3.36 – 3.31 (m, 2H), 3.29 – 3.25 (m, 4H), 3.00 (t, J = 7.3 Hz, 2H), 2.58 (t, J = 6.9 Hz, 2H), 2.06 (p, J = 7.4 Hz, 2H), 1.58 (p, J = 7.0 Hz, 2H). $^{13}\text{C NMR}$ (101 MHz, Methanol-*d*₄) δ 175.1, 158.1, 137.1 (2C),

135.3 (2C), 135.0 (2C), 132.9 (2C), 131.2 (2C), 122.4 (2C), 72.6, 40.4 (2C), 39.4, 38.4, 37.8, 36.0, 28.4, 27.1. **HRMS** (ESI): calcd for $C_{23}H_{27}Br_2Cl_2N_4O_2^+$ $[M+H]^+$ 618.9872, found 618.9878. **SFC**: 96.7%.



1,3-bis(3-aminopropyl)-5,5-bis(3,5-dibromobenzyl)imidazolidine-2,4-dione 2dA.

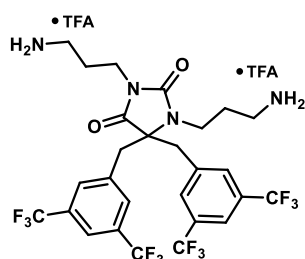
9d (149 mg, 0.25 mmol, 1.0 eq), *tert*-butyl (3-bromopropyl)carbamate **S7** (179 mg, 0.75 mmol, 3.0 eq), Cs_2CO_3 (244 mg, 0.75 mmol, 3.0 eq), TBAI (18 mg, 50 μ mol, 0.2 eq) and acetone (1.5 mL) were stirred at 65 °C for 70 h. Purification by column chromatography on silica gel with a gradient of 15-70% EtOAc in heptane delivered the impure intermediate Boc-**2dA** (169 mg, 159 μ mol, 74%) as a white foam. TFA (191 μ L, 2.50 mmol, 10.0 eq) and DCM (2.0 mL) were added and the solution was stirred at ambient temperature for 4 h. The crude was purified by RP chromatography with a gradient of 0-70% MeCN/H₂O + 0.1% TFA to yield the di-TFA salt of **2dA** (153 mg, 163 μ mol, 65% o2s) as a white solid. **¹H NMR** (400 MHz, Methanol-*d*4) δ 7.67 (t, J = 1.7 Hz, 2H), 7.36 (d, J = 1.7 Hz, 4H), 3.59 (dd, J = 8.5, 6.6 Hz, 2H), 3.41 – 3.33 (m, 2H), 3.27 (s, 4H), 3.00 (t, J = 7.2 Hz, 2H), 2.67 (t, J = 7.0 Hz, 2H), 2.06 (p, J = 7.3 Hz, 2H), 1.63 (p, J = 7.0 Hz, 2H). **¹³C NMR** (101 MHz, Methanol-*d*4) δ 174.9, 158.1, 140.0 (2C), 134.3 (2C), 133.0 (4C), 123.9 (4C), 72.5, 40.3 (2C), 39.3, 38.4, 37.9, 36.2, 28.5, 27.3. **HRMS** (ESI): calcd for $C_{23}H_{27}Br_4N_4O_2^+$ $[M+H]^+$ 706.8862, found 706.8856. **SFC**: >99.0%.



1,3-bis(3-aminopropyl)-5,5-bis((4-bromonaphthalen-1-yl)methyl)imidazolidine-2,4-dione 2eA.

9e (135 mg, 0.25 mmol, 1.0 eq), *tert*-butyl (3-bromopropyl)carbamate **S7** (179 mg, 0.75 mmol, 3.0 eq), Cs_2CO_3 (244 mg, 0.75 mmol, 3.0 eq), TBAI (18 mg, 50 μ mol, 0.2 eq) and acetone (1.5 mL) were stirred at 65 °C for 70 h. Purification by column chromatography on silica gel with a gradient of 10-25% EtOAc in heptane delivered the slightly impure intermediate Boc-**2eA** (208 mg, 244 μ mol, 98%) as a yellow solid.

TFA (191 μ L, 2.50 mmol, 10.0 eq) and DCM (1.5 mL) were added and the solution was stirred at ambient temperature for 3.5 h. The crude was purified by RP chromatography with a gradient of 0-70% MeCN/H₂O + 0.1% TFA to yield the di-TFA salt of **2eA** (132 mg, 150 μ mol, 60% o2s) as a yellow solid. **¹H NMR** (400 MHz, Methanol-*d*4) δ 8.33 – 8.22 (m, 4H), 7.77 (d, J = 7.8 Hz, 2H), 7.71 – 7.62 (m, 4H), 7.18 (d, J = 7.8 Hz, 2H), 4.05 (d, J = 15.3 Hz, 2H), 3.86 (d, J = 15.3 Hz, 2H), 3.79 – 3.69 (m, 2H), 3.10 (t, J = 6.8 Hz, 2H), 2.83 (t, J = 7.4 Hz, 2H), 2.14 (t, J = 6.8 Hz, 2H), 1.70 (p, J = 7.5 Hz, 2H), 1.01 (p, J = 6.8 Hz, 2H). **¹³C NMR** (101 MHz, Methanol-*d*4) δ 175.3, 158.2, 134.9 (2C), 133.4 (2C), 132.7 (2C), 130.4 (2C), 129.1 (2C), 128.8 (2C), 128.7 (2C), 128.3 (2C), 126.1 (2C), 123.7 (2C), 71.7, 39.7, 38.3, 37.4, 37.1 (2C), 35.7, 28.2, 26.7. **HRMS** (ESI): calcd for $C_{31}H_{33}Br_2N_4O_2^+$ $[M+H]^+$ 651.0965, found 651.0965. **SFC**: >99.0%.



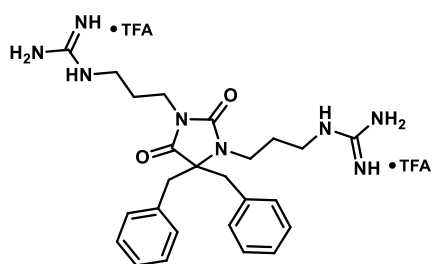
1,3-bis(3-aminopropyl)-5,5-bis(3,5-bis(trifluoromethyl)benzyl)imidazolidine-2,4-dione 2fA.

9f (200 mg, 0.36 mmol, 1.0 eq), *tert*-butyl (3-bromopropyl)carbamate **S7** (259 mg, 1.09 mmol, 3.0 eq), Cs_2CO_3 (354 mg, 1.09 mmol, 3.0 eq), TBAI (27 mg, 72 μ mol, 0.2 eq) and acetone (5.0 mL) were stirred at 65 °C for 72 h. Purification by column chromatography on silica gel with a gradient of 10-25% EtOAc in heptane delivered the slightly impure intermediate Boc-**2fA** (225 mg, 260 μ mol, 72%) as a white solid.

TFA (277 μ L, 3.63 mmol, 10.0 eq) and DCM (2.0 mL) were added and the solution was stirred at ambient temperature for 17 h. The crude was purified by RP chromatography with a gradient of 10-65% MeCN/H₂O + 0.1% TFA to yield the di-TFA salt of **2fA** (144 mg, 161 μ mol, 45% o2s) as a white solid. **¹H NMR** (400 MHz, Methanol-*d*4) δ 7.92 (s, 2H), 7.80 (d, J = 1.7 Hz, 4H), 3.72 (dd, J = 8.5, 6.5 Hz, 2H), 3.56 (d, J = 14.2 Hz, 2H), 3.45 (d, J = 14.3 Hz, 2H), 3.26 (dd, J = 7.9, 6.5 Hz, 2H), 3.06 (t, J = 7.3 Hz, 2H), 2.63 (t, J = 7.0 Hz, 2H), 2.14 (q, J = 7.3 Hz, 2H), 1.48 (p, J = 7.1 Hz, 2H). **¹³C NMR** (101 MHz, Methanol-*d*4) δ 174.5, 157.6, 138.8 (2C), 132.8 (q, J = 33.3 Hz, 4C), 132.1 – 131.8 (m, 4C), 124.7 (q, J = 272.1 Hz, 4C), 122.8 – 122.4 (m, 2C), 71.7, 40.3 (2C), 39.3, 38.4, 37.8, 36.2, 28.9, 27.0. **HRMS** (ESI): calcd for $C_{27}H_{27}F_{12}N_4O_2^+$ $[M+H]^+$ 667.1937, found 667.1940. **SFC**: 96.8%.

1.4.4 Synthesis of *N,N'*-dialkylated hydantoin 2G

The following compounds were prepared according to General Procedure D:

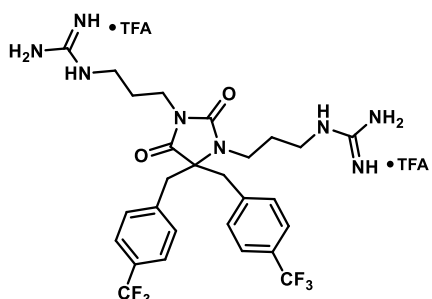


1,1'-((4,4-dibenzyl-2,5-dioxoimidazolidine-1,3-diyl)bis(propane-3,1-diyl))diguanidine **2aG**.

2aA (120 mg, 193 μmol , 1.0 eq), *N,N'*-Di-Boc-1*H*-pyrazole-1-carboxamide (150 mg, 482 μmol , 2.50 eq), DIPEA (134 μL , 771 μmol , 4.00 eq) and THF (1 mL) were stirred at 45 °C for 2.0 h. The crude was purified with a gradient of 10-45% EtOAc in heptane to yield Boc-**2aG** (126 mg, 143 μmol , 74%) as a white foam.

TFA (221 μL , 2.89 mmol, 15.0 eq) and DCM (2 mL) were added and the solution was stirred at ambient temperature for 24 h. The crude was

purified by RP chromatography with a gradient of 10-55% MeCN/H₂O + 0.1% TFA to yield the di-TFA salt of **2aG** (86 mg, 122 μmol , 63% o2s) as a white powder. ¹H NMR (400 MHz, Methanol-*d*₄) δ 7.31 – 7.21 (m, 6H), 7.16 (dd, *J* = 7.6, 1.9 Hz, 4H), 3.57 – 3.49 (m, 2H), 3.34 (d, *J* = 14.6 Hz, 2H), 3.25 (d, *J* = 14.5 Hz, 2H), 3.17 (dt, *J* = 11.1, 6.8 Hz, 4H), 2.58 (t, *J* = 6.9 Hz, 2H), 1.94 – 1.84 (m, 2H), 1.31 (p, *J* = 6.8 Hz, 2H). ¹³C NMR (101 MHz, Methanol-*d*₄) δ 176.1, 158.7, 158.6, 158.4, 135.9 (2C), 130.9 (4C), 129.6 (4C), 128.6 (2C), 73.4, 41.8 (2C), 40.2, 40.0, 39.4, 36.2, 29.4, 28.3. HRMS (ESI): calcd for C₂₅H₃₅N₈O₂⁺ [M+H]⁺ 479.2877, found 479.2868. SFC: >99.0%.

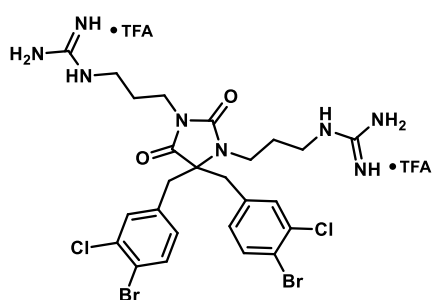


1,1'-((2,5-dioxo-4,4-bis(4-(trifluoromethyl)benzyl)imidazolidine-1,3-diyl)bis(propane-3,1-diyl))diguanidine **2bG**.

2bA (103 mg, 136 μmol , 1.0 eq), *N,N'*-Di-Boc-1*H*-pyrazole-1-carboxamide (105 mg, 340 μmol , 2.50 eq), DIPEA (95 μL , 543 μmol , 4.00 eq) and THF (1 mL) were stirred at 45 °C for 2.0 h. The crude was purified with a gradient of 10-52% EtOAc in heptane to yield Boc-**2bG** (120 mg, 118 μmol , 87%) as a white foam.

TFA (156 μL , 2.04 mmol, 15.0 eq) and DCM (1 mL) were added and the solution was stirred at ambient temperature for 24 h. The crude was purified by RP chromatography with a gradient of 10-60% MeCN/H₂O

+ 0.1% TFA to yield the di-TFA salt of **2bG** (89 mg, 106 μmol , 78% o2s) as a white powder. ¹H NMR (400 MHz, Methanol-*d*₄) 7.60 (d, *J* = 8.0 Hz, 4H), 7.38 (d, *J* = 8.0 Hz, 4H), 3.64 – 3.54 (m, 2H), 3.44 (d, *J* = 14.4 Hz, 2H), 3.39 (d, *J* = 14.4 Hz, 2H), 3.21 (dt, *J* = 9.2, 7.0 Hz, 4H), 2.70 (t, *J* = 6.9 Hz, 2H), 1.99 – 1.90 (m, 2H), 1.38 – 1.26 (m, 4H). ¹³C NMR (101 MHz, Methanol-*d*₄) δ 175.2 (2C), 158.3, 140.4 (2C), 131.8 (4C), 126.4 (q, *J* = 3.8 Hz, 4C), 72.8, 41.3 (2C), 40.2, 40.0, 39.4, 36.4, 29.6, 28.3. CF₃ carbon and the neighboring carbon were not observed due to too low intensity. HRMS (ESI): calcd for C₂₇H₃₃F₆N₈O₂⁺ [M+H]⁺ 615.2625, found 615.2626. SFC: >99.0%.

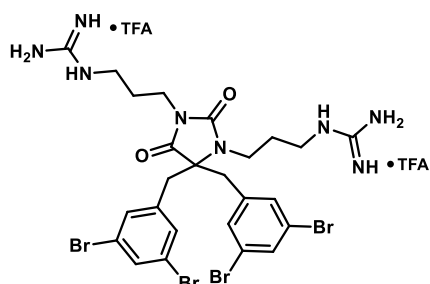


1,1'-((4,4-bis(4-bromo-3-chlorobenzyl)-2,5-dioxoimidazolidine-1,3-diyl)bis(propane-3,1-diyl))diguanidine **2cG**.

2cA (57 mg, 68 μmol , 1.0 eq), *N,N'*-Di-Boc-1*H*-pyrazole-1-carboxamide (53 mg, 170 μmol , 2.50 eq), DIPEA (47 μL , 272 μmol , 4.00 eq) and THF (1 mL) were stirred at 45 °C for 2.0 h. The crude was purified with a gradient of 10-52% EtOAc in heptane to yield impure Boc-**2cG** (120 mg, 109 μmol , 159%) as a white foam.

TFA (78 μL , 102 mmol, 15.0 eq) and DCM (1 mL) were added and the solution was stirred at ambient temperature for 24 h. The crude was purified by RP chromatography with a gradient of 10-60% MeCN/H₂O + 0.1% TFA to yield the di-TFA salt of **2cG** (44 mg, 47 μmol , 69%

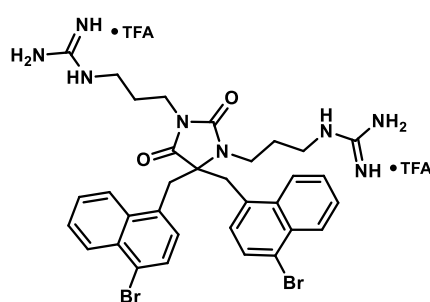
o2s) as a white powder. ¹H NMR (400 MHz, Methanol-*d*₄) δ 7.60 (d, *J* = 8.3 Hz, 2H), 7.33 (d, *J* = 2.1 Hz, 2H), 7.03 (dd, *J* = 8.3, 2.1 Hz, 2H), 3.59 – 3.50 (m, 2H), 3.29 – 3.20 (m, 8H), 2.78 (t, *J* = 7.0 Hz, 2H), 1.95 (p, *J* = 7.1 Hz, 2H), 1.39 (p, *J* = 7.1 Hz, 2H). ¹³C NMR (101 MHz, Methanol-*d*₄) δ 175.2, 158.7, 158.6, 158.0, 137.2 (2C), 135.4 (2C), 135.0 (2C), 132.9 (2C), 131.1 (2C), 122.4 (2C), 72.6, 40.4 (2C), 40.2, 40.0, 39.4, 37.8, 36.4, 29.7, 28.6. HRMS (ESI): calcd for C₂₅H₃₁Br₂Cl₂N₈O₂⁺ [M+H]⁺ 703.0308, found 703.0312. SFC: >99.0%.



1,1'-((4,4-bis(3,5-dibromobenzyl)-2,5-dioxoimidazolidine-1,3-diyl)bis(propane-3,1-diyl))diguanidine 2dG.

2dA (53 mg, 57 μ mol, 1.0 eq), *N,N'*-Di-Boc-1*H*-pyrazole-1-carboxamide (44 mg, 141 μ mol, 2.50 eq), DIPEA (39 μ L, 226 μ mol, 4.00 eq) and THF (1 mL) were stirred at 45 °C for 2.0 h. The crude was purified with a gradient of 10-52% EtOAc in heptane to yield Boc-**2dG** (60 mg, 50 μ mol, 89%) as a white foam.

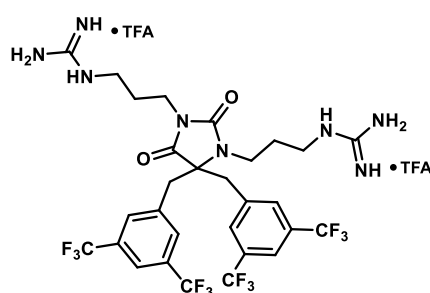
TFA (65 μ L, 848 μ mol, 15.0 eq) and DCM (1 mL) were added and the solution was stirred at ambient temperature for 24 h. The crude was purified by RP chromatography with a gradient of 10-60% MeCN/H₂O + 0.1% TFA to yield the di-TFA salt of **2dG** (50 mg, 49 μ mol, 87% o2s) as a white powder. ¹H NMR (400 MHz, Methanol-*d*4) δ 7.66 (t, *J* = 1.7 Hz, 2H), 7.34 (d, *J* = 1.8 Hz, 4H), 3.57 – 3.46 (m, 2H), 3.30 – 3.22 (m, 8H), 2.87 (t, *J* = 7.0 Hz, 2H), 2.01 – 1.90 (m, 2H), 1.46 (p, *J* = 7.1 Hz, 2H). ¹³C NMR (101 MHz, Methanol-*d*4) δ 175.1, 158.7, 158.6, 157.9, 140.1 (2C), 134.2 (2C), 133.0 (4C), 123.9 (4C), 72.7, 40.4 (2C), 40.2, 40.0, 39.5, 36.5, 29.7, 28.8. HRMS (ESI): calcd for C₂₅H₃₁Br₄N₈O₂⁺ [M+H]⁺ 790.9309, found 790.9310. SFC: >99.0%.



1,1'-((4,4-bis((4-bromonaphthalen-1-yl)methyl)-2,5-dioxoimidazolidine-1,3-diyl)bis(propane-3,1-diyl))diguanidine 2eG.

2eA (27 mg, 31 μ mol, 1.0 eq), *N,N'*-Di-Boc-1*H*-pyrazole-1-carboxamide (24 mg, 77 μ mol, 2.50 eq), DIPEA (21 μ L, 123 μ mol, 4.00 eq) and THF (1 mL) were stirred at 45 °C for 2.0 h. The crude was purified with a gradient of 10-45% EtOAc in heptane to yield Boc-**2eG** (27 mg, 24 μ mol, 77%) as a clear liquid.

TFA (35 μ L, 460 μ mol, 15.0 eq) and DCM (1 mL) were added and the solution was stirred at ambient temperature for 24 h. The crude was purified by RP chromatography with a gradient of 10-55% MeCN/H₂O + 0.1% TFA to yield the di-TFA salt of **2eG** (20 mg, 21 μ mol, 68% o2s) as a white powder. ¹H NMR (400 MHz, Methanol-*d*4) δ 8.28 (ddt, *J* = 7.7, 4.6, 2.2 Hz, 4H), 7.74 (d, *J* = 7.8 Hz, 2H), 7.70 – 7.60 (m, 4H), 7.16 (d, *J* = 7.8 Hz, 2H), 4.06 (d, *J* = 15.4 Hz, 2H), 3.85 (d, *J* = 15.3 Hz, 2H), 3.71 – 3.59 (m, 2H), 3.04 (dt, *J* = 10.4, 6.9 Hz, 4H), 2.32 (t, *J* = 7.0 Hz, 2H), 1.47 (p, *J* = 7.0 Hz, 2H), 0.72 (p, *J* = 7.0 Hz, 2H). ¹³C NMR (101 MHz, Methanol-*d*4) δ 175.7, 158.5, 158.3, 158.0, 135.0 (2C), 133.5 (2C), 132.7 (2C), 130.4 (2C), 129.0 (2C), 128.7 (2C), 128.6 (2C), 128.2 (2C), 126.1 (2C), 123.7 (2C), 71.7, 40.1, 40.1, 39.0, 37.0 (2C), 36.2, 29.2, 28.1. HRMS (ESI): calcd for C₃₃H₃₇Br₂N₈O₂⁺ [M+H]⁺ 735.1401, found 735.1393. SFC: >99.0%.



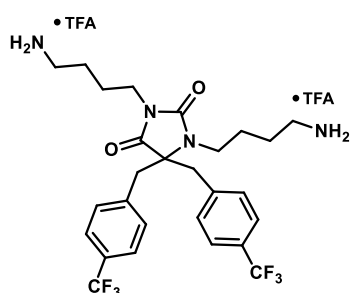
1,1'-((4,4-bis(3,5-bis(trifluoromethyl)benzyl)-2,5-dioxoimidazolidine-1,3-diyl)bis(propane-3,1-diyl))diguanidine 2fG.

2fA (83 mg, 93 μ mol, 1.0 eq), *N,N'*-Di-Boc-1*H*-pyrazole-1-carboxamide (72 mg, 232 μ mol, 2.50 eq), DIPEA (65 μ L, 371 μ mol, 4.00 eq) and THF (1 mL) were stirred at 45 °C for 2.0 h. The crude was purified with a gradient of 10-50% EtOAc in heptane to yield Boc-**2fG** (48 mg, 42 μ mol, 45%) as a clear liquid.

TFA (107 μ L, 1.39 mmol, 15.0 eq) and DCM (1 mL) were added and the solution was stirred at ambient temperature for 24 h. The crude was purified by RP chromatography with a gradient of 15-55% MeCN/H₂O + 0.1% TFA to yield the di-TFA salt of **2fG** (30 mg, 31 μ mol, 33% o2s) as a white powder. ¹H NMR (400 MHz, Methanol-*d*4) δ 7.94 – 7.89 (m, 2H), 7.83 – 7.76 (m, 4H), 3.67 – 3.60 (m, 2H), 3.57 (d, *J* = 14.3 Hz, 2H), 3.50 (d, *J* = 14.3 Hz, 2H), 3.30 (t, *J* = 6.8 Hz, 2H), 3.20 – 3.12 (m, 2H), 2.80 (t, *J* = 6.9 Hz, 2H), 2.07 – 1.96 (m, 2H), 1.34 – 1.19 (m, 2H). ¹³C NMR (101 MHz, Methanol-*d*4) δ 174.7, 158.8, 158.6, 157.5, 138.9 (2C), 132.8 (q, *J* = 33.3 Hz, 4C), 132.0 – 131.7 (m, 4C), 124.7 (q, *J* = 272.0 Hz, 4C), 122.6 – 122.4 (m, 2C), 72.3, 40.4 (2C), 40.2, 40.0, 39.2, 36.4, 29.8, 28.5. HRMS (ESI): calcd for C₂₉H₃₁F₁₂N₈O₂⁺ [M+H]⁺ 751.2373, found 751.2375. SFC: >99.0%.

1.4.5 Synthesis of *N,N'*-dialkylated hydantoin 6A

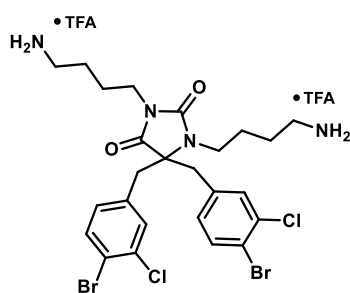
The following compounds were prepared according to General Procedure C:



1,3-bis(4-aminobutyl)-5,5-bis(4-(trifluoromethyl)benzyl)imidazolidine-2,4-dione 6bA.

9b (69 mg, 166 μmol , 1.0 eq), *tert*-butyl (4-bromobutyl)carbamate **S8** (104 mg, 414 μmol , 2.5 eq), Cs_2CO_3 (189 mg, 580 μmol , 3.5 eq), TBAI (6.1 mg, 17 μmol , 0.1 eq) and acetone (2.0 mL) were stirred at 75 $^\circ\text{C}$ for 72 h. Purification by column chromatography on silica gel with a gradient of 15-50% EtOAc in heptane delivered the impure intermediate Boc-**6bA** (110 mg, 145 μmol , 88%) as a colorless solid.

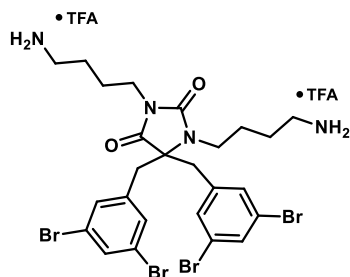
TFA (127 μL , 1.66 mmol, 10.0 eq) and DCM (1.5 mL) were added and the solution was stirred at ambient temperature for 24 h. The crude was purified by RP chromatography with a gradient of 15-55% MeCN/ H_2O + 0.1% TFA to yield the di-TFA salt of **6bA** (64 mg, 81 μmol , 49% o2s) as a white solid. $^1\text{H NMR}$ (400 MHz, Methanol-*d*4) δ 7.60 (d, J = 8.0 Hz, 4H), 7.38 (d, J = 8.0 Hz, 4H), 3.58 – 3.49 (m, 2H), 3.39 (s, 4H), 3.12 (t, J = 7.3 Hz, 2H), 2.97 (t, J = 7.2 Hz, 2H), 2.74 (t, J = 7.7 Hz, 2H), 1.82 – 1.64 (m, 4H), 1.31 – 1.18 (m, 2H), 1.05 (h, J = 7.4, 6.8 Hz, 2H). $^{13}\text{C NMR}$ (101 MHz, Methanol-*d*4) δ 175.1, 157.8, 140.5 – 140.4 (m, 2H), 131.9 (4C), 130.7 (q, J = 32.3 Hz, 2C), 126.3 (q, J = 3.9 Hz, 4C), 125.6 (q, J = 271.2 Hz, 2C), 72.5, 42.0, 41.3 (2C), 40.2, 39.7, 38.2, 27.2, 26.3, 25.6, 25.4. **HRMS** (ESI): calcd for $\text{C}_{27}\text{H}_{33}\text{F}_6\text{N}_4\text{O}_2^+$ $[\text{M}+\text{H}]^+$ 559.2502, found 559.2503. **SFC**: 96.6%.



1,3-bis(4-aminobutyl)-5,5-bis(4-bromo-3-chlorobenzyl)imidazolidine-2,4-dione 6cA.

9c (73 mg, 144 μmol , 1.0 eq), *tert*-butyl (4-bromobutyl)carbamate **S8** (91 mg, 360 μmol , 2.5 eq), Cs_2CO_3 (164 mg, 504 μmol , 3.5 eq), TBAI (5.3 mg, 14 μmol , 0.1 eq) and acetone (2.0 mL) were stirred at 75 $^\circ\text{C}$ for 72 h. Purification by column chromatography on silica gel with a gradient of 15-50% EtOAc in heptane delivered the impure intermediate Boc-**6cA** (92 mg, 108 μmol , 75%) as a colorless solid.

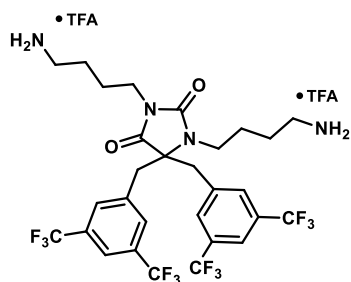
TFA (111 μL , 1.44 mmol, 10.0 eq) and DCM (1.5 mL) were added and the solution was stirred at ambient temperature for 24 h. The crude was purified by RP chromatography with a gradient of 15-55% MeCN/ H_2O + 0.1% TFA to yield the di-TFA salt of **6cA** (71 mg, 81 μmol , 56% o2s) as a white solid. $^1\text{H NMR}$ (400 MHz, Methanol-*d*4) δ 7.60 (d, J = 8.3 Hz, 2H), 7.34 (d, J = 2.1 Hz, 2H), 7.03 (dd, J = 8.3, 2.1 Hz, 2H), 3.48 (t, J = 7.5 Hz, 2H), 3.25 (s, 4H), 3.19 (t, J = 7.2 Hz, 2H), 2.98 (t, J = 7.2 Hz, 2H), 2.81 (t, J = 7.6 Hz, 2H), 1.81 – 1.65 (m, 4H), 1.35 – 1.23 (m, 2H), 1.20 – 1.08 (m, 2H). $^{13}\text{C NMR}$ (101 MHz, Methanol-*d*4) δ 175.1, 157.8, 137.2 (2C), 135.2 (2C), 135.0 (2C), 133.1 (2C), 131.2 (2C), 122.2 (2C), 72.4, 41.9, 40.4 (2C), 40.2, 40.1, 38.3, 27.3, 26.2, 26.0, 25.5. **HRMS** (ESI): calcd for $\text{C}_{25}\text{H}_{31}\text{Br}_2\text{Cl}_2\text{N}_4\text{O}_2^+$ $[\text{M}+\text{H}]^+$ 647.0185, found 647.0192. **SFC**: 97.3%.



1,3-bis(4-aminobutyl)-5,5-bis(3,5-dibromobenzyl)imidazolidine-2,4-dione 6dA.

9d (73 mg, 123 μmol , 1.0 eq), *tert*-butyl (4-bromobutyl)carbamate **S8** (77 mg, 306 μmol , 2.5 eq), Cs_2CO_3 (140 mg, 429 μmol , 3.5 eq), TBAI (4.5 mg, 12 μmol , 0.1 eq) and acetone (2.5 mL) were stirred at 75 $^\circ\text{C}$ for 72 h. Purification by column chromatography on silica gel with a gradient of 15-50% EtOAc in heptane delivered the impure intermediate Boc-**6dA** (91 mg, 97 μmol , 79%) as a colorless solid.

TFA (94 μL , 1.23 mmol, 10.0 eq) and DCM (1.5 mL) were added and the solution was stirred at ambient temperature for 24 h. The crude was purified by RP chromatography with a gradient of 15-55% MeCN/ H_2O + 0.1% TFA to yield the di-TFA salt of **6dA** (73 mg, 76 μmol , 62% o2s) as a white solid. $^1\text{H NMR}$ (400 MHz, Methanol-*d*4) δ 7.66 (t, J = 1.7 Hz, 2H), 7.34 (d, J = 1.7 Hz, 4H), 3.49 – 3.41 (m, 2H), 3.29 – 3.24 (m, 4H), 3.22 (d, J = 7.4 Hz, 2H), 3.02 – 2.95 (m, 2H), 2.87 (t, J = 7.6 Hz, 2H), 1.72 (p, J = 3.6 Hz, 4H), 1.40 (p, J = 7.4 Hz, 2H), 1.34 – 1.23 (m, 2H). $^{13}\text{C NMR}$ (101 MHz, Methanol-*d*4) δ 175.1, 157.6, 140.2 (2C), 134.2 (2C), 133.1 (4C), 123.9 (4C), 72.6, 42.0, 40.5 (2C), 40.3, 40.0, 38.5, 27.2, 26.2, 26.2, 25.6. **HRMS** (ESI): calcd for $\text{C}_{25}\text{H}_{31}\text{Br}_4\text{N}_4\text{O}_2^+$ $[\text{M}+\text{H}]^+$ 734.9175, found 734.9179. **SFC**: 96.1%.



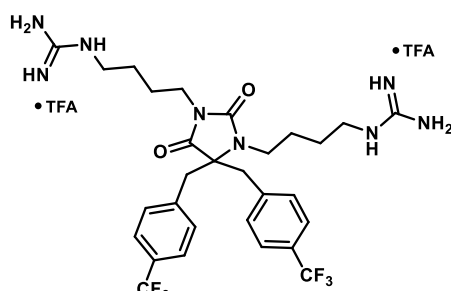
1,3-bis(4-aminobutyl)-5,5-bis(3,5-bis(trifluoromethyl)benzyl)imidazolidine-2,4-dione 6fA.

9f (72 mg, 130 μmol , 1.0 eq), *tert*-butyl (4-bromobutyl)carbamate **S8** (82 mg, 326 μmol , 2.5 eq), Cs_2CO_3 (149 mg, 456 μmol , 3.5 eq), TBAI (4.8 mg, 13 μmol , 0.1 eq) and acetone (2.0 mL) were stirred at 75 $^\circ\text{C}$ for 72 h. Purification by column chromatography on silica gel with a gradient of 15-50% EtOAc in heptane delivered the impure intermediate Boc-**6fA** (103 mg, 115 μmol , 88%) as a colorless solid.

TFA (100 μL , 1.30 mmol, 10.0 eq) and DCM (1.5 mL) were added and the solution was stirred at ambient temperature for 24 h. The crude was purified by RP chromatography with a gradient of 8-48% MeCN/ H_2O + 0.1% TFA to yield the di-TFA salt of **6fA** (96 mg, 104 μmol , 80% o2s) as a white solid. $^1\text{H NMR}$ (400 MHz, Methanol-*d*4) δ 7.92 (d, J = 2.0 Hz, 2H), 7.81 – 7.77 (m, 4H), 3.59 – 3.53 (m, 2H), 3.54 (d, J = 14.3 Hz, 2H), 3.49 (d, J = 14.3 Hz, 2H), 3.10 (dd, J = 8.4, 6.7 Hz, 2H), 2.96 (t, J = 6.8 Hz, 2H), 2.79 – 2.69 (m, 2H), 1.76 (p, J = 3.3 Hz, 4H), 1.37 – 1.25 (m, 2H), 1.08 (tt, J = 9.4, 6.5 Hz, 2H). $^{13}\text{C NMR}$ (101 MHz, Methanol-*d*4) δ 174.7, 157.2, 139.0 (2C), 132.7 (q, J = 33.2 Hz, 4C), 132.0 – 1.31.7 (m, 4C), 124.7 (q, J = 272.0 Hz, 4C), 122.6 – 122.4 (m, 2C), 72.2, 42.0, 40.5 (2C), 40.2, 39.7, 38.3, 27.4, 26.2, 25.7, 25.3. **HRMS** (ESI): calcd for $\text{C}_{29}\text{H}_{31}\text{F}_{12}\text{N}_4\text{O}_2^+$ [M+H] $^+$ 695.2250, found 695.2254. **SFC**: 95.5%.

1.4.6 Synthesis of *N,N'*-dialkylated hydantoin 6G

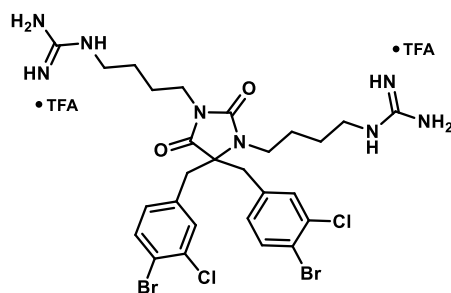
The following compounds were prepared according to General Procedure D:



1,1'-((2,5-dioxo-4,4-bis(4-(trifluoromethyl)benzyl)imidazolidine-1,3-diyl)bis(butane-4,1-diyl))diguanidine 6bG.

6bA (29 mg, 37 μmol , 1.0 eq), *N,N'*-Di-Boc-1*H*-pyrazole-1-carboximidine (29 mg, 92 μmol , 2.50 eq), DIPEA (26 μL , 148 μmol , 4.0 eq) and THF (0.75 mL) were stirred at 45 $^\circ\text{C}$ for 2.5 h. The crude was purified with a gradient of 20-55% EtOAc in heptane to yield pure Boc-**6bG** (38 mg, 36 μmol , 99%) as a clear solid.

TFA (85 μL , 1.11 mmol, 30.0 eq) and DCM (0.75 mL) were added and the solution was stirred at ambient temperature for 44 h. The crude was purified by RP chromatography with a gradient of 20-60% MeCN/ H_2O + 0.1% TFA to yield the di-TFA salt of **6bG** (25 mg, 29 μmol , 78% o2s) as a white powder. $^1\text{H NMR}$ (400 MHz, Methanol-*d*4) δ 7.59 (d, J = 8.1 Hz, 4H), 7.38 (d, J = 8.0 Hz, 4H), 3.54 (dd, J = 9.1, 6.7 Hz, 2H), 3.39 (s, 4H), 3.22 (t, J = 7.1 Hz, 2H), 3.14 (t, J = 6.5 Hz, 2H), 3.00 (t, J = 6.9 Hz, 2H), 1.82 – 1.69 (m, 2H), 1.69 – 1.58 (m, 2H), 1.15 – 1.02 (m, 4H). $^{13}\text{C NMR}$ (101 MHz, Methanol-*d*4) δ 175.3, 158.7, 158.6, 158.0, 140.5 (2C), 131.9 (4C), 130.8 (q, J = 32.3 Hz, 2C), 126.3 (q, J = 3.9 Hz, 4C), 125.6 (q, J = 271.4 Hz, 2C), 72.5, 42.2, 42.0, 41.5, 41.4 (2C), 38.4, 27.5 (2C), 26.5, 25.8. **HRMS** (ESI): calcd for $\text{C}_{29}\text{H}_{37}\text{F}_6\text{N}_8\text{O}_2^+$ [M+H] $^+$ 643.2938, found 643.2936. **SFC**: >99%.

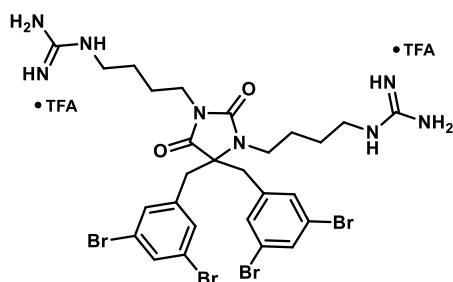


1,1'-((4,4-bis(4-bromo-3-chlorobenzyl)-2,5-dioxoimidazolidine-1,3-diyl)bis(butane-4,1-diyl))diguanidine 6cG.

6cA (28 mg, 32 μmol , 1.0 eq), *N,N'*-Di-Boc-1*H*-pyrazole-1-carboximidine (25 mg, 80 μmol , 2.50 eq), DIPEA (22 μL , 128 μmol , 4.0 eq) and THF (0.75 mL) were stirred at 45 $^\circ\text{C}$ for 2.5 h. The crude was purified with a gradient of 20-55% EtOAc in heptane to yield pure Boc-**6cG** (35 mg, 31 μmol , 97%) as a clear solid.

TFA (74 μL , 0.96 mmol, 30.0 eq) and DCM (0.75 mL) were added and the solution was stirred at ambient temperature for 44 h. The crude was purified by RP chromatography with a gradient of 20-60% MeCN/ H_2O + 0.1% TFA to yield the di-TFA salt of **6cG** (28 mg, 29 μmol , 91% o2s) as a white powder.

$^1\text{H NMR}$ (400 MHz, Methanol-*d*4) δ 7.59 (d, J = 8.2 Hz, 2H), 7.33 (d, J = 2.1 Hz, 2H), 7.03 (dd, J = 8.3, 2.1 Hz, 2H), 3.53 – 3.44 (m, 2H), 3.27 – 3.16 (m, 8H), 3.06 (t, J = 7.1 Hz, 2H), 1.81 – 1.69 (m, 2H), 1.69 – 1.58 (m, 2H), 1.25 – 1.06 (m, 4H). $^{13}\text{C NMR}$ (101 MHz, Methanol-*d*4) δ 175.2, 158.7, 158.6, 158.0, 137.3 (2C), 135.3 (2C), 134.9 (2C), 133.0 (2C), 131.2 (2C), 122.3 (2C), 72.4, 42.2, 42.1, 41.8, 40.5 (2C), 38.5, 27.6, 27.5, 26.5, 26.1. **HRMS** (ESI): calcd for $\text{C}_{27}\text{H}_{35}\text{Br}_2\text{Cl}_2\text{N}_8\text{O}_2^+$ [M+H] $^+$ 731.0621, found 731.0630. **SFC**: >99%.

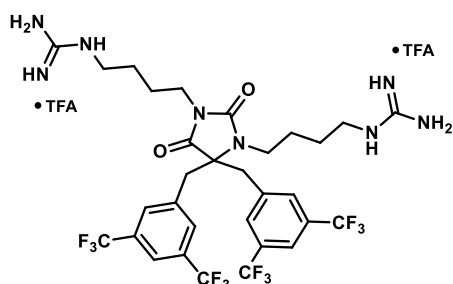


1,1'-((4,4-bis(3,5-dibromobenzyl)-2,5-dioxoimidazolidine-1,3-diyl)bis(butane-4,1-diyl)diguanidine **6dG**.

6dA (31 mg, 32 μmol , 1.0 eq), *N,N'*-Di-Boc-1*H*-pyrazole-1-carboximidine (25 mg, 80 μmol , 2.50 eq), DIPEA (22 μL , 129 μmol , 4.0 eq) and THF (0.75 mL) were stirred at 45 $^{\circ}\text{C}$ for 2.5 h. The crude was purified with a gradient of 20-55% EtOAc in heptane to yield pure Boc-**6dG** (36 mg, 29 μmol , 92%) as a clear solid.

TFA (74 μL , 963 μmol , 30.0 eq) and DCM (0.75 mL) were added and the solution was stirred at ambient temperature for 44 h. The crude was purified by RP chromatography with a gradient of 10-45%

MeCN/H₂O + 0.1% TFA to yield the di-TFA salt of **6dG** (25 mg, 24 μmol , 74% o2s) as a white powder. ¹H NMR (400 MHz, Methanol-*d*4) δ 7.65 (t, *J* = 1.7 Hz, 2H), 7.34 (d, *J* = 1.7 Hz, 4H), 3.45 (t, *J* = 7.7 Hz, 2H), 3.28 – 3.19 (m, 8H), 3.11 (t, *J* = 6.8 Hz, 2H), 1.79 – 1.57 (m, 2H), 1.34 – 1.17 (m, 4H). ¹³C NMR (101 MHz, Methanol-*d*4) δ 175.1, 158.7, 158.6, 157.8, 140.2 (2C), 134.1 (2C), 133.1 (4C), 123.9 (4C), 72.6, 42.2 (2C), 41.9, 40.5 (2C), 38.7, 27.5 (2C), 26.7, 26.4. HRMS (ESI): calcd for C₂₇H₃₅Br₄N₈O₂⁺ [M+H]⁺ 818.9611, found 818.9613. SFC: >99%.



1,1'-((4,4-bis(3,5-bis(trifluoromethyl)benzyl)-2,5-dioxoimidazolidine-1,3-diyl)bis(butane-4,1-diyl)diguanidine **6fG**.

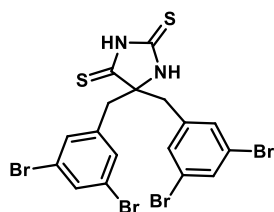
6fA (33 mg, 36 μmol , 1.0 eq), *N,N'*-Di-Boc-1*H*-pyrazole-1-carboximidine (28 mg, 89 μmol , 2.50 eq), DIPEA (25 μL , 143 μmol , 4.0 eq) and THF (0.75 mL) were stirred at 45 $^{\circ}\text{C}$ for 2.5 h. The crude was purified with a gradient of 20-55% EtOAc in heptane to yield pure Boc-**6fG** (40 mg, 34 μmol , 95%) as a clear solid.

TFA (82 μL , 1.07 mmol, 30.0 eq) and DCM (0.75 mL) were added and the solution was stirred at ambient temperature for 44 h. The crude was purified by RP chromatography with a gradient of 20-60%

MeCN/H₂O + 0.1% TFA to yield the di-TFA salt of **6fG** (31 mg, 31 μmol , 86% o2s) as a white powder. ¹H NMR (400 MHz, Methanol-*d*4) δ 7.91 (s, 2H), 7.81 – 7.77 (m, 4H), 3.60 – 3.52 (m, 2H), 3.55 (d, *J* = 14.3 Hz, 2H), 3.49 (d, *J* = 14.3 Hz, 2H), 3.23 (t, *J* = 7.0 Hz, 2H), 3.10 (t, *J* = 6.8 Hz, 2H), 3.00 (t, *J* = 6.8 Hz, 2H), 1.78 (q, *J* = 8.4, 7.7 Hz, 2H), 1.74 – 1.63 (m, 2H), 1.17 – 1.04 (m, 4H). ¹³C NMR (101 MHz, Methanol-*d*4) δ 174.8, 158.7, 158.6, 157.5, 139.0 (2C), 132.7 (q, *J* = 33.3 Hz, 4C), 132.0 – 131.7 (m, 4C), 124.7 (q, *J* = 272.1 Hz, 4C), 122.6 – 122.3 (m, 2C), 72.2, 42.2, 42.0, 41.5, 40.5 (2C), 38.5, 27.7, 27.5, 26.5, 25.9. HRMS (ESI): calcd for C₃₁H₃₅F₁₂N₈O₂⁺ [M+H]⁺ 779.2686, found 779.2689. SFC: >99%.

1.5 Synthesis of different core structures 3-5 and 15

1.5.1 2,4-Dithiohydantoin

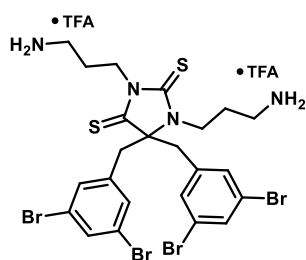


5,5-bis(3,5-dibromobenzyl)imidazolidine-2,4-dithione **16**.

Hydantoin **9d** (175 mg, 294 μmol , 1.0 eq) was mixed with anhydrous 1,4-dioxane (2.5 mL) in an oven dried vial under inert atmosphere. Lawesson's reagent (475 mg, 1.17 mmol, 4.0 eq) was added and the solution was stirred at 115 $^{\circ}\text{C}$ for 40 h. The mixture became yellow and clear at elevated temperature. The mixture was allowed to cool to ambient temperature and the solvent was removed under reduced pressure.

Purification by column chromatography on silica gel with a gradient of 10-15 % EtOAc in heptane and subsequent lyophilization delivered **16** (152 mg, 242 μmol , 82%) as a yellow solid.

¹H NMR (400 MHz, DMSO-*d*6) δ 12.91 (s, 1H), 10.97 (d, *J* = 1.7 Hz, 1H), 7.72 (t, *J* = 1.8 Hz, 2H), 7.37 (d, *J* = 1.8 Hz, 4H), 3.17 (d, *J* = 13.5 Hz, 2H), 3.10 (d, *J* = 13.5 Hz, 2H). ¹³C NMR (101 MHz, DMSO-*d*6) δ 206.5, 180.4, 138.5 (2C), 132.3 (4C), 132.2 (2C), 121.9 (4C), 80.6, 43.5. HRMS (ESI): calcd for C₁₇H₁₁Br₄N₂S₂⁻ [M-H]⁻ 622.7103, found: 622.7109.



1,3-bis(3-aminopropyl)-5,5-bis(3,5-dibromobenzyl)imidazolidine-2,4-dithione **4A**.

2,4-dithiohydantoin **16** (75 mg, 119 μmol , 1.0 eq), *tert*-butyl (3-bromopropyl)carbamate **S7** (92 mg, 388 μmol , 3.25 eq), Cs₂CO₃ (97 mg, 0.299 μmol , 2.5 eq), TBAI (8.8 mg, 24 μmol , 0.2 eq) and acetone (2.0 mL) were stirred at 55 $^{\circ}\text{C}$ for 72 h. The mixture was allowed to cool to ambient temperature before water and EtOAc were added. The layers were separated, and the aqueous layer was extracted with EtOAc twice. The combined organics were dried over MgSO₄, filtered and the solvent was removed under reduced pressure. Purification by automated flash column chromatography on silica gel with a

removed under reduced pressure. Purification by automated flash column chromatography on silica gel with a

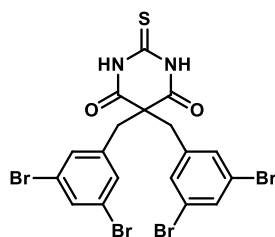
gradient of 10-45% EtOAc in heptane delivered the impure intermediate Boc-**4A** (169 mg, 159 μ mol, 74%) as a yellow foam.

Boc-**4A**, TFA (138 μ L, 1.79 mmol, 15.0 eq) and DCM (1.0 mL) were combined, and the mixture stirred for 24 h at ambient temperature. The solvent was removed and the crude purified by RP chromatography with a gradient of 20-60% MeCN/H₂O + 0.1% TFA to yield the di-TFA salt of **4A** (65 mg, 67 μ mol, 56% o2s) as a white solid.

Note: Peaks in the NMR that are not accounted for are likely to be the S-alkylated isomers.

¹H NMR (400 MHz, Methanol-*d*₄) δ 7.56 (t, *J* = 1.8 Hz, 2H), 7.31 (d, *J* = 1.8 Hz, 4H), 3.61 – 3.55 (m, 2H), 3.37 (t, *J* = 7.2 Hz, 2H), 3.36 (d, *J* = 13.0 Hz, 2H), 3.26 (d, *J* = 12.9 Hz, 2H), 3.17 (t, *J* = 7.2 Hz, 2H), 2.74 (t, *J* = 7.3 Hz, 2H), 2.25 (p, *J* = 7.2 Hz, 2H), 1.56 – 1.43 (m, 2H). ¹³C NMR *not obtained*. HRMS (ESI): calcd for C₂₃H₂₇Br₄N₄S₂⁺ [M+H]⁺ 738.8405, found: 738.8405. SFC: *not obtained*.

1.5.2 Thiobarbituric acid

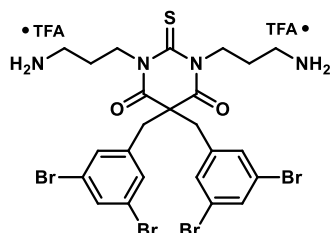


5,5-bis(3,5-dibromobenzyl)-2-thioxodihydropyrimidine-4,6(1H,5H)-dione **18**.

Diethyl 2,2-bis(3,5-dibromobenzyl)malonate^[11] (1.10 g, 1.67 mmol, 1.0 eq) was dissolved in 15 mL of anhydrous THF:DMF (2:1) under inert atmosphere and cooled to 0 °C. Thiourea (1.27 g, 16.7 mmol, 10.0 eq) and NaH (201 mg, 5.02 mmol, 3.0 eq, 60% in mineral oil) were added and the mixture was stirred at that temperature for 30 min. The suspension was then heated to 65 °C for 5 days, cooled to ambient temperature and EtOAc was added. The organic layer was washed with 5% LiCl_(aq) solution thrice, dried over MgSO₄, filtered and the solvent was removed under reduced pressure. The crude solids were purified by column chromatography on silica gel with 5% EtOAc in heptane to yield **18** (261 mg, 408 μ mol, 24%) as a yellow foam.

¹H NMR (400 MHz, Chloroform-*d*) δ 9.20 (s, 2H), 7.58 (t, *J* = 1.8 Hz, 2H), 7.23 (d, *J* = 1.8 Hz, 4H), 3.33 (s, 4H). ¹³C NMR (101 MHz, Chloroform-*d*) δ 174.0, 168.4, 137.6 (2C), 134.2 (2C), 131.6 (4C), 123.6 (4C), 59.9, 43.3 (2C). HRMS (ESI): calcd for C₁₈H₁₁Br₄N₂O₂S⁻ [M-H]⁻ 634.7280, found: 634.7275.

The following compound was synthesized according to General procedure C:



1,3-bis(3-aminopropyl)-5,5-bis(3,5-dibromobenzyl)-2-thioxodihydropyrimidine-4,6(1H,5H)-dione **5A**.

2-Thiobarbituric acid **18** (106 mg, 166 μ mol, 1.0 eq), *tert*-butyl (3-bromopropyl)carbamate **S7** (118 mg, 497 μ mol, 3.0 eq), Cs₂CO₃ (119 mg, 364 μ mol, 2.2 eq), TBAI (12 mg, 33 μ mol, 0.2 eq) and acetone (1.5 mL) were stirred at 70 °C for 87 h. Purification by automated column chromatography on silica with a gradient of 5-45% EtOAc in heptane delivered the impure intermediate Boc-**5A** (83 mg, 87 μ mol, 53%) as a yellow solid.

TFA (102 μ L, 1.33 mmol, 8.0 eq) and DCM (1.0 mL) were added and the solution was stirred at ambient temperature for 17 h. The crude was purified by RP chromatography with a gradient of 20-60% MeCN/H₂O + 0.1% TFA to yield two batches of a mixture of desulfurized (**1A**) and thionylated product (**5A**) as their di-TFA salts. Yield adjusted to pure **5A** (15 mg, 15 μ mol, 9% o2s) Analytical data is only referring to the thionylated product. *Note: De-sulfurization has taken place.*

Mixture 1: white solid, 2-thiobarbituric acid **5A** : barbituric acid **1A** 2.4:1.0^a,

Mixture 2: slightly yellow solid, 2-thiobarbituric acid **5A** : barbituric acid **1A** 1.0:1.7^a

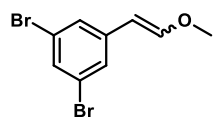
Analytical data for the 2-thiobarbituric acid derivative **5A**:

¹H NMR (400 MHz, Methanol-*d*₄) δ 7.65 (t, *J* = 1.7 Hz, 2H), 7.25 (d, *J* = 1.7 Hz, 4H), 4.26 – 4.18 (m, 4H), 3.48 (s, 4H), 2.94 (t, *J* = 7.3 Hz, 4H), 1.93 – 1.81 (m, 4H). ¹³C NMR (101 MHz, Methanol-*d*₄) δ 179.1, 169.8, 140.3 (2C), 134.7 (2C), 132.6 (4C), 124.2 (4C), 61.9, 46.5 (2C), 45.1 (2C), 38.3 (2C), 26.6 (2C). HRMS (ESI): calcd for C₂₄H₂₇Br₄N₄O₂S⁺ [M+H]⁺ 750.8583, found: 750.8592. SFC: *not obtained*.

Analytical data for desulfurized derivative was identical to the data obtained previously.^[12]

^a Ratio was determined by NMR

1.5.3 4-imidazolidin-2-one and its constitutional isomers

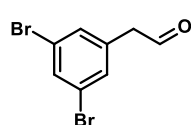


(E)/(Z)-1,3-dibromo-5-(2-methoxyvinyl)benzene **S9**.

(Methoxymethyl)triphenylphosphonium chloride (7.27 g, 21.2 mmol, 1.6 eq) was taken up in dry THF (40 mL) under inert atmosphere and cooled to -78 °C. NaHMDS (21.2 mL, 21.2 mmol, 1.6 eq; 1.0 M in THF) was added slowly and the resulting mixture was stirred at 0 °C for 30 min. The mixture was re-cooled to -78 °C and 3,5-dibromobenzaldehyde **10** (3.50 g, 13.2 mmol, 1.0 eq) was added slowly. Stirring was continued at -78 °C for 30 min and then at ambient temperature for another 2 h. Water and EtOAc were added and the layers were separated. The aqueous layer was extracted with EtOAc twice and the combined organics were dried over MgSO₄, filtered and the solvent was removed under reduced pressure. Heptane was added to the crude solids, and the suspension was sonicated for 5 min. The organic layer was decanted, and the procedure was repeated 3 times. The organic layers were combined, and the solvent was removed under reduced pressure. The crude product was purified by column chromatography on silica gel with 0-5% EtOAc in heptane to yield **S9** (3.54 g, 12.1, 91%) as a slightly yellow liquid. A 1.5 : 1.0 mixture of the *(E)*:*(Z)* isomers was obtained. **HRMS** (ESI): calcd for C₉H₉Br₂O⁺ [M+H]⁺ 290.9015 found: *not found*.

Cis-**ABML444**: ¹H NMR (400 MHz, Chloroform-*d*) δ 7.64 (d, *J* = 1.7 Hz, 2H), 7.41 (t, *J* = 1.8 Hz, 1H), 6.20 (d, *J* = 7.0 Hz, 1H), 5.08 (d, *J* = 7.0 Hz, 1H), 3.82 (s, 3H). ¹³C NMR (101 MHz, Chloroform-*d*) δ 150.3, 139.6, 130.9, 129.6 (2C), 122.7 (2C), 103.3, 57.0.

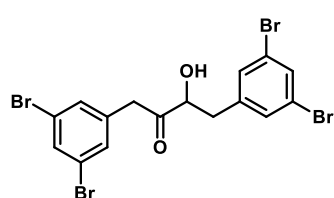
Trans-**ABML444**: ¹H NMR (400 MHz, Chloroform-*d*) δ 7.40 (t, *J* = 1.7 Hz, 1H), 7.28 (d, *J* = 1.8 Hz, 2H), 7.04 (d, *J* = 12.9 Hz, 1H), 5.65 (d, *J* = 12.9 Hz, 1H), 3.69 (s, 3H). ¹³C NMR (101 MHz, Chloroform-*d*) δ 151.0, 140.4, 130.9, 126.7 (2C), 123.2 (2C), 102.9, 57.0.



2-(3,5-dibromophenyl)acetaldehyde **11**.

The mixture of *(E)/(Z)*-**S9** (2.87 g, 9.83 mmol, 1.0 eq) was taken up in anhydrous MeCN (197 mL, *c* = 0.05 M) and NaI (3.09, 20.6 mmol, 2.1 eq) was added. To the vigorously stirring mixture TMSCl (2.63 mL, 20.6 mmol, 2.1 eq) was added and the suspension was stirred at ambient temperature for 110 min. A 0.5 M Na₂SO_{3(aq)} solution was added and the layers were separated. The aqueous layer was extracted with Et₂O thrice and the combined organics were dried over MgSO₄, filtered and the solvent was removed under reduced pressure. The crude solids were taken up in CCl₄, filtered and the solvent was removed under reduced pressure. The crude orange solids were quickly filtered over a short silica plug to yield aldehyde **11** (1.63 g, 5.68 mmol, 60%) as a white solid. *Note: The product decomposes on silica upon extended exposure.*

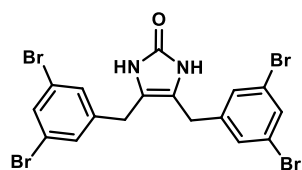
¹H NMR (400 MHz, Chloroform-*d*) δ 9.75 (t, *J* = 1.9 Hz, 1H), 7.62 (t, *J* = 1.8 Hz, 1H), 7.32 (d, *J* = 1.8 Hz, 2H), 3.67 (d, *J* = 1.9 Hz, 2H). ¹³C NMR (101 MHz, Chloroform-*d*) δ 197.5, 135.7, 133.4, 131.6 (2C), 123.5 (2C), 49.5. **HRMS** (ESI): calcd for C₈H₇Br₂O⁺ [M+H]⁺ 276.8858, found: *not found*.



1,4-bis(3,5-dibromophenyl)-3-hydroxybutan-2-one **12**.

Aldehyde **11** (1.63 g, 5.86 mmol, 1.0 eq) and 3-benzyl-5-(2-hydroxyethyl)-4-methylthiazolium chloride (119 mg, 440 μmol, 0.07 eq) were mixed with anhydrous PEG-400 (18 mL) under inert atmosphere. Triethylamine (409 μL, 2.93 mmol, 0.50 eq) was added and the resulting mixture was stirred at 80 °C for 5 h. The oil bath was removed ice-water was added and stirring was continued for 1.0 h. Water and BRINE were added and the aqueous layer was extracted with Et₂O thrice. The combined organics were washed with water twice, dried over MgSO₄, filtered and the solvent was removed under reduced pressure. The crude product was purified by column chromatography on silica gel with 10% EtOAc in heptane to yield **12** (635 mg, 1.14 mmol, 39%) as a yellow solid.

¹H NMR (400 MHz, Chloroform-*d*) δ 7.60 (t, *J* = 1.8 Hz, 1H), 7.57 (t, *J* = 1.8 Hz, 1H), 7.31 (d, *J* = 1.8 Hz, 2H), 7.24 (d, *J* = 1.8 Hz, 2H), 4.49 – 4.40 (m, 1H), 3.78 (d, *J* = 16.5 Hz, 1H), 3.72 (d, *J* = 16.4 Hz, 1H), 3.16 (s, 1H), 3.10 (dd, *J* = 14.2, 4.2 Hz, 1H), 2.79 (dd, *J* = 14.2, 7.7 Hz, 1H). ¹³C NMR (101 MHz, Chloroform-*d*) δ 207.0, 140.1, 136.2, 133.2, 132.9, 131.4 (2C), 131.2 (2C), 123.2 (2C), 123.1 (2C), 76.6, 44.3, 39.2. *Note: Residual EtOAc and heptane were observed.* **LRMS** (ESI): calcd for C₁₆H₁₁Br₄O₂⁻ [M-H]⁻ 550.7, found 550.7.



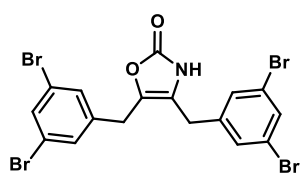
4,5-bis(3,5-dibromobenzyl)-1,3-dihydro-2H-imidazol-2-one **14**.

Acyloin **12** (543 mg, 0.98 mmol, 1.0 eq) was mixed with dry urea (205 mg, 3.42 mmol, 3.5 eq) in a heat dried flask. Glacial acetic acid (2 mL) and anhydrous PEG-400 (2 mL) were added and the mixture was heated to 130 °C for 110 min. After cooling to ambient temperature water was added and a white solid formed. The suspension was stirred for 45 min at ambient temperature, before the solids were filtered off. The residue was washed with water twice. The crude solids were purified by automated flash

column chromatography on silica gel with a gradient of 60-80% EtOAc/heptane + 2.5% MeOH. The title compound **14** (221 mg, 381 μ mol, 39%) was obtained as a white solid.

$^1\text{H NMR}$ (400 MHz, DMSO-*d*₆) δ 9.78 (s, 2H), 7.65 (t, *J* = 1.8 Hz, 2H), 7.39 (d, *J* = 1.8 Hz, 4H), 3.69 (s, 4H). *Note: Residual MeOH was observed at δ 4.10 (q, *J* = 5.3 Hz), 3.17 (d, *J* = 5.2 Hz).* $^{13}\text{C NMR}$ (101 MHz, DMSO-*d*₆) δ 154.2, 144.3 (2C), 131.2 (2C), 130.3 (4C), 122.4 (4C), 115.5 (2C), 28.4. *Residual MeOH was observed at 48.6.* **HRMS** (ESI): calcd for C₁₇H₁₃Br₄N₂O⁺ [M+H]⁺ 576.7756, found: 576.7756.

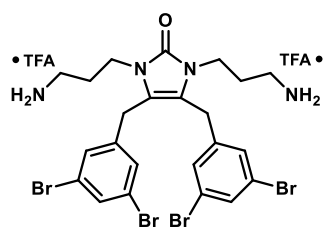
The following constitutional isomer was obtained from the reaction mixture of compound **14**:



4,5-bis(3,5-dibromobenzyl)oxazol-2(3H)-imine 13.

Same chemicals and procedure as for **14**. The title compound **13** (100 mg, 172 μ mol, 18%) was obtained as a white solid.

$^1\text{H NMR}$ (400 MHz, DMSO-*d*₆) δ 10.61 (s, 1H), 7.72 (t, *J* = 1.7 Hz, 1H), 7.71 (t, *J* = 1.8 Hz, 1H), 7.49 (d, *J* = 1.8 Hz, 2H), 7.41 (d, *J* = 1.7 Hz, 2H), 3.89 (s, 2H), 3.77 (s, 2H). $^{13}\text{C NMR}$ (101 MHz, DMSO-*d*₆) δ 155.0, 142.5 (2C), 133.5, 131.7, 131.7, 130.5 (2C), 130.4 (2C), 122.6 (2C), 122.5 (2C), 120.2, 28.5, 27.5. *Note: Residual CDCl₃ was observed at 79.3, 79.0, 78.6.* **LRMS** (ESI): calcd for C₁₇H₁₀Br₄NO₂⁻ [M-H]⁻ 575.9, found 575.7.



1,3-bis(3-aminopropyl)-4,5-bis(3,5-dibromobenzyl)-1,3-dihydro-2H-imidazol-2-one 3A.

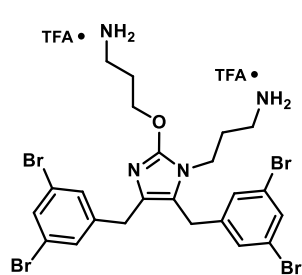
4-imidazolidin-2-one **14** (100 mg, 172 μ mol, 1.0 eq), *tert*-butyl (3-bromopropyl)carbamate **S7** (329 mg, 1.38 mmol, 8.0 eq), K₂CO₃ (135 mg, 0.98 mmol, 5.7 eq) and (*n*-hexadecyl)tri-*n*-butylphosphonium bromide (88 mg, 172 μ mol, 1.0 eq) were mixed with toluene (0.5 mL) and water (0.5 mL). The resulting mixture was heated under microwave irradiation to 130 °C for 90 min and then to 150 °C for 60 min. After cooling to ambient temperature, water was added and

the aqueous layer was extracted with toluene thrice. The combined organics were dried over MgSO₄, filtered and the solvent was removed. The crude yellow solid was purified by automated column chromatography on silica gel with a gradient of 15-45% EtOAc/heptane + 2.5% MeOH. Boc-**3A** (35 mg, 39 μ mol, 23%) was obtained as a slightly yellow solid.

Boc-**3A** (35 mg, 39 μ mol, 1.0 eq) was taken up in DCM (500 μ L) and TFA (75 μ L, 0.98 mmol, 25 eq) was added. The solution was stirred at ambient temperature for 20 h before removal of the solvent. The crude amine was purified by RP chromatography with a gradient of 20-55% MeCN/H₂O + 0.1% TFA. The title compound **3A** (30 mg, 33 μ mol, 19% o2s) was obtained as a white di-TFA salt.

$^1\text{H NMR}$ (400 MHz, Methanol-*d*₄) δ 7.60 (t, *J* = 1.8 Hz, 2H), 7.27 (d, *J* = 1.8 Hz, 4H), 3.99 (s, 4H), 3.72 (t, *J* = 6.8 Hz, 4H), 2.89 (t, *J* = 7.1 Hz, 4H), 1.77 (p, *J* = 6.9 Hz, 4H). $^{13}\text{C NMR}$ (101 MHz, Methanol-*d*₄) δ 155.5, 143.7 (2C), 133.7 (2C), 131.1 (4C), 124.4 (4C), 119.7 (2C), 39.2 (2C), 37.7 (2C), 28.6, 28.4 (2C). **HRMS** (ESI): calcd for C₂₃H₂₇Br₄N₄O₁⁺ [M+H]⁺ 690.8913 found 690.8924. **SFC**: >99%.

The constitutional isomer **15A** was obtained from the reaction mixture of **3A**:



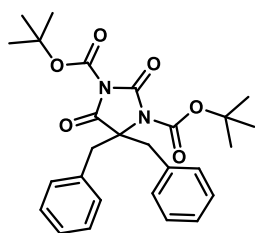
3-(2-(3-aminopropoxy)-4,5-bis(3,5-dibromobenzyl)-1H-imidazol-1-yl)propan-1-amine 15A.

Chemicals and procedure as stated above for **3A**. Boc-**15A** was obtained impure as a yellow foam (no yield determined).

After TFA treatment and purification by RP chromatography with a gradient of 20-60% MeCN/H₂O + 0.1% TFA, the di-TFA salt of **15A** (27 mg, 29 μ mol 17% o2s) was obtained as a white solid.

$^1\text{H NMR}$ (400 MHz, Methanol-*d*₄) δ 7.58 (t, *J* = 1.8 Hz, 1H), 7.54 (t, *J* = 1.8 Hz, 1H), 7.31 (d, *J* = 1.7 Hz, 2H), 7.17 (d, *J* = 1.8 Hz, 2H), 4.62 – 4.54 (m, 2H), 4.07 (s, 2H), 3.90 (s, 2H), 3.87 – 3.80 (m, 2H), 3.18 (t, *J* = 7.4 Hz, 2H), 2.91 (t, *J* = 7.9 Hz, 2H), 2.24 (p, *J* = 6.5 Hz, 2H), 1.90 (p, *J* = 7.8 Hz, 2H). $^{13}\text{C NMR}$ (101 MHz, Methanol-*d*₄) δ 151.4, 144.1, 143.1, 133.9, 133.4, 131.5 (2C), 131.1 (2C), 128.0 124.4 (2C), 124.1 (2C), 123.3, 70.6, 41.2, 37.9, 37.6, 31.3, 28.4 (2C), 28.0. **HRMS** (ESI): calcd for C₂₃H₂₇Br₄N₄O₁⁺ [M+H]⁺ 690.8913, found 690.8907. **SFC**: 96.5%.

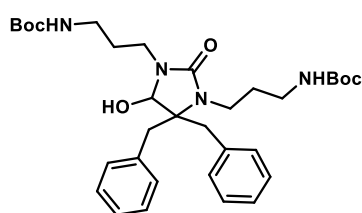
1.5.4 4-imidazolidin-2-one via *N*-acyliminium ion rearrangement



Di-tert-butyl 4,4-dibenzyl-2,5-dioximidazolidine-1,3-dicarboxylate Boc-9a.

5,5-disubstituted hydantoin **9a** (100 mg, 357 μmol , 1.0 eq) was taken up in THF (2.0 mL) and cooled to 0 °C. 4-DMAP (3.3 mg, 27 μmol , 0.1 eq) and Boc₂O (234 mg, 1.07 mmol, 3.0 eq) were added the cooling bath was removed and the resulting solution was stirred at 45 °C for 20 h. The solution was allowed to cool to ambient temperature and DCM was added. The organic layer was washed with 0.1 M HCl_(aq) thrice, dried over MgSO₄, filtered and the solvent was removed. The crude was purified by automated column chromatography on silica gel with a gradient of 10-38% EtOAc in heptane to yield Boc-**9a** (156 mg, 325 μmol , 91%) as a white solid.

¹H NMR (400 MHz, Chloroform-*d*) δ 7.29 – 7.20 (m, 6H), 7.15 – 7.09 (m, 4H), 3.69 (d, *J* = 13.7 Hz, 2H), 3.38 (d, *J* = 13.6 Hz, 2H), 1.63 (s, 9H), 1.43 (s, 9H). **¹³C NMR** (101 MHz, Chloroform-*d*) δ 170.1, 149.4, 146.9, 144.5, 133.9 (2C), 129.6 (4C), 128.8 (4C), 127.8 (2C), 85.9, 84.5, 71.8, 40.8 (2C), 28.1 (3C), 27.6 (3C). **HRMS** (ESI): calcd for C₂₇H₃₂N₂O₆Na⁺ [M+Na]⁺ 503.2153, found: 503.2155.

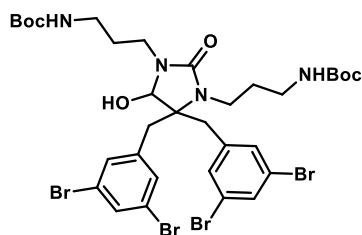


Di-tert-butyl ((4,4-dibenzyl-5-hydroxy-2-oxoimidazolidine-1,3-diyl)bis(propane-3,1-diyl))dicarbamate S2

Boc-**2aA** (226 mg, 380 μmol , 1.0 eq) was dissolved in anhydrous DCM (2.5 mL) under inert atmosphere and cooled to -78 °C. DIBAL-H (1 M in DCM, 570 μL , 570 μmol , 1.5 eq) was added and the resulting mixture was stirred at -78 °C for 3h. 10% Rochelle's salt_(aq) solution was added and the suspension was stirred at ambient temperature for 30 min. The aqueous layer was extracted with Et₂O thrice and the combined organics were washed twice

with 10% Rochelle's salt_(aq) solution, dried over MgSO₄, filtered and the solvent was removed under reduced pressure. The crude was purified by automated column chromatography on silica gel with a gradient of 15-60% EtOAc in heptane to yield **S2** (126 mg, 211 μmol , 56%) as a colorless solid.

¹H NMR (400 MHz, Chloroform-*d*) δ 7.53 – 7.45 (m, 2H), 7.37 – 7.23 (m, 3H), 7.22 – 7.12 (m, 3H), 6.95 – 6.81 (m, 2H), 5.60 (t, *J* = 6.9 Hz, 1H), 5.04 (d, *J* = 6.7 Hz, 1H), 4.73 (d, *J* = 6.8 Hz, 1H), 4.59 (s, 1H), 3.81 – 3.66 (m, 1H), 3.50 (d, *J* = 13.5 Hz, 1H), 3.43 – 3.31 (m, 1H), 3.26 – 3.14 (m, 1H), 3.10 – 2.98 (m, 1H), 2.84 (d, *J* = 14.1 Hz, 1H), 2.80 (d, *J* = 13.5 Hz, 1H), 2.80 – 2.58 (m, 4H), 2.48 (d, *J* = 14.1 Hz, 1H), 1.86 – 1.64 (m, 2H), 1.44 (s, 9H), 1.41 (s, 9H), 1.24 – 1.19 (m, 2H). *Residual DCM* (5.29, s), *EtOAc* (4.14 (q, *J* = 7.2 Hz), 2.06 (s), 1.27 (t, *J* = 7.1 Hz)) and *heptane* (0.93 – 0.86 (m, 1H)) were observed. **¹³C NMR** (101 MHz, Chloroform-*d*) δ 159.8, 156.7, 156.4, 136.9 (2C), 135.8 (2C), 131.1 (2C), 129.8 (2C), 128.6 (2C), 128.5 (2C), 127.0 (2C), 126.9 (2C), 84.2, 79.3, 79.2, 67.4, 40.6, 39.9, 37.7, 37.5, 37.3, 31.7, 29.5, 28.6 (3C), 28.6 (3C). *Residual EtOAc* (171.3, 60.5, 21.2, 14.2), *heptane* (32.0, 22.8, 14.3) and "grease" (29.1) were observed. **HRMS** (ESI): calcd for C₃₃H₄₉N₄O₆⁺ [M+H]⁺ 597.3647, found: 597.3647.

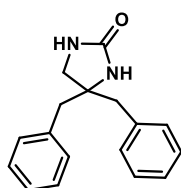


Di-tert-butyl ((4,4-bis(3,5-dibromobenzyl)-5-hydroxy-2-oxoimidazolidine-1,3-diyl)bis(propane-3,1-diyl))dicarbamate S3.

Boc-**2dA** (131 mg, 144 μmol , 1.0 eq) was dissolved in anhydrous DCM under inert atmosphere and cooled to -78 °C. DIBAL-H (432 μL , 432 μmol , 3.0 eq) was added and the resulting mixture was allowed to warm to 0 °C and stirred for 3h. 10% Rochelle's salt_(aq) solution was added and after stirring at ambient temperature for 60 min, the aqueous layer was extracted with DCM thrice.

The combined organics were washed twice with 10% Rochelle's salt_(aq) solution, dried over MgSO₄, filtered and the solvent was removed under reduced pressure. The crude was purified by automated column chromatography on silica gel with a gradient of 50-85% EtOAc in heptane to yield **S3** (92 mg, 101 μmol , 70%) as a white solid.

¹H NMR (400 MHz, Chloroform-*d*) δ 7.62 (d, *J* = 1.8 Hz, 2H), 7.59 (t, *J* = 1.7 Hz, 1H), 7.50 (t, *J* = 1.7 Hz, 1H), 7.01 (d, *J* = 1.7 Hz, 2H), 5.58 (s, 1H), 5.50 (s, 1H), 4.93 (t, *J* = 6.7 Hz, 1H), 4.75 (d, *J* = 6.3 Hz, 1H), 3.80 – 3.64 (m, 2H), 3.46 (d, *J* = 13.3 Hz, 1H), 3.42 – 3.31 (m, 1H), 3.19 – 3.09 (m, 2H), 3.09 – 2.80 (m, 5H), 2.77 (d, *J* = 14.0 Hz, 1H), 2.70 (d, *J* = 13.4 Hz, 1H), 2.40 (d, *J* = 14.0 Hz, 1H), 1.86 – 1.73 (m, 2H), 1.73 – 1.61 (m, 2H), 1.45 (s, 9H), 1.44 (s, 9H), 1.24 – 1.18 (m, 2H). *Residual heptane* was observed at 1.33 – 1.22 (m) and 0.90 – 0.85 (m). **¹³C NMR** (101 MHz, Chloroform-*d*) δ 159.5, 157.3, 156.4, 140.6, 139.5, 133.0 (3C), 132.7, 131.5 (2C), 123.1 (2C), 122.9 (2C), 83.7, 80.5, 79.4, 67.0, 40.5, 39.2, 37.8 (2C), 37.6, 37.4 31.8, 30.5, 28.6 (6C). *Residual heptane* was observed at 32.0, 29.2, 22.8, 14.3. **HRMS** (ESI): calcd for C₃₃H₄₄Br₄N₄O₆Na⁺ [M+Na]⁺ 930.9887, found: 930.9886.



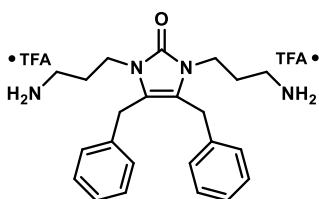
4,4-dibenzylimidazolidin-2-one S4.

Boc-**9a** (156 mg, 325 μmol , 1.0 eq) was dissolved in EtOH, NaBH₄ (61 mg, 1.62 mmol, 5.0 eq) was added and the mixture was stirred at ambient temperature for 16 h. 0.1 M HCl was added to destroy residual NaBH₄, followed by the addition of water. The aqueous layer was extracted with Et₂O thrice. The combined organics were dried over MgSO₄, filtered and the solvent was removed under reduced pressure. The crude was purified by automated column chromatography on silica gel with a gradient of 15-55% EtOAc in heptane to yield impure-**S1** (16 mg,

33 μmol , 10%) as a white solid. **S1** was obtained as a mixture of compounds having between zero to two Boc groups and was used without further purification.

S1 (16 mg, 33 μmol , 1.0 eq) was dissolved in anhydrous toluene (0.75 mL) in an oven dried flask under inert atmosphere and p-TsOH (1.6 mg, 8.3 μmol , 0.25 eq) was added. The resulting mixture was heated to 120 °C for 24 h. The mixture was allowed to cool to ambient temperature and the solvent was removed. To the resulting crude DCM (0.75 mL) and TFA (64 μL , 828 μmol , 25 eq) were added and the resulting solution was stirred at ambient temperature for 20 h. The solvent was removed and the crude product was purified by automated column chromatography on silica gel with a gradient of 15-55% EtOAc in heptane to yield impure **S4** (3 mg, 11 μmol , 24%) as a white solid.

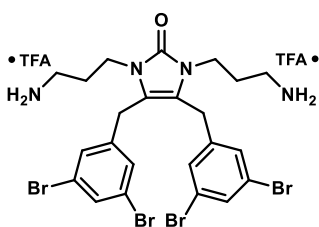
¹H NMR (400 MHz, Methanol-*d*₄) δ 7.37 – 7.20 (m, 10H), 4.19 (s, 2H), 2.97 (d, *J* = 13.8 Hz, 2H), 2.89 (d, *J* = 13.8 Hz, 2H). ¹³C NMR (101 MHz, Methanol-*d*₄) δ 161.8, 137.0 (2C), 131.7 (4C), 129.5 (4C), 128.1 (2C), 72.1, 62.6, 45.9 (2C). LRMS (ESI): calcd for C₁₇H₁₈N₂O⁺ [M+H]⁺ 267.1, found 267.1.



1,3-bis(3-aminopropyl)-4,5-dibenzyl-1,3-dihydro-2H-imidazol-2-one S5.

S2 (18 mg, 30 μmol , 1.0 eq) was dissolved in DCM (750 μL) and TFA (46 μL , 603 μmol , 20.0 eq) was added. The resulting clear solution was stirred at ambient temperature for 18 h. The solvent was removed under reduced pressure and the crude was purified by RP column chromatography with a gradient of 10-45% MeCN/H₂O + 0.1% TFA to yield the impure di-TFA salt of **S5** (15 mg, 25 μmol , 82%) as a slightly yellow solid.

¹H NMR (400 MHz, Methanol-*d*₄) δ 8.09 (s, 6H), 7.34 – 7.26 (m, 4H), 7.26 – 7.19 (m, 4H), 7.10 (d, *J* = 7.3 Hz, 4H), 3.86 (s, 4H), 3.64 (s, 4H), 2.71 (s, 4H), 1.48 (s, 4H). ¹³C NMR (101 MHz, Methanol-*d*₄) δ 154.9, 137.0 (2C), 129.3 (4C), 127.9 (4C), 127.5 (2C), 119.3 (2C), 37.6 (2C), 36.2 (2C), 29.2 (2C), 26.5 (2C). HRMS (ESI): calcd for C₂₃H₃₁N₄O⁺ [M+H]⁺ 379.2492, found: 379.2499.



1,3-bis(3-aminopropyl)-4,5-bis(3,5-dibromobenzyl)-1,3-dihydro-2H-imidazol-2-one 3A.

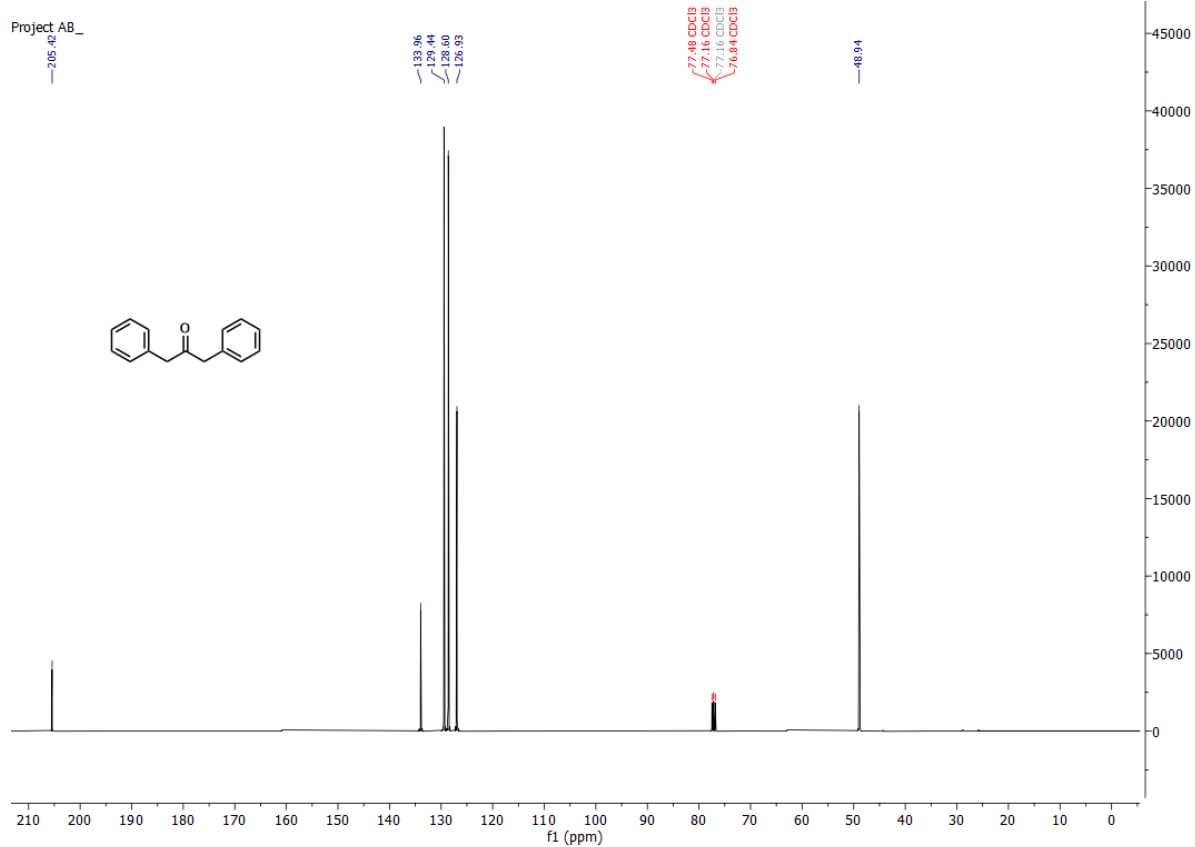
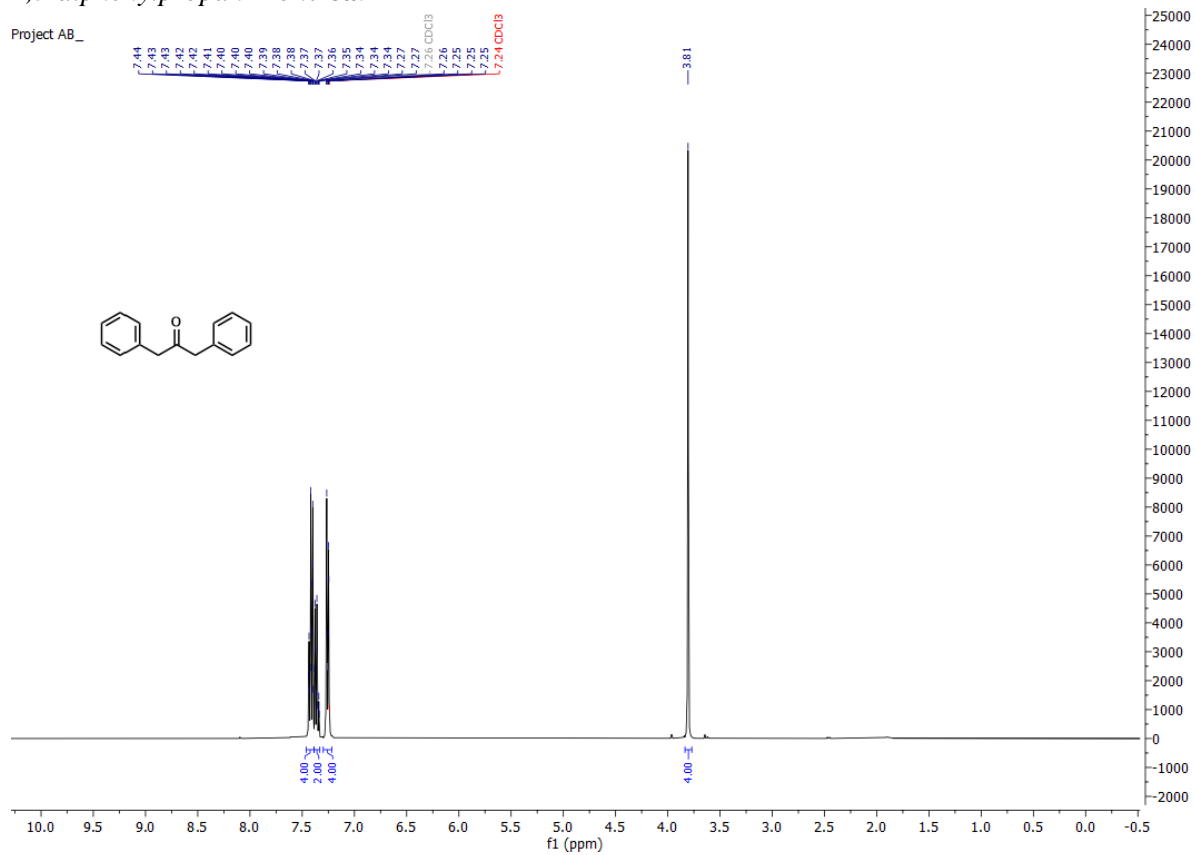
S3 (92 mg, 101 μmol , 1.0 eq) was dissolved in DCM (1 mL) and TFA (116 μL , 1.51 mL, 15.0 eq) was added. The mixture was stirred at ambient temperature for 22 h. A second portion of TFA (116 μL , 1.51 mL, 15.0 eq) was added and the mixture was heated to 45 °C for 20 h. The solution was allowed to cool to ambient temperature after a total of 42 h and the solvent was removed. The crude was purified by RP column chromatography with a gradient of 10-55% MeCN/H₂O +

0.1% TFA to yield the impure di-TFA salt of **3A** (40 mg, 43 μmol , 43%) as a slightly yellow solid. The spectroscopic data was identical to the ones reported (*vide supra*).

2. NMR spectra

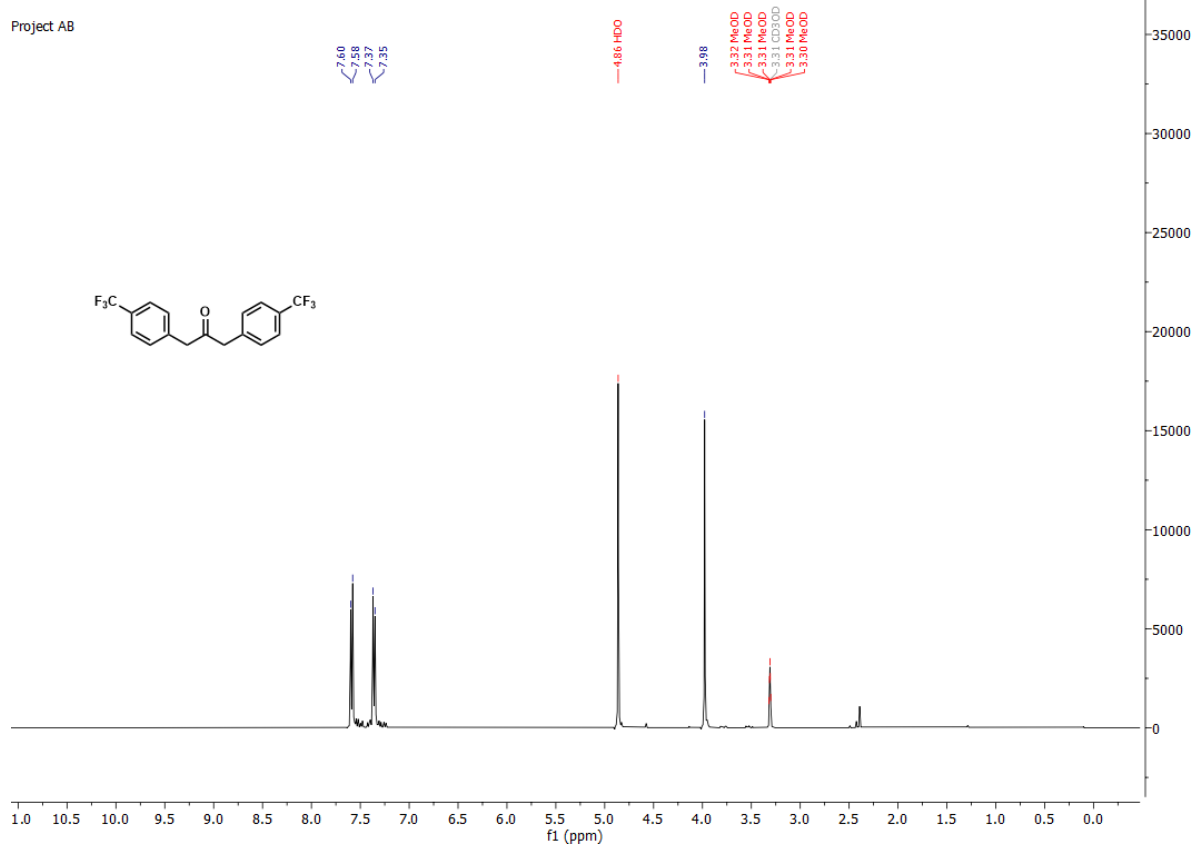
2.1 Symmetrical ketones 8

1,3-diphenylpropan-2-one **8a**.

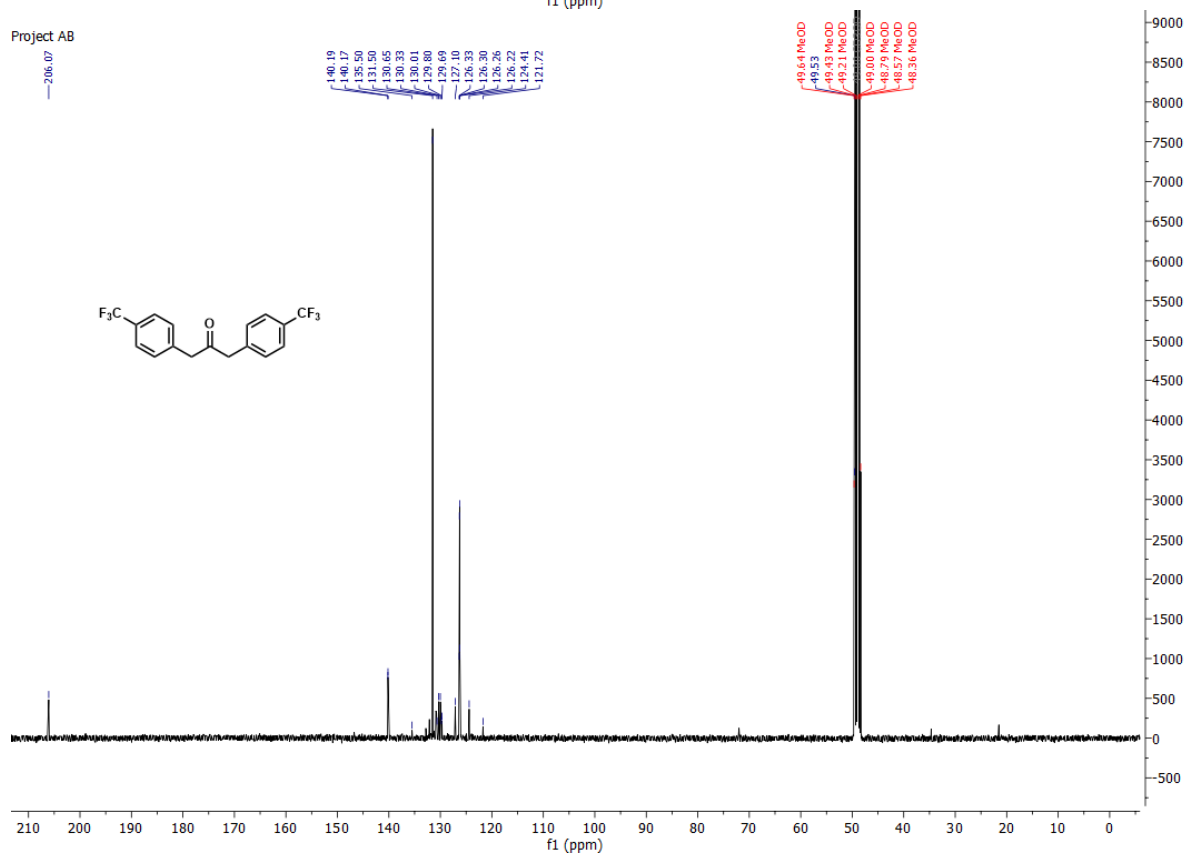


1,3-bis(4-(trifluoromethyl)phenyl)propan-2-one **8b**.

Project AB

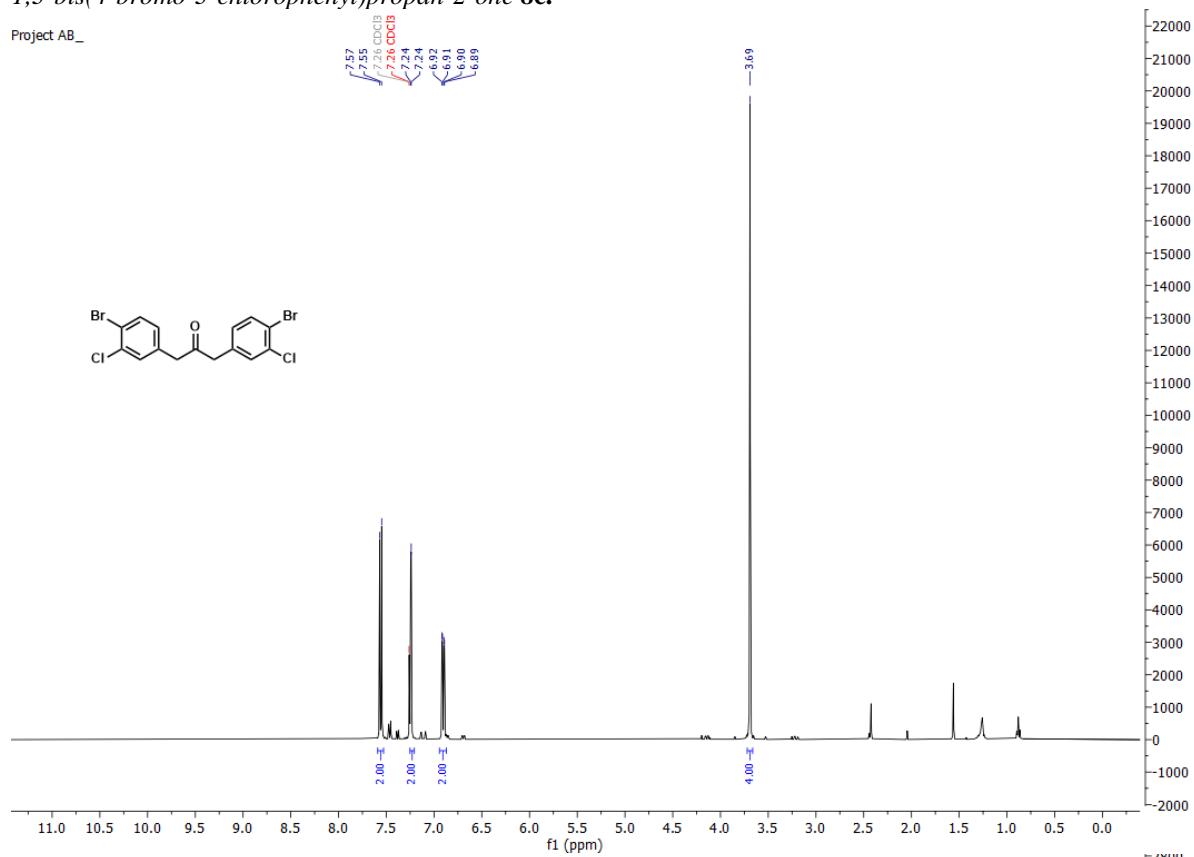


Project AB

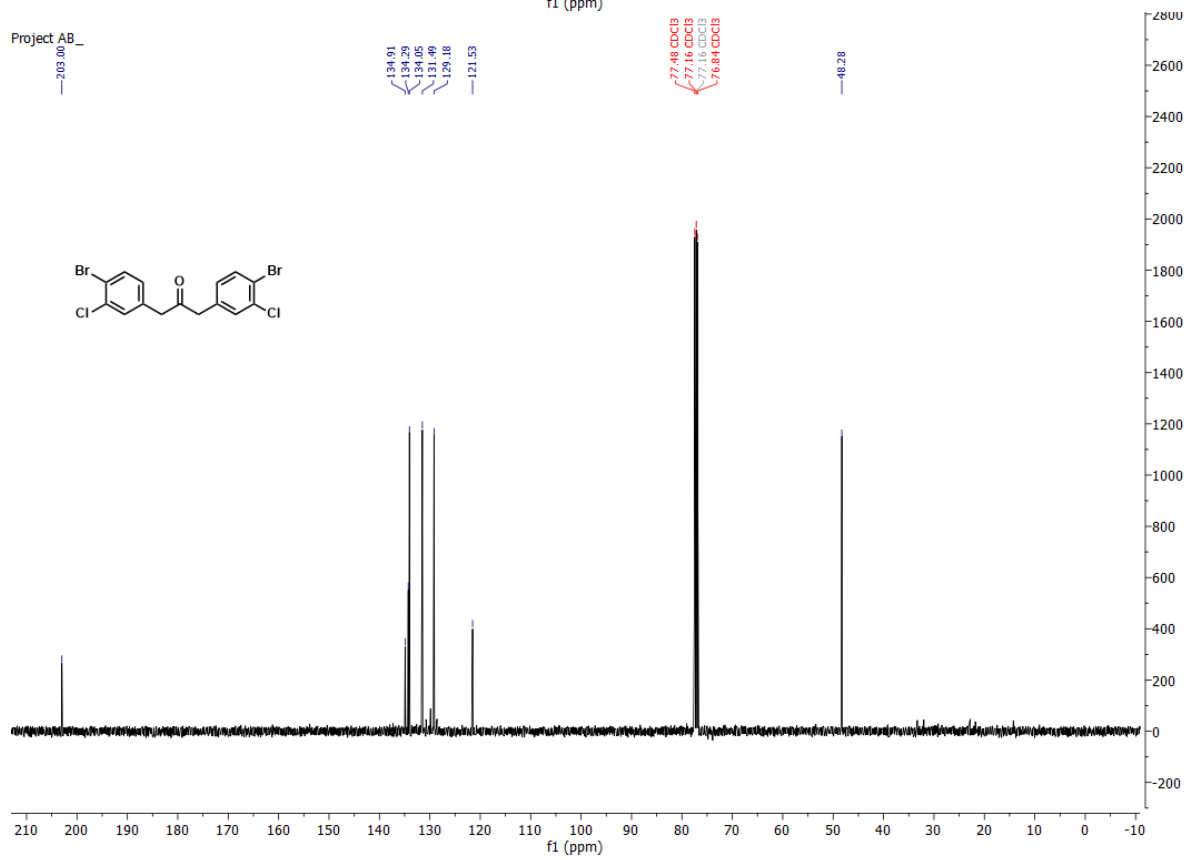


1,3-bis(4-bromo-3-chlorophenyl)propan-2-one **8c**.

Project AB_

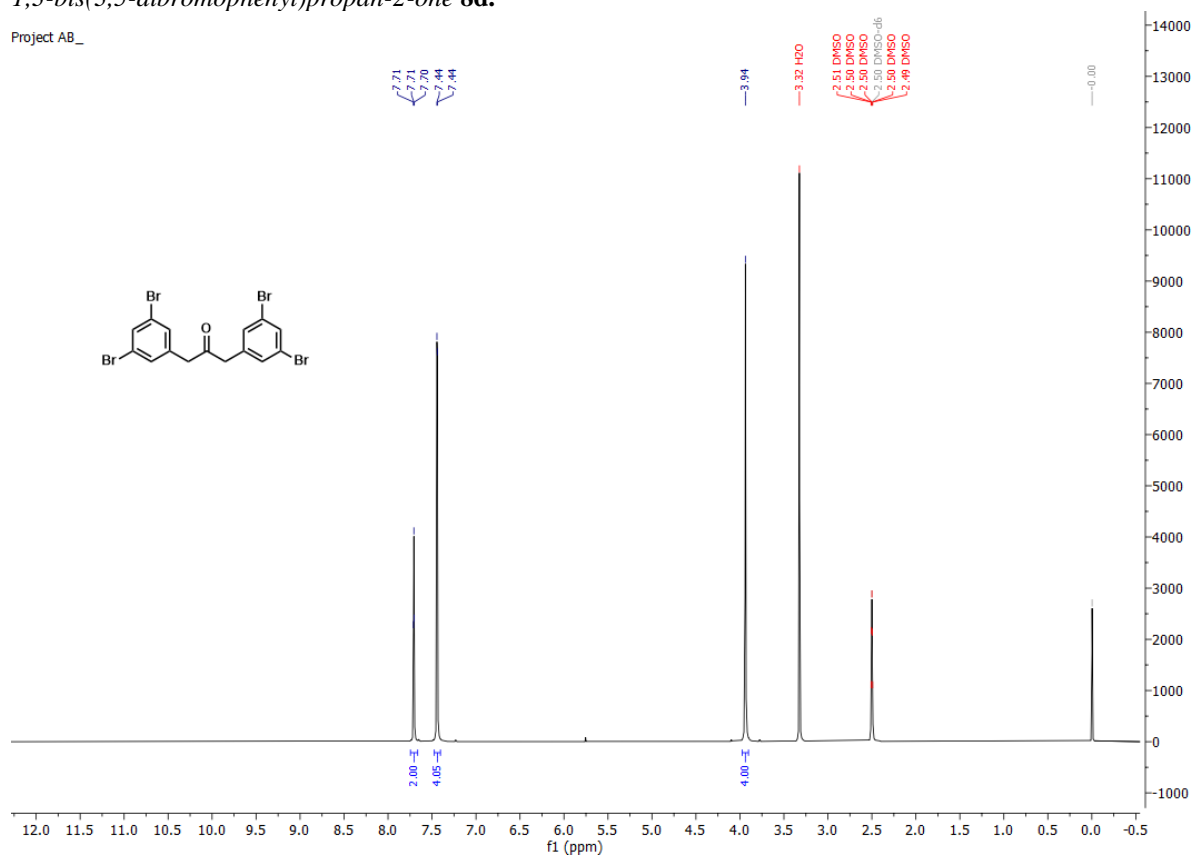


Project AB_

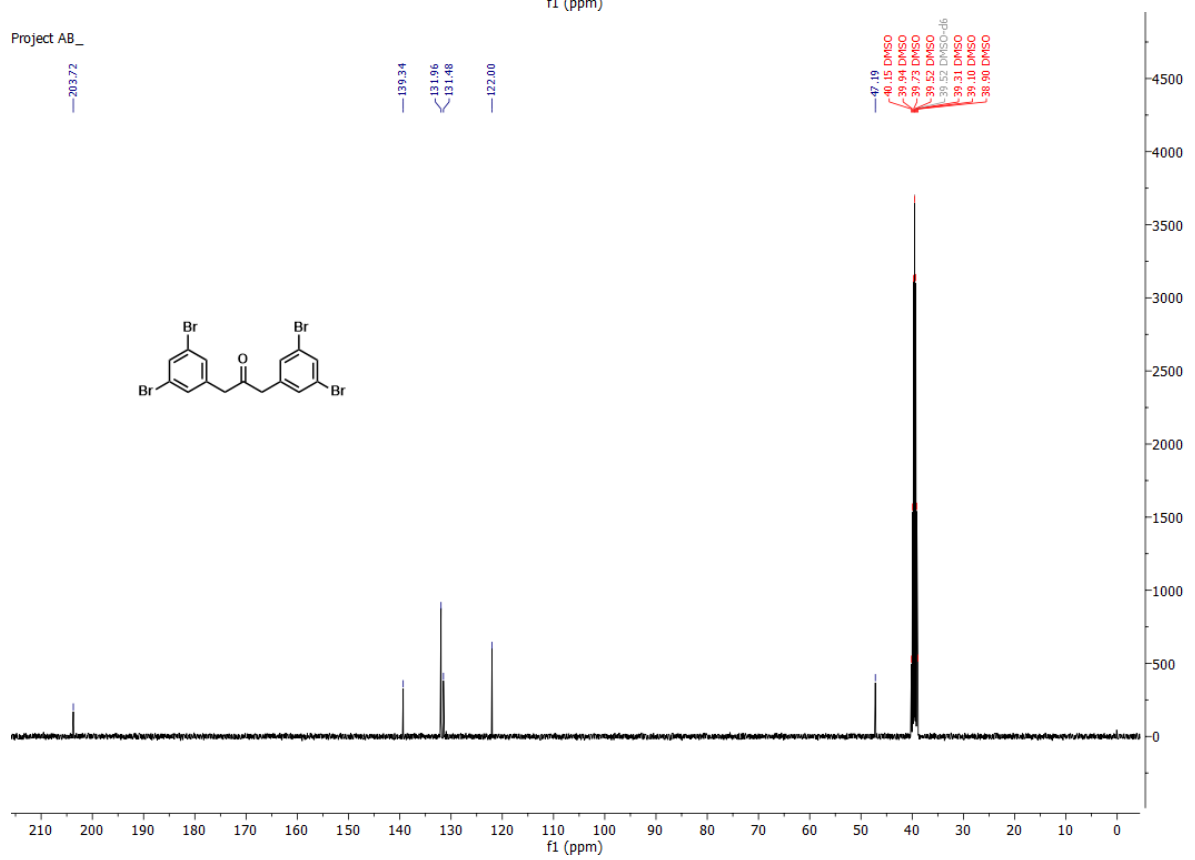


1,3-bis(3,5-dibromophenyl)propan-2-one **8d**.

Project AB_

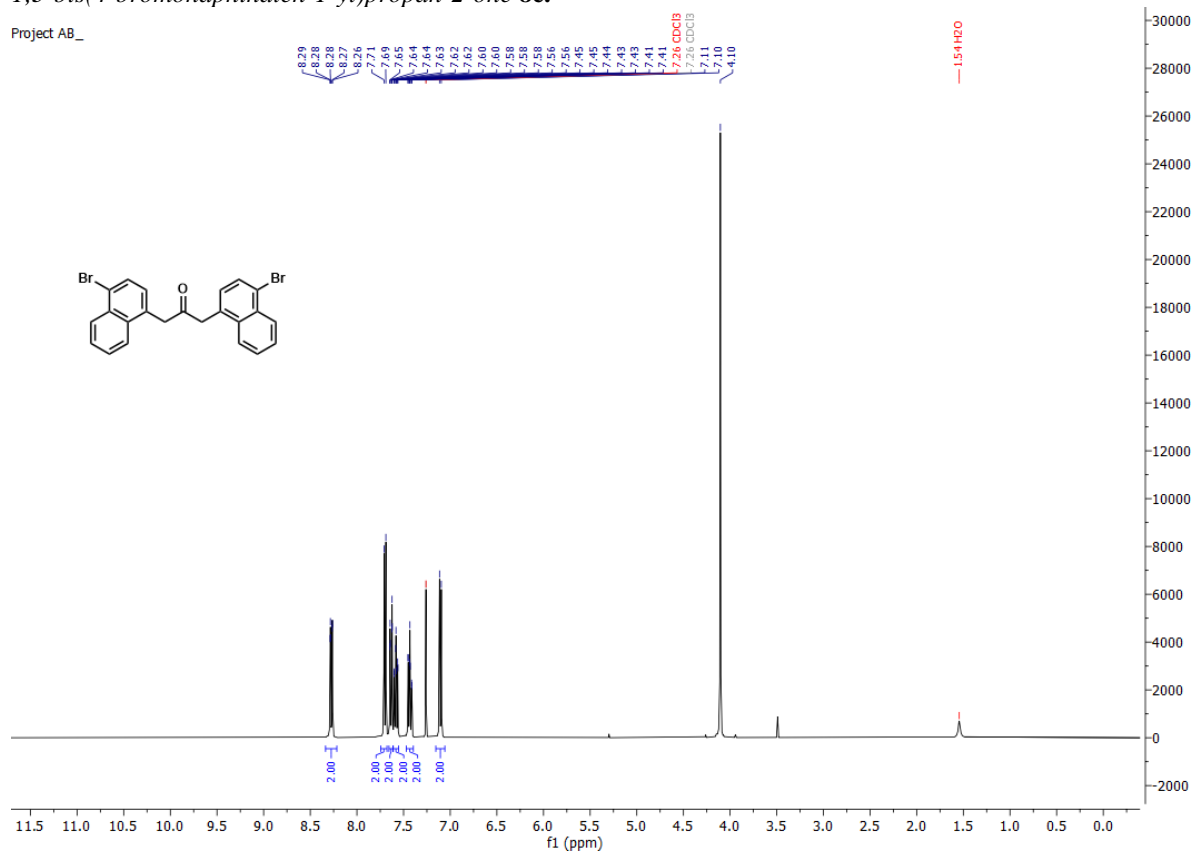


Project AB_

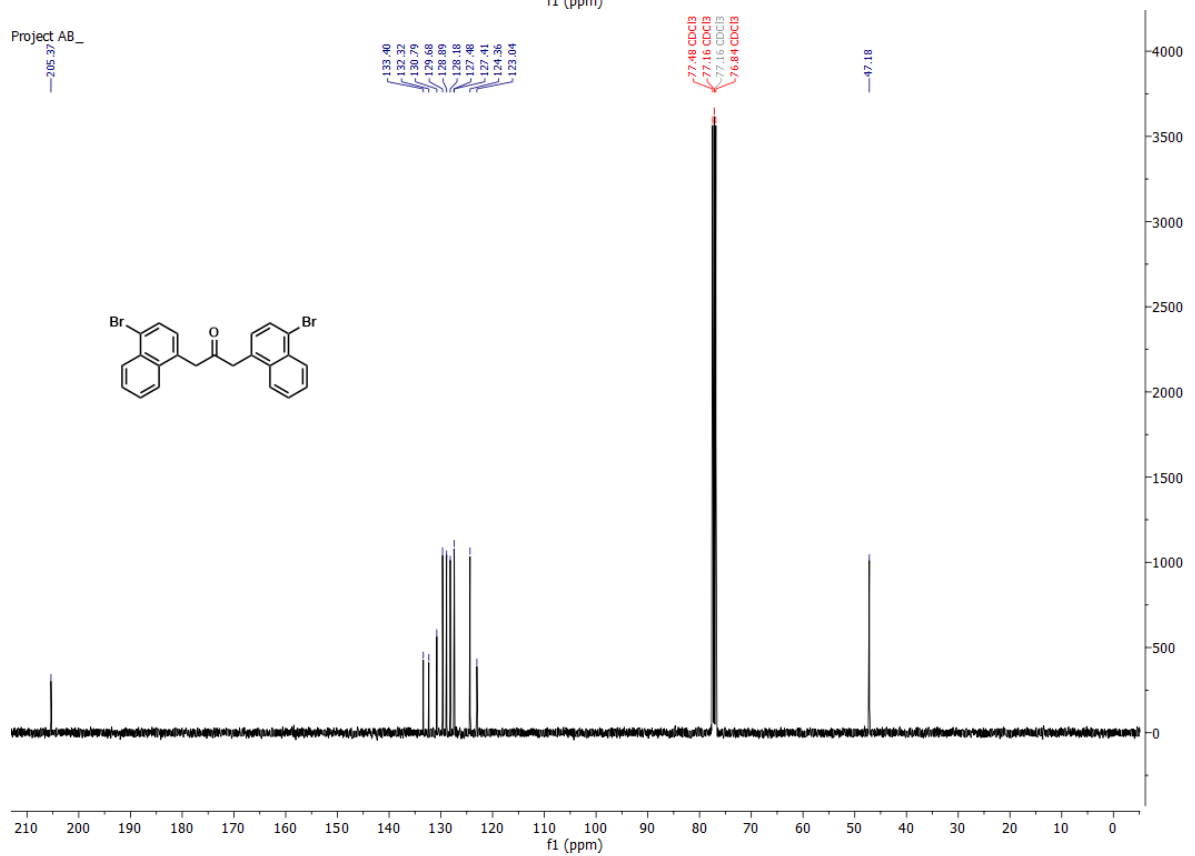


1,3-bis(4-bromonaphthalen-1-yl)propan-2-one **8e**.

Project AB_

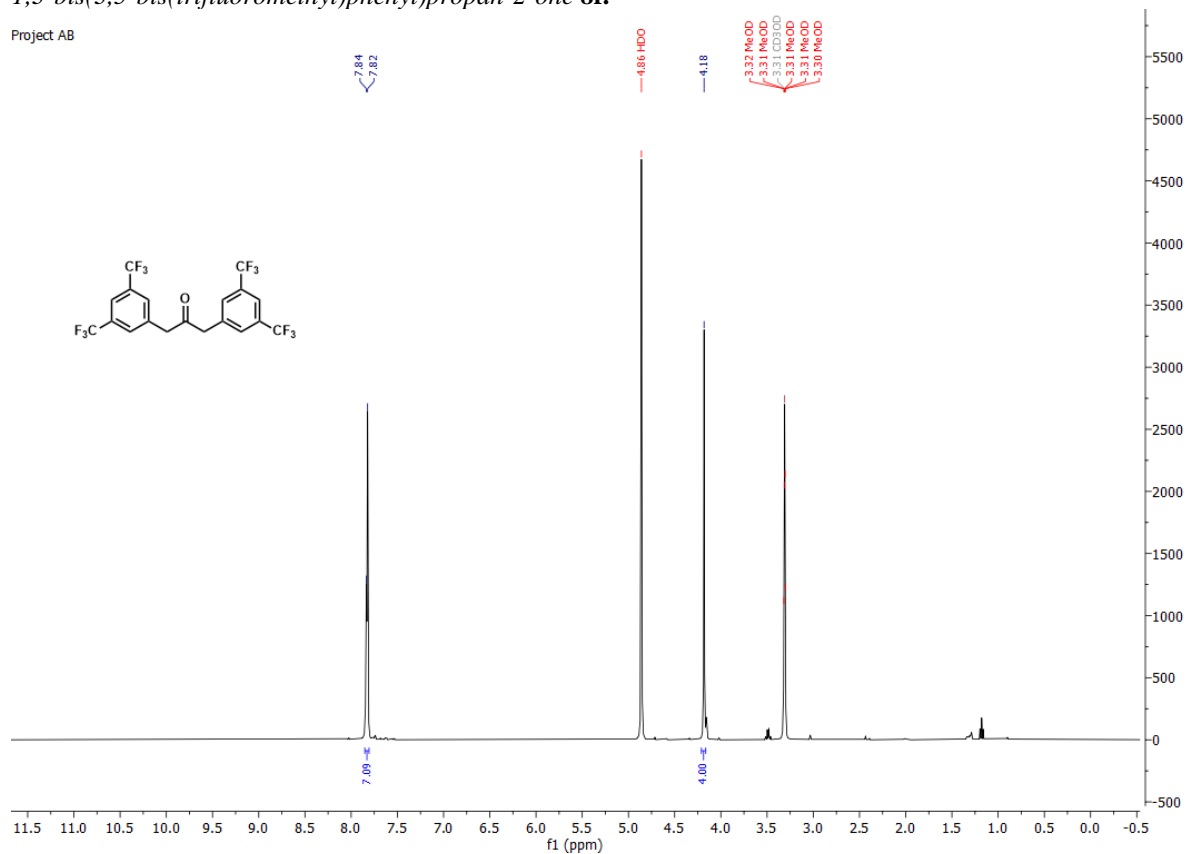


Project AB_

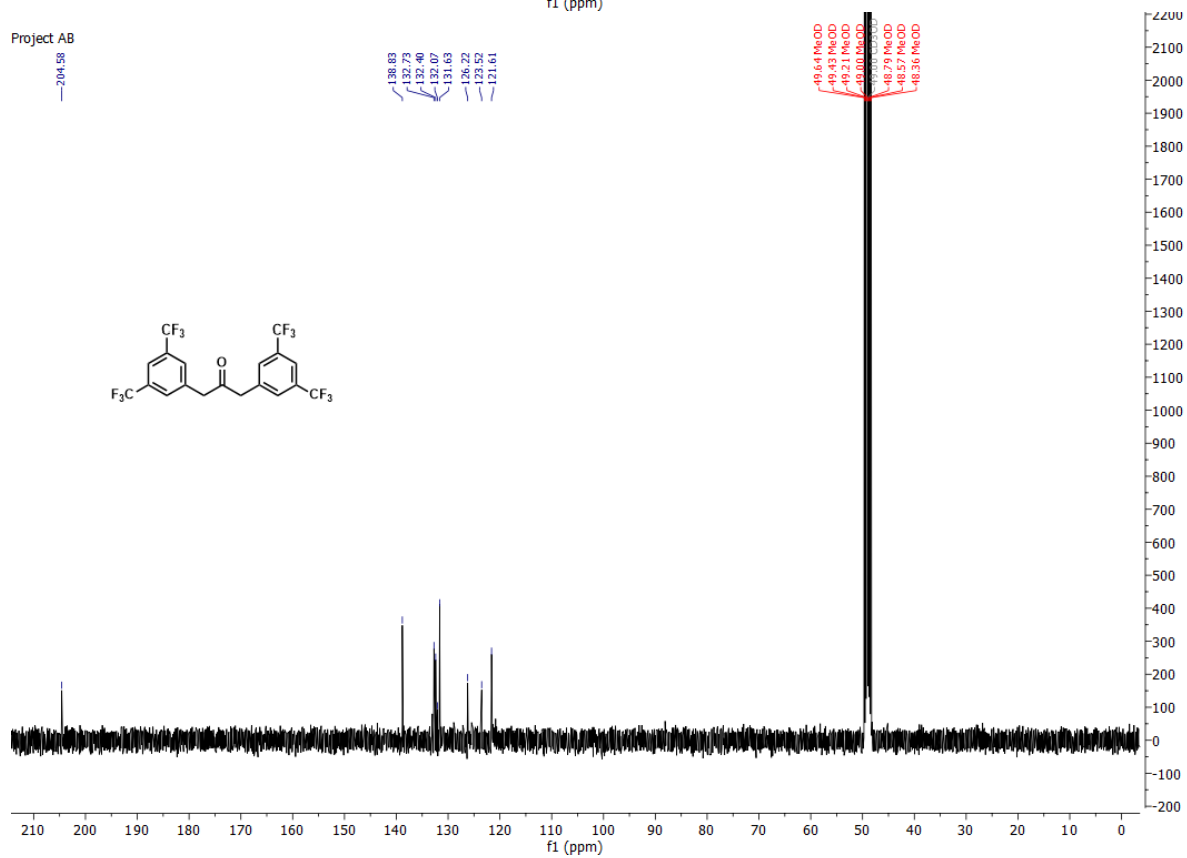


1,3-bis(3,5-bis(trifluoromethyl)phenyl)propan-2-one **8f**.

Project AB



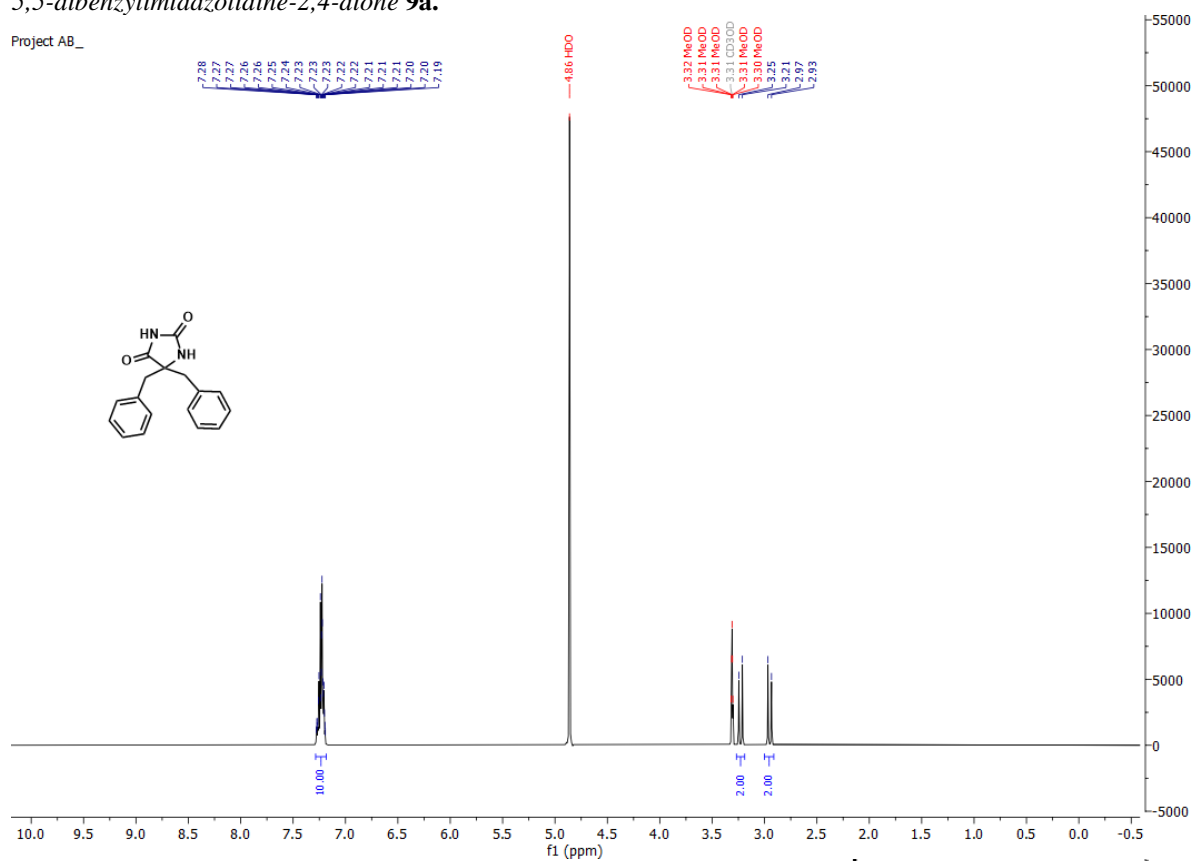
Project AB



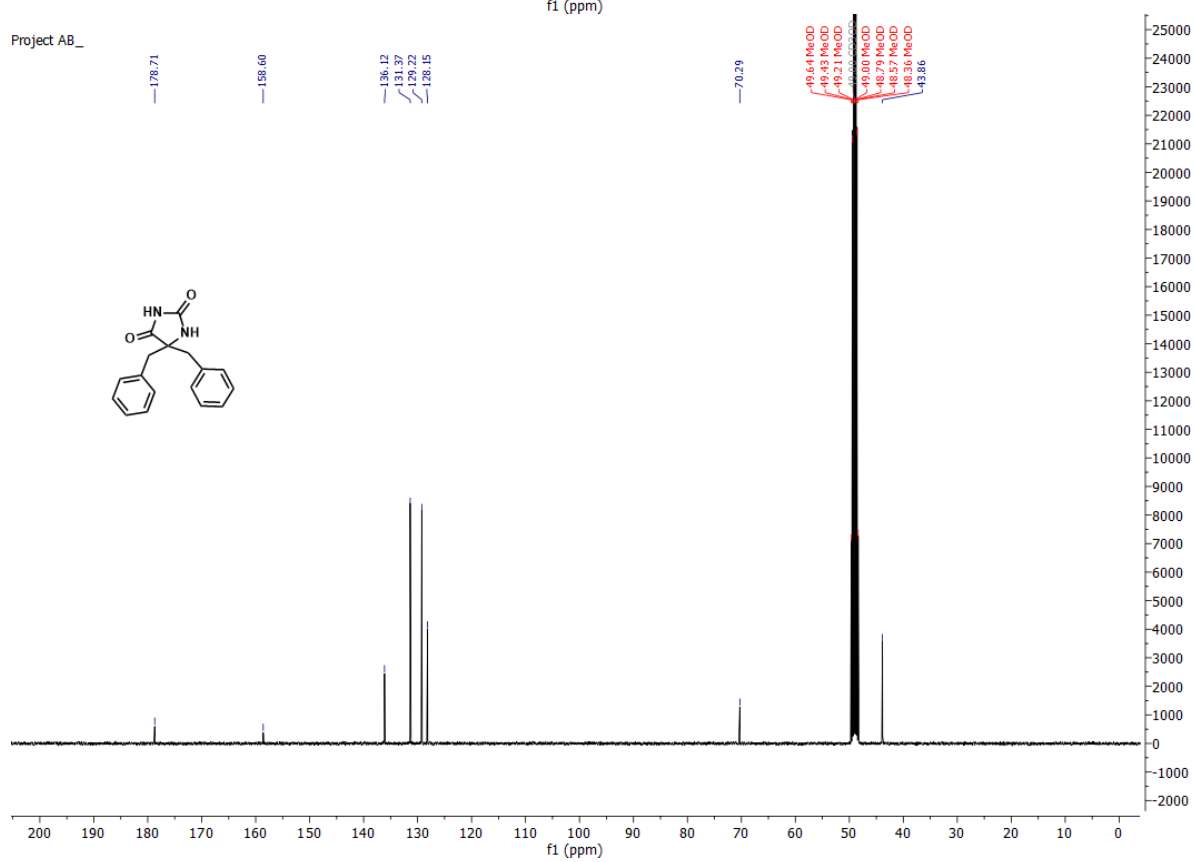
2.2 Hydantoins 9

5,5-dibenzylimidazolidine-2,4-dione **9a**.

Project AB_

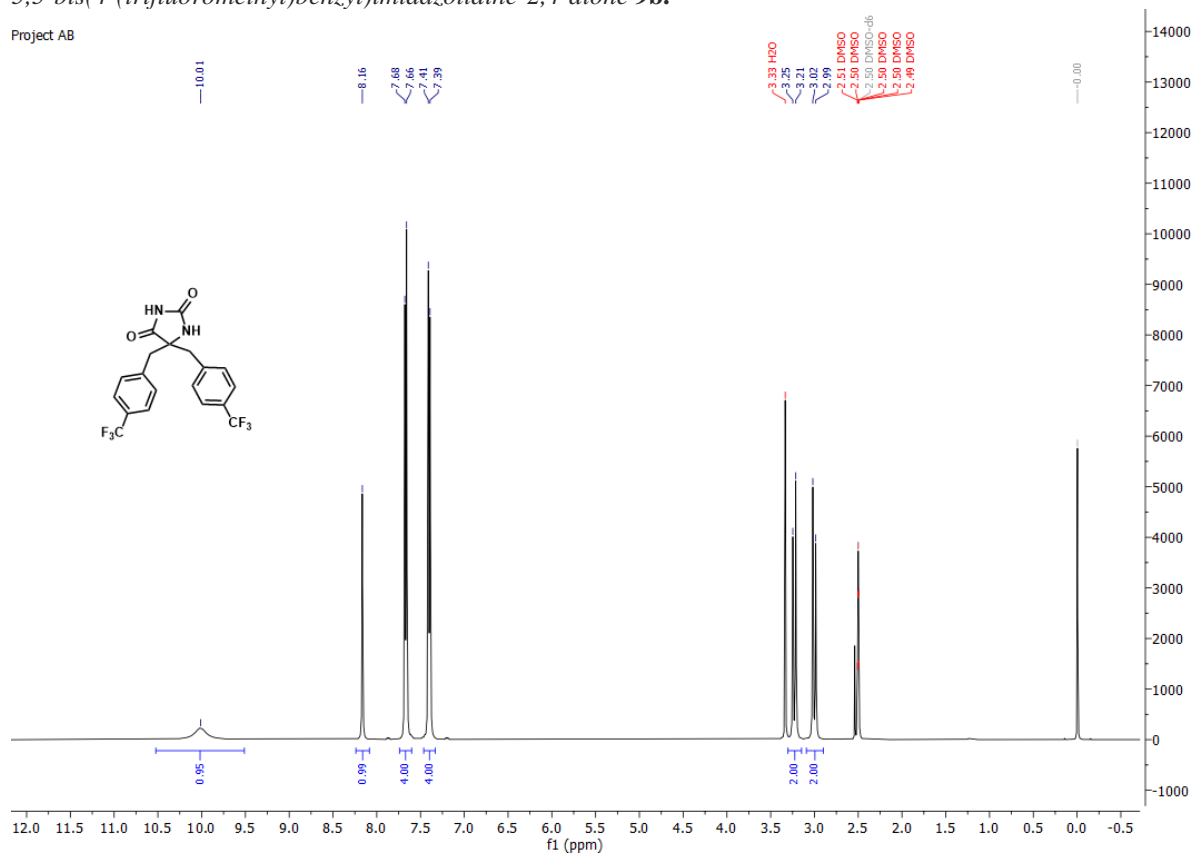


Project AB_

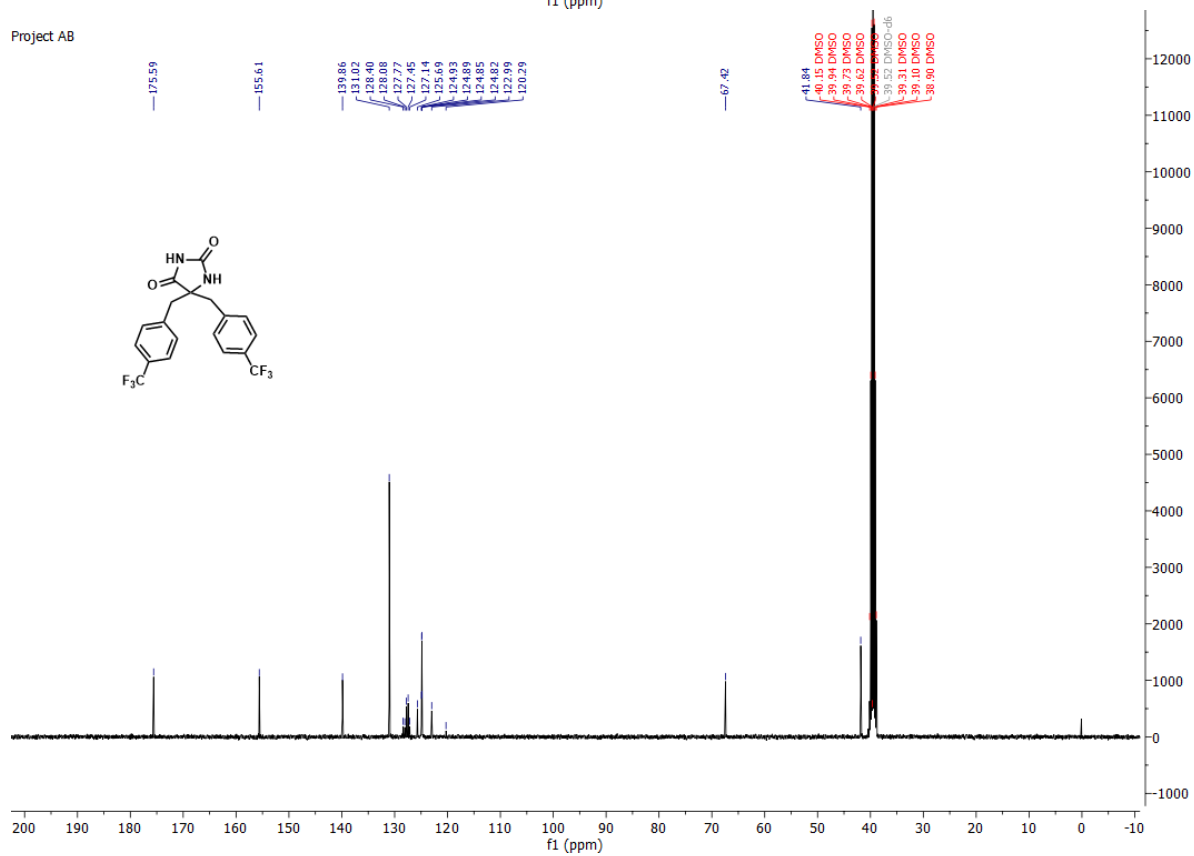


5,5-bis(4-(trifluoromethyl)benzyl)imidazolidine-2,4-dione **9b**.

Project AB

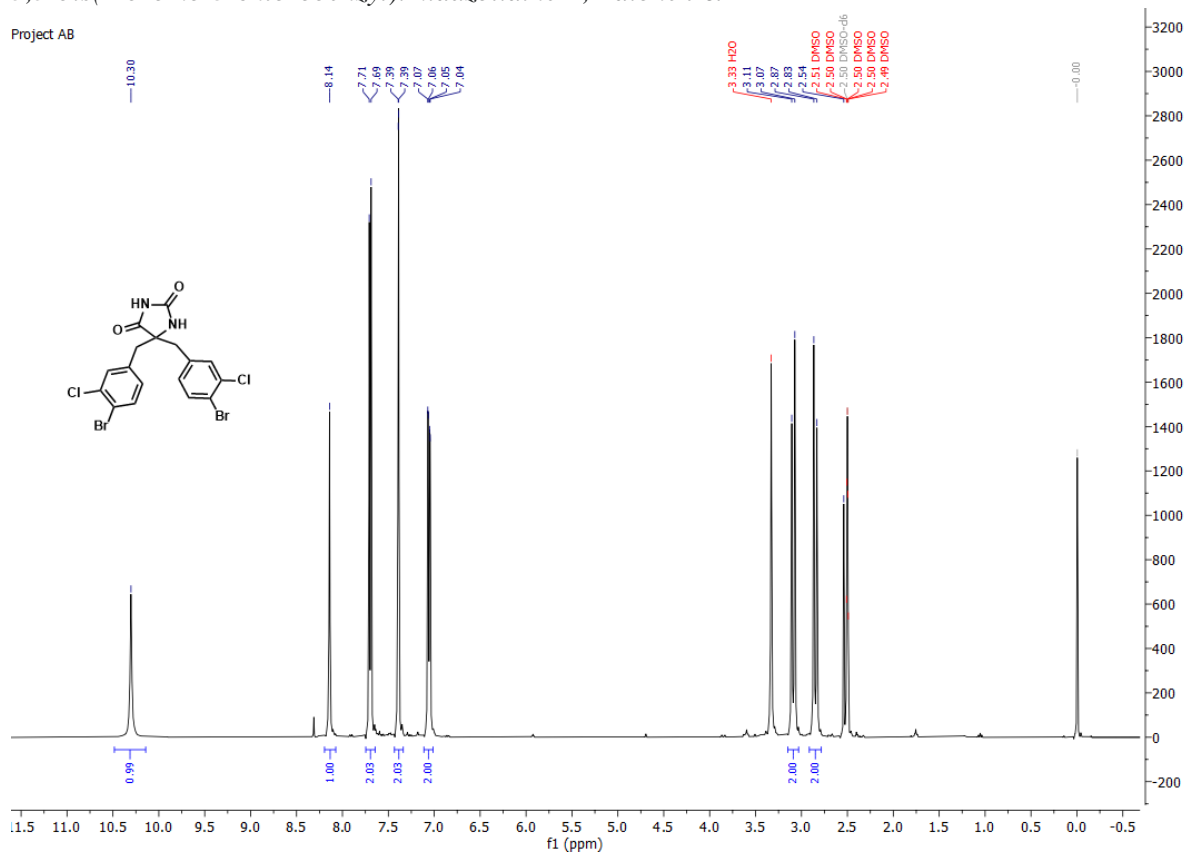


Project AB

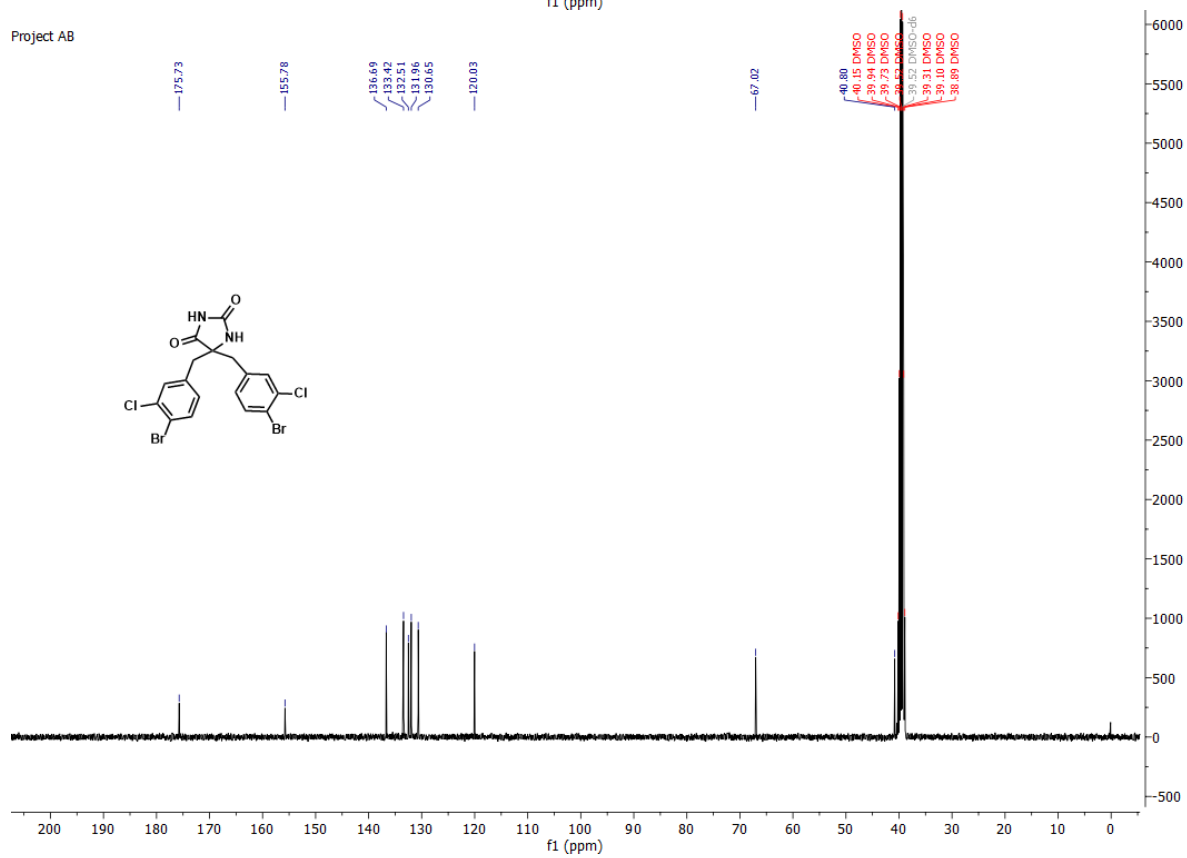


5,5-bis(4-bromo-3-chlorobenzyl)imidazolidine-2,4-dione **9c**.

Project AB

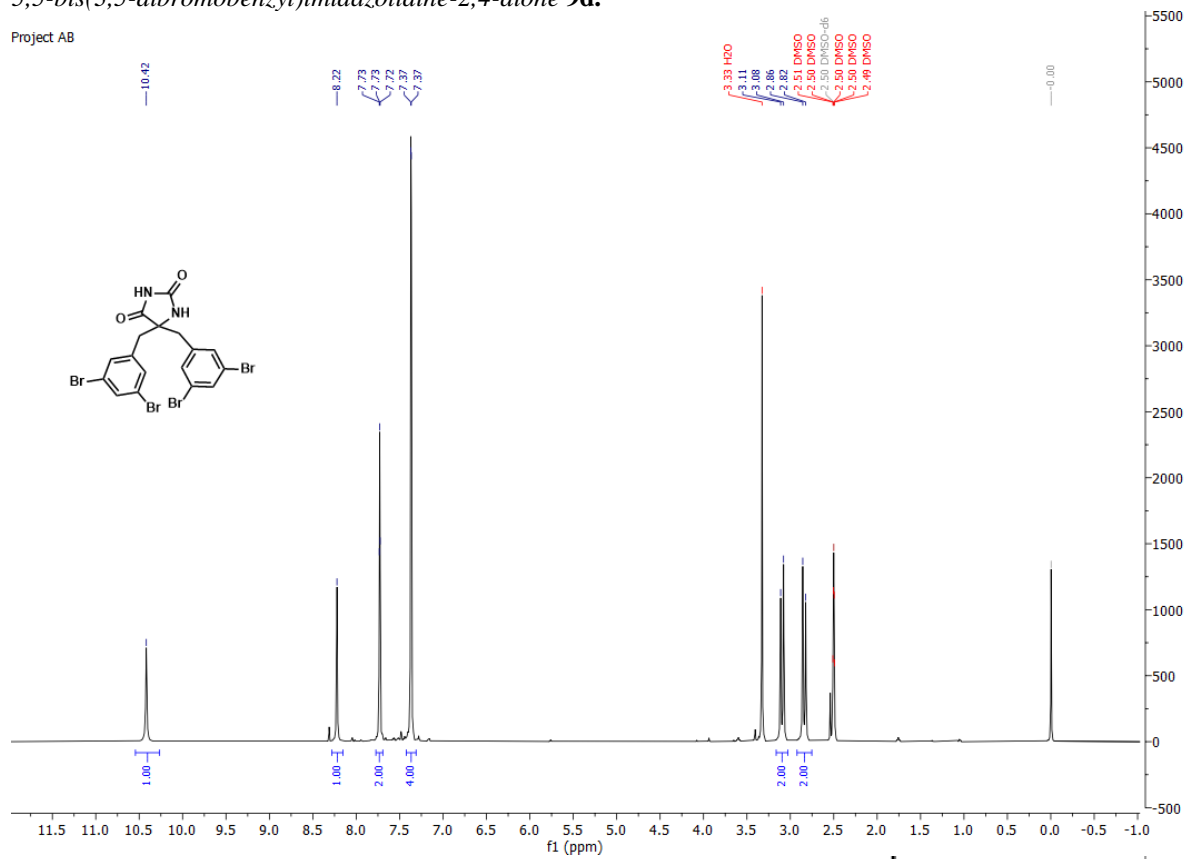


Project AB

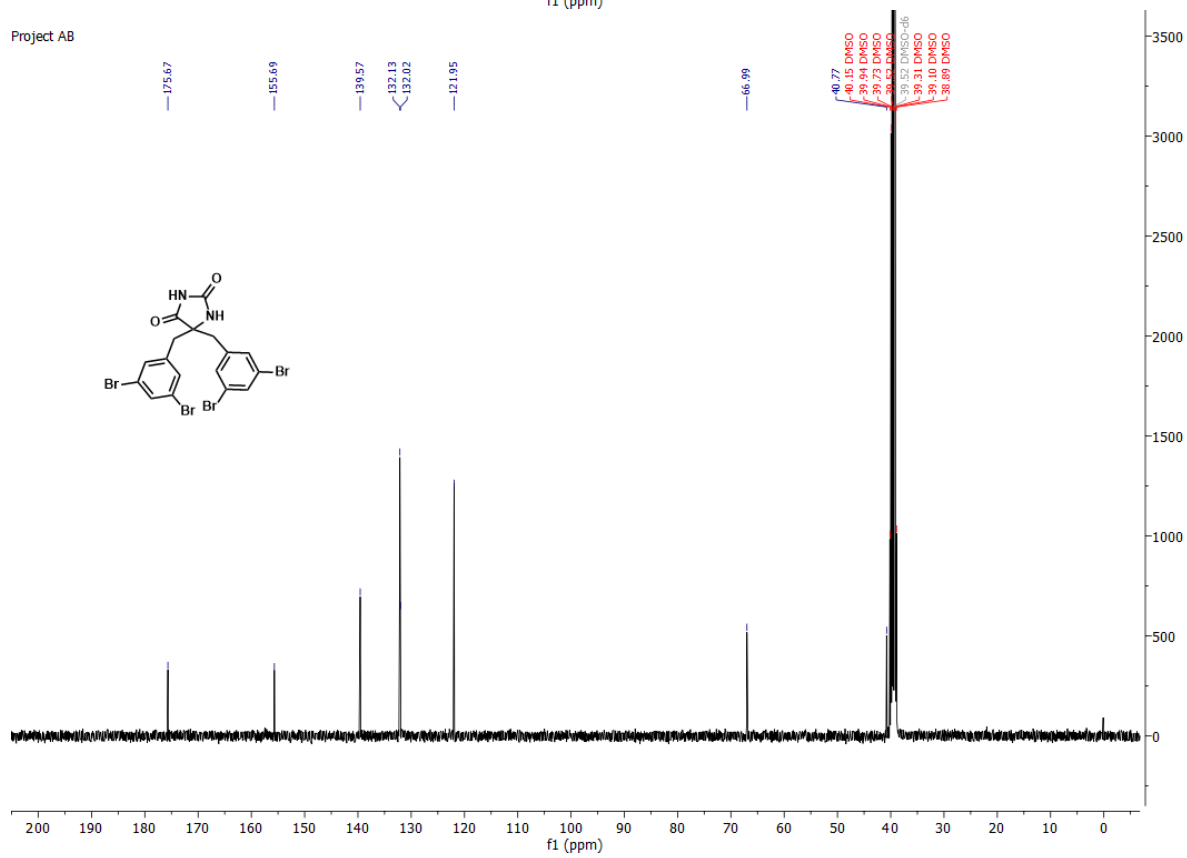


5,5-bis(3,5-dibromobenzyl)imidazolidine-2,4-dione **9d**.

Project AB

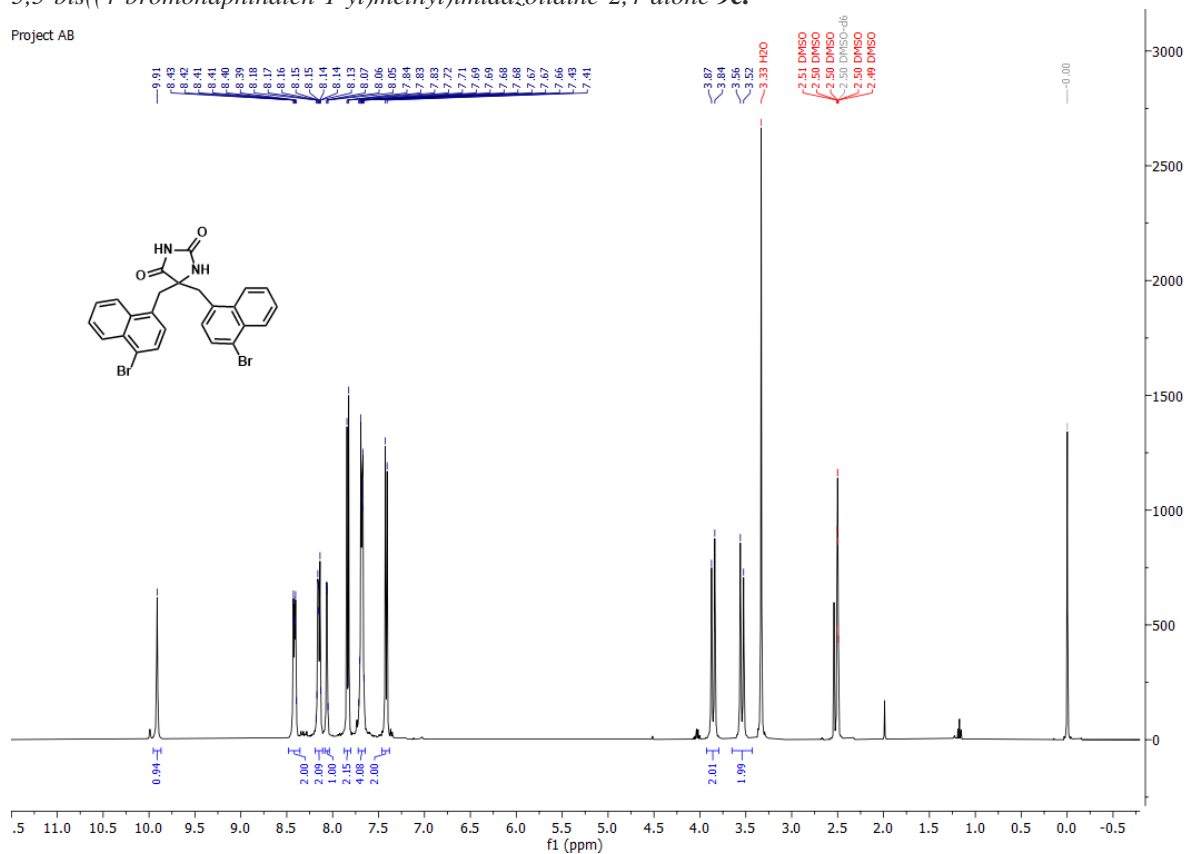


Project AB

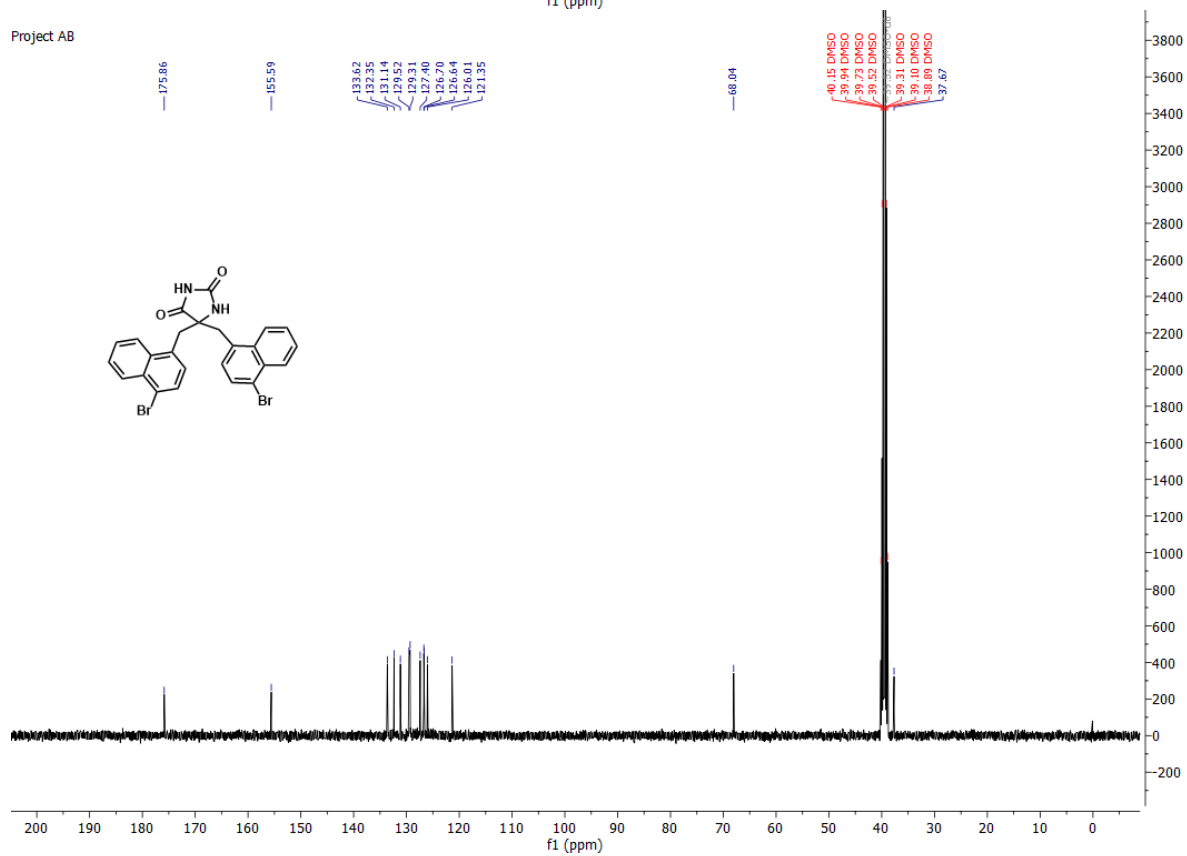


5,5-bis((4-bromonaphthalen-1-yl)methyl)imidazolidine-2,4-dione **9e**.

Project AB

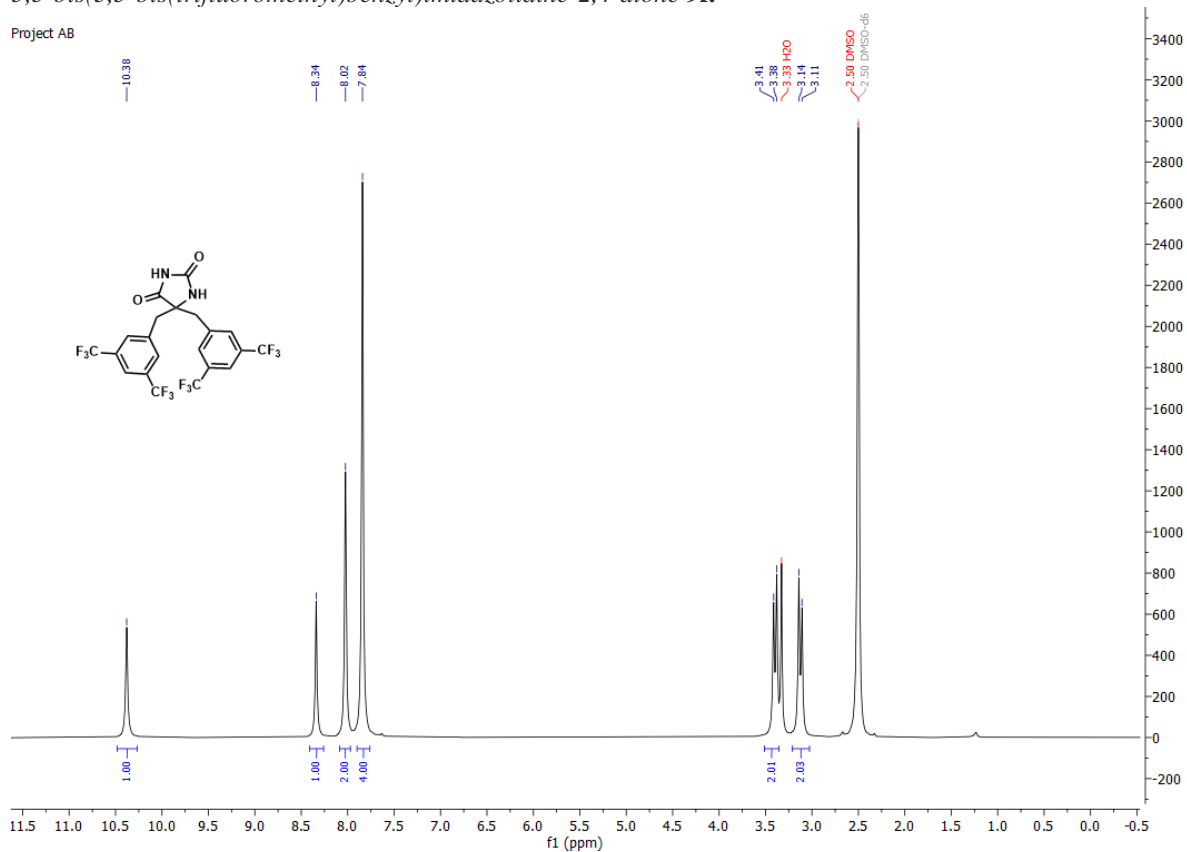


Project AB

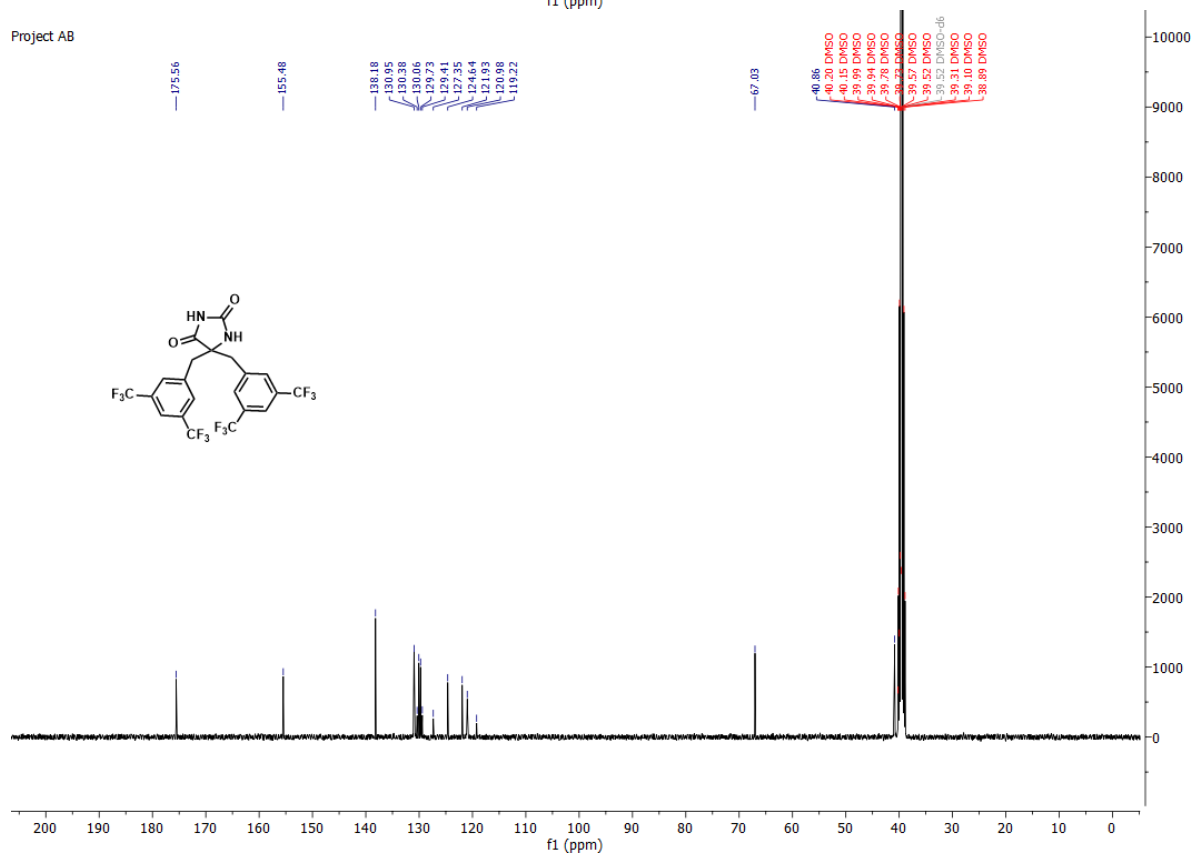


5,5-bis(3,5-bis(trifluoromethyl)benzyl)imidazolidine-2,4-dione **9f**.

Project AB



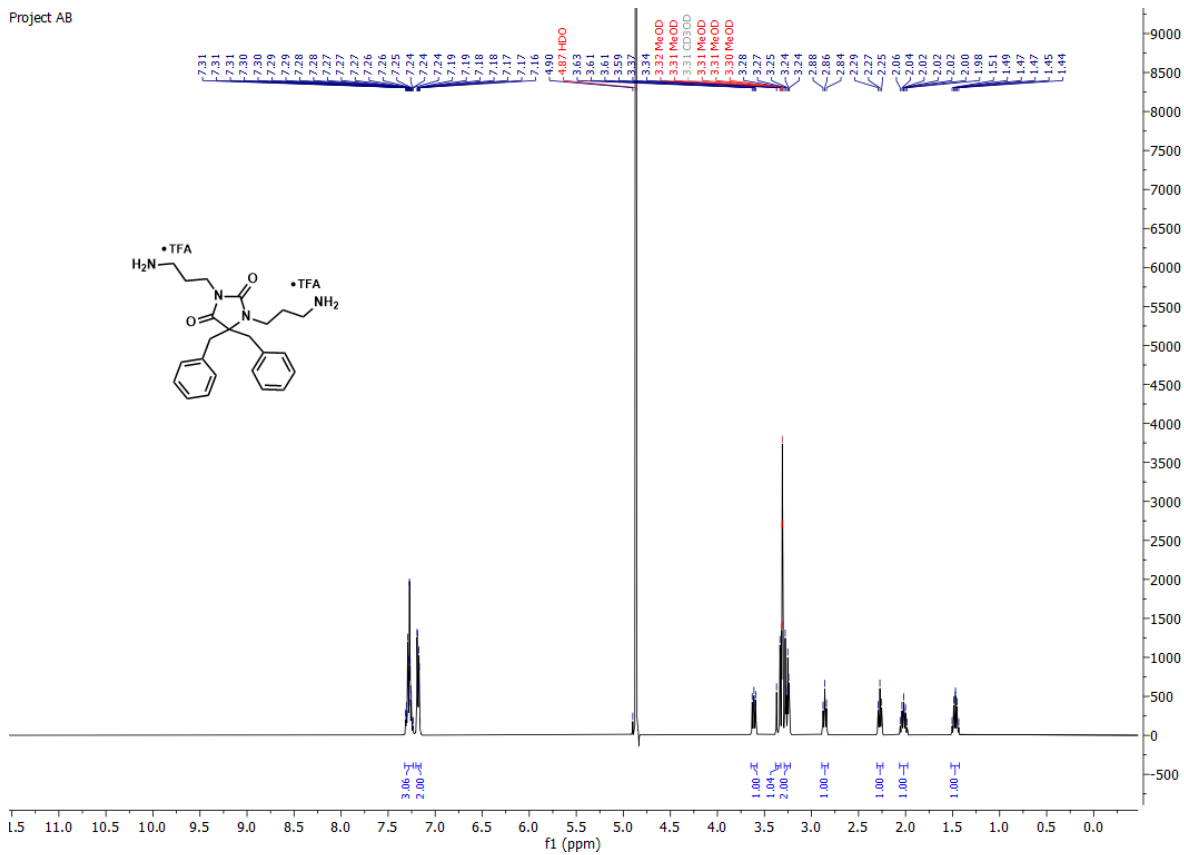
Project AB



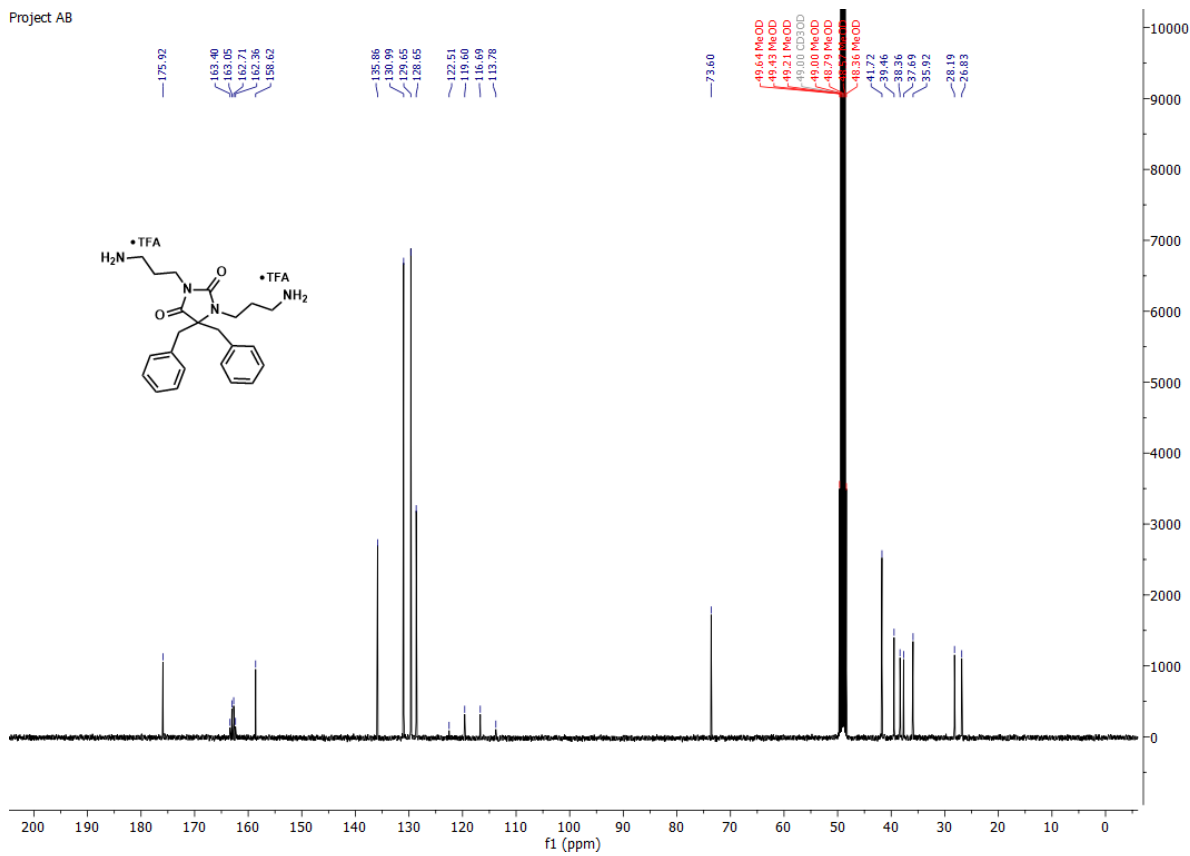
2.3 *N,N*-dialkylated hydantoin 2A

1,3-bis(3-aminopropyl)-5,5-dibenzylimidazolidine-2,4-dione **2aA**.

Project AB

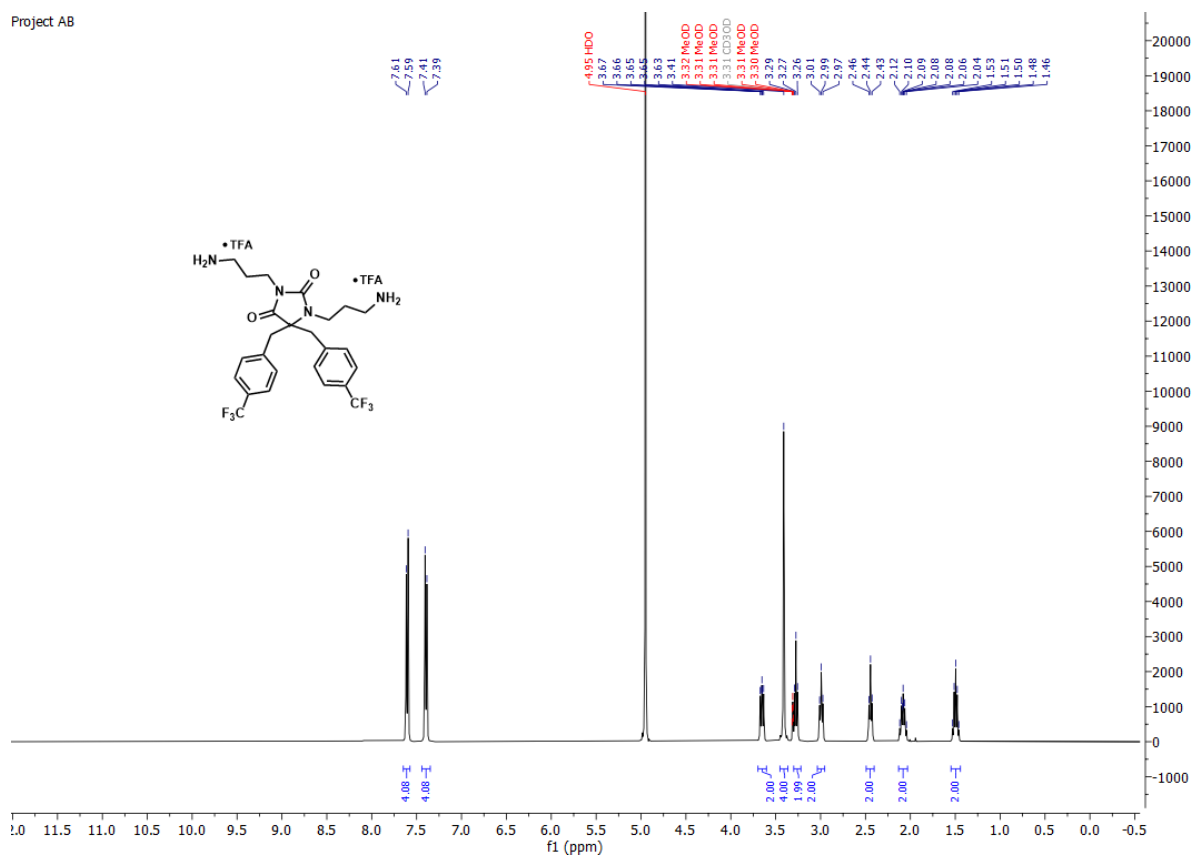


Project AB

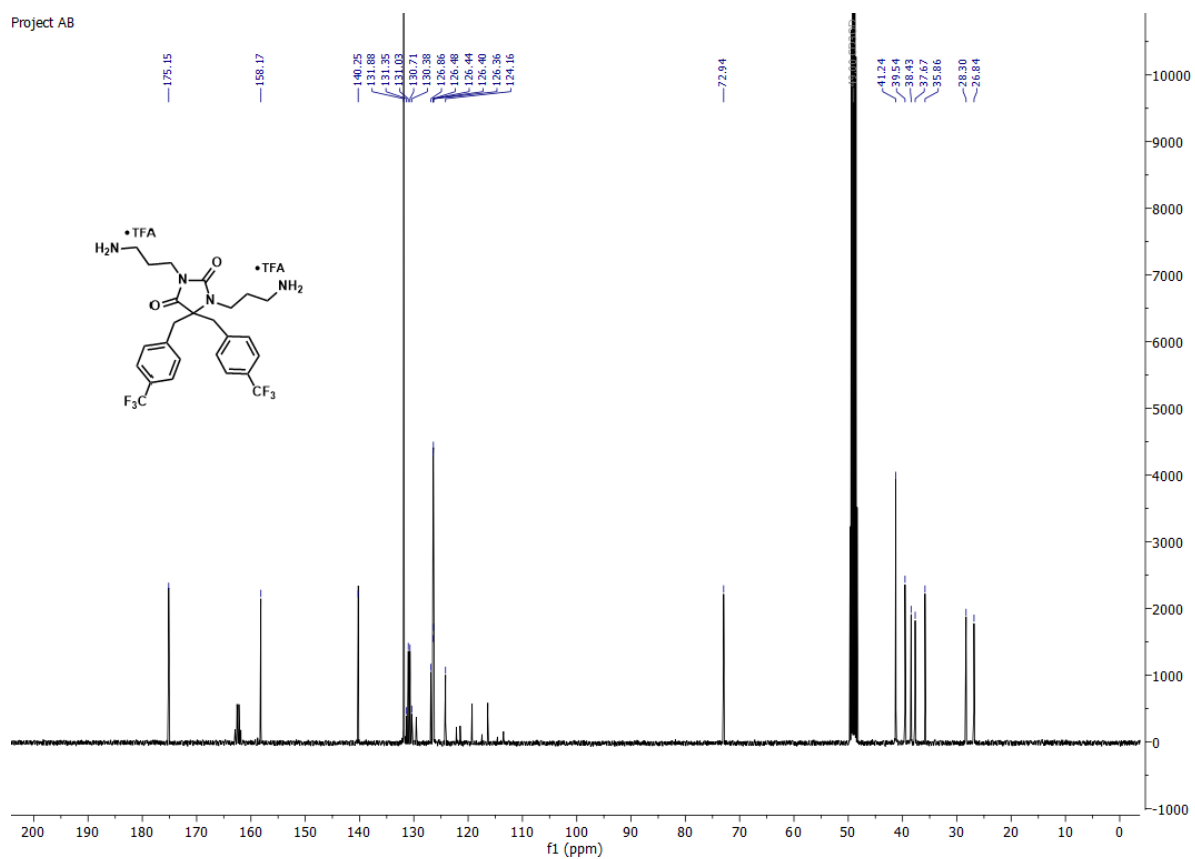


1,3-bis(3-aminopropyl)-5,5-bis(4-(trifluoromethyl)benzyl)imidazolidine-2,4-dione **2bA**.

Project AB

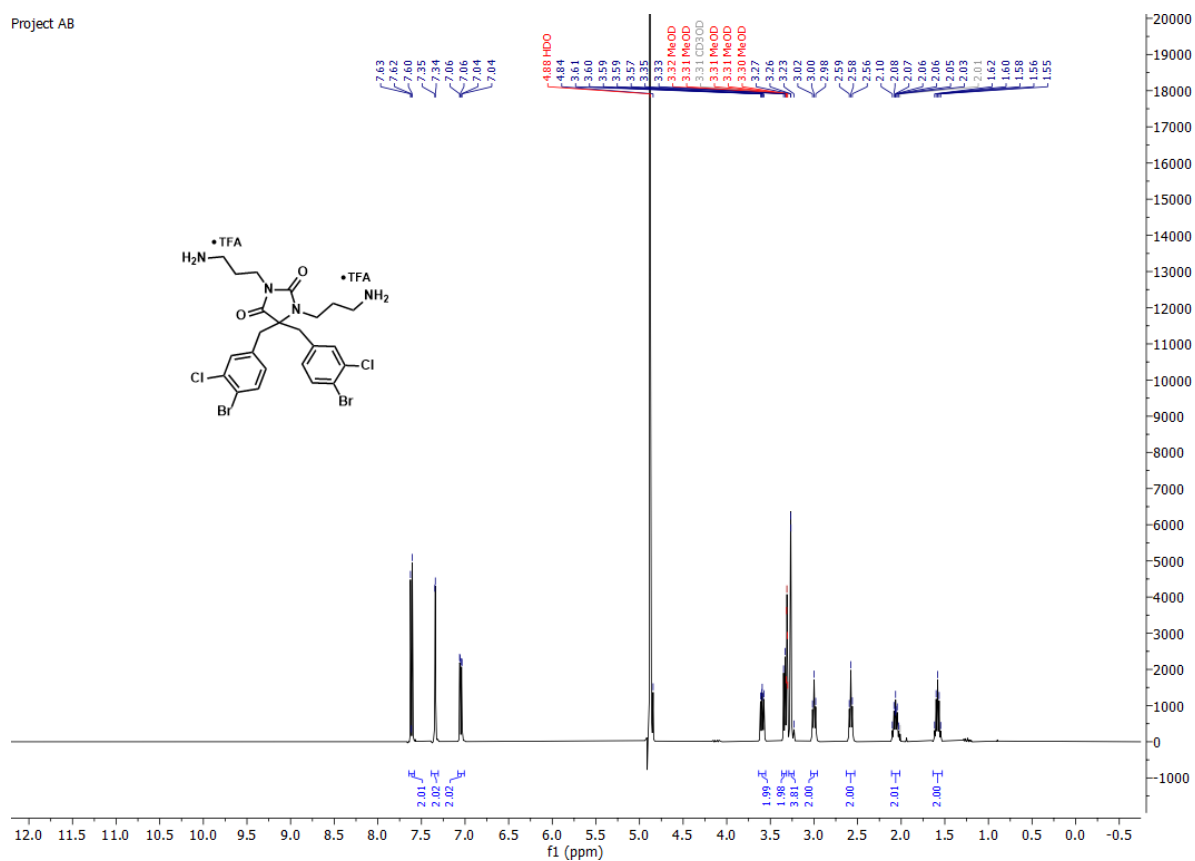


Project AB

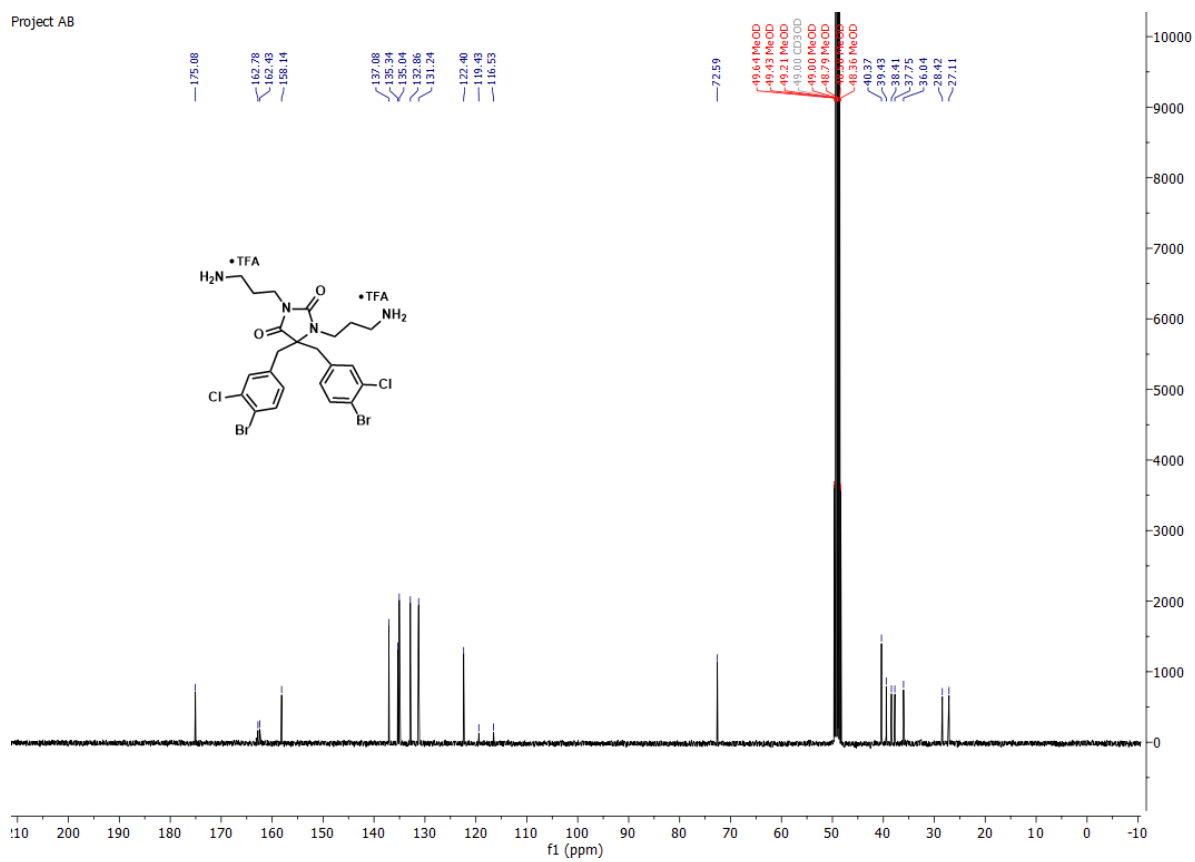


1,3-bis(3-aminopropyl)-5,5-bis(4-bromo-3-chlorobenzyl)imidazolidine-2,4-dione **2cA**.

Project AB

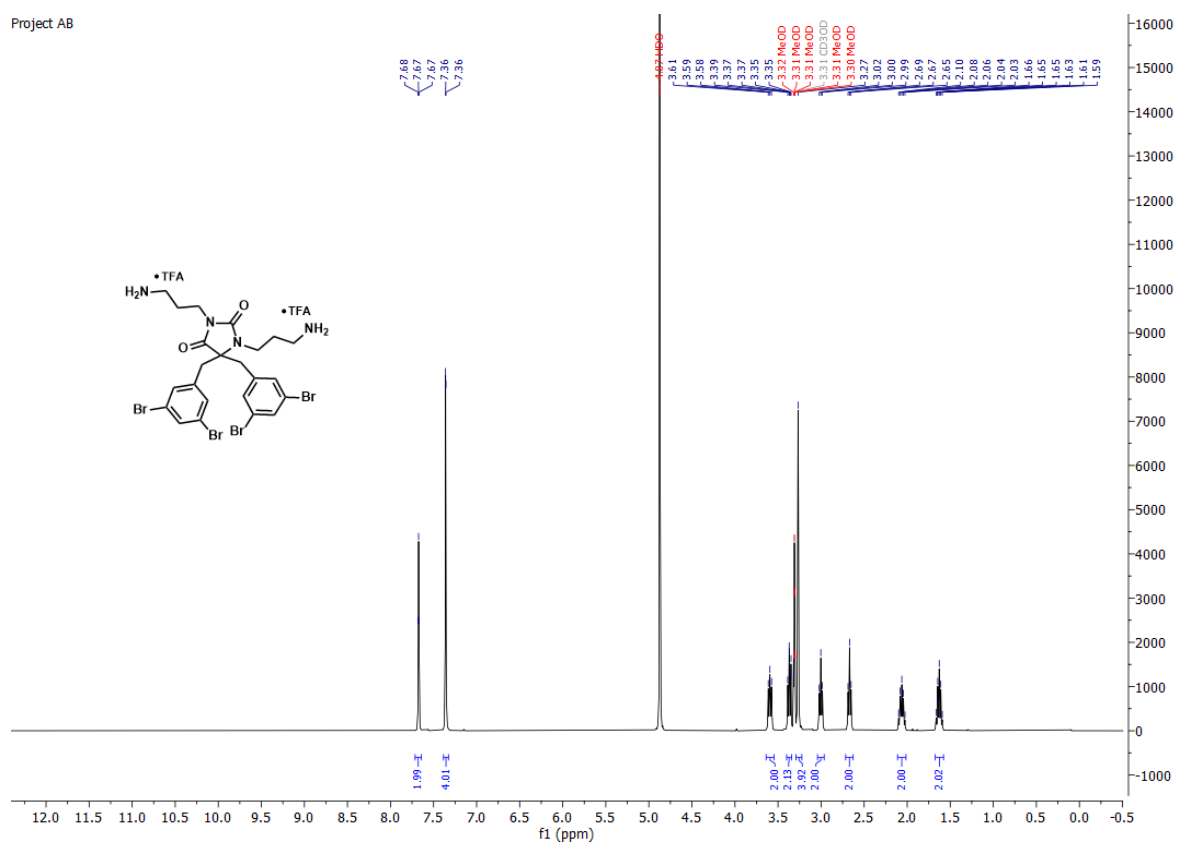


Project AB

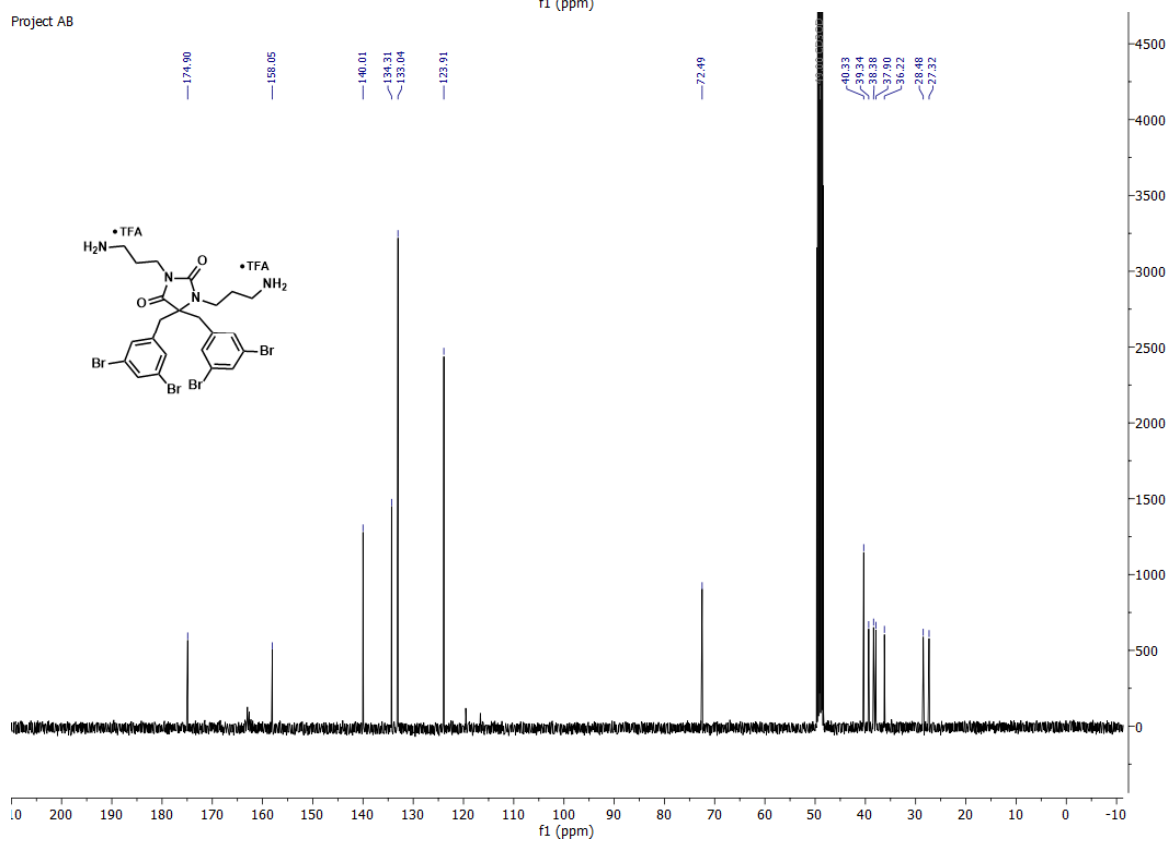


1,3-bis(3-aminopropyl)-5,5-bis(3,5-dibromobenzyl)imidazolidine-2,4-dione 2dA.

Project AB

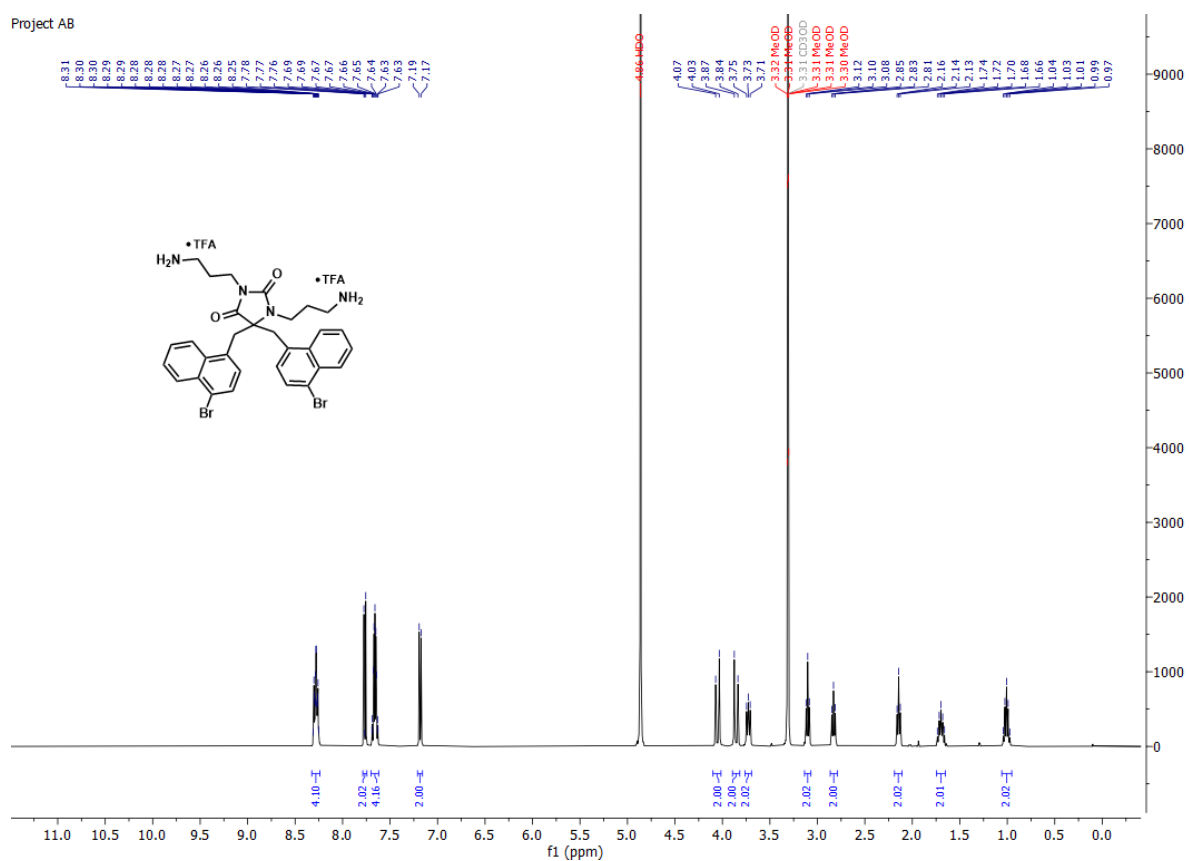


Project AB

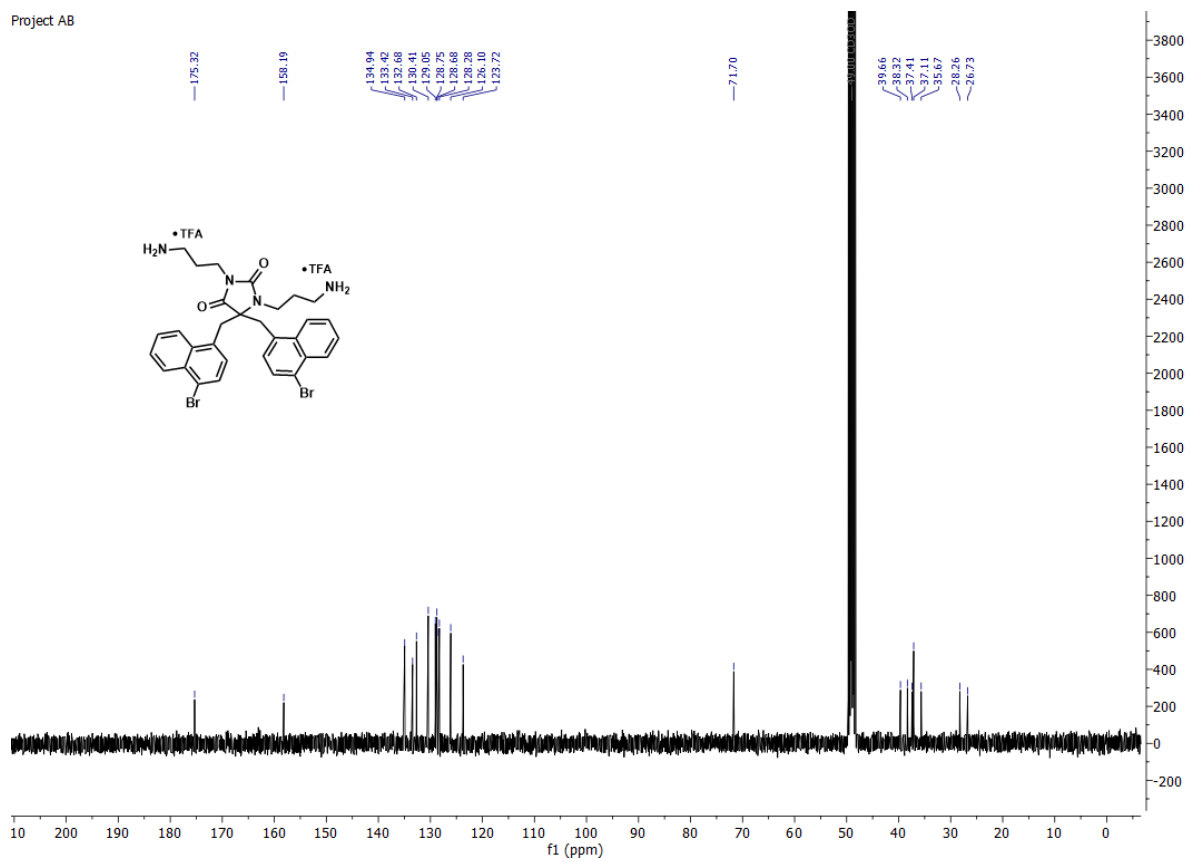


1,3-bis(3-aminopropyl)-5,5-bis((4-bromonaphthalen-1-yl)methyl)imidazolidine-2,4-dione 2eA.

Project AB

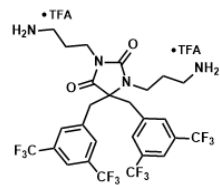
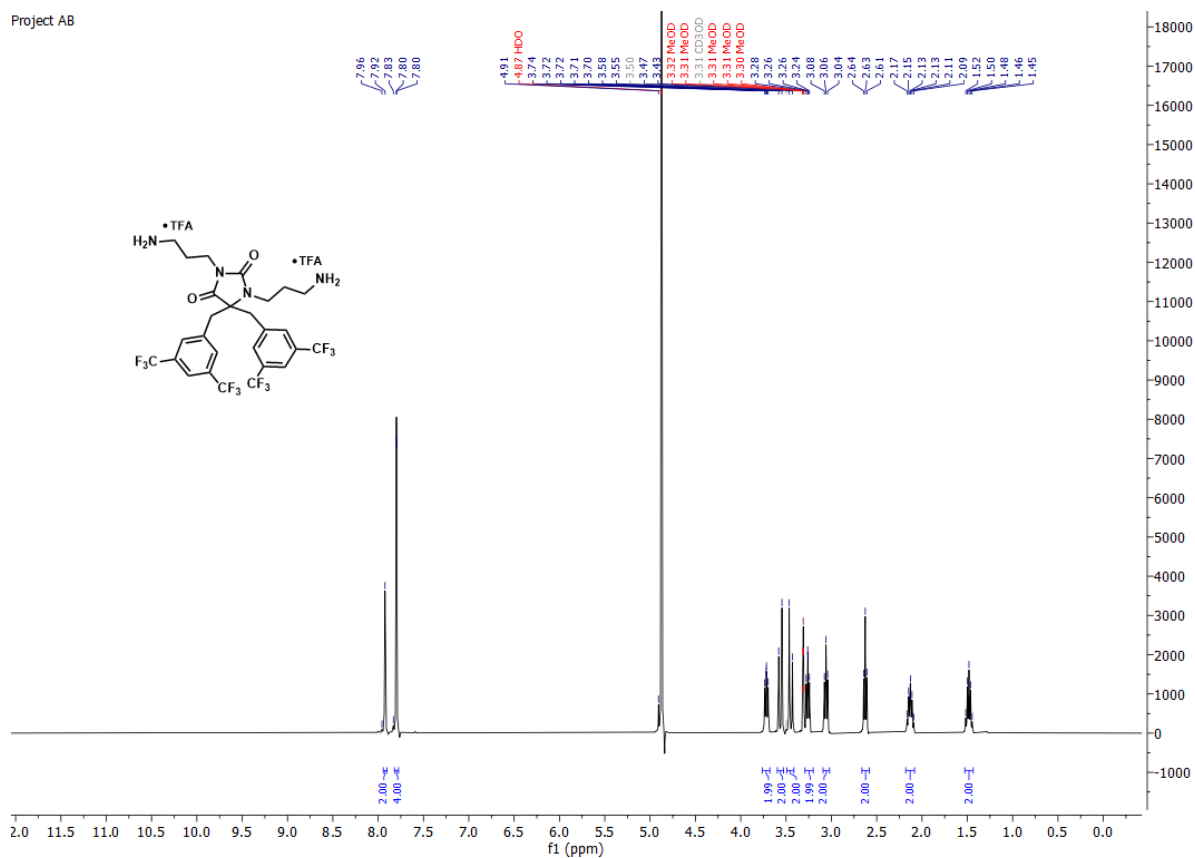


Project AB

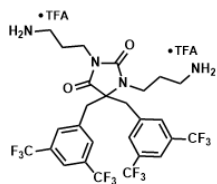
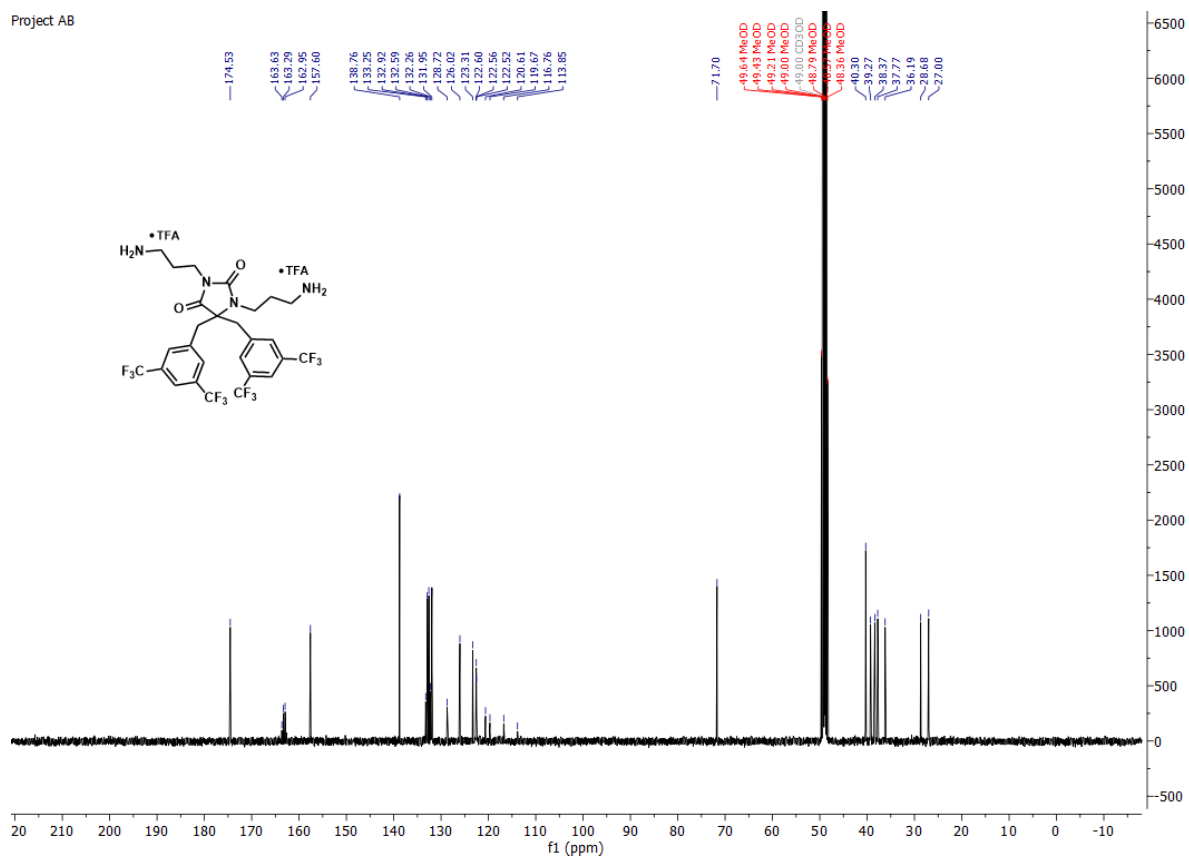


1,3-bis(3-aminopropyl)-5,5-bis(3,5-bis(trifluoromethyl)benzyl)imidazolidine-2,4-dione **2fA**.

Project AB



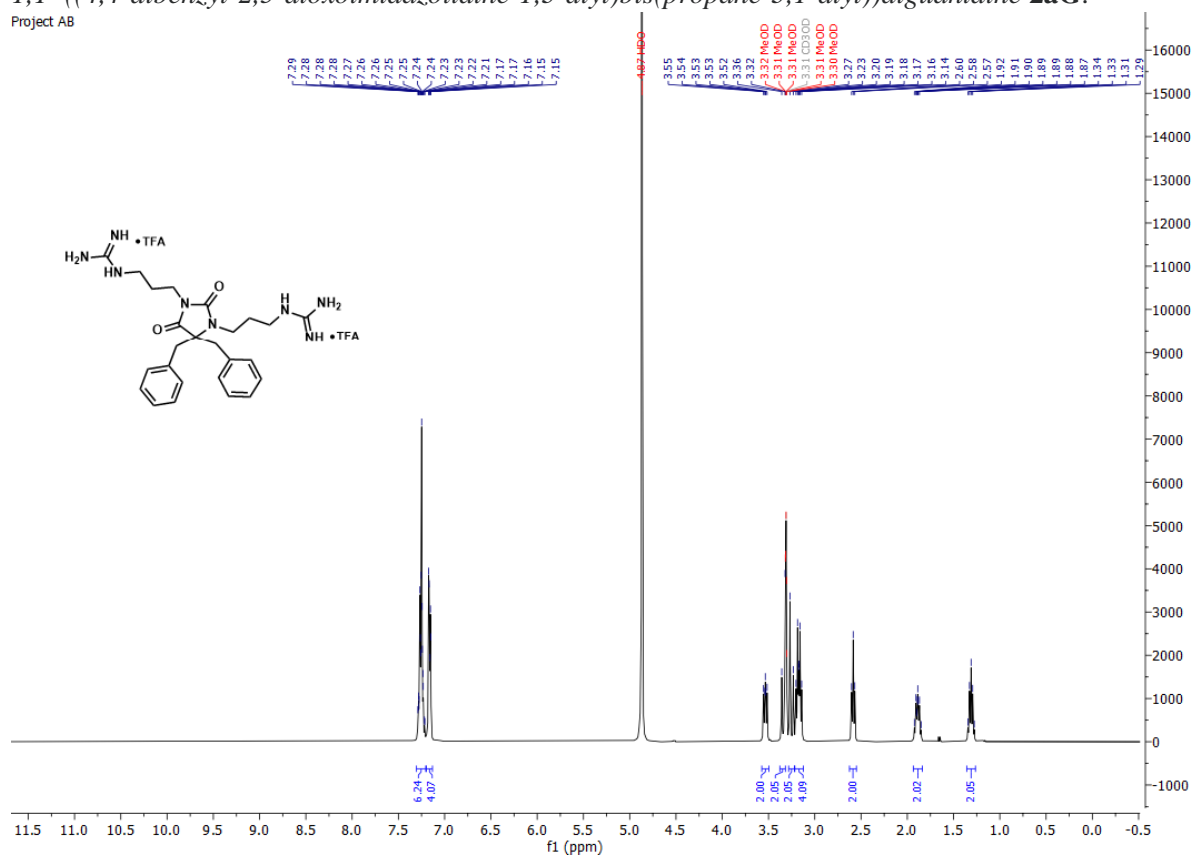
Project AB



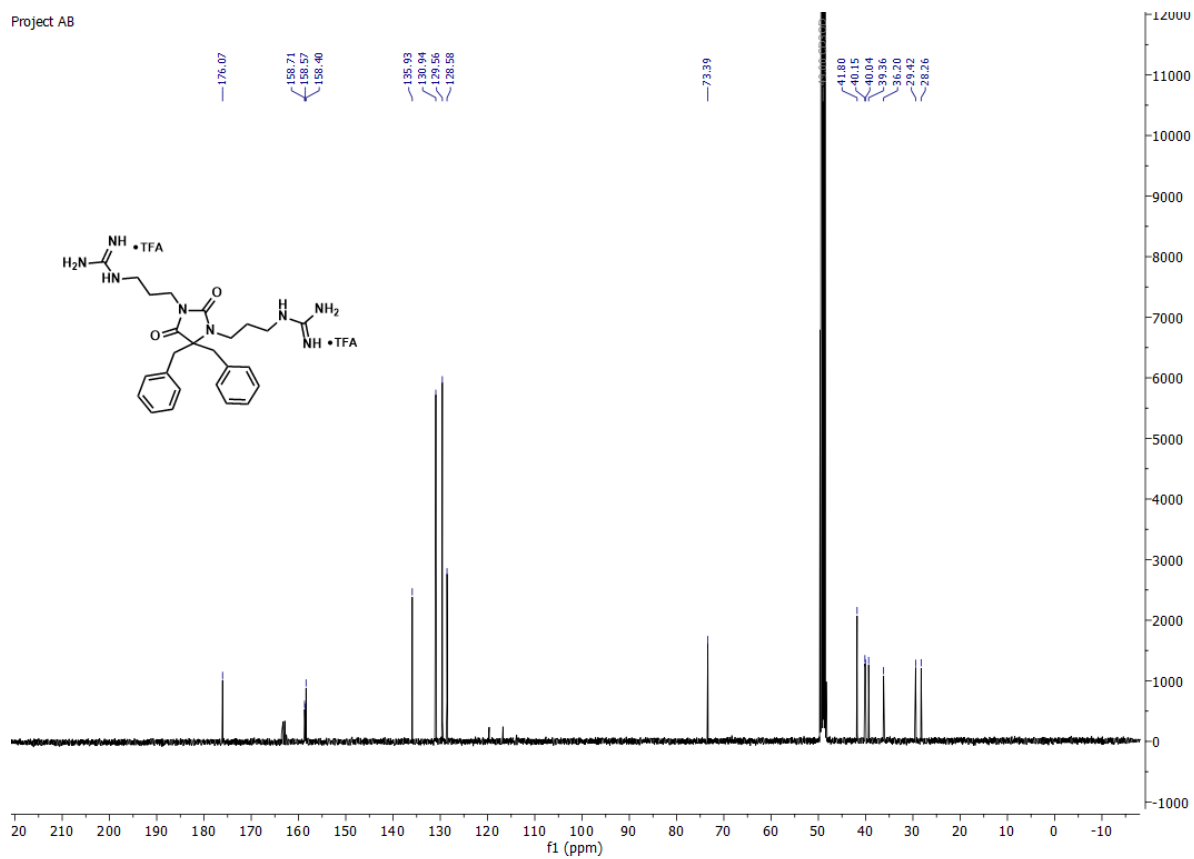
2.4 *N,N*-dialkylated hydantoin 2G

1,1'-((4,4-dibenzyl-2,5-dioximidazolidine-1,3-diyl)bis(propane-3,1-diyl))diguanidine **2aG**.

Project AB

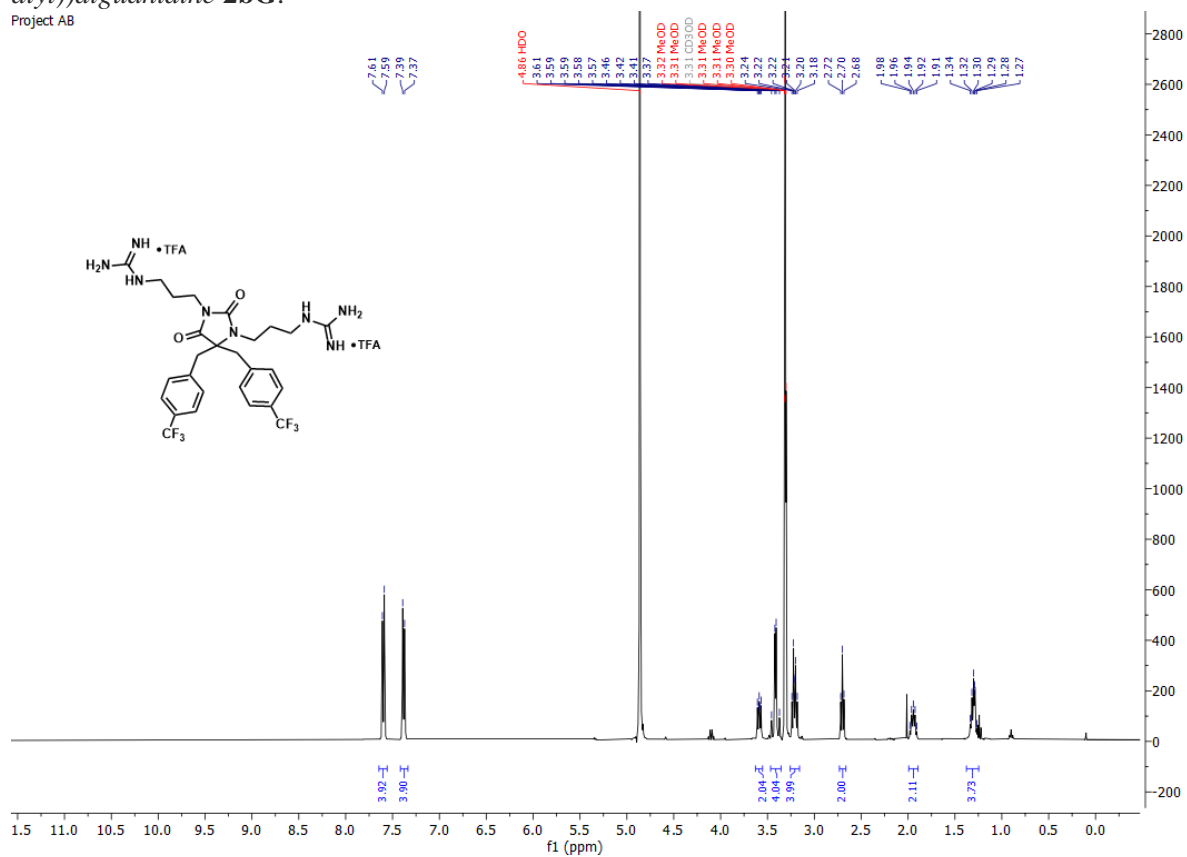


Project AB

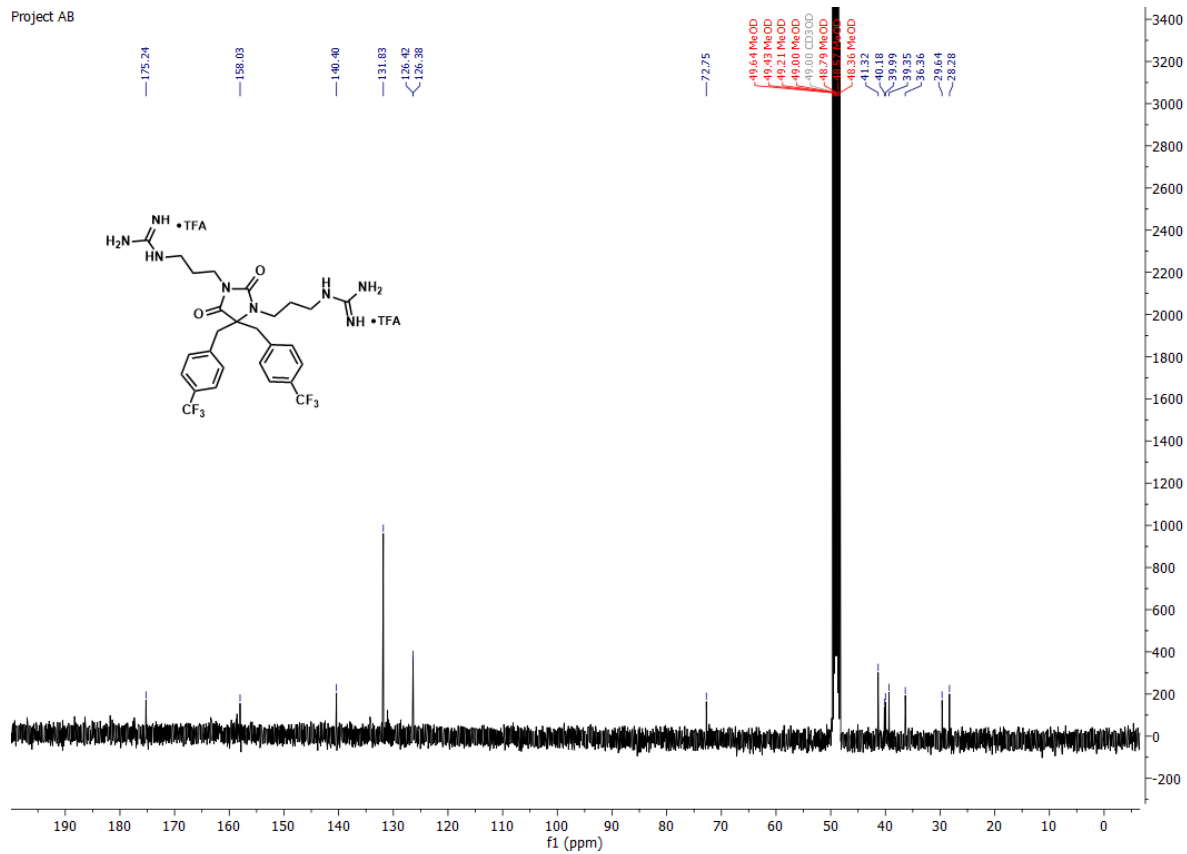


1,1'-((2,5-dioxo-4,4-bis(4-(trifluoromethyl)benzyl)imidazolidine-1,3-diyl)bis(propane-3,1-diyl))diguanidine **2bG**.

Project AB

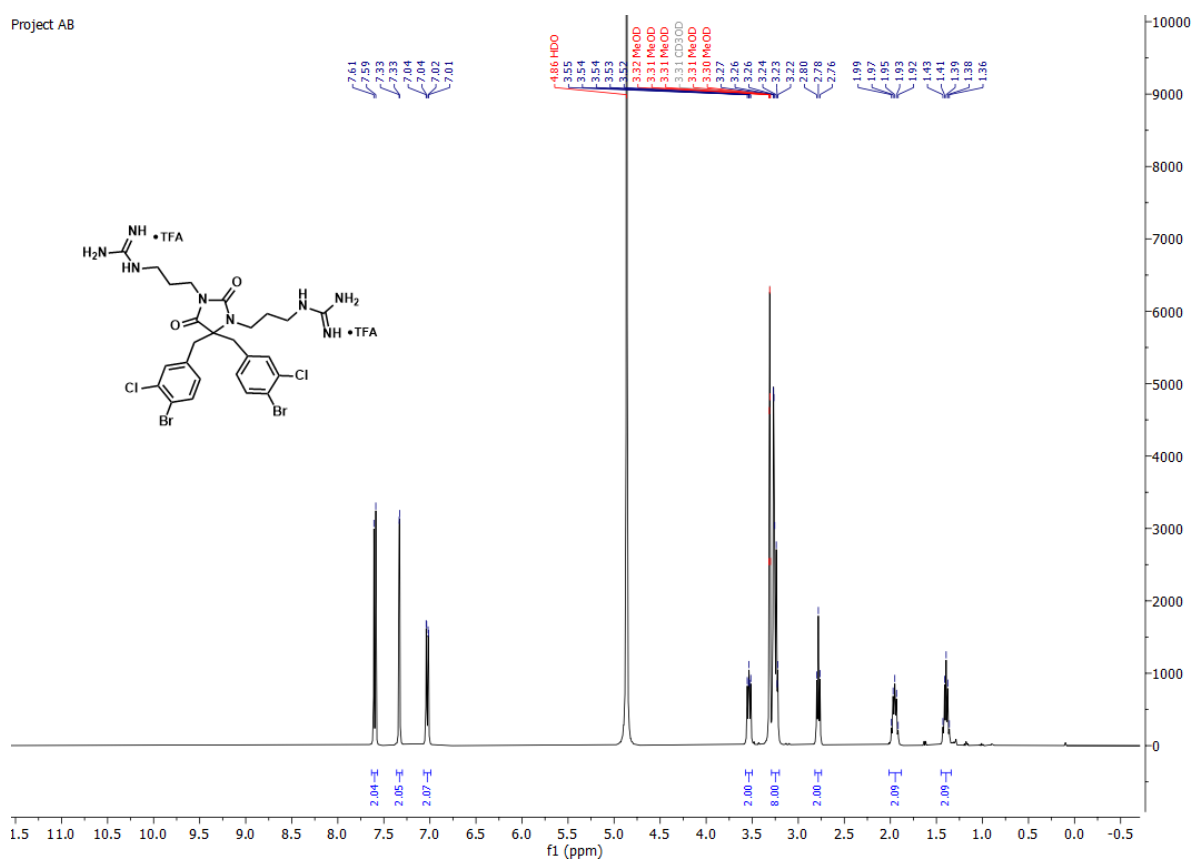


Project AB

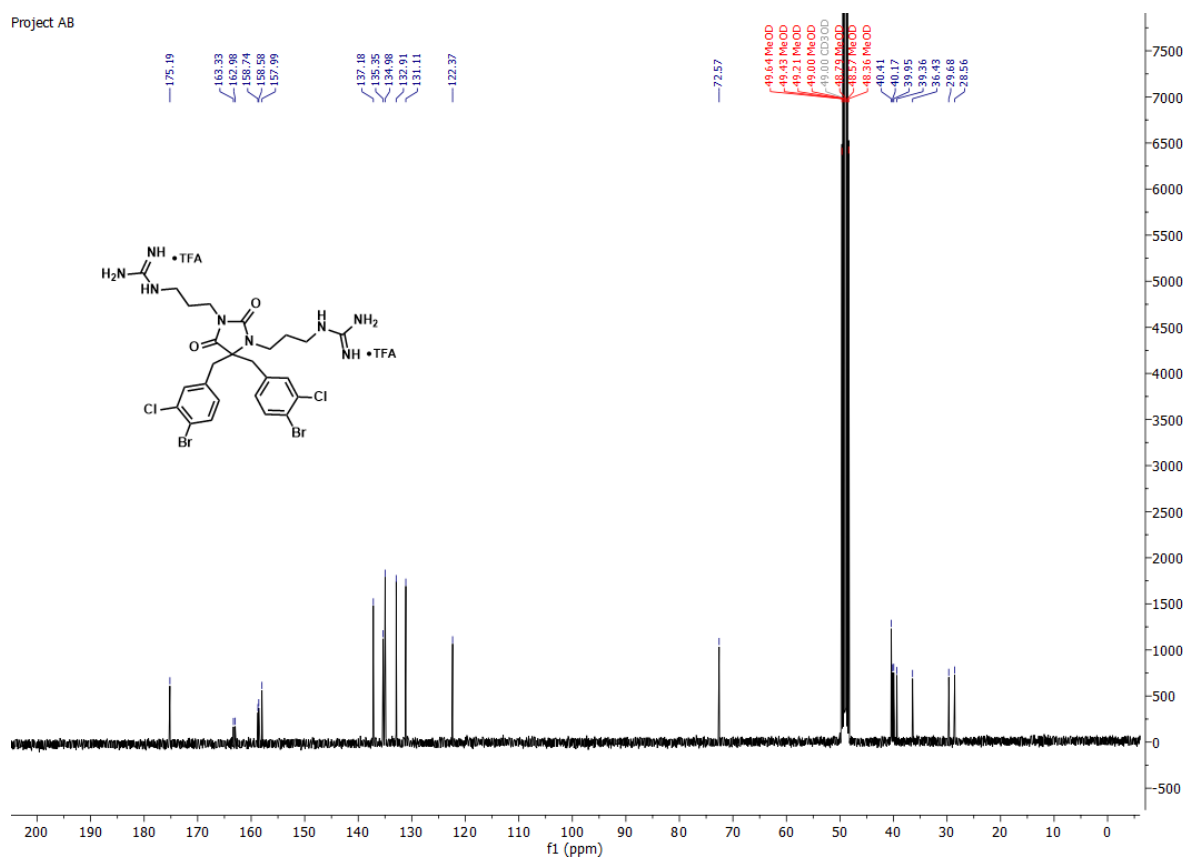


1,1'-((4,4-bis(4-bromo-3-chlorobenzyl)-2,5-dioximidazolidine-1,3-diyl)bis(propane-3,1-diyl))diguanidine **2cG**.

Project AB

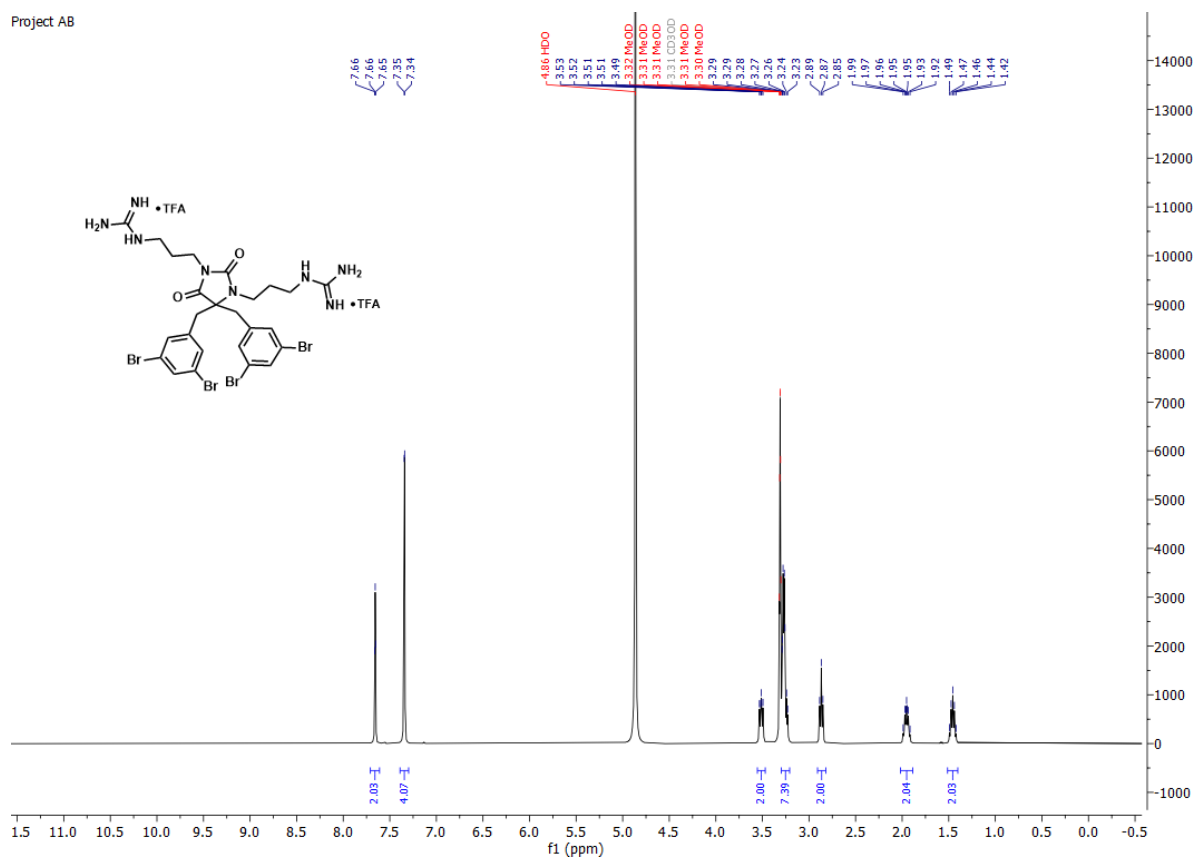


Project AB

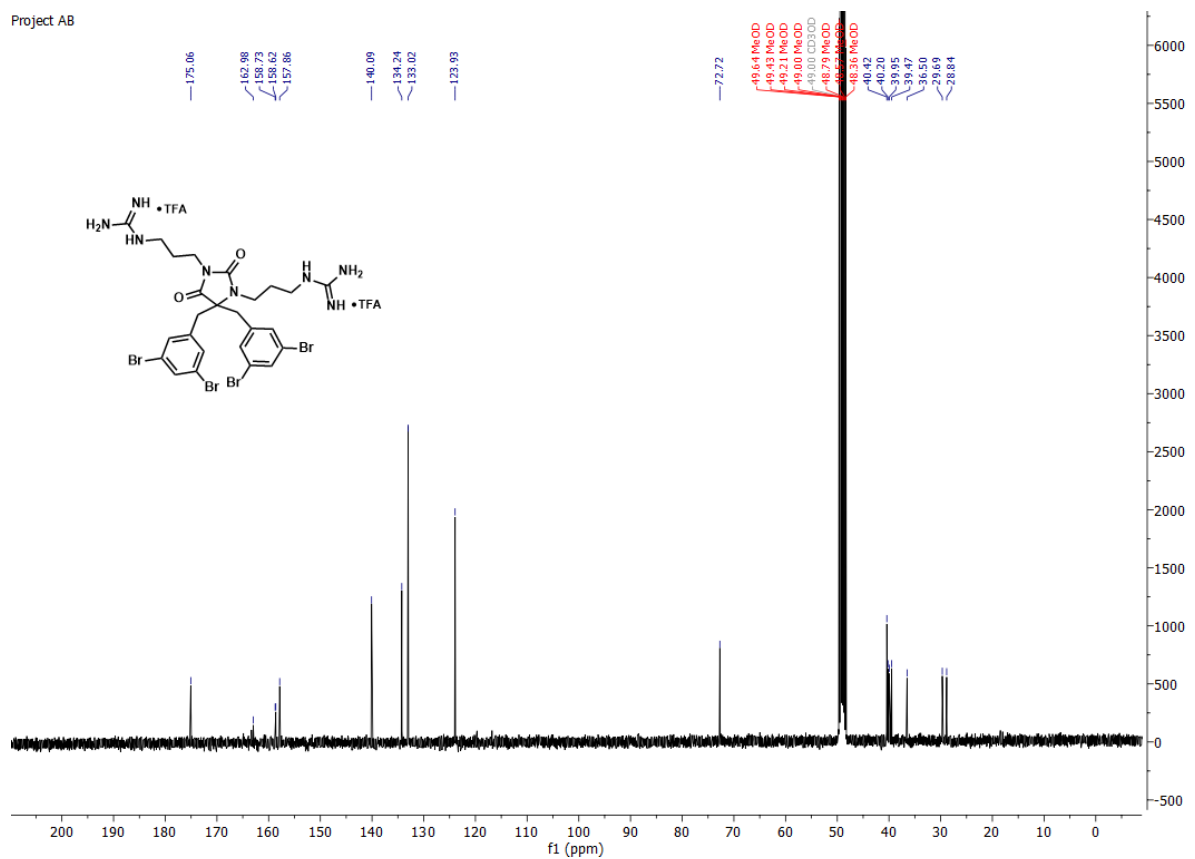


1,1'-((4,4-bis(3,5-dibromobenzyl)-2,5-dioximidazolidine-1,3-diyl)bis(propane-3,1-diyl)diguanine
2dG.

Project AB

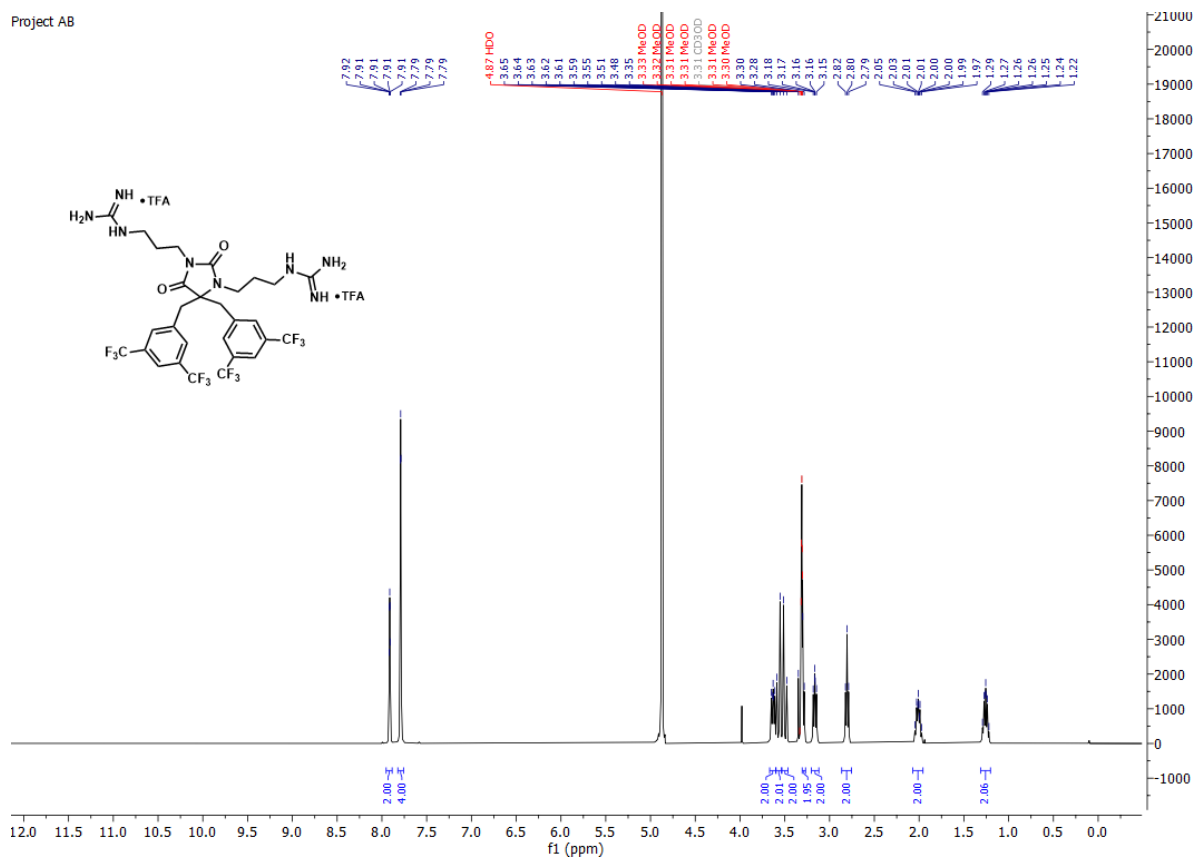


Project AB

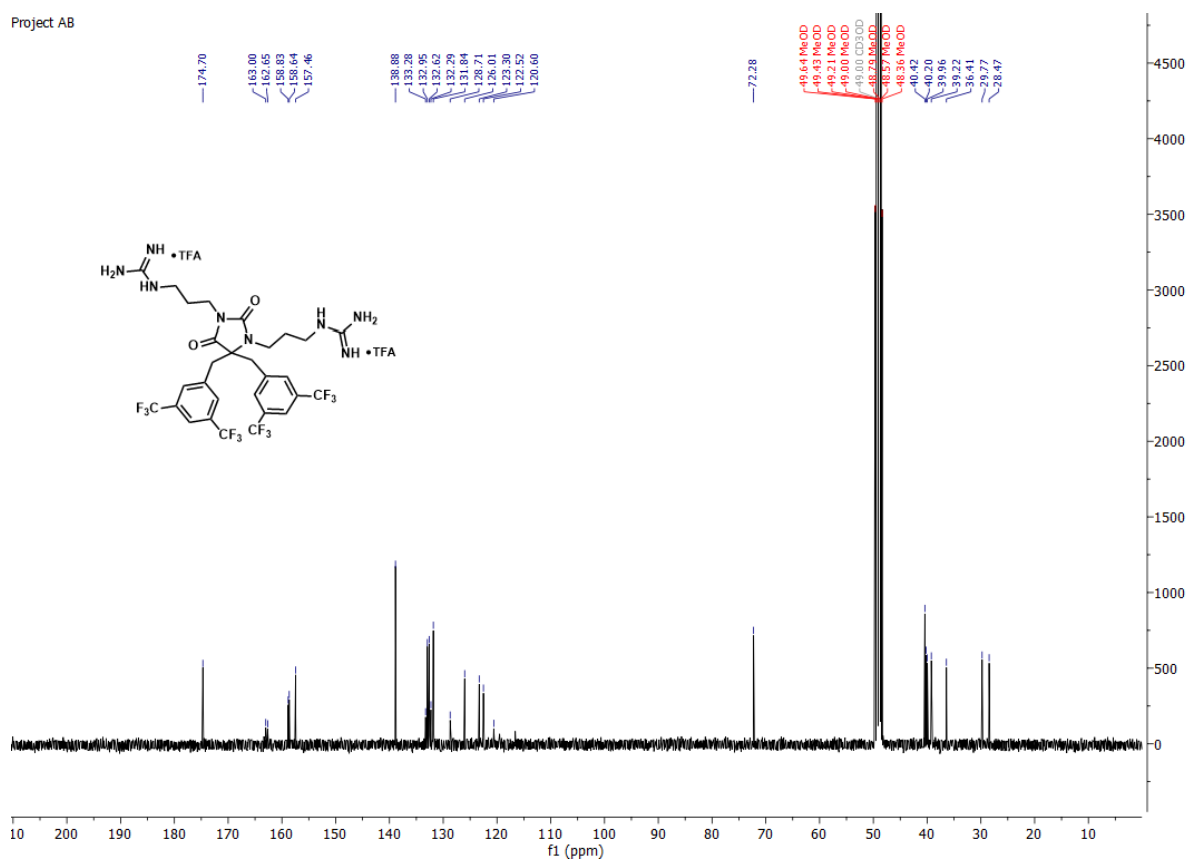


1,1'-((4,4-bis(3,5-bis(trifluoromethyl)benzyl)-2,5-dioximidazolidine-1,3-diyl)bis(propane-3,1-diyl))diguanidine **2fG**.

Project AB



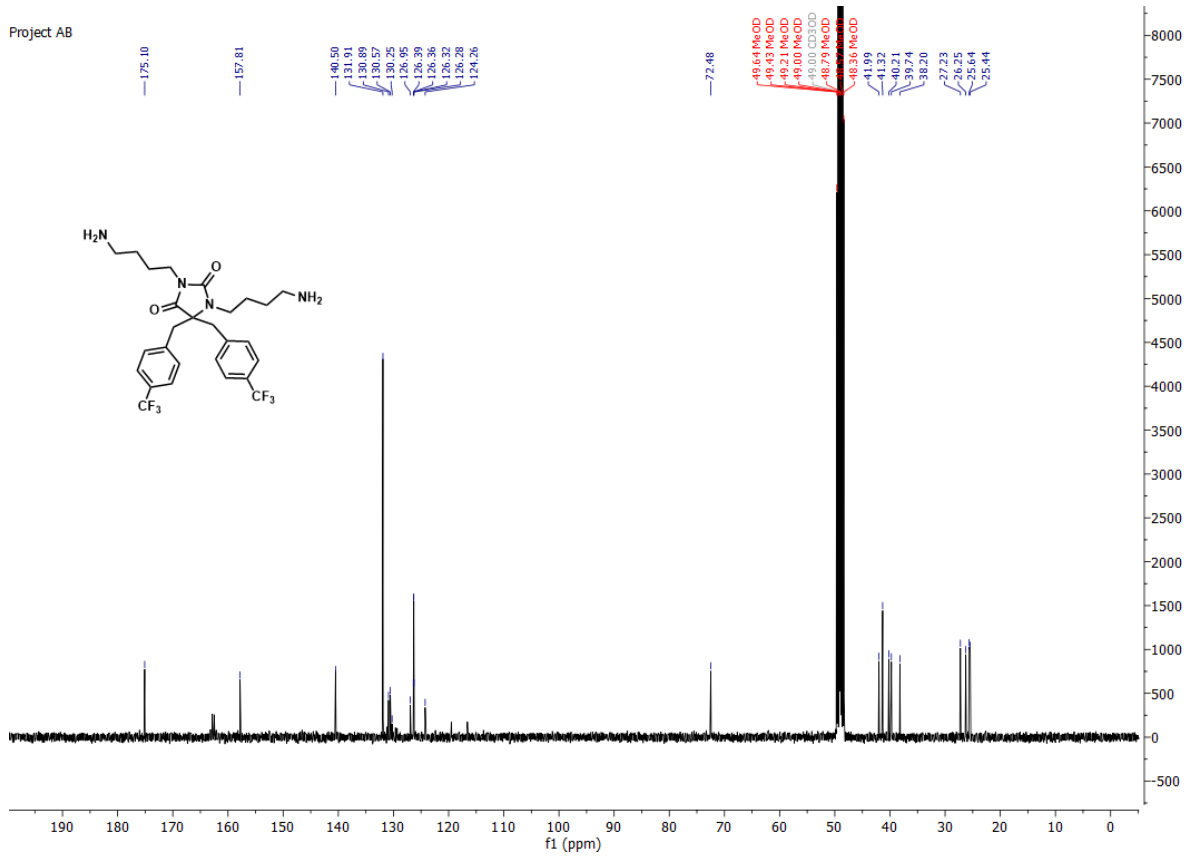
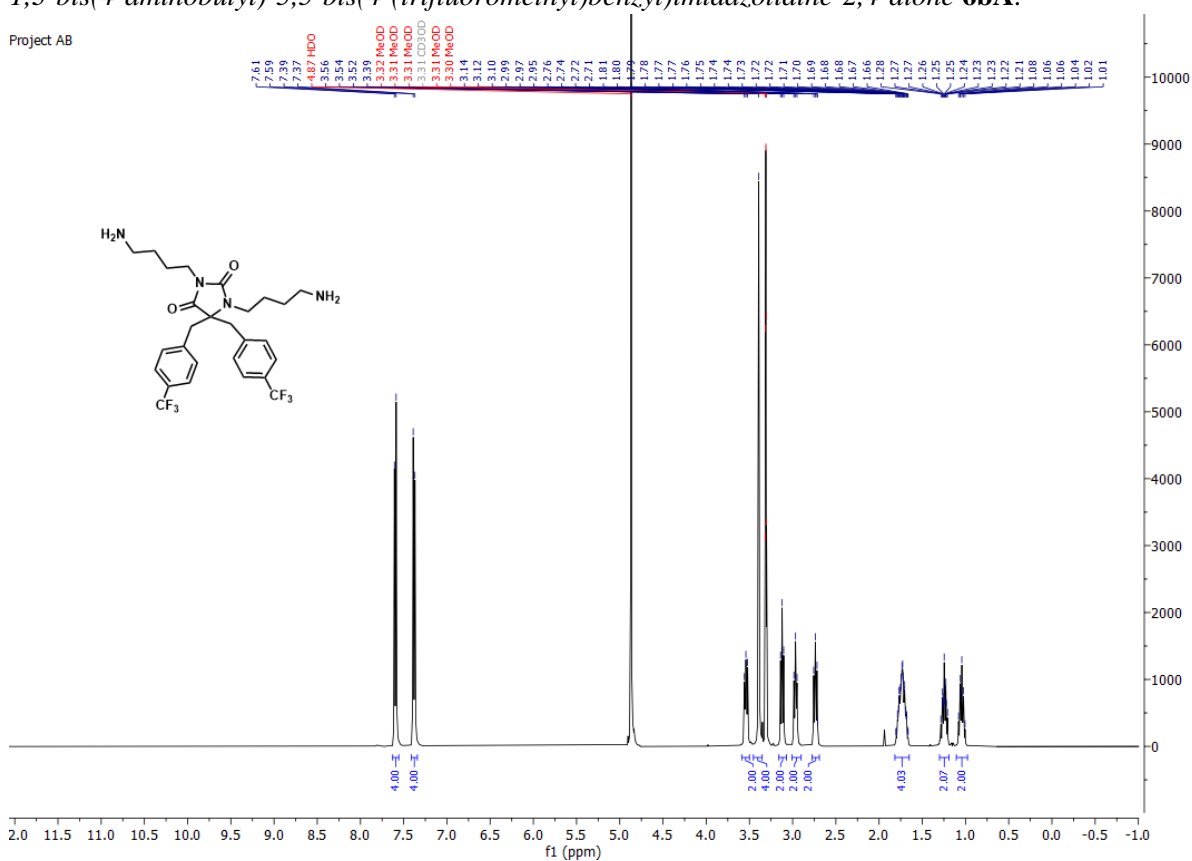
Project AB



2.5 *N,N*-dialkylated hydantoin 6A

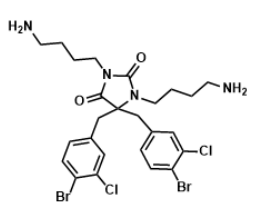
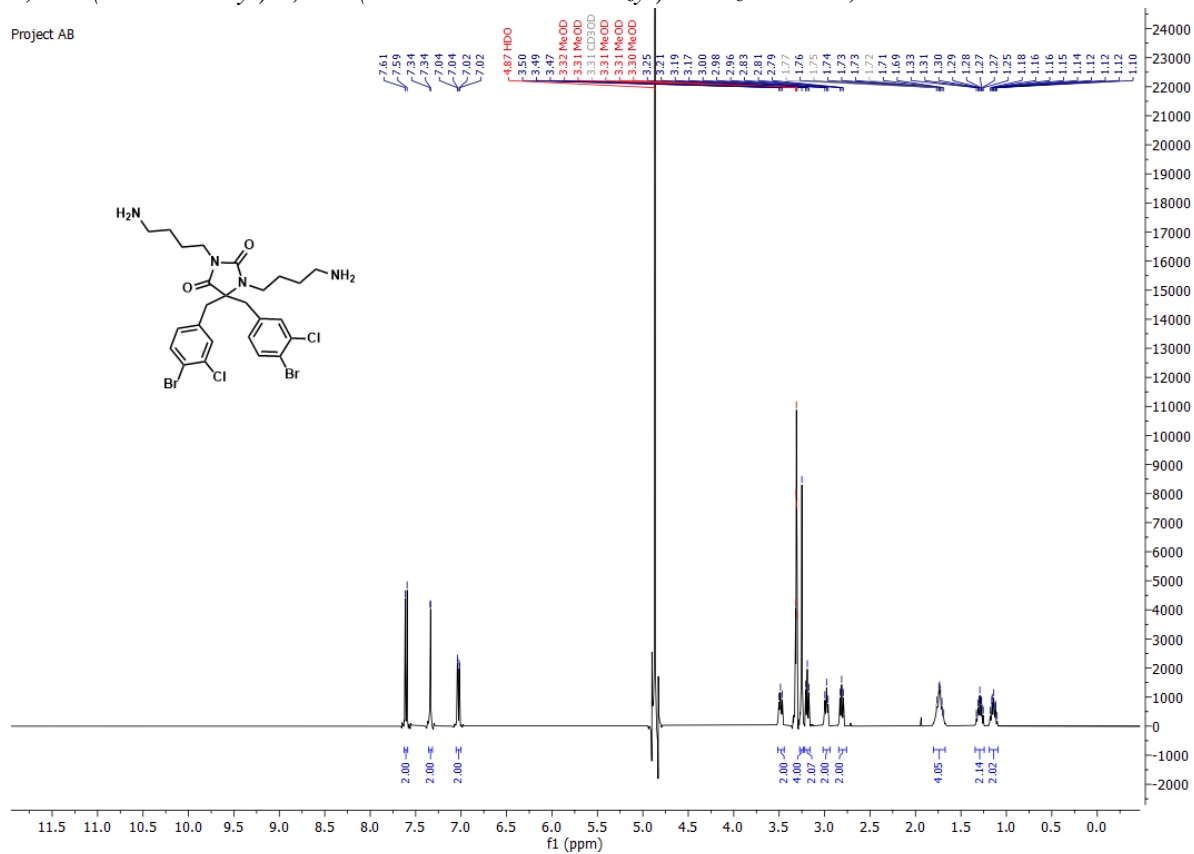
1,3-bis(4-aminobutyl)-5,5-bis(4-(trifluoromethyl)benzyl)imidazolidine-2,4-dione **6bA**.

Project AB

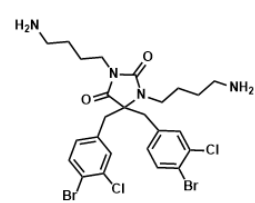
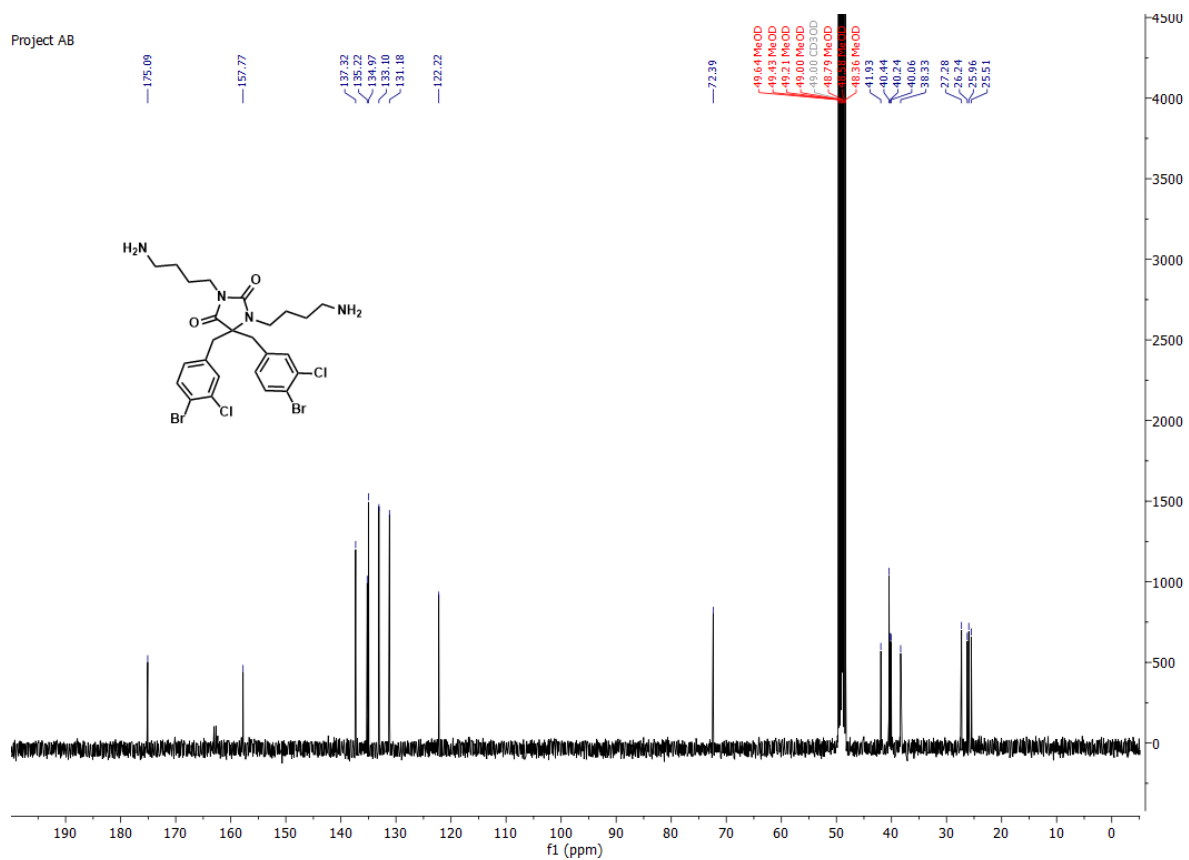


1,3-bis(4-aminobutyl)-5,5-bis(4-bromo-3-chlorobenzyl)imidazolidine-2,4-dione **6cA**.

Project AB

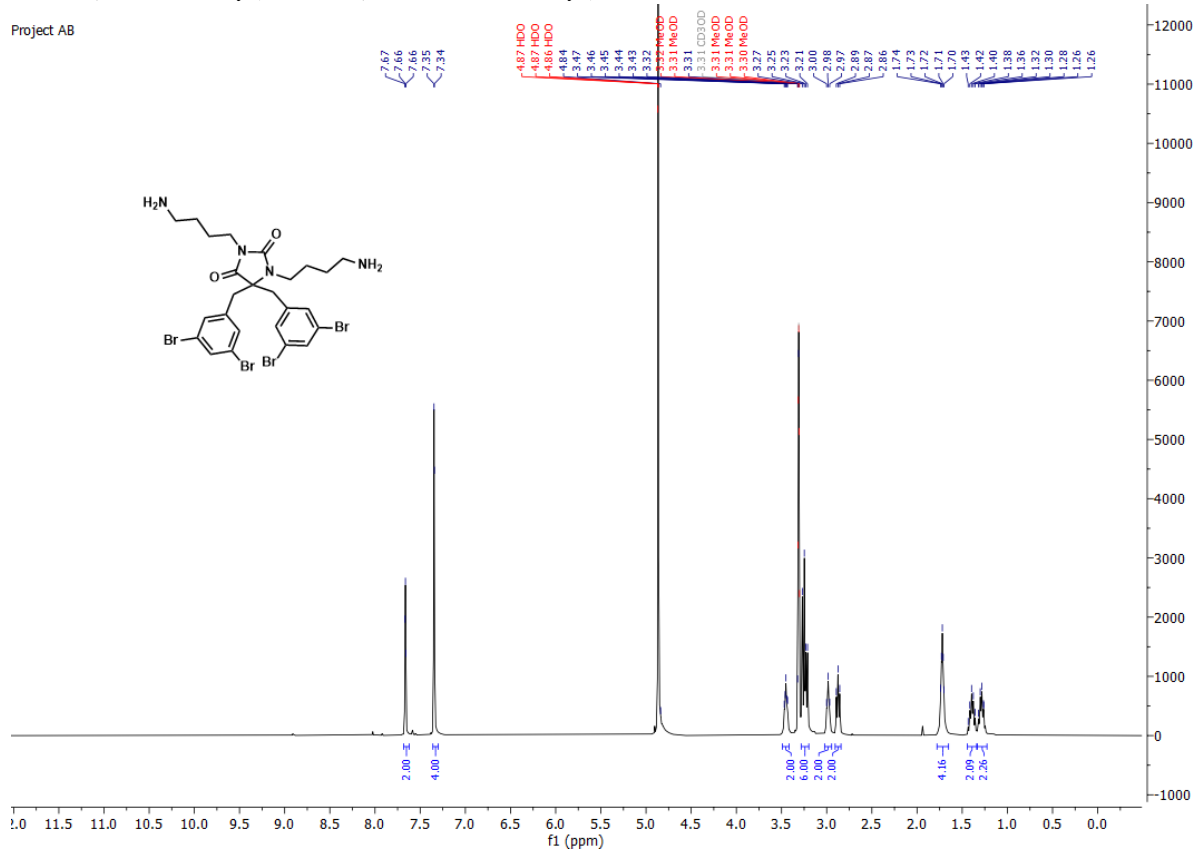


Project AB

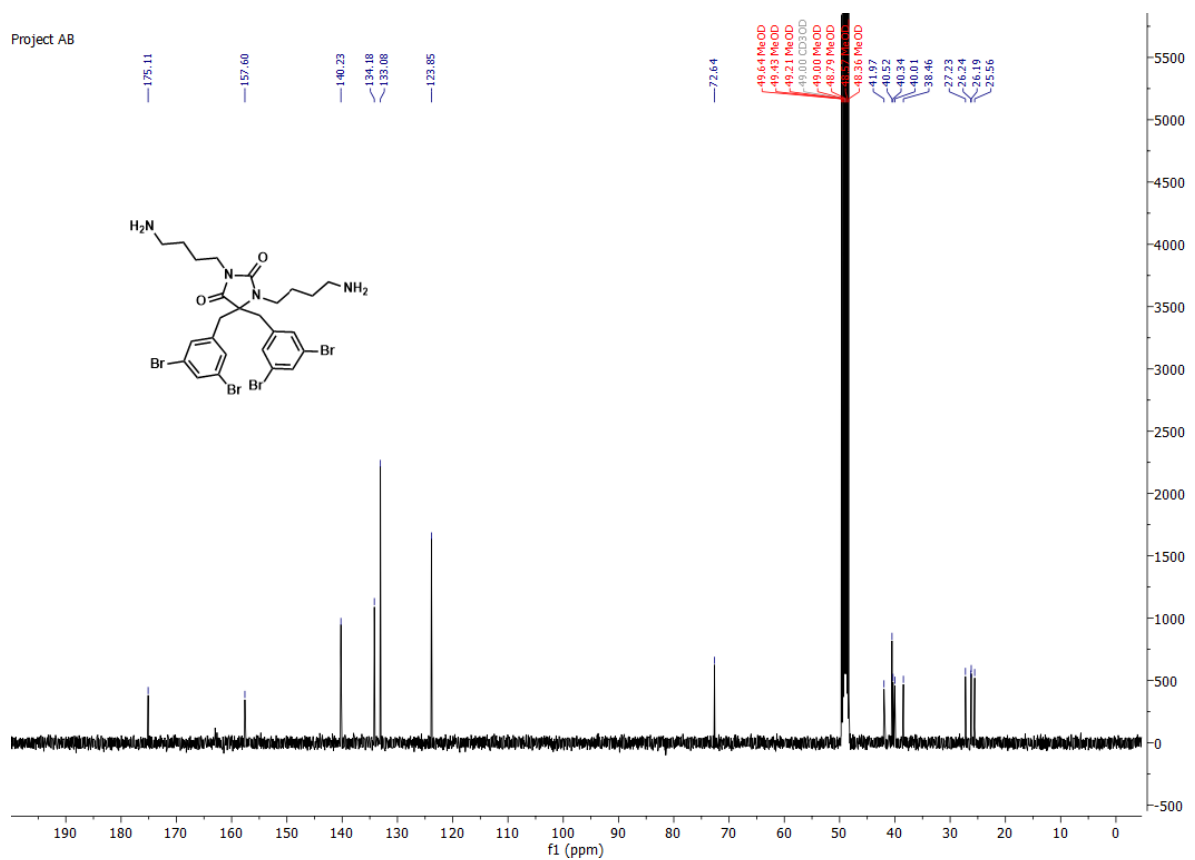


1,3-bis(4-aminobutyl)-5,5-bis(3,5-dibromobenzyl)imidazolidine-2,4-dion 6dA.

Project AB

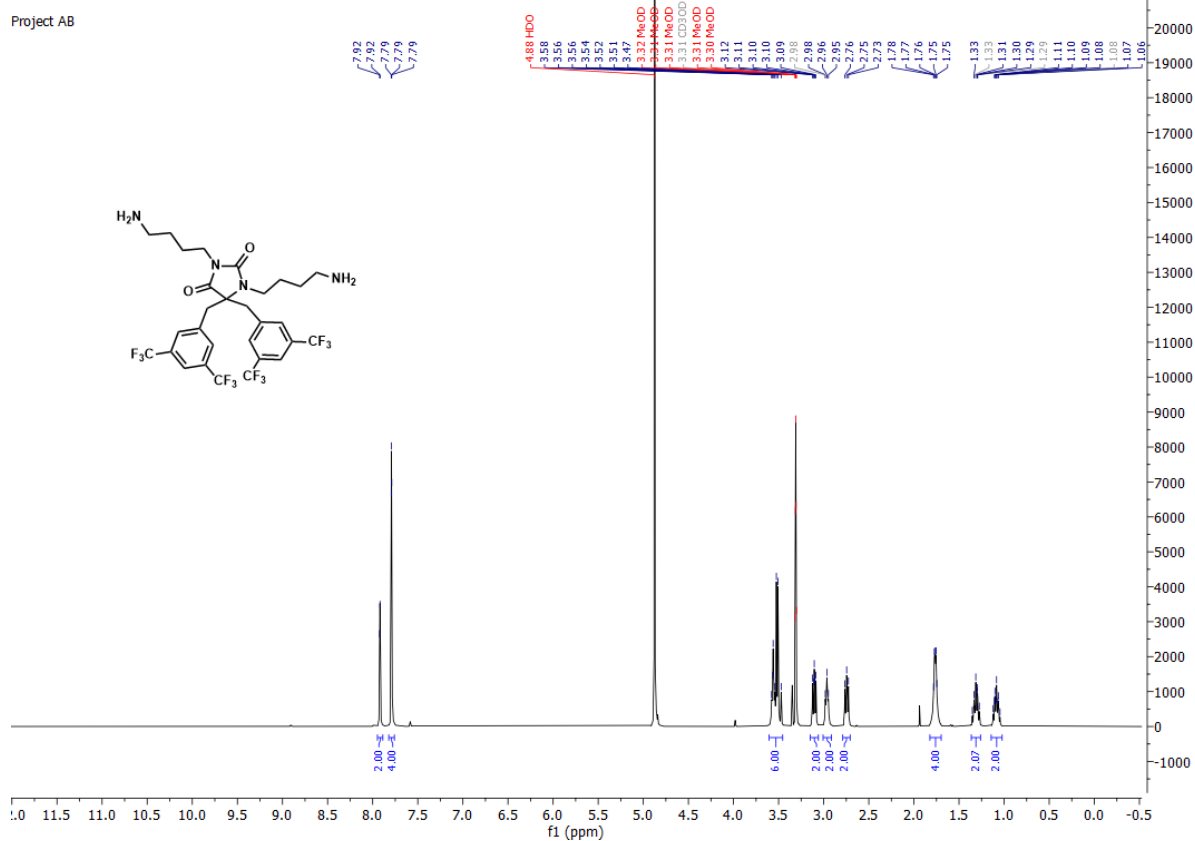


Project AB

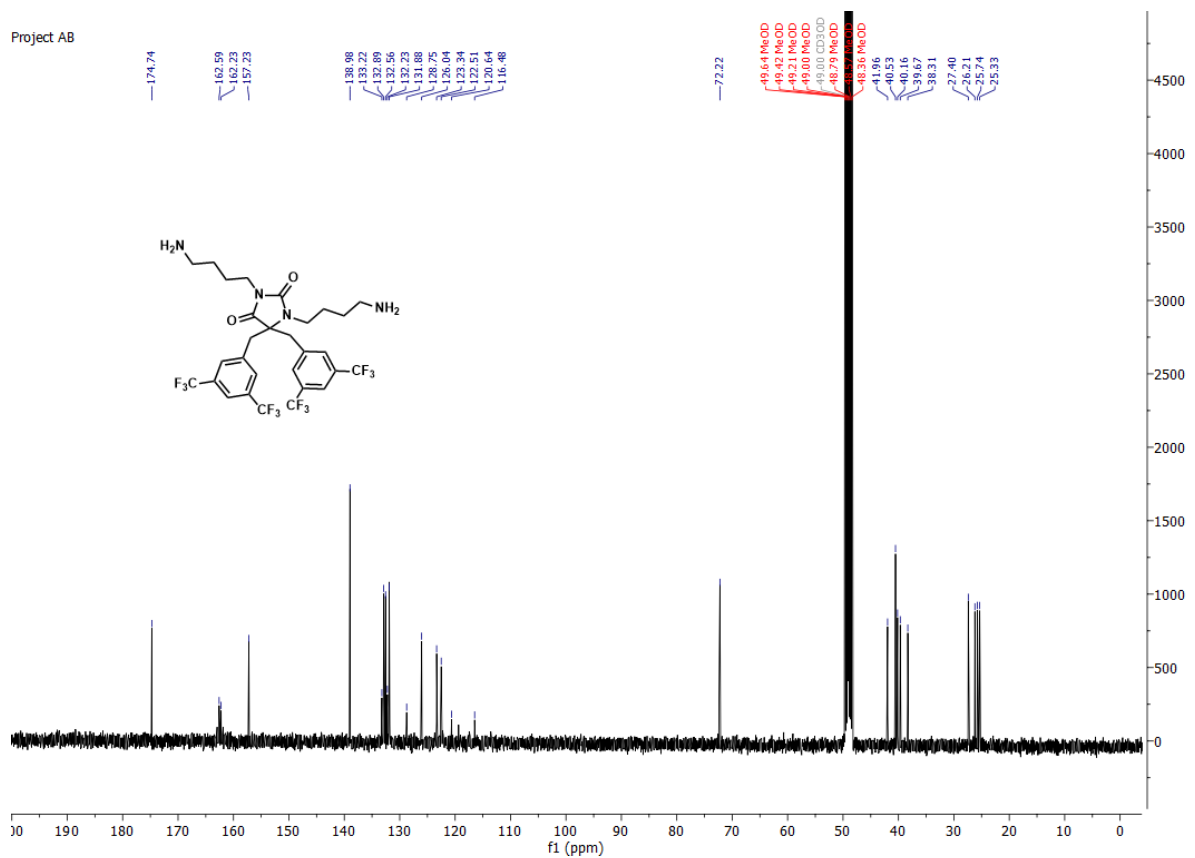


1,3-bis(4-aminobutyl)-5,5-bis(3,5-bis(trifluoromethyl)benzyl)imidazolidine-2,4-dione **6fA**.

Project AB



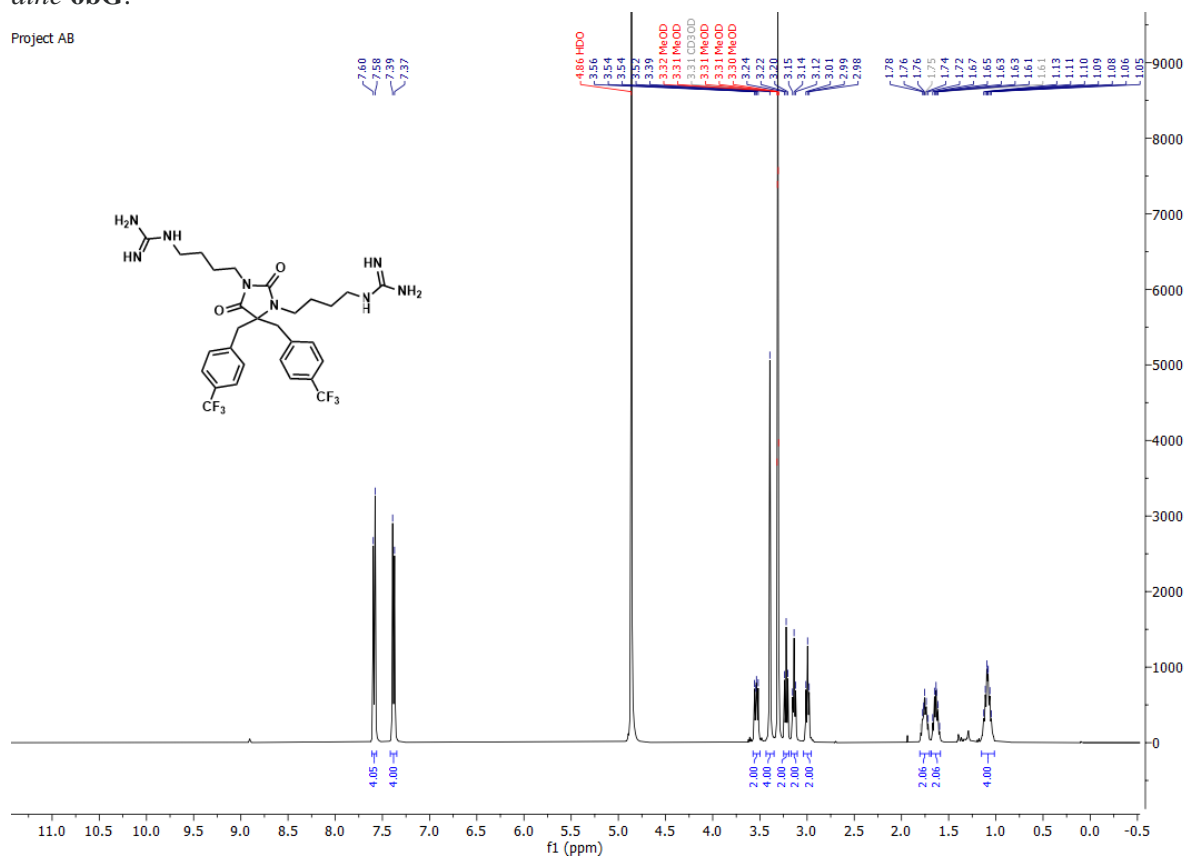
Project AB



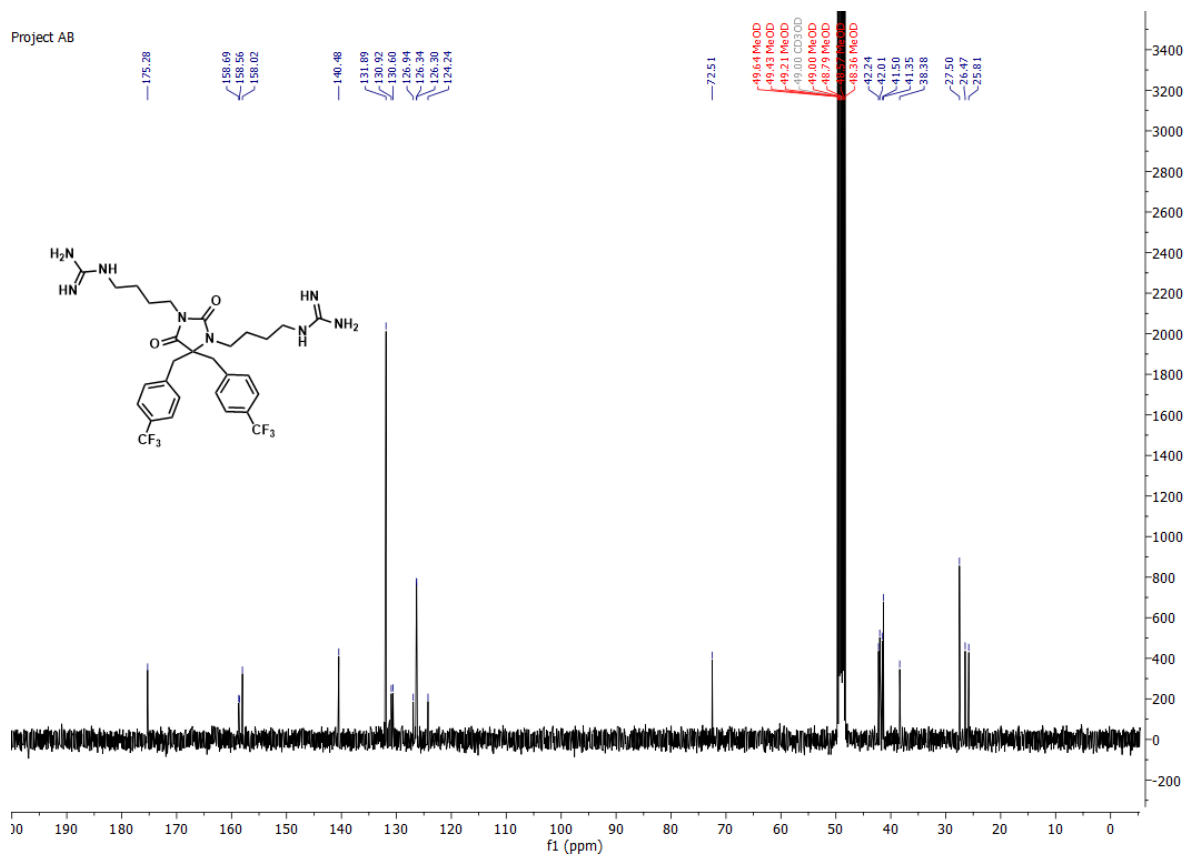
2.6 *N,N*-dialkylated hydantoin 6G

1,1'-((2,5-dioxo-4,4-bis(4-(trifluoromethyl)benzyl)imidazolidine-1,3-diyl)bis(butane-4,1-diyl))diguanidine **6bG**.

Project AB

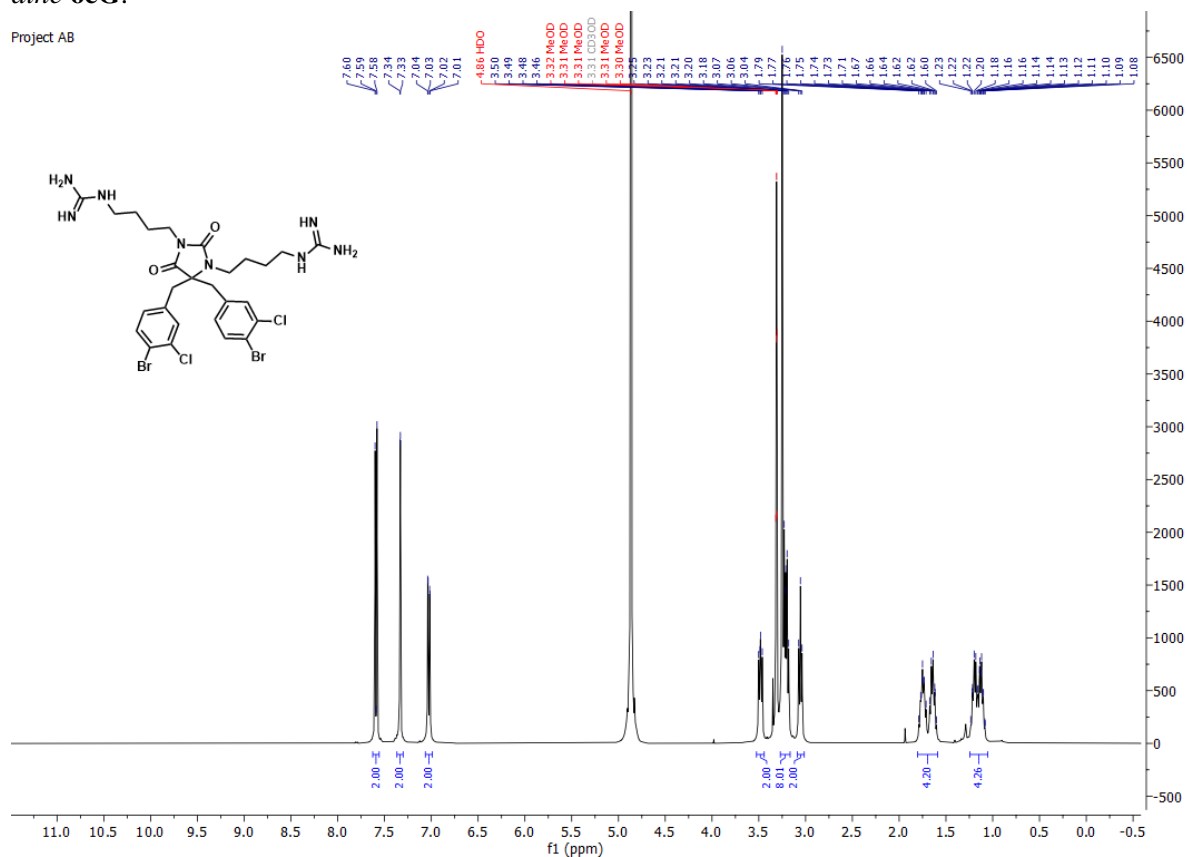


Project AB

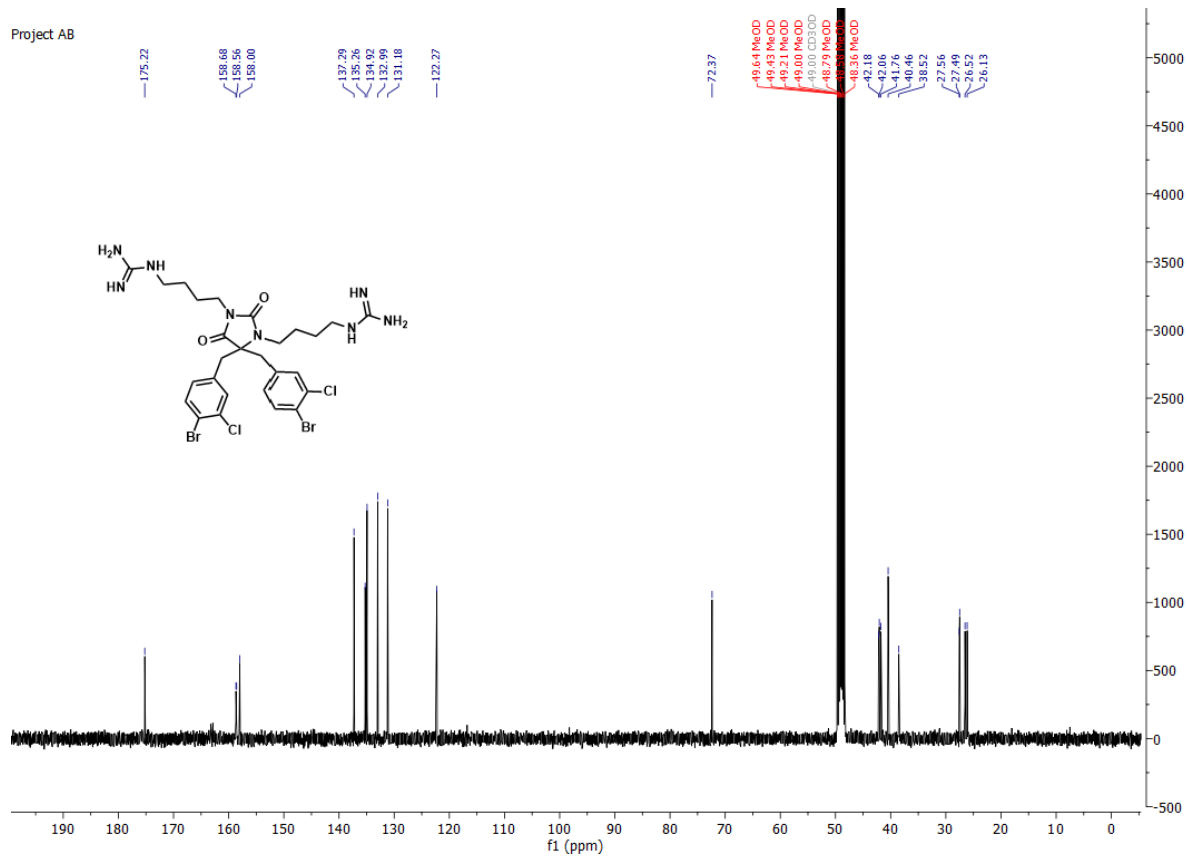


1,1'-((4,4-bis(4-bromo-3-chlorobenzyl)-2,5-dioximidazolidine-1,3-diyl)bis(butane-4,1-diyl)diguani-
dine **6cG**.

Project AB



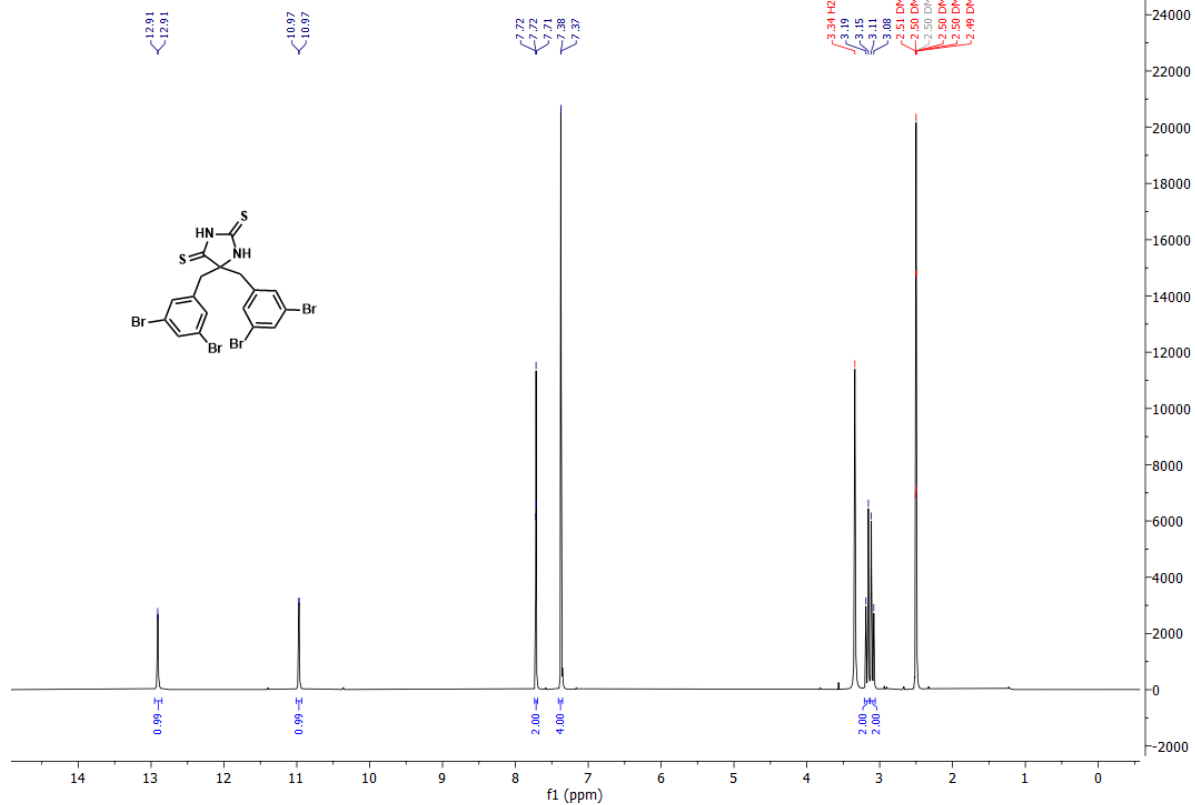
Project AB



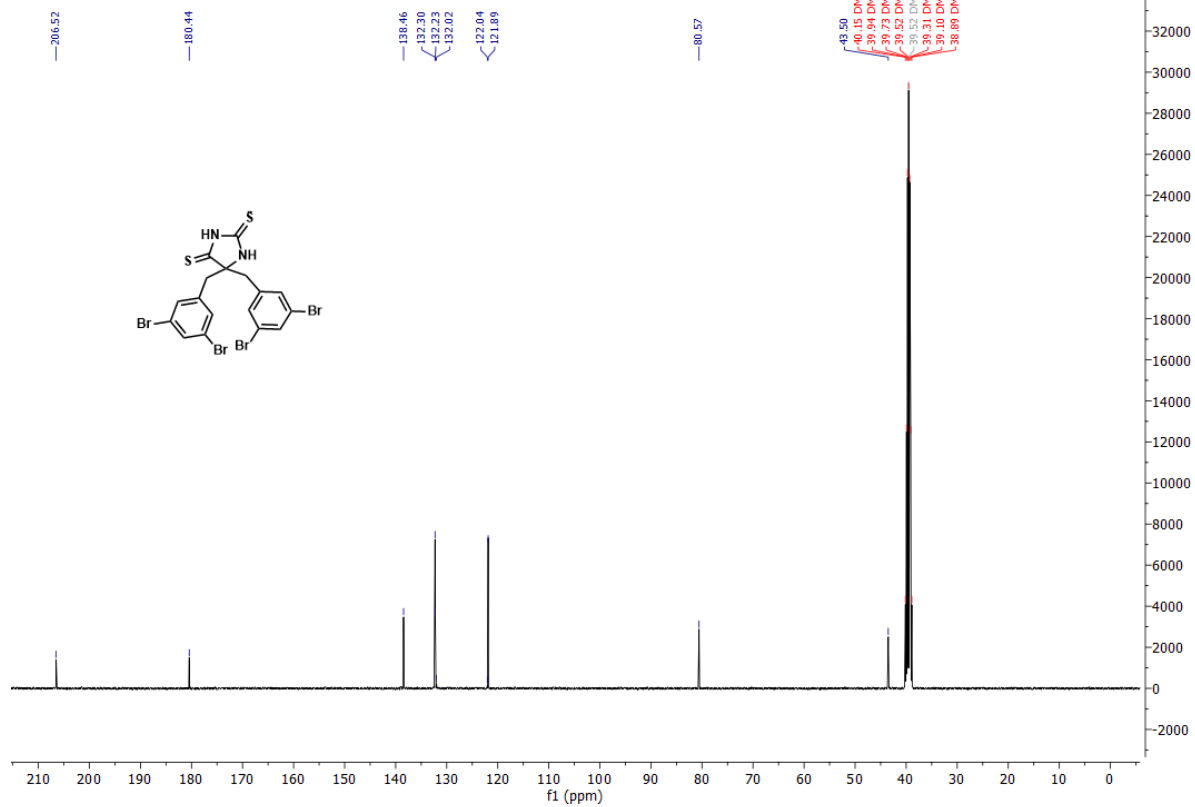
2.7 2,4-Dithiohydantoin core

5,5-bis(3,5-dibromobenzyl)imidazolidine-2,4-dithione **16**.

Project AB



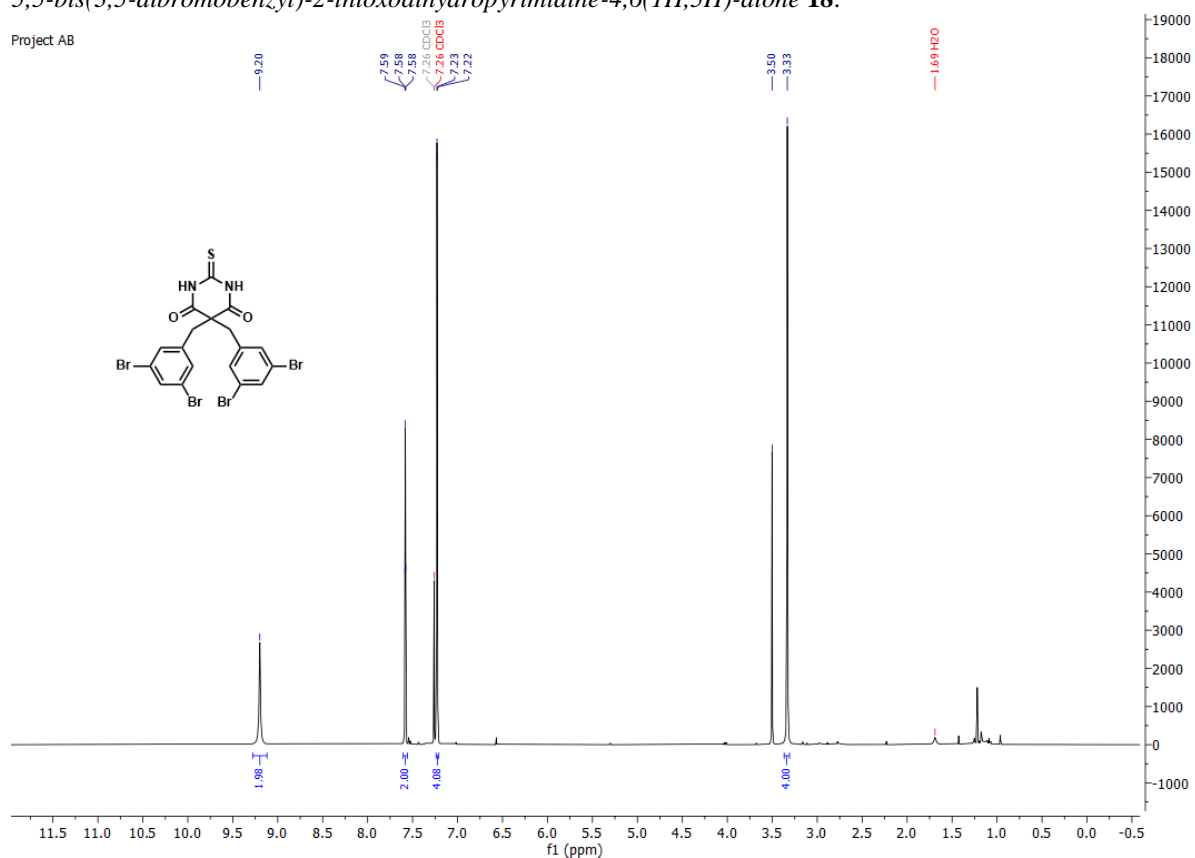
Project AB



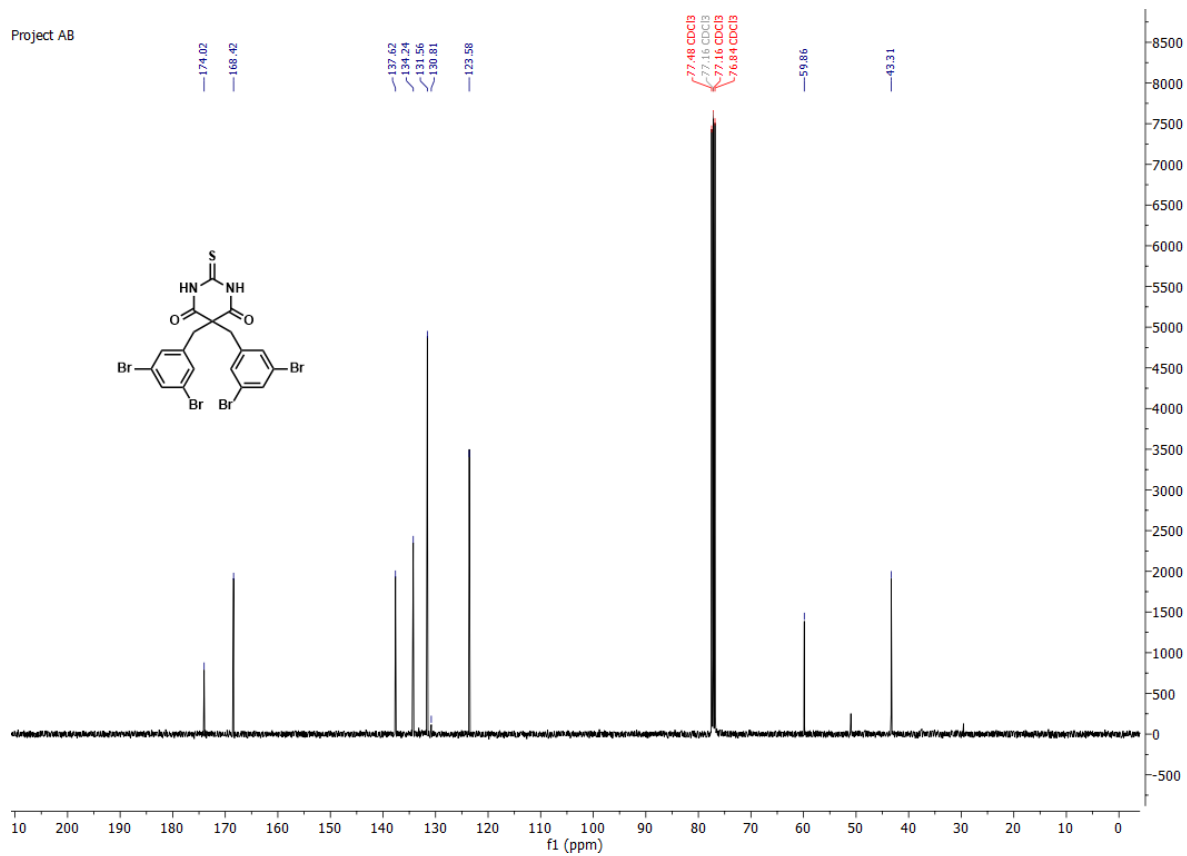
2.8 2-Thiobarbituric acid core

5,5-bis(3,5-dibromobenzyl)-2-thioxodihydropyrimidine-4,6(1H,5H)-dione **18**.

Project AB

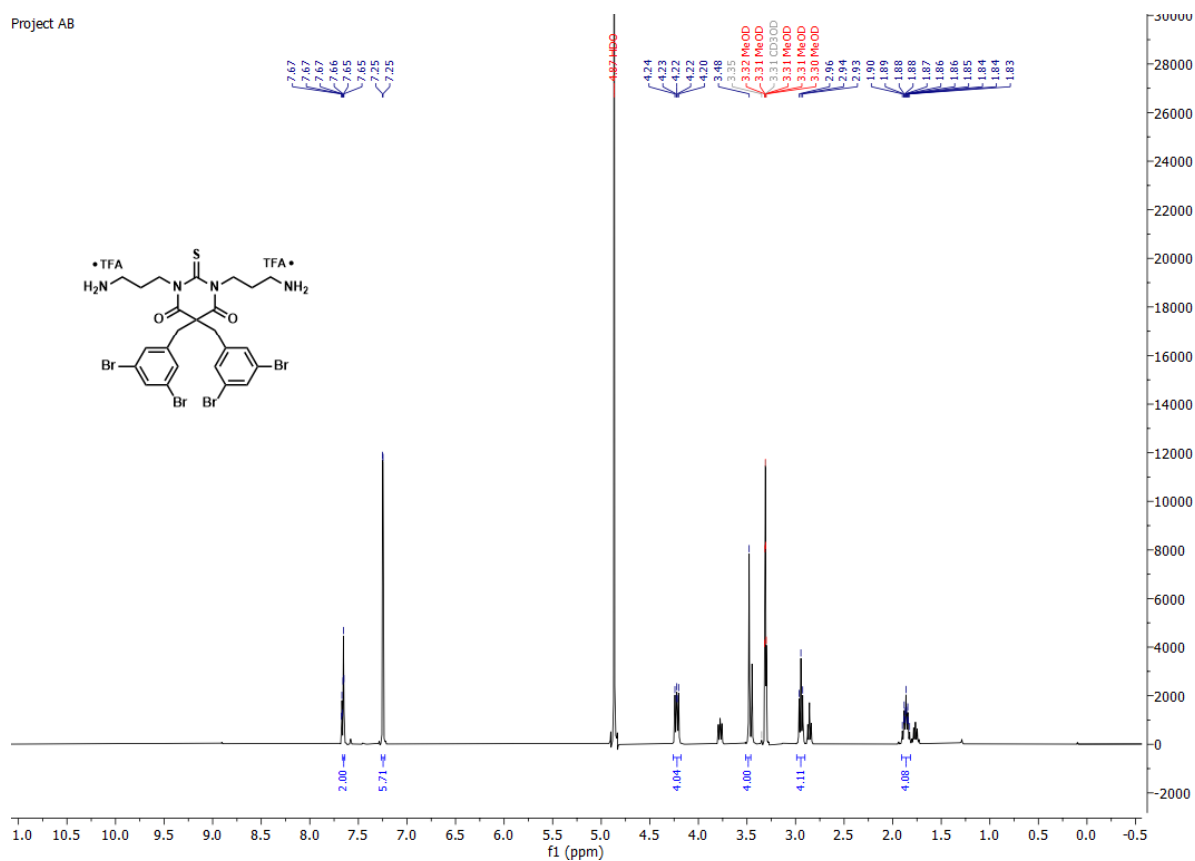


Project AB

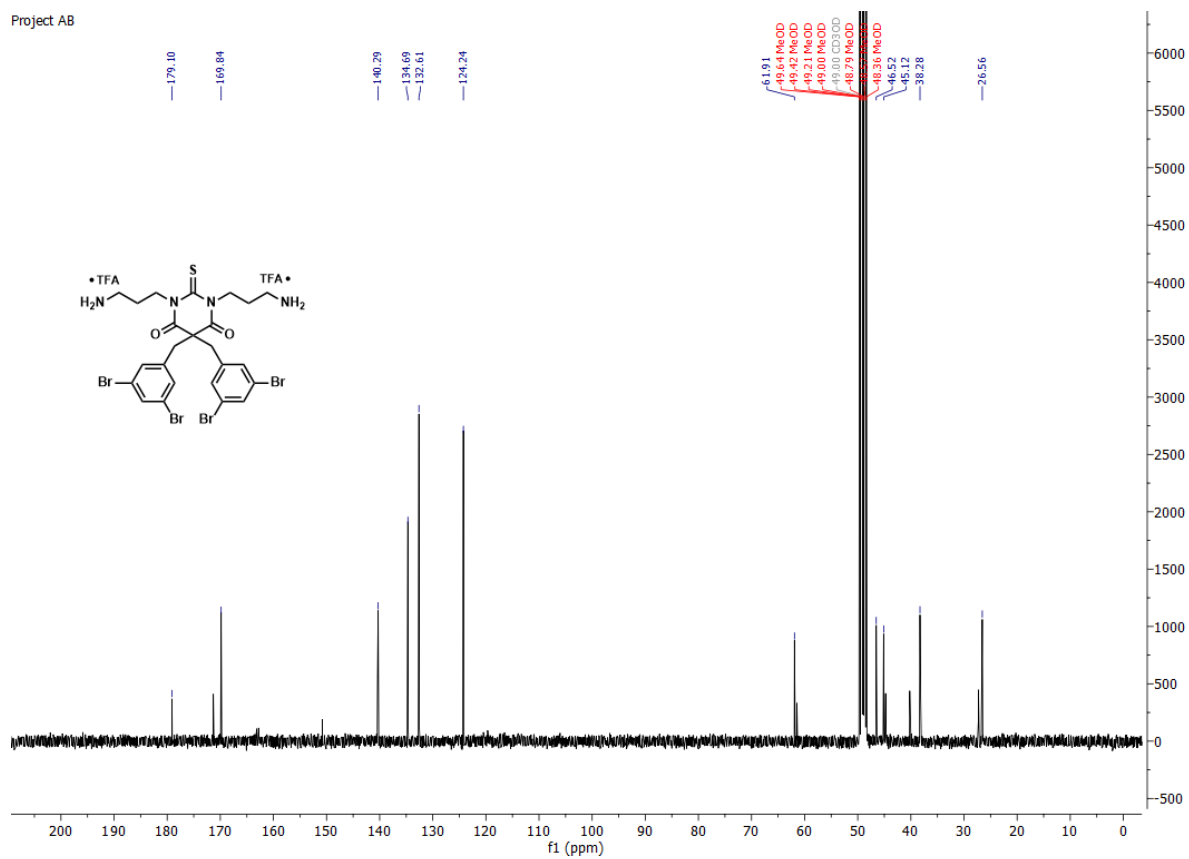


1,3-bis(3-aminopropyl)-5,5-bis(3,5-dibromobenzyl)-2-thioxodihydropyrimidine-4,6(1H,5H)-dione **5A**.

Project AB

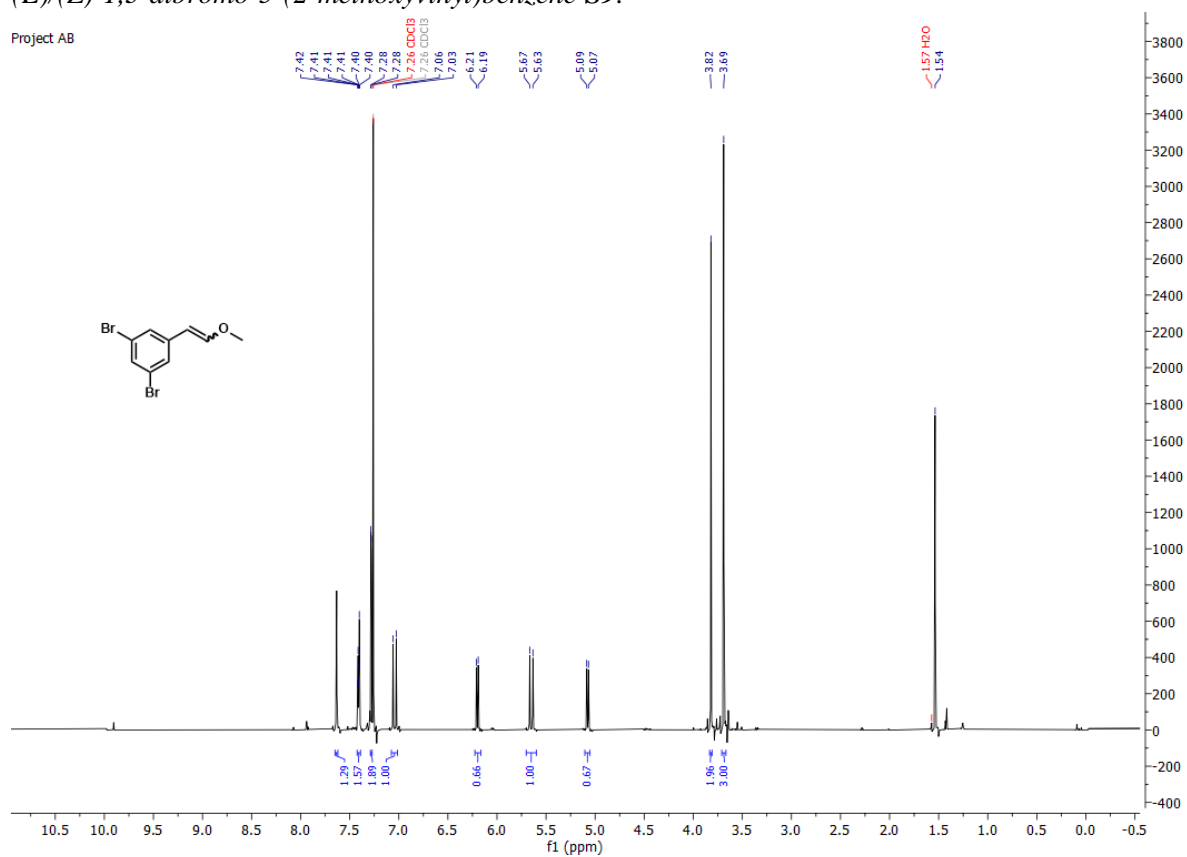


Project AB

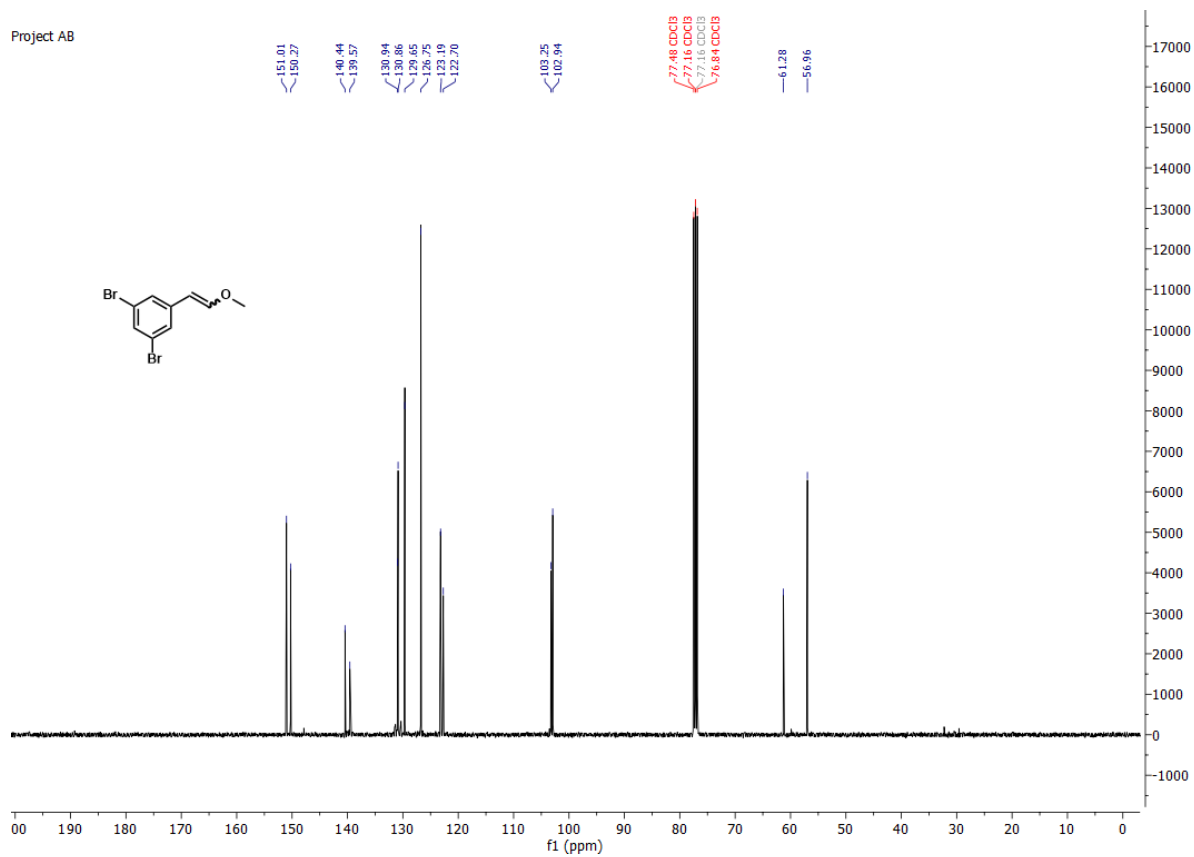


2.9 4-imidazolidin-2-one and its constitutional isomers
(E)/(Z)-1,3-dibromo-5-(2-methoxyvinyl)benzene **S9**.

Project AB

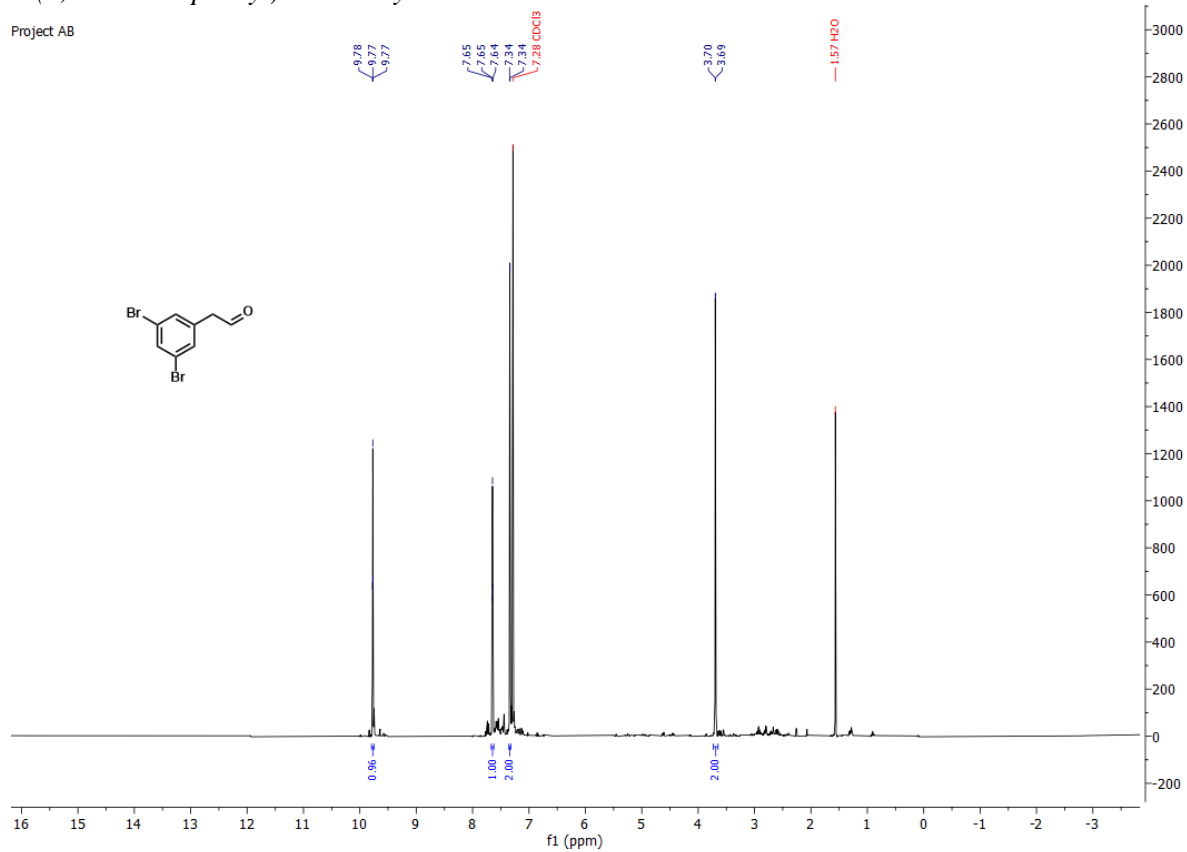


Project AB

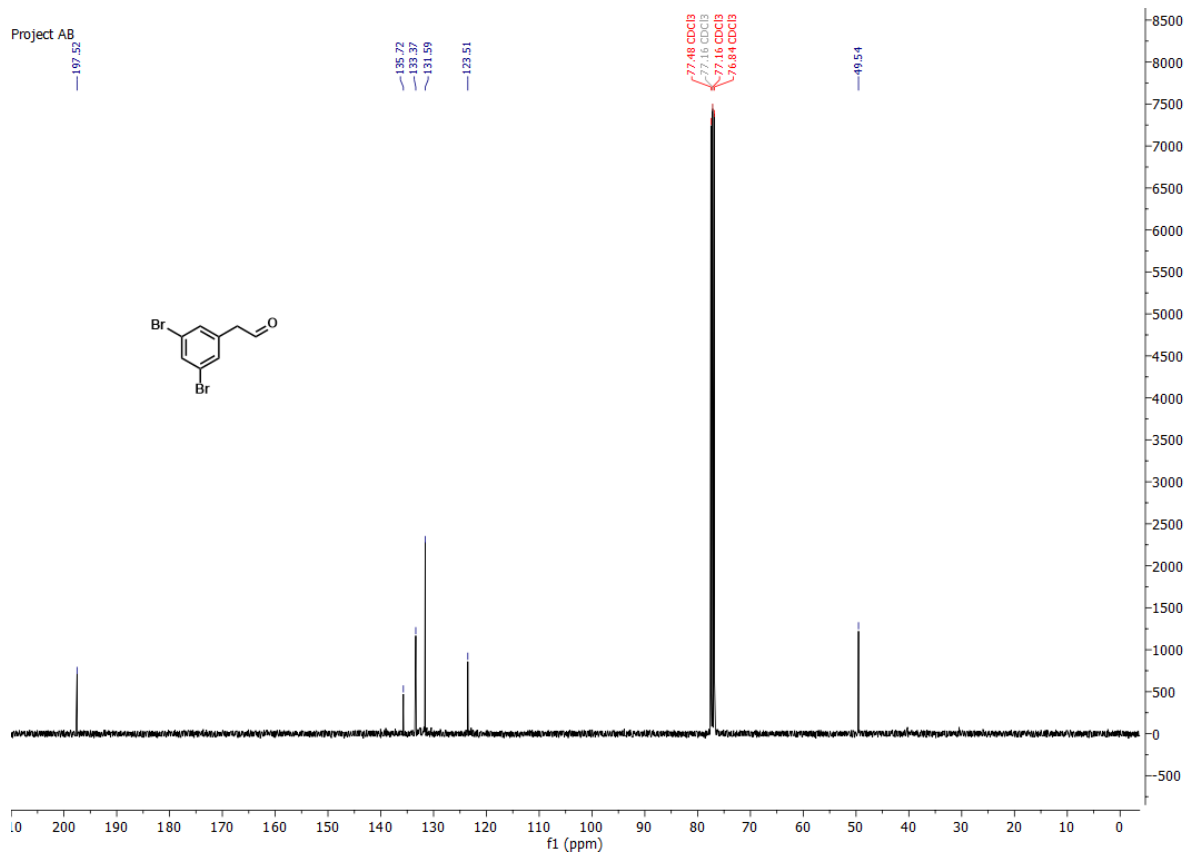


2-(3,5-dibromophenyl)acetaldehyde **11**.

Project AB

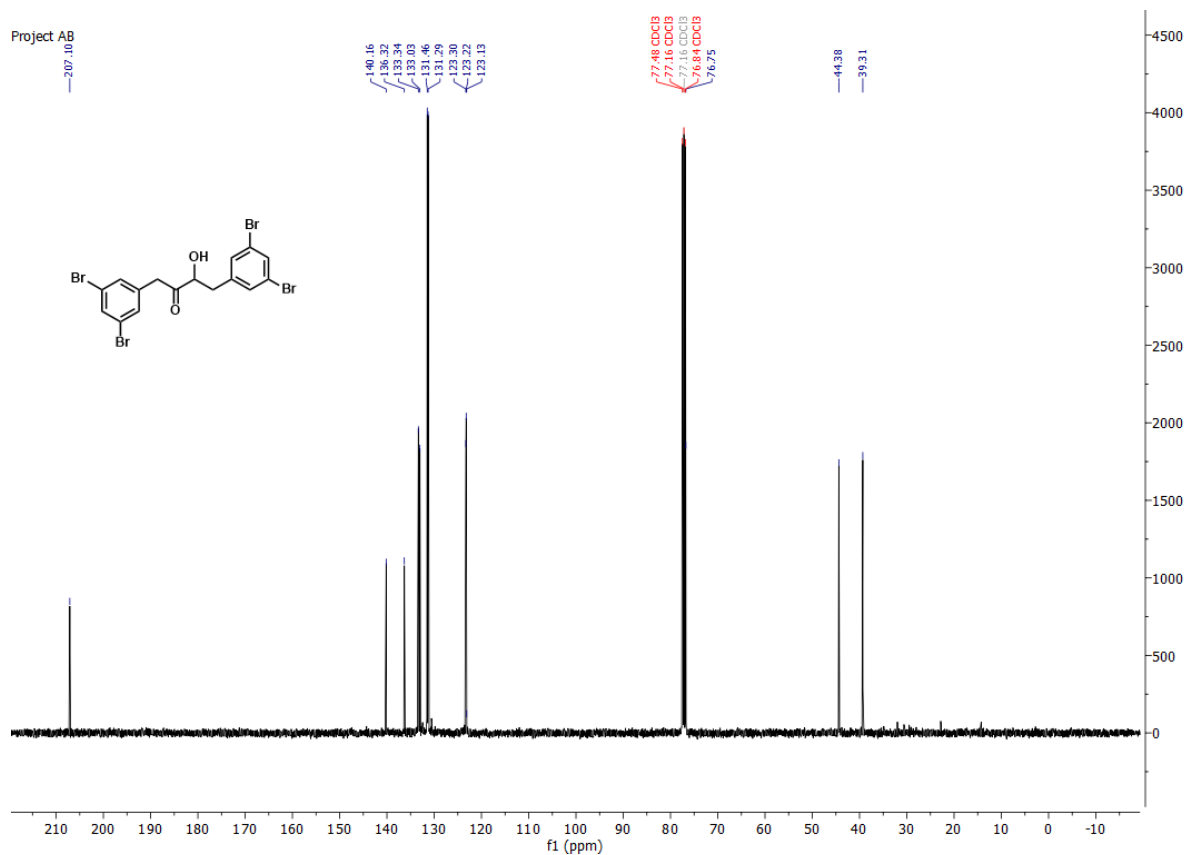
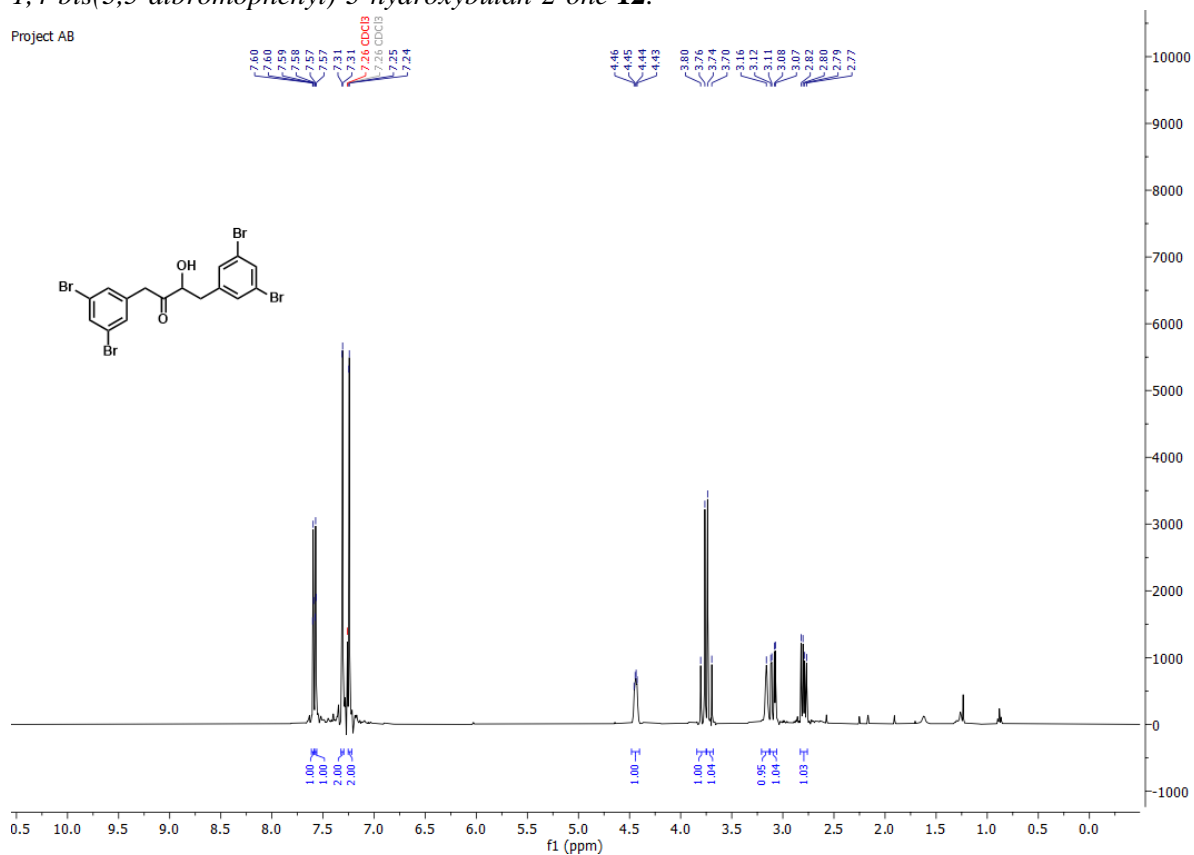


Project AB



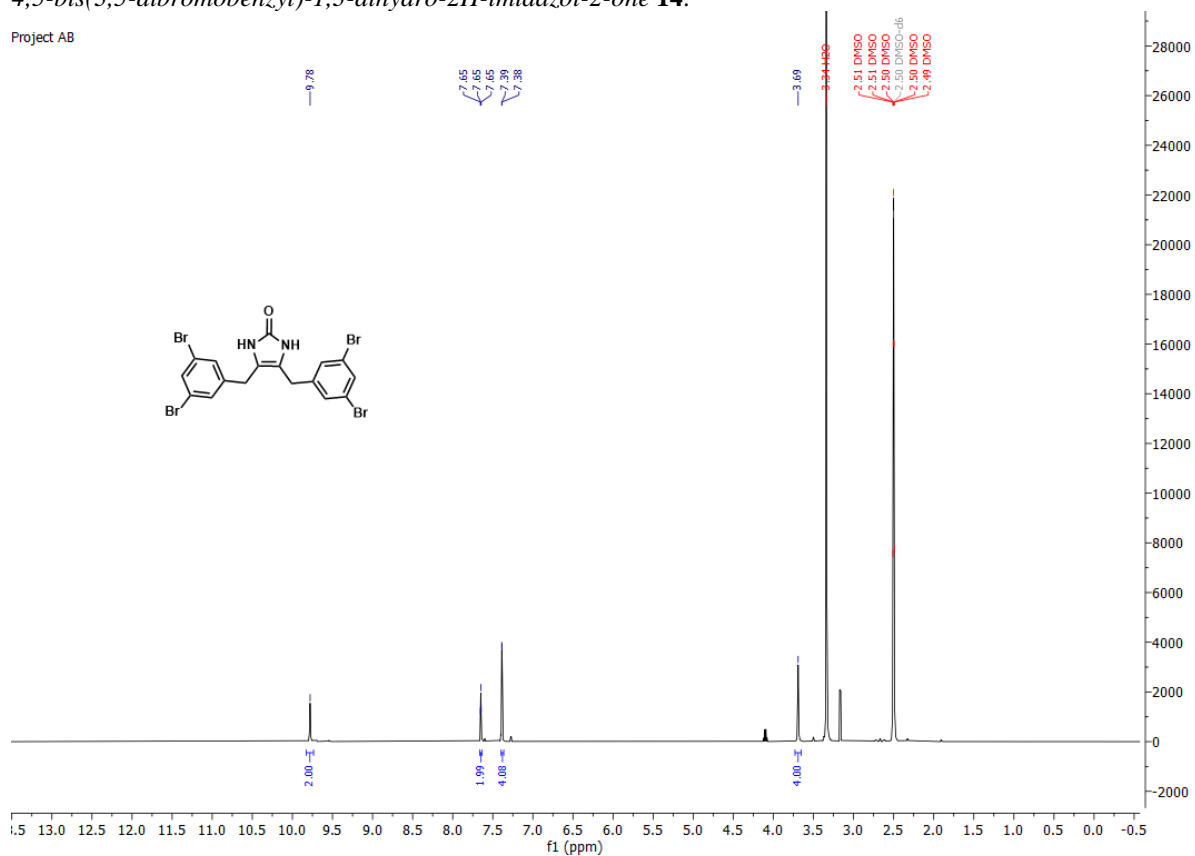
1,4-bis(3,5-dibromophenyl)-3-hydroxybutan-2-one 12.

Project AB

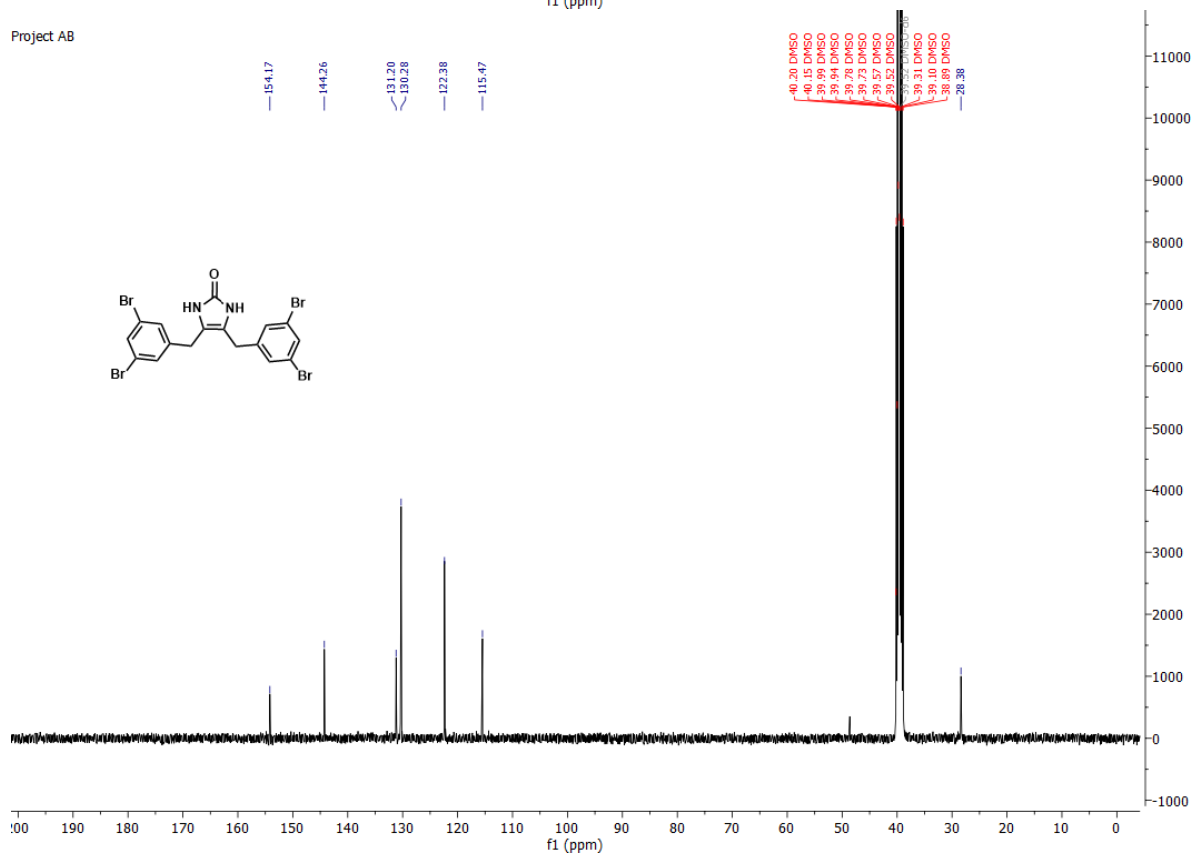


4,5-bis(3,5-dibromobenzyl)-1,3-dihydro-2H-imidazol-2-one **14**.

Project AB

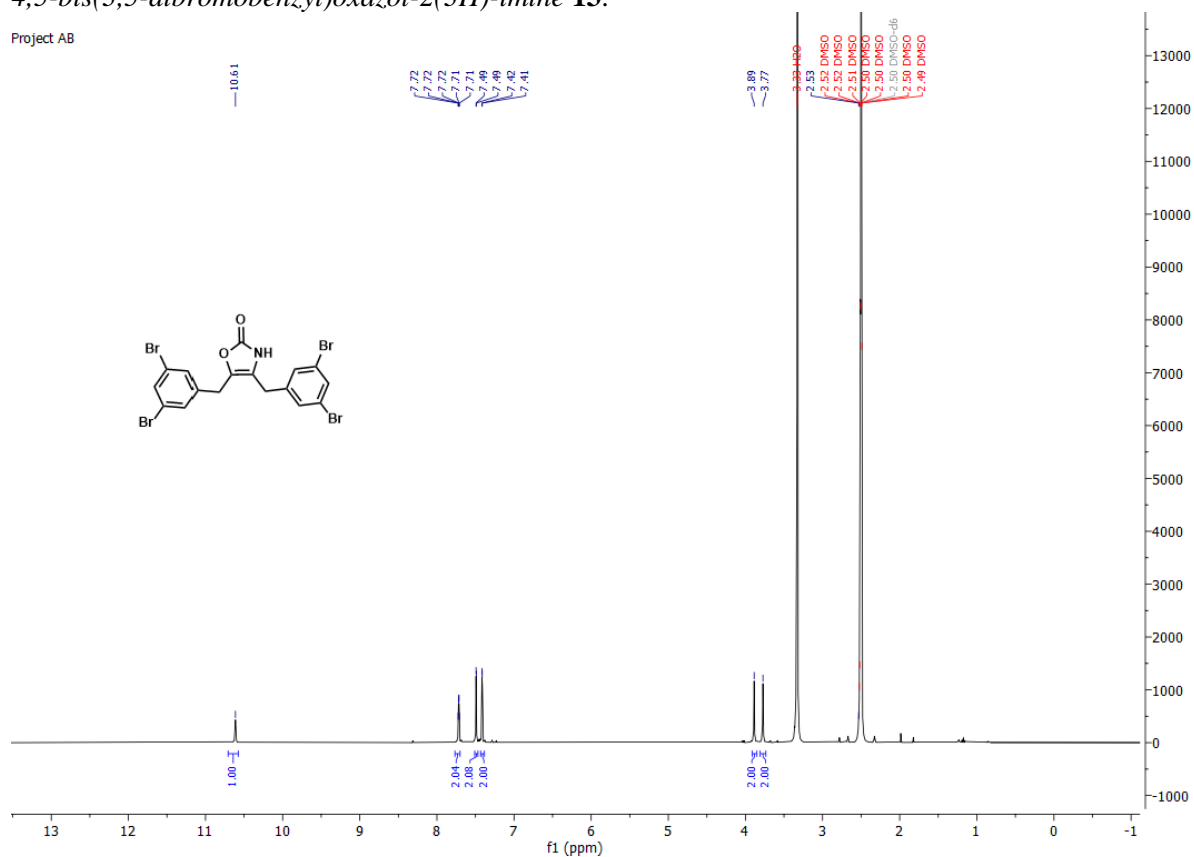


Project AB

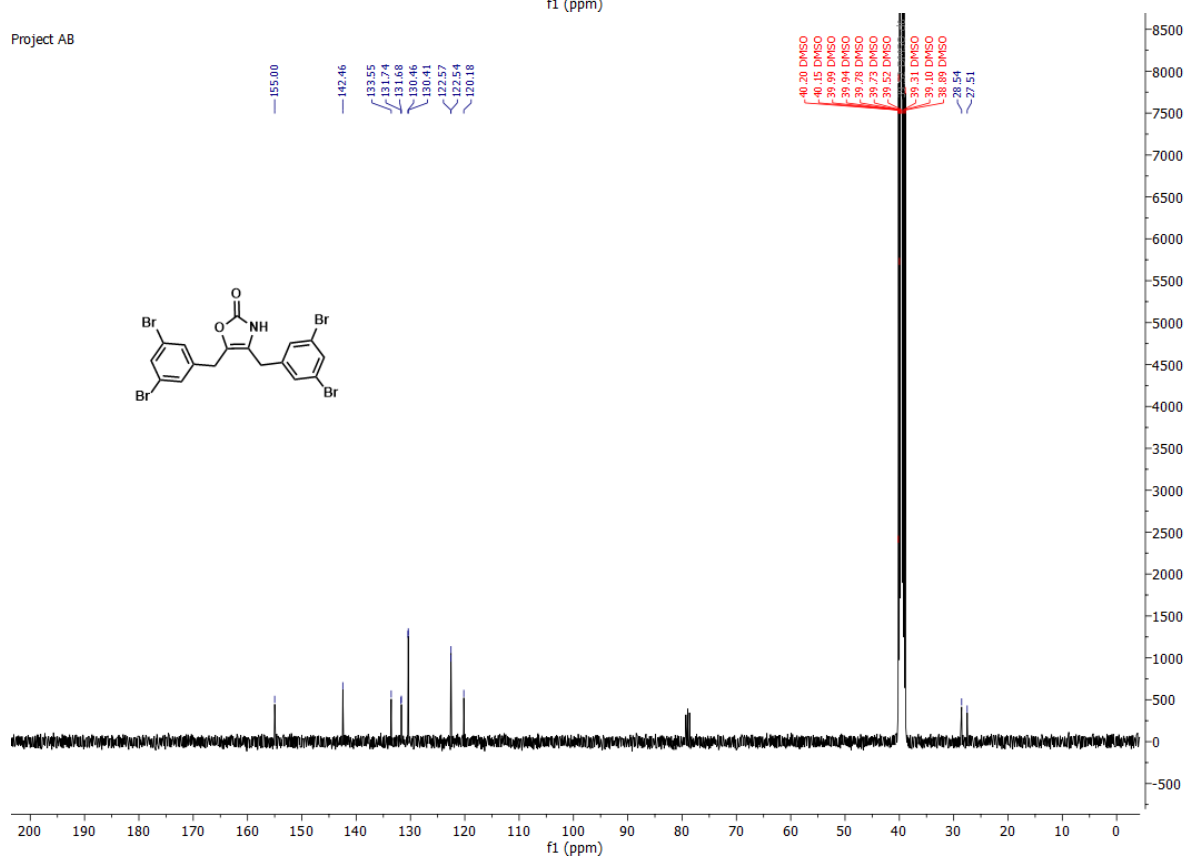


4,5-bis(3,5-dibromobenzyl)oxazol-2(3H)-imine **13**.

Project AB

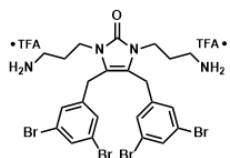
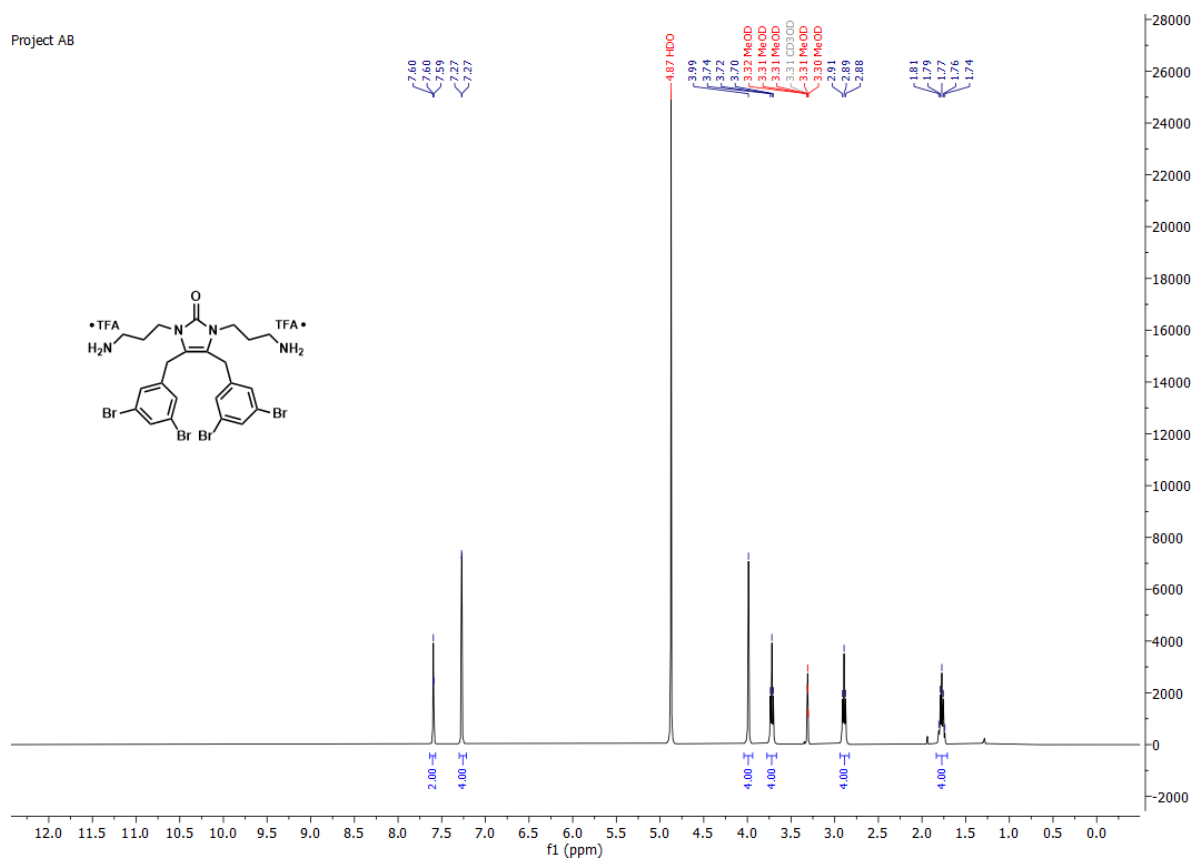


Project AB

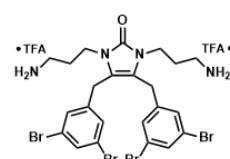
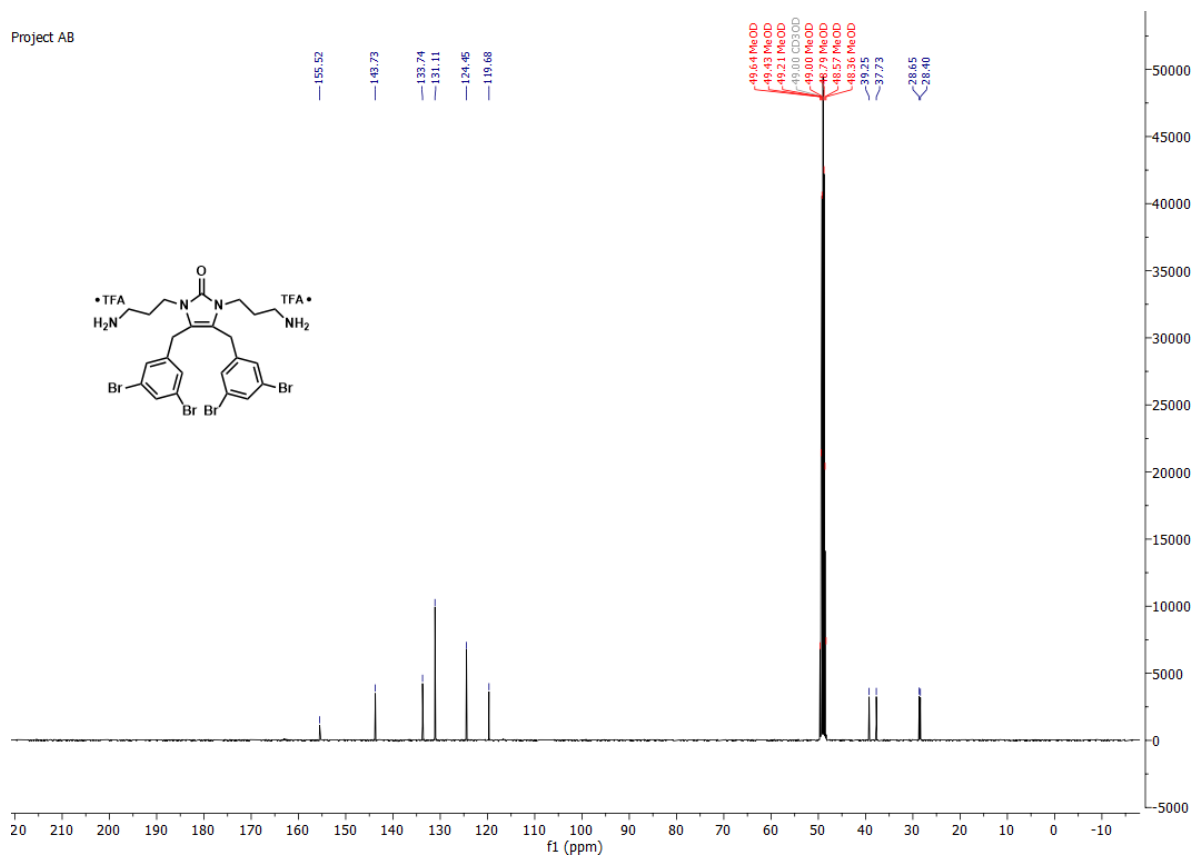


1,3-bis(3-aminopropyl)-4,5-bis(3,5-dibromobenzyl)-1,3-dihydro-2H-imidazol-2-one 3A.

Project AB

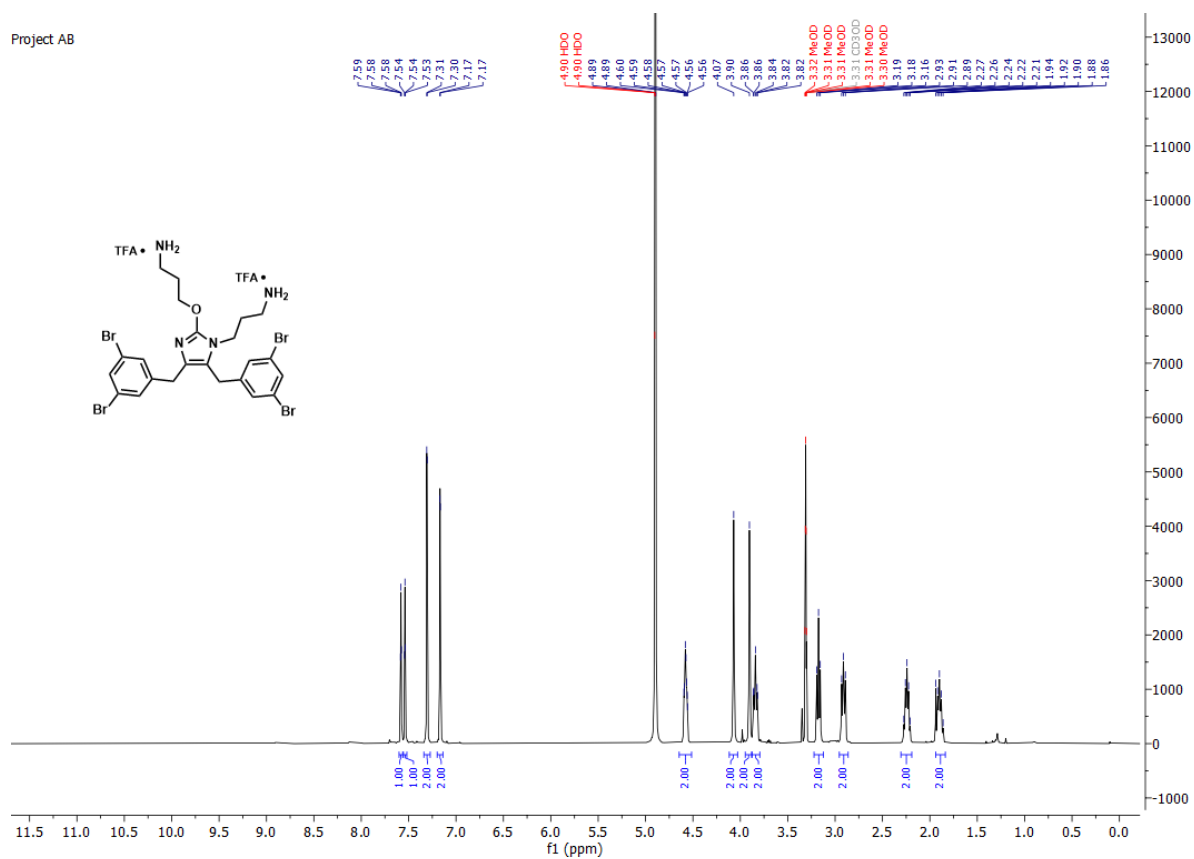


Project AB

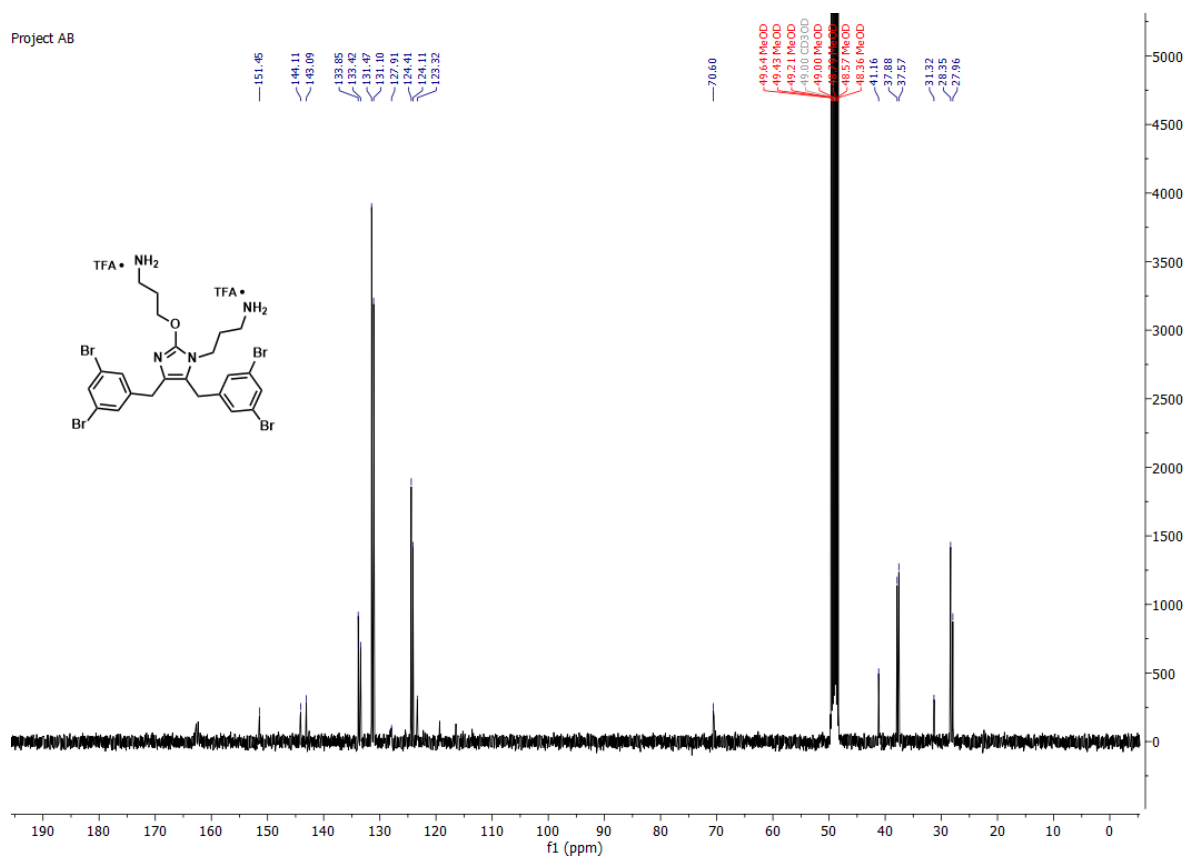


3-(2-(3-aminopropoxy)-4,5-bis(3,5-dibromobenzyl)-1H-imidazol-1-yl)propan-1-amine **15A**.

Project AB



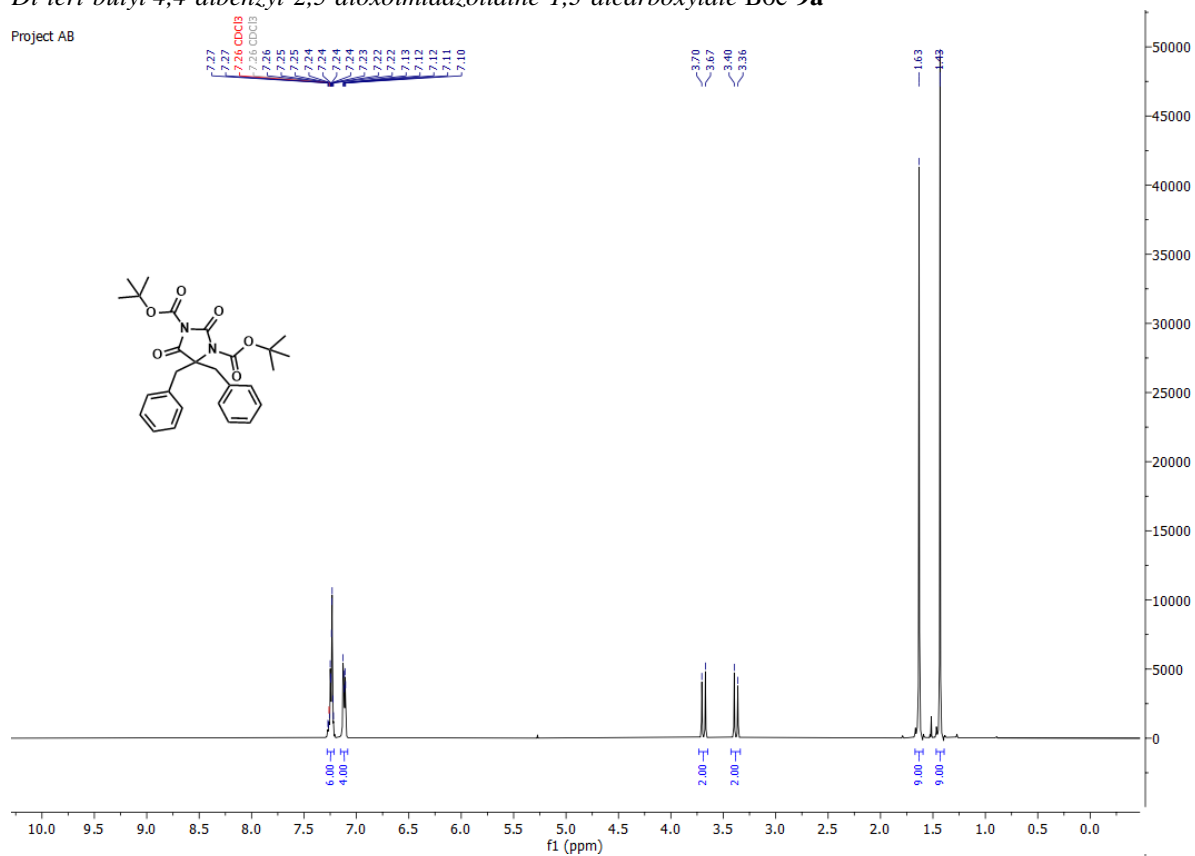
Project AB



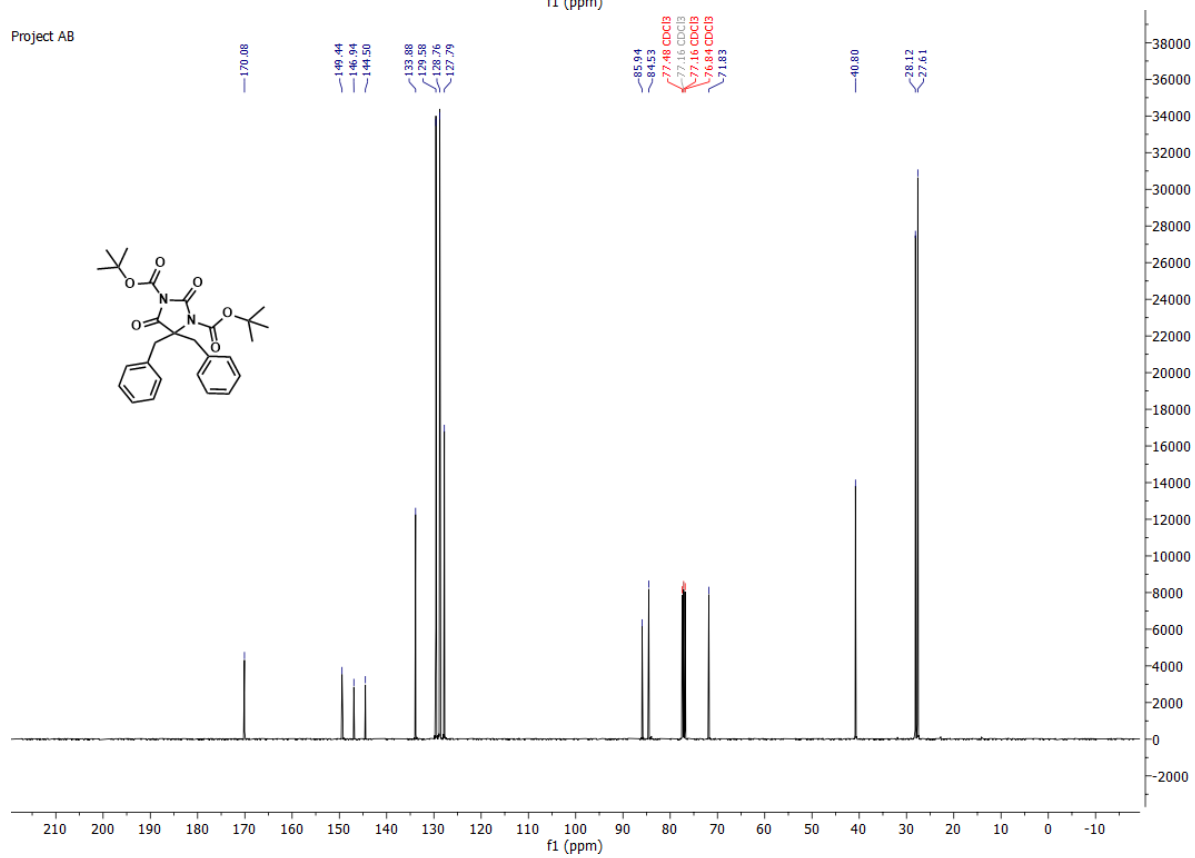
2.10 4-imidazolidin-2-one via *N*-acyliminium ion rearrangement

Di-tert-butyl 4,4-dibenzyl-2,5-dioximidazolidine-1,3-dicarboxylate Boc-9a

Project AB

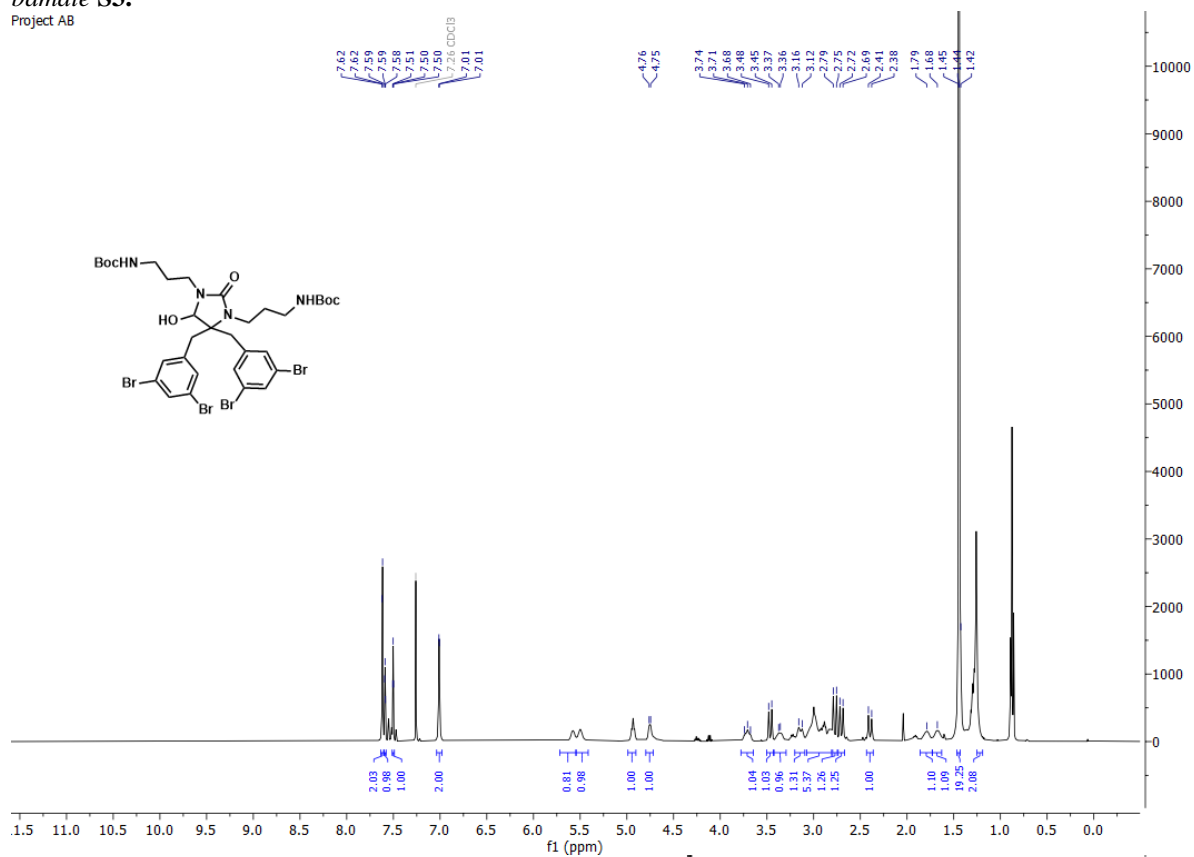


Project AB

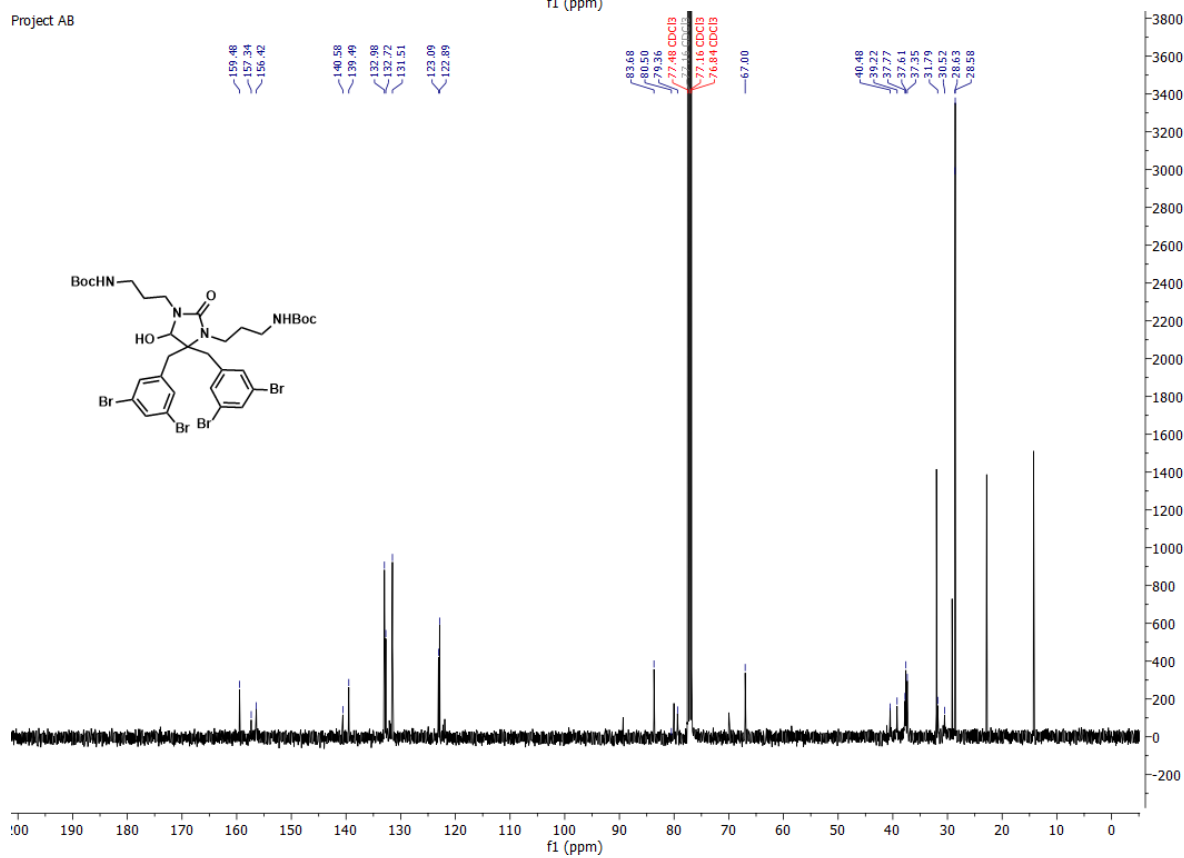


Di-tert-butyl ((4,4-bis(3,5-dibromobenzyl)-5-hydroxy-2-oximidazolidine-1,3-diyl)bis(propane-3,1-diyl))dicarbamate S3.

Project AB

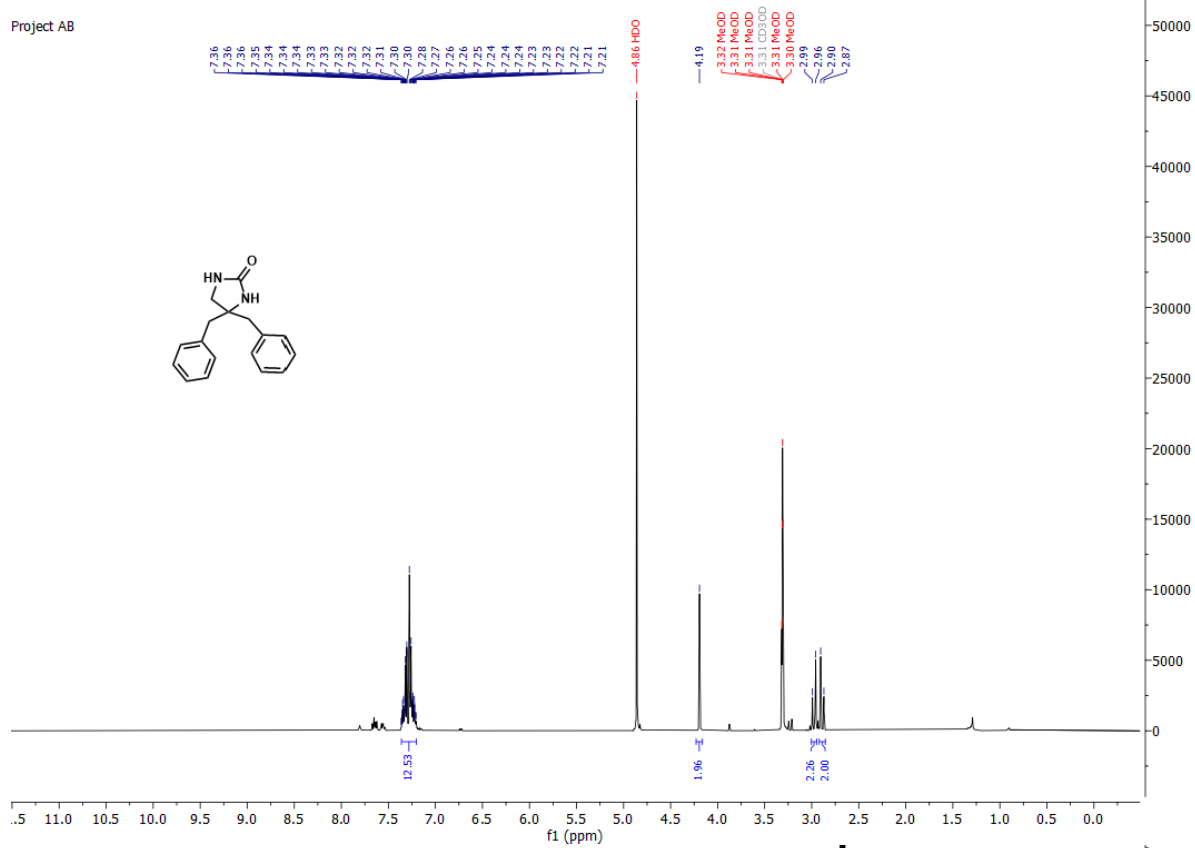


Project AB

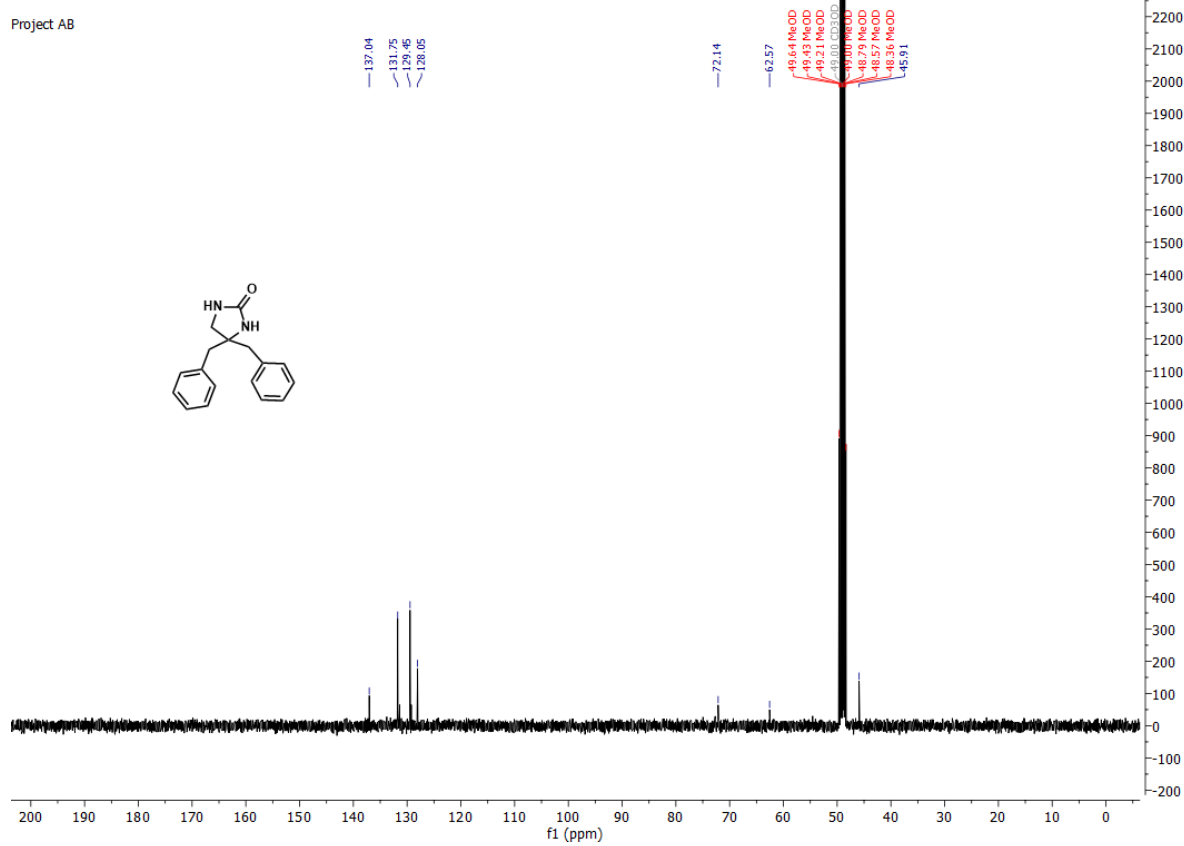


4,4-dibenzylimidazolidin-2-one S4.

Project AB

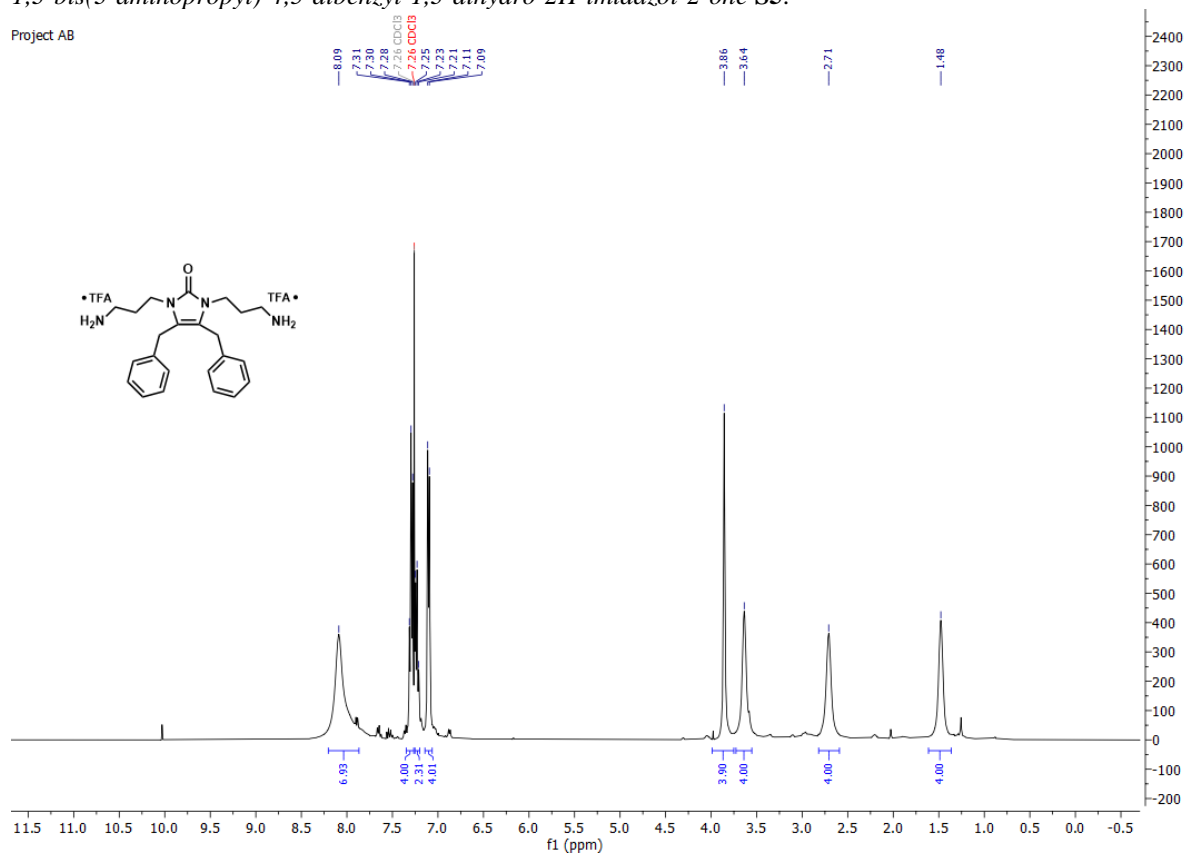


Project AB

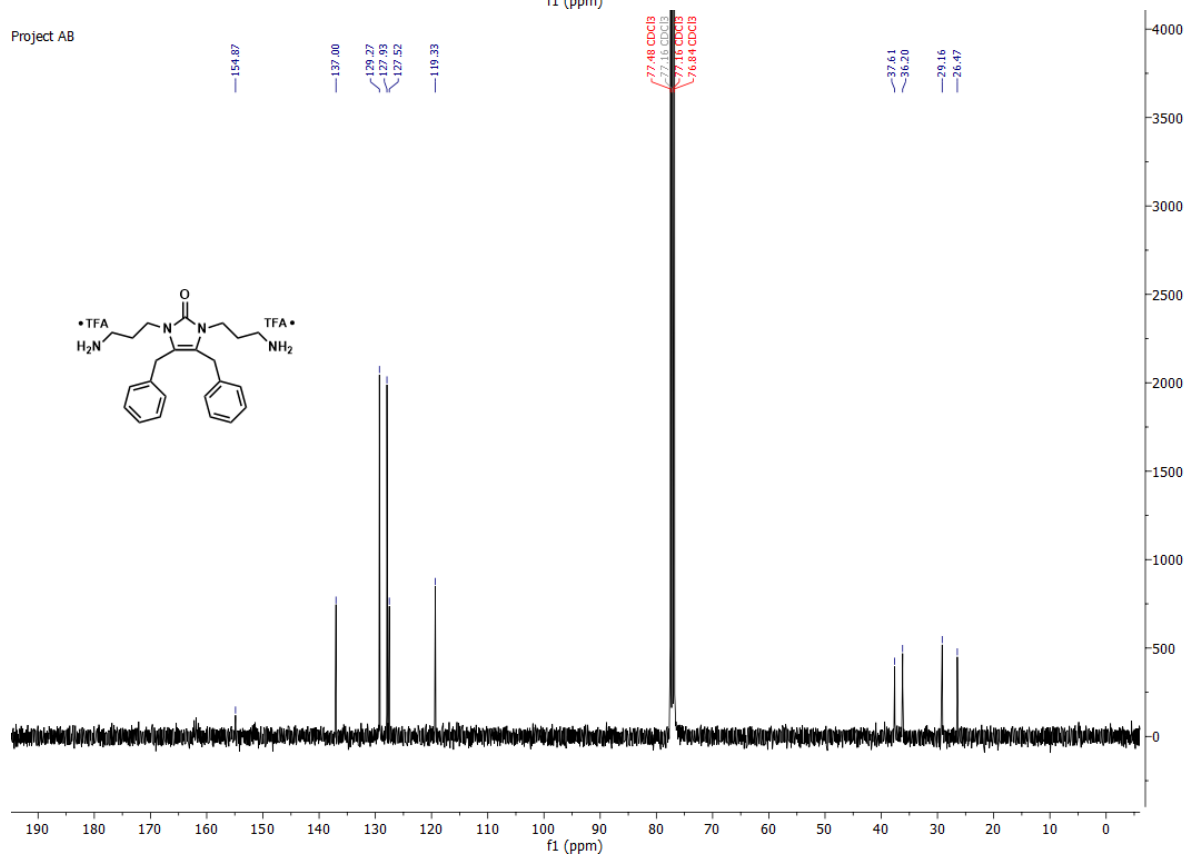


1,3-bis(3-aminopropyl)-4,5-dibenzyl-1,3-dihydro-2H-imidazol-2-one S5.

Project AB



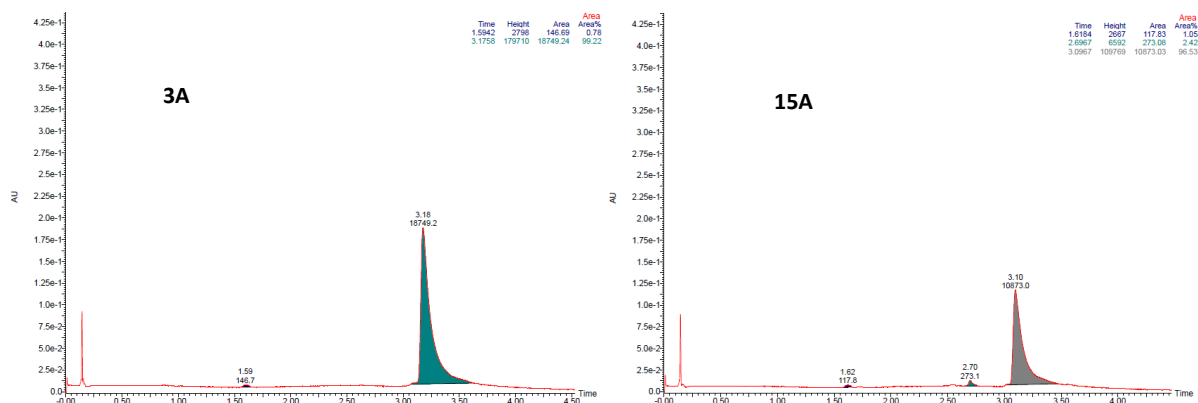
Project AB



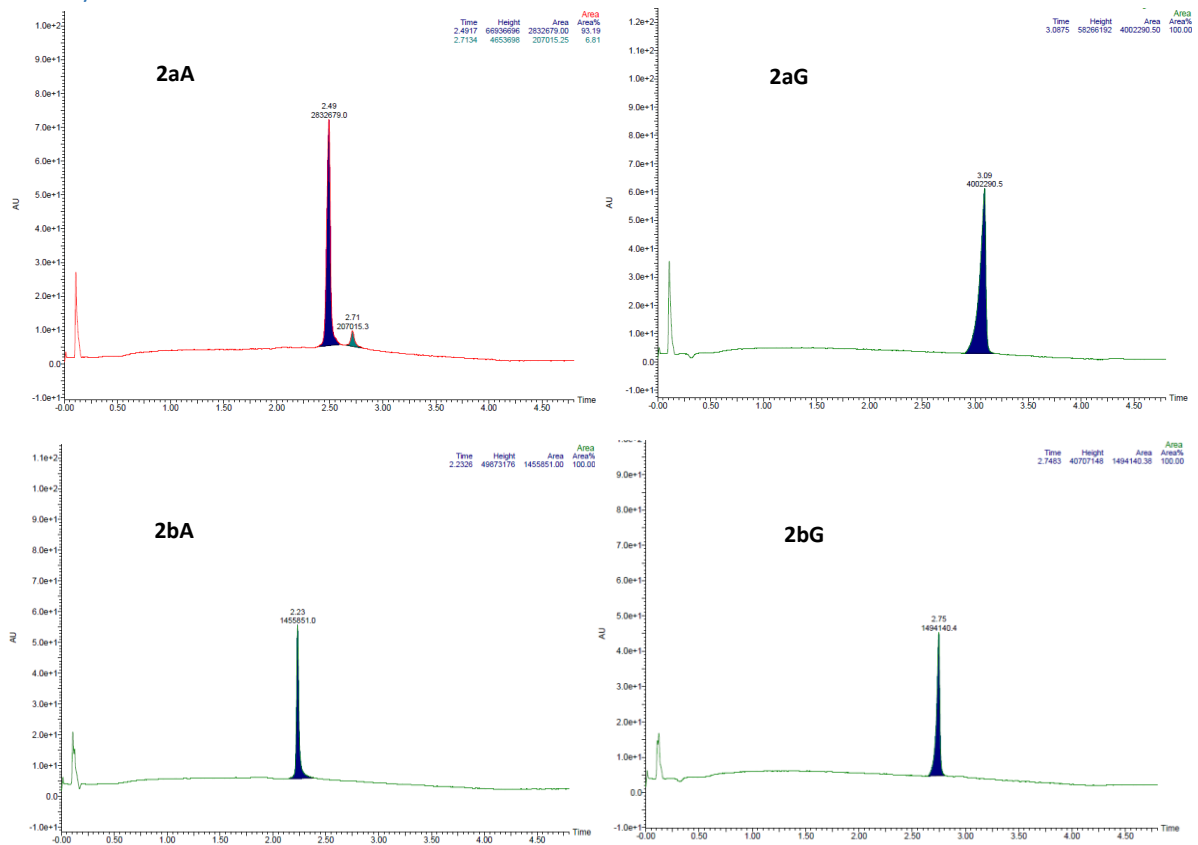
3. SFC traces

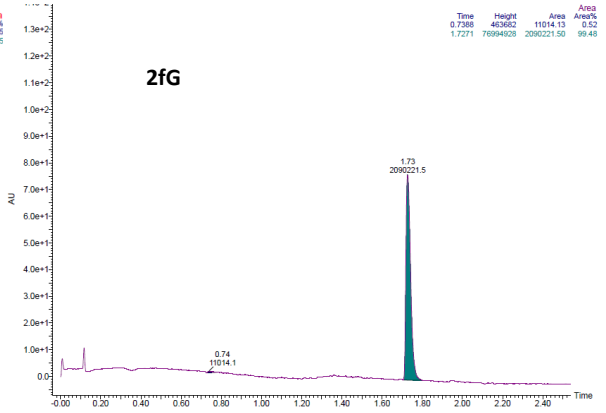
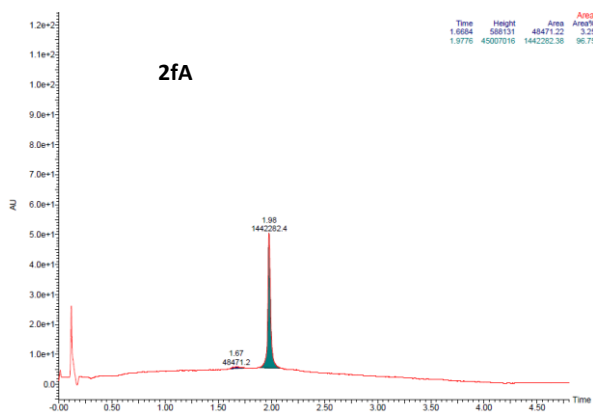
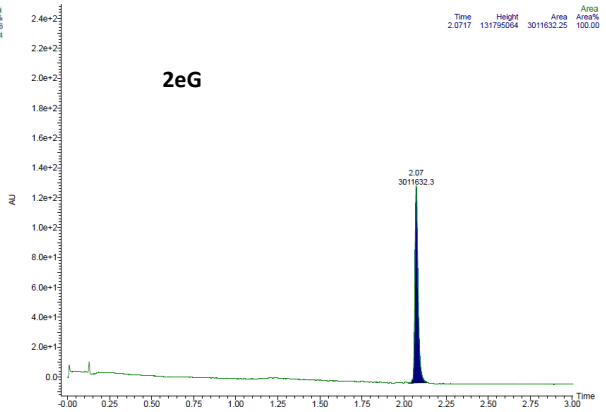
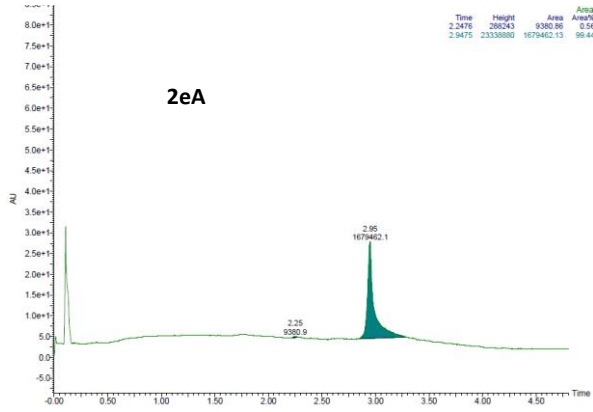
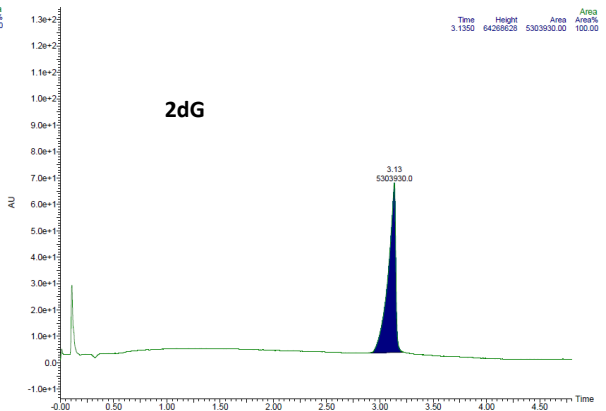
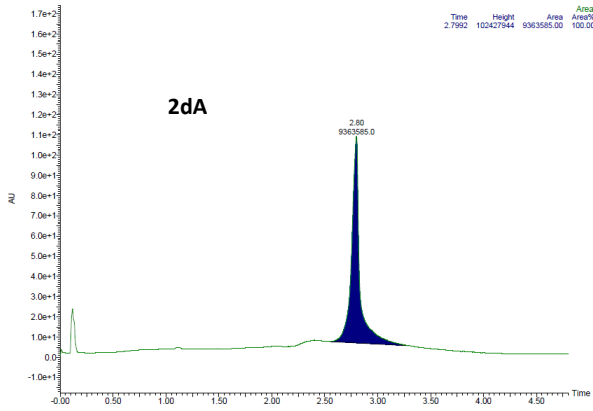
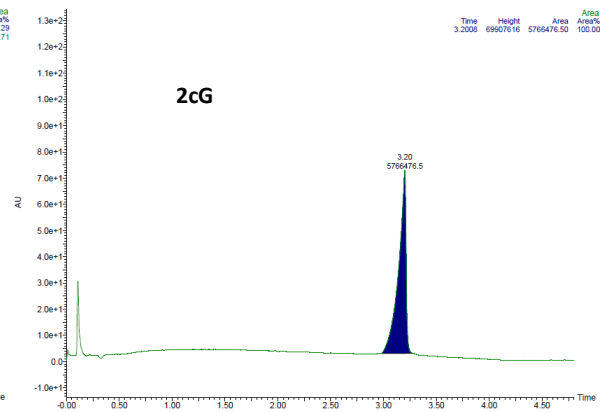
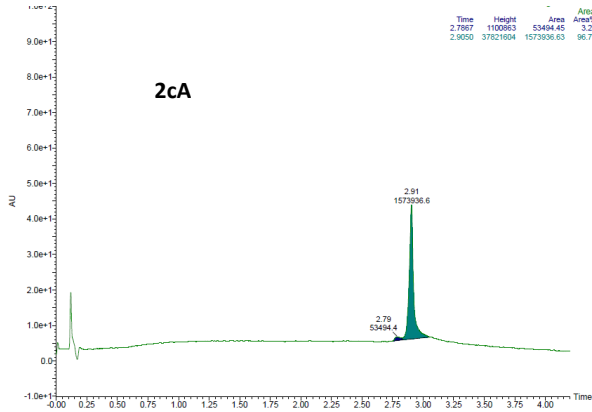
3.1 Scaffolds 3A, 4A, 5A and 15A

For compounds **4A** and **5A** no SFC traces were obtained.

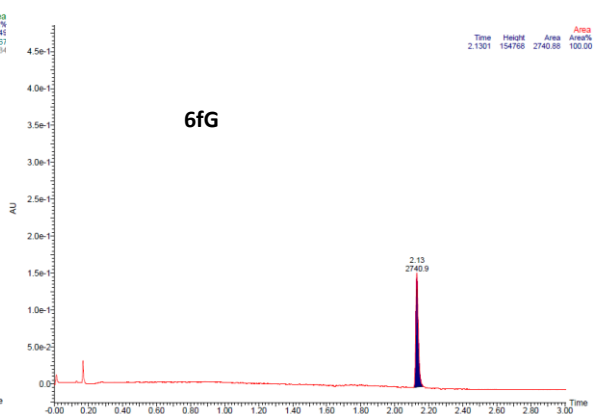
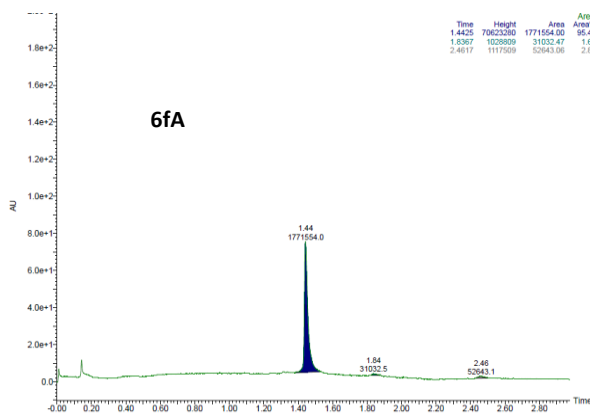
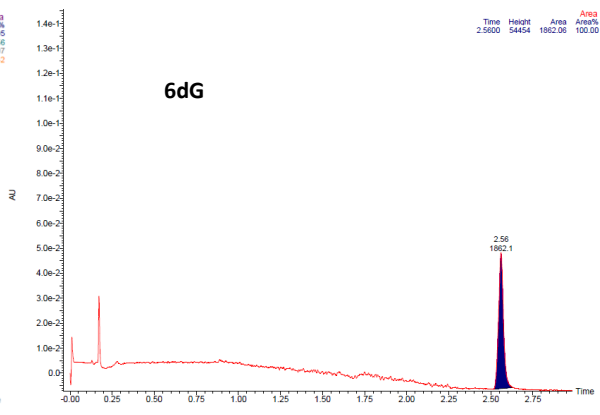
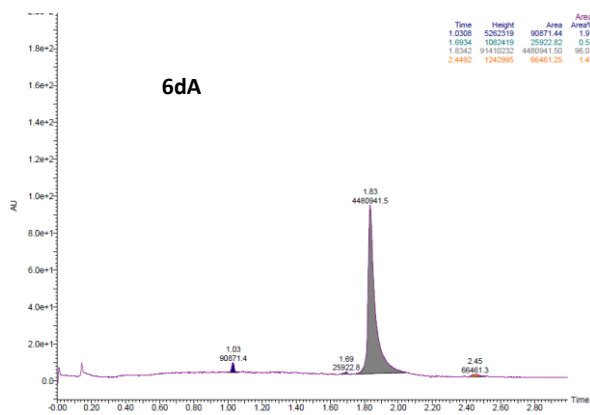
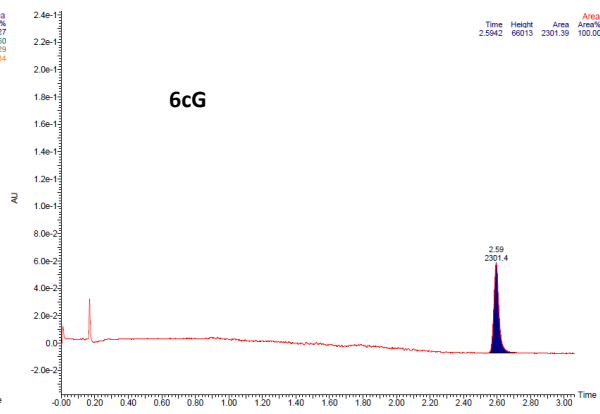
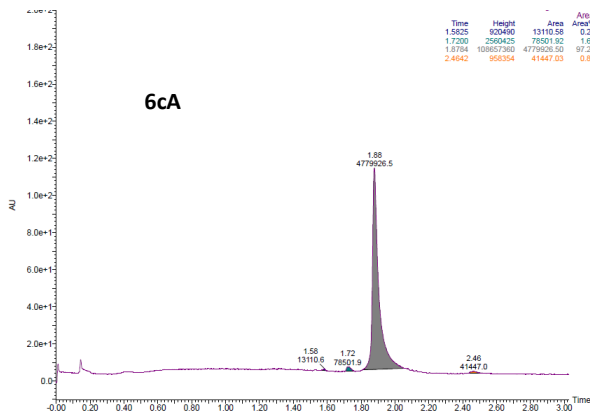
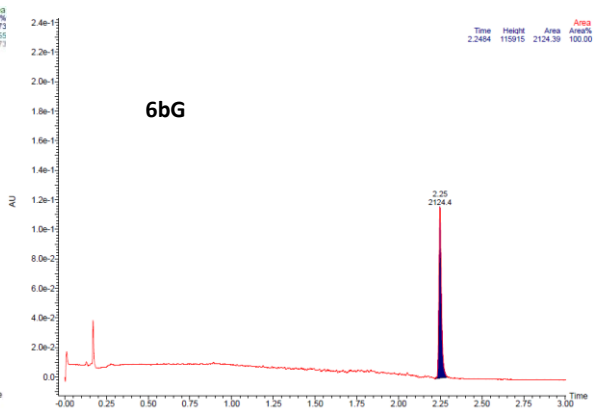
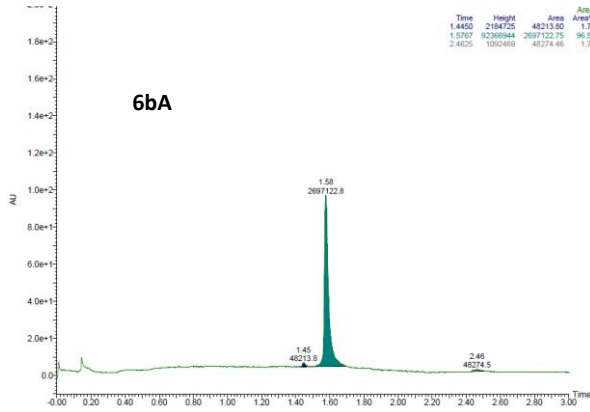


3.2 Hydantoin 2A and 2G





3.3 Hydantoins 6A and 6G



4. Full selectivity index table

Table S3. Selectivity index (SI) of all compounds towards all bacterial strains tested. EC₅₀ values are given in [µg/mL].

Code	Core	ClogP ^b	SI (MIC/EC ₅₀)				EC ₅₀ ^c
			S. a	B. s	E. c	P. a	
2dA	Hydantoin	-1.69	43	86	22	43	344
4A	2,4-dithiohydantoin	-1.22	48	48	24	-	385
3A	4-imidazolidin-2-one	-0.47	24	48	24	6	48
15A	2-(hydroxy)-1 <i>H</i> -imidazol	0.26	22	22	11	11	44
Mix 1	2-thiobarbituric acid	-0.10	38	76	76	19	305
Mix 2	2-thiobarbituric acid	-0.10	23	46	23	23	182
1A	Barbituric acid	-1.44	25	25	12	12	99

Code	Ar	Y	ClogP ^b	SI (MIC/EC ₅₀)				EC ₅₀ ^c	Code	SI (MIC/EC ₅₀)				EC ₅₀ ^c
				S. a	B. s	E. c	P. a			S. a	B. s	E. c	P. a	
2aA	(Ph)	<i>n</i> -propyl	2.64	-	-	-	-	>311	2aG	-	-	-	-	>353
2bA	(4-CF ₃ Ph)	<i>n</i> -propyl	3.52	-	>24	-	-	>379	2bG	>26	>65	-	-	>421
2cA	(3-Cl, 4-BrPh)	<i>n</i> -propyl	4.08	46	92	-	-	368	2cG	>234	>234	-	-	>467
2dA	(3,5-di-BrPh)	<i>n</i> -propyl	4.38	43	86	22	43	344	2dG	243	122	30	-	486
2eA	(4-Br-1-Nal)	<i>n</i> -propyl	4.68	17	17	6	6	69	2eG	103	103	26	-	206
2fA	(3,5-di-CF ₃ Ph)	<i>n</i> -propyl	5.03	25	50	25	25	399	2fG	>122	>245	-	-	>489

Code	Ar	Y	ClogP ^b	SI (MIC/EC ₅₀)				EC ₅₀ ^c	Code	SI (MIC/EC ₅₀)				EC ₅₀ ^c
				S. a	B. s	E. c	P. a			S. a	B. s	E. c	P. a	
6bA	(4-CF ₃ Ph)	<i>n</i> -butyl	3.52	-	>25	-	-	>393	6bG	>126	>126	-	-	>503
6cA	(3-Cl, 4-BrPh)	<i>n</i> -butyl	4.08	>55	>110	-	-	>439	6cG	87	172	22	44	347
6dA	(3,5-di-BrPh)	<i>n</i> -butyl	4.38	46	182	-	-	364	6dG	206	206	52	13	206
6fA	(3,5-di-CF ₃ Ph)	<i>n</i> -butyl	5.03	>29	>115	-	-	>461	6fG	192	192	48	-	384

Bacterial reference strains: S. a – *Staphylococcus aureus* ATCC 9144, B. s – *Bacillus subtilis* 168, E. c – *Escherichia coli* ATCC 25922, and P. a – *Pseudomonas aeruginosa* ATCC 27853. ^a -: No SI was calculated if MIC was >16 µg/mL.

5. Biological Methods

5.1 Minimum inhibitory concentration (MIC) assay

Based on the CLSI M07-A9 protocol,^[13] a modified broth microdilution sensitivity test^[14] was used to determine the minimum inhibitory concentration (MIC). Initially, a stock solution of water-soluble compounds was prepared by dissolving it in ultrapure water (Milli-Q H₂O, Millipore, MA, United States). Before being further diluted with ultrapure water, the less water-soluble compounds were first dissolved in 25 - 50 μ L 100% DMSO. The concentration of DMSO is always less than 1% in each compound's working concentration. The test components were then two-fold diluted with ultrapure water in polystyrene microplates with 96 wells of flat bottom (NUNC, Roskilde, Denmark). The bacterial inoculum was diluted into Mueller-Hinton broth (MHB, Difco Laboratories, USA) at 2.5×10^4 cells / ml and added to the different diluted compounds in a 1:1 ratio. In each experiment, positive control (ciprofloxacin, Sigma-Aldrich, USA), negative control (bacteria + water), and medium control (media + water) were included. The microplates were incubated in EnVision microplate readers at 35 °C for 48 hours (Perkin-Elmer, Turku, Finland). The lowest concentration of compounds that did not cause bacterial growth was defined as MIC by optical density measurements (OD600). All components have been tested in 3 technical repetitions.

5.2 Membrane integrity assay

5.2.1 Inner membrane

Bacillus subtilis 168 (ATCC 23857) and *Escherichia coli* K12 (ATCC MC1061) were used as test strains to perform the inner membrane integrity assay in real time. Both strains were transformed with the reporter plasmid pCSS962 containing the gene encoding eukaryotic luciferase (*lucGR* gene).^[15] D-luciferin, which was added externally, was used as a substrate for luciferase to detect light emissions. MH media supplemented with 5 μ g/mL chloramphenicol (Merck KGaA, Darmstadt, Germany) and a mixture of 20 μ g/mL chloramphenicol and 100 μ g/mL ampicillin (Sigma-Aldrich, USA), respectively, were used to suspend *B. subtilis* and *E. coli* colonies and grown overnight at RT. The overnight culture was further diluted and grown at RT for 2-3 hours until OD600 = 0.1. A final concentration of 1 mM of D-luciferin potassium salt (Synchem Inc., Elk Grove Village, IL, USA) was added to the bacterial cultures and the background light is measured before the actual tests. Black microtiter plates (96 wells, round-bottom; Nunc, Roskilde, Denmark) were prepared with a twofold series of dilutions of compounds (10 μ L per well) at final concentrations of 51.2 to 1.6 μ g/mL. MQ-H₂O and chlorhexidine acetate (Fresenius Kabi, Halden, Norway) were used as negative and positive control, respectively. The bacterial suspension was primed before loading the assay plate into the Synergy H1 Hybrid Plate Reader (BioTek, Winooksi, VT, USA). The 90 μ L bacterial inoculum with D-luciferin was injected sequentially (well by well) by automated injection into test wells. Light emission (luminescence) due to bacterial membrane disturbance was monitored every second for 3 minutes. Each study was conducted at least three times independently and the figures show a representative set.

5.2.2 Outer membrane

The integrity testing of the outer membrane was carried out in real time using *E. coli*, the integrity same strain used in the testing of the integrity of the inner membrane. 1-N-phenyl-naphthylamine (NPN), which was added externally, was used as a substrate for fluorescent detection. The MH medium was used to suspend *E. coli* colonies and grown overnight at RT. The overnight cultures were further diluted and grown in RT for 2-3 hours until OD600 = 0.1. NPN (Sigma-Aldrich, USA) was added to bacterial cultures at a final concentration of 20 μ M in glucose hepes buffer (5mM). Background fluorescence was measured before the actual assay. Black 96-well microtiter plates (round bottom) are prepared with a two-fold series of compounds (10 μ L per well) diluted at final concentrations between 51.2 and 1.6 μ g/mL. MQ-H₂O and chlorhexidine acetate were used as negative and positive control. The bacterial suspension was primed before the assay plate was loaded into the Synergy H1 hybrid plate reader. Bacterial inoculum (aliquots of 90 μ L) with NPN was sequentially (well by well) injected into the test wells by an automated injector. As a result of bacterial outer membrane disruption, light (fluorescence) emission was monitored every second for 3 minutes. Each study has been carried out independently at least three times and the figures show a representative set.

5.3 Viability assay

B. subtilis 168 and *E. coli* K12, the same strains used in the inner membrane integrity assay, were used to perform the bacterial viability assay in real time. However, *E. coli* K12 was transformed with the reporter plasmid pCGLS-

1 and *B. subtilis* 168 has a constitutively expressed lux operon as a chromosomal integration at the *sacA* locus (P_{liaG}).^[16] MH medium supplemented with 5 µg/mL chloramphenicol and a mixture of 20 µg/mL chloramphenicol and 100 µg/mL ampicillin, respectively, were used to culture *B. subtilis* and *E. coli*, the same way as the membrane integrity assay. The respective injector was primed with bacterial suspension and continuous light production by these biosensors was monitored in the Synergy H1 hybrid reader. 10 µL of each compound at the final concentration ranging from 51.2 to 1.6 µg/mL (two-fold dilutions) was prepared in black round-bottom 96-well microtiter plates. Chlorhexidine was used as a positive control and MQ-H₂O as a negative control. The automated injector added bacterial suspension (aliquot of 90 µL) consequently. Due to changes in bacterial viability, the reduction of light emission was monitored every second for 3 minutes. Each study was carried out at least three times individually and the figures show a representative set.

5.4 Red Blood Cell Haemolysis Assay

The protocol was adapted from Paulsen et al.^[11] Haemolysis was determined using a heparinized fraction (10 IU/mL) of freshly drawn blood. The blood collected in ethylenediaminetetraacetic acid-containing test tubes (Vacutest, KIMA, Arzergrande, Italy) was used for the determination of the hematocrit (hct). The heparinized blood was washed 3× with pre-warmed phosphate-buffered saline (PBS) and adjusted to a final hct of 4%. Derivatives in DMSO (50 mM) were added to a 96-well polypropylene V-bottom plate (NUNC, Fisher Scientific, Oslo, Norway) and serially diluted. The test concentration range was 500–4 µM with DMSO contents ≤1%. A solution of 1% triton X-100 was used as a positive control for 100% haemolysis. As a negative control, a solution of 1% DMSO in PBS was included. No signs of DMSO toxicity were detected. RBCs (1% v/v final concentration) were added to the well plate and incubated at 37 °C and 800 rpm for 1 h. After centrifugation (5 min, 3000g), 100 µL of each well was transferred to a 96-well flat-bottomed microtiter plate, and absorbance was measured at 545 nm with a microplate reader (VersaMax™, Molecular Devices, Sunnyvale, CA, USA). The percentage of haemolysis was calculated as the ratio of the absorbance in the derivative-treated and surfactant-treated samples, corrected for the PBS background. Three independent experiments were performed, and EC₅₀ values are presented as averages.

6. Membrane integrity and viability assay

Table 4. Summary of the membrane integrity and viability assay against *B. subtilis* 168.

Code	MIC ¹ (µg/mL, 24h)		MIA (activity and speed) ²	VA (effects) ³
	B. s	E. c		
2bG	8	128	+	-
2cA	4	32	++	+
2cG	2	32	+++	++
2dA	4	16	++	+
2dG	4	16	++++	++
2eG	2	8	+++	+++
2fG	2	32	+++	+
6bG	4	64	++	++
6cA	4	64	++	+
6cG	1	8	++++	+++
6dA	2	32	++	+
6dG	1	4	++++	+++
6fG	2	8	++++	+++
CHX	1.6	1.6	++++	+++

B. s: *Bacillus subtilis*, E. c: *Escherichia coli*

¹MIC assay was also performed in biosensor assay, and the value was similar.

²For membrane integrity assay: High active, fast speed (++++) Medium active, Intermediate speed (+++), Medium active, Slow speed (++) , Low active, Slow speed (+) and Not active (-).

³For viability assay: High effect (+++), Medium effect (++) , Low effect (+) and No effect (-). The highest concentration (51.2 µg/mL) was used to compare and evaluate the membrane integrity and viability assay results.

Table 5. Summary of the membrane integrity and viability assay against *E. coli* K12.

Code	MIC ¹ (µg/mL, 24h)		MIA (activity and speed) ²	VA (effects) ³
	B. s	E. c		
2dA	4	16	+	+
2dG	4	16	+	+
2eG	2	8	+	++
6cG	1	8	+	+
6dG	1	4	+	+
6fG	2	8	+	+
CHX	1.6	1.6	++++	+++

B. s: *Bacillus subtilis*, E. c: *Escherichia coli*

¹MIC assay was also performed in biosensor assay, and the value was similar.

²For membrane integrity assay: High active, fast speed (++++) Medium active, Intermediate speed (+++), Medium active, Slow speed (++) , Low active, Slow speed (+) and Not active (-).

³For viability assay: High effect (+++), Medium effect (++) , Low effect (+) and No effect (-). The highest concentration (51.2 µg/mL) was used to compare and evaluate the membrane integrity and viability assay results.

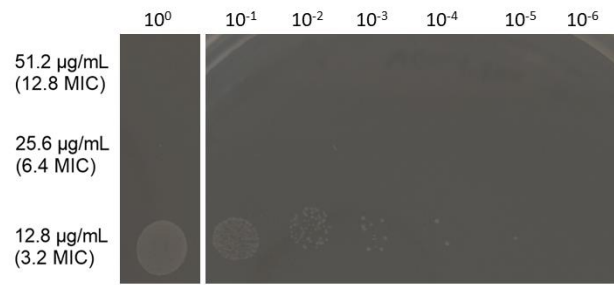


Figure S1. Bactericidal effect of hydantoin **2dA** against *E. coli* after the outer membrane study with NPN. Horizontal: Dilution of the bacterial load.

7. Literature

- [1] J. Dijkink, H. E. Schoemaker, W. N. Speckamp, *Tetrahedron Lett.* **1975**, *16*, 4043-4046.
- [2] H. Hiemstra, W. N. Speckamp, in *Alkaloids Chem. Biol.*, Vol. 32 (Ed.: A. Brossi), Academic Press, **1988**, pp. 271-339.
- [3] aD. J. Hart, T. K. Yang, *J. Org. Chem.* **1985**, *50*, 235-242; bH. Ent, H. De Koning, W. N. Speckamp, *J. Org. Chem.* **1986**, *51*, 1687-1691.
- [4] H. Kohn, Z. K. Liao, *J. Org. Chem.* **1982**, *47*, 2787-2789.
- [5] aD. Gupta, D. Bhatia, V. Dave, V. Sutariya, S. Varghese Gupta, *Molecules (Basel, Switzerland)* **2018**, *23*, 1719; bA. T. M. Serajuddin, *Adv. Drug Del. Rev.* **2007**, *59*, 603-616.
- [6] P. L. Gould, *Int. J. Pharm.* **1986**, *33*, 201-217.
- [7] C. Huixiong, L. Jean-Philippe, G. Nohad, G. Christiane, *Eur. J. Org. Chem.* **2006**, *2006*, 2329-2335.
- [8] M. Donnier-Maréchal, P. Carato, P.-E. Larchanché, S. Ravez, R. Boulahjar, A. Barczyk, B. Oxombre, P. Vermersch, P. Melnyk, *Eur. J. Med. Chem.* **2017**, *138*, 964-978.
- [9] J. Simonin, S. K. V. Vernekar, A. J. Thompson, J. D. Hothersall, C. N. Connolly, S. C. R. Lummis, M. Lochner, *Bioorg Med Chem Lett* **2012**, *22*, 1151-1155.
- [10] L. Tao, F. Luoyi, G. Hao, X. Zeming, Z. Yanpeng, J. Nianqiang, J. Long, L. Gaofeng, L. Yang, W. Jiaobing, *Angew. Chem. Int. Ed.* **2017**, *56*, 9473-9477.
- [11] M. H. Paulsen, M. Engqvist, D. Ausbacher, T. Anderssen, M. K. Langer, T. Haug, G. R. Morello, L. E. Liikanen, H.-M. Blencke, J. Isaksson, E. Juskewitz, A. Bayer, M. B. Strøm, *J. Med. Chem.* **2021**.
- [12] M. K. Langer, Rahman, A.; Dey, H.; Anderssen, T.; Zilioli, F.; Haug, T.; Blencke, H.-M.; Stensvåg, K.; Strøm, M. B.; Bayer, A., (*submitted Manuscript*) **2022**.
- [13] F. R. Cockerill, 9th ed. (Ed.: C. a. L. S. Institut), Wayne, Pa : Clinical and Laboratory Standards Institut, **2012**.
- [14] E. M. Igumnova, E. Mishchenko, T. Haug, H.-M. Blencke, J. U. E. Sollid, E. G. A. Fredheim, S. Lauksund, K. Stensvåg, M. B. Strøm, *Biorg. Med. Chem.* **2016**, *24*, 5884-5894.
- [15] M. Virta, K. E. O. Åkerman, P. Saviranta, C. Oker-Blom, M. T. Karp, *J. Antimicrob. Chemother.* **1995**, *36*, 303-315.
- [16] aJ. Radeck, K. Kraft, J. Bartels, T. Cikovic, F. Dürr, J. Emenegger, S. Kelterborn, C. Sauer, G. Fritz, S. Gebhard, T. Mascher, *J. Biol. Eng.* **2013**, *7*, 29; bS. Frackman, M. Anhalt, K. H. Nealson, *J. Bacteriol.* **1990**, *172*, 5767-5773.

Paper IV

**Stereocontrolled and Adaptable Synthesis of *ent*-Phenol A – one Protocol for the Formal
Synthesis of All Four Stereoisomers**

Manuel K. Langer, Annette Bayer

Manuscript

Stereocontrolled and Adaptable Synthesis of *ent*-Phenol A – one Protocol for the Formal Synthesis of All Four Stereoisomers

Manuel K. Langer^a, Annette Bayer^{a*}

^a Department of Chemistry, UiT – The Arctic University of Norway, NO-9037 Tromsø, NORWAY.

*Corresponding author.

MANUSCRIPT INFO	ABSTRACT
<p><i>Article history:</i></p> <p>Received: Received in revised form Accepted</p> <p>Available online</p> <p><i>Keywords:</i></p> <p>Aspergilone A Azaphilones 1,2-boron-ate rearrangement</p>	<p>Citrinin-type azaphilones, a class of fungal polyketides, are often known as mycotoxins, but beyond that offer a diverse assortment of biological activities. A degradation product is citrinin is phenol A, which can be found as a structural feature in many members of the citrinin-type azaphilones. We report an enantioselective formal synthesis towards all stereoisomers of phenol A, exemplified on its enantiomer <i>ent</i>-phenol A. The key conversion is double sequential 1,2-boronate rearrangement, with full stereocontrol. The di-<i>O</i>-demethylation of a resorcin-type intermediate was achieved by utilizing a counterattack reagent under basic conditions. <i>ent</i>-Phenol A was obtained enantiopure in >99% ee and 5% yield over 7 steps.</p>

1. Introduction

Azaphilones are a class of fungal polyketides, featuring an isochroman core and exerting a wide range of biological activities including antimicrobial, cytotoxic, antifungal, antiviral, antioxidant, anticancer, antifouling and anti-inflammatory.¹⁻⁴ The citrinin-type azaphilones are a structural subclass constituted of around 60 members^{1,4} and a selection of them is shown in Figure 1. The subclasses eponym, (-)-citrinin (**1a**), was first isolated in 1931⁵ and it was not before 1963 that the absolute configuration was determined (Figure 1).^{6,7} Albeit recognized for its antimicrobial activity, its general cytotoxicity limits its use for medical applications.^{8,9}

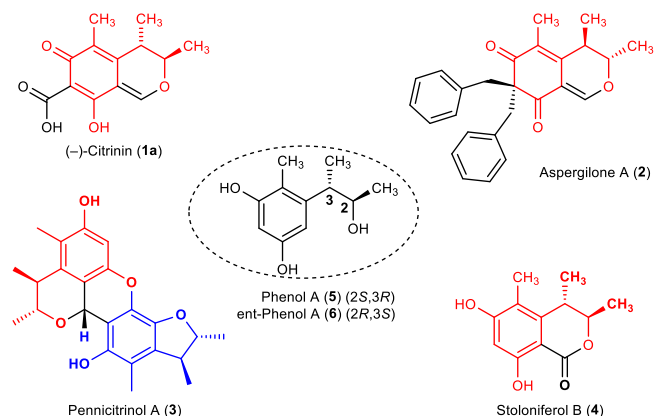


Figure 1. Chemical structures of (-)-citrinin (**1a**), aspergilone A (**2**), pennicitrinol A (**3**), stoloniferol B (**4**), phenol A (**5**) and (*ent*-)phenol A (**6**). The (*ent*-)phenol A is highlighted in red and blue in the natural products.

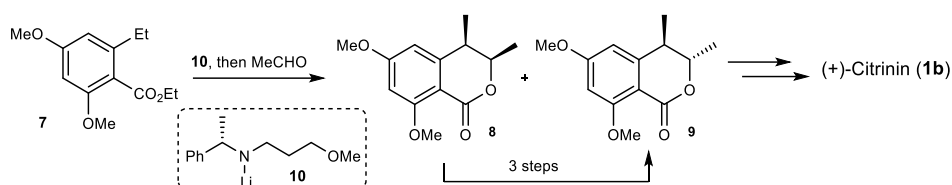
Phenol A (**5**) is a degradation product of **1a**,⁵ but no direct intermediate in the biosynthesis.^{10,11} It is a subunit found in many members of the citrinin subclass such as pennicitrinol A (**3**) and stoloniferol B (**4**), but its enantiomer *ent*-phenol A (**6**) can only be found in aspergilone A (**2**). Phenol A (**5**) and its stereoisomers

were used as the key intermediates in a number of total syntheses of (+)- and (-)-citrinin.¹²⁻¹⁵ To introduce the stereogenic centers, Regan et al.¹³ combined an *ortho*-toluate carbanion, generated with a chiral amide base **10**, and ethanal as an electrophile (Scheme 1). They obtained a mixture of the *erythro* and *threo* lactone (**8** and **9**) of which the former one could be transformed to the desired *threo* product **9** by a three-step process. Unfortunately, they discovered later that they had made the unnatural (+)-citrinin **1b**. When Rödel et al.¹⁴ employed an aryl Grignard and (2*S*)-*trans*-(-)-2,3-dimethyloxirane **12**, they obtained the *erythro* alcohol **13**, which needed to be converted to the desired *threo* configuration **14** by means of a Mitsunobu reaction (Scheme 1). Ohashi et al.¹⁶ synthesized stoloniferol B (**4**), employing a stereoselective Mukayama aldol reaction to introduce the *trans*-1,2-dimethyl structure and used then several manipulations to first built up the lactone and then the aromatic system.

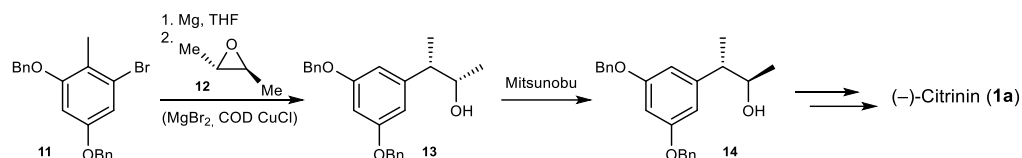
Spurred by our interest in aspergilone A (**2**) due to its antifouling and anticancer activity,³ we became interested in the development of a concise synthetic route towards *ent*-phenol A (**6**), which was envisioned to be an intermediate in the total synthesis. Moreover, it became evident that a facile and stereocontrolled synthesis of all phenol A stereoisomers, that would give access to a range of citrinin-type natural products and their unnatural isomers, was missing.

Herein, we report the enantioselective synthesis of the *ent*-phenol A (**6**) stereoisomer using a stepwise, stereoselective introduction of each methyl group by an anionic 1,2-boronate rearrangement¹⁷⁻¹⁹ (Scheme 1) exemplified by the enantioselective synthesis of the *ent*-phenol A (**6**) stereoisomer. As the 1,2-boronate rearrangement is known to be stereospecific and the outcome can be controlled completely by choice of the reagents, our protocol offers formal access to all four stereoisomers of phenol A without major adjustments.

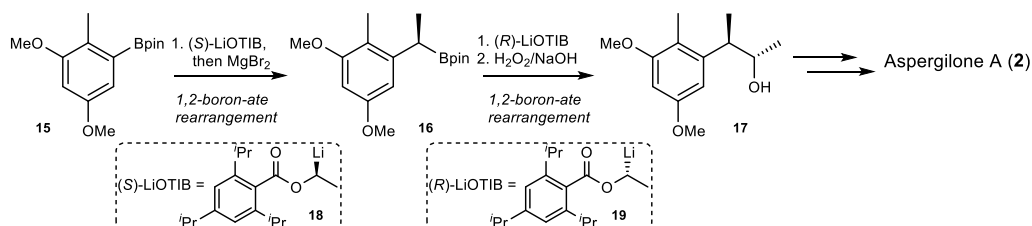
Regan et al. (1987):



Rödel et al. (1995):



Our approach:

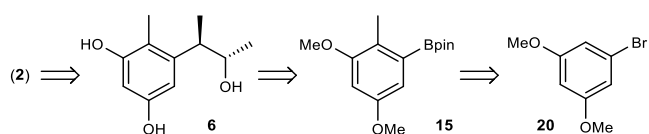


Scheme 1. Synthetic strategies for the introduction of the stereogenic centers.

2. Results and Discussion

2.1. Retrosynthesis

Ent-Phenol A (**6**) and its stereoisomers, key intermediates in the synthesis of a number of citrinin-type natural products were disconnected to the aryl boronic acid pinacol ester **15**. In the forward direction, this disconnection corresponds to the key transformation of our approach – two sequential 1,2-boronate rearrangements followed by oxidation of the boronic ester to the alcohol. Aryl boronic acid pinacol ester **15** should be attainable from the corresponding 1-bromo-3,5-dimethoxybenzene **18** in a three-step process consisting of formylation, deoxygenation and borylation with a boronic acid pinacol ester.



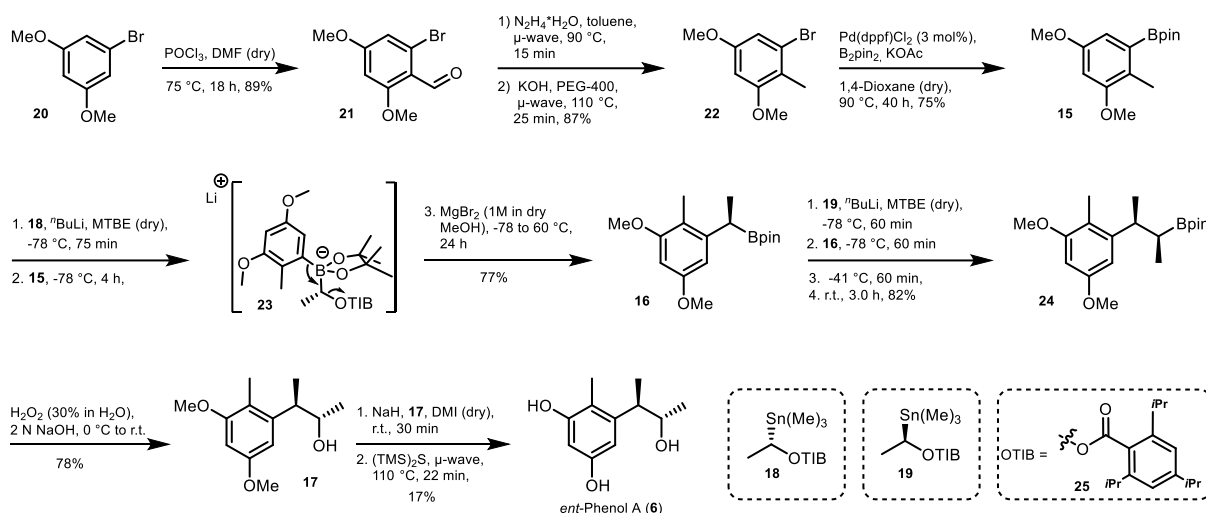
Scheme 2. Retrosynthetic analysis of *ent*-phenol A (**6**) and aspergiline A (**2**).

2.2. Synthesis

We started our endeavour from commercially available 1-bromo-3,5-dimethoxybenzene **20** and employed a modified literature protocol for the Vilsmeier-Haack formylation (Scheme 3).²³ We obtained the formylated product **21** in 89% yield. When employing toluene or PEG-400²⁴ as solvents in the following Wolff-Kishner reduction, either KOH or the starting material were insoluble, respectively, and low to no conversion was observed. Eventually we first made the hydrazone by mixing hydrazine and aldehyde **21** in toluene and then added KOH and PEG-400. Deoxygenated **22** was obtained in 87% yield. The amount of hydrazine and the reaction times could be greatly reduced by employing μ -wave

irradiation.²⁵ The aryl boronic ester **15** was obtained in good yields (75%) using Pd(dppf)Cl₂, bis(pinacolato)diboron (B₂pin₂) and potassium acetate under standard Miyaura borylation conditions. In the following key step, the stepwise, stereocontrolled introduction of the stereocenters, (*S*)-tin benzoate **18** was treated with *n*-BuLi at cryogenic temperatures to deliver the chiral secondary lithium alkyl.^{26, 27} Upon addition of aryl boronic acid pinacol ester **15**, boron-ate complex **23** was formed, and underwent an anionic 1,2-aryl shift, eliminating the benzoate leaving group **25**. The antiperiplanar arrangement of the aryl and the benzoate dictates the stereochemical outcome. Higher temperatures and Lewis acids are known to promote the rearrangement.¹⁹ Heating to reflux and the addition of 1.5 eq of MgBr₂ in methanol was imperative to obtain benzyl boronic acid pinacol ester **16** in yields of up to 77%. Following the same procedure and using (*R*)-tin benzoate **19** the second ethyl group was incorporated. Since alkyl boronic acids readily undergo the 1,2-rearrangement, no additional Lewis acid was needed in the second rearrangement.¹⁹ Alkyl boronic acid pinacol ester **24** could be obtained in up to 82% yield. Interestingly, we occasionally obtained the oxidized product (the alcohol) of mono-homologated **16** as side product in both homologation steps. Analysis of the alcohol by chiral SFC revealed ee values between 4-39%. The remaining of some enantiomeric excess excludes the formation of a benzylic cation as an intermediate. The mechanism of the formation of the alcohol remains, however, unknown.

Alkyl boronic acid ester **24** was oxidised under standard conditions with 30% H₂O_{2(aq)} and a 2 M NaOH_(aq) solution, delivering the di-*O*-methyl ether of *ent*-phenol A **17**. Chiral SFC indicated the presence of a single stereoisomer.



Scheme 3. Synthetic strategy towards *ent*-phenol A (**6**).

For comparison a small sample of **17** was treated with 2 N H₂SO₄, which is known to induce racemisation of phenol A *via* a phenyl cation by water elimination.^{5, 12} After 3 h the enantiomeric purity of the sample was reduced to 75% ee, clearly proving that alcohol **17** in fact was enantiopure.

The cleavage of phenolic *O*-methyl ethers is usually achieved with strong Lewis acids, such as BBr₃, AlCl₃ with NaI or TMSI.^{28, 29} However, those conditions might lead to racemization as iterated in the previous paragraph. We therefore intended to use those acidic conditions on compound **24**, reasoning that without a leaving group in the alkyl chain, the phenyl cation cannot be formed. We started our studies with more readily available boronic acid ester **15**. We were indeed able to cleave both, the *O*-methyl ethers and the Bpin ester of derivative **15** with AlCl₃ and *N,N*-dimethylaniline in toluene under microwave irradiation.³⁰ Unfortunately, even after optimizing the reaction conditions, no more than 35% NMR yield could be obtained. We then turned our attention to basic cleavage of the methyl ethers from intermediate **17** and used 3,5-dimethoxybenzyl alcohol as a first model system. Commonly, thiolate nucleophiles are employed, delivering the intermediate phenolates before quenching of the reaction.³¹ Unsurprisingly, this approach did not work in our model system as the final intermediate would be a tri-anionic species which should energetically be very unfavorable. When we finally employed hexamethyldisilathian ((TMS)₂S), a counterattack reagent,³² we could observe 3,5-dihydroxy benzyl alcohol in up to 60% NMR yield. Utilizing our optimized conditions with alcohol **17** delivered the desired product *ent*-phenol A (**6**), albeit in low yields (17%). Chiral SFC confirmed the presence of a single stereoisomer and the observed specific rotation was +34.5° (phenol A³³: -36.4°). We feel confident that the yields for the last transformation can be improved, to increase the efficiency of our synthetic approach.

3. Conclusion

We have developed a seven-step synthesis of *ent*-phenol A (**6**) with ee >99%. The protocol demonstrates the formal synthesis of all other stereoisomers of phenol

A by simply employing the suitable enantiomeric stannane in the right order. Additionally, analogues of phenol A, in which the aliphatic methyl groups are replaced by other moieties, may be accessible, due to the high versatility of the boron-ate rearrangement.

4. Experimental Section

For a detailed description of the experimental procedures and chemical analysis see the Supporting Information.

Author contributions

M.K.L and A.B. designed the synthetic strategy. M.K.L performed the compound synthesis and analysis. The manuscript was written through contributions of all authors. All authors have given approval to the final version of the manuscript.

Acknowledgements

MKL thanks for a PhD fellowship provided by UiT as part of the AntifoMar grant.

Declaration of competing interest

The authors declare no conflict of interests.

References

- Gao, J.-M.; Yang, S.-X.; Qin, J.-C., Azaphilones: Chemistry and Biology. *Chem. Rev.* **2013**, *113* (7), 4755-4811.
- Osmanova, N.; Schultze, W.; Ayoub, N., Azaphilones: a class of fungal metabolites with diverse biological activities. *Phytochem. Rev.* **2010**, *9* (2), 315-342.
- Shao, C.-L.; Wang, C.-Y.; Wei, M.-Y.; Gu, Y.-C.; She, Z.-G.; Qian, P.-Y.; Lin, Y.-C., Aspergilones A and B, two benzylazaphilones with an unprecedented carbon skeleton from the gorgonian-derived fungus *Aspergillus* sp. *Bioorg. Med. Chem. Lett.* **2011**, *21* (2), 690-693.

4. Chen, C.; Tao, H.; Chen, W.; Yang, B.; Zhou, X.; Luo, X.; Liu, Y., Recent advances in the chemistry and biology of azaphilones. *RSC Advances* **2020**, *10* (17), 10197-10220.
5. Hetherington, A. C. R., H., Biochemistry of microorganisms. XIV. Production and chemical constitution of a new yellow coloring matter, citrinin, produced from dextrose by *Penicillium citrinum*. *Trans. Roy. Soc. (London)* **1931**, *B220*, 269-296.
6. Mehta, P. P.; Whalley, W. B., 704. The chemistry of fungi. Part XLII. The absolute configuration of citrinin. *J. Chem. Soc. (Resumed)* **1963**, (0), 3777-3779.
7. Hill, R. K.; Gardella, L. A., The Absolute Configuration of Citrinin. *J. Org. Chem.* **1964**, *29* (3), 766-767.
8. Liu, B. H.; Wu, T. S.; Su, M. C.; Chung, C. P.; Yu, F. Y., Evaluation of citrinin occurrence and cytotoxicity in *Monascus* fermentation products. *J. Agric. Food Chem.* **2005**, *53* (1), 170-175.
9. Iwahashi, H.; Kitagawa, E.; Suzuki, Y.; Ueda, Y.; Ishizawa, Y.-h.; Nobumasa, H.; Kuboki, Y.; Hosoda, H.; Iwahashi, Y., Evaluation of toxicity of the mycotoxin citrinin using yeast ORF DNA microarray and Oligo DNA microarray. *BMC Genomics* **2007**, *8* (1), 95.
10. Colombo, L.; Gennari, C.; Scolastico, C.; Aragozzini, F.; Merendi, C., Biosynthesis of citrinin. *J. Chem. Soc., Chem. Commun.* **1980**, (23), 1132-1134.
11. Colombo, L.; Gennari, C.; Potenza, D.; Scolastico, C.; Aragozzini, F.; Merendi, C., Biosynthesis of citrinin and synthesis of its biogenetic precursors. *J. Chem. Soc., Perkin Trans. 1* **1981**, (0), 2594-2597.
12. Barber, J. A.; Staunton, J.; Wilkinson, M. R., A diastereoselective synthesis of the polyketide antibiotic citrinin using toluate anion chemistry. *J. Chem. Soc., Perkin Trans. 1* **1986**, (0), 2101-2109.
13. Regan, A. C.; Staunton, J., Asymmetric synthesis of (+)-citrinin using an ortho-toluate carbanion generated by a chiral base. *J. Chem. Soc., Chem. Commun.* **1987**, (7), 520-521.
14. Rödel, T.; Gerlach, H., Enantioselective synthesis of the polyketide antibiotic (3*R*,4*S*)-(-)-citrinin. *Liebigs Ann. Chem.* **1995**, *1995* (5), 885-888.
15. Bergmann, D.; Hübner, F.; Wibbeling, B.; Daniliuc, C.; Cramer, B.; Humpf, H.-U., Large-scale total synthesis of ¹³C₃-labeled citrinin and its metabolite dihydrocitrininone. *Mycotoxin Res.* **2018**, *34* (2), 141-150.
16. Ohashi, T.; Hosokawa, S., Total Syntheses of Stoloniferol B and Penicitol A, and Structural Revision of Fusaraisochromanone. *Org. Lett.* **2018**, *20* (10), 3021-3024.
17. Szymiest, J. L.; Dutheil, G.; Mahmood, A.; Aggarwal, V. K., Lithiated Carbamates: Chiral Carbenoids for Iterative Homologation of Boranes and Boronic Esters. *Angew. Chem. Int. Ed.* **2007**, *46* (39), 7491-7494.
18. Larouche-Gauthier, R.; Fletcher, C. J.; Couto, I.; Aggarwal, V. K., Use of alkyl 2,4,6-triisopropylbenzoates in the asymmetric homologation of challenging boronic esters. *Chem. Commun.* **2011**, *47* (47), 12592-12594.
19. Leonori, D.; Aggarwal, V. K., Lithiation-Borylation Methodology and Its Application in Synthesis. *Acc. Chem. Res.* **2014**, *47* (10), 3174-3183.
20. Cartwright, N. J.; Robertson, A.; Whalley, W. B., A Synthesis of Citrinin. *Nature* **1949**, *163* (4133), 94-95.
21. Warren, H. H.; Dougherty, G.; Wallis, E. S., The Synthesis of Dihydrocitrinin and Citrinin. *J. Am. Chem. Soc.* **1949**, *71* (10), 3422-3423.
22. Gore, T. S.; Talavdekar, R. V.; Venkataraman, K., A new partial synthesis of citrinin. *Curr. Sci.* **1950**, *19* (1), 20-21.
23. D'Agostino, L. A. S., Robert Tjin Tham; Niu, Deqiang; McDonald, Joseph John; Zhu, Zhendong; Liu, Haibo; Mazdiyasi, Hormoz; Petter, Russell C.; Singh, Juswinder; Barrague, Matthieu; Gross, Alexandre; Munson, Mark; Harvey, Darren; Scholte, Andrew; Maniar, Sachin Preparation of heteroaryl compounds as inhibitors of protein kinases WO/2014/144737, **2014**.
24. Wolfson, A. D., Christina, Glycerol as an alternative green medium for carbonyl compound reductions. *Org. Commun.* **2009**, *2* (2), 34-41.
25. Gadhwal, S.; Baruah, M.; Sandhu, J. S., Microwave Induced Synthesis of Hydrazones and Wolff-Kishner Reduction of Carbonyl Compounds. *Synlett* **1999**, *1999* (10), 1573-1574.
26. Still, W. C.; Sreekumar, C., α -Alkoxyorganolithium reagents. A new class of configurationally stable carbanions for organic synthesis. *J. Am. Chem. Soc.* **1980**, *102* (3), 1201-1202.
27. Burns, M.; Essafi, S.; Bame, J. R.; Bull, S. P.; Webster, M. P.; Balieu, S.; Dale, J. W.; Butts, C. P.; Harvey, J. N.; Aggarwal, V. K., Assembly-line synthesis of organic molecules with tailored shapes. *Nature* **2014**, *513* (7517), 183-188.
28. Vickery, E. H.; Pahler, L. F.; Eisenbraun, E. J., Selective O-demethylation of catechol ethers. Comparison of boron tribromide and iodotrimethylsilane. *J. Org. Chem.* **1979**, *44* (24), 4444-4446.
29. Ghiaci, M.; Asghari, J., Dealkylation of Alkyl and Aryl Ethers with AlCl₃ - NaI in the Absence of Solvent. *Synth. Commun.* **1999**, *29* (6), 973-979.
30. Subbaraju, G. V. M., M.; Mohan, H. R.; Suresh, T.; Ivanisevic, I.; Andres, M.; Stephens, K. Key intermediate for the preparation of stilbenes, solid forms of pterostilbene, and methods for making the same. US20110144212A1, **2011**.
31. Magano, J.; Chen, M. H.; Clark, J. D.; Nussbaumer, T., 2-(Diethylamino)ethanethiol, a New Reagent for the Odorless Deprotection of Aromatic Methyl Ethers. *J. Org. Chem.* **2006**, *71* (18), 7103-7105.
32. Hwu, J. R.; Tsay, S. C., Counterattack reagents sodium trimethylsilanethiolate and hexamethyldisilathiane in the bis-O-demethylation of aryl methyl ethers. *J. Org. Chem.* **1990**, *55* (24), 5987-5991.
33. Johnson, D. H.; Robertson, A.; Whalley, W. B., 580. The chemistry of fungi. Part XIII. Citrinin. *J. Chem. Soc. (Resumed)* **1950**, (0), 2971-2975.

Supporting Information
for
Stereocontrolled and Adaptable Synthesis of *ent*-Phenol A – one
Protocol for the Formal Synthesis of All Four Stereoisomers

Manuel K. Langer^a, Annette Bayer^{a*}

^a Department of Chemistry, UiT – The Arctic University of Norway, NO-9037 Tromsø, NORWAY.

*Corresponding author.

Table of Contents

1. Experimental Procedures	2
1.1 General Information	2
1.2 Materials and reagents.....	3
1.3 Synthesis of building blocks.....	3
1.4 Synthetic Procedures.....	5
2. NMR spectra	10
3. IR spectra	19
4. References.....	23

1. Experimental Procedures

1.1 General Information

Air and water sensitive reactions were carried out in heat-dried glassware under an argon atmosphere using standard Schlenk techniques. Anhydrous solvents were prepared from commercially available solvents and dried over molecular sieves of appropriate pore size.

Normal phase flash chromatography was carried out on VWR Silica Gel 40 – 63 μm . Automated flash chromatography was carried on an interchim[®] PuriFlash XS420 flash system with the sample preloaded on a Samplet[®] cartridge belonging to a Biotage SP-1 system or on a Biotage[®] Isolera One system with the sample preloaded on Celite. For both systems Biotage S_fär Silica columns were used. Thin layer chromatography was carried out using Merck TLC Silica gel 60 F₂₅₄ and visualized by short-wavelength ultraviolet light or by treatment with an appropriate stain.

NMR spectra were obtained on a Bruker Advance 400 MHz, Bruker Fourier 300 MHz and Bruker DPX 400 MHz NMR spectrometer at 20 °C. The chemical shifts (δ) are reported in parts per million (ppm) relative to the solvent residual peak (Chloroform-*d*: δH 7.26 and δC 77.16; Acetone-*d*₆: δH 2.05 and δC 29.84 or 206.26). ¹³C-NMR spectra were obtained with ¹H decoupling. Data is represented as follows: chemical shift, multiplicity (s = singlet, d = doublet, t = triplet, q = quartet, dd = doublet of doublet, dq = doublet of quartet, bs = broad singlet, m = multiplet), coupling constant (J, Hz) and number of protons.

High-resolution mass (HRMS) spectra were recorded from methanol solutions on a LTQ Orbitrap XL (Thermo Scientific) with electrospray ionization (ESI), a Waters Xevo G2-XS QToF with electrospray ionization (ESI), Thermo Scientific Q Exactive GC Orbitrap with electron ionization (EI) and chemical ionization (CI) or a ThermoScientific Vanquish UHPLC system coupled to a ThermoScientific Orbitrap Exploris 120 with electrospray ionization (ESI). Ultrapure MilliQ Water and HPLC grade solvents were used for the Vanquish UHPLC system. Water (A) and a 90/10/0.1 (v/v) mixture of MeCN/H₂O/formic acid (B) were used as solvents. Gradient: 0-70% (B) over 7 min, 100% (B) for 2 min, 0% (B) for 2 min. The molecular ion peaks are reported as molecular ion plus hydrogen [M+H]⁺ or molecular ion [M]⁺.

Infra-red (IR) spectra of the pure compounds were recorded on an Agilent Technologies Cary 630 FTIR. Selected absorption maxima (ν_{max}) are reported in wavenumbers (cm⁻¹).

Melting points were measured in degree Celsius (°C) using a Stuart SMP50 automatic melting point detector and are reported uncorrected.

Optical rotations were determined on an Optical Activity LTD AA-10R Automatic Polarimeter at 20 °C in a cuvette of 100 mm length with the sodium D-line (589 nm). The concentrations and solvents (HPLC grade) were adapted for each compound individually. The polarimeter was calibrated against the pure solvent. Concentrations are given in g/(100 mL).

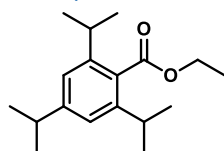
Chiral HPLC measurements were performed on a Shimadzu apparatus. The different modules were SIL-10ADVP (auto injector), LC-10ATVP (liquid chromatograph), FCV-10ALVP (pump), DGU-14A S2 (degasser), CTO-10ASVP (column oven), SCL-10AVP (system controller) and SPD-M10A (diode array detector). HPLC grade *n*-hexane and isopropanol were used as solvents. Separation was achieved on a Chiralcel OD-H S-5 μm (0.46 cm \varnothing × 25 cm) column.

Chiral SFC was performed on a Waters ACQUITY UPC² system equipped a Trefoil[™] CEL2, 2.5 μm , 3.0 x 150mm column coupled to a Waters ACQUITY PDA detector spanning from wavelengths 190 to 650 nm. HPLC grade solvents and CO₂ were used as the mobile phase. Solvent mixtures and gradients are specified for each compound individually.

1.2 Materials and reagents

Unless otherwise noted, purchased chemicals were used as received without further purification. Anhydrous Et₂O was dried over two columns of activated alumina^[1] in a solvent purification system (SPS) and stored over 3 Å mol sieves. Commercial anhydrous MTBE (Sigma-Aldrich) was kept over 4 Å mol sieves before usage. Solvents were degassed by vigorously bubbling argon through the solvent under ultrasonication. TMEDA, (-)-sparteine and (+)-sparteine were distilled over CaH₂ and stored under N₂ at -20 °C. The 1 M solution of MgBr₂ in anhydrous MeOH was prepared according to literature procedures^[2] and stored at -20 °C.

1.3 Synthesis of building blocks



Ethyl 2,4,6-triisopropylbenzoate **S1**.^[3]

A biphasic mixture of 2,4,6-isopropylbenzoic acid (10 g, 40.3 mmol, 1.0 eq), tetrabutylammonium iodide (892 mg, 2.42 mmol, 0.06 eq), NaOH (3.54 g, 88.6 mmol, 2.20 eq) and 1-bromoethane (15.8 mL, 221 mmol, 5.25 eq) in CHCl₃ (200 mL) and water (160 mL) was stirred vigorously for 5 d at ambient temperature. The layers were separated and the aqueous layer was extracted with DCM twice. The combined organics were dried over MgSO₄, filtered and the solvent was removed under reduced pressure. Pentane was added to the resulting clear liquid, upon which a white precipitate formed. The solids were filtered off and washed with pentane twice. The filtrates were combined and the solvent was removed under reduced pressure to yield **S1** (11.0 g, 40.0 mmol, 99%) as a clear colorless liquid.

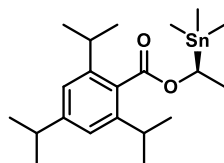
¹H NMR (400 MHz, Chloroform-*d*) δ 7.00 (s, 2H), 4.37 (q, *J* = 7.1 Hz, 2H), 2.88 (dq, *J* = 13.7, 7.0 Hz, 3H), 1.37 (t, *J* = 7.2 Hz, 3H), 1.25 (d, *J* = 6.8 Hz, 12H), 1.24 (d, *J* = 7.0 Hz, 6H).

¹³C NMR (101 MHz, Chloroform-*d*) δ 171.0, 150.2, 144.9 (2C), 130.8, 121.0 (2C), 60.9, 34.6, 31.6 (2C), 24.3 (4C), 24.1 (2C), 14.4.

HRMS: (ESI): calcd for C₁₈H₂₉O₂⁺ [M+H]⁺ 277.2162, found: 277.2158.

IR (ν_{max}/cm⁻¹, neat): 2960, 1724, 1250, 1075, 765.

R_f: 0.58 (10% EtOAc in heptane).



(S)-1-(trimethylstannyl)ethyl 2,4,6-triisopropylbenzoate **18**.^[3]

S1 (5.00 g, 18.1 mmol, 1.0 eq) and freshly distilled (-)-sparteine (5.4 mL, 23.5 mmol, 1.3 eq) were added to a flame dried reaction vessel under argon atmosphere. Anhydrous Et₂O (72 mL) was added, and the mixture was cooled to -78 °C. After 10 min equilibration time *sec*-BuLi (18.1 mL, 25.3 mmol, 1.4 eq) was added dropwise via syringe over 10 min. The mixture turned red and then brown. Stirring was continued for 4h at that temperature, during which a precipitate formed. Then Me₃SnCl (23.5 mL, 23.5 mmol, 1.3 eq) was added dropwise over 30 min and stirring was continued at -78 °C for 20 min. The solution was warmed to ambient temperature and stirred for 80 min at that temperature. 5% H₃PO_{4(aq)} solution was added and the biphasic mixture was stirred for 10 min. The layers were separated and the organic layer was washed twice with 5% H₃PO_{4(aq)} solution. The combined aqueous layers were extracted with Et₂O thrice and the combined organics were dried over MgSO₄, filtered and the solvent was removed. Stannane **18** (5.3 g, 12.1 mmol, 67%) was obtained as a white solid after recrystallization.

The crude was recrystallized from MeOH (2-3 mL/g crude). After solvent addition the mixture was heated until all solids dissolved. After crystallization, the solids were collected and the residual MeOH left for further crystallization. Two crops were obtained. The crops were combined and recrystallized once more from MeOH to yield 3 crops. Each crop was kept and used individually.

¹H NMR (400 MHz, Chloroform-*d*) δ 7.00 (s, 2H), 5.04 (q, *J* = 7.6 Hz and q, *J* = 7.6 Hz, 1H), 2.94 – 2.79 (m, 3H), 1.59 (d, *J* = 7.6 Hz and dd, *J* = 54.7, 7.7 Hz and dd, *J* = 57.8, 7.7 Hz, 2H), 1.24 (d, *J* = 6.8 Hz, 18H), 0.18 (s, 9H and d, *J* = 51.7 Hz and *J* = 54.1 Hz).

¹³C NMR (101 MHz, Chloroform-*d*) δ 171.4, 150.1, 145.0 (2C), 130.9, 120.9 (2C), 67.2, 34.5, 31.5, 24.5 (2C), 24.2 (2C), 24.1 (2C), 19.4, -8.1, -8.2, -9.8 (s and d, *J* = 320.3 Hz and d, *J* = 335.4 Hz, 1C).

HRMS (ESI): calcd for C₂₁H₃₇O₂Sn⁺ [M+H]⁺ 437.1806, found: 437.1797.

IR (*v*_{max}/cm⁻¹, neat): 2959, 1696, 1259, 1074, 765.

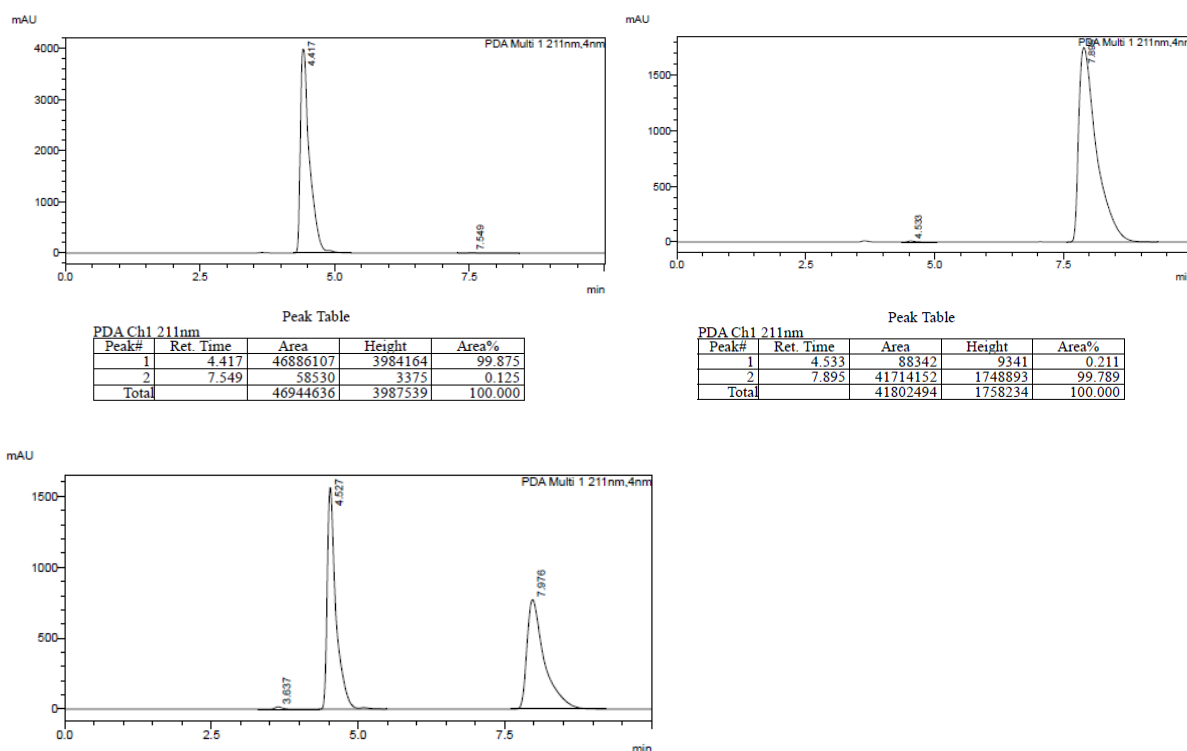
M_p: 48-51 °C.

R_f: 0.40 (5% EtOAc in heptane).

Chiral HPLC (Daicel Chiralcel OD-H, hexane, 0.9 mL/min, room temperature, 211 nm): *t_R* = 4.4 min (*S*-**18**), e.r. = 99.9:0.1; *t_R* = 7.9 min (*R*-**19**), e.r. = 99.8:0.2 for the first crop.

For the 2nd crop: *not determined*.

For the 3rd crop: (*S*), e.r. = 98.9:1.1, (*R*), e.r. = 98.2:1.8.

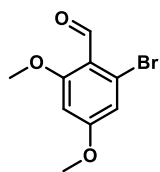


(*R*)-1-(trimethylstannyl)ethyl 2,4,6-triisopropylbenzoate **19** and the racemic compound **S2** were obtained by the same procedure using (+)-sparteine and TMEDA, respectively.

Preparation of MgBr₂ in anhydrous MeOH^[2]

Commercially available anhydrous MgBr₂ (Sigma-Aldrich) was placed in a heat dried round bottom flask together with a stirring bar. The flask was evacuated and backfilled with argon. The solids were heated to 200 °C under vacuum (1 mbar) for 3 h. The solids were allowed to cool to ambient temperature and anhydrous MeOH was added until a final concentration of 1 M was reached. Caution: Methanol starts boiling at the beginning of the addition due to strong heat evolution. A slightly grey solution was obtained with some precipitation. The solution was stored at -20 °C. Before usage, the flask was allowed to warm to room temperature and only the clear solution was used, carefully avoiding the solids.

1.4 Synthetic Procedures



2-bromo-4,6-dimethoxybenzaldehyde **21**.^[4]

POCl_3 (3.86 mL, 41.5 mmol, 6.0 eq) was added to anhydrous DMF (8.03 mL, 104.7 mmol, 15.0 eq) at 0 °C to yield a white slurry. Solid 1-bromo-3,5-dimethoxybenzene (1.50 g, 6.91 mmol, 1.0 eq) was added in one portion and the mixture was warmed to 75 °C for 18 h. The color changed to dark brown during the course of the reaction. The solution was allowed to cool to ambient temperature and water was added slowly under external cooling. The aqueous layer was extracted with EtOAc thrice and the combined organics were dried over MgSO_4 , filtered and the solvent was removed. The crude product was purified by column chromatography on silica gel with 50% EtOAc in heptane to yield **19** (1.51 g, 6.17 mmol, 89%) as a white solid.

$^1\text{H NMR}$ (400 MHz, Chloroform-*d*) δ 10.28 (s, 1H), 6.75 (d, $J = 2.3$ Hz, 1H), 6.41 (d, $J = 2.3$ Hz, 1H), 3.87 (s, 3H), 3.84 (s, 3H).

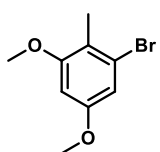
$^{13}\text{C NMR}$ (101 MHz, Chloroform-*d*) δ 189.3, 164.5, 163.7, 127.5, 116.9, 111.6, 98.2, 56.2, 56.0.

HRMS (ES): calcd for $\text{C}_9\text{H}_9\text{BrO}_3^+$ [$\text{M}+\text{H}$] $^+$ 244.9808, found: 244.9801.

IR ($\nu_{\text{max}}/\text{cm}^{-1}$, neat): 2872, 2780, 1082, 1590, 1556, 1450, 1413, 1229, 1203, 1136, 1051, 1026, 933, 826, 780.

M_p: 89 – 90 °C.

R_f: 0.53 (50% EtOAc in heptane).



1-bromo-3,5-dimethoxy-2-methylbenzene **22**.^[5]

To aldehyde **19** (1.29 g, 5.25 mmol, 1.0 eq) in toluene (16.5 mL) was added hydrazine hydrate (703 μL , 11.5 mmol, 2.20 eq; 80% in water) and the resulting mixture was heated to 90 °C for 15 min under μ -wave irradiation. Then PEG-400 and KOH (1.73 g, 31.5 mmol, 6.0 eq) were added and the mixture was heated to 110 °C for 25 min under μ -wave irradiation. Water and Et_2O were added and the layers were separated. The aqueous layer was extracted with Et_2O twice and the combined organics were dried over MgSO_4 , filtered and the solvent was removed under reduced pressure. The crude product was purified by column chromatography on silica gel with 10% EtOAc in heptane to yield **20** (1.06 g, 4.58 mmol, 87%) as a clear liquid.

$^1\text{H NMR}$ (400 MHz, Chloroform-*d*) δ 6.70 (d, $J = 2.4$ Hz, 1H), 6.38 (d, $J = 2.4$ Hz, 1H), 3.79 (s, 3H), 3.77 (s, 3H), 2.22 (s, 3H).

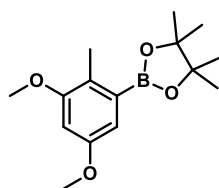
$^{13}\text{C NMR}$ (101 MHz, Chloroform-*d*) δ . 158.9, 158.7, 125.6, 119.3, 108.3, 98.0, 55.9, 55.7, 15.1.

HRMS (EI): calcd for $\text{C}_9\text{H}_{11}\text{BrO}_2^+$ [M] $^+$ 229.9937, found: 229.9939.

IR ($\nu_{\text{max}}/\text{cm}^{-1}$, neat): 2921, 2835, 1606, 1571, 1487, 1406, 1372, 1320, 1219, 1148, 1036, 933, 828, 815, 793, 747, 699.

M_p: 29 – 31 °C.

R_f: 0.50 (15% EtOAc in heptane).



2-(3,5-dimethoxy-2-methylphenyl)-4,4,5,5-tetramethyl-1,3,2-dioxaborolane **15**.

An oven dried flask was charged with PdCl_2dppf (102 mg, 140 μmol , 0.03 eq), KOAc (1.31 g, 13.4 mmol, 2.87 eq) and B_2pin_2 (1.90 g, 7.49 mmol, 1.61 eq) under argon. **20** (1.08 g, 4.65 mmol, 1.00 eq) was dissolved in anhydrous 1,4-dioxane (25 mL) and added to the flask. The resulting mixture was stirred at 90 °C for 40 h. After cooling to ambient temperature, the solvent was removed under reduced

pressure. Water and EtOAc were added, the layers were separated and the aqueous layer was extracted with EtOAc twice. The combined organics were dried over MgSO₄, filtered and the solvent was removed under reduced pressure. The crude was purified by column chromatography on silica gel with 2% EtOAc in heptane to yield **15** (965 mg, 3.47 mmol, 75%) as a white solid.

¹H NMR (400 MHz, Chloroform-*d*) δ 6.85 (d, *J* = 2.6 Hz, 1H), 6.52 (d, *J* = 2.6 Hz, 1H), 3.82 (s, 3H), 3.79 (s, 3H), 2.34 (s, 3H), 1.35 (s, 12H).

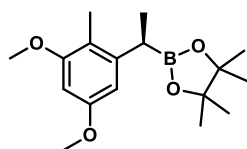
¹³C NMR (101 MHz, Chloroform-*d*) δ 158.6, 158.1, 130.2 (bs), 126.0, 109.9, 101.5, 83.7 (2C), 55.6, 55.6, 25.0 (4C), 14.0.

HRMS (ESI): calcd for C₁₅H₂₄B₁O₄⁺ [M+H]⁺ 278.1801, found: 278.1798.

IR (ν_{max}/cm⁻¹, neat): 2992, 2938, 2842, 1588, 1464, 1358, 1291, 1193, 1144, 1053, 966, 933, 834, 728.

M_p: 83 – 85 °C.

R_f: 0.27 (5% EtOAc in heptane).



(+)-(R)-2-(1-(3,5-dimethoxy-2-methylphenyl)ethyl)-4,4,5,5-tetramethyl-1,3,2-dioxaborolane **16**.^[6]

(*S*)-stannane **18** (924 mg, 2.10 mmol, 1.3 eq) was placed in a heat dried Schlenk flask under Argon. The flask was evacuated and backfilled with Argon one time. Anhydrous, degassed MTBE (10 mL) was added and the resulting clear solution was cooled to -78 °C. *n*-BuLi (841 μL, 2.10 mmol, 1.3 eq, 2.5 M in hexanes) was added dropwise to the mixture at -78 °C. The reaction mixture was stirred at that temperature for 75 min for the tin - lithium exchange to occur (the solution turned pale yellow, without any precipitate). Aryl boronic acid pinacol ester **15** (450 mg, 1.62 mmol, 1.0 eq), dissolved in anhydrous, degassed MTBE (3.2 mL, 0.5 M), was added dropwise to the reaction mixture at -78 °C. It was stirred at that temperature for 4 h. Then MgBr₂ (2.43 mL, 2.43 mmol, 1.5 eq, 1.0 M in anhydrous MeOH) was added and it was stirred 10 min at -78 °C. The cooling bath was removed and the reaction mixture was allowed to warm to ambient temperature over 20 min, before it was heated to 60 °C for 24 h. The suspension was allowed to cool to ambient temperature, filtered over a pad of Celite and the Celite was washed with Et₂O. The filtrate was collected and the solvent was removed under reduced pressure. Water (5 mL) was added and biphasic mixture was stirred for 5 min. The aqueous layer was extracted with Et₂O (3x), the organic phases were combined, dried over MgSO₄, filtered and the solvent was removed to yield a crude orange oil. A 1:20 mixture of **15**:**16** was obtained. The crude was purified on a Biotage Isolera system equipped with a silica column and gradient 0-15% EtOAc in petrol ether (PE) to yield the title compound **16** (381 mg, 1.24 mmol, 77%) as a clear oil.

¹H NMR (400 MHz, Chloroform-*d*) δ 6.42 (d, *J* = 2.5 Hz, 1H), 6.30 (d, *J* = 2.4 Hz, 1H), 3.79 (s, 6H), 2.59 (q, *J* = 7.5 Hz, 1H), 2.10 (s, 3H), 1.29 (d, *J* = 7.3 Hz, 3H), 1.23 (d, *J* = 4.9 Hz, 12H).

¹³C NMR (101 MHz, Chloroform-*d*) δ 158.5, 158.3, 145.4, 116.6, 104.5, 95.6, 83.4 (2C), 55.6, 55.3, 24.8 (4C), 22.5 (bs), 16.7, 11.2.

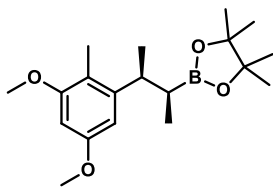
HRMS (ES): calcd for C₁₇H₂₈B₁O₄⁺ [M+H]⁺ 307.2084, found: 307.2081.

IR (ν_{max}/cm⁻¹, neat): 2970, 2933, 2835, 1731, 1605, 1588, 1459, 1312, 1201, 1143, 1103, 1069, 966, 939, 861, 676.

R_f: 0.41 (10% EtOAc in heptane).

[α]_D²⁰: +6.5° (*c* 0.99 CHCl₃).

Chiral SFC: not measured.



(+)-2-((2*S*,3*S*)-3-(3,5-dimethoxy-2-methylphenyl)butan-2-yl)-4,4,5,5-tetramethyl-1,3,2-dioxaborolane **24**.^[3]

(*R*)-Stannane **19** (193 mg, 441 μmol , 1.3 eq) was placed in a heat dried Schlenk flask under Argon. The flask was evacuated and backfilled with Argon one time. Anhydrous, degassed MTBE (2.2 mL) was added and the resulting clear solution was cooled to $-78\text{ }^\circ\text{C}$. *n*-BuLi (170 μL , 425 μmol , 1.3 eq, 2.5 M in hexanes) was added dropwise to the mixture at $-78\text{ }^\circ\text{C}$. The reaction mixture was stirred at that temperature for 60 min for the tin–lithium exchange to occur (the solution turned pale yellow, without any precipitate). Benzyl boronic acid pinacol ester **16** (100 mg, 327 μmol , 1.0 eq), dissolved in anhydrous, degassed MTBE (0.64 mL, 0.5 M), was added dropwise to the reaction mixture at $-78\text{ }^\circ\text{C}$. The resulting mixture was stirred at $-78\text{ }^\circ\text{C}$ for 60 min, to let the boron-ate form (the solution became colorless). The flask was transferred to a $-41\text{ }^\circ\text{C}$ cold cooling bath for 75 min to deplete residual lithium benzoate. The cooling bath was removed and the mixture was stirred at ambient temperature for 3.0 h. The suspension was filtered over a short plug of silica gel and the silica was washed with Et_2O . The filtrate was concentrated under reduced pressure. Water and Et_2O were added and the biphasic mixture was stirred for 5 min. The layers were separated and the aqueous layer was extracted thrice with Et_2O and the combined organics were dried over MgSO_4 , filtered and the solvent was removed to yield a crude yellow oil. The crude was purified on a Biotage Isolera system equipped with a silica column and gradient 0-15% EtOAc in PE to yield the title compound **24** (90 mg, 269 μmol , 82%) as a clear oil.

$^1\text{H NMR}$ (400 MHz, Chloroform-*d*) δ 6.38 (d, $J = 2.5\text{ Hz}$, 1H), 6.28 (d, $J = 2.4\text{ Hz}$, 1H), 3.78 (s, 3H), 3.77 (s, 3H), 3.03 (dq, $J = 9.4, 6.9\text{ Hz}$, 1H), 2.14 (s, 3H), 1.33 – 1.23 (m, 1H), 1.17 (d, $J = 6.9\text{ Hz}$, 3H), 1.02 (d, $J = 7.4\text{ Hz}$, 3H), 1.02 (s, 6H), 0.98 (s, 6H).

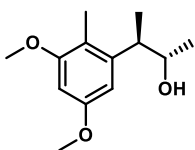
$^{13}\text{C NMR}$ (101 MHz, Chloroform-*d*) δ 158.3, 158.2, 148.4, 116.4, 103.1, 96.0, 82.7 (2C), 55.7, 55.4, 37.3, 25.2 – 23.7 (m), 24.5 (4C), 19.9, 13.3, 10.6.

HRMS (ES): calcd for $\text{C}_{19}\text{H}_{32}\text{B}_1\text{O}_4^+$ $[\text{M}+\text{H}]^+$ 335.2396, found: 335.2394.

IR ($\nu_{\text{max}}/\text{cm}^{-1}$, neat): 2960, 2874, 1605, 1590, 1459, 1381, 1361, 1312, 1201, 1143, 1069, 1045, 1012, 988, 938, 849, 833, 685.

R_f: 0.41 (10% EtOAc in heptane).

$[\alpha]_{\text{D}}^{20}$: +29.0° (c 0.9, CHCl_3).



(+)-(2*S*,3*R*)-3-(3,5-dimethoxy-2-methylphenyl)butan-2-ol **17**.

Alkyl boronic acid pinacol ester **24** (219 mg, 0.66 mmol, 1.0 eq) was taken up in degassed THF under inert atmosphere. The solution was cooled to $0\text{ }^\circ\text{C}$ and a degassed mixture of 2 N $\text{NaOH}_{(\text{aq})}:\text{H}_2\text{O}_2$ (30% in H_2O) (2:1, 6.0 mL) was added dropwise. The biphasic mixture was stirred for 2.0 h in the melting ice-water bath. 10 mL of 2 N $\text{NaOH}_{(\text{aq})}$ was added to quench the reaction. The layers were separated and the aqueous layer was extracted with Et_2O thrice and the combined organics were dried over Na_2SO_4 , filtered and the solvent was removed to yield a crude colorless oil. The oil was purified on an automated flash system equipped with a silica column and gradient 15-40% EtOAc in heptane to yield the title compound **17** (115 mg, 0.51 mmol, 78%) as a colorless oil.

$^1\text{H NMR}$ (400 MHz, Chloroform-*d*) δ 6.43 (d, $J = 2.5\text{ Hz}$, 1H), 6.35 (d, $J = 2.4\text{ Hz}$, 1H), 3.94 – 3.84 (m, 1H), 3.81 (s, 3H), 3.80 (s, 3H), 3.11 – 3.00 (m, 1H), 2.15 (s, 3H), 1.55 (d, $J = 2.6\text{ Hz}$, 1H), 1.27 (d, $J = 6.2\text{ Hz}$, 3H), 1.18 (d, $J = 7.0\text{ Hz}$, 3H).

$^{13}\text{C NMR}$ (101 MHz, Chloroform-*d*) δ 158.8 (2C), 143.9, 118.0, 102.5, 96.3, 72.3, 55.6, 55.4, 43.0, 20.5, 18.0, 10.9.

HRMS (ES): calcd for $\text{C}_{13}\text{H}_{21}\text{O}_3^+$ $[\text{M}+\text{H}]^+$ 225.1485, found: 225.1483.

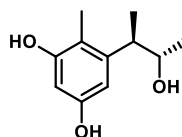
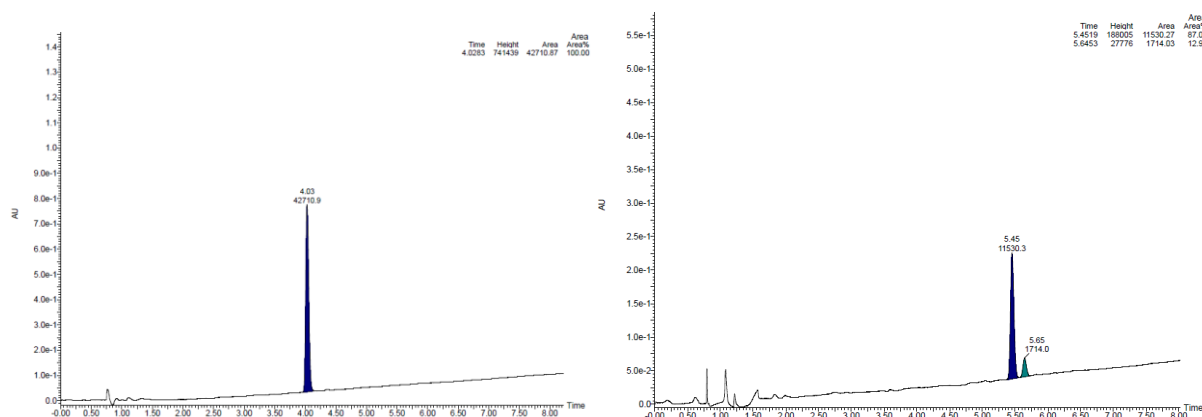
IR ($\nu_{\max}/\text{cm}^{-1}$, neat): 3434, 2965, 2935, 1586, 1454, 1307, 1201, 1145, 1084, 1027, 939, 920, 827, 729.

R_f: 0.38 (35% EtOAc in heptane).

[α]_D²⁰: +46.5° (*c* 0.8, CHCl₃).

Chiral SFC: (TrefoilTM, CEL2, 1.2 mL/min, 40 °C, 280 nm, solvent A: CO₂, solvent B: EtOH:PrOH:TFA 1:1:0.2%, gradient: 0 min: 25% B, 7.5 min: 35% B, 8 min 60% B, 9 min 60% B, 9.3 min 25% B, 11 min 25% B). t_R = 4.03 min (2*S*, 3*R*), e.r. = >99%

To (+)-alcohol **17** (3 mg) was added 2 M H₂SO₄ (1 mL) and it was stirred for 3 h to induce racemization.^[7] The acidic aqueous layer was extracted with EtOAc (3x), the organics combined and the solvent was removed. The obtained compound was again analyzed by chiral SFC using a slightly modified gradient: 0 min: 10% B, 7.5 min: 17% B, 8 min 60% B, 9 min 60% B, 9.3 min 10% B, 11 min 10% B). t_R = 5.45 min (2*S*,3*R*), e.r. = 87.1% and t_R = 5.65 (2*R*,3*S*), e.r. = 12.9%.



(+)-5-((2*R*,3*S*)-3-hydroxybutan-2-yl)-4-methylbenzene-1,3-diol (*ent*-Phenol A) (**6**).

NaH (19 mg, 470 μmol , 1.3 eq, 60% in mineral oil) was placed in a heat dried microwave vial. The vial was evacuated and backfilled with argon. To remove the mineral oil, anhydrous pentane (1.0 mL) was added to the solids, the tube was briefly shaken and the liquids were removed to yield pure white NaH. Alcohol **17** (81 mg, 361 μmol , 1.0 eq) was placed in a heat dried vial. The vial was evacuated and backfilled with argon and anhydrous 1,3-dimethyl-2-imidazolidinone (DMI, 1.0 mL) was added. The solution was transferred to the microwave vial and the resulting suspension was stirred at ambient temperature. After 45 min a slightly green solution was obtained and gas evolution has ceased. Hexamethyldisilathiane (152 μL , 722 μmol , 2.0 eq) was added and strong gas evolution was observed. The turbid mixture was stirred at ambient temperature for 15 min until gas evolution has ceased to deliver a dark blue, clear solution. The solution was heated to 220 °C for 22 min under microwave irradiation. After cooling, a dark brown, clear solution was obtained. Water was added and the pH was adjusted to pH = 3-4 with a 0.01 N HCl solution. The aqueous layer was extracted with EtOAc (4x). The combined organics were dried over MgSO₄, filtered and the solvent was removed to yield a crude, yellow-brown liquid. The crude was filtered over a short silica plug with a mixture of DCM:MeOH 95:5 (v/v) to remove DMI. The obtained yellow oil was purified by column chromatography on silica gel with 35-50% EtOAc in heptane to yield *ent*-phenol A (**6**) (12 mg, 61 μmol , 17%) a white solid.

The analytical data was identical to the previously reported data for synthetic phenol A.^[8]

¹H NMR (400 MHz, Acetone-*d*₆) δ 7.91 (s, 1H), 7.74 (s, 1H), 6.34 (d, *J* = 2.4 Hz, 1H), 6.25 (d, *J* = 2.4 Hz, 1H), 3.90 – 3.79 (m, 1H), 3.19 (d, *J* = 4.1 Hz, 1H), 3.04 (p, *J* = 7.0 Hz, 1H), 2.09 (s, 3H), 1.13 (d, *J* = 7.1 Hz, 3H), 1.10 (d, *J* = 6.2 Hz, 3H).

^{13}C NMR (101 MHz, Acetone-*d*₆) δ 156.6, 156.5, 145.8, 114.5, 105.8, 101.1, 71.4, 42.9, 20.2, 16.7, 10.9.

HRMS (ES): calcd for $\text{C}_{11}\text{H}_{17}\text{O}_3^+$ $[\text{M}+\text{H}]^+$ 197.1172, found: 197.1173

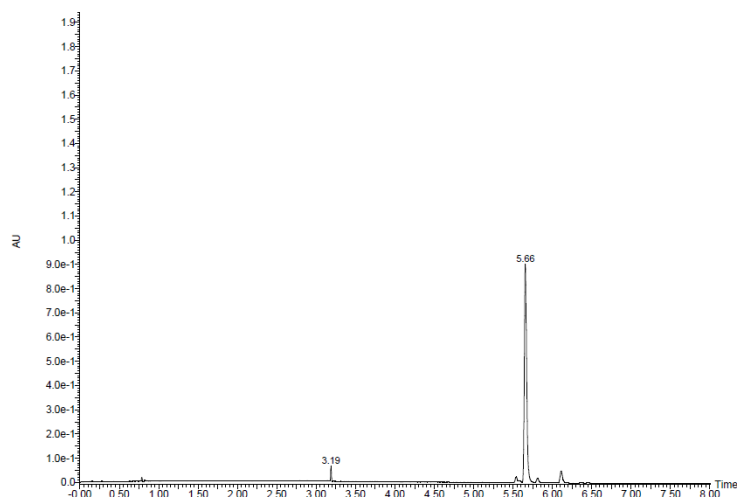
IR ($\nu_{\text{max}}/\text{cm}^{-1}$, neat): 3276, 2971, 2933, 1596, 1458, 1303, 1267, 1136, 1019, 918, 896, 842, 729.

M_p: 120-122 °C

R_f: 0.47 (70% EtOAc in heptane)

$[\alpha]_{\text{D}}^{20}$: +34.5° (c = 0.67, EtOH)

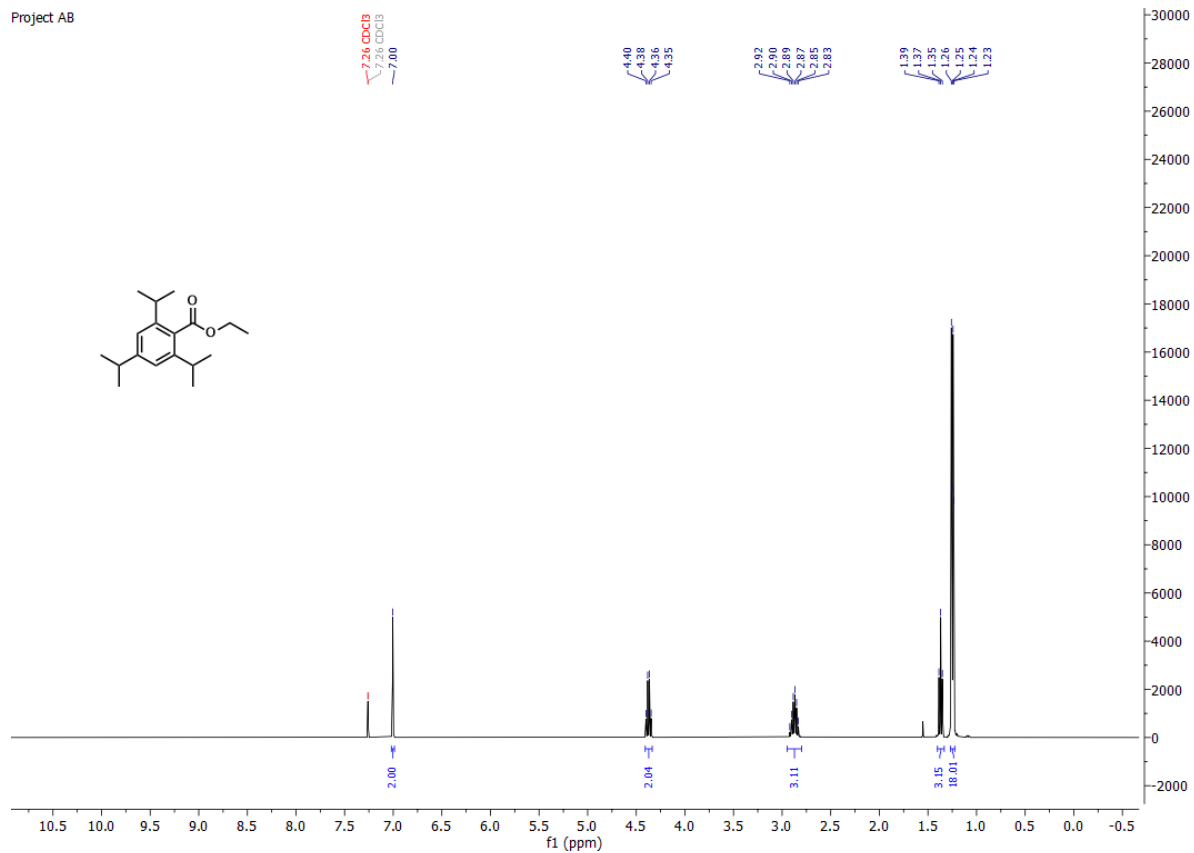
Chiral SFC: (TrefoilTM, CEL2, 1.2 mL/min, 40 °C, 280 nm, solvent A: CO₂, solvent B: EtOH:PrOH:TFA 1:1:0.2%, gradient: 0 min: 40% B, 2.0 min: 40% B, 6.50 min: 60% B, 7.50 min 60% B, 7.70 min 40% B, 9.0 min 40% B). t_R = 5.66 min (2*R*, 3*S*), e.r. = >99%.



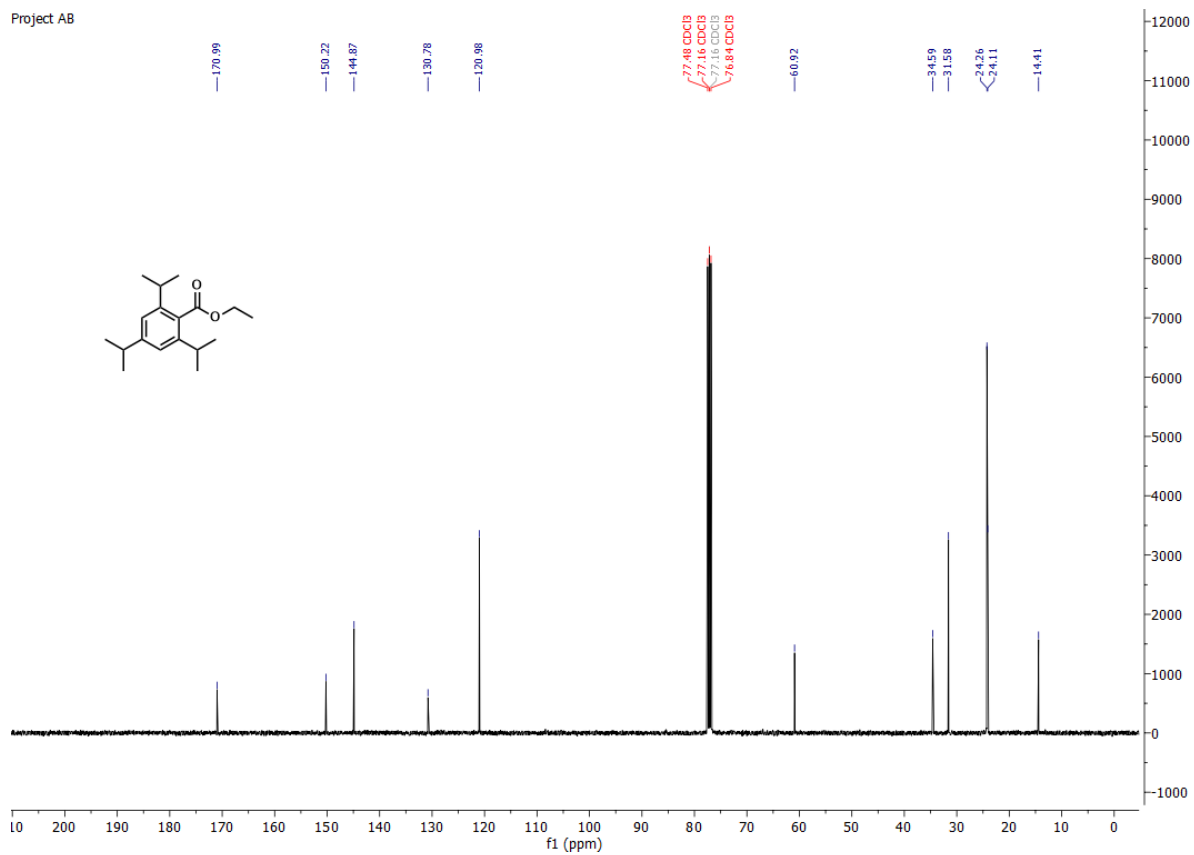
2. NMR spectra

Ethyl 2,4,6-triisopropylbenzoate **S1**.^[3]

Project AB

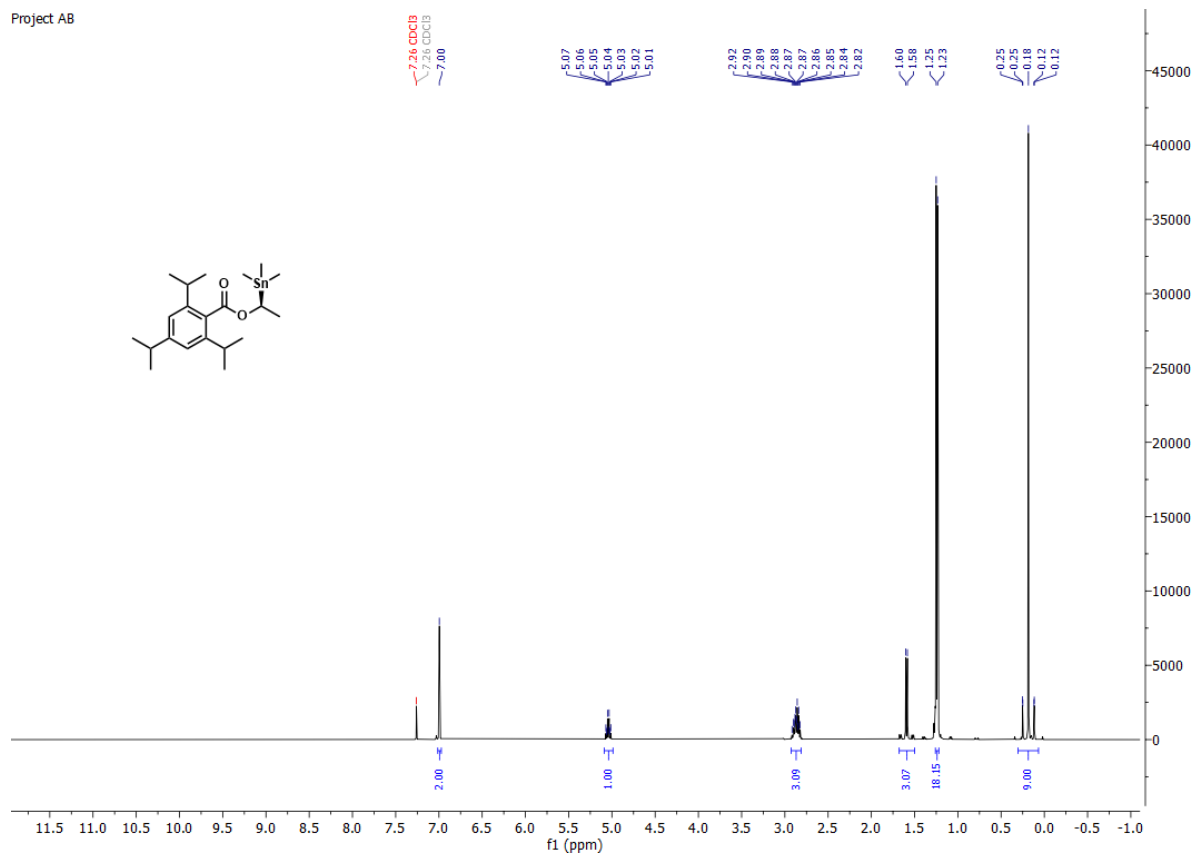


Project AB

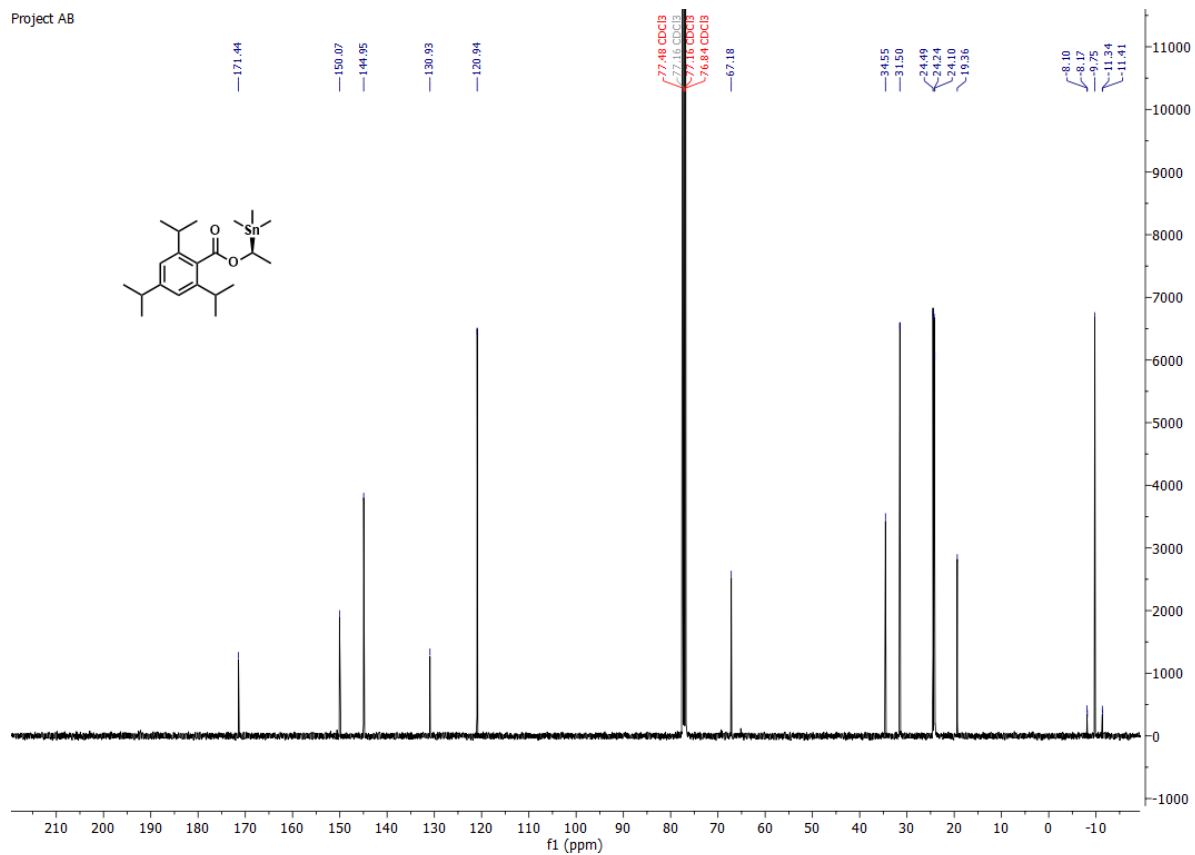


(S)-1-(trimethylstannyl)ethyl 2,4,6-triisopropylbenzoate **18**.^[3]

Project AB

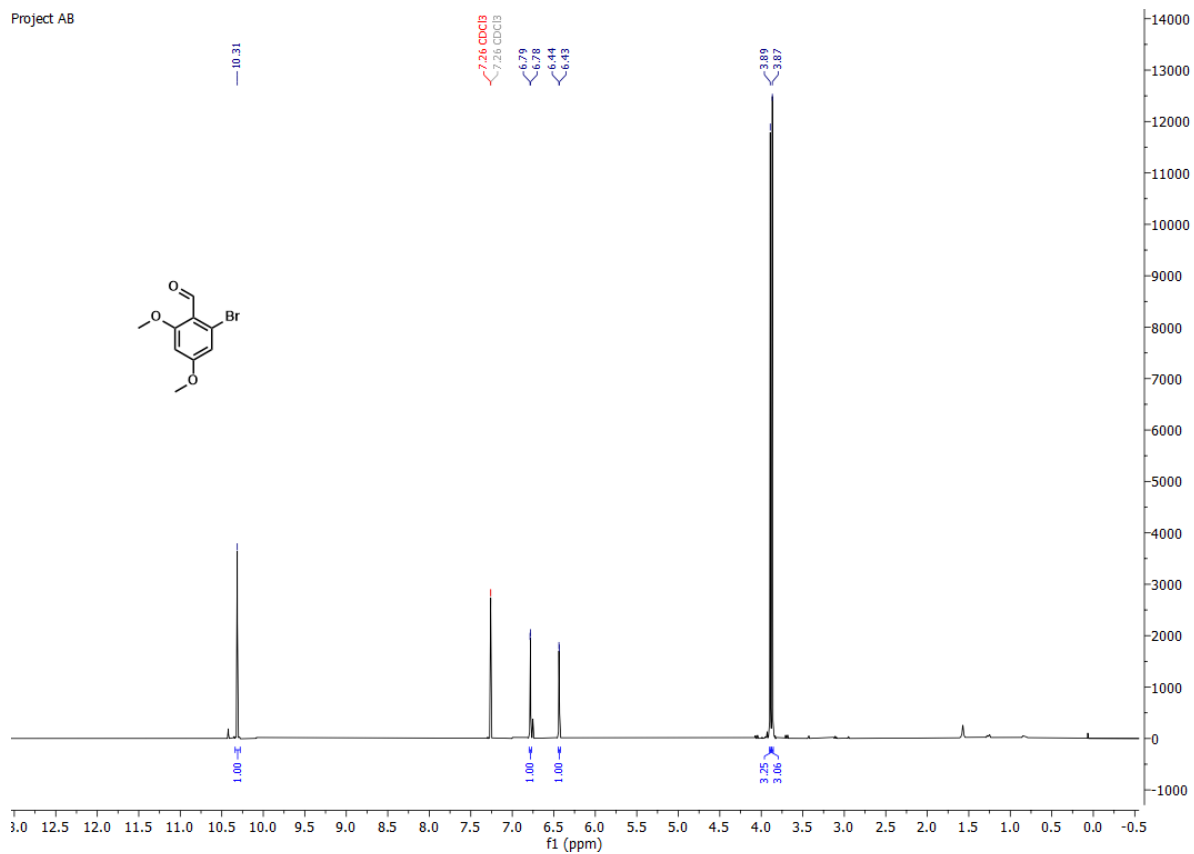


Project AB

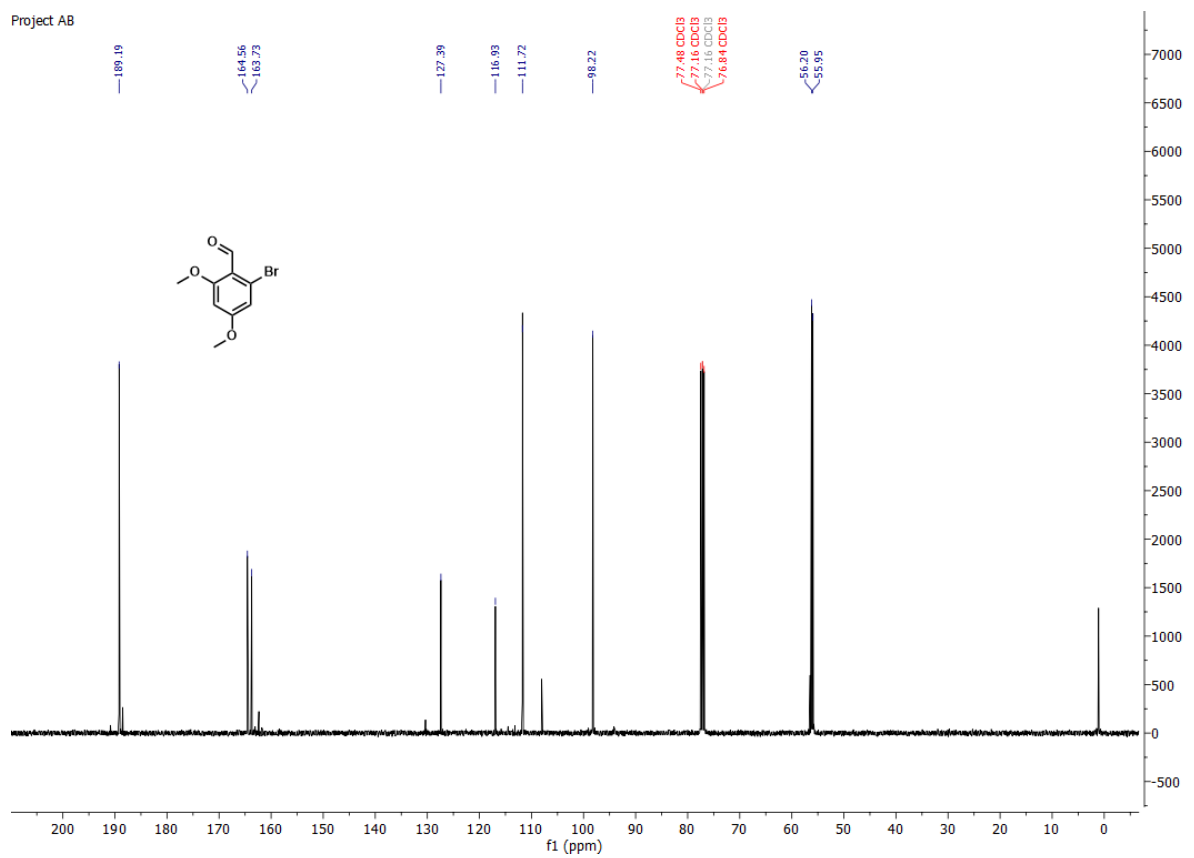


2-bromo-4,6-dimethoxybenzaldehyde **21**.

Project AB

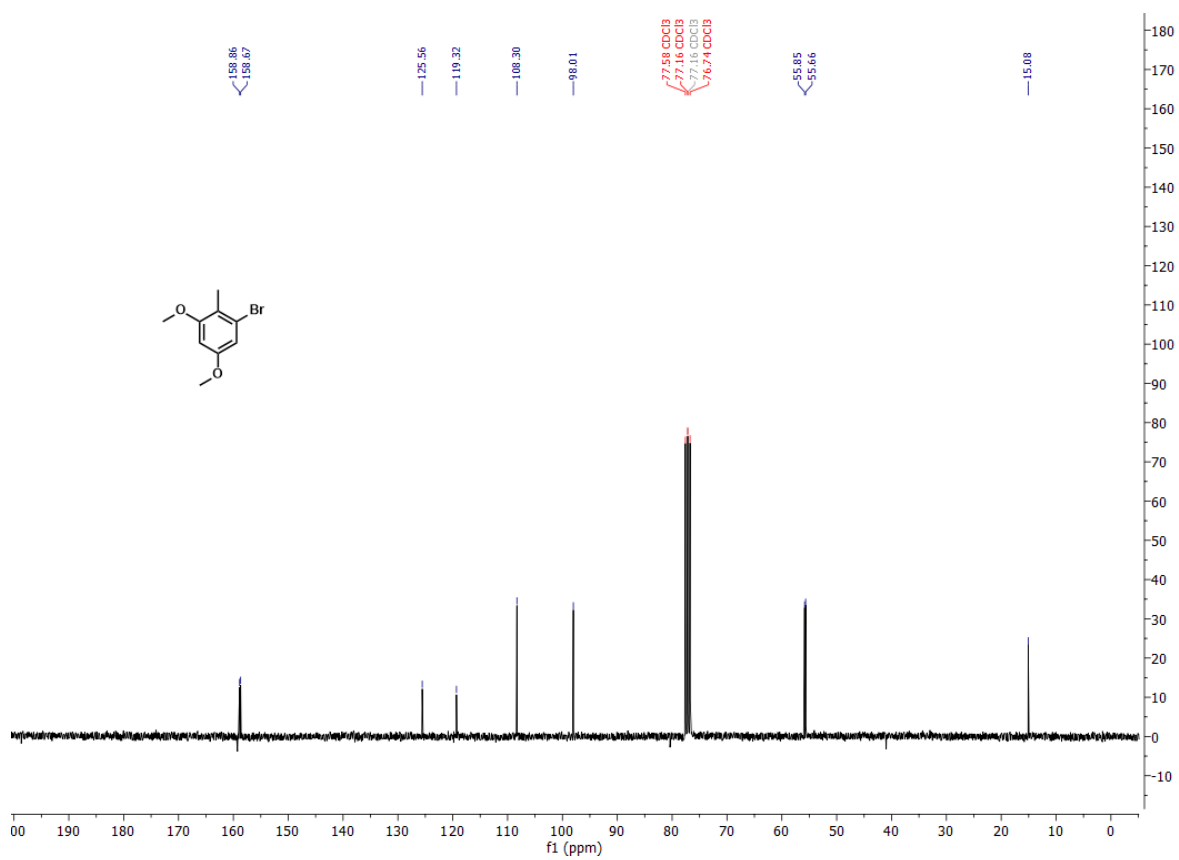
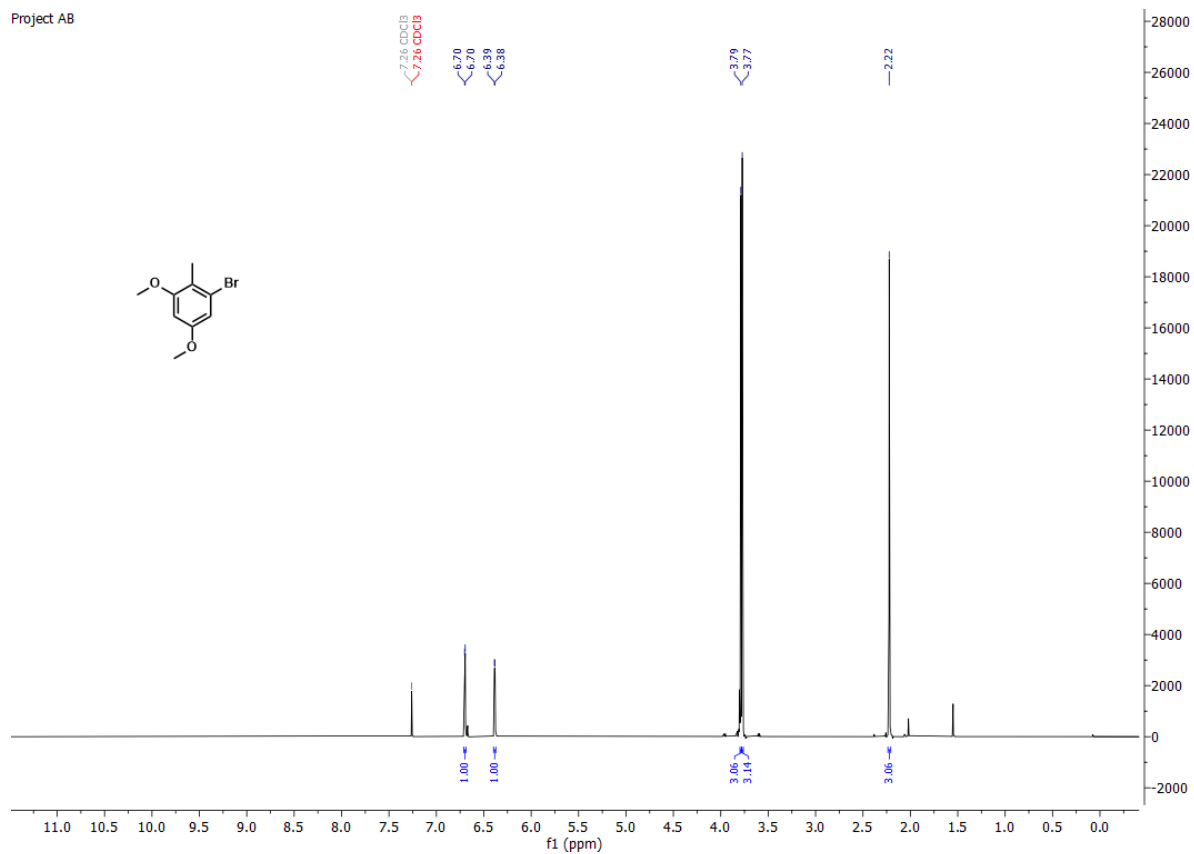


Project AB



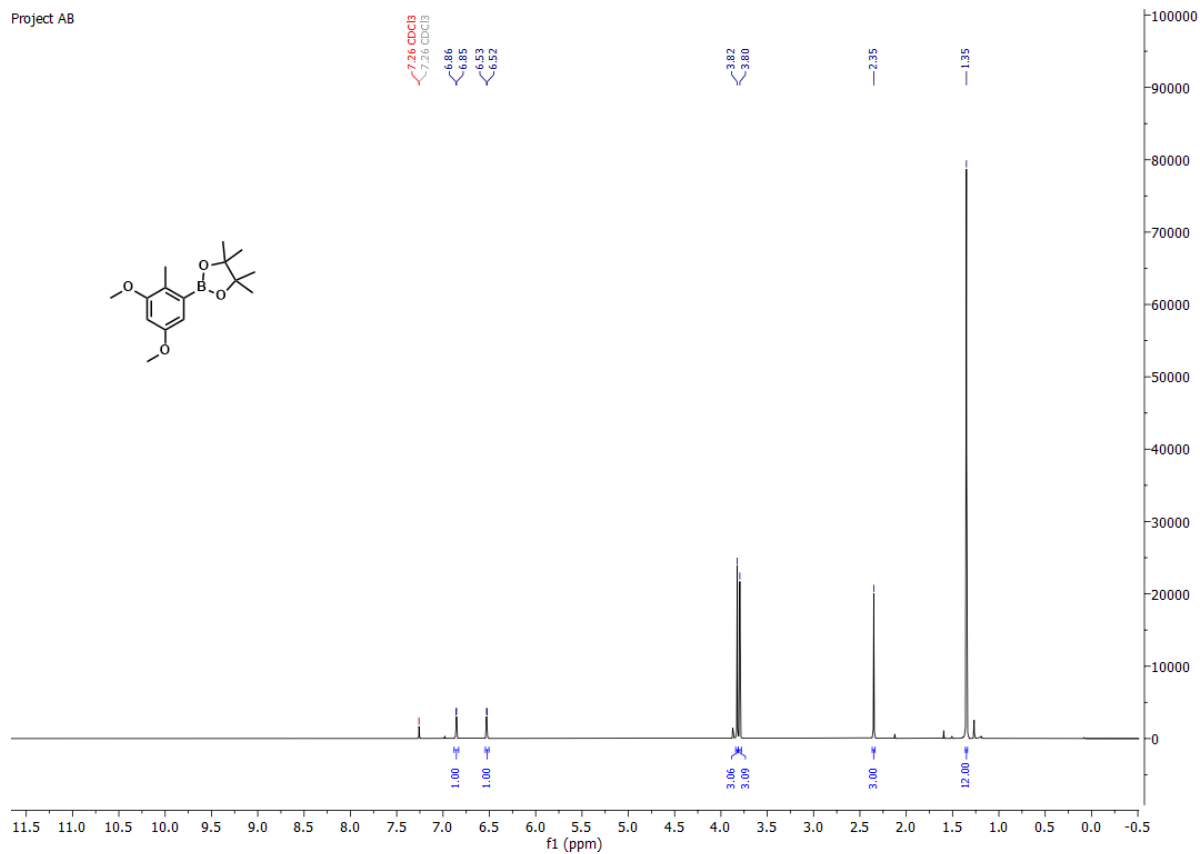
1-bromo-3,5-dimethoxy-2-methylbenzene **22**.

Project AB

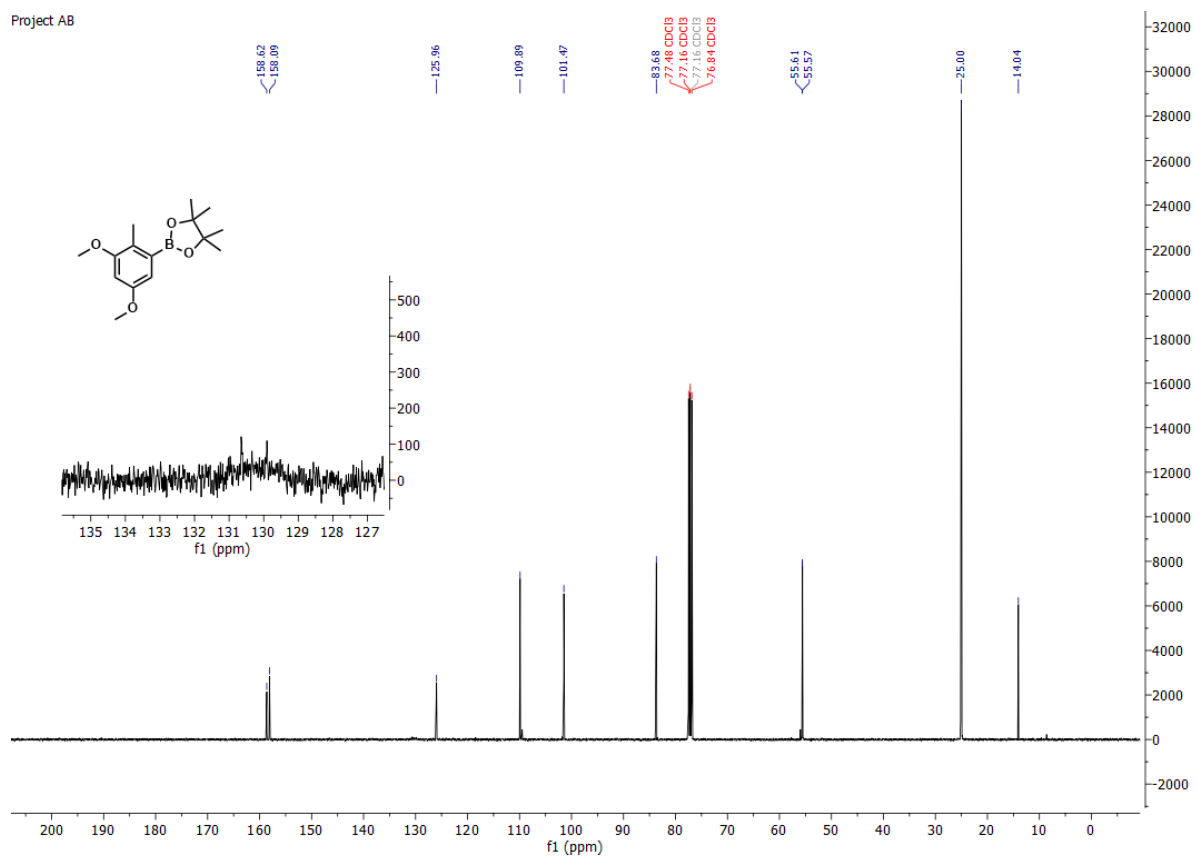


2-(3,5-dimethoxy-2-methylphenyl)-4,4,5,5-tetramethyl-1,3,2-dioxaborolane **15**.

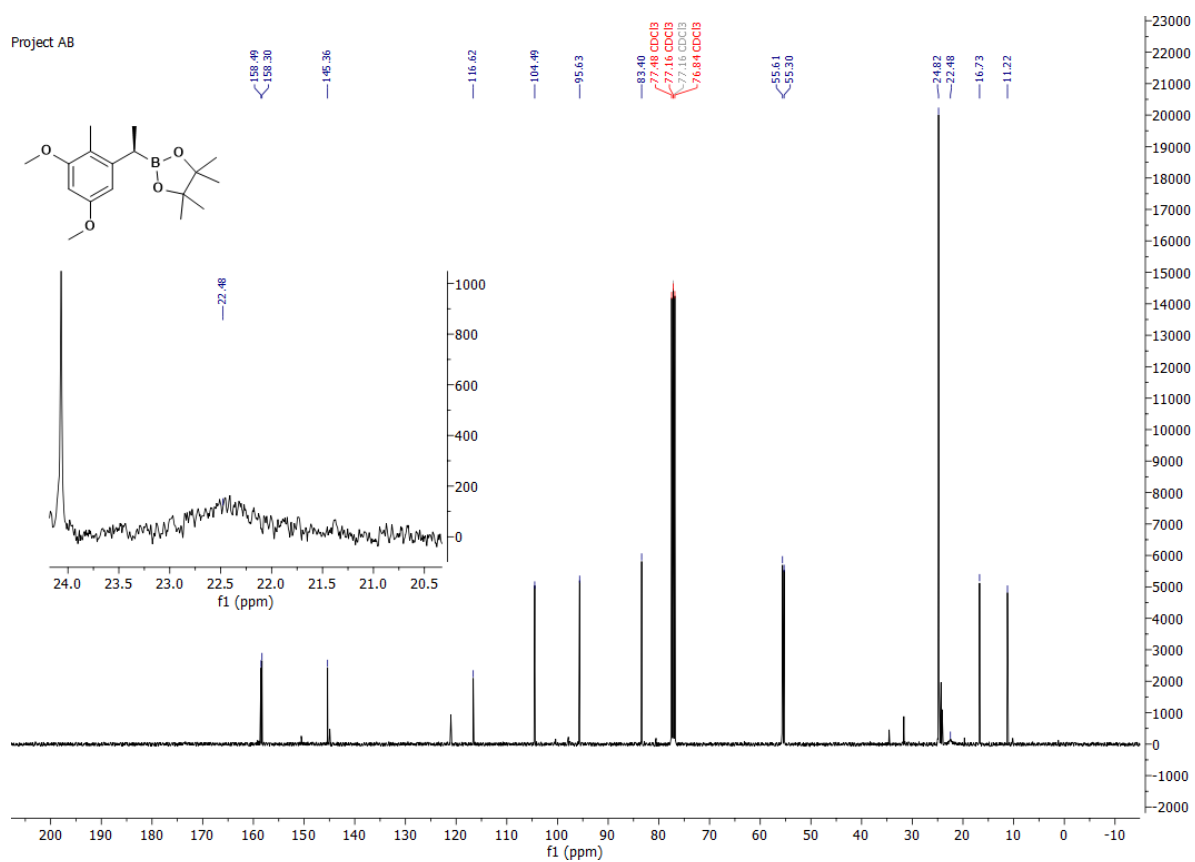
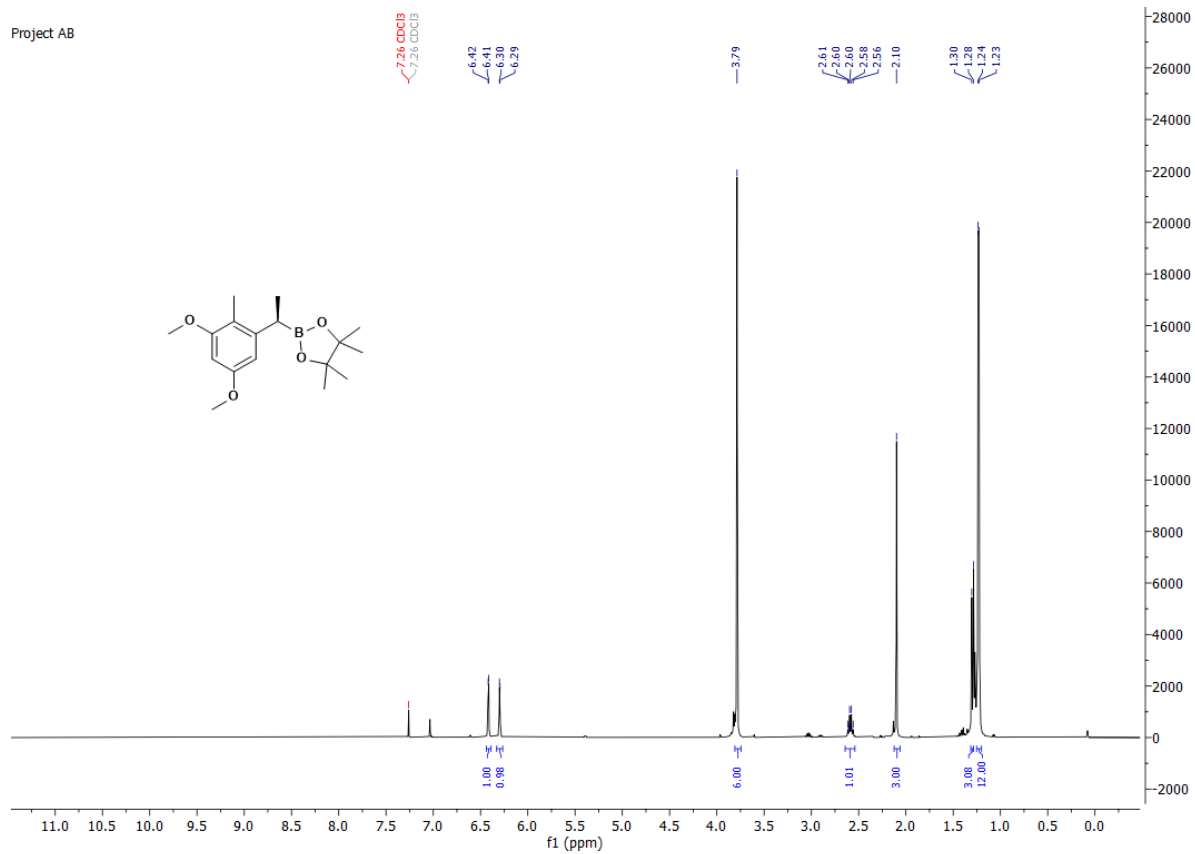
Project AB



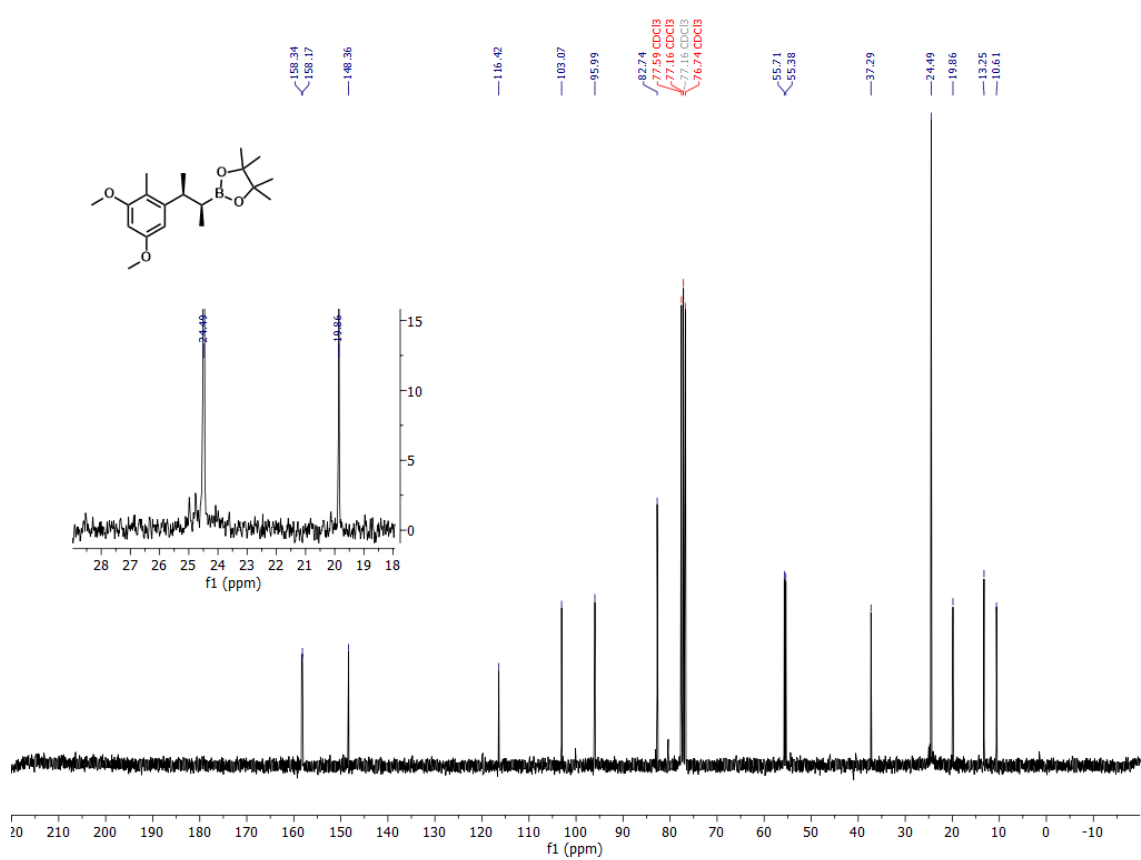
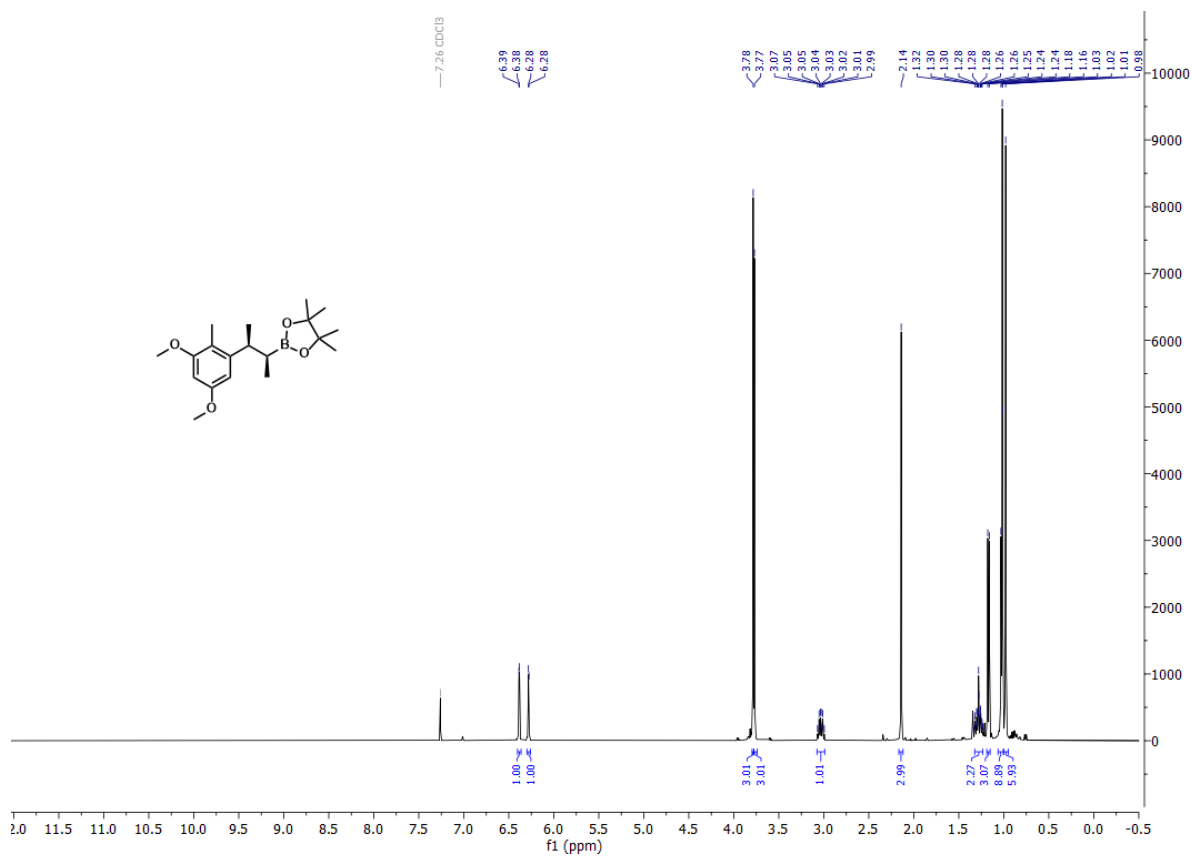
Project AB



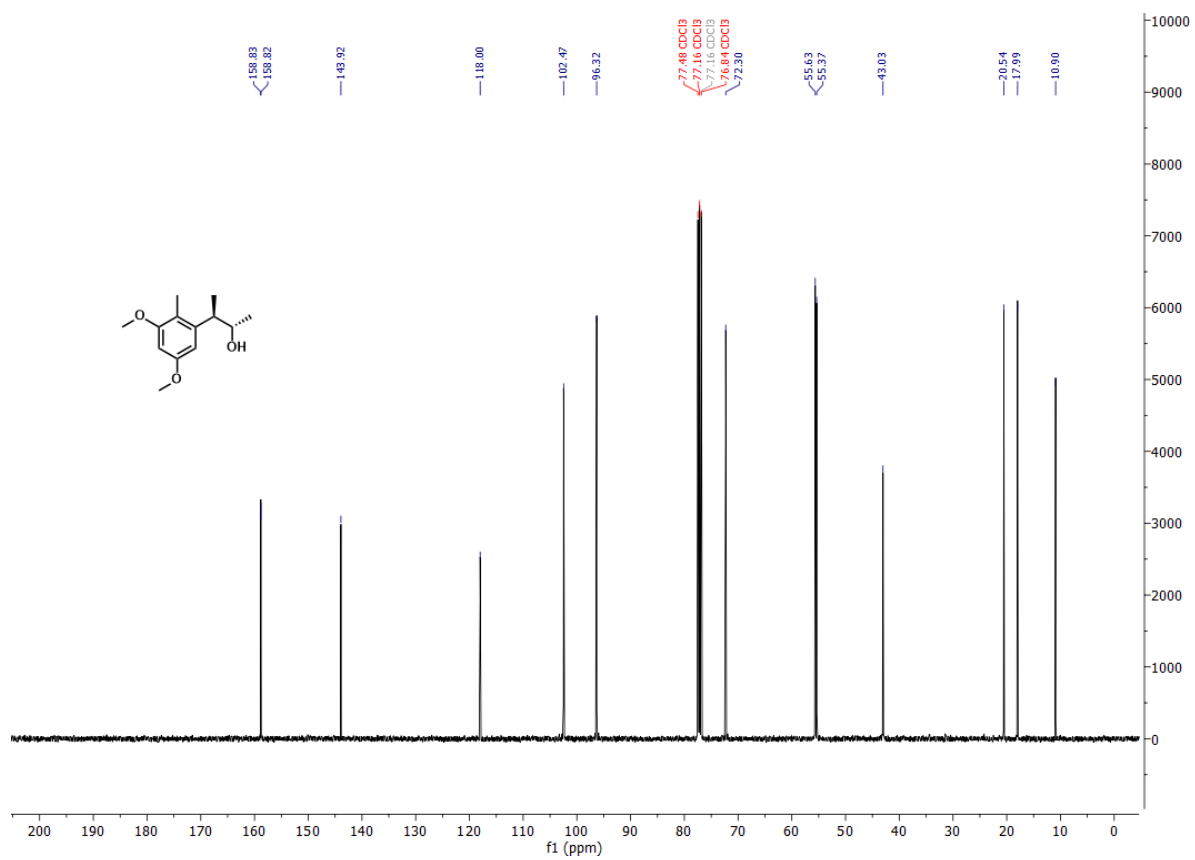
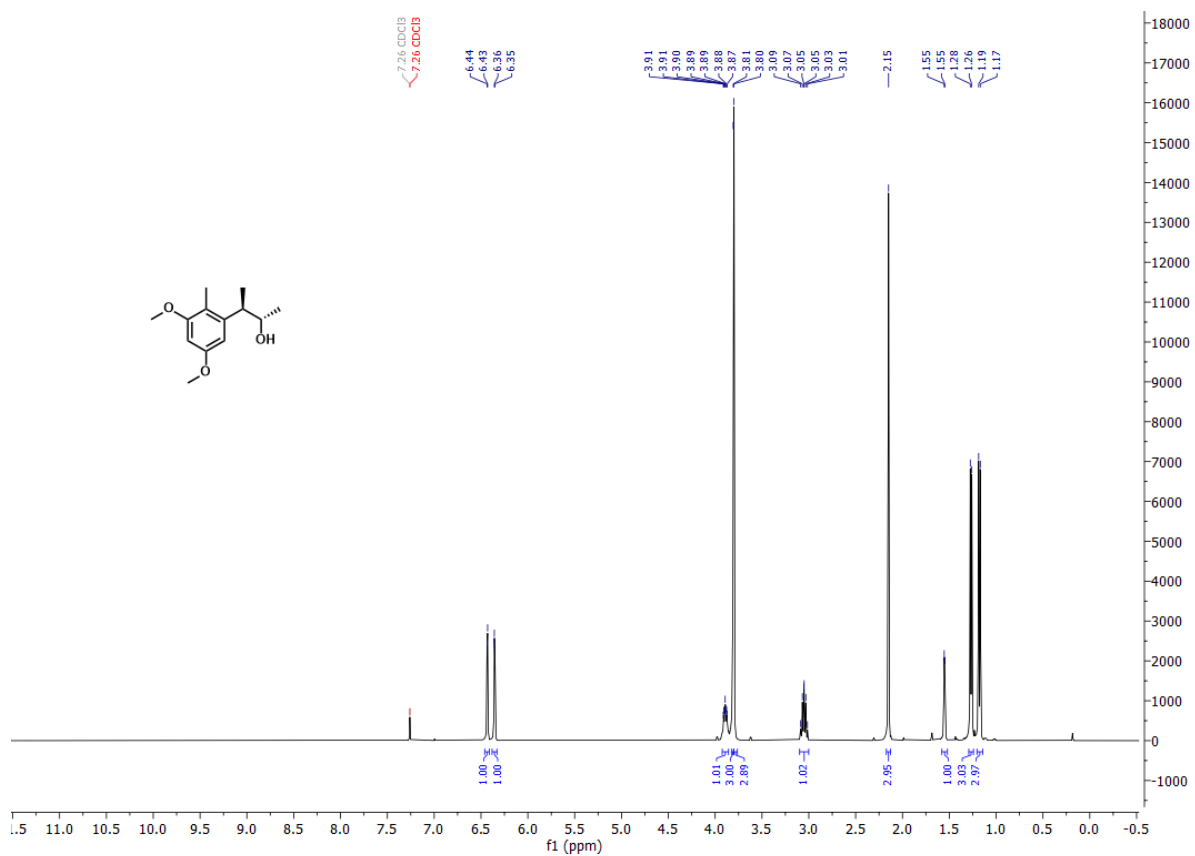
(R)-2-(1-(3,5-dimethoxy-2-methylphenyl)ethyl)-4,4,5,5-tetramethyl-1,3,2-dioxaborolane **16**.



2-((2S,3S)-3-(3,5-dimethoxy-2-methylphenyl)butan-2-yl)-4,4,5,5-tetramethyl-1,3,2-dioxaborolane **24**.

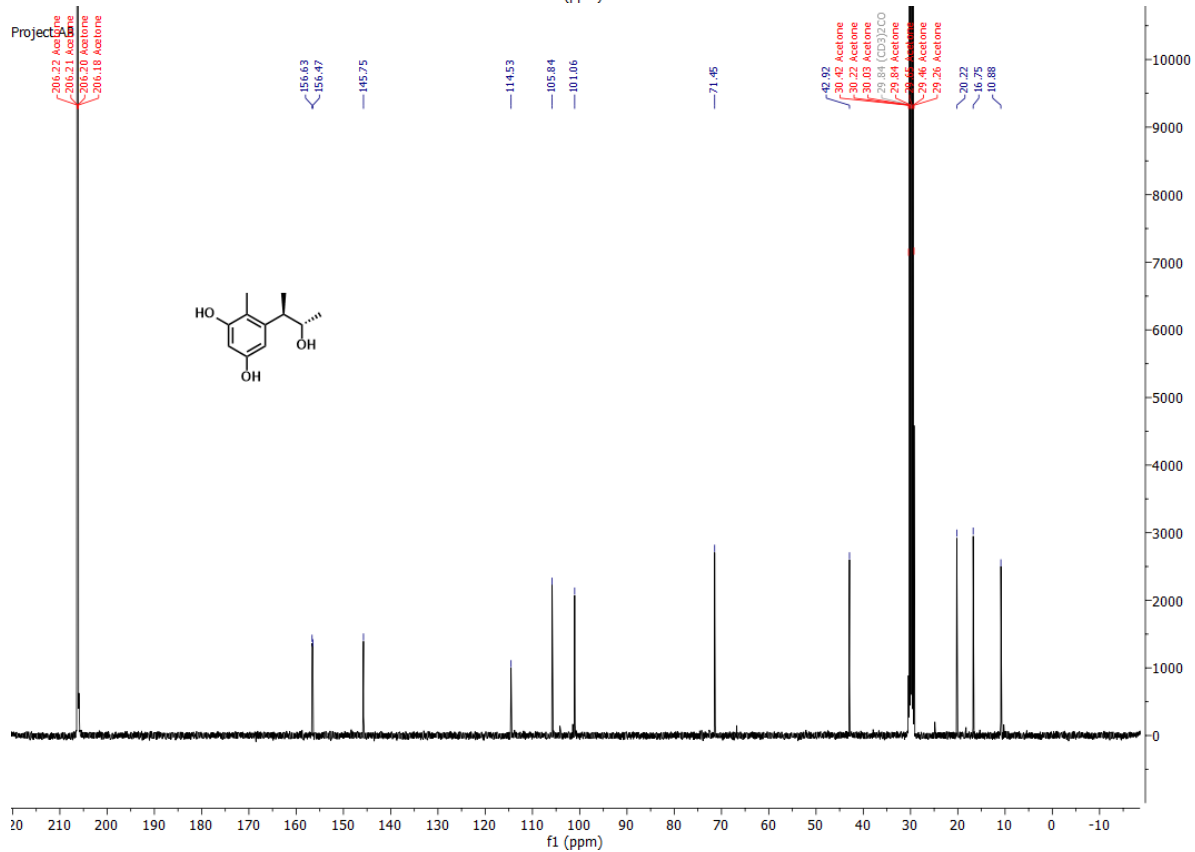
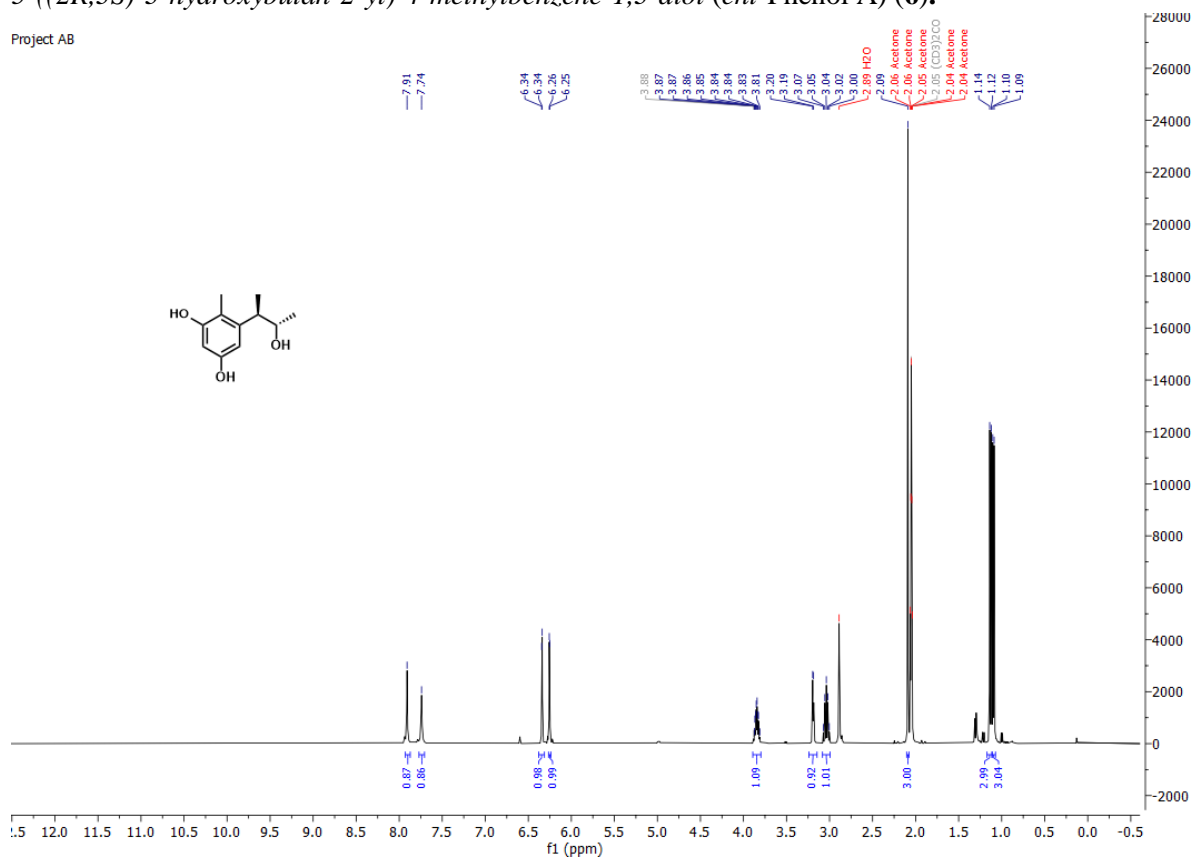


(2S,3R)-3-(3,5-dimethoxy-2-methylphenyl)butan-2-ol **17**.



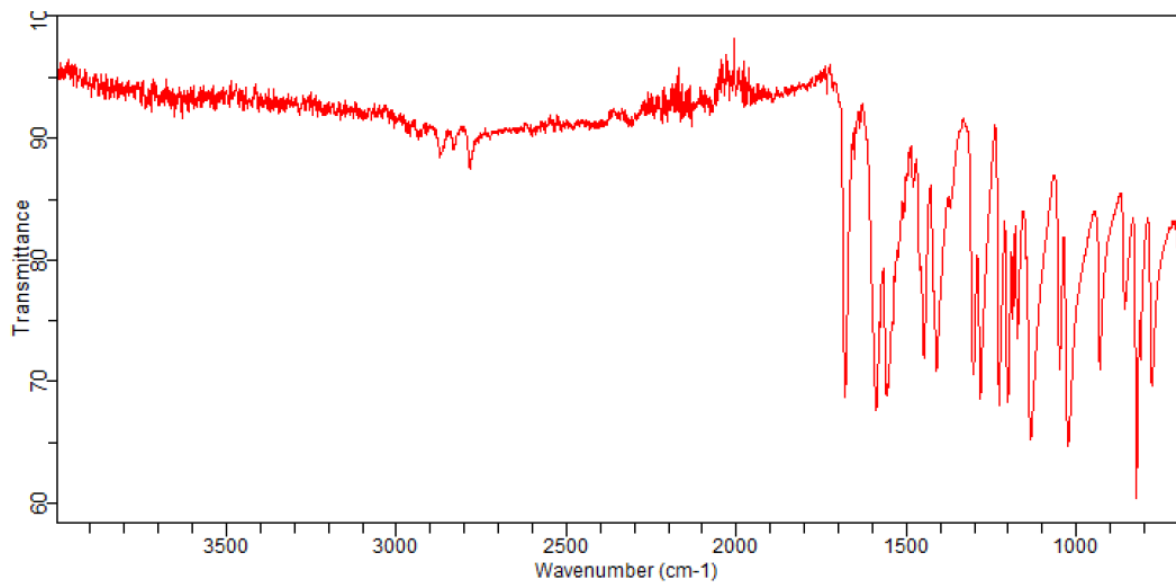
5-((2R,3S)-3-hydroxybutan-2-yl)-4-methylbenzene-1,3-diol (*ent*-Phenol A) (**6**).

Project AB

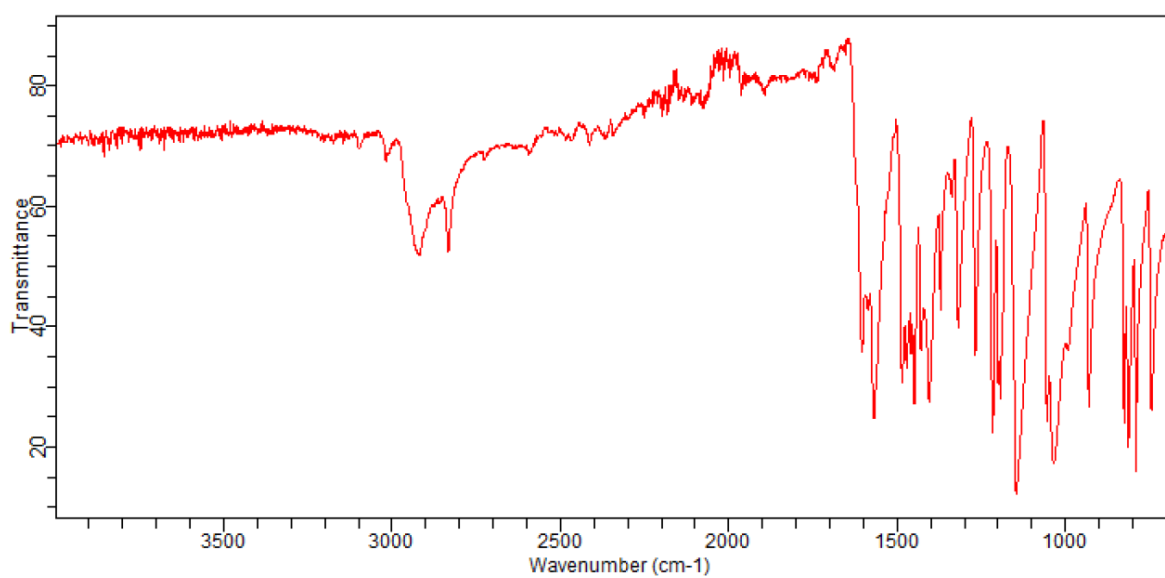


3. IR spectra

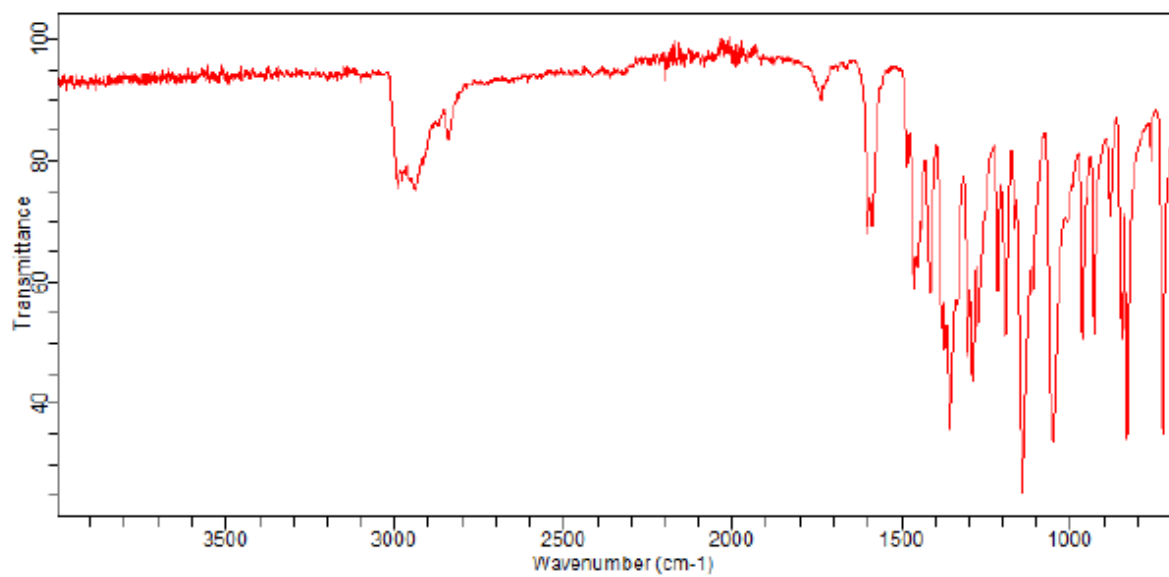
2-bromo-4,6-dimethoxybenzaldehyde **21**.



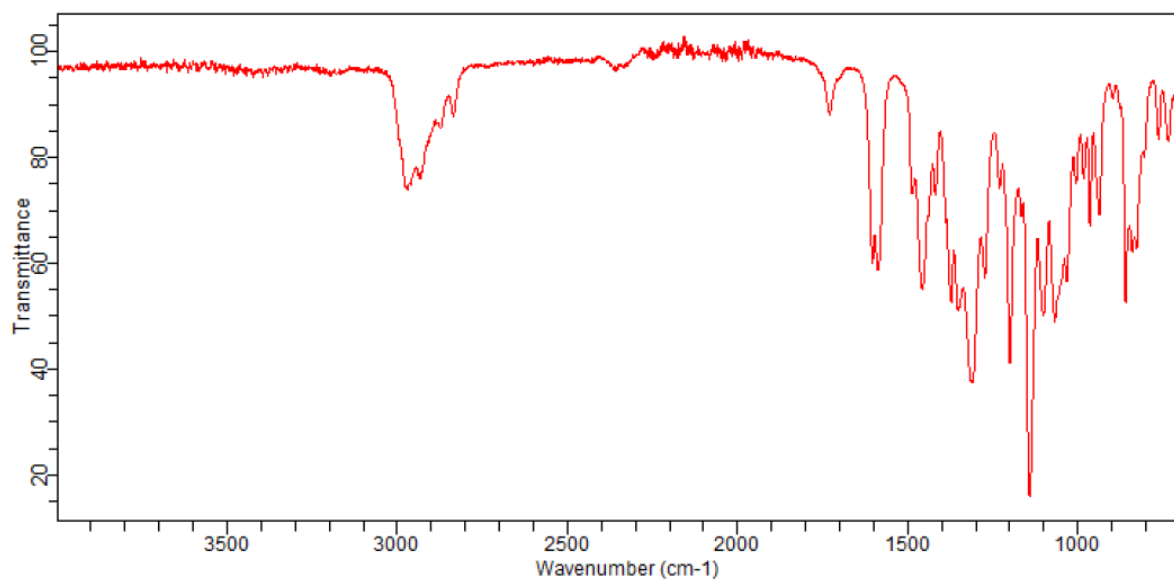
1-bromo-3,5-dimethoxy-2-methylbenzene **22**.



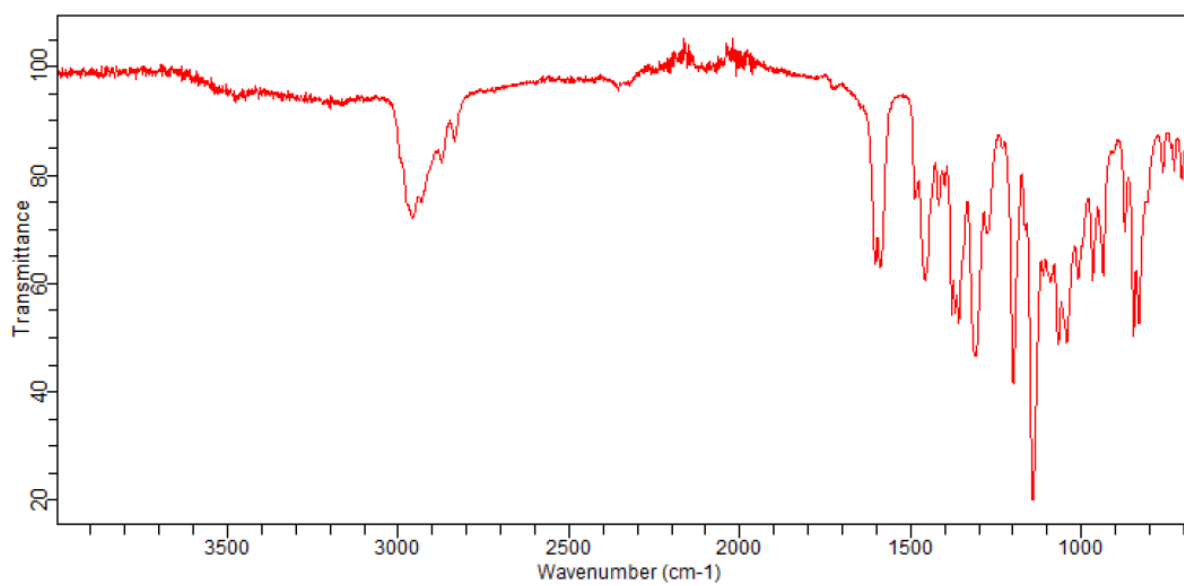
2-(3,5-dimethoxy-2-methylphenyl)-4,4,5,5-tetramethyl-1,3,2-dioxaborolane 15.



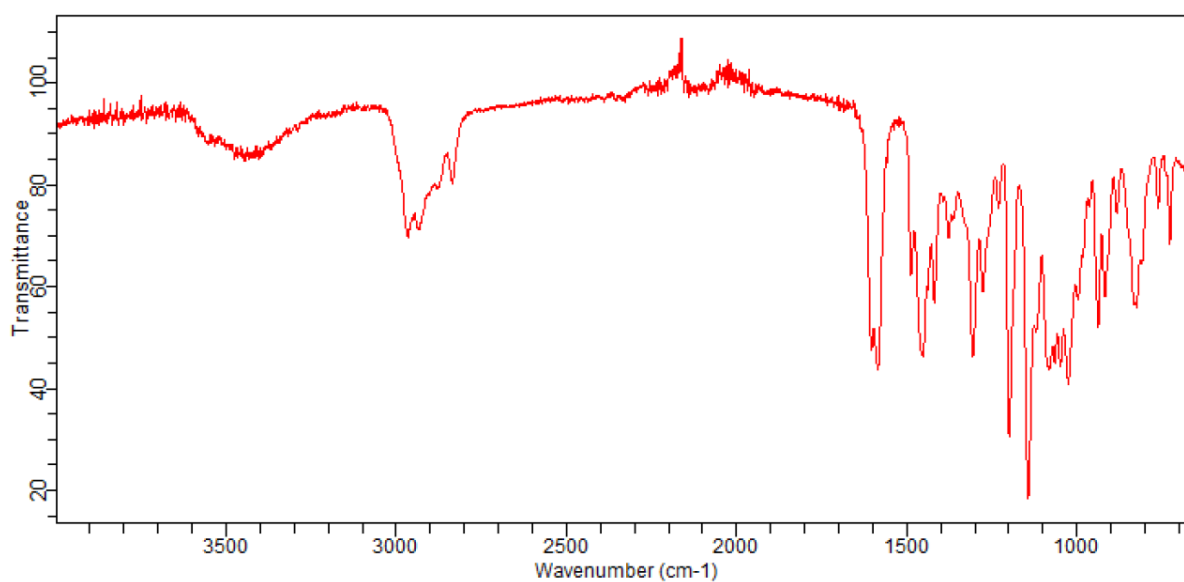
(R)-2-(1-(3,5-dimethoxy-2-methylphenyl)ethyl)-4,4,5,5-tetramethyl-1,3,2-dioxaborolane 16.



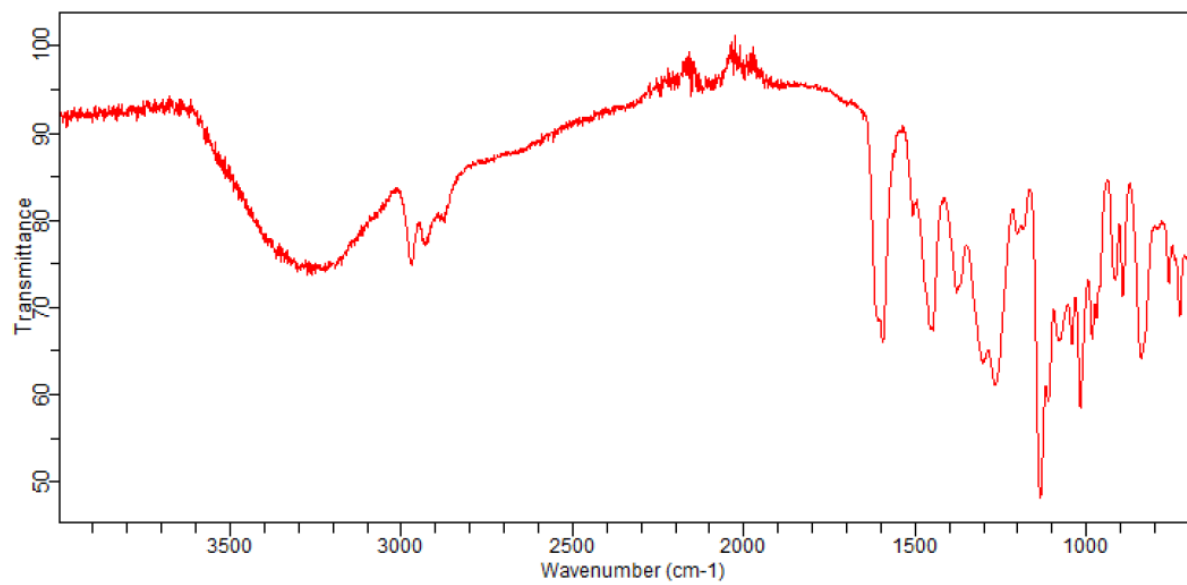
2-((2S,3S)-3-(3,5-dimethoxy-2-methylphenyl)butan-2-yl)-4,4,5,5-tetramethyl-1,3,2-dioxaborolane 24.



(2S,3R)-3-(3,5-dimethoxy-2-methylphenyl)butan-2-ol 17.



5-((2*R*,3*S*)-3-hydroxybutan-2-yl)-4-methylbenzene-1,3-diol (*ent*-Phenol A) (**6**).



4. References

- [1] A. B. Pangborn, M. A. Giardello, R. H. Grubbs, R. K. Rosen, F. J. Timmers, *Organometallics* **1996**, *15*, 1518-1520.
- [2] V. Bagutski, R. M. French, V. K. Aggarwal, *Angew. Chem. Int. Ed.* **2010**, *49*, 5142-5145.
- [3] M. Burns, S. Essafi, J. R. Bame, S. P. Bull, M. P. Webster, S. Balieu, J. W. Dale, C. P. Butts, J. N. Harvey, V. K. Aggarwal, *Nature* **2014**, *513*, 183-188.
- [4] A. H. Sommers, R. J. Michaels, A. W. Weston, *J. Am. Chem. Soc.* **1952**, *74*, 5546-5546.
- [5] S. Gadhwal, M. Baruah, J. S. Sandhu, *Synlett* **1999**, *1999*, 1573-1574.
- [6] R. Larouche-Gauthier, C. J. Fletcher, I. Couto, V. K. Aggarwal, *Chem. Commun.* **2011**, *47*, 12592-12594.
- [7] A. C. R. Hetherington, H., *Trans. Roy. Soc. (London)* **1931**, *B220*, 269-296.
- [8] T. Rödel, H. Gerlach, *Liebigs Ann. Chem.* **1995**, *1995*, 885-888.

